

*Proceedings of*

# SMAC 03

Stockholm Music Acoustics Conference

August 6-9, 2003

**Volume I**

*Edited by Roberto Bresin*

*2<sup>nd</sup> edition*



Copyright © 2003 by the authors. Permission is granted to copy, distribute and/or modify this document under the terms of the GNU Free Documentation License, Version 1.2 or any later version published by the Free Software Foundation; with no Invariant Sections, no Front-Cover Texts, and no Back-Cover Texts. A copy of the license is included in the section entitled “GNU Free Documentation License”.

The website of this book is <http://www.speech.kth.se/smac03>

Cover by Kjetil Falkenberg Hansen & Roberto Bresin

### **Contents**

**Volume I:** Opening Session - The Sundberg Session – Violins – Guitars – Pianos – Brasses – Woodwinds – Organs – Percussions - Physics-Based Modelling

**Volume II:** Singing Voice - Music Performance - Music Perception - Instrument Control - Miscellanea

Volume I: ISBN 91-7283-558-3

Volume II: ISBN 91-7283-559-1

TRITA-TMH 2003:8

ISSN 1104-5787

# CONTENTS

## VOLUME I

---

<i>Scientific advisory committee</i>	<i>xvi</i>
<i>Preface</i>	<i>xvii</i>
<i>Sponsors</i>	<i>xix</i>

### OPENING SESSION

Recent developments in musical sound synthesis based on a physical model ( <i>invited paper</i> ) <i>J O Smith III</i>	3
From musical acoustics to everyday acoustics: a physical modeling route ( <i>invited paper</i> ) <i>D Rocchesso</i>	7

### THE SUNDBERG SESSION

A marriage of the Director Musices program and the Conductor Program ( <i>invited paper</i> ) <i>M V Mathews, A Friberg, G Bennett, C Sapp, J Sundberg</i>	13
Expressiveness in music performance: analysis and modelling ( <i>invited paper</i> ) <i>G De Poli</i>	17
The voice as a musical instrument: fundamental differences between man-made and biological designs ( <i>invited paper</i> ) <i>Ingo R. Titze</i>	21
Why music does not produce basic emotions: A plea for changing the paradigm in studying the emotional effects of music ( <i>invited paper</i> ) <i>K R Scherer</i>	25

### VIOLINS

The bowed string as we understand it today ( <i>invited paper</i> ) <i>J Woodhouse</i>	31
Generalized normal mode violin acoustics ( <i>invited paper</i> ) <i>G Bissinger</i>	35

An acoustical comparison of flat- and round-backed double basses <i>A W Brown</i>	39
Operating deflecting modes of five conventional and two unconventional violins recorded with TV-holography <i>A Buen, O J Løkberg</i>	43
Numerical optimization of violin bows with varying densities of the wood material <i>P Carlsson, M Tinnsten</i>	47
Modeling Savart 's trapezoidal violin using a digital waveguide mesh <i>F Fontana, S Serafin</i>	51
Experiments with an automatic bowing machine <i>P M Galluzzo, J Woodhouse</i>	55
Psychoacoustic investigations on the possibility of aurally identical violins <i>P Geissler, O Martner, C Zerbs, M Schleske</i>	59
The influence of vibrato and noise on the assessment of violin tone <i>C Gough</i>	63
Bow speed or bowing position - which one influences spectrum the most? <i>K Guettler, E Schoonderwaldt, A Askenfelt</i>	67
The BH-hill and tonal quality of the violin <i>E V Jansson</i>	71
Inferring decision rules from jurors' ranking of competing violins <i>J Jelonek, E Łukasik, A Naganovski, R Slowinski,</i>	75
AMATI: A multimedia database of violin sounds <i>E Łukasik</i>	79
Unsupervised machine learning methods in timbral violin characteristics visualization <i>E Łukasik, R Susmaga</i>	83
Logarithmic damping decrement as the characteristic of physical acoustics for quality estimation of violin wedges <i>E Rajčan, S Urgela, M Čulík</i>	87
Effect of the width of the bow hair on the violin string spectrum <i>E Schoonderwaldt, K Guettler, A Askenfelt</i>	91
Bowed string simulation using an elasto-plastic friction model <i>S Serafin, F Avanzini, D Rocchesso</i>	95
Bowed string physical model validation through use of a bow controller and examination of bow strokes <i>S Serafin, D Young</i>	99
Determination of important wood properties for blanks for violin tops by the use of numerical optimisation <i>M Tinnsten, P Carlsson</i>	103

The admittance matrix of a cello <i>J Woodhouse, P E Courtney</i>	107
Wireless sensor system for measurement of violin bowing parameters <i>D Young</i>	111

## GUITARS

Guitar models for makers ( <i>invited paper</i> ) <i>B E Richardson</i>	117
Physical model of a complete classical guitar body <i>R Bader</i>	121
A comparative study of the vibro-acoustical behaviour of electric guitars produced in different decades <i>E Esposito</i>	125
Modal radiation from classical guitars: experimental measurements and theoretical predictions <i>T J W Hill, B E Richardson, S J Richardson</i>	129
New Designs for the kantele with improved sound radiation <i>J Pölkki, C Erkut, H Penttinen, M Karjalainen, V Välimäki</i>	133
The transient behaviour of guitar strings <i>J Woodhouse</i>	137

## PIANOS

Modeling the longitudinal vibration of piano strings <i>B Bank, L Sujbert</i>	143
Quality of treble piano tones <i>A Galembo</i>	147
Phase randomisation in piano bass tones <i>A Galembo, A Askenfelt</i>	151
Measurement and reproduction accuracy of computer-controlled grand pianos <i>W Goebel, R Bresin</i>	155
The piano action as the performer's interface: Timing properties, dynamic behaviour and the performer's possibilities <i>W Goebel, R Bresin, A Galembo</i>	159
The pretransient of the harpsichord sound <i>T Gäumann</i>	163
Sonological analyses of Harpsichord Sounds <i>A Schneider, A Beurmann</i>	167

The piano soundboard behaviour in relation with its mechanical admittance <i>J S Skala</i>	171
Experimental and theoretical studies of piano hammer <i>A Stulov</i>	175
Analysis of piano tones with soft and hard touches <i>H Suzuki, J Kanno, S Mikimoto</i>	179

## BRASSES

Brass instruments as we know them today ( <i>invited paper</i> ) <i>D M Campbell</i>	185
Harmonics: what do they do in the didjeridu? <i>N Amir</i>	189
Bridging instrument control aspects of brass instruments with physics-based parameters <i>M Bertsch</i>	193
Reproducibility and control of the embouchure of an artificial mouth for playing brass instruments <i>S R Bromage, O F Richards, D M Campbell</i>	197
Australian Aboriginal musical instruments -- the gum-leaf <i>N H Fletcher</i>	201
Studying lip oscillators of brass instruments: A distributed two dimensional lip model and its electrical equivalent circuit <i>W Kausel</i>	205
Physical modeling of the trombone player's lips <i>D O Ludwigsen</i>	209
Trumpet bell vibrations and their effect on the sound of the instrument <i>T R Moore, E T Shirley, A E Daniels</i>	213
Corrections to the plane-wave approximation for acoustic waves in rapidly flaring horns <i>C J Nederveen</i>	217
Gradient based optimisation of brass instruments <i>J O D Noreland</i>	221
Measurement of the force applied to the mouthpiece during brass instrument playing <i>J F Petiot</i>	225
Differentiation of trumpets' sound: experimental study with an adaptable depth mouthpiece <i>J F Petiot, E Poirson, J-L Le Carrou, J Gilbert</i>	229

Modelling the lip reed - computational and experimental investigations of two-mode inward/outward striking behaviour <i>O F Richards, D M Campbell, J Gilbert</i>	233
--	-----

## WOODWINDS

From sound synthesis to instrument making: an overview of recent researches on woodwinds and organs ( <i>invited paper</i> ) <i>B Fabre, A Hirschberg</i>	239
Experimental research on double reed physical properties and its application to sound synthesis <i>A Almeida, C Vergez, R Caussé, X Rodet</i>	243
The 'Virtual Flute': acoustic modelling at the service of players and composers <i>A Botros, J Smith, J Wolfe</i>	247
Relationship between blowing pressure, pitch, and timbre of a Scottish bellows blown bagpipe <i>S Carral, D M Campbell, T D Rossing</i>	251
The free reed coupled to a pipe resonator <i>J P Cottingham</i>	255
Waveguide modelling of the Panpipes <i>A Czyzewski, B Kostek</i>	259
Playing frequency shift due to the interaction between the vocal tract of the musician and the clarinet <i>C Fritz, J Wolfe, J Kergomard, R Caussé</i>	263
Influence of losses on the saturation mechanism of single reed instruments <i>J Gilbert, J-P Dalmont, M Atig</i>	267
Vibrato of single reed instruments <i>J Gilbert, L Simon, J Terroir</i>	271
Acoustical and psychoacoustical investigations of the effect of crook bore profile on the playability of bassoons <i>T J W Hill, D B Sharp</i>	275
RIAM (Reed Instrument Artificial Mouth): A computer controlled excitation device for reed instruments <i>A Mayer</i>	279
Experimental investigation of clarinet reed operation and its consequence on the non-linear characteristics of the mouthpiece <i>S Ollivier, J-P Dalmont</i>	283
Resonance curves and frequencies in multi-holed ocarinas <i>D R Peterson</i>	287
Modeling vocal-tract influence in reed wind instruments <i>G P Scavone</i>	291

Head joint, embouchure hole and filtering effects on the input impedance of flutes <i>J Smith, J Wolfe, M Green</i>	295
Flute performology; Statistical analyses and numerical simulation of flute tone excitation. <i>Jan Tro, Aslak Bjerkvik, Ulf Kristiansen</i>	299
Relating the harmonic-rich sound of the Chinese flute (dizi) to the cubic non-linearity of its membrane <i>C G Tsai</i>	303
Some effects of the player's vocal tract and tongue on wind instrument sound <i>J Wolfe, A Z Tarnopolsky, N H Fletcher, L C L Hollenberg, J Smith</i>	307

## ORGANS

CFD analysis of air jet deflection - Comparison with Nolle's measurements <i>S Adachi</i>	313
Breathing modes and sound radiation of metallic organ pipes <i>S Bergweiler, A Bergner, T Görne, M Wegener, R Gerhard-Multhaupt</i>	317
Particle image velocimetry (PIV) measurements of velocity fields at an organ pipe labium <i>E-L Johansson, L Benckert, P Gren</i>	321
Space and air economy in the organ low register <i>J Liljencrants</i>	325
Free reed instruments: clues for a physical model <i>L Millot</i>	329
Subjective evaluation of organ pipe timbre in the standard listener positions <i>V Syrový, Z Otčenášek, J Štěpánek</i>	333

## PERCUSSIONS

Making of a computer carillon <i>M Karjalainen, P A A Esquef, V Välimäki</i>	339
Normal modes of the elephant bell <i>R Perrin, B Deutsch, A Robinson, R Felce, T R Moore, G M Swallowe</i>	343
Rayleigh's bell model revisited <i>R Perrin, G M Swallowe</i>	347
The HANG: A hand-played steel drum <i>T D Rossing, U J Hansen, F Rohner, S Schärer</i>	351
Vibrational modes of five-octave concert marimbas <i>J Yoo, T D Rossing, B Larkin</i>	355

## PHYSICS-BASED MODELLING

Physics-based modeling of musical instruments ( <i>invited paper</i> ) <i>V Välimäki</i>	361
A power normalized non-linear lossy piano hammer <i>J Bensa, S D Bilbao, R Kronland-Martinet, J O Smith III</i>	365
Sound synthesis for three-dimensional objects: dynamic contact between two arbitrary elastic bodies <i>J Bensoam, R Caussé, C Vergez, N Misdariis, N Ellis</i>	369
Musical applications of multichannel generalized digital waveguides <i>C Burns, S Serafin, M Burtner</i>	373
Synthesis of voiced sounds by means of waveform adaptive physical models <i>C Drioli</i>	377
The development of a modular software paradigm for the physical modelling of musical instruments <i>I A Drumm</i>	381
The principle of closed wavetrains, resonance and efficiency: past, present and future <i>G Essl, P R Cook</i>	385
Real-time synthesis models of wind instruments based on physical models <i>P Guillemain, J Kergomard, T Voinier</i>	389
Time-domain physical modeling and real-time synthesis using mixed modeling paradigms <i>M Karjalainen</i>	393
A new method for the calculation of self-sustained oscillations: the perturbation of the Helmholtz motion <i>J Kergomard, S Divoir, S Farner, C Vergez</i>	397
Simulating the mechanism of sound generation in flutes using the lattice Boltzmann method <i>H Kühnelt</i>	401
Methods for synthesizing very high Q parametrically well behaved two pole filters <i>M V Mathews, J O Smith III</i>	405
Modeling and real-time synthesis of the kantele using distributed tension modulation <i>J Pakarinen, M Karjalainen, V Valimäki</i>	409
The estimation of birdsong control parameters using maximum likelihood and minimum action <i>T Smyth, J S Abel, J O Smith III</i>	413
<i>Author index</i>	417
<i>GNU Free Documentation License</i>	425



## VOLUME II

---

*Sponsors*

*xvii*

### SINGING VOICE

Singing voice modeling - as we know it today ( <i>invited paper</i> ) <i>M Kob</i>	431
Using imaging and modeling techniques to understand the relationship of vocal tract shape to acoustic characteristics ( <i>invited paper</i> ) <i>B H Story</i>	435
Sample-based singing voice synthesizer by spectral concatenation <i>J Bonada, A Loscos, H Kenmochi</i>	439
Acoustical effects of the core principles of the 'Bel Canto' method on choral singing <i>L Fagnan, X Rodet</i>	443
The influence of the practice of basso continuo on the intonation of a professional singer in the time of Monteverdi <i>G Faraone, S Johansson, P Polotti</i>	447
Acoustic pulse reflectometry for vocal tract measurement <i>C D Gray, D M Campbell, C A Greated</i>	451
On the use of electroglottography for characterisation of the laryngeal mechanisms <i>N Henrich, B Roubeau, M Castellengo</i>	455
Vocal fold resonances at low and high pitch tuning <i>S Hertegård, H Larsson, S Granqvist</i>	459
A capella SATB quartet in-tune singing: evidence of intonation shift <i>D M Howard</i>	463
Larynx closed quotients in a capella SATB quartet singing <i>D M Howard</i>	467
The effect of the hypopharyngeal and supra-glottic shapes for the singing voice <i>H Imagawa, K-I Sakakibara, N Tayama, S Niimi</i>	471
The effect of vocal vibrato on blending individual singer characteristic with hall acoustics <i>K Kato, D Noson, Y Ando</i>	475
Singer identification through dynamic modeling of vocal fold and vocal tract parameters <i>Y E Kim</i>	479

Spectral modeling of the singing voice using asymmetric generalized Gaussian functions <i>M E Lee, M J T Smith</i>	483
Comparison of directional sources in simulating a soprano voice <i>L Parati, F Otondo</i>	487
Neck muscle activation in professional classical singing <i>V Pettersen, R H Westgaard</i>	491
The laryngeal flow model for pressed-type singing voices <i>K-I Sakakibara, H Imagawa, S Niimi, N Osaka</i>	495
Acoustic and aerodynamic analyses of support and resonance demonstrated by an elite baritone singing teacher <i>R C Scherer, N Radhakrishnan, A Poulimenos, F Alipour</i>	499
Perceptual Relevance of the 5kHz spectral region to sex identification in children's singing voices <i>P J Sjölander</i>	503

## MUSIC PERFORMANCE

Large-scale performance studies with intelligent data analysis methods ( <i>invited paper</i> ) <i>G Widmer</i>	509
Studies of music performance: a theoretical analysis of empirical findings ( <i>invited paper</i> ) <i>P N Juslin</i>	513
Estimation of the note durations in a polyphonic piano transcription system <i>A M Barbancho, I Barbancho, L J Tardón</i>	517
Expressive Director: a system for the real-time control of music performance synthesis <i>S Canazza, A Rodà, P Zanon, A Friberg</i>	521
Expressiveness analysis of virtual sound movements and its musical applications <i>A de Götzen</i>	525
A statistical approach to expressive intentions recognition in violin performances <i>R Dillon</i>	529
Melodic characterization of monophonic recordings for expressive tempo transformations <i>E Gómez, M Grachten, X Amatriain, J L Arcos</i>	533
Measurements and models of musical articulation <i>J Jerkert</i>	537
The percussion instrument operation synchronized with the visual and/or auditory stimuli <i>T Kamitani, K Kouzuki, M Matsuda</i>	541

Aspects on time modification in score-based performance control <i>M Laurson, M Kuuskankare</i>	545
Interaction among physical acoustic knowledge and performance in the accordion and its educational side <i>R Llanos-Vazquez, J Alonso-Moral, M J Elejalde-Garcia, E Macho-Stadler</i>	549
Time domain note average energy based music onset detection <i>R Liu, N J L Griffith, J Walker, P Murphy</i>	553
Application of Bayesian Networks to automatic recognition of expressive content of piano improvisations <i>L Mion</i>	557
ESP - an interactive collaborative game using non-verbal communication <i>M L Rinman, A Friberg, I Kjellmo, A Camurri, D Cirotteau, S Dahl, B Mazzarino, B Bendiksen, H McCarthy</i>	561
Mapping a physical correlate of loudness into the velocity space of MIDI-controlled piano tones <i>T Taguti</i>	565
On the relation between performance cues and emotional engagement <i>R Timmers, A Camurri, G Volpe</i>	569
Analysis of jazz drummers' movements in performance of swing grooves - a preliminary report <i>C H Waadeland</i>	573
A singing transcription system using melody tracking algorithm based on Adaptive Round Semitone (ARS) plus music grammar constraints <i>C K Wang, R Y Lyu, Y C Chiang</i>	577
Learning to recognize famous pianists with machine learning techniques <i>P Zanon, G Widmer</i>	581

## MUSIC PERCEPTION

Automatic transcription of music ( <i>invited paper</i> ) <i>A P Klapuri</i>	587
Brain activity in perception and retention in memory of the pitch of music and speech <i>E Castro-Sierra, H A Poblano</i>	591
Looking at perception of continuous tempo drift - a new method for estimating Internal drift and Just Noticeable Difference <i>S Dahl, S Granqvist</i>	595
What can the body movements reveal about a musician's emotional intention? <i>S Dahl, A Friberg</i>	599
Time estimation: isochronous versus accelerated audio sequences <i>D Dall'Osto</i>	603

Timbral semantics and the pipe organ <i>A C Disley, D M Howard</i>	607
Hardness recognition in synthetic sounds <i>B L Giordano, K Petrini</i>	611
Categorical perception of microtonal intervals <i>E Huovinen</i>	615
Towards a virtual singer: contribution to the development of the teaching of sung diction through the intermediary of a functionalised system <i>M Nahas, H Huitric, J Kiss</i>	619
Musical sound parameters revisited <i>B Kostek, P Zwan, M Dziubinski</i>	623
Pitch measurements versus perception of South Indian classical music <i>A Krishnaswamy</i>	627
Relationships between musical audio, perceived qualities and motoric responses <i>M Leman, V Vermeulen, L De Voogdt, A Camurri, B Mazzarino, G Volpe</i>	631
User-dependent taxonomy of musical features as a conceptual framework for musical audio-mining technology <i>M Lesaffre, M Leman, K Tanghe, B De Baets, H De Meyer, J P Martens</i>	635
Consistency in listeners' ratings as a function of listening time <i>G Madison, B Merker</i>	639
Verbal description of musical sound timbre in czech language <i>O Moravec, J Štěpánek</i>	643
Development of a language for specifying saxophone timbre <i>A J Nykänen, Ö Johansson</i>	647
Influence of duration of tone stationary part on perception of starting transient <i>Z Otčenášek, J Štěpánek, V Syrový</i>	651
Perceived influence of changes in musical instrument directivity representation <i>F Otondo, B Kirkwood</i>	655
Effects of the grouping cue on the pitch shift of a pure tone induced by other tones <i>T Shirado, M Yanagida</i>	659
Listeners common and group perceptual dimensions in violin timbre <i>J Štěpánek, Z Otčenášek</i>	663
Pattern recognition of musical instruments using Hidden Markov Models <i>R Ventura-Miravet, F Murtagh, J Ming</i>	667
Influence of rhythmic, melodic, and semantic violations in language and music on the electrical activity in the brain <i>S Ystad, C Magne, S Farner, G Pallone, C Astesano, V Padeloup, R Kronland-Martinet, M Besson</i>	671

## INSTRUMENT CONTROL

Remutualizing the Instrument: Co-design of synthesis algorithms and controllers ( <i>invited paper</i> ) <i>P Cook</i>	677
Interactive music systems for everyone: Exploring visual feedback as a way for creating more intuitive, productive and learnable instruments ( <i>invited paper</i> ) <i>S Jordà</i>	681
Controlling the virtual bodhran - the vodhran <i>R Bresin, S Dahl, M Rath, M Marshall, B Moynihan</i>	685
The Radio Baton as configurable musical instrument and controller <i>R Bresin, K F Hansen, S Dahl</i>	689
DJ scratching performance techniques: Analysis and synthesis <i>K F Hansen, R Bresin</i>	693
Gesture-tactile controlled physical modelling music synthesis <i>D M Howard, S Rimell</i>	697

## MISCELLANEA

*Including* OPTICAL AND ACOUSTICAL MEASUREMENTS *and*  
TEACHING MUSIC ACOUSTICS TO MUSICIANS

Visualization of sound fields with application to musical instruments ( <i>invited paper</i> ) <i>N E Molin</i>	703
Breathing modes of woodwind bodies: Experimental detection with ring-shaped piezoelectric-polymer sensors <i>M Wegener, R Gerhard-Multhaupt, W Wirges, A Bergner, S Bergweiler</i>	707
Leak detection in musical wind instruments using acoustic pulse reflectometry <i>V Chilekwa, D B Sharp, T J W Hill</i>	711
An EDS modelling tool for tracking and modifying the musical signals <i>B David, G Richard, R Badeau</i>	715
Didactic resources for the teaching and popularisation of the physics of the music <i>M J Elejalde-García, E Macho- Stadler, A Franco-García, J Janariz-Larumbe</i>	719
Quantitative assessment of air flow from professional bass reflex systems ports by Particle Image Velocimetry and Laser Doppler Anemometry <i>E Esposito, M Marassi</i>	723
Computer-animated illustrations of vibrations and waves <i>D E Hall</i>	727

Musical acoustics courses in the education of music students in the U.S.A. <i>D E Hall</i>	729
Unusual motions of a nonlinear asymmetrical vibrating string <i>R J Hanson, H K Macomber, A C Morrison</i>	731
Reducing the source tube to improve the bandwidth of acoustic pulse reflectometry <i>A Li, D Sharp</i>	735
An apparatus for measuring string vibration using electric field sensing <i>J Pakarinen, M Karjalainen</i>	739
An ensemble method for automatic alignment of sound and its transcription <i>K Sjölander</i>	743
Measurement of the termination impedance of a tube using particle image velocimetry <i>D J Skulina, D M Campbell, C A Greated</i>	747
Direct measurement of the 3-D acoustic impedance in wind instruments near field <i>D Stanzial, D Bonsi</i>	751
Sound and vibration from a special musical instrument: the Mazzacorati theatre <i>L Tronchin, E Esposito, V Tarabusi</i>	755
Large-bandwidth measurement of acoustic impedance using two microphones and four calibrations <i>M O van Walstijn, D M Campbell</i>	759
Refractoscopic visualisation of sound in musical instruments <i>L Zipser, H Franke</i>	763
<i>Author index</i>	767
<i>GNU Free Documentation License</i>	775

## SCIENTIFIC ADVISORY COMMITTEE

### BRASS

**Dr. Joël Gilbert**

Laboratoire d'Acoustique de l'Université du Maine  
Le Mans, France

### STRINGS

**Prof. Knut Guettler**

Norwegian Academy of Music  
Oslo, Norway

### SYNTHESIS/MUSIC INSTRUMENT CONTROL

**Prof. David Howard**

Dept. of Electronics  
The University of York, UK

### PHYSICS-BASED MODELLING

**Prof. Matti Karjalainen**

Laboratory of Acoustics and Audio Signal Processing  
Helsinki University of Technology, Finland

### WOODWINDS – ORGANS

**Prof. Jean Kergomard**

Laboratoire de Mécanique et d'Acoustique  
Marseille, France

### SINGING VOICE

**Prof. Ronald Scherer**

Dept. of Communication Disorders  
Bowling Green State University, USA

### PIANOS – GUITARS

**Prof. Donald Hall**

California State University  
Sacramento, USA

### MUSIC PERFORMANCE

**Prof. Antonio Camurri**

Laboratorio di Informatica Musicale  
University of Genoa, Italy

**Prof. Nicola Bernardini**

Media Innovation Unit  
Firenze Tecnologia, Italy

### MUSIC PERCEPTION

**Prof. Peter Desain**

Music, Mind, Machine Group  
University of Nijmegen, The Netherlands

## PREFACE

The Stockholm Music Acoustics Conference, August 6 – 9, 2003 (SMAC 03) continues the series of music acoustics conferences in Stockholm, started 20 years ago. Following the tradition of SMAC 83 and SMAC 93, SMAC 03 covers the entire field of music acoustics, with musical instruments, singing voice, and music performance and perception as the three main themes. At the time of the first SMAC the number of conferences in music acoustics and related disciplines such as computer music science, music psychology, the voice in all its aspects, music technology, and digital audio processing was limited. Some of these areas were still in their infancy. Today the offer of conferences, symposia, and workshops is so rich that it is difficult even to get a good survey, much less to attend everything of potential interest. One good reason for keeping the broad perspective from earlier SMACs is to offer the possibility of at least a partial overview of the many fascinating research areas which address the wonderful combination of performing arts, physics, creativity, and life experience called *music*. In order to give this perspective, SMAC 03 features a number of invited presentations (the exact number being 22), in which outstanding researchers, old and young, will present overviews of their areas up to and including the research frontier. A unifying theme of these presentations is ‘as we know it today.’ All invited presentations will be published as full papers in scientific journals during 2004.

One session is special. *Johan Sundberg*, professor in Music Acoustics at KTH and the father of the continuing series of SMACs, retired formally a couple of years ago. We hasten to add that in reality very little has changed, Johan being busier than ever from early morning to late evening. However, SMAC 03 offered a natural opportunity to give a homage to his many contributions to date to the advancement of the sciences of the singing voice and music performance. His first scientific article, published in 1970, has been followed by more than 200 articles and numerous books. In passing we could mention that The Acoustical Society of America very recently came up with a similar idea, deciding to award him the Silver Medal in Musical Acoustics in the Fall of 2003 “.... for contributions to understanding the acoustics of singing and musical performance and for leadership in musical acoustics research.”

The last afternoon of SMAC 03 is devoted to *The Sundberg Session*. Five keynote speakers will present their view on research areas related to Johan Sundberg’s special interests, the singing voice and music performance. It goes without saying that number one on Johan’s wish list of speakers was Max Mathews, the great pioneer who has been of such significance to music acoustics, computer music, and Johan Sundberg personally.

Besides all scientific sessions SMAC 03 will include many memorable events, including a concert with young Swedish artists, workshops, a Swedish summer night banquet in the archipelago of Stockholm, and above all, numerous occasions to meet friends and colleagues, old and new.

WE WELCOME YOU ALL TO SMAC 03!

*Anders Askenfelt*

*Erik Jansson*

*Sten Ternström*

*Anders Friberg*

*Roberto Bresin*

Department of Speech Music Hearing, KTH

[www.speech.kth.se](http://www.speech.kth.se)

PS. The next SMAC will take place in August 2013. DS.





## SPONSORS

Stockholm Music Acoustics Conference, August 6 – 9, 2003 (SMAC 03) SMAC 03 was made possible due to generous grants from:



Royal Institute of Technology (KTH)  
[www.kth.se](http://www.kth.se)



The Wenner-Gren Foundations  
[www.wenner-grenstift.a.se](http://www.wenner-grenstift.a.se)



The Bank of Sweden Tercentenary Foundation  
[www.rj.se](http://www.rj.se)



The Swedish Research Council  
[www.vr.se](http://www.vr.se)

Helge Ax:son Johnsons Stiftelse



Royal Swedish Academy of Music  
[www.musakad.se](http://www.musakad.se)



Catgut Acoustical Society  
[www.catgutacoustical.org](http://www.catgutacoustical.org)



City of Stockholm  
[www.stockholm.se](http://www.stockholm.se)



The Italian Embassy  
[www.itemb.se/science/](http://www.itemb.se/science/)



The Italian Institute of Culture in Stockholm  
<http://www.italkult.com/>



The Swedish Radio  
[www.sr.se](http://www.sr.se)



# OPENING SESSION



## RECENT DEVELOPMENTS IN MUSICAL SOUND SYNTHESIS BASED ON A PHYSICAL MODEL

Julius O. Smith III (jos@ccrma.stanford.edu)

Center for Computer Research in Music and Acoustics (CCRMA)  
Department of Music, Stanford University  
Stanford, California 94305

### ABSTRACT

This paper gives an overview of selected recent developments in musical sound synthesis based on physical models of musical instruments.

### 1. INTRODUCTION

Musical sound synthesis has a long history spanning more than half a century [1]. Since the 1960s, efforts have been aimed at developing sound synthesis algorithms based on the musical acoustics of live instruments [2, 3]. In this paper, some recent developments in this area will be summarized.

Traditionally, physical vibrating systems such as musical instruments are modeled mathematically by means of *differential equations*. Computational models are then developed by discretizing these relations, and converting them to *finite difference equations* defined on a discrete space-time grid [4]. This approximation step in going from a differential equation to a difference equation is sometimes called *finite difference approximation* (FDA). These difference equations can be integrated numerically to obtain estimates of the acoustic field in response to external forces and boundary conditions. Numerical integration of FDAs is perhaps the most general path to *finite difference schemes* (FDS) yielding computational models of acoustic systems (see, e.g., [5, 6]).

In recent decades, an alternative approach to finite-difference simulation known as the “digital waveguide approach” has been developed [7]. Its characteristics are well matched to the problem of developing high-speed algorithms for digital sound synthesis based on physical models of musical instruments. The basic idea is to first digitize an *idealized* differential equation, and then introduce perturbations (usually in the form of digital filters) which can reintroduce formerly neglected phenomena such as amplitude attenuation and phase dispersion. This two-step procedure can yield finite difference schemes which are orders of magnitude less expensive computationally, relative to FDAs, without sacrificing sound quality in the acoustic simulation. Since the variables in the resulting FDS retain their physical interpretations, nonlinearities and time-varying parameters can be implemented in the same way as in the FDA method. The digital waveguide approach is most effective for modeling physical systems that support traveling waves and for which losses, dispersion, and any nonlinearities can be well modeled psychoacoustically at spatially localized

points. Fortunately, many acoustic musical instruments fit this description.

A third approach to FDS development is the “wave digital filter” (WDF) approach [8]. In this case, one begins with a *lumped* physical model consisting, conceptually, of masses, springs, dashpots, and their interconnections. Each individual element is replaced by a first-order digital filter that captures its behavior in discrete time. However, unlike the other methods mentioned above, the frequency axis is *warped* according to an arctangent function. This has the advantage of preventing *aliasing* of the high-frequency system response onto the low-frequency response, but the frequency warping can be an undesirable distortion. For example, when there are two or more resonance frequencies in the system, only one can be mapped to the desired frequency in the discrete-time simulation. In particular, harmonic resonances (as in a vibrating string or acoustic bore) are no longer harmonic after the frequency warping.

As a general rule, fundamentally distributed linear elements, such as vibrating strings, woodwind bores, pipes, horns, and the like, are most efficiently modeled using the digital waveguide framework. (From a modal synthesis point of view, digital waveguides are highly efficient for simulating large numbers of quasi-harmonic resonances.) On the other hand, systems having at most one important resonance (or anti-resonance) in the audio band, such as clarinet reeds, toneholes, and piano hammers, are best modeled using the FDA or WDF approach. Other situations arise as well, some of which will be noted below.

In the remainder of this paper, selected recent developments in sound synthesis based on musical acoustics will be cited. All are related in one way or another to the above three modeling frameworks. Due to space limitations, only the projects with which I have been most actively involved are mentioned in the text, with additional noteworthy recent publications appearing in the bibliography.

### 2. RECENT THESES (IN TIME ORDER)

Gary Scavone’s 1997 thesis [9] is concerned acoustic modeling of woodwind instruments. His work has recently focused on tonehole implementations [10, 11], vocal tract influences (see elsewhere in this proceedings), conical air column structures [12], and sound radiation directivity within a real-time synthesis context [13].

In his 1999 thesis [14], David Berners developed a novel formulation for wave scattering in acoustic horns based on

Sturm-Liouville (SL) theory. This formulation avoids the well known “growing exponentials” that can arise at the junction of conical acoustic tubes when each tube is characterized only by its (complex) wave impedance at the junction. In the SL theory, the growing exponentials are replaced by so-called “trapped modes.”

Stefan Bilbao’s 2001 thesis [15] is devoted to the study of finite difference schemes (FDS) for differential equations arising in musical acoustics and elsewhere. A unique contribution of his thesis is a unified formulation of both the wave digital and digital waveguide frameworks, deriving each as a special case of a more general framework. More recently, he has continued to obtain interesting and useful results in this area, including an improved second-order-in-time FDS applicable to piano strings [16, 17] and a power-normalized wave digital hammer [18], in which the nonlinear action of the hammer felt modulates a structurally lossless, power-normalized, scattering junction (common to both the “digital waveguide” and “wave digital” paradigms).<sup>1</sup> As a result, the hammer nonlinearities are constrained to conserve energy, irrespective of the degree of accuracy to which they are computed. An update on this research appears elsewhere in this proceedings.

Hui-Ling Lu, in her 2002 thesis [19], developed a model for the singing voice in which the driving glottal pulse train is estimated jointly with the vocal tract filter parameters. The model can be seen as an improvement over linear-predictive coding (LPC) of voice in the direction of a more accurate physical model of voice production, while maintaining a low computational cost relative to more complex articulatory models of voice production. In particular, the parameter estimation involves only convex optimization plus a one-dimensional (possibly non-convex) line search over a compact interval. The line search determines the so-called “open quotient” which is fraction of the time there is glottal flow within each period. The glottal pulse parameters are based on the derivative-glottal-wave models of Liljencrants, Fant, and Klatt. Portions of this research have been published in the ICMC-00 [20] and WASPAA-01 [21] proceedings.

Maarten van Walstijn’s 2002 thesis [22] is concerned with discrete-time modeling of brass and reed woodwind instruments, using a blend of wave digital and digital waveguide approaches. A JASA paper based on this research has recently appeared [23].

A high-quality computational model of the piano, partially based on physical modeling and suitable for high-quality real-time sound synthesis, has been recently developed by Julien Bensa in the context of his thesis work [24].

In the reasonably near future, we can expect dissertations from Stefania Serafin (CCRMA) on the topic of analysis and synthesis of friction-driven musical instruments [25], and Tamara Smyth (CCRMA) regarding synthesis of cicada and birdsong based on acoustic models [26].

CCRMA Ph.D. student Arvinth Krishnaswamy has developed an effective method for identifying selected control parameters in violin performance from measured audio spectra [27]. The essence of the method is to develop a forced classification scheme based on short-time power

spectra indexed by pitch class. In other words, for each pitch class, a small linear-discriminant-analysis database is developed which returns the estimated playing parameters (bow position, which string was played, whether plucked or bowed) as a function of the measured power spectrum. Related work determining the plucking point along a guitar string was carried out by Caroline Traube at CCRMA (now a Ph.D. student at McGill) [28].

In separate research [29], Arvinth et al. have proposed new, more physically accurate algorithms for simulating vibrating strings which strike against physical objects (for simulation of slap bass, tambura, sitar, etc.). Both a pure “waveguide approach” and a hybrid approach involving a “mass-spring” string model inside a digital waveguide are considered.

### 3. RECENT BOOKS

Perry Cook has recently published a book devoted to sound synthesis related to physical models [30]. The book is especially useful for getting going quickly with effective and practical synthesis models.

The following interlinked books have been published to the Web in HTML format:

1. **Math. of the Discrete Fourier Transform** [31]
2. **Introduction to Digital Filters** [32]
3. **Digital Waveguide Modeling of Musical Instruments** [7]

While only Book 3 is firmly within the scope of this paper, it relies heavily on the material in the first two (which can be regarded as prerequisites). In particular, Book 3 alone contains approximately 20,000 automatically generated hypertext links, most pointing into Books 1 and 2. The goal is that a person should be able to start reading “anywhere” (e.g., coming in from a Google search), and be able to click on any technical term to obtain its “home page,” or at least a clear definition with some development. This goal has not been fully realized, but substantial progress has been made to date.

### 4. OPEN DICTIONARY

The Open Dictionary<sup>2</sup> [33], developed by the author during a 1999 sabbatical leave, contains a browsable superset of the links installed automatically in the online books described in the preceding section. The intent is to provide a *link repository* where researchers around the world may combine their “link collections” for use in teaching and research. The appearance while browsing is that of a “hierarchical dictionary”.

Figure 1 illustrates examples of the Open Dictionary link submission syntax. Anyone may submit Web links as “definitions” for various terms to the Open Dictionary<sup>3</sup> and all reasonable submissions are accepted.

<sup>2</sup><http://www.opendict.org>

<sup>3</sup>Detailed submission instructions are available at <http://www.opendict.org>. However, email to [od@w3k.org](mailto:od@w3k.org) is presently equivalent.

<sup>1</sup><http://www-ccrma.stanford.edu/~jos/waveguide/-NormalizedScatteringJunctions.html>

Referring to Fig. 1, when two or more URLs are associated with the same KEY phrase, they must *compete* to “define” that key phrase. Presently, this arbitration is handled manually. It is planned that the URLs for a given term will be *ranked* democratically by “trusted” users (a peer group associated with each PATH).

Any PATH may be specified in a submission, and (KEY,URL) entries may be duplicated as many times as necessary to populate the alternative paths. In the future, it is planned that identical URLs detected in different paths will trigger automatic “see also” cross-references from each path to the others containing the same URL.

## 5. REFERENCES

- [1] J. O. Smith, “Viewpoints on the history of digital synthesis,” in *Proc. 1991 Int. Computer Music Conf., Montreal*, 1991, pp. 1–10, Computer Music Association, (keynote paper.) Available online at <http://www-ccrma.stanford.edu/~jos/kna/>.
- [2] P. M. Ruiz, *A Technique for Simulating the Vibrations of Strings with a Digital Computer*, Ph.D. thesis, Music Master Diss., Univ. Ill., Urbana, 1969.
- [3] L. Hiller and P. Ruiz, “Synthesizing musical sounds by solving the wave equation for vibrating objects. Part I,” *J. Audio Eng. Soc.*, vol. 19, no. 6, pp. 462–470, June 1971, Part II: vol. 19, no. 7, pp. 542–551, July/Aug. 1971.
- [4] J. Strikwerda, *Finite Difference Schemes and Partial Differential Equations*, Wadsworth and Brooks, Pacific Grove, CA, 1989.
- [5] A. Chaigne and A. Askenfelt, “Numerical simulations of piano strings. I. a physical model for a struck string using finite difference methods,” *J. Acoust. Soc. of Amer.*, vol. 95, no. 2, pp. 1112–1118, Feb 1994.
- [6] G. Derveaux, P. Joly, E. Bécache, and A. Chaigne, “Time-domain simulation of a guitar: Model and method,” *submitted for publication*, 2003.
- [7] J. O. Smith III, *Digital Waveguide Modeling of Musical Instruments*, <http://www-ccrma.stanford.edu/~jos/waveguide/>, 2003.
- [8] A. Fettweis, “Wave digital filters: Theory and practice,” *Proc. IEEE*, vol. 74, no. 2, pp. 270–327, Feb. 1986.
- [9] G. P. Scavone, *An Acoustic Analysis of Single-Reed Woodwind Instruments with an Emphasis on Design and Performance Issues and Digital Waveguide Modeling Techniques*, Ph.D. thesis, CCRMA, Music Dept., Stanford University, March 1997, available from [info@ccrma.stanford.edu](mailto:info@ccrma.stanford.edu) or <ftp://ccrma-ftp.stanford.edu/pub/Publications/Theses/-GaryScavoneThesis/>.
- [10] G. P. Scavone and P. R. Cook, “Real-time computer modeling of woodwind instruments,” in *Proc. Int. Symp. on Musical Acoustics (ISMA-98)*, Leavenworth, Washington, July 1998, pp. 197–202, available online at <http://www-ccrma.stanford.edu/~jos/tonehole.html>.
- [11] M. van Walstijn and G. Scavone, “The wave digital tonehole,” in *Proc. 2000 Int. Computer Music Conf., Berlin*, 2000, pp. 465–468, Computer Music Association, available online at <http://www-ccrma.stanford.edu/~jos/wdth/>.
- [12] G. P. Scavone, “Time-domain synthesis of conical bore instrument sounds,” in *Proc. 2002 Int. Computer Music Conf., Sweden*, 2002, pp. 9–15.
- [13] G. P. Scavone and M. Karjalainen, “Tonehole radiation directivity: A comparison of theory to measurements,” in *Proc. 2002 Int. Computer Music Conf., Sweden*, 2002, pp. 325–329.
- [14] D. P. Berners, *Acoustics and Signal Processing Techniques for Physical Modeling of Brass Instruments*, Ph.D. thesis, Elec. Eng. Dept., Stanford University (CCRMA), June 1999, available online at <http://www-ccrma.stanford.edu/~dpberner/>.
- [15] S. Bilbao, *Wave and Scattering Methods for the Numerical Integration of Partial Differential Equations*, Ph.D. thesis, Stanford University, June 2001, available online at <http://www-ccrma.stanford.edu/~bilbao/>.
- [16] J. Bensa, S. Bilbao, R. Kronlan-Martinet, and J. O. Smith III, “From the physics of piano strings to digital waveguides,” in *Proc. 2002 Int. Computer Music Conf., Sweden*, 2002.
- [17] J. Bensa, S. Bilbao, R. Kronlan-Martinet, and J. O. Smith III, “The simulation of piano string vibration: from physical models to finite difference schemes and digital waveguides,” *accepted for publication in J. Acoust. Soc. of Amer.*, August or September (expected) 2003.
- [18] S. Bilbao, J. Smith, J. Bensa, and R. Kronland-Martinet, “A power-normalized wave digital piano hammer,” *J. Acoust. Soc. of Amer., Program of the 144th Meeting, Cancun, Mexico, Dec. 2-6*, Dec. 2002, see paper on the conference CD-ROM.
- [19] H.-L. Lu, *Toward a High-Quality Singing Synthesizer with Vocal Texture Control*, Ph.D. thesis, Elec. Eng. Dept., Stanford University (CCRMA), July 2002, available online at <http://www-ccrma.stanford.edu/~vickyly/thesis/>.
- [20] H.-L. Lu and J. Smith, “Glottal source modeling for singing voice synthesis,” in *Proc. 2000 Int. Computer Music Conf., Berlin*, Aug. 2000, available online at <http://ccrma-www.stanford.edu/~vickyly/research/-glottalSource/glottal.htm>.
- [21] H.-L. Lu, , and J. Smith, “Estimating glottal aspiration noise via wavelet thresholding and best basis thresholding,” in *Proc. IEEE Workshop on Appl. Signal Processing to Audio and Acoustics*, New Paltz, NY, New York, Oct. 2001, IEEE Press.
- [22] M. O. van Walstijn, *Discrete-Time Modelling of Brass and Reed woodwind Instruments with Application to Musical Sound Synthesis*, Ph.D. thesis, Department of Physics and Astronomy, University of Edinburgh, 2002, available online at <http://www.ph.ed.ac.uk/~maarten/>.
- [23] M. O. Van Walstijn and D. Campbell, “Discrete-time modelling of woodwind instrument bores using wave variables,” *J. Acoust. Soc. of Amer.*, vol. 113, pp. 575–585, 2003.
- [24] J. Bensa, *Analysis and Synthesis of Piano Sounds using Physical and Signal Models*, Ph.D. thesis, Université de la Méditerranée, Marseille, France, 2003, available online at <http://www.lma.cnrs-mrs.fr/~bensa/>.
- [25] S. Serafin, P. Huang, S. Ystad, C. Chafe, and J. O. Smith III, “Analysis and synthesis of unusual friction-driven musical instruments,” in *Proc. 2002 Int. Computer Music Conf., Sweden*, 2002.
- [26] T. Smyth and J. O. Smith, “The syrinx: Nature’s hybrid wind instrument,” in *J. Acoust. Soc. of Amer., Program of the 144th Meeting, Cancun, Mexico, Dec. 2-6*, 2002.
- [27] A. Krishnaswamy, , and J. O. Smith, “Inferring control inputs to an acoustic violin from audio spectra,” in *Proc. Int. Conf. Multimedia Eng.*, New York, 2003, IEEE Press.



```

PATH = / Science / Physics / Acoustics / Musical Acoustics

KEY = Coupled Piano Strings
URL = http://www.speech.kth.se/music/5_lectures/weinreic/weinreic.html

PATH = / Music / Computer Music / Software

KEY = Planet CCRMA Software Package | Planet CCRMA at Home | Planet CCRMA
URL = http://www-ccrma.stanford.edu/planetccrma/software/
DSC = Linux software packages used at CCRMA for sound and music applications

KEY = Synthesis Tool Kit | STK
URL = http://www-ccrma.stanford.edu/software/stk/
DSC = A C++ tool kit for rapid prototyping of sound synthesis algorithms.

```

Figure 1: Open Dictionary submission syntax, sent via email to [od@u3k.org](mailto:od@u3k.org).

- [28] C. Traube and J. Smith, "Estimating the plucking point on a guitar string," in *Proc. Int. Conf. Digital Audio Effects (DAFx-00)*, Verona, Italy, Dec. 2000.
- [29] A. Krishnaswamy, , and J. O. Smith, "Methods for simulating string collisions with rigid spatial objects," 2003, submitted to WASPAA-03.
- [30] P. R. Cook, *Real Sound Synthesis for Interactive Applications*, A. K. Peters, L.T.D., 2002.
- [31] J. O. Smith III, *Mathematics of the Discrete Fourier Transform (DFT)*, <http://www-ccrma.stanford.edu/~jos/mdft/>, 2003.
- [32] J. O. Smith III, *Introduction to Digital Filters*, <http://www-ccrma.stanford.edu/~jos/filters/>, 2003.
- [33] J. O. Smith, "The Open Dictionary," 2003, <http://www-ccrma.stanford.edu/~jos/od/>.
- [34] A. Almeida, C. Vergez, R. Causs, and X. Rodet, "Applications of bioacoustics in physical modeling and the creation of new musical instruments," in *Proc. Int. Symp. on Musical Acoustics (ISMA-02)*, Mexico City, 2002, available online at <http://www.ircam.fr/equipes/instruments/almeida/articles/>.
- [35] F. Avanzini, S. Serafin, and D. Rocchesso, "Modeling interactions between rubbed dry surfaces using an elasto-plastic friction model," in *Proc. COST-G6 Conf. Digital Audio Effects (DAFx-02)*, Hamburg, Germany, September 2002, pp. 111–116.
- [36] C. Erkut, *Aspects in Analysis and Model-Based Sound Synthesis of Plucked String Instruments*, Doctoral thesis, Helsinki University of Technology, Espoo, Finland, November 2002, available online at <http://lib.hut.fi/Diss/2002/isbn9512261901/>.
- [37] C. Erkut, M. Karjalainen, P. Huang, and V. Välimäki, "Acoustical analysis and model-based sound synthesis of the kantele," *J. Acoust. Soc. of Amer.*, vol. 112, no. 4, pp. 1681–1691, October 2002.
- [38] G. Essl, *Physical Wave Propagation Modeling for Real-Time Synthesis of Natural Sounds*, Ph.D. thesis, Computer Science Dept., Princeton University, November 2002, available online at <http://ncstr1.cs.princeton.edu/expand.php?id=TR-659-02>.
- [39] M. Karjalainen, V. Välimäki, and P. A. A. Esquef, "Efficient Modeling and Synthesis of Bell-Like Sounds," in *the 5th Int. Conf. Digital Audio Effects*, Hamburg, Germany, September 26-28 2002, pp. 181–186.
- [40] P. Huang, S. Serafin, and J. Smith, "A waveguide mesh model of high-frequency violin body resonances," in *Proc. 2000 Int. Computer Music Conf.*, Berlin, Aug. 2000.
- [41] T. Hélie, C. Vergez, and X. Rodet, "Virtual musical instruments: Contribution to physical modeling and control of self-sustained instruments," in *Conférence Systemics Cybernetics and Informatics (SCI'2001)*, Orlando, Florida, 2001, vol. X, pp. 547–550.
- [42] L. Savioja and V. Välimäki, "Reducing the dispersion error in the digital waveguide mesh using interpolation and frequency-warping techniques," *IEEE Trans. Speech and Audio Processing*, pp. 184–194, March 2000.
- [43] M. Laurson, C. Erkut, V. Välimäki, and M. Kuuskankare, "Methods for Modeling Realistic Playing in Acoustic Guitar Synthesis," *Computer Music Journal*, vol. 25, no. 3, pp. 38–49, 2001.
- [44] X. Rodet and C. Vergez, "Nonlinear dynamics in physical models: Simple feedback-loop systems and properties; from basic models to true musical instruments," *Computer Music J.*, vol. 23, no. 3, pp. 18–49, 1999.
- [45] L. Trautmann, B. Bank, V. Välimäki, and R. Rabenstein, "Combining Digital Waveguide and Functional Transformation Methods for Physical Modeling of Musical Instruments," in *the AES 22nd Int. Conf. Virtual, Synthetic and Entertainment Audio*, Espoo, Finland, June 15-17 2002, pp. 307–316.
- [46] V. Välimäki, M. Laurson, and C. Erkut, "Commutated waveguide synthesis of the clavichord," *Computer Music Journal*, vol. 27, no. 1, pp. 71–82, Spring 2003.
- [47] M. van Walstijn and J. O. Smith, "Use of truncated infinite impulse response (TIIR) filters in implementing efficient digital waveguide models of flared horns and piecewise conical bores with unstable one-pole filter elements," in *Proc. Int. Symp. Musical Acoustics (ISMA-98)*, Leavenworth, Washington, June 28 1998, pp. 309–314, Acoust. Soc. of Amer., available online at <http://www-ccrma.stanford.edu/~jos/tiirts/>.
- [48] C. Vergez and X. Rodet, "New algorithm for nonlinear propagation of a sound wave application to a physical model of a trumpet," *Journal of Signal Processing*, 2000.
- [49] G. P. Scavone, Ed., *CCRMA Overview, April 2003*, Stanford University Department of Music Technical Report STAN-M-112, Apr. 2003, (62 pages) available from [info@ccrma.stanford.edu](mailto:info@ccrma.stanford.edu) or <http://www-ccrma.stanford.edu/overview/>.

## **FROM MUSICAL ACOUSTICS TO EVERYDAY ACOUSTICS: A PHYSICAL MODELING ROUTE**

*Davide Rocchesso*

Dipartimento di Informatica  
Università di Verona  
Davide.Rocchesso@univr.it

### **ABSTRACT**

Everyday sounds pose several challenging problems to the physical modeler. However, much of the knowledge gained in studies of musical acoustics and musical instrument modeling turn out to be useful when designing new physics-based models of everyday sound phenomena. We developed two classes of contact sound models, one based on impacts and one based on friction, that became the kernel of several simulations of rolling, sliding, squeaking, breaking, crumpling, walking, running, etc. .

### **1. INTRODUCTION**

In the year 2000, I started thinking about how the experience and knowledge gained in physical modeling from musical acoustics could be profitably used to model everyday sound phenomena. At that time, there were some remarkable success stories of non-musical non-speech sound synthesis [1, 2, 3]. However, I had the feeling that more fundamental research had to be done to obtain models that are capable of describing large families of sounds, being at the same time efficient and simple to control. This was the rationale behind the Sounding Object (SOB) EU project (<http://www.soundobject.org>).

We put together a group of researchers that started working from models inherited from our own experience in musical acoustics, and steered them toward everyday sound modeling by considering recent studies in applied mechanics and automatic control. Since everyday sounds are rarely produced by linearly-excited one-dimensional resonators, we departed from classic waveguide modeling to adopt a more general and manageable modal description of resonators. By imposing the appropriate parameters and control signals, we realized models of rolling, sliding, squeaking, breaking, crumpling, walking, running, etc., that are all based on a similar kernel impact or friction model. All the models are so efficient that many instances of them can run in real time and drive simultaneous interactive 3D graphics.

### **2. PRIOR ART**

Physically based models gives the possibility to synthesize naturally behaving sounds from computational structures that can easily interact with the environment and respond to physical input parameters.

The physical behavior of interacting objects can be modeled with different approaches. Van den Doel et al. [2, 3] adopted modal synthesis [4] as an efficient yet accurate framework for describing the acoustic properties of objects. The parameters of modal resonators can be derived from geometric and physical descriptions

of objects, or measured directly with scanning techniques [5]. The same synthesis technique has also been used by O'Brien et al. [6] in order to achieve real-time sound generation in interactive applications, where conventional rigid-body simulators are used. After a precomputation of shapes and frequencies of the modes, contact forces are used at runtime to drive the modal synthesizer, under the assumption that the sound-producing phenomena are linear, thus being representable as source - filter systems.

For some applications, it has been proposed to generate sound as a side effect of nonlinear finite element simulations [1], or by connection of a multitude of interacting particles [7, 8]. With these techniques, large amounts of computations are required for large structures, but many interesting nonlinear phenomena can be imitated.

Physical models are widely developed in the computer music community, where the waveguide simulation paradigm [9] is especially popular, but their main application has been the faithful simulation of existing musical instruments. The techniques used in those simulations, however, lack of generality, since each physical system needs its own model. Cook has proposed several waveguide-based simulations of everyday sounds [10], especially in the context of interactive systems, where computational efficiency is a major concern.

### **3. PHYSICS-BASED MODELS OF EVERYDAY SOUNDS**

Physical models, both in sound synthesis and computer graphics, are being used increasingly wherever the goal is a natural dynamic behavior. Moreover, with physical models it is possible to connect the model control variables directly to sensors and actuators, as the physical quantities are directly accessible in the model. There are several degrees of accuracy that can be used in developing a physics-based sound model. Using a finite-element model of interacting objects would make sense if tight synchronization with realistic graphic rendering is required, especially in the cases of fractures of solids or fluid-dynamic phenomena [1]. Most often, good sounds may be obtained by simulation of the rigid-body dynamics of objects described by piecewise parametric surfaces [3]. However, even in this case each impact results in a matrix of ordinary differential equations that have to be solved numerically. On the other hand, if the display is mainly auditory we can rely on perception to simplify the models significantly, without losing either their physical interpretability or veridical sound behavior.

As an example, consider the model of a bouncing ball. On one extreme, we can try to develop a finite-element model of the air cavity, of its enclosure, and of the dynamics of impact subject to gravity. On the other hand, if we have a reliable model of nonlin-

ear impact between a striking object and a simple mechanical resonator, we can model the system as a point-like source displaying a series of resonant modes. The source can be subject to gravity, thus reproducing a natural bouncing pattern, and the modes can be tuned to those of a sphere, thus increasing the impression of having a bouncing ball. Of course, this simplification based on lumping distributed systems into point-like objects introduces inevitable losses in quality. For instance, even though the ball can be turned into a cube just by moving the modal resonances to the appropriate places, the effect would not resemble that of a bouncing cube, just because the temporal pattern followed by a point-like bouncing object does not match that of a bouncing cube. However, we can introduce some controlled randomness in the bouncing pattern in such a way that the effect becomes perceptually consistent. Again, if the visual display can afford the same simplifications, the overall simulated phenomenon will be perceived as veridical [11].

The immediate benefit of simplified physics-based models is that they can run in real time in low cost computers, so that they can be interactively controlled by means of gestural or graphical interfaces. Figure 1 shows the graphical `pd`<sup>1</sup> “patch” of a bouncing object, where sliders can control the size, elasticity, mass, and shape. In particular, the shape slider allows continuous morphing between sphere and cube via superellipsoids, and it controls both the position of resonances and the statistical deviation from the regular temporal pattern of a bouncing ball. This kind of sound modeling leads to a sort of sonic cartoons [12, 13], these being simplified descriptions of sounding phenomena, with possible exaggeration of selected features. Visual as well as auditory cartoons are often preferred over realistic images and sounds because they ease our understanding of key phenomena by simplifying the representation and exaggerating the most salient traits, and this can lead to economy in realization and to the possibility of detailed control over the expressive content of the picture or sound.

#### 4. CONTACT SOUND MODELING

Many of the sounds that occur in every-day surroundings are based on contacts of solid bodies. The auditory perception of ecological attributes, like material and size of objects in contact, is common experience and has been examined by the SOb project [11]. Our works show that many typical forms of contact-interaction can be successfully modeled on the basis of a flexible and efficient one-dimensional impact or friction algorithm. Specific characteristics of the macroscopic phenomena which are of high perceptual relevance are modeled explicitly, for instance as macro-temporal distributions of micro-impacts.

##### 4.1. Impact

In contrast to most physical models of solid bodies in contact, focusing on the resonance behavior of interacting objects and widely ignoring the transient state of the event, our approach is based on a physical description of impact interaction processes [14]. This physical model involves a degree of simplification and abstraction that implies efficient implementation as well as adaption to a broad range of impact events.

We consider two resonating objects and assume that their interaction depends on the difference  $x$  of two variables, one variable for each object. In the standard case of examined movements

along a spatial direction,  $x$  is the distance variable in that direction. A compact efficient algorithm is described as follows. The impact force  $f$  is stated as a nonlinear term in  $x$  (and  $\dot{x}$ ) [15]:

$$f(x, \dot{x}) = \begin{cases} k(-x)^\alpha + \lambda(-x)^\alpha \cdot (-\dot{x}), & x < 0, \\ 0, & x \geq 0. \end{cases} \quad (1)$$

Here,  $k$  is the elasticity constant, the exponent  $\alpha$  shapes the dynamic behavior of the interaction, while  $\lambda$  controls the dissipation of energy during contact, accounting for friction loss. One inlet of the `impact...` modules takes a list of `interactor-parameters` containing the aforementioned values. The instantaneous cross relationship of resonator states is solved through a numerical strategy [16], that carefully avoids distorting artifacts.

The two interacting objects are built as modal resonators [4]. The modal formulation, while retaining an intuitive acoustic meaning, is general enough to be used in the description of any resonating objects. One resonator is here characterized by the number of its modes and, for each mode, by the three modal parameters: mode frequency, decay time, and level (“weight”) of the mode at the point of interaction. Accordingly, the `impact_2modal` modules have inputs for lists of frequencies, decay-times and weighting-factors of the two resonators. It is often convenient to use the modules `impact_modal`, where the first resonator is reduced to an inertial point mass and characterized only by one “mass” parameter. This practical and computational simplification parallels the notion that in many practical contact scenarios the vibration of one of the objects is hardly perceived.

In vibrating systems, the excitation and pickup points determine the relative weighting among the modes. Similarly, in our software modules each resonator can be accessed through an arbitrary number of pickup points, each being described by a list of weighting factors. The first pickup is coincident with the interaction point, and it always exists.

Finally, all modules have three other inlets. Two of these accept signals that are used to represent external forces on both resonators at the point of interaction. The third inlet is an additional positional offset, and it is used to impose surface profiles in rolling or sliding models.

##### 4.2. Friction

For friction modeling, we use a computational structure very similar to the one used for impacts. The `pd` plugin is called `friction_2modalb`.

The underlying model describes the average behavior of a multitude of micro-contacts made by hypothetical bristles extending from each of two sliding surfaces. When a modal decomposition is adopted for both interacting objects, the equations are [17, 18]

$$\begin{cases} m_{ei}\ddot{x}_{ei} + r_{ei}\dot{x}_{ei} + k_{ei}x_{ei} = f_{ee} - f_f, \\ m_{rj}\ddot{x}_{rj} + r_{rj}\dot{x}_{rj} + k_{rj}x_{rj} = f_{re} + f_f, \\ (i = 1 \dots N_e, j = 1 \dots N_r) \\ v = \sum_{i=1}^{N_e} t_{mi}\dot{x}_{ei} - \sum_{j=1}^{N_r} t_{lj}\dot{x}_{rj}, \quad (\text{relative velocity}) \\ \dot{z} = f_{NL}(v, z) = v \left[ 1 - \alpha(z, v) \frac{z}{z_{ss}(v)} \right], \\ f_f = \sigma_0 z + \sigma_1 \dot{z} + \sigma_2 v, \quad (\text{friction force}) \end{cases} \quad (2)$$

<sup>1</sup><http://www.pure-data.org>

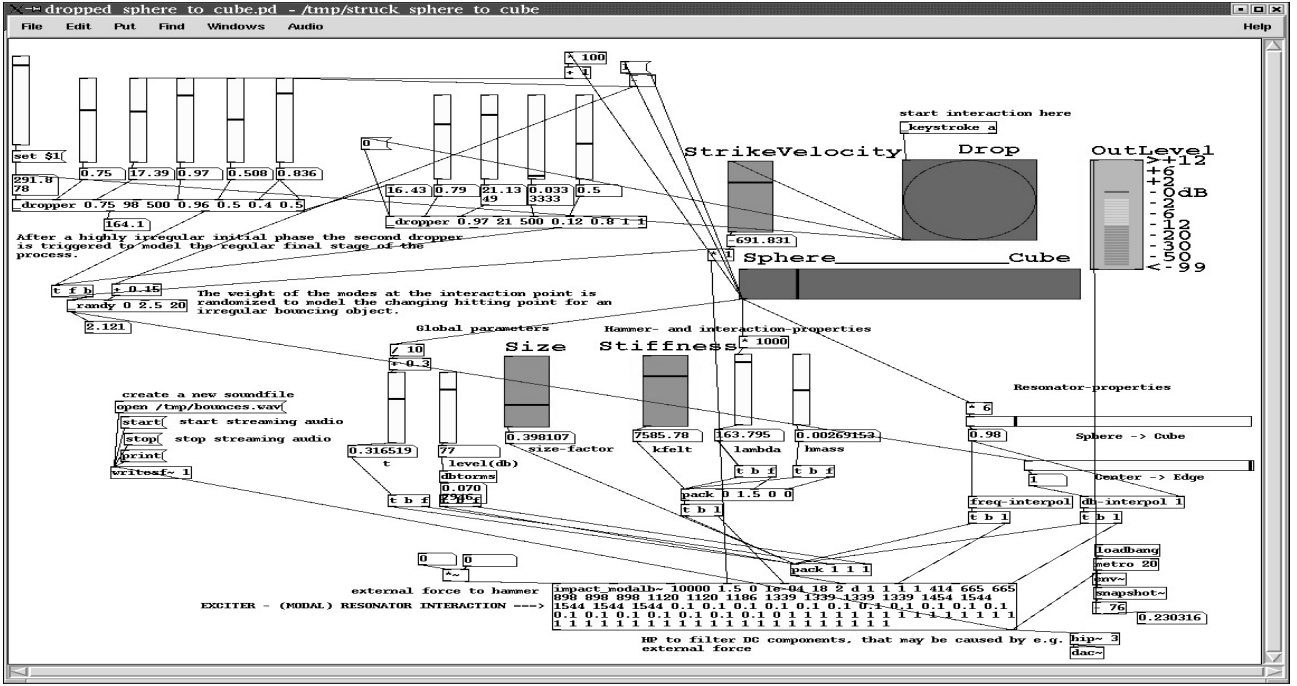


Figure 1: A pd patch for a bouncing object.

where the  $x$  variables represent the modal displacements, while  $z$  is the mean bristle displacement. The terms  $f_{ee}$  and  $f_{re}$ , as indicated by  $e$  in the second subscript, represent external forces. A pseudo-random fourth component  $\sigma_3 w(t)$  is also added to the friction force in order to account for noise due to surface roughness. The function  $\alpha(z, v)$  is an adhesion map that controls the rate of change of  $z$ . Specifically, when the bristle displacement  $z$  is smaller than a given breakaway displacement  $z_{ba}$  then  $\alpha$  is set to zero and the model possesses a purely elastic presliding regime (that is,  $\dot{z} = v$ ). Transition to the plastic regime occurs for larger bristle displacement. The function  $z_{ss}(v)$  has the typical shape used for interaction force in classic bowed string modeling [19], accounting for the so-called Stribeck effect, i.e. the decrease of the friction coefficient for increasing relative velocity of the two bodies in contact.

High-level interactions between the user and the audio objects rely mainly upon three interaction parameters. These are the external forces  $f_{ee}$  and  $f_{re}$  acting on each of the two objects, which are tangential to the sliding direction, and the normal force  $f_N$  between the two objects. The remaining parameters belong to a lower level control layer, as they are less likely to be touched by the user and have to be tuned at the sound design level.

Such low-level parameters can be grouped into two subsets, depending on whether they are related to the resonators' internal properties or to the interaction mechanism. As described for the `impact...` modules, each mode of the two resonating objects is tuned according to its center frequency and decay time, and a modal gain (which is inversely proportional to the modal mass) can be set for each resonator mode, to control the extent of excitation of that mode.

A second subset of low-level parameters relates to the interaction force specification. The triple  $(\sigma_0, \sigma_1, \sigma_2)$  define the interaction stiffness, the bristle internal dissipation, and the viscous friction,

and therefore affects the characteristics of signal transients as well as the ease in establishing stick-slip motion. A triple of parameters is used to set the shape of the curve  $z_{ss}$ . Specifically, the Coulomb force and the stiction force are related to the normal force through the equations  $f_s = \mu_s f_N$  and  $f_c = \mu_d f_N$ , where  $\mu_s$  and  $\mu_d$  are the static and dynamic friction coefficients. Finally, the breakaway displacement  $z_{ba}$  is also influenced by the normal force. In order for the function  $\alpha(v, z)$  to be well defined, the inequality  $z_{ba} < z_{ss}(v) \forall v$  must hold. Since  $\min_v z_{ss}(v) = f_c / \sigma_0$ , a suitable mapping between  $f_N$  and  $z_{ba}$  is

$$z_{ba} = c f_c / \sigma_0 = c \mu_d f_N / \sigma_0, \quad \text{with} \quad c < 1. \quad (3)$$

## 5. HIGHER-LEVEL SOUND MODELING

The models described in section 4 are complex and versatile enough to represent a wide class of contact sounds. For instance, the impact model can be tuned to render material properties of the resonators or to give different degrees of impact hardness, ranging from stiff to sticky. The continuous interaction achieved with the friction model is even more expressive. The continuously changing friction noises produced by rubbed glasses, braked wheels, or squeaky doors have been successfully simulated and used in interactive animations.

The ecological recognition of several contact events relies on temporal patterns that extend on a relatively large time scale. Examples of this kind are bouncing, breaking, rolling, crumpling, etc. [20, 11], and they can all be simulated by proper sequences of activation of the basic models. Such sequences are obtained by higher-level models, describing temporal dynamics at a slower rate. For instance, a rolling model is obtained by using a pseudo-random surface profile that acts on the offset parameter of the impact model. The sampling points of the surface profile are chosen

according to a simplified kinematics of the rolling ball.

An even higher level of abstraction is required when the gestures of human agents are taken into account. Gesture modeling for expressive rendering of animated sounds is a large playground for researchers in the years to come. In the SOb project, researchers at KTH–Stockholm did gesture analysis and modeling at several levels of complexity, ranging from the preparatory gestures of drummers, to walking and running patterns, to the rich gesture vocabulary used by DJ scratchers. Accurate, stable, and efficient low-level models provide the crucial ingredient for the success of these higher level models [13].

## 6. CONCLUSION

In the past forty years, the disciplines of sound synthesis, psychoacoustics, and music acoustics have always been mutually related. In recent years, the progress of physical modeling, ecological psychoacoustics, and auditory display for interactive applications, has steered many research efforts toward everyday sounds. This is a new exciting area for multidisciplinary research, where computer scientists, psychologists, acousticians, and sound designers can all give significant contributions.

## ACKNOWLEDGMENT

Many people directly or indirectly contributed to the SOb project. The authors of [20] have been heavily involved in the sound modeling work done at the University of Verona. Special thanks to Federico Avanzini and Matthias Rath for their contributions to this paper, and to Stefania Serafin for her contribution to friction modeling.

## 7. REFERENCES

- [1] J. O'Brien, P. R. Cook, and G. Essl, "Synthesizing Sounds from Physically Based Motion," in *Proc. ACM SIGGRAPH 2001*, Los Angeles, CA, 2001, pp. 529–536, ACM Press/ACM SIGGRAPH.
- [2] K. van den Doel and D.K. Pai, "Synthesis of shape dependent sounds with physical modeling," in *Proc. International Conference on Auditory Display*, Palo Alto, CA, 1996, ICAD.
- [3] K. van den Doel, P.G. Kry, and D.K. Pai, "Foleyautomatic: Physically-based Sound Effects for Interactive Simulation and Animation," in *Proc. of SIGGRAPH 2001*, Los Angeles, CA, 2001, pp. 537–544, ACM Press/ACM SIGGRAPH.
- [4] J. M. Adrien, "The Missing Link: Modal Synthesis," in *Representations of Musical Signals*, G. De Poli, A. Piccialli, and C. Roads, Eds., pp. 269–297. MIT Press, Cambridge, MA, 1991.
- [5] D.K. Pai, K. van den Doel, D. L. James, J. Lang, J. E. Lloyd, J. L. Richmond, and S. H. Yau, "Scanning Physical Interaction Behavior of 3D Objects," in *Proc. ACM SIGGRAPH 2001*, Los Angeles, CA, 2001, pp. 87–96, ACM Press/ACM SIGGRAPH.
- [6] J. O'Brien, C. Shen, and C. Gatchalian, "Synthesizing Sounds from Rigid-Body Simulations," in *Proc. ACM SIGGRAPH 2002 Symposium on Computer Animation*, San Antonio, TX, 2002, pp. 175–182, ACM Press/ACM SIGGRAPH.
- [7] C. Cadoz, A. Luciani, and J.-L. Florens, "Physical models for music and animated image. The use of CORDIS-ANIMA in Esquisses: a Music film by Acroë," in *Proc. International Computer Music Conference*, Aarhus, Denmark, 1994, ICMA.
- [8] Jamel Nouiri, Claude Cadoz, and Annie Luciani, "The physical modelling of complex physical structures. the mechanical clockwork: Motion, image, and sound," in *Proceedings of Computer Animation Conference*, Geneva, Switzerland, 1996, IEEE, pp. 36–46.
- [9] J.O. Smith, "Physical modeling using digital waveguides," *Computer Music Journal*, vol. 16, no. 4, pp. 74–91, 1992.
- [10] Perry R. Cook, Ed., *Real sound synthesis for interactive applications*, A. K. Peters, Natick, MA, 2002.
- [11] Davide Rocchesso and Federico Fontana, Eds., *the Sounding Object*, Mondo Estremo, Firenze, Italy, 2003, <http://www.soundobject.org>.
- [12] William W. Gaver, "How do we hear in the world? explorations in ecological acoustics," *Ecological Psychology*, vol. 5, no. 4, pp. 285–313, 1993.
- [13] Davide Rocchesso, Roberto Bresin, and Mikael Fernström, "Sounding objects," *IEEE Multimedia*, vol. 10, no. 2, pp. 42–52, 2003.
- [14] Federico Avanzini and Davide Rocchesso, "Modeling collision sounds: Non-linear contact force," in *Proc. COST-G6 Conference on Digital Audio Effects*, Limerick, Ireland, 2001, pp. 61–66.
- [15] D. W. Marhefka and D. E. Orin, "A Compliant Contact Model with Nonlinear Damping for Simulation of Robotic Systems," *IEEE Trans. Systems, Man and Cybernetics-Part A*, vol. 29, no. 6, pp. 566–572, Nov. 1999.
- [16] G. Borin, G. De Poli, and D. Rocchesso, "Elimination of Delay-free Loops in Discrete-Time Models of Nonlinear Acoustic Systems," *IEEE Transactions on Speech and Audio Processing*, vol. 8, no. 5, pp. 597–606, 2000.
- [17] P. Dupont, V. Hayward, B. Armstrong, and F. Altpeter, "Single State Elasto-Plastic Friction Models," *IEEE Transactions on Automatic Control*, vol. 47, no. 5, pp. 787–792, 2002.
- [18] Federico Avanzini, Davide Rocchesso, and Stefania Serafin, "Modeling interactions between rubbed dry surfaces using an elasto-plastic friction model," in *Proc. COST-G6 Conference on Digital Audio Effects*, Hamburg, Germany, 2002.
- [19] M. E. McIntyre, R. T. Schumacher, and J. Woodhouse, "On the oscillations of musical instruments," *Journal of the Acoustical Society of America*, vol. 74, no. 5, pp. 1325–1345, 1983.
- [20] Matthias Rath, Federico Avanzini, Nicola Bernardini, Gianpaolo Borin, Federico Fontana, Laura Ottaviani, and Davide Rocchesso, "An introductory catalog of computer-synthesized contact sounds, in real-time," in *Proc. Colloquium on Musical Informatics*, Firenze, Italy, 2003.

# THE SUNDBERG SESSION



## **A MARRIAGE OF THE DIRECTOR MUSICES PROGRAM AND THE CONDUCTOR PROGRAM**

*Max Mathews<sup>1</sup>, Anders Friberg<sup>2</sup>, Gerald Bennett<sup>3</sup>, Craig Sapp<sup>1</sup>, Johan Sundberg<sup>2</sup>*

<sup>1</sup>Stanford University

<sup>2</sup>KTH Royal Institute of Technology

<sup>3</sup>Zurich Musikhochschule

*m.v.mathews@att.net*

### **ABSTRACT**

This paper will describe an ongoing collaboration between the authors to combine the Director Musices and Conductor programs in order to achieve a more expressive and socially interactive performance of a midi file score by an electronic orchestra. Director Musices processes a “square” midi file, adjusting the dynamics and timing of the notes to achieve the expressive performance of a trained musician. The Conductor program and the Radio-baton allow a conductor, wielding an electronic baton, to follow and synchronize with other musicians, for example to provide an orchestral accompaniment to an operatic singer. These programs may be particularly useful for student soloists who wish to practice concertos with orchestral accompaniments.

### **1. INTRODUCTION**

This paper is intended to serve two purposes. It is a celebration of one facet of Johan Sundberg’s long and brilliant career which continues at an undiminished speed, despite his “nominal” retirement from KTH. It is also a progress report on the recent ongoing collaboration which the other authors have been privileged to have with Johan. One author (Mathews) felt that a paper describing this research would be both an appropriate vehicle to honor Johan and would also allow the world to share some of his recent results. It also seemed necessary and appropriate that he should be included as an author of this paper.

Because of its unusual dual objectives and because the authors are now on different continents, the paper is being drafted by one of the authors (Mathews) and he accepts full responsibility for any mistakes and for any possible misrepresentations of the other authors’ opinions.

### **2. THE QUEEN OF THE NIGHT ARIA**

In the mid 1970’s computer music was in the frustrating position of theoretically being capable of synthesizing any sound but practically unable to generate many timbres, particularly those of the human voice. Johan spent a few months at the newly formed IRCAM in Paris working with Gerald Bennett and Xavier Rodet [1] and Yves Potard. Together they developed an “analysis-by-synthesis” technique for synthesis of the singing voice. The result was the first professional quality singing voice synthesis. It depended on Johan’s knowledge of the human voice along with Rodet’s formant synthesis program, Bennett’s musical expertise. The detailed synthesis was mostly done by Potard.

### **3. BICYCLE BUILT FOR TWO**

The “queen” aria still is the most convincing example of computer singing which exists. It also illustrates the power of utilizing speech research knowledge for musical purposes. Johan, from his position in the KTH speech and music laboratory, has long been a prime example of the power of this liaison.

The first computer singing synthesis also depended on basic knowledge from KTH. The bicycle song, became famous in the movie “2001: A Space Odyssey” as the computer’s swan song. It was created by John Kelly and Carol Lochbaum at Bell Telephone Labs in 1960. They used the vocal tract area function data from Gunnar Fant’s famous book [2]. Their synthesis used a tube model of the vocal tract in which the areas of the tubes were manipulated by the computer to achieve the proper spectrum for both vowel and consonant sounds. Their program was the first example of the physical modeling approach which only became popular to create music timbres much later in the 1990s [play example in talk]

### **4. SYNTHESIS OF SINGING BY RULES**

The synthesis for both “queen” and “bicycle” involved hand tailoring the sounds, a very tedious process. This and the desire to better understand the rules singers use led Sundberg into studies of rule synthesis [3]. His experimental vehicle was a hybrid synthesizer, MUSSE, a formant analogue machine driven by a minicomputer.

Data for the rule synthesis consisted of a table of the first five target formant frequencies and the first three target formant bandwidths for both vowels and consonants (“queen” being a vocalise had no consonants which much simplified its synthesis). The target information for the sequence of vowels and consonants to be sung were then converted into smooth time functions by coarticulation and other rules in the minicomputer computer program.

The resulting time functions were sent to MUSSE. The resulting singing showed both that expressive rule synthesis is possible and that the rules that singers use are very complex and many factors in addition to formant frequencies and bandwidths must be evoked to achieve acceptable quality.

### **5. DIRECTOR MUSICES**

Johan later extended his interest in rule synthesis to rules for expressive performance of instrumental music [4]. By then sampling synthesizers had developed useful timbres for most



orchestral instruments and midi files had become a lingua franca for representing scores and playing them automatically with a computer and synthesizer. With sufficient effort, scores in general music notation can be converted to midi files. But most resulting midi files are too “square” to yield expressive performances when played directly on a “dumb” synthesizer. The performances lack the phrasing and dynamics that trained musicians would always add when performing from a traditional paper score. Director Musices ameliorates this limitation.

Director reads a “square” midi file and writes out a modified midi file where the times of starting and ending notes, the loudness of notes, and possibly the timbre quality of the notes are adjusted to create a more expressive performance.

Usually Director applies a pallet of about a dozen rules to the input midi file. The weight with which each of the rules is applied can be adjusted by the user from zero which produced no change to a maximum which produces unacceptably large changes. Negative weights can even be commanded by an iconoclastic musician.

Some rules only use the pitches and durations of the notes in the “square” input score—for example making high pitched notes louder or increasing the duration contrast between long and short notes. Other rules require additional information beyond what is in the midi file.

Phrasing rules require that phrase beginnings and endings be added to the midi file. Melodic and harmonic “charge” rules emphasize notes and chords that are unusual in the key of the music. These rules require a harmonic analysis be added to the midi file. Adding a harmonic analysis can be a substantial task.

## **6. THE CONDUCTOR PROGRAM**

The Conductor Program was conceived by Mathews at Bell Telephone Laboratories in the mid 1980s and further developed at CCRMA after 1987 [5]. It was intended as a mode of computer aided live performance. The model for the program was not a performer but rather a conductor leading an orchestra. A synthesizer provided a virtual orchestra and the Radio-Baton provided two batons with which the conductor controlled the synthesizer.

The score was an augmented midi file. The main augmentation was a conductor track added to the midi file with trigger points corresponding to expected baton beats. A baton beat causes the program to play the next beat’s worth of score in the midi file. The time between the previous two beats sets the tempo used to play the next beat’s worth of the midi file. Thus the conductor’s baton controls both onset of each beat’s worth of midi file and the tempo at which it is played.

The Conductor Program also requires a preamble score which defines how motions of the second baton control the dynamics and balance of the various voices in the orchestra.

Perhaps the most important strength of the conductor program is its precise control of time so that it can function as a social instrument playing with other instruments and supporting its share of the task of synchronizing with the other performers. It can provide orchestral accompaniments for soloists who can not afford real orchestras.

Its greatest weakness is the lack of intelligence of the synthesizer and midi file score compared to that of an orchestra of highly trained musicians.

## **7. MARRIAGE OF DIRECTOR MUSICES AND THE CONDUCTOR PROGRAM**

By 2000 Gerald and Verena Bennett in Switzerland had experimented for some time with the Radio-Baton and the Conductor Program accompanying piano students and singers. They were dissatisfied with the lack of musicality in the “square” midi file scores which were all that were available to them. Gerald believed that processing the midi files with Director Musices could greatly improve the accompaniments. He raised support to bring the authors of this paper together in Zurich for a total of four weeks in 2000 and in 2001 to develop and try his idea.

Although I much looked forward to the opportunity to work with Johan and Gerald, I had doubts that the marriage of our programs would work. I feared that the expressive control by the conductor during the live performance would fight with the expressive changes made in the midi file by Director. I also thought there might be computer conflicts in joining the two programs that we would not have time to solve during our short time together. I think Johan shared some of my concerns.

Happily my fears were unfounded. Thanks to midi files as a lingua franca, the programs worked together immediately. Also we were able to achieve useful compromises on who was in charge of various expressions.

Our working procedure started with a square midi file. Next a baton track of trigger points was added to the midi file. This required committing to the number of beats per measure which usually, but not always, corresponded to the time signature of the score. Occasionally we would double the number of trigger points to give the conductor finer control of timing. Extra trigger points could be added to terminate fermatas.

The augmented midi file was then passed through Director after choosing a trial set of weights for the pallet of rules. Director would adjust the loudness via the midi key velocity byte for each midi note in each voice. Director would also introduce pauses and timing changes by moving midi note start and end times forward or backward various numbers of midi file ticks. The same timing changes were made in all tracks so all the voices would remain synchronized including the baton track. Adding the baton track to the midi file before applying Director was necessary so baton trigger points would remain associated with the notes they were supposed to trigger.

In the live performance, the conductor completely controlled the performance times of the trigger points notes and the overall tempo at which the notes between two trigger points would be played. Director could adjust relative times of notes between trigger points.

With a baton, the Conductor could control the loudness and balance of the voices by varying the synthesizer volume control (C11 in midi terminology) for each voice. Since C11 is completely independent of the midi key velocity byte, no technical conflict could exist between Director and the conductor.

The sharing of expressive control which I just described worked better than we expected. It yielded performances that were both pleasant to conduct and lively to hear.

We mainly tried orchestra accompaniments for piano concertos and vocal pieces. Purely piano pieces did not prove to

be as satisfactory as orchestral pieces. We do not yet understand why.

Some of Director's rules depend only on information in the midi file. These can be used without much additional work. Other rules require that phrasing information be added. The Director program has provision for marking three levels of phrasing. Putting in phrase marks is not overly tedious.

Other rules, like those for harmonic and melodic charge, require a harmonic analysis of the score which may be more work than the user wishes or is able to invest. The interest in having a program to do this work motivated Craig Sapp to write a new harmonic analysis program which generates a two dimensional analysis. The X dimension is the usual performance time going from beginning to end of the composition. The Y dimension is the degree of aggregation over which a sub analysis is made. At the top of Y, the entire piece is analyzed to estimate the key of the piece. At the bottom of Y, each individual chord is classified. The data is shown as a two dimensional color plot. Sapp's program makes the use of harmonic analysis in Director much more practical. But in addition the program is interesting in its own right.

The program has not yet been integrated with Director and the Conductor Program. All programs use the same midi file as input, but the results of Sapp's analysis must be manually entered into the Director score, which is still time consuming. To make wide usage simple enough to be practical, Sapp's program needs to be combined with Director and Conductor.

## 8. CONCLUSIONS

The Director-Conductor-Baton system has been convincingly demonstrated at universities in Switzerland and Austria, in Stockholm at a meeting of pan European singers, at Stanford in student classes at CCRMA, and at the Bourges electronic music festival in France. The success these demonstrations encourage us to continue to develop a simple unified device which can accept a midi file and allow the conductor to play an expressive score without having to fight either equipment or computer programs. The hardware box would contain both a Radio-Baton and a synthesizer. Its output would be a stereo signal ready to be sent to a speaker-amplifiers. Director Musices, the Radio-Baton program, the Conductor Program, and a harmonic analysis program would be combined into a single program.

## 9. REFERENCES

- [1] Bennett,G and Rodet,X, Synthesis of the Singing Voice, CURRENT DIRECTIONS IN COMPUTER MUSIC RESEARCH, MIT press, Cambridge Massachusetts, 1989
- [2] Fant,G, ACOUSTIC THEORY OF SPEECH PRODUCTION, 1960, Mouton & Co,The Hague, Netherlands
- [3] Sundberg, J, Synthesis of Singing by Rule, CURRENT DIRECTIONS IN COMPUTER MUSIC RESEARCH, the MIT press, Cambridge Massachusetts, 1989
- [4] Friberg, A, Colombo,V, Fryden, L, and Sundberg, J (2000) Generating Musical Performances with Director Musices, Computer Music Journal, 24 (3), 23-29
- [5] Mathews, M, The Conductor Program and Mechanical Baton,CURRENT DIRECTIONS IN COMPUTER MUSIC RESEARCH,MIT press, Cambridge, Massachusetts, 1989



## **EXPRESSIVENESS IN MUSIC PERFORMANCE: ANALYSIS AND MODELING**

*Giovanni De Poli*

Centro di Sonologia Computazionale – Dept. of Information Engineering  
University of Padova  
depoli@dei.unipd.it

### **ABSTRACT**

Expression is an important aspect of music performance. It is the added value of a performance and is part of the reason that music is interesting to listen to and sounds alive. Moreover, understanding and modeling expressive content communication is important in many engineering applications. In human musical performance, acoustical or perceptual changes in sound are organized in a complex way by the performer in order to communicate musical content to the listener. The same piece of music can be performed trying to convey a specific interpretation of the score, by adding mutable expressive intentions. The analysis of these systematic deviations has led to the formulation of several models that try to describe their structures, and aim at explaining where, how and why a performer modifies, sometime in an unconscious way, what is indicated by the notation of the score. Modeling paradigms and problems are reviewed and issues for future research efforts are discussed.

### **1. INTRODUCTION**

Music is an important means of communication where three actors participate: the composer, the performer and the listener. The composer instils into his works his own emotions, feelings and sensations, and the performer communicates them to the listeners. The composer describes his/her musical ideas by a score or a process. The information contained in the score (or produced by the process) has a double function: a descriptive one, as a symbolic representation of the cognitive elements constituting the composition, and a functional one, as a mean to convey instructions to the performer. Other information is implicit in the score and regards performance style and interpretative conventions. The performer interprets these symbols, taking into account the implicit information and his/her personal artistic feeling and aim, and produces the sounds by using a musical instrument. Music performance includes all the human activity that lies between the symbolic score and the music instrument

Music performance is an interesting topic to study for its multidisciplinary valence. In this paper paradigms and issues emerged in research on modeling expressiveness in music performance will be reviewed and future research perspectives will be discussed. Due to space limitation, many references will be skipped. A more complete indication can be found in the bibliography of the few papers here quoted [1-7].

### **2. BASIC ISSUES**

#### **2.1 Models**

Frequently in science *models* are employed to evidence and abstract some relations that can be hypothesized, discarding details that are felt to be not relevant for what is being observed and described. Models can be used to predict the behavior in certain condition and compare these results with observations. In this sense, they serve to generalize the findings and have both a descriptive and predictive value.

In the study of music performance, models for describing music performance start being developed soon. The possibility, offered by technology, of implementing the models and to experiment with their behavior by simulation gave rise to an increased use of technology in music research. Moreover, computer science and music technology developed in many conceptual frameworks and practical tools the last decades, that are very useful for music performance investigation. For example artificial intelligence, knowledge engineering, soft computing methodologies, physics based models, MIDI instruments, signal processing analysis methods, computer controlled performance, motion capture devices, constitute paradigms and tools that are at the base of many performance models.

The idea of developing *computational models* of music performance dates back to the first music application of computers. It can be mentioned the Groove system by Max Mathews that allowed real time control and editing of performer actions described (graphically or symbolically) by time functions. The first models were mainly dedicated to music production and experimentation, and were embedded in computer programs for music synthesis or representation and for interactive performance. Their theoretical assumptions and conceptual foundation were often not explicit. Later models for performance understanding started to be developed (e.g. KTH performance rule system) and now we can expect a convergence of efforts toward models that are oriented toward both performance understanding and production.

#### **2.2 Expressiveness in music performance**

The communication of expressive content by music can be studied at three different levels: considering composer message, performer expressive intentions and listener perceptual experience. Studies of the first kind are historically more developed. Generally, they analyze the elements of the musical

structure and the musical phrasing that are critical for a correct interpretation of composer's message.

The contribution of the performer to expression communication has two facets: to clarify the composer's message enlightening the musical structure and to add his personal interpretation of the piece. A mechanical performance of a score is perceived as lacking of musical meaning and is considered dull and inexpressive as a text read without any prosodic inflexion. Indeed, human performers never respect tempo, timing and loudness notations in a mechanical way when they play a score: some deviations are always introduced.

Thus in general *expressiveness* refers both to the means used by the performer to convey the composer message and to his own contribution to enrich the musical message. However many music performance studies concentrate on the first aspect trying to understand the performer actions to better convey the musical structure. Simulation models are often evaluated by the musical acceptability of their results, or in other words how well a supposed ideal interpretation of that particular piece is approached.

Recently interest is growing also in taking into account the expression component added by the performer. Some aspects are still strongly related to the musical piece, as performer specific style, and influences of stylistic expectation based on cultural norm or actual performance situation. But other communicative aspects can be taken into account. Experiments are carried out by asking performers to play the same piece according diverse specific adjectives or nuances or trying to convey different content. The researcher then seeks to understand and model the strategies used in these performances. Often basic emotions are chosen as possible expressions (e.g. by Gabrielsson group) and in this case the term expressive performance refers to *emotional performance*. Notice that sometimes emotions the performer tries to convey can be in contrast with the character of the musical piece. A slightly broader interpretation of expression as KANSEI (Japanese term indicating sensibility, feeling, sensitivity) or affective communication is proposed in some Japanese or American studies. I prefer the broader term "*expressive intentions*" that include emotion, affects as well other sensorial and descriptive adjectives or actions. Furthermore this term evidences the explicit intent of the performer in communicating expression.

Understanding of specific *artistic intentions* of top level performers is more challenging. While artists aim to express aesthetic value, I feel that these qualities are probably impossible to model, without loosing their real essence.

### 2.3 Expressive deviations

Most studies of performance expressiveness aims at understanding the systematic presence of *deviations* from the musical notation as a communication means between musician and listener. Deviations, introduced by technical constraints (such as fingering) or by imperfect performer skill, are not normally considered part of expression communication and thus are often filtered out as noise.

The analysis of these systematic deviations has led to the formulation of several models that try to describe their structure, with the aim to explain where, how and why a performer modifies, sometimes unconsciously, what is indicated by the notation in the score. It should be noticed that, although deviations are only the external surface of something deeper and often not directly accessible, they are quite easily measurable, and thus widely used to develop computational models in scientific research and generative models for musical applications.

When we talk of deviation, it is important to define which is the *reference* used for computing deviation. Very often the score is taken as reference, both for theoretical (the score represents the music structure) and practical (it is easily available). However, the use of a score as reference has some drawbacks for the interpretation of how listeners judge expressiveness. Alternative approaches are the intrinsic definitions of expression (expressive deviations defined in terms of the performance itself) or non-structural approaches relating expression to motion, emotion, etc.. Our studies in expressive intention rendering yield best results using a *neutral* performance as reference [4].

## 3. MODELS OF / FOR MUSIC PERFORMANCE

Models are developed with different aims. A basic difference is between models for understanding (also called analysis models) and models able to produce music performances (also called synthesis models). In the following sections the main paradigms will be presented and discussed.

### 3.1 Analysis models

We may distinguish two strategies in developing the structure of the model and in finding its parameters: analysis-by-measurement and analysis-by-synthesis

In the first strategy, *analysis-by-measurement*, is based on the analysis of deviations measured in recorded human performances. The analysis aims at recognizing regularities in the deviation patterns and to describe them by means of a mathematical model, relating score to expressive values. Sometimes multidimensional analysis is applied to performance profiles (e.g. principal component analysis) in order to extract independent pattern. Often the hypothesis, that deviations deriving from different patterns or hierarchical levels can be separated and then added, is implicitly assumed. This hypothesis helps the modeling phase, but may be oversimplified.

Alternative to this method is that of performing controlled experiments: by manipulating one parameter in a performance (e.g. the instruction to play at a different tempo) the measurements reveal something of the underlying mechanisms.

*Machine learning* performance rules are another active research stream. The group of Widmer and of Katayose-Inokuchi use some AI inductive algorithms to infer performance rules from recorded performances. Another similar approach with AI algorithms using case-based reasoning was proposed by Arcos et al. and in that developed a system for the synthesis of expressive performances, and by Suzuki et al.. Several methodologies of approximation of human performances were developed using

neural network techniques by Bresin, fuzzy logic approach by De Poli et al., using a multiple regression analysis algorithm by Ishikawa, linear vector space theory by Zanon (see [5] for an overview of analysis models).

The second strategy derives models, which are described with a collection of rules, using an *analysis-by-synthesis* method. The most important is the KTH rule system [6-7]. The rules describe quantitatively the deviations to be applied to a musical score, in order to produce a more attractive and human-like performance than the mechanical one that results from a literal playing of the score. Every rule tries to predict (and to explain with musical or psychoacoustic principles) some deviations that a human performer is likely to insert. At first, rules are obtained based on the indications of professional musicians, using knowledge *engineering* paradigms. Then, the performances, produced by applying the rules, are evaluated by listeners, allowing further tuning and development of the rules. The rules can be grouped according to the purposes that they apparently have in music communication. *Differentiation rules* appear to facilitate categorization of pitch and duration, whereas *grouping rules* appear to facilitate grouping of notes, both at micro and macro level. As an example of such rules, let us consider the Duration Contrast rule: it shortens and decreases in amplitude the notes with duration between 30 and 600 ms, depending on their duration according to a suitable function. The value computed by the rule is then weighted by a quantity parameter  $k$ .

### 3.2 Performance synthesis models

While the models above described were developed mainly for analysis and understanding purpose, often they are used also for synthesis purpose. Starting from expressiveness models, several software systems for the computer *automatic generation* of musical performances were developed. Some examples are POCO by Honing, the RUBATO system by Mazzola and Zahorka, Director Musices by Friberg, et al., Super Conductor by Clynes and CaRo by Canazza, et al.. Moreover, many sequencers now implement functions, called humanizer, that add deviations to the score, computed in a random way or according to specific criteria.

The idea of automatic expressive music performance, especially when it is applied to the performance of classical music that was not written for this purpose, is questionable. Even if the models could be very accurate (and still they are not), some very important artistic aspects of this kind of music will be omitted. When we listen to a recording of a classic music performance, we are aware that it is just a reproduction of an event and not an experience of the music as it was conceived at its time. On the other hand, the possibility to fully model and render the artistic creativity implied in the performance is still to be demonstrated. For the moment, at best, we can expect a reproduction of a specific performance, without a real new creative contribution, that would make listening interesting. Or we can expect the rendering of some, hopefully relevant, aspects of a musically acceptable performance, but not sufficient for a full artistic appreciation.

Performers are particularly sensitive to these aspects and usually looks at performance synthesis in a very suspicious manner. An instinctive fear of a possible danger for their competence and

even their job can be guessed to contribute, but the cultural motivations are definitely true. On the other hand if we think to music applications, where a real artistic value is not necessary (even if useful as in many multimedia applications), and where the alternative is a mechanic performance of the score (as in many sequencers), automatic performance can be acceptable. From this point of view such models can be used for entertainment application or when it not necessary to preserve the exact artistic environment of the composition, as in popular music. However, in many occasions a human performer is not available and should be substituted in a certain way. Performance models or processing MIDI recorded performance could be a solution. Notice that the quality of performance processing is much higher when it is based on performance models and knowledge.

Another important application of performance models, even of classical music, is in *education*. The knowledge embodied in performance models can help the teacher to rationalize the performance strategies and to better convey his teaching effort.

### 3.3 Models for artistic creation

The situation is different when music is expressly created bearing in mind the use of technology. We are in the era of information society and artists are always more frequently using technology in their artworks. Since the beginning of last century, some musicians started to think how to enlarge the sound palette by using not conventional instruments. The availability of new electronic and computer generated sounds gave rise to a new kind of music. Artists exploited and innovated greatly the methods of producing and performing music. In the first period of computer music, a lot of research effort was dedicated to sound synthesis and modeling. New synthesis algorithms were discovered, such as frequency modulation, and new paradigms were developed for musical sound generation, such as spectral and physical models. On the other side, models for music representation and algorithmic composition were developed.

Less attention was being paid to the performance aspects. The music was automatically generated from the score as it was written by the composer or generated by the composition program. The composer had to take into account all the nuances often implicit in the score to communicate the expressive content of the music. In this situation, the composer must explicitly preview what the performer normally handles. The composer is also a performer and needs to formalize the performance process. A different approach, to overcome the limitations of computer generated music, was followed by music for live electronics where the performer interacts with technology on the stage transforming in real time the sound produced by traditional or synthetic instruments.

In both cases, a central challenge is the control of the sound synthesis or processing engines (systems, algorithms, etc.). This problem is a typical performance topic and it refers to the need of establishing and computing the relation of musical and compositional aspects with sound parameters, according to the expressive aim of the musician. The inputs are discrete events, as described in the score or generated by computer, and continuous signals, e.g. performer gestures. These inputs should be coordinated and merged to produce and process sound events. In

music technology the concept of mapping strategies, which describe these relations, is of great importance. The conventional (and simplest) aspect refers to specific relation; for example how to convert a pitch and loudness information into proper spectral and micro-timing values of a synthetic note. But the word strategies tends to refer to other possible choices and source of information as phrasing, musical character, mood of the performer, stylistic alternatives. All these aspects are typical music performance issues. Suitable music performance models are very desirable.

Recently people are becoming more aware of the need of a well-founded approach based on strong scientific knowledge. This aim can be faced from two complementary directions. One way is to start from the knowledge gained in classical music performance studies and formalized in performance models; then generalize their results and apply them to the performance of new music creation. The other direction starts from the practical knowledge of new music creators (often embodied in their music performance systems) in order to extract possible suggestions and proposals of new performance models. From the joint effort of scientists and musicians valid results can be expected and real new tools can be developed, not only inspired to problems and solutions of the past times.

#### 4. CONCLUSIONS

It can be noticed that music performance is an interesting topic for scientific investigation and for technology research: it involves human non-verbal communication, has artistic-creative finality, and requires strong cooperation between art and science - technology. Probably still more important is the fact that music is an immaterial art that has a strong tradition of symbolic representation and abstract thinking. This attitude may explain why musicians were the most enthusiastic and successful in promoting and contributing to the joint development of art and science since the beginning of computer science. In other arts, this collaboration started much later and very often it is restricted to the use of technology rather than a real contribution to joint development of knowledge and tools.

#### 3. REFERENCES

- [1] Gabrielsson, A. "The performance of music". In D. Deutsch (Ed.), *The psychology of music* (2nd ed.), San Diego: Academic Press, pp. 501-602, 1999.
- [2] Palmer, C., "Music Performance." *Annual Review Psychology*, vol. 48, pp. 115-38, 1997.
- [3] Clarke, E. F. "Expression in performance: generativity, perception and semiosis." In J. Rink (ed.), *The Practice of Performance: Studies in Musical Interpretation*, Cambridge: CUP, pp. 21-54. 1995.
- [4] Canazza S., De Poli G., Drioli C., Rodà A. and Vidolin A., "Modeling and control of expressiveness in music performance", *The Proceedings of the IEEE*, 2003
- [5] Zanon P., De Poli G. "Estimation of parameters in rule system for expressive rendering of musical performance" *Computer Music J.*, 27(1), pp. 29-46, 2003
- [6] Friberg, A., "Generative Rules for Music Performance: a Formal Description of a Rule System." *Computer Music Journal*, 15(2), pp. 56-71. 1991
- [7] Friberg, A., Colombo, V., Frydén, L. and Sundberg, J., "Generating Musical Performances with Director Musices." *Computer Music Journal*, 24(3), pp. 23-29, 2000.

## **"THE VOICE AS A MUSICAL INSTRUMENT: FUNDAMENTAL DIFFERENCES BETWEEN MAN-MADE AND BIOLOGICAL DESIGNS."**

*Ingo R. Titze, Ph.D.*

**Department of Speech Pathology and Audiology  
University of Iowa  
National Center for Voice and Speech  
Denver Center for the Performing Arts and University of Iowa  
[ingo-titze@dcpa.org](mailto:ingo-titze@dcpa.org)**

### **ABSTRACT**

Although the singing voice resembles string and wind instruments in many ways, there is a major size difference that forces the biological system to take advantage of nonlinearities. Both the length of the vocal fold and the length of the vocal tract are well below standard (in terms of musical instruments). Nature has compensated by creating a ligament "string" that has a nonlinear stress-strain relation and nonuniform cross-section to cover a wide pitch range. The vocal tract, being only 10-20 cm long, can only resonate one or two harmonics at a time at high pitches, but general harmonic reinforcement can be obtained by inertive source-resonator coupling, a nonlinear effect not often used in speech. But a price is paid for the heavy use of nonlinearity. The instrument becomes more difficult to control. Pitch and intensity, for example, are never independent. It requires a complex central nervous system to play the instrument. Furthermore, there are two critical pathways to deal with in laryngeal control, the speech motor pathways and the limbic system pathways. These pathways can interfere with each other in the production of musical sounds, but they can also be useful in the expression of emotion.



Figure 1

### **1.1 The Basic Design**

When acousticians design sound-producing instruments, the frequency of the instrument is inversely proportional to size. Large vibrators make low sounds, and small vibrators make high sounds. There is generally a sound-reinforcing structure, the size of which is also commensurate with the frequencies of production. Usually the entire instrument resonates. Humans compare in size to stringed instruments (Figure 1), but only a small part of the anatomy is used for sound generation and resonance. Our vocal cords are on the order of one centimeter long, one-hundredth of the average length of the violin or piano strings. Furthermore, the large soundboards are missing. Why not vibrate the chest, the belly, the back, or the buttocks, where surfaces are woofer size? (Figures 2 and 3). The problem is, these surfaces are like mush; they don't spring back like a speaker cone, or a drumhead, or a thin plate of spruce. Resonation and radiation from our body surfaces are quite poor.



Figure 2

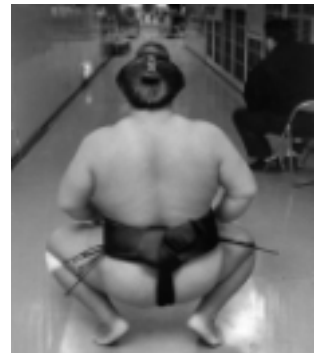


Figure 3

Our only sound reinforcing structure, the airway tube from larynx to lips is only about 17 centimeters long, with both surface and volume measures being tiny in comparison to those of stringed instruments. Even in comparison to the tubes and horns of brass and woodwind instruments, we are woefully undersized (Figures 4 and 5). If we uncoil the trumpet





Figure 4

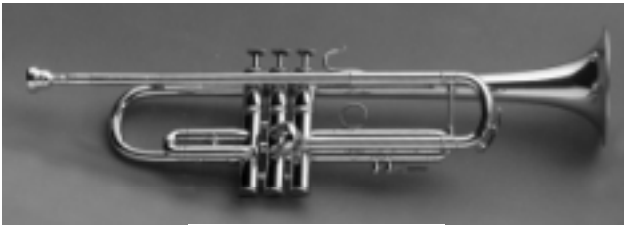


Figure 5

tube, its length is on the order of one meter, more than half the length of our body head to toe. The result of this undersizing of our airways is that we cannot resonate many harmonics of our sound source at any one time. By musical instrument standards, this should result in a rather dull and uninteresting instrument.

## 1.2 Questions of Interest

Given this larger size requirement for a good instrument, the question is, "Why has Mother Nature decided to put our sound-producing organ in the neck, the smallest and most constricted region of our body?" (Figure 6). Real estate is high-priced there, with competition arising from major nerves and blood vessels, the spine, and the food pipe.



Figure 6

Then comes the next dilemma. To raise pitch, we must tense our vocal folds. But, unlike in stringed instruments, in which tension is increased by wrapping the strings around pegs, we can only increase tension by stretching our tissues. But this stretching (or elongating) has the effect of lowering

pitch if tension is not increased dramatically, because longer strings have lower pitches.

The next problem is that pitch and loudness are not independent. In an easily playable musical instrument, we would like to increase loudness and keep pitch constant, or increase pitch and keep loudness constant. But our vocal folds are like a New Year's Eve noisemaker or a duck call; if we blow hard, the pitch rises. In speech, we have learned to accept that: as we raise our voice in loudness, we automatically raise our voice in pitch. But if a singer wants to sing a crescendo on a constant pitch, she has to make complicated adjustments in vocal fold tension to overcome the effect of greater blowing pressure.

The culprit in all of this is the amplitude-to-length ratio of the of the vocal cords (Figure 7). In stringed instruments, this is very small. A one-meter long string vibrates with about a one millimeter amplitude. In the voice, a one centimeter-long vocal fold also vibrates with a one-millimeter amplitude. In the voice, a one-centimeter long

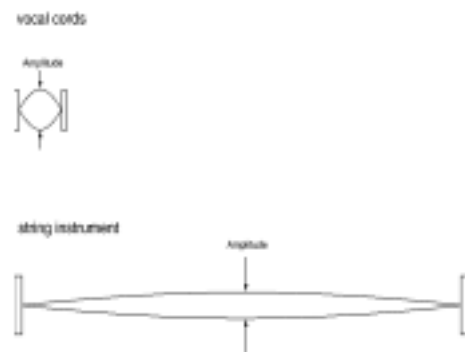


Figure 7

vocal fold also vibrates with a one-millimeter amplitude. This large amplitude-to-length ratio creates a lot of dynamic tension change in the vibrating system. And with dynamic tension nonlinearity, we have opened Pandora's chaos box. Chaos is always lurking in vocalization. Rather suddenly, a clean sound can turn into a dirty sound, with apparent randomness in vibration of the vocal folds.

We find the same dichotomy of rough and smooth vocalization among birds. Songbirds, like cardinals, produce periodic sounds, whereas crows and blue jays produce aperiodic sounds, which appear to result from chaotic vibrations. Also, birds do not have a larynx; they have a syrinx, which sits lower in the airways. Some birds have multiple folds they can vibrate.

Voluntary control of roughness is still poorly understood. Early indications are what vocalists detune the natural frequencies of coupled vocal folds that are otherwise



enhance vocal communication. They become the building blocks for speech. Others believe that the speech motor system is specially wired. Articulatory development, they would say, is part only of the human genetic code, independent of the limbic system, and unique to humans. If this is true, emotions may compete with speech for the use of the larynx and the lungs. When you bear emotional testimony and you “choke up”, your pitch sometimes rises in an uncontrollable fashion. A sob can block your respiration and phonation, and tears and extra mucus can cause you to misarticulate. That’s poor speech, but extraordinary vocal communication.

Another part of the nervous system that is deeply involved in vocalization is the spinal reflex system. Breathing, for example, requires no conscious voluntary action. Because the amount of air and carbon dioxide exchanged in the lungs must be regulated, there is an inherent feedback control between the lungs and the larynx. When we vocalize, the breathing rhythm is altered, and the reflex system may get in the way. Coughing is an example of a respiratory reflex.

The slightest touch on the vocal folds with a foreign object will elicit a cough reflex. But why don’t we cough when the vocal folds touch each other in collision? One theory is that the speech motor system must inhibit the reflex system (see the dashed line on Figure 10). If this is true, then some voice disorders may result from a malfunction of this inhibition of reflexes. The reflex system may be triggered too easily and the speech motor system gets tripped up by it. This may be the case in a symptom known as spasmodic dysphonia, where a person speaks with many interruptions and much tension.

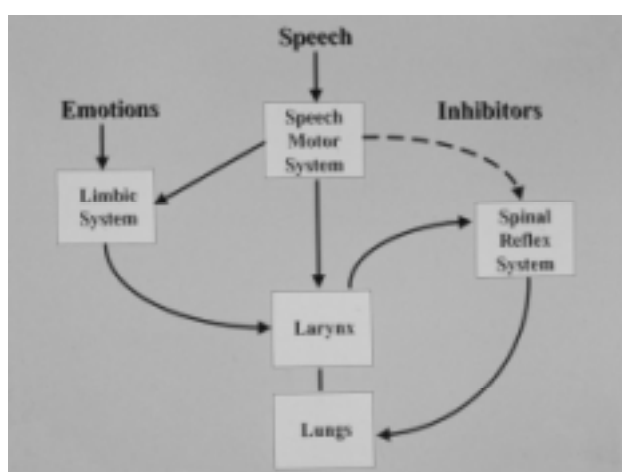


Figure 10

But, we have discovered that laryngeal reflexes also play a major role in producing vocal vibrato, trill, and trillo, three artistic ornaments in vocal music. These vocal tremors are like earth tremors, revealing much of what lies under the surface. Shakespeare wrote, “His voice was properties as all

the tuned spheres,” recognizing perhaps that if all the neural, aerodynamic, and acoustic systems are functioning in harmony like pulsating oscillators, human expression with our voice can be glorious.

## **WHY MUSIC DOES NOT PRODUCE BASIC EMOTIONS: PLEADING FOR A NEW APPROACH TO MEASURING THE EMOTIONAL EFFECTS OF MUSIC**

*Klaus R. Scherer*

Department of Psychology  
University of Geneva  
klaus.scherer@pse.unige.ch

### **ABSTRACT**

It is suggested that the study of emotional effects of music has been handicapped by two common misunderstandings: 1) the tendency to assume that "emotions" and "feelings" are synonyms, and 2) the tendency to assume that music evokes "basic" or "fundamental" emotions. As to 1), "feelings" can be profitably conceptualized as *one component of emotion*, albeit a very important one. The feeling component integrates all components of emotion and serves as the basis for the conscious representation of emotional processes and for affect regulation. As to 2), the notion of a limited number of basic or fundamental emotions is (correctly) based on the evolutionarily continuous adaptive function of emotion processes. However, in focusing on the small number of emotion classes that can be identified for a large number of different species, psychobiologists have downplayed the evolution of much more complex forms of emotional processes in humans, including specific affective feeling states produced by music. The use of a simple dimensional approach, using valence and activation judgments, or eclectic approaches to affect assessment, in the place of basic emotions, is also fraught with problems. It is proposed that a radical paradigm change, including the development of new measurement methodology, is required to enable researchers to study the emotional effects of music appropriately. Concretely, it is suggested that affect produced by music should be studied as (more or less conscious) feelings that integrate cognitive, physiological, and behavioral effects, which may be accounted for by widely different production rules. To select the verbal labels to be used in empirical research, music listeners' intuitions about which terms are best suited to describe their feelings are currently examined.

### **1. INTRODUCTION**

The notion that music expresses emotion has a venerable history and its validity is rarely debated. There is less agreement on *how* music expresses such affective content and exactly what emotions are most likely to be expressed. The related notion that music induces or produces emotions in listeners also has a venerable history but still generates frequent debates about its validity. The extensive literature on these two notions does not need reviewing here; the recent volume on "Music and Emotion" edited by Patrick Juslin and John Sloboda [1] provides an exhaustive collection of theory and research in this domain.

Rather, this contribution will inquire into the meaning of the term emotion in this context. Based on current psychological models of emotion, I will review the different kinds of affective phenomena and their characteristics and examine the likelihood that they will be expressed and/or produced by music. Apart from its obvious theoretical significance (as regularly debated by philosophers), this issue has direct relevance for the methodology in this area of research, particularly with respect to the affect categories or scales used to obtain listener judgments on the affect that is expressed or produced by musical stimuli.

One can distinguish three major schools of thought in this respect, the basic emotion, the emotional dimension, and the eclectic approach. The former two are more or less firmly rooted in established theories of emotion – discrete emotion theory and dimensional theory. Discrete emotion theory advocates the measurement of a small number of basic or fundamental emotions, such as anger, fear, joy, and sadness, whereas dimensional theories suggest ratings of valence (positive-negative) and activation (aroused-calm) experiences. The eclectic approach consists in choosing verbal labels that seem appropriate to the aims of a particular study, choosing terms from the rich affect vocabulary that seems particularly appropriate to the pieces of music used in a particular study (such as nostalgic, triumphant, or exhilarating). This diversity in the ways in which musical expressiveness or affective reactions to music are measured makes it very difficult to compare findings from studies using a different theoretical approach and different conceptualizations and measures of the affective phenomena under investigation. Apart from this difficulty, which impedes a systematic accumulation of knowledge, one may also ask which of the three theoretical approaches is best suited to examine the emotional effects of music on listeners. In this contribution I argue against the use of the two first approaches in music research and advocate a paradigm shift in the direction of making the eclectic approach more systematic by providing a theoretical basis for differentiating emotion and feeling and by developing instruments that are based on empirical research.

Before embarking on this task, I will attempt to clarify a major source of confusion in the field – the relationship between emotion and feeling. The fact that individuals can verbally report a multitude of qualitatively different feelings, as encoded in a rich emotion vocabulary, constitutes the most important facet of emotional episodes for many scholars in the field of emotion. These internal sensations, often considered as necessarily conscious experiences, are often called *qualia*, irreducible

qualities of feeling that are unique to the specific emotional experience of a particular individual. By adopting a component process approach to emotion [2, 3], the feeling component can be conceptualized as a reflection of all changes in components during an emotion episode, i.e., the results of event appraisal, motivational change, and proprioceptive feedback from motor expression and physiological reactions. It is important to differentially define the concepts in this fashion as the tendency to use emotion (the process as a whole) and feeling (one of its components) as synonyms results in confusion.

If we want examine whether music produces *emotions*, in the sense of the construct defined above, we need to measure all components, something that has not been attempted so far. Furthermore, if one subscribes to the notion that the changes in the components are highly synchronized during an emotion episode when they are coupled in the interest of optimal adaptation to the eliciting circumstances, the degree of coupling would need to be examined. Again, this has, to my knowledge, not been attempted so far. The large majority of studies on the emotional effects of music have requested verbal report of the consciously experienced emotion, in other words, the *subjective feeling* component, although there are a few studies on physiological patterns and action tendencies [4].

It is important to realize that measuring *feeling*, the subjective experience of an emotion episode, requires a different approach from measuring *emotion*, the synchronized pattern of responses in different organismic subsystems. This important distinction was already advocated by Wilhelm Wundt, one of the pioneers of experimental emotion research in the last century.

## **2. ARGUMENT**

### **2.1. Basic emotions: The issue of specificity**

Asking listeners to indicate to which extent a piece of music evokes emotions like joy, sadness, anger, fear, and similar basic emotions, presumes that the affective state produced by the music is comparable to similar emotions experienced in "real life", in the normal course of a person's activity, outside of a music-listening context. To evaluate this assumption, one needs to keep the nature and functions of such basic or fundamental emotions in mind.

The theorists in the discrete emotion model tradition suggest that during the course of evolution, a number of major adaptive emotional strategies have developed. These are seen to consist of a limited number, generally between 7 and 14, of basic or fundamental emotions with specific eliciting conditions and specific physiological, expressive, and behavioral reaction patterns. Thus, Plutchik [5] has proposed a set of basic emotions based on fundamental, phylogenetically continuous classes of motivation as identified by ethological research.

Many of the discrete emotion models are derived from Darwin [6] who illustrated the functionality, the evolutionary history, and the universality across species, ontogenetic states, and different cultures of some major emotions as labeled in the English language. Tomkins [7] extended Darwin's theorizing to argue that a number of basic or fundamental emotions could be conceived of as phylogenetically stable *neuro-motor programs*. While Tomkins did not describe the nature of these programs in detail, the assumption was that specific eliciting conditions

would automatically trigger a pattern of reactions ranging from peripheral physiological responses to muscular innervation, particularly in the face. Ekman [8] and Izard [9] extended the theory and attempted to obtain pertinent empirical evidence. Given the limited number of such basic or discrete emotions, theorists in this tradition assume a mechanism of emotion mixing or blending to explain the large variety of emotional states that are distinguished in the language. On the whole, the major theorists in this area have focused mostly on the prototypical reaction patterns (in particular facial expression and physiological responses) that are considered to be characteristic for a particular basic emotion. There has been much less concern with the elicitation and differentiation of the respective emotion, generally thought to be determined by eliciting situations that are again considered to be characteristic for the respective emotion (such as death of a close person in the case of sadness or encountering a severe threat for life or well-being in the case of fear).

There are a number of aspects of discrete emotion theory that make it seem suboptimal to describe the emotional effects of music. First, the small number of primary basic emotions seems ill adapted to describe the extraordinary richness of the emotional effects of music reported in both fictional and scientific accounts. A restriction of this extraordinary gamut of potential experiences to 7-14 states constitutes a serious impoverishment and a lack of resolution in the measurement instrument with respect to the phenomenon to be assessed. This is particularly true since emotion blends, as postulated by some theorists in this domain, are virtually never studied in discrete-emotion-based research on the emotional effects of music. Second, according to discrete emotion theory, the elicitation of the basic emotions is due to prototypical situations such as loss, threat, etc. While there is no doubt that in all cultures music often accompanies socially significant events that generate strong emotions, the latter are generally elicited by the nature of the event rather than the music itself. Listening to music for pleasure, one of the prime achievements of human culture, can hardly be considered to be comparable to such typical emotion-eliciting events and situations, many of which are considered to reflect similar motivational states across species. In addition, music appreciation in itself cannot account for the extraordinary differentiation of emotional effects. Third, listening to music is unlikely to evoke a limited number of neuro-motor programs resulting in highly emotion-specific facial expressions or physiological response patterns. In fact, except for facial expression portrayals by actors, such response specificity is rarely found in laboratory studies of emotional induction [10].

It would seem, then, that discrete emotion models are not the best theoretical basis to study emotional effects of music nor do they provide categories and measurement instruments that are well suited to research in this area. Why is it, then, that the use of basic or fundamental emotion categories is so popular in studies on emotional effects of music? The work of Tomkins, Izard, and Ekman has been responsible for the renaissance of work on emotion in modern psychology which was first dominated by behaviorism and then by cognitivism. Therefore, much of present day emotion psychology is in one way or another strongly influenced by the assumption of discrete fundamental emotions. Obviously, this idea is strongly supported by the existence of verbal labels with very high frequency of

usage, such as anger, fear, sadness, and joy, which serve to describe overarching concepts or prototypes.

Many researchers using a list of so-called fundamental emotions in their research may be convinced that this list provides comprehensive and representative coverage of the emotion domain. Given the disagreement as to the number and identity of "basic" emotions [11], this is a vain hope, especially since most theorists do not provide credible criteria for including certain emotions in their list. One exception is the list of defining criteria suggested by Ekman [8], who requires, among other things, that a basic emotion must be very brief (2-3 minutes) and be characterized by a specific, interculturally stable facial expression pattern. It is unlikely that these criteria are optimally suited to describe music-induced affect. Finally, researchers who like to describe their favorite list of basic emotions as the "Big Six" (with the set of six varying over researchers) seem to draw a parallel to the "Big Five" in personality measurement. This constitutes a serious category error, given the major differences in the nature of the underlying domain and in the measurement operations used, as well as the absence of evidence for a single robust six-factorial structure of emotion terms.

## **2.2. Valence and activation: The issue of discrimination**

Wundt suggested to distinguish between three dimensions of feelings -- pleasantness-unpleasantness, rest-activation, and tension-relaxation. This three-dimensional model has had a strong impact on the psychology of affect and emotion. Since the third dimension has been difficult to establish reliably in an empirical fashion via factor analyses, feeling is often defined in terms of a two-dimensional space formed by valence and activation. Such two-dimensional models have some appeal in that they allow illustrating similarities between different feelings in terms of neighborhood in space [12].

The use of two-dimensional valence-activation models has become very widespread in the affective sciences and is well represented in research on emotional effects of music. This approach has some obvious advantages. It is simple, easily understood by participants in experiments, and highly reliable. In addition, the valence dimension maps directly into the classic approach-avoidance action tendencies that have direct relevance for behavior. Unfortunately, there are also some disadvantages.

First, specifying the quality of a feeling only in terms of valence and activation does not allow a very high degree of differentiation -- qualitatively rather different states can be close neighbors in valence-activation space (e.g., panic fear and hot anger). This is particularly important in research on music, where one may expect a somewhat reduced range of both the unpleasantness and the activation of the states produced by music. In consequence, adopting a valence by activation approach, asking listeners to rate their state on these two dimensions, may not allow a very fine-grained separation of the emotional effects of different pieces of music.

Second, a valence by activation approach is entirely descriptive in nature, focusing exclusively on a fairly undifferentiated end result of the entire process. It does not encourage the development of theoretical predictions as to the mechanism underlying the affective functions of music.

## **2.3. Wanted: A scale for music-generated affective feeling**

The discussion so far suggests that the two most popular approaches to studying emotional effects of music, asking listeners to choose between basic emotion labels or rating feeling states on positive-negative/active-passive dimensions are not optimally suited for the task. While music making and listening to music certainly have a strong evolutionary basis, and music often plays a major part in social situations that provoke strong emotions, it is unlikely that listening to pieces of music in the concert hall or from CD, will provoke powerful basic emotions like anger, fear, disgust, or desperation. Since the emotional effects of music are generally studied in this kind of listening situation, a more adequate conceptualization and measurement approach is required. Valence-activation systems cannot fill the void, given their low degree of resolution and differentiation as well as the complete absence of explanatory frameworks helping to identify the underlying mechanisms. Unfortunately, the third approach regularly encountered in this research area, the use of eclectic scales containing verbal affect labels deemed pertinent by a particular researcher for a particular study, does not provide a desirable alternative. There is no guarantee that the labels chosen can be reliably judged, that they cover affective phenomena likely to be produced by music, or that they are organized in an economical, non-redundant manner. Most importantly, they render the comparison of data from different studies or a systematic accumulation of findings impossible.

Therefore, the field needs the development of a judgmental rating scale for emotional feeling states that is uniquely adapted to the needs of music research. It should be developed in a principled rather than an eclectic manner and it should be thoroughly pretested for its psychometric properties. The Geneva Emotion Research Group, in a project directed by Prof. Marcel Zentner, has embarked upon the development of such a scale. This development is essentially driven by an effort to discover which verbal affect labels listeners find most appropriate to label the affect state produced by the listening to widely different pieces of music. Starting with a pool of over 500 terms, we are in the process of progressively reducing the eligible expressions to a smaller number to obtain a representative set of a realistic size that can be expressed in about 8-10 factors. In the process, we are examining potential differences in the appropriateness of terms depending on whether the listener has to describe the character of the music, i.e., what is expressed by the music, or the nature of the affective change in feeling that has been produced by the music. We conduct studies in the laboratory, in homes, and at the occasion of public concerts, studying jazz, rock, and pop in addition to classical music. While the examination of the psychometric qualities of such a new scale is relatively straightforward, its validation is more of a problem. Currently we define two major criteria, 1) the agreement between different listeners to characterize similar pieces with similar scale items, 2) the ability of the scale items to discriminate different pieces of music in multidimensional space (defined by the fit of higher-order dimensional or cluster analyses and the relative distance of the musical pieces from the cluster centers). We will soon propose such a new scale, constructed according to clearly specified principles, to the research community. If we could convince our colleagues of the utility of such a scale and if it were to be widely adopted, two

major objectives could be achieved: 1) the comparison of results over studies and a systematic accumulation of findings, and 2) the measurement of emotional feeling dimensions that are uniquely adapted to the effects of music.

In the discussion above, the established conceptual and methodological approaches in this area, basic emotion and dimensional theories, have been found wanting with respect to their ability to help identify and assess the mechanisms that might underlie emotional effects of music. Given that the scale currently constructed in Geneva is based on principled, but strictly empirical criteria, one may wonder to what extent it can inform the search for mechanisms.

While we are not sufficiently advanced in the development of the new instrument for a final assessment, I can suggest some preliminary observations.

First, the restricted set of affect labels that survives our rigorous selection procedure includes many different types of affect descriptions. Many of these echo the fact that, as theoretically argued above, feeling states can be considered as reflecting the changes in all components of an emotion episode by making reference to cognitive (e.g., nostalgic), physiological (e.g., tense), or motivational, action-related (e.g., feeling like wanting to dance) components. This can be explained by the fact that the basis for the verbal labeling of emotional states consists of the changes in conscious subjective feeling states. While this feeling component may reflect the changes characterizing an emotion process in all of the organismic subsystems, verbal labels often represent only a salient part of those changes, those that reach awareness [3]. In many cases this process of becoming aware of a change and labeling it may be restricted or give prominence to individual emotion components. For example, the term "tense" which is frequently used as an affect descriptor seems to refer almost exclusively to a special tonic state of the somatic nervous system, the striated musculature.

Second, many of the expressions are reminiscent of the potential mechanisms underlying affect induction through music that we have called *production rules* [4]. We suggested that music can induce emotion via a central route including appraisal, memory associations, or empathy, and via a peripheral route, for example via proprioceptive feedback. Thus, some of the expressions in our final list of candidates (e.g., filled with wonder or feeling transcended) suggest new criteria for appraisal, especially with respect to the appraisal of intrinsic esthetic qualities and of levels of reality. Others (like nostalgic or affectionate) suggest memory associations to places or relationships. Still others (such as comforted) may be linked to processes of empathy. The peripheral route consists of mechanisms which are based on motor induction of peripheral arousal (e.g., sympathetic changes via rhythm or action tendency induction) and a change of feeling state due to consequent proprioceptive feedback. Terms like "feeling like dancing", feeling energetic or strong but also calm suggest this type of mechanism.

### 3. CONCLUSION

Using the criterion of what listeners find most appropriate as labels to describe emotional effects of music listening may provide more promising leads for the inquiry into the underlying mechanisms than established basic emotion lists or valence-

activation dimensions. In consequence, measurement instruments constructed on this basis to fit the conceptual, theoretical, and methodological needs in this research area would be most welcome.

### 4. REFERENCES

- [1] P. N. Juslin and J. A. Sloboda, "Music and emotion: Theory and research,".: London, Oxford University Press. (2001).
- [2] K. R. Scherer, "On the nature and function of emotion: A component process approach," in *Approaches to emotion*, K. R. Scherer and P. Ekman, Eds. Hillsdale, N.J.: Erlbaum, 1984, pp. 293-318.
- [3] K. R. Scherer, "Appraisal considered as a process of multilevel sequential checking," in *Scherer, Klaus R. (Ed); Schorr, Angela (Ed); et al. (2001). Appraisal processes in emotion: Theory, methods, research. Series in affective science. (pp. 92 120). London, Oxford University Press.*
- [4] K. R. Scherer and M. R. Zentner, "Emotional effects of music: Production rules," in *Juslin, Patrik N. (Ed); Sloboda, John A. (Ed). (2001). Music and emotion: Theory and research. Series in affective science. (pp. 361 392). London, Oxford University Press.*
- [5] P. Plutchik, *Emotion: A psychobioevolutionary synthesis*. New York: Harper & Row, 1980.
- [6] C. Darwin, *The expression of emotions in man and animals*, 3rd. edition, P. Ekman (ed.). London: HarperCollins, 1997 ed. London: John Murray, 1872.
- [7] S. S. Tomkins, "Affect theory," in *Approaches to emotion*, K. R. Scherer and P. Ekman, Eds. Hillsdale, N.J.: Erlbaum, 1984, pp. 163-196.
- [8] P. Ekman, "An argument for basic emotions," *Cognition and Emotion*, vol. 6, pp. 169-200, 1992.
- [9] C. E. Izard, *The psychology of emotions*. New York, NY: Plenum Press, 1991.
- [10] G. Stemmler, M. Heldmann, C. A. Pauls, and T. Scherer, "Constraints for emotion specificity in fear and anger: The context counts," *Psychophysiology*, vol. 38, pp. 275-291, 2001.
- [11] A. Ortony and T. J. Turner, "What's basic about basic emotions?," *Psychological Review*, vol. 97, pp. 315-331, 1990.
- [12] L. F. Barrett and J. A. Russell, "The structure of current affect: Controversies and emerging consensus," *Current Directions in Psychological Science*, vol. 8, pp. 10-14, 1999.

# VIOLINS





## THE BOWED STRING AS WE UNDERSTAND IT TODAY

J. Woodhouse

Cambridge University Engineering Department  
Trumpington St, Cambridge CB2 1PZ, UK  
jw12@eng.cam.ac.uk

### ABSTRACT

The vibration of a bowed string has been studied since the 19th century, and today this problem is the only example of vibration excited by friction that can claim to be reasonably well understood. Theoretical models now embody many of the complicating features of real strings, instruments and bows, and detailed comparisons with experimental studies are allowing fine tuning of the models to take place. The models can be used to explore questions directly relevant to instrument makers and players. This paper will review the history of bowed-string research, and highlight recent developments and current issues. Probably the main unresolved question at present concerns an accurate description of the frictional behaviour of rosin, since recent results have shown that none of the friction models used in the existing literature is entirely credible.

### 1. INTRODUCTION

A musical instrument is a device for converting motor actions which we are capable of performing into sounds which we like to hear. For an instrument like the violin which has had a stable design for a long time, we may suppose that the best examples are close to an optimum on both counts. By taking advantage of motor actions up to the limits of what we are able to perform, a range of sounds can be produced which occupy regions of perceptual space where our discrimination is most acute. This double optimality makes musical acoustics a demanding discipline: one is frequently confronted with rather subtle physical effects which result in sounds which our auditory system happens to be able to process with great acuity.

Non-specialists usually imagine that the goal of violin research is to understand the *sound* of a Stradivarius. However, rather few people are able to tell an outstanding violin from a good one just by listening. Apart from anything else, a skilled player will compensate for many of the shortcomings of a lesser instrument so that the sounds may be quite similar. The player, though, will be well aware which is the preferred instrument, since he or she is inside the feedback loop governing the compensation process. Thus if one is trying to understand the musically-significant differences between instruments, the playing behaviour may be as important as the sound *per se*. “Playability” is a much better starting point for physical research than “sound”: we can construct theoretical models of a bowed string and ask questions which are of interest to instrument makers (“Will it be easier to play if I change this detail?”) and to players (“What is the best bowing gesture to achieve this effect?”).

The study of bowed-string motion began with Helmholtz [1], who first described the periodic vibration pattern of a string

when bowed “normally”. In this “Helmholtz motion”, at any given instant the displacement of the string consists of two straight sections, separated by a “corner” that shuttles back and forth along the length of the string at the frequency of the note being played. While the corner travels from the bow to the player’s finger and back the string is sticking to the bow-hair, and while it travels the shorter distance from bow to bridge and back the string is slipping rapidly along the hairs of the bow. The arrival of the corner at the bow triggers the transitions between these two states.

The player controls four quantities when bowing: the bow speed, the normal force between bow and string, the position of the bow on the string, and the degree to which the ribbon of bow-hair is tilted relative to the string. A consequence of the Helmholtz motion is that, to a first approximation, the steady vibratory motion of the string is the same, regardless of these details of bowing. The player’s ability to influence the sound quality of a note depends on three things. First, if the bowing parameters fall outside a certain range the Helmholtz motion is not possible at all, and something else (usually undesirable) happens. Second, within the range for which Helmholtz motion occurs, the fine details of the string motion *do* depend somewhat on the bowing parameters, enough for audible variations to be produced for musical effect. Third, our perception of sound quality is influenced by the length and detailed nature of the transients by which the note begins and ends, and different bowings produce different transients.

### 2. MODELS FOR BOWING

The most basic model of a bowed string must take account of transverse vibration of the string, and of the friction force from the bow applied to the string. Some energy dissipation must also be included, otherwise all possible periodic motions are unstable [2]. The earliest such model was studied by Raman early in the 20th century [3], but his model was a very special case which is now known to give unrealistic predictions [4]. A more sophisticated model of this type arose from the work of Cremer and Lazarus, reported in [5], and grew into an efficient algorithm for time-stepping simulation which was first presented in the 1970s [6]. This approach has since spawned a family of more complicated models based on the same principle. A number of features need to be considered in constructing a fully believable model, all of which have received research attention during recent years:

- Bending stiffness of the string, which makes successive string overtones progressively sharp compared to an ideal harmonic series [7,8];

- Torsional motion of the string, because the friction force from the bow is applied tangentially to the string's surface rather than through its centre [9];
  - Coupling of the string motion to modes of the instrument body, since this is the only route by which two instruments may differ in "playability" [6];
  - Dynamics of the bow and its hair, since it is well known that different bows affect both sound and playability on a given instrument [10];
  - Finite width of the contact region between bow-hair and string [11,12];
  - Correct modelling of the frictional characteristics of the rosin applied to the bow-hair [13];
  - Realistic bowing gestures, required as input patterns of bow speed and force for the simulation of string motion [14,15].
- Most of these can now be incorporated with some confidence into the theoretical models, although questions remain to be answered about many of them

It is straightforward in principle to simulate a particular transient and study its details, but this does not in itself reveal much about playing the violin. The more interesting questions generally involve asking how the string motion varies as some parameter is changed. Early examples of the use of theoretical models to study portions of the player's parameter space were Schelleng's analysis of the parameter combinations necessary in order that the Helmholtz motion of the string is possible [7], and Cremer's study of how the waveform of steady Helmholtz motion varies when the bow force is changed [5].

These studies represent first attempts to quantify what "playability" might mean. The simplest possibility concerns the range between maximum and minimum bow force for steady playing: perhaps an "easy to play" instrument, or particular note, has an unusually wide range. Schelleng's study was a response to this idea. Alternatively, perhaps "ease of playing" relates to the extent of variations between different notes or strings on a given instrument, because large differences require extensive player compensation, and thus produce a perception of difficulty [16]. However, when players comment on problems of playability they are usually referring to problems associated with *transients*. For example, a note may be "slow to start", or it may be "unreliable" because it tends to squeal during rapid passages, or it may be difficult to play very softly, and so on.

It is natural to investigate such questions by using computer simulations of bowed-string motion. We can perform many runs of the computer program, each simulating a slightly different bowing gesture, and see which ones produce a Helmholtz motion and which ones do not. For those which do, we can ask how long Helmholtz motion took to be established to assess "ease of speaking". By plotting the results in some chosen parameter plane, regions showing qualitatively different behaviour may be revealed.

Two examples are illustrated here. The first is a study of a family of bowing gestures in which the bow speed remains constant, while the force varies in time [17]. One parameter is the final value of the bow force, and the second is the ratio of initial bow force to asymptotic force: the force is allowed to start higher or lower than its asymptotic value, and then to approach it with an exponential transient. Simulation results

for a portion of the plane of these two parameters are shown in Fig. 1. Black pixels indicate runs which never reached Helmholtz motion, while others are shaded with a gray level indicating the length of transient before Helmholtz motion was established. It is clear that both parameters have a significant influence on behaviour.

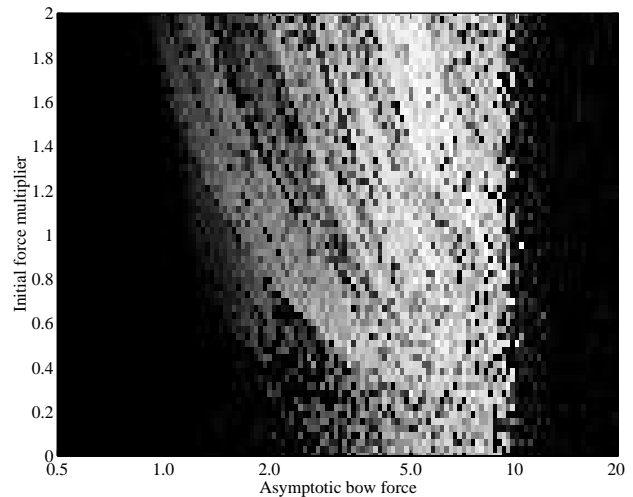


Figure 1: *Simulated transient lengths from [17]. Each pixel denotes a simulation, with a bowing gesture having constant bow speed. The bow force tends asymptotically towards the value on the x-axis, while the initial force has this value multiplied by the y-axis value. Black pixels show transients which did not produce Helmholtz motion. Others are grey-shaded to indicate the transient length, white being shortest.*

The second example is due to Guettler [18]. He pointed out that most of the bowing gestures simulated in Fig. 1 are not in practice possible. Either the bow speed or the bow force must start from zero: a human player cannot "switch on" force and speed instantaneously. Guettler therefore advocated a family of transients with steady force and varying speed, starting from zero with a constant acceleration. Figure 2 shows his results in the plane of bow force and acceleration. Again, the gray scale indicates the length of transient. The white wedge labelled 2 shows a region of "perfect starts", in which Helmholtz motion is established immediately from the first slip of the string. To the left, in region 1, progressively longer transients are seen in which the early behaviour is irregular (described as "creaky" sounds). To the right, in region 3, longer transients are seen with a different nature: whereas Helmholtz motion involves a single slip per cycle of the string against the bow, these transients begin with a spell with two or more slips per cycle. Alongside these computed results, Guettler also analysed the mechanisms determining the boundaries of the "white triangle", an important step towards understanding bowed-string transients.

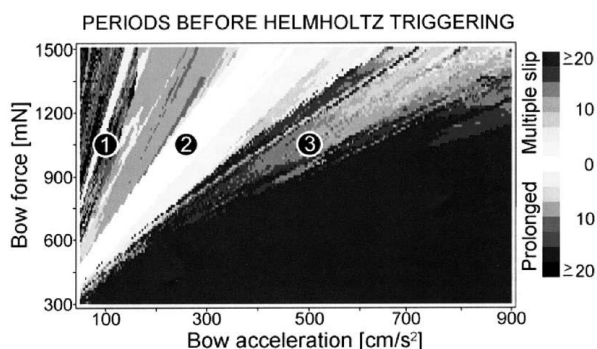


Figure 2: Simulated transient lengths from [18].

Each pixel denotes a simulation, with a bowing gesture having constant acceleration from rest with value given on the x-axis. The force is constant at the value given on the y-axis. Black pixels show transients which did not produce Helmholtz motion. Others are grey-shaded to indicate the transient length, white being shortest.

### 3. EXPERIMENTAL STUDIES

Alongside the development of computer models for simulating the bowed string, there have been experimental investigations into various aspects of the problem.

#### 3.1. Gestures

The first family of experimental studies concerns the bowing gestures employed by string players. First, Askenfelt used an instrumented bow to record the force, speed and bow-bridge distance in a variety of bowings [14,15]. This gives valuable input information to the computer models. A second study, by Guettler and Askenfelt [19], addressed the question raised by Figs 1 and 2: what length of transient is acceptable in musical practice? They looked at two types of data: the distribution of actual transient lengths when professional players were asked to play simple passages (without being told the purpose of the test), and the judgements of a panel of listeners on a range of single-note transients produced with a mechanical bowing machine. The first test revealed that the players were very good at their job. They achieved transients of less than 10 ms duration about 50% of the time, and virtually all transients within the acceptance limits revealed by the second test: “creaky” transients should be of less than 50 ms duration, while multiple-slipping transients were judged acceptable up to about 90 ms.

A different gestural study by Guettler and Askenfelt [20] examined two particular styles of bowing, spiccato and ricochet. They found that a particular phase relation was necessary between the translational and rotational bow motion to produce a perfect sequence of spiccato notes. They also obtained good confirmation of the results from computer simulation, an encouraging indication of the growing realism of these models. One might hope that more studies of this type will be undertaken, looking at the details of other bowing styles.

#### 3.2. Friction measurements

An entirely different set of recent experimental studies concerns the frictional behaviour of rosin, the material applied to bow hair to promote stick-slip friction. Until quite recently, all writers agreed on a theoretical model to describe the frictional behaviour of rosin. This traditional model is illustrated by the dashed line in Fig. 3: it shows the coefficient of friction varying as a function of the relative sliding speed between bow and string, with high friction at low speeds falling to much lower values with fast sliding. However, when a measurement was made of the frictional force during a stick-slip vibration, the results told a different story. As illustrated by the solid curve in Fig. 3, the friction force describes a hysteresis loop, no part of which follows the steady-sliding curve [21]. Similar measurements were subsequently made using a different method, involving a real bowed string, and these gave broadly similar results [22].

It is immediately clear that the friction force must depend on some variable other than sliding speed, and from a variety of evidence it has been suggested that this extra variable is temperature at the sliding interface. Theoretical models have been proposed based on this idea [13]. These show promise but they do not yet reproduce all the phenomena observed in experiments. It is already clear that the final model may have to be quite complicated: for example, micrographs of the track left in a rosin surface after stick-slip events show a range of behaviour from viscous flow during fast sliding to brittle fracture at the end of a fairly long interval of sticking [22].

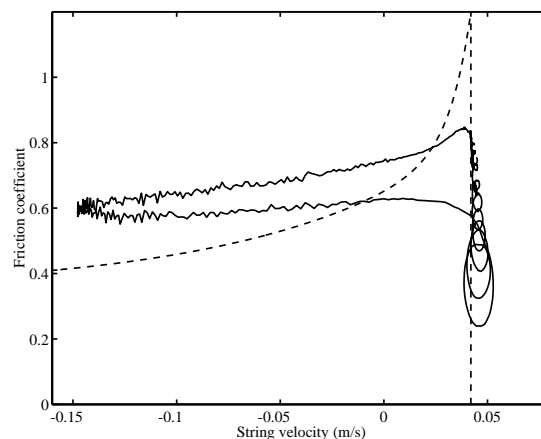


Figure 3: Friction models

Alternative friction models for rosin. The dashed line shows the traditional “friction curve model” in which friction coefficient is a function of sliding speed only. The plotted values were measured in a steady-sliding experiment [21]. The solid line shows the result of a measurement of the friction force and sliding speed during a stick-slip vibration, using the same rosin used to calibrate the dashed curve. The hysteresis loop is traversed in the anticlockwise direction. The loops during the sticking phase, towards the lower right, are an artefact of the measurement method [21].

### 3.3. Validation of simulation models

We have seen that theoretical models are being developed which embody many of the features of real violins and bows. These have the potential to be used to explore questions directly relevant to instrument makers and players, but it is first necessary to have confidence in the accuracy of predictions. This requires experimental work to test and calibrate the models. To perform experimental scans over a region of parameter space to be compared with Figures 1 and 2 goes beyond the abilities of a human player and requires an automatic bowing machine. Such a machine has been built and tested, and is producing results which are allowing the simulation models to be fine-tuned [23].

## 4. THE CHALLENGE

For some years now there has been a good qualitative understanding of the bowed string. The many regimes of periodic motion were studied by Raman [3] and various later workers (e.g. [24,25]). When the early simulation models were developed, several observed phenomena were shown to be predicted by these models. Three examples can be mentioned. First, the variation with bow force of the sharpness of the Helmholtz corner was one of the motivations for developing the model [5], and is well described by simulations. Second is the “wolf note” which arises, especially in the cello, when playing a note coinciding with a strong body resonance. The body motion cyclically takes energy out of the Helmholtz motion, forcing it to change to double-slipping motion, and then feeds it back in to produce Helmholtz motion again [6]. Third, an instability discovered mathematically by Friedlander [2] proved to have a physical origin, associated with subharmonics of the Helmholtz motion. In a real string these subharmonics are not unstable, but under some circumstances they are faintly audible.

The challenge for the subject now is to turn this qualitative understanding into something quantitatively accurate. Once the computer models can be trusted to predict more or less correct transient details under a wide range of bowing gestures, the task of exploring “design” questions by simulation can begin in earnest. Perhaps by SMAC2013 we will be able to design the “most playable” string, or rosin, or bow, or violin setup.

## 5. REFERENCES

- [1] Helmholtz, H.L.F., *On the sensations of tone*, Dover, New York, 1954 (reprint).
- [2] Friedlander, F.G., “On the oscillations of the bowed string”, *Proc. Cambridge Phil. Soc.* 49:516–530, 1953.
- [3] Raman, C.V., “On the mechanical theory of vibrations of bowed strings”, *Indian Assoc. Cult. Sci. Bull.* 15:1–158, 1918.
- [4] Woodhouse, J., “Idealised models of a bowed string”, *Acustica* 79:233–250, 1993.
- [5] Cremer, L., *The physics of the violin*, MIT Press, Cambridge MA, 1985.
- [6] McIntyre, M.E., Woodhouse, J., “On the fundamentals of bowed-string dynamics”, *Acustica* 43:93–108, 1979.
- [7] Schelleng, J.C., “The bowed string and the player”, *J. Acoust. Soc. Am.* 53:26–41, 1973.
- [8] Woodhouse, J., “On the playability of violins: Part 1”, *Acustica* 78:125–136, 1993.
- [9] Woodhouse, J., Loach, A.R., “The torsional behaviour of cello strings”, *Acustica/acta acustica* 85:734–740, 1999.
- [10] Schumacher, R.T., “Some aspects of the bow”, *Catgut Acoust. Soc. Newsletter* 24:5–8, 1975.
- [11] Pitteroff, R., Woodhouse, J., “Mechanics of the contact area between a violin bow and a string, Part II”, *Acustica/acta acustica* 84:744–757, 1998.
- [12] Pitteroff, R., Woodhouse, J., “Mechanics of the contact area between a violin bow and a string, Part III”, *Acustica/acta acustica* 84:929–946, 1998.
- [13] Woodhouse, J., “Bowed string simulation using a thermal friction model”, *Acustica/acta acustica* 89:355–368, 2003.
- [14] Askenfelt, A., “Measurement of bow motion and bow force in violin playing”, *J. Acoust. Soc. Am.* 80:1007–1015, 1986.
- [15] Askenfelt, A., “Measurements of the bowing parameters in violin playing: II bow-bridge distance, dynamic range and limits of bow force”, *J. Acoust. Soc. Am.* 86:503–516, 1989.
- [16] Woodhouse, J., “On the playability of violins: Part 2”, *Acustica* 78:137–153, 1993.
- [17] Schumacher, R.T., Woodhouse, J., “Computer modelling of violin playing”, *Contemp. Phys.* 36:79–92, 1995.
- [18] Guettler, K., “On the creation of the Helmholtz motion in bowed strings”, *Acustica/acta acustica* 88:970–985, 2002.
- [19] Guettler, K., Askenfelt, A., “Acceptance limits for the duration of pre-Helmholtz transients in bowed-string attacks”, *J. Acoust. Soc. Am.* 101:2903–2913, 1997.
- [20] Guettler, K., Askenfelt, A., “On the kinematics of spiccato and ricochet bowing”, *J. Catgut Acoust. Soc.* 3(6):9–15, 1998.
- [21] Smith, J.H., Woodhouse, J., “The tribology of rosin”, *J. Mech. Phys. Solids* 48:1633–1681, 2000.
- [22] Woodhouse, J., Schumacher, R.T., Garoff, S., “Reconstruction of bowing point friction force in a bowed string”, *J. Acoust. Soc. Am.* 108:357–368, 2000.
- [23] Galluzzo, P.M., Woodhouse, J. “Experiments with an automatic bowing machine”, elsewhere in this volume.
- [24] Lawergren, B., “Harmonics of S-motion on bowed strings”, *J. Acoust. Soc. Am.* 73:2174:2179, 1983.
- [25] Kubota, H., “Kinematical study of the bowed string”, *J. Acoust. Soc. Japan* 43:301:310, 1987.

## GENERALIZED NORMAL MODE VIOLIN ACOUSTICS

George Bissinger

Physics Department  
East Carolina University  
bissinger@mail.ecu.edu

### ABSTRACT

A constantly growing violin normal mode database presents significant opportunities to relate specific modal properties such as the 1<sup>st</sup> corpus bending mode frequencies to violin quality. Perhaps more interesting however is the prospect of extracting *general* aspects of violin sound related to quality classes such as “good” or “bad”. Frequency-related trends for various measured properties, viz., total damping, radiation efficiency and damping, and internal damping, are of fundamental interest because of their connection to the vibratory energy expenditure of the violin. For example, (aggregate) violin internal damping obtained by subtracting radiation damping from total damping was surprisingly insensitive to violin quality, while the parent dampings were not. Because damping trendlines for each energy loss path are independent of excitation particulars, they provide insights into the spectral balance of radiation from the violin while sidestepping the role of the intermediate bridge-corpus energy transfer, i.e., a “bridge-less” violin. Computing the fraction-of-vibrational-energy-radiated from the radiation-total damping ratio up to 8 kHz reveals a mechanism related to the critical frequency for a “good” violin radiating more in the 3 kHz region relative to a “bad” violin. Finally some aspects of f-hole vs. structure radiation to the far-field will be presented.

### 1. INTRODUCTION

The violin enjoys few scientific simplicities. Among these are the transmutation of the complicated, non-linear stick-slip, bow hair-string interaction into approximately a sawtooth driving force, with a harmonic strength falling as  $1/n$ ,  $n = 1, 2, 3, \dots$ . Another is the violin itself being a linear system, hence its dynamics are describable as a sum of individual normal modes dynamics. And finally the underlying regularity in normal mode radiation efficiency  $R_{\text{eff}}$  trends from low to high frequencies [1]. A non-scientific simplicity is the “good-bad” violin quality rating by excellent violinists.

Part of the VIOCADEAS Project is the normal-mode databasing of violins of varying quality [2]. Each violin can be parameterized by at least 20 different normal-mode-based quantities, some particular to an individual mode, some averaged over a band, some based on trendlines through the data. Typically, searching through “signature” mode (cavity modes A0 and A1, CBR the mode with the shear-like plate motion in the C-bout region [3], 1<sup>st</sup> corpus bending modes B1<sup>-</sup> and B1<sup>+</sup>) frequencies and dampings for quality dependent trends is the aspect most people would consider most important, but another less obvious perhaps but equally important aspect is tracing the energy flow out of the violin via damping.

### 2. THE “VIOLIN EQUATION”

For this undertaking it is instructive to write a simplified equation for the energy flow through the violin that captures the influence of major paths, from the string, through the bridge to the acoustic field (without mode summation and phases) [4],

$$I(\omega) \propto F(\omega)^2 \cdot \langle Y(\omega_i)^2 \rangle \cdot R_{\text{eff}}^i \quad (1)$$

On the left hand side, the acoustic intensity  $I(\omega) \propto p^2$  ( $p$  = pressure). On the right hand side the 1<sup>st</sup> term is the energy input to the bridge (typically via a ~sawtooth forcing function). The 2<sup>nd</sup> term is the mean-squared over-the-corpus (top+back+ribs) mobility ( $Y$  = velocity/force) transfer function that is a measure of how effectively the energy input at the bridge is transferred to each corpus normal mode. The 3<sup>rd</sup> term is the radiation efficiency, a normal mode parameter that “intermediates” the conversion of corpus vibrational energy into acoustic energy (averaged over a sphere). The separation of the energy path into two sequential, independent parts implies that the acoustic energy output is the product of these. The violin equation underscores a fundamental inability to work backwards from the sound of the violin to the mechanical construction. That is, given  $I(\omega)$  how do we determine  $Y(\omega)$  (or  $R_{\text{eff}}$  for that matter) separately?

$R_{\text{eff}}$  is a dimensionless quantity that relates the radiation for each normal mode relative to a baffled piston of the same area and same mean-squared velocity. It is computed mode-by-mode from [1]

$$R_{\text{eff}} = \frac{1}{\rho_o^2 c^2} \cdot \frac{A}{S} \cdot \frac{\langle p^2 \rangle}{\langle v^2 \rangle} \quad (2)$$

where  $\rho_o$  is the density of air,  $c$  the speed of sound,  $A$  the area of the measurement microphone sphere ( $18.1 \text{ m}^2$ ),  $S$  the surface area of the corpus ( $\approx .13 \text{ m}^2$ ), and  $\langle p^2 \rangle$  and  $\langle v^2 \rangle$  are the mean-squared pressures/velocities over the microphone sphere/corpus. (Our radiativities (pressure/force) and mobilities, measured simultaneously, were substituted for  $\langle p^2 \rangle$  and  $\langle v^2 \rangle$  in the ratio.) Typically  $R_{\text{eff}}$  is always low when the sound wavelength is  $\gg$  dimensions of the source, and reaches a “plateau” value of 1 for structures when the bending wave velocity in the structure makes the transition from subsonic to supersonic at the critical frequency.

Neglecting the energy input to the violin (1<sup>st</sup> 2 terms in eq. (1), energy loss paths are parameterized straightforwardly by the various damping categories for the violin.

### 3. DAMPING

#### 3.1 Total damping

The total damping measured for the violin,  $\zeta_{\text{tot}}$ , includes the true internal (heat) losses as well as losses to acoustic radiation and to the support fixture and any additional damping whose purpose is to suppress certain substructure vibrations, e.g., the strings. The support fixture for the violin in the anechoic chamber was purposely designed to have very low damping ( $\leq 5\%$  of total damping) [5]. No string damping was used, and chin and shoulder rests were removed. Consequently energy loss paths other than internal and acoustic radiation can be neglected. The total damping (in percent of critical damping - %crit) for each mode is derived from a "global" (average-over-the-violin) fit to the mobilities. These values can vary widely from mode to mode but always show an overall drop-off trend as frequency increases.

A scatter plot of  $\zeta_{\text{tot}}$  for over 400 modes up to 4 kHz is shown in Figure 1. The plot has been specifically chosen to be a log-log plot. If the data fall off linearly on a log-log plot then the parametric dependence is power-law, i.e.,  $\zeta_{\text{tot}} = C f^x$ . Even with the data spray seen in Figure 1 a linear trend is observable. While most of the mode dampings shown are for the corpus modes, a few substructure (neck-fingerboard, tailpiece, bridge – but not strings) modes have been left in the data array to show their lower damping values (hatched areas). Also shown in Figure 1 are modal averages over 250 Hz bands. These averages band both simplify the data analysis and provide via a standard deviation computation a simple numerical measure of the range of damping values. Note that this standard deviation is *not* an experimental error for the total damping or radiation efficiency measurements, both of which are about  $\pm 10\%$ .

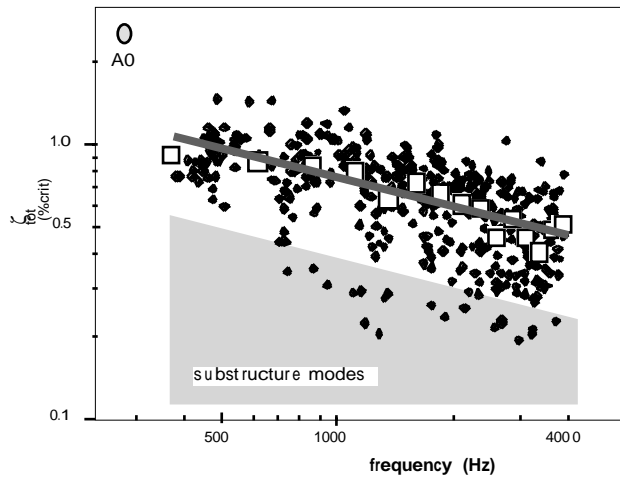


Figure 1: Total damping (%crit) collected for 9 violins up to 4 kHz. Hatched region highlights substructure mode region. Boxes show 250-Hz-band-averages, trendline power-law fit to band-averaged points. A0 result (averaged) shown as oval disk ( $f$  and  $\zeta_{\text{tot}}$  standard deviations represented by disk spreads).

This violin damping fall-off behavior contrasts sharply with the measured damping trends for the isolated top and back plate substructures. Measurements of total damping trends for 10 top and back plates, with and without varnish, show almost no change with frequency, being almost constant up to 4 kHz. This is consistent with measurements for individual strips, or other very simple geometry samples.

Power law fits to all violins gave  $x = -0.34 \pm 0.05$ . Separating the violins into two quality groups – the 3 best (= "good") and 3 worst (= "bad") – only, gave  $x = -0.29 \pm 0.05$  for the "good", and  $x = -0.45 \pm 0.05$  for the "bad", a significant difference. However it is not clear where this difference originates, i.e., is the internal damping higher for good violins or bad? Or is the radiation damping higher? Or both?

#### 3.2 Radiation damping

The radiation damping was measured independently of the total damping using a microphone array to sweep over a sphere around the violin to capture the acoustic energy emissions. The radiation efficiency  $R_{\text{eff}}$  has an additional, fundamental importance here: it is needed to compute the radiation damping  $\zeta_{\text{rad}}$  (%crit) for each mode of a structure, using the equation [1]

$$\zeta_{\text{rad}} = 50 \cdot \frac{\rho_o c}{2\pi} \cdot \frac{S}{M} \cdot \frac{R_{\text{eff}}}{f} \quad (3)$$

where  $M$  is the mass of the violin, nominally 0.43 kg, and  $f$  is the mode frequency. ( $\zeta_{\text{rad}}$  (%crit) =  $50/Q$ ). The inverse dependence on violin mass (not expected for internal damping) is important because – all other things being equal (although being wood, they never are) – the lighter the violin the more it radiates, over all frequencies; this is even more interesting trend-wise.

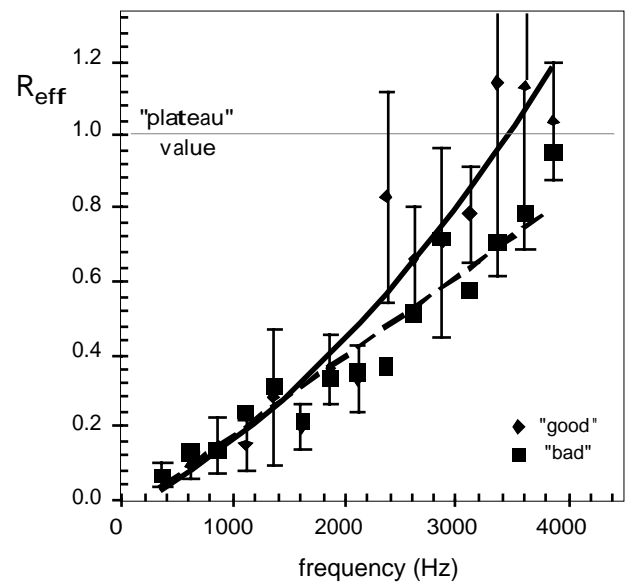


Figure 2: Modal average radiation efficiency for "good" and "bad" violins, with trendlines. (range standard deviation for "good" only)

Experimental 250-Hz-band averaged  $R_{\text{eff}}$  values for “good” and “bad” violins are shown in Figure 2. The more rapid rise for the “good” violins is apparent. The trendlines shown are  $\leq 2^{\text{nd}}$  order polynomial fits – where the minimum order with equivalent  $r$ -correlation coefficient was always chosen. These trendlines for  $R_{\text{eff}}$  can also be used in eq. (3) to compute  $\zeta_{\text{rad}}$  trendlines. With  $\zeta_{\text{rad}}$  and  $\zeta_{\text{tot}}$  it is possible to compute both the internal damping of the violin, or the fraction-of-vibrational-energy-radiated  $F_{\text{RAD}}$ , mode-by-mode or with trendlines. General behaviors of  $R_{\text{eff}}$  and  $\zeta_{\text{rad}}$  with frequency are shown in Figure 3.

$R_{\text{eff}}$  trendlines also provide an important additional benefit: a way to estimate the critical frequency for “good” and “bad” violins by solving the trendline equation for  $R_{\text{eff}} = 1$ . This procedure provides critical frequency estimates of  $\sim 3.4$  kHz for the “good” and  $\sim 4.8$  kHz for the “bad” violins. Our generalized normal-mode acoustics approach then “attaches” the  $R_{\text{eff}} = 1$  plateau at the “knee”. As Figure 3 shows the  $\zeta_{\text{rad}}$  trendline then undergoes a fundamental change at the critical frequency/ $R_{\text{eff}}$  “knee” region: the onset of the  $1/f$  falloff and consequently a peak appears in  $\zeta_{\text{rad}}$ . A “good-bad” critical frequency *shift* also implies a change in the spectral balance of sound between violin quality classes.

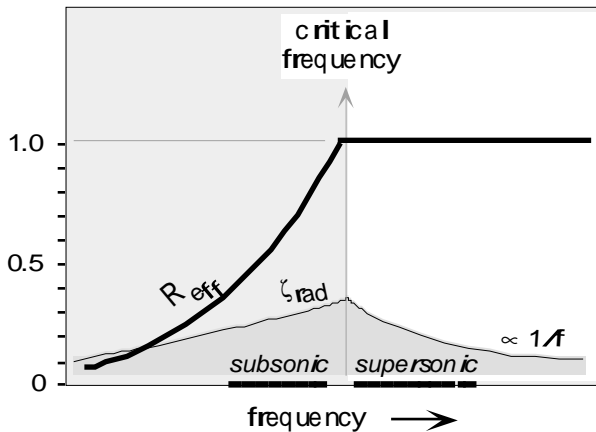


Figure 3: Generalized radiation efficiency (dimensionless - solid curve) and radiation damping (%crit - shaded curve) trends with frequency (realistic values - both parameters)

### 3.3 Internal damping

“True” internal damping is a “new” quantity for the violin due to the fact that the measured (= sum of all energy loss paths, i.e., total) damping for a violin must have radiation damping subtracted to extract it. With our  $\zeta_{\text{rad}}$  and  $\zeta_{\text{tot}}$  results it is straightforward to compute an aggregate internal damping [6],

$$\zeta_{\text{int}} \approx \zeta_{\text{tot}} - \zeta_{\text{rad}} \quad (4)$$

The internal damping computed from eq. (4) is shown in Figure 4 for the band-averaged dampings. Each data point has an “error” bar derived from the standard deviations computed to represent *ranges* of total and radiation damping. (Note that

the total damping and radiation damping have estimated *experimental* errors of  $\pm 10\%$  for each mode, so errors computed for the damping **difference** will also appear relatively large.)

The power law behavior observed in Figure 1 has been extended to the internal damping both because it is a reasonable parameterization of the experimental data and because it is well behaved outside the fit region. This provides a reasonable basis to extrapolate up to 8 kHz to cover the important acoustic range of the violin. The power law fits for the “good” and “bad” violin are superimposed on 250-Hz-band modal average results. Given the large “errors” expected in the internal damping calculation it is clear that there is no obvious difference between the “good” and “bad” violin internal dampings.

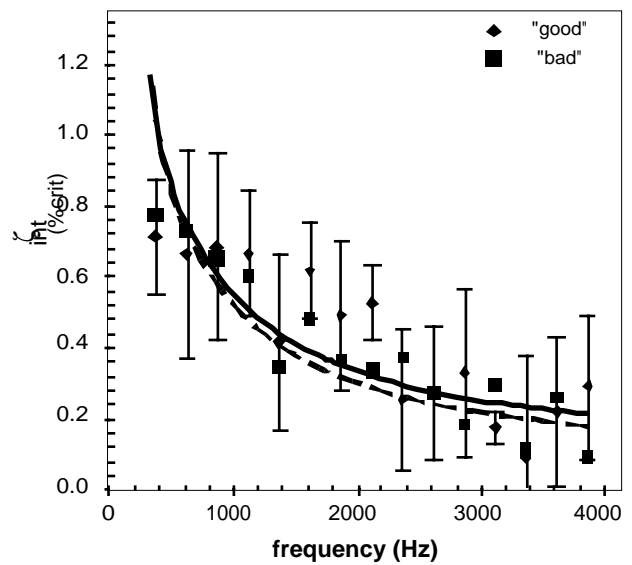


Figure 4: Internal damping for “good” and “bad” violins from total and radiation damping differences (range standard deviation for “good” only); power law trendlines (solid “good”, dashed “bad”).

### 4. $F_{\text{RAD}}$

The fraction-of-vibrational-energy-radiated  $F_{\text{RAD}}$  is computed simply from our damping results as

$$F_{\text{RAD}} = \frac{\zeta_{\text{rad}}}{\zeta_{\text{tot}}} \quad (5)$$

Values of  $F_{\text{RAD}}$  were computed from experimental  $\zeta_{\text{tot}}$  and  $\zeta_{\text{rad}}$  250-Hz-band averages using eq. (5) and are shown in Figure 5 for “good” and “bad” violins. The results are surprisingly close, indicating that “bad” violins pretty much radiate just as effectively as “good” ones. (Reminder – no consideration of how effectively input energy is transferred from the strings to the violin body is in the damping analysis.) It might seem that  $F_{\text{RAD}}$  should be substantially different between the two since



$\zeta_{\text{rad}}$  is ~50% larger for the “good” violins near the critical frequency. However by rewriting the equation for  $F_{\text{RAD}}$

$$F_{\text{RAD}} = \frac{1}{1 + \frac{\zeta_{\text{int}}}{\zeta_{\text{rad}}}} \quad (6)$$

If we discuss  $F_{\text{RAD}}$  behavior using eq. (6) in the modal average sense in each band, it is clear that the ratio of internal to radiation damping is what governs the behavior of  $F_{\text{RAD}}$ . Since  $\zeta_{\text{int}}$  is the same for each mode - “good” or “bad” in a band - and it dominates the total damping up to ~2 kHz, while the radiation dampings are also very similar below 2 kHz and slowly increasing,  $F_{\text{RAD}}$  will be very similar below 2 kHz, starting small and slowly increasing. In the  $R_{\text{eff}}$  plateau region ( $R_{\text{eff}} = 1$ ) the radiation damping in each band is the same, as is the internal damping, so again no differences in  $F_{\text{RAD}}$  are expected. It is only in the region between 2 kHz and the higher critical frequency where the radiation damping differs the most that significant  $F_{\text{RAD}}$  differences should occur, i.e., around 3 kHz, the most sensitive region for our hearing.

Also note an A0  $F_{\text{RAD}}$  value in Figure 5. Cremer estimated that radiation and viscous damping losses for A0 were approximately the same [7], hence  $F_{\text{RAD}} \approx 0.5$ .

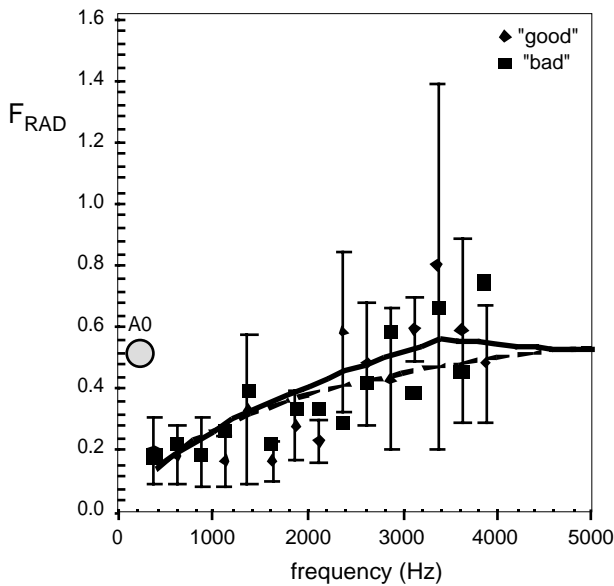


Figure 5: Fraction of vibrational-energy-radiated for good and bad violins ( $F_{\text{RAD}}$  range standard deviation - good only). Trendlines: “good” (solid), “bad” (dashed)

## 5. APERTURE VS. STRUCTURE

The first “patch” near-field acoustic holography measurements on f-hole radiation offer a surprising result [8]. Not only A0 radiates effectively through f-holes, the 1<sup>st</sup> corpus bending modes do too. This appears to reveal a new feature of

“structure” modes – volume changes over a cycle creating substantial volume flows through the f-holes.

## 6. CONCLUSIONS

What particular feature distinguishes “good” from “bad” violins? All have basically the same modes in the same order in the pitch range of the open strings. They radiate in similar ways and within any 250 Hz band have overlapping standard deviations for their modal-average total and internal dampings, and radiation efficiencies. In retrospect this is no surprise. All instruments were constructed within a fairly constricted “material-geometry” range, and thus in the normal mode sense must be quite similar in behavior. (This conclusion holds for properly scaled instruments too, e.g., the violin octet [3].)

However, the more rapid rise of the radiation efficiency, i.e., a slightly different trend, for “good” violins, leads to a lower critical frequency, dropping the peak in the radiation damping curve into the region near 3 kHz, making  $F_{\text{RAD}}$  a maximum where the ear has its maximum sensitivity. Nevertheless the significance of this difference becomes clear only when the “good” violin trends are compared to the “bad” violin trends.

The support of the National Science Foundation for this research (DMR-9802656) is gratefully acknowledged. We would also like to acknowledge discussions with Frank Fahy and Jim Woodhouse.

## 7. REFERENCES

- [1] Fahy, F. *Sound and Structural Vibration: Radiation, Transmission and Response* (Academic Press, 1987, paperback, New York)
- [2] Bissinger, G. “Toward a normal-mode understanding of the violin”, *Catgut Acoust. Soc. J.*, vol.3, no.6(Series II), 21-22 (1998)
- [3] Bissinger, G. “Modal analysis of a violin octet”, *J. Acoust. Soc. Am.* **113**, 2105-2113 (2003)
- [4] Bissinger, G. and Keiffer, J. C., “Radiation damping, efficiency, and directivity for violin normal modes below 4 kHz”, *Acoust. Res. Lett. Online* **4**, 7-12 (2003).
- [5] Ye, K., and Bissinger, G., “Attaining ‘free-free’ normal mode frequency and damping conditions for the violin”, *Proc.18<sup>th</sup> Intern. Modal Analysis Conf.- Soc. Exp. Mechanics*, Bethel, CT, 2000, pp. 398-403.
- [6] Bissinger, G., “Extracting internal damping from total damping and radiation efficiency measurements”, *Proc.21<sup>st</sup> Intern. Modal Analysis Conf.- Soc. Exp. Mechanics* (CD only), Bethel, CT, 2003, paper #160.
- [7] Cremer, L., *The Physics of the Violin*, (MIT Press, Cambridge, 1984).
- [8] Williams, E. G. and Bissinger, G., “Analysis of the radiation from the violin f-holes using patch near-field acoustical holography”, *J. Acoust. Soc. Am.*

## AN ACOUSTICAL STUDY OF FLAT- AND ROUND-BACKED DOUBLE BASSES

Andrew W. Brown

Institut für Wiener Klangstil, University of Music and Performing Arts Vienna, Austria

brown@mdw.ac.at

### ABSTRACT

The form of the violin has prevailed as the standard for the violin, viola and violoncello, but not for the double bass. Surveys reveal that while some tendencies exist among instrument makers and musicians, opinions about the sound of the two main types of basses, flat- and round-backed, often conflict. Several new double basses of nearly identical form and extremely similar materials were created especially for this study, presenting a unique opportunity to define acoustical characteristics of flat-backed and round-backed basses. The pairs of instruments differ, in theory, only in the form of the back. Laser vibrometry, analysis of audio recordings made in an anechoic chamber, and listening test surveys were used to delineate differences between the types concerning radiation characteristics and timbre. A special flat back for an existing violoncello was also made, tested and compared to a similar instrument of the standard form. Room acoustics and psychoacoustical considerations are discussed along with experimental results to offer an explanation about why the double bass is the only modern bowed instrument in use that has a flat back.

### 1. INTRODUCTION

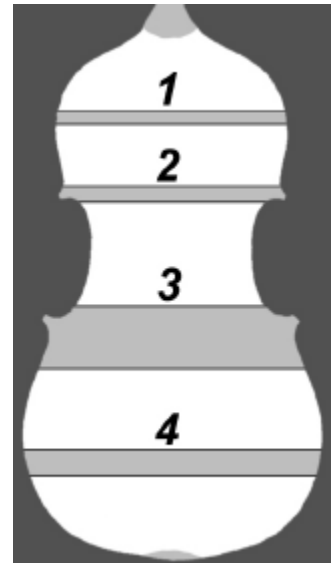
Though many aspects of the modern double bass have yet to be standardized, currently used instruments may be divided into two main categories: those with a flat back, and those with a rounded ("carved") back. The flat backed double bass has its roots in the design of the viol. An important feature of this type is not only the flat back plate, which is most often uniformly thick, but the size and configuration of internal bracings (Figure 1) which support the soundpost and add stiffness to the plate. Rounded backs have no such supports and are graduated like violins.

A survey of instrument makers and musicians shows no overwhelming preference for one type at this time, though many have opinions about the instruments' static and acoustical properties. According to the surveys, the flat back plate is prone to shrinkage problems because the perpendicular spruce braces do not allow the plate to expand and contract freely with atmospheric changes. On the other hand, flat backs require less material to make, and are less labor intensive if the bass is made by hand. Of the few makers and players who had an opinion, the majority described flat backed basses as sounding "more direct", "boomier", and rounded backs as "rounder (!)" and "warmer".

Papers on the acoustics of the flat double bass back were written by Wall [1] and Traeger [2], but do not present a

comparison to the round back design. The standard literature on instrumental acoustics has not up till now made a distinction between these two types of basses.

*Figure 1: A bracing pattern often seen in flat backed basses, including the test basses, which are arbitrarily numbered here. The braces are made generally of spruce and glued onto the interior side of the back with the grain perpendicular to the years of the plate. Any number of variations on this pattern have been reported: one, two or three braces, an "x" formed support under the soundpost, or even this standard pattern carved out of a round back!*



#### 1.1. Experimental setup

Ten instruments were measured during this study. Five are basses made especially for this test by a Bavarian luthier that have nearly identical design features and accessories, such as strings, tailpiece and fingerboards, except for the backs. Two were made in poplar and spruce and two in maple and spruce. The fifth has a plywood back with maple ribs. The poplar basses, which were cut from the same tree, are the focus of this paper. The components were manufactured by a large CCD milling machine, thinned by hand partially at the edges of the top plate and assembled. The bridges and soundposts are of similar materials and were fitted to the same positions. The instruments are not varnished.

Examination with a magnetic gauge revealed that thicknesses among the basses were generally within a  $\pm 0.5$  mm tolerance, with two important exceptions: the thickness of the top plate at the upper and lower widths inside the purfling was found to vary in the range between 3.0 and 4.7 mm, and braces 1, 2 and 4 (Figure 1) of the maple flat back were double the thickness of the poplar flat back (20 mm as opposed to 10 mm).

For measurements, each instrument was mounted on an artificial endpin affixed to a stone plate, allowing the instrument to stand firmly without any other contact. A B&K shaker 4810 on a heavy mounting sat on the stone plate, driving the bridge on the bass side. For audio recordings of sine sweeps, the

instrument was placed in a quasi-anechoic room with the strings dampened with foam. Five AKG CK92 spherical characteristic microphones were arranged in a half circle at a distance of 100 cm to the vibrating surface at the height of the bridge. A B&K accelerometer 4374 (0.65g) was placed on the bridge next to the shaker contact point as a reference. A sine sweep from 40 –3500 Hz over sixty seconds was recorded onto six channels (five audio + one reference) and repeated, then the instrument and shaker were rotated 180° and the process repeated. The resulting audio files for 000°, 045°, 090°, 135°, 180°, 225°, 270°, and 315° and two reference channels (front and back measurements) were RMS analyzed, yielding response curves.

For measurements using the Polytec laser vibrometer, the instrument and shaker were mounted as above, in a relatively small room with smooth concrete walls. A periodic chirp from 5-2000 Hz was used, the bridge was driven on the treble side and the strings were not dampened. No additional audio data was collected.

## 1.2. Audio Analysis

Attempting measurement of low frequencies in an anechoic environment is problematic. The repeated microphone channels at angles 090° and 270° show that audio signals below 100 Hz may vary by  $\pm 15$  dB and by  $\pm 5$  dB above 100 Hz. Since the soundpost and bridge set-up and other conditions were controlled as closely as possible, the measured differences between both instrument types should still have their origins in the design or materials. Consideration of the near- and far-field is also an important aspect of double bass acoustics, but the acquisition of sufficient signal levels at greater distances in larger rooms is difficult.

At the time of writing, many casual but no methodical listening tests have been performed. Playing a few bowed notes on both basses in the anechoic chamber yielded material for a few informal listening tests. When various recorded excerpts were played for “blind” colleagues, the result was quite entertaining: one said the first bass sounded “rounder”, while the second sounded “flatter” (“*flächig*”). Since then, any number of informal tests have shown that there is some sound difference, but no one has been able to recognize or consistently identify one or the other in blind tests, whether or not the research topic is known to them. The general response to the flat-backed ‘cello was that it “had a nice sound” but that the modulation of the tone color was difficult or impossible.

## 1.3 Radiation and Mobility Analysis

All flat-backed stringed instruments measured, including four basses, the special ‘cello, and a ‘cello-sized viola da gamba, are characterized by narrow band peaks and valleys in the response curve showing extreme amplitude differences within the range of middle body modes. The poplar flat-back bass shows troughs in forward-radiated energy occurring at 175, 205, and 260 Hz which do not occur in its round-backed twin (Fig. 2). The four

round-backed instruments recorded have a smoother response curve in this range.

The signal of the accelerometer waxed onto the bridge near the shaker’s needle yields a kind of input admittance curve, assuming that the input force remains constant. This curve, referred to here perhaps imprecisely as “mobility”, was used to help identify some air mode differences between the two models: the A0 mode at 67 Hz appears as expected in the radiation curve stronger than in the mobility curve. The T1/A1 mode appears at 115 Hz in both instruments, as its frequency is dependent on the body dimensions. The next appearance of an apparent air mode is the suspected A2 at 150 Hz in the flat-back and 158 Hz in the round-back. High mobility and low radiation is found in both basses at ca. 100 Hz, indicating blind power. Such values are also found in the flat-back at 175 Hz and 250 Hz and in the round-back at 230 Hz.

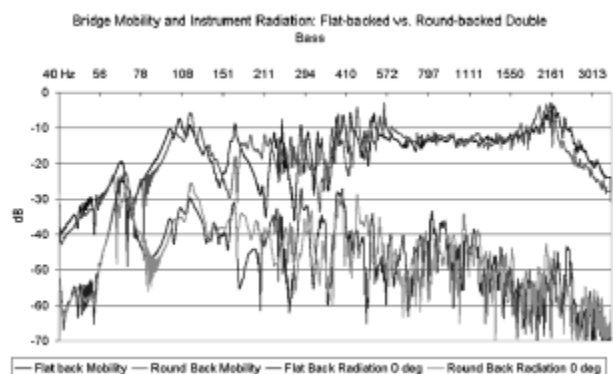


Figure 2: comparison of curves between the two poplar test instruments: Mobility above, radiation below.

Fig. 3 shows the response curves of the two flat-backed instruments (left) and the two round-back basses averaged over all eight audio channels. Several peaks are significantly different between the two flat-backed models, probably due to the thickness differences in braces 1, 2 and 4. The round-back models conform to one another more closely. This seems to indicate that the choice of poplar or maple for the back and ribs has little influence on the response curve.

## 1.4 Laser Vibrometry Analysis

Given the large amount of literature on the modal behavior of the violin, it was entertaining to discover many of the same patterns in the round-backed double bass and sometimes in the flat model. Due to technical difficulties, the first useful laser measurements occur above 80 Hz, so the first corpus bending modes and A0 mode are not well visible. The T1/A1 mode is very clear at 115 Hz in both basses, corresponding to the response curves of this study and illustrations from related literature. It is however remarkable that the top plate in both models vibrates as the violin

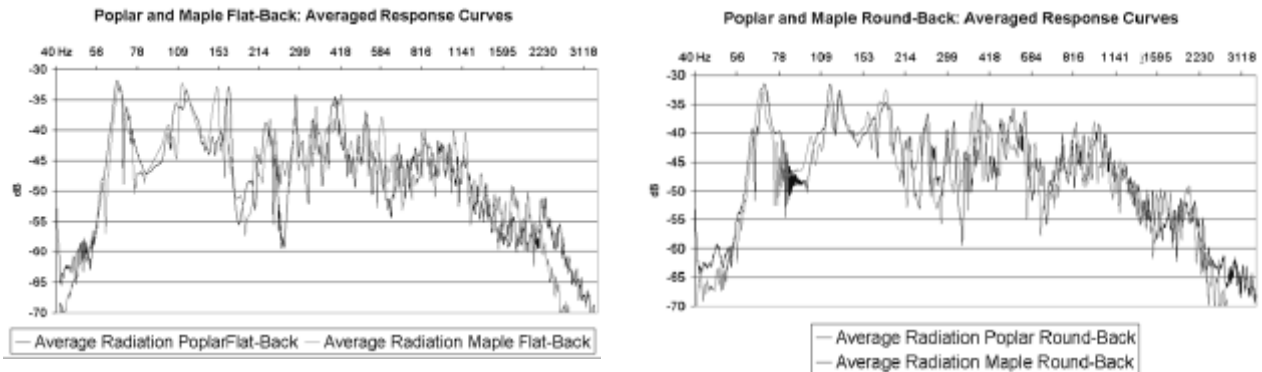


Figure 3: Averaged response curves of two flat-backed basses (left) and two round-backed basses, in poplar and maple.

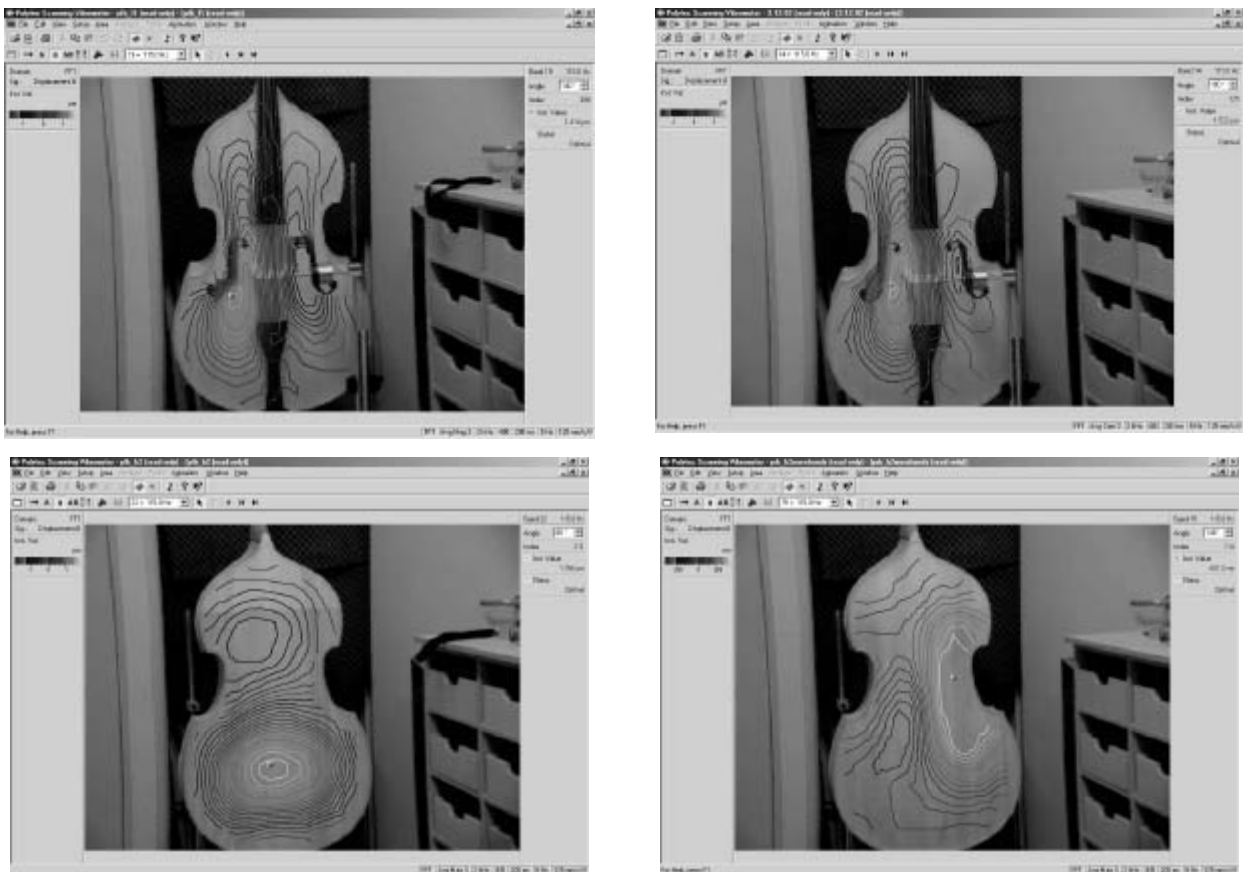


Figure 4: The T1/A1 mode at 115 Hz, flat back at left. Which pattern doesn't fit?

does [3], but that the back plates vibrate completely differently: the rounded back seems to behave as a large violin while the flat back with braces behaves presumably like a gamba (Fig. 4). Patterns of the backs remain different to varying degrees throughout the measured range. A ring pattern in the rounded back is present at a lower frequency (125 Hz) relative to the violin (650-700 Hz), and remains dominant in a broad band reaching to 160 Hz. The flat back, in contrast, goes through a rapid transition between deflection patterns within

narrow bandwidths. This appears to be the cause of the smoother response curve in the case of the rounded back: in the range of about 90-300 Hz the braces of the flat back sharply dampen narrow frequency bands and resonate in others. It is also characteristic of the flat back to vibrate symmetrically along the vertical axis, divided into sections by the braces, while the rounded back shows asymmetrical patterns along the length of the back, apparently due to the influence of the soundpost. An FFT of the vibration in both backs over the entire bandwidth reveals this tendency (Fig. 5).

In progressively higher frequency ranges, the modal patterns for both models get predictably more intricate. A more detailed list of deflection patterns and frequencies for both bass types will soon be available from the IWK.

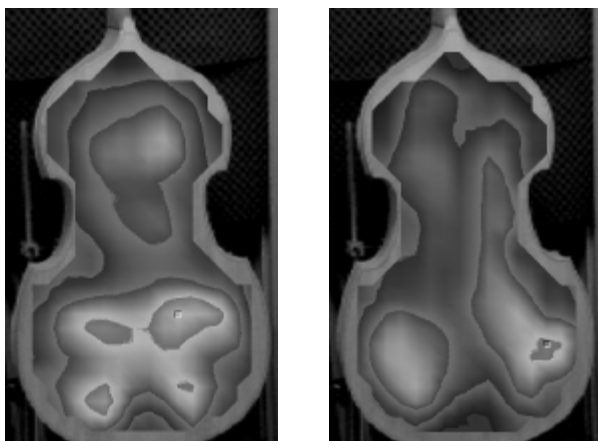


Figure 5: Laser vibrometry FFT of velocity over the entire bandwidth of 5-2000 Hz, flat back left, round back right. The maximum value (marked) for the flat back is 1.49 mm/s and for the round back 1.37 mm/s.

## 2. CONCLUSIONS

Analysis of radiated sound and laser vibrometer data has shown that there are remarkable differences in the resonance characteristics of two types of bowed instrument backs. The measured flat-backed instruments are characterized by narrow-band resonance peaks and troughs in the low and middle range of response curves. The flat backs demonstrate completely different operational deflection patterns than their rounded counterparts, which share many similarities with the violin. It is therefore remarkable that on the whole, both types are used equally often by bassists today. It is suggested that in spite of the large measurable differences observed between the two types, these differences are less significant in practice on account of psycho-acoustical and room-acoustical factors, but this must be confirmed with pending systematic listening tests.

## 3. REFERENCES

- [1] Wall, E., "Preliminary Studies of Flat-Backed Basses", JCAS Nr. 44, 1985, pp. 28-33.
- [2] Trager, C., "Tuning flat backs", CASJ, Vol. 3, Nr. 2 (Series 2), 1988, pp. 40-44, 198.
- [3] Moral, J.A. und E.V. Jansson (1982). *Eigenmodes, Input Admittance, and the Function of the Violin*, in *Acustica*, S. Hirzel Verlag, Stuttgart, Jahrgang 50, Nr. 5, S. 329-337.

# OPERATING DEFLECTION MODES IN FIVE CONVENTIONAL AND TWO UNCONVENTIONAL VIOLINS

Anders Buen\* and Ole Johan Løkberg\*\*

\*Brekke & Strand akustikk as, Hovfaret 17, NO-0275 Oslo, Norway

\*\*NTNU, Dept. of Physics, NO-7491 Trondheim, Norway  
anders.buen@bs-akustikk.no

## ABSTRACT

Operating deflecting modes in seven violins were studied using TV-holography and acceleration measurements. Two violins had a special inner support system. Mode shapes, vibration phase, -frequencies, levels and Q-values were recorded for frequencies below ~1,5kHz. Generally corresponding modes of the violins looked similar, though differences were seen, especially in the vibration phase. Combinations between modes were observed as the rule. The vibration levels was lower on the special violins up to around 600Hz, from then on they were comparable to the normal violins. The Q-values for the two special and an unvarnished violin were slightly higher than for the other violins.

## 1. INTRODUCTION

The dynamic response of violin bodies plays an important role in the sound production, the playability and the instrument quality [1,2]. The analysis of modes also gives meaningful information in the process of making and modeling instruments [3,4]. The violin has been studied by scientists and makers in at least 250 years.

Two of the violins studied here are versions of a violin developed in Norway [5]. Basically it is a version of the "Chrotta", where the right foot of the bridge rest directly on the sound-post which is not in contact with the top plate [7,8]. Such instruments sound like violins, but how do they acoustically compare to a normal violin?

In this study we have used acceleration  $a(\omega)$  over force  $F(\omega)$  measurements and TV-holography for visualization of vibration shapes, levels and Q-factors in seven violins as seen in Table 1. We also have seeked answers if anything can be said about the connection between acoustical measures and instrument quality.

Violin	Builder and some information	Quality
V1	An unvarnished violin made by the author	Bad
V2	Joseph Baldantoni, Germany, 1834	Fair
V3	Violin tonally rebuild by Buen senior, 1965	Good
V4	French violin tonally rebuild by Buen senior	Concert
V5	Gaetano Guadagnini (II), Italy, ca 1800	Concert
V6	Mikal Hagertrø no 39, 1993	Fair
V7	Mikal Hagertrø, unvarnished plywood, 1994	Fair

Table 1: The studied violins.

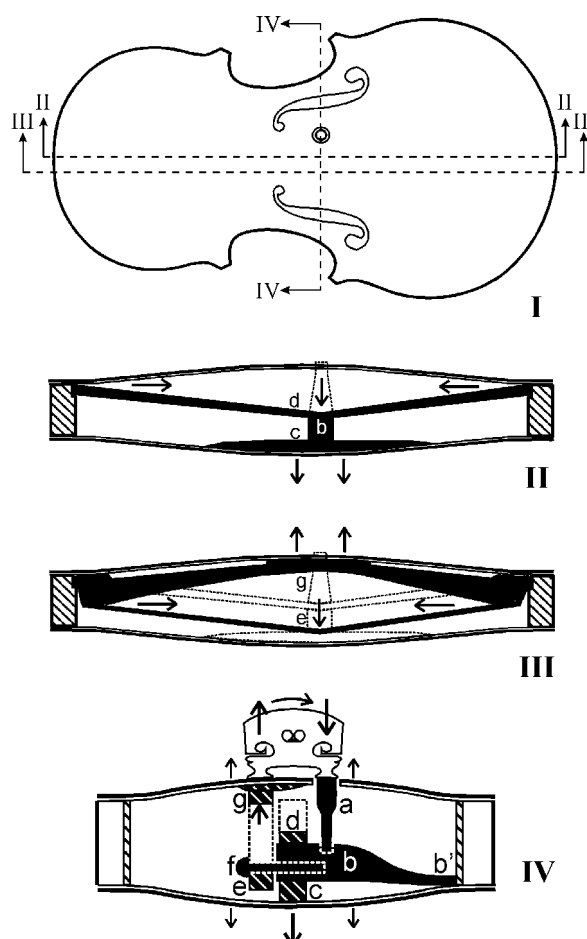


Figure 1: The principle for the inner support system of special violins V6 and V7. Pressing down the sound post (a) causes the cross member (b) – fastened at (b') – to bend down (see IV).

This forces the longitudinal member (c) and the back plate (d) down, while the support (d), the wooden pin (f), and chord (e) follow (see II and III). The lowering of (e) pulls the neck and the tailpiece blocks together, which causes the trestle (g) to bend up. An expansion of the body has been achieved. Pressing down the bridge on the reverse side gives the reverse effect. Most of the string tension is taken up by the support (d) while (a), (b), (f), (e) and (g) counteract the vertical component, leaving both plates virtually unchanged. [6]

## 1.1 The investigated violins

The investigated instruments were given quality ranking by a professional player as summarized in Table 1. The ranking sequence were like this (best violin first): V5, V4, V3, V2, V6, V7 and V1. V1 had rather thick plates, ~4mm in the top and ~6mm in the back, and it was unvarnished. V2 to V5 were normal varnished violins while special designs, V6 and V7, had the special inner support system as seen in Figure 1. The bar system was designed for a "breathing" motion of the violin body and it took up much of the string tension.

The plywood instrument, V7, had plates made of three crossed layers of spruce for the top and maple for the back. The laminating process with glue and arching of the plates was made simultaneously by cold pressing in a mould. The plate thickness were as low as 1,5-2mm or even thinner in some places, i.e. close to the thinnest areas in the conventional instruments made. V7 was not varnished.

## 2. THE MEASUREMENT METHODES

### 2.1 Transfer inrtance

The acoustical measurements were made with a set up as seen in Figure 2. The violin was supported in a rig simulating holding for playing. The acceleration signal  $a(\omega)$  was picked up behind the left bridge foot. The violin was driven by a light impulse hammer hitting the upper left bridge side. The excitation force  $F(\omega)$  during the impulses was recorded so the transfer inrtance curve  $a(\omega)/F(\omega)$  [ $\text{g}^{-1}$ ] could be calculated and presented by a dual channel FFT analyzer.

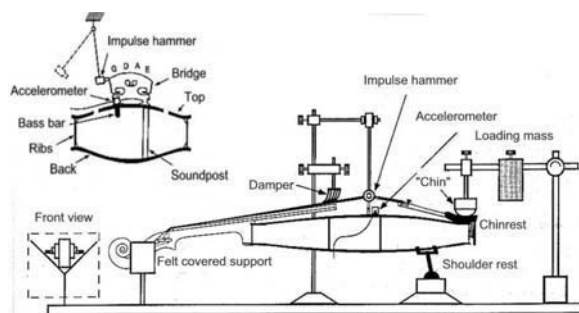


Figure 2: The inrtance measurement system. An impulse hammer hit the left bridge side and a tiny ( $< 1\text{g}$ ) accelerometer picked up the vibrations just behind the left bridge foot.

### 2.2 TV Holography

The optical measurements were made with the violin supported as seen in Figure 3. The static deflection of the foam rubber just to the left of the tailpiece was 4mm. Because of this soft vibration isolator it was expected that the measured modal frequencies was disturbed less than about 1Hz. At the same time the violin settled enough for the sensitive holography measurements to be accomplished. An angled mirror made the back side of the instrument visible to the TV-holography system. Details about the holography instrument can be found in [9].

The varnished violins were covered with talcum to increase the reflectivity and diffused possible glaring spots from the laser light. Excitation was a sinusoidal signal fed through a light piezoelectric disc ( $m < 1\text{g}$ ), a "buzzer", waxed to the top just behind the left bridge foot. The excitation was normal to the top plate.

The recording of the operating deflection modes was fully automated and typically made within a minute, depending on the wanted resolution and repetitions.

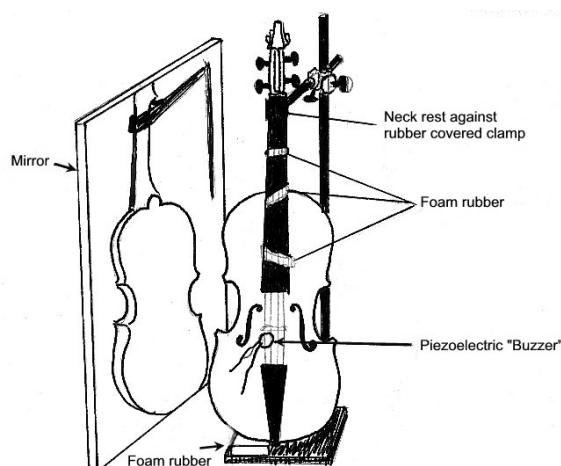


Figure 3: The violin setup for TV-holography measurements.

## 3. RESULTS

### 3.1 Transfer inrtance

Figure 4 show the inrtance curves of the best three violins, V3 to V5. They all have the high resonance level and width around 550Hz (the C3 mode, see Figure 9) typical of better violins [2]. The frequency region under about 600Hz is quite similar. In the old Italian, V5, the C3-resonance give significant response over a frequency width of about 170Hz. That is about five to six musical semitones. The C3 cover more than 10% of the played fundamentals and first harmonics in the best three violins. About 48% of played fundamentals are below 666Hz, this region is definitely very important.

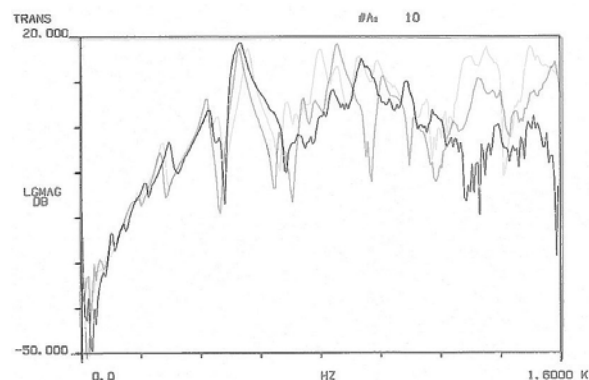


Figure 4: Transfer inrtance of the best three violins, V3 (light gray), V4 (darker) and V5 (black).

In Figure 5 is shown the two special violins, V6 and V7, compared to the old Italian, V5. The stiffness region below 400Hz is 5-10dB weaker in the special designs. Around C3 the difference is 10-20dB. From about 600Hz the special designs are equal or higher in level.

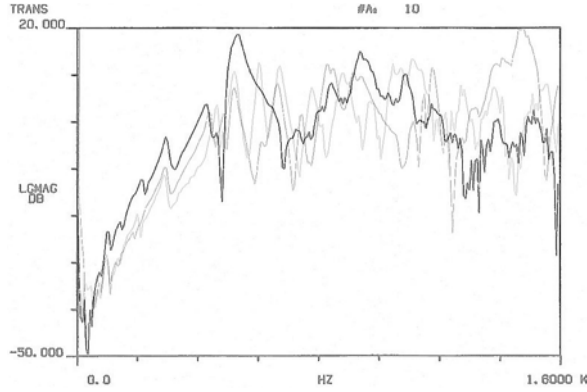


Figure 5: Transfer inductance of V5 (black) and the special instruments, V6 and V7 (lightest gray).

### 3.2 Holographic recordings

#### Velocity levels of modes

Figures 6 and 7 show the recorded levels of the modes in the top plates and back plates respectively. Figure 6 shows velocity levels relative to the top plate level of violin V1 at A0, the first air resonance. We see the trend that special violins are 6-10dB weaker up to about 600Hz. From 600Hz to 1kHz they are about equal. From 1-1.2kHz they are weaker again, because the modal overlap became evident. Special violins were not recorded beyond 1,2kHz.

We see that also the back plate vibrations are significantly lower in the special designs. Generally back plates are about 4dB weaker than the top plates reflecting the higher density of maple (about 25%), higher thickness (about 20%) and stiffer boundaries (no f-holes).

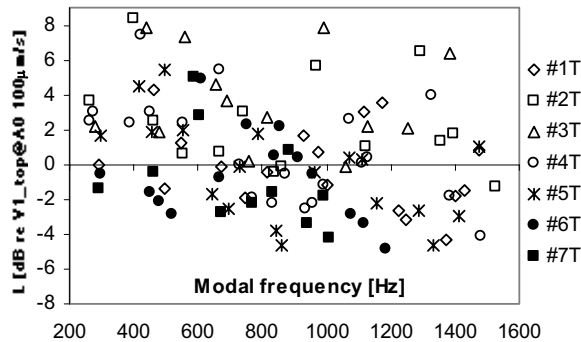


Figure 6: Velocity levels of modes at the top plates measured with TV-holography. To compare with the inductance curves:  
 $a(\omega) = \omega \cdot v(\omega)$ .

We see from the spread of levels that the natural variation between the instruments is about 8-10dB. These differences in levels will definitely be clearly audible by playing.

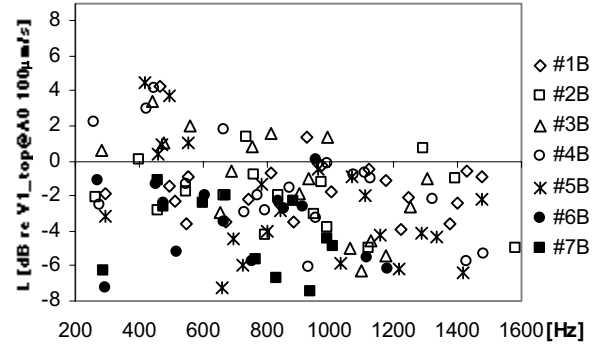


Figure 7: Maximum velocity levels of modes at the back plates measured with TV-holography

#### Q-factors

The measured Q-factors from each mode in the top plates are shown in Figure 8. We see the increasing trend with increasing frequency. Because of the thin plates and higher modal overlap in the special violins they are in the higher end. From linear regression the “Q-factor lines” follow this sequence in increasing order: V5, V3, V2, V1, V4, V7 and V6 respectively. For the back plates the sequence was: V5, V2, V6, V3, V4, V7 and V1. The unvarnished instruments, V1 and V7, seem to have higher Q-values than the varnished violins. Special designs V6 and V7 have slightly higher Q's than the mean.

The old Italian instrument had the lowest Q-values reflecting a rather fat varnish. May be everyday use cause higher exposure to humidity and thus lower Q-values as well.

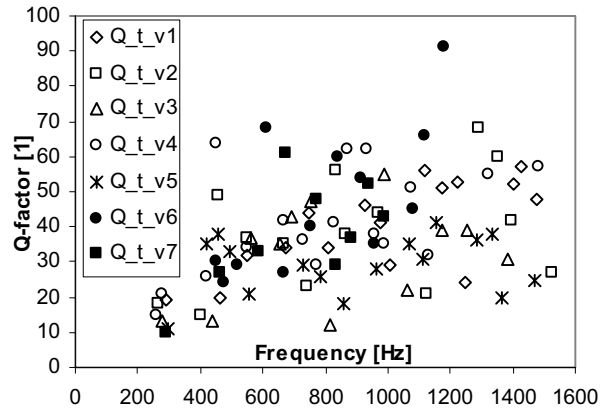


Figure 8: Q-factors of modes measured with TV-holography

#### Operational deflecting modes

Typical mode forms are shown in figure 9. They look similar to those seen in other publications [1,2]. Generally the vibrating shapes of the special violins were more complicated because of combinations of modes. Phase mappings show continuously changing phase over the structure like a shaken carpet or a flipping coin. Amplitude mappings show nodal *points* rather than nodal *lines* with areas 180° out of phase. The reason for less “clean” vibrations are probably parasitic vibrations in the



inner bar structure, different boundary conditions like a cross stiffening bar and no support at the normal sound post position and thinner plates. "Clean" modes cannot be "a must" as e.g. the old Italian violin had a conglomerate of four resonances involving C2, A1 (first longitudinal cavity air resonance) and T1. The phase mappings show traveling waves typical of combinations. Because the string fundamental and harmonics seldom will be exact at a body resonance, we may expect the normal violin vibrations during playing to be combinations rather than "clean modes".

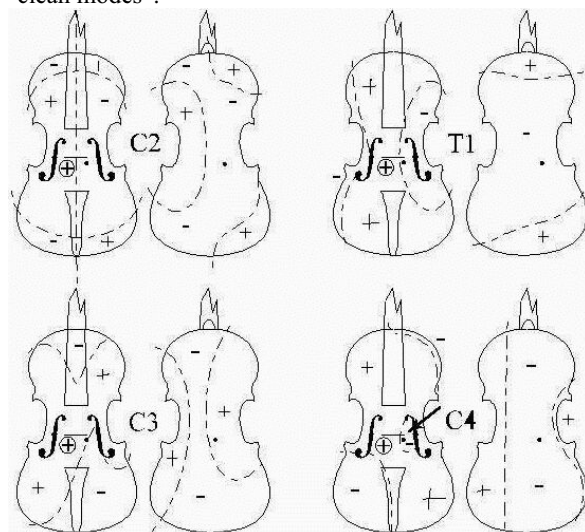


Figure 9: Typical operating deflecting modes of violins measured with TV-holography. The arrow show a version of "the Ireland" of L Cremer in the C4 mode [8].

The special violins had breathing C3- (~550Hz) and C4- (~670Hz) modes. The best two normal violins did show the same. Such pulsating modes should increase the sound radiation compared to plates vibrating in phase.

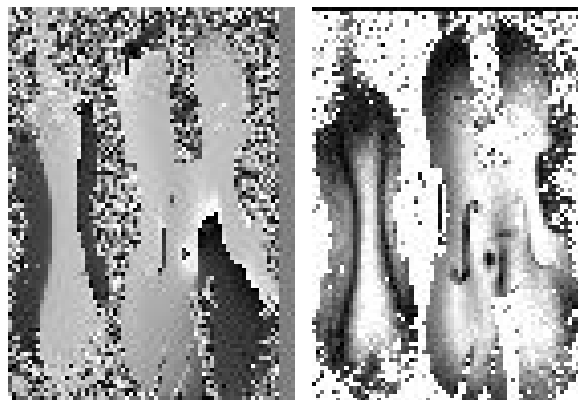


Figure 10: Vibration phase (left) and amplitude (right) of a "breathing" C4 resonance in V7 at 672 Hz. Grey and black areas are 180° out of phase. Black areas in the amplitude plot are at rest, white areas show high activity.

There were similar modes seen at two or three maxima recorded in all violins indicating coupling between vibrating structures. The better instruments had stronger coupling with a larger width between the maxima, thus extending the mode over a larger frequency region. Such coupling may reduce the risk for a "wolf" and smooth the

response when fitted at high peaks. T1 was double in V3, V4 and V5. C4 was double in V3 and V5, several other higher modes as well.

The fingerboard was damped. The coupling might be with the tailpiece, although the phase mappings did not show clear vibrations here. Activity in the tailpiece should be highest between the splitted resonances. But there is a possibility that the plates themselves might give a resonance split due to mutual coupling. Possibly the right type of plate tuning may give this effect, similar observations have been found for the guitar [1].

#### 4. CONCLUSIONS

The measurements have shown considerable differences between normal violins and special designs. Levels were 5-20dB lower for frequencies < 600Hz, vibration shapes were less "clean" and Q-factors somewhat higher in the special violins. From about 600Hz to 1kHz the levels were similar and the special design had "breathing" C3- and C4- modes equal the two best normal violins.

Later versions of the special violins sound more dark and better than the two special violins that have been tested, indicating improved low frequency response. Investigations into radiation indicate slightly higher radiation efficiency than in a normal violin [10], but also need for improvement in the "body hill" region around 2-3kHz.

More investigations should be made concerning splitted modes, higher frequencies including the "body hill", the normal variation of levels in a larger set of instruments more studies of damping and instrument timbre.

#### 5. REFERENCES

- [1] Fletcher and Rossing: "The physics of Musical instruments", Second edition, Springer, 1998, 756 p.
- [2] Jansson, E.V: "Acoustics for Violin and Guitar makers", KTH, Dept. of Speech, Music and Hearing, Fourth edition 2002, [www.speech.kth.se/music/acviguit4/](http://www.speech.kth.se/music/acviguit4/)
- [3] Schleske, Martin: "Empirical tools in Contemporary Violinmaking Part (I and) II, CASJ, Vol 4, No.6 (Series II), November 2002
- [4] Buen Anders: "Vibration modes in violins", M. Sc. thesis, NTH, February 1994, 135 p, (In Norwegian).
- [5] PCT International publication no WO 97/04438, "Inner support structure for a stringed instrument", Hagetrø fioliner AS, NO-7332 Løkken, NORWAY
- [6] Güettler Knut: "The Hagetrø violin", CASJ Vol 4, No. 2 (Series II), November 2000.
- [7] Heron Allen, E: Violin making as it was and is", Ward lock, London 1885.
- [8] Cremer, Lothar: "The Physics of the violin", MIT-press 1984.
- [9] Ellingsrud, S., Løkberg, O.J: "Full Field Amplitude and Phase Measurement of Loudspeakers using TV-Holography and Digital Image Processing" J. Sound Vib. 168(2), pp 193-208 (1993)
- [10] Morset, L-H: Measurements of radiation efficiency and internal mechanical loss applied to violins, ICA.

## NUMERICAL OPTIMIZATION OF VIOLIN BOWS WITH VARYING DENSITIES OF THE WOOD MATERIAL

Peter Carlsson and Mats Tinnsten

Department of Information Technology and Media  
Mid Sweden University, Östersund

Peter.Carlsson@mh.se

### ABSTRACT

The wood material for violin bows from the pernambuco tree (*Caesalpinia echinata*) has large individual variations in the density. For high quality bows, the higher densities are preferred, but since pernambuco is rather rare and expensive, it is of interest to investigate if it is possible to compensate for density variations in the wood material, at the same time as important qualities of the bow are unchanged. In this study, numerical optimization is used to recover the static and dynamic properties of a reference bow, on a bow with 10% lower density. The structural calculations of the bows are made with a numerical model in the finite element program ANSYS, which in its is coupled to an external, gradient based optimization routine. The automatic optimization process is performed with a routine called the Method of Moving Asymptotes (MMA).

### 1. INTRODUCTION

Since the days of the famous bow maker François Tourte (1747-1835), see Figure 1, the best violin bows are made of heart wood from the Brazilian hardwood pernambuco (*Caesalpinia echinata*).



Figure 1: François Tourte (1747-1835), creator of the modern violin bow.

For high quality bows, sticks with high density and high Young's modulus are favoured, but since pernambuco is rather rare and expensive, it is of interest to investigate if it is possible to make good bows of wood with lower densities, at the same time as important qualities of the bows are preserved. Another thing of interest to investigate is how quality bows with other material in the stick than pernambuco could be designed.

#### 1.1. Relation between physical properties and the quality of the bow

According to Askenfelt and other authors [1], [2], the quality of a bow can be divided into the "playing properties" and the "tonal properties" of the bow. The former quality can be connected to static properties as mass, centre of gravity and mass moment of inertia, while the latter probably is connected to the eigenfrequencies and perhaps also to the internal damping of the wood material in the stick. Both qualities are highly related to the material distribution and the Young's modulus in the fibre direction of the stick.

### 2. ANALYSIS AND OPTIMIZATION

Analysis is performed with a finite element model of the bow, and the honeycomb model of the wood material [3], [4], is used to estimate the effect on the material parameters when the density of the stick is altered. Since a bow has its main dimension in the fibre direction of the wood material, we are primarily interested in the relations between the density and the modulus in the fibre or axial direction. From the honeycomb model we get the relation

$$E_a = C \cdot \frac{\rho}{\rho^c} \quad (1)$$

where  $E_a$  is the modulus in the axial direction,  $C$  is a constant,  $\rho$  is the actual density of the wood, and  $\rho^c$  is the (almost constant) density of the cell wall in the wood fibre.

The analysis program is coupled to an optimization routine, and automatic optimization is made against the playing and tonal qualities of a reference bow of good quality.

#### 2.1. Analysis

A reference bow by Petzel, a younger player's bow with a total weight of 54 [g] and a length of 739 [mm], was measured and modelled in the commercial finite element program ANSYS [5]. Density and Young's moduli of the bow is estimated but the internal damping of the wood material is not considered in the model. Only the part of the stick from the upper side of the frog to the tip is modelled. The stick is fixed rigidly at the upper end of the frog and free to move in all directions at the tip, see Figure 3. Bow-hair is not included. The 3D finite element model consists of 310 volume elements (the eight node, SOLID45-

element), of which 18 elements are used to build up the tip, see Figure 2. The wood material of the stick is modelled as an orthotropic material, and the fibre direction of the wood follows the curve of the stick.



Figure 2: Finite element model of the stick.

For the sake of the optimization, the thickness of the stick can be easily changed during the automatic process. The rather dense discretization of the elements makes it possible to perform proper calculations of the wanted eigenfrequencies and the static properties, and to make necessary changes of the material distribution along the stick during the automatic optimization process.

## 2.2. Numerical Optimization

Optimization can be performed in many ways and with several techniques. The result of the optimization is often dependent of the problem definition, and different methods may demand different problem formulations. The optimization of the bow has been carried out with both stochastic and gradient based methods, but in this paper, only optimization with a gradient based method is presented.

The method used is the nonlinear, gradient based MMA routine (MMA, Method of Moving Asymptotes, Svanberg [6]) which has been used with great success in a variety of applications from structural, wood drying, fluid-flow, and acoustic optimization [7], [8], [9]. The MMA routine is connected to the analysis program ANSYS, and necessary derivatives are calculated numerically as finite differences. Optimization is performed against a reference bow of good quality, and in this study the optimization problem is to recover the static and dynamic properties of the reference bow, on a bow with the same length but with a different density. Design variables are the thickness of the tip at the bow-hair, and the diameter of the stick at certain locations, see Figure 3. In order to give a nice shape to the new bow, the MMA routine is forced to create a shape as similar to the reference bow as possible. This is made by choosing the minimal geometrical deviation from the reference bow as the goal or objective function of the optimization problem (2). The constraints (3) – (5) takes care of the static properties, while the three constraints in (6) are responsible for the fulfilling of the dynamic properties of the bow.

In mathematical terms, the optimization problem is formulated as follows:

Minimize (the so called objective function)

$$f(\theta) = \sum_i \left( \frac{\theta_i - \theta_i^{ref}}{\theta_i^{ref}} \right)^2 \quad (2)$$

such that (the constraints)

$$g_1(\theta, t) \equiv \left( \frac{m - m_{ref}}{m_{ref}} \right)^2 \leq \varepsilon_m^2 \quad (3)$$

$$g_2(\theta, t) \equiv \left( \frac{\bar{x} - \bar{x}_{ref}}{\bar{x}_{ref}} \right)^2 \leq \varepsilon_x^2 \quad (4)$$

$$g_3(\theta, t) \equiv \left( \frac{I - I_{ref}}{I_{ref}} \right)^2 \leq \varepsilon_I^2 \quad (5)$$

$$g_{4-6}(\theta, t) \equiv \left( \frac{f^j - f_{ref}^j}{f_{ref}^j} \right)^2 \leq \varepsilon_f^2, j=1-3 \quad (6)$$

where  $\theta$  is a vector of the design variables  $\theta_i$ , i.e. the diameter of the stick at position  $i$  (see Figure 3),  $t$  is the thickness of the tip at the bow-hair,  $m$  is the mass,  $\bar{x}$  is the position of the centre of mass,  $I$  is the mass moment of inertia about an axle perpendicular to, and through the upper end of the frog, and  $f^j$  is eigenfrequency  $j$  ( $j=1-3$ ) for the stick. Index  $ref$  is used for properties of the reference stick and the  $\varepsilon$ 's are small numbers.

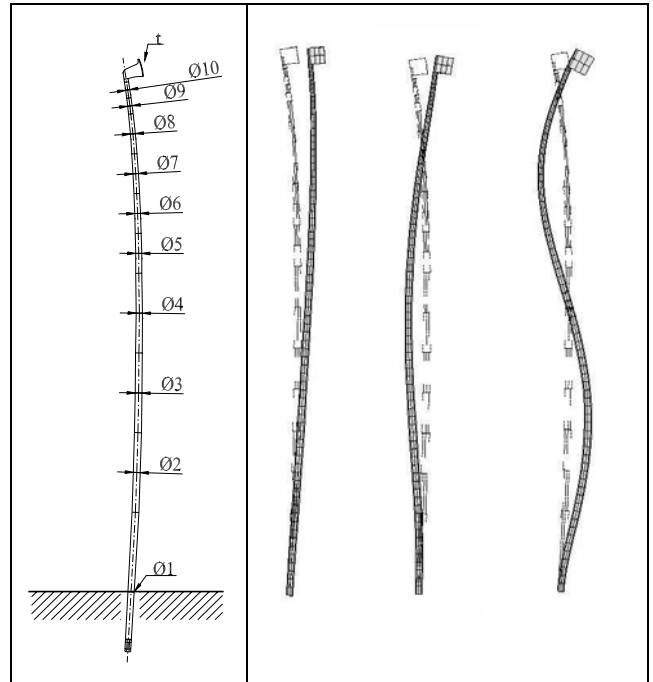


Figure 3: To the left: Design variables and fixing of the stick.

Only the part above the fixation is modelled. To the right: Studied eigenmodes of the stick (all modes oscillates in a plane parallel to the flat side of the frog). From left to right: Mode 1 corresponding to frequency  $f^1$ , mode 2 corresponding to frequency  $f^2$ , mode 3 corresponding to frequency  $f^3$ . (the undeformed stick is outlined as a broken line).

The choice of the objective function may seem strange, but practical experiences has shown that the outer shape of the stick will be less attractive if the design variables are left without any restrictions: the material will otherwise tend to amass at certain

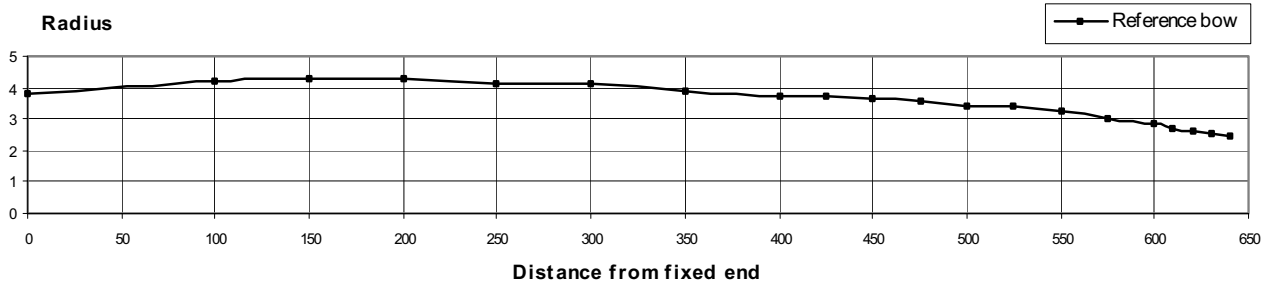


Figure 4: Measured radiuses on the reference stick. Range of measurement from upper part of the frog to the beginning of the tip, see Figure 3.

places of the optimized stick. Furthermore, in problems where eigenvalues like eigenfrequencies are calculated, the risk of local minima must also be considered. This is of particular importance when gradient based optimization methods are used. An objective function based only on the eigenfrequencies in (6) would surely give such problems.

The natural way to write the constraints, if constraint  $g_1$  (3) is taken as example, would be something like

$$g_1(\theta, t) \equiv m = m_{ref} \quad (7)$$

but since MMA only allows inequality constraints, the constraint is formulated as in equation (3). However, during the optimization process, the value of the  $\varepsilon$ 's are gradually decreased, and therefore, in the end of the process, the constraints are almost fulfilled as in the equality formulation in (7). The constraints and the terms in the objective function are also normalized in order to make them more equal in numerical size.

During optimization, only the thickness variables  $\theta$  along the stick and the thickness of the tip  $t$  are altered, see Figure 3. The outer shape of the bow, *i.e.* the curve of the bow, is constant during the whole process since separate calculations has shown that it has a negligible influence of the result.

### 3. NUMERICAL RESULTS

The thickness distribution and the outer shape of the reference bow by Petzel was measured. The bow has radiuses according to Figure 4, and a thickness of 10 [mm] at the tip at the bow-hair. The density and Young's modulus of the reference bow in the fibre direction was estimated to  $\rho_{ref} = 900$  [kg/m<sup>3</sup>] and  $E_a^{ref} = 17$  [Gpa] respectively (other material parameters, of less importance for the calculations, are not presented here). A calculation in ANSYS gave the following reference values of the parameters of interest in this study:  $m_{ref} = 0.02623$  [kg],  $\bar{x}_{ref} = 0.32015$  [m] from the fixed end,  $I_{ref} = 0.00370$  [kgm<sup>2</sup>] about an axis through the upper end of the frog,  $f_{ref}^1 = 11.1$  [Hz],  $f_{ref}^2 = 56.4$  [Hz], and  $f_{ref}^3 = 150.9$  [Hz].

The bow to be optimized was given a 10% lower density of  $\rho = 810$  [kg/m<sup>3</sup>], and, according to the honeycomb model (1), a Young's modulus of  $E_a = 15.3$  [Gpa] in the fibre direction. As an

initial design for the optimization, the bow was given the same shape as the reference bow.

Design variables was ten diameters along the stick and the thickness of the tip at the bow-hair, see Figure 3. Upper and lower limits was set on the design variables, and the small numbers  $\varepsilon$  in equations (3) – (6) were all gradually decreased from 3% to 0.8% during the optimization process.

With the new material in the stick, but with unchanged dimensions, initial calculations with ANSYS gave a 10% lower mass and mass moment of inertia as expected, while the centre of mass was unchanged and the eigenfrequencies was almost the same. The latter result can be explained by a simplified analogy there the sticks are treated as two homogenous bars with constant cross section and length: if the Young's modulus ( $E_a$ ) in the fibre direction is proportional to the density ( $\rho$ ) of the material, as in the honeycomb model, the eigenfrequency is only proportional to the (constant) term  $\sqrt{E_a / \rho}$ .

The task for the MMA-routine is now to recover the static and dynamic properties of the reference bow (as defined here) with small changes of the geometry. After 32 iterations in the MMA-routine, the shape of the bow has converged to a shape according to Figure 5. The thickness of the tip has increased from 10.0 to 11.25 [mm] at the bow-hair. The optimized shape of the bow gave values of the static and dynamic properties shown in Table 1.

Table 1. Comparison of static and dynamic properties between optimized bow and reference bow.

Property	Opt. bow	Ref. bow	Difference
$m$ [kg]	0.02646	0.02623	0.84%
$\bar{x}$ [m]	0.32056	0.32015	0.13%
$I$ [kgm <sup>2</sup> ]	0.00367	0.00370	-0.84%
$f^1$ [Hz]	11.1	11.1	-0.47%
$f^2$ [Hz]	56.8	56.4	0.74%
$f^3$ [Hz]	152.1	150.9	0.76%

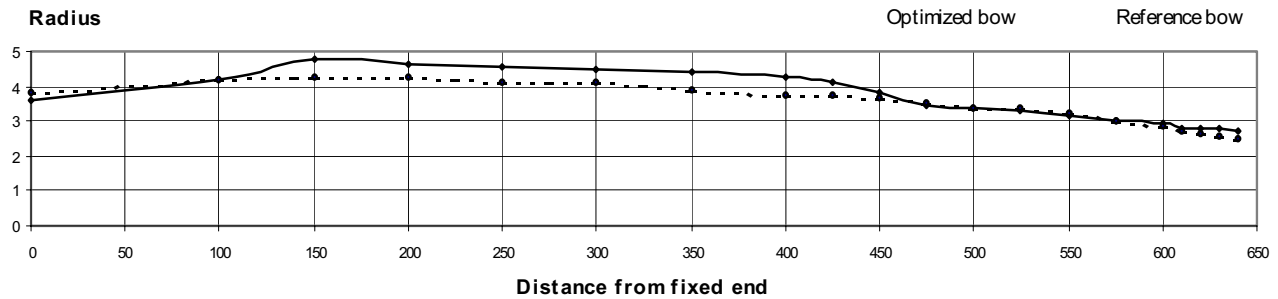


Figure 5: Radiuses of the optimized stick together with radiuses of the reference stick, marked as a dashed line. Range of measurement from upper part of the frog to the beginning of the tip, see Figure 3.

An interesting observation is that the main result of the optimization was achieved as the fulfilments of the constraints, while the final value of the objective function at optimum is of less importance. But, as mentioned before, with gradient based optimization routines as MMA, it is essential to avoid problem formulations with risk of several local minima on the way to the optimum solution. How close the solution is to the global or absolute optimum is hard to say. A possible way to test an achieved solution, when the analytical solution of the problem is unknown, is to start the optimization process from different starting points, in this case different initial shapes of the bow, and see if the solution converges to the same shape.

#### 4. DISCUSSION AND CONCLUSION

The optimization problem was to recover the static and dynamic properties of a reference bow, on a bow with 10% lower density and Young's modulus in the fibre direction. The properties to recover was the mass, the centre of mass, the mass moment of inertia, and the first three eigenfrequencies in a plane parallel to the flat side of the frog. The optimization problem should be solved with a minimum geometrical deviation from the thickness distribution of the reference bow, which also was chosen as the objective function. The results are quite promising, and indicates that optimization might serve as a valuable tool also in bow making.

The density and Young's modulus of the bows was only estimated in this study, but in a sharp calculation both values can be determined without any damage of the reference bow. A "naked" stick might be weighed and measured carefully. After transformation of the stick to a finite element model, the output from the FEM-program gives the volume of the stick, and after that the density of the stick is easily determined. Young's modulus can be determined from experimental determination of the eigenfrequencies, the same way as the material parameters are determined on a violin top in [10] where Young's moduli are calculated by an optimization routine coupled to a finite element program.

#### 5. FUTURE CONSIDERATIONS

The outcome of an optimization need to be verified against a real bow, made from the geometrical specifications of the

calculations described above. The optimization should in that case be made on a blank with known material parameters, determined as described in [10]. If the reference bow is a bow of good quality, it would be interesting to see how close the optimized bow is to the reference bow in playing and tonal properties, when it is tested by professional violinist.

In this paper, the calculations are only performed on bows made of pernambuco. The numerical model might, however, be easily adapted to bows made of other wood species or other materials as reinforced material with carbon or glass fibres.

#### 6. REFERENCES

- [1] Askenfelt, A. "Observations on the Dynamic Properties of Violin Bows". STL-QPSR 4/1992.
- [2] Caussé, R., Maigret, J.P., Dichtel, C. and Bensoam, J. "Study of Violin Bow Quality", IRCAM,
- [3] Gibson, L.J. and Ashby, M.F. "Cellular Solids, Structure and Properties". Pergamon Press, Oxford. pp. 69-119. 1998.
- [4] Carlsson, P. and Tinnsten, M. "Optimization of a Violin Top with a Combined Laminate Theory and Honeycomb Model of Wood". *Holzforschung* 57, pp. 101-105. 2003.
- [5] Finite element program, ANSYS Inc. Southpointe 275 Technology Drive, Canonsburg. [www.ansys.com](http://www.ansys.com).
- [6] Svanberg, K. "MMA – Method of Moving Asymptotes – A new Method for Structural Optimisation". *Int. Journal for Numerical Methods in Engineering* 24. pp. 359-373. 1987.
- [7] Carlsson, P. and Tinnsten, M. "Optimization of Drying Schedules Adapted for a Mixture of Boards with Distribution of Sapwood and Heartwood". *Drying Technology*, 20(2). pp. 403-418. 2002.
- [8] Dahlén, L. and Carlsson, P. "Numerical Optimization of a Distributor Valve". Submitted to *Journal of Fluid Power*, 2003.
- [9] Tinnsten, M. "Numerical Prediction of Acoustic Response – a Numerical and Experimental Comparison". *Structural Optimization* 19. pp. 122-129. 2000.
- [10] Tinnsten, M. and Carlsson, P. "Determination of Important Wood Properties for Blanks for Violin Tops by the use of Numerical Optimization". SMAC-03, proc.

## MODELING SAVART'S TRAPEZOIDAL VIOLIN USING A DIGITAL WAVEGUIDE MESH

Federico Fontana

Department of Information Engineering  
University of Padova, Italy  
fontana@sci.univr.it

Stefania Serafin

CCRMA, Department of Music,  
Stanford University, Stanford, CA  
serafin@ccrma.stanford.edu

### ABSTRACT

We propose a real-time computer model of Savart's trapezoidal violin. The model, which uses a three dimensional waveguide mesh, is applied to a bowed string physical model.

### 1. INTRODUCTION

The tone quality of a violin is largely determined by the normal modes of vibration of the violin body, which filters vibrations that propagate from the string through the bridge. The current shape of the violin body has evolved from different ancient bowed instruments such as the rebec, the gigue, the lyra and the vielle [1].

Different attempts were made in order to perfect the violin. At the beginning of the 19th century Savart tried to simplify the shape proposing a trapezoidal body without arches, with straight sound holes, and a bass bar in the middle of the front [2]. A violin similar to the one proposed by Savart is shown in figure 2. This violin was never adopted, even if documents of the time claim that the Academies of Sciences and of Arts approved the design and the sonorities [2].

In this paper we propose a digital implementation of the trapezoidal violin proposed by Savart. Section 2 describes the resonances of a traditional violin's body, section 3 proposes an overview of previous research on body modeling, section 4 describes Savart's trapezoidal violin, section 5 describes how to build a trapezoidal three dimensional mesh, and section 6 describes how to apply the mesh to a bowed string physical model.

### 2. VIOLIN BODY RESONANCES

The violin body acts as a resonator for the vibration generated from the strings. The coupling of air cavity modes and top and back plate modes produces the complex filtering which contributes strongly to the characteristic timbre of the violin. At lower frequencies (below 3kHz), the wood modes predominate, and at higher frequencies (above 3kHz) the air modes predominate.

The impulse response of a violin body is shown in 1. The response was obtained by exciting the body vertically with an impulse hammer in an anechoic chamber. The bottom of the figure shows the frequency response. Note the high number of resonances that are a characteristics of the body. Modeling these resonances is a challenge in sound synthesis by physical modeling, as described in the following section.

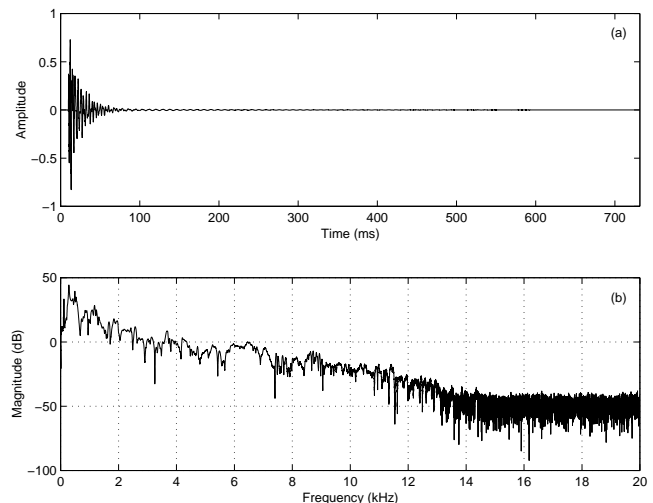


Figure 1: (a) impulse response of a violin body. (b) frequency response of a violin body.

### 3. PREVIOUS RESEARCH ON VIOLIN BODY MODELING

In real-time synthesis of a violin, there is some difficulty in modeling the body because of a tradeoff between accuracy and computational cost. If all the resonances of the body are accounted for by modeling each one with its own pair of filter poles, the computational cost is too high. On the other hand, one cannot implement too few filter poles and neglect the large number of resonances, because the complex filtering of the body contributes strongly to the characteristic timbre of the violin.

In order to solve the problem of computational cost and maintain an efficient implementation that runs in real-time, in [3] a technique called *commuted synthesis* is proposed. The idea behind commuted synthesis is to combine the complex impulse response of an instrument's body with the excitation. This technique is a computationally efficient solution that avoids to model excitation and body resonances separately. Instead of the classical path excitation-string-body, the combined excitation and body resonances are the input to the string model; this is the reason why the synthesis is called *commuted*.

Commuted synthesis works well for linear systems, in which this permutation is mathematically justified. For nonlinear systems, such as a bow excited by a string, other solutions need to be found.

Huang et al.[4] proposed to use a waveguide mesh to model high frequency modes of a violin. The dimensions of the mesh were chosen in order to match perceptually and statistically the resonances of a violin's body. Since the rectangular mesh was not providing the right low-frequency resonances required by a violin's body, the complete body model was made of a combination of second order resonant filters for low-frequencies and a waveguide mesh for high frequencies.

#### 4. SAVART'S TRAPEZOIDAL VIOLIN

In this paper we choose to model a violin's body using the waveguide mesh approach. We choose a mesh whose dimensions correspond to the ones proposed by Savart for his trapezoidal violin. In this way the mesh design is motivated and justified by historical reasons.

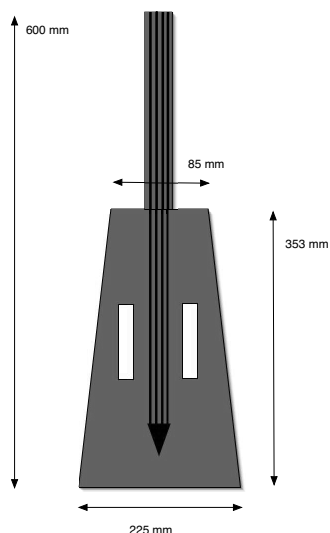


Figure 2: Savart's trapezoidal violin.

As shown in figure 2, the dimensions of the original violin were 600 mm of total length, 353 mm of body length, 225 mm of body width in the lower part and 85 mm of length for the higher part of the body. The violin had two rectangular holes in each side, which correspond to the f-holes in the traditionally shaped violin.

#### 5. MODELING SAVART'S TRAPEZOIDAL VIOLIN

In order to create a digital model of Savart's violin we used a three dimensional trapezoidal waveguide mesh.

The trapezoidal mesh is an extension of the original two dimensional rectangular mesh [5] in which the horizontal dimension decreases in size from bottom to top, according to the design proposed by Savart.

The dimensions of the mesh are chosen in order to match the dimensions of Savart's violin.

Figure 3 shows the impulse response (top) and frequency response (bottom) of the trapezoidal mesh. Notice how the frequency response shows some strong peaks in the frequency range until about 5000 Hz. This is not compatible with the perceptual research on violin body's resonances (see, for example, [6]). One

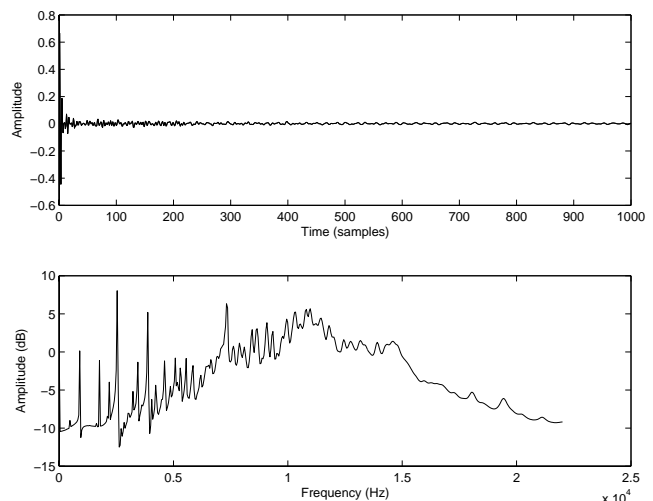


Figure 3: Top: impulse response, bottom: frequency response of Savart's trapezoidal violin with no holes.

characteristic of the *good tone* of a violin is, in fact, an equal distribution of peaks and valleys, which is obviously not the case in the spectrum of the trapezoidal mesh shown in figure.

To cope with this problem, we added a model of the two violin's holes, as described in the following section.

#### 5.1. Accounting for the violin's holes

We added the holes to the trapezoidal mesh using the same technique adopted to model toneholes in woodwind instruments [7]. Figure 4 shows the impulse and frequency response of the trapezoidal mesh that accounts for the holes.

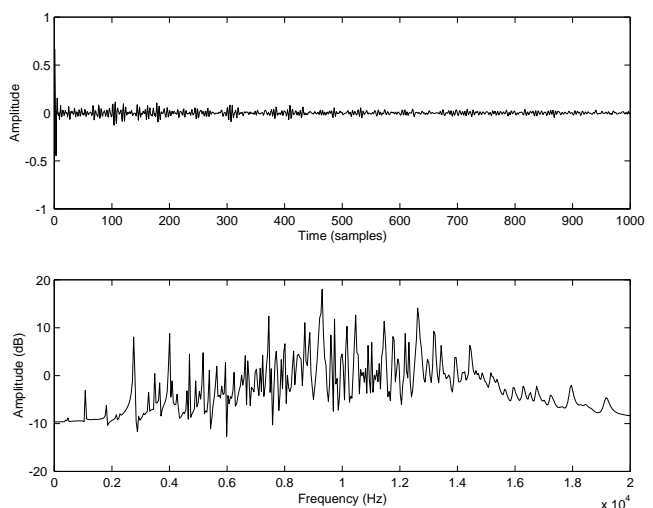


Figure 4: Top: impulse response, bottom: frequency response of Savart's trapezoidal violin with the holes.

Note how the peaks and valleys in the frequency response are more equally distributed.

## 6. APPLICATION TO A BOWED STRING PHYSICAL MODEL

The violin's body model was applied to the digital waveguide model of a bowed string proposed in [8]. The input parameters of the model are bow pressure  $f_b = 0.2$  N, bow velocity  $v_b = 0.05$  m/s and normalized bow position  $b_p = 0.1$  (where 0.5 represents the middle of the string, and 0 represents the bridge). In this simulation a cello  $D$  string ( $f_0 = 147$  Hz) was used.

The outgoing velocity at the bridge point  $v_{ob}$  was filtered through the resonances of the trapezoidal mesh, as shown in figure 5.

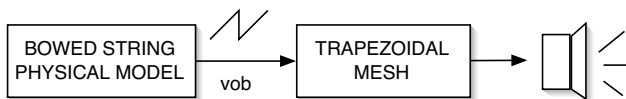


Figure 5: Simplified block diagram of the combination of the physical model and the trapezoidal mesh.

Figure 6 shows the result of applying the trapezoidal mesh to the bowed string physical model. The top of figure 6 represents the outgoing velocity at the bridge  $v_{ob}$  before being filtered by the body resonances, while the bottom of figure 6 shows the output of the bowed string physical model after being filtered by the body resonances. The waveforms were captured after steady state motion was achieved.

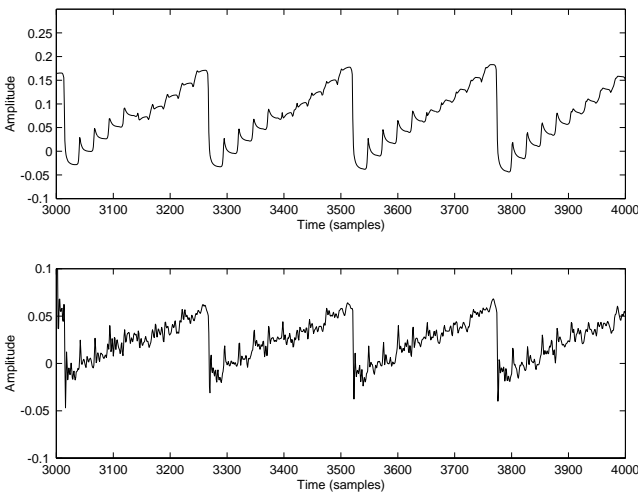


Figure 6: Top: outgoing velocity at the bridge before being filtered by the body resonances; bottom: outgoing velocity at the bridge after being filtered by the body resonances.

As expected, the regularity of the Helmholtz motion is broken when the waves are filtered through the body. This is the same behavior that can be observed when looking at the bridge velocity in an oscilloscope, before and after being filtered by the body resonances. This difference can be noticed also in the spectrum of the resulting waveforms, shown in figure 7.

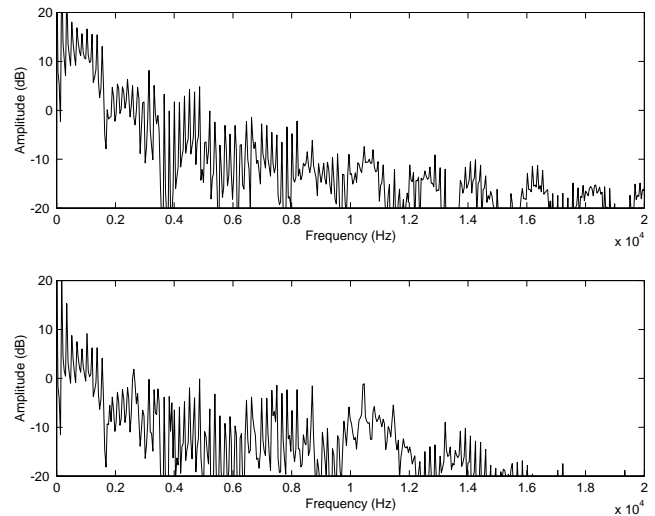


Figure 7: Top: spectrum of the outgoing velocity at the bridge before being filtered by the body resonances; bottom: spectrum of the outgoing velocity at the bridge after being filtered by the body resonances.

## 7. CONCLUSIONS

We proposed a digital model of Savart's trapezoidal violin using three dimensional waveguide meshes. The model has been applied to a bowed string physical model. The combination of the bowed string and the body model is efficient enough to run in real-time on a personal computer.

## 8. REFERENCES

- [1] E. Leipp, *The violin*, University of Toronto Press, Toronto, 1969.
- [2] F. Savart, "Memoire sur la construction des instruments a cordes et á archet," Tech. Rep., Paris, Deterville, 1819.
- [3] M. Karjalainen and J.O. Smith, "Body modeling techniques for string instrument synthesis," in *Proc. International Computer Music Conference*. Aug. 1996, Computer Music Association.
- [4] P. Huang, S. Serafin, and J. O. Smith, "Modeling high-frequency modes of complex resonators using a waveguide mesh," in *Proc. DAFX*. Dec. 2000, Verona, Italy.
- [5] S. A. Van Duyne and Julius O. Smith, "Physical modeling with the 2-D digital waveguide mesh," in *Proc. ICMC*. 1993, pp. 40–47, Computer Music Association.
- [6] M. Mathews and J. Kohut, "Electronic simulation of violin resonances," *Journal of the Acoustical Society of America*, vol. 53, no. 6, pp. 1620–1626, 1973.
- [7] Gary Scavone and Julius O. Smith, "Digital waveguide modeling of woodwind toneholes," *Presented at the 132nd meeting of the Acoustical Society of America, Honolulu*, Dec. 1996.
- [8] Stefania Serafin, Julius O. Smith, III, and Jim Woodhouse, "An investigation of the impact of torsion waves and friction characteristics on the playability of virtual bowed strings," in *Proc. WASPAA*, New York, Oct. 1999, IEEE Press.





## EXPERIMENTS WITH AN AUTOMATIC BOWING MACHINE

*P. M. Galluzzo and J. Woodhouse*

Department of Engineering  
Cambridge University  
pmg26@eng.cam.ac.uk

### ABSTRACT

In order to validate and develop theoretical models of the action of a bowed string, careful experimental work is needed. It is already known that current models predict behaviour which is qualitatively plausible, but can they predict accurately the details of the transient response to specific bowing gestures? A computer-controlled bowing machine has been developed which allows reproducible gestures to be made, in which the bow speed and bow force can be specified. This allows systematic experiments to be made in which a portion of parameter space is explored by varying parameters in small steps. These results can be compared directly to corresponding simulated results, and identical automatic processing of each set of data can be applied so that the comparison is fair. This comparison reveals that some aspects of behaviour are quite well captured by current models, but that other features are not reproduced. Careful study of the results can guide further development of the theoretical models.

### 1. INTRODUCTION

When a string is bowed with appropriate speed and force so as to produce a clear and full tone, its vibration pattern counter-intuitively comprises two straight segments of string joined by an abrupt corner (see e.g. [1]). This motion, known as Helmholtz motion, is undetectable by the human eye because the position of the corner joining the two segments of string moves rapidly back and forth. Helmholtz motion is unique and distinctive, and the sound that it invokes from the instrument by exciting the bridge and hence the body of the instrument is also distinctive; a violinist would describe a violin as ‘speaking’ during Helmholtz motion.

Alternatives to Helmholtz motion which may be elicited by incorrect levels of bow force and speed are either too quiet, too shrill, or too ‘crunchy’, and would rarely qualify as acceptable to a violinist. A desirable property of a violin is therefore how easily a player can make it speak, or, more precisely, the range of bow speed and force on a given instrument which reliably and quickly lead to Helmholtz motion. Manufacturers of instruments, strings, bows and rosin would benefit from the knowledge of how the design of a musical instrument can be made more conducive to the production of Helmholtz motion; players and teachers also stand to benefit from a better understanding of the physics behind ‘correct’ bowing gestures.

Theoretical models have been developed which predict the formation of Helmholtz motion although, crucially, even the most sophisticated models lack the refinement required to predict detailed patterns of transient string vibration. Before one can use these theoretical models to explore the contributing factors to the ease

of production of Helmholtz motion, it is critical that they first be systematically tested against experimental data.

### 2. DESCRIPTION OF BOWING MACHINE

A computer-controlled bowing machine has been built, whose purpose is to redress the lack of experimental validation of theoretical models of the bowed string. In this section, the design of the bowing machine is outlined, with emphasis on its ability to maintain a constant bow force while moving with a constant acceleration.

#### 2.1. Controlling bow force

The task of pushing the bow against the string was initially achieved by attaching the bow to a torque motor, designed to mimic a player’s wrist. However, subsequent efforts to control the bow force were impeded by the inevitable friction in the moving parts of the motor, and a friction-free solution was devised involving the use of a leaf spring and shaker: see Figure 1.

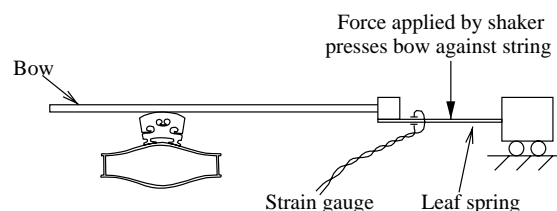


Figure 1: *Schematic diagram of the method used to press the bow against the string. The bow is held in a clamp attached to a leaf spring, which is pressed upon by a shaker; the bow is hence pressed against the string as shown. The strain gauge, measuring bending strain, is used to deduce the magnitude of the bow force.*

The normal force (referred to as ‘bow pressure’ by players) cannot be directly measured, and so it was deduced from the output of a strain gauge, also shown in Figure 1. Bow force was controlled by the following means:

- The required level of bow force was converted into an equivalent quantity of strain.
- Feedback compensation was used to ensure that the strain gauge output equalled that quantity.

The snag of this system is however that the level of strain required to maintain a constant bow force changes as the bow moves (it increases during down-bows and decreases during up-bows); the time delay in the feedback loop thus means that the bow presses into the string too lightly during down-bows and too hard during up-bows. To rectify this problem, the required level of strain was anticipated by  $\Delta$  seconds before being used as input for the feedback compensator, where  $\Delta$  equals the time delay of the controller.

Figure 2 demonstrates the ability of the force controller to hold force constant as the bow accelerates from rest: the bow force is seen to remain within 3% of the demand signal.

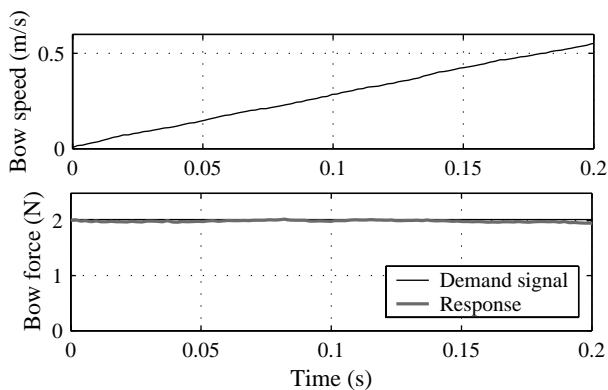


Figure 2: Attempt to hold the bow force (bottom plot) constant while the bow accelerates (top plot). The acceleration used here is  $2.77\text{m/s}^2$ , which is not far from the largest value ever used in the experiments, of  $3.2\text{m/s}^2$ .

## 2.2. Controlling bow speed

The moving parts of the bowing machine were mounted onto a linear motor, which provides a thrust proportional to applied current to move the bow back and forth. A proportional-differential feedback controller was used to determine the applied current, with the position of the bow as the controlled variable. Bow position is controlled rather than bow speed itself, because the force controller described previously requires the current value of position to convert force demand signals to strain demand signals; integrating the output of a velocity transducer or accelerometer for this purpose would lead to low-frequency drift problems.

Position was measured using an optical encoder, whose signal to noise ratio is far superior to analogue alternatives. With the resulting lack of noise in the position signal, the bandwidth of the proportional-differential controller could be made large: the response time of the feedback controller to a change in demand signal is only 0.03 seconds.

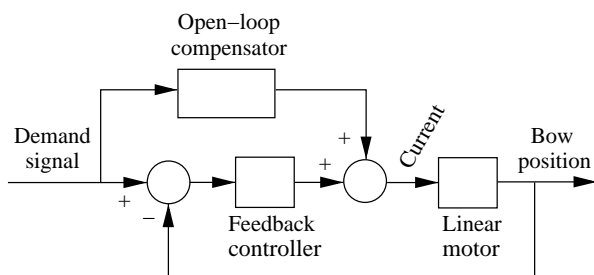


Figure 3: The configuration of the open-loop and feedback compensators used to control the bow speed. ( $u$  is current.)

Although a time delay of 0.03 seconds is already quicker than is possible for a human violinist, an additional open-loop compensator was designed which effectively reduces the time delay to nothing. The open-loop compensator, implemented in parallel with the feedback compensator as shown in Figure 3, outputs an estimate of what the current input to the linear motor should

be based on trial and error tests. The feedback controller itself is only henceforth responsible for compensating for slight errors in the open-loop compensator, and for resisting external disturbances. Figure 2 (top plot) demonstrates the effectiveness of this scheme: bow speed matches the demand signal within  $\pm 0.005\text{m/s}$  at all times.

All controllers were digitally implemented using the dSpace DS1102 floating-point controller board, with a sampling rate of 512Hz. A photograph of the completed bowing machine is shown in Figure 4.

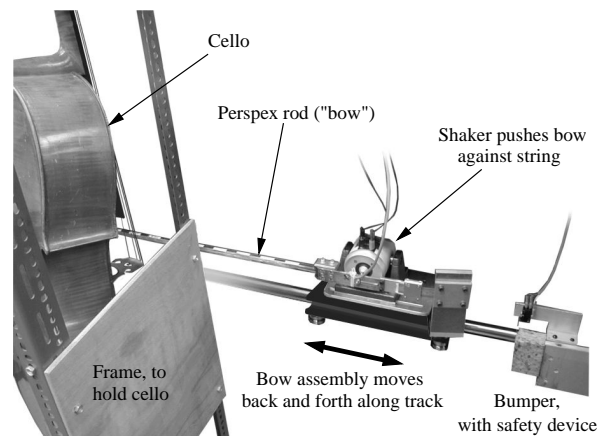


Figure 4: Photograph of apparatus.

## 3. COMPARING EXPERIMENT AND THEORY

Recent simulations of the bowed string may be broadly divided into two classes: those that include the effect of temperature on the tribology of rosin and those that do not. Smith et. al [2] proposed that, during periods of slipping, the rosin layer between the bow and the string may be modelled as a plastically deforming solid, such that the bow/string friction force equals the shear yield strength of rosin multiplied by the area of contact. Noting that rosin is already near its glass-transition temperature at room temperature, Smith proposed that the value of the shear yield strength will fall as its temperature increases. This model of bow/string friction is known as the 'plastic thermal model' of friction, whereas the previous model of friction comprising a single (temperature-independent) curve to describe the dependence of friction coefficient upon relative sliding speed is known as the 'friction curve model'.

Very little experimental evidence exists which can discriminate between these two models. Indeed, there is very little quantitative experimental validation of the use of either friction model in bowed string simulations at all: for example, Schelleng's famous map of regions of Helmholtz motion production on the force-distance plane [3] has never before been experimentally reproduced.

### 3.1. Experimental setup

The bowing machine is capable of playing any member of the stringed instrument family including violins, violas and cellos. The experimental results which follow are generated by bowing a Thomastik 'Dominant' D-string on a full-sized cello using a stiffened perspex rod in place of a bow. A Dominant cello D-string was

used because their torsional and transverse properties have been measured by past researchers [4], and a rod was used in place of a bow because it contacts the string at a single point instead of over a finite width of string – perspex was selected for use because it has similar thermodynamic properties to ordinary horse hair [2].

### 3.2. Bridge-force measurement

The vibration of the string is detected using a piezo-electric force transducer mounted in the bridge of the cello which is sensitive only to the transverse component of string tension, referred to as ‘bridge-force’. Different string vibration waveforms leave characteristic patterns in the bridge-force. Helmholtz motion, for example, causes a “saw-tooth” waveform (as seen in Figure 6, top and bottom); the bridge-force gradually rises as the bow pulls the string during sticking, and then abruptly falls back as the “Helmholtz corner” reflects from the bridge. “Double-slipping” motion is characterized by a “double saw-tooth” waveform; the string now has two travelling corners corresponding to two slips, and each one causes an abrupt drop in bridge-force as it reflects from the bridge. Further details may be found in [5].

### 3.3. Time to Helmholtz motion in the force-acceleration plane

Loosely defining the ‘playability’ of a stringed instrument as the ease with which Helmholtz motion can be created, a measure of playability is the range of bow speeds and forces which a player may choose from which rapidly lead to Helmholtz motion. In this spirit, Guettler [6] conducted a series of computational simulations in which the bow accelerated from rest at rate  $a$  and the bow force  $F$  was held constant, and plotted the time taken to produce Helmholtz motion in the  $F$  vs.  $a$  plane. With short pre-Helmholtz transients indicated using light colors and long pre-Helmholtz transients indicated by dark colors, one may correlate the playability of an instrument with the extent of light-colored area.

Using data from the bridge-force sensor described previously a ‘Guettler diagram’ has been plotted in Figure 5, alongside simulated versions using the two friction models. To ensure an unbiased treatment of all data, the same automatic pattern identification algorithm was used in each vibration transient to identify the occurrence of Helmholtz motion. Figure 5 demonstrates that the friction curve model and the plastic thermal model both predict the formation of Helmholtz motion, although the latter is evidently more successful at predicting when it forms.

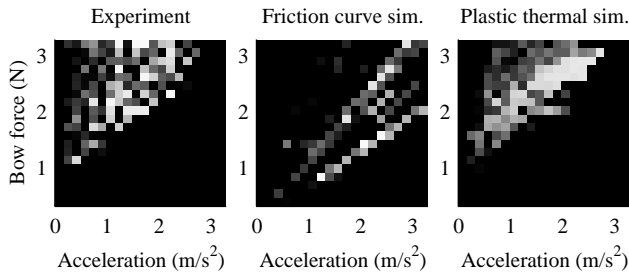


Figure 5: ‘Guettler diagrams’, experimental and simulated. The shade of each pixel denotes the time taken to reach Helmholtz motion; white pixels indicate that Helmholtz motion formed immediately after the first slip and black pixels indicate that Helmholtz motion took twenty or more period lengths to form.

### 3.4. Details of initial transient string vibration

From a diagnostic point of view, a closer look at the transient vibration of the string can be more revealing. Figure 6 shows experimental and simulated bridge-force waveforms, for the case of  $F=2.32\text{N}$ ,  $a=1.394\text{m/s}^2$  and  $\beta=0.08$  (where  $\beta$  is the fractional distance of the bowed point from the bridge). In this case, the friction curve model (middle plot of Figure 6) predicts a rather noisy transient, whereas the plastic thermal model (bottom plot of Figure 6) predicts the formation of Helmholtz motion. The latter is clearly closer to the experimental measurement, although there are still differences around the time of the first slip.

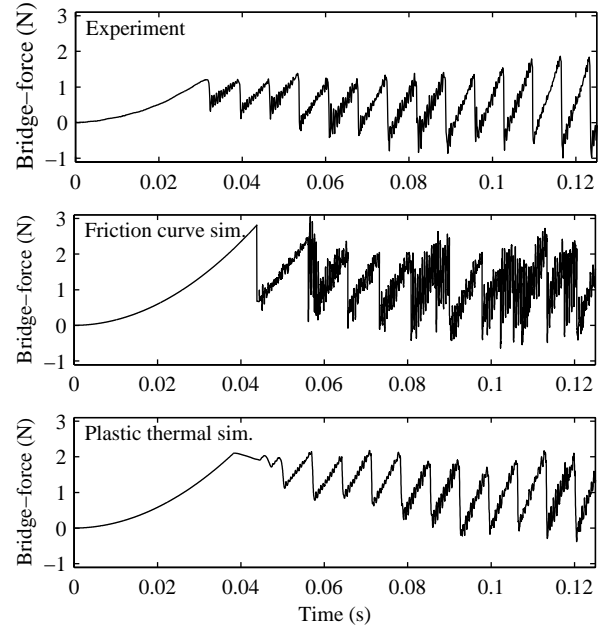


Figure 6: Experimentally measured and simulated bridge-force waveforms, all with  $\beta=0.08$ , acceleration= $1.394\text{m/s}^2$  and bow force= $2.32\text{N}$ . The two simulated transients are based on different models of bow/string contact friction: the middle plot uses the classical ‘friction-curve’ model, and the bottom plot uses the ‘plastic thermal model’ proposed by Smith et. al [2]. Of the two friction models, clearly the latter outperforms the former: not only does the plastic thermal model predict Helmholtz motion (signified by the saw-tooth waveform), it also correctly predicts several details of the secondary waves superimposed on Helmholtz motion; the friction curve model does neither of these things. The most obvious draw-back of the plastic thermal model seen here is the failure of the string to ‘fly back’ immediately after the first slip.

Although this is only a one-off example of the detailed performance of bowed string simulations, it is broadly typical of their behavior: the plastic thermal model frequently captures the essential characteristics of the string vibration despite anomalies around the time of the first slip, whereas the friction curve model is frequently too ‘twitchy’.

### 3.5. Overheating in the thermal model

Although the plastic thermal model for friction is clearly promising, in its current form it fails to capture every nuance of the friction behavior. An example of its shortcomings becomes apparent

at high bow speeds, where the simulated rosin can reach unlikely temperatures of around 100°C. Under these conditions the (simulated) rosin is unable to sustain the friction required for Helmholtz motion, resulting in a bridge-force waveform which is a ‘rounded’ version of the recognizable saw-tooth waveform associated with Helmholtz motion. Such a waveform has never been observed when the same conditions (bow speed, force etc.) are reproduced with the bowing machine; one may therefore conclude that this behavior is not physical. See Figure 7.

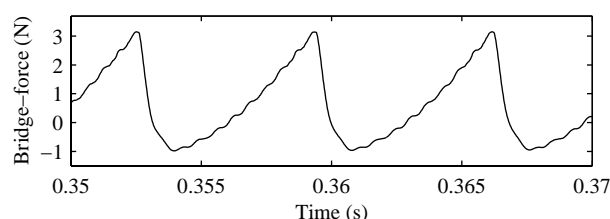


Figure 7: Close-up view of a typical bridge-force waveform from a simulation based on the plastic thermal model in which the rosin has overheated. The bow speed in this case is 0.5m/s, and the waveform has degenerated from the recognizable saw-tooth waveform of Helmholtz motion. This behavior has never been observed in experiment.

#### 4. IMPROVEMENTS TO THE THEORETICAL MODEL

The weakest link in the theoretical model of the bowed string is the description of the friction between bow and string. Both friction models considered here stand to be improved in the light of experimental data, although the options are limited for the friction curve model. One can only hope that, perhaps with the aid of a nonlinear optimization routine, a different  $\mu(v_{sliding})$  relationship might be found which leads to more ‘benign’ behavior. Failing that, any realistic simulations of the bowed string must rely on a thermal model of rosin.

The plastic thermal model for friction, being more complicated than the friction curve model, has much more room for improvement. Several minor alterations seem appropriate on the basis of experimental evidence:

- In the present model, rosin takes too long (typically two cycles) to warm up by frictional heat generation, and as a result the friction coefficient remains very high for too long. Incorporating a fracture model whereby the friction drops whenever slipping starts, thus ensuring a larger initial sliding speed, sufficient heat would be generated to rapidly raise the rosin temperature and accelerate the drop in friction. Such a model has been tested, with the results shown in Figure 8.
- The thermodynamic model of rosin proposed by Smith et. al [2] predicts that the rosin takes several seconds to cool back down to near ambient temperature following a bowing gesture. It is possible therefore that the rosin used in the experiment had itself not cooled to room temperature; the measurement shown in the top plot of Figure 6 was taken only twelve seconds after a similar previous measurement. As such, it may be appropriate to start simulations from a higher temperature. This too has been tested; the bridge-force transient shown in Figure 8 starts with the rosin already around 6°C above ambient at the time of the first slip.

- The bridge-force at the time of the first slip, and hence the limiting value of static friction coefficient, is too large, and should be decreased. This may be corrected by lowering the value assumed in simulations for the shear yield strength of rosin at low temperatures.
- Overheating, as in Figure 7, could be readily avoided by lowering the friction coefficient at large temperatures. This physically plausible modification would suppress heat generation, and hence further temperature rise, at high temperatures.
- Recent evidence suggests that, during nominal sticking periods, rosin tends to creep. This is slightly visible in the top plot of Figure 6 where the bridge-force, before the first slip, is slightly less than the parabola that it would follow if uniformly accelerating. Accommodating creep in the simulation is straightforward.

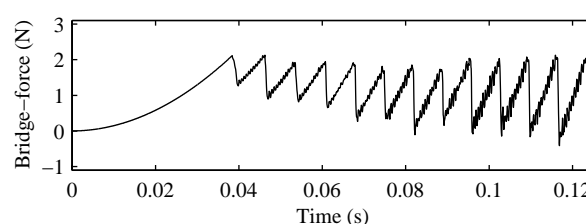


Figure 8: Same as Figure 6, but with the plastic thermal model modified to include a fracture strength and with the simulations started from slightly above ambient temperature. The drop in bridge-force at the first slip seen here represents an improvement in the realism of the simulation model.

#### 5. CONCLUSIONS

An automatic bowing machine has been constructed which can accurately control the speed and force of a bow. Initial measurements of transient string vibration have been presented which, when compared with simulated equivalents, already provide many useful clues as to the accuracy of bowed string simulations.

A number of methods for improving the simulation model have been suggested, although there are several other logical modifications that one might make besides these. Work is in progress to establish a definitive theoretical description of the bowed string, and it is intended that this model will play a major part in future investigations into the playability of stringed instruments.

#### 6. REFERENCES

- [1] Galluzzo, P. M., “Helmholtz motion”, [http://www2.eng.cam.ac.uk/~pmg26/hpage/Helm\\_motion.html](http://www2.eng.cam.ac.uk/~pmg26/hpage/Helm_motion.html), 2003.
- [2] Smith, J. and Woodhouse, J., “The tribology of rosin”, *J. Mech. Phys. Solids*, Vol. 48, pp. 1633-1681, 2000.
- [3] Schelleng, J. C., “The bowed string and the player”, *J. Acoust. Soc. Am.*, Vol. 53, pp. 26-41, 1973.
- [4] Woodhouse, J. and Loach, A. R., “Torsional behaviour of cello strings”, *Acustica*, Vol. 85, pp. 734-740, 1999.
- [5] Woodhouse, J., “Bowed string simulation using a thermal friction model”, *Acustica*, Vol. 89, pp. 355-368, 2003.
- [6] Guettler, K., “On the creation of Helmholtz motion in bowed strings”, *Acustica*, Vol. 88, pp. 970-985, 2002.

## PSYCHOACOUSTIC INVESTIGATIONS ON THE POSSIBILITY OF AURALLY IDENTICAL VIOLINS

*Paul Geissler<sup>1)</sup>, Otto Martner<sup>1)</sup>, Carsten Zerbs<sup>1)</sup>, Martin Schleske<sup>2)</sup>*

<sup>1)</sup>Müller-BBM GmbH, Planegg near Munich, Germany

<sup>2)</sup>Meisteratelier für Geigenbau, Munich, Germany

PGeissler@MuellerBBM.de

### ABSTRACT

“Is it possible to make sound copies of violins?” To answer this question one needs to know the ingredients which make two violins judged by musicians to be aurally identical. Using a questionnaire among 54 musicians verbal attributes related to sound quality characteristics of violins were collected and ranked. Subjective listening tests were carried out to check which verbal attributes are suitable and do evoke the same meaning in different persons. Useful attributes for the ranking could be found using statistical measures for consistency and concordance. Additionally, it was found that the measurement uncertainty of frequency response measurements today is smaller than the analysis resolution of the human ear in regard to frequency and amplitude in the frequency range important for the hearing sensation and for room acoustic situations typical for a violin maker’s workshop. The results give strong indications that the psychoacoustics characteristics of the human ear and the vibroacoustic characteristics of the violin body in combination with the attributes judged to be important for violin sound quality will in principle allow for the idea of making sound copies of a given violin.

### 1. INTRODUCTION

#### 1.1. What are sound copies?

Professional musicians sometimes use the sound quality characteristics of a given instrument as a reference and asks the violin maker “Can you make me a violin that sounds like this instrument?”. To be even more precise: if the customer holds, say one of the famous old Italian violins in his hand, the question would be “Can you make me a new violin that sounds like this masterpiece in my hand?”

The focus is on the verb “sound”. A violin maker learns how to make geometrical copies of masterpieces. This is certainly useful to get a violin body to start with. Of course, due to the differences in the wood material the geometrical copies do in general not sound like the masterpieces.

But if a violin maker is able to build with up-to-date wood material a new violin whose modal characteristics, the eigenfrequencies, damping factors and mode shapes, are identical to the modal characteristics of the reference violin with its old wood material, it should in principle be possible. If the modal identity can be attained, one could expect that the copy also has the same radiation characteristics as the reference violin and hence - for

the same listener in the same room - the same hearing impression for both instruments. This concept of modal copies or “tonal copies” has recently been tackled by Schleske [1].

#### 1.2. Can the procedure be simplified?

How accurate must these modal copies be built? Are differences between the modal characteristics of the copy and the reference violin allowed? Taking into account the finite resolution of the human hearing perception and the always present statistical fluctuations in the reverberant sound field of a room one could imagine that the copying procedure can eventually be simplified, if only the differences between copy and reference violin are smaller than the audible differences.

It should also be noted that the question which is formulated here for violins is a fundamental question in sound quality investigations of other products and services as well. The ability to evaluate if two physically not 100% identical products do evoke the same hearing impression for potential customers is the basis for product sound design. Telephone and broadcasting are two branches where simplification procedures based on the human hearing perception have been investigated and applied successfully.

#### 1.3. Acknowledgements

The results of this paper are based on work carried out within the research project „Material investigations and advanced methods of production and quality control of bowed instruments“ (VIOLIN) funded by the European community under contract BRST-CT98-5465. The project was structured into different working groups. The „Meisteratelier für Geigenbau Martin Schleske“ and the company „Müller-BBM“ formed the working group „sound“.

The team members of the working group “sound” thank Helmut A. Müller for help, comments and fruitful discussions.

### 2. QUALITY ATTRIBUTES

#### 2.1. Questionnaire

The musician’s evaluation of a violin is based on a number of perceived sensations and attributes. The sound received at his ears is one of the most important criteria but there are also additional criteria such as playability, reaction of the instrument and others. The interests of the musician certainly play a role,

too. Beginners tend to weigh attributes such as playability and reaction much higher than professional musicians. The professional musician usually is much more interested in the sound because he is able to fully control the instrument at hand.

As a first step psychoacoustic investigations were carried out to find out relevant attributes used by musicians for the evaluation of the sound of a violin.

A questionnaire asking for relevant acoustic attributes of violins and the attribute's ranking was designed. The questionnaire was mailed to about 100 musicians in Germany. 54 musicians (26 female, 28 male) sent answers. The musicians were asked: "Please list attributes you would choose to evaluate a violin in respect to sound and playability" and "Please rank the above attributes according to the importance that you personally give them".

For analysis the more than 70 different attributes (or attribute pairs) were grouped empirically into different general features. For example the attributes *bright/dark* (hell/dunkel), *warm/cold* (warm/kalt) or *round/soft* (rund/weich) were grouped to the general feature *timbre* (Klangfarbe), while attributes such as *easy/difficult* (leicht/schwer) or *direct* (direkt) were grouped to the general feature *reaction* (Ansprache). A weight of 1 was assigned to the attribute ranked highest, the second rank was given a weight of  $\frac{1}{2}$  and so on.

## 2.2. Results of the questionnaire analysis

The final result of the analysis, together with some interpretation concerning the correlated physical response quantity, is shown in table 1.

feature	%	physical response quantities correlated
timbre	38	spectral distribution of frequency response
reaction	19	coupling between player and violin
sustain	13	coupling between violin and room
balance	11	balance of spectral distribution
loudness	9	energy of frequency response
modulation	7	dynamic range of frequency response
others	3	colour, optics and other attributes

Table 1: Features, physical meaning and percentile contribution.

The results show that *timbre* with a contribution of 38% together with the 11% contribution of *balance* (Ausgeglichenheit) of timbre are judged by musicians to be the most important criteria for sound quality. *Loudness* (Lautstärke) contributes only 9%. Of nearly equal importance is *modulation* (Modulierbarkeit) with 7% contribution: a feature that stands for the variability of the timbre and a large dynamical range between forte and piano playing, with the piano passages still markedly above the "operational noise floor" given by the mere bow/string interaction. It is believed that all these features are closely related to the structural dynamic characteristics of the violin itself. These features make a total of 66% of the sound quality features.

*Sustain* (Tragfähigkeit) is judged to be important as well (13%). It is assumed that this feature is related to the coupling between the violin and the room acoustical situation. One could also argue, however, that sustain is for a given room a feature

linked with the power of the violin itself. In this case nearly 80% of the features refer to sound quality characteristics of the violin.

A very important feature is *reaction* which is not a pure listening criterion but takes the feedback of the instrument on the player's action into account. However, this feature is in parts also related to the modal characteristics of the violin. "Other" features (3%) were mostly optical attributes.

The results show that the majority of the selected quality attributes refer to variables linked with frequency response functions. An example relevant in this context is the frequency response function that relates the sound pressure at the listener's ear to the force at the bridge in bowing direction.

It is important to recognize that there are today psychoacoustic models that allow us to calculate from the measured or calculated sound pressure as a physical quantity psychoacoustic quantities that relate to the various aspects of the hearing perception. For example, for the evaluation of the loudness one has the models of Moore [2] or Zwicker [3], for the evaluation of timbre one has models of Benedini [4] and v. Bismarck [5],[6].

Knowing that we can calculate and evaluate the attributes related to the relevant hearing perception once we know the sound pressure at the ear, it is useful to investigate into the scaling of psychoacoustical criteria and into consequences for the determination of frequency response functions during the violin making.

## 3. LISTENING TEST

### 3.1. Setup

Based on the results of the questionnaire a listening test was developed and carried out. Because the main interest here was methodological, the listening test was carried out with only 3 female and 7 male test persons, aged between 30 and 45. It was executed as a complete paired comparison test.

For the listening test the attributes *bright* (hell), *nasal* (nasal), *pleasant* (angenehm), *reaction* (Ansprache), *balanced* (ausgeglichen), *colourful* (farbenreich) and *passionate* (leidenschaftlich) were selected because they were typical for the different features of the questionnaire analysis.

For each of the selected attributes a characteristic sound example was recorded. Sound recordings of 8 different violins played by 2 different professional musicians were made. The binaural recordings were made with an artificial head system. They encompassed short pieces from violin compositions, scales and tones. Using an audio editor short sequences were compiled from these recordings. A time period of 5 seconds duration of this sound was prepared for all eight violins (played by the same musician).

The consistency of the decisions of the listeners was checked. The results showed the difficulties to assess the attributes selected. It was further analysed how the test persons ranked the instruments for all the attributes of interest. As a measure of the concordance between the judgements of different test persons the concordance coefficient [11] was determined. It was found that the concordance coefficient in the ranking was relatively high for the attributes *pleasant* and *reaction*, medium for *bright* and *balanced* and relatively low for *nasal*, *colourful* and *passionate*.

Not all values were found to be significant on a level of at least 5%, i. e. with an hypothesis error probability  $\alpha < 5\%$ .

Table 2 shows the concordance coefficient for all test persons and for those with consistent answers.

attributes	$W_a$	$\alpha_a$ (%)	$W_c$	$\alpha_c$ (%)
bright	0.3	0.5	0.5	3.5
nasal	0.2	8.5	0.1	> 40
pleasant	0.7	$\approx 0$	0.7	$\approx 0$
reaction	0.7	$\approx 0$	0.7	$\approx 0$
balanced	0.2	20	0.5	3.0
colourful	0.2	4.5	0.3	> 40
passionate	0.3	1.5	0.7	20

Table 2: Values (rounded to one significant digit) for the concordance coefficient  $W_a$  for all test persons and  $W_c$  for consistently answering test persons (6 or less circular triples, with the exception for passionate: 9 or less circular triples) and values for the hypothesis error probability  $\alpha_a$  and  $\alpha_c$ , respectively [11].

The results show that the attributes *pleasant* and *reaction* are rated approximately equal among the test persons. For these attributes the understanding of what pleasant or (good) reaction means was equal among the test persons. On the other hand for *colourful* or *nasal* the value is lower: obviously the understanding of these attributes is different among the different test persons or the test persons had no clear image about these attributes.

For the scaling of the ranking evaluation the BTL-method [12] was chosen. The scale values were on an interval scale with an arbitrary reference value. The reference value was set to 0.0.

The results for the BTL-scale based upon the consistent decisions is shown in the following table 3 and figure 1.

violin	bright	nasal	pleasant	reaction	balanced	colourful	passionate
no. 1	0.7	0.30	3.0	3.0	0.9	0.6	0.3
no. 2	0.0	0.0	2.8	3.5	2.0	1.5	0.6
no. 3	1.8	0.3	2.0	1.0	2.8	1.4	0.0
no. 4	2.0	0.5	0.0	1.9	1.6	0.0	0.6
no. 5	2.0	1.0	1.2	2.4	2.2	1.1	0.6
no. 6	1.1	0.7	0.7	1.8	1.2	1.2	1.2
no. 7	2.3	0.1	0.7	0.4	1.3	1.4	0.7
no. 8	2.1	1.5	2.6	0.0	0.0	0.0	1.7

Table 3: BTL – scaling values, calculated from the cumulated preference frequency of the consistently answering test persons.

According to table 3 violin no. 1 is not particularly bright (0.67) but sounds very pleasant (2.96) and has a good reaction (2.96). On the other hand violin no. 7 is ranked to be very bright (2.34) but ranked low for pleasant (0.69) and reaction (0.44).

Table 3 also shows that the violins in the test have no significant difference in the ranking concerning the attribute nasal.

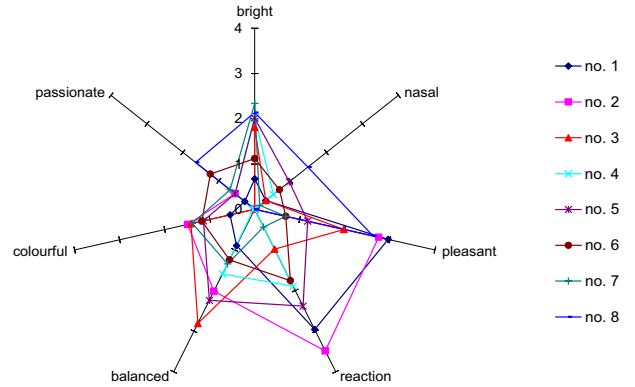


Figure 1: BTL-scaling values of consistently answering test persons for violin no. 1 to 8.

The results are to be interpreted from a methodological perspective. They show that one can find attributes like *pleasant*, *reaction*, *bright* and *balanced* that do evoke approximately the same meaning within different persons. They are obviously not only important but can additionally be used for scaling and ranking of the sound quality of different violins, whereas attributes like *passionate*, *colourful* or *nasal* evoke a different understanding in different persons. They can not be properly scaled properly and should therefore be omitted for the ranking of violins.

#### 4. FREQUENCY RESPONSE FUNCTIONS

The above results show that the majority of features is implicitly described by the frequency response characteristics of a violin, measured e. g. as the frequency response function of the sound pressure at a specific point in the room (e. g. at the listener's ear) related to the force input at the bridge in bowing direction. Conceptually such a frequency response function can be subdivided into the structural frequency response functions of the acceleration or velocity of various points on the violin body in normal direction related to the force input at the bridge, and the vibroacoustic frequency response functions of the sound pressure at the specific point in the room related to the accelerations or velocities at the violin body.

How accurate must the frequency response characteristics of the copy meet those of the reference? It is known that the sound pressure frequency response level of a room, when it is excited by a sinusoidal sweep, shows irregularities due to the overlap of the modes and phases. Cremer and Müller [10] showed, based on results from Kuttruf and Thiele [8] and Schröder [9] that the number of level maxima  $n_R$  in a given frequency band  $\Delta f$  can be written as

$$n_R = \frac{T}{6.7} \Delta f \quad (1)$$

with  $T$  being the reverberation time of the room.

From this result one can estimate the number of level maxima in the 1/12-octave centred around a half-tone  $f_H$ ,  $n_{RH}$ , to be approximately  $n_{RH} \approx 0.009 \cdot T f_H$ .



In a concert hall with a typical reverberation time of 2 s this results approximately in 4 level maxima for the band around the lowest tone of a violin (G3,  $f_H \approx 200$  Hz) and 115 level maxima for the band around the highest tone, five octaves above the lowest tone, (G8,  $f_H \approx 6400$  Hz). For a reverberation time of 0.5 s – which is typical for a small living room or a violin maker's workshop – one would have about 1 level maximum per half-tone at 200 Hz and about 29 maxima per half-tone at 6400 Hz.

A violin has typically only 1 mode, the so-called Helmholtz-resonance, in the frequency range 200 Hz to 400 Hz. The number of level maxima per half-tone for a violin,  $n_{VH}$ , in this frequency range can be estimated from the above result to be approximately  $n_{VH} \approx 0.0003 \cdot f_H$ . For 400 Hz this number is 0.12. It is considerably smaller than the number of level maxima for a room. Therefore it is important to match the Helmholtz-resonance of the copy exactly to the Helmholtz-resonance of the reference violin.

For frequencies between 400 Hz and 800 Hz one usually observes 2 to 4 modes in frequency response curves of sound radiated from violins. For 4 modes the number of level maxima per half-tone would be  $n_{VH} \approx 0.0006 \cdot f_H$ . For 800 Hz one would calculate the number of level maxima per half-tone to be roughly 0.5, which is still smaller than the equivalent number for rooms. The exact matching of eigenfrequencies in the copy is important in this frequency range, too.

The exact matching of eigenfrequencies becomes less important, however, when  $n_{VH} \geq 1$ , i. e. when there is at least one mode in the violin body per half-tone. Estimates based on the modal density of a 5 mm flat plate indicate that this happens at about 1500 Hz. Woodhouse reports similar results based on estimates of modal overlap factors [13], and observations from mobility measurements show that the transition frequency where  $n_{RH} \geq 1$  can be even lower. Above approximately 1500 Hz the exact matching of single modes is not very important as long as the overall modal density and damping are preserved.

The limits in the resolution of human hearing can be stated by the so-called just-noticeable sound changes. Data for just-noticeable sound changes vary to a certain extent between different authors. In [7] it is stated that the just-noticeable relative frequency difference for pure tones between the 500 Hz and 2000 Hz octave presented to a listener for 500 ms or longer is roughly  $0.002 \times \text{frequency}$ , i. e. about 2 Hz around 1000 Hz. For octaves below 500 Hz and above 2000 Hz these values are larger. Also, for a shorter duration of the tone presentation – which is likely when one evaluates the sound quality of different violins – these differences increase and are for a duration of 10 ms approximately 10 times higher than the values stated above, i. e. 20 Hz around 1000 Hz. Concerning the sound level it is stated that the just-noticeable level difference for white noise is about 0.5 dB for levels above 25 dB.

With an optimised measurement procedure, using a hammer pendulum system, one is able to measure frequency response functions, including the radiated sound pressure, up to 3 kHz with an uncertainty of 0.5 dB (and from 3 kHz to 10 kHz with an uncertainty of 2 dB). The frequency resolution is typically dependent upon the measurement time but can be selected so that the frequency resolution is smaller than the above mentioned just-noticeable changes.

## 5. CONCLUSIONS

It was shown that there are sound quality features of violins that are relevant for musicians and do evoke similar perceptions in different listeners. These features can be scaled and used for consistent sound quality ranking of violins. The features can be analysed from measured frequency response functions using psychoacoustic models. For frequencies below 1500 Hz the modal characteristics of the “tonal copy” and the reference violin must be identical or very similar. For higher frequencies the average modal density and damping must be preserved. The uncertainty of the frequency response measurement is smaller than the just-noticeable changes of our hearing perception. Thus a violin maker can in principle measure the modal characteristics of the copy for the final instrument and during the working progress and evaluate if the sound quality is already “near enough” – i. e. aurally indistinguishable – to the reference violin.

## 6. REFERENCES

- [1] Schleske, M., “Empirical tools in contemporary violin making: Part I. Analysis of design, materials, varnish and normal modes”, *J. Catgut Acoust. Soc.*, vol. 4, no. 5 (Series II), p. 50-64, 2002.
- [2] Moore, B. C. J., Glasberg, B. R., Baer, T., “A model for the prediction of thresholds, loudness and partial loudness”, *J. Audio Eng. Soc.* 45, 1997.
- [3] Zwicker, E., “A program for calculating loudness according to DIN 45631 (ISO 532 B)”, *J. Acoust. Soc. Japan (E)*, 12, p. 39-42, 1991.
- [4] Benedini, K., “Ein Funktionsmodell zur Beschreibung von Klangfarbenunterschieden”, *Biol. Cybernetics* 34, p. 111-117, 1979.
- [5] v. Bismarck, G., “Timbre of steady sound. A factorial investigation of its verbal attributes”, *Acustica* 30, p. 146-159, 1974.
- [6] v. Bismarck, G., “Sharpness as an attribute of the timbre of steady sounds”, *Acustica* 30, p. 159-172, 1974.
- [7] Zwicker, E., Fastl, H., *Psychoacoustics - Facts and Models*, 2nd revised edition, Berlin, 1999.
- [8] Kuttruff, H., Thiele, R., “Über die Frequenzabhängigkeit des Schalldrucks in Räumen”, *Acustica* 4, p. 614, 1954.
- [9] Schröder, M., “Die statistischen Parameter der Frequenzkurven von großen Räumen”, *Acustica* 4, p. 594, 1954.
- [10] Cremer, L., Müller, H. A., *Die wissenschaftlichen Grundlagen der Raumakustik, Band II, Teil 4, Wellentheoretische Raumakustik*, 2. Auflage, Stuttgart, 1976.
- [11] Bortz, J., Lienert, G. A., Böhnke, K., *Verteilungsfreie Verfahren in der Biostatistik*, Berlin, 2. Auflage, 2000.
- [12] Bradley, R. A., Terry, M. E., “Rank analysis of incomplete block design. I. The method of paired comparison.” *Biometrika*, Vol. 39, p. 324-345, 1952.
- [13] Woodhouse, J., “Body vibration of the violin – what can a maker expect to control?”, *J. Catgut Acoust. Soc.*, vol. 4, no. 5 (Series II), p. 43-49, 2002.

## THE INFLUENCE OF VIBRATO AND NOISE ON THE ASSESSMENT OF VIOLIN TONE

*Colin E. Gough*

School of Physics and Astronomy  
University of Birmingham, B15 2TT, UK

c.gough@bham.ac.uk

### ABSTRACT

We investigate the influence of vibrato and noise on the perception of the tonal quality of a violin in two ways. First, we consider recorded sound of both high and poor quality violins. By continuous repetition of single period waveforms, we remove the frequency, amplitude and noise fluctuations introduced by the performer playing the instrument, whilst retaining the sampled spectral information relating to the resonances of the particular instrument being played. Audio demonstrations underline the importance of the fluctuations in frequency, amplitude and spectral timbre as identifying the sound as that of a violin. We argue that, since such fluctuations are important in identifying the instrument as a violin rather than any other instrument, then such fluctuations must be equally important in any subjective assessment of the quality of tone of individual violins.

To investigate such correlations, we have developed computational models, which enable the listener to judge the importance of vibrato amplitude and modulation frequency on a “virtual” instrument with multi-resonant modes similar to those of a real violin. In particular, we demonstrate how the influence of vibrato depends on the Q-values and density of the structural resonances excited.

Such factors are clearly global characteristics of the violin that are closely related to the “quality” of the wood used in a violin’s construction and the skill of the luthier in adjusting the thickness of the plates to accommodate differences in the properties of the woods used in an instrument’s construction. The addition of stochastic bowing noise, which is filtered by the multi-resonant spectrum of the violin body is also shown to be an important “global” contribution to the quality of the sound produced by a particular instrument.

### 1. INTRODUCTION

The waveform and spectral content of the sound produced by the bowed violin varies widely from one note to the next, and even within a single note when played with even a small amount of vibrato. Nevertheless, the tone of an individual violin as judged by player and listener alike can appear to be remarkably uniform.

This suggests there must be global factors that do not change from note to note, which define the quality of a particular instrument, as emphasised by Benade amongst others.

The exact placing of body resonances, fingerboard, tailpiece and higher order air modes, etc. cannot therefore be important in determining the quality of an instrument over its whole playing range, though it may well affect the quality of particular notes, such as the wolf-note on a cello or violin.

Furthermore, we listen to violins played in a room or concert hall, which adds its own signature to the overall sound spectrum of the perceived sound. Feedback from the room acoustics can certainly affect the quality of sound produced by the player. However, a good instrument still sounds like a good instrument, just as an individual’s voice is instantly recognised, whatever the room acoustic. As Woodehouse[1] has noted, the use of the precedence effect in recognising initial transients is almost certainly an important factor in the identification of instruments (and voices) and their quality assessment, which largely circumvents problems from room acoustics. The same arguments are probably valid true for the recognition of fluctuations in the sound of a continuously played note.

Weinreich[2] has recently argued the importance of the binaural perception of the sound of a violin, with variations in spectral content associated from small movements of the player and listener’s head arising from the large differences in directivity of the sound radiated by different structural resonances. However, a fine violin still sounds like a fine instrument on a mono-recording listened to with a single monaural headphone. Although the spatial dependence of the sound produced by a violin may well be an important factor in determining the difference between a really fine violin sound and simply a good sound, just as it is in determining the quality of sound in a concert hall, it cannot be the determining factor in the differentiating the sound of a violin from any other instrument.

Although, it is well known that recognition of any musical instrument is strongly influenced by the starting transients, the sound still sounds like a violin when the initial transients are removed and the steady state tone is allowed to build up smoothly from zero. However, within the steady tone, there are inevitable fluctuations from the stochastic noise always present in the bowing mechanism and in the ubiquitous use of vibrato by the modern international soloist. Indeed, when one listens critically to the quality of sound produced by a great player, one cannot

escape recognizing the enormous influence that vibrato has on the quality of the sound produced. The response of violin to the use of vibrato is almost certainly a major characteristic of importance to the performing artist in choosing an instrument. Even the most idealistic players of the baroque violin, for whom the use of any vibrato can be anathema, cannot escape small amounts of frequency and amplitude modulation in the sound they produce. This inevitably tells the listener they are playing a violin rather than, say, a wind instrument. Vibrato is very important in the concert hall, because the continuous variation of sound attracts the attention of the ear and allows an instrument to be heard over the rather blander “chorus” sound of the rest of the string section.

In this paper, we demonstrate that the frequency and amplitude fluctuations produced on a normally played instrument are essential factors in defining the sound of a violin and hence, we argue, the ultimate quality of a particular instrument. We demonstrate that the sound of a repetitively sounded single waveform of a continuously bowed tone of a great instruments played by a concert artist has none of the characteristics that we might identify with that of a violin. The sound produced by such a model is clearly identical to the simple physicist’s model of the violin as a multi-resonant structure excited at the bridge by a saw-tooth waveform. However, the sound produced has none of the characteristics of a real violin. The sound is indistinguishable from that produced by a frequency synthesiser or from the continuously repeated waveforms of quite different instruments.

We therefore argue that it has to be the fluctuations in amplitude, frequency and spectral content, when the instrument is played by a real performer rather than when excited artificially by, say, an electromechanical driver, that define the sound of a violin. If such fluctuations characterise the sound of a violin, it follows that they must also be important in determining the quality of individual instruments. Such fluctuations may therefore be a major “global” factor in determining violin quality.

In addition to the fluctuations in sound from the use of vibrato, the finite width of the bow hairs and resultant variations in the “sticking point” in the slip stick mechanisms, give rise to a random noise, superimposed on any regular saw-tooth force on the bridge (McIntyre, Schumacher and Woodehouse[3]). This noise is broad band and gives rise to a noise spectrum in the radiated sound that reflects the characteristic response of the violin. One would not expect this noise to vary significantly from note to note. Indeed, it is possible that this noise contributes to the “husky, velvety” quality of many early “Italian” instruments admired by both chamber musicians and soloists alike, rather than the rather “bright and solid” sound of, say, a typical nineteenth century French instrument.

In this paper, we present an account of some preliminary measurements on fluctuations of amplitude and noise using both both real and computer synthesised instruments. The ultimate aim of this research is to assess the importance of vibrato,

spectral content and noise in defining “violin sound” and the perceived quality of individual instruments.

## 2. VIBRATO

The use of vibrato, the cyclic variation in pitch of a note by rolling the finger backwards and forwards about its stopped position on the string, is a very important aspect of modern violin technique. It adds “warmth” and carrying power to the sound. We will argue that the response of a violin to the use of vibrato that is one of the key factors in the performer’s perception of the “responsiveness” of a particular instrument.

An example of this is illustrated in Figure 1, which shows the envelope, waveforms and spectral content of a note of perceived “amazing, wonderful, vibrant and amazing tone” taken from a BBC recording of Tasmin Little playing the exceptionally fine Stradivarius violin played by Milstein (Gough[4]). In addition to the cyclic variations in pitch associated with the use of a large amplitude vibrato, there are even more dramatic cyclic changes in amplitude, waveform and spectral content. It is quite clear from the complete recording, in which the performer kept coming back to this note with the largest cyclic changes, that the response of the violin to the use of vibrator was a major factor in determining both the player’s and listener’s perception of its tone quality.

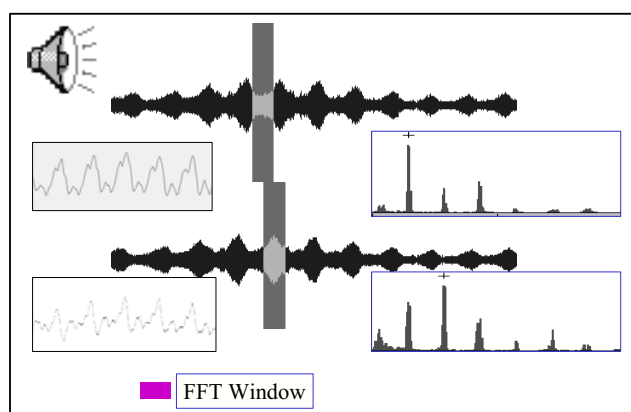


Figure 1: *Vibrato modulation*

. Envelope and sections of the wave form and associated spectra of Milstein’s Stradivarius violin played by an international soloist on the note D (~300 Hz) on the g-string illustrating the marked influence of the use of vibrato on both waveforms and spectra within an individual bowed note.

The large variations in amplitude on a violin that accompany the cyclic changes in pitch was recognised long ago by Matthews [5] and Meyer[6] amongst others. A recent detailed investigation of such effects with both computer simulations and listener perception tests has been reported by Mellody and Wakefield[7]. Psychoacoustic research has shown

that the ear is much more sensitive to fluctuations in amplitude than to fluctuation in pitch (see Moore[8]). This is easily demonstrated by synthesising amplitude and frequency modulated tones by mixing in equal amplitude side bands in phase and in phase-quadrature respectively. Contrary to what most players and listeners believe, it is amplitude and spectral variations rather than frequency variations that are most important in the perception of notes played with vibrato.

The amplitude variations are easily understood in terms of the usual model of sound production by the bowed violin. This produces a saw-tooth waveform force at the bridge with equally spaced harmonic components  $f_n$  with amplitudes decreasing as  $1/f_n$ . This force excites the various structural resonances of the instruments. After taking their radiation patterns into account, the spectral content of the sound produced varies wildly from one harmonic to the next depending on its proximity of a particular harmonic to nearby coupled structural resonances. Vibrato changes the frequency of all the harmonics by the same fraction value. The amplitudes of each individual component will therefore increase and fall as the frequency crosses individual resonances, reflecting the strong peaks and troughs in the frequency response of an individual instrument. This leads to changes in amplitudes of individual harmonics and the overall spectral content in the sound produced, as illustrated in Figure 1.

We can use such data to assess the relative importance of the vibrato in assessment of the tone quality of an instrument. We have based our preliminary investigations on a recording of Perlmann playing the opening sections of the Max Bruch concerto, which conveniently covers a wide range of solo notes on the violin. The individual notes all show strong amplitude and spectral variations arising from the use of vibrato and even notes played on the lowest open-G show significant amplitude fluctuations within the note.

Individual waveforms of one period length are extracted from the recording at the peaks and troughs in amplitude of individual notes sampled well away from their starting transient. When such waveforms are played repetitively, they have none of the characteristics of a violin sound. However, when the different waveforms at the two limits of the vibrato are first modulated by a sine and cosine wave at a chosen vibrato frequency and then added to simulate the affect of vibrato, the sound is much more realistic. The influence of vibrato speed and amplitude of spectral modulation can be investigated by taking the two "beating waveforms", adjusting their repetition frequency to the mid-frequency and adding them together. This centre-frequency signal can then be mixed with varying amounts of the sinusoidally modulated extreme waveforms to produce a note with a controlled amount of spectral modulation. The affects of "turning" on the vibrato by controlled amounts can then be assessed.

The addition of vibrato changes the sound from that of a crude synthesiser to something approaching that of a violin. In practice, the amplitude of the variations in amplitude and spectral content associated with the use of vibrato will vary with the "peakiness" of the instrument's frequency response. The amplitudes will be governed by both the density of resonant

states and their quality factors. The larger the Q-factor of the resonances, the larger will be the amplitude and spectral variations, which we argue are important factors in determining the tone of an instrument. The perceived tonal quality of an instrument will therefore depend on two important global factors - the tonal quality (Q-factor) of the wood used in the construction of the violin and its detailed mechanical structure determining the density of resonant states. Neither of factors will surprise the skilled luthier. However, it does suggest that it is these factors, rather than the placing of individual resonances (particularly at the higher frequencies), that largely determine the overall quality of an instrument.

Although the above model goes some way towards simulating a more realistic violin sound, it is deficient in two major respects. It assumes a sinusoidal variation in the spectral content from one waveform to the other and it fails to include the stochastic variations from the bowing action, which leads to both noise and frequency fluctuations.

In practice, the modulation of individual harmonic components are uncorrelated, with some harmonics rising while other fall. A more realistic model assumes a saw-tooth waveform at the bridge, varying cyclically in frequency with vibrato, and treats the sound output from each harmonic component separately. In such an analysis, it is important to consider the dynamics of the shock excited resonances, not simply their steady state response. An alternative procedure, which we are currently investigating, uses the recorded sound from tap-tones at the bridge (the impulse response) in combination with computer simulated sawtooth waveforms to simulate the real sound of violins. The logical extension of this procedure would be to use recorded forces at the bridge on, say, an electronic violin or a particular instrument, when played in the normal way with vibrato. This could then be used with the recorded acoustic impulse response of other instruments to synthesise the sound that they produce under identical recording conditions.

### 3. NOISE

As McIntyre et al [9] have shown, stochastic variations in the slip-stick mechanism on the bowed string results in wide band-noise in the force at the bridge, and hence wide-band noise in the sound produced by an instrument. The radiated sound will be wide-band but modulated by the spectral response of the instrument. Even though the noise is typically around 40 dB lower intensity than the individual harmonics of the bowed string, it is distributed over the whole frequency range. The integrated noise power is therefore quite significant, so that such noise can easily be distinguished in the sound of the violin. In listener tests, Mellody and Wakefield[7] have shown that the inclusion of noise is an important factor in giving verisimilitude to the sound of a synthesised violin sound even when the affects of vibrato are taken into account. As the spectrum of the noise reflects the overall spectral response of the individual violin, this may be yet another global factor that enables the ear to distinguish one violin from another.

Figure 2 shows the sound spectra from the open-G string played at relatively large amplitude on a Vuillaume violin with and without a soft rubber mute placed on the bridge. The spectral amplitude is plotted on a logarithmic scale with the noise providing a rather broad platform (due to the expected fluctuations of the fluctuation spectrum at individual frequencies).

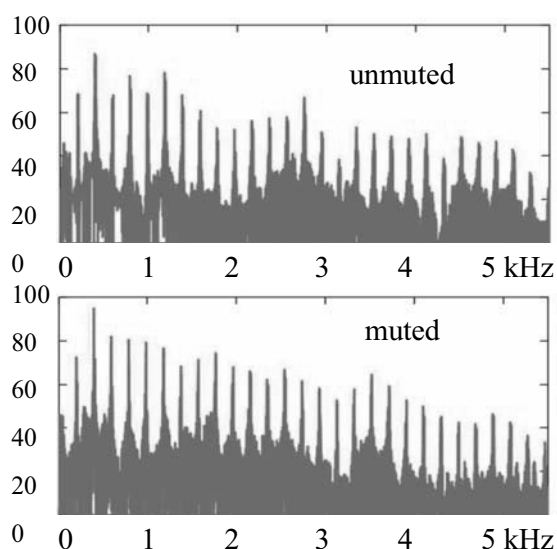


Figure 2: Noise spectra of bowed open string

*Spectra of open G on Vuillaume violin on an arbitrary dB scale with and without a soft rubber mute on the bridge, showing strong correlation between amplitude of harmonic modes excited and background noise spectrum*

Both the individual harmonics and the noise reflect the presence of individual structural resonances, their coupling and acoustic radiation strengths and density of states. The amplitude of individual components is strongly correlated with the noise spectrum. Strong peaks in the noise floor are observed between the air resonance at  $\sim 300$  Hz and the main body resonances at around 4-500 Hz, with other fairly broad peaks in resonance densities just above 1 kHz and around 2.6 kHz, with considerable structure at higher frequencies. Placing the mute on the bridge has a significant affect on both the amplitudes of the individual harmonics excited and the sound from the instrument and the noise spectrum.

In both the muted and un-muted cases, the relative heights of the individual components, with input amplitudes varying as  $1/f_n$ , decrease with increasing frequency relative to the noise spectrum. This is consistent with the noise over this frequency range being fairly constant, consistent with short impulse noise.

We have investigated the affect of varying the amount of noise on the output waveform, by subtracting the spectral components for amplitudes just above the noise floor and then adding the subtracted “noise” signal in variable amounts to the original signal minus the noise signal. In this way we are able to listen to the sound in the complete absence of any background noise and to the background noise itself. We can also use the “noise removed signal” to investigate the affect of adding various computer synthesised noise signals.

As previously noted by Mellody and Wakefield [7], the addition of noise improves the verisimilitude of computer synthesised violin sounds; however, they only included low frequency noise. Here, we emphasise the importance of noise over the whole frequency range, with a spectrum that reflects the spectral response of the instrument.

## 2. CONCLUSIONS

In a number of preliminary investigations, we have demonstrated the importance of vibrato in producing the amplitude and spectral variations that characterise the sound of the violin and thereby the quality of a particular instrument. In addition we have noted the importance of wide-band noise. Both factors contribute to the global factors that must help determine the quality of particular instruments.

## 3. REFERENCES

- [1] Woodehouse, J., *Catgut Acoust. Soc. Newsl.*, Vol 39: 22—24, 1983
- [2] Weinreich, G., *J. Acoust. Soc. Am.*, Vol.101: 2338—2346, 1997
- [3] McIntyre, M.E., Schumacher, R.T., and Woodehouse, J., “Aperiodicity in bowed-string motion.”, *Acustica*, Vol 49: 13—32, 1981
- [4] Gough, C.E. *The Physics of the Violin*, Physics World, Vol 1999
- [5] Matthews, M.V., and Kohut, J., “Electronic simulation of violin resonances.”, *J. Acoust. Soc. Am.*, Vol.53(6): 1620-1626, 1973
- [6] Meyer, J., “New aspects of the violin vibrato.”, *J. Acoust. Soc. Am.*, Vol.89: 1901-1902, 1991
- [7] Mellody, M. and Wakefield, G.H., “The time-frequency characteristics of violin vibrato: Modal distribution analysis and synthesis.”, *J. Acoust. Soc. Am.*, Vol. 107: 598—611, 2000
- [8] Moore, B.C., “An Introduction to the Psychology of Hearing”, Academic Press, 4<sup>th</sup> Edition, 2003, pp97-100

# BOW SPEED OR BOWING POSITION— WHICH ONE INFLUENCES SPECTRUM THE MOST?

K Guettler<sup>1</sup>, E Schoonderwaldt<sup>2</sup>, A Askenfelt<sup>2</sup>

<sup>1</sup>Norwegian Academy of Music, Oslo, Norway

knut.guettler@samson.nmh.no

<sup>2</sup>KTH, Dept. of Speech, Music and Hearing, Stockholm, Sweden

schoondw@speech.kth.se; andersa@speech.kth.se

## ABSTRACT

Raman and Schelleng analyzed waveform properties of the bowed string as function of bow speed, bow force, and bow position (the distance between bow and bridge). Schelleng also described spectral changes caused by alterations of the bow force alone. This phenomenon was further explained by Cremer, and referred to as "rounding of the Helmholtz corner". In this study it is shown that of the remaining two parameters, it is the bow's speed rather than its position that bears a potential of changing the shape of the string's spectral envelope. This contrasts to the popular belief that by bringing the bow closer to the bridge, the sound automatically becomes more brilliant.

## 1. INTRODUCTION

Every string player has experienced that by bringing the bow closer to the bridge, the sound becomes more brilliant. In the case of pizzicato, a similar effect is observed when the point of plucking is approaching one of the string's termination points. One might thus easily jump to the (hasty) conclusion that changing the point of excitation alone alters the spectral envelope in both cases.

In his JASA paper of 1973, Schelleng[1] utilized a diagram to describe the requirements for maintaining the Helmholtz motion in terms of the bow's force and position, provided a given speed and defined string properties. He also brought the concept of timbre variation into the picture, introducing the two terms "brilliant" and "sul tasto" in his diagram. ("Sul tasto" literally means "by the fingerboard", but appears here, presumably, as reference to soft tone color.) It is, however, not immediately apparent from the figure whether these timbre differences are caused by change of bowing *position* (the two expressions are marked at different bow positions within the Helmholtz area), or by change of bowing *force* (the expressions are positioned at different values with respect to the ordinate).

In the discussion that followed, Schelleng showed how the waveform of the string velocity under the bow changes with the *bow force*. Cremer [2] analyzed this more in depth, and established the theory of "the rounded corner".

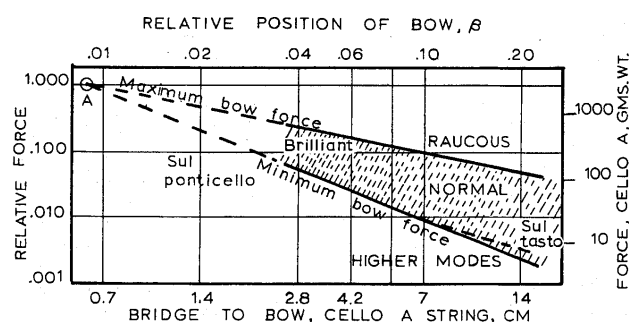


Figure 1:

Diagram from Schelleng's JASA paper. Given a fixed bow speed, the triangle sets the borders for maintaining Helmholtz motion in a bowed string. Two timbre expressions, "Brilliant" and "Sul tasto", are included in the figure, within the triangle.

## 2. ANALYSIS OF FORCE ON THE BRIDGE DURING PIZZICATO AND ARCO

In pizzicato, the force exerted on the bridge during each individual period is in principle an off-set square pulse with a width equal to  $\beta/f_0$  ( $\beta$  being the relative position of excitation, and  $f_0$  the fundamental frequency). For large  $\beta$ , the spectral slope is generally  $-6$  dB/oct., corresponding to an envelope of decaying lobes. The first lobe, however—the width of which is determined by  $\beta$ —will provide a number of partials with amplitudes near unity (see Figure 2).

So is not the case in arco: The force signal exerted on the bridge during an ideal Helmholtz motion remains a perfect sawtooth wave, irrespectively of which  $\beta$  chosen. As long as the Helmholtz corner is "sharp", the deviation from the ideal sawtooth shape are steps due to "missing partials" or "...node frequencies" i.e., frequencies having a node at the position where the bow excites the string (see Appendix). The sawtooth wave itself creates no spectral lobes, but decays smoothly at a rate  $-6$  dB/oct. (Lobes are seen, however, in the spectrum of string velocity under the bow.)

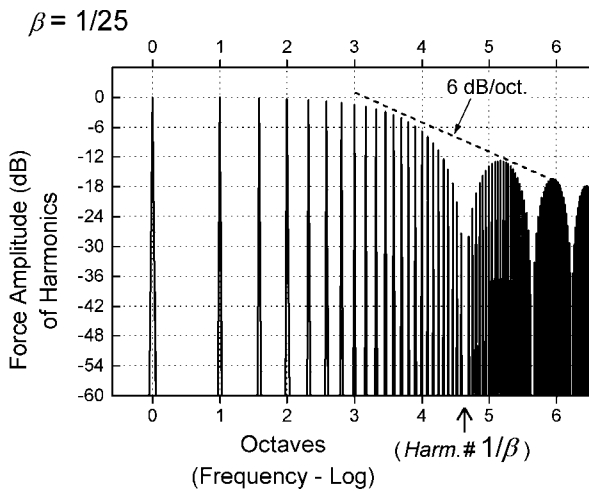


Figure 2:

Spectrum of the force acting on the bridge in pizzicato. As  $\beta$  becomes smaller, an increasing number of (lower) partials will approach unity in magnitude—relative to the width of the first spectral lobe.

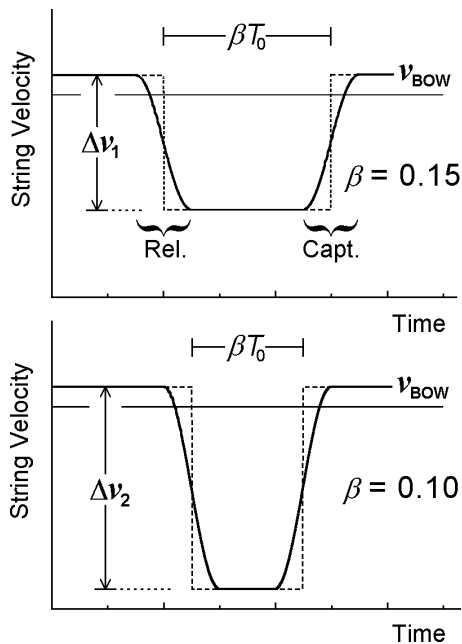


Figure 3:

Example of string velocity under the bow for two different  $\beta$ , but with the same bow speed and identical transition functions from stick to slip and vice versa. ( $T_0$  = the fundamental period;  $\Delta v = v_{BOW}/\beta$ , while  $\beta$  = the ratio between the bow-to-bridge distance and the total string length.)

As was already shown by Schelleng, it is the transitions at release and capture at the bow that carry the potential of softening or sharpening the rotating corner, and thus distinctly changing the tone color. Figure 3 shows idealized examples of such transitions.

String stiffness and the frictional characteristics of the rosin—as well as previous rounding of the rotating corner—cause the string release to spread out over a small transition interval before the full negative velocity is reached at slip. Accordingly, a comparable transition takes place at capture. (In practice the transition at capture is often shorter than the one at release—see Figure 4.) It can be shown that as long as these *transition functions* are independent of the bowing position, the force signal's spectral slope, i.e., the shape of the envelope, will remain entirely unaffected by  $\beta$ .

### 3. EFFECT OF BOW SPEED ON SPECTRUM.

Figure 4 and 5 show measured string velocity during slip, and spectral content for an open violin D-string [3] bowed by a bowing machine with bow force = 400 mN, and three different bow speeds, respectively. When averaged over a large number of periods, a modest prolongation of the slipping interval was observed as bow speed was increased. But more importantly: the string's deceleration and acceleration took slightly lower values.

The effect of that is quite visible when regarding the amplitude spectrum of the string velocity under the bow. When normalizing the energy of the first harmonic to zero dB, increasing the bow speed from 3 to 5 through 10 cm/s gave average amplitude reductions of 1.3 and 5.2 dB, respectively, in the range 16<sup>th</sup> to 65<sup>th</sup> harmonic. Increasing the bow speed further, from 10 to 30 cm/s, reduced the amplitudes only slightly more: in average another reduction of 0.8 dB to 6.0 dB, for that same harmonic range. It is probably correct to say the influence of bow speed on spectrum has its greatest impact at low speeds within the Helmholtz regime.

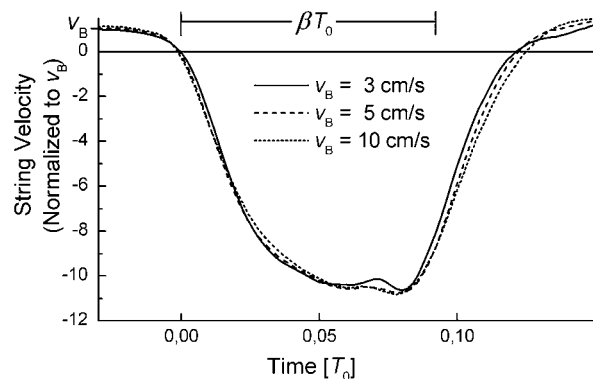


Figure 4:

Averaged string-velocity under the bow during slip for three different bow speeds. Stick/slip transitions are slowed down as the bow speed is increased. (Bow force = 400 mN;  $\beta = 1/10.833$ ; bow-hair width = 8 mm; all strokes performed with bowing machine).

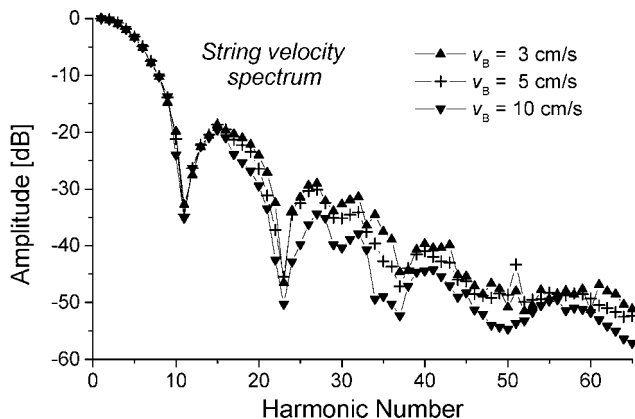


Figure 5:

*Spectrum of string velocity for the three strokes referred to in Figure 4 (normalized to 0 dB for the first harmonic). It can be seen that the lowest bow speed gives the highest (relative) amplitudes for the upper partials. In each case the spectrum was averaged over several strokes with constant bowing parameters.*

These spectrum data were obtained by averaging the FFTs of a Bluestein [4]-filtered (the filter allowing for an arbitrary number of elements in the FFT), moving Hann window of width equal to five nominal periods of the waveform under investigation. This procedure minimizes the danger of spectral peaks of higher harmonics being reduced or “averaged” due to the small frequency fluctuations that are always present in a bowed-string signal—but less so when the bow speed is high, or the bow force low.

The string-velocity signal was recorded as the voltage induced in the (steel) D-string when moving in a fixed magnetic field provided by a permanent magnet right under the string at the point of bowing. The magnet’s diameter (6 mm) was later compensated for in the calculations of spectra. Sampling frequency was 44.1 kHz (resampled to 148 kHz for Fig 4).

Apart from the “natural aperiodicity” [5] of the bowed string, no pitch flattening was observed with the bowing parameters employed in these tests. Earlier experiments and simulations have shown, however, that when pitch flattening is introduced as result of excess bow force or too low speed, higher partials tend to fade out, while mid-range partials are still emphasized.

#### 4. EFFECT OF BOW POSITION ON SPECTRUM

To see the effect of moving the bowing point over a large range while maintaining all other parameters unchanged, a series of simulations was performed. The string model included torsion and a “quasi plastic” friction algorithm (all data similar to String I of ref. [7]). The resulting spectra of force on the bridge are shown in Figure 6. Apart from the local deviations seen for “node frequencies” or frequencies close to these, the general spectral envelope remains unchanged for all simulations. There is no trend in the direction of greater brilliance for lower  $\beta$ . Other string models give similar results.

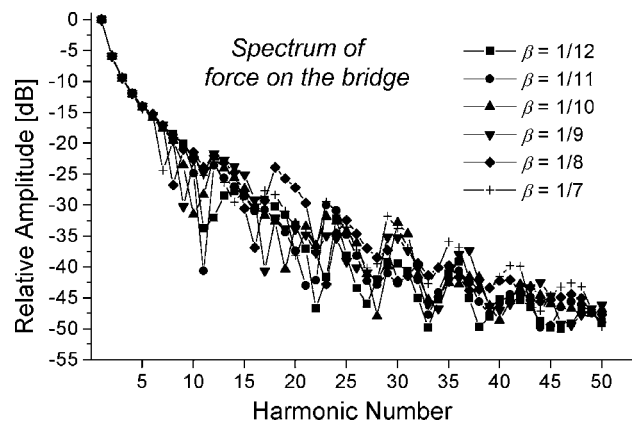


Figure 6:

*Simulated spectral changes as the bow is moved from  $\beta = 1/7$  to  $\beta = 1/12$  while keeping other bowing parameters unaltered—the first harmonics normalized to 0 dB. (From ref. [6].)*

#### APPENDIX

In a purely resistive system like the one studied by Raman [8] and Schelleng, the “sawtooth” force signal working on the bridge will consist of a number of steps rather than one ramp. This number can be found as the lowest value of  $n$  that holds for the expression below:

$$n(1 - \beta) = \text{integer}, \quad (\beta < 0.5; n = 1, 2, 3, \dots). \quad (1)$$

During the buildup of the Helmholtz motion, slip waves “rotate” on each side of the bow with frequencies  $\beta/f_0$  and  $(1-\beta)/f_0$ , respectively (see ref [7]). In this process, the string’s reflection pattern will repeat in time intervals equal to  $n(1 - \beta)/f_0$ . Examples: for  $\beta = 1/6$ ,  $\beta = 1/6.1$ , and  $\beta = 1/6.5$ , the force signal will consist of 6, 51 and 13 (individually sized) force steps per period, respectively. It follows that for an irrational  $\beta$ , the force on the bridge will take the form of a true sawtooth—after an infinitely long transient.

#### ACKNOWLEDGMENT

The authors are indebted to the Swedish Research Council who supported this work.

#### REFERENCES

- [1] Schelleng, J. C. (1973) The bowed string and the player, J. Acoust. Soc. Amer. 53(1), pp 26-41
- [2] Cremer, L. (1972 and 1973) The influence of “bow pressure” on the movement of a bowed string. Part I



and II. NL. Catgut Acoust. Soc. #18 pp. 13-19 and #19, 21-25.

- [3] Steel-core violin D-string by Prim.
- [4] Bluestein L. I., (1968) A linear filtering approach to the computation of the discrete Fourier transform. 212—Nerem records.
- [5] McIntyre, M. E. et al. (1981) Aperiodicity in bowed-string motion, *Acustica Vol.* 49, pp 13-32.
- [6] Guettler, K., (2003) A closer look at the string player's bowing gestures. *Journal of Catgut Acoust. Soc. Vol.* 4, No.7 (Series II) pp. 12-16.
- [7] Guettler, K. (2002). On the Creation of the Helmholtz Motion in Bowed Strings. *Acustica - Acta Acustica* 88(6), 970-985.
- [8] Raman, C. V., (1918) On the mechanical theory of the vibrations of bowed strings and of musical instruments of the violin family, with experimental verification of the results. Part I. Indian Assoc. for the Cultivation of Science, Bull 15, pp 1-158.

## **THE BH-HILL AND TONAL QUALITY OF THE VIOLIN**

*Erik V Jansson*

Department of Speech Music and Hearing  
Kungl Tekniska Högskolan  
erik@speech.kth.se

### **ABSTRACT**

In the frequency range of maximum sensitivity of the ear the so-called BH-hill can be found. The BH-hill can not be confined to the violin bridge only. A normal bridge and a plate bridge (a bridge with only feet tips but no cutting outs as heart, ear etc) give mainly the same BH-hill. The same bridge on a Stradivarius violin and a new violin gives differently shaped BH-hills. A couple of forces (two forces in opposite directions) at the bridge feet gives a BH-hill, both for normal bridge and bridge plate. A momentum applied at the central line of the top plate gives no BH-hill. The BH-hill is much affected by the distance between the two feet, i.e. the two forces of the couple. The cross-stiffness of the top plate also gives a large influence. The importance of the bridge hill will be demonstrated by playing two violins, one with a normal BH-hill and another violin with no BH-hill. Thus it has been demonstrated that the BH-hill is very important and that it is mainly set by the bridge feet distance and the top plate properties at the bridge feet.

### **1. INTRODUCTION**

The main question at issue of our work is to understand the main function, the physics of the violin and to explain how the violin works – not as a help to copy the works of the old masters but supplying a fundament for further development of the violin. The practical and artistic work will be left to the maker, the artist. Bridge mobility of a violin is fairly easily measured. In the frequency range of maximum sensitivity of the human ear, 2-3 kHz, the so-called BH-hill can be found. Experiments have indicated that the BH-hill, is very important perhaps the most important for the tonal quality. Therefore it is important to understand the mechanics of the BH-hill and practically understand how it can be adjusted. The violin bridge on rigid support has its first in-plane resonance at about 3 kHz [1]. Experiments have shown that the BH-hill can not be confined to the violin bridge only, and specifically not to this resonance [2]. The design of a normal bridge and of a plate-bridge (a bridge shaped plate with feet tips but without cutting-outs as heart, ears etc) are shown in figure 1. The normal bridge has its first in-plane resonance at 3 kHz and the plate bridge its first in-plane resonance at 7.6 kHz. The bridge mobility of the normal bridge and the plate-bridge on a violin N92 was measured see figure 2. The bridge mobility curves are close to identical with few exceptions. The main part of the BH-hill remains the same in spite of the different first in-plane resonance frequencies of the two bridges (main difference is a minor, but sharp peak at 2.3 kHz). Thus the BH-hill is not confined to the violin bridge only and especially not to the first in-plane resonance only.

### **2. BH-HILL IN TOP-PLATE VIBRATIONS**

The BH-hill is found in the bridge vibrations, but these should not radiate sound very efficiently. Can the BH-hill be found in vibrations of the violin body? Single resonances of a violin body should not be possible to separate in this frequency region. Bridge mobility of several violins and vibrations at the bridge feet were measured. The same BH-hill might be found both in the bridge vibrations and at the bridge feet for the same bridge excitation (mechanical impulse by an impulse force hammer in a pendulum arrangement [3]). Thus the experiments indicate that the BH-hill vibrations are transferred to the violin top plate (c.f. [4]), but more evidence is needed for the final conclusion.

### **3. BH-HILL AND BRIDGE FEET DISTANCE**

A major question is: Can the BH-hill be perturbed by the bridge and is this clearly perceived? The bridge plate open possibilities for simple and informative experiments. A set of similar plate bridges are easily made with only varying distances between the two bridge feet-tips. The feet-tips can be adjusted to fit a violin. A violin (N92) and a plate bridge with normal feet distance gives a clear BH-hill, see figure 3, but a violin (PW96) and a plate-bridge with no feet distance gives no BH-hill, see figure 4. The first violin (N92) sounds like a violin but hardly the second violin (PW96). The simple experiment indicates that the BH-hill and the feet distance are very important. Further experiments with several violins indicate that increased feet distance gives higher frequency but lower level of the BH-hill.

### **4. BH-HILL - THE SAME BRIDGE BUT DIFFERENT VIOLINS**

Does the violin body not influence the BH-hill? Two violins were measured with the same bridge. First the bridge mobility of a Stradivarius 1709 violin was measured, see figure 5. The same bridge was set on the N92 violin and the bridge mobility violin was measured again, see figure 6 (on the Stradivarius violin a new bridge had been fitted). A look at the mobility curves shows clear differences in spite of the same bridge. The BH-hill of the Stradivarius has a smooth BH-hill and corresponding smooth phase shift, which are typical for old violins [5]. The N92 violin has a marked peak with a corresponding phase step. The differences between the two BH-hills result from differences built into the violins (the bridge fitted fairly well for both violins). Thus we can again see that the BH-hill is not confined to the bridge only.

## 5. CONCLUSIONS

The experiments have shown that the BH-hill can be perturbed by the distance between the bridge feet. A practical test with normal and no distance, i.e. a typical BH-hill and none, respectively, results in a violin with a normal sound and a one with rather odd sound. Thus we have found that the BH-hill is important for the tonal quality of a violin. The BH-hill can be somewhat perturbed by the distance between the bridge feet - higher frequency but lower level with increased feet distance. But the BH-hill is very dependant on the properties built into a violin, too.

**Final conclusion:** Bridge feet distance can to a certain extent be used for obtaining a suitable BH-hill but built-in properties of the violin can not be neglected.

## 6. REFERENCES

- [1] Cremer, L., "The Physics of the Violin" MIT press, Cambridge Massachusetts, 1984.
- [2] Jansson, E.V. and Niewczyk, B.K., ". On the acoustics of the violin: Bridge or body hill", CASJ May 1999, pp. 23-27.
- [3] Jansson, E., "Acoustics for Violin and Guitar Makers" <http://www.speech.kth.se/music/acviguit4/index.html>
- [4] Jansson, E.V. Molin, N.-E. an'd Wåhlin, A.O., "Transientwave response of the violin body", J Acoust Soc Am 88 (1990), pp. 2479-2481.
- [5] Jansson, E.V., " Admittance Measurements of 25 High Quality Violins", Acustica united with Acta Acustica 83 (95), pp. 337-341.



Figure 1: Normal violin bridge with first in-plane resonance at 3 kHz (left) and plate bridge with first in-plane resonance at 7.6 kHz (right).

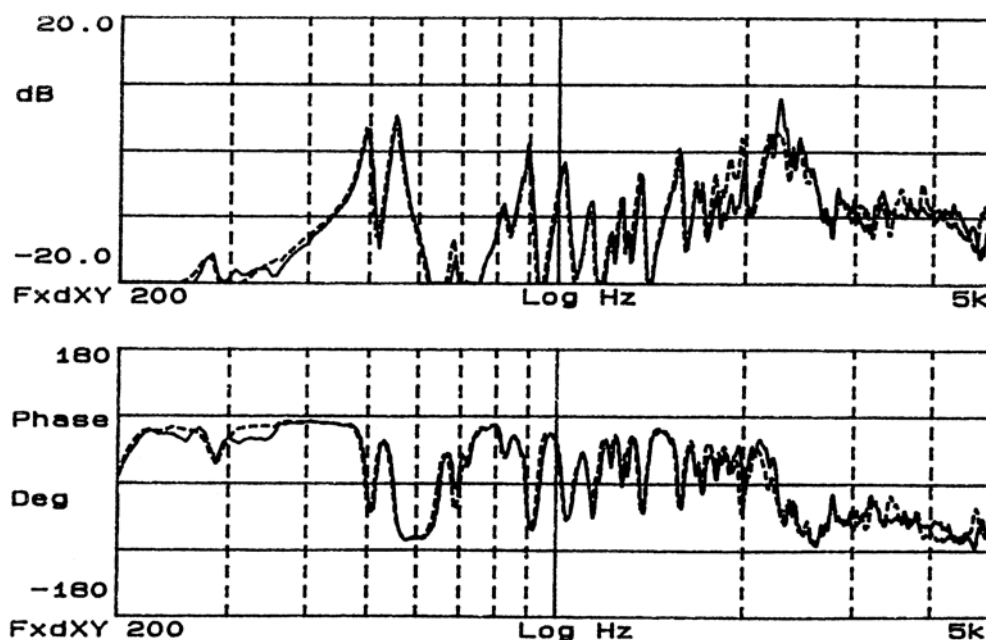


Figure 2: Bridge mobility of violin N92 with normal bridge (full line) and plate bridge (dashed line).

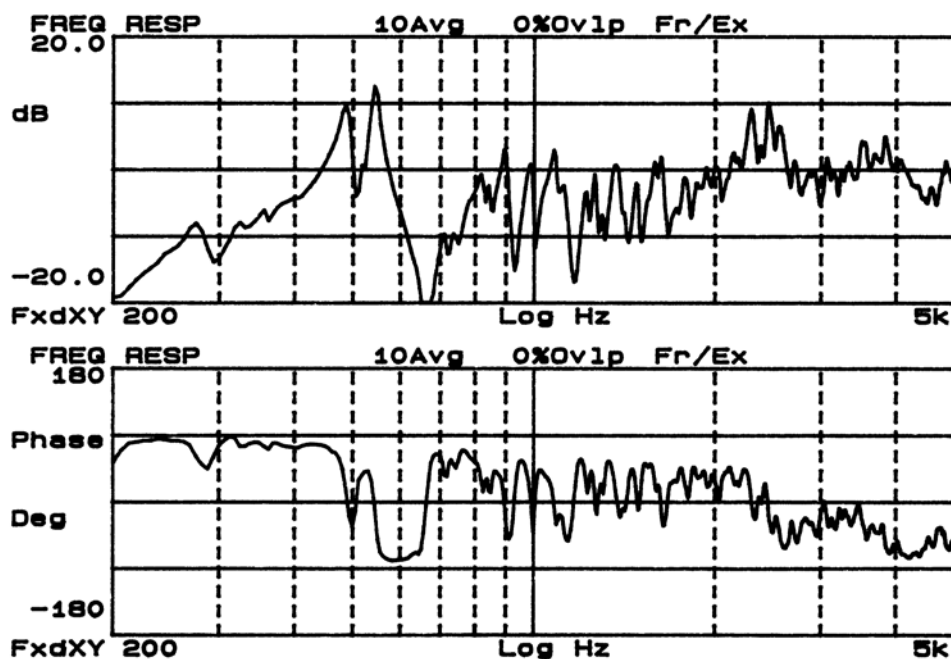


Figure 3: Bridge mobility of violin N92 with plate bridge with normal feet distance.

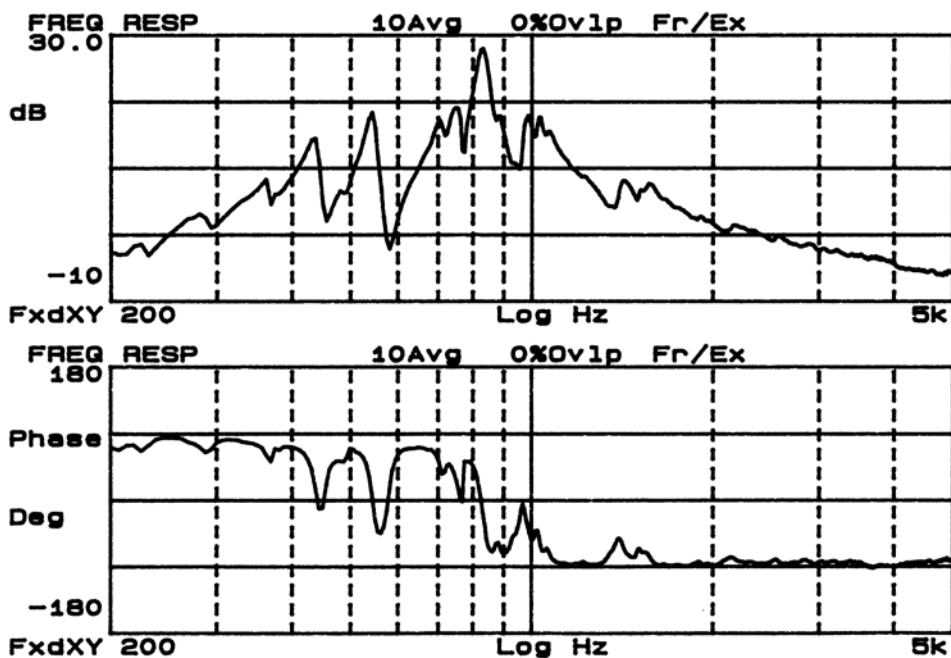


Figure 4: Bridge mobility of violin PW96 with plate bridge with no feet distance.

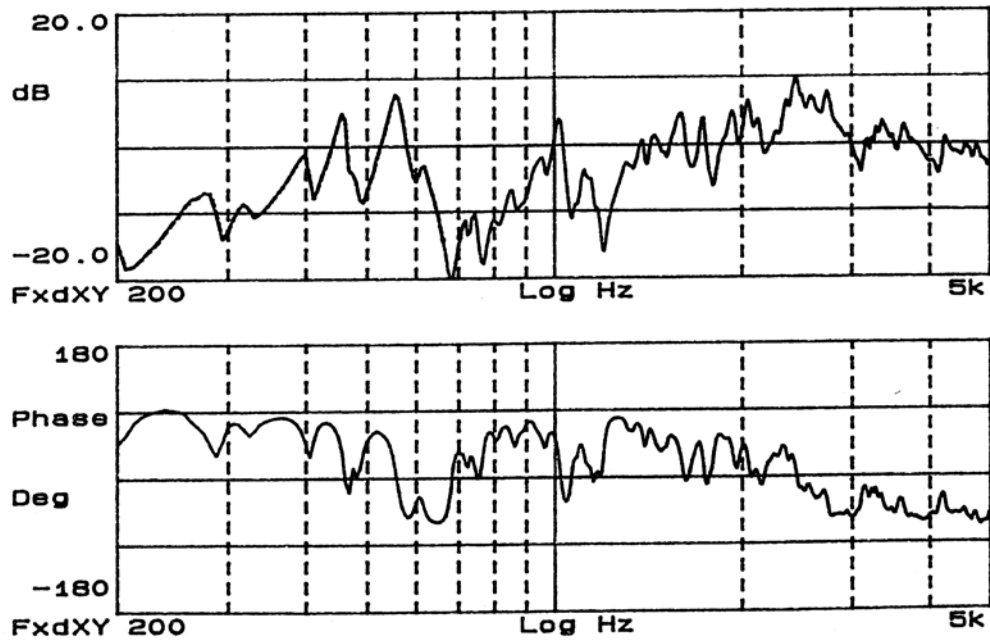


Figure 5: Bridge mobility of a Stradivarius 1709 violin.

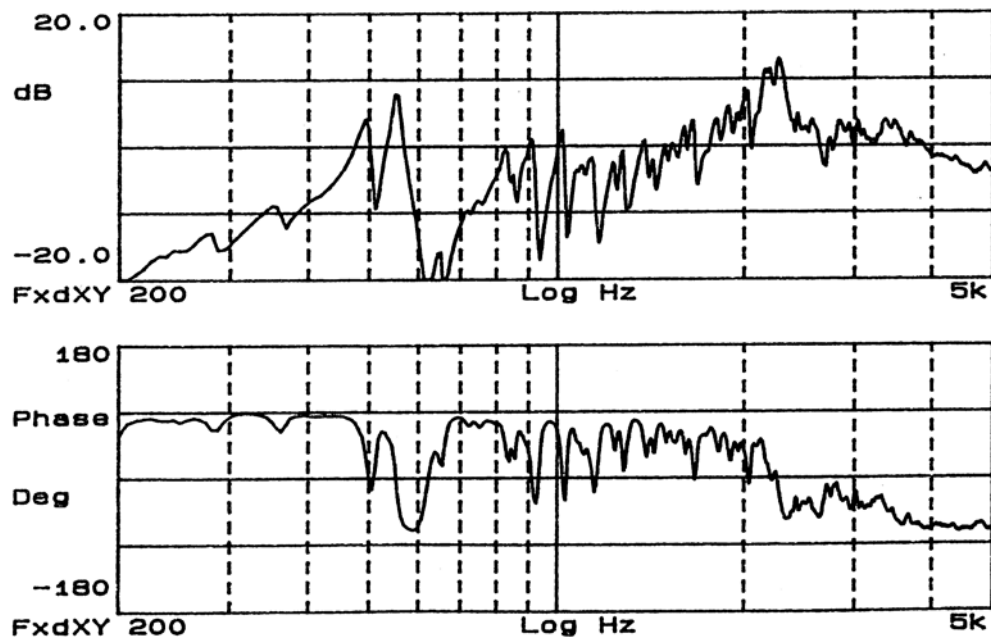


Figure 6: Bridge mobility of violin N92 with the bridge from the Stradivarius 1709 violin.

## INFERRING DECISION RULES FROM JURYS' RANKING OF COMPETING VIOLINS

Jacek Jelonek, Ewa Łukasik, Aleksander Naganowski, Roman Slowinski

Institute of Computing Science, Poznan University of Technology, 60-965 Poznań, Poland

jacek.jelonek@cs.put.poznan.pl

### ABSTRACT

A set of violins submitted to a competition has been evaluated by the jury from the viewpoint of several criteria and then ranked from the best to the worst. The sound of the instruments played by violinists during the competition has been recorded digitally and then processed to obtain sound attributes, e.g. cepstral coefficients, harmonics based spectral parameters and attributes based on the Lyon's cochlear model. Given the jury's ranking of violins according to sound quality criteria, we are inferring from the sound characteristics a preference model of the jury in the form of "if..., then..." decision rules. This preference model should explain the given ranking and should also permit to build a ranking of a new set of violins according to this policy. The inference follows the scheme of an inductive supervised learning. For this, we are applying a special computational tool called Dominance-based Rough Set Approach (DRSA).

### 1. INTRODUCTION

A set of violins submitted to 10<sup>th</sup> International Henryk Wieniawski Violinmakers Competition in Poznań has been evaluated by the jury on a set of criteria including [4]:

- a) volume of sound,
- b) timbre of sound,
- c) ease of sound emission,
- d) equal sound volume of strings,
- e) accuracy of assembly,
- f) individual qualities.

Criteria a), b), d) refer mainly to quality of the violin's sound while c), e), f) are related rather to quality of the violin's assembly. The sound of the instruments played by violinists during the competition has been recorded digitally and then processed to obtain sound attributes: cepstral coefficients, spectral perceptive parameters (e.g. brightness, odd/even relation, tristimuli [5]) and attributes based on the Lyon's cochlear model (averaged output values of auditory filters and their reduced, selected or aggregated forms).

Given the jury's rankings of violins according to sound quality criteria a), b), d), we are inferring a preference model of the jury in the form of "if..., then..." decision rules from the sound characteristics. This preference model should explain the rankings with respect to criteria a), b), d), in terms of the most relevant sound characteristics. It should also permit to build a ranking with respect to a), b), d) of a new set of violins in accordance with the jury's policy.

The inference follows the scheme of an inductive supervised learning. For this, we are applying a special computational tool called Dominance-based Rough Set Approach (DRSA) [1,2,3].

First, using the judgments of the members of the jury, we are constructing rough approximation of the preference relation known from a ranking on criterion a), or b), or d). The rough approximation of the preference relation is a starting point for inducing the decision rules in terms of the acoustic features of the violins. The rules can serve: (i) to explain the decision policy of the jury, i.e. to reconstruct the ranking with respect to a given criterion by using rules to the violins from the competition, and (ii) to build a new ranking for a new set of violins characterized by acoustic features. Application of a set of decision rules to a set of violins gives a preference graph where nodes correspond to violins and arcs are preference relations for pairs of violins. Positive and negative flows are calculated for each node (violin), giving arguments about its relative strength and weakness. Aggregation of both arguments leads to a final ranking of violins, either partial or complete. The approach can also be useful for discovering subsets of acoustic features being relevant for the final ranking.

The paper is organized as follows: in the next section, the dominance-based rough set approach is outlined; then, the acoustic data are characterized and, finally, the results are presented in terms of relevant acoustic features and decision rules.

### 2. THE ROUGH SET APPROACH TO VIOLIN'S DATA ANALYSIS

Consider a data table whose rows correspond to objects (violins) and columns to attributes describing the objects. Among the  $n+1$  attributes there are  $n$  condition attributes based on sound features and one decision attribute corresponding to a ranking by the jury. It is assumed that some attributes have preference-ordered domains (cardinal scales) and for this reason they are called *criteria*. A dedicated heuristic algorithm is used to search for such attributes. Moreover, it is assumed that there exists a *semantic correlation between* condition criteria and the decision criterion (ranking). In general, semantic correlation between condition criteria and the decision criterion requires that object  $x$  dominating object  $y$  on all condition criteria (i.e.  $x$  having evaluations at least as good as  $y$  on all condition criteria) should also dominate  $y$  on the decision criterion (i.e.  $x$  should have evaluations at least as good as  $y$  on the decision criterion). This principle is called *dominance principle* (or Pareto

principle). In this case, the data table provides a preferential information of the jury in a multicriteria ranking problem; in consequence, the comprehensive preference relation characterized by decision rules discovered from this data can be considered as a *preference model* of the jury. It may be used to explain a decision policy of the jury and to recommend a preference ranking with respect to new objects.

### 2.1. Pairwise comparison table (PCT) as preferential information and a learning sample

Let  $A$  be a set of objects (violins) evaluated by a finite set of criteria  $C$ . The preferential information concerning the multicriteria ranking of objects can be transformed to a pairwise comparison table (PCT) including *pairs of objects* from  $A \times A$ , described by preference relations on particular criteria and a comprehensive preference relation, for example, a large preference relation called *outranking relation*. The comprehensive preference relation is calculated from the jury's ranking of objects according to a given decision criterion. If for any pair of objects  $(x, y) \in A \times A$ , object  $x$  is placed not worse than object  $y$  in the ranking, then  $x$  outranks  $y$ ; otherwise,  $x$  does not outrank  $y$ . In the following,  $xSy$  will denote the presence, while  $x \not S y$  the absence of the outranking relation for a pair  $(x, y) \in A \times A$ .  $S$  is reflexive, but neither necessarily transitive nor complete.

An  $m \times (n+1)$  Pairwise Comparison Table  $S_{PCT}$  is then created on the base of this information. Its first  $n$  columns correspond to criteria from set  $C$ . The last,  $(n+1)$ -th column of  $S_{PCT}$ , represents binary relation  $S$  or  $S^c$ . The  $m$  rows are pairs from  $A \times A$ . Assuming the *gain* preference direction on each criterion  $i \in [1; n]$ , an inner element of  $S_{PCT}$  is a difference:

$$\Delta_i(x, y) = g_i(x) - g_i(y)$$

calculated using evaluations  $g_i(x)$  and  $g_i(y)$  of objects  $x$  and  $y$  on criterion  $i$ .

### 2.2. DRSA analysis of the PCT

Given  $P \subseteq C$  ( $P \neq \emptyset$ ),  $(x, y), (w, z) \in A \times A$ , the pair of objects  $(x, y)$  is said to *dominate*  $(w, z)$ , taking into account criteria from  $P$  (denoted by  $(x, y)D_P(w, z)$ ), if  $x$  is preferred to  $y$  at least as strongly as  $w$  is preferred to  $z$  with respect to each  $i \in P$ . Precisely, "at least as strongly as" means "by at least the same difference":

$$\Delta_i(x, y) \geq \Delta_i(w, z) \Rightarrow (x, y)D_P(w, z)$$

Let  $D_{\{i\}}$  be the dominance relation confined to the single criterion  $i \in P$ . The binary relation  $D_{\{i\}}$  is reflexive  $((x, y)D_{\{i\}}(x, y))$ , for every  $(x, y) \in A \times A$ , transitive  $((x, y)D_{\{i\}}(w, z) \text{ and } (w, z)D_{\{i\}}(u, v) \text{ imply } (x, y)D_{\{i\}}(u, v))$ , for every  $(x, y), (w, z), (u, v) \in A \times A$ , and complete  $((x, y)D_{\{i\}}(w, z) \text{ and/or } (w, z)D_{\{i\}}(x, y))$ , for all  $(x, y), (w, z) \in A \times A$ . Therefore,  $D_{\{i\}}$  is a complete preorder on  $A \times A$ . Since the intersection of complete preorders is a partial preorder and  $D_P = \bigcap_{i \in P} D_{\{i\}}$ ,  $P \subseteq C$ , then the

dominance relation  $D_P$  is a partial preorder on  $A \times A$ .

Let  $R \subseteq P \subseteq C$  and  $(x, y), (u, v) \in A \times A$ ; then the following

implication holds:

$$(x, y)D_P(u, v) \Rightarrow (x, y)D_R(u, v).$$

Given  $P \subseteq C$  and  $(x, y) \in A \times A$ , we define:

- a set of pairs of objects dominating  $(x, y)$ , called *P-dominating set*,  $D_P^+(x, y) = \{(w, z) \in A \times A : (w, z)D_P(x, y)\}$ ,
- a set of pairs of objects dominated by  $(x, y)$ , called *P-dominated set*,  $D_P^-(x, y) = \{(w, z) \in A \times A : (x, y)D_P(w, z)\}$ .

The  $P$ -dominating sets and the  $P$ -dominated sets defined on  $B$  for all pairs of reference objects from  $B$  are "granules of knowledge" that can be used to express  $P$ -lower and  $P$ -upper approximations of comprehensive outranking relations  $S$  and  $S^c$ , respectively:

$$\underline{P}(S) = \{(x, y) \in B : D_P^+(x, y) \subseteq S\},$$

$$\overline{P}(S) = \bigcup_{(x, y) \in S} D_P^+(x, y).$$

$$\underline{P}(S^c) = \{(x, y) \in B : D_P^-(x, y) \subseteq S^c\},$$

$$\overline{P}(S^c) = \bigcup_{(x, y) \in S^c} D_P^-(x, y).$$

It has been proved in [1] that

$$\underline{P}(S) \subseteq S \subseteq \overline{P}(S), \quad \underline{P}(S^c) \subseteq S^c \subseteq \overline{P}(S^c).$$

Furthermore, the following complementarity properties hold:

$$\underline{P}(S) = A \times A - \overline{P}(S^c), \quad \overline{P}(S) = A \times A - \underline{P}(S^c),$$

$$\underline{P}(S^c) = A \times A - \overline{P}(S), \quad \overline{P}(S^c) = A \times A - \underline{P}(S).$$

The  $P$ -boundaries ( $P$ -doubtful regions) of  $S$  and  $S^c$  are

$$Bn_P(S) = \overline{P}(S) - \underline{P}(S), \quad Bn_P(S^c) = \overline{P}(S^c) - \underline{P}(S^c).$$

From the above it follows that  $Bn_P(S) = Bn_P(S^c)$ .

The coefficient

$$\gamma_P = \frac{|\underline{P}(S) \cup \underline{P}(S^c)|}{|A \times A|}$$

defines the *quality of approximation of  $S$  and  $S^c$  by  $P \subseteq C$* . It expresses the ratio of all pairs of objects  $(x, y) \in A \times A$  correctly assigned to  $S$  and  $S^c$  by the set  $P$  of criteria to all the pairs of objects contained in  $A \times A$ . Each minimal subset  $P \subseteq C$ , such that  $\gamma_P = \gamma_C$ , is called a *reduct* of  $C$  (denoted by  $RED_{S_{PCT}}$ ). Let us remark that  $S_{PCT}$  can have more than one reduct. The intersection of all reducts is called the *core* (denoted by  $CORE_{S_{PCT}}$ ).

It is also possible to use the Variable Consistency Model on  $S_{PCT}$  [3] allowing that some of the pairs in positive or negative dominance sets belong to the opposite relation but at least  $l$  percent of pairs belong to the correct one. Then the definition of lower approximations of  $S$  and  $S^c$  boils down to:

$$\underline{P}(S) = \left\{ (x, y) \in A \times A : \frac{|D_P^+(x, y) \cap S|}{|D_P^+(x, y)|} \geq l \right\}$$

$$\underline{P}(S^c) = \left\{ (x, y) \in A \times A : \frac{|D_P^-(x, y) \cap S^c|}{|D_P^-(x, y)|} \geq l \right\}$$

### 2.3. Searching for criteria

As mentioned before, there is no explicit knowledge, whether a specified attribute can be considered as a criterion or not. In order to detect criteria among attributes, we propose to use a special coefficient  $Q_p$  within DRSA:

$$Q_p = (1 - \alpha)\gamma_p + \alpha \left( 1 - \frac{|Edge(S)| + |Edge(S^c)|}{|A \times A|} \right)$$

It is a weighted sum of two components – the quality of approximation  $\gamma_p$  and the relative number of incomparable objects in each approximation expressed by the cardinality of edges:

$$Edge_p(S) = \{ (x, y) \in S : |D_p^-(x, y)| = 1 \}$$

$$Edge_p(S^c) = \{ (x, y) \in S^c : |D_p^+(x, y)| = 1 \}$$

The weight  $\alpha \in [0; 1]$  permits to tune the relative importance of the two components. The value of the coefficient  $Q_p$ , from the range  $[0; 1]$ , may be treated as a measure of the *semantic correlation* between the acoustic features and the decision criterion (ranking). We consider a feature as a criterion if the value of the coefficient  $Q_p$  is relatively high (close to 1.0).

The search for the best criteria subset is made in a *wrapper* loop where groups are formed by adding features one by one. In each iteration, all groups (future subsets) are evaluated using the  $Q_p$  coefficient.

### 2.4. Induction of decision rules from rough approximations of outranking and non-outranking relations

Using the rough approximations of  $S$  and  $S^c$  defined in 2.2, it is then possible to induce a generalized description of the preferential information contained in a given  $S_{PCT}$  in terms of suitable decision rules.

In case of Variable Consistency Model, described in 2.2, the decision rules have then the following syntax [1,3]:

#### 1) $D_{\geq}$ -decision rules:

if  $\Delta_{i1}(x, y) \geq r_{i1}$  and...  $\Delta_{ie}(x, y) \geq r_{ie}$ , then  $xSy$ ,

where  $P = \{i1, \dots, ie\} \subseteq C$ ; these rules are supported by pairs of objects from the  $P$ -lower approximation of  $S$  only;

#### 2) $D_{\leq}$ -decision rules:

if  $\Delta_{i1}(x, y) \leq r_{i1}$  and...  $\Delta_{if}(x, y) \leq r_{if}$ , then  $xS^c y$ ,

where  $P = \{i1, \dots, if\} \subseteq C$ ; these rules are supported by pairs of objects from the  $P$ -lower approximation of  $S^c$  only;

Each rule is characterized by two parameters: *strength* (the number of pairs from  $S_{PCT}$  covered by the rule) and *confidence* (the ratio of the number of pairs concordant with the conclusion to the number of all pairs from  $S_{PCT}$  covered by the rule – it should not be less than  $l$ ).

### 2.5. Use of decision rules for decision support

The decision rules induced from a given  $S_{PCT}$  describe the

comprehensive preference relations  $S$  and  $S^c$ , that is the jury's ranking. A set of these rules covering all pairs of  $S_{PCT}$  represent a preference model of the jury. Application of these decision rules on a new set  $M$  of objects induces a specific preference structure on  $M$ .

In fact, any pair of objects  $(u, v) \in M \times M$  can match the decision rules in one of four ways:

- at least one  $D_{\geq}$ -rule and no  $D_{\leq}$ -rule,
- at least one  $D_{\leq}$ -rule and no  $D_{\geq}$ -rule,
- at least one  $D_{\geq}$ -rule and at least one  $D_{\leq}$ -rule,
- no decision rule.

These four ways correspond to the following four situations of outranking, respectively:

- $uSv$  and not  $uS^c v$ , i.e. *true* outranking ( $uS^T v$ ),
- $uS^c v$  and not  $uSv$ , i.e. *false* outranking ( $uS^F v$ ),
- $uSv$  and  $uS^c v$ , i.e. *contradictory* outranking ( $uS^K v$ ),
- not  $uSv$  and not  $uS^c v$ , i.e. *unknown* outranking ( $uS^U v$ ).

The four above situations, which together constitute the so-called *four-valued outranking* [1], have been introduced to underline the presence and absence of *positive* and *negative* reasons for the outranking. Moreover, they make it possible to distinguish contradictory situations from unknown ones.

A final ranking can be obtained upon a suitable exploitation of this structure, i.e. of the presence and the absence of outranking  $S$  and  $S^c$  on  $M$ . A possible exploitation procedure consists in calculating a specific score, called Net Flow Score, for each object  $x \in M$ :

$$S_{nf}(x) = S^{++}(x) - S^{+-}(x) + S^{-+}(x) - S^{--}(x), \text{ where}$$

$$S^{++}(x) = \text{card}(\{y \in M : \text{there is at least one rule that affirms } xSy\}),$$

$$S^{+-}(x) = \text{card}(\{y \in M : \text{there is at least one rule that affirms } ySx\}),$$

$$S^{-+}(x) = \text{card}(\{y \in M : \text{there is at least one rule that affirms } yS^c x\}),$$

$$S^{--}(x) = \text{card}(\{y \in M : \text{there is at least one rule that affirms } xS^c y\}).$$

The recommendation in ranking problems consists of the total preorder determined by  $S_{nf}(x)$  on  $M$ .

## 3. THE VIOLIN'S ACOUSTIC DATA

The sounds for the analysis have been selected from the set of digital recordings gathered in AMATI database [4]. Namely these were individual sounds played on open strings, G, D, A, E. They have been repeated twice in each direction of a bow movement. The same player played all sounds, performing them with the equal bow position, speed, angle and pressure. The recording session took place in the chamber hall used by the jury during the audition. The microphone has been placed 1m from the player. Experiments concerned attributes of 25 instruments from the collection, ranked by the musicians as the best, average and the worst. Numbers that we use in the records stood for instruments identifiers during the competition. The following principles of awarding points for acoustic properties that we use as a set criteria have been used:

- volume of sound – maximum 20 points (5 points per string),
- timbre of sound – maximum 20 points (5 points per string),
- equal sound volume of strings – maximum 15 pts.



#### 4. THE RESULTS

Our acoustic analyses that lead to generation of features, include cepstral coefficients, often giving good results in solving discrimination problems of sound data. In one of the experiments we used 25 cepstral coefficients for each string as a base set of features (100 values per violin). As we present below, it is possible to approximate jury's rankings with an acceptable precision, using only a small subset of these all 100 values. The criteria were selected by using the algorithm described before.

	Subset of criteria	$\gamma_P$	$Q_P$	No. of rules	Ranking distance
A	A14, E13, D12, G16	0.94	0.86	62	1.57
B	E13, D15, G4, G17, D5	0.94	0.85	99	2.00
D	D20, D15, A24, D10	0.98	0.87	64	2.26

These results were obtained for a selected group of 23 instruments, arranged in three different rankings, called A, B, D, according to sound quality criteria a), b), d) (see Section 1). For each ranking, one of the best subsets of criteria was chosen – the letter in the criterion name corresponds to the string name and the number is the index of the cepstral coefficient. The quality of approximation and the  $Q_P$  coefficient were calculated for the  $S_{PCT}$  with *variable consistency* level equal to 0.95. Three sets of rules were generated on the base of these subsets using the *DomLEM* algorithm [2], which is a *minimal cover* rule induction algorithm. To reduce the size of the sets of rules, they were induced with *consistency level* equal to 0.9. A distance between the jury's original ranking and the ranking obtained by applying rules is calculated as an average position shift for one object.

To present an example application of the induced rules, we have chosen three violins (no. 43, 24 and 15), from the top of the original ranking B (timbre of sound). The values on all criteria (with the *gain* preference direction) from the subset selected before are as below:

Viol. no.	Orig. rank.	E13	D15	G4	G17	D5
43	1	-0.0268	0.0167	0.0526	-0.0003	0.0715
24	2	-0.0040	-0.0695	0.0176	0.0382	0.0632
15	3	-0.0660	0.0008	0.0157	0.0364	0.0503

From among the rules induced from rough approximations of  $S$  and  $S^c$ , the following match pairs of the violins selected:

Pair	Rule
(24, 15)	$[\Delta(E13) \geq 0.0596] \Rightarrow S$
(43, 24)	$[\Delta(E13) \geq -0.0228] \wedge [\Delta(D15) \geq 0.0704] \Rightarrow S$
(43, 15)	$[\Delta(E13) \geq 0.02] \wedge [\Delta(D15) \geq 0.0110] \Rightarrow S$
(43, 43) (24, 24) (15, 15)	$[\Delta(D15) \geq -0.0098] \wedge [\Delta(G4) \geq -0.0004] \wedge [\Delta(G17) \geq -0.0049] \Rightarrow S$
(15, 24)	$[\Delta(E13) \leq -0.0592] \Rightarrow S^c$
(15, 43)	$[\Delta(E13) \leq -0.0097] \wedge [\Delta(D15) \leq -0.0146] \Rightarrow S^c$
(24, 43)	$[\Delta(D15) \leq -0.0834] \wedge [\Delta(D5) \leq -0.0083] \Rightarrow S^c$

Note that the conditions are defined on differences between values on the specified criteria, since rules are applied on rows

of  $S_{PCT}$ . According to the NFS score the resulting order is concordant with the jury's decision:

Violin no.	Original ranking	NFS score	Resulting ranking
43	<b>1</b>	4	<b>1</b>
24	<b>2</b>	0	<b>2</b>
15	<b>3</b>	-4	<b>3</b>

#### 5. CONCLUSIONS

The presented approach permits to create rankings of instruments that are almost identical to the original ones, which means that the jury's preferences are well approximated. The approach permitted moreover, to discover a small but relevant subset of acoustic features ensuring a good approximation of the rankings. By induction of decision rules from available data, we are able to represent a decision policy of the jury in easily interpretable terms.

The rough set approach including the quality coefficient  $Q_P$  permits to deal with a set of features for which it is not explicitly known if attributes are criteria, i.e. attributes with preference-ordered domains. We are continuing this research to discover other interesting acoustic features than cepstral coefficients on a larger set of violins.

#### ACKNOWLEDGEMENTS

The authors wish to acknowledge the financial support from the State Committee for Scientific Research, KBN research grant 4 T11F 002 22.

The authors would like to express their gratitude to Henryk Wieniawski Musical Society in Poznań for making accessible the judgments of the jury and for enabling recordings of violins. The words of appreciation are addressed to the management of the Museum of Musical Instruments, branch of National Museum in Poznań, for the entire help during the realization of the project.

#### 6. REFERENCES

- [1] Greco, S., Matarazzo, B., Slowinski, R.: "Rough sets theory for multicriteria decision analysis". *European J. of Operational Research* 129 (2001) no.1, 1-47.
- [2] Slowinski, R., Greco, S., Matarazzo, B.: "Rough set based decision aiding". [In]: E. Burke and G. Kendall (eds.), *Introductory Tutorials on Optimization, Search and Decision Support Methodologies*, Kluwer Academic Publishers, Boston, 2003, chapter 16.
- [3] Slowinski, R., Greco, S., Matarazzo, B.: "Mining decision-rule preference model from rough approximation of preference relation". [In]: Proc. 26<sup>th</sup> IEEE Annual International Conference on *Computer Software & Applications*, 26-29 August 2002, Oxford, England, pp. 1129-1134.
- [4] Łukasik, E., Multimedia Database of Violin Sounds, submitted to SMAC'03.
- [5] Kostek, B., "Soft Computing in Acoustics", Physics Verlag, Heidelberg, 1999.

## **AMATI – MULTIMEDIA DATABASE OF VIOLIN SOUNDS**

*Ewa Łukasik*

Institute of Computing Science, Poznań University of Technology, 60-965 Poznań, Poland

`Ewa.Lukasik@cs.put.poznan.pl`

### **ABSTRACT**

The database AMATI is entirely devoted to the violin voices. The instruments recorded are master quality and represent international schools of violinmaking. They were competitors of the 10<sup>th</sup> International Henryk Wieniawski Violinmaker Competition, held in Poznań, in autumn 2001. There are 17 000 sound files saved in the database. The collection of sounds comprises material similar to the one, that the jury of musicians examined during the audition. It includes open string bowed and plucked sounds, the entire range of notes across a chromatic scale on each string, a range of notes of diatonic scale and a fragment of J.S. Bach's piece of music. For each instrument the basic information is provided, including a photo, an emblem, the violinmaker's nationality, etc. The averaged scores of musical jury judgments constitute the unique and important element of the database, making possible e.g. the search for relationships between objective and subjective measures. The database contains harmonics based parameters for each sound. Parameter values may be visualized and compared in multiple configurations using a variety of charts created on-line. Signal waveforms, spectra and spectrograms are also available. Numerical values of parameters may be exported and used for further study. The database is an open source product (My SQL) and may be distributed among researchers.

### **1. INTRODUCTION**

The violin sound characteristics and its quality have been a research problem for a long time [1]. Studies have been devoted to historical (Italian), contemporary (master) and factory-made instruments recorded usually in the place, where the work took place (e.g. [2], [3]). There exist several musical databases on CDs or in the Internet (e.g. McGill University[4], SHARC [5], Studio en Ligne, IRCAM [6], B. Kostek [7]) containing, among others, the violin sounds performed with different articulation. In this paper we present the project AMATI, entirely devoted to violin sound. The instruments recorded are of superior quality and represent international schools of violinmaking - they were competitors during the 10<sup>th</sup> International Henryk Wieniawski Violinmaker Competition, held in Poznań, Poland, in autumn 2001. 70 instruments from 16 countries that were qualified to the second stage of the competition are represented in the database. The project has been developed in the Institute of Computing Science, Poznań University of Technology in the cooperation with Henryk Wieniawski Musical Society and Museum of Musical Instruments (branch of the National Museum) in Poznań. The collection of sounds comprises material similar to the one the Jury examined at the second stage of the competition. The averaged scores of musical jury judgments constitutes important and exceptional element of the database enabling correlation of objective and subjective measures to qualify the

instrument tone. The research in this domain has already started and some results are reported in [8] and [9].

The database is an open source product (My SQL) and may be distributed among researchers.

### **2. AMATI PROJECT PREREQUISITIES**

The sound quality of musical instrument depends upon a great number of factors. Both playing and recording methods may cause differences in analyzed sound. Generally speaking, no real instrument produces an accurate repetition of the same basic pattern. Both frequency and time domain representations of a steady state of an instrument are difficult. However human listeners judge the instrument quality in concert halls, and during competitions. Therefore it is still of interest to search for the relationship between objective and subjective judgments. The jury members of various competitions concerning art often say that the prize is given in a particular place and time and the same piece of art could be scored in absolutely different way given other milieu.

#### **2.1. The goal**

The main idea was to catch particular place and time of violinmaker competition to record the tone of a variety of international violins for further study. A starting point was analysis of the competition regulation concerning judgments of the acoustic properties of instruments performed by the jury of musicians and analysis of the way the actual audition proceeded. As a result a recording session has been organized in the environment maximally reproducing the one during the competition: the same chamber hall, microphones positioned in the places where jury members worked, the same violinist for all recordings (the player that tested instruments in the third stage of the competition). Also the sound collection was similar to that the jury members worked on. Together with the jury scores we got the substantial material for further study.

#### **2.2. Violinmakers Competition rules**

The 10th, edition of International Henryk Wieniawski Violinmaker Competition, was organized by Henryk Wieniawski Musical Society in Poznań in collaboration with Polish Violinmaker Association and Museum of Musical Instruments - a branch of National Museum in Poznań, in September 2001. The Competition was open to professional violinmakers of all nationalities and ages. Eligible for participation in the competition was an instrument that was an original piece of work, constructed not earlier than in 1998, being the property of the violinmaker who participated in the Competition, and was not awarded prizes at other competitions. The main objective of

the Competition was to select instruments of supreme acoustic qualities and exhibiting supreme artistry of violinmaking. The course of the Competition was as follows.

In stage 1, jury members - violinmakers - performed a general overview of the submitted instruments and eliminated those that did not meet the criteria of the Rules and Regulations.

In stage 2, members of the jury pronounced individual judgments on instruments admitted to the stage: violinmakers judged the violinmaking qualities, musicians judged the functional and acoustic properties. At this stage of the competition, the jury members used a 100-point scale. The following principles of awarding points for acoustic properties have been introduced:

- volume of sound (maximum 5 points per string (20 in total),
- timbre of the sound (maximum 5 points per string (20 in total),
- ease of sound emission (maximum 20 points),
- equal sound volume of strings (maximum 15 points),
- accuracy of assembly (maximum 10 points),
- individual qualities (maximum 10 points).

Basing on the highest scores awarded in stage 2, the jury determined a dozen of instruments admitted to stage 3 of the competition. In this stage, the jury in its full composition performed acoustic evaluation of instruments at public concerts in chamber and in concert hall. This part of the competition featured invited violin player - soloist (later performing recordings for AMATI project).

The AMATI database contains collection of sounds of 70 violins qualified to the second stage of the competition.

### 2.3. Recordings

The competition rules and regulation, as well as the procedure of performing musical judgments by musicians - members of the Jury influenced the way sounds for AMATI database were collected.

The recording sessions have been performed in the chamber hall of the Museum of Musical Instruments, branch of the National Museum in Poznan both in the near field (1 meter from the player) and in the far field (ca 10 meters from the player, in the place, where jury members worked).

The recording equipment consisted of capacity microphone DPA 4011 with cardioid characteristic (for recordings in the near field) and Tonsil MC 358 with supercardioid characteristic (for recordings in the far field), preamplifier – Sonosax SX-M2, digital CD recorder Philips CDR 880. All recordings were monofonic but performed simultaneously in two channels: one for near field and one far field. The sampling frequency was 44100 Hz.

The same player has played the sounds with the same bow during three sessions within five days, to make all recording conditions the most alike possible. The list of sounds was inspired by the second stage audition and is as follows:

- individual sounds played in detached mode on open G-string, D-string, A-string and E-string (four repetitions, two in each direction of the bow movement: up and down),
- plucked sound on four open strings, repeated once,
- the entire range of notes across a chromatic scale (two octaves) on G-string, from G3 to G5 (25 notes),

- the entire range of notes across a chromatic scale (two octaves) on D-string, from D4 to D6,
- the entire range of notes across a chromatic scale two octaves) on A-string, from A4 to A6,
- the entire range of notes across a chromatic scale two octaves) on E-string, from E4 to E6,
- a range of notes of diatonic scale from G3 to G6,
- a fragment of Johannes Sebastian Bach's Partita no 2 in d-minor, BWV 1004, part 3 - Sarabande.

## 3. AMATI DATABASE DESCRIPTION

The database contains over 17 000 templates - sounds of 70 competing instruments. They are accompanied by additional textual information, photos of violins and some charts created on line, representing sound waveforms, spectra and spectrograms, as well as displaying values of the set of chosen parameters. Names of violinmakers are not available. Instruments are identified by their specific numbers they got at the second stage of the competition. For enabling the user a rough insight into the instruments' characteristics, the database contains values of harmonics based parameters describing spectral features of individual sounds.

### 3.1. Database functions

The whole system is composed of the database and the application that communicates with the database and transfers queries from the user. User has on his/her disposal a range of operations, starting from the selection of sounds for analysis. Selection applies to the following attributes:

- instruments from the list (Figure1),
- sound (note) or the whole range of scale notes (Figure 2),
- microphone position,
- parameters and a range of their values.

Other operations include:

- reviewing text information and photos of instruments (Figure 3),
- playing selected sounds,
- displaying time-frequency representation of sounds - waveforms, spectrograms and spectra (Figure 4) and saving their bitmaps to the file,
- generating tables comprising numerical values of parameters and creating appropriate files,
- exporting selected sounds to the disc,
- creating bar chart of chosen parameter values for an entire scale or for selected sounds (Figure 5) ,
- creating a two dimensional separability charts (Figure 6),
- saving charts to the files,
- creating and printing reports containing selected data in numerical form.

The sounds contained in files are fully identified by file names. It is rather traditional, but very clear way of annotating sounds. In this way a compact and distinct names are assured for sounds exported from the database. The names contain violin number identifier (e.g. 75), sound type (e.g. de - détaché, pi - pizzicato, ch - chromatic scale, dia - diatonic scale), string name (G, D, A, E), sound within the chromatic scale (e.g. dis2 in notation used

in Poland), bowing direction (up, down), number of the repetition (1 or 2), microphone position (nf - near field, ff - far field). Below there are some examples:

- 75\_de\_G\_up\_2\_nf - violin no 75, separate sound played détaché on G-string with the bow movement up, second repetition, microphone placed in the near field,
- 75\_pi\_G\_nf - violin no 75, separate plucked sound (pizzicato) on G-string, microphone in the near field,
- 75\_ch\_G\_ff, the whole range of chromatic scale on G-string, microphone in the far field,
- 75\_ch\_G\_d2\_ff - violin no 75, separate sound d2 in notation used in Poland (D4 from the chromatic scale played on G-string), far field,
- 75\_dia\_ff - violin no 75, diatonic scale, far field,
- 75\_Bach\_ff - violin no 75, piece of music of Johannes Sebastian Bach, far field.

The database is of relational model and tuples do not need to preserve the file names.

### 3.2. Parameters calculation

The database contains FFT-based parameters pre-computed for each note. In the first version of the system these parameters have been calculated for the specific while of the sound evolution, which could be treated as a steady state. This while has been marked manually after tone waveforms and spectra analysis and marker position (the sample number, starting point for the FFT analysis) has been saved in the database. Improved FFT algorithm [10], has been used to calculate high precision frequency and amplitudes of harmonics. In the prototype version of the database the harmonics based spectral parameters that proved useful for musical instruments classification [7] have been provided: relative energy of the first harmonic (modified Tristimulus 1), relative energy of mid-frequency harmonics (modified Tristimulus 2), relative energy of high frequency harmonics (modified Tristimulus 3), brightness, relative energy of even harmonics, relative energy of odd harmonics, RMS and first three cepstral coefficients..

These parameters have been chosen for preliminary categorization of instruments. Deep analysis of violin sounds requires more advanced methods.

### 3.3. Technical concept

In order to make the database broadly available it was assumed that it will be realized in MS Windows environment using the open source MySQL relational database [11]. The application communicating with MySQL server has been created in MS Visual C++ 6.0 environment.

AMATI system operates as the interface to the database, enabling construction of queries to sound database and numerical values of selected parameters. It also enables generating reports and creating tables, charts and lists in response to queries.

The database server stores data and serves queries. The AMATI application has a function of a database client that operates on the data received. The client - server communication is performed using MySQL++. For on-line calculation of

spectral representation of sounds the Intel Signal Processing Library has been used, formerly available at Intel www site.

The system has been realized as a student team project under the supervision of the author.

## 4. CONCLUSIONS

In the paper the multimedia database of violin sounds has been presented. The recorded material consists of the sounds, spectra based parameters and jury scores of instruments presented at the 10<sup>th</sup> International Henryk Wieniawski Violinmakers Competition held in Poznań, Poland, in 2001. It is an open source product that may be distributed among researchers. Further development of functionality is planned. The sound material from the database will be of interest for violinmakers and students, as well as for research conducted in the domains of musical signal processing and machine learning.

## 5. ACKNOWLEDGEMENTS

The author wish to acknowledge the financial support from the State Committee for Scientific Research, the KBN grant no 4 T11F 002 22.

The author also feels grateful to Henryk Wieniawski Musical Society in Poznań and the management of the Museum of Musical Instruments, branch of National Museum in Poznań, for enabling recording of competing violins, for the access to the judgments of the jury and for the entire help during the realization of the project.

## 6. REFERENCES

- [1] Hutchins, C.M., "A history of violin research", J. Acoust. Soc. Amer., vol.73, pp. 1421-1432, 1983.
- [2] Meyer, J., "The tonal quality of violons", *Proc. SMAC'83*, Stockholm, pp. 69-78, 1985.
- [3] Harajda, H., "Violin timbre in relation to its spectra and transient characteristics" (in Polish), Ph.D. Thesis, Adam Mickiewicz University, Poznań, Poland, 1964.
- [4] *McGill University Master Samples*, <http://lecaine.music.mcgill.ca/MUMS/Html/Mums.html>.
- [5] *STUDIO EN LIGNE*, IRCAM, <http://www.ircam.fr>.
- [6] *Sandell Harmonic Archive SHARC Timbre Database*, <http://sparcy.parmly.luc.edu/sharc>.
- [7] Kostek B., *Soft Computing in Acoustics*, Physica-Verlag, Springer-Verlag, 1999.
- [8] Łukasik E., Susmaga, R., "Unsupervised machine learning methods in timbral violin characteristics visualization", *Proc. of SMAC'03*, Stockholm, 2003.
- [9] Jelonek J., Łukasik, E., Naganowski, A., Slowinski R., "Inferring Decision Rules from Jurys' Ranking of Competing Violins", *Proc. of SMAC'03*, Stockholm, 2003.
- [10] Desainte-Catherine, M., Marchand, S., "High - Precision Fourier Analysis of Sounds Using Signal Derivatives", *Journal of the AES*, 48, 7/8, pp. 654-667, 2000.
- [11] MySQL www site, <http://www.mysql.com>.

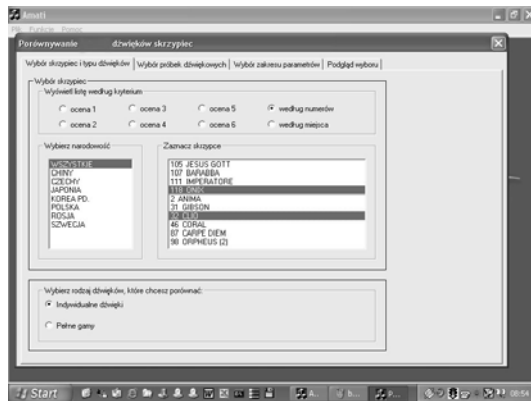


Figure 1: Violin selection.

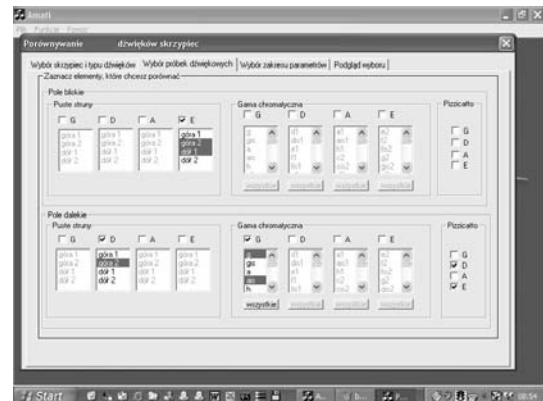


Figure 2: Selection of a particular sound.

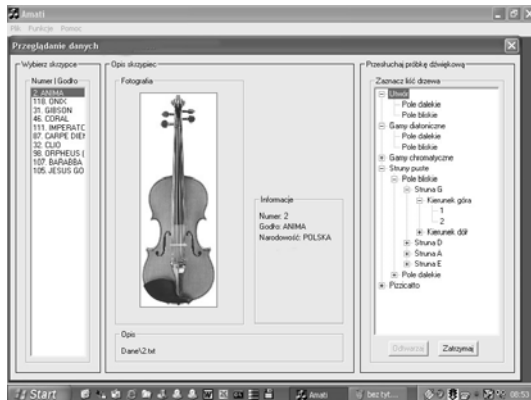


Figure 3: Description of the violin ANIMA (playing sound is possible)



Figure 4: Graphical representation of waveforms, spectra and spectrograms (playing sound is possible)

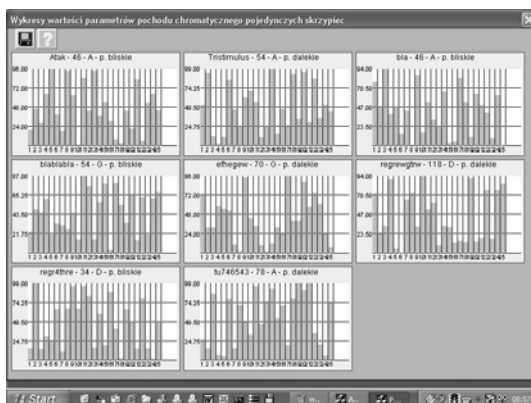


Figure 5: Visualization of parameter values for 25 sounds of a chromatic scale

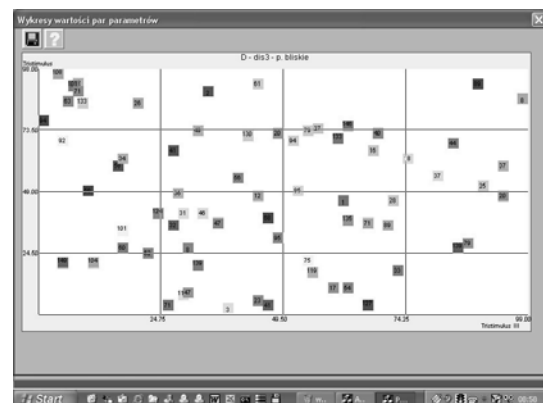


Figure 6: 2-D representation of a pair of parameter values for selected instruments

## UNSUPERVISED MACHINE LEARNING METHODS IN TIMBRAL VIOLIN CHARACTERISTICS VISUALIZATION

*Ewa Łukasik, Robert Susmaga*

Institute of Computing Science, Poznań University of Technology, 60-965 Poznań, Poland

Robert.Susmaga@CS.PUT.Poznan.PL

### ABSTRACT

We apply a mixture of unsupervised learning and statistical methods to find and illustrate similarity and dissimilarity factors in the timbre of violin voices. Our data come from the AMATI sound database that contains digitized recordings of 70 musical instruments presented at the Henryk Wieniawski 10th International Violinmakers Competition in Poznań, Poland, 2001. The raw sound data served to extract various sets of features, including harmonic based parameters (e.g. brightness, tristimulus, even and odd harmonics content), spectral parameters (e.g. energy, moments of various order), mel and linear scale cepstral coefficients, spectral envelope features (maxima and minima) and human ear auditory model features (the Lyon's model). We demonstrate machine ability to perceive the differences of violin timbre by applying multidimensional scaling (MDS) paradigm to the results of both classic and enhanced clustering methods. The MDS-based visualization leads to better perception and comprehension of the analyzed multi-dimensional space of the timbre characteristics. The ultimate MDS result is finally enhanced by the introduction of Voronoi diagrams, which can be displayed in form of both planar and spherical maps.

### 1. INTRODUCTION

The problem of defining the idea of musical timbre has been of interest to many researchers starting from Helmholtz [11]. Being aware of the impact of the way in which sound commences or terminates, he directed his attention to the musical part of the tone, which corresponded to a 'uniformly sustained and regularly periodic motion of the air'. Other definitions have been published by Fletcher (1934), and many others, including recently e.g. Grey (1975), Handel or Kendall, [8, 9, 14], who used the term *timbre* to refer to perceptual qualities of objects or events, that is to 'what it sounds like'. The most used is the ASA definition of timbre (1960): 'Timbre is that attribute of auditory sensation in terms of which a listener can judge that two sounds similarly presented and having the same loudness and pitch are dissimilar'. A further note was added in 1973: 'Timbre depends primarily on the spectrum of the stimulus, but it also depends upon the waveform, the sound pressure, the frequency location of the spectrum, and the temporal characteristics of the stimulus'. Although there has been some criticism of this definition, e.g. from Bregman [1], who argues that in this way we cannot define the timbre of the sounds that do not have pitch and who claims that the proper vocabulary of timbre should include labels for salient dimensions that should 'act in

psychologically simple ways and should have straightforward physical definition'. The timbre definition of Pratt and Doak is following [22]: 'Timbre is that attribute of auditory sensation so that a listener can judge that two sounds are dissimilar using any criteria other than pitch, loudness or duration'.

The history of the study of acoustic properties of the violin is very long [12]. Let us recall here only the investigations performed in Kungl Tekniska Högskolan by Sundberg, Janssen and Askenfeld [13], in Physikalisch-Technische Bundesanstalt in Braunschweig by Meyer [20] and some research in Poznań, Poland, performed by Kwiek and Harajda [10, 16]. As a result the relationship of the timbre and physical attributes has been examined in deep, still however leaving room for further investigations. With the advances of machine learning methods in the last few years, the problem has got a new dimension – it grew into the more general problem of automatic recognition of sound sources, including recognition of musical instruments (e.g. [2, 7, 15, 23]). This paper presents the problem from a new perspective, trying to benefit from the visualization of differences of the violin voices features.

### 2. THE METHODOLOGY

It has been shown beyond doubt that successful analysis of real-world objects cannot be properly performed without multi-dimensional description of these objects, as hardly ever a single coefficient can completely and exhaustively describe all the considered properties of the objects. In result, multi-dimensional descriptions of objects occur in most scientific analyses. The sheer multi-dimensionality of the description, however, prevents humans from getting proper and clear insight into the nature of such data.

That is why perceiving the data structure in multiple dimensions is one of the central objectives in all data analysis techniques. This objective can be reached by assisting the analyst in understanding higher dimensions, by effective reduction of the number of dimensions or by a skilled combination of the two.

The procedure applied in this particular set of experiments included (but was no limited to):

- clusterization of both unprocessed as well as PCA-transformed representations of the sounds,
- actual visualization, which implies either visualization of the results of clustering (in case of successful clusterization) or visualization of individual objects (otherwise).

The achieved results were visualized using the combination of multidimensional scaling, MDS, [4] and Voronoi diagrams [3].

## **2.1. Planar visualization**

Multi-dimensional scaling is a method that allows perceiving relative distances between objects described in high-dimensional data sets. Since seeing the relative positions of objects in the multi-dimensional space of attributes is impossible the method suggests specific positions (the x-y co-ordinates) of the considered objects in two-dimensional space. The two-dimensional positions are chosen in such a way that the distances between the objects in this two-dimensional space match as well as possible the distances between the objects in the original, multi-dimensional space. And although the structure represented by the positions of objects in the new, two-dimensional plane is not the same as the structure of their positions in the original, multi-dimensional space, such a 'map' of objects may be treated as a good approximation of this multi-dimensional structure.

It turns out that visualization of such maps may be greatly enhanced by the introduction of Voronoi diagrams (the process also known as the Dirichlet tessellation). Performing the tessellation of a planar map of  $n$  objects (in this context referred to as centres) resolves itself into partitioning the plane into  $n$  convex polygons such that each polygon contains exactly one centre and every polygon is defined by the points that are closer to its centre than to any other one.

It turns out that applying the Dirichlet tessellation to the results of MDS is especially fortunate in case when the MDS served to visualize the results of non-agglomerative clustering methods (e.g. the c-means clustering algorithm). This is because the result of the tessellation partitions the two-dimensional map into regions that are sets of points closest to their respective centers. A similar rule applies to the result of the c-means algorithm: clusters are also sets of observations that are closest to their respective centres. Thus the Voronoi polygons may be treated as some two-dimensional approximations of the clusters.

The above reasoning has some noticeable flaws, one of them being the fact that the Voronoi polygons have sharp boundaries while the clusters may or may not have such boundaries. The latter concerns in particular the fuzzy c-means algorithm, which (as opposed to the classic c-means algorithm) provides a model in which each observation may belong to more than one cluster, and thus rendering fuzzy clusters.

Of course applying MDS and the Voronoi diagrams need not be limited to visualizing the results of a clustering algorithm. The technique may also be used to illustrate the relative positions of individual objects. But it may be difficult with some data sets because when the number of objects increases, MDS encounters problems with finding proper two-dimensional co-ordinates of these objects. Fortunately, this difficulty may often be eased by visualizing representatives of clusters instead of objects. Again, this confirms that MDS, the Voronoi diagrams and a clustering tool turn out to be a very useful combination.

## **2.2. Spherical visualization**

As it turns out, applying the tessellation to a planar result of MDS have a particular disadvantage. It is characteristic to the planar representation of any group of objects that some of them have internal positions, while the other ones are distributed

towards the edge of the configuration. This makes no difference in MDS where only relative positions of the centres are taken into account, but can pose a problem when the corresponding Voronoi polygons are additionally added. This is because the areas of the polygons corresponding to the external centres are actually unbounded. In result, comparing their areas makes no sense, as the relative areas depend on the mere scale of the drawing.

The unfortunate problem of unbounded Voronoi polygons does not occur when the polygons (and their centres) are represented on a sphere. In such case each Voronoi polygon is bounded and the areas of all polygons may be successfully compared to one another. The topology of the sphere proves much more useful in this respect than the topology of the plane.

On the other hand, spherical scaling seems to have some drawbacks, one of them being the fact that the sphere cannot be easily represented in two dimensions. It is true that a sphere may be successfully projected onto a plane but, in fact, any static projection of a sphere onto a plane partially destroys the advantages of spherical scaling. The problem, however, is strictly a technical one and can easily be solved with a computer, which can successfully render three-dimensional, dynamic images of revolving spheres (another possibility would be to create a real model of Voronoi polygons on a sphere, i. e. in form of a colourful ball). The analysis of the regions in this case is not more difficult than in case of the planar representation.

Another, more important difference between planar and spherical visualization is that of the distance. The distances between points on the resulting two-dimensional map are always Euclidean (this measure is not to be confused with the measure chosen to calculate the distance between object in the original, multi-dimensional space of attributes, where many different measures can be used, including non-Euclidean ones). Introduction of spherical topology requires that this Euclidean distance should be substituted with spherical distance.

In the spherical MDS the locations of points on the sphere are chosen in such a way that the distances between the objects on the sphere match as well as possible the distances between the objects in the original, multi-dimensional space. The final result has the form of a spherical map of objects.

As it is also the case of planar scaling, the spherical scaling may have no ideal solution, i.e. there may exist no configuration of points on a sphere such that spherical distances among those points would be exactly equal to the distances contained in the input matrix of multi-dimensional distances. In this situation the proximity of solution may be characterised by the measure of stress. Low values of stress may indicate that the achieved solution, although not ideal, remains usable.

## **3. THE DATA AND EXPERIMENTS**

Actual recordings are individual sounds of equal length performed by an expert violinist on open strings, repeated several times with the same bow speed, bow pressure and bow position. Undoubtedly, the repeatability of such sounds could have been reached with only limited precision, as the human performer is influenced by many factors (including non-acoustic ones [20])

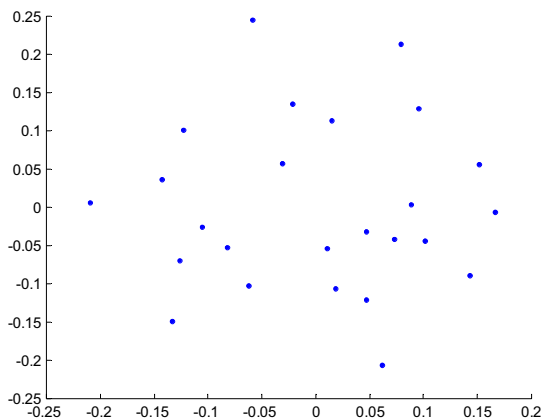


Figure 1: A planar result of the MDS procedure – the map of 25 violins, which illustrates their relative distances in the multidimensional space of attributes.

### 3.1. The creation of attributes

The bedrock of violin sound parameterisation is the harmonic-based spectral analysis of a steady-state of individual sounds. It has to be pointed out that it is hard to define the steady state of a string instrument sound, as it changes continuously. Therefore the parameters values have been calculated in the middle point of signal duration, where the amplitude reached its maximum.

The tristimulus method introduced in [21] and widely used in [15] has been adopted for this purpose giving first three parameters, the next being brightness, even/odd harmonics relation [15] and the four initial cepstral coefficients. Another set of features was related to the spectral envelope of the sounds. In this case the spectrum was calculated for the whole duration of the sound, averaging the influence of the evolution of sound on the features.

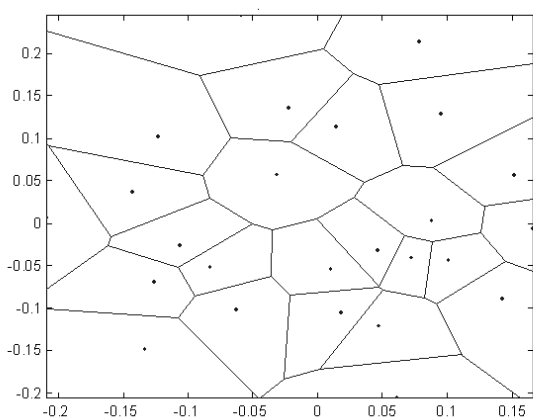


Figure 2: A planar Voronoi diagram of the 25 violins. Points indicate positions of the polygons' centres.

Cepstral coefficients in the linear mel-scale have been considered as the features responsible for spectral envelope shape. More exact form of representing envelope characteristics was maxima and minima of the envelope calculated as the inverse DFT of cepstral coefficients. They approximated the formants positions of the sound. The last set of features was based on the Lyon's cochlear model [19]. The features were calculated as the averaged outputs of filters modelling human auditory system. Their reduced and aggregated versions have also been taken into account [17].

### 3.2. Exemplary results

The experiments were carried on set of instruments selected from AMATI. This particular sets contained 25 violins, including those ranked as the best, average and the worst. The analysis proceeded with several representations of their sounds. As the different clusterization attempts (different methods, different control parameters) applied to these instruments produced rather poor results, the main problem of the visualization was to demonstrate relations between individual objects.

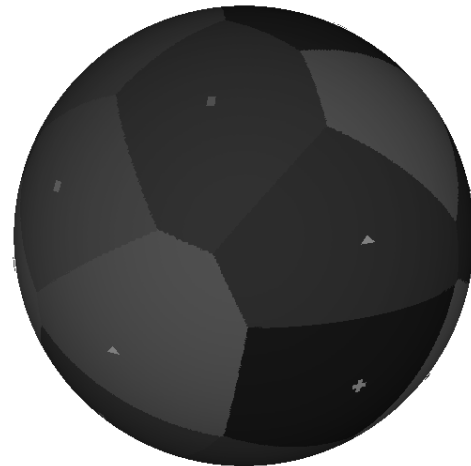


Figure 3: A spherical Voronoi diagram of the 25 violins. Markers indicate the position of the centres.

This kind of visualization is fully appreciated only when the sphere may be freely rotated using computer graphics.

The failure of the various clusterization algorithms to detect clusters despite the many different sound representations could be due to several reasons. First of all, the attributes in each of the considered attribute sets were not free of noise and some amount of randomness. Noise and randomness characterizes many real-life data and is unavoidable. Secondly, even when all the instruments possess unique qualities as far as the timbre of their sounds is concerned, the differences between particular pairs of instruments may be approximately equal and provide too little variety to deliver distinct clusters. Finally, such a result may be due to the performer/player of the sounds, whose influence of the performed on the sound of the violin is unavoidable.



Of course not every characteristic of a particular violin could be entirely determined by the player, as this is not the case. If needed, meticulous examinations of violins can be done with automatic sound uttering systems, which makes the analysis player independent. But it should be borne in mind that violins could never be fully appreciated and admired without their maestro-players, just as the maestro-players could never be fully appreciated without their instruments.

#### 4. CONCLUSIONS

The combination of MDS and the Voronoi diagrams has proved been very helpful in effectively illustrating the configurations of objects in the multi-dimensional space of attributes, and helping the analyst to better understand the relations between these objects. This concerns, in particular, the situation in which the objects are different representations of the sounds of violins.

Thanks to the planar illustration all relative dissimilarities between the instruments, understood as the difference in timbre, are evident. At the same time, instruments characterised by Voronoi polygons of large areas, which may be interpreted as big individuality of their timbre, are instantly identifiable. It is also easy to discover groups of similar – and as such relatively non-characteristic – instruments (despite the fact that no distinct clusters could be established in the analysed data set).

At least equally interesting results could be achieved with spherical representation of the Voronoi diagrams. In case of spherical representation all the polygons are bounded and their areas, now fully comparable to one another, can be estimated with even better confidence.

#### ACKNOWLEDGEMENTS

The authors wish to acknowledge the financial support from the State Committee for Scientific Research, KBN, research grant 4T11F 002 22. We would also like to express our gratitude to Henryk Wieniawski Musical Society in Poznań for the recordings of violins and to the Museum of Musical Instruments, branch of the National Museum in Poznań, for the lasting help received throughout the realization of the project.

#### 5. REFERENCES

- [1] Bregman, A., *Auditory Scene Analysis*, MIT Press, 1990.
- [2] Brown J.C., 'Computer Identification of Musical Instruments Using Pattern Recognition with Cepstral Coefficients as Features', *JASA*, 105, 1999.
- [3] Brown, K.Q., 'Voronoi Diagrams from Convex Hulls', *Information Processing Letters*, 9, 5, pp. 223–228, 1979.
- [4] Cox T.F., Cox M.A.A., *Multidimensional Scaling*, Chapman and Hall, London, 1994.
- [5] Fayyad U., Grinstein G.G., Wierse A., *Information Visualization in Data Mining and Knowledge Discovery*, Morgan Kaufmann, 2002.
- [6] Fletcher, H., 'Loudness, pitch and the timbre of musical tones and their relation to the intensity and the overtone structure', *JASA*, 6, pp. 59–69, 1934.
- [7] Fujinaga I., MacMillan K., 'Real Time Recognition of Orchestral Instruments', *Proc. of the Int. Computer Music Conference*, pp. 141–143, 2000.
- [8] Grey J.M., 'Timbre discrimination in musical patterns', *JASA*, 64 (2), pp. 467–72, 1978.
- [9] Handel, S., 'Timbre perception and auditory object identification', in Moore B.C.J. (Ed.), *Hearing – Handbook of Perceptual Cognition*, 1995, pp. 423–461.
- [10] Harajda, H., 'Classification of violin timbre' (in Polish), *Zeszyty Naukowe UAM w Poznaniu*, 4, 1964.
- [11] Helmholtz, H., *On the Sensation of Tone as a Psychological Basis for the Theory of Music*, 2nd English edition, Dover Publications, 1962.
- [12] Hutchins C.M., 'A history of violin research'. *JASA*, 73, pp. 1421–1432, 1983.
- [13] Jansson E., Bork I., Meyer J., 'Investigations into the Acoustical Properties of the Violin', *Acustica*, 62, 1986.
- [14] Kendall R.A., Carterette E.C., 'Difference Thresholds for Timbre Related to Spectral Centroid', *Proc. of the IV Int. Conference on Musical Perception and Cognition*, pp. 91–95, 1986.
- [15] Kostek B., *Soft Computing in Acoustics*, Physica Verlag, Heidelberg, 1999.
- [16] Kwiek M., Harajda H., Kamiński W., Urbański R., 'An attempt to the objective assessment of violin voices using spectral analysis of sounds', (in Polish), *Materiały X Otwartego Seminarium z Akustyki*, 1963.
- [17] Ligocka A., Łukasik E., 'Audio Features Extraction and Reduction Using Auditory Model – Application to Violin Voices Discrimination', accepted for ECCTD, 2003, Cracow, Poland.
- [18] Łukasik, E., 'AMATI – Multimedia Database of Violin Sounds', *Proc. of SMAC'03*, Stockholm, 2003.
- [19] Lyon R.F., 'A computational model of filtering, detection, and compression in the cochlea', *Proc. of the ICASSP'82*, Paris, IEEE, pp. 1282–1285, 1982.
- [20] Meyer J., 'The Tonal Quality of Violins', *Proc. of SMAC'83*, Stockholm, pp. 69–82, 1983.
- [21] Pollard H.F., Jansson E., 'A tristimulus method for the specification of musical timbre', *Acustica* 51 (3), pp. 162–171, 1982.
- [22] Pratt, R.I., Doak, P.E., 'A subjective rating scale for timbre', *Journal of Sound and Vibration*, 4, pp. 317, 1976.
- [23] Schreier E. D., 'Music Listening Systems', Ph.D. Thesis, MIT, 2000.

## LOGARITHMIC DAMPING DECREMENT AS THE CHARACTERISTIC OF PHYSICAL ACOUSTICS FOR QUALITY ESTIMATION OF VIOLIN WEDGES

Rajčan, E., Urgela, S., Čulík, M.

Technical University, SK – 96053 Zvolen, Slovakia  
emil@vsl.d.tuzvo.sk

### ABSTRACT

The quality evaluation of elements assessed for bowed instruments making is important for forest economists, wood businessman as well as for music instrument makers. In order to get the more complex data for violin wedges evaluation, to the trinity of characteristics of physical acoustics, measured in previous experiments (the density, modulus of elasticity, acoustical constant) the measurement of logarithmic damping decrement was added. After construction and evaluation of experimental violins made from the samples investigated, the more close linkage between materials characteristics and quality of instruments should be expected.

### 1. INTRODUCTION

In Europe and especially in Central Europe, high-quality maple (*Acer pseudoplatanus L.*) wood used for back plates of string instruments is relatively expensive. It can therefore be useful to find new maple sources and to compare perfect wood coming from traditional localities with that from new or unknown areas. For this reason, the experimental study of such maple wood is a current matter.

The question from the viewpoint of materials science inherent to musical instruments making solved here can be also formulated as follows: We have a piece of material (maple). Is it suitable for manufacturing a bowed string musical instrument? If yes, what is the grade of material? This statement corresponds with the question: what level of quality of the final product could be anticipated? The grading of maple for this purpose is the main object of this study.

When wood material is selected, properties of maple, which should determine the constructional and acoustical characteristics of a string musical instrument, are in most cases evaluated by sensory tests using empirical knowledge of a manufacturer. After visual control regularity and width of annual rings and casual occurrence of defects as knots, resin, ducts, fungi attach, etc., by means of the tapping test [1] a violin maker finds out information about acoustical properties of the material [2]. For high quality (master) instruments, curly maple is preferred. This attribute, as it has been generally known since the age of old Italian violin makers, represents one of the basic aesthetic criteria in order to classify an instrument as a top-quality product, e.g., [3].

The wavy grain in maple is considered as a natural defect. In case its acceptance for musical instruments making, this enhances the commercial value of timber [4]. Existing standards for lumbering and assortment, e.g., [5], are regarded to be more or less a framework and are not strictly applied for selection and price estimating. Producers of the instruments, in respect to the lack of maple, are willing to give up the recommendations of

standards and to pay a lot for a piece of wood assumed to be cut properly to obtain the plates or forms for other parts with sufficient dimensions [6].

Recently, significance of exact methods of wood examination based on physical acoustics laws has increased along with the subjective empirical experience. Modal analysis [7, 8] is one of the basic methods for vibration investigation. The Chladni method and holographic interferometry have been shown to be helpful for investigation of rectangular wooden plates, violin plates and string instrument modes [e.g. 9]. Extensive study by using the modal analysis method applied to wood was carried out by McIntyre and Woodhouse [10].

Application of the mentioned methods of the physical acoustics could contribute to successful selection of wood material for musical instruments making. The concept and application of the material selection charts was described by Ashby [11]. Similar 2D graphic plots for spruce and maple wood for bowed musical instrument were independently invented by Rajčan [12] and later improved to 3D graphic plots [13]. As a part of the AKUSTOMAT system, the 3D graphic charts support evaluation or grading of wood for manufacturing of bowed musical instruments. Comparing with the previous experiments (where the triplet of characteristics density, A-constant and E-modulus were measured), the present study is oriented on the quantities triplet: density, A-constant and the logarithmic damping decrement.

This study is devoted to an experimental research of maple wedges from a company GLEISSNER – Tone woods, as material for back of violins. The data obtained were compared with experimental data obtained on two sets of maple evaluated by experts for violin manufacturing as high- and lower-quality.

### 2. THEORETICAL NOTE

When a plate or a stick is excited by an acoustic wave, the standing bending wave can arise in it. In the case of a plate with free edges, the so-called first bending beam mode can be quite easily generated. The natural frequency  $f$  corresponding to this mode enables us to determine the Young's modulus  $E$  using the formulae [10].

$$E \approx 0.947 \frac{f^2 \rho a^4}{h^2}, \quad (1)$$

where  $\rho$  is density,  $a$  – length,  $h$  – thickness of the plate. For the calculation of the acoustic constant  $A$  the relation [14]

$$A = \sqrt{\frac{E}{\rho^3}}. \quad (2)$$

and for logarithmic damping decrement the equation [e.g. 15]

$$\vartheta = \pi(f_2 - f_1) / \sqrt{3} \cdot f \quad (3)$$

(where  $f_2$  and  $f_1$  are the frequencies at which the amplitudes of oscillations have half value of the amplitude at the resonant frequency  $f$ ) were used.

### 3. EXPERIMENT

Experimental measurements were done on the system AKUSTOMAT [13]. Its mechanical part is shown on the fig.1.

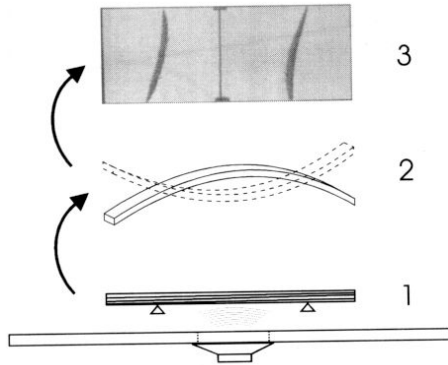


Figure 1: Layout of first bending beam mode generated in a plate. 1 – test specimen supported at nodes, 2 – shape of the bending beam mode, 3 – so-called Chladni pattern of the mode.

The data calculated using the equations (1) and (2) from the measured values of mass, dimensions and frequencies, were plotted in 3D material selection charts with co-ordinates  $\rho$ ,  $\vartheta$ ,  $A$ . The results were compared with the reliable standards for back plates of string bowed musical instruments. Afterwards, estimation of investigated maple wood was performed. The evaluation in 3D plots were supported by mathematical-statistical tests.

#### 3.1. Results

The quality of actual wedges can be demanded on the base of appreciation of the position inherent point, representing result of measurement of characteristics of physical acoustics in 3D. The next figures show basic tendencies of high-quality (HQ), lower-quality (LQ) maple and comparison of the examined set with HQ and LQ standards.

From these measurement – as it is obvious from fig. 2 – the HQ set (together with the waviness of annual rings) is characterized by higher density, lower A-constant and greater decrement in comparison with the LQ-set (with very low or absent waviness). This basic tendency can be used on the evaluation of actual set of maple wedges

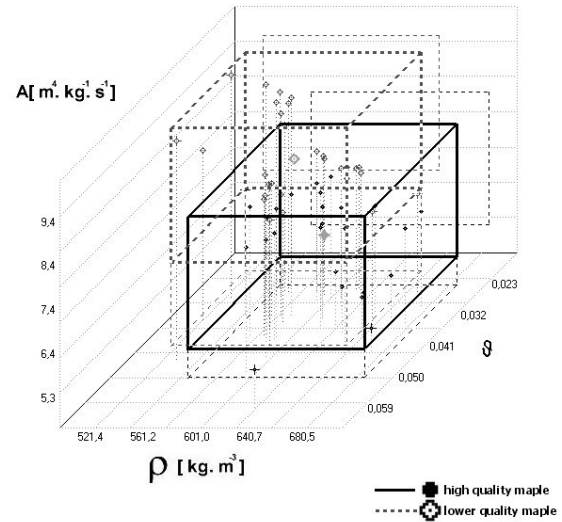


Figure 2: The density  $\rho$ , the acoustic constant  $A$  and the logarithmic damping decrement  $\vartheta$  of individual test specimens of high-quality and of lower-quality maple for a violin back plate in 3D. For each quantity, the mark of the test specimen is distinguished regarding its reference inside or outside the interval of the mean value  $\pm 2$  standard deviation. Material was selected by an experienced expert for violin making.

### 4. DISCUSSION

From the comparison of the examined set with HQ and LQ standards it implicates that the examined set from the viewpoint of used triplet of characteristics is somewhere between HQ and LQ. Except others the examined set is characterised by relatively high dispersion of the damping decrement.

Based on the position of individual wedges in the given 3D it is possible to appreciate and rank their quality; to negotiate the price of particular material. So the AKUSTOMATical measurements and their following display in 3D enables more competent appreciation of wood as material for musical instrument making. The results of such measurements are not in contradiction with the empirical knowledge, but bring possibility more precisely wood quality grading.

### ACKNOWLEDGMENTS

This research was supported by Slovak Grant Agency, project No 1/7567/20.

The authors thank to R. Igaz and P. Statdrucker and V. Bahyl for technical help.

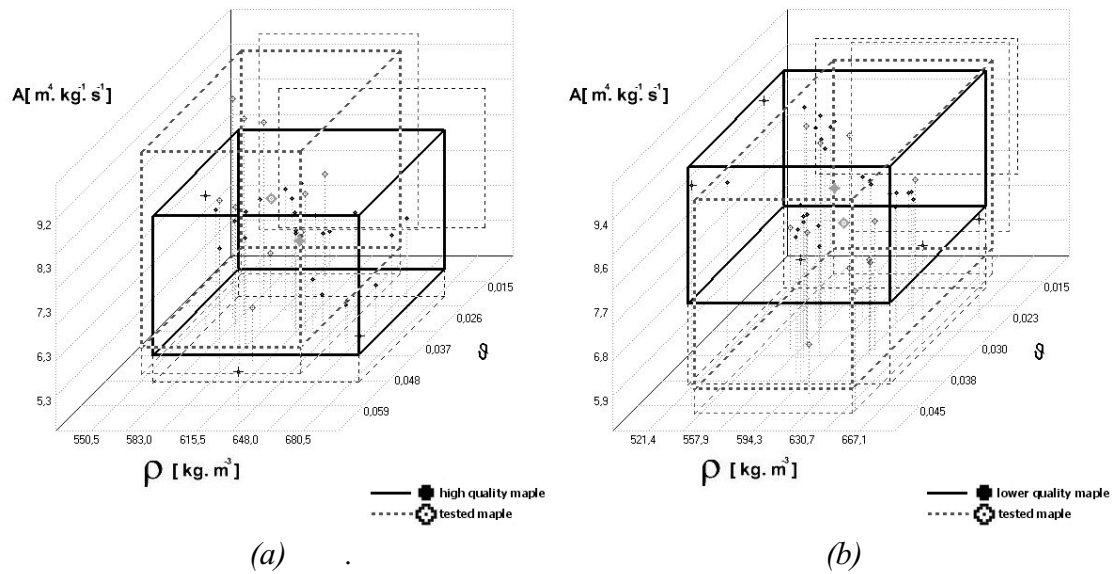


Figure 3: The characteristics  $\delta$ ,  $A$  and  $\rho$  of HQ set and the tested set of maple.

## 5. REFERENCES

- [1] E. Jansson: Acoustics for violin and guitar makers. Webpage: <http://www.speech.kth.se/music/acvigit4/index.html>
- [2] V. Pilař and F. Šrámek: The art of violinmakers. Panton, Praha, Czech, 1989, 1<sup>st</sup> ed.
- [3] M. Gleissner: Tonholzer. Personal communication to authors, 1999, Bubenreuth
- [4] V. Bucur, Acoustics of wood. CRC Press, Boca Raton–New York–London–Tokyo, 1995, 1<sup>st</sup> ed.
- [5] STN 48 0056. Broad leaved assortments of raw wood. Technical requirements Vydavatelství UNM Praha, Slovak, 1985, p. 15
- [6] J. Holíš: Manager of AKORD KVINT – private bowed instruments' manufacturing company. Personal communication to authors, Luby u Chebu, 1999
- [7] K. Wogram: Schwingungsuntersuchungen an Musikinstrumenten. In: Fortschritte der Akustik, Plenarvorträge und Fachbeiträge der 20. Deutschen Jahrestagung für Akustik, DAGA 94 – Dresden, Teil A, 53–64
- [8] M. A. Hutchins: Acoustical parameters for violin and viola back wood. Catgut Acoustical Society Newsletters **36**, 1981, 29–31
- [9] E. V. Jansson, N. E. Molin and H. O. Saldner: On eigenmodes of the violin – Electronic holography and admittance measurements. J. Acoust. Soc. Am. **95**, 1994, 1100–1105
- [10] M. E. McIntyre and J. Woodhouse: On measuring wood properties, part I, II, III. Journal of the Cutgut Acoustical Society **42**, 1984, 11–15, **43**, 1985, 18–24, **45**, 1986, 14–23
- [11] F. Ashby: Materials Selection in Mechanical Design. Pergamon Press. Oxford–New York–Seoul–Tokyo, 1993, Reprinted (twice) with corrections
- [12] E. Rajčan: Die Physikalisch – akustischen Charakteristiken von Holz als Material für die Produktion von Streichinstrumenten. INSTRUMENTENBAU ZEITSCHRIFT. MUSIK INTERNATIONAL **45**, 1991, 44–47
- [13] E. Rajčan: Applications of acoustics in some problems of material science related to the making of musical instruments. ACUSTICA united with acta acustica **84**, 1998, 122–128.
- [14] N. N. Andreev: On the wood for musical instruments. In Collection of Works of Scientific Research Institute of Musical Industry. Issue 1, Moscow–Leningrad, 1938, 13–18
- [15] E. Rajčan: Acoustics I. Technical University in Zvolen, Slovak, 1998, 1<sup>st</sup> ed.



## EFFECT OF THE WIDTH OF THE BOW HAIR ON THE VIOLIN STRING SPECTRUM

Erwin Schoonderwaldt<sup>1</sup>, Knut Guettler<sup>2</sup>, and Anders Askenfelt<sup>1</sup>

<sup>1</sup>KTH, Dept. of Speech, Music and Hearing, Stockholm, Sweden

{schoondw, andersa}@speech.kth.se

<sup>2</sup>Norwegian Academy of Music, Oslo, Norway

knut.guettler@samson.nmh.no

### ABSTRACT

Violinists often claim that tilting the bow provides greater brilliance. By tilting, the effective width of the bow hair is reduced and the bow force distribution across the bow hair ribbon is changed. Considering that the width of the bow hair of a violin bow is roughly 1/32 of the string length (about 10 mm), and that the relative bow-bridge distance in playing typically varies between 1/8 and 1/32, an effect of the width of the hair on the slip-stick process seems reasonable. Pitteroff [1] has reported simulations and measurements showing that the slipping intervals become progressively shorter as the width of the bow hair ribbon is decreased. However, the effect, which mainly was attributed to a faster transition from stick to slip at release, was small. In this study, evidence gained in experiments using a bowing machine is presented, showing that a decrease of the width of the bow hair may boost the string spectrum considerably for higher harmonics. A gain in partial amplitudes of 3–6 dB has been observed above partial 20. Besides increased brilliance, it is clear that there are several other reasons for violinists to tilt the bow. For example, tilting the bow hair facilitates gentle note attacks due to a gradual buildup in string contact.

### 1. INTRODUCTION

String players often tilt the bow by leaning the stick towards the fingerboard. A line through the centers of the stick and bow hair will then no longer be perpendicular to the string plane, as in the case when the bow is placed flat on the string. There are several good reasons for tilting the bow, which applies both to playing in soft and loud dynamics. For a moderate tilting all hairs will remain in contact with the string, and the distribution in bow force across the width of the bow hair will decrease from a higher value at the edge towards the fingerboard (outer) to a lower value at the edge towards the bridge (inner) [1]. For strong tilting the effective width of the bundle of bow hair, which makes contact with the string is reduced. For a sufficiently high force the bundle of hair will twist so much that the entire width of the hair is brought in contact with the string, except when playing close to either the frog or the tip.

Pitteroff [1] showed through simulations that tilting in the correct way (the stick leaning towards the fingerboard) is advantageous by increasing the safety margins for Helmholtz motion, see Fig. 1. The distribution in bow force across the bow hair obtained by correct tilting reduces the penetrating depth of backward partial slips into the bow hair. (Backward slips are due to reflections from the bridge during nominal stick but do usually not reach through the entire width of the bow hair). This reduces the risk of total secondary slips, resulting in a division

of the period into fractions of the fundamental. Also, with a tilted bow the partial slips will be less pronounced in the bridge force waveform. For strong tilting, the reduction in the width of the hair in contact with the string brings the bowing situation closer to the point-bow case. This reduces the discrepancy in string slopes at the inner and outer edges of the bow hair, weakening the strength of backward partial slips.

The simulations indicated that the duration of the release and recapture (the transitions from stick to slip and vice versa)

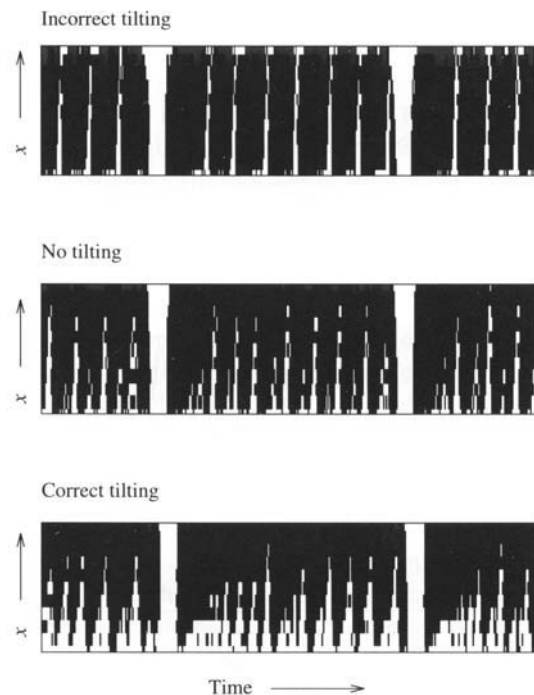


Figure 1: Simulation of the effects of tilting the bow; bow flat on string (middle), bow tilted in the correct way towards the fingerboard (bottom), and bow tilted the wrong way (top). The panels are "friction maps" showing the contact conditions across the width of the bundle of bow hair vs. time with white color indicating "slip" and black "stick" (the edge of the hair towards the bridge at the bottom). The large white passages reaching through the entire width of the hair are the main slips of the Helmholtz motion. The smaller white encroachments are backward partial slips caused by reflections arriving from the bridge during nominal stick. Bow force 1500 mN,  $\beta = 1/23.2$ . (From Pitteroff [1])

decreased when tilting the bow, while not affecting the total duration of the slip. This observation suggests a possibility for an influence on string spectrum.

## 2. METHOD

The velocity of a violin string was recorded under controlled bowing conditions using a PC-controlled bowing machine. The string velocity was picked up at the point of bowing by mounting a magnet (diameter 6 mm) under the string, and stored digitally with a sample frequency of 44.1 kHz. A carbon-fiber composite bow (Spiccato Solo) was used, playing a violin D string (Prim, steel core) mounted on a custom-designed monochord of dural. The design of the monochord copied the dimensions of a violin closely, including bridge height, and the speaking length of the string ( $L = 325$  mm,  $f_o = 293$  Hz). Spectra of selections from the steady-state part of 10 strokes were averaged. Each selected part had a duration 0.5 s, and corresponded to 5 to 15 cm of a bow stroke between the middle and tip. The spectra were calculated using a moving Hann window of width 1764 points, yielding a bandwidth of 50 Hz.

The spectral envelopes were obtained from the harmonic peaks, and compensated for the influence of the width of the magnet.

Data for a set of three *widths* of the bow hair (4, 8, 15 mm), three *bow forces* (400, 550, 800 mN), and three *bow velocities* (10, 20, 30 cm/s) were collected. The bow-bridge distance was 30 mm, corresponding to a  $\beta$  close to 1/11. The 9 combinations of bow forces and velocities spanned a reasonable large range from “light” bowing with high velocity to “heavy” bowing at low speed, showing pitch flattening. The combination of high bow force and low velocity (800 mN/10 cm/s) gave non-Helmholtz motion (raucous).

The original width of the bow hair was 8 mm. The wide bow hair condition (15 mm) was implemented by spreading the hairs evenly with the aid of two small pieces of a densely spaced louse comb at the tip and middle of the bow. The narrow bow (4 mm) was obtained by lifting the outer parts of the bow hair from the contact path with the string by inserting small pieces of cardboard in the bundle of bow hairs at the tip and middle.

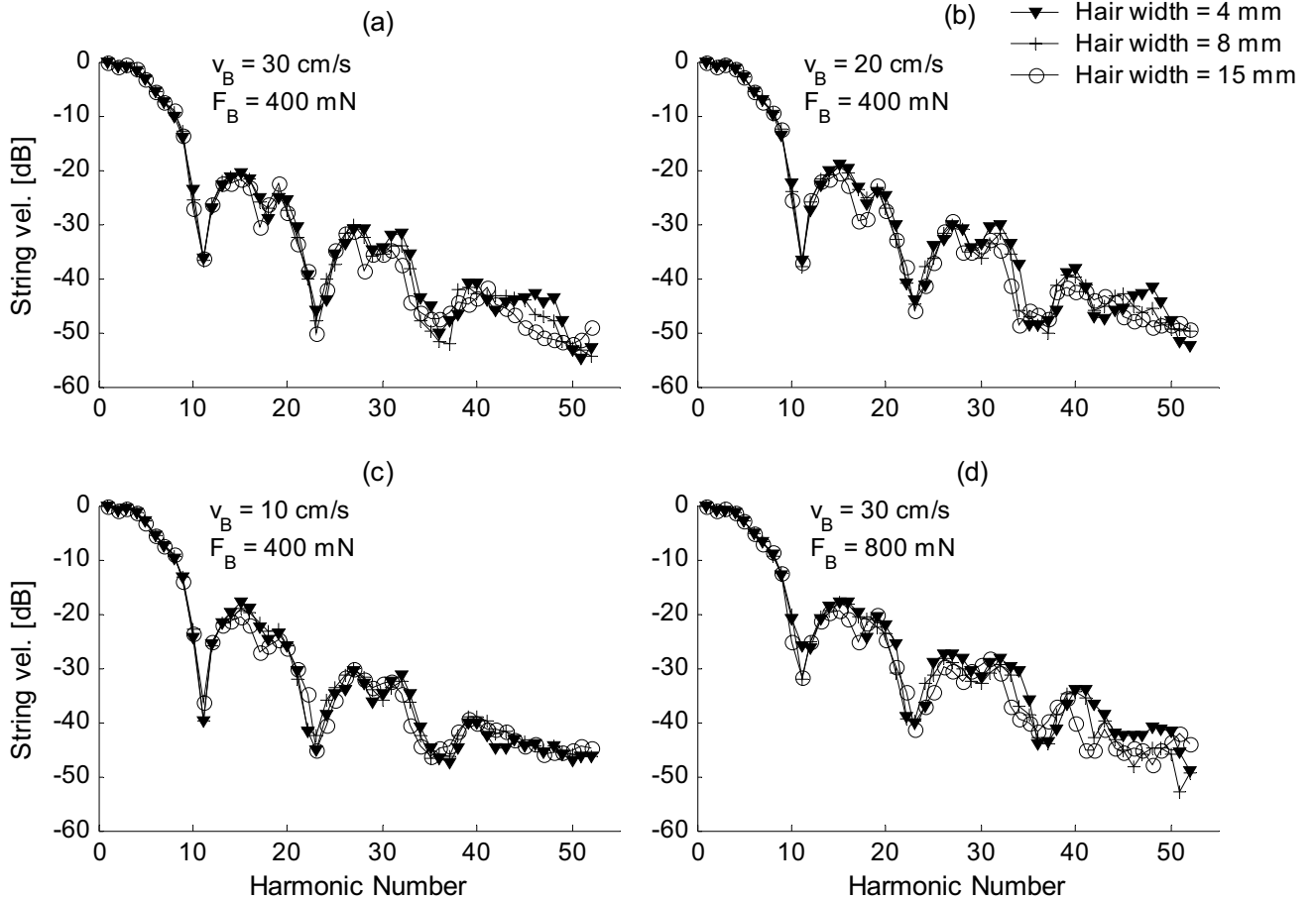


Figure 2: Influence of width of bow hair on string spectrum for low bow force (400 mN) and a bow velocity of (a) 30 cm/s, (b) 20 cm/s, (c) 10 cm/s, and (d) high bow force (800 mN) and high velocity (30 cm/s). The width of the bow hair was 4 mm ( $\blacktriangledown$ ), 8 mm ( $+$ ), and 15 mm ( $\circ$ ). Each spectrum is an average across 5 s of recorded bow strokes. The partial amplitudes have been normalized to the fundamental.

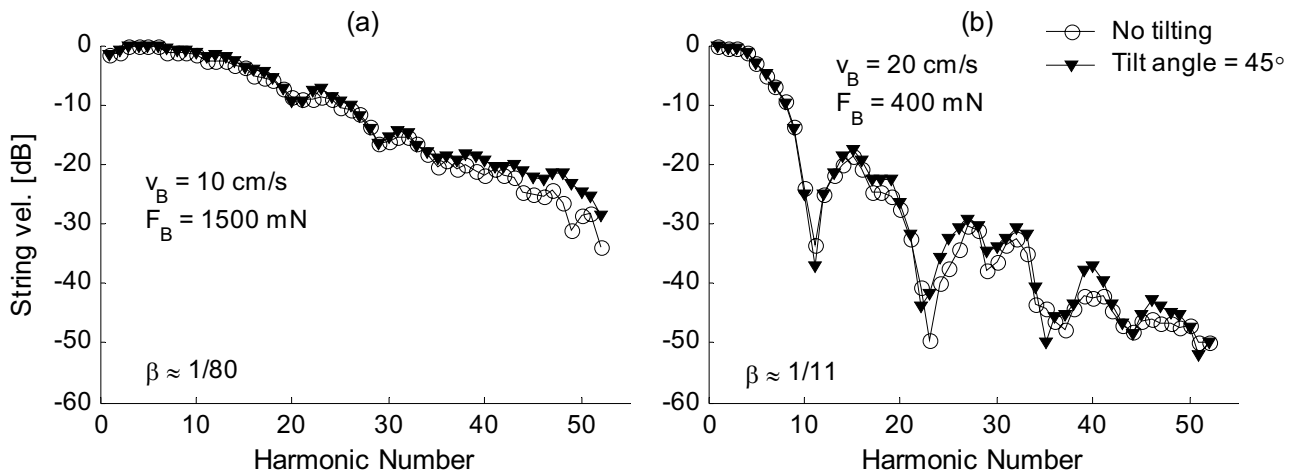


Figure 3: Influence of tilting the bow. Comparison of string velocity spectra when playing (a) very close to the bridge (4 mm from bridge to center of bow hair) with a high bow force (1500 mN, 10 cm/s), and (b) at a normal bow-bridge distance (30 mm) with low bow force (400 mN, 20 cm/s). The curves compare the case of the bow flat on the string ( $\circ$ ) with a tilting of  $45^\circ$  in the correct way ( $\blacktriangledown$ ). For the tilted condition, the width of the hair in contact with the string was larger in (a) than in (b) due to the high bow force.

### 3. RESULTS

#### 3.1 Influence of bow width

Changing the width of the bow hair (while keeping the bundle of hairs flat on the string) had a clear influence on the string spectrum. A reduced hair width gave generally higher amplitudes of the high-frequency partials (see Fig. 2). The effect was most pronounced for the highest bow velocity (30 cm/s). Starting above the first “node frequency” (partial 11), the boost was typically 2–4 dB at 30 cm/s for both cases of reduction in bow width, from 8 to 4 mm, and from 15 to 8 mm. The effect increased more or less continuously in the frequency range observed (up to partial 50, ca 15 kHz), with individual gain in partials up to 6 dB. A high bow force enhanced the differences. At 10 cm/s the effect was marginal, and not possible to verify within the accuracy of the measurements.

#### 3.2 Influence of tilting

Reducing the width of the bow hair by tilting gave a consistent boost of the amplitudes of higher partials. The situation when playing very close to the bridge with a high bow force (1500 mN) is illustrated in Fig. 3 (a). In this condition the inner bow hairs touch the bridge and  $\beta$  varies under the bow from 1/40 (outer edge of hair) to about 1/80 (center). A tilt of  $45^\circ$  in the correct way with the stick leaning towards the fingerboard, gave a boost in string partial amplitudes of about 1 dB from partial 6, continuously increasing to more than 5 dB at partial 50 (16 kHz). Tilting also had a clear effect on the quality of the attacks. With the bow placed flat on the string the tone was often unstable with persisting aperiodic pre-Helmholtz transients. Tilting of the bow resulted in a more “free” tone quality with reasonably long attacks.

Also when playing farther away from the bridge a clear effect of tilting was observed. Fig. 3 (b) shows a case with the same bow-bridge distance as in Fig. 2 (30 mm) and low bow force (400 mN). The tilting gives a gain in the partial amplitudes, typically 2–4 dB, starting at about partial 11. Tilting the bow in the incorrect way (the stick leaning towards the bridge) also gave a gain in high-frequency partials but slightly less consistent than for the correct way of tilting.

#### 3.3 Influence of bow force

The influence on string spectrum available to the player by changing the bow force is shown in Fig. 4. As described by Schelleng [2] and Cremer [3] an increase in bow force boosts the high-frequency partials. The observed spectral changes when increasing the bow force from 400 to 550 to 800 mN,

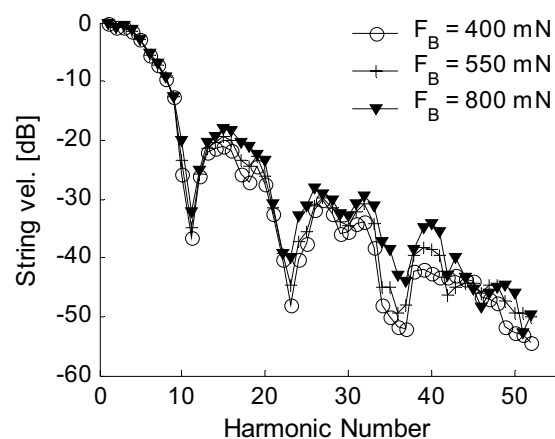


Figure 4: Influence of bow force on string spectrum, 400 mN( $\circ$ ), 550 mN( $+$ ) and 800 mN( $\blacktriangledown$ ) (hair width 8 mm, velocity 30 cm/s, bow-bridge distance 30 mm).



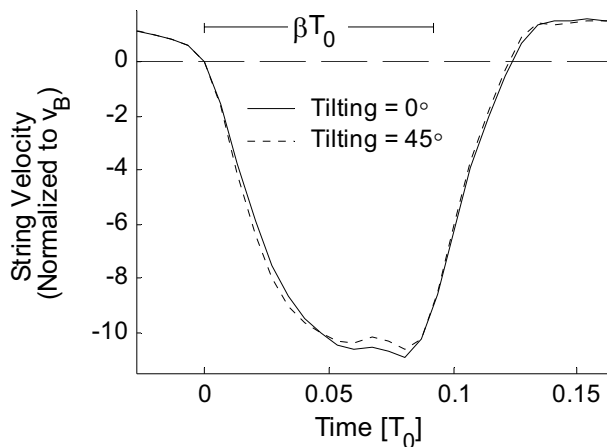


Figure 5: String velocity under the bow during slip for the two cases in Fig. 3 (b) with the bow hair placed flat on the string and with the bow tilted  $45^\circ$  in the correct way towards the fingerboard (400 mN, 20 cm/s, bow-bridge distance 30 mm). Each curve is averaged across 10 periods.

respectively, are of the same magnitude as the changes induced by reducing the width of the bow hair from 15 to 8 to 4 mm. A gain in partial amplitudes of 4 – 6 dB is observed, with maxima of about 6 dB. However, when increasing the bow force the effect is relatively large even at lower partials (from partial 11 and up) and more consistent compared to the effect of reduced hair width and tilting. When decreasing the hair width the general trend of a gain in partial amplitudes is occasionally punctuated by reductions in individual partials (cf. Fig. 2).

### 3.4 Influence of bow velocity

The influence on string spectrum by changing the bow velocity (30, 20, 10 cm/s) was of the same magnitude as changing the width of the bow hair (4, 8, 15 mm). In contrast to a widely spread belief, a gain in higher partials is achieved by lowering the bow velocity, rather than by bringing the bow closer to the bridge [4]. The effect of velocity changes was slightly larger at the lowest bow force (400 mN).

## 4. DISCUSSION

The results show that a reduction of the width of the bow hair, either by tilting or by a modification of the bundle of bow hair gives a boost in high-frequency partials. This applies to low as well as high bow forces and velocities. The effect can be traced in the velocity waveforms during slip (see Fig. 5). Reducing the width of the hair gives a faster transition from stick to slip, and a marginally faster transition from slip to stick in, both in line with the simulations by Pitteroff [1].

In playing, bow-bridge distance, bow force, bow velocity, and the width of the hair (tilting) are rarely varied one by one. As shown in studies of violinists' performances, a key characteristic in string playing is a continuous coordination of all the bowing parameters [5]. Even when drawing long *steady* notes the bow pressure, bow bridge distance, and also tilting is

varied as the contact point moves from frog to tip in order to maintain what is considered as a uniform timbre. The results of this study and an accompanying study [4] indicate that there might be a substantial combined effect on the spectral slope by bringing the bow closer to the bridge while simultaneously increasing the bowing force, lowering the bowing velocity, and adjusting tilting.

Perceptually tilting is claimed to increase brilliance and giving a more "free" tone quality (as opposed to "pinched" or "pressed"). The tilting is considered especially important when approaching the frog [6].

Besides the influence on spectrum and timbre of sustained tones described above, there are other good reasons for tilting the bow. A tilting may facilitate clean attacks by reducing the influence of secondary backward slips. By tilting, the note is started with a more point-like bow, successively bring the full width into play after the Helmholtz motion has started. In this way, the risk of long-lived pre-Helmholtz transients might be reduced.

## ACKNOWLEDGEMENTS

Work supported by the Swedish Research Council.

## 5. REFERENCES

- [1] Pitteroff, R. & Woodhouse, J., "Mechanics of the contact area between a violin bow and a string. Part III: Parameter dependence", *Acta Acoustica*, Vol. 84 No. 5, pp. 929-946, 1998.
- [2] Schelleng, J. C., "The bowed string and the player", *J. Acoust. Soc. Amer.* 53(1), pp 26-41, 1973
- [3] Cremer, L. (1972 and 1973) "The influence of "bow pressure" on the movement of a bowed string" (Part I and II), *NL. Catgut Acoust. Soc.* #18 pp. 13-19 and #19, 21-25.
- [4] Guettler, K., Schoonderwaldt, E. & Askenfelt A., "Bow speed or bow position – which one influences spectrum the most?", *Proc. of the Stockholm Music Acoustics Conference (SMAC 03)*, Stockholm, Sweden, 2003.
- [5] Askenfelt A., "Measurement of the bowing parameters in violin playing II: Bow-bridge distance, dynamic range, and limits of bow force", *J. Acoust. Soc. Am.*, Vol. 86, pp. 503-516, 1989.
- [6] Galamian, I., "Principles of violin playing and teaching", Prentice-Hall, Inc., Englewood Cliffs, N. J., 1962

## BOWED STRING SIMULATION USING AN ELASTO-PLASTIC FRICTION MODEL

Stefania Serafin

CCRMA, Dept. of Music  
Stanford University  
The Knoll, 660 Lomita  
3Stanford, CA, 94309

serafin@ccrma.stanford.edu

Federico Avanzini

Dip. Ing. dell'Informazione  
University of Padova  
Via Gradenigo 6/A,  
5131 - Padova, Italy

avanzini@dei.unipd.it

Davide Rocchesso

Dip. Informatica  
University of Verona,  
Strada Le Grazie, 15  
37134 - Verona, Italy

rocchesso@sci.univr.it

### ABSTRACT

This paper proposes a digital waveguide model of a bowed string in which the interaction between the bow and the string is modeled using an elasto-plastic friction model. The interaction model is presented, and its advantages with respect to usual static models are discussed. Details about the numerical implementation are addressed. Numerical simulations show that a hysteresis loop in the friction versus velocity plane is created, which is qualitatively compatible with experiments on real instruments and with the behavior of a recently proposed thermodynamical friction model applied to bowed string simulations.

### 1. INTRODUCTION

The bow-string interaction is a complex phenomenon that belongs to the larger field of frictional induced vibrations. The most widely accepted theoretical models of the bow-string interaction assume that the excitation ideally occurs at a single point and that the frictional force at the contact point is a function of the relative sliding velocity between the bow and the string (see for example [1, 2]). Many relevant features of the bowed string motion are successfully explained by these *static* models.

Recently, Smith and Woodhouse [3] proposed a more sophisticated model, based on the observation that the interfacial rosin layer exhibits plastic deformation at the contact point due to fast temperature changes within one oscillation period. For this reason, they proposed a model called *plastic*, in which friction depends on the “thermal history” around the contact zone. As a consequence, the model exhibits an hysteresis loop in the force versus velocity plane.

Outside musical acoustics studies, a plethora of friction models are available from the literature of robotics and haptics, as well as automatic control. *Dynamic* models have been proposed, in which the dependence of friction on the relative sliding velocity is given by a differential equation [4, 5, 6, 7], which is meant to account for transient behaviors.

In this paper we apply a class of *elasto-plastic* dynamic friction models to the simulation of a bow exciting a string. An earlier attempt to use this model in the context of bowed string simulation has been already proposed in [8]. However, the numerical implementation used by the authors does not allow accurate simulations of the model, and introduces instability problems. The numerical scheme adopted here provides an accurate yet efficient numerical implementation of the non-linear equations. The very same numerical model has been applied elsewhere to simulate frictional

interaction between modal resonators [9], and applied to the design of “everyday” (non-musical) sounds [10].

Section 2 describes the interaction model and compares it with the plastic approach proposed by Smith and Woodhouse. Section 3 presents numerical simulations from both models, and shows that they provide qualitatively similar behaviors. Ideas for future work are sketched in the concluding section 4.

### 2. DYNAMIC FRICTION MODELS

In order to adequately describe friction phenomena at low velocities (i.e., stick-slip motion, presliding behavior, frictional memory, etc.) researchers have recently developed dynamic models that describe the dependence of friction on the relative velocity between two contacting bodies through a differential equation. Dynamic models are able to take into account presliding behavior for very small displacements, where the friction force increases gradually with the displacement.

The first attempt to describe presliding is due to Dahl (see [4] for a review): the Dahl model successfully simulates presliding displacement, but does not account for the sliding regime and related features (e.g., the Stribeck effect, i.e. the dip of the force at low relative velocities). The LuGre model [5] extended Dahl's work in order to include such effects. However, it was shown that this model exhibits drift for arbitrarily small external forces, which is not physically consistent. This effect has been explained in [7] by observing that LuGre does not allow purely elastic regime: therefore, a class of *elasto-plastic* models has been proposed in [7], where the drawbacks of LuGre are overcome.

Before addressing the elasto-plastic approach in section 2.2, we briefly review in section 2.1 the plastic model by Smith and Woodhouse.

#### 2.1. The plastic friction model

Experimental results reported by Smith and Woodhouse [3] show that, in stick-slip conditions, the measured friction force versus the sliding speed exhibits large hysteresis loops, i.e. the instantaneous sliding speed does not determine the friction force during the oscillation. This hysteresis loop suggests that the contact force has a dependence on some additional variables, and that the system state must be enlarged in order to account for this phenomenon.

In [3], the authors argued that the contact temperature during the oscillation cycle plays an important role by affecting the coefficient of friction of the interfacial rosin layer. They developed a method for measuring the varying coefficient of friction during

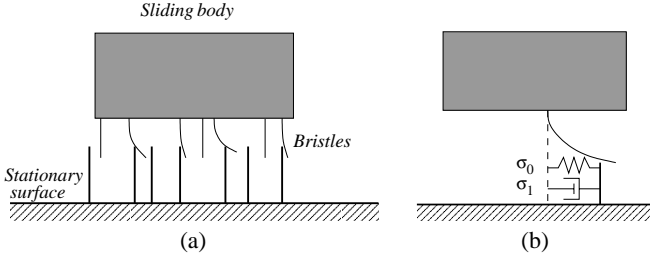


Figure 1: (a) bristle interpretation of the friction mechanism; (b) the LuGre model as an averaged description of the bristle behavior.

individual cycles of stick-slip vibrations, and proposed a model that includes this information. The authors called this model *plastic*, since it accounts for plastic deformations of the rosin layer according to temperature variations.

In this model, friction is therefore given by:

$$f = \text{sgn}(v) F_N \cdot \mu(T), \quad (1)$$

where  $F_N$  is the normal bow force,  $\mu(T)$  is a temperature dependent friction coefficient as described in [3], and  $v$  is the relative velocity between the bow and the string.

It is shown in [3] that this model reproduces the experimentally observed hysteresis loops in the force versus velocity plane.

## 2.2. The elasto-plastic model

Let us consider two facing surfaces in frictional contact. The friction between the two surfaces can be interpreted to be caused by a large number of bristles, each contributing a fraction of the total friction load, as shown in figure 1(a). The load contributed by each bristle is proportional to the strain of the bristle. When the strain exceeds a certain level the bond is broken.

The LuGre model [5] makes use of this interpretation, and describes the deflection of the bristles in an averaged way through a single degree of freedom  $z$ . When a tangential force is applied, the bristles are assumed to be subject to restoring elastic and dissipative forces (see figure 1(b)). If the deflection is large enough, the bristles start to slip.

Denoting by  $z$  the average bristle deflection, the model is given by:

$$\begin{aligned} \dot{z}(v, z) &= v - \sigma_0 \frac{|v|}{g(v)} z, \\ F &= \sigma_0 z + \sigma_1(v) \dot{z} + f(v), \end{aligned} \quad (2)$$

where  $\sigma_0$  is the stiffness of the bristles, and  $\sigma_1(v)$  is the damping. The function  $g(v)$  describes the steady state displacement for constant sliding velocities ( $\dot{z} = 0$ , then  $z = 1/[\sigma_0 g(v)]$ ).

The physical interpretation of this model is as follows: contact surfaces are very irregular at microscopic level, and we visualize this as two rigid bodies that make contact through elastic bristles. When a tangential force is applied, the bristles will deflect like springs and dampers which give rise to the friction force. The average deflection of the bristles corresponds to the internal state of the dynamic friction model  $z$ .

One drawback of the LuGre model is that it exhibits drift for arbitrarily small external forces: this is not a physically consistent behavior, and is rather due to inaccurate modeling of the presliding behavior. The *elasto-plastic* class of models [7] is also based

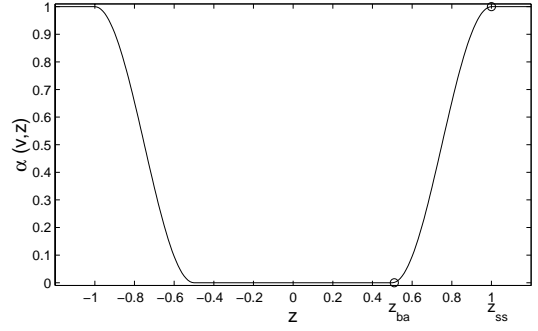


Figure 2: Smooth elastic-to-plastic transition provided by the function  $\alpha(v, z)$ .

on the bristle interpretation of friction, and overcomes the drawbacks of LuGre by using the following formulation for the bristle displacement:

$$\dot{z} = v \left[ 1 - \alpha(z, v) \frac{z}{z_{ss}(v)} \right]. \quad (3)$$

Compared to equation (2), the new ingredient is the function  $\alpha(z, v)$ . This is an adhesion map which controls the rate of change of  $z$  to avoid drift. Following Dupont *et al.* [7], we use a function  $\alpha(z, v)$  parametrized as

$$\alpha(v, z) = \begin{cases} 0 & |z| < z_{ba}, \text{sgn}(v) = \text{sgn}(z) \\ \alpha_m(v, z) & z_{ba} < |z| < z_{ss}(v), \text{sgn}(v) = \text{sgn}(z) \\ 1 & |z| > z_{ss}(v), \text{sgn}(v) = \text{sgn}(z) \\ 0 & \text{sgn}(v) \neq \text{sgn}(z) \end{cases}, \quad (4)$$

where  $z_{ba}$  is the breakaway displacement below which the presliding is purely elastic, and

$$\alpha_m(v, z) = \frac{1}{2} \left[ 1 + \sin \left( \pi \frac{z - \frac{1}{2}(z_{ss}(v) + z_{ba})}{z_{ss}(v) - z_{ba}} \right) \right] \quad (5)$$

ensures a smooth transition between elastic and plastic behavior (see figure 2). Indeed, for small displacements  $\alpha = 0$  and consequently  $\dot{z} = v$  (elastic presliding), while for larger displacements mixed elastic-plastic sliding is entered. Finally, at steady state purely plastic regime is achieved with  $\alpha = 1$ ,  $\dot{z} = 0$ , and  $z = z_{ss}$ .

We use the following steady-state friction characteristic  $z_{ss}$ , defined as in [5]:

$$z_{ss}(v) = \frac{\text{sgn}(v)}{\sigma_0} \left[ f_c + (f_s - f_c) e^{-(v/v_s)^2} \right], \quad (6)$$

where  $f_c, f_s$  are the Coulomb force and the stiction force respectively, while  $v_s$  is the Stribeck velocity.

Equations (6) and (4) are just two possible parametrizations for the functions  $z_{ss}(v)$  and  $\alpha(z, v)$ . In practice, significant deviations from these curves can be tolerated without affecting the model behavior significantly.

## 3. APPLICATION TO BOWED STRING SIMULATIONS

In order to obtain a comparison with the plastic model proposed in [3], we applied our model to the simulation of a string excited by a bow.

### 3.1. Coupling exciter and resonator

The string resonator is modeled here using one dimensional digital waveguides while the bow is represented as an ideal lumped mass. The equations for the bow are discretized using the bilinear transformation, that corresponds to trapezoid integration of continuous-time functions [11]. It can be verified that the discrete-time relative velocity  $v(n)$  is given by

$$v(n) = \tilde{v}(n) + \mathbf{k}(1)\dot{z}(n), \quad (7)$$

where  $\tilde{v}$  is a computable quantity (i.e. a linear combination of variables that are known at time  $n$ ). The coefficient  $\mathbf{k}(1)$  isolates the dependence of  $v(n)$  upon  $\dot{z}(n)$  at the current time instant  $n$ . The bristle equation of dynamics is also discretized using the bilinear transformation, with time step  $T_s = 1/F_s$ :

$$\begin{aligned} z(n) &\approx \underbrace{z(n-1) + \frac{T_s}{2}y(n-1) + \frac{T_s}{2}\dot{z}(n)}_{\tilde{z}(n)} + \mathbf{k}(2)\dot{z}(n) \\ &\triangleq \tilde{z}(n) + \mathbf{k}(2)\dot{z}(n) \end{aligned} \quad (8)$$

where  $\mathbf{k}(2) = T_s/2$ . Again, the term  $\tilde{z}(n)$  represents a computable quantity.

Note that when the two interacting objects are coupled through the non-linear friction interaction, a delay-free path is generated in the computation: namely, the relative velocity  $v(n)$  and the bristle displacement  $z(n)$  depend on the term  $\dot{z}(n)$ , which in turn depends non-linearly on the pair  $(v(n), z(n))$  through equation (3). This problem is well studied in the literature of physical modeling. In [8], the authors chose the same numerical implementation used in [6], which introduces one sample delay to solve computational problems. However, this solution is known to introduce inaccuracies and even instability in the simulations. Here we adopt the approach proposed in [12]: at each time step the value  $\dot{z}(n)$  is found as a function of the pair  $(\tilde{v}, \tilde{z})$ , and is computed using Newton-Raphson iterations by finding a local zero of the function  $g(\dot{z}) = [\dot{z}(\tilde{v}(n) + \mathbf{k}(1)\dot{z}(n), \tilde{z}(n) + \mathbf{k}(2)\dot{z}(n)) - \dot{z}]$  (see also [10] for numerical details). Since simulations show that seven iterations of the Newton-Raphson algorithm typically allow to converge to the solution, the iterative zero-finding procedure is computationally efficient for real-time implementation.

### 3.2. Simulations

The control parameters that are typically used to drive a bowed string instrument are the bow velocity  $V_b$  and bow force  $F_N$ . In order to perform meaningful comparisons between the elasto-plastic and the plastic [3] models, the relationship between the low-level parameters of equations (3–6) and the pair  $(V_b, F_N)$  must be found.

As described in section 3.1, in our modeling approach the bow is treated as a lumped mass. As such, it can only be controlled by the user through external driving forces, and the bow velocity  $V_b$  can not be directly set. For this reason, the simulations described in this section have been obtained using a slightly different version of the model: in this formulation, no external forces are used and the state of the bow is explicitly updated at each time-step by forcing the bow velocity to assume the control value  $V_b$ .

The parameters  $(f_c, f_s)$  are related to  $F_N$  through the static and dynamic friction coefficients as  $f_s = \mu_s F_N$  and  $f_c = \mu_d F_N$ . Reasonable values for the static and dynamic coefficients in violin bows are  $\mu_s \approx 0.4 \dots 0.5$  and  $\mu_d \approx 0.2$ , respectively (see [13]).

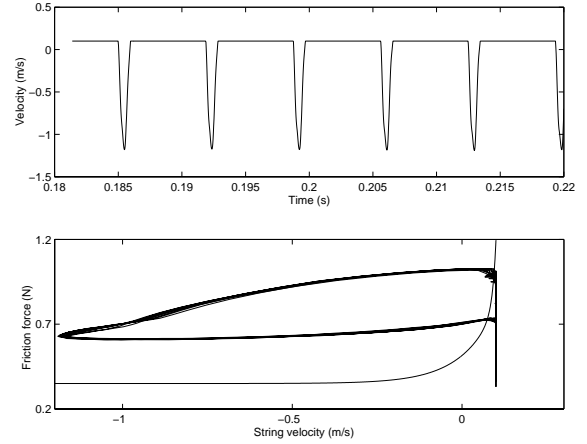


Figure 3: Top: velocity at the bow point for a cello D string (147 Hz) bowed with  $V_b = 0.1$  m/s and  $F_N = 1.1$  N. Bottom: velocity versus coefficient of friction. Both plots are generated using the model proposed in [3]. Courtesy of Jim Woodhouse.

The remaining parameters are taken from the literature. Note that  $\sigma_0$  defines the “degree of dynamicity” of the dynamic model (for  $\sigma_0 \rightarrow \infty$  the bristles do not move anymore) or, equivalently, the magnitude of the allowed presliding displacement, while  $\sigma_1$  describes the internal dissipation of vibrating bristles.

Figure 3 shows the results of applying the plastic model [3] to the simulation of a cello D string, tuned to 147 Hz, with a  $Q$  factor of 500 and a stiffness coefficient  $B = 0.0003$  N m<sup>2</sup>. The upper plot of figure 3 shows the snapshot of the time-domain velocity waveform at the bowing point obtained during the steady state portion of the motion, for  $V_b = 0.1$  m/s and  $F_N = 1.1$  N. Note that the Helmholtz motion, i.e. the ideal motion of the bowed string, is achieved. The lower plot of figure 3 shows hysteresis loop in the friction versus velocity characteristics.

Figure 4 shows the same signals as in 3, obtained using the elasto-plastic model, with parameters  $\sigma_0 = 6000$  and  $\sigma_1 = 0$ . Note that the behavior of the two models is qualitatively similar. The snapshot of the time-domain velocity waveform at the bowing point (upper plot) shows that, as before, the Helmholtz motion is achieved. More interestingly, the two models exhibit similar hysteretical behaviors of the friction versus velocity curve.

One noticeable difference between the two models is that the plastic model assumes an “ideal” ( $v \equiv 0$ ) stick phase, which can be noticed in the horizontal segments of the upper plot in figure 3. On the other hand, the corresponding plot in figure 4 shows that the ideal condition  $v \equiv 0$  is never achieved, and small oscillations occur even during the stick phase. This phenomenon is also noticed in the lower plot of figure 4, specifically in the small ripples around  $v = 0$ .

This transient behavior affects the sound quality dramatically. Figure 5 shows the result of elasto-plastic simulations with the same parameters as before, but with a larger value for the  $\sigma_1$  coefficient. Note that the waveforms are similar. However, since the parameter  $\sigma_1$  controls the internal bristle dissipation and consequently affects the transient behavior, the resulting micro-oscillations during the stick phase are also affected and the perceptual results are noticeably different.

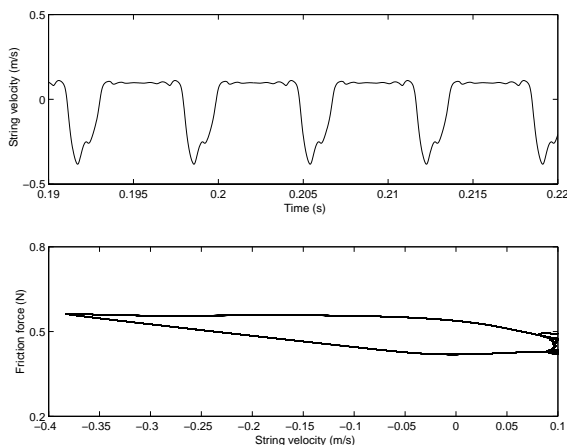


Figure 4: Top: velocity at the bow point for a cello D string (147 Hz) bowed with  $V_b = 0.1$  m/s and  $F_N = 1.1$  N,  $\sigma_0 = 6000$ ,  $\sigma_1 = 0$ . Bottom: velocity (m/s) versus friction force (N).

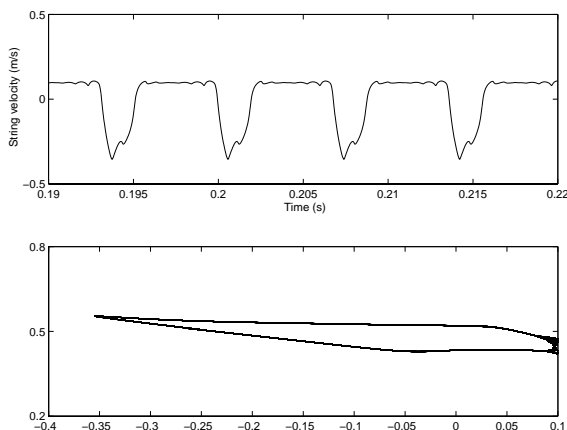


Figure 5: Top: velocity at the bow point for a cello D string (147 Hz) bowed with  $V_b = 0.1$  m/s and  $F_N = 1.1$  N,  $\sigma_0 = 6000$ ,  $\sigma_1 = 0.5$ . Bottom: velocity (m/s) versus friction force (N).

#### 4. DISCUSSION

We have presented a new physical model of the bowed string, which bases upon a waveguide string excited by a sophisticated elasto-plastic friction model. An accurate numerical implementation has been developed and applied to simulations of a bowed-string system.

The results presented in section 3.2 show that the model exhibits a physically consistent behavior, specifically the force versus velocity characteristics has a hysteretical behavior that has been observed in experiments on real instruments.

Preliminary comparisons with the plastic model by Smith and Woodhouse [3] show that the two models behave in qualitatively similar ways, although they have been derived under very different physical assumptions. Further work is required to develop quantitative comparisons between the two models. Specifically, non-linear identification techniques such as those described in [14] may be used in order to study whether parameters values of the elasto-

plastic model can be found such that the model behavior reproduce accurately that of the plastic model.

#### 5. REFERENCES

- [1] M. E. McIntyre and J. Woodhouse, "On the fundamentals of bowed string dynamics," *Acustica*, vol. 43, no. 2, pp. 93–108, Sept. 1979.
- [2] R. T. Schumacher and J. Woodhouse, "Computer modelling of violin playing," *Contemporary Physics*, vol. 36, no. 2, pp. 79–92, 1995.
- [3] J. H. Smith and J. Woodhouse, "The tribology of rosin," *J. Mech. Phys.Solids*, vol. 48, pp. 1633–1681, 1999.
- [4] H. Olsson, K. J. Åström, C. Canudas de Wit, M. Gäfvert, and P. Lischinsky, "Friction models and friction compensation," *European J. of Control*, vol. 4, no. 3, pp. 176–195, 1998.
- [5] C. Canudas de Wit, H. Olsson, K. J. Åström, and P. Lischinsky, "A new model for control of systems with friction," *IEEE Trans. Autom. Control*, vol. 40, no. 3, pp. 419–425, 1995.
- [6] V. Hayward and B. Armstrong, "A new computational model of friction applied to haptic rendering," in *Experimental Robotics VI*, P. Corke and J. Trevelyan, Eds., pp. 403–412. Springer-Verlag, 2000.
- [7] P. Dupont, V. Hayward, B. Armstrong, and F. Altpeter, "Single State Elasto-Plastic Friction Models," *IEEE Trans. Autom. Control*, vol. 47, no. 5, pp. 787–792, may 2002.
- [8] S. Serafin, C. Vergez, and X. Rodet, "Friction and Application to Real Time Physical Model of a Violin," in *Proc. Int. Computer Music Conf. (ICMC'99)*, Beijing, Oct. 1999.
- [9] F. Avanzini, S. Serafin, and D. Rocchesso, "Modeling Interactions Between Rubbed Dry Surfaces Using an Elasto-Plastic Friction Model," in *Proc. COST-G6 Conf. Digital Audio Effects (DAFx-02)*, Hamburg, Sept. 2002, pp. 111–116.
- [10] F. Avanzini, M. Rath, and D. Rocchesso, "Low-level sound models: resonators, interactions, surface textures," in *The Sounding Object*, D. Rocchesso and F. Fontana, Eds., pp. 119–148. Mondo Estremo, 2003, In press. Freely distributed under the GNU Free Documentation License, <http://www.soundobject.org/SObBook>.
- [11] A. V. Oppenheim and R. W. Schaffer, *Discrete-time Signal Processing*, Prentice-Hall, Englewood Cliffs, NJ, 1989.
- [12] G. Borin, G. De Poli, and D. Rocchesso, "Elimination of Delay-free Loops in Discrete-Time Models of Nonlinear Acoustic Systems," *IEEE Trans. Speech Audio Process.*, vol. 8, no. 5, pp. 597–606, 2000.
- [13] A. Askenfelt, "Measurement of the bowing parameters in violin playing. II: Bow-bridge distance, dynamic range, and limits of bow force," *J. Acoust. Soc. Am.*, vol. 86, no. 2, pp. 503–516, Aug. 1989.
- [14] F. Altpeter, *Friction Modeling, Identification and Compensation*, Ph.D. thesis, École Polytechnique Fédérale de Lausanne, 1999.

## BOWED STRING PHYSICAL MODEL VALIDATION THROUGH USE OF A BOW CONTROLLER AND EXAMINATION OF BOW STROKES

Stefania Serafin

CCRMA, Department of Music  
Stanford University, Stanford, CA, USA  
serafin@ccrma.stanford.edu

Diana Young

MIT, Media Lab,  
Cambridge, MA, USA  
young@mit.media.edu

### ABSTRACT

Combining a physical model with a bow controller, we propose a technique to validate bow strokes in a virtual instrument.

### 1. INTRODUCTION

Bowed string physical models have achieved a level of completeness that allows their performance to be favorably compared to that of their real instrument counterparts. These comparisons are facilitated by the use of refined bow controllers that detect all the subtle changes in motion and force that are experienced by a bow while in contact with a string and give expressive playing its characteristic sound.

In the bowed strings' literature, research on playability has focused both on aspects related to musical acoustics and to musical controllers.

In these different domains the word *playability* has different definitions. For example, according to Jim Woodhouse [1], playability of virtual instruments means that the acoustical analysis of the waveforms produced by the model fall within the region of the multidimensional space given by the parameters of the model. This is the region where *good tone* is obtained. In the case of the bowed string, *good tone* refers to the Helmholtz motion, i.e. the ideal motion of a bowed string that each player is trying to achieve. The Helmholtz motion is given by an alternation of stick-slip-stick-slip, in which the string sticks to the bow hair for the longest part of its period, slipping just once. Experiments show that simulated bowed strings have the same playability as real bowed strings as calculated by Schelleng [2].

Further experiments also show that the playability of virtual bowed strings increases when accurate friction models that account for the thermodynamical properties of rosin are taken into account [3].

In these experiments, in fact, the input parameters that drive the bowed string model corresponding to the right hand of the player are kept constant for each simulation. This is a situation that is clearly not the same as that which occurs in violin performances. As in performance it is the continuous evolution of the input parameters that constitute the nuance that are the characteristics of an expressive performance.

In order to address this issue, Askenfelt [4] studied the contribution of bowing parameters in different bow strokes, trying to determine the physical limits of the input parameters in order to achieve a specific stroke. He determined the maximal duration of the pre-Helmholtz attack allowed in order to judge a particular stroke as acceptable. The previous definition of playability is the one we are interested on examining in this paper. Similar work

with a stronger focus on performance issues rather than acoustical validation was proposed in [5]. In this research the combination of the input parameters of a bowed string physical model was used to reproduce different bow strokes such as *detaché*, *legato* and *spiccato*. Although the goal was to reproduce a particular sound specific to a certain performer's gesture, no real-time input controller was used. Definitions of playability more related to performance issues are described in [6].

In this paper we are interested in exploring the possibility of reproducing traditional bowing techniques using a bow controller that behaves in a manner as closely related to that of a traditional violin bow as possible. This allows us to validate both the model and the controller by comparing it to the behavior of the traditional instrument.

We therefore used a real-time bowed string physical model and a wireless bow controller to reproduce the bow strokes that are most fundamental to the right hand technique of an accomplished bowed string player, such as *legato*, *detaché staccato*, *spiccato*, and *balzato*. We discuss the integration of the two components of these experiments and illustrate how the bow controller is used to control the physical model of the violin in order to faithfully reproduce these strokes. Moreover, we compare the range of input parameters that determine these strokes in the model with the values for these parameters measured on real violins, showing how synthetic instruments may present the same playability regions as real instruments.

The ultimate goal of this research is to create a bowed string instrument able to reproduce the behavior of a traditional instrument as well as to create extended performance techniques for bowed string players. In the following section the bowed string physical model used in the simulations is described.

### 2. A BOWED STRING PHYSICAL MODEL

We built a bowed string physical model that combines waveguide synthesis [7] with latest results on bowed string interaction modeling [8].

A schematic representation of the model is shown in Figure 1. In this model, the bow excites the string in a finite number of points, which represent the bow width. The frictional interaction between the bow and the string is modeled considering the thermodynamical properties of rosin, using the so-called plastic model proposed in [9], given by:

$$\mu = \frac{Ak_y(T)}{N} \text{sgn}(v) \quad (1)$$

where  $A$  is the contact area between the bow and the string,  $N$  is

the normal load, and  $k_y(T)$  is the shear yield stress as a function of temperature  $T$ . The temperature  $T$  of the shearing rosin layer can be estimated from the current sliding velocity  $v$  by passing it through an appropriate linear filter [9].

The bow width is modeled by discretizing the region of the string in contact with the bow using finite differences and calculating the coupling between the waves propagating along the string and the frictional interaction between the bow and the string at each point. Once the velocity of the string at the contact point has been calculated, the waves propagating along the string are modeled using digital waveguides. More precisely, transversal and torsional waves propagating toward the bridge and the fingerboard are modeled as pairs of one dimensional digital waveguides.

The outgoing velocity at the bridge is filtered through the body's resonances and corresponds to the output waveforms perceived by the listener. A preliminary version of this model has been described in [3].

The block diagram structure of the complete bowed string physical model is shown in Figure 2. In it delay lines correspond to traveling waves propagating from the bow point to the bridge and the nut; LP and AP represent respectively the lowpass filters that simulate losses and the allpass filters that simulate dispersion. The input parameters of the model corresponding to the right hand of the player are bow position relative to the bridge (normalized between 0 and 1, where 0 corresponds to the bridge, 1 corresponds to the nut, 0.5 corresponds to the middle of the string), bow pressure, bow velocity, and amount of bow hair in contact with the string. The model has been implemented as an external object in the Max/MSP environment.

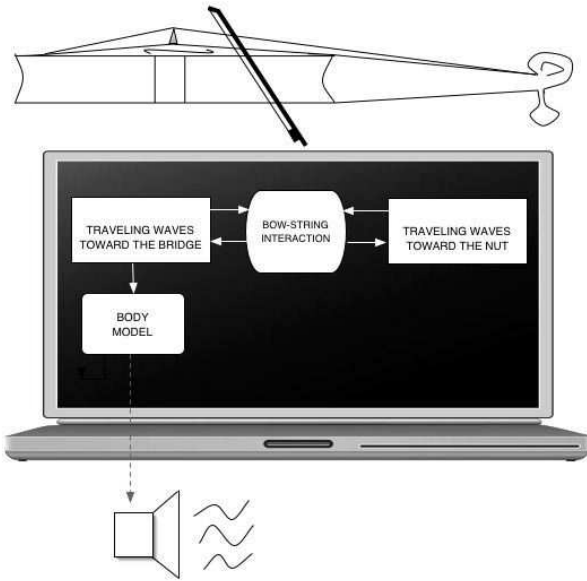


Figure 1: Simplified structure of the bowed string physical model used in the simulation.

### 3. A BOW CONTROLLER

The bow controller used in these experiments is a commercial carbon fiber bow, adapted by adding a custom measurement system.

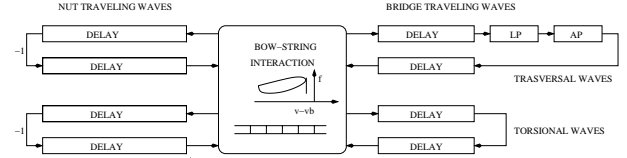


Figure 2: Refined block diagram structure of the bowed string physical model used in the simulations.

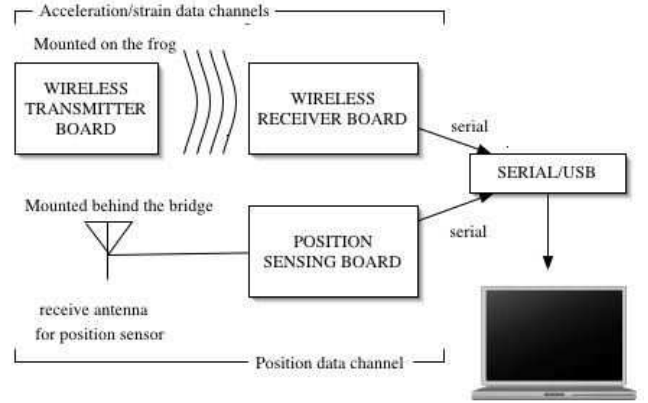


Figure 3: Data flow for the violin controller.

The system is comprised of an electric field sensor for measuring bow position (tip-frog / bow-bridge distance), commercial accelerometers for detecting 3D acceleration, and foil strain gauges for measuring the strain in the bow stick proportional to normal force on the string and the orthogonal force corresponding to flexion toward and away from the scroll.

From these sensors, the parameters of bow velocity, bow-bridge distance, downward force, and bow width (using tilt information provided by the accelerometers and the second strain sensor) may be isolated from bowing gestures and used as input to the physical model.

The implementation of the measurement system is minimal and maintains the playability of the interface in most scenarios. Though somewhat heavier than usual (almost 30g heavier, including battery), the resulting bow has a reasonable balance point and remains wireless.

The microcontroller, battery, RF transmitter, and accelerometers are housed on an electronics board mounted on the frog, while the strain sensors are mounted directly to the bow stick around the midpoint of the bow. The acceleration and strain data is transmitted wirelessly to a bay station board.

The bow board also sends two square wave signals to either end of a resistive strip that runs the length of the bow stick, acting as an antenna for the position measurement. The resultant signal is received by an antenna mounted behind the bridge of the violin, and this signal is connected via a cable to a small bay station board that determines the different amplitudes of the two received signals. The position information is then combined with the acceleration and strain data stream and output through a serial bus to the computer running the physical model.

The compactness of this gesture measurement system allows for an easy test setup in a laboratory or performance environment.

For a detailed description of the bow controller, see [10].

#### 4. EXPERIMENTAL SETUP

In these experiments we used a Macintosh G4 computer to run the Max/MSP implementation of the bowed string physical model. The gestural data from the bow controller was connected via a serial/USB converter to a USB port of the computer.

The antenna used for the measurement of bow position was mounted behind the bridge of an electric violin (Jensen). This violin was chosen for these tests for ease of audio recording, as well as the ability to play the audio produced by the model and the unamplified violin sound together.

Recordings of both the violin audio and the bow controller data were made simultaneously within the Max/MSP environment. The gesture data was then used to drive the physical model, which produced waveforms that were also recorded.

This setup was simple enough to allow fast and easy recording and testing, and was used to reproduce some of the bow strokes that are fundamental to the right hand technique of an accomplished bowed string player, such as legato, détaché, and balzato.

The waveforms of the violin were then qualitatively compared to those produced by the model using both time and spectral domain evaluation and perceptual evaluation. The experimental setup used is shown in Figure 4.

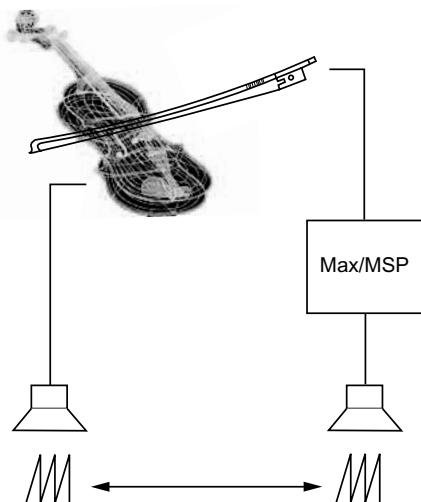


Figure 4: Setup used for the experiments.

##### 4.1. Playing with Downward Force

We began the integration of the bow controller hardware with the software model by addressing one input parameter at a time. In the first trial we used the downward strain sensor to control the downward force parameter for the bowed string model.

With the model parameters of bow-bridge distance, bow velocity, bow width, and frequency held constant, we varied the downward force between 0 and 5 N.

Other than setting a threshold appropriate for the sensor range, it was unnecessary to perform any adjustments to this mapping.

Using the bow controller to play a single string on the test violin, we were able to compare the sound produced by the model with that of the test violin. We were able to quickly produce sonorities from the model that sounded appropriate for the amount of pressure we applied to the bow.

Interestingly, the model produced sounds that seemed perceptually correct for long sustained strokes as well as for short strokes with sharp attacks and decays.

##### 4.2. Adding Velocity and Bow-Bridge Distance

Next we added the bow velocity and bow-bridge distance controls by using the data from the bow position sensor. By taking the data values corresponding to the tip and the frog, the transverse bow position was determined, and from this the velocity value was derived. The bow-bridge distance was taken as the sum of the tip and the frog values.

We were able to change the sound of the tones produced by the model by adjusting bow pressure, speed, bow-bridge distance, and by simply changing the bow direction. As the sound of the test violin offered an easy comparison to the model, we experimented by playing two open strings (of the test violin) while controlling a single tone of the model tuned to different intervals above and below the higher string. Playing the small duet between real and virtual violins we were able to make small adjustments in the mappings so that the timbers sounded as though they were all three emanating from the test violin.

#### 5. COMPLETE MAPPING

In order to build an expressive virtual musical instrument, the capture of the gesture of the performance is as important as the manner in which the mapping of gestural data onto synthesis parameters is done. In the case of physical modeling synthesis, a one-to-one mapping approach of control values to synthesis parameters makes sense due to the fact that the relation between gesture input and sound production is often hard-coded inside the synthesis model [?]. Because both the physical model and the bow controller are developed according to physical input and output parameters, the complete mapping between the two is straightforward. Figure 5 shows how all the data sent by the bow controller were mapped to the input parameters of the physical model. Downward bow force of the controller is directly mapped into bow force in the physical model. Bow velocity and bow-bridge distance were captured by measuring the horizontal and vertical position of the bow respectively. Moreover, lateral strain sensors were mapped onto the amount of bow hair in contact with the bow.

##### 5.1. Bow strokes

As mentioned in the previous paragraph, the evaluation of the bow strokes using the experimental setup was done by comparing the output of the electric violin to the output of the physical model, using the same input parameters. This evaluation was first performed by comparing the shape of the time domain and frequency domain waveforms produced by the two instruments. This evaluation, however, did not seem very effective: not surprisingly, waveforms with quite different shapes in some cases turned out to sound similar.

Inspection of waveforms alone was not sufficient to determine the similarity between sounds. We therefore started performing



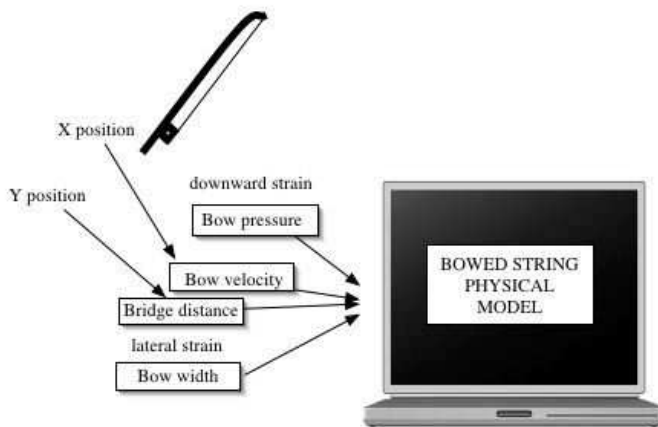


Figure 5: Final mappings of the bow controller to the bowed string physical model.

listening tests to evaluate the accurateness of the overall setup.

## 6. CONCLUSIONS

We proposed the combination of a bowed string physical model and a bow controller to examine how different bow strokes can be achieved in a virtual bowed string instruments. Preliminary experiments show that the bow strokes that a beginner's violin player learns after few years of practice are easily reproduced. More accurate listening tests and comparisons between all the variations of input parameters and bow strokes need to be tested in order to fully validate the playability of our instrument.

## 7. REFERENCES

- [1] James Woodhouse, "On the playability of violins. Part I: Reflection functions. Part II: Minimum bow force and transients," *Acustica*, vol. 78, pp. 125–136, 137–153, 1993.
- [2] John C. Schelleng, "The bowed string and the player," *Journal of the Acoustical Society of America*, vol. 53, no. 1, pp. 26–41, Jan. 1973.
- [3] Stefania Serafin, Julius O. Smith, III, and Jim Woodhouse, "An investigation of the impact of torsion waves and friction characteristics on the playability of virtual bowed strings," New York, Oct. 1999, IEEE Press.
- [4] Anders Askenfelt, "Measurement of the bowing parameters in violin playing," *Journal of the Acoustical Society of America*, vol. 86, no. 2, pp. 503–516, August 1989.
- [5] David Jaffe and Julius Smith, "Performance expression in commuted waveguide synthesis of bowed strings," in *Proc. International Computer Music Conference. ICMA*, 1995, pp. 343–346.
- [6] D. Young and S. Serafin, "Playability evaluation of a virtual bowed string instrument," in *Proc. NIME*, Montreal, CA, 2003.
- [7] Julius O. Smith, "Physical modeling using digital waveguides," *Computer Music Journal*, vol. 16, no. 4, pp. 74–91, Winter 1992.
- [8] R. Pitteroff, "Mechanics of the contact area between a violin bow and a string. part i: reflection and transmission behaviour. part ii: Simulating the bowed string. part iii: Parameter dependance," in *Acustica-Acta Acustica*, 1998, pp. 543–562.
- [9] Jonathan H. Smith and James Woodhouse, "The tribology of rosin," *J. Mech Phys. Solids*, vol. 48, pp. 1633–1681.
- [10] Diana Young, "The hyperbow controller: Real-time dynamics measurement of violin performance," in *Proc. NIME*, 2002.

## DETERMINATION OF IMPORTANT WOOD PROPERTIES FOR BLANKS FOR VIOLIN TOPS BY THE USE OF NUMERICAL OPTIMIZATION

Mats Tinnsten and Peter Carlsson

Department of Information Technology and Media  
Mid Sweden University  
mats.tinnsten@mh.se

### ABSTRACT

In the strive of understanding how different parameters affects the vibration properties and the characteristics of the sound emanating from a violin, i.e. what makes a good violin good, numerical methods as FEM (finite element method) and BEM (boundary element method) are used. Numerical models of whole violins and/or part of it is created and studied. Crucial for the results from these studies is the correctness of the input data for the numerical analysis.

One important group of input data is the wooden material parameters for the part of the violin subjected to analysis. In this study a new method for determining these important material parameters for blanks for violin tops is proposed. In the proposed method a FEM-code is linked together with a stochastic optimization algorithm in order to, in an automatic fashion, determine the material parameters. The method requires the geometrical dimensions, the density, and measured normal modes for the blank and it consider the fact that the Young's modulus in the axial direction varies with respect to the radial direction.

### 1. INTRODUCTION

The characteristics of the sound emanating from a vibrating structure and its vibration properties, as mode shapes and eigenfrequencies, depends of its design properties and if these are changed the sound characteristics and the vibration properties are also changed. The influence of changes in structural design variables such as geometric dimensions [1], shell thickness [2], material parameters [3], discrete masses [4], and, for fiber reinforced material, fiber orientation [5] have been studied earlier with interesting results but more research is needed in order to understand how musical instruments, especially wooden, should be modeled to give numerical results to correspond to measured ones.

An instrument made out of wood comprises a very complex material where the material parameters, which also have a natural distribution, have great influence on the vibration properties and the characteristics of the sound emanating from it. Earlier studies, [6], on blanks for violin tops gives a good idea of the sensitivity of the vibration properties with respect to the material parameters and it stands clear that even if the material in the blank is regarded as othotropic there is no simple answer on how to determine the different material parameters in order to get acceptable correspondence between measured and calculated results. In [6] the different material parameters were assumed to be constant with regard to spatial coordinates and with the help of the sensitivity analyses, the values of the parameters were determined to give correspondence between measured and calculated results. This is not an easy task and it has proven in earlier analyses, [7], that even if the number of

variables is low it is hard to determine the values of each variable by the use of sensitivity analysis to get acceptable results.

In this study the possibility to estimate these important material parameters, for an individual blank, by the use of optimization methods is investigated. Firstly, a material model for wood the so-called honeycomb model, [8], is used in order to determine the material parameters that then is used in the blank for numerical modal analysis. The results are thereafter compared with the measured results according to [6]. The next step is to use an optimization method in order to determine the material parameters that give the correct eigenfrequencies and mode shapes according to the measurements in [6]. Here the material parameters are assumed to be constant with regard to spatial coordinates. Finally optimization is used in order to determine the parameters when the Young's modulus in the first direction is allowed to vary linearly with respect to the second direction, see Figure 1.

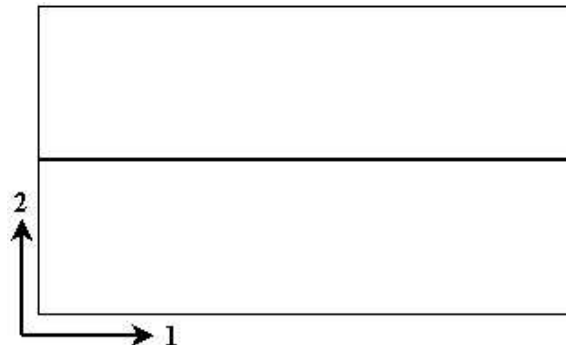


Figure 1: Blank for a violin top. The first direction indicates the axial direction (the direction of the fibre) and the second the radial direction.

### 2. ANALYSIS METHOD

It is possible to change the vibration properties as mode shapes and eigenfrequencies, and the characteristics of the sound emanating from a vibrating structure, by changing structural design variables. Of course, changes in one or more of these variables will result in changes in other structural characteristics. To find the best design, i.e. the one that satisfies all the demands put upon the structure is a question of optimization. This often requires a multi disciplinary approach, i.e. analytical tools from different disciplines

must be used in concert. A typical problem formulation could be: minimize the structural weight under the constraints that the sound intensity in certain spatial domains and the maximum stress in the structure do not exceed some given values.

The modal analysis in this investigation has been performed with the commercial finite element code Ansys 7.0 (mode extraction method: block Lanczos). The FE-code has been linked together with the stochastic optimization algorithm simulated annealing (SA) [9] in order to, in an automatic fashion, determine the different material parameters. The method requires the geometrical dimensions, the density, and the measured normal modes for the individual blank.

### 3. IMPORTANT MATERIAL PARAMETERS FOR BLANKS

Wood has a cellular structure. If knots, annual rings and other deviations are neglected, a hexagonal honeycomb model gives a good description of the mechanical properties of wood (see [8] for more detailed information). If the wood material is modeled with the honeycomb model it is possible to show that the mechanical properties of wood depend primarily on the properties on the cell wall, the cell wall density, and the shape of the cells. Although wood as balsa or beech differs a lot in density, mechanical properties, and strength, the properties of the material in the cell wall itself are still about the same. This fact makes it possible to estimate several global wood properties from information on the cell wall.

#### 3.1. Reference material parameters determination

In the following equations, the thickness of the cell wall is related to the density of the wood (the density of the wood is proportional to the actual cell wall thickness). The honeycomb model gives the following approximate equations for some mechanical properties of wood:

$$\frac{E_1}{E_S} = \frac{\rho}{\rho_S}, \quad \frac{E_2}{E_S} = 0.81 \left( \frac{\rho}{\rho_S} \right)^3 \quad (1)$$

$$\frac{G_{12}}{E_S} = 0.074 \frac{\rho}{\rho_S} \quad (2)$$

where  $E_1$  and  $E_2$  are the Young's modulus in axial (first direction) and radial directions (second direction) of the wood (blank), see Figure 1,  $G_{12}$  the shear modulus,  $E_S$  the axial Young's modulus for the cell wall,  $\rho_S$  the density of the cell wall, and  $\rho$  the density of the actual wood. From Eq. (1) we note that the axial Young's modulus ( $E_1$ ) is proportional to the density (i.e. the relative density), while the radial modulus ( $E_2$ ) is proportional to the cube of the density. The values for  $E_S$  and  $\rho_S$  were taken as 35 [GPa] and 1500 [kg/m<sup>3</sup>] respectively, [8], and the value of  $\rho$  to 482 [kg/m<sup>3</sup>], [6]. These values together with (1) and (2) gives the reference material parameter set according to:  $E_1=11.2467$ ,  $E_2=0.9406$ ,  $G_{12}=0.8323$  [GPa]. The Poisson's ratio  $\nu_{12}$  was chosen to 0.02, [6].

#### 3.2. The use of optimization in determining the actual material parameters

Earlier studies, [7], on the use of optimization in connection to violins suggests that it could be possible to compensate for changes in the material parameters (from one top to another) by adjusting the thickness distribution and the arching on the violin top in

order to retrieve a desired vibrational behavior. In [7] the material parameters were assumed to be known and the variables in the optimization analyses were the thickness distribution and the arching on a top. The objective with the optimization was to calculate the compensation in these variables when the material parameters for the top slightly was changed. Also in [7] the honeycomb model according to section 3.1 was used to calculate the changes in the Young's modulus when the density in the top material was changed. In the present investigation however optimization is used in order to determine the actual material parameters for the blank so that desired (or measured) normal modes are obtained. In the optimization analysis performed here there is no variables concerning geometrical dimension, instead the variables here are the material parameters.

### 4. PROBLEM DEFINITION

The optimization (which comprises modal analyses) is performed on a blank for a violin top (spruce). The blank has the following geometrical dimensions, vibrational properties, and weight, [6]: length = 386, width = 215, height at edge = 8.5, and height at centerline = 20 [mm] where length and width is the geometrical extension in the first and second direction respectively (Figure 1). The density of the blank is 482 [kg/m<sup>3</sup>]. The value of the measured three first eigenfrequencies are:  $f_1=272$ ,  $f_2=562$ , and  $f_3=631$  [Hz]. The nodal lines (white) from the measurements are showed in the figures in section 5. In the FE analysis (the modal analysis) an orthotropic four-node shell element is used and the analysis is performed on a free blank, i.e. without any supports.

#### 4.1. Reference material (given by the honeycomb material model)

The reference material set given by the honeycomb model is according to section 3.1:  $E_1=11.2467$ ,  $E_2=0.9406$ ,  $G_{12}=0.8323$  [GPa] and the Poisson's ratio  $\nu_{12}$  is chosen to 0.02. Here no optimization is carried out, only a modal analysis on the blank.

#### 4.2. Constant material parameter distribution

This optimization is performed with the assumption that the Young's modulus in both directions ( $E_1$  and  $E_2$ ) are constant with respect to spatial dimensions. The objective with the optimization is to minimize the difference of the three first eigenfrequencies and the difference of the nodal line for mode 2 compared to the measured ones [6]. The optimization comprises four variables:  $E_1$ ,  $E_2$ ,  $G_{12}$ , and  $\nu_{12}$ .

#### 4.3. Varying material parameter distribution

Here one variable is added in allowing the Young's modulus in the first direction,  $E_1$ , to vary linearly with respect to direction 2. The objective with the optimization is the same as in section 4.2 with the difference that the optimization comprises five variables:  $E_1$ ,  $E_2$ ,  $G_{12}$ ,  $\nu_{12}$ , and the variation of  $E_1$ : *evar*.

## 5. RESULTS

#### 5.1. Reference material

The modal analysis with this material set gives the following eigenfrequencies:  $f_1=288.9$ ,  $f_2=500.6$ , and  $f_3=610.3$  [Hz] (to be compared with the measured ones:  $f_1=272$ ,  $f_2=562$ , and  $f_3=631$  [Hz]).

The nodal lines for mode 2 and 3 (the first mode correspond with the measured) are showed in Figure 2 and 3.



Figure 2: Reference material. Nodal lines for mode 2 (white curved lines represent measured nodal lines and black calculated).

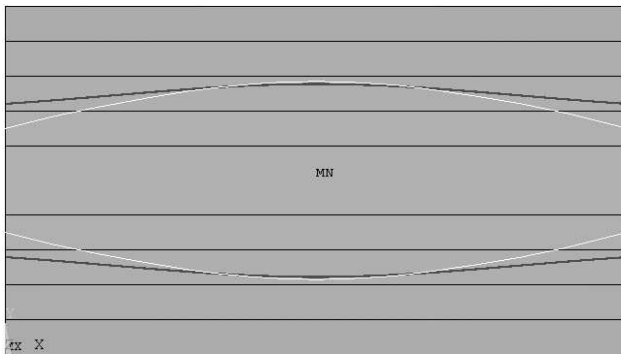


Figure 3: Reference material. Nodal lines for mode 3 (white curved lines represent measured nodal lines and black calculated).

## 5.2. Constant material

The initial (the starting point for optimization) material parameters is set to the values according to the reference material (section 3.1) and the optimization converged to the following results:  $f_1=272.0$ ,  $f_2=562.0$ , and  $f_3=631.0$  [Hz] (to be compared with the measured ones:  $f_1=272$ ,  $f_2=562$ , and  $f_3=631$  [Hz]). The variable set for the optimal state is:  $E_1=14.4720$ ,  $E_2=0.9984$ ,  $G_{12}=0.7251$  [GPa], and  $\nu_{12}=0.0189$ . The nodal lines for mode 2 and 3 (the first mode correspond with the measured) are showed in Figure 4 and 5.

## 5.3. Varying material

Also here the initial (the starting point for optimization) material parameters is set to the values according to section 3.1 and the optimization converged to the following results:  $f_1=271.9$ ,  $f_2=562.0$ , and  $f_3=631.0$  [Hz] (to be compared with the measured ones:  $f_1=272$ ,  $f_2=562$ , and  $f_3=631$  [Hz]). The variable set for the optimal state is:  $E_1=11.7230$  (at the edge),  $E_2=0.9844$ ,  $G_{12}=0.7276$  [GPa],  $\nu_{12}=0.0246$ , and  $evar=39.1\%$ . The nodal lines for mode 2 and 3 (the first mode correspond with the measured) are showed in Figure 6 and 7.

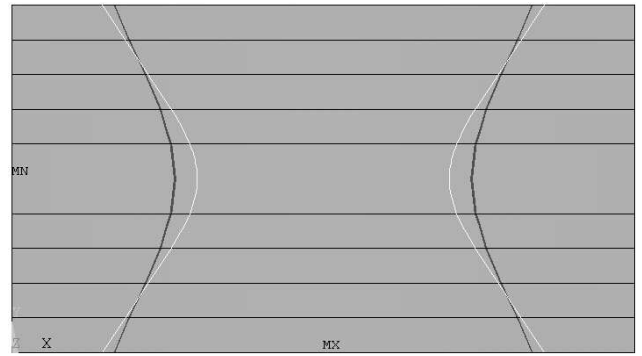


Figure 4: Constant material. Nodal lines for mode 2 (white curved lines represent measured nodal lines and black calculated).

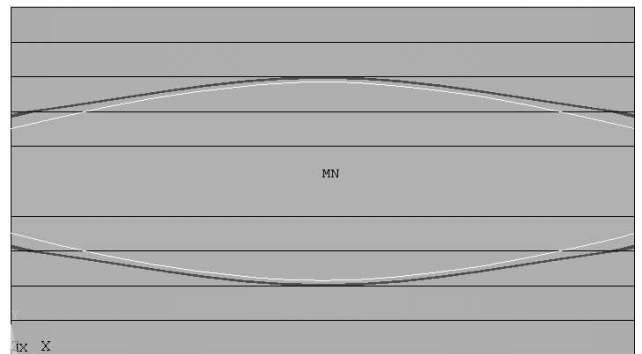


Figure 5: Constant material. Nodal lines for mode 3 (white curved lines represent measured nodal lines and black calculated).

## 6. DISCUSSION AND CONCLUSIONS

Present investigation on blanks for violin tops has been performed on a blank with the same geometrical dimensions and weight (see section 4) as was used in [6]. The FE-analyses in [6] was performed with the finite element code FEMP developed at Luleå University of Technology and the blank was discretized with triangle (shell) element. The method proposed in [6] resulted in the following material parameters for the blank in question:  $E_1=15.50$ ,  $E_2=1.03$ ,  $G_{12}=0.75$  [GPa], and  $\nu_{12}=0.02$ . The FE-analysis (FEMP) gave the following values for the first three eigenfrequencies:  $f_1=277$ ,  $f_2=553$ , and  $f_3=644$  [Hz]. In the present investigation the commercial FE-code Ansys 7.0 has been used and the first analysis here was on a blank discretized in triangle elements with the same material parameters as above and exactly the same pattern as in [6]. This analysis gave the following values for the first three eigenfrequencies:  $f_1=276.8$ ,  $f_2=580.9$ , and  $f_3=645.5$  [Hz]. If we compare the results we see that the first and third value correspond quite well but there is a significant difference in the second value. In spite of this we decided to rely on the results from Ansys 7.0. Generally the four-node elements give more accurate results than the three-node element and because of this the former element type has been used in this investigation. An analysis on the blank with the same material parameters as above but discretized with four-node elements gave the following results:  $f_1=276.8$ ,  $f_2=579.6$ ,

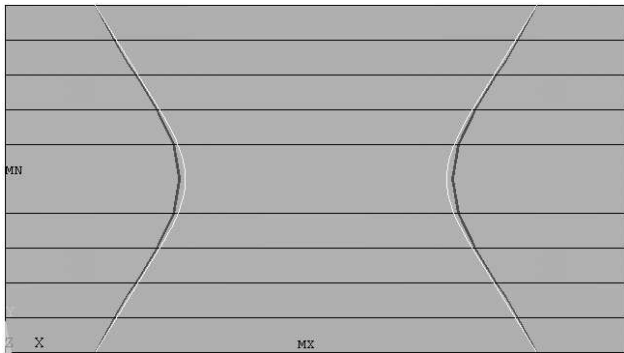


Figure 6: *Varying material. Nodal lines for mode 2 (white curved lines represent measured nodal lines and black calculated).*

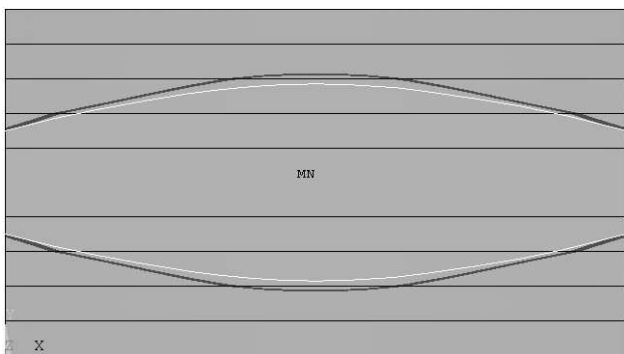


Figure 7: *Varying material. Nodal lines for mode 3 (white curved lines represent measured nodal lines and black calculated).*

and  $f_3=642.6$  [Hz] which seems to be in order since triangle elements tends to give a stiffer structure (overstiff) than four-node elements. In all the presented modal results in this investigation, the Ansys 7.0 four-node shell element (SHELL63) has been used.

In the optimization analyses performed here the objective has been to determine a material set (material parameters in different direction) that gives the values of the first three eigenfrequencies and the nodal line for mode 2 according to measured results [6].

From the modal analysis on the blank with material parameters determined by the honeycomb model (section 5.1 and Figure 2 and 3) it can be concluded that this model is not sufficient to this application since both the values of the eigenfrequencies and the mode shapes differs significantly.

The first optimization analysis with constant material parameters (with regard to spatial dimensions), section 5.2, gives quite interesting results. Here the values of the eigenfrequencies correspond very well with the measured ones but the mode shapes, especially for mode 2, differs significantly (see Figure 4 and 5).

In the second optimization analysis (section 5.3) the Young's modulus in the first direction was allowed to vary linearly with respect to the second direction and this variation was added to the variable set. The results from this analysis are quite promising, the values of the eigenfrequencies corresponds very well with the measurement and also the mode shapes correspond quite well (see Figure 6 and 7).

It seems that the variation of  $E_1$  is needed to get both the values of the eigenfrequencies and the mode shapes to correspond with measured results. The optimization determined this variation to 39.1% which could seem as a high value on a distance not longer than 10.75 [cm] but there is support in the literature for variation of these levels [10].

## 7. REFERENCES

- [1] Tinnsten, M., "Optimization of acoustic response – a numerical and experimental comparison", *Struct. Opt.*, Vol. 19, pp. 122–129, 2000.
- [2] Belegundu, A.D., Salagame, R.R., and Koopmann, G.H., "A general optimization strategy for sound power minimization", *Structural Optimization*, Vol. 8, pp. 113–119, 1994.
- [3] Lamancusa, J.S. and Eschenauer, H.A., "Design optimization methods for rectangular panels with minimal sound radiation", *AIAA J.*, Vol. 32, pp. 472–479, 1994.
- [4] Constants, E.W., Belegundu, A.D., and Koopmann, G.H., "Design approach for minimizing sound power from vibrating shell structures", *AIAA J.*, Vol. 36, pp. 134–139, 1998.
- [5] Tinnsten, M. and Jonsson, M., "Acoustic optimization of plate vibration – a numerical example", *Proc. Vibration, Noise & Structural Dynamics '99*, Venice, Italy, pp. 71–78, 1999.
- [6] Molin, N.E., Tinnsten, M., Wiklund, U., and Jansson, E., "A violinmaker's practical test of wood properties suggested from FEM-analysis of an orthotropic shell", *J. Catgut Acoust. Soc.*, Vol. 46, pp. 24–26, 1986.
- [7] Tinnsten, M. and Carlsson, P., "Numerical optimization of violin top plates", *Acta acustica*, Vol. 88, pp. 278–285, 2002.
- [8] Gibson, L.J. and Ashby, M.F., "Cellular solids, structure and properties", Pergamon Press, 1998.
- [9] Goffe, W.L., Ferrier G.D., and Rogers J., "Global optimization of stastical functions with simulated annealing", *J. Econ.*, Vol. 60, pp. 65–100, 1994.
- [10] Dahlbom, O., Petersson, H., and Ormarsson, S., "Characterization of modulus of elasticity", Improved spruce timber utilization, Final report subtask AB 1.7, FAIR CT 96-1915, Lund University, 2000.

## THE ADMITTANCE MATRIX OF A CELLO

*J Woodhouse and P E Courtney*

Cambridge University Engineering Department  
Trumpington St, Cambridge CB2 1PZ, UK  
jw12@eng.cam.ac.uk

### ABSTRACT

The  $3 \times 3$  admittance matrix at the centre of a cello bridge has been measured directly, using a miniature impulse hammer and laser vibrometer. This contrasts with earlier work, in which the matrix was determined (for a violin) by an ingenious but indirect method [1]. Data exhibiting good coherence and correct reciprocal behaviour has been obtained up to 3 kHz (corresponding to 9 kHz on the violin). The admittances for excitation parallel to the strings show unfamiliar features, which are explored. Longitudinal string resonances and out-of-plane resonances of the bridge are seen, together with an apparently new vibration mode of the cello structure at about 400 Hz.

### 1. INTRODUCTION AND MEASUREMENTS

If a single measurement is to be made to characterise the behaviour of an instrument of the violin family, then the most natural choice is the input admittance at the bridge. This is the only aspect of the body behaviour which influences the string, and hence the only aspect which can contribute to variations of “playability” between instruments [2]. The admittance does not relate directly to the radiated sound of the instrument, but it does govern how much energy is taken from the string by the body and so contains partial information about the radiated sound intensity. Several researchers have reported measurements of input admittance, or at least an approximation to it, in the direction of bowing: for example Beldie reported by Cremer [3], and Jansson [4,5]. However, the bridge of a violin or cello can move in all three dimensions, and a full characterisation of the input admittance as experienced by a single string at its contact point in the bridge notch requires a  $3 \times 3$  matrix.

This matrix is not easy to measure without adding significant mass, which would distort the results: a violin mute may weigh only a few grams, and yet has an obvious effect on the sound of the instrument. Boutillon and Weinreich [1] made a virtue of this problem, and measured the matrix using an ingenious method involving a comparison of behaviour with and without a known added mass, which removed the necessity to measure the applied forces. In this paper, by contrast, a direct measurement is described, using a miniature impulse hammer and laser vibrometer, neither of which adds any mass to the system.

The measurement was simplified by choosing a cello rather than a violin. A special bridge was made, illustrated in Figure 1. A normal bridge blank was fitted to the test cello and carved into the conventional form, except that a small rectangular block of wood was left between the two middle

strings. This did not interfere with bowing, so that it could be verified that the cello still sounded normal rather than muted.

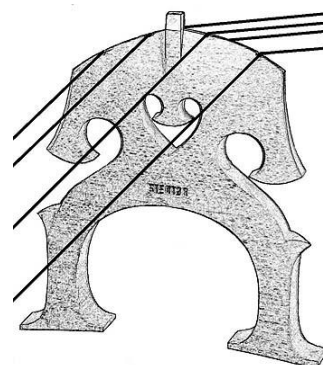


Figure 1: *The modified cello bridge.*

The faces of the block offer orthogonal surfaces for hammer impact and laser reflection. All measurements will be described in terms of a coordinate system based on the block faces: the direction through the axis of the block (vertical when the cello is lying on its back) is denoted *X*, the horizontal direction in the plane of the bridge (approximately the bowing direction) is denoted *Y*, and the direction approximately parallel to the strings is denoted *Z*. The PCB miniature impact hammer was held in a pendulum rig similar to that described by Jansson [4]. This makes it easy to ensure that the impact occurs perpendicular to the face being struck, to avoid frictional impulses which could distort the result [1]. The cello was supported in a frame which could be laid flat or stood vertically, so that any of the block faces could be presented in a vertical plane suitable for impact by the hammer-pendulum. A Polytec laser vibrometer was then aligned on a face oriented in the direction to be measured, and several impacts recorded by a data-logging PC so that an averaged transfer function could be determined. In all but one of the nine configurations needed to measure the full matrix, the laser illuminated a different face to that impacted by the hammer. The exception is the input admittance in the *X* direction, for which the laser spot had to be adjacent to the hammer on the same face of the block. The input admittances in the other two directions could be measured with the hammer and laser on opposite sides. The admittance measurements were calibrated in the usual way, by comparison with an identical admittance measurement on a known mass.

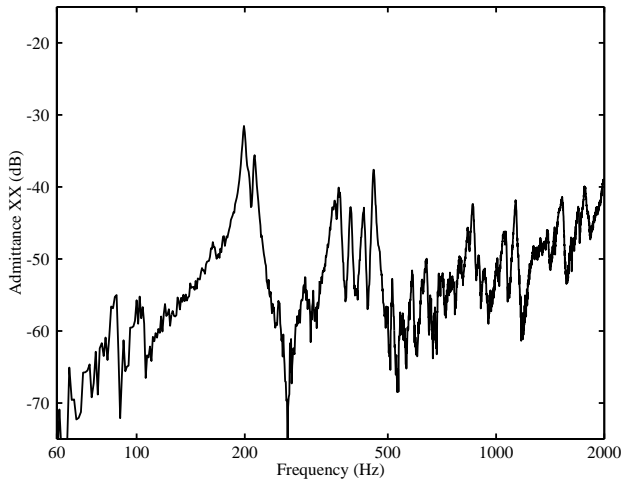


Figure 2a: The XX admittance.

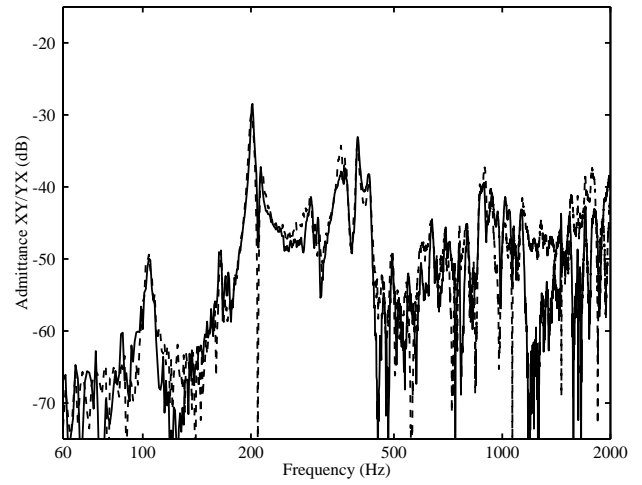


Figure 2d: The XY/YX admittances.

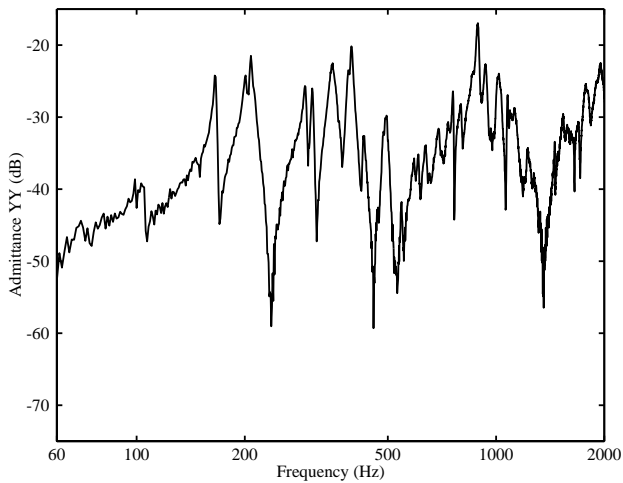


Figure 2b: The YY admittance.

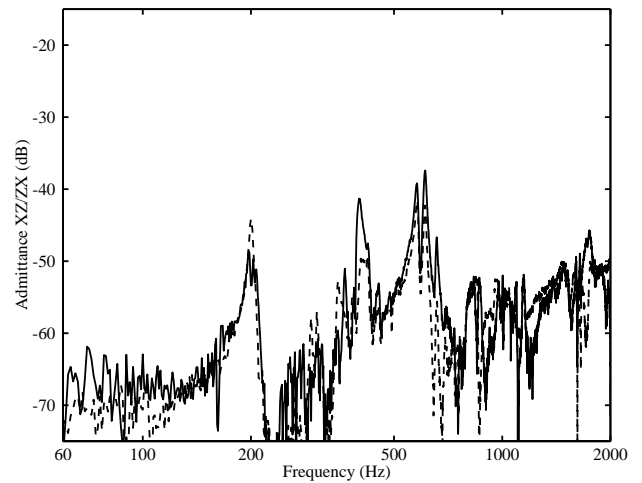


Figure 2e: The XZ/ZX admittances.

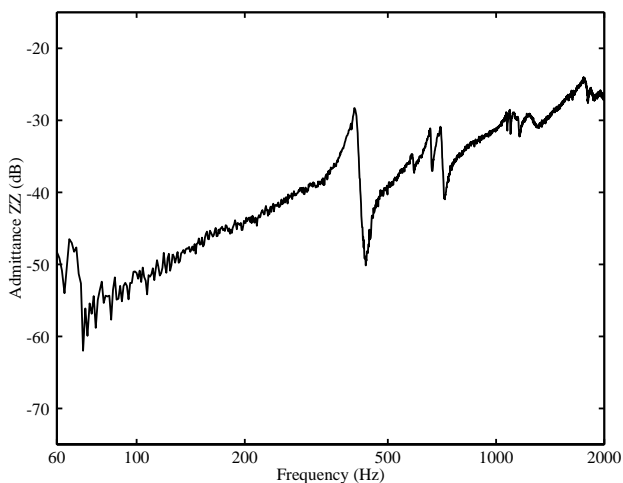


Figure 2c: The ZZ admittance.

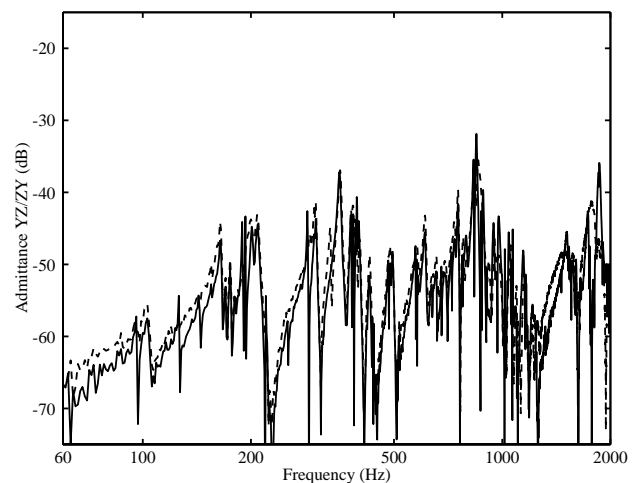


Figure 2f: The YZ/ZY admittances.

A full set of results is shown in Fig. 2. Good coherence was obtained up to approximately 3 kHz: except near antiresonances the XY-plane results showed coherence above 0.9, and those involving the Z direction were above 0.8. The frequency limit is determined by the impact dynamics of the hammer on the relatively soft wood of the block. A first check on accuracy of the results comes from verifying that the real part of the diagonal terms, Figs. 2a, 2b and 2c, show all-positive behaviour. Figure 3 illustrates both the coherence and the real part check on a direct admittance. A second accuracy check comes from the fact that the off-diagonal terms of the matrix should be symmetric, by the reciprocal theorem. It can be seen from Fig. 2d that the XY/YX admittances show excellent reciprocity, while Figs. 2e and 2f show reasonably good reciprocal behaviour in the two admittances involving the Z direction. As will be discussed shortly, the Z direction shows very different behaviour to that in the XY plane, and getting acceptable results for these cross terms required some care with experimental details.

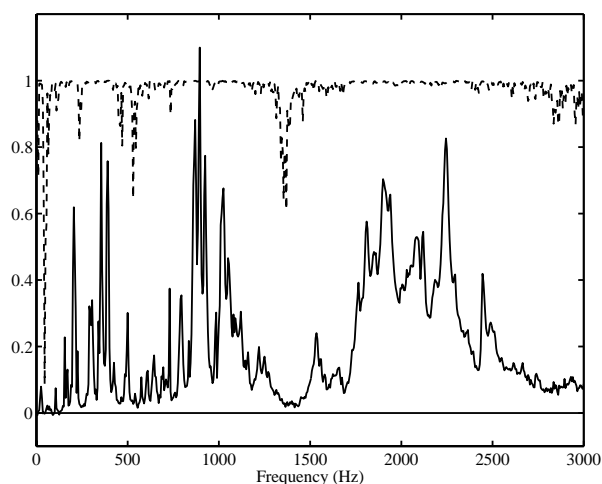


Figure 3: Accuracy checks on YY admittance. Solid line: real part of the YY admittance, multiplied by 10 for convenience of scale; dashed line: coherence associated with the measurement of this admittance.

## 2. INTERPRETATION

The results obtained in the XY plane do not require special comment, since they show features which are familiar from earlier measurements on cellos and violins. The three admittances in this plane show the same set of resonance peaks with different amplitudes, corresponding mainly to body resonances of the instrument. The low-frequency body modes of instruments of the violin family have been quite extensively studied: e.g. Marshall [6], Bissinger [7].

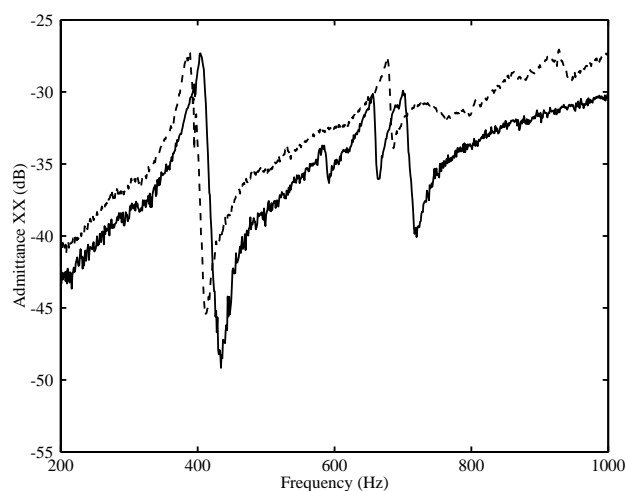


Figure 4: Effect of removing D string. Portion of the ZZ admittance, showing the effect of removing the D string of the cello. Solid line: original plot with all strings present but damped; dashed line: equivalent plot with D string removed.

The ZZ admittance is obviously quite different. It shows a rather small number of strong peaks, which do not align obviously with strong peaks in the XY-plane results. Further measurements were made on the test cello to establish the source of these peaks. The first possibility to be examined is that some of the peaks might be associated with longitudinal resonances in the strings. To test this, the ZZ admittance was measured with each string in turn removed from the instrument. A typical result is shown in Fig. 4, with the D string removed. Removing a string decreases the stiffness in the Z direction, so the resonant peaks have generally shifted down in frequency, and the admittance level has increased somewhat. More strikingly, of the cluster of peaks around 700 Hz in the original measurement, the middle one has disappeared completely, suggesting that it was a longitudinal resonance of the D string. In a similar way, some other peaks were associated with particular strings of the instrument (which were all steel-cored). Resonances of the two middle strings, G and D, show up more conspicuously in this admittance measurement than resonances of the outer strings, but that is an artefact of the placement of the measurement block on the bridge.

The next stage was to perform a modal analysis of motion in the Z direction at various points on the bridge. This revealed that some of the peaks seen in Fig. 2c arise from bending resonances of the bridge. The first two of these are sketched in Figure 5. The lowest resonance, associated with the peak around 700 Hz also visible in Fig. 4, is approximately a pinned-pinned resonance of the bridge, rotating about a line running approximately through the string notches of the two middle strings. It shows up in the admittance measurement because the block stands above this line.



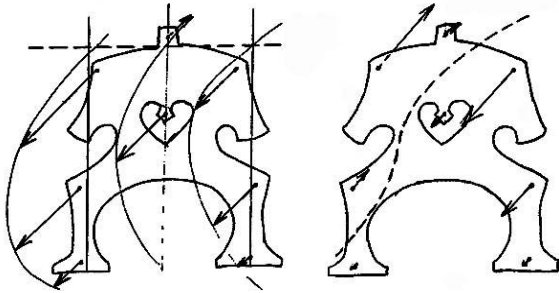


Figure 5: Bending resonances of the bridge.

The first two out-of-plane bending resonances of the cello bridge, revealed by modal analysis with hammer impact in the Z direction. Dashed lines indicate the approximate position of nodal lines. Left: resonance at 700 Hz, with a nodal line close to the string notches. Right: resonance at 940 Hz, showing a combination of bending and twisting.

These two tests accounted for all the peaks in Fig. 2c except the strong resonance around 400 Hz. After exploring a number of possibilities, this peak was eventually found to be a resonance of the cello structure of a rather surprising nature. Schematic results of a Z-direction modal test are shown in Fig. 6: all the auxiliary components (strings, bridge, fingerboard, tailpiece) are moving in phase with the applied force, while the body and scroll move in antiphase. This suggests bending/shearing motion of the entire structure, but the precise details are still far from clear and further investigation of this resonance would be of interest. For example, does a violin show a similar mode?

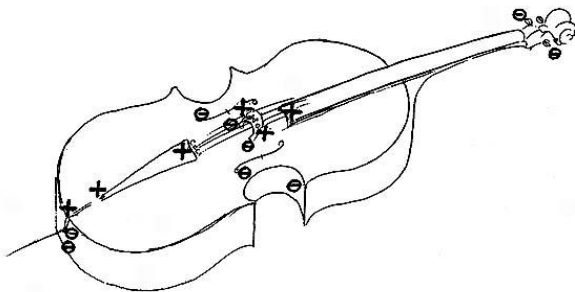


Figure 6: Body mode at 404 Hz.

Sketch of the results of a modal analysis with hammer impacts in the Z direction on the bridge, observing at various points on the body and attached components which allowed a laser reflection in the Z direction: the four corners of the bridge, the end of the fingerboard, the tailpiece, the pegbox, and points on the body near the endpin and the upper corners. Plus signs and minus signs (in circles) denote the phase of the observed motion at the 404 Hz resonance relative to the applied force.

### 3. CONCLUSIONS

A range of measurements have been made on a cello, fitted with a modified bridge to allow the complete admittance matrix to be measured at essentially a single point using an impulse hammer

and a laser vibrometer. The admittance matrix shows, as already noted by Boutillon and Weinreich [1], that the off-diagonal terms are not negligible and might have an influence on the playing behaviour of the instrument. Such an influence would arise most plausibly by the generation of Y-direction motion of the string, which could lead to some modulation of the normal force at the bow. The lateral compliance of the bow-hair may be able to accommodate this without any very drastic consequences arising, but it is an issue which might usefully be explored in bowed-string simulations.

The other results reported here concern the features seen in the ZZ admittance, seen in Fig. 2c. This has a very different appearance to the other two direct admittances, showing a small number of resonant peaks at frequencies with no obvious correspondence to those influencing XY-plane behaviour. By a series of experimental tests, three sources for these ZZ peaks were identified: longitudinal string resonances, out-of-plane bending resonances of the bridge, and a resonance of the cello body at about 400 Hz which appears to involve bending and/or shearing motion, with the auxiliary components (strings, bridge, fingerboard, tailpiece) moving in phase with the applied force while the body and scroll move in antiphase. Whether any of these resonances have a significant influence on the sound or playability of the cello is not known: one might speculate that the most likely route for influence would be by acting as “tuned absorbers”, increasing the energy dissipation near their resonant frequency in the same manner as many designs of “wolf eliminator” for the cello.

### 4. REFERENCES

- [1] Boutillon, X. and Weinreich, G., “Three-dimensional mechanical admittance: theory and new measurement method applied to the violin bridge”, J. Acoust. Soc. Am. 105:3524–3533, 1999.
- [2] Woodhouse, J., “On the playability of violins, Part I reflection functions”, Acustica 78:125–136, 1993.
- [3] Cremer, L., The physics of the violin, MIT Press, Cambridge MA, 1985.
- [4] Jansson, E.V., Molin, N.-E. and Saldner, H.O., “On eigenmodes of the violin — electronic holography and admittance measurements”, J. Acoust. Soc. Am. 95:1100:1105, 1994.
- [5] Jansson, E.V., “Admittance measurements of 25 high quality violins”, Acustica 83:337–341, 1997.
- [6] Marshall, K.D., “Modal analysis of a violin”, J. Acoust. Soc. Am. 77:695:709, 1985.
- [7] Bissinger, G., “Modal analysis of a violin octet”, J. Acoust. Soc. Am. 113:2105–2113, 2003.

# WIRELESS SENSOR SYSTEM FOR MEASUREMENT OF VIOLIN BOWING PARAMETERS

Diana S. Young

Media Lab  
Massachusetts Institute of Technology  
Cambridge, MA, USA  
diana@media.mit.edu

## ABSTRACT

We present a new system to measure the position and force parameters most relevant to violin bowing technique. It is stable and reliable, and as it allows players to perform without impediment and consists of minimal equipment, it is also suitable for use in professional performance settings. This measurement system, implemented on a carbon fiber bow, relies on an electromagnetic field sensing technique for detecting both transverse bow position and bow-bridge distance and foil strain gauges for downward force measurement. The position data is collected using an antenna that is located behind the bridge and mounted from the tailpiece of an acoustic violin. The strain gauges are permanently mounted around the midpoint of the bow stick, and the force data is collected and sent to a remote computer via a wireless transmitter mounted at the frog. The resultant bow remains wireless, and the placement of the sensors and electronics ensures a balance point that remains within the normal range for traditional bows. We describe several experiments illustrating the usefulness of this system for continued studies of bowing parameters, as well as inspection of musical performance style and pedagogical applications.

## 1. INTRODUCTION

The measurement system presented in this paper was originally developed as an enhancement of a carbon fiber violin bow to create a new electronic music interface, or controller. Specifically, it was designed for the purpose of measuring various aspects of right hand bowing technique in order to enable real-time control of effects processing and synthesis algorithms in electroacoustic music performances [1]. This work was related to previous projects involving the modification of traditional string instruments to create new electronic music instruments for expert performers [2, 3, 4].

Despite its beginnings as a performance interface, this bow sensing system shows promise for use in scientific studies of bowing parameters. The limits of the bowing parameters of bow force, bow velocity, and bow-bridge distance are discussed in [5, 6, 7]. This work presents the inspection of bowing parameters as a means of understanding distinctions between different musical performances and musical styles. Because the system described here originated as a bow controller suitable for use in performance scenarios and environments, we suggest it as a tool for such studies.

In the following sections we describe the architecture of the sensor system and its operation. A closer inspection of the strain sensor measurement relating to downward force is detailed, which includes details of its range and performance. Finally, downward strain in the stick (corresponding to downward force), position and

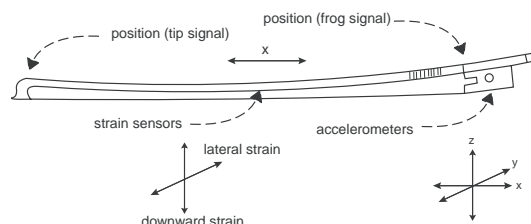


**Figure 1:** The measurement system for the bow includes accelerometers, mounted at the frog of the bow, to give acceleration data for all three axes of bow movement, two strain sensors, mounted around the middle of the stick, for downward (normal to the strings) and lateral (parallel to the strings) strains, and the outputs for the two signals necessary for position sensing (parallel to the bridge), located on the stick at the extreme ends of the bow hair.

velocity, and acceleration data is shown for simple *detaché* bow-strokes.

## 2. MEASUREMENT SYSTEM

The violin bow measurement system discussed in this paper consists of three kinds of sensors. An electromagnetic field sensor [8] is used to measure bow position (transverse), foil strain gauges are used to detect both downward and lateral strain in the bow stick, and accelerometers are used to measure 3D acceleration.

The accelerometers are housed on an electronics board mounted on the frog, while the strain sensors are mounted directly to the bow stick around the midpoint of the bow. The bow board also sends two square wave signals to either end of a resistive strip that runs the length of the bow stick, acting as an antenna for the position measurement. Figure 1 shows the relative positions of the sensors on the carbon fiber bow.

The basic schematic for the bow board is shown in Figure 2, and the bay station schematic is shown in Figure 3.

The implementation of this sensing system is minimal and maintains the playability of the bow as much as possible. Though the sensors and electronics add a considerable amount of weight (almost 30 g), the balance point is still within the normal range, and the bow remains wireless. Details concerning the hardware design may be found in [1, 9].

For the purposes of the work in this paper, only the downward strain sensor, and the position sensor are necessary, though transverse acceleration ( $x$ ) is a convenient indicator of changes in bowing direction. The downward strain sensor is used to reflect

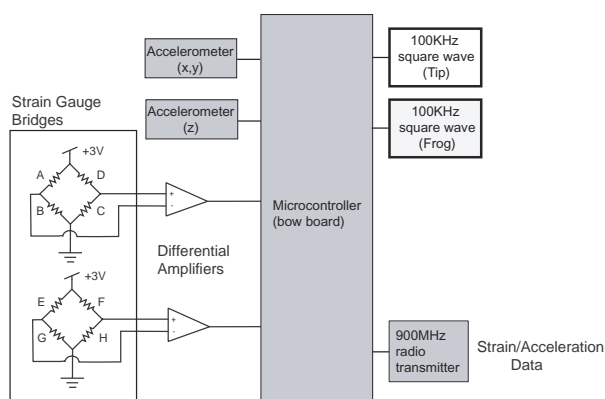


**Figure 2:** The electronics board mounted to the frog of the bow houses a microcontroller, two 2-axis accelerometers, and an RF transmitter. The microcontroller outputs the two square wave signals for the position measurement and receives the signals from the strain sensors as inputs to its internal A/D converter.

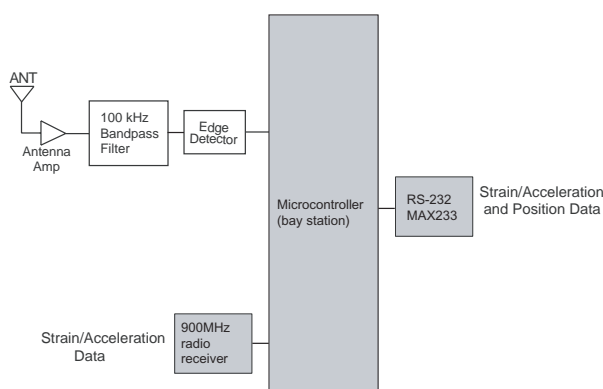


**Figure 3:** Bay station schematic. Signal radiating from resistive strip on bow received by electrode antenna mounted behind the bridge of the test violin. The signal is then passed through a bandpass filter and edge detector and into the A/D of the microcontroller. The position data values for the tip and the frog ends of the bow are then added to the stream of data carrying the strain sensor and accelerometer information (which is received via an RF module).

bow force, and the position sensor data is used to measure bow velocity and bow-bridge distance.

As depicted in Figure 4, the strain and acceleration data is transmitted from the bow wirelessly to the bay station, and the position sensor data is carried from the antenna mounted on the violin to the board via a cable. The microcontroller in the bay station combines the two data streams and sends the result to the serial port of the computer for analysis. Currently, the sampling rate of the bow data is about 40 Hz.

### 3. STRAIN SENSOR TESTS

In order to characterize the response of the downward strain sensor, the sensor data was recorded while force was applied directly to the bow stick by an Instron universal testing machine (4400 series). To accomplish this, the bow was secured by a clamp on either end (tip and frog). Unfortunately, this arrangement was not ideal and probably contributed to the error in the measurements, as the

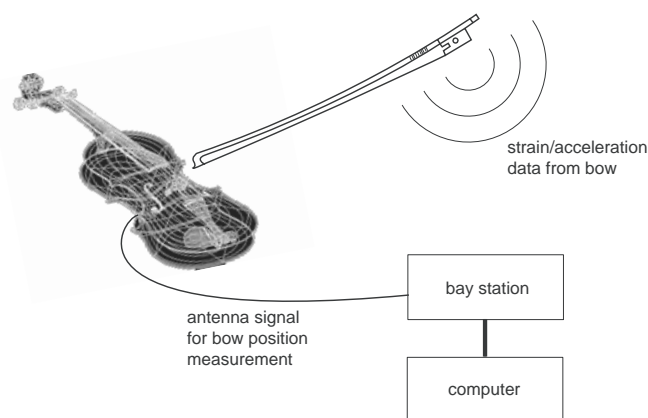


**Figure 4:** The bay station for the bow measurement system contains an RF receiver that receives the strain and acceleration data from the bow. An antenna cable also carries the position sensor signal to the board, and both data streams are combined into one and sent out of the serial port to the computer for analysis.

bow may have slipped during the experiments. Despite this likelihood, we proceeded with the measurements in order to estimate the range of the strain sensor.

Figure 5 shows plots of strain data taken for force applied at three different points along the length of the bow. Each plot shows the curve corresponding to increasing force on the stick, as well as decreasing force. Clearly, these measurements indicate definite hysteresis in the sensor. However, it is likely that hysteresis in the bow itself may be a large contributing factor to this behavior, as it is easy to observe that the stick is slow to recover to its original position after being held in a flexed position.

The experiment was repeated at the location around the mid-point of the bow for a smaller range in applied force, corresponding to the normal range of bow force discussed in [5, 6]. Figure 5(d) shows that for this smaller measurement range the hysteresis is significantly reduced.

Though the results of these experiments are limited, the data shown clearly indicates that the downward strain sensor is capable of reflected the full range of downward force used in normal violin playing.

Further tests should be done in order to correctly calibrate the stain sensor to properly reflect changes in downward bow force. Clearly, the setup used here was insufficient, due to the manner in which the bow was secured for data collection. Not only was the bow not held tightly enough during the experiment, but these measurements should be taken while the bow is held only at the frog. Therefore, we hope to repeat a series of similar experiments using a computer-controlled bowing machine. After doing so, a calibration curve relating the strain data to downward bow force for different bowing points should be attained.

#### 4. POSITION SENSOR TESTS

Gesture data for simple bow strokes was recorded in order to illustrate the performance of the position sensor. As discussed in [8], the amplitudes of the signals emitted from the tip and frog may be used to determine the transverse bow position and bow-bridge distance. Bow position is found to be equal to the difference of the two values divided by the sum of the two values. In Figure 6, the bow position is plotted for bowstrokes of about 30 cm in length around the midpoint of the bow. The plot of the acceleration in this direction is also included to indicate the changes in bow direction.

These results are encouraging, as they indicate that the position sensor is quite linear in its response. Though the strain sensor data does not yet indicate the downward force parameter, its plot shows consistency and repeatability in the measurement.

Bow-bridge distance is not depicted here, but depends on the same data as the position measurement. In future, much more testing will be done to correlate the gesture data measured by the bow system with different strokes in order to further investigate the performance of the sensors.

#### 5. CONCLUSIONS AND FUTURE WORK

We have presented a new kind of measurement system for bowing parameters that is suitable for use in performance scenarios and environments. Such a system could facilitate studies of musical style and may even be useful for pedagogical applications in which the monitoring of bowing parameters is used for training purposes.

Experiments were described that indicate that the downward strain sensor located around the middle of the bow stick is capable of reflecting the range of downward force used in normal violin playing. Also, the data from the position sensor was shown to be consistent and linear.

There is a great deal of work yet to be done toward a full characterization of the sensor system presented here, which should include experiments using a computer-controlled bowing machine. A thorough study of different bow strokes and musical performances should follow.

#### 6. ACKNOWLEDGEMENTS

Special thanks to Yael Maguire and Jonathan Polimeni for their help with the data-recording and figures.

#### 7. REFERENCES

- [1] D. S. Young, "New frontiers of expression through real-time dynamics measurement of violin bows," Master's thesis, M.I.T., 2001.
- [2] T. Machover and J. Chung, "Hyperinstruments: Musically Intelligent and Interactive Performance and Creativity Systems," in *Proceedings of the 1989 International Computer Music Conference*, (San Francisco, CA), pp. 186–190, 1989.
- [3] T. Machover, "Hyperinstruments: A progress report 1987-1991," tech. rep., MIT Media Laboratory, 1992.
- [4] J. A. Paradiso, "Electronic Music Interfaces: New Ways to Play," *IEEE Spectrum*, vol. 34, no. 12, pp. 18–30, 1997.
- [5] A. Askenfelt, "Measurement of bow motion and bow force in violin playing," *Journal of the Acoustical Society of America*, vol. 80, no. 4, pp. 1007–15, Oct. 1986.
- [6] A. Askenfelt, "Measurement of the bowing parameters in violin playing. II. Bow-bridge distance, dynamic range, and limits of bow force," *Journal of the Acoustical Society of America*, vol. 86, no. 2, pp. 503–16, Aug. 1989.
- [7] J. Woodhouse, "On the Playability of Violins. II. Minimum Bow Force and Transients," *Acustica*, vol. 78, no. 3, pp. 137–53, April 1993.
- [8] J. A. Paradiso and N. A. Gershenfeld, "Musical applications of electric field sensing," *Computer Music Journal*, vol. 21, no. 3, pp. 69–89, 1997.
- [9] D. S. Young, "The hyperbow controller: Real-time dynamics measurement of violin performance," in *Proceedings of the 2002 Conference on New Interfaces for Musical Expression (NIME-02)*, 2002.

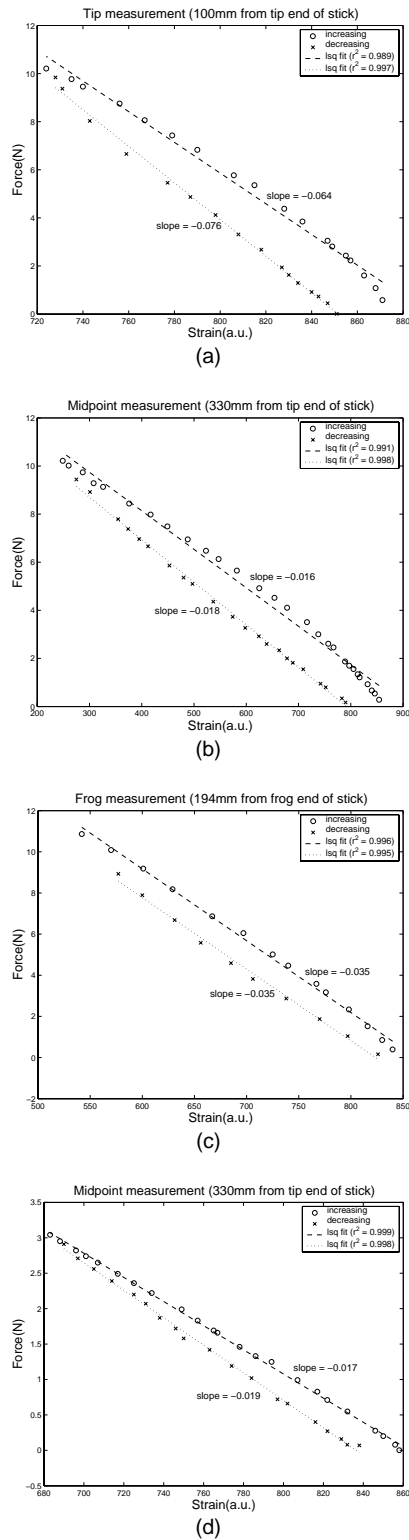


**Figure 5:** In order to calibrate the downward strain sensor, a force was applied directly to the bow as the sensor data was recorded. Data was taken for an increasing force of approximately 0–10 N, and then a force decreasing to zero. The exercise was performed for three points along the length of the bow at (a) 100 mm from tip, (b) 330 mm from tip, and (c) 194 mm from frog end. The measurement reveals a significant hysteresis effect. (d) The force calibration exercise was repeated for the midpoint position for a range of 0–3 N. It can be seen that the hysteresis observed in the previous plots is smaller for the lower range of applied force.

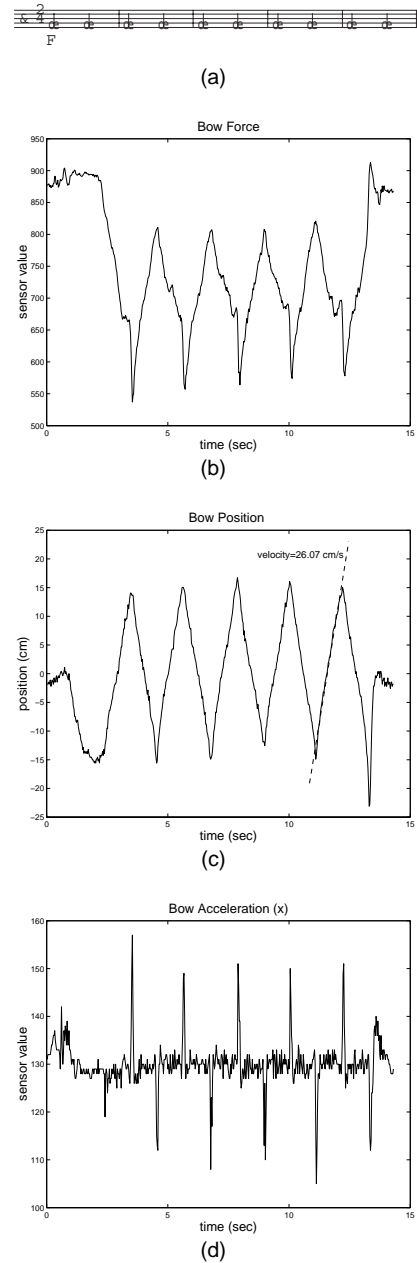


**Figure 6:** Gesture data was taken for a series of *detaché* bowstrokes, played on the open D string of the test violin. The figure shows (a) repeated strokes on the open D string, played at a steady *mf* dynamic level; (b) downward bow force reflected by the strain sensor measurement; (c) bow position over a range of about 30 cm around the midpoint of the bow stick, as well as the bow velocity indicated by the slope of the graph; and (d) data from the accelerometer indicating the changes in bow direction.

# GUITARS



## GUITAR MODELS FOR MAKERS

*Bernard E. Richardson*

Musical Acoustics Group, Department of Physics and Astronomy, Cardiff University  
P.O. Box 913, Cardiff CF24 3YB, United Kingdom

RichardsonBE@Cardiff.ac.uk

### ABSTRACT

Science has given a remarkable insight into the mechanical and acoustical action of stringed instruments such as the guitar. Techniques such as holographic or speckle interferometry or the finite element method give detailed information about the vibrations of the wooden body and their dependence on materials and construction. More recently, there has been interest in measuring and modelling sound radiation fields from guitars. Studies have also been made of the player's interaction with the instrument and of the listener's response to modelled or real sounds. One would expect that by now science could answer that innocent question so often posed by makers: "How do I make better guitars?". This paper aims to give an overview of the acoustics of the guitar as we know it today. It will take a look at both experimental and theoretical attempts to find relationships between guitar construction and the musical performance of the instrument. It will also explore some useful models which might be used for quality control or for the exploration of new musical sounds and go, at least some of the way, towards answering the many practical questions posed by makers.

### 1. INTRODUCTION

To establish relationships between the "tone quality" of an instrument and its constituent materials and dimensions first requires a thorough understanding of the important perceptual features in the radiated sound. These can be summarised by reference to Figure 1, which shows the time dependence of the sound spectrum of a single guitar note.

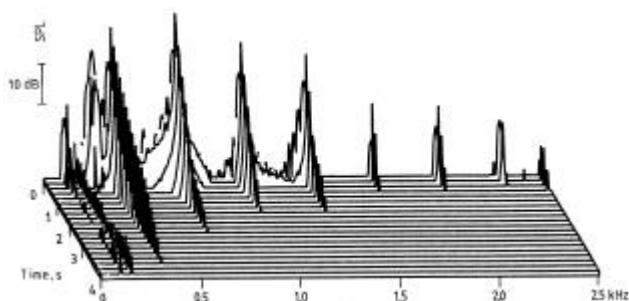


Figure 1: *Short-term FFT analysis of a guitar note (open top string  $E_4$  with other strings damped).*

It is convenient, though strictly physically incorrect, to break the spectrum down into two sets of components: the near-harmonically related and relatively long-lived "string" partials which result from the standing waves on the string, and short-lived "noise" components which result from the relaxation of the body on release of the string. The former determine the pitch of the sound and the latter add a perceptually important percussive element to the sound. The peak heights and decay rates of the "string" components depend crucially on the coupling of the strings to the body and the body's structural dynamics and its interaction with the internal and external surrounding air, but the player can also exercise considerable control through choice of plucking position, fingertip interaction and release velocity (trajectory and speed). The angle of release is particularly important since the bridge responds very differently to forces applied parallel or perpendicular to the bridge.

In the nylon-strung classical guitar the decays of the "string" vibrations are dominated by internal damping in the strings themselves, though spectacularly rapid decays occur when "string modes" coincide with "body modes" (the so-called "wolf notes"). The strong coupling which occurs on these occasions produces substantial inharmonicity (sizeable fractions of semitones – in general far more than introduced by finite string stiffness or string imperfections). Over-coupling between string and body (or insufficient impedance mismatch) is a major problem in modern guitar design [1]. Decays often have a single exponential decay factor (linear decay on a log plot), but it is not uncommon to see dual decays and beating decays. These are caused by coupling effects between different string polarisations and or between "sympathetic" strings. (The latter provides a very idiomatic flavour to the sound of the guitar but it should never be relied upon to provide sustain in a properly constructed guitar.) There are also some non-linear effects concerned with longitudinal string forces. Recent work by David [2] suggests that the bridge typically provides up to six degrees of freedom, highlighting the complex physics at this crucial point.

It must be stressed that whilst Figure 1 is representative of the spectrum of a guitar note, there is huge variation even from one note to the next on a single instrument. This begs the question "What defines a guitar sound?". It is clearly not sufficient to work at the single-note level to answer this question. The more pertinent question of what constitutes a "good" guitar sound might then be seen to be related more to relationships



between notes and to the dynamic and tone ranges rather than simply “harmonic content”, “harmonicity” and “sustain”. This is clearly a field ripe for further psychoacoustical investigation.

Finally there is an issue of the “feel” of the guitar under the players’ fingertips. Measurements and models by Pavlidou and Lewney [3] show that the players’ interactions are complex, involving rolling and sliding of the string over the fingertip, but attempts to quantify the instrument’s “feel” have so far eluded our investigations.

## 2. GUITAR MODE STUDIES

The maker modifies the sound of an instrument by using different materials or modifying the dimensions of the guitar. The most practical way to analyse and comprehend these changes is in terms of the instrument’s modes of vibration and sound radiation fields; these are ultimately what determine the acoustical function of the guitar.

Huber [4] was the first to propose using frequency-response curves for quality control in guitars. These show resonance peaks in sound pressure or input admittance. In the spirit of the time, it was assumed that these graphs contained the “signature” of an instrument, but it is fair to say that nowadays we have less faith in using these “one-dimensional measures” for quality control, though combinations of pressure response and input admittance can give great insight into the mechanics of stringed musical instruments. Practical mode studies truly came of age in the early 1970s when holographic interferometry was first used to visualise guitar modes [5].

Whilst not exclusively so, a common preoccupation for both makers and scientific researchers has been investigations of the influence of soundboard strutting on the response of the guitar. Some of the earliest systematic experiments were performed over a ten year period by Jovicic and Jovicic (e.g. see [6],[7]), who investigated the development and modification of body modes and radiated sound spectra with various structural changes. Similarly, Meyer [8] performed a set of experiments involving practical modifications of real instruments with an associated psychoacoustical research programme which allowed him to recommend particular strutting systems for factory-made guitars. Richardson and Roberts [9] showed that the combination of holographic and speckle interferometry and the finite element method could be used to help develop numerical models to give insight into the importance of specific changes in the guitar’s structure (see also Walker [3]). Recent studies by Elejabarrieta *et al.* [10],[11] have taken advantage of modern computing power to extend these models; their models of structural and air-cavity interactions [12] are particularly illuminating.

Practical measurements of sound radiation from guitars has received considerably less attention until recently [13]. Attempts to model sound radiation include simple monopole-radiation models by Christensen [14] and boundary element models, e.g. Brooke [3]. Increasingly, research is being

undertaken on computationally efficient methods for computing radiation [15] or for modelling both the instrument and radiation fields [16]; this is no doubt an area where we will see intense activity in the next few years and one which potentially might answer some of the questions posed here.

Mode studies usually present data on the gross features of mode shapes and resonance frequencies only. In this form they are superb educational tools for makers – they show graphically which parts of the instrument are vibrating and allow informed choice about where and how to introduce significant modification. But to return to an earlier line of questioning, “What modes should a good guitar have?”. The problem here is that, in the author’s experience, mode shapes and frequencies of “good” and “bad” guitars are very similar. To some extent this is a basic demonstration that the physical differences between instruments is small, but it also indicates that we might not necessarily be measuring the right thing.

## 3. A MODEL FOR STRING-BODY INTERACTION

Finite element models are very exciting, but they are unwieldy, complex and labour intensive – hardly the thing for a maker to be involved with on a daily basis. Current models also do not handle damping very well. Given the relatively small differences between instruments, perturbation methods may provide greater insight (this approach was advocated by Stetson [17] many years ago). In work at Cardiff we have taken a semi-analytical approach using a generic model in which various acoustical parameters can be modified. This at least gives some insight into what “dimensions” of the modes might be important. In turn, the changes in acoustical parameters can be referenced back to constructional features.

Based on the work of Christensen [14] and Gough [18], Wright [3],[19] constructed a “free-oscillator” model of the guitar for the low- to mid-frequency range (up to about 2 kHz). The model included a plane-polarised plucked string (with damping) coupled to a body described in terms of simple harmonic oscillators, the bridge dynamics being specified in terms of the mode frequencies, Q-values (damping), effective masses and monopole radiation coefficients of each mode. (The latter two parameters reflect the mode shape as will be described later.) Starting with parameters derived from real instruments and adjusting each parameter in turn through realistic ranges, Wright used this model in psychoacoustical experiments to determine which of the modal properties had significant effects on the sound quality of the instrument.

An updated, transmission-line model representing a string stretched between points 0 and  $L$  (the bridge) is presented in Equation (1). The mechanical properties of the body at the bridge are described by the load impedance  $Z_L(\omega)$ , which is simply the reciprocal of the input admittance at the bridge (Equation (1) in [13]). The input admittance at the plucking point at position  $x$  is then given by

$$Y(\omega) = \frac{\sin(k'x)}{Z_L(\omega) \sin(k'L) + iZ'_0 \cos(k'L)}, \quad (1)$$

where  $k'$  and  $Z'_0$  are “lossy” versions of the wavenumber for transverse waves on the string ( $k = \omega/c$ ) and the string’s characteristic impedance ( $Z_0$ ) respectively, given approximately by  $k' = k\sqrt{1+i/Q_s}$  and  $Z'_0 = Z_0\sqrt{1+i/Q_s}$ , where  $Q_s$  is the Q-value of the string. This formula predicts, in the frequency domain, all the frequency shifts, decay-rate modifications and transient noise elements described earlier. Straightforward Fourier tricks allow conversion to the time domain. With the addition of suitable “radiation terms” and summed over the range of modes of interest, it can be used to synthesise plucked-string sounds containing all the principal features described in Section 1. In principle, there is no reason why this model cannot be extended to incorporate higher-order radiation terms, as described in [13].

Wright’s psychoacoustical experiments clearly demonstrated that, contrary to popular belief, neither the mode frequencies nor the damping of modes were particularly important. Shifts in mode frequencies are perfectly audible, particularly in the dominant, low-order modes, but they were basically *localised* effects; what they essentially do is to modify the position of “wolf notes”, which arguably might be of concern to players (see also comments in [13]). The parameters which proved to be much more important because they induced *global* effects were the effective masses and the radiativities of modes. With these factors in mind we can begin to re-appraise the important features of the guitar’s modes.

#### 4. THINKING ALOUD

Figure 2 shows an interesting comparison of a single guitar plate strutted in various configurations. Superficially the mode shapes appear to be the same – a uni-phase motion of the plate centred on the bridge. The different configurations add varying amounts of stiffness either along and or across the grain promoting different resonance frequencies. In the context of the previous discussions, however, what is of more interest is the variations in the effective masses of the plates (the physical masses are virtually identical). Bearing in mind that both strong response and strong radiativities require low effective masses of modes (within reason of course!), we note that Configuration III – the lattice-braced guitar – has a great deal of potential. When we further note that in more sensitive hands this plate could have been made about 25% thinner to reduce the mode frequency to that of the “standard” Torres model (Configuration II) thereby reducing the effective mass even further, we understand immediately why this type of bracing has found considerable favour in recent years in the manufacture of high-quality concert guitars [20]. It is straightforward to show that effective masses

and radiativities are both functions of mode shapes, as explored at some length in another publication [21].

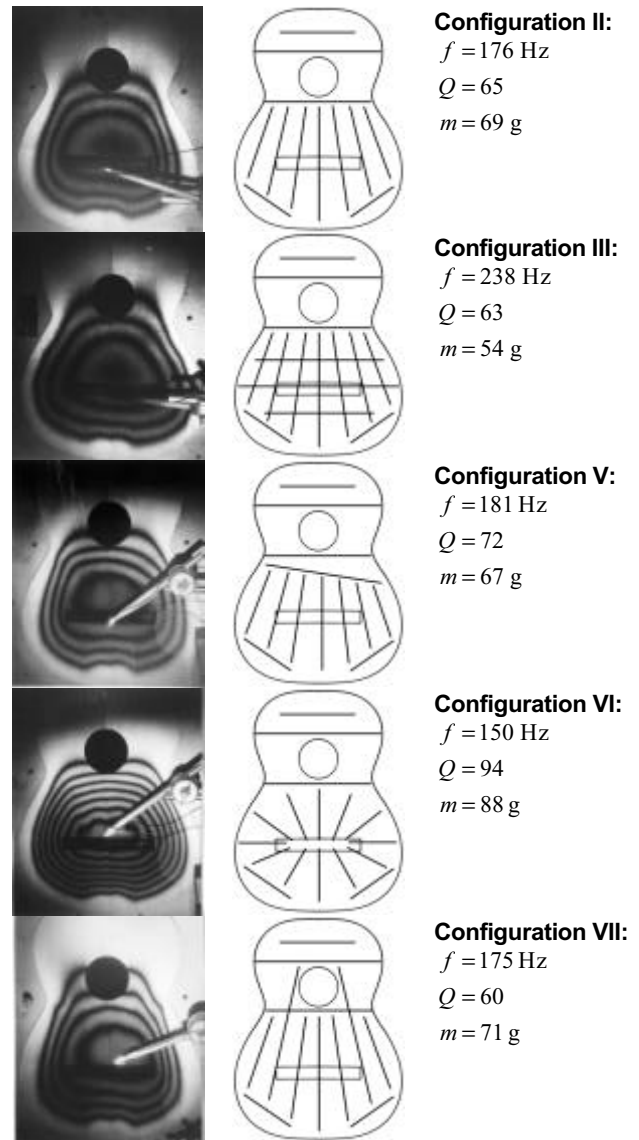


Figure 2: The fundamental soundboard mode for each of five strutting configurations. The same soundboard, glued to a “rigid” edge constraint, was used throughout these experiments; only the bracing was modified. The measurements shown here are for the soundboard without a backing cavity. The configurations are: II “standard Torres”, III Lattice, V “Ramirez”, VI Radial and VII Extended Torres (the numbering system is for consistency with other experimental work in progress). Note that the amplitudes are chosen arbitrarily. Data from Lewney [3].

Unfortunately, neither effective masses nor radiativities are quite so user-friendly as mode shapes and resonance frequencies. In situations where there is little departure from a fixed design with standard materials, mode frequencies are probably as good

an indicator of consistency as any tests based on effective masses. When experimenting with new designs and materials, however, these broader concepts should be considered.

Finally, we might speculate on some useful future work. Modes of guitars are “separable” up to about 1 or 2 kHz. Input admittance measurements above these frequencies show a gradual flattening effect with significant modal overlap. Sound pressure response shows highly complex structure because of increased directionality of the radiation. It is quite likely that statistical models would be perfectly adequate to describe these regions, but the high-frequency ranges of guitars require much more attention. It is interesting to speculate whether the “periodic” spacing of the fan struts produces cut-off frequencies for waves propagating on the soundboard. This type of effect would explain why thin soundboards with thick struts and thick soundboards with thin struts which have comparable properties at low frequencies produce quite different sounding instruments.

Our recent work on radiation has shown the importance of dipole radiation and also the strong dipole contributions from low-order modes (which have previously been considered primarily monopole radiators). These observations appear to raise an old issue of the importance of interactions between the soundboard, ribs, back plate and air cavity, a problem which could surely be resolved with a good finite element model.

## 5. ACKNOWLEDGEMENTS

We gratefully acknowledge financial support for our recent work from the Leverhulme Trust (ref: F/407/R). We would also like to thank the many makers and players who have given their time and loaned instruments for these and other studies. The author also acknowledges the hard work and effort from past students and research assistants which has driven the musical acoustics work at Cardiff.

## 6. REFERENCES

- [1] Richardson, B.E., “The acoustical development of the guitar”, *J. Catgut Acoust. Soc.*, Vol. 2(5), pp. 1-10, 1994.
- [2] David, M.B., *Caractérisations acoustiques de structures vibrantes par mise en atmosphère raréfiée*, PhD Thesis de l’Université Paris 6, 1999.
- [3] Details of PhD studies undertaken in the Musical Acoustics Group at Cardiff are available from the following web site: [www.astro.cf.ac.uk/groups/acoucomp/](http://www.astro.cf.ac.uk/groups/acoucomp/).
- [4] Huber, J., “The application of acoustical testing methods to the guitar”, *Catgut Acoust. Soc. Newslett.*, No. 11, pp. 15-18, 1969.
- [5] Jansson, E.V., “A study of acoustical and hologram interferometric measurements of the top plate vibrations of a guitar”, *Acustica*, Vol. 25, pp. 95-100, 1971.
- [6] Jovicic, J., “Spectres sonores de la guitare de concert”, *Acustica*, Vol. 18, pp. 113-118, 1967.
- [7] Jovicic, O., and Jovicic, J., “Le rôle des barres de raidissement de la table de résonance de la guitare: II. Leur effet sur les nœuds de la table (étude holographique)”, *Acustica*, Vol. 38, pp. 180-185, 1977.
- [8] Meyer, J., *Akustik der Gitarre in Einzeldarstellungen*, Verlag E. Bockinsky, Frankfurt, 1985.
- [9] Richardson, B.E., and Roberts, G.W., “The adjustment of mode frequencies in guitars: a study by means of holographic interferometry and finite element analysis”, *SMAC '83*, Vol. II, Publication of the Royal Swedish Academy of Music, No. 46:2, pp. 285-302, 1985.
- [10] Elejabarrieta, M.J., Ezcurra, A., and Santamaría, C., “Evolution of the vibrational behaviour of a guitar soundboard along successive construction phases by means of modal analysis techniques”, *J. Acoust. Soc. Am.*, Vol. 108, pp. 369-378, 2002.
- [11] Elejabarrieta, M.J., Ezcurra, A., and Santamaría, C., “Vibrational behaviour of the guitar soundboard analysed by means of finite element analysis”, *Acustica united with Acta Acustica*, Vol. 87, pp. 128-136, 2001.
- [12] Elejabarrieta, M.J., Ezcurra, A., and Santamaría, C., “Coupled modes of the resonance box of the guitar”, *J. Acoust. Soc. Am.*, Vol. 111, pp. 2283-2292, 2002.
- [13] Hill, T.J., Richardson, B.E., and Richardson, S.J., “Modal radiation from classical guitars: experimental measurements and theoretical predictions”, see elsewhere in these Proceedings, 2003.
- [14] Chistensen, O., “An oscillator model for analysis of guitar sound pressure response”, *Acustica*, Vol. 54, pp. 289-295, 1984.
- [15] Pichon, A.L., Berge, S., and Chaigne, A., “Comparison between experimental and predicted radiation of a guitar”, *Acustica united with Acta Acustica*, Vol. 84, pp. 136-145, 1998.
- [16] Derveaux, G., *Modélisation numérique de la guitare acoustique*, PhD Thesis de l’École Polytechnique, Paris, 2002.
- [17] Stetson, K.A., “The effect of thickness perturbations of the vibration modes of plates”, *Catgut Acoust. Soc. Newslett.*, No. 28, pp. 28-34, 1977.
- [18] Gough, C.E., “The theory of string resonances on musical instruments”, *Acustica*, Vol. 49, pp. 124-141, 1981.
- [19] Wright, H.A.K., and Richardson, B.E., “On the relationships between the frequency response of the guitar body and the instrument’s tone”, *Proc. Inst. Acoust.*, Vol. 19(5), pp. 149-154, 1997.
- [20] Morrish, J., *The Classical Guitar: a Complete History*, Outline Press Ltd., 1997.
- [21] Richardson, B.E., “Simple models as a basis for guitar design”, *J. Catgut Acoust. Soc.*, Vol. 4(5), pp. 30-36, 2002.

## PHYSICAL MODEL OF A COMPLETE CLASSICAL GUITAR BODY

Rolf Bader

Musikwissenschaftliches Institut Universität Hamburg  
Neue Rabenstr. 13, 20354 Hamburg R.Bader@t-online.de

### ABSTRACT

A complete model of a classical guitar is built in a software with the method of finite-differences FDM. It allows all coupling between the guitar parts as well as coupling between longitudinal and transversal waves. The time stepping algorithm leads to time series in a sound field or taken from any part of the guitar body. The aim is to find explanations of some guitar behaviours, as known from the analysis of recorded guitar sounds. As two examples, the amplitude modulation of overtones of real sounds are shown here to appear after an impulse struck at the back, even without the coupling of the back to any other part of the body. One reason for this is given. Also the curvature of the back due to its geometrical tension is simulated. The frequency response of the curved back has a raised overtone structure. The reason for this can be seen in the coupling between longitudinal and transversal waves in the plate. As the guitar parts are visualised in this software, the observation of the guitar body moving in 'slow motion' is of great help in finding the explicit reason for the observed behaviour. Also the produced sound can be heard and judged as a plausible result of the simulation.

### 1. INTRODUCTION

Musical instruments often have complicated geometries, for which the formulation of differential equations is practically no more possible. The fundamental mode of a guitar i.e. is a combination mode. It comes into existence through the top plate, the back plate and the air enclosed into the guitar interacting and so are forming an own combined vibration. Next, the guitar has a so called fan bracing, on the top plate to stabilize the wood. A Torres fan bracing i.e. consists of seven small wooden bars glued at the bridge part of the top plate. So this plate cannot longer be treated as one continuous piece. Also the boundary conditions of a guitar are not the known ones of fixed, free or clamped. The top plate and the back are connected to the ribs, which take over the vibrations and vice versa. So the connections of the guitar parts has to be taken as another format between fixed and clamped.

The finite element method FEM and the finite difference method FDM are two possible formulations of such a problem. The FDM is used here because it is transient in the first place and because it not assumes global behaviour of the system like eigenvalues, but results in a time series, from which the frequencies can be obtained later. Again this is done for two reasons. A very important part of musical sounds is the initial. It can be that short, that the notion of a frequency comes with a large uncertainty. Also the frequencies change a lot in their values and amplitudes during the initial. Secondly in pre-tests, a balinese bronze plate with a complicated structure showed more eigenvalues during the initial, then could be detected with sophisticated FEM calculations (unpublished up to now, PERMAS used as FEM program).

### 2. METHOD

The guitar is divided into top plate, back plate, ribs, neck and the air cavity in the guitar. The radiation is simulated as a delay function, the strings are a waveguide for convenience.

Each guitar part is simulated with longitudinal and transversal waves (except the air, which only has longitudinal waves). The basic idea is a lattice as shown in Fig. 1.

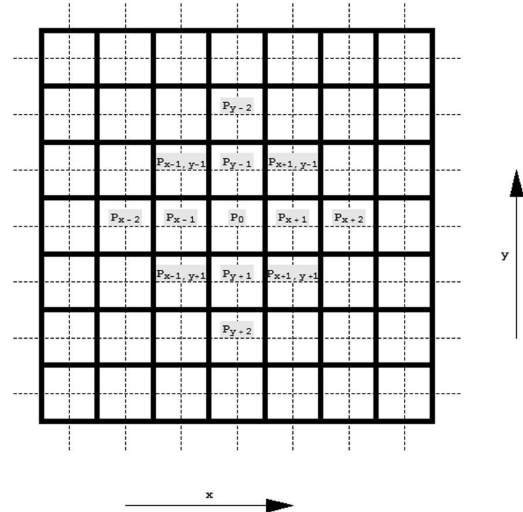


Figure 1: Two dimensional lattice. The thick lines are the element boundaries, the dotted lines are the connections of the element middle points.  $P_0(x, y)$  is the middle element, for which the calculation takes place. All other elements refer to  $P_0$ .

The elements can be seen as the thick lines. The dotted lines show the connections of the element middle points. The displacements of these middle points have to be determined by the calculation. All elements are taken as two-dimensional, except the air enclosed.

#### 2.1. Longitudinal waves

The longitudinal wave is a differential equation of second order. It is  $a = \frac{Fm}{s}$ , with  $a$  as acceleration,  $F$  as force and  $m$  as the mass of the element. Now,  $F$  is determined from the definition of Youngs modulus:

$$F = A * E * \frac{\Delta s}{s}, \quad (1)$$

Here  $A$  is the area between two elements. As the thickness of all elements can be different, it has to be calculated for all neighbours of  $P_0$  separately.  $E$  is Youngs modulus,  $s$  the distance between two element middle points and  $\Delta s$  the change of that distance due to displacements. As the differential equation of longitudinal waves is of second order, next to  $P_0$  as the middle element, we only need  $P_{x-1}$  and  $P_{x+1}$  for the displacement calculation in the x-direction.

But not only the change of distances of the neighbour elements of  $P_0$  causes a displacement in the x-direction. Two more factors come into place, the shearing and the lateral contraction.

There is a shearing, when  $P_{y-1}$  and  $P_{y+1}$  move in x-direction. Then it can happen, that these two will tear  $P_0$  in their direction.

The lateral contraction is given by Poissons number. Here, the elements  $P_{x+1,y+1}$ ,  $P_{x+1,y-1}$ ,  $P_{x-1,y+1}$  and  $P_{x-1,y-1}$  come into place. E.i., will  $P_{x+1,y+1}$  and  $P_{x+1,y-1}$  move closer together, then they contract  $P_0$  in the negative x-direction. The same holds for  $P_{x-1,y+1}$  and  $P_{x-1,y-1}$  for the positive x-direction. Both have to be taken into consideration, because they can cancel out or strengthen each other.

Now, is the change of length known for  $P_0$ , then  $F$  can be calculated and with it also the acceleration, velocity and displacement for the next time step.

$$P_{0,longitudinal_{x,new}} = P_{0,longitudinal_{x,old}} + v_{new} * \Delta t \quad (2)$$

$\Delta t$  is the time step of iteration. Here the fraction of CD-quality sampling rate is used.

$$\Delta t = \frac{1}{44,1kHz} \quad (3)$$

## 2.2. Bending waves

The iteration of bending waves is more complicated then the one for longitudinal vibrations. The differential equations of bending is of fourth order.

$$\frac{\partial^2 y}{\partial t^2} = -\frac{E * K^2}{\rho} * \frac{\partial^4 y}{\partial x^4} \quad (4)$$

From the derivation of this equation we know, that the fourth order is the curvature of the moment. Using the definition of curvature  $\frac{\partial^2 y}{\partial x^2} = \frac{1}{r}$  and the definition of Youngs modulus Gl. (1) we get

$$F = E * A * \frac{\partial^2 y}{\partial x^2} * z \quad (5)$$

We assume here, that the beam, which is bent here as a neutral axis, which is a middle area in the beams direction. This neutral axis does not change its length while the beam is bending.  $F$  is the force that arises, when the beam with the cross section  $A$  and the curvature  $\frac{\partial^2 y}{\partial x^2}$  in y-distance  $z$  above the neutral axis is displaced. Integration by  $z$  leads to a moment, which uses the radius of gyration  $\int \int z^2 dA$ .

$$M = F * z = E * \frac{\partial^2 y}{\partial x^2} * \int \int z^2 dA \quad (6)$$

This moment does not cause the backdriving force. Only if this moment  $M$  along the beam changes, we get a cross-force. But

this cross force also is not the backdriving, because equal cross-forces cancel out themselves. Just a change of this cross-forces leads to the backdriving force.

So the algorithm for calculating the acceleration in the case of the bending waves is clear now. We need two cross-forces, which we sum up and divide by two along the x-direction. We get these cross forces again by summing of three bending moments. These moments arise out of the curvatures. In discrete mechanics, a curvature can be calculated out of three displacements. For a curvature, we need three points. Because of similarities, we only need five points for all three curvatures, here the points  $P_{x-2}$ ,  $P_{x-1}$ ,  $P_0$ ,  $P_{x+1}$ ,  $P_{x+2}$ . But for the bending waves, not the x-, but the z-displacements have to be used, because bending takes place in z-direction. We get

$$M_1 = E * A * K(P_{x-2}, P_{x-1}, P_0) \quad (7)$$

$$M_2 = E * A * K(P_{x-1}, P_0, P_{x+1})$$

$$M_3 = E * A * K(P_0, P_{x+1}, P_{x+2})$$

$$F_{cross1} = \frac{M_1 - M_2}{s(P_{x-1}, P_0)}$$

$$F_{cross2} = \frac{M_2 - M_3}{s(P_0, P_{x+1})}$$

and finally

$$F_{back} = \sum_{x,y} \frac{F_{cross2} - F_{cross1}}{s(P_{x-1}, P_{x+1})} \quad (8)$$

Here  $K$  is curvature for the different points and  $s$  is the distance also for these points.

## 2.3. The ribs

The ribs of the guitar are curved within themselves. So we need a higher order differential equation to solve the problem here. Each element of the ribs here is for itself in a x/y plane with a bending displacement in z-direction. After the geometry of the guitar is inserted into the program, it calculated the curvature of every element of the ribs separately. The curvature is used for reasons of higher programming ease and to get the coupling to the neighbour elements.

Now as a curvature as mentioned above can be expressed by a second order derivation, a bending displacement will only take place in such an element, when there is a second order difference of the moments of the basic geometry curvature. In other words, if there is a curvature of a curvature of a curvature. As all elements of the ribs have a different curvature, there is an element curvature of constant  $P_C$ , which comes into the equation for bending of the ribs.

$$\frac{\partial^2 z}{\partial t^2} = -\frac{E * K^2}{\rho} P_C \frac{\partial^6 z}{\partial x^6} + \frac{\partial^4 z}{\partial y^4} \quad (9)$$

In the iteration process, we obtain the momenti from the curvature of the surrounding of  $P_0$  as usual, taking the basic curvature of this rib area into consideration. So after a first step of geometry curvature consideration, we arrive at the known fourth order differential equation. Note, that Eq. 9 only holds for one element. It cannot be used as a meta-equation for the whole rib. This is one of the strength of the FDM, that these complicated geometries can be calculated quite simple.

In Eq. 9  $P_C$  is only applied to the x-directional term. The rib is not curved along the y-direction, which means along the height of the guitar. So here still holds the normal fourth-order differential equation and both have to be summed up.

But this is not the final equation. Imagine a z-displacement orthogonal to the tangential geometry curvature direction of a place on the ribs. Now the neighbour element is displaced in its z-direction (which is not the same as the z-direction of the first element, the coordinate systems are local Lorentzian, so to say). Now the neighbour element is just displaced in z-direction as much, as the overall curvatures of these two elements is. The rest of the z-displacement of one element tears the neighbour in the neighbours x-direction. But this means nothing but also causing the neighbour to vibrate now longitudinally.

The same holds vice versa. The longitudinal displacement of the neighbour will act as a z-displacement according to the curvature.

$$\frac{\partial^2 z}{\partial t^2} = -\frac{E * K^2}{\rho} P_C \frac{\partial^6 z}{\partial x^6} + \frac{\partial^4 z}{\partial y^4} - P_L \frac{E}{\rho} \frac{\partial^2 w}{\partial x^2} \quad (10)$$

Eq. 10 takes that into consideration.  $P_L$  is now the curvature coupling constant for longitudinal wave to transversal ones. Here the displacement in x-direction is assumed to be w.

## 2.4. Coupling of guitar parts

The guitar parts are coupled by using the same principle as with the ribs. There is a sudden "curvature" so to say, where the top plate is glued to the ribs. The 90 degree change of geometry couples bending waves completely into longitudinal ones. Because the displacement of the top plate in its z-direction will tear the ribs in their y-direction, which is a longitudinal one. The opposite is also true. The longitudinal displacement of the top plate in a combination of x- and y- directions (tangential to the top plate boundary) displaces the ribs in their z-direction, which causes a bending wave. The same is true vice versa in the coupling of the ribs to the top plate and of course is true for the coupling of the back to the ribs. The reason, why not all energy suddenly disappears in the ribs and the back from the top plate is, that the connections of top plate to ribs is strengthened with the rims. So the overall mass is much larger there and weakens the coupling so.

The air in the guitar has just longitudinal waves. It couples with all the guitar body parts simply tangential to the body surface.

The neck is glued to the ribs with a lot of mass there. So the main coupling takes place by the top plate. The neck reaches the sound hole of the guitar and is glued to the top plate all over. So it can be seen as a thicker part of the guitar in the region of the top plate and only later on acts as an own vibration system, taking over longitudinal and bending waves of the top plate.

The strings are simulated as a waveguide acting on the bridge and the nut of the guitar alike. There is a back coupling from the top plate to the string.

## 3. RESULTS

Although there are many possible explanations for the vibrating structure of guitars, which can be looked at in this model - coupling parameters, different thickness, static analysis due to string tension ect. - in the scope of this paper, only a few results can be shown.

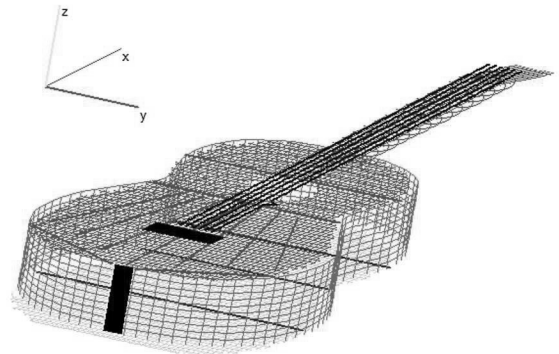


Figure 2: Visualisation of the whole guitar. It is realised in this view with a 50x50 Matrix of the top and back plate, which leads to frequencies up to ca. 15 kHz.

From earlier investigations of guitar sounds, analysing the time fine structure of overtones, there always appeared an amplitude modulation. This is periodic and not caused by any beating between neighbouring modes. Theoretically, this beating should not appear and may only be caused by some coupling with of the top and back plate to the ribs and the enclosed air. But this ribbling of the overtones could be found even with the back plate not coupled to any other parts of the system. The plate was struck at the lower side in the middle - opposite to the bridge. This means, that initial conditions were given, where a field of 5x5 points were given an initial displacement of 0, 1cm and of a velocity of 10cm/s, which is realistic. One could apply a simple Dirac delta impulse to just one element. But here an initian was preferred, which is close to the knocking on the sound board. Both, displacement and velocity was applied, because an initial displacement leads to the attraction of higher partials, the velocity to the lower ones.

Fig. 3 shows a Wavelet-Transform of that initian. This view is linear in both scales for best visualisation. The partials of the back, clearly show an amplitude modulation. The first overtone comes in after the higher partials. The fundamental is struggling at the beginning. The wavelet transform has artifacts at the beginning and end of the transform as already can be seen here, so no lower frequencies are displayed here. This seems surprising at first sight, but gets explained, when watching the back move in slow motion, which is implemented in the program. As the back in round at all borders, the travelling wave is not reflected precisely at the boundaries. So some energy is transferred to another direction, while energy from another direction, scattered elsewhere, is supplied into the mode again. This is one observed explanation, others may be found.

The used struck was applied to a back, which was not under tension, to make it as simple as possible. The tension of the back is now applied. It is assumed, that the back at all borders is 1mm larger, that the geometry of the ribs all around. So it will curve, which is said to make the guitar sound brighter. This curvature, when applied in the program can only occur due to coupling be-

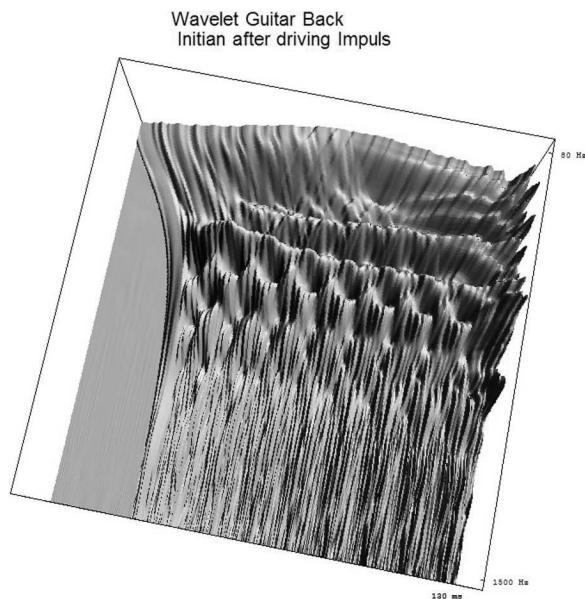


Figure 3: Wavelet-Transform of the impulse response of a struck on the back plate of the guitar at the middle opposite to the bridge. An overtone fluctuation is observed, which was not expected theoretically, but observed in recorded sound of physical guitars.

tween longitudinal and bending waves. As the back is too large but fixed at the ribs, the force acting on it is longitudinal, so the back would just be compressed. But just a small displacement in z-direction will result in a curved back, when we assume, that the bending backdriving force is equal to the expending longitudinal force due to compression. The result is a much more stable structure.

To reach that structure, we assume the back with an initial displacement and start the time stepping algorithm. One can watch the back move and finally get to rest at this shown position in Fig. 4. So this curvature is realistic, when we assume the proposed algorithm to act in a plate. This curvature is round even in the tail regions of the back. This only comes into place, when the bracing is applied to the back. Otherwise, the tail region shows a saddle. Also the curvature changes, if we assume different relations between the Youngs modulus in and cross the wood fibres. Here a relation of 12.8 is assumed[?], but five different relations known from literature have been tried.

Also the frequencies of impulse responses of the curved back are higher than those of the flat one. This seam to be because of the more stable structure, where part of the transversal backdriving force is supplied by the longitudinal compression energy.

#### 4. CONCLUSIONS

The method of just assuming basic equations of elasticity and couple them to a complex structure not only lead to new results, but also helps to explain basic behaviour of the vibrating guitar, when analysing the time evolution of the system by means of signal processing tools as much as by just watching the system move and change its initial conditions. This is just a small fraction of results shown here and ongoing research may help to discover more and more items.

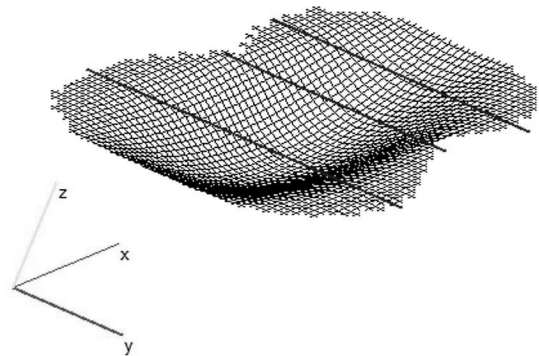


Figure 4: The curved back of the guitar. The structure is reached through a time stepping process and reaches its final state, because the back is supposed to be 1mm larger than the ribs all around the border.

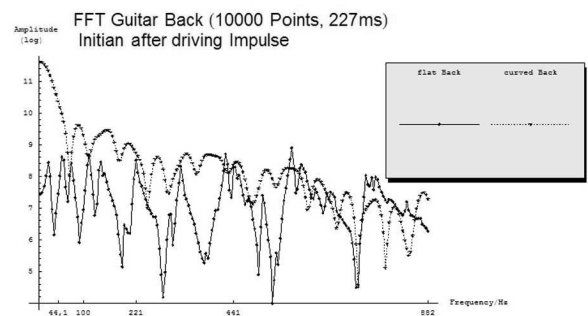


Figure 5: FFTs of impulses applied to the flat and to the curved back plate. The frequency modes are risen a bit due to the curved structure being more stable.

#### 5. REFERENCES

- [1] Tolonen, T., Välimäki, V & Karjalainen, M, "Evaluation of Modern Sound Synthesis Methods." Report 48, Helsinki University of Technology. 1998.
- [2] Cook, P.R., "Real Sound Synthesis for Interactive Applications." Natick, 2002.
- [3] Schneider, A., "Tonhöhe, Skala, Klang". Bonn 1997.
- [4] Meyer, J., "Verbesserung der Klangqualität von Gitarren aufgrund systematischer Untersuchungen ihres Schwingungsverhaltens." Physikalisch-Technische Bundesanstalt Braunschweig, Forschungsvorhaben Nr. 4490, 1980.
- [5] Hughes, Th.J.R., "The Finite Element Method", Mineola, NY, 1987, 2000.

## **A COMPARATIVE STUDY OF THE VIBRO-ACOUSTICAL BEHAVIOUR OF ELECTRIC GUITARS PRODUCED IN DIFFERENT DECADES.**

*E Esposito*

Department of Mechanics  
Polytechnic University of Marche – Ancona (I)  
espo@mehpl.univpm.it

### **ABSTRACT**

The date of the invention of the electric guitar is uncertain, but maybe ascribed to Loyd Loar who worked for Gibson from 1920 to 1924 and there developed the first pick-up.

As we will describe later, there followed many years of development, but a milestone was posed in 1950 when Leo Fender started to market the "Telecaster", the first industrially produced two pick-ups modern solid body. At that point the essence of the modern electric guitar was in place. As we see, the history of the electric guitar spans eight decades, and it is practically impossible to study all guitar types and models, so in our work we will investigate the vibro-acoustical behaviour of a single well known guitar, the Fender "Stratocaster". Our aim is to define some measurable parameters that undoubtedly characterize the sound of different guitars and that reflect the human judgement of "good" or "bad" guitar. We have tested Strats from the 50's to the 90's of different price ranges, including one sample of the first ever series produced in 1954. Vibration modes have been investigated by laser Doppler vibrometers, using different types of excitation to study both steady and transient state. Finally, also a commercial Sound Quality software package has been employed to evaluate the psychoacoustics parameters of live played guitars.

### **1. INTRODUCTION**

In 1923 Lloyd Loar invented the first pickup and the history of music changed, because it was possible to amplify the relatively weak sound of acoustic guitars. Around 1931 George Beauchamp, working with Adolph Rickenbacker, produced an improved electromagnetic pickup that, introduced on a lap-steel known as the "Frying Pan", made this guitar the first commercially viable electric.

After the 1930's, the electric guitar was developing itself due to names like Les Paul (real name Lester William Polfus), who created the first solid-body electric guitar, the "Log", mounting strings and pickups on a solid block of pine, Leo Fender, who made one of the most traditional guitar enterprises, and Seymour Duncan, the most famous guitar pickup creator. Fender invented the Broadcaster (1949), later renamed Telecaster, the first success of the company and the first solid body to be mass produced. Eventually, Leo would create the world's very first instrument amplifiers with built-in tone controls and then the legendary Fender Stratocaster (1954), preceded by another historical guitar, the Gibson Les Paul (1952). In 1958 Ted McCarty introduced the Gibson ES-335, a semi-hollow body guitar designed to incorporate the best of both the hollow body, and solid body designs. It quickly became

popular and used by such influential guitarists as B.B. King and Chuck Berry. By 1961 the electric guitar was in its full maturity. Gibson had introduced "Humbucking" pickups into the Les Paul, designed to eliminate unwanted hum from the magnetic coils. Humbucking pickups utilize two coils wrapped out of phase so as to cancel out the common mode hum introduced by previous designs. Both Gibson and Fender had introduced futuristic looking designs, in particular the Gibson SG (1961). But it was the Fender Stratocaster that topped at cult status by becoming the guitar of choice used by Jimi Hendrix, the first guitarist since Charlie Christian to completely revolutionize the way the guitar was played.

Although there have been a handful of other manufacturers in addition to Gibson and Fender such as The Fred Gretsch Co. formed in Brooklyn in 1883, who have contributed to the development of the electric guitar, the electric guitar as it exists today is for all practical purposes the same now as it was by 1961.

Generally guitar bodies and necks are made of compact, highly resistant woods, with a frequency range of fundamentals extending from 82 Hz to 1318 Hz for a 24 frets guitar. As in the case of electric basses, strong low frequency vibrations are induced in the instrument structure while playing, and lowest modes may be sensed by hand. Moreover, the normal environment for electric guitars sees the presence of extremely high sound levels (peak levels of 135 dB are not an exception [1], [2]), this also leading to the possibility of obtaining high vibration levels. Guitars are generally played using a plastic plectrum, but there exist noteworthy exceptions of guitarists using their fingers, for example Mark Knopfler of Dire Straits, or unusual playing styles like Jeff Healey, a blind player that has the guitar on his lap and plays with his fingers almost perpendicular to the fretboard. Playing style is also important, because the plectrum may be used, for example, in a strong upward fashion to add power and color to notes or with rapid shuffling strokes to produce the well known "funky" sound of many 70's records. We must also mention that to obtain some particular sounds, the guitarist will bend the guitar neck, temporarily detune the instrument, or will tap on the strings to enrich the sound with higher harmonics. Jimmy Page from Led Zeppelin used a violin bow to develop a longer sustain while most guitarist will use also a set of electronic effects (rack mounted or "stomp boxes" standing on the floor) to shape the frequency response of the guitar and to modify its time response characteristics.

We thus see which incredible number of variables is inherent in the study of this instrument, and our aim is to help clarify some fundamental aspects that can help in the objective judgment of a "good" or a "bad" guitar.



## 2. MEASUREMENTS ON SAMPLE GUITARS

Three sets of vibration measurements have been conducted on three guitars, each set differing for the excitation method: a loudspeaker, an electro-dynamical shaker and a custom built mechanical exciter. In all cases a Scanning Laser Doppler Vibrometer – SLDV [3] has been employed to measure body and neck vibration levels.

Other measurement sessions have been conducted in a anechoic chamber to record four guitarists playing live. Although the use of the chamber will eliminate any reverberation, thus giving an unusual acoustic feel to acquired signals, its use will avoid disturbing surrounding people and will also allow acquiring audio signals in a well-defined and controlled environment. Acquisition parameters and set ups have been implemented following the indications on frequency bands and acoustic levels presented in a different paper [4], also because at present it is hard to find material on vibration measurements of electric guitars. Much more attention is devoted to acoustic ones [5], [6], [7] and, although some noteworthy exceptions there exist, the most interesting material is found on the WEB [8].

### 2.1. Equipment and measurement set-ups

Schemes of the measurement set-ups that have been implemented are reported in Figure 1.

In Figure 1 (a) the set up based on the mechanical exciter is shown. The exciter consists of a small motor with a wood disc mounted on its axis and a guitar plectrum glued on it. The plectrum would struck the guitar repeatedly simulating the effect of a real one. The electrical output of the guitar has been used as the reference signal and triggered the laser acquisitions. The second set up, Figure 1 (b), employs acoustic excitation of the guitars, trying to emulate a real life excitation input of these instruments. During the measurement sessions a sound meter has been used to measure the sound field and supply the reference signal. A professional PA system, an FBT MaxX4a, has been employed to guarantee about 105 dB SPL for the duration of the laser scans, using as input signals both 5 kHz band limited white noise and sinusoids. Two different SLDV systems have been employed, namely an Ometron VPI 4000 and a Polytec PSV 200; in the former case, the signal generator is included in the laser controller, in the latter case it is not, so an external generator has been included in the measurement chain. The scheme based on the shaker is conceptually identical to the latter one, the only difference being a shaker fixed to the guitar body with an interposed load cell to measure input force. We examined three guitars: a standard Stratocaster, a Stratocaster Ultra, and a Stratocaster from the first production year (from now on simply called 1954).

Model	Neck wood	Body wood	Fingerboard wood	Estimated value (€)	Year
1954	maple	ash	maple	A lot!	1954
Ultra	maple	alder	ebony	1,800	1992
Standard	maple	alder	maple	800	1992

Table 1: Characteristics of examined Stratocasters.

Measurements have been taken at the back of the instruments to avoid complications due to the presence of pick-ups, knobs, strings et cetera; guitars have been suspended by elastic bands to a steel parallelepiped frame, with longer rods filled with sand to add weight and damping. Additional steel weights have been added to the base and at the middle of the longer rods and all the structure rested on a thick rubber mat. Finally, guitars had to be brushed with titanium oxide powder to avoid mirror-like reflections due to their shiny surface finish.

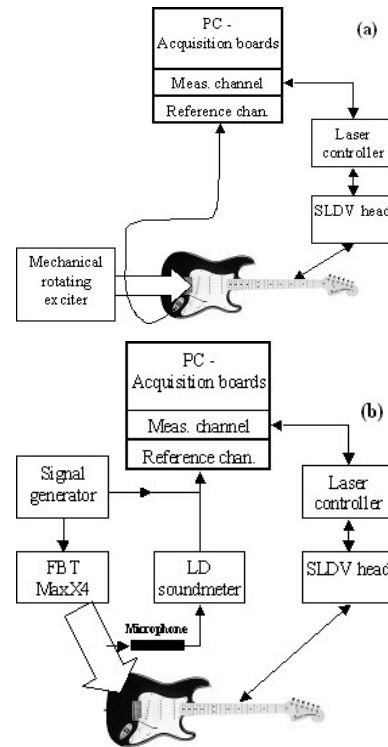


Figure 1: Schematics of measurement set-ups.

### 2.2. Live recordings

We mentioned that also a series of live recordings were performed in the Department anechoic chamber to evaluate the psychoacoustics parameters of the sound produced by amplified electric guitars. This chamber has been verified to be truly anechoic down to 100 Hz so it almost perfectly fits in the frequency range we are interested in.

All measurements have been implemented using a Bruel & Kjaer Sound Quality system, based on a 4100 Head And Torso Simulator – HATS, a Pulse multi channel acquisition analyzer and a Type 7698 software package; in Figure 2 we show a photo of the actual set-up. For this test we also employed other guitars, namely a Cort, and an Ibanez, while the power amplifier has always been a Marshall 100 W one preceded by a digital multieffect stomp box. Using this set up, guitarists played different styles of songs, going from gentle arpeggios to heavily distorted solos and rhythm patterns. Recordings have been exported as WAV files and a jury test has been implemented using both guitar players and not musically trained persons;

judges had to select the best guitar in paired comparisons and also to submit a preference rating based on a 1 to 5 scale. Finally, the results of these human based tests were compared with the psychoacoustics parameters calculated by the 7698.



Figure 2: HATS and guitarist in the anechoic chamber.

## 2.3 Measurements results

### 2.3.1. Vibration modes

Using the equipment described in paragraph 2.1, we performed many tens of measurements on the three Fender guitars and were able to identify most relevant vibration modes.

Because of its extremely high cost, the 1954 guitar has been examined using only acoustic excitation, and, to allow proper comparison, we show in Figure 3, maps of guitars vibrations in terms of surface velocity amplitude and phase obtained in the same way. An example of the results derived from the use of the rotating exciter is shown in Figure 4. In this case, due to the type of excitation, we are observing modes or operational deflection shapes that are always related to guitar strings fundamentals; for example, the examined frequency coincides with the second harmonic of the A string.

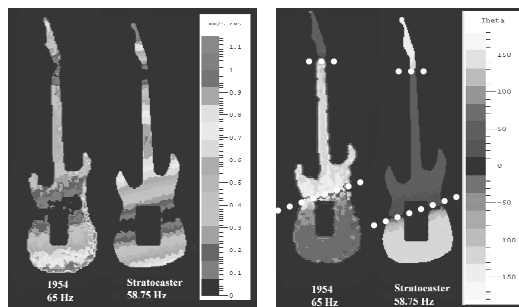


Figure 3: First modes of Stratocaster and 1954 excited by loudspeaker. Left: amplitude, right: phase (white dotted lines mark nodal lines).

### 2.3.2. Sound quality assessment

From assembling the results of the jury preference test, it emerged a scale that is reported below, going from the “best” to the “worst” sounding guitar.

Of course from such a simple test it is not possible to derive any absolute conclusion and we are not suggesting any technical judgment on guitars, but our aim was to see if it was possible to

establish any correlation with the Sound Quality software results. For this scope, in Table 3 we ordered the guitars from left to right according to the above scale presenting the values of their psychoacoustics parameters.

Worst guitar				Best guitar
1954	Cort	Ultra	Ibanez	Stratocaster
Average score on preference test				
2.56	3.08	3.08	3.11	3.23

Table 2: Preferences of jury test.

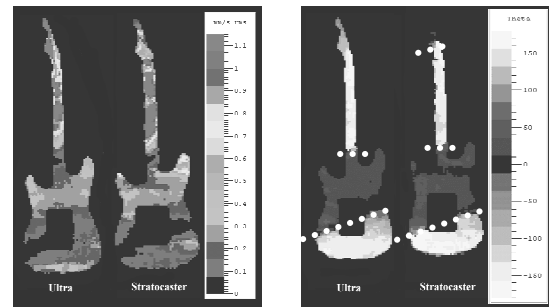


Figure 4: Ultra and Stratocaster modes at 220 Hz excited by rotating plectrum. Left: amplitude, right: phase (white dotted lines mark nodal lines).

	1954	Cort	Ultra	Ibanez	Stratocaster
<b>Mean Loudness (sone)</b>	150.06	143.50	129.00	145.12	125.58
<b>Mean Sharpness (acum)</b>	1.96	1.73	1.608	1.65	1.77
<b>Roughness (asper)</b>	2.18	1.61	1.84	1.67	1.95
<b>Fluctuation Strength (vacil)</b>	1.88	2.11	2.23	1.64	2.10
<b>Tone-to-Noise Ratio (dB)</b>	3.64	37.57	37.65	38.78	18.22
<b>Crest factor</b>	16.06	17.01	16.70	16.37	17.54

Table 3: Sound Quality parameters of tested guitars.

## 3. CONCLUSIONS

Looking at the results obtained by vibration measurements, it is not easy to appreciate important differences among guitars but only really subtle ones. For example, in Figure 4 the only relevant difference is the upper nodal line, which is not present in the Ultra.

For this reason, we are also investigating new approaches, mainly based on transient response and signal dynamic characteristics. In Figure 5 we show the response of the Ultra

body as measured on a single point by the SLDV after a short pulse given by a small hammer on the body itself, and the correspondent frequency response. In Figure 7 we present similar data for the 1954: it is possible to immediately note a moderately lower crest factor, and an upward shift of resonance frequencies. Similar measurements have been conducted on all Fender guitars and results are still to be collected and examined closely; however we think that this type of characterization should always be used to better individuate the unique characteristics of every guitar.

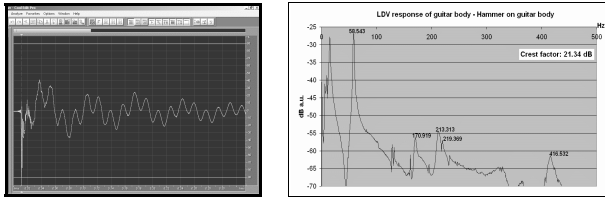


Figure 5: Time and frequency response of the Ultra after an impact hammer hit.

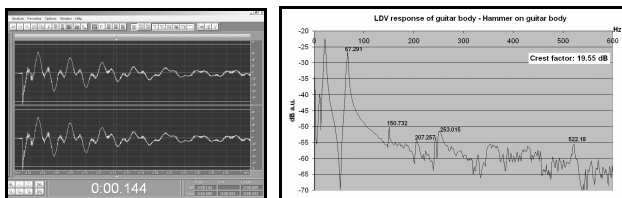


Figure 6: Time and frequency response of the 1954 after an impact hammer hit.

As regards sound evaluation procedures, an immediate relationship between the results of the jury test and the results of the evaluation done by the Sound Quality software is not evident. However, if we observe that four guitars, Cort, Ultra, Ibanez, and Stratocaster, have obtained preference scores that do not differ of more than 5%, we could consider them as a uniform group in comparison with the 1954. In this case, three parameters clearly differentiate these two classes of guitars, namely Sharpness, Roughness, and Tone-to-Noise Ratio. However, the last one presents a large spread of values and appears to be of little significance to our analysis; we later added to our calculations a somewhat similar parameter, the Prominence Ratio, which showed more limited variations as reported in Table 4, but nevertheless it also does not allow any correlation with the preference test.

	1954	Cort	Ultracaster	Ibanez	Stratocaster
Prominence Ratio (dB)	2.61	4.31	-2.41	0.12	1.67

Table 4: Prominence Ratio of tested guitars.

We may also note that generally the three Fender guitars have a higher Roughness than the others with a value spread limited to about 15%; this is probably due to a higher hum

deriving from the single coil pick-ups. This leaves us with the Sharpness as the only parameter apparently able to classify the sound of guitars, with a proposed acceptance range for “good” guitars of 1.6-1.8 acum. We cannot avoid to point out that the results of our investigation were a little bit surprising, because we had to reject many people eagerly asking for the possibility of playing the 1954 Stratocaster, a legendary guitar that will always be in the dreams of every guitarist. However, a somewhat systematic approach to the problem and jury tests allowed to put in evidence the objective characteristics of this guitar sound, that has also received comments of the type “thin”, “screechy”, “hummy”. For this reason, the final step of our research will consider a meeting with highly respected guitarists that will not repeat the jury test, but will help us to translate this kind of subjective sentences to Sound Quality parameters, in order to help mapping everyday speaking to meaningful numbers. In the end we think that our investigations could be very helpful for musical instruments industries willing to find out a scientific approach for the evaluation of their new products, to avoid “bad” guitars hitting the market, but we also think that, luckily, there will always remain myths and legends regarding some guitars that will stay there forever.

#### 4. ACKNOWLEDGEMENTS

I wish to express all my gratitude to Sergio and Davide Tomassone, owners of the famous shop in Bologna (I), who gave us the 1954 (and a 1966 as well) and generally contributed a lot with their experience. A grateful thanks also to Emanuele and Christian, two students who helped a lot taking many measurements and playing their guitars.

#### 5. REFERENCES

- [1] "TRIPLA" system specifications, Outline snc, Flero (I).
- [2] 650-R2 Concert Series Subwoofer specifications, Meyer Sound, Berkeley, CA (USA).
- [3] Castellini, P., Revel, G.M., and Tomasini, E. P., “Laser Doppler vibrometry: a review of advances and applications”, The Shock and Vibration Digest, Vol. 30, 1998, pp. 443-456.
- [4] Esposito, E., Santolini, C., and Scalise, L., “Axe work II: vibro-acoustical study of solid body electric guitars”, Proc. 5<sup>th</sup> International Conference on Vibration Measurements by Laser Techniques, Ancona, Italy, SPIE Vol. 4827, pp. 207-218, 2002.
- [5] Boulosa, R. R., “Vibration measurements in the classical guitar”, Applied Acoustics, Vol. 63, 2002, pp. 311-322.
- [6] French, M., and Bissinger, G., “Testing Of Acoustic Stringed Musical Instruments”, Experimental Techniques, Jan/Feb. issue, 2001, 40-43.
- [7] Hill, T. J. W., Richardson, B. E., and Richardson, S. J., “Measurements of acoustical parameters for the classical guitar”, Proc. International Symposium on Musical Acoustics - ISMA, Perugia, Italy, pp. 417-420, 2001.
- [8] Prof. Daniel A. Russell, Kettering University, MI, USA, <http://www.kettering.edu/~drussell/>, Mr. Don Tillman, Palo Alto, California, USA, <http://www.till.com/>. Reference site: [www.harmony-central.com/](http://www.harmony-central.com/).

## **MODAL RADIATION FROM CLASSICAL GUITARS: EXPERIMENTAL MEASUREMENTS AND THEORETICAL PREDICTIONS**

*T.J.W. Hill, B.E. Richardson and S.J. Richardson*

Acoustics Group, Department of Environmental and Mechanical Engineering, Open University,  
Milton Keynes, MK7 6AA, United Kingdom

Musical Acoustics Group, Department of Physics and Astronomy, Cardiff University,  
Cardiff, CF24 3YB, United Kingdom

T.J.Hill@open.ac.uk, RichardsonBE@cf.ac.uk

### **ABSTRACT**

In this paper we present input admittance data taken at string positions on the bridge and measurements of the complex sound pressure fields taken on spheres surrounding the guitar. Measurements of input admittance allow the determination of the resonance frequencies, Q-values and effective input masses for each mode. Measurements of the sound field, when an individual mode is predominantly excited, allow the orthogonal monopole and dipole radiation coefficients to be determined and hence the effective modal area and equivalent source radius to be deduced. The combination of these parameters allows the complex-pressure frequency response to be predicted theoretically and this is shown to agree well with experimental data. It is apparent that monopole and dipole contributions from a few, key, low-frequency modes are responsible for the majority of features in the pressure response at low frequencies and that these modes also determine the general response at high frequencies. Evaluation of this small set of acoustical parameters therefore enables the acoustical performance of different instruments to be modelled and compared quantitatively. If coupled with a model of the string-finger interaction, this theory has significant potential for psychoacoustical exploration of the effects that these acoustical parameters have on the tone quality and musical value of instruments.

### **1. INTRODUCTION**

Research carried out at Cardiff on the acoustical properties of classical guitars in the low to middle frequency range has focused on characterising the performance of guitars in terms of a small set of parameters that quantitatively describe each mode [1]. Psychoacoustical experiments have shown which of these parameters have the greatest influence on the sound and the judged musical quality of an instrument [2,3]. In this paper we report and discuss data from three of the ten guitars investigated to date. These are high quality instruments played by professionals and made by master craftsmen. Their differences in design and construction, and subsequently the acoustical parameters that characterise them, point to the wide range in players' subjective value judgements and the many possible approaches to, and the difficulty of, the task the craftsman faces when attempting to satisfy players' requirements.

### **2. METHODS**

We will only briefly discuss the experimental methods by which the set of acoustical parameters have been obtained as they are detailed elsewhere in the literature [1, 2].

Resonance frequencies,  $f_0$  (or  $\omega_0$ ), Q-values,  $Q$ , and effective masses,  $M$ , were measured using standard impedance-head techniques to measure the input impedance. The instrument was excited by a swept sine wave using a miniature electromagnetic driver attached at string positions on the bridge. The complex admittance data was fitted using a single-degree-of-freedom, peak-picking method and thereby the parameters for each mode were extracted. The admittance is given by

$$y(\omega) = \frac{i\omega}{M(\omega^2 - \omega_0^2 + i\omega_0\omega/Q)}. \quad (1)$$

The sound radiation properties were measured using an approach similar to that of Arnold and Weinreich [5]. Prior investigation of the mode shapes using speckle and holographic interferometry suggested optimal locations for excitation of predominantly one mode at a time. The instrument was then driven at resonance at this position and the complex sound field measured in anechoic conditions on the surface two concentric spheres surrounding the instrument using a pair of travelling microphones. The out-going wave, and subsequently the radiativity for each spherical harmonic component, were determined [1] by performing a spherical harmonic decomposition of the 324-point data from each measurement sphere. This enabled the monopole, dipole and higher order components to be determined. The higher order terms (quadrupoles and octupoles) are small in comparison with the monopole and dipole terms and will not be considered. The dipole terms are expressed in terms of dipoles oriented along the three cartesian axes. Thus the pressure response for a particular spherical harmonic component from a particular mode from at a certain point in the field is given by

$$\frac{p_{lm}(r, \theta, \varphi)}{F} = \frac{\rho_0 c}{4\pi} k^{(l+2)} y(\omega) Y_{lm}(\theta, \varphi) h_l(kr), \quad (2)$$

where  $k=\omega/c$  is the wavenumber,  $\omega$  the angular frequency,  $c$  the speed of sound in air,  $\rho_0$  the density of air,  $G_{lm}$  are the radiativities for each spherical harmonic  $Y_{lm}(\theta, \varphi)$ , and  $h_l(kr)$  is the spherical Hankel function. The radiativities are scaled for excitation at a string position by performing a transfer admittance measurement between the string position and that at

which a particular mode is excited. We define  $G_{00}$  as the monopole radiativity and  $G_{Ix}$ ,  $G_{Iy}$  and  $G_{Iz}$  as the dipole radiativities along the  $x$ ,  $y$  and  $z$  axes respectively for excitation at a specified string position. Summing equation (2) for contributions from all guitar modes and all required values of  $l$  and  $m$  enables the complex-pressure frequency response to be calculated at positions in the field determined by spherical coordinates  $r$ ,  $\theta$  and  $\phi$ . Further modification of the model to incorporate finite sized, rather than point, sources gives a better fit to the roll-off in response found in the high frequency range but makes little difference in the region in the low frequency range [1].

One advantage of this set of acoustical parameters is that they can be incorporated in a straightforward manner into a theoretical model that includes a plucking component. This would allow the model to be played and sounds generated at the listener's position which could be used in subsequent psychoacoustical testing to evaluate the influence of particular parameters.

### 3. RESULTS

Sets of acoustical parameters were measured for the lower-order modes of three high-quality instruments. The instruments were SA121 by Simon Ambridge, JLR677 by José Romanillos, and PF952 by Paul Fischer. Input admittance at string positions on the bridge are shown in Figure 2. The acoustical parameters that characterize these modes (resonance frequencies,  $Q$ s, effective masses and monopole and dipole radiativities) are given in Table 1. The pressure frequency-responses reconstructed from these acoustical parameters are shown in Figures 4 and 5 along with the measured response. A few selected mode shapes imaged using holographic interferometry and their respective sound fields are shown in Figure 3.

### 4. DISCUSSION

The key point that unites the three instruments for which we present data in this paper is that all three are high-quality instruments made by top British makers. The instruments are of nominally the same size and are built to the highest standards. Two of them (JLR677 and PF952) are instruments chosen and played by professional players. The markedly different design philosophies are born out in their significantly different responses and corresponding sets of acoustical parameters.

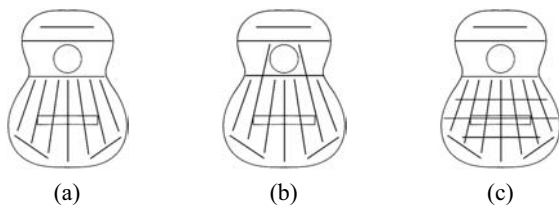


Figure 1: Three top plate strutting patterns.

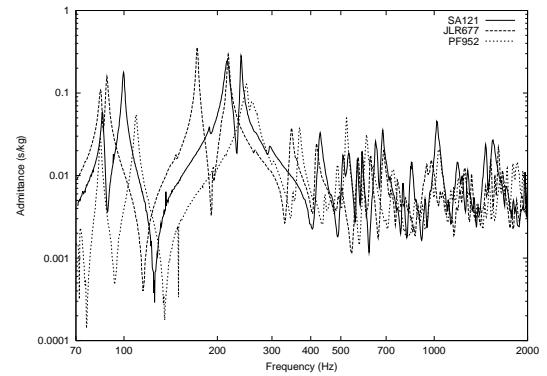


Figure 2: Input Admittance data at the top E string position on the bridge for guitars SA121, JLR677 and PF952.

Mode	$f_0$ (Hz)	$Q$	$M$ (kg)	$G_{00}$ (m <sup>2</sup> ) $\times 10^{-3}$	$G_{Ix}$ (m <sup>3</sup> ) $\times 10^{-3}$	$G_{Iy}$ (m <sup>3</sup> ) $\times 10^{-3}$	$G_{Iz}$ (m <sup>3</sup> ) $\times 10^{-3}$
Guitar							
SA121							
T(1,1) <sub>1</sub>	100	64	0.589	-19.4	-8.0	0.3	9.2
T(1,1) <sub>2</sub>	214	31	0.100	24.3	4.2	-0.6	-1.0
T(2,1)	238	85	0.180	2.8	0.2	-2.8	0.1
T(1,2) <sub>2</sub>	429	51	0.509	-34.3	-5.5	-0.3	3.9
T(3,1)	528	37	0.776	-47.8	-7.5	0.4	-4.5
JLR677							
T(1,1) <sub>1</sub>	88	63	0.722	-21.7	-15.3	0.3	9.2
T(1,1) <sub>2</sub>	172	74	0.191	3.6	2.5	-0.6	-1.0
B(1,2) <sub>1</sub>	212	35	0.750	-61.2	-13.2	-2.8	0.1
T(2,1)	219	65	0.163	-2.9	-0.5	-0.3	3.9
T(1,2) <sub>1</sub>	347	48	0.591	-11.1	-1.2	0.4	-4.5
T(1,2) <sub>2</sub>	419	54	0.847	41.4	9.4	0.5	3.4
T(2,2)	475	55	1.800	-29.7	-3.7	2.9	-1.3
T(3,1)	568	68	1.110	2.5	0.5	-0.1	0.3
PF952							
T(1,1) <sub>1</sub>	109	52	1.375	-73.9	-20.0	2.0	-32.1
T(1,1) <sub>2</sub>	248	37	0.182	51.7	6.3	-0.2	1.6
T(1,2) <sub>1</sub>	259	21	0.166	-37.0	2.2	-0.4	1.4
T(1,2) <sub>2</sub>	369	56	0.632	-1.0	-0.6	0.1	0.3
B(3,1)	445	72	1.658	-25.2	-8.5	-0.6	3.9
T(3,1)	460	55	0.528	4.9	-0.7	-0.0	0.6
T(2,1) <sub>1</sub>	522	86	0.517	-2.3	-0.5	-2.6	-0.7
T(2,1) <sub>2</sub>	606	59	0.504	4.5	0.8	-3.8	0.5

Table 1: Acoustical parameters

The instrument by Ambridge, SA121, is best described as a conventional "Torres construction" with "fan-shaped" internal soundboard strutting (similar to Figure 1a), which is found on many instruments, both hand-made and factory-made. The instrument by Romanillos, JLR677, uses another design pioneered by Torres, in which the cross strut has portions removed to allow two of the fan struts to run continuously up into the upper bout region of the top-plate (similar to Figure 1b).

The instrument by Fischer, PF952, adopts a totally different approach to the strutting by employing a lattice of thinner, criss-cross struts (similar to Figure 1c). In this design the sound-hole is also relocated, being raised and split either side of the fingerboard.

Players broadly require a wider dynamic range, responsiveness and sustain. Consequently, makers explore various designs with expectations of achieving particular sounds or improved response. Design philosophies that have permeated makers' thinking are (1) thinner, lighter sound boards will respond better, generating more sound more easily, making the instrument louder and more responsive, (2) increasing the vibrating area of the sound board will make the instrument louder, (3) the position, or tuning, of particular resonances is important. With hindsight it seems that there is not always a strong physical basis for making these assumptions and there is always the difficulty that structural changes rarely affect only one attribute of the sound but more usually involve trade-offs between one feature and another. With images of the mode-shapes and tables of the key acoustical parameters we can begin to quantify and comment on the differences produced by the three different guitar designs investigated in this paper.

Firstly, it is worth pointing out that even with the relocated sound hole of PF952 the general mode shapes of the three instruments are much the same as for most guitars. This is as one would expect, given that they are all have the same outline shape, the strings attach at much the same position and they all have similar substantial cross-braces in the upper bout.

The strutting found on most instruments, and on SA121, acts so as to stiffen the instrument against the longitudinal tension of the strings and produce additional stiffness across the instrument around the opening of the sound hole, where there is an obvious structural weakness. The strutting pattern of instrument JLR677 can be assumed to be an attempt to encourage the top plate to vibrate more in the region of the upper bout. The thinness of the plate in PF952, which might be construed as a device to create a more responsive and louder instrument, necessitates a suitable strutting pattern to maintain structural integrity. In addition, the relocation of the sound hole, might also be inferred to be a way of increasing the radiating surface area.

The frequencies of the five modes identified for SA121 (Table 1) and their corresponding mode shapes are representative of many instruments studied in this and other projects. These modes are driven strongly by the strings and contribute significantly to the overall response of the instrument. The cut-away strutting of JLR677 has the effect of lowering the resonance frequencies of the lower modes ( $T(1,1)_1$  and  $T(1,1)_2$ ) and perturbs the mode shape with slightly more plate motion occurring in the waist and upper bout. The addition of a thin bridge plate maintains the bending stiffness and keeps the  $T(3,1)$  at a more conventional frequency.

The resonance frequencies of PF952 are significantly different compared with both the more conventional Torres strutting of SA121 and the modified strutting of JLR677. For PF952 they are generally much higher and also the order in which the modes occur is different.

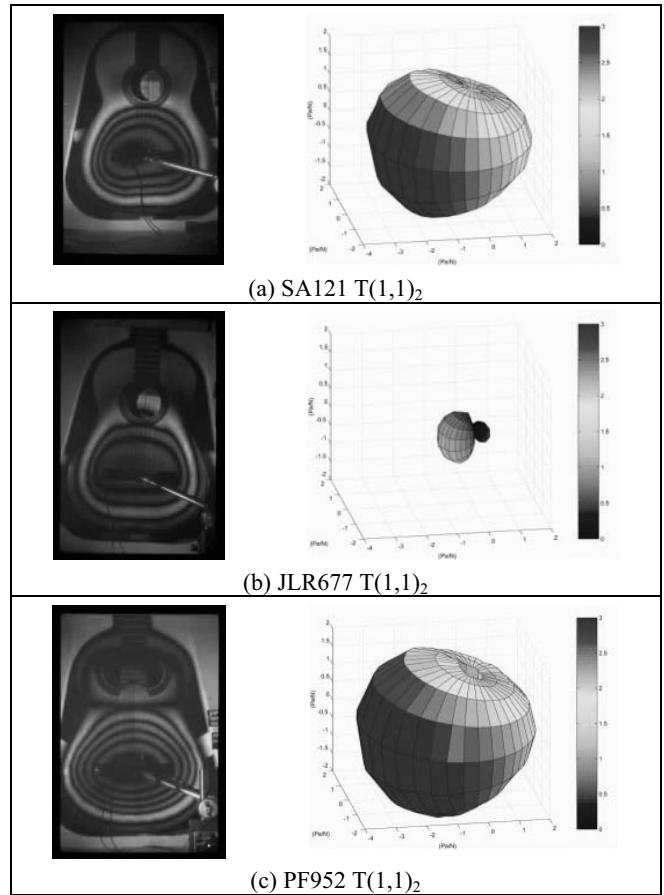


Figure 3: Mode shapes and sound fields for the  $T(1,1)_2$  mode of (a) SA121, (b) JLR677 and (c) PF952.

Turning to the other measured acoustical parameters we find that the  $Q$ -values lie in broadly the same range, 30 to 80, for all three instruments, however, more obvious differences are found between them when one examines the effective masses,  $M$  and the monopole radiativity  $G_{00}$ . In SA121, and many other instruments, the  $T(1,1)_2$  is usually the most dominant mode. The acoustic radiation from this mode is strongly monopole, as the mode shape might suggest, characterised by  $G_{00}Q/M$  at resonance and  $G_{00}/M$  above resonance. Its generally low effective mass, around 0.1 kg, means that the strings couple to it strongly, often producing a "wolf" note at the resonance frequency. The effective masses for the  $T(1,1)_2$  modes of JLR677 and PF952 are much higher at around 0.2 kg. This results in a less pronounced "wolf" note and a more even response. The modal sound fields measured for the  $T(1,1)$  modes of the three instruments exhibit yet more differences. For the  $T(1,1)_1$  the fields are much the same. The  $T(1,1)_2$  for JLR677 is found to be considerably weaker than those of SA121 and PF952. This is partly because there is increased structural interaction with the back plate in JLR677 resulting in a cancellation effect.

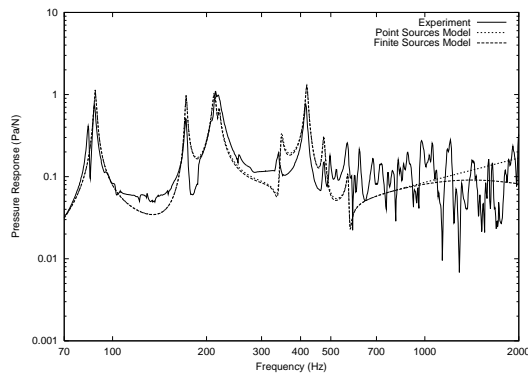


Figure 4: Experimental and reconstructed pressure responses for JLR67,  $r=0.45m$ ,  $\theta=45^\circ$ , and  $\phi=-45^\circ$ .

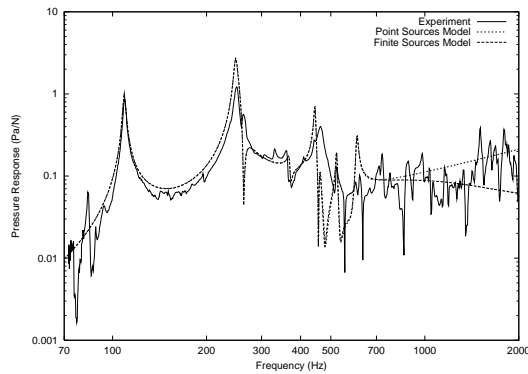


Figure 5: Experimental and reconstructed pressure responses for PF952,  $r=0.45m$ ,  $\theta=45^\circ$ , and  $\phi=-45^\circ$ .

Interestingly, it might be argued that the combined effect of

the thinner plate, lattice bracing and relocation of the sound-hole in PF952 in order to attempt to increase the potential radiating surface and area and hence increase the overall output has achieved this not by the means envisaged. The lattice bracing, which extends closer to the ribs (guitar side walls) increases the stiffness right out to the edge of the plate. Likewise, the extra plate area gained by relocating the sound hole increases stiffness in that region. The net result is that the active, moving plate area is actually reduced. However, the top plate now behaves more like a plate with clamped edges and the ratio of the displaced volume to effective mass (i.e.  $G_{00}/M$ ), which is a measure of its effectiveness to radiate energy, is found to increase.

It is clear from Table 1 that the T(2,1) and T(1,2) modes exhibit significant dipole radiation, as one might expect, given their respective mode shapes. The dipole contribution to the pressure response above resonance has also been found to be significant [1]. In instrument PF952 the T(2,1) mode, which is split due to coupling with a similar mode on the back plate, has frequencies of 522 Hz and 606 Hz, which are over an octave higher than those found on most guitars.

The pressure responses (Figures 4 and 5), reconstructed using the acoustical parameters of Table 1 according to equation (2) show the main experimentally observed features for JLR677 (experimental data for SA121 is not available, but see

[1] for a similar Torres style instrument). The pressure response for PF952 is much more complex and is not reproduced as well by the parameters of Table 1. This is because modes with more complex mode shapes (e.g. T(2,2)) for which sound fields were not easily measured appear mixed in with the lower order modes and so there is some information on the contribution of these modes. Broadly speaking, all three guitars exhibit peaks in their responses at the T(1,1)<sub>1</sub>, T(1,1)<sub>2</sub>, B(1,1) (sometimes coincident with the T(2,1)) and T(3,1) which are the modes that have stronger monopole radiativities (or are not dipole radiators).

## 5. CONCLUSIONS

We have demonstrated that with this small set of parameters we can characterize the low-order frequency modes and broadly predict the pressure response of the instrument in both the low and higher frequency ranges. In this paper we have also shown that three instruments made to the highest standards, each with their own unique playing qualities, have widely differing values of the key acoustical parameters that characterise them, in particular the resonance frequencies. Having said that, these three instruments still accommodate the requirements of professional performance. These findings, along with those of others [3, 4], suggest that mode frequencies play a less important role in determining the quality of an instrument than has been previously suggested in the literature. The question that now faces us is "if these instruments are so different then what are the features, or combination of features that lead to players rating then so highly?". This suggests possible avenues involving more refined psychoacoustical testing with listeners and, more importantly, players.

## 6. ACKNOWLEDGEMENTS

We gratefully acknowledge financial support from the Leverhulme Trust (ref: F/407/R) and from the EPSRC (SJR). We would also like to thank Simon Ambridge, John Taylor and John Mills and the other makers and players who have loaned us their instruments for these studies.

## 7. REFERENCES

- [1] Hill, T.J.W., Richardson, B.E. and Richardson, S.J., "Acoustical parameters for the classical guitar", *Acustica*, accepted for publication.
- [2] Richardson, S.J., "Acoustical parameters for the classical guitar", PhD Thesis, University of Wales, 2001.
- [3] Wright, H.A.K., "The acoustics and psychoacoustics of the guitar", PhD Thesis, University of Wales, 1996.
- [4] Wright, H.A.K. and Richardson, B.E., "On the relationships between the response of the guitar body and the instrument's tone quality", *Proc. Inst. Acoustics, UK*, 19(5), pp 149-154, 1997.
- [5] Weinreich, G. and Arnold, E.B., "Method for measuring acoustic radiation fields", *J. Acoust. Soc. Amer.*, Vol. 68, 1982, pp 404-411.

## NEW DESIGNS FOR THE KANTELE WITH IMPROVED SOUND RADIATION

Jyrki Pölkki<sup>1</sup>, Cumhur Erku<sup>2</sup>, Henri Penttinen<sup>2</sup>, Matti Karjalainen<sup>2</sup>, and Vesa Välimäki<sup>2</sup>

<sup>1</sup> Soitinrakentajat AMF, Tuikkalantie 2, 79100 Leppävirta, Finland  
jyrki.polkki@estelle.fi

<sup>2</sup> Helsinki University of Technology, Laboratory of Acoustics and Audio Signal Processing  
P.O. Box 3000, FIN-02015 HUT, Espoo, Finland

### ABSTRACT

The kantele is a plucked string instrument belonging to the family of zithers that are used in traditional folk music in Finland, Northwest Russia, and the Baltic states. We propose design rules for a kantele that has a higher loudness than traditional models and present acoustical analysis results to confirm the amplification. The guidelines for making a plucked string instrument louder are to increase the string tension, to add more radiating surface area, and to isolate the top plate from the sound-box with an air gap. We investigate the increased string tension analytically, and show the benefits of the enlarged radiating surface and the isolated top plate experimentally, by acoustical measurements. The input force and the resulting SPL are measured in an anechoic chamber at several points around the instrument, and the measured SPL values are converted to loudness estimates using a computational model. All results are compared against similar figures for a traditional kantele. A playability test, where a professional kantele player is asked to play as softly and as loudly, as she/he feels comfortable, reveals how much we have been able to widen the dynamic range. Finally, the effect of the structural modifications on the timbre is evaluated.

### 1. INTRODUCTION

There is a great variety in string quantities, box models, and sizes among the stringed musical instruments that are called the "kantele". A common feature is the special timbre that is caused by the way the steel strings are attached, especially the knot [1, 2]. A kantele has typically 5 to 36 steel strings, which form a fan over the top plate. Fig. 1 shows a traditional 10-string Finnish kantele. The narrow end, on the right in Fig. 1, is called the 'ponsi'. At the right end of Fig. 1, each string is attached by a special knot to a metal rod called the 'varras'. At the wide end of the string fan (on the left in Fig. 1), the strings go around the tuning pins.

For Finns, the kantele is closely connected to the oldest layers of their music and poetry. Nowadays, the kantele is used more

and more often in concerts, but the traditional Finnish models are usually not heard without amplification. On the stage, the kantele needs to be louder than traditional models, and it is of interest to examine what can be done without electrical amplification. These are some of the motivations for this research.

Musical instrument makers usually consider designs, where strings are attached to a wooden box that has a sound hole. The main radiator of acoustic energy is the top plate. The mid-part of the top plate is able to vibrate strongly, while the regions at the edges are nearly fixed. There is a long and wide research tradition of stringed instruments with wooden vibrating plates, such as violins, pianos, and guitars, and it helps us to better understand the kantele, too. From the functional point of view, the guitar and the kantele have similarities: they both get an impulsive excitation from the player's finger, and they cannot produce very loud sounds.

In this paper, we propose novel design rules for a kantele that has a higher loudness than traditional models. The main goal of the new design is the improved radiation efficiency. At the same time, an improved balance between the low and high tones is attempted. A large variety of ringing, fluctuating tone colors can be achieved by a skilled kantele player, and we do not want to lose these possibilities when increasing the dynamic range. We investigate the benefits obtained by the increased string tension, an enlarged radiating surface, and an isolated top plate.

The first kanteles of the new design were built in the summer of 1999. Different sizes have been tested: 11-string piccolos one octave higher than the traditional one described above, 5-string models, and two larger 20 or 21-string models with a large compass and deep bass with the lowest tone D2. Based on evaluations by several pairs of ears, all these designs have been promising. Especially the low bass tones sounded deeper in quality and stronger in amplitude than those of the comparable, good-quality traditional models. An 11-string kantele produced according to the new design is shown in Fig. 2.

The idea for a freely vibrating top plate comes from the old 5-string museum kanteles: some of them have a closed box while



Figure 1: The traditional 10-string kantele.



Figure 2: The modified 11-string kantele.



others are carved from a single piece of wood so that they have a top with sides along its edges, but no bottom. The bottomless design is clearly louder of the two, and it has a warmer timbre. The favorable features of the bottomless model come from an extended radiating area, as reported in [3]. Our practical experiments showed that the old bottomless design could be further improved by taking the idea of a "bottomless box" to the direction of a reinforced plate. An experimental bottom, fixed to the top at the center and separated with a small gap at the boundaries sounded promising. At the same time, the top plate was made 1.5 to 3 times thicker than before. This appeared to help maintaining the characteristics of the attack and the decay of the tone.

The two kanteles under detailed analysis reported in this paper are representatives of large groups of similar instruments. The traditional model is a good one among its type, produced in thousands. The new design is one of about 50 experimental instruments. For these two instruments, we present measurement results that demonstrate their differences and then explain those differences. In Section 2 of this paper, we examine in detail the changes in string tension and body structure. Section 3 reports measurements of the mechanical admittance and radiation efficiency. A playability test and a loudness comparison are presented in Section 4. Section 5 concludes the paper and suggests ideas for future research.

## 2. DESIGN GUIDELINES

### 2.1. Guidelines for strings

Our first step towards an improved design was to increase the tension of the strings. In practice, this is equivalent to keeping the fundamental frequencies of the strings constant, and increasing their lengths. The fundamental frequency  $f$  of a stretched string is related to its length  $L$  and its nominal tension  $T$  by the following well-known relation

$$f_0 = \frac{1}{2L} \sqrt{\frac{T}{\rho_1}} \quad (1)$$

where  $\rho_1$  is the linear mass density of the string. In the modified design, all the string lengths have been increased. The lengths of the strings in both designs are tabulated in Table 1. In order to achieve the diatonic scale, an additional string has been added in the modified design (String 2 in Table 1). Since the same set of strings is used for both designs, the relative tension change is obtained using Eq. (1). On the average, the nominal tension is increased % 27 in the modified design.

The transversal force exerted on the tuning pin at the end of the string is given by

$$f(L) = T \frac{dz}{dx} \Big|_{x=L} \quad (2)$$

where  $L$  is the length of the string along the longitudinal direction  $x$  and  $z$  is the transversal displacement of the string, so that the term  $\frac{dz}{dx}$  is the slope of the string. The slope is determined by the player and it is closely related to the tension of the string. Using the initial slopes determined by a professional player in the playing tests (these are discussed in Section 4) and inserting the tension change values of Table 1 into Eq. (2), we conclude that the force input to the modified design is increased 20 % on the average.

Depending on the mechanical input admittance  $Y(\omega)$ , this force component sets the instrument body into motion. The admittance

S#	Tuning	$f_0$ (Hz)	$L_n$ (cm)	$L_m$ (cm)	$L\%$	$T\%$
1	D5	587.3	32.5	34.3	6	11
2	C#5	554.4	-	36.8	-	-
3	B4	493.9	35	39.7	13	29
4	A4	440.0	37.5	42.7	14	30
5	G4	392.0	40.5	45.8	13	28
6	F#4	370.0	43.5	49.5	14	29
7	E4	329.6	47	53.3	13	29
8	D4	293.7	50.5	57.6	14	30
9	C#4	277.2	54.5	62	14	29
10	B3	246.9	58.5	66.7	14	30
11	A3	220	63.5	72.2	14	29

Table 1: The string lengths  $L_n$  and  $L_m$ , fundamental frequencies  $f_0$ , relative length and tension change percentages,  $L\%$  and  $T\%$ , respectively, of the normal (index n) and modified (m) kantele.

is determined by the structural properties of the instrument. Therefore, before presenting the measured admittance functions and following the energy flow from the strings to the mechanical vibrations of the body in Section 3, we summarize the structural design guidelines in the next subsection.

### 2.2. Structural design guidelines

During an earlier set of measurements on a five-string kantele [2], we observed that a considerable amount of the soundboard vibration was being transferred to the sides, and consequently, to the back-plate of the instrument. The preliminary tests on the 10-string kantele also confirm this observation. In a typical performance condition, where the player holds the instrument on his/her lap, the vibrations of the side plates are damped so that some portion of the mechanical energy is lost. The first structural design goal was to reduce this energy loss. This goal is achieved by isolating the top-plate, i.e., by fixing the back-plate to the instrument in the middle area and by leaving the top-plate edges free by a small air gap. Note that this design introduces a cavity, which is further discussed in Section 3.

Another design goal was to improve the radiation efficiency, i.e., the ratio between the input power and sound intensity. This is achieved by increasing the total radiating surface area. The free edges obtained by isolating the top-plate, as discussed above, also add to the total radiating surface. The result is an improvement over the traditional design, where the hinged boundaries of the top-plate do not contribute to the radiation at all (see, for instance, the TV holography measurements reported in [3]).

## 3. BODY VIBRATIONS AND RADIATION

### 3.1. Admittance and input power

The mechanical admittance, defined as the ratio of the velocity and the force spectra  $Y(\omega) = V(\omega)/F(\omega)$ , provides a useful presentation of the body vibration. Since it is also related to the total input power, the measurement of the admittance function has a paramount importance for our discussion.

Recall that the power spectral density is defined as

$$p(\omega) = \Re\{F^*(\omega)V(\omega)\} \quad (3)$$

and within the frequency range  $\omega \in [\omega_1, \omega_2]$ , the total power is calculated by

$$P = \int_{\omega_1}^{\omega_2} p(\omega) d\omega \quad (4)$$

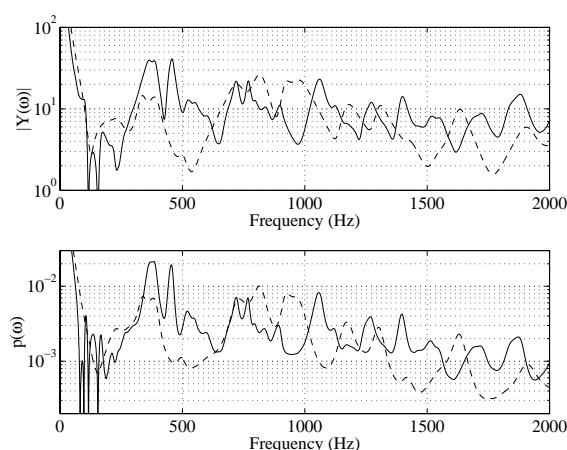


Figure 3: The admittance moduli (top) and the power spectral densities of the normal (dashed) and modified (solid) designs.

It can be shown that the power spectral density  $p(\omega)$  is related to the real part of the admittance function  $\Re\{Y(\omega)\}$  by a weight factor  $w(\omega)$ , which is the autocorrelation of the input force.

In order to follow the energy flow from the strings to the body and determine the input power for both designs, we conducted the following experiment. We mounted a small accelerometer (PCB 309A) on the top-plate of each instrument near the tuning pin, where String 7 (see Table 1) is terminated. With an impulse hammer (PCB 086C02), we exerted a force on the tuning pin, and measured the acceleration. The instruments were supported as in typical playing condition. We also recorded the autocorrelation of the force. For accuracy, 25 individual hits were averaged. During the measurements, we checked the coherence and only the successful hits were included in the averaging. The acceleration is converted to the velocity by integration.

This method allowed us to obtain admittance functions for both designs up to 2000 Hz. The admittance functions thus obtained are illustrated in the top part of Fig. 3, where the dotted curve indicates the admittance function of the normal design, and the solid curve indicates the admittance function of the modified design. The two admittance functions differ mostly around the low-frequencies (below 500 Hz). Above 750 Hz they are comparable in magnitude, however the modified design has a higher density of the resonances. The power spectral densities that are shown at the bottom part of Fig. 3 are obtained by multiplying the corresponding force autocorrelation by the real part of each admittance function. The numerical integration of the densities between 200 Hz and 2000 Hz according to Eq. (4) indicates that the total input power is increased by 26 % in the modified design.

### 3.2. Radiation

The final step in the energy flow chain is the transduction of the mechanical vibrations to the acoustical waves. In order to test the radiation properties of the new design, we have conducted the following experiment. Both instruments were excited by the impulse hammer in an anechoic chamber, as described in Sec. 3.1. The sound field was measured with a microphone (B&K 4145), placed one meter above the top plate of each instrument. Simultaneous SPL readings were recorded for microphone calibration. The results of this experiment are illustrated in Fig. 4, which shows the force to SPL transfer functions of the normal (dashed curve) and

modified (solid curve) kantele.

In Fig. 4 the modified-design transfer function exhibits two low-frequency peaks that are absent in the admittance plots (see Fig. 3). These peaks are associated with the cavity of the modified design, and will be further discussed in the next subsection. Similar to the admittance measurements, but more pronounced here, the characteristics differ mostly at the low-frequencies (below 500 Hz). It should be noted that the measured SPL is related to but different from the perceived loudness. In other words, by inspecting the radiation characteristics shown in Fig. 4, one cannot conclude that the modified design is louder. We will revisit the estimation of the loudness using a computational model in Section 4.

### 3.3. Cavity resonances

The cavity introduced in the modified design differs from that of a typical plucked string instrument (e.g., guitar) in the sense that it cannot be considered a simple Helmholtz resonator with a single opening. Although there is a sound hole under the ponsi, a continuous opening under the extended range (see Fig. 2) complicates the determination of the air modes of the instrument. Here, we report a simple experiment, in which we mounted a small loudspeaker near the sound hole under the ponsi. The loudspeaker was driven by a signal generator, and the cavity response was measured with a microphone placed at the continuous opening. During the measurement, the body of the instrument and the strings were damped. A frequency sweep allowed us to roughly determine the frequencies of the cavity resonances by inspecting the microphone signal level. Then, the input frequency was controlled manually, and two lowest cavity resonances was observed around 160 Hz and 270 Hz. The frequencies of these resonances, as well as the observed signal levels, match the characteristics of the lowest peaks in Fig. 4.

## 4. PLAYABILITY AND LOUDNESS ESTIMATE

A playability test was conducted where both playing and verbal feedback was recorded. The player was asked to play as quietly and as loudly as she felt comfortable with both instruments. Initially, the player had difficulties to adjust her left-hand position because of the extended wing, and to balance the instrument, especially when her right hand is released from it. However, after some warm-up time, she adapted to the conditions imposed by the new design.

The recordings were made in an anechoic chamber, with a microphone (B&K 4145) at the distance of one meter from the instrument, in regular playing position. First we recorded the piano

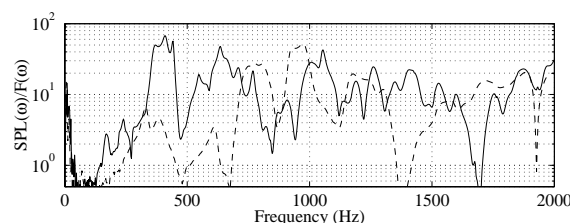


Figure 4: Comparison of the transfer functions of the modified and normal designs, indicated by solid and dashed curves, respectively.

and forte playing for approximately two minutes each, on both instruments. Then a set of notes were recorded while increasing the loudness at each step. In addition, the deflection of the string from its rest position was measured in a regular and loud pluck situation. Marks on the instrument were done while the player was asked to deflect the string, but not to release it. The markings were confirmed by visually evaluating a real plucking event, and they have been converted to the initial slope estimates. These initial slope estimates are used in Section 2.1 to calculate the input power.

In the dynamics test, the SPL is increased approximately 9 dB with the modified design. In addition, the dynamic range has been widened, as confirmed by the player. She suggested that the normal design has dynamically saturated in the series of plucks, whereas the new design responded to the increasing dynamics. Our SPL measurements confirmed her suggestion.

In the playability test, the player reported a physical discomfort during the continuous forte playing on both instruments. Therefore, the forte data has been discarded, and piano data has been analyzed. One minute segments have been used for the average RMS power calculation, using 1 ms windows. The SPL values for the normal and modified designs are 66.2 dB and 69.1 dB, respectively, indicating an SPL difference of 2.9 dB.

Short excerpts of the data are analyzed using the HutEar toolbox [4] for loudness estimates based on a computational model proposed in [5]. This model attempts to calculate the average loudness that would be perceived by a large group of listeners with normal hearing. The excitation patterns in the model are calculated from the auditory filter shapes, and they are transformed to specific loudness, i.e., loudness estimates per critical band. The overall loudness (in sones) is calculated by integrating the specific loudness. The estimation results are illustrated in Fig. 5. The model gives overall loudness estimates of 23 and 27 sones, for the normal and modified instruments, respectively. We thus conclude that the loudness is increased in the modified design.

As a last remark, the player noted a difference in the timbre and indicated that the 11-string design sounds like a kantele equipped with a microphone. This is probably because of the vibration of the extended part of the top plate.

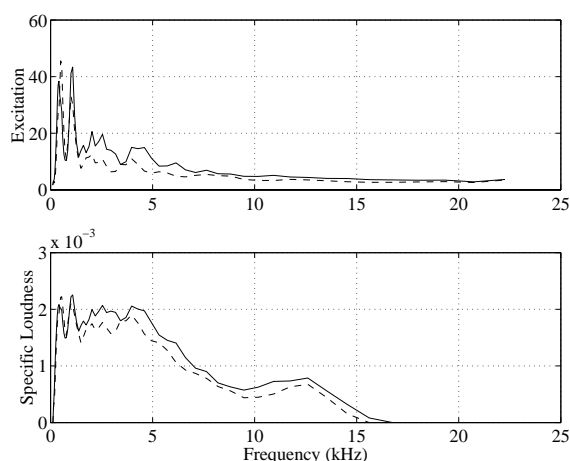


Figure 5: Comparison of the excitation patterns (top) and the specific loudness estimates (bottom) for the modified and normal designs, indicated by solid and dashed curves, respectively. The estimates are based on the loudness model proposed in [5].

## 5. CONCLUSIONS

In this paper, we propose design guidelines for a kantele with a higher loudness than the traditional model. These guidelines include the increase of the tension of the strings, the isolation of the top plate, and the increase of the radiating area. We have confirmed the effectiveness of these rules by following the energy path from the string vibrations to the radiated sound, and by conducting preliminary experiments for quantitative description of the improvement. We found that the total input power is increased by 26 % in the modified instrument, and using a computational model, we concluded that the overall SPL is increased by 2.9 dB. In addition, we have reported results of a preliminary playability test.

The new design ideas naturally can be applied to other stringed instruments. Among all the musical instruments there seem not to be clear examples of free edge plates or a separate bottom of the baffle type. There should not be great problems in trying these principles in other instruments whose sound radiation is based on a plate. At the time of writing this paper (May 2003), we have not conducted experiments with instruments other than the kantele.

Our future directions include a detailed analysis of the vibrations of the body, the air modes within the cavity, and the radiation characteristics of the modified instrument. The analysis of the vibration characteristics using experimental modal analysis or holographic techniques would extend the understanding of the proposed design principles. In addition, the acoustic intensity measurements could provide a quantitative description of the radiation efficiency in the new design. These measurements are left out as challenging future tasks.

## 6. ACKNOWLEDGMENTS

The authors wish to thank Dr. Marc Schönwiesner for his script<sup>1</sup> that is used for computing the specific and total loudness of the measured signals, and Dr. Arja Kastinen for participating in the playability test. Dr. Aki Härmä is also highly acknowledged for his HutEar toolbox. Henri Penttinen's work has been financially supported by the Pythagoras Graduate School.

## 7. REFERENCES

- [1] M. Karjalainen, J. Backman, and J. Pölkki, "Analysis, modeling, and real-time sound synthesis of the kantele, a traditional Finnish string instrument," in *Proc. ICASSP*, vol. 1, (Minneapolis, Minnesota, USA), pp. 125–128, Apr. 1993.
- [2] C. Erkut, M. Karjalainen, P. Huang, and V. Välimäki, "Acoustical analysis and model-based sound synthesis of the kantele," *J. Acoust. Soc. Am.*, vol. 112, pp. 1681–1691, Oct. 2002.
- [3] A. Peekna and T. D. Rossing, "The acoustics of Baltic psaltery," in *Proc. Int. Symposium on Musical Acoustics (ISMA)*, vol. 2, (Perugia, Italy), pp. 437–442, Sept. 2001.
- [4] A. Härmä and K. Palomäki, "HutEar—a free Matlab toolbox for modeling of human hearing," in *Proc. Matlab DSP Conference 1999*, (Espoo, Finland), pp. 96–99, Nov. 1999. Available at <http://www.acoustics.hut.fi/software/>.
- [5] B. Moore and B. Glasberg, "A revision of Zwicker's loudness model," *Acustica*, vol. 82, pp. 335–345, 1996.

<sup>1</sup>Available online at <http://www.uni-leipzig.de/~neuro/schoel/loudness.html>

## THE TRANSIENT BEHAVIOUR OF GUITAR STRINGS

*J. Woodhouse*

Cambridge University Engineering Department  
Trumpington St, Cambridge CB2 1PZ, UK  
jw12@eng.cam.ac.uk

### ABSTRACT

By analysing the body vibration or the radiated sound from plucked notes on a guitar, two questions can be addressed. First, how much can be learned about the behaviour of strings and body by analysing played notes only? Second, how accurately do the results match theoretical models of coupled string/body vibration? From the set of overtone frequencies, string stiffnesses and intonation errors can be determined. From the pattern of overtone decay rates as a function of frequency, the coupling between strings and body can be explored. By analysis of plucks with accurately controlled position and polarisation angle, comparisons can be made with theoretical models which reveal good agreement in some areas, but anomalies of detail, some of them quite puzzling.

## 1. OVERVIEW OF SYNTHESIS METHODS

### 1.1. Introduction

When a guitar string is plucked the player creates certain initial conditions of displacement and velocity in the string and the guitar body, then releases the string so that they vibrate freely. The resulting vibration is given by a superposition of the transient responses of the various coupled string/body modes of the instrument. The player can, to a certain extent, control the amplitudes making up the mixture, but the frequency, decay rate and radiation behaviour of each mode are governed by the instrument's construction and stringing, and the player can only exert a very minor influence on them for musical effect. Somewhere in the details of these transient decaying sounds lies the information which determines perceptual judgements of instrument quality.

To investigate such issues requires synthesis of the transient response to a pluck over the frequency range of interest for musical applications. This is not a simple task. The radiated sound from a typical note on a classical guitar shows clear spectral peaks up to at least 5 kHz. This corresponds to about the 60th harmonic of the lowest note on a normal guitar (82 Hz). Each of these isolated string "harmonics" can appear in two polarisations. A typical guitar body structure has of the order of 250 vibration modes in this range (plus a roughly comparable number of modes of the internal air cavity [1]). Assembling these numbers, it is clear that an accurate synthesis method may have to account correctly for several hundred degrees of freedom.

There are several viable approaches to synthesis. The fastest and most accurate ones are summarised here. All methods start from the same basic information about the

system. The string is characterised by its tension, mass per unit length, bending stiffness and damping. For the body, the most direct characterisation of dynamic behaviour is via the input admittance at the point on the bridge where the string makes contact, or more generally via the admittance matrix at this point. We may choose to process this admittance to extract modal properties: each mode has an effective mass, effective stiffness, damping factor, and angle of movement at the bridge. It also has a radiation efficiency and pattern, which would be relevant if the desire was to synthesise the sound field.

### 1.2. Modal synthesis

The first class of synthesis methods works by computing the coupled string/body modes, together with appropriate frequencies and damping factors, then using modal superposition to construct the transient response. The simplest modal approach proceeds in four stages. First, the system mass and stiffness matrices are worked out. Second, the modes and natural frequencies of the coupled string/body system are computed in the absence of damping by standard eigenvalue/eigenvector analysis. Third, a suitable Q-factor is calculated for each mode using a small-damping argument based on Rayleigh's principle [2]. Finally, the transient response to an ideal pluck at a given position on the string can be calculated using a standard modal superposition result.

The method just outlined is precisely what is used in the vast majority of calculations of the vibration response of complex structures. For example, almost all Finite-Element calculations work this way. Unfortunately, as pointed out by Gough [3], this method does not always give a good approximation to the correct answer. To avoid the problem, it is necessary to compute the modal behaviour of the coupled, damped system. The usual method is to recast the equations into first-order form [4]. This gives an eigenvalue/eigenvector problem which yields the (complex) mode vectors and associated complex natural frequencies, and there are then standard formulae for frequency response functions and impulse response functions in terms of modal sums ([4], Chapter 8).

Modal synthesis methods share certain advantages. First, they work in terms of degrees of freedom which are very natural: loosely, "string mode amplitudes" and "body mode amplitudes". Second, once the modes have been computed, the desired transient response is given by an explicit formula which introduces no further approximations or numerical difficulties. A disadvantage of these methods is that they require the body response to be expressed in terms of modal properties over the entire frequency range. This is simple and natural at low frequencies, but by frequencies of the order of 500 Hz in a

typical classical guitar the modal overlap factor of the body starts to become significant and above that it is neither easy nor unambiguous to fit reliable modal parameters to a measured admittance [5].

### 1.3. Frequency domain synthesis

A completely different approach to the synthesis problem is to deal with the string/body coupling in the frequency domain, and then use an inverse FFT to create the required time-varying transient response. This method is attractive because the string and the body are coupled together at a single point, and there is a very simple method which can be applied to any such problem: if two systems have input admittances  $Y_1(\omega)$  and  $Y_2(\omega)$  and they are then rigidly connected at the points at which these admittances are defined, then the coupled system has an admittance  $Y$  at that point satisfying

$$Y^{-1} = Y_1^{-1} + Y_2^{-1}. \quad (1)$$

The body is naturally described in terms of its admittance (or admittance matrix), as already described. By calculating the corresponding admittance at the end of a string, this result can be applied immediately to give the impedance or impedance matrix of the strung guitar at the bridge.

To use this to derive a pluck response, use can be made of the reciprocal theorem of vibration response. We wish to find the body vibration which results from a step function of force applied at a given position on the string. Reciprocally, we can consider applying the force at the bridge, and calculate the resulting motion at the relevant point on the string (and in the relevant direction there, if string polarisations are to be taken into account). To solve this reciprocal problem, we simply have to multiply two transfer functions together. The first is the coupled admittance just calculated, which give the velocity at the bridge when a force is applied there. The second is the dimensionless transfer function between a given displacement applied at one end of a string and the corresponding displacement at the point where the pluck is to be applied.

The advantages of this frequency-domain approach are that it is very simple, and that it gives the choice of expressing the body admittance in terms of modes, as before, or of using the measured admittance directly, thus avoiding the complication of modal fitting at high frequencies. The main disadvantage of the method is its reliance on inverse Fourier transformation at the final stage. However, a sufficiently causal result can be achieved with care, and that makes this method very attractive. It is significantly faster to compute than the modal method.

## 2. COMPARISONS WITH MEASUREMENTS

Pluck responses synthesised by the methods just outlined can be compared with measured ones, either obtained by normal playing or from more controlled plucks using a loop of fine copper wire which is pulled until it breaks. First, calibration data is needed on the guitar body vibration, in the form of a measurement of the input admittance, done with a miniature impact hammer and a laser vibrometer so that no mass loading was added by the measurement hardware. This admittance can

be curve-fitted to yield modal parameters, at least at low frequencies. To obtain a modal model at higher frequencies, a “statistical fit” to the measurements has been used: broadly plausible mode frequencies, amplitudes and damping factors can be calculated using a random number generator, given statistical information about the modal density, and the range of damping factor and modal masses. A typical result is compared to the measured input admittance in Figure 1.

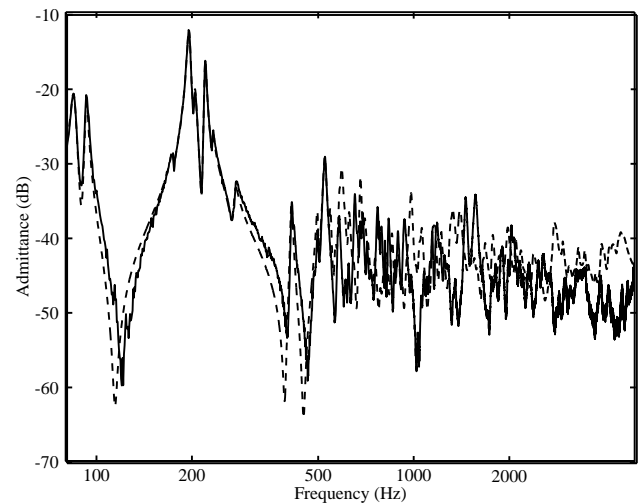


Figure 1: *Body input admittance.*

The input admittance at the bridge near the bottom E string, for the guitar used in the tests. Solid line: measured admittance; dashed line: modal fit based on exact fitting up to 500 Hz and “statistical fitting” above that.

A powerful way to extract information from a pluck response is by time-frequency analysis. Overlapping portions of the data, Hanning windowed, are analysed by FFT. The resulting time-frequency plot reveals the decaying “harmonics” of the string. Each one can be located, and the decay profile extracted. A decay rate can be determined by linear regression on the log amplitude, and an accurate frequency can be determined by linear regression on the phase variation. This process can be carried out automatically, so that many notes can be played, and the frequencies and decay rates of all strong overtones calculated. Various interesting information can then be extracted.

From the frequencies, the bending stiffness of the string can be found. This is most easily done from a plot of frequency divided by mode number, as illustrated in Fig. 2. The measured points follow a parabolic curve, as predicted by the theory of a stiff string [6]. A polynomial fit yields the value of the bending stiffness, which can then be used as input to the synthesis algorithms. Notice that in the example plotted, the 9th overtone does not lie on the parabolic curve. As will be discussed in the next subsection, this is not a processing error but an indication of something unexpected happening.

Another calibration requirement for the synthesis models is the frequency dependent string damping. Damping falls slightly from DC up to 1 kHz or so, but rises steeply so that by 15 kHz it has risen by about two orders of magnitude. The measured

data can be used to fit a model of the type described by Valette [6], which matches these characteristics quite well.

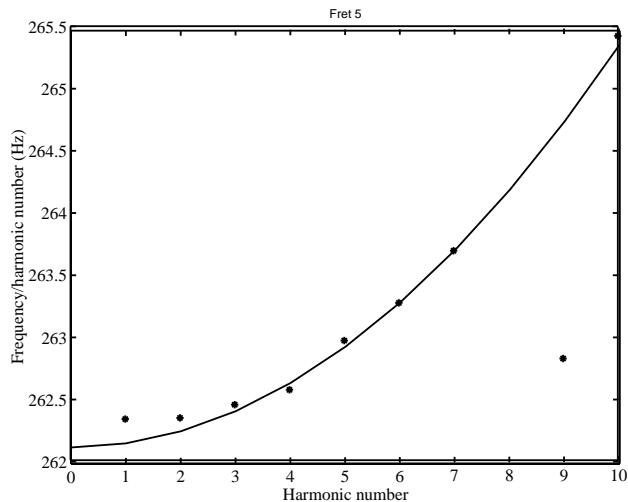


Figure 2: Frequencies and stiffness fit.

For the note C at the 5th fret of the 3rd string of the test guitar, frequency divided by harmonic number plotted against harmonic number (points). The line shows the best fit of the quadratic function predicted by theory, which yields a value for the bending stiffness of the string. The lowest overtones are perturbed by coupling to the body. Higher ones should not be perturbed much, and the anomalous point at the 9th overtone is a discrepancy discussed in the text

From the same data, another revealing plot is shown in Fig. 3a: modal damping factors are plotted against frequency, for all overtones below 2 kHz of all notes up to the 12th fret on the bottom E string of the test guitar. Corresponding results are shown in Fig. 3b from a set of plucks synthesised by the frequency domain method using the “statistical-fitted” admittances, for a pluck at 45° to the plane of the soundboard. The two plots correspond in a very broad sense, but the detailed agreement is not impressive. The “floor” level matches quite well, because the damping model described above is fitted to this. Some discrepancies are due to missing points in one plot or the other — the automatic algorithm only includes strong peaks which show an accurate fit to exponential decay. The two points at low frequency in Figure 3b which show very high damping may be ignored: these correspond to “body modes” rather than “string modes”, captured erroneously by the algorithm. Above 500 Hz, recall that the fine details are not expected to agree because of the “statistical fit” of admittance. But even so, there are certainly real discrepancies between these figures, pointing to inadequacies of the current synthesis model despite efforts to calibrate it carefully to this guitar. Possible sources of these are discussed below.

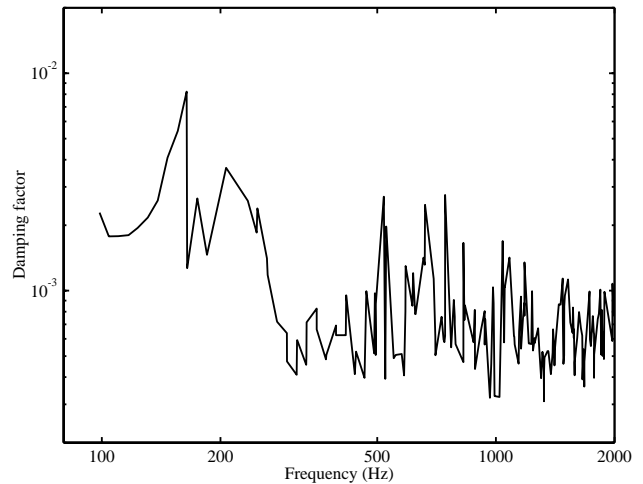


Figure 3a: Decay rates for 6th string (E).

Decay rates versus frequency, for all detected harmonics of each note up to the 12th fret on the 6th string (E) of the test guitar.

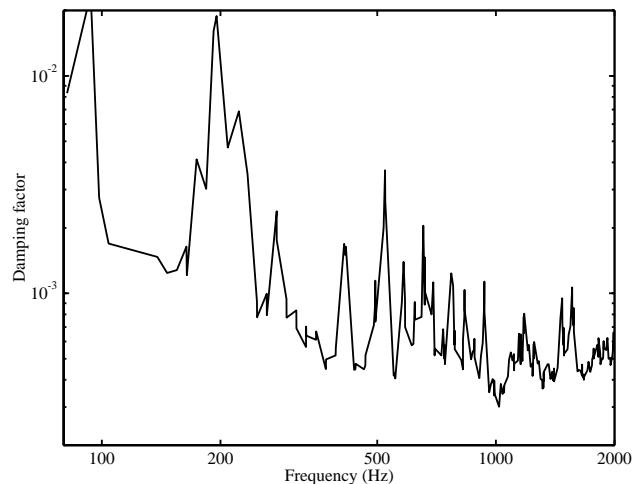


Figure 3b: Decay rates for 6th string (E).

As Figure 3a, but showing results for synthesised plucks on the test guitar. The points with high damping at low frequencies correspond to “body modes” rather than “string modes”, caught accidentally by the automatic processing algorithm.

A different view is given of the experiment/synthesis comparison by looking in the frequency domain. Figure 4a shows that at low frequencies, a good measure of agreement is obtained. At higher frequencies, though, discrepancies again appear. Figure 4b shows a typical example. The theory predicts that high overtones of the string are only very weakly coupled to the body, so that the synthesised spectrum shows string resonances with very little obvious sign of body effects. The measurement, though, shows some anomalous resonance peaks in unexpected places. One such peak accounts for the “rogue” point in Fig. 2: the automatic algorithm caught the “wrong” peak.

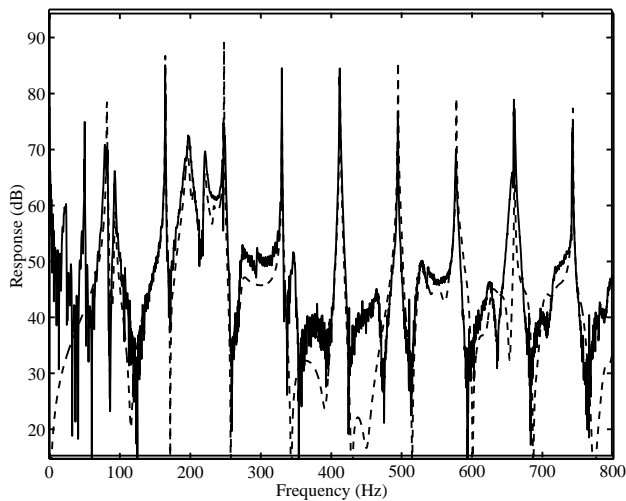


Figure 4a: Frequency spectrum of pluck.

The low frequency part of the spectrum of a pluck on the open 6th string (E) of the test guitar. Solid line: measured pluck with breaking wire; dashed line: corresponding synthesised pluck.

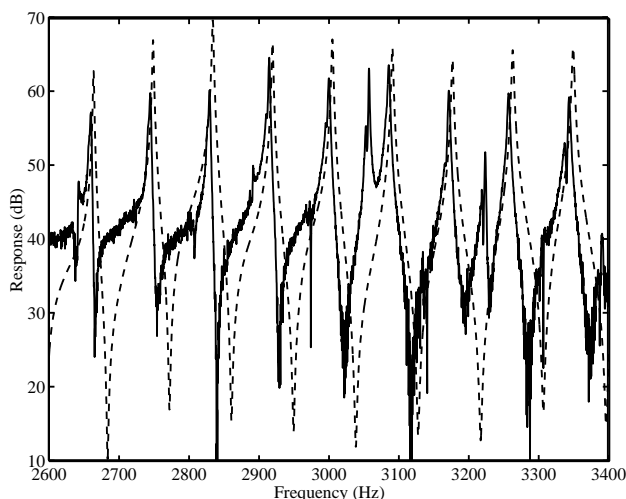


Figure 4b: Frequency spectrum of pluck.

As Figure 4a, showing the same two plucks in a higher frequency range. The slight mismatch of peak positions arises because the guitar was not perfectly in tune compared to equal temperament. The measurement shows anomalous additional peaks which are as yet unexplained.

The source of these discrepancies is still somewhat of a mystery, but some possibilities can be listed. The low-frequency differences seen in Fig. 3 might possibly be caused by the low modes of the guitar being somewhat affected by the fixture which held the guitar for measurement. It is even possible that the behaviour had actually changed a little because of temperature and humidity variations. Another factor missing from these syntheses is coupling of the string to the body through the fret, as well as through the bridge, but this is

expected to be a minor effect. However, none of these explanations can account for the behaviour seen in Fig. 4b. The anomalous peaks do not arise from sympathetic resonance of other strings, because they were all damped. These peaks appear to be a real physical phenomenon rather than a measurement artefact of some kind. Is the string perhaps slipping sideways on the fret? Does the manufacturing process for the string perhaps produce some axial variation of properties, such as in the density of windings on this wrapped string? Neither of these ideas sounds entirely plausible, and further investigation is needed.

### 3. CONCLUSIONS

Algorithms for synthesis of guitar transients have been reviewed. The two methods which give best results are (i) modal synthesis using the first-order method, and (ii) frequency-domain synthesis. The latter is significantly faster to compute, and offers the possibility of using measured admittance behaviour directly, without needing a modal fit.

When synthesis results are compared with measurements, moderately good general agreement is seen. Many such comparisons have been made, of which only a very small sample can be shown here. However, a number of discrepancies emerge, highlighted in data illustrated. These may well have audible consequences. It is mildly surprising that such a “simple” problem as the coupled vibration of a guitar string and body does not conform more readily to the type of theory which is universally used to analyse the behaviour. Further work is needed to identify the source of the discrepancies and incorporate the effects in the synthesis models.

### 4. REFERENCES

- [1] Weinreich, G., “Vibration and radiation of structures with application to string and percussion instruments”, in “Mechanics of musical instruments”, ed. A. Hirshberg, J. Kergomard and G. Weinreich, Springer-Verlag, Wien, 1995.
- [2] McIntyre, M.E. and Woodhouse, J., “The influence of geometry on linear damping”, *Acustica* 39:209-224, 1978.
- [3] Gough, C.E., “The theory of string resonances on musical instruments”, *Acustica* 49:124-141, 1981.
- [4] Newland, D.E. “Mechanical vibration analysis and computation”, Longman Scientific, New York, 1989.
- [5] Woodhouse, J., “Body vibration of the violin — what can a maker expect to control?”, *J. Catgut Acoust. Soc. Series II* 4(5):43-49, 2002.
- [6] Valette, C., “The mechanics of vibrating strings”, in “Mechanics of musical instruments”, ed. A. Hirshberg, J. Kergomard and G. Weinreich, Springer-Verlag, Wien, 1995.

**PIANOS**





## MODELING THE LONGITUDINAL VIBRATION OF PIANO STRINGS

*Balázs Bank and László Sujbert*

Department of Measurement and Information Systems  
Budapest University of Technology and Economics  
bank@mit.bme.hu, sujbert@mit.bme.hu

### ABSTRACT

This study is motivated by the physical modeling of the longitudinal string vibrations in the piano. Informal listening tests show that the longitudinal vibrations play an important role in the attack of the sound, and are responsible for the metallic character of low notes. First, a simple mathematical model is developed for qualitative understanding. Detailed analysis is given for sinusoidal transversal displacement with non-rigid termination, clarifying the generation of phantom partials. To investigate how these effects develop in more natural circumstances, finite-difference string and hammer models are used, with parameters taken from real pianos. For real-time sound synthesis purposes, an efficient modeling approach is presented. The model extends the digital waveguide string model by implementing two additional string models, one for the phantom partials and one for the longitudinal modes.

### 1. INTRODUCTION

Physical modeling of the piano has been an interesting field of research in the last decades, see, e.g. [1, 2, 3]. As faster processors emerge, real-time implementations become possible. However, the quality of synthesized piano sound is still far from perfect. The digital waveguide [4] used in these models is capable of producing a quasi-periodic sound, which is built up by exponentially decaying sinusoids. Conversely, when the spectra of a real piano sound is observed, other components can also be noticed. These correspond to either the longitudinal modes of the string [5], or to the “phantom” partials generated by nonlinear mixing [6]. We believe that these two phenomena should be treated together.

The motivation of this research was to refine the quality of our piano model. However, as no detailed analysis can be found in the literature on the generation of these phenomena, first the underlying physics has to be understood before efficient physical models are developed. The paper is organized as follows: first, prior work is presented and the basic properties of phantom partials and longitudinal modes are described. This is followed by the analysis of steady-state motion and by the investigation of the transient response by a numerical model. Emphasis is given on the explanation of phantom partials. For real-time sound synthesis, an efficient algorithm is presented by applying digital waveguide string models.

### 2. PRIOR WORK

By observing the spectrum of piano sound, “phantom” partials can be found between the normal, inharmonic partial series [6]. They are generated by nonlinear frequency mixing, thus, their frequencies can be computed as the sum or difference of the normal par-

tial frequencies. Those, which appear at the double frequency of a normal partial, called “even” phantoms. Accordingly, “odd” phantoms appear at the sum or difference of two different partial frequencies. In a perfectly harmonic instrument, these sum and difference frequencies will correspond to the frequencies of “normal” partials, thus, phantom partials do not influence the sound significantly. However, when the transversal vibration has an inharmonic frequency series, which is the case for the piano, phantom partials will depart from the normal partials. As measurements show, odd phantoms are generally produced by adjacent parents (e.g.,  $5 + 6$ , rather than  $4 + 7$ ) [6]. That paper does not describe the reason of this fact, nor the detailed mechanism how these phantoms arise.

Somewhat earlier, a second series (the “lower series”) of partials were extracted from the spectrum of a piano in [7]. This lower series of partials has a lower inharmonicity. The inharmonicity coefficient  $B$  has been found to be around the fourth of the one for normal partials. Explanation of this fact is not given in the paper. Moreover, the authors argue that the lower series is possibly generated by the string vibration parallel to the soundboard. However, there is no physical reason why the string should have a different dispersion in the two transversal polarizations. We believe that the “lower series” is equivalent with the phantom partials generated by nonlinear mixing.

Some phantom partials are displayed in Fig. 1 for an  $A_4^\sharp$  note with circles. The marked phantoms appear at the frequencies in terms of the normal partial series at  $f_4 + f_5$ ,  $2f_5$ ,  $f_6 + f_7$ , and  $f_7 + f_8$ . These phantom partials may play a part in differentiating the timbre between pianos by emphasizing the effect of inharmonicity with the beats produced between them and the normal partials [6].

The longitudinal modes of the piano string may have a more significant perceptual effect. In the low range of the piano, the pitch of these components can be perceived by the listener, and the subjective quality of the instrument is highly dependent on the frequency of these modes [5]. The longitudinal modes are a nonlinear function of the transversal vibration, which justifies the assumption that they are excited by the string stretching due to a transversal vibration of a finite amplitude [8].

### 3. THE BASIC EQUATION

A real piano string is vibrating in two transversal planes, and in the longitudinal direction as well. Principally, piano hammers excite one polarization of the string, the other two are gaining energy through coupling. Throughout the vibration, these polarizations interact with each other, as a result of nonlinear behavior of the string.

For simplicity, let us assume that the string is vibrating in one plane, thus, one transversal and one longitudinal polarization is

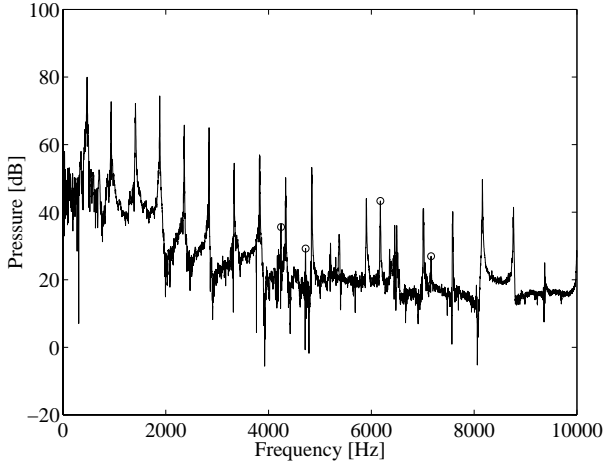


Figure 1: Spectrum of an  $A_4^\sharp$  piano tone with some phantoms marked by circles.

present. When there is a transversal displacement on the string, the string elongates. This results in a force exciting a longitudinal wave in the string. The longitudinal wave modulates the tension along the string, which influences the transversal vibration. As we are interested in the generation of longitudinal waves, a further assumption is made: the influence of the longitudinal polarization on the transversal one is neglected.

The equations describing the interaction of the two transversal and the longitudinal polarizations are developed e.g., in [9]. After some approximations, the longitudinal motion can be characterized by the following equation:

$$\mu \frac{\partial^2 \xi}{\partial t^2} = ES \frac{\partial^2 \xi}{\partial x^2} + \frac{1}{2} ES \frac{\partial \left( \frac{\partial y}{\partial x} \right)^2}{\partial x} \quad (1)$$

where  $y = y(x, t)$  and  $\xi = \xi(x, t)$  are the transversal and longitudinal displacement of the string with respect to time  $t$  and space  $x$ . The mass per unit length is referred by  $\mu$ ,  $E$  is the Young's modulus and  $S$  is the cross-section area of the string. Eq. (1) is the standard wave equation with an additional force term depending on the transversal vibration of the string, according to a second-order nonlinearity.

#### 4. STEADY STATE SOLUTION

By applying the above equations, the coupling between the transversal and longitudinal string vibration can be computed analytically for sinusoidal transversal vibration. This corresponds to describing the origin of phantom partials of [6] or the "lower series" of [7].

##### 4.1. Sinusoidal transversal wave

Considering one single transversal mode of a lossy string with rigid terminations, the transversal string displacement will be [9]:

$$y(x, t) = A_k \sin(2k\pi f_0 t) e^{-\frac{t}{\tau_k}} \sin\left(\frac{k\pi}{L} x\right) \quad (2)$$

where  $A_k$  stands for the initial amplitude, and  $\tau_k$  for the decay time of mode  $k$ . The length of the string is referred by  $L$ , and  $f_0$

is the fundamental frequency, i. e., the frequency of mode  $k = 1$ . According to Eq. (1), the longitudinal excitation force-distribution  $F_{l,e}(x, t)$  can be obtained as follows:

$$F_{l,e}(x, t) = ES \frac{k^3 \pi^3}{4L^3} A_k^2 (\cos(4k\pi f_0 t) - 1) e^{-\frac{2t}{\tau_k}} \sin\left(\frac{2k\pi}{L} x\right) \quad (3)$$

From this, some interesting observations can be made. The force can be separated to a decaying cosine and to a decaying static force. The amplitude of the force  $F_{l,e}(x, t)$  is proportional to the square of initial transversal displacement  $A_k$ , the decay time is the half of  $\tau_k$ , and the frequency of force variation is the double of the transversal vibration frequency  $k f_0$ . Concerning the spatial distribution of  $F_{l,e}(x, t)$ , a transversal mode  $k$  produces an excitation force corresponding to a longitudinal mode  $k_l = 2k$ .

The normal modes of the longitudinal vibration can be written similarly to Eq. (2). Now the question is if  $F_{l,e}(x, t)$  can excite the longitudinal mode  $k_l$  of the string. For efficient coupling, two conditions has to be met: the spatial distribution of  $F_{l,e}(x, t)$  should not be orthogonal to the longitudinal-mode shape  $\sin\left(\frac{k_l \pi}{L} x\right)$ , and the frequency of the excitation  $2k f_0$  should be close to that of the longitudinal mode  $k_l f_{l,0}$ . Coming from the first condition, a transversal mode  $k$  can only excite a longitudinal mode  $k_l = 2k$ . Thus, a force with a frequency of  $2k f_0$  should excite a longitudinal mode with a frequency of  $2k f_{l,0}$ . As  $f_{l,0}$  is of an order higher than  $f_0$  in practice, this results in a small longitudinal motion only, although it might reach the air through the soundboard.

In reality, the string is terminated with a finite impedance. Therefore, the normal modes do not have a node at the termination. This can be taken into account in Eqs. (2) and (3) by substituting  $L$  with  $L + \delta L$ , while  $0 \leq x \leq L$  still holds. We can still assume that the termination is perfectly rigid in the longitudinal direction. The result will be that the force  $F_{l,e}(x, t)$  is not orthogonal to any of the longitudinal mode shapes, thus, it excites all of them, although in a different way. If the frequency of the excitation is near to a longitudinal-mode frequency, i.e.,  $2k f_0 \approx k_l f_{l,0}$ , strong longitudinal vibration emerges. For example, if  $f_{l,0} \approx 10 f_0$ , then the fifth transversal mode can excite the first longitudinal mode strongly. This is in a good accordance with the measurements of [6], where some cases phantom partials with frequencies near to the longitudinal mode have produced larger sound pressure than the neighboring transversal ones.

As the excitation force of Eq. (1) is known, the corresponding longitudinal vibration could be analytically calculated by the help of the Green's function [9]. However, as the role of this section is to help qualitative understanding, these derivations are not included in the paper.

##### 4.2. Mode pairs

In practice, the transversal vibration is made up of several modes. Hence, the excitation force  $F_{l,e}(x, t)$  will contain terms with the sum and difference frequencies of all the transversal modal frequencies, coming from the second-order nonlinearity of the coupling. When  $N$  normal transversal partials are present, they generate  $N^2$  phantom partials. However, these are not all noticeable in the spectrum: generally the phantoms produced by transversal parents with consecutive mode numbers (e.g., 5 + 6) appear [6]. Let us examine the reason in detail.

As the nonlinearity is of second order, it is enough to explain the phenomena for the sum of two sinusoids. When the excitation force  $F_{l,e}(x, t)$  is calculated for the sum of two exponen-

tially decaying sinusoids described by Eq. (2), the force distribution  $F_{l,e}(x, t)$  with the sum and difference frequencies will be the following:

$$F_{l,e}(x, t) = -ES \frac{k_1 k_2 \pi^3}{4L^3} A_1 A_2 F_{l,e}(t) \times \\ \times \left( \sin\left(\frac{k_1 + k_2}{L} \pi x\right) (k_1 + k_2) + \sin\left(\frac{k_2 - k_1}{L} \pi x\right) (k_2 - k_1) \right) \quad (4)$$

where  $F_{l,e}(t)$  is the time dependent component containing two cosine functions with the sum and difference frequencies of transversal mode  $k_1$  and  $k_2$ . Note that Eq. (4) does not include the double-frequency terms for clarity (they are the same as for the single sine case of Eq. (3)).

We have seen that a longitudinal mode  $k_l$  is significantly excited only if the spatial distribution of  $F_{l,e}(x, t)$  is not orthogonal to the longitudinal mode shape  $\sin(\frac{k_l \pi}{L} x)$ , and the excitation frequency is close to the modal frequency  $k_l f_{l,0}$ . The sum frequency of the lower (e.g.,  $k < 10$ ) transversal modes are around the frequency of the first longitudinal mode  $k_l = 1$ . Accordingly, those  $k_1 + k_2 = m$  combinations will be present in the longitudinal motion, where  $k_2 - k_1 = 1$ , since in the spatial distribution of  $F_{l,e}(t)$  the  $\sin(\frac{\pi}{L} x)$  term will be present. In the case of higher phantom partials, higher longitudinal modes should be excited, thus, the parents will be transversal modes with mode numbers  $k_2 - k_1 > 1$ .

It has to be noted that a phantom generated by modes  $k_2 - k_1 = 1$  appears almost at the same frequency where the one produced by mode  $k_2 - k_1 = 3$  appears, if  $k_1 + k_2 = m$  is the same for the two case. This is because the sum frequencies produced by the frequency pairs  $k_1 + k_2$  are not distributed evenly on the frequency axis, but have a larger density around the center frequency determined by  $k_2 - k_1 = 1$  (the deviation from this center frequency is proportional to  $(k_2 - k_1)^2$ ).

By knowing that odd phantoms are mainly produced by adjacent parents, and that even phantoms can be found at the double frequencies of normal partials, we can easily explain why the inharmonicity coefficient  $B$  is the 1/4 part of the value for normal partials. We can calculate the frequencies  $f_m$  of even phantoms  $m = 2k$  easily, by the help of the inharmonicity formula of [10]:

$$f_m = 2f_k = 2f_0 k \sqrt{1 + Bk^2} = f_0 m \sqrt{1 + \frac{1}{4} Bm^2} \quad (5)$$

For even phantoms, the expression is accurate. For odd phantoms,  $k = m/2$  is not an integer number, but Eq. (5) can be still applicable, since we can assume that the inharmonicity curve is smooth enough.

These theoretical results were justified by a finite difference model based on Eq. (1) with losses added. The transversal vibration has been analytically computed, which have made it easy to experiment with different transversal mode numbers and vibration frequencies. For low transversal mode numbers ( $k_1, k_2 < 10$ ) adjacent parents ( $k_2 - k_1 = 1$ ) produced 15-20 dB higher longitudinal motion compared to other combinations of  $k_1 + k_2 = m$ .

Those sum terms which do not form a phantom partial ( $k_2 - k_1 \gg 1$ ), together with the difference components, form a dense, noise-like excitation spectrum with thousands of partials. These are measured in the sound spectrum as broadband noise. However, when a frequency of a term is close to that of a longitudinal mode, it can excite that mode effectively. As the excitation force spectrum is dense, it is very probable that the longitudinal modes of the string will be excited throughout the vibration. Note that for a

perfectly harmonic instrument the excitation force spectrum would contain some distinct peaks, exciting the longitudinal modes only in special constellations of the longitudinal and transversal fundamental partial frequencies.

## 5. TRANSIENT RESPONSE

Up to now, only the phenomenon of phantom partials has been considered, which is the forced motion of the longitudinal modes. However, as the excitation in a real piano is not steady-state, the free vibration of the longitudinal modes will also appear.

A finite-difference string model has been realized for calculating the transversal vibration with hammer excitation. The parameters of the model were taken from [11]. The transversal displacement produced by the model serve as an input for the finite-difference longitudinal string model. The longitudinal string model is based on Eq. (1), with losses added. Both in the transversal and longitudinal string models 100 elements were used. A high sampling frequency ( $f_s = 441$  kHz) was necessary to maintain the numerical stability of the longitudinal string model.

The output of the model has shown that the longitudinal vibrations excited by the hammer strike are the most significant components of the longitudinal motion. Figure 2 displays the spectrum of the force at the bridge in the direction of the strings for a  $C_2$  piano string, with the parameters of [11]. The Young's modulus  $E$  and the cross section area of the string  $S$  were set according to values found in real pianos. The impact velocity of the hammer was set to 5 m/s.

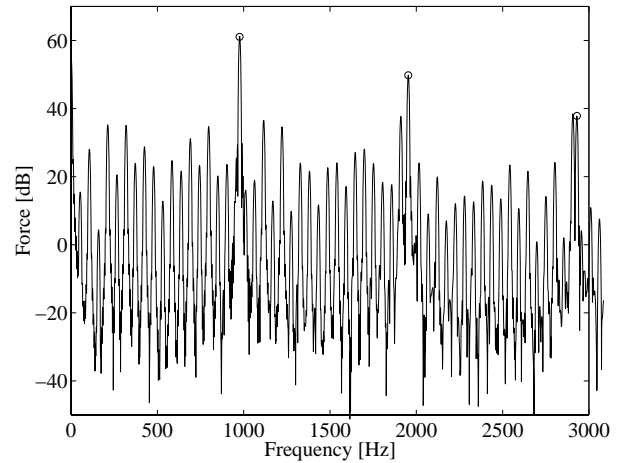


Figure 2: Force spectrum of the longitudinal vibration of a  $C_2$  note. The longitudinal modal frequencies are marked by circles.

The components of the free longitudinal vibration are marked by circles in Fig. 2. It can also be seen that around these frequencies the phantom partials are emphasized, producing beating with the longitudinal modes. Note that in real pianos the longitudinal modes are not in a perfect harmonic series, and simulating them in this way produces poor sonic results. Further research is needed to determine whether the "inharmonicity" of the longitudinal modes are produced by the finite impedance or caused by the properties of the string.

## 6. THE ROLE OF FEEDBACK

In some cases the simulation produced unexpected results, where the longitudinal vibration had very large amplitudes. This happens when a phantom partial lies very close to a longitudinal mode, exciting it with its eigenfrequency. This cannot occur in reality, since the transversal modes lose energy when they excite the longitudinal motion. When the effect of the longitudinal vibration on the transversal one is also taken into account, the same longitudinal modes behave as expected. The wave equation for the transversal motion can be written by approximating the formulas of [9]:

$$\mu \frac{\partial^2 y}{\partial t^2} = T_0 \frac{\partial^2 y}{\partial x^2} + ES \frac{\partial \left( \frac{\partial y}{\partial x} \frac{\partial \epsilon}{\partial x} \right)}{\partial x} \quad (6)$$

It can be seen that the components coming from the longitudinal motion are the sum and difference frequencies of one transversal and one longitudinal mode. Let us assume that the transversal modes  $k_1 + k_2$  excite a longitudinal mode strongly with a frequency  $f_{l,k} = f_0(k_1 + k_2)$ . Now the difference frequencies between the longitudinal and transversal modes can react with the other modes of the mode pair  $k_1$  and  $k_2$ , since  $f_{l,k} - f_0 k_1 = f_0 k_2$  and  $f_{l,k} - f_0 k_2 = f_0 k_1$ . Further investigations are required to understand how this feedback can diminish the energy of the modes  $k_1$  and  $k_2$ .

## 7. THE DIGITAL WAVEGUIDE MODEL

A finite-difference string model would require unacceptable computational costs for real-time sound synthesis. A highly efficient string modeling technique, the digital waveguide modeling [4] reduces this complexity by an order of 100. However, implementing the interaction of the longitudinal and transversal polarizations is not a straightforward task.

One option is calculating the transversal vibration by a digital waveguide model, and running a finite-difference longitudinal string model in parallel with the excitation force calculated from the transversal displacement. The required computational complexity can be reduced by implementing only 5-10 string elements in the longitudinal model, since the task is to simulate the first few longitudinal modes. The longitudinal vibration must be made slightly inharmonic by e.g., applying inhomogeneous string parameters. This model produces acceptable quality at a reasonable computational cost, but in some cases the longitudinal vibration can be unexpectedly large, similarly as described in Sec. 6. Feedback from the longitudinal vibration to the transversal one is not an option here, since the stability of the system cannot be maintained because of the large number of approximations.

A simpler, but less physical solution is implementing the phantom partials and the free vibration of the longitudinal modes directly with two other string models. As we have seen in Sec. 4.2, the phantom series has a similar inharmonicity curve as the normal partials, but with inharmonicity coefficient  $B/4$ . This can be easily realized with a second digital waveguide in parallel. Moreover, informal listening tests show that this second waveguide can be perfectly harmonic, so there is no need for a high-order dispersion filter. To render the nonlinear dependence of the amplitudes of phantom partials on the strike velocity, the hammer force calculated by the basic string model is squared before lead to the phantom string model. The longitudinal vibrations are simulated in a similar way, but in that case a perfectly harmonic waveguide produces poor results. Therefore, either an allpass filter is needed

to alter the modal frequencies, or the small number of required partials are modeled by a parallel resonator bank. The model produces good sound quality, although the longitudinal modes sound to be separated from the main tone in some cases. This can be overcome by increasing the number of partials to produce an inharmonic tone, thus, a less definite pitch.

## 8. CONCLUSIONS

We have described the phenomenon how the longitudinal vibration of a string is excited by the transversal vibration with a simplified mathematical model. The longitudinal motion of a string is made up of the free vibration of the longitudinal modes and the forced vibration coming from the transversal displacement with a quadratic nonlinearity. The generation mechanism of phantom partials was described in detail. The theoretical results were verified by computer simulations with a finite-difference string model. For sound synthesis purposes an efficient digital waveguide based solution has been presented.

## 9. REFERENCES

- [1] Julius O. Smith and Scott A. Van Duyne, "Commutated piano synthesis," in *Proc. Int. Computer Music Conf.*, Banff, Canada, September 1995, pp. 335-342.
- [2] Gianpaolo Borin, Davide Rocchesso, and Francesco Scalcon, "A physical piano model for music performance," in *Proc. Int. Computer Music Conf.*, Thessaloniki, Greece, September 1997, pp. 350-353.
- [3] Balázs Bank, "Physics-based sound synthesis of the piano," M.S. thesis, Budapest University of Technology and Economics, Hungary, May 2000, Published as Report 54 of HUT Laboratory of Acoustics and Audio Signal Processing, URL: <http://www.mit.bme.hu/~bank>.
- [4] Julius O. Smith, "Physical modeling using digital waveguides," *Computer Music J.*, vol. 16, no. 4, pp. 74-91, Winter 1992.
- [5] Harold A. Conklin, "Design and tone in the mechanoacoustic piano. Part III. Piano strings and scale design," *J. Acoust. Soc. Am.*, vol. 100, no. 3, pp. 1286-1298, June 1996.
- [6] Harold A. Conklin, "Generation of partials due to nonlinear mixing in a stringed instrument," *J. Acoust. Soc. Am.*, vol. 105, no. 1, pp. 536-545, January 1999.
- [7] I. Nakamura and D. Naganuma, "Characteristics of piano sound spectra," in *Proc. Stockholm Music Acoustics Conf.*, 1993, pp. 325-330.
- [8] N. Giordano and A. J. Korte, "Longitudinal vibrations and the role of the bridge," *J. Acoust. Soc. Am.*, vol. 100, no. 6, pp. 3899-3908, December 1996.
- [9] Philip M. Morse and K. Uno Ingard, *Theoretical Acoustics*, McGraw-Hill, 1968.
- [10] Harvey Fletcher, E. Donnell Blackham, and Richard Stratton, "Quality of piano tones," *J. Acoust. Soc. Am.*, vol. 34, no. 6, pp. 749-761, June 1962.
- [11] Antoine Chaigne and Anders Askenfelt, "Numerical simulations of piano strings. II. Comparisons with measurements and systematic exploration of some hammer-string parameters," *J. Acoust. Soc. Am.*, vol. 95, no. 3, pp. 1631-1640, March 1994.

## QUALITY OF TREBLE PIANO TONES

Galembo, A.

Setchenov Institute of Evolutionary Physiology and Biochemistry, St. Petersburg, Russia  
alex@speech.kth.se

### ABSTRACT

In this study it is shown that the quality of a treble tone of the piano is defined primarily by the temporal dynamics of the perceptually competing impact noise (“knock element”) and the string-born “tonal element” (the partials responsible for pitch sensation). The relation between the two elements depends primarily on the parameters of the hammer-string contact, and not so much on the soundboard properties. The knock component is “colored” by the metal frame, in particular by the choice of material. Two ways (mechanical and electronic) of experimentally separating the knock and the tonal element in a real piano tone for listening tests and demonstrations are shown. (The paper presents results of previous industrial research conducted in the acoustic laboratory of the Leningrad Piano Factory, Russia to English readers.)

### 1. INTRODUCTION

The treble range (about two highest octaves) is a weak link in many pianos. Consistent high quality of the treble tones is, as a rule, an index of a high-class maker and a careful production technology, because in this range the piano “works” at the limit of its acoustical capacity for a long, clear tone, because:

- – The strings are extremely short;
- – The hammer-string contact duration exceeds a half-period of the string fundamental, thus causing the hammer to damp the string vibrations after the initial excitation;
- – The hammer-string contact point is critically close to the string support;
- – The fundamental frequency and overtones are located in a frequency range of low sensitivity of the ear.

Compared to other registers, treble tones are characterized by the noisiest attack and the fastest decay. It would be fair to say that the treble tones are the most non-steady ones in the piano, but with the most perceptually important transients [1,2]. Subjectively, the attack of a treble tone contains a distinct “knock”, which masks the string-born pitch and might even cause difficulties in tuning.

### 2. EXPERIMENTAL RESULTS

A typical spectrogram of a piano treble tone obtained using Key Elemetric type 730 sonagraph, is presented in Fig. 1. It shows the highest tone of the standard piano compass (C8 = 4 186 Hz), with level contours added at each 6 dB level.

The tone starts with a low frequency noise (AB fragment), which precedes the hammer-string contact. This noise is caused by the finger-key collision and following noisy contacts between the parts of the key action.

The BC fragment starts from the moment of hammer-string contact, and consists of a sharp attack noise with a wide spectrum up to the ultrasound frequencies. This noise suddenly drops at higher frequencies but not so in the lower frequency range, where the noise might be heard up to the end of the tone.

Over this noisy background the strings start to vibrate at their mode frequencies. The higher overtones of treble strings are highly inharmonic, but they are few and have very high frequencies. As they are located in a frequency range of low sensitivity of the ear, their inharmonicity is not perceptually significant.

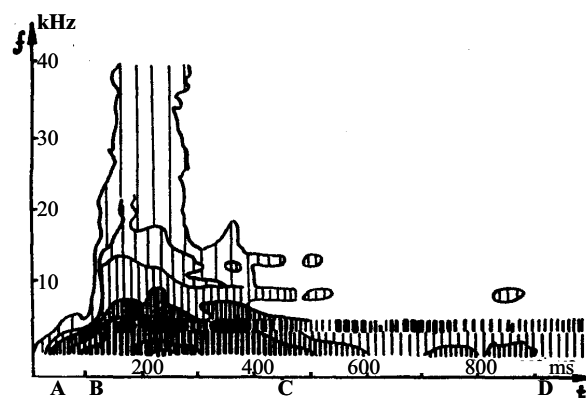


Figure 1: Spectrogram of a C8 piano tone (here recorded from a model Л-104 upright piano made by the Leningrad piano factory), contoured in 6 dB steps [3]

Being initially hidden in the noisy background, the string partials are almost free from the surrounding noise in the CD fragment. They become even more distinct after D, provided that the decay is not too fast.

When listening to the AB fragment only (e.g. by means of a sound file editor), it is perceived as a click. The BC fragment resembles a xylophone. The rest of the sound, when separated, is associated with something like a flute and has a distinct pitch.

When pianists are interviewed on the tone quality of treble tones, they often complain about “short-living” tones and a “deficiency of pitch clarity”, exposed in fast treble passages. Other definitions of low-ranked treble tones are “husky”, “knocky”, “glassy”, etc.

A plausible explanation of these impressions might be found in a non-optimal distribution of impact energy between the iron frame and the string [3]. Part of the hammer energy in a form of a wide-band short pulse, is transmitted via the very short part of the strings (down to about 1 mm long in the upper treble) directly to the iron frame and to a less extent – via a much longer part of the string – to the bridge and the soundboard. This creates

the initial knock in the piano tone (“knock element”). Another part of the hammer energy excites the transversal string modes that provide the pitch sensation (“tonal element”)<sup>1</sup>. While the hammer remains in the contact with the strings, its energy is transmitted both to the knock response of the piano structure and to the string vibrations. The longer the hammer contacts the strings (compared to the string period), the longer it serves as a damper blocking the string vibrations, and thus the later, weaker and shorter living will be the tonal element as compared to the concurrent knock element in the perceived tone. That is why the knock element is relatively more intensive in higher tones.

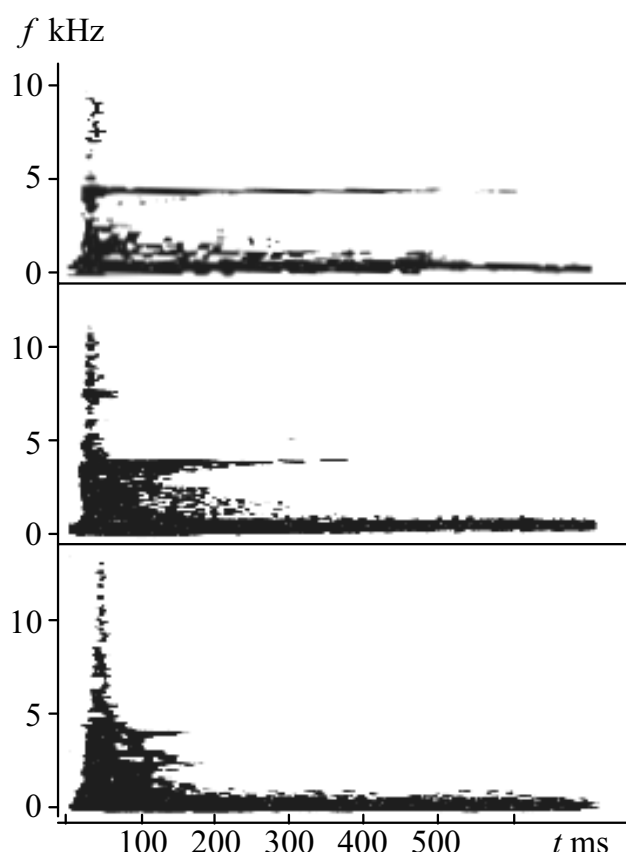


Figure 2: Sonograms of three C8 tones from: Steinway D concert grand, (top); Leningrad Piano Factory concert grand (middle); and a small upright made by Leningrad Piano Factory (bottom). The judged tone quality as obtained in listening tests decreases from top to bottom [1]

The sonograms in Fig. 2 allow comparison of C8 tones played on three pianos and rated as different in quality. The sonograms indicate that in a treble tone of higher quality we should expect:

- – The noise element is shorter-lived, of less intensity, and with narrower spectrum;
- ▣ The tonal element is longer-living, more intense, and less surrounded by noise.

<sup>1</sup> In later terminology by Serra [4] they would be called “stochastic” and “deterministic” elements, respectively.

So, the pitch of the treble tone manifests itself not immediately after the first moment of hammer-string contact, but after some weakening of the knock element.

Since the hammer blow is transferred to the metal frame almost directly (but delayed and modified when delivered to the soundboard) it is logical to expect that the audible response of the iron frame to the hammer blow defines the primary part of the knock element in treble tones. Several experimental evidences of that have been compiled:

1. Listening tests including tones from upright pianos of the same model but differing in the material of the frame (regular cast iron vs. an aluminum alloy) were conducted. It was easily recognizable that treble tones of these pianos differed in the “knock color”, while it was not so between two instruments with the same material of the frame.
2. It is possible to separate the knock from the tonal components of the tone mechanically just by dampening the strings by felt strips and adjusting the position of the hammer to hit the V-bar of the frame directly. For the A7 note of two pianos, the knock was separated and recorded in this manner, as well as regular tones. Fig. 3, showing the spectrum of the tones, obviously suggests that (a) the frequencies of the spectral maxima of the aluminum frame (“knocky” response) are quite different compared to those of the iron frame; and (b) these maxima are clearly present in the regular A7 tone of the same instrument.

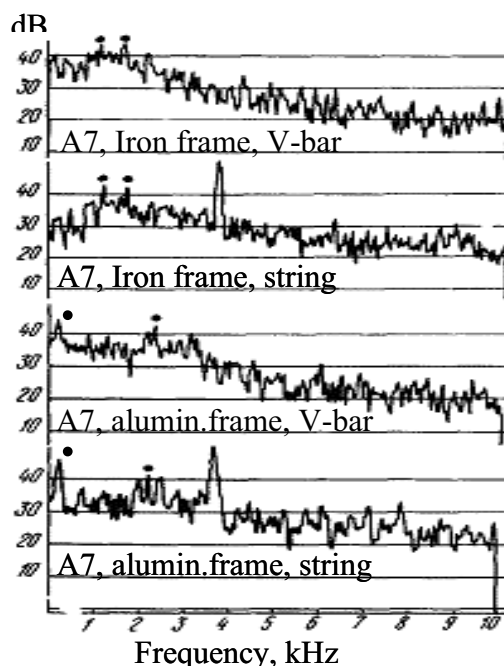


Figure 3: Spectral envelopes of A7 piano tones from two upright pianos. The upper pair relates to a piano with a cast iron frame, the lower pair to a piano with an aluminum alloy frame. The lower spectrum in each pair is an ordinary tone, while the upper is made with the hammer adjusted to hit against the V-bar directly with the strings damped by felt strips. The spectral maximum of the knock is obviously associated with the frame material [3]

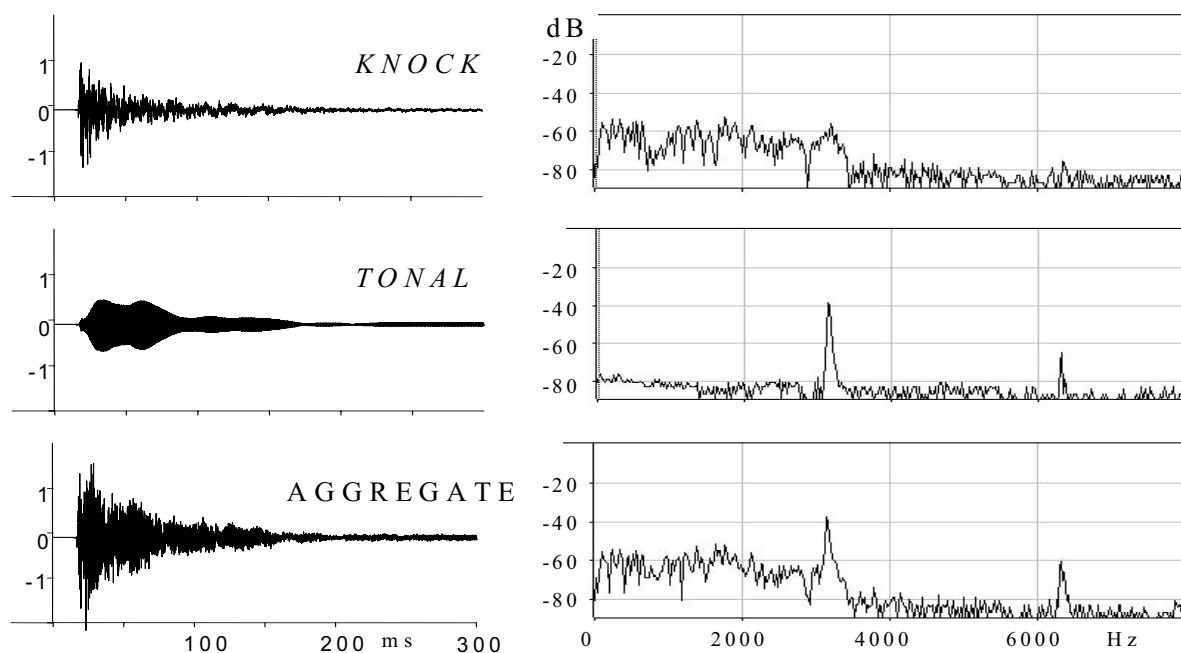


Figure 4: Waveform (left) and spectral envelope (right) of the knock and tonal element of a G7 piano tone

3. Six professional piano tuners (voicers) were presented with two different A7 knocks from the two (with aluminum and cast iron frame) pianos, followed by a regular tone from one of the pianos. The task was to recognize which of the two knocks were present in the tone. All tones in the C6 to C8 range from both pianos (50 tones altogether) were presented in a random order. No errors were made above G6. In the lower tones the errors were rather few. It was concluded that “it is perfectly clear that the knocks present in the treble tones are similar within each piano and differ between the two pianos. This difference is clearly associated with the different material of the metal frame”.

Another way to decompose the tonal and knocky elements in the frequency domain is by comb filtering. In this way time histories of a “signal-noise” ratio of the tones are obtained, which allowed to roughly discriminate between treble piano tones of different quality [5, 6]. Modern sound editing software allows an easy and effective sound demonstration [7] of the knock and tonal elements, first separated and then combined to form a real piano tone (Fig. 4). It was observed that both mechanical and electronic separation give the same sound result.

These data confirm our general conclusion that the quality of treble tones is connected with the temporal development of the energy ratio between the tonal element and the knock. The faster the “signal” prevails over the noise – the better is the attack. Another desired element of the treble quality is a durable tonal element – the longer the better. This duration in turn depends on the remaining energy of the string modes after it has been damped by the hammer, and on the losses due to dissipation at the string supports beyond the speaking length.

As the knock color of the treble tones is often attributed to the initial soundboard response to the hammer blow on the string

[2, 11], we refer to another pilot experiment conducted at the Leningrad piano factory. Six professional piano tuners (voicers) were asked to try two new upright pianos of the same model (104 cm high). Next, in absence of the subjects, 50 wooden wedges were tightly inserted into one of the pianos between the vertical beams of the wooden frame and the soundboard ribs in order to stiffen the soundboard. The subjects were informed about that something in the design related to the soundboard had been modified. Then the subjects were asked to play downward chromatic scales on both pianos, starting on the highest note (C8), until they had detected in which of the instruments the sound was unnormal. No subject could define that before he reached the 5th octave (below C6). In the lower registers the stiffening of the soundboard dramatically influenced the tone quality.

This experiment suggests that in the treble range the soundboard behaves as a part of the rigid wooden frame of the piano (the carcass) rather than as a membrane. This suggestion has later been supported by the results of a study by Kindell and Wang [12] who performed modal analysis and finite element analysis of a Baldwin concert grand (model SD-10). They found a low activity in the treble part of the soundboard.

After the earliest reports of these results [3, 5, 8-10] other authors have reported simple methods for objective assessment of treble tone quality. The first publication was by Smurzynski [13], who proposed as a physical correlate of quality of piano treble tones, a “dullness coefficient of the hammer impact,” defined as the squared ratio between the sound level of the tone with the partials removed, and the sound level of the original tone.

Another simplification was offered by Revvo [14], who suggested to judge the treble tone quality by the ratio between



the levels of the original tone and the same tone modified by mechanical damping of the strings.

Although simplification is useful in industrial applications, the methods by Smurzynski and Revvo do not include the transient character of the pitch formation in treble tones. Their simplified methods might be used only for evaluation of some "averaged" relative pitch clarity, which in the highest treble tones will not always correlate with a subjective rating of the tone quality. As seen from the sonograms on Fig. 1, the duration of the tonal element is important in treble tones, but it is not reflected in the overall envelope over the duration of the tone. Nevertheless, both Smurzynski and Revvo reported a significant correlation of the measured data with subjective ratings of the tone quality.

### 3. CONCLUSIONS

1. In the treble range, the pitch clarity (in present terminology paralleling "pitch strength") is an important subjective criterion of the tone quality, together with loudness and duration,
2. Objectively, the pitch clarity of a piano treble tone depends on how soon the fundamental tone and its overtones become audible above the initial transient noise (knock) to form a clear pitch sensation.
3. The iron frame is the most important design element defining the "color" of the knock in treble piano tones.
4. The hammer parameters, the location along the string (striking distance), and the duration of the hammer-string contact, are the primary adjustable factors determining the knock intensity and duration.

### 4. ACKNOWLEDGMENTS

Authors are indebted to the Wenner-Gren Foundation for the Visiting Professorship grant and to the Swedish Institute for the Visiting Research grant given to the first author, thus having made this publication possible.

### 5. REFERENCES

- [1] Galembo, A., The quality of piano tones, Legkaya Industriya Press, Moscow, 1987.
- [2] Bork, I., Marshall, H., and Meyer, J., "Zur Abstrahlung des Anschlag-geräusches beim Flügel. *Acustica* 81: 300-308, 1995.
- [3] Galembo, A. and Ivanovskaia, L., "Spectral time structure and noise sources in the high treble of the piano (in Russian)," Proc. 9th USSR Acoustical Conference, Moscow, pp. 37-40, 1977.
- [4] Serra, X., 'Sound hybridization techniques based on a deterministic plus stochastic decomposition model', Proc. Intl. Computer Music Conference, Aarhus, Denmark, 1994.
- [5] Galembo, A., "A method for objective evaluation of the timbre in the piano treble (in Russian)", Proc. 18th Acoustical Conference of Czechoslovakia, Český Krumlov, pp. 45-48, 1979.
- [6] Galembo, A., Askenfelt, A., Cuddy, L. L. (1998). "Inharmonicity and quality of piano ton," in Proc. of the International Symposium on Musical Acoustics (ISMA'98), Leavenworth WA, June 26 - July 1, 1998, p. 241-246.
- [7] Galembo, A., "Several demonstrations with piano tones," Invited report at the conference "Physics of Musical Instruments 2", Brighton, Great Britain, 2000.
- [8] Galembo, A., "Development of the methods for evaluation of a pitch clarity in musical (piano) sounds (in Russian)", doctoral diss., St. Petersburg Institute of Cinema and Television, 1995. Abstract in *J. Acoust. Soc. Am.* 101(4): 2397, 1995.
- [9] Galembo, A., "Device for evaluation of musical instrument quality", Invention certificate No. 828215, Cl. G 10 1/02, 1981. Bulletin for discoveries, inventions, trademarks and industrial designs (USSR), No. 17, p. 215, 1981.
- [10] Galembo, A., "Some data on the tonal structure of pianos (in Russian)", Proc. 4th USSR Scientific Technological Conference on Electrical Musical Instruments, part 1, Moscow, pp. 49-55, 1981.
- [11] Kondrashin, P., "Musical instruments at a microphone (in Russian)", *Zvukoregisser*, No. 1, pp. 45-50; No 3, pp. 62-68; No 4, pp. 56-62, 2001.
- [12] Kindell J. and Wang I., "Modal analysis and finite element analysis of a piano soundboard", Proc. 5th Intl. Modal Analysis Conference (IMAC), London, pp. 1545-1549, 1987.
- [13] Smurzynski J., "Objective and subjective measurements on treble piano sounds", Proc. Conference on Acoustical and Technical Aspects of Musical Instruments, Kraslice, Czechoslovakia pp. 91-95, 1983.
- [14] Revvo, A., "Criteria for objective quality evaluation of piano sounds (in Russian)", in book: *Novelties of musical instrument industry*, Scientific Research and Design Technological Institute of Musical Industry, Moscow, p. 180, 1988.

## PHASE RANDOMISATION IN PIANO BASS TONES

*Galembo, A.*

Setchenov Institute of Evolutionary Physiology and Biochemistry, St. Petersburg, Russia  
alex@speech.kth.se

*Askenfelt, A.*

Department of Speech Music and Hearing, Kungl Tekniska Högskolan  
andersa@speech.kth.se

### ABSTRACT

It has been shown that the timbre of synthesized multi-component harmonic bass tones with steady magnitude spectrum depends on the phase spectrum, particularly on the randomness of the relative phases between partials. For inharmonic spectra (as in a piano), the waveform is non-stationary due to the temporal evolution of the phase relations. This creates audible attack transients, which are characteristic for the particular starting phases [1].

The relevance of these findings for the perception of real piano tones has been unclear. A piano tone shows a complex dynamic evolution of the spectrum during attack and decay, which, besides inharmonicity, is influenced by the properties of the soundboard and room reverberation.

In this pilot study it is shown that frequency sweeps and associated pitch glides due to phase rotation introduced by string inharmonicity are present in real piano bass tones. The evidence of frequency sweeps is clear in the string and bridge velocities, and also in the radiated sound close to the piano, although to a lesser extent.

### 1. SYNTHESIZED TONES

A set of piano-like A0 tones was synthesized with two levels of spectral inharmonicity and five different starting phase relations between partials (Sine, Sine-Cosine alternate, Random, Schroeder and negative Schroeder).<sup>1</sup>

The spectrum of a real piano bass tone was mimicked by:

- Introducing inharmonicity typical for pianos (two extreme levels corresponding to a large grand and a small upright);
- Letting the spectrum envelope roll off gradually from maximum at the fundamental to almost zero at the 100-th partial;
- Punctuating the spectral envelope by a grouping of the partials with 7-8 partials in each group;
- Giving a progressive decay rate towards higher partials, resulting in a spectrum that gets narrower with time.

Analysis of the waveforms obtained (Fig. 1) revealed presence of frequency sweeps within each period (half-period for the alternate-phase tone), similar to those in the inharmonic tones with a steady flat spectrum [1], but more concentrated at the starting portion of the tone, where the spectrum is the widest.

---

<sup>1</sup> Schroeder-phase tones have monotonically increasing or decreasing phase across frequency (partial order).

Subjective evaluation of the tones presented over headphones (Sennheiser HD580 Precision) showed that:

- The pitch structure and timbre were less influenced by the starting phase relations compared to tones with flat steady magnitude spectrum, but all the perceptual characteristics found in these earlier cases remained audible.
- Tones with minimum inharmonicity ( $B = 60 \cdot 10^{-6}$ ) had different timbre of the attack and the decaying part, depending on a starting phase spectrum. The alternate-phase tone was perceived as higher in pitch compared to the other tones, or being brighter. The random-phase tone had a smooth timbre without specific clicks or pitch glides. Pitch glides were most audible in the Schroeder and negative-Schroeder tones.
- For the tones with maximum inharmonicity ( $B = 600 \cdot 10^{-6}$ ), the differences were even more reduced. The small differences that remained were concentrated to the attack part. The alternate-phase tone was sometimes reported as being somewhat brighter.

In short, in the synthesized tones we observed:

- The presence of quasi-periodic downward frequency sweeps. These sweeps are physical indications of the regularity of the initial phase spectrum<sup>2</sup>
- An audible timbral effect of well-behaved initial phase "rotation" by inharmonicity consisting of downward pitch glides. This effect disappears after a short time due to further phase randomisation.

Therefore, in our investigation of real pianos we will look for a presence of these frequency sweeps in the waveform and spectrogram of a tone.

### 2. IMPLICATION FOR PIANO ACOUSTICS

In a slightly simplified view, the string vibrations in the piano starts with zero displacement, the hammer impact exciting all string modes in one direction at the striking point. It is logical to expect that the piano string starts to vibrate with a regular phase spectrum, showing groups of in-phase partials.

---

<sup>2</sup> Podlesak and Lee [2] were probably the first to notice pitch glides in piano bass tones picked up from the string, while surprisingly being not found in the radiated tone. Recent studies revealed that these pitch glides are due to a dephasing of partials by string inharmonicity [1].

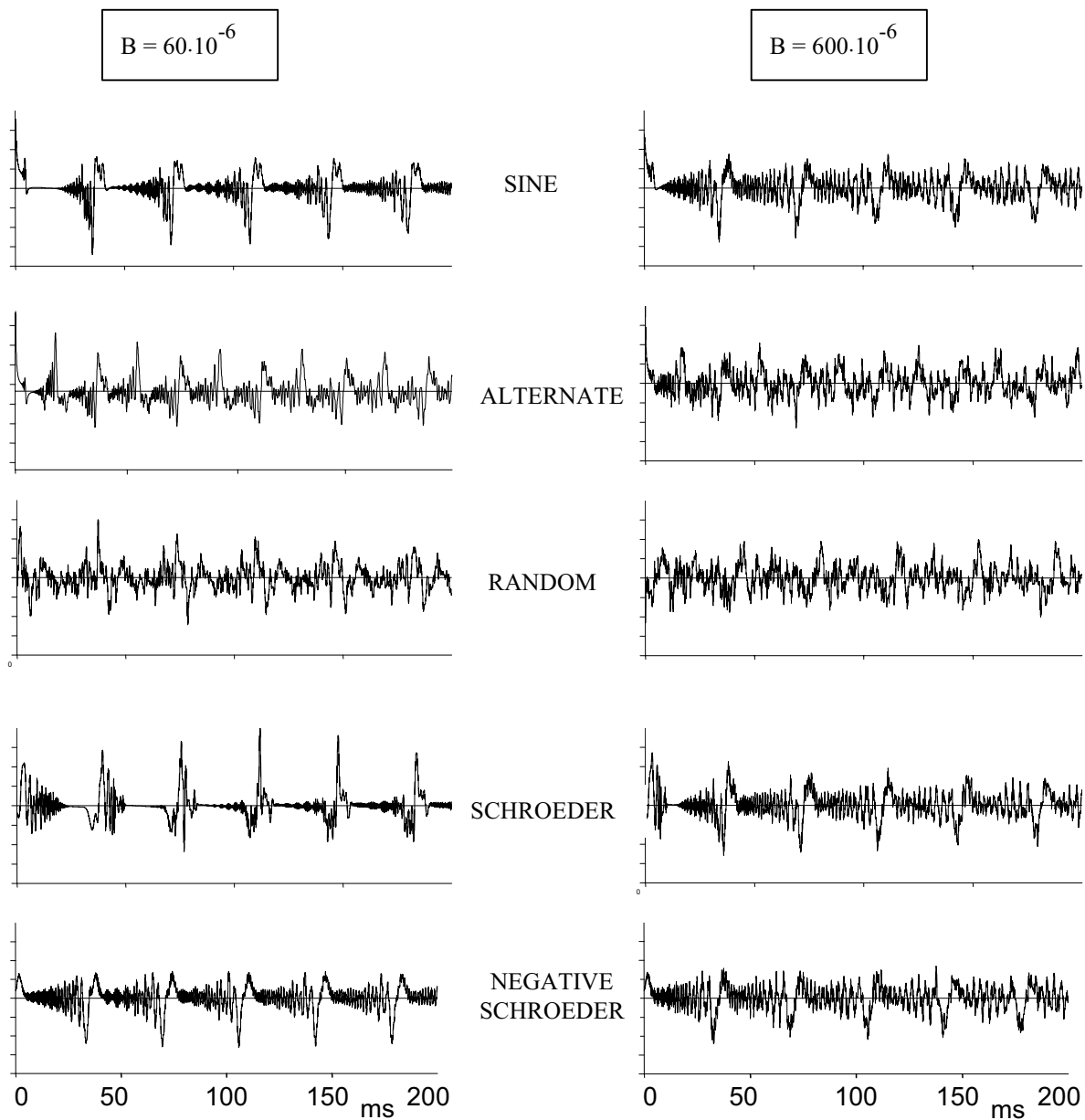


**Figure 1.** Waveforms of the first 200 ms of ten A0 tones consisting of 100 consecutive inharmonic partials with piano-like spectral dynamics. The tones differ in starting phases and amount of inharmonicity. The left column shows tones with low inharmonicity ( $B = 60 \cdot 10^{-6}$ ) and the right column tones with high inharmonicity ( $B = 600 \cdot 10^{-6}$ ). The starting phases are from the top: Sine, alternate, random, Schroeder, and negative Schroeder.

There are several active sources of phase randomisation in the formation of the piano tone after the string started to vibrate:

- The first is inharmonicity due to the string stiffness. The lower the inharmonicity coefficient and the lower the pitch, the slower the phases will be randomised, and the more distinctively the pitch glides will be audible as a temporal process.
- Another source of phase mixing is the soundboard, a distributed radiator. Waves in the soundboard, initiated at the bridge, propagate outwards and reflect repeatedly at irregularities in the soundboard (e.g. ribs, internal stress boundaries) and the edges.
- A specific source of phase mixing is the internal volume of the case of upright pianos.
- The last phase mixer is the room. A distant listener is exposed to all the mixing processes, while the pianist,

situating close to the soundboard, experiences the direct sound in higher proportion.

### 3. REAL PIANO TONES

For our pilot experiment we made multi-channel recordings of Bb0 tones (28.9 Hz) from a grand piano (Steinway C, 2.24 m) in a room with rather long reverberation time. The following signals were registered:

- the string velocity close to the hammer-string contact point (15 mm towards the agraffe), measured as the voltage generated across the string, vibrating between the poles of a magnet;
- the velocity of the bridge at the inner bridge pin, measured by an accelerometer;
- the sound pressure 20 cm above the point where the string crosses the bridge.

For reference and comparisons we synthesized a Bb0 multicomponent tone with a piano-like spectral dynamics (as explained above) having the same fundamental frequency (28.93 Hz) and inharmonicity coefficient ( $181 \cdot 10^{-6}$ ) as measured in the real piano tone. The waveform and spectrogram of the synthesized tone are presented in Fig. 2. The waveforms of the three measured signals and the synthesized tone are given in Fig. 3 for comparison. The corresponding spectrograms can be compared in Figs. 2 and 4.

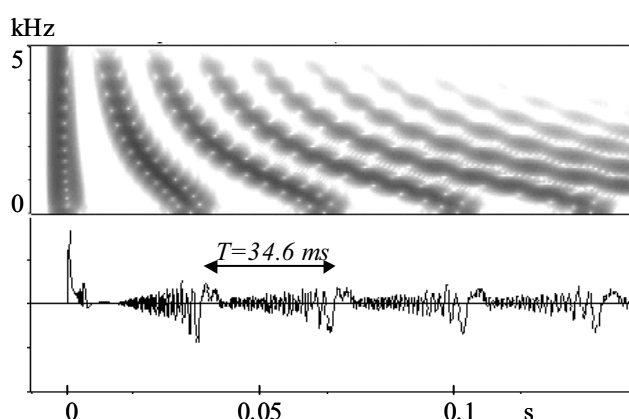


**Figure 2.** Synthesized Bb0 piano-like tone. Notice frequency sweeps due to the phase rotation by inharmonicity. The sweeps become slower, longer and more overlapping with time

Listening to the tones showed that the pitch glides, corresponding to the frequency sweeps in the spectrograms and waveforms, were most distinct in the synthesized tones, less audible in the signal picked up from the string, weakly audible in the signal picked up at the bridge, and not audible in the radiated sound at some distance from the piano.

### 4. DISCUSSION AND CONCLUSIONS

In this study, we have explored some effects of phase on pitch and timbre, which may be of relevance for bass piano tones. The evolution of the waveform and phase relations in the synthesized piano-like tone and real piano tones have noticeable similarities. The main observation is frequency sweeps in waveforms and spectrograms and corresponding pitch glides in the tone.

The experiments indicate that:

- Piano bass strings start to vibrate with regular phase relationships between partials;
- Inharmonicity induces frequency sweeps which repeat every fundamental “period” of the string;
- The frequency sweeps are better separated in time and thus more clear and distinct in the beginning of the tone, progressively overlapping over time;
- Frequency sweeps observed in the measurement data correspond to the pitch glides, which are most audible in the synthesized tone, but also heard in the signals picked up from the string and the bridge.

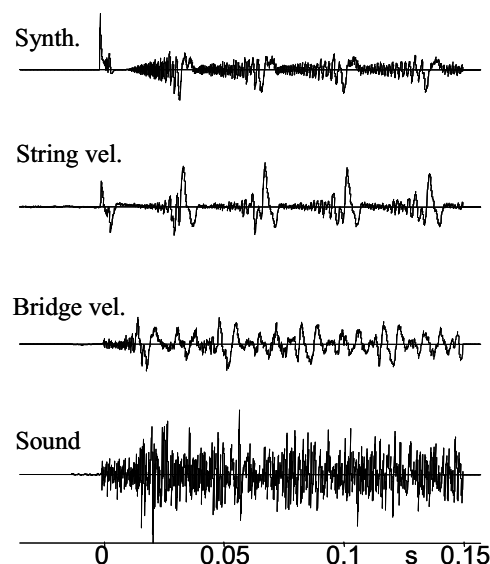


**Figure 3.** Comparison of signals (Bb0) picked up at three points in a grand piano and the synthesized tone (top)

Weak traces of frequency sweeps are identifiable even in the spectrogram of the radiated tone recorded close to the piano (20 cm above the string), but the corresponding pitch glides were not possible to hear out. This can partly be explained by the long reverberation of the room, in which the experiment was conducted. Absence of audible pitch glides in the radiated tone does not exclude a timbral effect of phase regularities in the tone – but this effect is much more difficult to investigate.

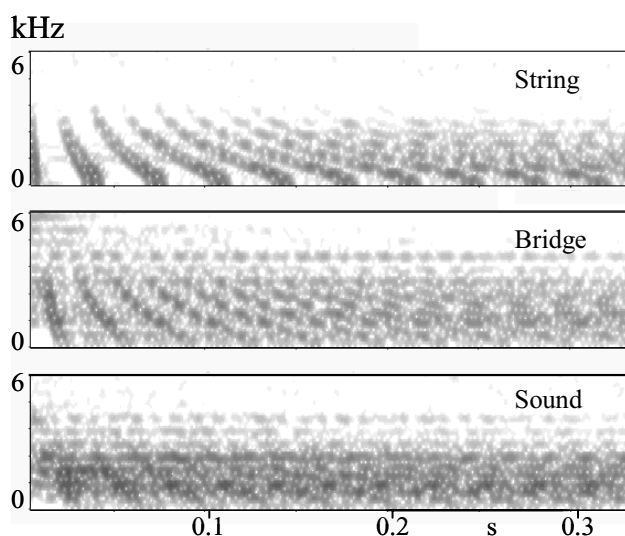


**Figure 4.** Spectrogram of a grand piano tone (Bb0) picked up at three stages of the tone formation. Notice that repeating frequency sweeps are distinct in the string and at the bridge vibration, and to some extent also present in the sound near the piano. Cf. the synthesized tone in Fig. 2.

Logically, there are more chances to hear out the timbral effect of phase mixing in a large grand piano, than in a small upright. The phase effect is concentrated to the attack, and a large soundboard gives a larger gap between the initial wave and the reflections from the edges of the soundboard, and consequently a slower phase mixing process. Further, a lower inharmonicity in the bass range, which is a characteristic of larger pianos, “rotates” the phases slower. The case of upright piano contributes to the rate of the phase mixing process. Narrower spectral bandwidth and less regular spectral envelop typical for small upright pianos are also expected to speed up the phase randomisation, making it less resolvable in time by the ear and thus weakening the impact of phase effects.

The influence of inharmonicity on the phase spectrum may explain, at least partly, the importance of the position of the pick-up on the soundboard when a piano is prepared with a contact microphone for amplification or recording. As the phase mixing effect due to the soundboard is lost, pitch glides can be recognised in the contact microphone signal for certain positions of the pick-up, for example when placed close to the bass bridge.

Another difference in the quality of piano bass tones that might be based on phase effects arises when listening to recorded piano music. The impression may be quite different when listening over loudspeakers (even of high quality) compared to listening over headphones, because the latter have much better phase characteristics [3].

We mentioned elsewhere [4] that due to the phase randomising in natural sounds by a reverberant environment, phase regularity between partials (defining the peak structure of the waveform) might convey evolutionary important distance information in species with phase-sensitive hearing.

A similar “distance” approach might be reasonable when discussing the quality concept of musical instruments. Tests of the quality of musical instruments, in particular the piano, often

show dramatic differences in judgement of the tone between the musician who is playing and a listener situated at some distance from the instrument. Some other psychological reasons for this difference have been presented recently [5, 6]. One probable acoustical reason might be that the pianist, being closer to the instrument, hears the tone with less randomised phase relations between partials than does the listener.

## 5. ACKNOWLEDGMENTS

Authors are indebted to the Wenner-Gren Foundation for the Visiting Professorship grant and to the Swedish Institute for the Visiting Research grant given to the first author, thus having made this publication possible.

## 6. REFERENCES

- [1] Galembo, A., Askenfelt, A., Cuddy, L. L., and Russo, F. A., "Effects of relative phases on pitch and timbre in the piano bass range", *J. Acoust. Soc. Amer.*, Vol. 110(3): 1649-1666, 2001.
- [2] Podlesak, M. and Lee, A. R., "Effect of inharmonicity on the aural perception of initial transients in low bass tones", *Acustica*, Vol. 68: 61-66, 1989.
- [3] Blauert, J. and Laws, P., "Group delay distortions in electroacoustical systems", *J. Acoust. Soc. Amer.*, Vol. 64: 1478-1483, 1978.
- [4] Galembo, A., Askenfelt, A., and Cuddy, L. L., "Observations on the effects of phase on pitch and timbre in the piano bass range", *Speech, Music and Hearing Laboratory Quarterly Progress and Status Report*, Dept. of Speech Communication and Music Acoustics, Royal Institute of Technology, TMH-QPSR 4/1998: 61-83, 1998.
- [5] Galembo, A., Askenfelt, A., and Cuddy, L.L., "On the acoustics and psychology of piano touch and tone", *Proc. 16th Intl. Congress on Acoustics*, Seattle, USA, 1998.
- [6] Galembo, A., "Perception of Musical Instrument by Performer and Listener (with application to the piano)", *Proc. of Intl. Workshop on Human Supervision and Control in Engineering and Music*, Kassel, Germany, pp. 257-266, 2001.

## MEASUREMENT AND REPRODUCTION ACCURACY OF COMPUTER-CONTROLLED GRAND PIANOS

Werner Goebel<sup>1,2</sup> & Roberto Bresin<sup>2</sup>

<sup>1</sup> Austrian Research Institute for Artificial Intelligence (ÖFAI), Vienna

<sup>2</sup> Department of Speech, Music, and Hearing  
Royal Institute of Technology (KTH), Stockholm

werner.goebel@oefai.at, roberto@speech.kth.se

### ABSTRACT

The recording and reproducing capabilities of a Yamaha Disklavier grand piano and a Bösendorfer SE290 computer-controlled grand piano were tested, with the goal of examining their reliability for performance research. An experimental setup consisting of accelerometers and a calibrated microphone was used to capture key and hammer movements, as well as the acoustic signal. Five selected keys were played by pianists with two types of touch (*staccato* and *legato*). Timing and dynamic differences between the original performance, the corresponding MIDI file recorded by the computer-controlled pianos, and its reproduction were analysed. The two devices performed quite differently with respect to timing and dynamic accuracy. The Disklavier's onset capturing was slightly more precise ( $\pm 12$  ms) than its reproduction (from  $-20$  to  $+30$  ms). The Bösendorfer performed generally better, but its timing accuracy was slightly less precise for recording ( $-9$  to  $3$  ms) than for reproduction ( $\pm 2$  ms). Both devices exhibited a systematic (linear) error in recording over time. In the dynamic dimension, the Bösendorfer showed higher consistency over the whole dynamic range, while the Disklavier performed well only in a wide middle range. Neither device was able to capture or reproduce different types of touch.

### 1. INTRODUCTION

Current research in expressive music performance mainly deals with piano interpretation because obtaining expressive data from a piano performance is easier than from other instruments. Pianists are able to control only a few parameters on their instruments. These are the tone<sup>1</sup> onsets and offsets, the intensity (measured as the final hammer velocity), and the movements of the two pedals<sup>2</sup>. Computer-controlled grand pianos are a practical device to record and to measure these expressive parameters and simultaneously provide a natural and familiar setting for pianists in a recording situation. Two systems are most commonly used in performance research: the Yamaha Disklavier and the Bösendorfer SE system.

The measurement results for the Yamaha Disklavier were already reported elsewhere [1] and are compared here with data from a Bösendorfer SE290 computer-controlled grand piano.<sup>3</sup>

<sup>1</sup>The onset of a sounding tone is very often called 'note onset', because of the MIDI world's terminology. In this paper, the terms 'tone' and 'note' are used synonymously, since we are not talking about musical notation.

<sup>2</sup>The middle or *sostenuto* pedal only prolongs certain tones and is not counted as an individual expressive parameter.

<sup>3</sup>For further introductory references, refer also to [1].

### 2. METHOD

The two computer-controlled grand pianos were the same as in [2]. For the experimental setup, equipment, calibration, and procedure, please also refer to [2].

In addition to the readings reported in [2], the **MIDI note onset time**, and the **MIDI velocity value** were taken from the MIDI file or the corresponding internal file format of the Bösendorfer. The onset differences between the original recording and the MIDI file, and those between the original recording and its reproduction were calculated<sup>4</sup>. Since the three measurements (original recording, MIDI file, and reproduction) were not synchronised in time by the measurement procedure, their first attacks were defined as being simultaneous. Care was taken that the first tones always were loud attacks in order to minimise synchronisation error, since timing error was smaller the faster the attack was. If there was a soft attack at the beginning, the files were synchronised by the first occurring louder attack (hammer velocity over 1 m/s).

### 3. RESULTS & DISCUSSION

#### 3.1. Timing accuracy

In Figure 1, the note onset delays of the MIDI file in comparison to the original recording are plotted against the recorded time separately for the two pianos. It is evident that both MIDI files show a constantly increasing anticipation over time. This timing error in the MIDI file was larger for the SE system than the Disklavier. The origin of this systematic timing error is yet unknown, but it is likely that the internal counters of the systems (in the case of the SE system, it is a personal computer) did not operate in exactly the desired frequency, probably due to a rounding error.

To illustrate the recording accuracy without this systematic error, the residual timing error (the differences between the fitted lines and the data) is plotted in Figure 2 separately for the two pianos against recorded MIDI velocity.<sup>5</sup> The variance was larger for the Disklavier than the SE system (Yamaha mean: 1.4 ms, standard deviation (SD): 3.8 ms; Bösendorfer mean: 0.2 ms, SD: 2.1 ms), but for both pianos, the residual timing error bore a trend with respect to the loudness of the recorded tones. The Disklavier tended to record softer tones later than louder ones, the SE showed the opposite trend, but to a smaller extent and with much less variation (Figure 2).

<sup>4</sup> $Delay_{MIDI} = t_{MIDI} - t_{orig}$ ;  $Delay_{repro} = t_{repro} - t_{orig}$ .

<sup>5</sup>In an earlier conference contribution, a different normalisation method was applied on the same data of the Disklavier [1].

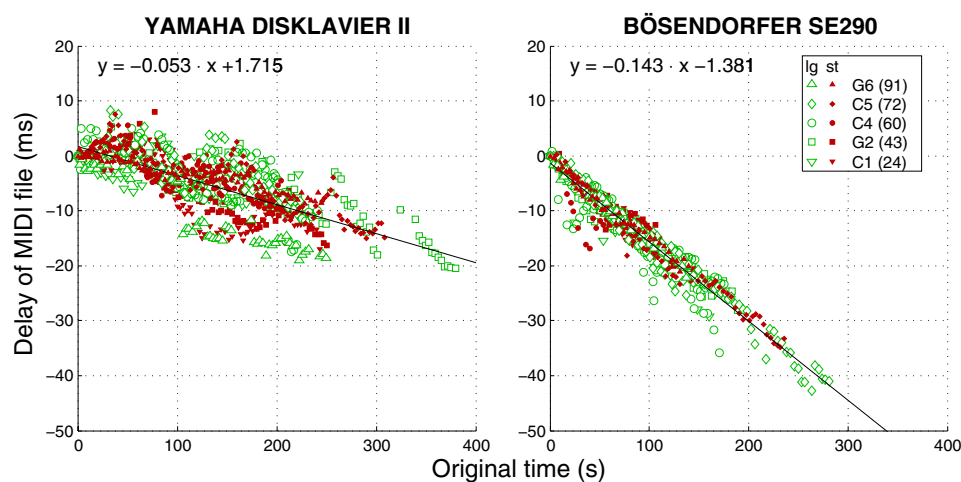


Figure 1: Timing delays (ms) as a function of recorded time (s) between the original recording and the MIDI file as recorded by the computer-controlled grand pianos for two types of touch: *legato* ('lg') and *staccato* ('st'). Negative values indicate that an onset in the MIDI file was earlier than in the original recording. The straight lines are linear fits of the whole data.

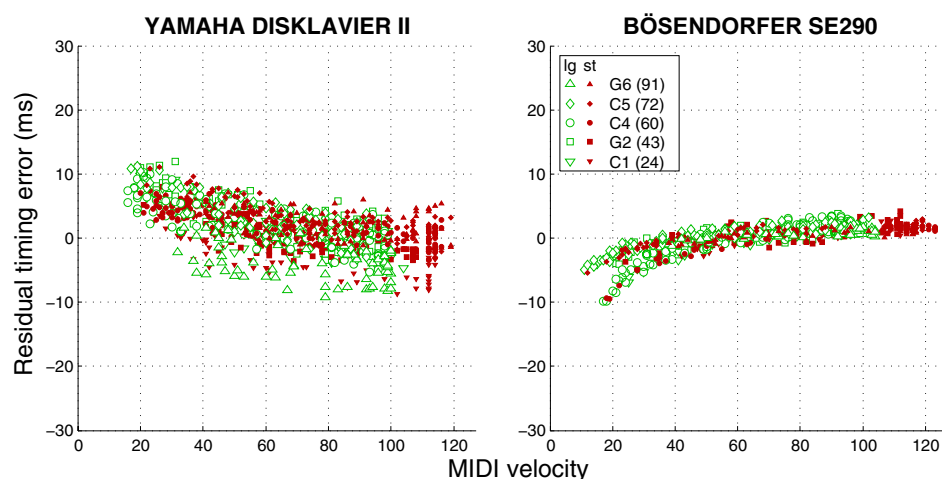


Figure 2: The residual timing error (ms) between the MIDI file and the original recording as a function of MIDI velocity, as recorded by the computer-controlled pianos. Again, negative values indicate onsets too early in the MIDI data, in comparison to the original file.

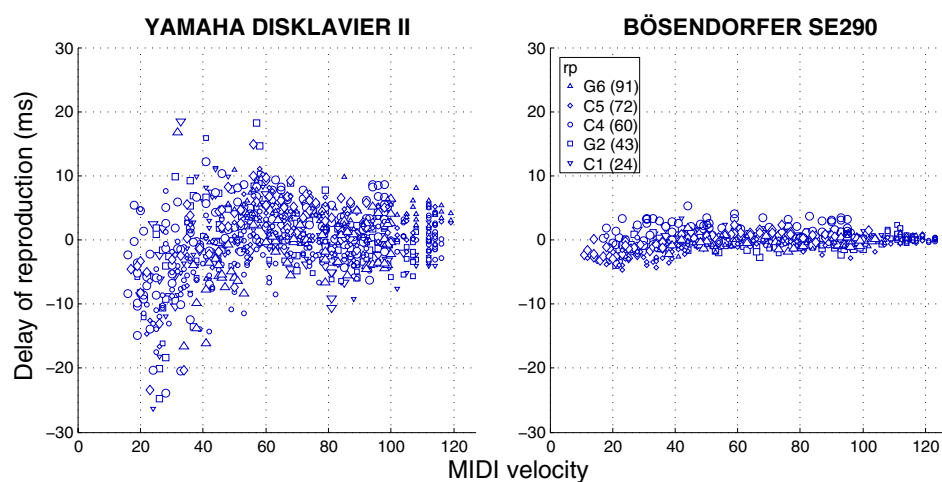


Figure 3: Timing delays (ms) between the original and its reproduction by the computer-controlled piano. (No systematic trend had to be removed.)

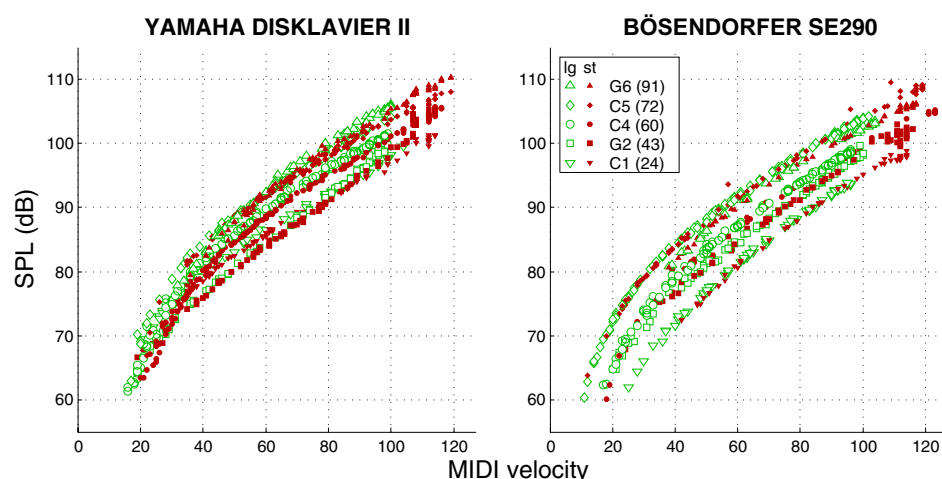


Figure 4: Peak sound pressure level (dB) against MIDI velocity as recorded by the two computer-controlled pianos. Different markers denote the five tones, different grey scales *legato* ('lg') and *staccato* ('st') touch.

The timing delays between the original recording and its reproduction are plotted in Figure 3 separately for the two pianos. There was no systematic timing error to remove in the data; the error in recording was evidently cancelled out by the same error in reproduction. The difference between the two systems becomes most evident in this display. While the reproduced onsets of the Disklavier can differ as much as +20 and −28 ms (mean: −0.3 ms, SD: 5.5 ms) from the actual played onset, the largest timing error of the SE system rarely exceeded  $\pm 3$  ms with a tendency of soft notes coming up to 5 ms too soon (mean: −0.1 ms, SD: 1.3 ms). Interestingly, the recording accuracy of the SE system was lower than its reproduction accuracy. Obviously, its internal calibration function aimed successfully to absolute precise reproducing capabilities. It could also be that the SE takes the first trip point (5 mm before the strings) as being the note onset, but calibrates itself correspondingly to overcome this conceptual mistake. However, this assumption was contradicted by information obtained by the SE's developer, W. Stahnke [3].

### 3.2. Dynamic accuracy

The second of the investigated parameters was dynamics which was measured in terms of the speed of the hammer hitting the strings (m/s) or peak sound pressure level (dB). Due to the limited space, we report here on the dynamic recording and reproduction capabilities only in terms of peak sound pressure level (dB–SPL). In Figure 4, dB–SPL is displayed against MIDI velocity units as recorded by the reproducing systems. On both instruments, different pitches exhibited different curves. The higher the pitch, the louder the radiated sound at the same MIDI velocity.

Peak dB–SPL as measured from the reproductions by the systems is plotted against dB–SPL as measured from the pianists' original recordings in Figure 5. It becomes evident that the Disklavier's solenoids were not able to reproduce very strong tones above a certain intensity. This varied slightly between keys, e.g. the G6 (with less hammer mass than hammers at a lower pitch) could be reproduced properly up to 107 dB, whereas a C1 (with a comparatively heavy hammer) only up to 93 dB. On the SE system, this ceiling effect could not be observed and there was no obvious effect of pitch as for the Disklavier. The superior reproduction of very loud tones for the Bösendorfer was due to its stronger solenoids. However, this does not explain why soft tones were reproduced considerably louder by the Disklavier, but very consistently by the Bösendorfer. Even silent notes were reproduced by the Bösendorfer, while this was not the case for the Disklavier.

## 4. GENERAL DISCUSSION

In this study, we measured the recording and reproducing accuracy of two computer-controlled grand pianos (Yamaha Disklavier, Bösendorfer SE) with an accelerometer setting in order to determine their precision for piano performance research. Both devices showed a systematic timing error over time which was most likely due to a rounding error in the system clock (the internal hardware at the Disklavier, a common personal computer at the SE). This linear error removed, the Bösendorfer had a smaller (residual) timing error than the Disklavier, but both exhibited a certain trend with respect to the loudness of the tones. The Disklavier tended to record soft tones too late whereas the SE had the tendency to record soft tones too early. But within these tendencies, the SE was more consistent. During reproduction, the superior performance of the Bösendorfer became more evident: the timing error was smaller than during recording whereas the Disklavier increased in variance in comparison to its recording.

The important point for performance research is the recording accuracy of these systems. Apart from the systematic error that only marginally affects the measured tempo value (0.0053% or 0.014%, resp.), the residual timing error (Fig. 2) was considerably large for the Disklavier and smaller for the Bösendorfer. The measurement precision could be improved by calculating out these trends using polynomial curve approximations.

To examine reproducing accuracy in the loudness dimension, we used peak sound pressure level as a measure. Here, the SE system revealed a much more precise reproducing behaviour over the whole dynamic range than the Disklavier. For the latter, the dynamic extremes flattened out, soft tones were played back too loudly and very loud tones too softly. The Disklavier's poor reproduction of loud tones was due to its smaller solenoids. Its reproduction of soft notes was limited, because the tested Disklavier prevented very soft tones from being silently reproduced with a minimum velocity matrix, adjustable by the internal control unit. It was also due to this function that the Disklavier was not able to reproduce silent notes at all, a crucial feature especially for music of the 20<sup>th</sup> century. The Bösendorfer exhibited linear reproducing behaviour over the whole dynamic range (from 60 to 110 dB SPL).

As another, and indeed very important criterion of recording and reproducing capability, we did not investigate the two pedals.<sup>6</sup>

<sup>6</sup>We are talking only of the right and the left pedal of grand pianos, since the middle pedal—the *sostenuto* pedal—only varies the tone length of certain keys depressed during its use, which is recorded and reproduced



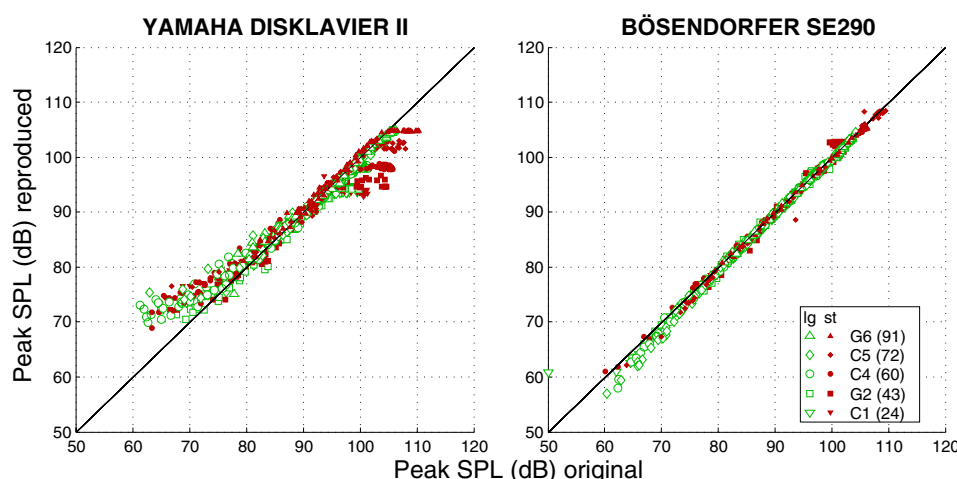


Figure 5: Peak sound pressure level (dB) as measured in the tones performed by the pianists (x axes) and reproduced by the computer-controlled pianos (y axes).

Both the Disklavier and the SE system are based on the same underlying principle. That is, to measure and reproduce movement of the piano action (and the pedals), in particular the final speed of the hammer before touching the strings. This principle is fundamentally different to what a performing artist does when playing expressively. The artist controls his/her finger and arm movements in order to reproduce a certain mental image of the sound by continuously listening to the resulting sound and by feeling the haptosensory feedback of the keys [4]. In this way, the performer is able to react to differences in the action, the voicing, the tuning, and the room acoustics, just to mention a few variables that have a certain influence on the radiated sound. On the other hand, a reproducing piano aims to reproduce a certain final hammer velocity independently of whether room acoustics, tuning, or voicing changed since the recording or not. Even if the reproduction takes place on the same piano and immediately after the recording, the tuning might not be the same anymore and the mechanical reproduction, as good as it might be, does not result in an identical sounding performance as the pianist played it before. This obvious limitation of such devices becomes most evident when a file is played from a different piano in a different room. Especially, if the damping point (the point of the right pedal where it starts to prevent the strings from freely oscillating) is a different one on another piano, the reproduction could sound too ‘wet’ or too ‘dry’. One possible solution to this problem could be a reproducing device with ‘ears’, in other words, the piano should be able to control its acoustical output via a feedback loop through a built-in microphone. If put into a different room, the device could check the room acoustics, its pedal settings, and its current tuning and voicing before the play-back starts, much the same as a pianist warming up before a concert. Such a system would require a representation of loudness or timbre other than MIDI velocity, indicating at what relative dynamics a certain note was intended to sound in a pianist’s performance.

The Disklavier measured in this study is certainly not the top model produced of the Yamaha corporation. Since then, Yamaha issued the Mark III series and the high end series, called ‘Pro’ (e.g., the special ‘Pro2000 Disklavier’). The latter series uses an extended MIDI format (with a velocity representation using more than 7 bits), and additional measures like key release velocity to reproduce the way the pianist released a particular key. It can be expected that these newer devices perform significantly better than the tested Mark II grand piano. Since these more sophisticated de-

vices were not available for the authors or were too far away from the accelerometer equipment, which was too costly to transport, this has to remain subject for future investigations.

## 5. ACKNOWLEDGEMENTS

This study was supported by the European Union (Marie Curie Fellowship, HPMT-GH-00-00119-02, the *Sounding Object* project (SOB), IST-2000-25287, <http://www.soundobject.org>, and the MOSART IHP network, HPRN-CT-2000-00115) and the START program from the Austrian Federal Ministry for Education, Science, and Culture (Grant No. Y99-INF). The Austrian Research Institute for Artificial Intelligence acknowledges basic financial support from the Austrian Federal Ministry for Education, Science, and Culture. We are indebted to Alf Gabrielsson and to the Bösendorfer company for providing the two instruments, and to Tore Persson and Friedrich Lachnit for maintaining and servicing them. Special thanks are due to Anders Askenfelt, Simon Dixon, Alexander Galembo, and Erik Jansson.

## 6. REFERENCES

- [1] Werner Goebel and Roberto Bresin, “Are computer-controlled pianos a reliable tool in music performance research? Recording and reproduction precision of a Yamaha Disklavier grand piano,” in *Workshop on current research directions in computer music, November 15–17, 2001*, Claudia Lomeli Buyoli and Ramon Loureiro, Eds., p. 45–50. Audiovisual Institute, Pompeu Fabra University, Barcelona, Spain, 2001.
- [2] Werner Goebel, Roberto Bresin, and Alexander Galembo, “The piano action as the performer’s interface: Timing properties, dynamic behaviour, and the performer’s possibilities,” in *this volume*, 2003.
- [3] Werner Goebel, “Melody lead in piano performance: Expressive device or artifact?,” *Journal of the Acoustical Society of America*, vol. 110, no. 1, pp. 563–572, 2001.
- [4] Alexander Galembo, “Perception of musical instrument by performer and listener (with application to the piano),” in *Proceedings of the International workshop on Human Supervision and Control in Engineering and Music, September 21–24, 2001*, p. 257–266. University of Kassel, Kassel, Germany, 2001, <http://www.engineeringandmusic.de/>.

by simply holding down the corresponding keys the same time this pedal was depressed.

## THE PIANO ACTION AS THE PERFORMER'S INTERFACE: TIMING PROPERTIES, DYNAMIC BEHAVIOUR AND THE PERFORMER'S POSSIBILITIES

Werner Goebel<sup>1,2</sup>, Roberto Bresin<sup>2</sup>, and Alexander Galembo<sup>2</sup>

<sup>1</sup> Austrian Research Institute for Artificial Intelligence (ÖFAI), Vienna

<sup>2</sup> Department of Speech, Music, and Hearing (TMH)  
Royal Institute of Technology (KTH), Stockholm

werner.goebl@oefai.at, {roberto,alex}@speech.kth.se

### ABSTRACT

A concert pianist is able to produce a wide range of imaginable nuances of musical expression by actuating the 88 keys on a piano, none of which travel through a distance greater than one centimeter. In this study, we investigated the temporal behaviour of grand piano actions from different manufacturers using different types of touch ('legato' versus 'staccato'). An experimental setup consisting of accelerometers and a calibrated microphone was used to capture key and hammer movements, as well as the acoustic signal. Five selected keys were played by pianists with the two types of touch. The analysis of the three-channel data was automated by computer software. Discrete measurements (e.g., finger–key, hammer–string, and key bottom contact times, hammer velocity) were extracted for each of the over 4000 recorded tones in order to study several temporal relations. Travel times of the hammer (from finger–key to hammer–string) as a function of hammer velocity varied clearly between the two types of touch, but only slightly between pianos. A travel time versus hammer velocity function found in earlier work [1] derived from a computer-controlled piano was replicated. Key bottom contact times exhibited larger variability between types of touch and pianos. However, no effect of touch type was found in the peak sound level (in dB as a function of hammer velocity).

### 1. INTRODUCTION

The grand piano action is a highly elaborate and complex mechanical interface, whereby the time and the speed of the hammer hitting the strings is controlled by varying the manner and the force of striking the keys. Its temporal parameters have been studied in detail [2, 3]. However, only exemplary data was reported so far.

The present study aims to collect a large amount of measurement data from different pianos, different types of touch, and different keys, in order to determine benchmark functions for performance research. The measurement setup with accelerometers was the same as used by [4], but the data processing procedure was automated with specially developed computer software in order to obtain a large and reliable data set. With the present setup, various temporal properties (travel time, key bottom time, time of free flight) and acoustic properties (peak sound level, rise time) were determined, only a few of which can be discussed here.

In a performance study on melody lead [1], finger–key onset times were inferred from the hammer–string onset times through an approximation of the travel times of the hammer (from finger–key to hammer–string contact) as a function of hammer velocity.

This travel time function was approximated from data of an internal chip of a Bösendorfer SE290 reproducing system. The present study also aims to reconsider that approximation.

### 2. METHOD

#### 2.1. Material

Three grand pianos by different manufacturers were measured in this study: A **Steinway grand piano**, model C, 225 cm<sup>1</sup>, a **Yamaha Disklavier grand piano** DC2IIXG, 173 cm<sup>2</sup>, and a **Bösendorfer computer-controlled grand piano** SE290, 290 cm<sup>3</sup>. Immediately before the experiments, all three instruments were tuned, and the piano action and—in the case of the computer-controlled pianos—the reproduction unit serviced.

#### 2.2. Equipment

The tested keys were equipped with two accelerometers: one fastened on the key<sup>4</sup> and one on the bottom side of the hammer shank.<sup>5</sup> Each of the accelerometers was connected with an amplifier<sup>6</sup> with a hardware integrator inside. Thus, their output was velocity in terms of voltage change. A sound level meter (Ono Sokki LA-210) placed above the strings of that particular key (approximately 10 cm distance) picked up the sound. The velocities of the key and the hammer as well as the sound were recorded on a multi-channel digital audio tape (DAT) recorder (TEAC RD-200 PCM data recorder) with a sampling rate of 10 kHz (16 bit). The DAT recordings were transferred onto computer hard disk into multi-channel WAV files (with a sampling frequency of 16 kHz). Further evaluation of the recorded data was done in Matlab programming environment with routines developed for this purpose (by the first author). The recording sessions were preceded by a calibration

<sup>1</sup>Situated at KTH-TMH in Stockholm (#516000, built in Hamburg, approx. 1992; this particular grand piano was already used in [5]).

<sup>2</sup>Situated at the Dept. of Psychology at Uppsala University (#5516392, built in Japan, approx. 1999; this series issued 1997 by Yamaha).

<sup>3</sup>Situated at the Bösendorfer Company in Vienna (#290-3, built in Vienna in 2000). The *Stahnke Electronics* (SE) system dates back to 1983 [6], but this particular grand piano was built in 2000. The same system used to be installed in an older grand piano (internal number 19-8974, built in 1986), but was put into a newer one for reasons of instrumental quality.

<sup>4</sup>Brüel & Kjær Accelerometer type 4393; 2.4 g; #1190913.

<sup>5</sup>ENDEVCO Accelerometer Model 22; 0.14 g; #20845.

<sup>6</sup>Brüel & Kjær Charge Amplifier Type 2635.

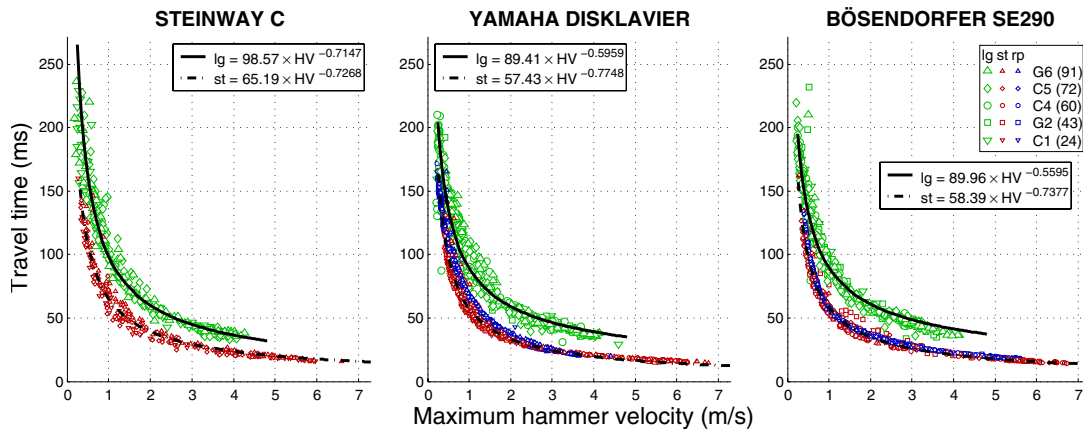


Figure 1: **Travel time** (from finger–key to hammer–string contact) against maximum hammer velocity for the three grand pianos (three panels), different types of touch (*legato*, *staccato*, and reproduction by the piano), and different keys (from C1 to G6, see legend). The two types of touch ('lg'–'st') were approximated by power functions (see legends). The travel time functions by the reproducing devices were similar to those produced by *staccato* touch.

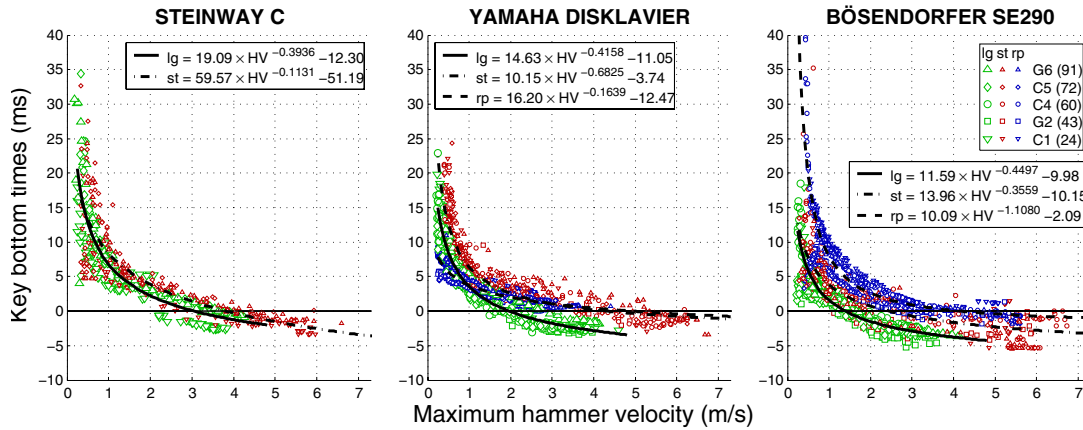


Figure 2: **Key bottom time** relative to hammer–string contact against maximum hammer velocity. Negative key bottom values denote instants *preceding* hammer–string contact. Legends list power curve fits of the data separately for legato ('lg'), staccato ('st'), and reproduction ('rp').

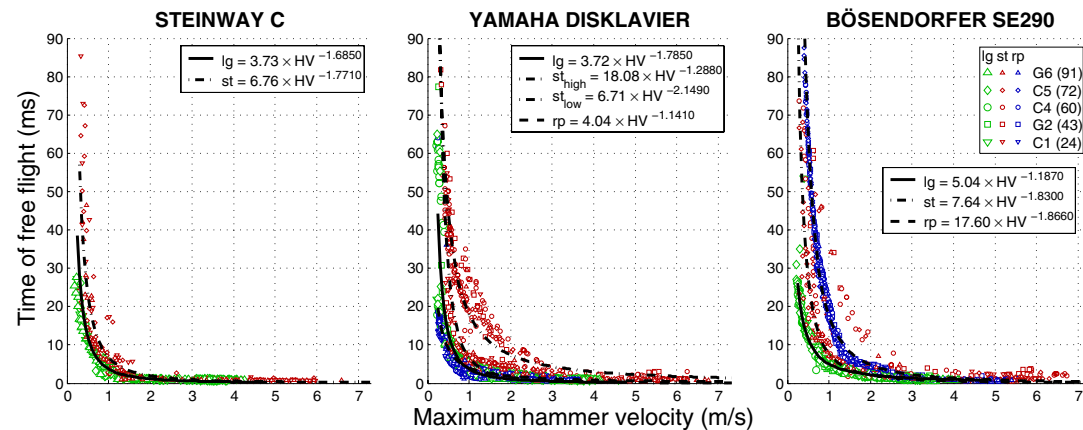


Figure 3: **Time of free flight of the hammer.** Time intervals between the point of maximum hammer velocity and hammer–string contact are plotted against maximum hammer velocity. Power functions were approximated for each type of touch ('lg', 'st', 'rp'). Two functions were fitted for the staccato data of the Yamaha.

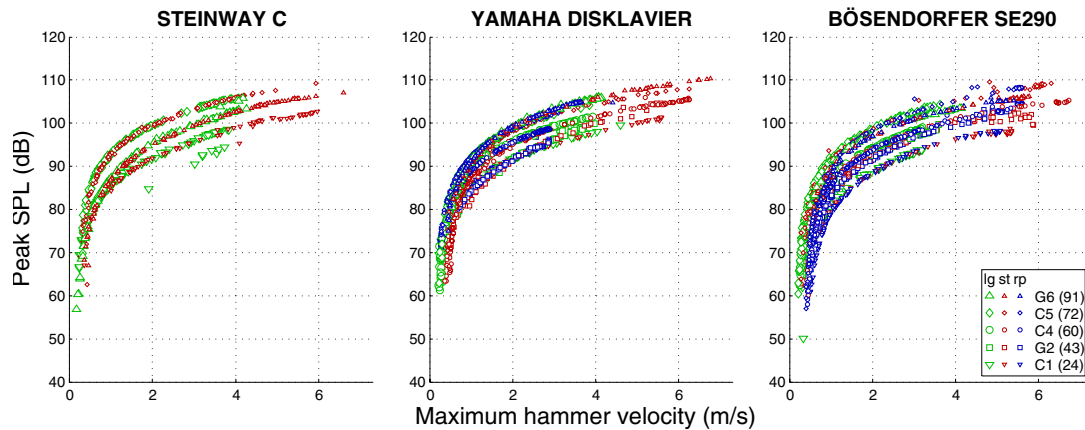


Figure 4: **Peak dB–SPL** values as a function of maximum hammer velocity for the three grand pianos (three panels), different types of touch (*legato*, *staccato*, and reproduction by the piano), and different keys.

procedure which allowed conversion from voltage changes into required units like meters per second or dB–SPL.

### 2.3. Procedure

Five keys distributed over the whole range of the keyboard were tested: C1 (MIDI note number 24), G2 (43), C4 (60), C5 (72), and G6 (91)<sup>7</sup>. The first two authors served as pianists to perform the recorded test tones. Each key was hit in as many different dynamic levels (hammer velocities) as possible, in two different kinds of touch: once with the finger resting on the surface of the key (*‘legato touch’*), once hitting the key from a certain distance above (*‘staccato touch’*), striking the key already with a certain speed.

Parallel to the accelerometer setting, the two reproducing pianos recorded these test tones with their internal device on computer hard disk (Bösendorfer) or floppy disk (Disklavier). For each of the five keys, each player played in each type of touch from 30 to 110 individual tones, so that a sufficient amount of data was recorded. Immediately after each recording of a particular key, the recorded file was reproduced by the grand piano, and the accelerometer data was recorded again onto the multi-channel DAT recorder. For the Steinway, 595 individual sound events were recorded, for the Yamaha Disklavier 1992, and for the Bösendorfer 1512 (including the reproduced keystrokes).

### 2.4. Data analysis

For each keystroke, several instants in time were defined as listed below and obtained automatically from the recorded data with the help of Matlab scripts.

The **hammer–string contact time** was defined as the moment of maximum deceleration (minimum acceleration) of the hammer shank (hammer accelerometer) which corresponded well to the physical onset of the sound, and conceptually with the ‘note on’ command in the MIDI file. In mathematical terms, the hammer–string contact is the minimum of the first derivative of the measured hammer velocity.

The **finger–key contact time** was defined to be the moment when the key started to move. It was obtained by a simple thresh-

old procedure applied to the key velocity track. In mathematical terms, it was the moment when the (slightly smoothed) key acceleration exceeded a certain threshold which varied relative to the maximum hammer velocity. Finding the correct finger–key point was not difficult for *staccato* tones (they showed typically a very abrupt initial acceleration). However, automatically determining the correct moment for soft *legato* tones was sometimes more difficult and needed manual correction. When this procedure failed, it failed by several tens of milliseconds—an error easy to discover in explorative data plots.

The **key bottom contact time** was the instant when the downwards travel of the key was stopped by the keybed. This point was defined as the maximum deceleration of the key (MKD). In some keystrokes, the MKD was not the actual keybed contact, but a rebound of the key after the first key bottom contact. For this reason, the time window of searching MKD was restricted to 7 ms before and 50 ms after hammer–string contact. The time window was iteratively modified depending on the maximum hammer velocity until the correct instant was found. MKD as indicator was especially clear and non-ambiguous when the key was depressed in a range of medium intensity.

The **maximum hammer velocity** (in meters per second) was the maximum value in the hammer velocity track before hammer–string contact. An **intensity value** was derived by taking the maximum energy (RMS) of the audio signal immediately after hammer–string contact, using a RMS window of 10 milliseconds. It was calibrated in order to obtain dB–SPL.<sup>8</sup> Data were controlled and inspected for errors with the help of an interactive tool that displayed simultaneously key and hammer velocity and the sound signal for each keystroke.

## 3. RESULTS & DISCUSSION

Travel times are plotted against the maximum hammer velocity in Figure 1 together with power curve approximations separately for the pianos and type of touch. It can be seen that the travel time functions varied considerably between the types of touch (the difference was of the order of 20 ms in the middle range), but only marginally between pianos. The travel time function of the

<sup>7</sup>Only three keys were tested at the Steinway piano (C1, C5, G6).

<sup>8</sup>B&K Sound Level Calibrator Type 4230; test tone 94 dB, 1 kHz.

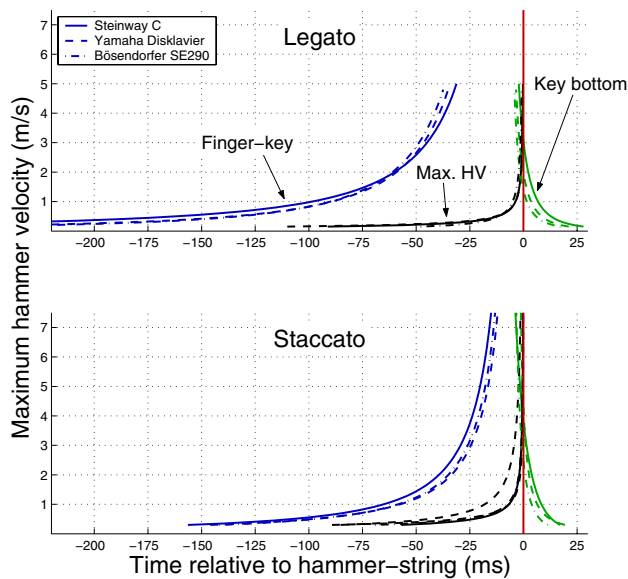


Figure 5: Temporal properties of three grand piano actions. Power curve approximations for the three pianos (line style), the two types of touch (panels), and for finger-key (left), maximum hammer velocity (max. HV, middle), and key bottom times (right).

Bösendorfer replicated the curve used in [1]. Legato keystrokes needed longer time to produce a sound than staccato keystrokes that produced equally fast attacks. Moreover, the softest notes were performed with legato touch, the loudest with staccato. Accelerating the keys in legato manner did not allow to generate hammer velocities far beyond 4 m/s.

Key bottom times are plotted relative to hammer-string contact in Figure 2 (negative values denote key bottom contact *preceding* the hammer-string contact). The data for legato, staccato, and reproduction were approximated by power functions. The data clusters were clearly distinct for the two types of touch on the Yamaha and the Bösendorfer, but almost overlapping on the Steinway.

The instant of the escapement was calculated as the maximum of the hammer velocity. This was a good estimation for strong and medium keystrokes but not for keystrokes when the escapement can occur before the hammer maximum velocity. The time interval between the escapement and the hammer hammer-string contact was calculated (Figure 3). With escapement, the pianist loses control over the tone. The point of maximum hammer velocity coincided well with the escapement point for medium and fast keystrokes, but was earlier for slow keystrokes. The time of free flight was almost zero beyond hammer velocities of 1.5 m/s for the Steinway, and beyond 3 m/s for the Yamaha and the Bösendorfer. On the Yamaha, the staccato data splits into two groups at medium intensities: maximum hammer velocity occurred at two different instants (Figure 3, middle panel).

In Figure 4, peak SPL values are plotted against maximum hammer velocity. The data formed different groups for different tones, but overlapped almost entirely between legato and staccato keystrokes. This indicates that the sound level of the tones does not depend on the way the tone was produced, but exclusively on the hammer velocity.

In Figure 5, all approximations reported above are plotted in a

single display. It becomes evident that type of touch affected the shape of the curves more than the instrument.

#### 4. CONCLUSIONS

This contribution provided benchmark data for the temporal properties of different grand pianos under two touch conditions. The temporal properties varied considerably between type of touch, only marginally between pianos, and not at all between the different tested keys. The temporal differences between a *pp* and a *ff* tone can become as large as 200 ms, between types of touch about 20–30 ms. A pianist must not only adapt to the intended dynamic level, but also to the kind of touch in order to control the precise timing of the produced tone.

Generally, a keystroke starts for the pianist kinesthetically with finger-key contact (the acceleration impulse by the finger) and ends at key bottom, but for the audience it starts with the hammer-string contact. Although these three points in time can be apart from each other as far as 200 ms, they might not be perceived as separate events. The intrinsic timing properties of a particular piano might be an important factor pianists have to get acquainted with when they ‘warm up’ on a yet unknown instrument.

#### 5. ACKNOWLEDGEMENTS

This study was supported by the European Union (Marie Curie Fellowship, HPMT-GH-00-00119-02, the *Sounding Object* project (SOB), IST-2000-25287, <http://www.soundobject.org>, and the MOSART IHP network, HPRN-CT-2000-00115) and the START program from the Austrian Federal Ministry for Education, Science, and Culture (Grant No. Y99-INF) and a visiting grant from the Swedish Institute for the third author. The Austrian Research Institute for Artificial Intelligence acknowledges basic financial support from the Austrian Federal Ministry for Education, Science, and Culture.

#### 6. REFERENCES

- [1] Werner Goebel, “Melody lead in piano performance: Expressive device or artifact?,” *Journal of the Acoustical Society of America*, vol. 110, no. 1, pp. 563–572, 2001.
- [2] Anders Askenfelt and Erik V. Jansson, “From touch to string vibrations,” in *Five Lectures on the Acoustics of the Piano*, Anders Askenfelt, Ed., vol. 64, pp. 39–57. Publications issued by the Royal Swedish Academy of Music, Stockholm, 1990.
- [3] Anders Askenfelt and Erik V. Jansson, “From touch to string vibrations. I. Timing in grand piano action,” *Journal of the Acoustical Society of America*, vol. 88, no. 1, pp. 52–63, 1990.
- [4] Anders Askenfelt and Erik V. Jansson, “From touch to string vibrations. II. The motion of the key and hammer,” *Journal of the Acoustical Society of America*, vol. 90, no. 5, pp. 2383–2393, 1991.
- [5] Anders Askenfelt and Erik V. Jansson, “From touch to string vibrations. III. String motion and spectra,” *Journal of the Acoustical Society of America*, vol. 93, no. 4, pp. 2181–2196, 1992.
- [6] Robert A. Moog and Thomas L. Rhea, “Evolution of the keyboard interface: The Bösendorfer 290 SE recording piano and the Moog multiply-touch-sensitive keyboards,” *Computer Music Journal*, vol. 14, no. 2, pp. 52–60, 1990.

## THE PRETRANSIENT OF THE HARPSICHORD SOUND. I. THE VERTICAL MOVEMENT OF THE PLECTRUM.

Tino Gäumann

Laboratoire de chimie physique moléculaire  
Ecole Polytechnique Fédérale de Lausanne  
tino.gaeumann@epfl.ch

dedicated to Nicole Hostettler

### ABSTRACT

The harpsichord time transient on the microphone starts after the string excited bridge and soundboard. These processes take a few milliseconds. However a small “pretransient” precedes the main transient on the microphone. According to the position of the microphone, it can even appear before the string has excited the bridge. It is shown that at least part of this pretransient match the vibration of the plectrum after the string jumped off. Whereas the transient signal is practically independent of the type of the plectra and the player, and reflects only the vibrating string, transformed by the frequency dependent impedances of the bridge and soundboard, this pretransient depends on the quality of the plectrum and the player. The first and in most cases the largest contribution is in the frequency range between 3 and 8kHz and corresponds to the vibration of the plectrum. It is tentatively proposed that this precursor is responsible for the particularities of the instrument and the harpsichordist.

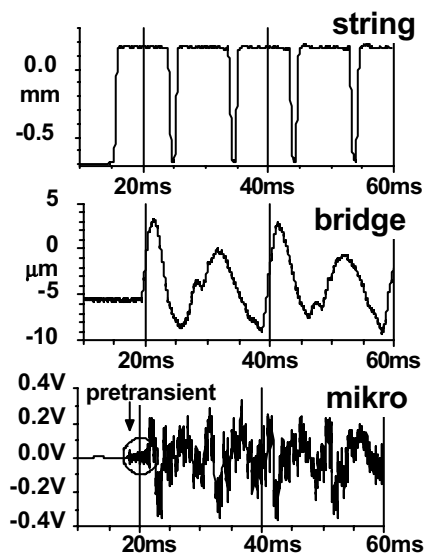


Figure 1: The time signal of the vertical movement of the string (A2), the bridge, and the microphone, crow quill plectrum.

### 1. INTRODUCTION

In the harpsichord a plectrum, usually of Delrin or crow quill, lifts and jumps off the string that transmits its pulsing vibration to the bridge, where it excites the emitting soundboard. It results a very fast rising transient that decays in a few seconds. It embraces the characteristic harmonic spectrum of the triangular form of the excited string that extends to the ultrasound region. The vertical and the horizontal movement of the string are excited simultaneously in a ratio of roughly 2:1 that depends on the instrument. This transient is very reproducible and allows no dynamic variation. The form of the time signals of string, bridge and microphone is shown in Figure 1. The frequency dependent impedances of the bridge and soundboard transform the pulsed string movement. The time signals of bridge and microphone are delayed by a few milliseconds from the jump-off of the plectrum. However an exact inspection of the microphone signal discloses the presence of a smaller signal that precedes the main transient and does not show up in the bridge signal.

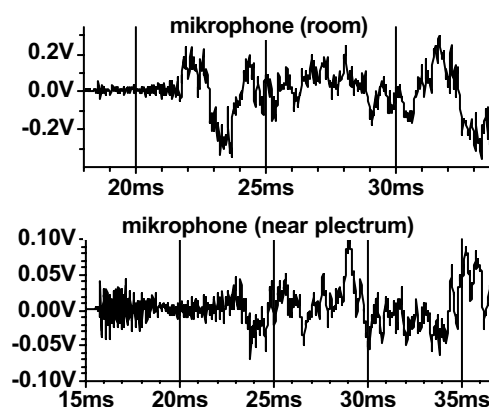


Figure 2: The enlarged time signal for two positions of the microphone: at 1m above the soundboard and at 7cm from the plectrum.

We call it the pretransient. It is to be distinguished from the pretransient that can be observed before the string changes its direction of movement as it is described by Valette & Cuesta [1].



This signal in the kHz range depends strongly of the hardness of the touch of the player. In the present work a smooth touch of the key was always used such that the pretransient described by these authors does not show up.

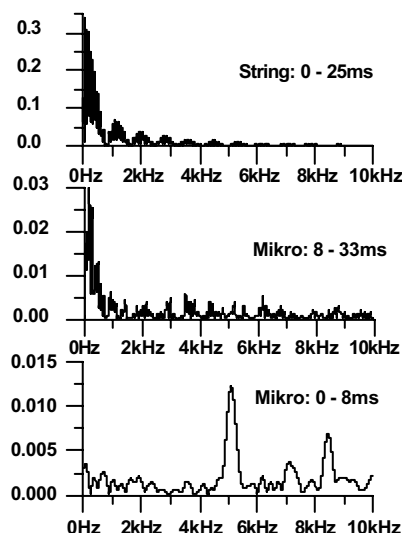


Figure 3: The Fourier Transform of the signals of string, microphone and the pretransient of the microphone.

## 2. SEPARATION OF PRETRANSIENT AND TRANSIENT

The amplitude of the pretransient is – depending on the position of the microphone – up to a factor of ten smaller than that of the transient. It precedes the transient by several milliseconds, but it extends also into the transient; this makes an analysis difficult (Figure 2, mikro room). Since the emission of the pretransient does not pass through the bridge, a placement of the microphone near the plectrum should favor the pretransient as is demonstrated in Figure 2. Two things are visible: firstly are the main frequencies in the pretransient much higher (in the kHz range) than the lower harmonic of the string signal (period of the 1<sup>st</sup> harmonic 10ms), secondly several signals with different start times contribute to the pretransient. It is possible that signals that do not originate near the plectrum are not visible in this case. It may also be mentioned that the contribution of the higher harmonics in the transient signal is relatively important in the start of the transient, but their decay is very fast.

## 3. THE FREQUENCY DOMAIN

The Fourier Transform (FT) of the signals of string, transient and the “separated” pretransient are presented in Figure 3. The string amplitudes correspond to a Fourier series of a triangular waveform. The maximum amplitude as a function of the measurement position on the string increases linearly from zero from the nut on the wrestplank to the plectrum position, stay

constant up to a point that corresponds to the distance front-plectrum, but measured from the bridge, and then decreases linearly to nearly zero on the bridge (see [1], Figure 2.6a). The maximum string amplitude is about 4mm in the bass and 0.35mm in the treble range.

The FT of the microphone signal in the room contains mainly the different harmonics of the fundamental, albeit with different intensities, depending on the position of the microphone in the room and the conditions of the FT. A closer inspection of the frequency range reveals the presence of a number of “nonharmonic” frequencies with smaller amplitudes; some of them correspond to combination frequencies of lower harmonics [2, 3], harmonics of the longitudinal frequency and their modulation with the vertical frequency, and some of unknown origin. However, none agrees within the error limits to the frequencies that are observed in the pretransient (see later).

The FT signal for the pretransient suffers from the very low frequency resolution of the FT because of the short pretransient signal. This has also the effect of a highpass filter. The most important frequencies are an isolated nonresolved group around 5kHz.

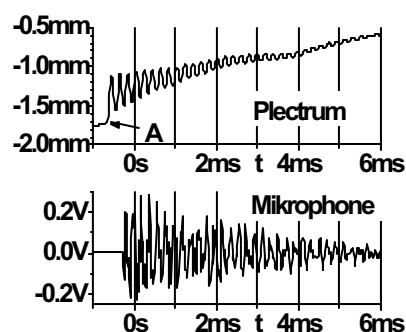


Figure 4: The time signals for a Delrin plectrum and a microphone placed near this plectrum.

## 4. THE ORIGIN OF THE PRETRANSIENT

When the plectrum touches the string, it acts as the tangent of the clavichord and excites a vertical movement. This movement corresponds to a frequency that is about 10% higher than the fundamental vertical frequency. Its presence is badly reproducible and difficult to see. Also a longitudinal frequency between ten and twenty times higher than the vertical frequency is sent to the bridge; its transmission to the bridge is faster than the vertical movement and can be easily observed with an accelerometer on the bridge nut.

The movement of the plectrum has been measured with Laser trigonometry (see later). In the moment the plectrum lets go the string it makes an upward jump of about 0.6mm (A in Figure 4) and starts to vibrate with an initial amplitude of 0.4mm and frequency of about 5kHz. This signal decays with a time

constant of 2ms and its frequency increases with time by 20Hz/ms. This movement is shown in Figure 4, together with the pretransient observed on the microphone. It can be seen that the same signals are observed on the plectrum and the microphone: it just follows that the microphone picks up the signal from the plectrum. Thus at least part of the pretransient signal corresponds to the vibration of the plectrum after the jump-off of the string.

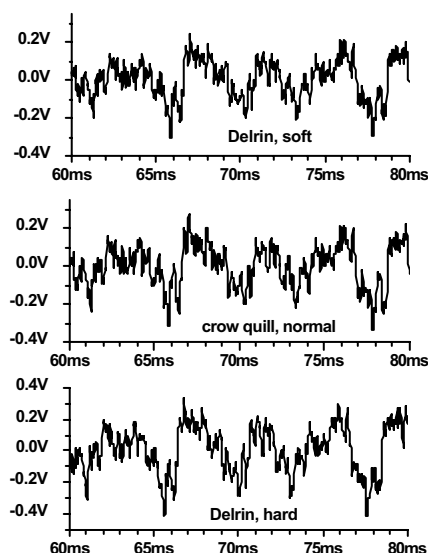


Figure 5: The microphone signal of the transient for different plectra.

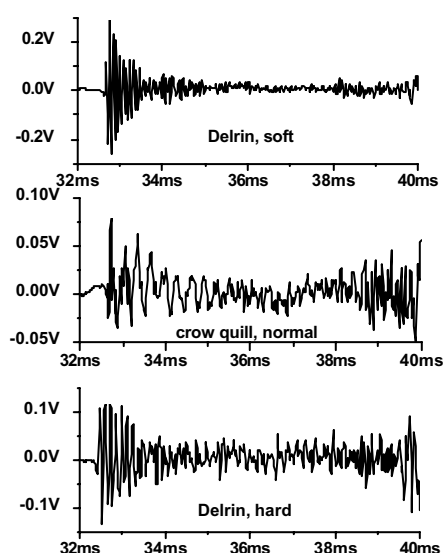


Figure 6: The microphone signal of the pretransient for different plectra.

## 5. THE INFLUENCE OF THE PLECTRUM

Several plectra of Delrin or cow quill were prepared; the width of one Delrin plectrum is very narrow and gives rise to a “soft” tone, another is thicker and wider resulting in a “hard” tone. The crow quill plectrum corresponds to the “normal” plectrum of the instrument. Part of the time transients of these three plectra are shown in Figure 5: it is astonishing to realize that with the exception of an amplitude difference for the “hard” plectrum that results in a somewhat “louder” tone the transients are identical: the tone quality does not change with the quality of the plectrum within reasonable limits! This does not seem to correspond to the experience one gets when voicing a harpsichord.

This situation changes drastically when the pretransient is measured (Figure 6). The three plectra differ in their vibration and the time constant of decay as well. Other frequencies are seen.

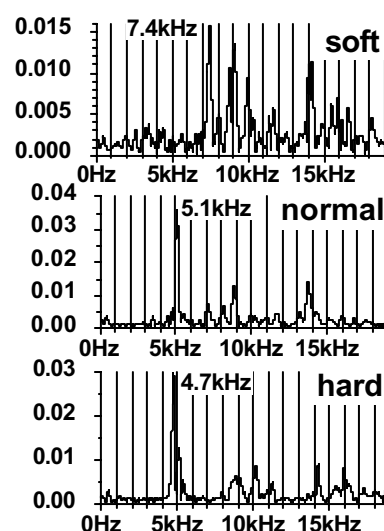


Figure 7: The Fourier Transform of the pretransient (8ms) for Delrin plectra of different design.

## 6. FREQUENCIES OF PRETRANSIENTS

The FT of three different Delrin plectra was measured. The same plectrum material was used for all three in order to have similar conditions for the pretransient. In addition, length and windowing of the FT were identical. Especially windowing has the effect of increasing the weight of the central position of the transient. It can be noticed in Figure 7 that one single frequency between 4 and 8kHz stems out. It corresponds to the vibration frequency of the plectrum that depends heavily on its geometry. However other frequencies of unknown origin are also present.

FT of short transients suffers among other defaults from the low frequency resolution. The Matrix Pencil method (MP [4,5]) has the advantage to offer a higher resolution; but it has several other defects that are not inherent in FT. So it may be expected



that the use of both methods might yield a good average of reality. Results for the initial amplitude and its decay time for the pretransients of the microphone and the plectrum signal are presented in Figure 8. It is evident that the “plectrum” signal contains several neighboring frequencies that are not discernible in Figure 7. Knowing this, one can try to resolve the FT signal around 5kHz into several Gaussian peaks. The results are given in Figure 9. The nonlinear approximations that are used in deconvoluting a peak are not very trustworthy, but the results correspond to the outcome obtained with the help of the MP method; thus they seem to be real.

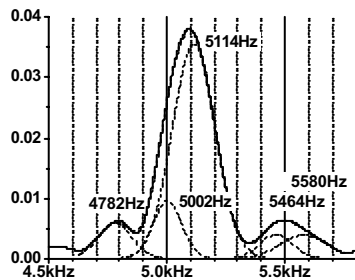


Figure 8: Some Matrix Pencil results (initial amplitude and decay time-constant (circles)) for the movement of a Delrin plectrum and its corresponding microphone signal.

## 7. EXPERIMENTAL

The harpsichord is an instrument of an Italian type, one manual, two 8' registers, constructed by von Nagel, Paris. Plectra of Delrin and crow quill of different design were used. The left string of A2 (104Hz, brass, 0.33mm diameter) was measured. The vertical elongation of the string, bridge and plectrum were determined by laser triangulation, with laser ranges from 0.5 to 4mm, 5-10kHz bandwidths, and corresponding noise levels between 0.04 and 0.3μm. The signals were digitized with 18bit resolution and a sampling frequency of 51kHz.

The frequency transformation was performed either by Fourier transform (FT) (several times zero padded, Kaiser windows of different orders) or by the Matrix Pencil method (MP) [4,5]. For short transients with mostly nonstationary signals, FT suffers from very low frequency resolution and the enhancement of the middle part of the time transient when windowing is used. The frequency value depends on the marginal conditions. The MP method is based on the Eigenvalue determination of rectangular matrices that limits its use to less than  $N < 10k$  data points because of computer capacity. The larger dimension of the matrices is  $N-1$ , the smaller optimally  $\sim N/3$ . The number of positive Eigenvalues used corresponds roughly to the double of the number of frequencies searched for (a rather vague value!) and their decay constant  $\tau_0$  that is assumed to be exponential. A least-squares calculation yields the initial amplitude  $A_0$  and the phase. The assumptions of the MP

method are not less stringent than FT, but different and the frequency resolution is higher.

## 8. CONCLUSIONS

The tone of a harpsichord can be divided into a small, short pretransient and a transient. The latter is responsible for the main portion and substance of the harpsichord sound. It is typical for the vibrating string within the instrument. The pretransient, which lasts less than 20ms, is characteristic for the voicing of the instrument and the touch of the player.

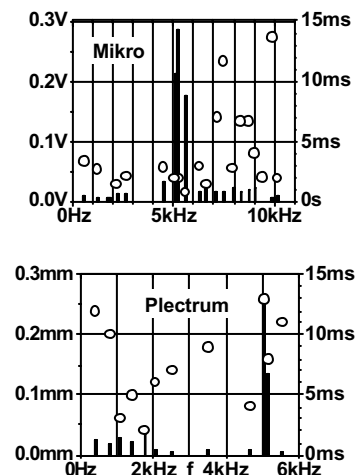


Figure 9: The deconvolution of the main peak in the FT of a pretransient into different Gaussian peaks. Compare with Fig. 8.

## 9. REFERENCES

- [1] Valette, Claude, and Cuesta, Christian., “Mécanique de la corde vibrante”, HERMES, Paris, 1993.
- [2] Conklin, Harold A. jr., “Piano design factors – their influence on tone and acoustical performance”, “The acoustics of the piano”, Ed. Askenfelt, Anders, Royal Swedish Academy of Music, Publ. No. 64, 1990, pp. 190-238
- [3] Conklin, Harold A. jr., “Piano string and “phantom” partials”, J. Acoust. Soc. Amer., Vol. 102, 1997, p. 659.
- [4] Hua Yingbo, and Sarkar, Tapan K., “Matrix Pencil Method for Estimating Parameters of Exponentially Damped/Undamped Sinusoids in Noise”, IEEE Trans. Acoustics, Speech and Signal Processing, Vol. 38, 1990, pp.814-824.
- [5] Laroche, Jean, “The use of the matrix pencil method for the spectrum analysis of musical signals”, J. Acoust. Soc. Amer., Vol. 94, 1993, pp. 1958-1965

## SONOLOGICAL ANALYSIS OF HARPSICHORD SOUNDS

Andreas Beurmann and Albrecht Schneider

Institute of Musicology, University of Hamburg, Germany  
Aschneid@uni-hamburg.de

### ABSTRACT

Sounds recorded from four historical harpsichords were subjected to sonological analysis. The aim is to investigate as well as to document sound characteristics of historical instruments. Sound analysis has been complemented by some vibroacoustic measurements.

### 1. INTRODUCTION

The acoustics of harpsichords have been the focus of a number of studies published over the past 25 years. Besides a general description of design and performance parameters relating to the string, the soundboard, string-soundboard coupling, etc. [1], special investigations have addressed, among other topics, attack transients, string velocity and the interaction of longitudinal and transversal string forces [2, 3, 4, 5, 6], the impedance of the bridge [7], the response of soundboards to external excitation [8] and the role of air and structural modes found in historical harpsichords as well as in modern replicas [7, 8, 9]. Methods employed include impulse response measurements and modal analysis in particular of soundboards [e.g., 7, 8, 9], yet also registration of the string velocity by means of induction [6]. The temporal evolution of longitudinal and transversal string forces acting on the bridge have been studied in a model to explain, among other phenomena, „precursor“ components found in the string motion immediately after excitation [4, 5, 12]. Sounds recorded from instruments have been subjected to spectrum analysis. Also, the directivity pattern of sound energy radiated from a particular harpsichord has been investigated. Though our knowledge of harpsichord acoustics has been greatly improved over the past decades, a full understanding of all relevant mechanisms of vibration including linear and nonlinear coupling between parts, damping factors etc. will be difficult to achieve because of the complex geometry of harpsichords as well as the number of parts which can contribute to the overall pattern of vibration.

The data presented in this paper were obtained from investigations of historical harpsichords housed in the collection of one of the authors [10]. The instruments chosen for this study are a one-manual Italian harpsichord made in Livorno by a certain Pierluigi ..., in 1579, a two-manual instrument built in the Flemish tradition by Andreas Ruckers (senior), in 1628, a two-manual French harpsichord whose maker is Nicolas Pigalle (Dijon 1771), and a two-manual English Jacob Kirckman which was built in London, in 1766 [11].

The basic mechanism of sound generation in a harpsichord is fairly well understood from the theory of plucked strings [1, 6, 7]. Depressing a key leads to raising the respective jack which carries a plectrum. This plectrum plucks the string which is first raised (whereby its shape becomes triangular, and both the length and the tension of the string increase), and then slips from

the tip from the plectrum which itself undergoes bending downwards. The amount of bending down to the position where the string is actually released depends on the shape of the plectrum as well as on material parameters (stiffness, static friction of the plectrum's surface). Both the bending of the plectrum and the restoring force of the string can be assumed to be roughly proportional to the deflection of the string. The deflection process of the string, the relevant forces, and the wave propagation in the string are discussed in [4, 5, 7, 12]. Because of the string slipping sideways from the plectrum, in addition to transversal motion perpendicular to the soundboard also parallel motion and even some torsional motion of the string seem possible. Further, longitudinal modes of the string can be detected in the short segment of vibration preceding transversal string motion known as „precursor“ [5, 13].

### 2. MEASUREMENTS

#### 2.1 Stationary spectrum

In the long term average spectra (LTAS) of harpsichord sounds notches occur where partials due to the actual relation of string length  $L$  to plucking point  $l$  are weak or completely cancelled out. Since a pulse travels on the string from the point of excitation to the bridge and to the nut (where it is reflected), the spectrum of the string has minima for partial frequencies at ratios  $L/l = k, 2k, \dots, nk$ . As an example, Figure 1 shows the spectrum of the  $C_2$  (tuned to 52 Hz) recorded from the Ruckers. Since the relation of  $L:l$  is 1672:182 mm or 9.187:1 for  $C_2$ , partials no 9, 18, 28, 37, 46, 55 etc. are weak or even disappear. Hence the spectrum is more or less periodic with maxima and minima of energy.

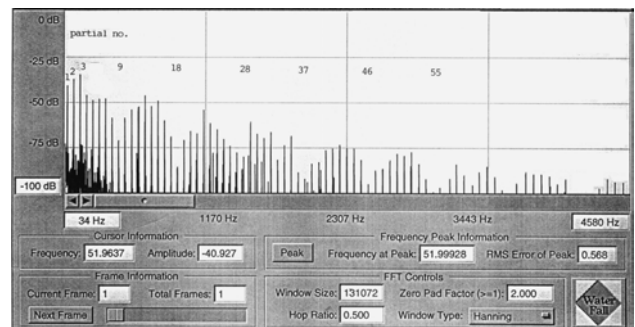


Figure 1: LTAS (131072 pts, Hanning), Ruckers 1628,  $C_2$ , (recording: U 67, V 76, 48 kHz/16bit).

## 2.2 Soundboard and bridge: aspects of excitation

Impulse responses of the soundboard (basically a thin plate clamped at the edge) of the Italian harpsichord, the Ruckers and the Pigalle were measured in that impulses were applied along the length of the 8'-bridge by means of an impact hammer. The response was recorded with an accelerometer placed, in most cases, at that part of the soundboard which has minimum stiffness [9]. In many 8'+4'-instruments, this is the region between the 8' bridge and the 4' hitchpin rail (e.g., Ruckers, Pigalle), in instruments having only one or two 8' registers, the part of the soundboard which can vibrate more freely is larger, and is found stretching from close to the bridge almost halfway to the nut.

As a rule, responses yield many discrete modes as can be seen, for example, in the spectrum of a response recorded from the Livorno 1579. Figure 2 shows eigenmodes in the frequency band from 0 to 2 kHz. For 14 peaks in the range from 100 to 420 Hz, the frequency readings are given in Fig. 2.

Since the soundboard (spruce) is thin, it adapts rapidly to forced vibrations transmitted to it from the string via the bridge. Therefore, the periodicity inherent in the string vibration is soon established also in the vibration pattern of the soundboard. This process is illustrated in Figure 3 which shows the autocorrelation function (ACF) for the note  $C_2$  played on the Livorno 1579. The vibration of the soundboard has been recorded with an accelerometer. The ACF clearly reflects the period  $T$  of the note  $C_2$  which is  $T \sim 870$  samples  $\sim 18$  ms  $\sim 55$  Hz. However, within the three initial periods  $T_1 - T_3$  (Fig. 3) there is considerable variation which can be attributed to the still transient nature of the vibration before a stable regime sets in.

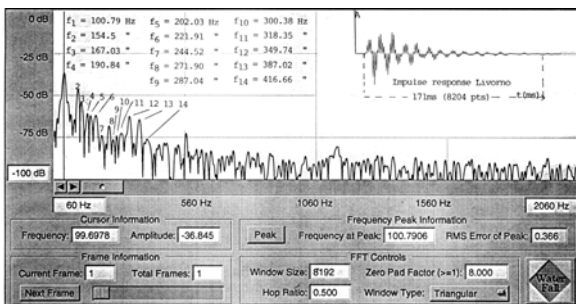


Figure 2: Livorno 1579, impulse response of soundboard, 0-2 kHz.

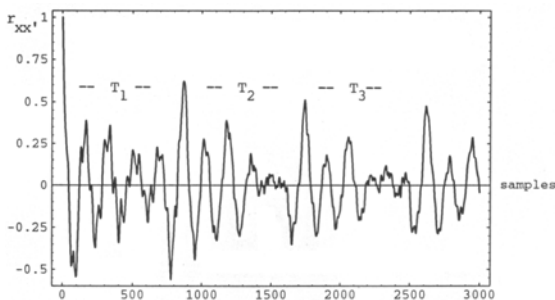


Figure 3: Livorno 1579, ACF for  $C_2$ , accelerometer on soundboard, 3000 samples

Since soundboard vibration can incorporate a multitude of eigenmodes, excitation can be achieved well with a pulse from the string which contains many partials. For example, the spectrum of the excitation pattern observed at the 8'-bridge of the Pigalle immediately after vibration has been started through energy transfer from the string in fact includes a large number of partials. In Figure 4, the spectrum of the note  $C_2$  ( $f_1 \approx 52.54$  Hz in the tuning chosen, with  $A_4 = 372$  Hz) measured with a small accelerometer (weight 0.7 g) placed against the side of the 8' bridge contains considerable energy up to almost 18 kHz. The spectrum is fairly periodic; its centroid is close to 7 kHz.

## 2.3 Attack transients

When recording sounds from a harpsichord with a condensor microphone sensitive to small changes in sound pressure, the initial portion of the time function of such sounds typically can be segmented into four phases: (A) the noisy sound of the spectrum pressed against the string before it is released to vibrate; (B) the time from the point of release to the beginning of periodic vibration, that is, the transient portion during which coupling of longitudinal and transversal motion can generate unstable vibrations (including precursors); (C) first full period, which sometimes is a bit distorted in waveshape as compared to (D) stable periodic vibration. The process sketched here is illustrated in Figure 5, which in its lower part gives the time function for the note  $A_1$  (fundamental freq.  $\approx 51$  Hz in the tuning chosen, with  $A_4 = 408$  Hz) recorded from the Kirkman 1766 (8', lower manual). Section A lasts for 11 ms, the attack section B covers another 11 ms, followed by the first full period C which is about 19 ms long (since  $T = 1/f$ , with  $f_1 \approx 51$  Hz,  $T$  must be close to 19 ms). From D on, vibration is quasiperiodic with small variation in waveshape and period length, respectively.

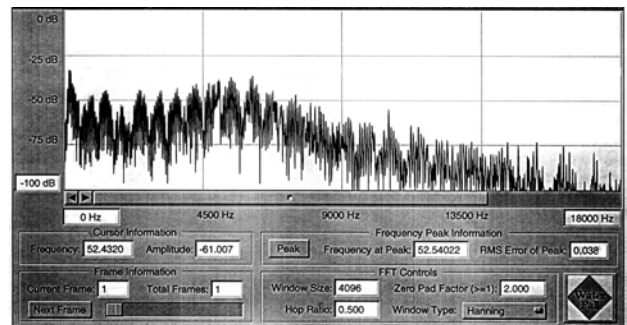


Figure 4: Pigalle 1771, excitation pattern recorded with accelerometer at the bridge, 0-18 kHz

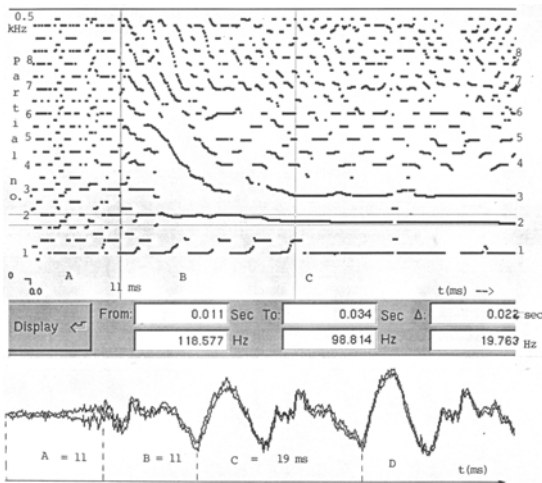


Figure 5: Kirckman 1766, A<sub>1</sub>, time function and attack transients. Wigner-Ville-transform (2048 pts, Hop: 7 pts ~ 0.146 ms), LPC (Markel & Gray), 0-0.5 kHz

This sound has been subjected to an analysis based on the Wigner-Ville-transform [14] to allow for better temporal resolution than would be possible with conventional STFT. A LPC algorithm which traces spectral peaks has been employed. Most of the spurious components resulting from Wigner cross terms  $W_{xy}(t, \omega)$  have been suppressed so that eight partials can be identified in the spectrogram (frequency range 0 – 500 Hz) which can be segmented into sections A (11 ms), B and C in regard of the temporal and spectral evolution of the sound in question. From the Wigner spectrogram it appears that during the transient attack portion there are some downward frequency shifts of partials as can be expected from the release of the string after it had been elongated. Since the tension of the string increases up to the point of release, the frequencies of partials should be higher at the onset of vibration as well, and should decrease with time. The process is documented in Figure 6 which traces the fundamental frequency of the note C<sub>2</sub> ( $f_1 \approx 60.8$  Hz) recorded from the Kirckman. Readings have been obtained from 20 frames of DFT of 4096 pts each; with a hop ratio of 0.1, thus ca. 252 ms of sound have been covered. The frequency at peak for  $f_1$  for each frame is calculated using parabolic interpolation.  $F_1$  of the note C<sub>2</sub> drops from 62.97 Hz in frame 1 down to 60.26 Hz in frame 20 which means a glide of ca. 76 cents.

The sharp attack of harpsichord sounds results from the deflection and sudden release of the string which itself contains many partials in its spectrum after onset of vibration. For example, the Bb<sub>2</sub> string of the Ruckers ( $L/l = 1344:159$  mm, tuned to ca. 90 Hz) when recorded with a magnetic pickup placed over the jack has some 70-80 partials (which result from transversal motion of the string) in its spectrum which contains energy up to 8.4 kHz. Since transversal motion of the string effects most of the energy transfer to the bridge and the soundboard, the 80 or so partials cause the bridge and soundboard to vibrate in various modes. (The input impedance of the bridge for the Bb<sub>2</sub> of the Ruckers is rather low compared to most of the neighbouring notes [7]). Hence the sound radiated from the instrument can be expected to contain a large number

of spectral components in particular at the moment of excitation as is shown in Figure 7 (see next page) for the first 200 partials of the Bb<sub>2</sub> recorded with a microphone ca. 0.5 m above the soundboard. In the 3D-plot, section A is the time where the plectrum rests against the string that is thereby raised with the tension growing; section B spans from the actual release of the string to 1 sec. of the recording. In section B the exponential decay of higher harmonics soon after the attack can be seen.

The spectral centroid (Figure 8) for 200 harmonics goes up to 4.9 kHz in section A, and to ca. 7.3 kHz for the very short attack phase at the beginning of B after which it falls rapidly to be followed by a smooth decay curve.

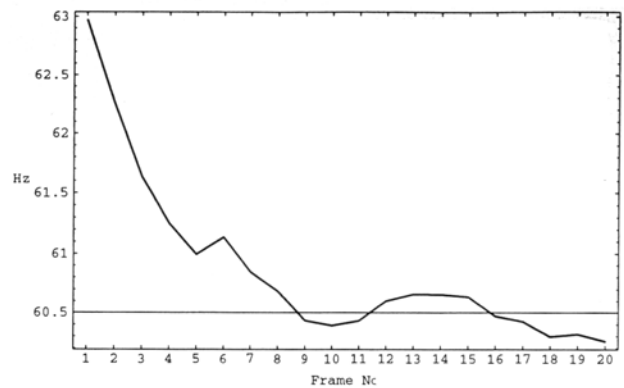


Figure 6: Kirckman 1766, C<sub>2</sub>, down glide of fundamental frequency after onset, ca. 63 – 60.3 Hz (20 frames ≈ 250 ms sound)

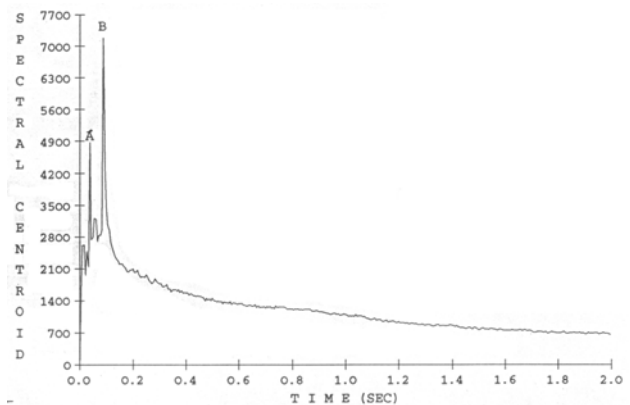


Figure 8: Ruckers 1628, B<sub>2</sub>, spectral centroid ./ time

### 3. CONCLUSION

The measurements presented aim at an analysis of spectral and temporal features of sounds recorded from historical harpsichords. These data have been viewed in regard of sound production and vibration mechanisms such as soundboard impulse response and excitation patterns. Another part of our investigation which studies sound characteristics of musical chords played in different tunings on historical harpsichords, will be presented elsewhere.

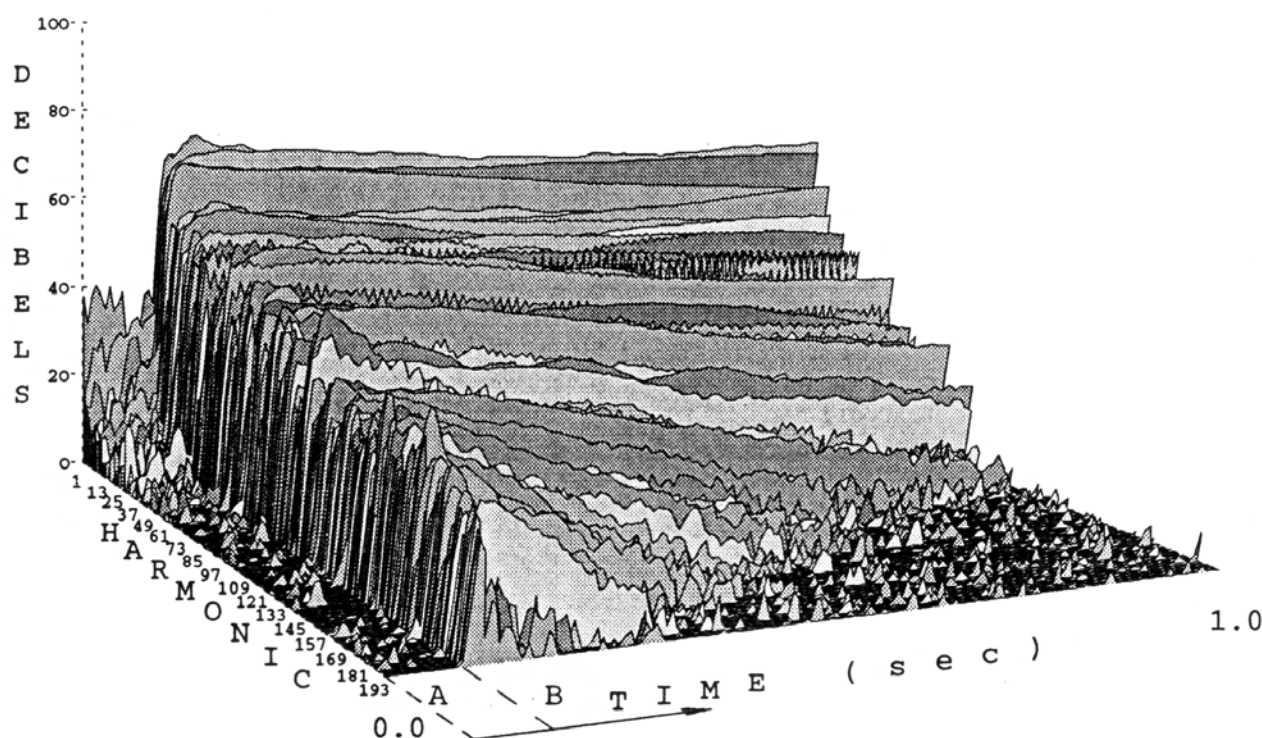


Figure 7: Ruckers 1628, B<sub>2</sub>, section A: spectrum rests again string; section B: attack (release of string), Phase Vocoder, 200 harmonics,  $f_1 = 90.15$  Hz,  $f_{200} = 18030$  Hz

#### 4. REFERENCES

- [1] Fletcher, N.H., „Analysis of the design and performance of harpsichords“. *Acustica* 37:139-147, 1977.
- [2] Weyer, R.D., „Time-frequency structures in the attack transients of piano and harpsichord sounds I“. *Acustica* 35:232-252, 1976.
- [3] Weyer, R.D., „Time-varying amplitude-frequency-structures in the attack transients of piano and harpsichord sounds II“. *Acustica* 36:241-258, 1976/77.
- [4] Cuesta, C. and Valette, C., „Evolution temporelle de la vibration des cordes de clavecin“, *Acustica* 66:37-45, 1988.
- [5] Cuesta, C. and Valette, C., „Le transitoire d'attaque des cordes de clavecin“. *Acustica* 68:112-122, 1989.
- [6] Gätjen, B., *Der Klang des Cembalos. Historische, akustische und instrumentenkundliche Untersuchungen*, Gustav Bosse Verlag, Kassel, 1995.
- [7] Elfrath, Th., *Physikalische Untersuchungen über die qualitätsbestimmenden Einflußgrößen bei Cembali*. Report No. 6795, Physikalisch-Technische Bundesanstalt, Braunschweig, 1990.
- [8] Kottick, E.L., „The Acoustics of the harpsichord: response curves and modes of vibration“. *Galpin Soc. Journ.* 38:55-77, 1985.
- [9] Savage, W.R., Kottick, E.R., Hendrickson, Th.J., and Marshall, K.D., „Air and structural modes of a harpsichord“. *Journ. Acoust. Soc. Am.* 91:2180-2189, 1992.
- [10] Beurmann, A.E., *Historische Tasteninstrumente. Cembali. Spinette. Virginal. Clavichorde*. Prestel, Munich, London, New York, 2000.
- [11] Detailed descriptions of all instruments except the Pigalle are found in [10].
- [12] Cuesta, C. and Valette, C., „Théorie de la corde pincée en approximation linéaire“. *Acustica* 71:28-40, 1990.
- [13] Giordano, N. and Korty, A.J., Motion of a piano string: longitudinal vibrations and the role of the bridge. *Journ. Acoust. Soc. Am.* 100:3899-3908, 1996.
- [14] Mertins, A., *Signal analysis. Wavelets, filter banks, time-frequency transforms and applications*. Wiley, Chichester, New York, 1996.

# **The PIANO SOUNDBOARD BEHAVIOUR IN RELATION WITH ITS MECHANICAL ADMITTANCE**

*Jan Skala*

*Department of Research  
PETROF, SPOL SRO*

skala@petrof.com

## **ABSTRACT**

The piano soundboard input mechanical admittance was investigated in wide frequency range. In lower frequency range strong differences between peak and pit values have been observed. With the increasing frequency, the wrinkled character of soundboard admittance is changed to more smooth one due to a coupling of modes. The idea was to compare a piano soundboard behavior on side-by-side peak and pit on admittance characteristic (mode + antinode). The soundboard was driven with shaker supplied with pure sinusoidal signal. The measurement was made on soundboard fixed to backframe and iron frame without strings. We expect that on antinode frequency the soundboard radiation will be very poor. The final perceived sound volume differs less than it has been expected. A discussion if rest of sound energy can be leaked out more either on other frequency partials by soundboard or by other piano parts (iron frame, rim) is included. This effect is one (but not only one) reason for we can hear a piano tone with frequency in which level of the soundboard admittance is very low.

## **1. INTRODUCTION**

The goal of this work was to follow differences in behavior of piano soundboard on frequencies with high and low mechanical admittance. One old unanswered question "How piano play its lower tones?" was the motif.

## **2. ABOVE FIRST MODE**

### **2.1. Admittance**

Piano soundboard is from tone point of view characterized by mechanical admittance in connecting point between strings and the bridge on the soundboard.

You imagine yourself the following experiment. The piano element i.e.(clamped piano soundboard with bridges on rim) without strings. For instance in point where bridge crosses with strings of A4 (440Hz) we fixed small steel plate for better shaker

connecting through force sensor. Now we can excite the soundboard by shaker and measure the mechanical admittance.

Be specific - on our tested instruments first mode resonance peak of admittance was found at 65 Hz. Antiresonance pit of admittance can be found slightly higher. Admittance on antiresonance pit is 48dB lower in level comparing to the resonance peak.

	<i>exciting frequency [Hz]</i>	<i>admittance MAG [dB]</i>
peak	65	-31,3
pit	104,5	-79,8

Table 1: Mode and antinode levels

### **2.2. Sound radiation**

Now we replace acceleration sensor by microphone (perpendicular to soundboard) or set of microphones around element and observe the sound radiation.

Now let us assume (of course inexactly) linear relation between soundboard velocity and acoustic pressure.

If soundboard was rigid (hypotetic presumption i) and we excited soundboard from given point by pure harmonic signal (presumption ii) to level SPL 50 dB, then after frequency change into admittance minimum we would hear signal about 2 dB (nearly nothing).

Hypotetic presumption i) is nonsense, of course. If soundboard was rigid, it could not have the antiresonance. Presumption ii) is in effect also not satisfied. Our laboratory cannot excite soundboard by pure harmonic force now. But it is not the key.....

We will excite the soundboard for instance by such strong signal to obtain 60dB on frequency of first admittance resonance peak. Now without changing signal generator amplitude we change frequency to the antiresonance. The sound pressure level decreases 22 dB instead of 48 dB.

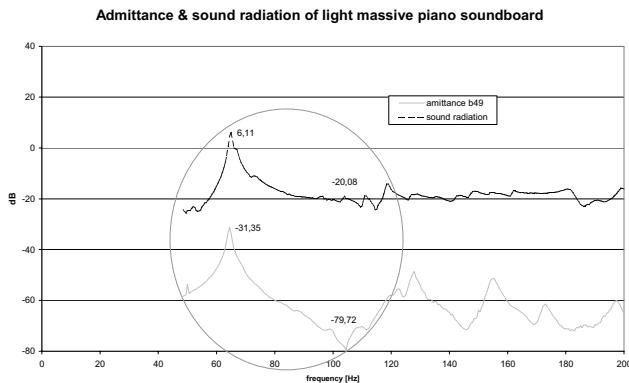


Figure 1: Admittance and sound radiation detail.

Dynamic tension component of string force acting to bridge can be on short trajectory high (comparing to force given by shaker).

From numerical simulations [1] perpendicular force is of order 10N for 1-mm string amplitude (for 25 N by hammer). Maximal perpendicular force of our laboratory minishaker is 10N for sine peak. But measurement uses pseudorandom noise exciting with spectral lines about 1-3mN2. Of course output mechanical impedance of shaker differs from string impedance. We can observe 50% difference between forces in admittance peak and pit. String maybe can play such partial which has antimode in connecting point, nicely, with long decay.

EMA of whole acoustic element (rim clamped soundboard with bridge and iron frame) shows 1<sup>st</sup> mode at 65 Hz and 2<sup>nd</sup> mode at 110,4Hz. Antirezonance frequency matches 2<sup>nd</sup> mode. Individual admittance measurement on bridge can yield information only about the sound radiation on 1<sup>st</sup> mode.

Now we compare directional characteristic measurement result for admittance peak and pit. Instrument was driven by constant amplitude sine signal. Graph shows SPL levels for 12 microphones around the element.

Computed Average SPLs from all microphones give similar results as Tab1.

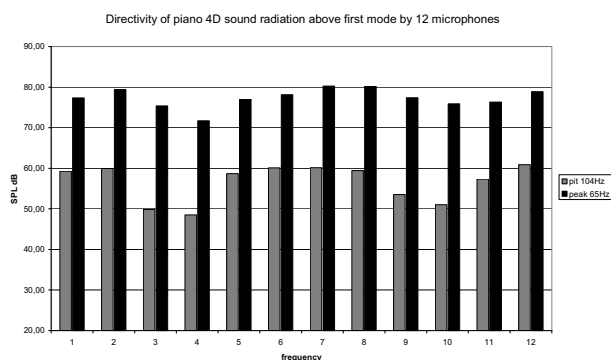


Figure 2: Directional characteristic of sound radiation at admittance peak and pit.

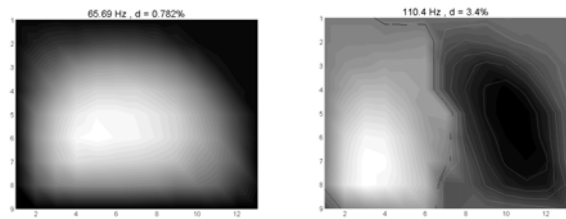


Figure 3: Soundboard mode shapes at 65,6Hz and 110,4Hz.

Giving to context EMA results - peak was found on mode shown on Fig. 3 left and pit on mode shown at Fig. 3 right.

With respect to microphone arranging symmetry we can expect in Fig. 2 difference between level for mic 6-7 and 12-1 for peak and pit. Expectations are satisfied only for mic 1. Mode is not accurately symmetric and for observing decrease it is needed to hit relatively accurately right sensing position.

The key for validation, whether really string can good radiate at soundboard antiresonance it will be measuring on whole instrument.

### 3. VERY LOW FREQUENCY RANGE

Let us start observing situation on lower side from first resonance peak. Usually we assume no instrument modes below the first soundboard mode.

#### 3.1. Admittance and Sound Radiation

Analogous model is based on low frequency filter. As frequency decreases, than magnitude of transfer function decreases also. Despite it, we can found some difference between decrease of admittance and decrease of SPL.

Following graph shows difference between decrease of admittance and decrease of SPL during frequency tuning from frequency of 1<sup>st</sup> soundboard mode to 1<sup>st</sup> piano tone.

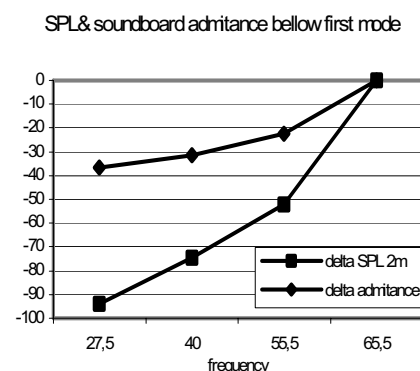


Figure 4: difference between decrease of admittance and decrease of SPL during frequency tuning from frequency of 1<sup>st</sup> soundboard mode to 1<sup>st</sup> piano tone.

In this case SPL falls more quickly than admittance and presumption i) seems to be bad. Speed of admittance decrease depends theoretically only on damping.

This situation can simply be presented on differences between spectral admittance and sound radiation curves. Their decrease is not monotonic. In detail look we can find some small hills, peaks and pits. Some of them can response to nonidentified noise source in chamber, some of them can response to vibrations of whole instrument body. (rim & frame bending) .

Sound radiation decrease monotonically from peak to about 2/3 of its frequency. In band from 1/3 to 2/3 of this frequency is

sound radiation amplitude approximately constant with inexpressive hillocks. Below 1/3 decrease probably continue but we have not reliable measurement here due to some low frequency noise in chamber.

We have to mention that volume of our anechoic chamber (168m<sup>3</sup>) allows measuring down to 80 Hz. Sound measurement in range between 27 Hz and 80Hz can be slightly unreliable.

Described hillocks have no consequence with nonlinearity of shaker, anyway shaker is really nonlinear apparatus, producing next harmonic components.

### Detail of piano soundboard sound radiation below first mode

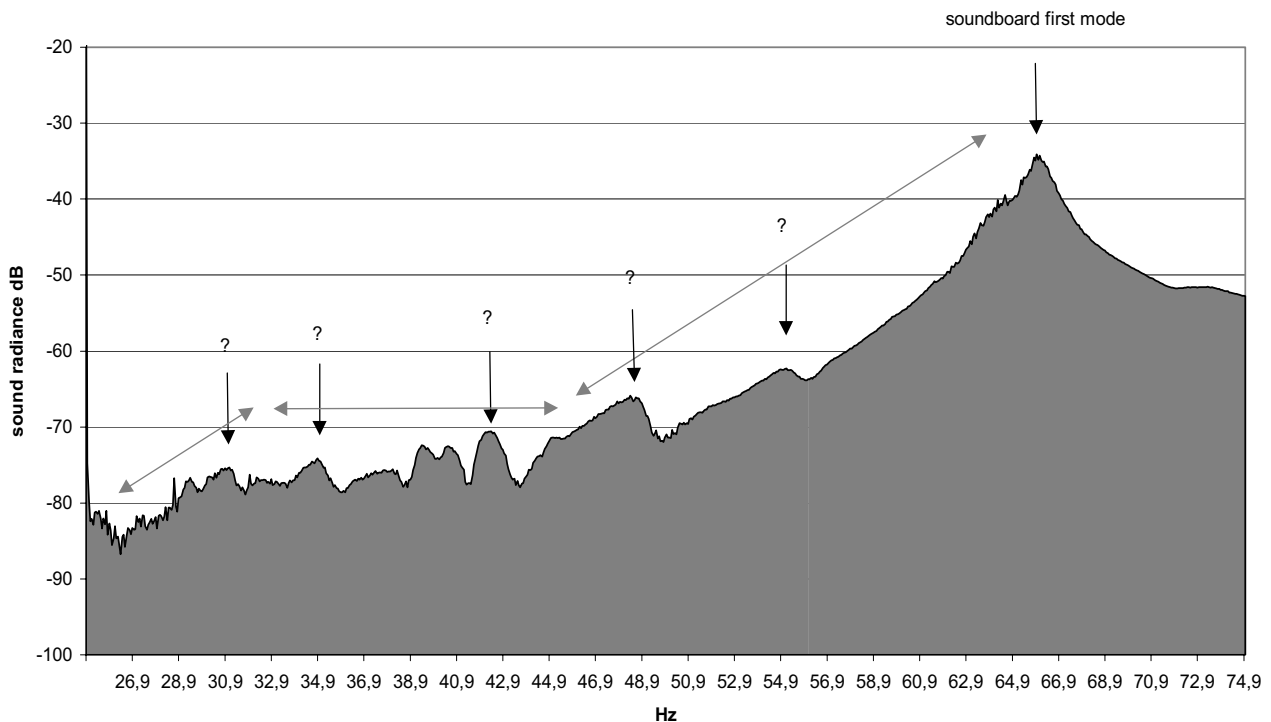


Figure 5: Element sound radiation – detail.

### 3.2 Element directional characteristics

Directional characteristics were obtained by computing SPL levels from 12 microphone signals. Soundboard was excited by pure harmonic signal with constant amplitude. In this case we must mention that role of shaker nonlinearity has some small influence. Directivity shape for 55 Hz is well following the trend for peak at 65 Hz. Expressive change was registered by microphone No 11 and 12 on frequency slightly lower (48 Hz).

Shape returns to shape for peak during next frequency decrease. Notice coincidence and difference for 40 and 38 Hz. Difference occurs on left side on element. Something really happen.

Repeated detailed EMA of instrument element without string shows weak mode bending whole element at 32 Hz.



### Directivities of piano sound radiation below first mode

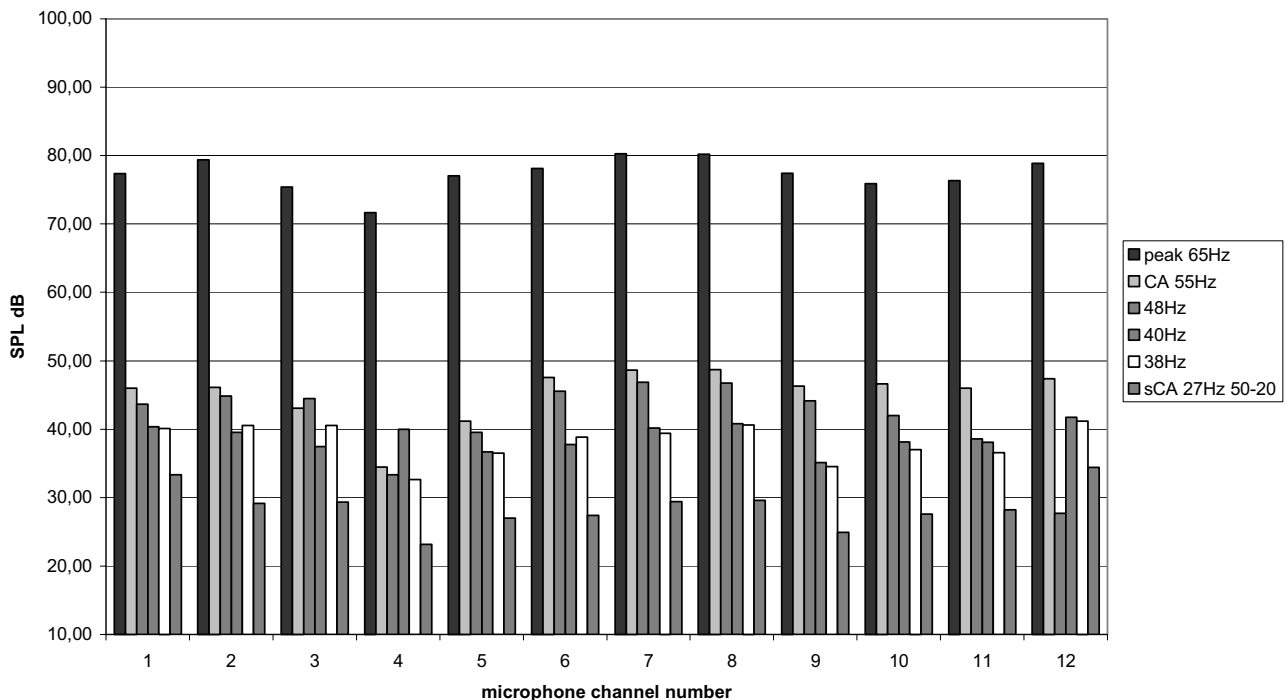


Figure 6: Element sound radiation directivity below first mode.

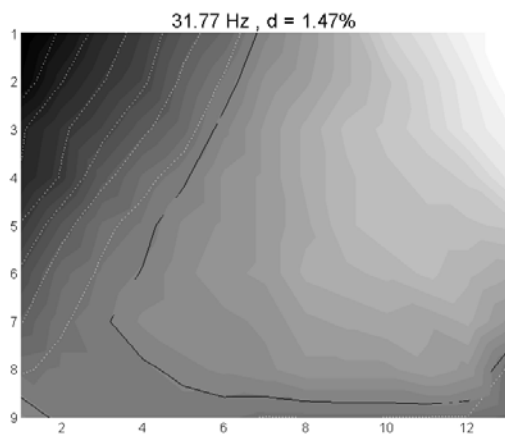


Figure 7: Element bending mode at 32Hz.

After assembling of element and piano cabinet this mode probably will change amplitude and frequency but cannot disappear. Maybe this is one member of whole complex of causation why we can relatively well hear lower piano tones.

## 4. CONCLUSIONS

Relationship between mechanical admittance and sound radiation was followed at two frequency bands. In first band, above first soundboard mode, differences between level of admittance and sound radiation for peak and pit of admittance were measured and explained. It needs to continue here with measurement on finished instrument.

In 2<sup>nd</sup> observed band - range of very low frequency, situation was explained by existence of whole instrument bending mode.

## 5. REFERENCES

- [1] Raffaj, A, "The Piano String Vibration and its Simulation", International Acoustic Conference -Acoustics2002 Banska Stiavnica, Proc, 225-227, 2002.
- [2] Giordano N, "Mechanical impedance of piano soundboard", J.Acoust. Soc. 103 (4) , 1998

## EXPERIMENTAL AND THEORETICAL STUDIES OF PIANO HAMMER

Anatoli Stulov

Institute of Cybernetics at Tallinn Technical University  
Centre for Nonlinear Studies  
Akadeemia tee 21, 12618 Tallinn, Estonia  
stulov@ioc.ee

### ABSTRACT

Based upon the large number of experimental data obtained using a special piano hammer testing device, it has been shown, that all the present-day piano hammers have as a quality the hysteretic type of the force-compression characteristics. This not a chance because such a hysteretic character has been developed step-by-step following the history of evolution of piano hammers since the instrument was created.

The dynamical behaviour of the modern piano hammer can be described by different mathematical hysteretic models. In addition to the four-parameter nonlinear hysteretic model of piano hammer, another new three-parameter hysteretic model was developed. It is very similar to the nonlinear Voigt model and permits a description of the dynamical hammer felt compression that is consistent with experiments. The both models are based on an assumption that the hammer felt made of wool is a microstructured material possessing history-dependent properties. The equivalence of these models is proved for all the realistic values of hammer velocity.

The continuous dependencies of the hammer parameters on the key number are obtained, which is the first known case of such an analysis. The application of hysteretic models to numerical simulation of the grand piano hammer-string interaction is demonstrated. The flexible string vibration spectra excited by different piano hammers are analyzed. All that together, leads to a new method for piano stringing-scale design.

### 1. INTRODUCTION

During for two last years the piano hammer testing device [1, 2, 3] was intensively used for piano hammer studies. The several whole sets of piano hammer were compared, and the dozens of piano hammers produced by various firms (*Schneider, Renner, Abel, Immadigawa*) were tested. The effect of the mechanical treatment (hammer voicing) on the piano hammer parameters, and the air humidity influence on the stability of these parameters were also investigated.

The method of the piano hammer parameters determination was based on the hysteretic (hereditary) model of the hammer felt [5]. It has been experimentally shown [2, 3, 4] that physical assumptions related to the history-dependent properties of the hammer are confirmed by the experiment. It was experimentally proved that the hereditary constitutive model of felt clarifies the dynamical features of piano hammers rather well.

The theoretical ground of the studies was the piano hammer model derived in [5] in the form

$$F(u(t)) = F_0 \left[ u^p(t) - \frac{\varepsilon}{\tau_0} \int_0^t u^p(\xi) \exp\left(-\frac{\xi-t}{\tau_0}\right) d\xi \right]. \quad (1)$$

Here  $F(u)$  is the force exerted by a hammer and  $u$  is the hammer compression. The instantaneous hammer stiffness  $F_0$  and compliance nonlinearity exponent  $p$  are the elastic parameters of a hammer, and constants  $\varepsilon$  and  $\tau_0$  are the hereditary parameters. This analytical four-parameter model describes the dynamical behaviour of the microstructural material, and for some certain set of the hammer parameters represent the unique force-compression curve. But, in spite of this evident fact, the numerical simulation of this model (1) demonstrates very similar force-compression curves, obtained for the different sets of hammer parameters. A close and subtle analysis of this phenomenon results the new more simple hysteretic model of piano hammer.

### 2. THREE-PARAMETER HAMMER MODEL

The impact of the hammer can be described by the equation of motion

$$m \frac{d^2 u}{dt^2} + F(u) = 0, \quad (2)$$

with the initial conditions

$$u(0) = 0, \quad \frac{du}{dt}(0) = V. \quad (3)$$

Here  $m$  and  $V$  are the hammer mass and the velocity respectively, and  $F(u)$  is defined by Eq. (1).

The equation (2) with the function (1) may be written also in the form

$$m \frac{d^2 u}{dt^2} + m\tau_0 \frac{d^3 u}{dt^3} + F_0 \left[ (1-\varepsilon)u^p + \tau_0 \frac{d(u^p)}{dt} \right] = 0. \quad (4)$$

The analysis of this equation shows that the second term is much smaller than the first one, and also the other terms. This fact corresponds to the non equality  $F(t) \gg \tau_0 dF/dt$ , which is valid for all the known values of  $\tau_0$  ( $< 10 \mu\text{sec}$ ), and for any reasonable value of the piano hammer velocity – up to 10 m/s. Therefore, the second term may be ignored, and introducing the new parameters

$$Q_0 = F_0(1-\varepsilon), \quad \alpha = \tau_0/(1-\varepsilon), \quad (5)$$

we have

$$m \frac{d^2 u}{dt^2} + Q_0 \left[ u^p + \alpha \frac{d(u^p)}{dt} \right] = 0. \quad (6)$$

Thus, according to Eq. 2 we can determine the new piano hammer model in the form

$$Q(u(t)) = Q_0 \left[ u^p + \alpha \frac{d(u^p)}{dt} \right], \quad (7)$$

where  $Q(u)$  is the force exerted by a hammer,  $Q_0$  is the static hammer stiffness, and  $\alpha$  is the retarded time. This hysteretic model is very similar to nonlinear Voigt model and permits a description of the hammer felt compression that is consistent also with experiments.

For very slow deformation, the loading and unloading of the hammer felt occur near the limit curve that is the same curve for both hysteretic models (Eqs. (1) and (7)). Due to the equalities (5), this curve is (see also [5]) determined by

$$F(u) = F_0(1 - \varepsilon)u^p = Q(u) = Q_0u^p. \quad (8)$$

However, for very fast loading these two models are quite different. The limit curve for the first model is described [5] by equation

$$F(u) = F_0u^p. \quad (9)$$

With the increasing rate of loading the position of this curve is not changed, but only the amplitude is increased. Instead of this, for the fast loading the limit curve in a frame of the second model does not exist at all, because the force  $Q(u)$  exerted by hammer is proportional to the hammer velocity  $V$  and its value is unlimited

$$Q(u) = p\alpha V Q_0 u^{p-1}. \quad (10)$$

For this and some other reasons, which are not discussed here, the first model (Eq. 1) is more physical and reasonable by nature, than the second (Eq. 7) one. Nevertheless, the three-parameter model, which is more simple, describes the dynamical behaviour of piano hammer also rather well for the hammer velocity up to 10 m/s.

### 3. PIANO HAMMER QUALITY

All the piano hammers tested in experiments were presented by Tallinn Piano Factory. The several series of measurements were carried out in order to compare the various types of piano hammers. Here the result of one of the tests is presented.

The four different hammers produced by *Abel* (Ab), *Immadi-gawa* (Im), and two *Renner's* hammers - old type (Or) and new type (Nr) were tested. The mass of each hammer was in the range 9.2 - 9.7 g. Such hammers correspond to  $E_2$  -  $A_2$  notes. The hammer velocity just prior to impact was approximately 1 m/s (different for each hammer to obtain the equal upper level of the acting force). The results of experiments are presented comparatively in Figure 1. The numerical simulation of experiment was provided by using both the hammer models. In Table 1 are displayed the values of the numerically determined hammer parameters for all hammers and the exact values of hammer velocities.

Parameter	Hammer type			
	Ab	Or	Nr	Im
$F_0$ (kN/mm <sup>p</sup> )	44.0	31.4	16.3	23.2
$\tau_0$ ( $\mu$ s)	2.30	2.0	1.82	2.0
$p$	3.80	3.70	3.73	3.80
$\varepsilon$	0.998	0.998	0.996	0.997
$Q_0$ (N/mm <sup>p</sup> )	88.0	62.8	65.4	69.6
$\alpha$ ( $\mu$ s)	1150	1000	455	667
$p$	3.80	3.70	3.73	3.80
$V$ (m/s)	1.05	1.12	1.15	1.13

Table 1: Piano hammer parameters.

Because the hammer parameters within frame of two models are related to each other by equalities (5), in Figure 1 there are no noticeable differences between the curves obtained using by each model.

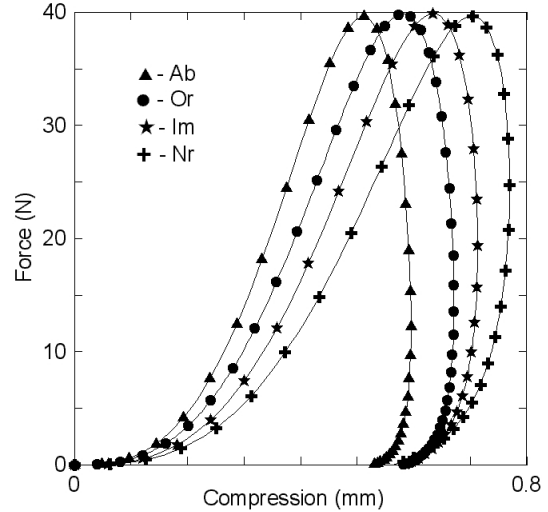


Figure 1: The measured (various symbols) and simulated (solid lines) force-compression characteristics of various piano hammers.

All the hammers considered are of different age and produced by different firms using the particular manufacturing technology. It seems, they have the quite different form of the force-compression characteristics, and the hammer parameters are not the same for each hammer. Nevertheless, the comparison of these hammers in frequency - domain, provided also in [3] demonstrates the similarity of hammers.

In Figure 2 is presented the result of the numerical simulation for note  $F_2$  ( $f=87.3$  Hz). The following set of the flexible string

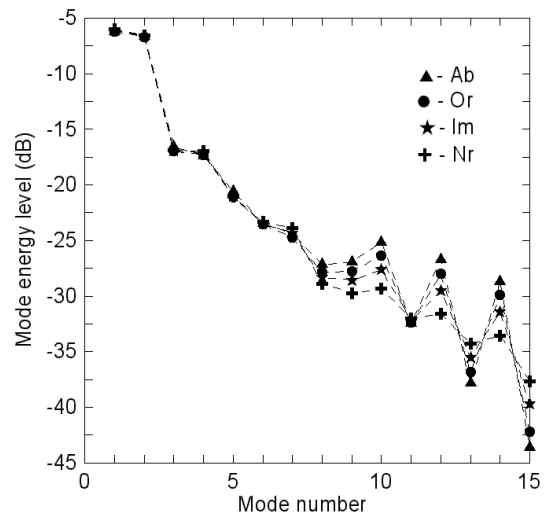


Figure 2: The simulated spectra of the string vibrations excited by various piano hammers.

parameters were used: the string length  $L=1.826$  m, the fractional striking point parameter  $r=0.118$ , the string diameter  $d=1.175$  mm. The linear mass density of this string is equal to  $\mu=8.51$  g/m, and for the simulation note frequency  $f=87.3$  Hz the string tension is equal to  $T=865$  N. The hammer parameters are the same as in Table 1.

The result of the spectra comparison presented in Figure 2 shows, that up to the 8th harmonic, the distinction between the hammers in frequency-domain is not essential. The largest difference of the mode energy level at  $n=15$  is equal to 6 dB. It is interesting, that the newest hammer (Nr) provides the most uniform spectrum of the string vibrations.

In our opinion, the main reason why the spectra of all the different hammers considered look similar is not a fortuity. It is obvious, that the dynamical features of the hammers produced by various firms are very similar indeed, for the various rates of loading. Thus we may state, that in spite of the different technologies that the manufacturers of the piano hammers are using, the mechanical features of their hammers are rather comparable. In particular, the evolution of the hammer manufacturing technology was developed so, to obtain namely the same modern hammer that we have now. And this one is the piano hammer which is made of the material with memory and possesses the hysteretic features.

#### 4. PIANO HAMMER SET

The procedure of the experimental testing of the whole hammer set gives a possibility to obtain the continuous dependencies of the hammer parameters on the key number. The experimentally measured force-compression characteristics of some hammers from the set of *Abel's* hammers were presented in [4], and displayed here in Figure 3. The hammer number  $N$  is displayed in Figure 3 near the corresponding curve.

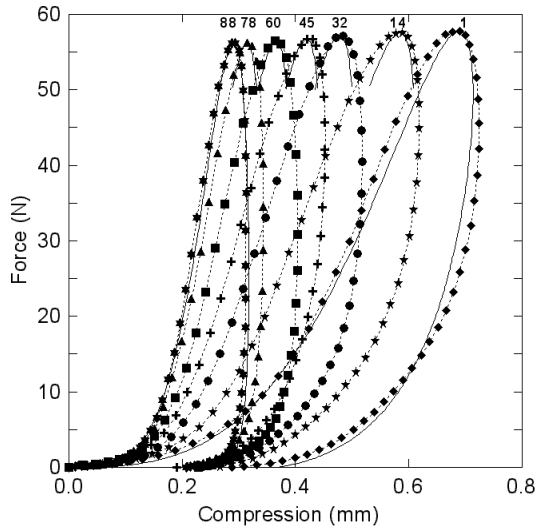


Figure 3: The measured (various symbols) and simulated (solid lines) force-compression characteristics of the hammer set.

During the measurements the initial hammer velocity  $V$  was not a constant value, but it was decreased with the hammer number  $N$ , to obtain approximately the same maximum value of the acting

force for the each hammer tested. Finally, the dependence of the hammer velocity on the hammer number  $N$  is determined as

$$V = 0.849 - 0.004N. \quad (11)$$

The velocity of the 88th hammer is equal to  $V = 0.5$  m/s.

Not all the data observed are used for determining the continuous dependencies. The rejected data corresponded either to possible errors in measurements (strong variation of data), or to hammers with defects. The total number of tests for one set is approximately 80. The percentage of rejected data is nearly 20%. We hope that further experiments should clarify these rejected data, which at the moment still bear certain marks of free choice.

Keeping the dependencies which form and position have qualitatively an obvious trend, we witness clearly regularity dependencies. The number of curves used for the analysis is certainly much more than seven shown in Figure 3, where the curves shown are the typical samples of the observed trend.

The hammer parameters were obtained by numerical simulation using the four-parameter model. In Figure 3 are also presented the simulated curves (solid lines) for the first and last hammers, and only the parts of the simulated curves (near the function maximum) for the others. The continuous dependencies of the hammer parameters on the key number are approximated as

$$p = 3.7 + 0.015N, \quad (12)$$

$$\varepsilon = 0.9894 + 8.8 \cdot 10^{-5}N, \quad (13)$$

$$\tau_0 = 2.72 - 0.02N + 9 \cdot 10^{-5}N^2, \quad (14)$$

for each hammer number  $1 \leq N \leq 88$ .

Regarding the hammer stiffness  $F_0$ , for this set of hammers, it is a linear function in logarithmic scale. The equation of this dependence is the function

$$F_0 = 15.5 \exp(0.059N). \quad (15)$$

Here the unit for relaxation time  $\tau_0$  is ( $\mu$ s), and the unit for  $F_0$  is ( $\text{kN/mm}^p$ ).

In Figure 4, the hammer parameters calculated for the three-parameter model are presented.

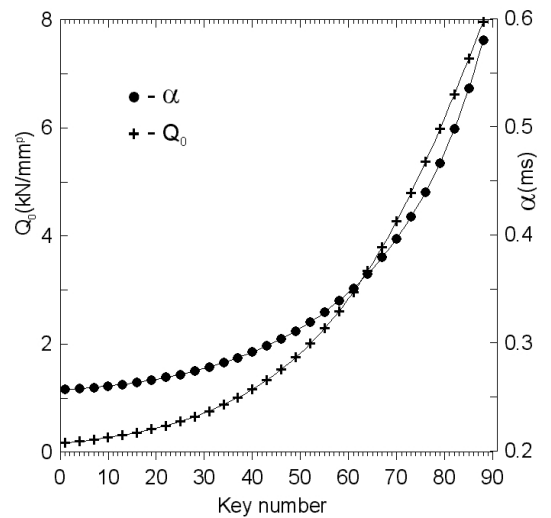


Figure 4: Hammer parameters.

These dependencies of the static hammer stiffness  $Q_0$ , and the retarded time  $\alpha$  were derived from (13) - (15), using (5). For numerical calculations the values of these parameters may be approximated as

$$\alpha = 248 + 1.83N - 5.5 \cdot 10^{-2}N^2 + 8.5 \cdot 10^{-4}N^3, \quad (16)$$

$$Q_0 = 183 \exp(0.045N). \quad (17)$$

Here the unit for retarded time  $\alpha$  is ( $\mu s$ ), and the unit for  $Q_0$  is ( $N/mm^p$ ). For the three-parameter model we must choose the same value of the compliance nonlinearity exponent  $p$  (Eq. 12), as for the four-parameter model.

Most likely, for a good high-quality set of piano hammers the dependencies of the hammer parameters on the key number must be continuous and regular as in Figure 4. On the contrary, if the measured values of the hammer parameters do not show such regular dependencies we may suppose that the hammer set is not of a good quality.

## 5. HAMMER-STRING INTERACTION

The numerical simulation of the hammer-string interaction considered in Section 3, is based on the mathematical model described in [6]. The application of this method for the case of hysteretic hammer was presented also in [7]. It was shown, that for calculation of the string vibration spectra the type of the hammer model is very important. In particular, the influence of the fractional striking point parameter on the sound spectra for the four-parameter model was discussed.

Here we want to demonstrate the importance of the hammer-string interaction study for the piano strings and scale design. No doubt that there are many approved, tested in practice and well tried methods, which are used for creation of a good configuration of tonally related structural parts of the grand piano. But for all that the dynamical features of the piano hammers were not taking into account due to the absence of good models.

Now we have the suitable piano hammer models, and the hammer parameters are also the known values. Thus, we may simulate the hammer-string interaction for the purpose of matching the hammers to some piano scale. Quite the contrary, we may use our knowledge to design of a string scale in according to the piano hammer used. For example, in Figure 2 are presented the simulated spectra for notes  $A_2$  (curves 1 and 2) and  $A_2^\sharp$  (curve 3). These are the neighbor notes, but the first note  $A_2$  consists of two strings, and the second one of three strings per note. Thus, we have a problem how to choose the string tension for each note.

Initially, the following set of the string parameters for note  $A_2$  were used: the string length  $L=1.218$  m, the fractional striking point parameter  $r=0.125$ . This is the wrapped string  $d=0.950$  mm with the winding wire  $d=0.200$  mm. The linear mass density of this string is equal to  $\mu=10.36$  g/m. For note  $A_2^\sharp$  the string parameters are: the string length  $L=1.201$  m, the fractional striking point parameter  $r=0.125$ , the string diameter  $d=1.125$  mm. The linear mass density of this string is equal to  $\mu=7.81$  g/m. For these strings the spectra difference (curves 1 and 3) is approximately equal to 5 dB at 11th and 13th harmonics. Nevertheless, if we choose for note  $A_2$  the another wrapped string:  $d=0.975$  mm with the winding wire  $d=0.250$  mm (curve 3), the spectra difference of the string vibrations may be neglected at all.

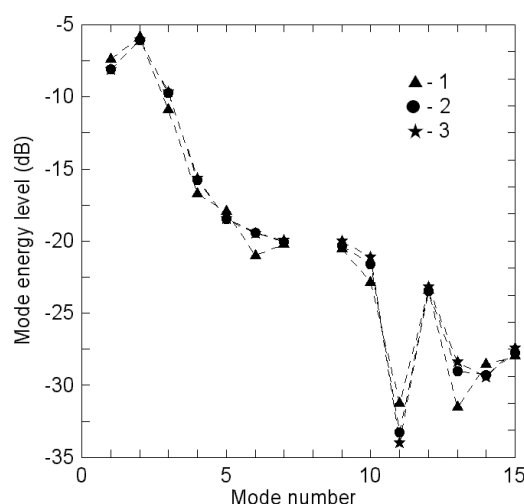


Figure 5: The simulated spectra of the various string vibrations excited by new type of Renner hammer.

## 6. CONCLUSIONS

The new three-parameter hysteretic model of piano hammer developed may be successfully used for description of the hammer-string interaction for a broad range of hammer velocities. The comparison of the different piano hammers produced by various firms shows that in spite of the different manufacturing technologies, the dynamical features of dissimilar hammers are rather comparable. The regular dependencies of the piano hammer parameters on the key number were obtained. The knowledge of the hammer parameters gives the possibility to predict the string vibration spectrum. Apparently, the results obtained will serve as a basis for a new method for piano stringing-scale design.

## 7. REFERENCES

- [1] Stulov, A. and Mägi, A., "Piano hammer testing device", Proc. Estonian Acad. Sci. Engin., Vol. 6, pp. 259-267, 2000.
- [2] Stulov, A. and Mägi, A., "Piano hammer: Theory and experiment", Proc. of the International Symposium on Musical Acoustics, ISMA'2001, Vol. 1, pp. 215-220, 2001.
- [3] Stulov, A., "Experimental and computational studies of the piano hammer I: Piano hammer testing device", Institute of Cybernetics at TTU, Tallinn, Estonia, Research Report (Mech 242/02), 2002.
- [4] Stulov, A., "Experimental and computational studies of the piano hammer II: Experimental testing and numerical determination of the piano hammer parameters", Institute of Cybernetics at TTU, Tallinn, Estonia, Research Report (Mech 243/02), 2002.
- [5] Stulov, A., "Hysteretic model of the grand piano hammer felt", J. Acoust. Soc. Amer., Vol. 97, pp. 2577-2585, 1995.
- [6] Hall, D., "Piano string excitation VI: Nonlinear modeling", J. Acoust. Soc. Amer., Vol. 92, pp. 95-105, 1992.
- [7] Stulov, A., "Comparison of string vibration spectra excited by a different piano hammers", Proc. Institute of Acoustics, ISMA'97, Vol. 19, Part 5, book 1, pp. 231-238, 1997.

## **ANALYSIS OF PIANO TONES WITH SOFT AND HARD TOUCHES**

*Hideo Suzuki*

Department of Information and Network Science, Chiba Institute of Technology  
Tsudanuma, Narashino 275-0016, Japan  
suzuki@net.it-chiba.ac.jp

*Jun Kanno*

Concert pianist, professor at Juan Pedro Carrero Music School in Barcelona, Spain

*Sumiko Mikimoto*

Researcher of piano playing method, Shinjuku, Japan

### **ABSTRACT**

For more than 70 years, the relation between the tone quality and the touch of the piano has been a topic of arguments. Notes G3, G4, and G5 were played with two types of touches, i.e., "soft" and "hard" touches. A key was pressed and recorded with the soft touch for several times until the peak level was within a target range, for example  $90 \text{ dB} \pm 0.3 \text{ dB}$ . Next, the same was repeated with the hard touch. This combination was repeated 10 times. Individual sounds recorded on a digital recorder were transferred onto a personal computer and edited so that all sounds have the same onset time and duration. The digital signals were analyzed by use of the FFT technique. Meaningful spectrum differences were observed for G5. The instantaneous envelope and instantaneous frequency analysis were also applied to analyze the signals around the attack. The instantaneous frequency showed an interesting difference between the two touches.

### **1. INTRODUCTION**

Can the touch affect the quality of a piano tone or not? This has been a topic of arguments for a long time [1-2]. The touch, here in the narrow sense, may be defined as a way a person presses a key to produce a single piano tone with an intention to add some character to the tone quality. Since the piano tone has a nonlinear characteristic (the tone gets brighter as it gets louder), one need to compare piano tones with different touches while keeping the peak levels constant or at least within a negligible difference. Pianists in general think that they can change the tone quality by the touch. On the other hand, physicists tend to think that there is no way to control the interaction between the hammer and the string except the hammer speed. The reason is that the hammer travels with a constant speed (neglecting the effect of the gravity and a mechanical loss) after a release from the acceleration by the key. The latter assumes that the hammer consists of a pure mass and a spring. If this is true, it can be concluded that there is no way to control the tone quality as far as the tone level is kept constant.

However, the observation of the hammer motion with a high-speed movie camera shows that the shank bends significantly after the contact. This indicates that the hammer shank may bend even before the contact due to the acceleration by the key. Following this result, Suzuki analyzed the effect of the initial shank deformation on the spectrum of the impact force of the hammer [3]. Experimental results obtained by Askenfelt and Jansson clearly show that the touch affects the motion of the hammer [4].

The aim of the present study is to find whether there is any difference between the spectral distributions of piano tones with soft and hard touches. One of the authors, a professional pianist, played the piano and tones were recorded with a digital recorder and they were analyzed after editing.

### **2. RECORDING OF THE PIANO SOUND**

The recording took place at Tomono Hall, a privately owned concert hall in Shinjuku, Tokyo. A scene of the recording is shown in Fig.1. The size of the hall is  $13\text{m} \times 9.2\text{m} \times 4.8\text{m}$ . A block diagram of the recording system is shown in Fig.2. A piano and measuring instruments used for recording are listed below.

piano : Model D (Steinway & Sons)

microphone : CU-41 (Sanken Microphone)

mixing amp : SX-PR (Sonosax)

digital recorder : D1624mkII (Fostex)

DAT : DTC-2A5ES (Sony)

sound level meter : LA-5111 (Ono Sokki)



Fig.1 Scene of recording at Tomono Hall in Tokyo.

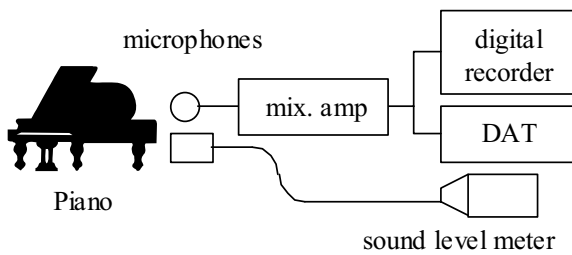


Fig.2 A block diagram of the recording system

Microphone CU-41 is designed for professional use and its frequency response is flat up to 30kHz. Digital recorder D1624mkII has specifications of 96kHz sampling and 24bit resolution as well as 48kHz sampling and 16bit resolution. A setup with the former values was used for recording. Digital audio tape deck DTC-2A5ES (DAT) is used only for a back-up of the digital recorder. The sound level meter played an important role in this experiment. In order to keep the played sound levels within a tolerance range, peak levels of individual tones were monitored by the sound level meter. Only those within  $\pm 0.3\text{dB}$  of a target level (98, 97, and 90dB for G3, G4 and G5, respectively) were used for later analysis.

The whole process was as follows:

- (1) A single note was played several times with a "soft" touch until the peak level fell inside the tolerance range.
- (2) The same was repeated with a "hard" touch.
- (3) Processes (1) and (2) were repeated ten times.

The above process gives ten pairs of tones for comparison. The hard touch is defined as pressing the key while keeping the shoulder, elbow, wrist and finger as firm (tight) as possible. The soft touch is defined as its opposite.

### 3. EDITING AND ANALYSIS METHODS

Since each piano tones are recorded for roughly 5 seconds, they must be edited before the analysis so that edited signals have the

same onset and duration. A time window  $w(t)$  used for this purpose is shown in Fig.3. The time window is defined as:

$$w(t) = \begin{cases} \sin^2(\pi t / 2T_1) & 0 \leq t \leq T_1 \\ 1 & T_1 \leq t \leq T_3 \\ \cos^2[\pi(t - T_3) / 2(T_4 - T_3)] & T_3 \leq t \leq T_4 \end{cases}$$

$T_2$  is the time at which the instantaneous sound pressure of the piano tone shows its maximum.  $T_1$ - $T_4$  used for G3, G4, and G5 are shown in Table 1. Examples of waveforms before and after the windowing are shown in Fig.4. The waveform of the onset of the piano tone is not affected by the windowing. However, the tail of the waveform is gradually reduced to zero so that the duration of the signal becomes equal to  $2.73067\text{s}$  ( $=2^{18}/96,000$ ). Note that the time axis of the signal after editing in Fig.4 is extended to -1s only for comparison.

In order to compare the spectrum differences, the fast Fourier transform (FFT) was applied to individual signals  $x(t)$  after editing. The number of sampling point is  $2^{18}$  ( $=262,144$ ). Since the sampling frequency is 96kHz, the duration of the signal is  $2.73067\text{s}$ . After FFT, a moving average is applied to the power spectra, i.e., the new spectra are given by:

$$|X'(k)|^2 = \left[ \sum_{i=-3}^3 |X(k+i)|^2 \right] / 7 \quad k \geq 3$$

This averaging was applied since the signal is transient and, therefore, the harmonics have spreading in the frequency domain. Peak levels that correspond to individual harmonics were extracted from spectrum data. Those values for soft and hard touches were compared to find out if there is any spectrum difference due to the touch.

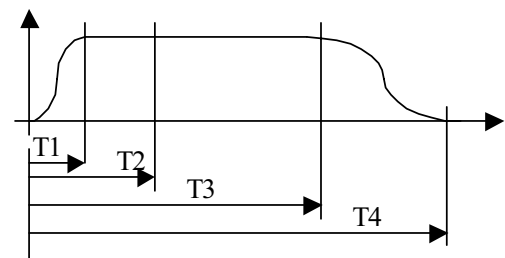


Fig.3 Time window used for editing

Table 1 Values of T1-T4

	T1	T2	T3	T4
G3	0.04	0.16	2.52	2.731
G4	0.04	0.16	2.52	2.731
G5	0.04	0.1	2.23	2.731

Another analysis method used here is the instantaneous envelope and frequency analysis [5,6,7]. The analytic signal  $x_a(t)$  of a signal  $x(t)$  is defined as:

$$x_a(t) = x(t) - jx_h(t)$$

where  $x_h(t)$  is a Hilbert transform of  $x(t)$ . The analytic signal is represented by:

$$x_a(t) = A(t)e^{j\phi(t)}$$

where  $|A(t)|=|x_a(t)|$  and  $\phi(t)$  are the instantaneous envelope and phase, respectively. Then, the instantaneous frequency is given by:

$$f_i(t) = [d\phi(t) / dt] / 2\pi$$

An example of the instantaneous envelope (abbreviated as IE) is shown in Fig.5. In the next section, one example of IE and instantaneous frequency (abbreviated as IF) during the period indicated by the two vertical lines in Fig.5 will be shown.

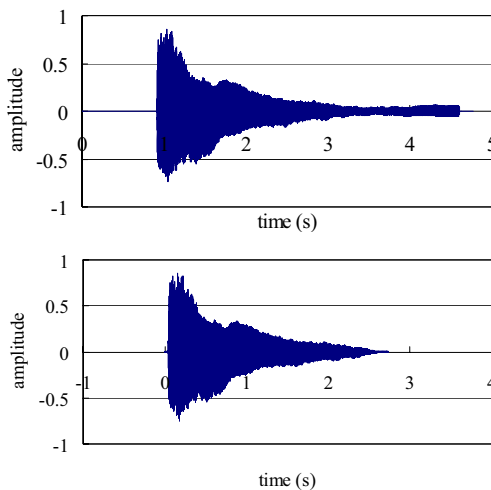


Fig.4 Waveforms of G3 before (top) and after (bottom) editing

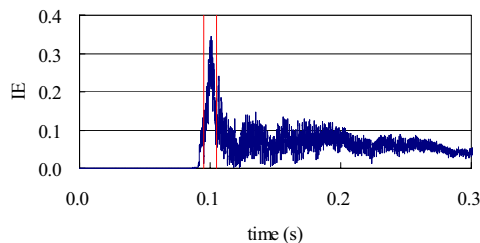


Fig.5 An example of the instantaneous envelope of G5 (hard touch).

## 4. RESULTS AND DISCUSSIONS

In order to show general spectral patterns of G3, G4, and G5 tones, examples of harmonic levels of tones (with the hard touch) are shown in Fig.6. The harmonic levels are adjusted so that the maximum levels of each notes become equal to 100dB. The highest orders of analysis (25, 17, and 10 for G3, G4, and G5, respectively) were determined from the reliability of peak level extraction.

The level differences between the hard and soft touches ( $L_{hard} - L_{soft}$ ) are shown in Fig.7. Top, middle, and bottom charts are for G3, G4, and G5, respectively. The narrow lines are the results for each comparison pairs and the thick lines show their averaged results. In the recording, ten comparison pairs were obtained but some of them (1, 2, and 2 pairs for G3, G4, and G5, respectively) showed abnormal values from other pairs and were removed. From the results, it may be concluded that there is no differences between soft and hard touches for G3 and G4 notes. For G5, however, it may be concluded that the hard touch produces larger harmonic levels than the soft touch. From and above the 4th harmonic, seven pairs out of eight have positive values meaning that the hard touch produces larger harmonics in magnitude than the soft touch. The variation of the results among pairs may be due to the variation how the key is pressed in each trial. The level differences on average are approximately 1dB above 5th harmonic, which may be audible for experienced people. One can see that the levels of the harmonics of G3 decrease slightly as the order of harmonics increases. However, since the level differences are much smaller than the variances, it will be safe to conclude that there is no difference for G3. G4 has small differences between the soft and hard touches for all harmonics.

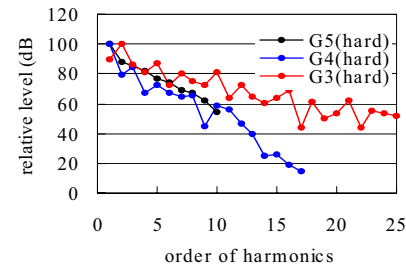


Fig.6 Levels of harmonics of G3, G4, and G5.

If the touch can affect the hammer-string interaction, how is it possible? The only possible reason is the shank deformation as mentioned in the INTRODUCTION. Depending on the touch, the key and the hammer are accelerated with different timings before the hammer hits the string. The shank may be deformed upwards or downwards at the time of contact. If the shank is deformed upwards, the force/time pattern gets narrower and gives larger harmonics [3]. The hammer geometries are different for different keys giving different resonance frequencies or periods. This may cause the difference on the effect of the touch for different keys. It seems that higher keys (G5) can reflect the intention of the pianist than the lower keys (G4, G3).



One pair of tones of G5 with large harmonic level differences was analyzed using the instantaneous envelope and frequency technique. The analysis was applied to the whole signal length (2.73s) but only the results between  $0.095s < t < 0.105s$  (see Fig.5) are shown in Fig.8. From the instantaneous envelope (top chart), one can see that the two envelopes match quite well with each other except that the signal level of the hard touch (red curve) is slightly lower than the soft touch (blue curve). This may be due to the recording level difference. On the other hand, the instantaneous frequency (bottom chart) of the hard touch varies wider than that of the soft touch. Since the levels of higher order harmonics of the hard touch are larger, this result seems reasonable. It is interesting to note that the average magnitude of the instantaneous frequency is close the fundamental frequency of note G5 (784Hz).

## 5. CONCLUSIONS

Ten pairs of piano tones of G3, G4, and G5 with soft and hard touches were recorded keeping the peak levels almost the same. Spectrum levels of harmonics between the soft and hard touches were compared. A meaningful difference (approximately 1dB on average) for higher harmonics of G5 was observed but not for G4 and G3. The instantaneous envelopes and frequencies of one pair of G5 that showed large differences in spectrum were calculated and compared. The instantaneous envelopes were almost the same for the tones with the soft and hard touches. The instantaneous frequency of the tone with the hard touch showed larger variation than that of the soft touch.

As a future study, a similar experiment with lower sound levels should be conducted. Also hearing tests should be conducted to find if there is an audible difference between the hard and soft touches.

## 6. ACKNOWLEDGEMENT

We would like to thank Mr. Eiichi Shinohara for his work to help us in recording piano tones and analyzing data.

## 7. REFERENCES

- [1] W.B White, "Human elements in piano tone production," J.Acoust.Soc.Am. 1, 357-367 (1930).
- [2] H. Hart, M. Fuller and W. Lusby, "A precision study of piano touch and tone," J.Acoust.Soc.Am. 6, 80-94 (1934).
- [3] H. Suzuki, "Vibration analysis of a hammer-shank system," Interim Report of CBS Technology Center (1983).
- [4] A. Askenfelt and E.V. Jansson, "From touch to string vibrations. II: The motion of the key and the hammer," J.Acoust.Soc.Am. 90, 2383-2393 (1991).
- [5] J.B. Thomas, An Introduction to STATISTICAL COMMUNICATION THEORY, John Wiley & Sons, Inc. New York (1968).
- [6] H. Suzuki and S. Morita and T. Shindo, "On the perception of phase distortion," J.Audio Eng.Soc. 28 (9), 570-574 (1980).
- [7] M. Toyama, H. Suzuki, and Y. Ando, The Nature and Technology of Acoustic Space, Academic Press, London (1995).

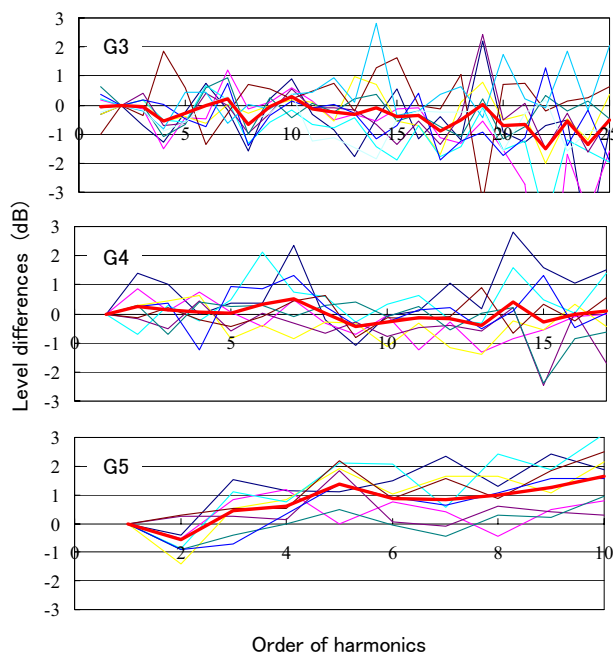


Fig.7 Level differences between hard and soft touches of each comparison pairs (hard-soft). The thick lines show the average differences.

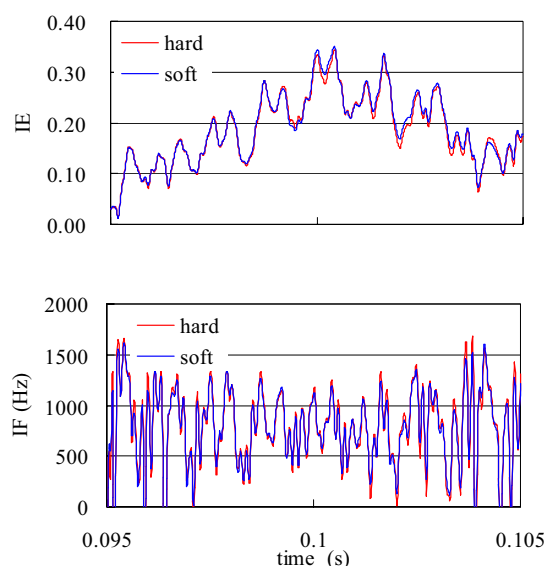


Fig.8 Instantaneous envelope (IE) and instantaneous frequency (IF) of the comparison pair during the period  $0.095s < t < 0.105s$ .

**BRASSES**



## **BRASS INSTRUMENTS AS WE KNOW THEM TODAY**

*Murray Campbell*

School of Physics  
University of Edinburgh  
d.m.campbell@ed.ac.uk

### **ABSTRACT**

Since the time of Helmholtz, brass instrument models have treated the lips of the player as a pressure-controlled flow valve coupled to the instrument's resonating air column. This coupled system is a classic problem in non-linear dynamics. A simple one degree of freedom model of the lip valve has been shown to yield surprisingly realistic trumpet sounds, but many more subtle features of brass playing are not captured. Attention is currently focused on developing more sophisticated lip models, guided by experiments using artificial lip excitation systems and visualisations of human lip motion during playing. Modelling of the air column must take account of non-planar modes in rapidly flaring tubes, and non-linear propagation in longer instruments. Resonances of the player's windway can also be important, especially in wide bored instruments like the didjeridu.

### **1. INTRODUCTION**

At first sight, a brass wind instrument seems a very straightforward acoustical device. It consists of a tube of cylindrical symmetry, usually with openings only at each end. The tube may terminate in a flaring bell, but it is a favourite party trick of expert players to demonstrate that an elaborate piece such as a Mozart horn concerto can be played on a length of hosepipe. It is tempting to propose a straightforward linear model for such a simple system, in which the player selects a lip vibration frequency to excite one of the harmonically related passive air column resonances.

The reality is much more complicated (and interesting). The modes of vibration of the air column are not in general members of an exact harmonic series; the sounding pitch is determined not solely by the air column resonance frequency, but by a non-linear feedback interaction between the air column and the lips. By altering the lip resonance properties the player can significantly alter the pitch of the sounded note.

Many of the most characteristic features of brass instrument technique derive from the detailed nature of the non-linear coupling between lips and air column. The development of realistic models of this interaction in recent years has relied heavily on inputs from two related areas of research: studies of mechanical reed woodwind instruments (mainly the clarinet), and attempts to model the human vocal folds. There is an important distinction to be drawn between the approaches normally adopted in these two areas. The clarinet reed can be modelled with considerable success as a single-mode oscillator, since the second mode of the reed is normally very much higher in frequency than the playing range of the instrument. The complexity of behaviour in the clarinet comes from the strongly non-linear nature of the relationship between the mouthpiece pressure and the flow through the reed. The coupling

between vocal tract resonances and behaviour of the vocal folds is usually neglected in vocal models: the vocal tract is treated as a passive resonator. However, relatively complex vocal fold models incorporating two or more coupled mass-spring systems are common.

Section 2 of this paper reviews attempts to model brass instruments by analogy with the clarinet, assuming a "one mass model" of the lips. Section 3 considers experimental evidence obtained from stroboscopic filming of lip motion, and from studies of brass instruments excited by artificial lip mechanisms. This evidence highlights the limitations of the one mass model. Section 4 surveys lip models with more than one degree of freedom, showing that a two mass model derived from vocal fold studies is already capable of explaining many of the experimentally observed features of the playing of real and artificial lips. In Section 5 the different types of resonating air column used in brass instruments are surveyed. Possible musical consequences of non-linear acoustical phenomena in the air column, and of wall vibrations, are also discussed. Finally, the role of the other resonating air column always present in a brass instrument - the player's windway - is reviewed.

### **2. MODELLING BRASS INSTRUMENTS USING A SINGLE MASS MODEL**

The modelling of reed wind instruments was first put on a firm footing by Helmholtz [1]. He identified two different classes of reed mechanism, which he defined by the geometry of the reed structure relative to the direction of flow: an "inward striking" reed is one in which the motion of the reed blade in the direction of flow results in a decrease in the reed opening, while an "outward striking" reed is one in which the motion of the reed blade in the direction of flow results in an increase in the reed opening. Later writers have generalised the definitions to take account of different geometrical arrangements. It is commonly stated that an increase in mouth pressure tends to close an inward striking reed, but to open an outward striking reed; it should however be borne in mind that this is true only for driving frequencies below the natural resonance frequency of the reed.

Bouasse [2] recognised that the operation of the reed as a non-linear flow control valve could result in the coupling of several air column modes in a regenerative regime. This idea was further developed by Benade and Gans [3] and Fletcher [4]. In an important study of excitation mechanisms in wind instruments, Fletcher [5] followed Helmholtz in identifying the brass player's lips as an outward striking reed. He showed that, in order to achieve regeneration, an outward striking reed must play at a frequency which is above both the nearest acoustical resonance frequency of the air column and the natural resonance frequency of the reed, whereas

the inward striking reed must play at a frequency which is below both air column and reed resonances.

The first attempt to provide a detailed model of the lip-reed flow control valve was that of Backus and Hundley [6]. Elliott and Bowsher [7] observed that Backus and Hundley had failed to take into account the turbulent nature of the flow through the lip channel, and presented a carefully worked out model of regeneration in brass instruments which has been the basis for all subsequent studies. Although Elliott and Bowsher retained the assumption that the lip-reed was predominantly outward-striking, they noted that the Bernoulli force in the lip channel introduced an alternative flow control mechanism with an inward-striking character. This aspect of the model was clarified by Hirschberg et al [8], [9], who emphasised the importance of a detailed understanding of the separation of the flow at the exit of the lip channel.

Several researchers followed Elliott and Bowsher in developing one-mass models of the lip reed. It became customary to refer to the outward-striking model of the lip-reed as the “swinging door” model, and to the inward-striking version as the “sliding door” model. Saneyoshi et al [10] proposed that the lip-reed motion was predominantly of the sliding door type. Adachi and Sato [11] tested simulations using both types of model, and reported musically satisfactory results from each. Dietz and Amir [12], Msallam [13], and Vergez [14] all achieved good musical performance using simulations based on sophisticated versions of the swinging door model.

### **3. EXPERIMENTAL STUDIES OF REAL AND ARTIFICIAL LIPS**

Although one-mass lip models have been widely adopted in the physical modelling synthesis of brass instrument sounds, there is much experimental evidence that musically significant aspects of the motion of the lips of a real brass instrument player cannot be captured by such a simple model. It has not proved possible to identify the brass player’s lips as unambiguously either inward or outward striking. Yoshikawa [15] studied the phase difference between lip motion and mouthpiece pressure in horn and trumpet players; he concluded that the lip reed had an outward-striking character for the lowest played modes, but changed to an inward-striking (or “upward-striking”) at around the third air column mode. Chen and Weinreich [16] used a specially constructed single mode “brass instrument” consisting of a Helmholtz resonator with active feedback and a trumpet mouthpiece. They identified the lip-reed as inward or outward striking by noting whether the playing frequency was below or above the measured resonance frequency of the resonator. They found that with extreme effort the player could sound notes either below or above the air cavity resonance, but that the “most comfortable note” was almost always above.

Measurements carried out by the author on the cornetto, a lip-reed instrument with side holes [17] showed that, for notes towards the bottom of the playing range, the player could easily adjust the embouchure (the setting of the lip parameters) to pull the playing frequency either above or below the resonance frequency of the nearest acoustic mode. In consonance with the common experience of brass instrument players, it was found to be easier to “lip” the note downwards in pitch than upwards.

It is very difficult to measure the mechanical resonance behaviour of the human lip-reed, and even more difficult to produce predefined and reproducible changes in such properties as the lip

resonance frequency. Ayers [18] has described an approach in which a special trumpet mouthpiece was used with a shunt hole in the backbore. The player first sounded a note with the shunt hole open. In this condition the mouthpiece cup was effectively decoupled from the low frequency resonances of the trumpet air column; the lip resonance frequency was taken to be the frequency of the sounded note. The shunt hole was then closed quickly without interrupting the sound, and the playing frequency for the complete instrument was determined. It was found that for the second air column mode the relationship between playing frequency and lip frequency was well described by a sliding door (inward-striking) model, but that for higher modes the behaviour could not be modelled by a lip model with only one degree of freedom.

A problem with any measurement involving a human player is that it is almost impossible to ensure that the player’s musical instincts do not consciously or subconsciously influence the performance of the prescribed task. To avoid this problem, several researchers have turned to artificial lip mechanisms [19], [20], [21]. Cullen et al [22] used a pair of water-filled latex lips to excite a trombone, and showed that the behaviour of the artificial lips corresponded in many respects with the performance of a human player. In particular, the gradual extension of the trombone slide with a fixed embouchure caused the played frequency to slide smoothly downwards. At one extreme the played frequency was below the acoustic resonance frequency (inward-striking behaviour); at the other extreme the played frequency was above the acoustic resonance frequency (outward-striking behaviour). The mechanical response of the lips was measured, and resonance peaks with both inward and outward phase characteristics were identified. These observations provided strong confirmation that a single mode mechanical oscillator could not model the observed behaviour of the lip reed.

The relatively complex nature of the motion of the brass player’s lips has also been noted in stroboscopic video recordings using mouthpieces with transparent walls or fibre optic inserts [23], [24], [25]. These visualisations of lip motion have consistently shown that the normal motion of the lips has components parallel and perpendicular to the flow direction which are comparable in magnitude. In addition, surface waves have been observed which propagate in the flow direction and which may be significant in the valving action of the lips [24].

### **4. LIP MODELS WITH MORE THAN ONE DEGREE OF FREEDOM**

The one mass model is the simplest member of a class of lumped parameter models which has been considerably developed in vocal fold research. In view of the complexity of motion revealed by visual studies of lip motion, it could be argued that modelling of the lips requires a finite element method rather than an extension of the lumped parameter approach. There are, however, considerable attractions in attempting to find the simplest model, with the minimum number of independent parameters, which adequately captures particular features of lip-reed behaviour. Physical insights are likely to emerge more clearly from such an approach, and a relatively simple model is clearly attractive from the point of view of real-time synthesis.

Adachi and Sato [26] have proposed a model which retains a single mass, but incorporates two degrees of freedom by allowing for both swinging and sliding door motions. This model can incorporate the observed orbital motion of the lips, involving compo-

nents of motion both parallel and perpendicular to the flow direction. It cannot however model the observed surface wave, which requires two independent masses in order to allow for a phase difference between the motions at the front and the back of the lip channel. Nevertheless, the hybrid model of Adachi and Sato has had some success in modelling low-frequency lip-reed behaviour [18].

In experiments with artificial lip excitation of a trombone-like instrument, Neal [27] has shown that the lipping of notes above and below the acoustical resonance frequency can be associated with a pair of mechanical lip resonances, the lower frequency resonance having outward-striking character and the higher frequency resonance having inward-striking character. A model with two independent masses has been shown to be capable of reproducing this lipping behaviour [28].

In general, two mass models used in vocal fold studies involve two masses each with a single degree of freedom. The two mass model proposed by Loos [29] incorporates in its framework the possibility of two degrees of freedom for each mass, but in the application described only one degree of freedom per mass is active. Vilain et al [30] pointed out that to properly take into account the mechanical boundary conditions in either vocal fold or lip-reed modelling will in general require four degrees of freedom. A two mass model with only two degrees of freedom has been shown to be incompatible with consistent application of realistic boundary conditions [31]. However, it appears that a four degree of freedom lip model is sufficient to explain a great deal of the experimentally observed behaviour of the artificial lips, including the detailed structure of the lip opening height impulse response curve [32].

## 5. RESONATORS OF BRASS INSTRUMENTS

The brass instrument family encompasses a wide diversity of resonator shapes. This subject has been well reviewed by Myers [33], who has discussed possible classification schemes for brass instruments based on the acoustical properties of different bore shapes. The nature of the non-linear aeroelastic coupling between lip-reed and air column discussed in Section 2 means that a played note on a brass instrument normally involves the simultaneous interaction of several air column modes. A set of mode frequencies with a close approximation to a harmonic series encourages mode-locking, and the development of a strong regime of oscillation. The ways in which different types of brass instrument achieve this are explained in several textbooks (e.g. [34], [35]).

A common assumption in the discussion of the propagation of sound in wind instruments is that only the plane wave mode need be considered. The limitations of this approach should be borne in mind: even at low frequencies evanescent higher modes will be generated at discontinuities in the bore, and in the rapidly flaring bell section of a trumpet or horn the assumption of planar wavefronts clearly breaks down. The treatment of non-planar modes, and their implications for the musical performance of brass instruments, have been discussed by several authors [36], [37], [38].

Another assumption which needs qualification is that propagation in the resonator is linear. Beauchamp [39] first questioned this assumption on the basis of measurements of the transfer function of a trombone. The reality of non-linear wave steepening in the trombone air column, leading to the formation of shock waves in loud playing, was confirmed by the measurements of Hirschberg et al [40], and the musical implications of non-linear propagation for trumpet timbre have been further explored by Fletcher and Ta-

mopolsky [41]. The significance of localised non-linearities such as vortex shedding at the bell end of brass instruments [9], and acoustic streaming at side holes in instruments such as the cornetto and the serpent, requires further investigation.

A topic which has been hotly contested for many decades [35], and which is still a matter of controversy, is the extent to which wall vibrations in the resonator of a brass instrument have a perceptible influence on the radiated sound. Hoekje [42] has estimated that the sound power radiated from structural vibrations in trumpets and trombones is about 40 dB lower than the energy radiated directly from the air column, although the body radiation is enhanced at high frequencies by the increased modal density of the structure. On the other hand, Moore [43] has reported that the acoustic power of a particular harmonic can change by as much as 3 dB when the bell of a trumpet is immobilised.

In all lip-reed instruments, the lips are in fact coupled to two resonators: downstream is the tube of the instrument, and upstream is the player's windway. In most of the modelling studies described earlier, the assumption has been made that the pressure in the mouth of the player remains constant. This assumption is not fully satisfied for most brass instruments: Elliott and Bowsher [7] found that the acoustic pressure in the mouth of a trombone player was between 5% and 20% of the pressure in the mouthpiece. Variation of the windway impedance (for example, by moving the tongue) could thus influence the behaviour of the lip reed.

While the significance of mouth shape on the timbre of notes played on orchestral brass instruments remains to be further explored, there is no doubt that it is a dominating factor in the performance technique of the Australian didgeridu. Fletcher et al [44] have pointed out that the characteristic impedance of the wide tube of the didgeridu is usually considerably less than that of the vocal tract, so that modifications of the vocal tract exert an important influence on the flow. In addition, the lips normally remain closed for a significant part of each vibration cycle, emphasising the high frequency content of the sound. Thus the normal assumptions of brass instrument modelling have to be seriously revised in dealing with the didgeridu: further study of this fascinating instrument is expected to throw fresh light on the nature of the lip-reed air column interaction.

## 6. REFERENCES

- [1] Helmholtz, H.I.F., *On the Sensations of Tone*, translated by Ellis, A.J., Dover, New York, 1954.
- [2] Bouasse, H. *Instruments à Vent*, Delagrave, Paris, 1929.
- [3] Benade, A.H. and Gans, D.J., "Sound production in wind instruments", *Ann. New York Acad. Sci.* **155**, 247-263, 1968.
- [4] Fletcher, N.H., "Mode locking in non-linearly excited inharmonic musical oscillators". *J. Acoust. Soc. Am.* **64**, 1566-1569, 1978.
- [5] Fletcher, N.H., "Excitation mechanisms in woodwind and brass instruments", *Acustica* **43**, 63-72, 1979.
- [6] Backus, J. and Hundley, T.C., "Harmonic generation in the trumpet", *J. Acoust. Soc. Am.* **49**, 509-519, 1971.
- [7] Elliott, S.J. and Bowsher, J.M., "Regeneration in brass wind instruments", *J. Sound Vib.* **83**, 181-217, 1982.
- [8] Pelorson, X., Hirschberg, A., van Hassel, R.R., Wijnands, A.P.J. and Auregan, Y., "Theoretical and experimental study of quasi-steady flow separation within the glottis during

- phonation; application to a two mass model", J. Acoust. Soc. Am. **96**, 3416-3431, 1994.
- [9] Hirschberg, A., Kergomard, J. and Weinreich, G., *Mechanics of Musical Instruments*, Springer-Verlag, New York, 1995.
- [10] Saneyoshi, J., Teramura, H., and Yoshikawa, S., "Feedback oscillations in reed woodwind and brasswind instruments", *Acustica* **62**, 194-210, 1987.
- [11] Adachi, S. and Sato, M., "Time-domain simulation of sound production in the brass instrument", *J. Acoust. Soc. Am.* **97**, 3850-3861, 1995.
- [12] Dietz, P.H. and Amir, N., "Synthesis of trumpet tones by physical modeling", *Proceedings of the International Symposium on Musical Acoustics*, Dourdan, France, 472-477, 1995.
- [13] Msallam, R., Dequidt, S., Causse, R. and Tassart, S., "Physical model of the trombone including non-linear effects; application to the sound synthesis of loud tones", *Acustica* **86**, 725-736, 2000.
- [14] Vergez, C. and Rodet, X., "Dynamical systems and physical models of trumpet-like instruments", *Acustica* **86**, 147-162, 2000.
- [15] Yoshikawa, S., "Acoustical behaviour of brass player's lips", *J. Acoust. Soc. Am.* **97**, 1929-1939, 1996.
- [16] Chen, F.-C. and Weinreich, G., "Nature of the lip reed", *J. Acoust. Soc. Am.* **99**, 1227-1233, 1996.
- [17] Campbell, D.M., "Non-linear dynamics of musical reed and brass wind instruments", *Contemporary Physics* **40**, 415-431, 1999.
- [18] Ayers, A.D., "Basic tests for models of the lip reed", *Proc. ISMA2001*, Perugia, Italy, 83-86, 2001.
- [19] Gilbert, J., Ponthus, S. and Petiot, J.-F., "Artificial buzzing lips and brass instruments: experimental results", *J. Acoust. Soc. Am.* **104**, 1627-1632, 1998.
- [20] Vergez, C., *Trompette et trompettiste: un système dynamique non linéaire analysé, modélisé et simulé dans un contexte musical*, PhD Thesis, Université de Paris VI, 2000.
- [21] Ehara, F., Nagai, K. and Mizutani, K., "Relationships between vibration of artificial lips and sound frequency of a trumpet", *Proc. ISMA2001*, Perugia, Italy, 513-516, 2001.
- [22] Cullen, Gilbert, J. and Campbell, D.M., "Brass instruments: linear stability analysis and experiments with an artificial mouth", *Acustica* **86**, 704-724, 2000.
- [23] Copley, D.C. and Strong, W.J., "A stroboscopic study of lip vibrations in a trombone", *J. Acoust. Soc. Am.* **99**, 1219-1226, 1996.
- [24] Ayers, R.D., "New perspectives on the brass instruments", *Proc. International Symposium on Musical Acoustics*, Leavenworth, U.S.A., 129-134, 1998.
- [25] Yoshikawa, S. and Muto, Y., "Lip-wave generation in horn players and the estimation of lip-tissue elasticity", *Acta Acustica* **89**, 145-162, 2003.
- [26] Adachi, S. and Sato, M., "Trumpet sound simulation using a two-dimensional lip vibration model", *J. Acoust. Soc. Am.* **99**, 1200-1209, 1996.
- [27] Neal, M.A., Richards, O., Campbell, D.M. and Gilbert, J., "Study of the reed mechanism of brass instruments using an artificial mouth", *Proc. ISMA2001*, Perugia, Italy, 99-102, 2001.
- [28] Neal, M., Richards, O., Campbell, M. and Gilbert, J., "Experimental measurements of the reed type of a brass player's lips using an artificial mouth", submitted to *J. Acoust. Soc. Am.*
- [29] Loos, N.J.C., Hofmans, G.C.J., Veldhuis, R.N.J. and Hirschberg, A., "A symmetrical two-mass vocal fold model coupled to vocal tract and trachea, with application to prosthesis design", *Acustica* **84**, 1135-1150, 1999.
- [30] Vilain, C., Le Marrec, L., Op 't Root, W., Willems, J., Pelorson, X. and Hirschberg, A., "Towards a new brass player's lip-model", *Proc. ISMA2001*, Perugia, Italy, 107-110, 2001.
- [31] Vilain, C.E., Pelorson, X., Hirschberg, A., Le Marrec, L., Op't Root, W. and Willems, J., "Contribution to the physical modelling of the lips. Influence of the mechanical boundary conditions", accepted for publication in *Acta Acustica*.
- [32] Richards, O., private communication.
- [33] Myers, A., *Characterization and taxonomy of historic brass musical instruments from an acoustical standpoint*, PhD thesis, University of Edinburgh, 1998.
- [34] Fletcher, N.H. and Rossing, T.D., *The Physics of Musical Instruments*, 2nd ed., Springer-Verlag, New York, 1998.
- [35] Campbell, M. and Greated, C., *The Musician's Guide to Acoustics*, Oxford University Press, Oxford, 1987.
- [36] Jansson, E.V. and Benade, A.C., "On plane and spherical waves in horns with nonuniform flare. II: Prediction and measurements of resonance frequencies and radiation losses", *Acustica* **31**, 185-202, 1974.
- [37] Pagneux, V., Amir, N. and Kergomard, J., "A study of wave propagation in varying cross-section waveguides by modal decomposition. Part I. Theory and Validation", *J. Acoust. Soc. Am.* **100**, 2034-2048, 1996.
- [38] Kemp, J., *Theoretical and experimental study of wave propagation in brass musical instruments*, PhD thesis, University of Edinburgh, 2002.
- [39] Beauchamp, J.W., "Analysis of simultaneous mouthpiece and output waveforms", *Audio Engineering Society Preprint No. 1626*, 1-11, 1980.
- [40] Hirschberg, A., Gilbert, J., Msallam, R. and Wijnands, A.P.J., "Shock waves in trombones", *J. Acoust. Soc. Am.* **99**, 1754-8, 1996.
- [41] Fletcher, N.H. and Tamopolsky, A., "Blowing pressure, power, and spectrum in trumpet playing", *J. Acoust. Soc. Am.* **105**, 874-881, 1999.
- [42] Hoekje, P.L., "SEA applications to wind instruments", *J. Acoust. Soc. Am.* **113**, 2315, 2003.
- [43] Moore, T.R., "The effects of bell vibrations on the acoustic spectrum of the trumpet", *J. Acoust. Soc. Am.* **113**, 2315, 2003.
- [44] Fletcher, N., Hollenberg, L., Smith, J. and Wolfe, J., "The didjeridu and the vocal tract", *Proc. ISMA2001*, Perugia, Italy, 87-90, 2001.

## **HARMONICS: WHAT DO THEY DO IN THE DIDJERIDU?**

*Noam Amir*

Department of Communication Disorders  
Sackler School of Medicine  
Tel Aviv University  
noama@post.tau.ac.il

### **ABSTRACT**

The characteristic timbre of the Australian didjeridu varies over a much wider range than that of most wind instruments, due to two factors: 1) the large variability in bore shape between instruments, 2) the great extent to which the player can control the timbre of the instrument. In this study we wish to examine several aspects of this timbre. Analyzing recordings of several instruments, each played over a range of possible timbres, we track the amplitudes of a large number of harmonics. Using this data we attempt to define the components of the timbre that are governed mainly by the instrument, which give the didjeridu its recognizable color, as opposed to those that are more easily controlled by the player. This is carried out both by visual examination of the harmonic tracks, and also through selective resynthesis. The same analysis is performed over instruments judged by a professional player to be of inferior quality, and used to give at least a partial explanation of the shortcomings found in these instruments

### **1. INTRODUCTION**

The didjeridu is a surprisingly versatile instrument, given the simplicity of its design, or even “non design”. A didjeridu is basically a hollowed out branch, or a tube made out of other material, with a rudimentary mouthpiece intended to bring the diameter at the playing end to a size that conveniently fits the lips. No mechanism for changing the effective length is present, therefore the didjeridu is played at one pitch, that of the lowest resonance, though it is sometimes overblown briefly at its second resonance for punctuating effects.

The didjeridu is used as a drone and rhythm instrument, employed by proficient players in ways that create interesting and intricate sounds that are far beyond that which such a simple structure might suggest. In fact, since the instrument and the vocal tract have impedances on the same order, the tone of the didjeridu is affected to a very large extent by the configuration of the vocal tract. This allows the player to vary the timbre considerably, probably more than in most western instruments.

The tone is further enhanced by overblowing and adding vocalizations through use of the vocal chords. Apart from these are two basic manners in which the didjeridu is played. The first is in playing long drone notes, in which the timbre is changed by manipulating the vocal tract. The second is in playing various rhythms, creating a variety of transient sounds through sudden changes in pressure – either in the lungs or by creating stops of the throat, tongue and lips. The playing qualities of a didjeridu can differ when used in either of these manners: e.g. an

instrument that has a less interesting timbre might be useful for creating drum-like rhythm sounds, while an instrument with a rich steady-state tone might be less suited for fast rhythms.

Traditionally, a didjeridu is made by selecting a eucalyptus branch hollowed out by termites, shortening it to the desired length, and adding a mouthpiece. Modern makers manufacture instruments from branches hollowed out manually, either from wood, or often from the stalks of Agave plants, which have a reasonably hard exterior and a soft balsa-like interior. This leaves a very large degree of freedom to the instrument maker, which raises a number of interesting questions: what qualities of the didjeridu create its recognizable timbre, that distinguish it from low brasses, for example? What separates a “good” instrument from a “bad” instrument? Given a specific design, which aspects of the timbre are governed by the instrument, and which are controllable by the player?

Previous studies on the didjeridu are very few, mostly carried out by Fletcher and his associates [1,2,3]. An acoustic analysis was carried out in these studies in some detail, showing the presence of a voicelike “formant” in the spectrum of the didjeridu sound, which can be shifted by the player through manipulation of the vocal tract. A meticulous and detailed comparative analysis of various instruments has not been published previously, to the best of our knowledge.

In the present study we address some of the questions raised above. We analyze the various timbres obtained from several instruments in quasiperiodic playing, i.e. with slowly varying timbre. Our purpose is to give some general properties of the didjeridu timbre, and examine the ways in which it can vary. Our main focus is in examining the last question above: to what extent can the player control the timbre, as opposed to the extent to which a certain instrument constrains it. Finally, we give some general characterizations of better vs. inferior instruments.

### **2. EXPERIMENTS**

#### **2.1. Instruments and player**

Six instruments were played: 3 eucalyptus didjeridus [EN, EM, EY], judged to be of high quality: easy to play, responsive to variations in timbre, with an agreeable and typical didjeridu sound. Two agave didjeridus constructed by the author [AB, AS]: AB was judged by both players as being of reasonably quality and the other found to be unresponsive and dull sounding. Finally, one plastic didjeridu [P] was used, made of PVC plumbing tubes. Both players found it easy to play, but not



as responsive to change of timbre, and having a basic “booming” sound quality which was too strong.

One player participated in the study. This player is a very proficient amateur, with several years of experience and good control over playing timbre.

## 2.2. Recordings

A Sony ECM 999PR microphone, used in mono mode with moderate (90 degree) directionality was placed several centimeters from the end of each instrument. Recordings were carried out on a PC with a standard sound card, at a sampling rate of 22050 Hz. The player was requested to play for about a minute, performing gradual changes in timbre, characteristically called “nasalisation” by many players. This refers to the rather nasal timbre which can be achieved by reducing the size of the mouth cavity. An excerpt was then taken from each recording, of approximately 5 seconds in length, containing a representative sweep of timbres.

In addition, a recording of “hand slapping” each instrument was carried out. An FFT of this signal can provide the resonance frequencies of the instrument to a high degree of accuracy, as shown previously by the authors [4].

## 2.3. Analysis and synthesis techniques

Analysis was carried out using the Short Time Fourier Transform (STFT): an FFT was performed on successive overlapping windows, and the underlying line spectrum was recovered from the peaks in the resultant graph. This procedure is quite sensitive to window length and type, especially in signals containing both very strong and very weak spectral components. After some experimenting, the following parameters gave optimal results: signal segments of 4 fundamental periods (approximately 50 ms for the instruments being studied), with overlap of 3 periods between successive windows. Since the pitch was very nearly constant throughout the recordings, the window size could be kept constant. A Blackman weighting window was applied before FFT. Though this is not a very common choice, the very low spectral side lobes of this window proved advantageous, due to the presence of both strong and weak harmonics next to each other. The FFT length was 65536 (2 to the 16<sup>th</sup> power), giving a spectral resolution of 0.336 Hz.

The first 50 peaks in the spectrum were located, and the amplitude, phase and frequency of each was stored. In cases where resynthesis was carried out, it was performed on successive windows twice the size of the analysis stepsize, each successive synthesized window multiplied by a Hamming weighting window, and overlapped at half the window length. This scheme has been used successfully on speech signals, giving results that are nearly indistinguishable from the original [5].

The program was implemented in a convenient graphic user interface, so that clicking on various parts of the signal displayed the local spectrum and its peaks. Resynthesis could be performed using the entire spectrum, or on a selected set of harmonics.

## 3. RESULTS

### 3.1. Stationary spectra

Some spectra obtained from two instruments are presented in Figures 1 and 2.

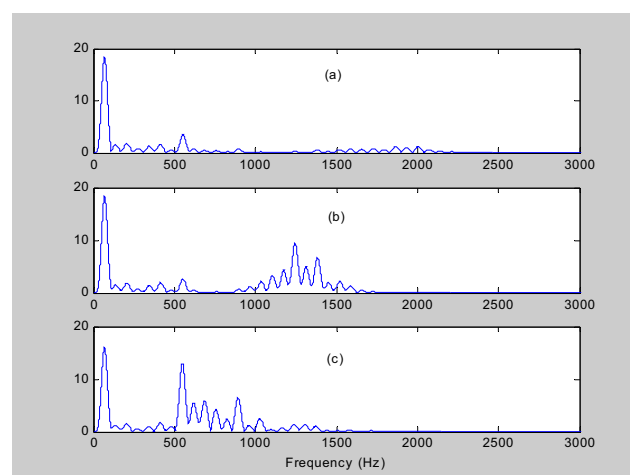


Figure 1: Spectra from beginning, end and middle of EN excerpt.

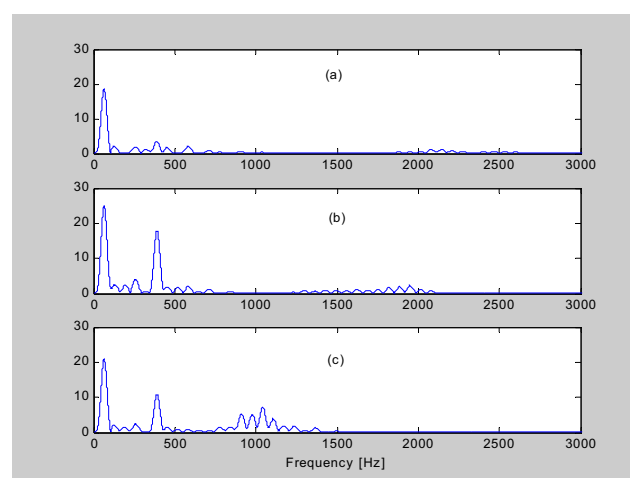


Figure 2: Spectra from beginning, end and middle of AB excerpt.

The most striking result from analysis of all the instruments under all playing conditions, was that the fundamental tone was nearly always the strongest component in the sound. This is rather surprising, considering that the didjeridus examined had nearly no flare at the radiating end, with a terminating diameter of 10 cm. at the most, far less than that of the low brass instruments. Only in the recording of instrument EN, the 13<sup>th</sup> harmonic was very briefly stronger than the fundamental.

This is probably due to the lack of a mouthpiece with a narrow backbore, which is known to create a form of “high pass” characteristic in brass instruments.

Another characteristic property of most instruments was the weakness of the next few harmonics after the fundamental, regardless of the degree of nasalization. This effect was more prominent in some instruments than in others, among the eucalyptus and agave instruments. In the plastic didjeridu (P), on the other hand, the second harmonic was very strong, which is the probable source of the exaggerated “booming” quality of this instrument.

These results led us to hypothesize that maybe the second resonance in instrument (P) was aligned with the second harmonic, whereas in other instruments it was not. Given that in the better instruments the first few harmonics above the fundamental were all quite weak, this property might be in fact advantageous, as opposed to brass instruments.

Analyzing the hand slapping recordings for the first five resonances in each instrument gave the following results:

Inst.	First res. Freq.	2'nd res. ratio	3'rd res. ratio	4'th res. ratio	5'th res. ratio
P	70.66	2.04	3.11	5.09	6.16
EN	67.29	2.80	4.73	6.52	8.35
EM	67.29	2.69	4.78	6.37	8.6
AB	63.25	2.83	4.59	6.30	7.77
AS	67.96	2.51	3.93	5.58	6.64

Table 1: Lowest resonance frequency and ratios of higher resonance to this frequency for all instruments

We note that the first resonance of EN and EM are the same by complete coincidence. Interestingly, the above table shows that instrument D has the second resonance very well aligned with the first, whereas this is not the case at all with the other instruments. The third resonance is also well aligned with the 5'th harmonic for this instrument. The only other reasonable alignments found in the table are the 5'th harmonic for AB, and the 4'th harmonic for AS. These resonance peaks are probably less influential, though it should be mentioned that these two instruments were judged to be poorer than EN and EM – especially AS.

Mean playing frequencies were: 70.33, 68.92, 68.17, 65.07, 68.19 for instruments P, EN, EM, AB, AS respectively. Aside from instrument P, these are all slightly above the first resonance frequency. This is more marked for the agave didjes, which gave the player a subjective feeling of being less “focused”, i.e. their pitch was too easy to “lip” up or down in frequency. Though a detailed analysis of this is not the subject of this paper, we remark that this is probably correlated to the height of the resonance peaks. This shows up also in the handslapping recordings – instrument P had a very resonant and slowly decaying response, which is probably too resonant for a good instrument. In the agave instruments, which have a rough,

untreated interior, the response decayed much faster, as shown in figure 3.

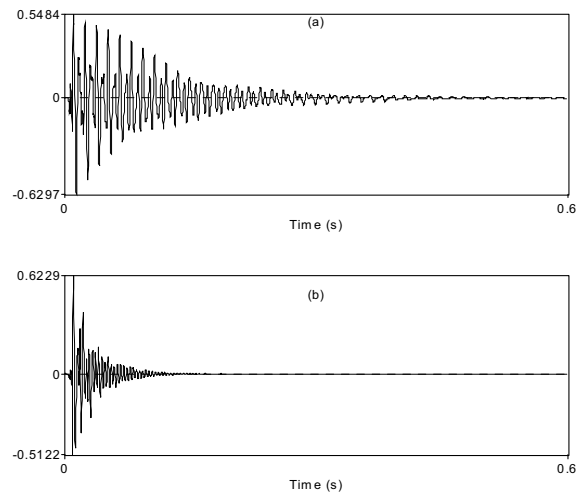


Figure 3: “slap response” of P (a) and AS (b) instruments.

### 3.2. Time dependent spectra

The spectral “snapshots” in figures 1 and 2 show that lower parts of the spectrum seem to be relatively stationary, while the higher harmonics change in amplitude, in a manner resembling a formant. This has been remarked upon previously by Fletcher [1].

In the present study we chose to observe the detailed behavior of the harmonics over time through a three dimensional plot showing the trajectory of each harmonic amplitude, instead of using a spectrogram which is often used in speech analysis. This type of graph gives a much more accurate representation. Due to the fact that the fundamental is usually very strong and that its amplitude was found to change very little, it was excluded from the graphs. Some examples are presented in figures 4 and 5. For lack of space we omit similar graphs for the other instruments.

A number of interesting conclusions can be drawn from these figures. The eucalyptus didjeridus have very weak harmonics up to the 5'th or sixth harmonic, regardless of the degree of nasalization. Instrument P is once more very different from this. Besides the extremely strong second harmonic (not shown in the graph, for reasons of scaling), the following several harmonics are very strong compared to the harmonics excited by nasalization, in contrast to the eucalyptus instruments. The agave instruments are not shown here for lack of space, but they are closer to the eucalyptus instruments in this respect.

Some subjective experiments were carried out, resynthesizing the signals with a limited number of harmonics. Synthesizing with the lower harmonics gave a sound with no nasalization, of course, retaining some of the information particular to the “signature” of each instrument. Resynthesizing instrument P with harmonics 2,3 and 4 removed gave a more eucalyptus like sound, with less of the booming quality.

Finally, we note that the formant-like clustering of highly excited upper harmonics commented in by Fletcher exhibits some peculiar behavior. Though nasalization strengthens some harmonics, it seems as if nearby harmonics are not influenced, or influenced to a much lesser degree. This could be influenced by an interplay of the formant like structure imposed by the mouth cavity and anti-resonances of the instrument itself. This is an interesting point that should be examined by physical modeling as proposed by Fletcher et al [3].

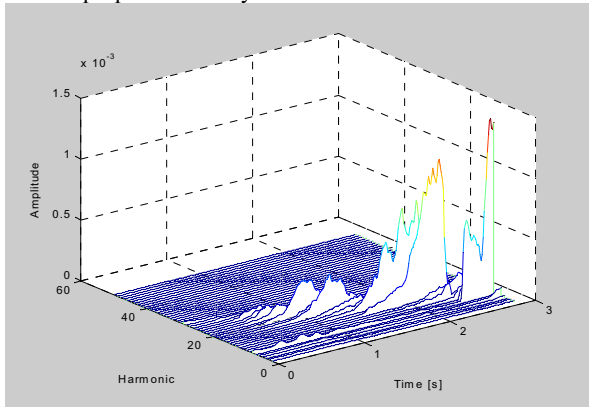


Figure 4: Harmonics 3-50 of inst. EN.

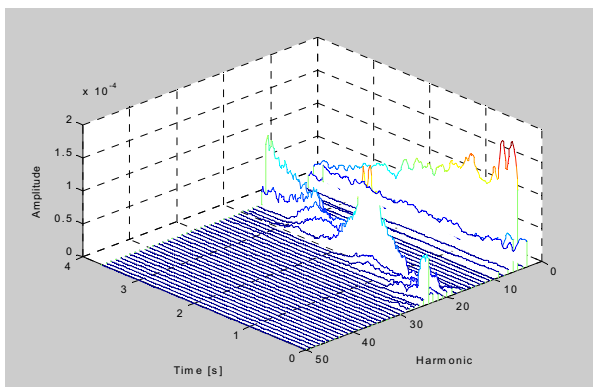


Figure 5: Harmonics 3-50 of inst. P.

#### 4. CONCLUSIONS

Various aspects of the didjeridu spectrum have been discussed, based on recordings of basic playing effects on a number of instruments. We have shown some evidence that points to the conclusion that the lower part of the spectrum is more influenced by the intrinsic structure of the instrument than the higher part, which can more easily be manipulated by the player. We have also shown that one characteristic of the recognizable didjeridu sound is the presence of a strong fundamental followed by approximately 5 or 6 very weak harmonics. The harmonics after these are those influenced by nasalization, though there behaviour is not purely formant-like.

Much further work can be carried out on this subject. The detailed dependence of the spectrum on higher resonances should be examined in detail. It would be very interesting to determine how the excitation mechanism shapes the overall

spectrum in its interaction with the lowest resonance, and to what degree this is modified by the higher resonances.

A more detailed examination of higher pitched instruments should also be carried out, as these often have a rather different timbre than the low pitched instruments examined here, with a fundamental lower than low C#.

Further examination of transients in the didjeridu would also be interesting, since these are used very often in didjeridu playing. The ease with which different transients can be evoked from a certain instrument are an important quality to players.

#### 5. REFERENCES

- [1] Fletcher, N. H., "Acoustics of the Australian didjeridu", Australian Aboriginal Studies, Vol. 1, 1983, pp 28-37
- [2] Fletcher, N. H., "The didjeridu (didgeridoo)", Acoustics Australia, Vol. 24, 1996, pp. 11-15
- [3] Fletcher, N. H., Hollenberg, L., Smith, J., Wolfe, J., "The didjeridu and the vocal tract", Proceedings of ISMA 2001, Perugia
- [4] Amir, N., Alon, Y., "A study of the didjeridu: normal modes and playing frequencies", Proceedings of ISMA 2001, Perugia
- [5] R.J. McAulay and T.F. Quatieri, "Sinusoidal Coding" in *Speech Coding and Synthesis*, W. B. Kleijn and K.K Paliwal, Ed., pp. 121-170. Elsevier, 1998.

## **BRIDGING INSTRUMENT CONTROL ASPECTS OF BRASS INSTRUMENTS WITH PHYSICS-BASED PARAMETERS**

*Matthias Bertsch*

Institute for Musical Acoustics (IWK), University of Music Vienna, Austria

*Bertsch@mdw.ac.at*

### **ABSTRACT**

Is there a connection between what we feel when playing an instrument and what we can measure? Physical models and measuring tools have been developed to provide a better understanding of brass instruments and objective physical documentation of their acoustics.

Musicians and instrument makers still criticize the enormous gaps between the physics-based parameters and the empirically reported feelings of brass players on quality aspects of their instruments. Deviations between played and measured parameters like intonation and their variability have already been focused on in earlier studies. Attempts at finding a theoretical explanation of these deviations using physical modeling continue.

For musicians, one of the most important quality factors of a brass instrument is its response. A new series of playing tests has been designed to correlate empirical data with objective physical parameters (impedance measurements). International instrument makers provided special test instruments (modular trumpets). This paper will examine the difficulties in defining response and setting up suitable playing tests.

### **1. INTRODUCTION**

Brass instrument makers produce and customize their brass instruments for players who have many different requirements and expectations of their ideal instrument. The manufacturing knowledge has developed through the centuries. Today, there are many good instruments on the market and the selection is large. One can choose between “rather similar” instruments built in large series by factories and custom-made smaller series or even handmade or adjusted “singular instruments”. So how can one find his optimal instrument without testing all of them? For beginners it is usually the advice of the teacher or the dealer, which narrows the choice. Those who start to test instruments usually quickly realize how difficult this procedure is. There are many criteria. On the one hand there is the sound quality and on the other hand there are the many aspects of instrument control parameters. The main criterion for the musician in choosing his instrument is the specific sound and timbre. Preferences about sound quality are individual and hard to describe with verbal attributes. It also depends on the specific interaction with the input of the player. Instrument makers’ descriptions of instrument parameters are for the most part very similar: perfect intonation, easy speaking, full sound, good response and more or less resistance. Of course, there are differences between those instruments, but there is little experience in labeling the parameters. You cannot simply look at a table and compare

features as you do when you shop for a car or loudspeaker. Quality control of brass instruments is still chiefly done through subjective criteria of test players. Reproducibility is difficult to control.

#### **1.1 Measurement tools and previous studies**

Since the 1980s, acousticians have been asked to deliver objective quality control tools. Meanwhile there are hardware and software systems that can measure the input impedance of brass instruments, which are easy to use [1]. The impedance measurement data represents an acoustic fingerprint of the total behavior of an instrument. One curve corresponds to one physical geometry of an instrument. But what do these curves tell the musician?

One feature of the impedance curve had almost immediately been translated into musical terms. The positions of the peaks correspond with the intonation of the notes. The measurement allows the detection of deviations to a reference intonation. The Brass Instrument Analysis System (BIAS) developed at the Institute for Musical Acoustics (IWK) at the Music University in Vienna can accurately show the intonation of all playable notes of a brass instrument. Earlier studies by the author have been done to determine the intonation properties of trumpets [2]. Empirical data of played trumpets have been compared with different theoretical tuning systems and with the intonation, which was calculated by means of input impedance measurements. The results showed great differences amongst players even playing the same reference instrument. The arithmetic mean over all trials correlated best with the calculated objective intonation. This information is already a big help for both makers and players in evaluating instruments. Additionally, new optimization tools can already help to correct problems of existing instruments by bore profile modifications and they can be used in developing new instruments by calculating the intonation with computer models before the instrument is built.

#### **1.2 More questions remain**

So what about other instrument control aspects? Do they also correspond to physics-based parameters? Acousticians expect that they do. Thomas Moore wrote in his article for trumpet players: “the sound and feel of every horn is definitely determined by its impedance spectrum” [3]. But how can you measure the feel of the horn? The language of musicians describing instrument properties is not easily translated into physical terms. Even when they use the same words, the meaning can be different. So far, it is not clear that what all players label “good response”, “easy speaking” or “low resistance” are the same. Also, most players have little

theoretical understanding about tone production. Our approach is to find a common language for players to report tone control parameters and to translate them into acoustical terms. The objective is to find an answer for a simple question: which factors make a trumpet speak well? What does the player, the mouthpiece, the bore, the shape or even the material have to do with it all? What can be changed to improve the response of a given instrument? The following example of practical relevance can show the need for these answers: While writing this introduction I received a phone call from an instrument maker. There is an almost perfect horn played by professional musician. The intonation is perfect; except that one note does not speak well if played piano. He asked what he should change on the instrument. I gave an answer, but I hope that we find a better answer as the ongoing project progresses.

### 1.3 Aims

The aims of the trumpet research project (TRP) are to define what 'response' can mean (there are many varying meanings), and to find physical parameters that can be used in further calculations and measurements. Preferences of different player types (classical, jazz, etc.) for these physical parameters are searched. This would allow computerized optimization of real instruments. Bridging the languages of musicians ("this trumpet feels good"), acousticians ("how much impedance is at this frequency") and instrument makers ("I could use a wider bore or different material") will help to create tools for developing better instruments.

## 2. METHODS

Several methods are used in this ongoing study. The planned methods include playing tests, input impedance measurements, bore reconstructions and finally the correlation of all data.

### 2.1 Playing tests setup

Blind performance tests and regular playing tests with outstanding professional trumpet players and with groups of musicians in Austria, Finland and the USA will deliver empirical data on specific test instruments. Different international instrument makers provide the test instruments. Playing tests are made with Bb trumpets with Périnet valves and German system trumpets with rotary valves. Some instruments are built modularly, such that the leadpipe, tuning slide and the bell can be changed. Information about makers is kept confidential during the playing tests so that players do not know what brand, model or setup of modular instrument they are playing. Tests are performed in a dark room (or with blindfold) and a questionnaire for each setup is answered. Information on the experience and preferences of the players are also requested. All data are organized in a database with search, sort and export functions.

### 2.2 Playing test questionnaire

Instrument control aspects are highly trained competence of musicians, but the knowledge is developing without unified verbal attributions. This is a well known problem of acoustician to deal with. Earlier tests by Wogram [4] have been taken into account. A new approach in this study is to proceed with the support of "images" and visualization. The player gives answers

and the tester fills out the questionnaire. Sometime this includes translating expressed feelings. A typical difficulty is to quantify the value of a given aspect. In this questionnaire the player has five possible values ("-2", "-1", "0", "+1", "+2"), but he can use his own personal reference. The answer "0" corresponds to "neutral, normal". Answers of "+1" indicate more, "+2" much more of a given aspect (respectively "-1" is less and "-2" is much less). During testing the player develops his own scale.

Questions about the subjective sound preference and description of the sound quality:

- Dynamic range: small - normal - large
- Timbre: dark - neutral bright
- Timbre: dull - neutral - brilliant
- Small sound - normal - full sound
- Boring, hard to modulate, - normal - rich colors
- I don't like it - Don't know - I like it
- Sound volume: small - normal - large
- Sound projection: poor - normal - good
- Tendency to sound brassy: low - normal - high

Questions about the starting phase of a note: (The question focus specifically on g4 and g5 as open series and with valve 1 and 3 engaged):

- How fast is the attack (soft versus quick onset)
- Ease of staccato and repetitions, How quickly can you repeat very fast notes pp and ff
- Soft versus abrupt slurs (B4-C5, C5-Eb5)
- Easy to play ppp? How much effort do you need to play a note? How easy does it speak?

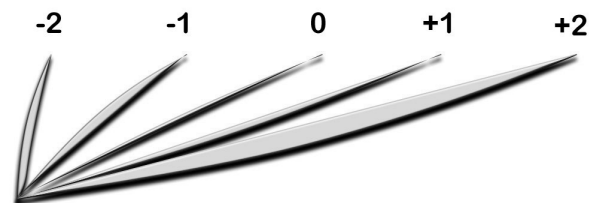


Figure 1: Schematic representation to ask for the attack: "How fast do you get feedback when you start blowing"

Question about the control aspects of a sustained note:

- Blowing resistance (forte)
- Air volume: Amount of energy (air) needed to sustain a note.
- Intonation of given notes
- Slotting pitch: enough or too much flexibility (how easy can you "lip up" and "lip down"?)



Figure 2: Schematic diagram to ask for slotting pitch. The deepness and shape represents the flexibility of the pitch center.

Classification of the instrument. The players are asked to judge about:

- Adequate user player level (beginner, student, pro),

- The type of music this instrument is best suited for (classical, jazz/pop or both)
- The applicability for all ranges, high or low register

Additional questions on mechanical and optical aspects (not in blind tests) are asked (Fast valve action... lightweight / heavyweight, Conception and assembly; finish) Finally the total preference is asked.

## 2.2 Measurements

All instruments and combinations of modular parts are measured with the BIAS system [2]. Several physics-based parameters are extracted from the input impedance measurement. Besides the peak frequencies, the shape of the peaks and the “0” phase position are taken into account. For each peak, the following values are calculated:

- **Offset:** Intonation given by the impedance peak center frequency. Intonation error related to the equal temperature in Cent. Tuning reference frequency is adjusted in order to minimize the overall intonation error of all playable notes.
- **Envelope:** Absolute peak height of impedance peak in MegOhm
- **Curvature:** Absolute value of the 2nd derivative of impedance curve at peak center in MegOhm/Hz<sup>2</sup>. Calculated as parabolic fit using the Savitzky-Golay convolution.
- **Low3dbLimit:** Distance of left peak edge (-3dB) from peak center in Cent.
- **High3dbLimit:** Distance of right peak edge (-3dB) from peak center in Cent
- **Bandwidth:** Low3dbLimit plus High3dblimit. (Inverse Q factor in Cent)
- **Phase:** Phase value at peak center in Rad. Should be close to zero at least for prominent peaks.
- **Groupdelay:** Group delay, 1st derivative of impedance phase at peak center in Rad/Hz.
- **ZeroPhase:** Intonation given by zero phase frequency. Intonation error related to the equal temperature in Cent. Tuning reference frequency is adjusted in order to minimize the overall intonation error of all playable notes.

For a detailed analysis of input impedance peaks, the shift of the position and of the amplitudes of all higher peaks has to be taken into account. Weighting Functions in the BIAS system allow considering the sum function of the excitation spectra of the lip.

## 2.3 Bore reconstruction:

Different impedance curves correspond to different bore profiles. Recent studies of Kausel [5,6,7] in calculating the profile from input impedance measurements demonstrate a further development in this technique. To compare these data with special leadpipes used for playing tests, digital X-RAY measurements have been done to document their geometrical difference. Small changes in the bore and mouthpiece have strong impact on difference “response” parameters.

## 2.4 Correlation:

The main step is to correlate the data of the playing tests to those of the input impedance, and to the bore profiles. The questionnaire delivers values, which can be used for calculations. First, it will be necessary to find dependent and independent variables. As documented in earlier studies, reasons for variability in trumpet sounds are enormous [8].

# 3. PRELIMINARY STUDIES

## 3.1 Three leadpipes



Figure 3: Three different leadpipes for a rotary trumpet.

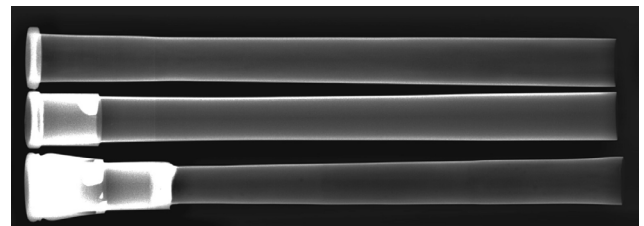


Figure 4: X-RAY images of above leadpipes

Different leadpipes can influence many aspects of a given instrument. Timbre, intonation, and several response factors are changed together with the input impedance. Figure 5 shows the impedance of trumpet #27 with the three leadpipes shown in Fig. 3 and 4. The absolute height and the shape of the peak that corresponds to the note g4 are different. This note can also be played with valve combination 1+3. The impedance peaks for this fingering is also plotted in Fig. 5. Musicians testing these instruments feel and hear differences, and more tests are necessary to find dependent and independent variables. A large number of tests repeated without knowledge of the players will determine the reproducibility of the tests.

## 3.2 Extra keys for response support

Some professional players and students in Vienna use rotary trumpets with additional keys (see Fig. 6) to support the response of tones in the high register. As can be seen in Fig. 7, the keys have a similar function to those on (non-original) historic trumpets. When the additional key is engaged, e.g. the “C” key, the impedance at this note is similar, while those at the neighbor’s frequencies are much more changed. For this instrument, the peak height of the played note increased with two keys and decreased with two other keys. More tests should be done to find to what extent these keys help psychologically for the “high note syndrome”, or if they actually improve the response. (The keys are pressed only to start a note and not to sustain it!)

## 4 SUMMARY

Preliminary studies have been done in 2002 for setting up the large-scale tests. The playing tests are being performed from March to June 2003 in Vienna and further tests with the same instruments are planned in other countries (Finland, USA,) to evaluate regional preferences and variations of schools. Playing tests are very difficult sensory evaluation tests, which depend on many aspects. Several psychological aspects have to be taken into account. Therefore, the tests will be performed without seeing the instrument and knowing about brand names; otherwise the expectations about brands and visual impressions can easily dominate the “feeling” of the musician. The expected results will help musicians to find their individual ideal instrument and deliver new tools for instrument makers.

## 5 REFERENCES

- [1] Widholm, Gregor. BIAS 5.1 Manual. Vienna: IWK (MA), 2001.
- [2] Bertsch, M. Intonation on trumpets. Proceedings of ISMA '98 (International Symposium on Musical Acoustics). Leavenworth: ASA, Catgut, 1998. p. 135-140.
- [3] Moore, T. What is Impedance and why do we care?. ITG-Journal. Vol. 27 Nr. 1. Westfield, USA: International Trumpet Guild, 2002. p. 70 - 71.
- [4] Wogram, Klaus. Information on playing tests performances for the German music instrument award. Braunschweig: Email correspondence to M. Bertsch (unpublished Material), 2003.
- [5] Kausel, W. Optimization of Brasswind Instruments and its Application in Bore Reconstruction. Journal of New Music Research. Nr. 1 Vol. 30. Swets & Zeitlinger, 2001. p.69-82.
- [6] Kausel, W. Bore reconstruction from measured acoustical input impedance: equipment, signal processing, algorithms and prerequisites. Proceedings of ISMA '2001 (International Symposium on Musical Acoustics). Vol. 2 Perugia: Musical and Architectural Acoustics Lab. FSSG-CNR Venezia, 2001. p.373-378.
- [7] Kausel, W. and Anglmayer, P. A Computer Program for Brass Instrument Optimization - Part I. Concept and Implementation. in: Proceedings of the 137th Meeting of the ASA and 2nd Convention of the EAA Forum Acusticum. DEGA, ASA, EAA, 1999.
- [8] Bertsch, M. Variability in Trumpet Sounds. Proceedings of the International Symposium of Musical Acoustics [ISMA 1997]. Vol 2. St Alban (UK): Institute of Acoustics, 1997. p.401-406.

Further information can be found through the website of the Institute for Musical Acoustics:

<http://www.bias.at/TRP>

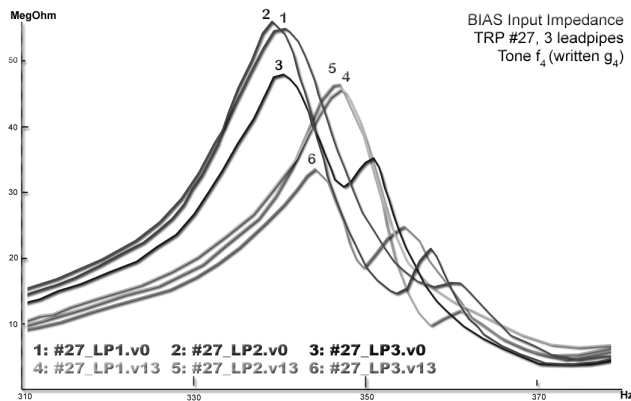


Figure 5: Impedance peaks for g4 (written f3) at 340 Hz. of one trumpet with three leadpipes. The peaks 1-3 are without valves and peaks 4-6 are with valve 1+3 engaged.

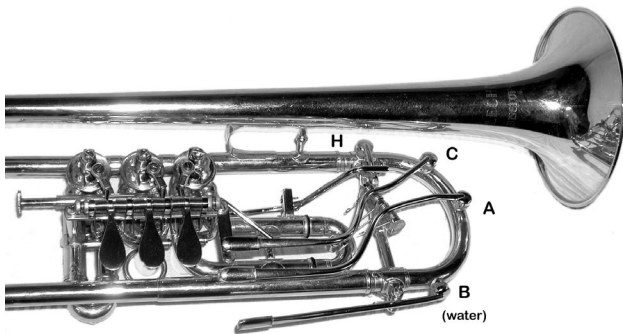


Figure 6: rotary trumpet with additional keys to support the response of higher tones. The regular water key is used for “Bb5” and “D6”, additional ones for “A5” “C6” and “H5”.

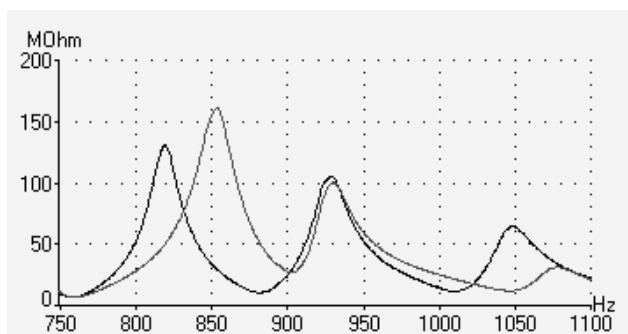


Figure 7: Impedance for the written c5 (sounding Bb4) at 930Hz with (red) without (black) the addition C-key engaged. The peak at this frequency changes slightly compared to dramatically changes of the total curve. The shift of the position and amplitude of all higher peaks has a significant influence on the played note.

## REPRODUCIBILITY AND CONTROL OF THE EMOUCHURE OF AN ARTIFICIAL MOUTH FOR PLAYING BRASS INSTRUMENTS

*S.R. Bromage, O.F. Richards, D.M. Campbell*

School of Physics  
University of Edinburgh  
seona@ph.ed.ac.uk

### ABSTRACT

Artificial mouths, based on the modelling of lips with latex tubes, have been extensively used in studies of brass instruments. The ability to make accurate comparisons between instruments, for example in spectral or listening studies, relies on the reproducibility and control of the embouchure (the static configuration of the lips). The mechanical resonance behaviour of the lips of an artificial mouth is related to characteristic parameters of the embouchure. These parameters include the rest position and internal pressure of the lips, and the extent to which the lips are squeezed by the pressure of the mouthpiece. Measurements of the mechanical response of the lips and the spectrum of the radiated sound were studied for a range of different embouchure settings. These indicate that the frequencies of the resonance peaks are well reproduced for repeated resetting of the embouchure parameters. However, the magnitudes of the peaks are less well reproduced. Reasons for this variability, and possible improvements aimed at its reduction, are discussed.

### 1. INTRODUCTION

#### 1.1. The Artificial Mouth

The sound produced when playing a brass instrument is the result of the coupling of the resonator, that is the instrument itself, the flow of air, and the resonances of the player's lips. Any study of how an instrument plays is affected by the method used to produce the initial vibration. Particularly when comparing different instruments, it is important to have a controllable playing mechanism that is as reproducible as possible. Artificial mouths have been developed to play wind instruments so as to remove many of the variations inherent in human playing.

#### 1.2. The Mechanical Response

Most musical reeds can be described as exhibiting either *inward* or *outward striking* behaviour depending on how the reed responds to an increase in blowing pressure. However, studies[1][2][3] have shown that the lips of a brass player seem to act as both inward and outward striking reeds, so allowing the player to produce notes above, below and at the resonant frequencies of the instrument.

The criteria for self-sustained oscillation dictate the phase relationships, given in equation 1, between  $h(\omega)$  the oscillating component of lip opening and  $\Delta P(\omega)$  the oscillating pressure difference across the lips. For inward striking behaviour the phase difference  $\angle C(\omega) = +\pi/2$  and for outward striking  $\angle C(\omega) = -\pi/2$ . By examining the magnitude and phase of the response of

the lips to an applied acoustic pressure it is possible to identify resonant peaks that correspond to inward and outward striking modes of vibration.

$$\angle C(\omega) = \angle h(\omega) - \angle \Delta P(\omega) \quad (1)$$

### 2. EXPERIMENTAL SETUP

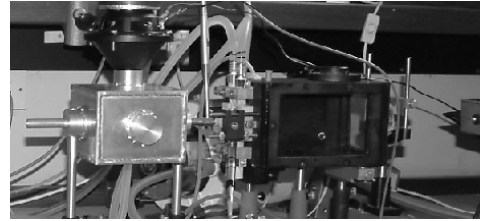


Figure 1: *Experimental apparatus.*

There exist several designs of artificial mouth for playing brass instruments. The design used in this study (see figures 1 and 2) is that used by Richards et al[2]. It differs from designs used in earlier studies mainly in that the lips are mounted externally. This makes the mouth compatible with a wide variety of mouthpieces and enables easy adjustment of the embouchure. The parameters which can be adjusted are the rest position of the lips as determined by the position of the two lip guides (shown in figure 2), the internal water pressure of the lips, and the extent to which the lips are squeezed by the pressure of the mouthpiece, determined by the position of the mouthpiece relative to the mouth.

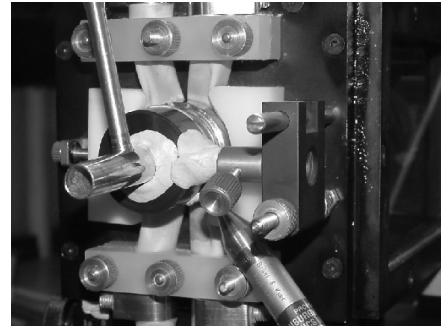


Figure 2: *Close up of artificial lips, showing lip guides and mouthpiece attachment.*



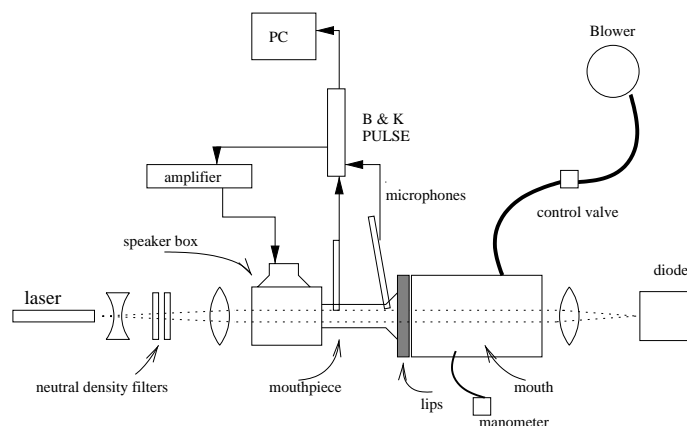


Figure 3: Experimental setup.

In this study the various parameters which determine the embouchure were set, changed and reset. Comparisons of results give some measure of the reproducibility of the system.

The overall setup is shown in figure 3. The lips were excited from the downstream side by an acoustic pressure provided by a speaker mounted on a box adapted to fit the mouthpiece shank (see figure 4). The signal used was a chirp over the frequency range 30Hz - 750Hz. Data was collected using the Brüel and Kjær PULSE system. The driving pressure was measured in the mouthpiece with a Brüel and Kjær probe microphone and the amplitude of the lip response was measured using a photodiode. The PULSE system calculates the magnitude and phase of the response of the lips to the applied acoustic pressure. By supplying a static overpressure in the mouth, above threshold, the playing frequency could be measured and the sound in the mouthpiece shank was recorded using a Brüel and Kjær  $\frac{1}{4}$ " microphone and the PULSE system.

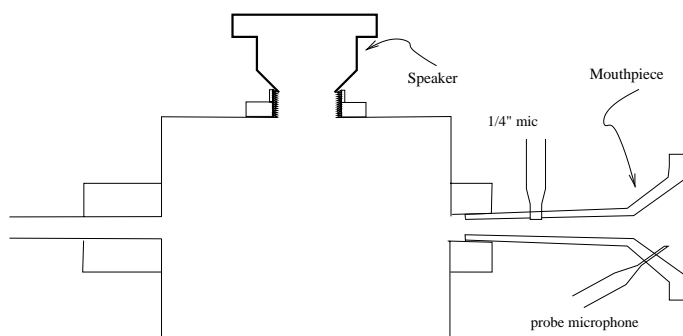


Figure 4: Speaker box and mouthpiece.

A program developed by Cullen[1] was used to fit curves to each of the resonances in the mechanical response. This program then outputs the frequency, quality factor and maximum value of each of the fitted curves.

### 3. RESULTS

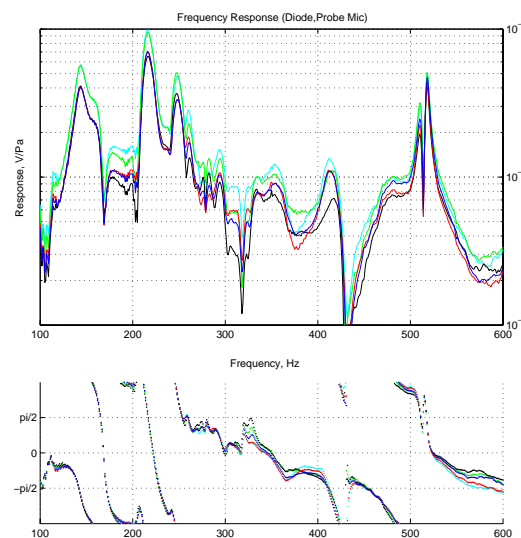


Figure 5: Five responses taken immediately one after the other.

Figure 5 shows five repeated measurements of the mechanical response, taken immediately one after the other. There are small variations in the magnitudes of the resonance peaks; for example, the peak at 216 Hz varies from 6.5 to 9.9 mV/Pa. Frequencies were constant within experimental accuracy (1Hz resolution) and quality factors varied by around 10%. Figure 6 shows that similar variations are observed when the system is played between each mechanical response measurement.

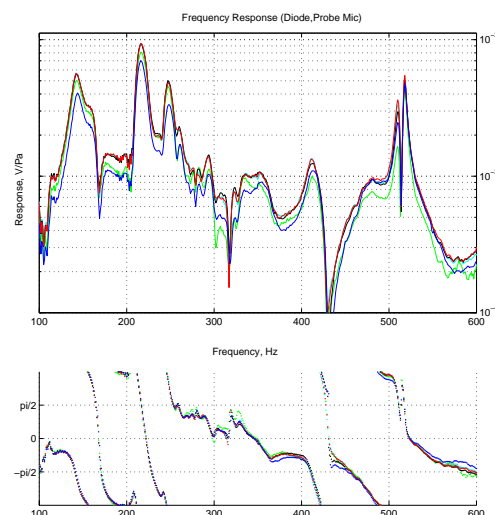


Figure 6: Five repeated responses, playing between.

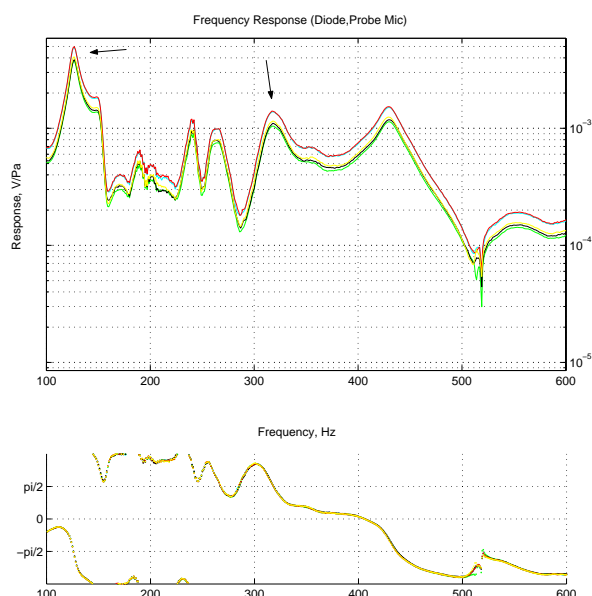


Figure 7: Five repeated responses, playing between.

Figure 7 again shows repeated measurements of the mechanical response, playing between measurements, but for a different initial embouchure. Values for the marked resonance peaks are given in Table 1. Examination of the spectrum of the sound measured in the mouthpiece shank shows that the levels of the first seven harmonic peaks are within 4dB, which should not be noticeable[4] and the other peaks detectable above the noise level vary by less than 8dB. The overall sound level varied by less than 0.5dB and the playing frequency was constant within the 1Hz resolution.

Dataset colour	Frequency Hz	Response mV/Pa	Quality factor
black	127.0	3.9	15.5
green	126.5	3.7	15.0
cyan	127.0	4.8	15.0
red	126.5	4.9	15.0
yellow	126.5	4.0	15.0
black	318.5	1.1	15.5
green	318.5	1.0	14.0
cyan	318.5	1.4	14.5
red	318.0	1.4	16.0
yellow	318.5	1.1	14.5

Table 1: Values for five responses shown in figure 7.

Similar small variations are observed when resetting the lip pressure though it has been found in practice that in order to make an effective change in the static position of the lips the mouthpiece must first be removed and then replaced to avoid the lips sticking to the mouthpiece surface. Greater variations are observed when the mouthpiece is moved and then replaced against the lips. Figure 8 shows five examples of this for the same initial embouchure as in figure 7. Again Table 2 gives values for the marked peaks.

Dataset colour	Frequency Hz	Response mV/Pa	Quality factor
red	126.5	4.0	15.0
green	125.5	5.0	16.0
cyan	123.0	7.9	16.5
black	122.0	7.5	16.0
yellow	124.5	5.2	16.5
red	318.5	1.1	14.5
green	316.5	1.5	17.0
cyan	316.0	1.1	23.5
black	315.5	.83	34.0
yellow	316.0	.72	—

Table 2: Values for five responses shown in figure 8.

Here the sound level measured in the mouthpiece shank varied by 11.3 dB. One possible reason for this variation is the lack of rigidity in the lips. As they are released (by removing the mouthpiece) and squashed again (by replacing the mouthpiece) they are able to settle into a number of different equilibrium positions. In order to achieve the same embouchure it is necessary to have a specific procedure which causes the lips to settle into the same position. Lubricating the surface of the latex lips with talcum powder could help avoid them 'sticking' to the mouthpiece and so being pulled into different positions.

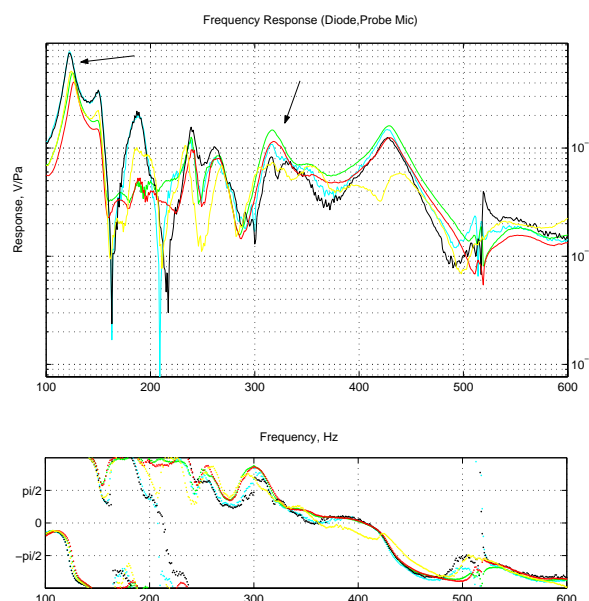


Figure 8: Five repeated responses, resetting mouthpiece position.

The nature of a resonance peak, not just its frequency, is important as it affects the output sound obtained. Looking at the five response curves in figure 8, variations in the Q factors of the dominant resonance peak (around 320Hz) seem to correlate well with the level of the radiated sound. With the black and cyan curves (Q factors 34 and 23.5) the sound was much louder (+4.4dB and +4.6dB) than with the red and green curves (Q factors 14.5 and

17). With the yellow curve it was much quieter (-6.7dB) and no curve could be matched to the peak as it was so poorly defined.

The process of connecting the mouthpiece shank to the speaker box is another possible source of variation. Figure 9 shows variations in the mechanical response curves obtained by moving and replacing the speaker box while the mouthpiece remains fixed in place. The exact cause of these variations is unclear but the process of reconnecting the box and mouthpiece seems to 'nudge' the mouthpiece slightly, suggesting that a more rigid mouthpiece support is required.

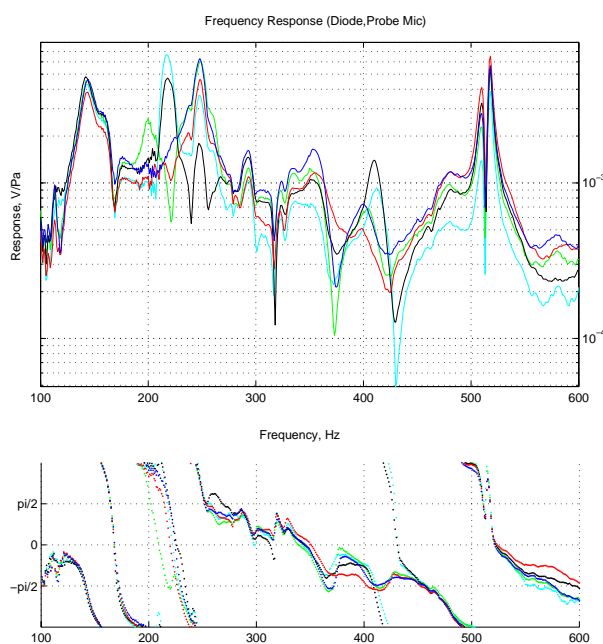


Figure 9: Five repeated responses, resetting speaker box position.

One major source of variation is in the simple design of the lip guides. While they effectively provide support for the lips and to a certain extent they determine the static lip separation, they do not fully constrain the position of the lips. When the mouthpiece is in place the lips can be 'prodded' into a wide range of positions. Figure 10 shows examples of different responses obtained in this way; playing frequencies ranged from 232Hz to 451Hz. Alternative designs of lip guides (both external and internal) are being developed as a possible solution to this problem.

#### 4. CONCLUSIONS

This design of artificial mouth was developed to play a variety of instruments and to more easily allow changes to the parameters that define the embouchure. While gaining this greater flexibility some control has been lost. Several improvements have been suggested to allow a wide variety of more reproducible embouchures.

It should be remarked that the parameters chosen in this study come from a relatively restricted set which have been found to give robust and stable playing behaviour.

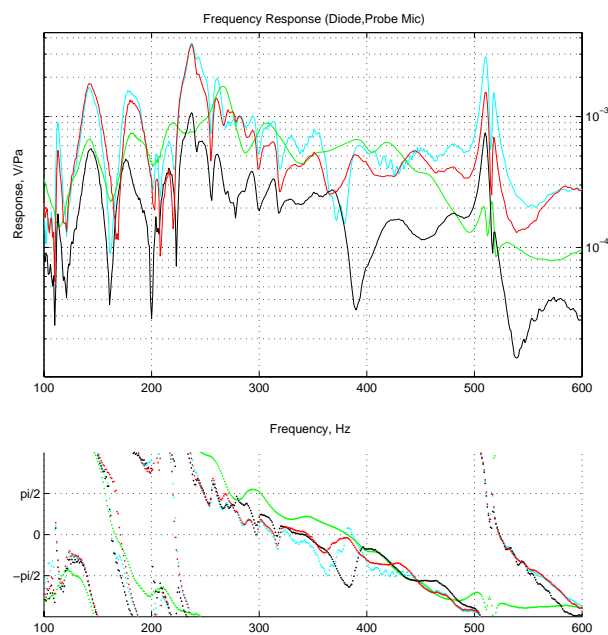


Figure 10: Five repeated responses, 'prodding' the lips.

#### 5. REFERENCES

- [1] Cullen, J.S., A study of brass instrument acoustics using an artificial reed mechanism and other techniques. Ph.D. thesis. The University of Edinburgh, 2000.
- [2] Richards, O.F, Campbell, D.M., Gilbert, J., and Neal, M.A., "Use of experimental studies in determining a two-mass lip model", SEVILLE Proc., 7(6):697-708, 2002.
- [3] Neal, M.A, Richards, O.F, Campbell, D.M., and Gilbert, J. "Study of the lip reed destabilisation using an artificial mouth", Proc. IoA 2002, March 2002.
- [4] Carral, S., Campbell, D.M., "The influence of the mouthpiece throat diameter on the perception of timbre of brass instruments", Proc. ISMA 2002 Mexico City, December 2002.
- [5] Cullen, J.S., Gilbert, J., and Campbell, D.M., "Brass instruments: Linear stability analysis and experiments with an artificial mouth." J. Acoust. Soc. Amer., 86:704-724, 2000.
- [6] Campbell, D.M., "Nonlinear dynamics of musical reed and brass wind instruments", Contemporary Physics, 40:415-431, 1999.
- [7] Brüel and Kjær "PULSE Manual" 2000.

## **AUSTRALIAN ABORIGINAL MUSICAL INSTRUMENTS: THE DIDJERIDU, THE BULLROARER AND THE GUMLEAF**

*Neville H. Fletcher*

Research School of Physical Sciences and Engineering, Australian National University,  
Canberra 0200, Australia, and also  
School of Physics, University of New South Wales, Sydney 2052, Australia

neville.fletcher@anu.edu.au

### **ABSTRACT**

The Australian Aboriginal people developed three musical instruments – the didjeridu, the bullroarer, and the gum-leaf. Most well known is the didjeridu, a simple wooden tube blown with the lips like a trumpet, which gains its sonic flexibility from controllable resonances of the player's vocal tract. The bull-roarer is a simple wooden slat whirled in a circle on the end of a cord so that it rotates about its axis and produces a pulsating low-pitched roar. The gum-leaf, as the name suggests, is a tree leaf, held against the lips and blown so as to act as a vibrating valve with "blown-open" configuration. Originally intended to imitate bird-calls, the gum-leaf can also be used to play tunes.

### **1. INTRODUCTION**

The Australian Aboriginal people have lived in this country for more than 40,000 years with almost no contact with the outside world. During that time they developed sophisticated tools such as the woomera spear-thrower and the returning boomerang. They also developed three musical instruments – the didjeridu, usually spelt "didgeridoo" in the non-academic literature and actually called a yidaki or yiraki in the Aboriginal language of the region where it originated, the bull-roarer, and the gumleaf. The didjeridu is a simple wooden tube blown with the lips like a trumpet, which gains its sonic flexibility from controllable resonances of the player's vocal tract. The bull-roarer, called by other names in Aboriginal languages, is a simple wooden slat whirled in a circle on the end of a cord so that it rotates about its axis and produces a pulsating low-pitched roar. The gum-leaf, as the name suggests, is a leaf from a Eucalypt tree, held against the lips and blown so as to act as a vibrating valve with "blown-open" configuration, denoted by (+,-). The sounding pitch is controlled by vocal tract resonances and is typically about an octave above the female singing voice. Originally intended to imitate bird-calls, the gum-leaf can also be used to play tunes. This paper will briefly describe each of these instruments.

### **2. THE DIDJERIDU**

The didjeridu originated in Arnhem Land on the northern coastline of central Australia, and has some similarity to bamboo trumpets and even bronze horns developed in other cultures, though it pre-dates most of these by many millennia. The characteristic feature is that the didjeridu, which is a slightly flaring wooden tube about 1.5 metres in length, is simply hollowed out by natural termites ("white ants") from the trunk of

one of the small trees of the region. After cutting down, the instrument is cleaned out with a stick, the outside refined by scraping and then painted with traditional designs, and the blowing end smoothed by adding a rim of beeswax.

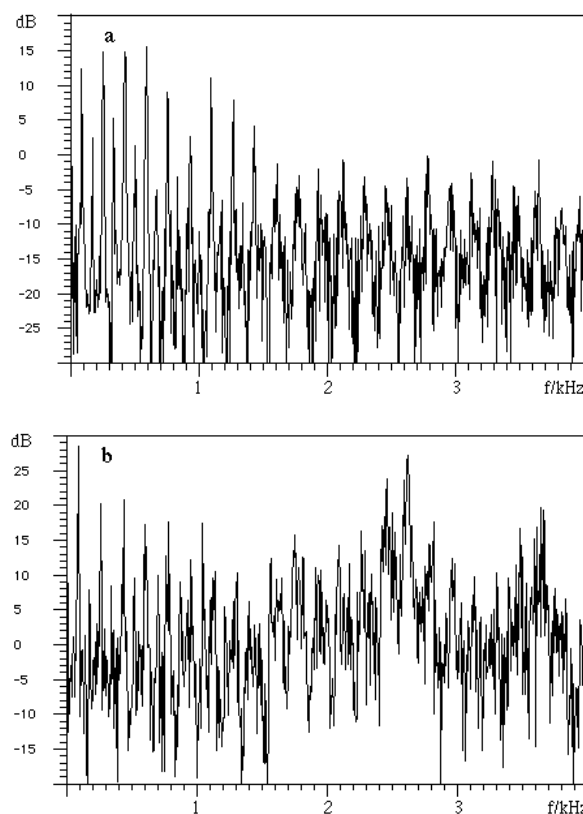


*Figure 1. Spectra of didjeridu sound. (a) an uninflected drone, and (b) a drone with two prominent formant bands. (From [4])*

The predominant sound of the didjeridu is a low-pitched drone with frequency around 70Hz, but depending significantly upon the length of the instrument and the flare of its bore. The second mode of the tube, with frequency a little less than 1.5 times that of the fundamental (because of the tube flare) is used sparingly as an accent to the sound, and the main variation comes from production of pronounced formant bands, the frequencies of which can be adjusted by the player over a range

from about 1kHz to 3kHz, as shown in Fig. 1. In traditional use, the didjeridu, with clap-sticks for emphasis, accompanies songs or illustrates traditional stories about ancestors and animals [1]. Recently, however, its use has spread into the popular music domain and has had world-wide influence [2].

The acoustics of the didjeridu tube is simple. Because of the irregular shape and general slight flare, the upper resonances (impedance maxima) are not well aligned with odd harmonics of the fundamental, and the main determinant of quality is the smoothness of the walls, on a sub-millimetre scale, and the absence of cavities. The diameter of the blowing end, typically about 30mm, must also match the expectations of the player.

The real acoustic interest comes from the techniques by which unusual sounds are made [3]. The prime technique is one involving adjustment of the impedance maxima of the vocal tract, as judged from the vibrating lip valve, since this impedance is effectively in series with the comparable impedance of the didjeridu tube itself. The player achieves this adjustment by raising the tongue to narrow the airway near the lips and further adjusting the spacing between the rear of the tongue and the hard palate [4]. Some further results of research on this subject are presented in another paper at this conference [5]. The main reason that these techniques are so effective in the didjeridu, compared with other lip-driven instruments, is that the diameter of the instrument bore near the lips is quite similar to that of the upper vocal tract, and there is no intervening mouthpiece cup to isolate one from the other.

The other impressive contribution to didjeridu sound comes from a technique in which vocalisation occurs simultaneously with normal lip-generated drone. There are then two pressure-operated valves, the vocal folds and the lips, acting in series upon the air flow. Because the operation of each valve is nonlinear, since the air flow is essentially governed by a Bernoulli equation, this generates multiple sum and difference frequencies  $n f_1 \pm m f_2$  in the sound output [3]. If the player sings a note a musical tenth above the drone, so that  $f_2 = (5/2) f_1$ , then in particular the sub-octave  $f_1/2$  is generated, giving a deep "growl". In addition, the player may insert many other transient sounds to mimic the cries of dingoes or birds, with marked dramatic effect.

### 3. THE BULLROARER

Since there are no bull-like animals in Australia, this is a misnomer for the Aboriginal instrument, but the actual word used is "secret-sacred" and not shared with non-Aboriginal people. The instrument itself consists of a simple wooden slat, 30 to 40cm in length and 5 to 7cm wide that is whirled around in a circle on the end of a length of cord. The slat rotates under the influence of aerodynamic forces and generates a pulsating sound with a frequency typically around 80Hz. This sound is an important feature of Aboriginal initiation ceremonies.

The instrument itself is by no means unique to Australia, and similar sound generators have been used by populations as diverse as those of ancient Egypt and the Inuit of Northern Canada. An Australian instrument is shown in Fig. 2.

The aerodynamics of sound generation in the bullroarer has been described in detail elsewhere [6], and only an outline will be given here. Since the quasi-static aerodynamic forces and torques on the slat balance out over a single period of its

revolution, the aerodynamic torque driving its rotation depends upon the rate of rotation itself. There is one rotation-inducing torque term that is linear in slat rotation speed, and also a drag term proportional to the square of the rotation speed. These lead to a threshold rotation rate that must be exceeded to begin the process, and then to an upper limit to the rotation rate. The steady angular rotation rate  $f$  of a rectangular slat of width  $W$  swung through the air on a string of length  $L$  with rotation frequency  $F$  can be shown to be approximately

$$f \approx 1.1 LF/W - 5.$$

Each rotation of the slat creates an oscillating flow dipole and, from considerations of symmetry, the dipole oscillation frequency, and thus the radiated sound frequency, is  $2f$ . The radiated acoustic power  $P$  is approximately

$$P \approx 3 (\rho/c^3) H^2 V^6$$

where  $H$  is the length of the slat,  $\rho$  is the density of air,  $c$  is the speed of sound in air, and  $V=2\pi LF$  is the speed of the slat through the air. From these two equations we see that wide slats produce sound of lower frequency but that the radiated power is independent of slat width. Sound frequency is, however, proportional to airspeed and thus to arm rotation rate, and the radiated power is a strong function of this arm rate. For typical conditions, the radiated power is a few milliwatts for an arm rotation rate of 120 r.p.m., which is about as fast as can normally be achieved. Sound radiation is nearly omnidirectional.

Because the output power is a strong function of airspeed  $V$ , and the arm rotation is normally faster on the down-sweep than on the up, the sound pulsates with a frequency typically between 1 and 2Hz. There is an additional slower pulsation with a period of several seconds that derives from the fact that the slat rotation gradually twists the cord, providing a contrary torque which eventually stops the rotation and re-launches it in the opposite sense.

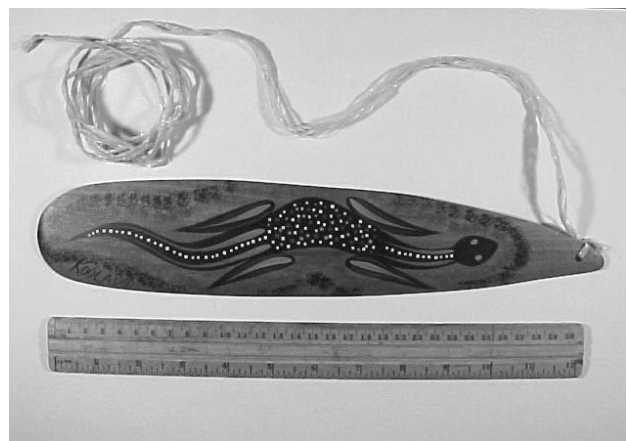


*Figure 2. An Australian bullroarer. Note the decorations, which show the totemic symbol of the tribe of the maker. (From [6])*

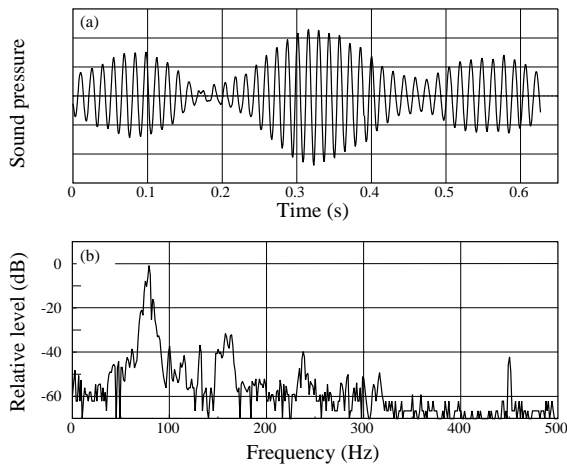


Figure 3. (a) The pressure waveform of sound from a bullroarer, showing typical pulsations. (b) Frequency analysis of this sound, showing low harmonic development. (From [6])

Analysis of the sound, as in Fig. 3, shows little harmonic development, the second-harmonic peak being about -30dB relative to the fundamental. The peaks are, however, somewhat broadened because of the variable rotational speed of a human arm.

#### 4. THE GUMLEAF

The gumleaf is altogether more primitive as a musical instrument, since it consists simply of a leaf, the shape of which is illustrated in Fig. 4(a), from one of the various species of Eucalypt trees growing throughout Australia, held against the lips using the fingers of both hands. It does, however, have a long tradition and culture [7].

In the normal playing configuration, shown in Fig. 4(b), the leaf is held tightly against the lower lip and, in a bent shape, lightly against the upper lip [8]. It is stretched rather tightly between the two hands. When air pressure is applied through the mouth, it tends to lift the top of the leaf away from upper lip and allow air to escape, so in this sense the valve can be described as an “outward-swinging door”, which is given the symbol (+,-), indicating the effect on the flow of applying pressure from the supply side (+) and from the exhaust side (-). Its configuration is thus similar to that of the valve constituted by the lips of a brass-instrument player, although these are sometimes (+,+) as in a sliding door, and the opposite of the reed of a clarinet, which is (-,+), as in an inward-swinging door. The acoustic behaviour of valves of each of these types has been examined elsewhere [9,10], and this treatment provides the basis for the present discussion.

Although it takes a good deal of trial and error for a beginner to even produce a sound from a gumleaf held as indicated in Fig. 4(b) above, a skilled player can control the pitch with good accuracy over a range of more than an octave and play simple tunes with ease, the pitch range being typically from about 500 to 1000Hz. Interest therefore centres on exactly how this is done.

Theory [9] and experiment [10] agree that for a valve with configuration (+,-) to oscillate, the sum of the up-stream and

down-stream acoustic impedances must have a negative imaginary component. Since the downstream impedance is essentially zero in this case, this implies that the mouth and vocal tract must present a compliant (capacitive) impedance at the lips. When this condition is satisfied, the valve will oscillate provided the applied air pressure exceeds a certain threshold and the losses are not too great. The actual oscillation frequency is necessarily higher than the mechanical resonance frequency of the elastically braced leaf, and is further determined by the magnitude of the impedance presented by the mouth to the leaf. If the imaginary part of this impedance is negative and large, corresponding to a small enclosed air volume in the mouth and a narrow passage to the lower vocal tract, then the oscillation frequency of the valve will be much higher than its natural frequency. In many ways, then, the technique for varying the mouth and vocal tract when playing the gumleaf is similar to that used in whistling.

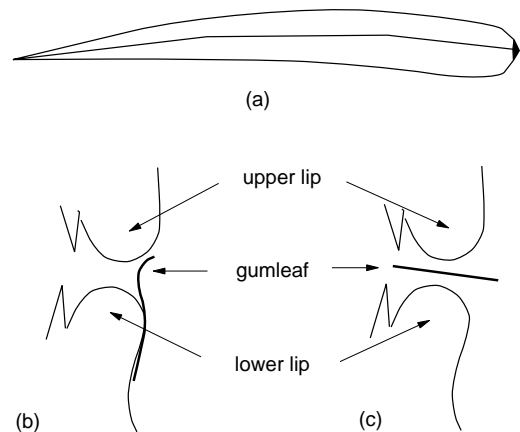


Figure 4. (a) The shape of a typical gumleaf from a Eucalypt tree. (b) In normal playing, the leaf is held firmly against the lower lip and rested lightly against the upper lip, and it is the upper edge of the leaf that vibrates. (c) A variant way of holding the leaf that results in a raucous quasi-chaotic sound.

As the gumleaf valve opens and closes, so the pressure in the mouth falls and rises, with a phase advance of about  $\pi/2$  relative to the lip opening. Because the airflow through the valve is in turn proportional to its opening area and to the square root of the driving pressure, this nonlinear relationship generates harmonics of the fundamental frequency, and the sound is rich in upper partials and has an incisive quality.

There is one other way of playing the gumleaf that is also worthy of mention. The configuration used is shown in Fig. 4(c), with the leaf simply lying parallel to the slot between the lips. As a variant, the leaf is sometimes held vertically between the sides of two opposed thumbs, which are pressed against the lips to create essentially the same configuration. The aerodynamic behaviour is now very different, and laboratory investigations suggest that the leaf, which is essentially flat, moves backwards and forwards in the slot and, at the same time, twists about its longitudinal axis. This motion repeatedly narrows and widens the flow channel at a frequency equal to twice the mechanical oscillation frequency of the leaf and so has

a similar effect on the air flow and thus on the emitted sound. In a larger-scale laboratory experiment the motion could be made simple and regular, but in most playing situations the leaf makes irregular contact with the lips or the thumbs and this upsets the motion. The resulting sound, while having a predominant pitch, is rough and quasi-chaotic. It is useful for special effects, such as imitating the cry of the native sulphur-crested cockatoo [11], but has no obvious musical value.

## 5. CLAPSTICKS

As in most cultures, the Aborigines also used percussive instruments in their ceremonies. Often these were simply two boomerangs clashed together, but they also made special shaped sticks for this purpose. Because the wood used is a fine-grained hardwood, the clapsticks are physically long-lasting and produce a sharp and well defined sound.

In their usual form, these sticks are about 200mm in length and 20mm in diameter and are shaped to a long point at each end. One stick is held in each hand and they are struck together at about the mid-point of each. The pointed ends ensure that the fundamental transverse vibration has a high frequency, so that the percussive effect stands out well above the drone of the didjeridu.

## 6. CONCLUSION

Ethnomusicology is a very interesting field, and it is made even more interesting when allied with a study of the acoustics of the musical instruments that were developed by the society under study. The musical instruments of the Australian Aboriginal people have come into world prominence because of the popularity of the didjeridu, both as a tourist item and as a musical instrument. It is only recently that we have begun to have an appreciation of the acoustical subtleties associated with performance on this and other ancient instruments.

## REFERENCES

- [1] Jones, T.A., "The didjeridu" *Studies in Music* (University of Western Australia) Vol 1, 23–55, 1967.
- [2] Neuenfeld, K. (ed.) *The Didjeridu: From Arnhem Land to Internet*, John Libbey & Co, Sydney, 1997.
- [3] Fletcher, N.H. "The didjeridu (didgeridoo)" *Acoustics Australia*, Vol. 24, 1–11, 1996.
- [4] Fletcher, N., Hollenberg, L., Smith, J., and Wolfe, J., "The didjeridu and the vocal tract" *Musical Sounds from Past Millennia*, Proc. ISMA-2001, Perugia, ed. D. Bonsi, D. Gonzales and D. Stanzial, Vol. 1, 87–90, 2001.
- [5] Wolfe, J., Tarnopolsky, A.Z., Fletcher, N.H., Hollenberg, L.C.L., and Smith, J., "Some effects of the player's vocal tract and tongue on wind instrument sound" *Proc. Stockholm Music Acoustics Conference, SMAC03*, KTH, Stockholm, 2003.
- [6] Fletcher, N.H., Tarnopolsky, A.Z., and Lai, J.C.S., "Rotational aerophones" *J. Acoust. Soc. Am.*, Vol. 111, 1189–1196, 2002.
- [7] Ryan, R., 'A Spiritual Sound, A Lonely Sound': *Leaf Music of Southeastern Aboriginal Australians, 1890s–1990s*. PhD thesis, School of Music, Conservatorium, Monash University, Clayton, Australia, 1999.
- [8] Patten, H. *How to Play the Gumleaf*, (booklet and CD) Currency Press, Strawberry Hills, NSW, Australia 1999.
- [9] Fletcher, N.H., "Autonomous vibration of simple pressure-controlled valves in gas flows" *J. Acoust. Soc. Am.*, Vol. 93, 2172–2180, 1993.
- [10] Tarnopolsky, A.Z., Fletcher, N.H., and Lai, J.C.S., "Oscillating reed valves — An experimental study" *J. Acoust. Soc. Am.*, Vol. 108, 400–406, 2000.
- [11] Fletcher, N.H., "A class of chaotic bird calls?" *J. Acoust. Soc. Am.*, Vol. 108, 821–826, 2000.

## STUDYING LIP OSCILLATORS OF BRASS INSTRUMENTS: A DISTRIBUTED TWO DIMENSIONAL LIP MODEL AND ITS ELECTRICAL EQUIVALENT CIRCUIT.

Wilfried Kausel

Department of Musical Acoustics  
University of Music, Vienna, A-1010, Austria  
Phone: (43) 1-71155-4311, email: kausel@mdw.ac.at

### ABSTRACT

In order to understand the mechanism of sound production in brass wind instruments, valuable theoretical and experimental work has been published by several authors. They proposed to model lips as outward or inward striking doors [1], opened by positive or negative pressure differences between mouth and mouthpiece, or as sliding doors, driven by the Bernoulli pressure between the lips [2]. All three simple models exhibit self sustained oscillations when combined with a pressure source (lung) and an input impedance (instrument).

Anyhow, the fact that a human player can easily play above as well as below the air resonances of an instrument cannot be reproduced by any of the simple models [3]. Therefore a combination of two simple models (stretchable outward striking door) has been proposed by Adachi [4]. This combined model exhibits the observed bi-directional pitch controllability at least for the two lowest played notes.

In order to enable application of more realistic complex models, a simulation environment based on electrical equivalent circuits has been proposed by the author and a one dimensional distributed wave guide model of the lip has been presented [5].

In this paper a two dimensional distributed lip model is proposed which is able to exhibit surface waves travelling between the teeth and the mouth piece rim. Surface waves are interacting with forces originating from the pressures in the mouth, in the mouthpiece and in the lip orifice. Phase speed depends on the tension of the lip.

### 1. INTRODUCTION

Since Helmholtz [1] classified wood wind instruments as having reeds operating like inward striking doors tending to close with increased mouth pressure, many attempts have been made to find a corresponding simple model for the oscillator of brass wind instruments.

Although it seems obvious, that the lip reeds of brass wind instruments are operating like outward striking doors, opening with the blowing pressure, it was found that some experimental evidence is in contradiction to that simple assumption [3]. According to that model tones would always sound sharper than the corresponding air resonance and it would be impossible to 'lip' them down. To excite air resonances, lip resonances are always required to be slightly lower.

Treating the lip as inward striking door tending to close with increased mouth pressure would yield the opposite result. A lip tension resulting in a lip resonance well above the air column res-

onance would be required and the sounding pitch would always be flatter than the air resonance.

Experimental evidence indicates that both mechanisms are in action simultaneously and good players seem to be able to control, which effect is dominating. Anyhow, it is not straight forward to understand, how the lip orifice can be closed by a higher blowing pressure.

In 1982 Elliot and Bowsher [6] raised the question about the role of the time-varying Bernoulli pressure, which has the ability to close the valve by applying a force perpendicular to the direction of air flow. This idea was elaborated by Saneyoshi et al. [2] introducing a third concept, which is now referred to as transverse model.

The three concepts are illustrated in figure 1, which was taken from publications of Adachi [7][4], where a much deeper investigation of these models can be found. In [7] a direct comparison between the sliding and outward-striking door models has been made. In [4] Adachi simulated trumpet sound using a model combining both effects.

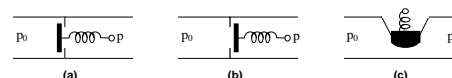


Figure 1: Classification of sound production mechanisms.

A linear theory of self-oscillation was published, reviewed and extended in [8][6][4]. A unified discussion of oscillation conditions for all three classes of oscillators was presented by Fletcher in [9].

The inward striking door model of figure 1 (a) is usually applied to woodwind instruments like clarinet and oboe. The door closes just because of a positive pressure difference between upstream and downstream region. The reed resonance must always be higher than the played frequency in order to meet the  $-\pi$  phase condition required for self sustained oscillation.

The outward striking door model of figure 1 (b) was originally applied to lip reed instruments. The door opens with a positive pressure difference between upstream and downstream region. The lip reed resonance must always be lower in order to meet the  $-\pi$  phase condition.

### 2. TRANSVERSE LIP REED MODELLING

The transverse model of figure 1 (c) is related to the inward striking door model. Closing the valve is accomplished by the Bernoulli force due to the under-pressure caused by quickly flowing fluids.



Stationary the Bernoulli pressure  $p_{lip}$  is proportional to the square of the air flow  $U$  through the area of the lip orifice  $S_{lip}$  according to [7]

$$p_0 - p_{lip} = \frac{1}{2}\rho\left(\frac{U}{S_{lip}}\right)^2 + \frac{\rho d}{S_{lip}}\frac{\delta U}{\delta t}, \quad (1)$$

where  $\rho$  is the average air density,  $d$  the length of the flow path through the lip orifice and  $p_0$  the blowing pressure.

On the other side the Bernoulli pressure  $p_{lip}$  is connected to the mouthpiece pressure  $p$  by [7]

$$p_{lip} - p = -\rho U^2 \left( \frac{1}{S_{cup} S_{lip}} - \frac{1}{S_{cup}^2} \right), \quad (2)$$

with  $S_{cup}$  as the cross-sectional area of the mouthpiece entryway.

Adding equation 1 and equation 2 yields an equation for the airflow  $U$ . After the decay of some transients (neglecting the inertia) it will become proportional to the square root of the pressure difference  $p_0 - p$  between mouth and mouthpiece:

$$U = S_{cup} S_{lip} \sqrt{\frac{2(p_0 - p)}{\rho(S_{cup}^2 - 2S_{cup} S_{lip} + 2S_{lip}^2)}} \quad (3)$$

If the sliding door tends to close with increasing air flow  $U$ , it closes with increasing pressure difference  $p_0 - p$ . This explains, why the transverse model is considered to show similar behavior like the inward striking reed [6]. In [7] f.e. it exhibits self sustained oscillations only below the corresponding air resonances requiring lip resonance frequencies well above the sounding frequency.

But this is not necessarily the case. Simulations of a transverse model presented by the author [5] showed the opposite behavior. The self sustained oscillations occurred only above the corresponding air resonances with lip admittance peaks well below the sounding frequencies. This characteristic is normally attributed to the swinging door model and therefore more investigations have been made.

## 2.1. Stability Analysis of One-Dimensional TL-Model

In order to exhibit self sustained oscillations in any closed feedback loop, it is necessary, that the open loop gain exceeds unity at an oscillation frequency, where the phase shift reaches  $\pi$ . If the static open loop gain is  $\geq 1$ , that means the circuit's DC-gain is greater 1 but inverting, then the circuit will unconditionally oscillate as soon as it is closed. If this is not the case, a small temporary stimulus signal has to be applied, to excite a self sustained oscillation. If a broadband initial excitation signal like a short pulse is applied, usually the lowest frequency, which meets the oscillation condition, will be triggered.

Let us start the investigation of a lip reed oscillator according to the transversal model at the air pressure  $p_{lip}$  in the lip orifice. This pressure applies a force to the lip perpendicular to its surface. This force is proportional to area of the lip surface, which is exposed to this pressure.

The lip itself acts as a distributed mass-stiffness system with a complex input admittance function. A maximum of the input admittance magnitude corresponds to a mechanical resonance of the lip. In a one dimensional approximation it is assumed that this input admittance is identical at all points of the lip surface.

The lip admittance converts the time varying force  $f_{lip}$  applied by the Bernoulli pressure into a surface velocity  $v_{lip}$ , which can be integrated in order to obtain the lip displacement  $x_{lip}$ . This modulates the cross-section of the lip orifice  $S_{lip}$ .

The cross-section of the lip orifice modulates the acoustic flow  $U$ , which enters the mouthpiece, where it meets the input impedance of the instrument. The input impedance of the instrument converts the flow  $U$  into the mouthpiece pressure  $p$ . The pressures  $p_0$  and  $p$  together with the flow  $U$  and the area of the lip orifice  $S_{lip}$  must fulfill equation 3 (this neglects the influence of the inertia of the air in the lip orifice).

Now a new Bernoulli pressure of the open loop can be calculated according to equations 1. If there are frequencies meeting the oscillation condition, self sustained oscillations will occur.

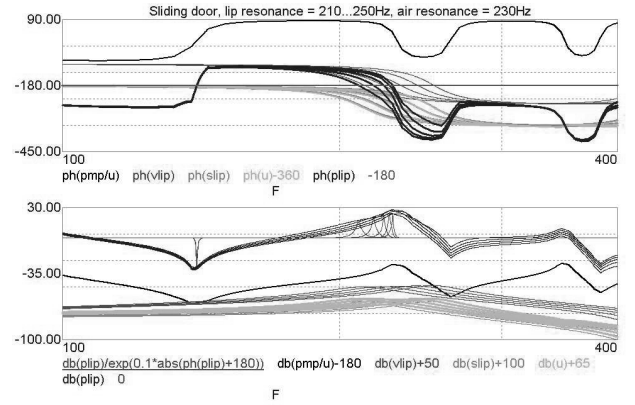


Figure 2: Stability Analysis Transversal Model.

The results of a linear stability analysis of the model which was presented in [5] is shown in figure 2. In the frequency range between 100Hz and 400Hz it displays phases (top) and gains (bottom) of some intermediate signals along the open loop as described above, when the lip resonance is varied from below to above the air column resonance of about 230Hz.

The curves labelled  $ph(pmp/u)$  and  $db(pmp/u)$  represent phase and dB gain of the input impedance function of the instrument. The curves labelled  $vlip$ ,  $slip$ ,  $u$  and  $plip$  correspond to the signals  $v_{lip}$  – the lip surface velocity –,  $S_{lip}$  – the cross-sectional area of the lip orifice –,  $U$  – the flow – and  $p_{lip}$  – the resulting Bernoulli pressure.

The sharp positive spikes in the gain plots represent the oscillation condition. They mark points of  $p_{lip}$ , where the gain is greater than 1, when the open loop phase crosses the  $-180^\circ$  line.

We can see, that the phase of  $v_{lip}$  below the lip resonance frequency is  $-90^\circ$  to become  $-270^\circ$  above it, crossing the x-axes not very steeply from up down. The slope is moderate because significant damping has been assumed. We can define a lip mobility  $\frac{v_{lip}}{p_{lip}}$  which has below its resonance a rising velocity during positive pressures and a falling velocity during negative pressures. At resonance velocity and pressure are of opposite phase.

The integration of  $v_{lip}$  into  $x_{lip}$  resp.  $S_{lip}$  subtracts  $90^\circ$  from the loop phase, while  $U$  is almost in phase with  $S_{lip}$ .

The conversion of  $U$  to  $p_{lip}$ , mainly by the input impedance, has zero phase at the resonance,  $90^\circ$  above and  $-90^\circ$  below. Much less damping is involved causing a steeper zero crossing.

In total we have  $-90^\circ$  below both resonances and at least about  $-270^\circ$  above the air resonance. The lip resonance can shift the  $-180^\circ$  phase transition point down but never up. It will shift it down even if the lip resonance is well above the air resonance because of its low Q-factor. Oscillation will take place at the phase inversion point as long as there is an open loop gain greater 1.

## 2.2. Transient Analysis of One-Dimensional TL Model

The linear stability analysis does not show any indication for the unexpected behavior of the circuit during a time domain analysis. Anyhow the effect is repeatable and could be reproduced with one and the same equivalent circuit, which was linearly analyzed above.

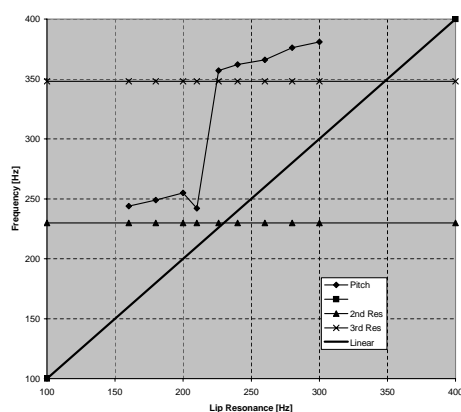


Figure 3: 2D Lip Model, Transmission Line.

The sounding pitch is plotted against the lip resonance frequency in figure 3. If there is no undetected error in the circuit, then there must be some nonlinear effect causing a transition from one side of the air resonance to the other. Further analysis is required to clarify, if oscillation regimes involving higher air or lip resonances could be a possible explanation.

## 3. TWO DIMENSIONAL LIP MODELLING

### 3.1. Equivalent Circuit

Extending the electrical equivalent circuit published by the author in [5] a two dimensional lip model has been added. The cross-section of the lip surface has been modelled as a transmission line with two reflecting terminations as shown in figure 4. One end is the point where the lip touches the teeth, the other one, where the lip is fixed by the mouthpiece rim.

The voltage waves travelling back and forth the transmission line between the two grounded end points are interpreted as Rayleigh type transversal surface waves, similar to those, which can be seen, when buzzing lips are observed under the light of a slightly desynchronized stroboscope as presented by Ayers et. al. in [10].

The waves are stimulated by and interacting with forces, related to the mouth pressure, the mouthpiece pressure and the Bernoulli pressure at several equally spaced positions along the flow path through the lip orifice. The forces are represented by currents while surface velocities correspond to voltages. The parameters of the transmission line have been chosen according to experimental data published by Yoshikawa and Muto in [11]. The phase speed of the surface waves is the independent parameter and is determined by the lip tension.

The fluid dynamical equation 1 describing the relationship between pressure drop, laminar flow and cross-sectional area has been implemented five times as shown in figure 5. Equation 1 has been split into two parts. The part proportional to the derivative of the flow, which represents the inertia of the air between the

lips, has been implemented as inductor with time varying inductance controlled by the lip displacement  $x_{lip}$ . The remaining part has been modelled by a nonlinear voltage source, controlled by the quadratic term containing  $U$  and  $x_{lip}$ . The lip displacement  $x_{lip}$  can vary along the lip orifice just like the pressure between the lips.

The expansion region, where a jet is formed and flow energy is dissipated is implemented as dependent voltage source controlled by equation 2. The load impedance is a theoretical input impedance of a Bb-Trumpet specified in the frequency domain.

For a detailed description of the simulation environment and all other components of the equivalent circuit please refer to [5].

### 3.2. Results and Conclusions

A transient analysis of the circuit described above has been made using the circuit simulator SPICE. In a first attempt the built in lossy transmission line model has been used for the segments between the points, where the pressures interact. Unfortunately this method does not allow to vary the TL parameters during one transient analysis run. Yet it is possible to step them and run the simulation automatically for many different lip tensions.

An example of the resulting wave forms is shown in 6. In this case the pedal tone has been stimulated if fortissimo (6kPa blowing pressure). The top graph contains the pressure wave forms starting with pm (mouth pressure) downstream to pmp (mouthpiece pressure). The pressure drop in between can be traced as signals pl1 to pl5, drawn with increasing gray value. With the assumptions used for the throat impedance and mouth capacitance, the mouth pressure looks still fairly constant at this playing condition.

The other graphs show lip surface velocities, displacements and lip opening areas at five points along the lip orifice.

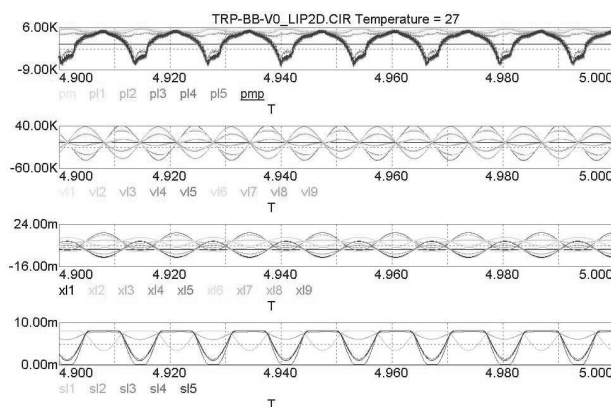


Figure 6: Time Signals of Pedal Tone.

Anyhow this approach does not simulate the real situation, where a player varies his embouchure in order to play a sequence of tones and to adjust intonation. Therefore an equivalent circuit for a lossy transmission line has been built, similar to those, which are used by telecom engineers to simulate the conditions of long telephone lines.

With this approach it was possible to vary the values of lip surface phase speed and lip damping even during one simulation run. By continuously increasing the lip tension a whole harmonic series starting with the pedal tone has been produced. Figure 7 shows the time domain signals of this "musical event".

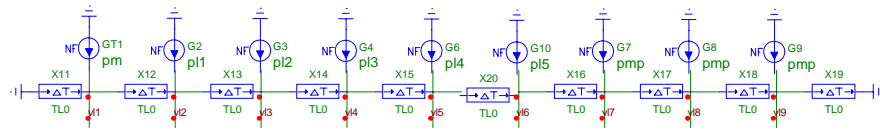


Figure 4: 2D Lip Model, Transmission Line.

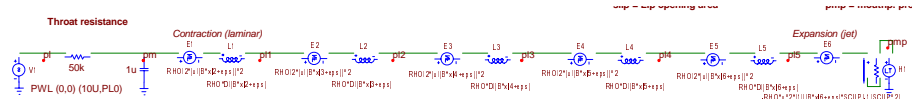


Figure 5: 2D Lip Model, Flow Path Coupling.

Now the mouth and throat parameters have been adjusted to reasonable values, so even the mouth pressure exhibits oscillations in the expected range. On top of the pressure signals the flow is plotted, appropriately scaled in order to make it visible. Below the displacements of the various lip surface points are plotted.

The  $xlq$  signal is the quiescent lip opening distance, which is controlled by a circuit in order to keep the average lip opening area proportional to the amplitude. Ideally it should set the bias value such, that the lips are closing just for a moment during any period. The negative signal parts of the  $xl_i$  are clipped, before the area  $S_{lip}$  is calculated. The average of the clipped signal parts is driving the circuit controlling  $xlq$ .

Figure 8 shows the moving lip cross-section during one period of the first resonance found in figure 7. The left side is the entry side where the teeth are fixing the lip edge. The right lip edge is fixed by the mouthpiece rim. The flow magnitude is represented by the length of the arrow and the pressure distribution along the air path by the gray value of the background. If the shape is animated nice surface waves can be observed travelling along the lip orifice.

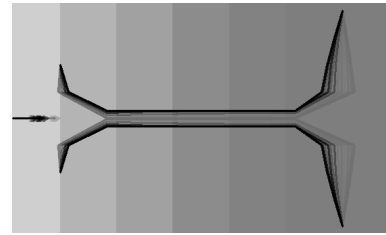


Figure 8: Lip Movement of Pedal Tone.

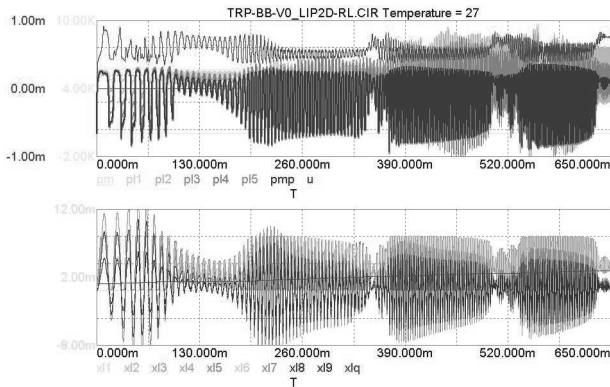


Figure 7: Time Signals of first 4 Resonances.

#### 4. REFERENCES

- [1] H. Helmholtz, *On the Sensation of Tone as a Physiological Basis for the Theory of Music*. New York: Dover, 1954.
- [2] J. Saneyoshi, H. Teramura, and S. Yoshikawa, "Feedback oscillations in reed woodwind and brass wind instruments," *Acustica*, vol. 1987, no. 62, pp. 194–210, 1987.

- [3] M. Campbell and C. Greated, *The Musicians's Guide to Acoustics*. New York: Oxford University Press, 1987.
- [4] S. Adachi and M. Sato, "Trumpet sound simulation using a two-dimensional lip vibration model," *Journal of the Acoustical Society of America (JASA)*, vol. 99, no. 2, pp. 1200–1209, 1996.
- [5] W. Kausel, "An attempt to use an electrical circuit simulator to better understand the relationship between a brass player's intonation and the instrument's input impedance," in *Revista de Acustica (Proceedings of Forum Acusticum Sevilla)*, E. A. Association, Ed. Sevilla: Sociedad Espanola de Acustica, 2002, pp. MUS-06–013.
- [6] S. J. Elliott and J. M. Bowsher, "Regeneration in brass wind instruments," *Journal of Sound and Vibration*, vol. 83, no. 2, pp. 181–217, 1982.
- [7] S. Adachi and M. Sato, "Time-domain simulation of sound production in the brass instrument," *Journal of the Acoustical Society of America (JASA)*, vol. 97, no. 6, pp. 3850–3861, 1995.
- [8] N. H. Fletcher, "Excitation mechanisms in woodwind and brass instruments," *ACUSTICA*, vol. 43, pp. 63–72, 1979.
- [9] —, "Autonomous vibration of simple pressure-controlled valves in gas flows," *Journal of the Acoustical Society of America (JASA)*, vol. 93, no. 4, pp. 2172–2180, 1993.
- [10] R. D. Ayers, R. P. Birkemeier, and L. J. Eliason, "Rayleigh wave model for the lip reed: Qualitative aspects," *Proceedings of the 137th Meeting of the ASA and 2nd Convention of the EAA Forum Acusticum, Abstract in Acustica*, vol. 85, p. 13, 1999.
- [11] S. Yoshikawa and Y. Muto, "Lip-wave generation in horn players and the estimation of lip-tissue elasticity," *Acta Acustica*, vol. 89, no. 1-2/2003, pp. 145 – 162, 2003.

## PHYSICAL MODELING OF THE TROMBONE PLAYER'S LIPS

*Daniel O. Ludwigsen*

Department of Science and Mathematics  
Kettering University

dludwigs@kettering.edu

### ABSTRACT

Physical modeling techniques are employed in this effort to better understand the behavior of the lips in a trombone/player system. The lip model incorporates the geometry and physical properties of the tissue in a solid model subject to finite element analysis. To drive the model dynamically, a simplified aerodynamic model applies pressure from the mouth, the mouthpiece, and the aperture between the lips. Feedback from the instrument informs the mouthpiece pressure. The resulting oscillation of the lip structure may be compared with that of previous models and experimental studies, and is seen to depend on both the instrument feedback and player control, as modeled by material properties of the lip tissue.

### 1. INTRODUCTION

The development of our understanding of the lip reed found in brass instruments has been a story of increasingly complex models. Helmholtz [1] described the lip reed as a particular kind of one-dimensional valve that uses pressure to regulate gas flow. That model, often called the outward-striking reed, has framed much of the discussion since. This outward-striking reed is one of three possible one-dimensional valves modeled by a mass on a spring.

#### 1.1. Lumped-element models

The other one-dimensional lumped-element models are that of the upward-striking reed and the inward-striking reed. The inward-striking reed, which will close with greater pressure upstream than downstream, describes the mechanical reed of the woodwinds.

The upward-striking reed gained greater applicability through the work of Saneyoshi, Teramura, and Yoshikawa [2], [3]. With both a modeling effort and experimental support, this group showed the behavior of the upward-striking reed must be considered in a description of the lip reed.

A hybrid lumped-element model was presented by Strong and Dudley [4], and brought to fruition by Adachi and Sato [5]. The lip mass is allowed to move in two dimensions via both swinging and stretching motions, combining the outward- and

upward-striking models. The latter work established that there is a transition in model behavior, from that of an outward-striking valve near the first mode of the instrument to an upward-striking valve for higher modes. Evidence for this transition arises primarily from phase relationships; trajectories of a point on the lip do not make as strong a case for a shift in phase. Experimental trajectories from videostroboscopy in the trombone mouthpiece [6] display prominent vertical motion. The trumpet mouthpiece may not be large enough to allow that much tissue displacement, but the trombone trajectories combine upward motion with outward swinging, with a relative phase difference that creates almost elliptical trajectories.

#### 1.2. Vocal fold model development

Lumped-element models of the vocal folds have also developed with increasing complexity and many degrees of freedom. Another approach, however, has yielded insight in the modeling of vocal fold dynamics. By creating a solid model of the continuous structure, then applying finite element analysis to that structure, many degrees of freedom can be incorporated in an elegant way. The geometry and material properties parameterize the model, based on a first-principles understanding of the physics of the vocal folds. The results of this approach have produced not only support for the utility of simpler lumped-element models, but have been used to try to understand abnormal oscillation and chaotic motion of the folds [7]. This work is a first step toward a similar study of the dynamics of the lips.

## 2. PHYSICAL MODEL

### 2.1. Continuous modeling of the lip reed

The structure of the lip is shown in cross section in Figure 1. The salient features to note are the outer layers (epithelium or skin, and mucuous membrane inside), inner muscle (orbicularis oris), and the intermediate layer of the dermis. The solid model has two distinct areas to represent muscle and dermis/skin/mucous membrane.

The solid model based on this structure is shown in Figure 2, meshed with 2-d solid finite elements (shades of gray indicate areas of two distinct types of tissue). These elements incorporate

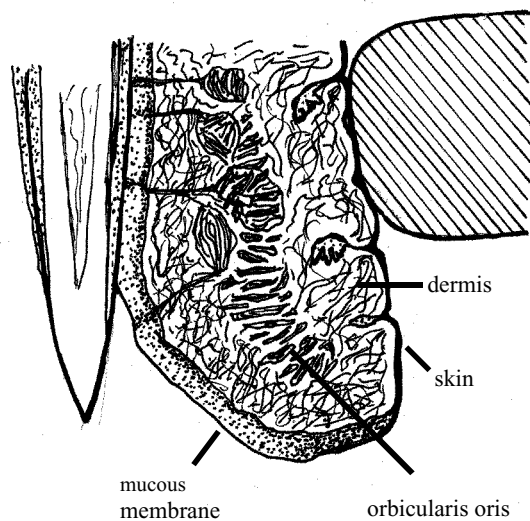


Figure 1: *The structure of the lip in cross section. Teeth and the mouthpiece rim are also shown. The essential elements of the lip structure are labeled.*

linear shape functions and isotropic governing equations from linear elastic theory. The inputs to the solid model are the parameters from elastic theory: mass density, Young's modulus, shear modulus, and Poisson's ratio. With isotropic tissue, shear modulus is found from the other two. These can be specified for distinct areas to represent the active muscle tissue and the passive outer layer.

The boundary conditions on the structure are of two types. The first is a zero-displacement constraint imposed on the upper edge of the upper lip, and lower edge of the lower lip. This serves as a first approximation to the effect of the mouthpiece rim and teeth squeezing the lip tissue. The second include the various pressure loads applied to the lip surface, dynamically specified by the aerodynamic model.

## 2.2. Aerodynamic model

The aerodynamic model traces the volume flow of air from the player's lungs, through the vocal tract, to the aperture created by the lips, and into the instrument. Most of this model can be easily understood using an equivalent impedance circuit, where pressure is analogous to voltage.

The lungs are modeled as a constant pressure source, with a gradual increase from zero at the beginning of the simulation. The lung pressure is one of the input parameters to the model. The vocal tract is represented by a pure resistance, independent of frequency. The aerodynamics of the lip aperture follow equations presented by Adachi and Sato in their model [8], with laminar flow upstream of the lips, and jet formation downstream.

The trombone resonator plays a dual role; with volume flow input at the mouthpiece, the instrument both radiates sound energy and provides feedback to the mouthpiece pressure, which has great influence on lip behavior. This is modeled by

convolutions of volume flow with two impulse response functions. The first is found from the ratio of radiated pressure (at the bell) to pressure in the mouthpiece. This ratio in the frequency domain is transformed to the time domain to give the pressure at the bell, given an injection of airflow at the mouthpiece. The second is similar, but gives the pressure at the mouthpiece as a function of time, in response to the injection of airflow. These functions were calculated from measurements of the trombone [9]. The convolutions are calculated in brute force discrete sums in a C routine which is called by the finite element package.

Other C routines keep track of all aerodynamic variables at each time step such as volume flow, mouth pressure, pressure between the lips, pressure in the mouthpiece, and pressure at the bell. Those pressures which influence lip behavior are incorporated as input loads on the structure for the next time step.

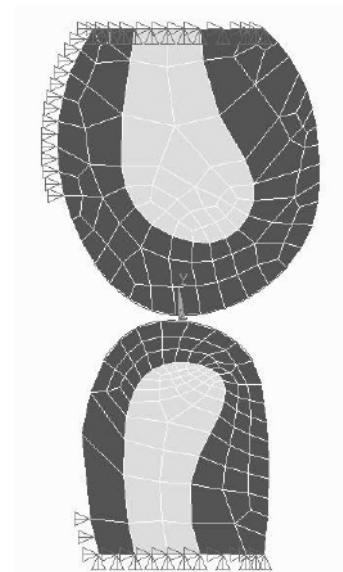


Figure 2: *The meshed solid model of the lips in cross section. Distinct tissue areas are shown by shades of gray, and zero-displacement constraints are shown with triangles. Those on the sides represent the effect of the teeth for the 117-Hz simulation.*

## 3. MODAL RESULTS

### 3.1. Mode shapes

Specifying the geometry and material properties of the lip structure is all that is needed for modal analysis of the model. Typical mode shapes are shown in Figure 3; arrows indicate maximum displacement of nodes. The material properties were chosen to approximate fairly loose lips, with Young's modulus values of  $1 \times 10^6$  and  $5 \times 10^6$  dynes/cm<sup>2</sup> for outer layer and muscle tissue, respectively. Poisson's ratio was set at 0.49 (nearly incompressible) and the mass density was 1.00 g/cm<sup>3</sup>.

The lowest mode shape for each lip has an outward swinging motion, and the second lowest mode has an upward swinging motion (possibly with some rotary motion as well).

### 3.2. Mode frequencies

The six modes shown in Figure 3 have frequencies given in Table 1.

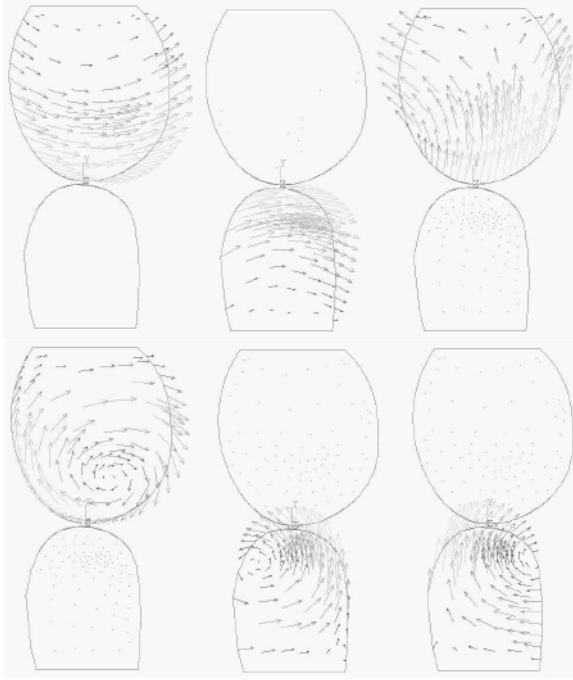


Figure 3: The lowest six modes of the fairly loose lip model. Read from top, left to right, in order of increasing mode frequency.

Mode shape	Frequency (Hz)
Upper – swinging	59.2
Lower – swinging	82.7
Upper – stretching	184
Upper – rotary	196
Lower – rotary/stretch	237
Lower – rotary/stretch	246

Table 1: The frequencies of modes with the mode shapes in Figure 2. Material properties were chosen to represent fairly loose lips.

Modes beyond these six embody increasingly complex patterns, which may lead us to believe they are less important to the control of airflow. Empirical eigenfunction analysis of dynamic simulations with this model show the lowest

eigenfunctions, similar to these mode shapes, are responsible for most of the motion.

### 3.3. Calibration of the lip model

The material properties, the geometry of the structure, and imposed boundary conditions determine the natural modes of oscillation. The process of calibrating the lip model requires choosing these to align closely with modes of the instrument. The set used for the modes described above provide a simulation of a pedal tone near 60 Hz.

In order to simulate tones near the second instrument mode at 117 Hz (used for playing the note B<sup>b</sup>2), stiffening the muscle tissue alone was not sufficient. Additional zero-displacement constraints on the surface of the lip, where teeth would have prohibited motion, was helpful in shifting the frequency of the upper lip swinging mode to 116 Hz. Further constraints on both the teeth side of the outer layer and the muscle tissue (where the rim might squeeze), together with an increase in stiffness for the inner layer, shifted that upper lip swinging mode to 169 Hz. This is near the instrument mode at 171 Hz (F3).

## 4. DYNAMIC MODEL RESULTS

### 4.1. 117 Hz instrument mode

The time series results of the dynamic model for the 117 Hz B<sup>b</sup>2 are shown in Figure 4. The lung pressure was set to 25 kdynes/cm<sup>2</sup> to simulate a mezzo-piano or mezzo-forte tone. This sets the maximum mouth pressure (mpre) seen in the third plot from the top. The lip opening area waveform bears some resemblance to the measured area waveform of Copley and Strong [6], but has greater time spent with the lips closed together. Volume velocity (flow) through the aperture is shown in the second plot. Finally, the lower two plots are, mouthpiece pressure (tpre) and radiated pressure (rpre).

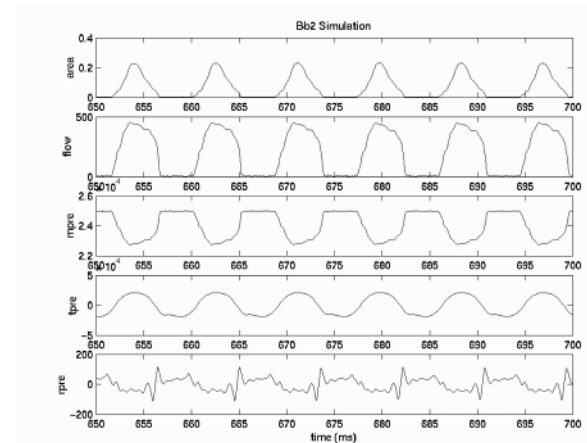


Figure 4: The waveforms from the simulation of B<sup>b</sup>2 at 117 Hz. From the top, the plots show area, volume velocity, mouth pressure, mouthpiece pressure, and radiated pressure. All units are cgs.

The extended closure of the lips is a major criticism of these results. This closure time occurs while the upper lip swings back slightly into the mouth, making contact with the lower lip. There is significant inertia which lengthens the time it takes for the upper lip to reverse its motion and open again. This delay affects the other waveforms; for example, the mouthpiece pressure “dip” is longer here than in published measurements [10].

Eigenvalue analysis (i. e., finding principal components) indicates that the swinging motion similar to the first mode is associated with 97% of the motion in the simulation. This is not surprising, since the lip structure was calibrated to employ the swinging lip mode near the 117 Hz instrument mode. However, the pure swinging motion cannot, by itself, produce the open or elliptical trajectory recorded by Copley and Strong. In this simulation, the tip of the lip returns along roughly the same path as it followed in extension.

#### 4.2. 171 Hz instrument mode

The waveforms of the F3 simulation are shown in Figure 5. Again the area plot features rather extended periods of closure, but the rapid rise and more gentle closing do replicate the experimental results of Copley and Strong. Similar concerns about the trajectory exist in this simulation as well; it too is comprised primarily of swinging motion (98%) with a closed trajectory.

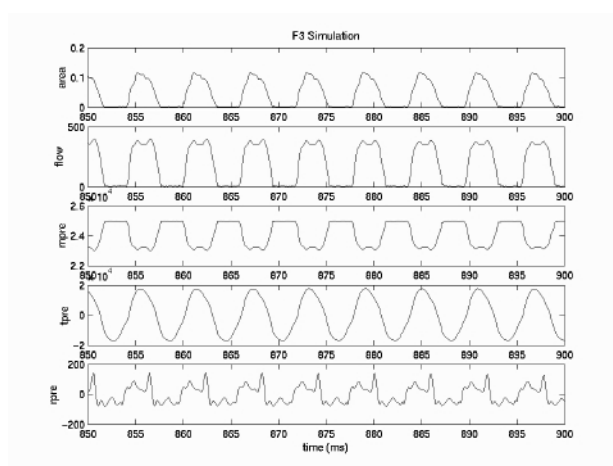


Figure 5: The waveforms produced by the simulation of F3 at 171 Hz. Axes are similar to those of Figure 4.

#### 5. CONCLUSIONS

The primary goal of this effort was to create a dynamic simulation of the lip reed in a trombone/player system featuring a finite element model of the lip reed. One measure of success is that the model produced self-sustained oscillation. From constant lung pressure, the valve action of the model's lips

created the unstable flow necessary to produce oscillation when coupled with the instrument feedback.

However, work remains to be done before this continuous model can be relied upon for guiding us to greater understanding of the behavior of the lip reed. The model structure exhibited problems of too much closure time during the cycle and poor agreement with observed trajectories of real lip motion. Both of these may stem from issues of geometry. A two-dimensional lip may not completely represent the dynamics of continuous lip structure.

A key feature missing from this work, and seen in vocal fold dynamics, is mode entrainment. Two modes of the structure sufficiently shift mode frequency during simulation so that both are involved in its motion at a particular playing frequency. This kind of combination of modes could enable both an outward and upward motion to occur at once, opening the trajectory into a more elliptical shape.

Finally, the model produced waveforms that may be auditioned. Realism is lacking in most raw simulation results, and these are somewhat flat, artificial tones. However, signatures of a brass tone can be heard, and subtle numerical artifacts add to the realism of the output waveforms.

#### 6. REFERENCES

- [1] Helmholtz, H. L. F., “*On the Sensation of Tones*,” translated by A. J. Ellis (reprinted by Dover, New York, 1954), pp. 390-394, 1877.
- [2] Saneyoshi, J., Teramura, H., and Yoshikawa, S., Feedback oscillations in reed woodwind and brasswind instruments, *Acustica*, Vol. 63, 1987, pp. 194-210.
- [3] Yoshikawa, S., Acoustical behavior of brass player's lips, *J. Acoust. Soc. Am.*, Vol. 97, 1995, pp. 1929-1939.
- [4] Strong, W. J., Dudley, J. D., Simulation of a brass player's lips, *Proceedings of the Stockholm Musical Acoustics Conference (SMAC 93)*, 1993, pp. 520-524.
- [5] Adachi, S., Sato, M., Trumpet sound simulation using a two-dimensional lip vibration model, *J. Acoust. Soc. Am.*, Vol. 99, 1996, pp. 1200-1209.
- [6] Copley, D. C., Strong, W. J., A stroboscopic study of lip vibrations in a trombone, *J. Acoust. Soc. Am.* Vol. 99, 1996, pp. 1219-1226.
- [7] Berry, D. A., Titze, I. R., Normal modes in a continuum model of vocal fold tissues, *J. Acoust. Soc. Am.* Vol. 100, 1996, pp. 3345-3354.
- [8] Adachi, S., Sato, M., Time-domain simulation of sound production in the brass instrument, *J. Acoust. Soc. Am.* Vol. 97, 1995, pp. 3850-3861.
- [9] Copley, D. C., A computational and experimental study on the physical modeling of the trombone for musical synthesis, Master's thesis, Brigham Young University, 1995.
- [10] Elliott, S. J., and Bowsher, J. M., Regeneration in brass wind instruments, *J. Sound Vib.*, Vol. 83, 1982, pp. 181-217.

## TRUMPET BELL VIBRATIONS AND THEIR EFFECT ON THE SOUND OF THE INSTRUMENT

Thomas R. Moore, Erin T. Shirley, and Amy E. Daniels

Department of Physics  
Rollins College  
Winter Park, Florida 32789  
tmoore@rollins.edu

### ABSTRACT

The acoustic spectrum of a modern trumpet with the bell section heavily damped has been compared to the spectrum of the same instrument with the bell section left free to vibrate. Measurements of the amplitude of vibration indicate that the damping significantly reduces the movement of the metal, and a corresponding change in the acoustic spectrum between the two cases is found. It is shown that the relative power may change by as much as a factor of two in some of the harmonics. The experimental results can be explained by assuming that the vibration of the bell causes a change in the viscous boundary layer within the bell.

### 1. INTRODUCTION

The effect of the vibrations of the bell on the sound of brass instruments, or lack thereof, has been the topic of debate for many years. Musicians almost universally believe that the material and thickness of the bell section has a great effect on the sound of the instrument due to the enhancement or damping of the resonant vibrations of the metal. Scientists, on the other hand, disagree, and there is conflicting evidence in the scientific literature.

Pyle has reported that something as insignificant as lacquering the bell of a French horn can make a noticeable difference. [1, 2] However, Smith has reported that something as important as changing the material of the bell has no effect on the sound of trombones.[3] On the other hand, Lawson and Lawson have reported that the effect of annealing the bell of a French horn on the radiated sound is exceptionally strong.[4] Hoekje, et al. has theoretically investigated the contribution of bell vibrations to the sound field of a trombone and concluded that vibrations may make a small contribution if the symmetry of the modes is broken, however, this contribution is 30 to 40 dB less than the contribution due to the air column.[5, 6, 7] These conflicting reports leave both the musician and the musical acoustician in the position of being unable to conclusively comment on the importance of bell vibrations to the sound of the instrument.

In order to conclusively determine the effects of bell vibrations on the acoustic spectrum of brass instruments, we have studied the effects of damping the bell vibrations of a modern trumpet. Our results indicate that the bell vibrations do indeed have a large effect on the acoustic spectrum, however, we propose that the effects are not due to the radiation of sound from the bell as is often believed. Our data indicate that more subtle effects are responsible for the change in the acoustic spectrum that occurs when the bells of brass instruments vibrate.

### 2. EXPERIMENT

In order to determine the influence of the bell vibrations on the acoustic spectrum of brass wind instruments we chose the modern trumpet as a typical instrument on which to experiment. The trumpet used in our experiments was a *Silver Flair* model made by the King Instrument Company circa 1970.

The instrument was securely mounted to the experimental table, and played with a set of artificial lips. The lips used were significantly different from those reported by Gilbert, et al., [8] in that these lips were made of rubber, and formed from molds of actual human lips. The lips were mounted on a mouth made of plexiglas, and during any individual experiment the orientation of the lips and the internal pressure of the mouth cavity were not changed. By using an artificial mouth and lips we were able to damp the vibrations of the bell while the instrument was playing, thus eliminating the need for multiple human subjects and the inherent uncertainty associated with them.

In order to determine the effects of the bell vibrations, the power spectrum of the acoustic field approximately one meter from the bell was measured with the bell free to vibrate, and then measured again with the bell heavily damped by sandbags that were placed around and over the bell section. The vibrations of the trumpet bell during play were measured to be  $200 \pm 20 \mu m$ . When the bell was damped with the sandbags the bell vibrations were reduced to  $20 m \pm 10 \mu m$ .

It is well known that the trumpet radiates in all directions during play. It is therefore plausible that the addition of the sandbags themselves may affect the acoustic spectrum recorded by the microphone, even when the experiments are performed in an anechoic chamber. In order to eliminate this concern, and ensure that any difference between the two spectra were actually attributable only to the vibrations of the bell, we placed the microphone inside a small anechoic chamber. The anechoic chamber measured approximately 1 x 1.3 x 1.5 meters and was completely tiled inside with sound absorbing foam. The trumpet was placed outside of the chamber, with the bell of the instrument flush with the outside wall. A hole approximately two millimeters in diameter larger than the bell allowed the radiation from the bell to enter into the chamber. This arrangement ensured that any changes detected by the microphone were due to a change in the instrument and not due to a change in the environment.

Thirty-eight different experimental trials were recorded; each trial consisted of between five and ten separate measurements of the power spectrum with the bell free to vibrate and with the bell vibrations damped. Within each experimental trial the the lips con-



tinued to play without adjustment of the trumpet as the bell was damped and undamped. However, to ensure that the results were not unique to a specific orientation of the lips, the trumpet was removed from the lips between experimental trials and then reoriented before the next trial.

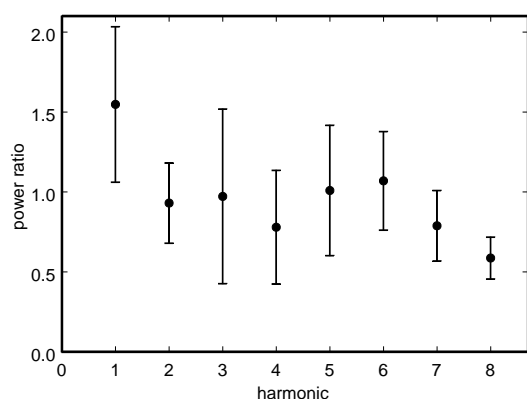


Figure 1: Ratio of the normalized power in each harmonic with the bell vibrations damped versus with the bell left free to vibrate.

Each of the spectra were normalized to the total power, and then the normalized power in each harmonic measured with the bell of the trumpet damped was divided by the power in the harmonic measured with the bell freely vibrating. The results are shown in Figure 1. Note that the power in the first harmonic is increased by up to 3dB when the bell is damped, while the power in the eighth harmonic is reduced by approximately the same amount.

### 3. ANALYSIS

The results shown in Figure 1 conclusively show that the vibrations of the bell section of a trumpet can significantly affect the acoustic spectrum. However, there is good evidence that the sound radiated by the bell is insignificant when compared to the sound attributable to the resonance of the air column; although, there may be enhanced radiation of the sound in the case where there are asymmetries in the bell.[6, 7]

Extensive investigation of the normal modes of vibration using electronic speckle pattern interferometry have shown that all of the normal modes of vibration of the trumpet bell used in these experiments were symmetric about the center of the bell. This indicates that there is little air to bell coupling due to the short circuiting between adjacent anti-nodes, and we therefore can ignore the effects of the sound attributable directly to the bell vibrations in the far-field.

The large uncertainty seen in the data shown in Figure 1 is not indicative of error, but is truly uncertainty caused by a large scatter in the data. This large uncertainty is only seen when the lips are reoriented between trials, and if several trials are made without reorienting the lips then the uncertainty is significantly smaller than that shown in Figure 1. This indicates that the change in relative power in any given harmonic before and after the bell is damped is dependent upon the actual position of the lips. We take this to indicate that the presence or lack of bell vibrations changes the input

impedance of the trumpet.

The actual etiology of the change in impedance is still under investigation, however, we believe that the effect can be adequately explained by a change in the viscous and thermal boundary layer in the bell section that occurs when the bell vibrates.

The thickness of the viscous boundary layer is given by [9]

$$\delta = \sqrt{\frac{2\eta}{\rho\omega}}, \quad (1)$$

where  $\eta$  is the shear viscosity,  $\rho$  is the density of air, and  $\omega$  is the angular frequency. Using the values for these parameters for air at room temperature, the thickness of the viscous boundary layer is approximately  $72\mu m$ . The thickness of the thermal boundary layer can be found by dividing the viscous boundary layer by the square root of the Prandtl number, which for air is approximately 0.84. [10]

The viscous and thermal boundary layers affect both the velocity of sound and the absorption coefficient, and the input impedance is dependent upon both of these values. For the case where the boundary layer is much smaller than the radius of the pipe, the change in the speed of sound and the absorption coefficient both vary linearly with the thickness of the boundary layer.

In light of this dependence we propose that the bell vibrations change the boundary layer, which in turn can significantly change the input impedance of the trumpet. It is reasonable, however, to ask if a change in the boundary layer in the last 14 centimeters can significantly affect the input impedance of an instrument that is comprised of approximately 1.4 meters of tubing.

In order to answer this question, we have designed a computer model of a trumpet that calculates the input impedance. The model assumes that the trumpet is made of a series of cylindrical sections and uses the equations presented by Benade to calculate the input impedance.[10] The equations include the effects of both the thermal and viscous boundary layers, and the length of the cylindrical sections vary depending upon the curvature of the wall. Our model is similar to others reported in the literature, and while we recognize the limitations of the model, it is sufficient to indicate how important a small change in the boundary layer near the bell may be.[11] Indeed, we have validated our model by comparing the predictions with experiments on cylindrical pipes connected to a trumpet mouthpiece and leadpipe, and we find that the predictions are within several percent at the point of largest deviation.

The computer model includes a mouthpiece, leadpipe, cylindrical tubing, and a bell. There is no attempt made to include the effects of bends in the tubing. The equations used to describe the mouthpiece and the leadpipe are the same ones used to make the actual pieces on a computer-controlled lathe. The bell shape is approximated by a Bessel horn shape that is similar to that found on the trumpet used in our experiments.

Figure 2 is a graph of the normalized impedance of a trumpet calculated by this model. Also shown in Figure 2 is the normalized impedance of the same trumpet with the viscous and thermal boundary layer increased by a factor of ten in the final 14 centimeters of the bell section. Note that there is a significant difference in the two impedance curves, with the input impedance being lower in the presence of the extended boundary layer. We propose that this lowering of the impedance decreases the feedback to the lips at the lower frequencies, thus producing a decrease in the power contained in the lower harmonics when the boundary layer is increased. There is no equivalent lowering of the impedance in the higher frequencies because the thickness of the boundary layer

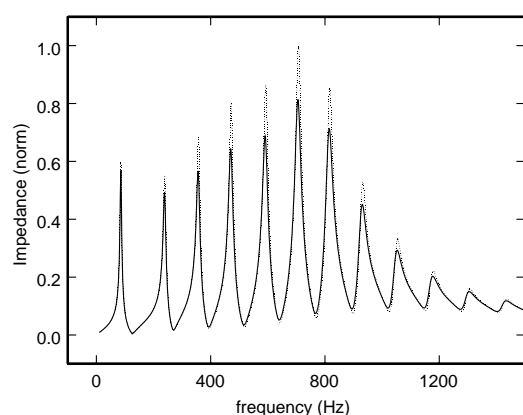


Figure 2: Calculated normalized impedance for a trumpet with rigid walls (dotted line), and for the same instrument with the boundary layer increased by a factor of ten in the final 14 centimeters of the bell section.

is proportional to the inverse of the square-root of the frequency as can be seen in equation (1), and therefore the increase in the boundary layer has significantly less effect at frequencies above 1 kHz.

Although an increase in the boundary layer near the end of the bell of a factor of ten may seem large, it is probably reasonable. If one naively considers the boundary layer to be estimated by the amplitude of vibration of the metal, the vibration of the metal itself is a full five times the estimated boundary layer thickness for a rigid-walled tube. A comparison of the calculated normalized input impedance for the B-flat resonance of a trumpet is shown in Figure 3, with the change in input impedance shown for increases in the boundary layer of the final 14 centimeters by a factor of five, ten, and fifty. Note that the response to an increase in the boundary layer is nonlinear, and that much of the decrease in impedance occurs within the first factor of five.

#### 4. CONCLUSIONS

We have conclusively shown that the vibrations of the bell of a trumpet do indeed affect the spectrum when played. The data shown in Figure 1 clearly indicate a large difference in the spectra when the bell vibrations are damped compared to when they are not, and the results are in agreement with the anecdotal evidence presented by brass instrument players; that is, damping the bell vibrations increases the relative power in the lower harmonics.

It is not immediately clear why the bell vibrations have such an affect on the spectrum. Numerous studies have shown that the radiation from the bell is not sufficient to explain even a small portion of the difference in spectra. However, we have shown that a change in the viscous boundary layer that may occur when the bell is damped can account for the different spectra. An increase in the boundary layer that may occur when the bell is free to vibrate will decrease the input impedance seen by the lips, leading to a reduced output in the lower harmonics. This decrease in impedance is not seen in the higher harmonics due to the inverse root-square dependence of the boundary layer on the frequency.

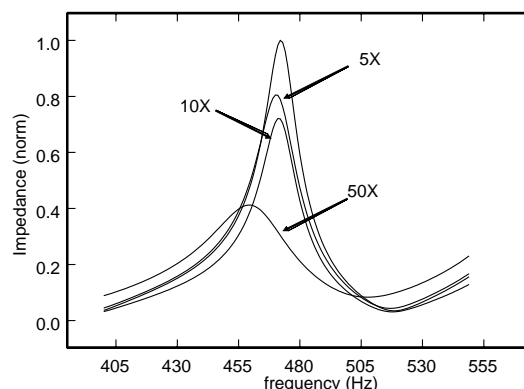


Figure 3: Calculated normalized impedance for the B-flat resonance of a trumpet with rigid walls, and for the same instrument with the boundary layer increased by a factor of five, ten, and fifty in the final 14 centimeters of the bell section.

Experiments are ongoing to determine if indeed the change in the spectrum can be unequivocally attributed to this effect.

#### 5. REFERENCES

- [1] Pyle, R., "The effect of lacquer and silver plating on horn tone," *Horn Call*, Vol. 11, 1981, pp. 26-29.
- [2] R. Pyle, "How brass instruments are built: art, craft, perhaps even science," *J. Acoust. Soc. Am.*, Vol. 101, 1997, p 3056.
- [3] R. Smith, "The effect of material in brass instruments: a review," *Proc. of the Inst. Of Acoust.*, Vol. 8, 1986, pp. 91-97.
- [4] B. Lawson and W. Lawson, "Acoustical characteristics of annealed French horn bell flares," *J. Acoust. Soc. Am.*, Vol. 77, 1985, pp. 1913-1916.
- [5] P.L. Hoikje, C.A. Payne, and D.N. Kjar, "Brass instrument bell vibrations and coupling to air modes," *J. Acoust. Soc. Am.* Vol 94, 1993, p. 1806.
- [6] A. Morrison and P.L. Hoekje, "Internal sound field of vibrating trombone bell," *J. Acoust. Soc. Am.*, Vol. 101, 1997 p 3056.
- [7] P.L. Hoekje, "Finite element analysis of vibrating trombone bell," *J. Acoust. Soc. Am.*, Vol. 105, 1999, p. 1126.
- [8] J. Gilbert, S. Ponthus, and J. Petiot, "Artificial buzzing lips and brass instruments: Experimental results," *J. Acoust. Soc. Am.*, Vol. 104, 1998, p 1627-1632.
- [9] L.E. Kinsler, A.R. Frey, A.B. Coppens, and J.V. Sanders, *Fundamentals of Acoustics*, (Wiley, New York, 2000)
- [10] A.H. Benade, "On the propagation of sound waves in a cylindrical conduit," *J. Acoust. Soc. Am.*, Vol. 44, 1968, pp. 616-623.
- [11] R. Causse, "Input impedance of brass musical instruments-Comparison between experiment and numerical models," *J. Acoust. Soc. Am.* Vol. 75, 1984, pp. 241-254.



# CORRECTIONS TO THE PLANE-WAVE APPROXIMATION FOR ACOUSTIC WAVES IN RAPIDLY FLARING HORNS

Cornelis J. Nederveen

Acacialaan 20, 2641 AC, Pijnacker, The Netherlands

## ABSTRACT

Calculating the input impedance of the air column of horns on wind instruments is simple as long as the flare is low: the wave equation can be solved assuming plane waves. A one-dimensional transmission-line (TL) method, in which the horn is described as a succession of short cones, is adequate. For a large flare, cross flow demands energy, effectively increasing the inertance. The magnitude of this inertance was numerically determined by a finite difference method, where space was filled with a fine grid. Studied were conical, hyperboloid and catenoidal horns. The additional inertance can be expressed as a simple fit-formula applicable to any horn shape. It is applied as a correction in the TL method. The formula can also be used for a sudden diameter change and for a flange (which is a horn of zero length). For most geometries found on wind instruments the correction is accurate within the detection threshold of the ear, 0.2% in frequency.

## 1. INTRODUCTION

The input impedance spectrum of a wind instrument gives importance information on its resonance behaviour. Calculating the input impedance accurately is difficult because of the many deviations from mathematically attractive shapes of the geometry. For some of these (for example side holes, diameter jumps, flanges) corrections are available [1, 2], but still lacking is a way to treat the various horns found on wind instruments. Some of these horns cover a large part of the length, other instruments only have a short horn near the open end. The sound field inside a horn is not accurately known, at least not to the accuracy sufficient for a musical instrument.

Studied were three horns, for which some mathematics is available, namely the conical, catenoidal and hyperboloid horn. Figure 1 shows the diameter as a function of the distance from the throat for these three horns, each with the throat radius  $a$ , mouth radius  $b$  and length  $L_H$ . For comparison two extremes, cylinder and flange, are also drawn. When a horn is slowly flaring, the wave fronts are approximately plane and the horn then can be described conveniently as a succession of short cones. The input impedance can be calculated. When the horn flares more quickly, wave fronts become curved, cross-sectional flow takes up energy, and the transmission line approach becomes inaccurate. Now the wave equation must be solved in three dimensions, which is cumbersome. Some analytical approaches are known, in some cases numerical methods have been used [2, 3, 4].

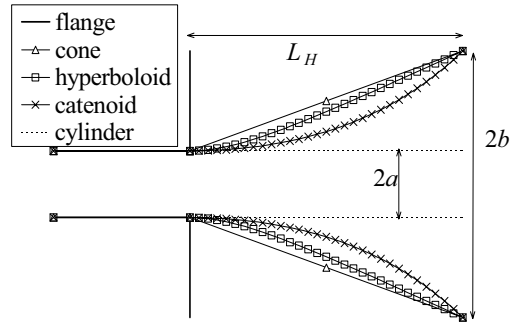


Figure 1. Shapes of the three horns investigated, with flange and cylinder as a comparison

## 2. THEORY

Neglecting losses, the wave equation for the pressure amplitude  $p$  is  $\nabla^2 p + k^2 p = 0$ , where  $k = \omega/c$  is the wave number,  $\omega$  the angular frequency and  $c$  the sound speed. For some special cases solutions are possible.

First consider a catenoidal horn with radius

$$r(x) = r_0 \cosh(mx), \quad (1)$$

where  $r_0$  is the radius at the throat,  $x$  the distance to the throat, and  $m$  the flare constant. For small flare and low frequencies the input impedance of a horn of length  $L_H$ , terminated by an open end without flange is [5, 6]

$$Z_{in} = (j\rho c/S)(k/m) \tanh[(L_H + 0.613 b)m]. \quad (2)$$

For a conical horn, the radius is given by

$$r(x) = r_0 (1 + x/x_0), \quad (3)$$

where  $x_0$  is the truncated part of the cone. Looking from left to right in the cone at a position where its section is  $S$  and the distance to the apex is  $R$ , its input admittance  $Y$  is [1, 7]

$$Y = (S/j\rho c)[1/kR - \cot(kR + k\delta)], \quad (4)$$

where  $\delta$  is a constant determined by the admittance at the mouth, the right hand end.

In a hyperboloid horn [7], or sometimes called hyperbolic horn [8, 9], the radius is

$$r(x) = \sqrt{r_0^2 + (x \tan \theta_0)^2}, \quad (5)$$

where  $\theta_0$  is the semi-top-angle of the limiting cone. The coordinates can be separated and the resulting differential equation can be solved numerically by a Runge Kutta method.

For a plane circular flange a fit formula is available for the end correction for a flange with radius  $b$ , mounted on a cylinder with radius  $a$ , [2] (the formula in the paper is different, but results are the same)

$$L_f/a = 0.821[1 - (a/b)]^Q + 0.613 (a/b), \quad (6)$$

where  $Q = 0.9$  for a good fit. Setting  $Q = 1$  greatly simplifies the application in a fit formula to be used later, while errors remain less than 0.03.

For an abrupt change in diameter a length correction must be applied to the tube with the smallest diameter  $a$  [1, 10],

$$L_f/a = 0.821(1 - a/b)^Q, \quad (7)$$

where  $Q = 1.5$  for the best fit, but errors remain below 0.1 when  $Q = 1$ .

In the transmission line (TL) method, conical pipe pieces are put in series and the impedance is calculated in steps, repeatedly using eq. (4). For zero frequency and a pipe with an open mouth the procedure is simplified. The length of the tube piece is  $L_{ba}$ . The terminating correction or “output length” at the outer end  $b$  is  $L_b$ . At position  $a$  the “input length” of the pipe section,  $L_a$ , which equals the terminating correction to the next pipe, using  $R_a/R_b = a/b$ , becomes

$$L_a = (a/b)[L_{ba} + (a/b)L_b]. \quad (8)$$

In the finite difference method (FDM) a grid is fitted in the sound field in and outside the horn. The wave equation is written as a discretized condition between the centre and its neighbouring points. The resulting matrix is solved, yielding the sound field in the horn [2, 11]. The geometry is circular symmetric, so a two-dimensional grid suffices. Two types of grid were employed, one using a cylindrical co-ordinate system, another using a co-ordinate system fitting the shape of the horn. Figs 2 and 3 show the two grids for a hyperboloid horn. Not drawn is the grid outside the horn; it was progressively stretched to further reduce the number of unknowns. Grid sizes were varied. Various techniques based on the “Richardson Extrapolation” were used to extrapolate the boundary to infinity and the grid size to zero [2, 12]. Formulating the conditions at the walls where the normal derivative is zero can be tricky [11].

The present report only describes investigations with zero frequency.

### 3. CALCULATIONS

Input impedances of the three horns were calculated with the TL method and with the FDM; for the catenoidal also with eq. (2), and for the hyperboloid horn by solving the partial differential equation (PDE). This was done for the zero-frequency case, for horns with ratio  $a/b = 0.3, 0.5$  and  $0.7$ . Calculated was the

relative “input length”  $L_{in}/a$  as a function of the relative (geometrical) horn length  $L_H/a$ . Results for all horns followed the same general pattern. These for the hyperboloid horn for  $a/b = 0.5$  are given in Figures 4 and 5. Figure 5 is an enlargement of Figure 4 of the part for the shorter horns. Results for the conical and the catenoidal horns are plotted in Figures 6 and 7, respectively, for relative horns lengths up to 5.

Results for the TL method are indicated by crosses. The horns were divided in 20 sections; this was sufficient: it appeared that increasing the number of sections gave changes of less than 0.1%.

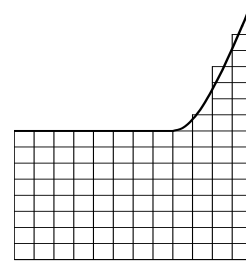


Figure 2. Grid in horn based on cylindrical coordinates

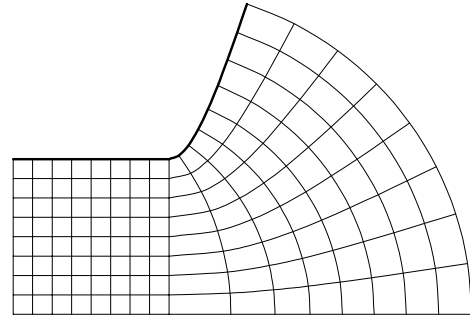


Figure 3. Grid in horn based on coordinates following the horn shape

The FDM results are plotted with open circles for the cylindrical grid (FDM 1) and filled circles for the grid following the horn wall (FDM 2).

The Runge Kutta solutions (PDE) for the hyperboloid horn and the analytical solutions for the catenoidal horn [eq. (2)] are plotted with squares.

The values for long horns are the same for all methods, though small differences remain (the FDM method becomes inaccurate because of the very large number of points in the tube length).

For short horns results are different, as appears from Figures 5, 6 and 7. The deviations from the FDM results are substantial.

A first remark can be made on the differences between the two FDM grids as appears from Figure 5. The second grid, presumably being the better choice, shows a slight hump near  $L_H/a = 0.25$ . For reasons of continuity, this does not seem very likely, so contrary to the expectation, the curved-coordinate method seems to be inferior. Possibly the orthogonality of the grid near the sharp bend is not sufficiently ensured.

The PDE solution fails dramatically for short hyperboloid horns. The analytic solution for short catenoidal horns is also strongly in error.

At very short horns, the effective length of a tube of zero length should become equal to the correction for a circular flange with an  $a/b$  ratio of 0.5,  $0.74a$  [2]. But the TL method gives values about half as large, which is definitely wrong. Searching for a way to correct this, inspiration was found in the expression for the flange, eq. (6).

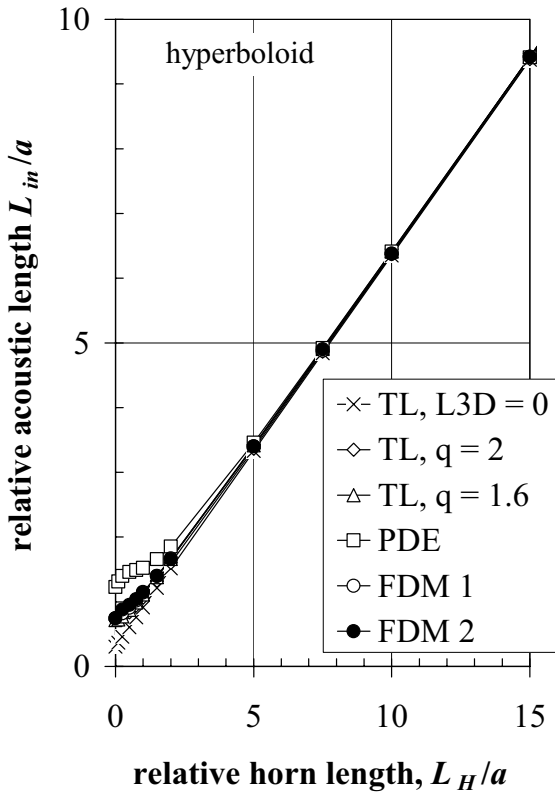


Figure 4. Relative acoustic input length as a function of relative horn length for a hyperboloid horn,  $a/b = 0.5$ , for zero frequency.

An extra correction term,  $L_{3D}$ ,

$$L_{3D} = \sqrt[q]{L_{ba}^q + (0.821(b-a))^q} - L_{ba}, \quad (9)$$

was added to the TL expression, eq. (8):

$$L_a = (a/b)[L_{ba} + (a/b)L_b + L_{3D}]. \quad (10)$$

Suitable values for  $q$  are in between 1.6 and 2. A convenient way to apply the correction is to add it to the termination length, as follows

$$L_a = (a/b)\{L_{ba} + (a/b)[L_b + (b/a)L_{3D}]\}. \quad (11)$$

New TL calculations were performed including the correction. Results are plotted in Figures 4, 5, 6 and 7 (diamonds and triangles). The correction can be seen to be reasonably successful. It brings the results close to those of the FDM. By trial and error it was found that the best fit was obtained for  $q = 1.6$ , although even  $q = 2$  is still acceptable. The largest error is 0.05, which has a nearly negligible effect on the tuning since short horns cover only a small fraction of the total length of the instrument.

Selamet [4] investigated a number of pipe terminations by a boundary element method. The end corrections obtained for a cylinder terminated by a horn with a bellmouth with different radii of curvature were measured from Selamet's Figure 10, and appeared to correspond, within measurement error, with TL calculations including the 3D correction. Dalmont et al. reported a measurement on a catenoidal horn  $L_H/a = 1$ ,  $a/b = 0.5$ , which also corresponds with the present findings [2].

In the formulation according to eq. (11) the extra length correction is related to an impedance in series with the termination impedance of the pipe end. In this way it can be added to the TL circuit for finite frequencies. This has been successfully done, but is not reported here.

When using the method for finite frequencies, it can be questioned whether also a correction must be applied for possible changes in the compressibility in rapid bore changes. It can be shown that this is not necessary: the TL approach suffices for the compressibility contribution.

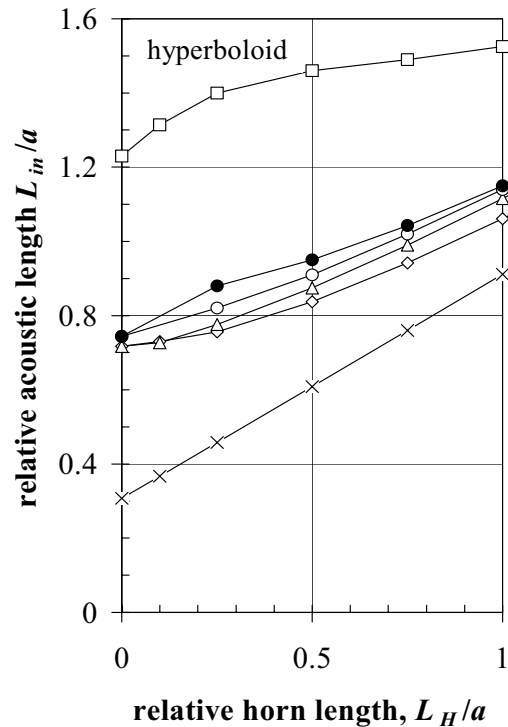


Figure 5. Relative acoustic input length as a function of relative horn length for a hyperboloid horn,  $a/b = 0.5$ , for zero frequency. For explanation of symbols see Figure 4

#### 4. CONCLUSION

The simple and straightforward TL calculation is very convenient for calculating the input impedance of horns. For rapidly flaring horns systematic errors are found. To compensate for this, a “3D”-correction can be introduced, adding a certain amount of extra mass. This correction is obtained from comparison with FDM results and written as a fit formula. It appears even applicable to extreme cases as flat circular flanges or diameter jumps. Accuracy is sufficient for most practical situations found on wind instruments, which means 0.2% in frequency or 3 cents.

We intend to further verify the theory with experiments. This is not easy: a high accuracy is necessary for measuring this higher order effect. Also, when wavelengths become comparable to the cross-dimensions cross-resonances may appear and modify the simple picture.

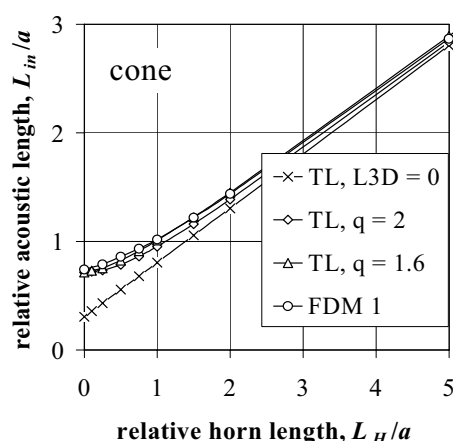


Figure 6. Relative acoustic input length as a function of relative horn length for a conical horn,  $a/b = 0.5$ , for zero frequency.

#### 5. ACKNOWLEDGEMENTS

The author wishes to thank Jean-Pierre Dalmont and Jos Jansen for useful discussions and suggestions.

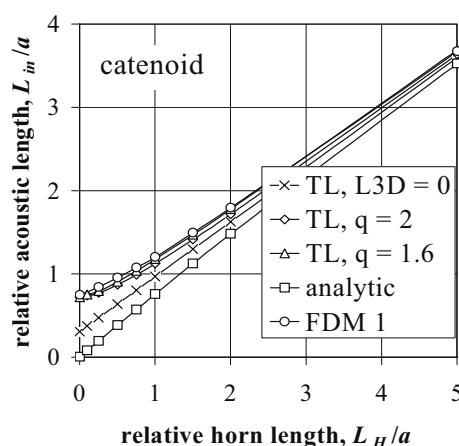


Figure 7. Relative acoustic input length as a function of relative horn length for a catenoidal horn,  $a/b = 0.5$ , for zero frequency.

#### 6. REFERENCES

- [1] Nederveen, C.J., Acoustical aspects of woodwind instruments, 2nd edition. De Kalb: Northern Illinois University Press, De Kalb, Ill, 1998.
- [2] Dalmont, J.-P., Nederveen C.J., and Joly, N. “Radiation impedance of tubes with different flanges: numerical and experimental investigations”, J. Sound Vib. Vol. 244, 2001, pp. 505–534.
- [3] Noreland, D., “A numerical method for acoustic waves in horns”, Acta Acustica/Acustica Vol. 88, 2002, pp. 576–586
- [4] Selamet, A., Ji, Z.L., and Kach, R.A., “Wave reflections from duct terminations”, J. Acoust. Soc. Am. Vol. 109, 2001, pp. 1304–1311.
- [5] Morse, P.M. Vibration and sound, McGraw-Hill, 1948. Reprint Acoustical Society of America, Woodbury, New York, 1976.
- [6] Pierce, A.D., Acoustics. An introduction to its physical principles and applications. Acoustical Society of America, New York, 1989.
- [7] Fletcher, N.H., and Rossing, T.D., The physics of musical instruments. Springer Verlag, New York, 1991.
- [8] Freehafer, J.E., “The acoustical impedance of an infinite hyperbolic horn”, J Acoust. Soc. Am. Vol. 11, 1940, pp. 467–476.
- [9] Keefe, D.H., and Barjou, A., “Acoustic propagation in flaring, axisymmetric horns: II Numerical results, WKB theory, and viscothermal effects”, Acta Acustica/Acustica Vol. 85, 1999, pp. 285–293.
- [10] Kergomard, J., and Garcia, A., “Simple discontinuities in acoustic waveguides at low frequencies: critical analysis and formulae”, J. Sound Vib Vol. 114, 1987, pp. 465–479.
- [11] Patankar, S.V., Numerical heat transfer and fluid flow. Taylor & Francis, London, 1980
- [12] Zwillinger, D., Handbook of Differential equations. New York: Academic Press Second Edition, 1898

## GRADIENT BASED OPTIMISATION OF BRASS INSTRUMENTS

D. Noreland

Department of information technology  
Uppsala University  
daniel@tdb.uu.se

### ABSTRACT

This paper presents the application of numerical shape optimisation to brass instruments. The instruments are modelled using a one-dimensional transmission line analogy with segments shaped as truncated cones. Using the end diameters of the segments as design variables, the task to find a design with desired input impedance peak frequencies and magnitudes is formulated as a non-linear least squares problem. This problem is solved using the Levenberg-Marquardt minimisation algorithm. The necessary gradient of the objective function is found by analytic manipulation of the transmission line model. Through the use of an appropriate design variable transformation, it is possible to quickly find smooth horn profiles, and to prevent the minimiser from getting stuck in local minima corresponding to irregular or jagged designs.

### 1. INTRODUCTION

Considerable effort has been spent on methods for the analysis of acoustic horns found in musical instruments (c.f [1], [2], [3]). However, very little has been reported about algorithms for automated design of wind instruments, or for improvement of existing instruments. To the author's knowledge, the only published work in the field of brass instrument optimisation is a paper by Kausel[4], in which genetic algorithms, and a zeroth order search method are employed in order to perform intonation and response optimisation. A lot of information regarding the intonation, response and tonal colour of a wind instrument is contained in its input impedance spectrum, and particularly in the locations and the magnitudes of the impedance peaks. A starting point for the formulation of a brass instrument optimisation problem is therefore to optimise the shape with respect to these the most interesting properties of the input impedance spectrum. This approach is different from the inverse problem of determining the shape of a horn from its entire input impedance spectrum. If the task is e.g. to improve the intonation of an existing instrument, the input impedance curve of the resulting instrument is not known a priori—only certain features of it, such as the peak frequencies. The fact that comparatively little information about the impedance curve is specified leaves a lot of freedom in the design. This freedom can be used in order to find geometrically appealing shapes. Jagged and irregular horn profiles are neither aesthetically pleasing nor feasible from a manufacturer's point of view.

There are essentially two difficulties associated to shape optimisation. Firstly, a detailed description with many degrees of freedom requires heavy computations, since each evaluation of the objective function entails the solution of a forward problem, that is to analyse the instrument with whatever method chosen for its modelling. Secondly, local optimisation routines run the risk of

getting stuck in local minima corresponding to unsatisfactory designs.

### 2. THE OPTIMISATION PROBLEM

#### 2.1. Objective function

The first step in the formulation of the optimisation problem is to define the objective function. In this work, concerned in the first place with intonation, the optimisation problem is formulated as a non-linear least squares problem, where the square sum of the deviations in the impedance peak frequencies and magnitudes from their desired values, is minimised by varying a set of design parameters. Finding the frequencies of the maxima of  $|Z_{in}|$  is computationally expensive. As an alternative, the observation that<sup>1</sup>  $\text{Im}(Z_{in}) = 0$  at the maxima can be exploited, suggesting the objective function

$$J(\alpha) = \frac{1}{2} \sum_{k=1}^n (\text{Im}(Z_{in}(f_k))^2 + \text{Re}(Z_{in}(f_k) - Z_{\text{peak}_k})^2), \quad (1)$$

where  $\alpha \in \mathbb{R}^m$  is the set of design variables,  $f_k$ ,  $k = 1, \dots, n$  are the desired peak frequencies, and  $Z_{\text{peak}_k}$ ,  $k = 1, \dots, n$  are the corresponding peak levels. Formulated as a non-linear least-squares problem, minimisation of Eq. (1) corresponds to the minimisation problem

$$\alpha_* = \arg \min_{\alpha \in \mathbb{R}^m} J(\alpha) = \arg \min_{\alpha \in \mathbb{R}^m} \frac{1}{2} \mathbf{F}^T \mathbf{F}, \quad (2)$$

where  $\mathbf{F}$  is commonly denoted the *residual*, here given by

$$\mathbf{F} = \begin{bmatrix} \text{Im}(Z_{in}(f_1)) \\ \text{Re}(Z_{in}(f_1) - Z_{\text{peak}_1}) \\ \text{Im}(Z_{in}(f_2)) \\ \text{Re}(Z_{in}(f_2) - Z_{\text{peak}_2}) \\ \vdots \end{bmatrix}. \quad (3)$$

Additional requirements, such as the value of the impedance between the peaks, can also be incorporated in  $J$  in order to adjust peak bandwidths etc.

In order to achieve rapid convergence, the Levenberg-Marquardt minimisation algorithm[5] is used. This requires the gradient of  $J$  with respect to the components of  $\alpha$ , which in turn requires differentiation of  $Z_{in}$ .

<sup>1</sup>To a very good approximation.



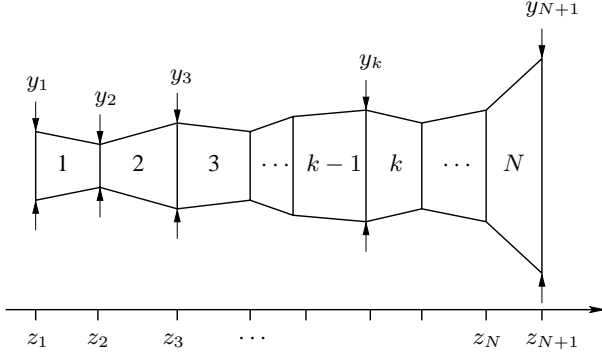


Figure 1: A horn approximated as a series of truncated cones.

## 2.2. Mathematical model of the horn

An established method for the computation of the input impedance  $Z_{in}$  of wind instruments is the one-dimensional transmission line analogy[2], where the instrument is approximated as a series of  $N$  truncated cones, as in Fig. 1. This model is accurate for moderately flaring horns. Denoting by

$$\mathbf{H} = \begin{bmatrix} H_{11} & H_{12} \\ H_{21} & H_{22} \end{bmatrix} \quad (4)$$

the transfer matrix of the instrument, the input impedance is given by

$$Z_{in} = \frac{H_{12} + H_{11}Z_L}{H_{22} + H_{21}Z_L}, \quad (5)$$

where  $Z_L$  is the radiation impedance.  $\mathbf{H}$  is approximated by the product of the transfer matrices of the individual sections[6];

$$\mathbf{H} = \prod_{j=1}^N \mathbf{H}_j(y_j, y_{j+1}, z_j, z_{j+1}). \quad (6)$$

In this paper, an expression according to Beranek[7] is used to approximate  $Z_L$ .

## 2.3. Computation of $\nabla Z_{in}$

Possible design variables for the horn approximated as in Eq. (6) are the end diameters  $y_1, \dots, y_{N+1}$ , and the positions  $z_1, \dots, z_{N+1}$ . The gradient of  $Z_{in}$  needs to be computed in an accurate and computationally inexpensive way. This precludes the use of finite differencing of the form

$$\frac{\partial Z_{in}}{\partial y_k} \approx \frac{Z_{in}(y_k + \varepsilon) - Z_{in}(y_k)}{\varepsilon}, \quad \varepsilon > 0,$$

since then the computational cost of the gradient grows as  $N^2$ . Fortunately, it is possible to differentiate Eq. (5) symbolically. This operation requires, in turn, differentiation of  $\mathbf{H}$ . Introducing

$$\mathbf{\Pi}_{j,k} = \mathbf{H}_j \mathbf{H}_{j+1} \cdots \mathbf{H}_k, \quad k > j,$$

the product rule for differentiation yields for  $3 \leq k \leq N-2$

$$\begin{aligned} \frac{\partial \mathbf{H}}{\partial y_k} &= \frac{\partial}{\partial y_k} (\mathbf{\Pi}_{1,k-2} \mathbf{H}_{k-1} \mathbf{H}_k \mathbf{\Pi}_{k+1,N}) = \\ &= \mathbf{\Pi}_{1,k-2} \left( \frac{\partial \mathbf{H}_{k-1}}{\partial y_k} \mathbf{H}_k + \mathbf{H}_{k-1} \frac{\partial \mathbf{H}_k}{\partial y_k} \right) \mathbf{\Pi}_{k+1,N}. \end{aligned} \quad (7)$$

Similar expressions apply for  $k = 1, 2, N, N+1$ , and for differentiation with respect to  $z_k$ . In a computer implementation, the products  $\mathbf{\Pi}_{1,1}$ ,  $\mathbf{\Pi}_{1,2}$ ,  $\dots$ ,  $\mathbf{\Pi}_{1,N-1}$ , and  $\mathbf{\Pi}_{N,N}$ ,  $\mathbf{\Pi}_{N-1,N}$ ,  $\dots$ ,  $\mathbf{\Pi}_{2,N}$  can be computed in a total of  $2N-3$  matrix multiplications. All intermediate cumulative products are stored for later retrieval in the evaluations of Eq. (7). It is also necessary to differentiate  $Z_L$  with respect to  $y_N$  and  $y_{N+1}$ .

## 3. FINDING SMOOTH SOLUTIONS

### 3.1. Optimisation with $\{y_k\}$ as design variables

The most straightforward choice of design variables is simply the set  $\{y_k\}$  itself. As Fig. 1 suggests, the number of design variables equals the number of segments. In a first experiment, the lowest three impedance peaks of a Bessel horn (Fig.2) of length 0.5 m were lowered by 10 Hz.  $y_1$  and  $y_{N+1}$  were kept fixed, as well as the segment lengths. Although the inequality bound  $y_k > 0$  is natural, it is not imposed in this, and the subsequent, experiments due to limitations of the used Levenberg-Marquardt implementation. This works surprisingly well, presumably because narrow horn profiles usually make the objective function diverge quickly. This can often prevent the optimisation from continuing in the direction of negative values of  $y_k$ .

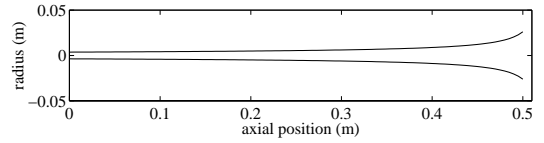


Figure 2: Model horn of Bessel type.

Figure 3 shows the shapes obtained for three values of  $N$ . Although a moderate impedance peak displacement was requested, the resulting shapes are infeasibly irregular. Refining the resolution seems to relieve the problem somewhat, but a considerable amount of ripple remains even for  $N = 400$ . The problems become even more severe if larger peak displacements are tried. An effort to shift the peaks as above, but by 20 Hz, fails due to a complete breakdown of the optimisation. It is thus not practical to optimise directly with respect to the segment end diameters.

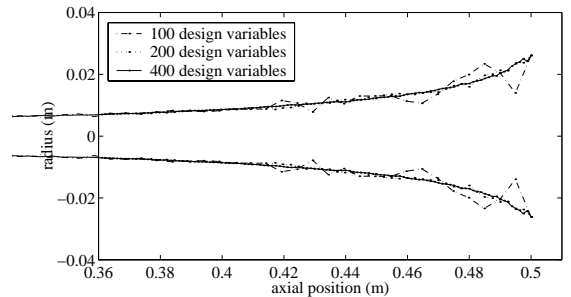


Figure 3: Resulting shapes for an intonation experiment with optimisation directly with respect to the segment end diameters.

### 3.2. Constraining the search space

Smooth designs can be enforced by reducing the search space to include only designs of desired smoothness. This can be done by parametrising the design boundary using some appropriate function. A brass instrument bell may for instance be designed by determining the coefficients in the expression for a Bessel horn [8],

$$y(z) = \frac{B}{(D_0 - z)^m}. \quad (8)$$

Consider a general case where the geometry is defined by the parameterisation

$$y = y(\alpha; z), \quad \alpha = (\alpha_1, \alpha_2, \dots, \alpha_m)^T. \quad (9)$$

The horn is as before discretised using  $N$  elements. The chain rule then yields

$$\frac{\partial Z_{in}}{\partial \alpha_k} = \sum_{j=1}^N \frac{\partial Z_{in}}{\partial y_j} \frac{\partial y_j}{\partial \alpha_k}, \quad (10)$$

which expression is evaluated using the results from section 2.3 and by differentiation of Eq. (9).

As an experiment, a simple instrument was constructed by attaching the Bessel horn defined in Eq. (8) to a conical lead pipe. The length of the pipe and the parameters  $B$ ,  $D_0$ , and  $m$  were then determined in order to give an instrument with eight harmonically related resonance frequencies, starting at 110 Hz. Figure 4 shows the result, which brings in mind the tuba. A slightly different ob-

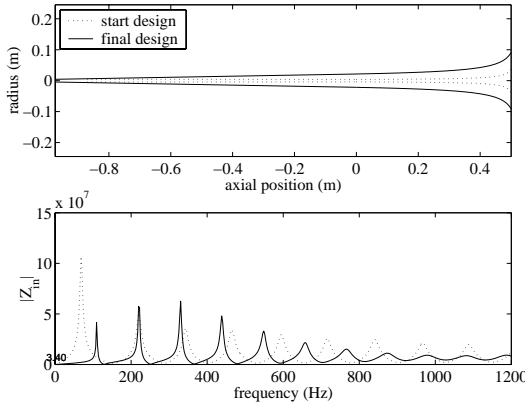


Figure 4: Harmonic instrument constructed of a Bessel horn attached to a conical pipe. Interestingly, although only four degrees of freedom were used, none of the eight first resonance frequencies deviates by more than eight musical cents from its desired value.

jective function was used here. The impedance peak magnitudes were not specified, but the objective function was defined from the actual deviations of the zeros of  $\text{Im}(Z_{in})$ . This requires some extra computations, but increases the convergence radius of the optimisation greatly, since there is no ambiguity in the identification of the zeros.

### 3.3. Smoothing

A different strategy is to retain the size of the search space, but to introduce a change of variables with the property that the optimiser is given a preference to search for smooth designs. In the

continuous case, the principle is to introduce the following change of variables[9],

$$\begin{cases} y''(z) &= \eta(z), \quad z \in [0, a] \\ y(0) &= y_0 \\ y(a) &= y_a, \end{cases} \quad (11)$$

for a horn of length  $a$ , and then optimise with respect to  $\eta$ . The idea of optimising with respect to the right hand side of a Poisson type equation is that the change of variables essentially represents a low pass filtering from the design variable  $\eta$  to the physical variable  $y$ . Equation (11) defines an isomorphism between  $\eta$  and  $y$ , and a minimum of  $\partial J / \partial \eta$  will also be a minimum of  $\partial J / \partial y$ . Thus, the change of variables preserves optimal solutions.

The continuous Eq. (11) has to be discretised in order to be applicable to the transmission line model. In this work, a one-dimensional finite element approximation is used. This yields the relation

$$\mathbf{y} = \mathbf{A}\boldsymbol{\eta} + \mathbf{b} \quad (12)$$

between the discrete variables  $\mathbf{y} = (y_0, y_1, \dots, y_{N+1})^T$  and  $\boldsymbol{\eta} = (\eta_0, \eta_1, \dots, \eta_{N+1})^T$ . The matrix  $\mathbf{A}$  and the vector  $\mathbf{b}$  depend on the discretisation and the boundary values of Eq. (11).  $\mathbf{A}$  can be interpreted as a discretisation of an operator that essentially integrates its operand twice. The use of the transformation (12) yields, together with the chain rule, the expression

$$\frac{\partial J}{\partial \boldsymbol{\eta}} = \mathbf{A}^T \frac{\partial J}{\partial \mathbf{y}}$$

for the gradient of  $J$ .

The experiments of section 3.1 were repeated with the smoothing applied. Figure 5 shows the resulting horn shapes, each of them obtained in 20 iterations. This time, all three designs are smooth. The shape does not seem to converge as  $N$  increases however, which is due to the large number of design variables compared to the number of terms (six, counting peak frequencies and magnitudes) in the residual.

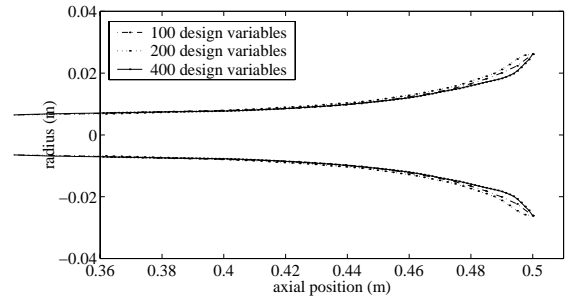


Figure 5: Resulting shapes for an intonation experiment with smoothing applied.

If large deformations are required in order to meet the intonation requirement, also the optimisation with smoothing may get stuck in a local minimum or fail to converge at all. A remedy to these problems is to perform the optimisation in two steps. In the first step, the design is changed so that the frequencies of the peaks get the desired values. In the second step, the peak magnitudes are adjusted. A challenging problem was formulated in order to test this approach. A 0.5 m long Bessel horn as given by Eq. (8) with  $B = 0.005$ ,  $m = 0.6$ , and  $D_0 = 0.52$  was analysed with respect

to its first nine impedance peaks. The aim was then to reproduce the shape of this horn from an initial design shaped as a truncated cone with the same length and end diameters as the original Bessel horn. The number of segments  $N$  was 100. The properties of the start design (the cone) and the desired horn (the Bessel horn) are shown in table 1. After 121 iterations, the shape shown in Fig. 6

start impedance		goal impedance	
freq. (Hz)	magn. ( $\Omega$ )	freq. (Hz)	magn. ( $\Omega$ )
290.3	$6.5 \cdot 10^7$	266.5	$2.0 \cdot 10^8$
591.3	$8.0 \cdot 10^7$	594.0	$1.4 \cdot 10^8$
904.4	$7.2 \cdot 10^7$	921.8	$9.5 \cdot 10^7$
1226	$5.9 \cdot 10^7$	1249	$6.6 \cdot 10^7$
1553	$4.8 \cdot 10^7$	1574	$4.6 \cdot 10^7$
1883	$4.0 \cdot 10^7$	1900	$3.3 \cdot 10^7$
2215	$3.4 \cdot 10^7$	2225	$2.5 \cdot 10^7$
2549	$3.0 \cdot 10^7$	2550	$2.1 \cdot 10^7$
2883	$2.7 \cdot 10^7$	2874	$1.8 \cdot 10^7$

Table 1: Start and goal properties for a reconstruction experiment with nine peaks. The figures refer to the impedance peak frequencies and magnitudes.

was obtained. Indicated are also the initial shape and the original Bessel horn. The optimiser has found a shape that is very close to the original one. Some wiggles of the contour remain, but on the whole it is remarkable that the specification of only nine impedance peak frequencies and magnitudes yields a shape so close to the original design.

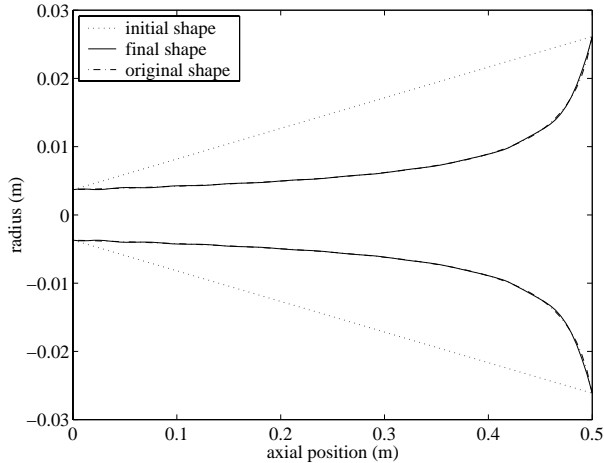


Figure 6: Original shape, and the shape obtained after optimisation considering the frequencies and magnitudes of the nine first impedance peaks.

#### 4. COMPUTATIONAL PERFORMANCE

The computer code of this project has been written in MATLAB, utilising optimisation routines from the Optimization toolbox. Although the interpreting language used is far from optimal in terms of execution speed, a typical intonation experiment with 100 design variables takes only in the order of one minute on a personal

computer. This figure can probably be reduced considerably by porting the code to a compiling language, such as fortran.

#### 5. CONCLUSIONS

Gradient based minimisation is effective for brass optimisation, provided that a suitable choice of design variables is chosen. The demands on computational power can be satisfied with a modern desktop computer. Still, the algorithms work fast enough to make them tractable as a hands-on virtual laboratory, with possibilities to interactive experimentation.

Although the algorithms presented here are primarily intended for intonation optimisation that require rather small changes of the initial shape, they have been used successfully for more difficult design problems. For a systematic use of the presented methods in wind instrument design “from scratch” it would, however, be beneficial to combine them with global minimisation algorithms.

A limitation of the transmission line model is the degraded accuracy for high frequencies, where modal conversion in the rapidly flaring part of the bell is considerable. Future development of the algorithm presented here may involve the use of a finite element description of the outermost part of the bell. Gradient based optimisation for such a model has been reported in [9].

#### 6. REFERENCES

- [1] A. H. Benade and E. V. Jansson. On plane and spherical waves in horns with nonuniform flare. i. theory of radiation, resonance frequencies, and mode conversion. *Acustica*, 31:79–98, 1974.
- [2] R. Caussé, J. Kergomard, and X. Lurton. Input impedance of brass musical instruments—Comparison between experiment and numerical models. *J. Acoust. Soc. Am.*, 75:241–254, 1984.
- [3] V. Pagneux, N. Amir, and J. Kergomard. A study of wave propagation in varying cross-section waveguides by modal decomposition. Part I. Theory and validation. *J. Acoust. Soc. Am.*, 100:2034–2048, 1996.
- [4] W. Kausel. Optimization of brasswind instruments and its application in bore reconstruction. *Journal of New Music Research*, 30:69–82, 2001.
- [5] J. J. Moiré. The Levenberg-Marquardt algorithm: Implementation and theory. In G. A. Watson, editor, *Numerical Analysis*, pages 105–116. Springer Verlag, New York, 1977.
- [6] D. Mapes-Riordan. Horn Modeling with Conical and Cylindrical Transmission-Line Elements. *J. Audio Eng. Soc.*, 41:471–483, 1993.
- [7] L. Beranek. *Acoustics*. McGraw-Hill, New York, 1954.
- [8] A. H. Benade. *Fundamentals of Musical Acoustics*. Dover Publications, New York, 1990.
- [9] E. Bängtsson, D. Noreland, and M. Berggren. Shape optimization of an acoustic horn. *Computer Methods in Applied Mechanics and Engineering*, 192:1533–1571, 2003.

## MEASUREMENT OF THE FORCE APPLIED TO THE MOUTHPIECE DURING BRASS INSTRUMENT PLAYING

Jean-François PETIOT

Institut de Recherche en Communications et Cybernétique de Nantes (UMR CNRS 6597 - Equipe MCM)- Ecole Centrale de Nantes, 1 rue de la Noë, BP 92101, 44321 Nantes Cedex 3 France  
Jean-Francois.Petiot@irccyn.ec-nantes.fr

### ABSTRACT

In order to assess the load produced on the lips of the musician during brass instrument playing, a measuring system was developed. It permits the recording in real time of the axial force created on the mouthpiece, and allows the players to perform on their own instrument and mouthpiece, in their usual manner. Tests involving 3 categories of players (professional – advanced – beginners) were conducted with various musical phrases, articulations and nuances. For all players, the force between the mouthpiece and instrument always increases with increasing loudness and ascending pitch, but in different proportions. After an analysis of the causes of this force, the extent of these variations is described and an interpretation of the results is proposed. These measurements are particularly interesting for musicians and physicist as well, in order to understand what the control parameters of the embouchure are, and how to manage them.

### 1. INTRODUCTION

Wind instruments (with the exception of those with a flute-like embouchure) are acoustic sources using a valve effect: the acoustic oscillation is the result of a destabilisation of a mechanical element whose movement changes the entrance cross-section of the instrument. This destabilisation is the result of a complex aeroelastic coupling between the mechanical element (the reed of a clarinet or the lips of a trombonist), the air flow entering the instrument as a result of the static overpressure in the mouth of the musician, and the instrument itself (the acoustic resonator) [1].

In the case of brass instruments, the vibrations of the lips of the musician are controlled both by the musician and the instrument itself [2]. When we focus on the musician as a “system”, several control parameters, which condition the natural frequency of the lips, have to be considered (tension, geometry, visco-elastic properties, ...). A great variety of musical sounds are obtained by the control and the management in “real time” of these parameters, this after several years of daily practice for the musician.

Using a systemic approach, the embouchure of the musician can be seen as a particular system, which performs a *function*, or process, which results in an *output*. The block diagram of the embouchure is described figure 1. This diagram shows the output, input and control data of the system. The input is the static overpressure in the mouth of the musician, created in the lungs by

the diaphragm. The output is the acoustic pressure in the mouthpiece, which generates a regime of oscillation in the instrument.

Many parameters control this process. Firstly, the instrument reacts on the lips of the musician, according to the acoustic characteristics of the instrument body (mainly the internal geometry or “bore”). The playing frequency of the note is thus strongly attracted toward the resonance frequency of the instrument [2]. Secondly, the musician can make vary the characteristics of the tone by controlling the tension of the muscles which position the lips. This is the crucial point of the learning of brasses, and succeeding in this lips’ control can take many years of hard practice. Finally, a third parameter control the embouchure of the musician: the force applied by the mouthpiece on the lips.

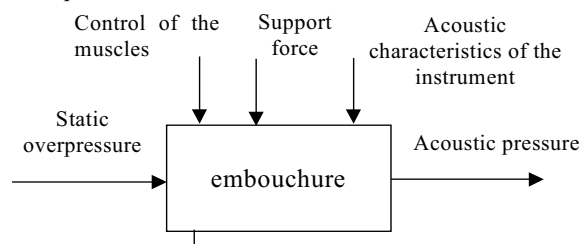


Figure 1: Block diagram of the embouchure of a musician.

For all brass musicians, lips are a very sensitive area because they are often hardly solicited. Every musician is subjected to the phenomena of lips’ weakness, where it’s no longer possible to play, and where a rest is necessary. This phenomena is caused on the one hand by the fatigue of the muscles of the embouchure, whose tension must always be controlled, and on the other hand by the support of the mouthpiece on the lips, which marks and traumatises the tissues. All brass teachers agree on the fact that the force on the mouthpiece must be as weak as possible, and various techniques (“no pressing”) are developed so as to reduce its magnitude. But this force exists at various degrees for several reasons:

- The force is necessary for the static airtightness between the lips and the mouthpiece; it avoids the air from escaping around the edges of the mouthpiece. This is inherent to the way brass instruments are played, and for having airtightness, the force cannot be nullified,
- The force can be used to modify the mechanical behaviour of the lips. When one presses on the lips, the tissues becomes

artificially more stiff, the mechanical characteristics of the oscillator are then modified, and the regime of vibration of the lips can be altered. In the same way, the variation of the force can modify the boundary conditions of the lips, and can eventually change the regime of vibration. We have clearly observed this phenomena with artificial mouths, where an increase of the force on the lips leads most of the time to a modification of the played note [2].

The support force on the mouthpiece can thus be used so as to compensate the inefficiency (or the fatigue) of the lips' muscles. This force can momentarily overcome a lack of technique or an excessive fatigue. But even if musicians are trained to carefully control this force, all of them use it at various degrees during playing.

Previous studies on the embouchure of the brass player have specifically focused on the mouthpiece forces during playing. In [3], recordings of the mouthpiece pressure and air pressure variations by representative musicians are presented. For all players, the mouthpiece pressure increases with the pitch of the tones. A transducer for measuring the force applied to the mouthpiece is described in [4]. This transducer gives both the axial and sagittal forces created by the player on the mouthpiece. The magnitude of the force was not significantly related to the proficiency or playing style of the player. Another system, which allows simultaneously the recording of mouthpiece forces and teeth (incisor) deflection is proposed in [5]. Various brass instruments was studied, and authors conclude that lip tension must be responsible for the difference in teeth displacements, and is of major importance in stressing the incisors during brass instrument playing.

We present in this article some results of our experiments on the study of the force created on the mouthpiece during brass playing. In order to better know this phenomena, how it appears and what are the influential factors, we developed a system for the measurement of the force while playing a particular brass: the fluegelhorn [6]. For recording purposes, the system was connected to a PC based data acquisition system. We investigated the influence on the magnitude of the force of factors like proficiency, dynamic of the tone, articulation, pitch and duration of the note, context of the note in the musical phrase.

## 2. EXPERIMENTAL STUDY

### 1.1. Description of the system

The measuring system has been adapted on a fluegelhorn, by replacing the tuning slide of the instrument by a tube which can glide freely in the mouthpipe. It is composed of the following elements (see figure 2):

- A tube, which glides in the instrument body,
- A ring 1, clamped to the tube,
- A ring 2, clamped to the instrument body,

- A force captor (button load cells with strain gauges), located between the rings. Range: 0 - 10daN, precision: 0.1%

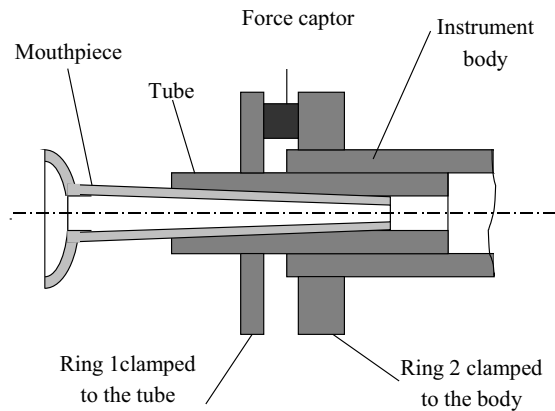


Figure 2: Description of the force captor.

The force captor is glued to ring 2 and presses on ring 1. When one presses on the mouthpiece, the axial force is directly transmitted to the captor, the friction between the parts being neglected. With this system, the measurement of the axial force on the mouthpiece can be made under normal playing conditions: the musician can use his/her usual performing technique while measurements are made, and he/she is not very disturbed by the system. The synoptic of the PC based data acquisition system is presented figure 3.

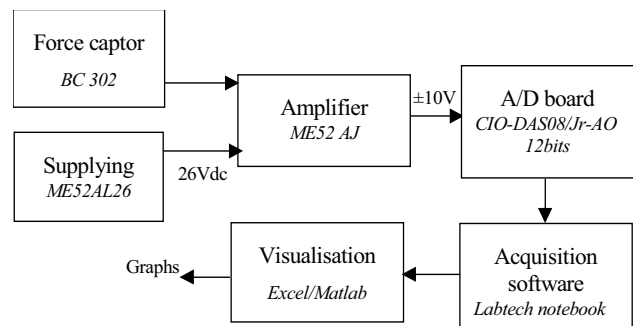


Figure 3: Synoptic of the acquisition system.

The measurement error is mainly due to the friction between the tube and the body of the instrument, and the gap between the position of the captor and the axis of the mouthpiece. A mechanical modelling of the friction between the parts leads to an estimation of this error of about 5%.

### 1.2. Experiments

Three brass musicians participated in the study. One was highly proficient (*professional*), being full time professional player in jazz big bands (5 hours per day); one was of advanced proficiency (*advanced*), having at least 20 years of practice as amateur (5 hours per week), and the last one of medium

proficiency (*medium*), with 5 years experience of the instrument (2 hours per week). The musicians used their own mouthpiece for the tests.

The tests consisted in playing successively an ascending and descending two octaves arpeggio (with no valves operated) in different style (staccato and legato), and different intensities (*mezzo forte*, *fortissimo*). The tempo was around 60 per quarter note for all tests.

### 1.3. Results

Each musician performed several attempts. We did not represent the average value of the force because it “smoothes” the curves, and the time scale was not exactly the same for all attempts. Even if the results presented concern particular tries, they are representative of the behaviour of the musician. Figures 4, 5, 6, 7 present the magnitude of the mouthpiece force as a function of time for various arpeggios and intensities.

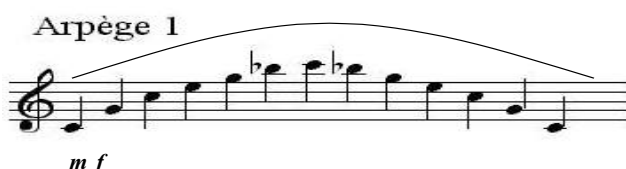
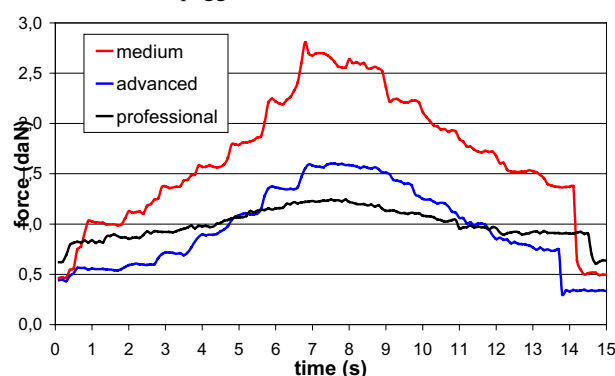


Figure 4: *force(time)* for arpeggio 1, dynamic *mf*.

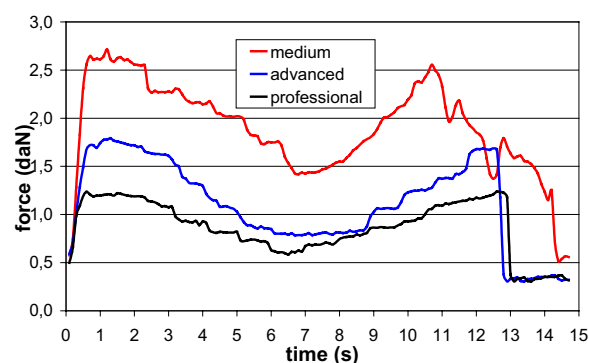


Figure 5: *force(time)* for arpeggio 2, dynamic *mf*.

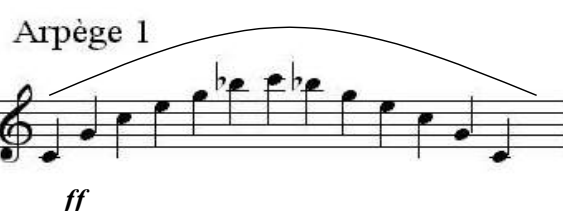
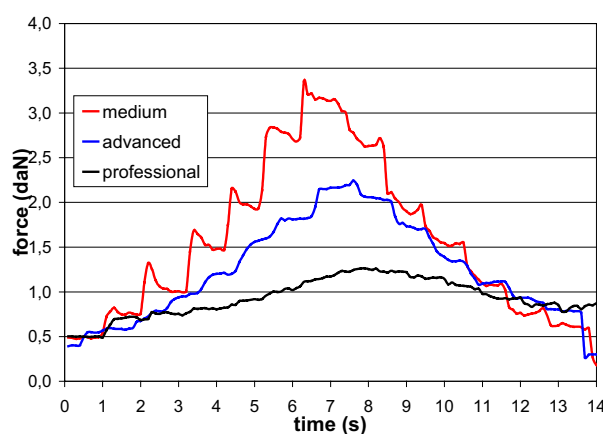


Figure 6: *force(time)* for arpeggio 1, dynamic *ff*.

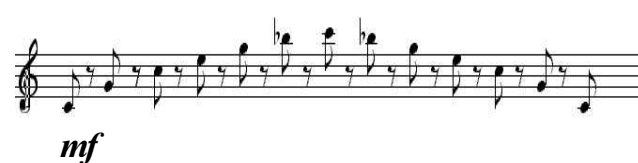
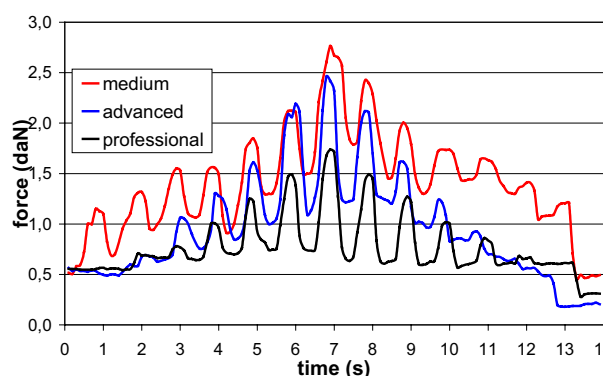


Figure 7: *force(time)* for arpeggio 3, dynamic *mf*.

### 3. DISCUSSION

For all tests and all musicians, the magnitude of the force always increases when the pitch of the note increases. This observation is in accordance with the intuition, and with previous studies [3, 4, 5]. The magnitude of the force varies according to the proficiency of our set of musicians. Higher is the level, weaker is the maximum force.

We think that an intensive and regular practice of the instrument leads to a sharp control of the playing parameters: control of the embouchure, control of the air pressure and the air flow. The “professional” musician use a force two or three time

less in average than the “medium” musician, and can in this way increase the duration of playing without having rest.

The magnitude of the force increases with the intensity of the tones (up to +20% from *mf* to *ff*). As the air pressure increase with the intensity, an increasing of the force is necessary to maintain the static airtightness between the lips and the mouthpiece.

On figure 6, peaks in the force curve can be observed for the “medium” musician. These peaks appear before each changing of notes. The “medium” musician uses a brief increase of the force for helping the changing of note. This behaviour is typical of a musician who does not have a strong control of his/her embouchure. In fact, among the playing parameters of the fluegelhorn (control of the embouchure, control of the air pressure and the air flow, control of the force on the mouthpiece), a beginner will use the most instinctive and easiest controllable parameter: the force on the mouthpiece. This phenomena, which increases with the intensity of the notes, is absent for the professional musician, who learned to change the note by modifying the embouchure, mainly by pressing the lips vertically against each others. Furthermore, the force generated by the “medium” musician for the emission of a note is generally greater than the force used for the sustain of this note (figure 6).

On figure 7, when notes are played separately, the magnitude of the force between two notes decreases with the proficiency of the musician. The “medium” musician keep on pressing the mouthpiece even if no note is played. This point is of major importance for having endurance and resistance during a session.

For all musicians, the force used for notes played separately is globally higher than the force needed for slurring notes. This can be explained by the fact that the musician can control continuously the parameters during slurred playing. Conversely, for notes played separately, a continuous control of the parameter is no longer possible, because no tone precedes the emission. A increasing of the force could then be necessary so as to insure the emission.

For all tests (figure 4, 5, 6, 7), force curves are not symmetrical (at various degrees), whereas all musical phrases are symmetrical. The tendency is that descending intervals need a greater force than the same ascending intervals. The control of the release of the embouchure and the air pressure during descending intervals seems to be more difficult than the control of the contraction (this is confirmed by many brass players). The musician has recourse to an increasing of the force so as to insure a descending interval.

#### 4. CONCLUSIONS

We have presented in this paper a system for the measurement of the force applied on the mouthpiece during brass instrument playing. The system is easy to use and does not necessitate complex modifications in the case of the fluegelhorn. We are going to adapt the device to the trumpet. Several measurements

have been made, with various musical phrases. We have presented the results for three musicians of different proficiency. The analysis of the measurements allows a better understanding of the playing parameters of the fluegelhorn. The main result is that the mouthpiece pressure was related, with our musicians, to their proficiency. The mouthpiece pressure seems to be in many case a substitute for muscular tension and embouchure control. The device could be used by beginners to feel that this pressure is undesirable when it takes over what muscular tension should do. The findings have to be tested with large scale tests with several subjects, in order to prove the significance of the observations (statistical analysis).

#### 5. ACKNOWLEDGMENTS

We acknowledge the help of Yannick Neveu, professional trumpet player, for his participation.

#### 6. REFERENCES

- [1] Fletcher, N.H. and Rossing, T. D. “The physics of musical Instruments”, Springer Verlag, New-York, 1991.
- [2] Gilbert, J., Ponthus, S., Petiot, J.F., “Artificial buzzing lips and brass instruments : experimental results”, J. Acoust. Soc. Am. 104, 1627-1632, 1998.
- [3] Henderson, H.W., “An experimental study of trumpet embouchure”, J. Acoust. Soc. Am, Vol. 13, pp 58-64, 1942.
- [4] Bardenel, J-C., “Mouthpiece forces produced while playing the trumpet”, Journal of Biomechanics. Vol. 21, No.5, pp. 417-424, 1988.
- [5] Borchers, L., Gebert, M., Jung, T., “Measurement of tooth displacements and mouthpiece forces during brass instrument playing, Med. Eng. Phys., Vol.17, No.8, pp 567-570, 1995.
- [6] Petiot, J-F. and Besnard, F., “Mesures de la force d'appui de l'embouchure sur les lèvres lors du jeu des cuivres”, Revue trimestrielle *Médecine des Arts* ISSN 1240-3784. N° 34 pp 7-9. December 2000.

## **DIFFERENTIATION OF TRUMPETS' SOUNDS: EXPERIMENTAL STUDY WITH AN ADAPTABLE DEPTH MOUTHPIECE**

*Jean-François PETIOT<sup>(1)</sup>, Emilie POIRSON<sup>(1)</sup>, Jean-Loïc LE CARROU<sup>(1)</sup>, Joël GILBERT<sup>(2)</sup>*

(1) Institut de Recherche en Communications et Cybernétique de Nantes  
UMR CNRS 6597 - Equipe MCM - Ecole Centrale de Nantes  
1 rue de la Noë, BP 92101, 44321 Nantes Cedex 3 France

(2) Laboratoire d'Acoustique de l'Université du Maine  
UMR CNRS 6613, Av. O. Messiaen, 72085 Le Mans Cedex 9, France

Jean-Francois.Petiot@ircrcyn.ec-nantes.fr

### **ABSTRACT**

In order to study the perceptual differentiation of trumpet's sounds, we developed a device for controlling one of the influencing variables of the sound quality of brass instruments: the mouthpiece depth. Using this mouthpiece, whose depth can be easily and continuously adjusted from "deep" to "shallow", and the same trumpet, we generated a "set" of instruments which differ from an acoustical point of view, and which produce sounds with subtle perceptual differences. In parallel, we developed by the past several "artificial mouths", which allow the playing of an instrument with a realistic and reproducible embouchure.

In this paper, we study the ability of the artificial mouth to show perceptively noticeable differences between sounds produced by instruments with small variations of the mouthpiece depth. For that, hearing tests with a set of subjects were performed, with sounds generated either by the artificial mouth or with a real player. An analysis of the sensitivity of sound differentiation for each sound generation procedure is presented. Secondly, an evaluation of the "brightness" of the sounds is performed by the subjects, in order to interpret a posteriori the differences observed between the sounds.

### **1. INTRODUCTION**

Studying the quality of musical instruments is particularly interesting to help their development and to improve quality assessment procedures. In [1], a study of the subjective assessment of brass instruments is proposed. Tests performed by musicians and listeners are described, using classical methods in sensorial analysis (multidimensional scaling, semantic differential method). In [2], authors discuss an objective approach for the assessment of the quality of brass. This approach necessitates to establish correlations between subjective responses given by a musician (which represent certain dimensions of the quality), and measurements extracted from the impedance curve of a set of instruments. These experiments are difficult to make, because one must finely control what parameters vary between the set of instruments, in order to be sure that the differences observed in the subjective assessment are effectively due to these variations. Many mathematical expressions, which aggregate information of the input impedance, are proposed to predict with more or less

success certain qualities of brasses [3]. But controlling and predicting the quality of an instrument by objective measurements is actually a very complex problem because it needs the establishing of links between two kind of variables, very different in essence: on one side, the "subjective quality", relative to the assessment of a musician or a listener, and controlled by the subject's perceptions; on the other side, the "objective quality", represented by the physical characteristics (or measurements) which are supposed to govern and influence the subjective quality, and mainly dependent on the instrument geometry. The main problem in this approach, based on correlations between objective and subjective assessments, is isolating sufficiently the influencing variables in order to control their variation and separate their effects.

We adopt in this paper another perspective for the study of brass quality, based on comparisons of sounds produced by the artificial mouth and a trumpet player. In previous studies [4], we shown that the artificial mouth is able to produce noticeable differences between two trumpets, and could be used as a test bench for comparing instruments. These differences concern objective measurements, namely the playing frequency, the threshold pressure, the output level in the bell.

We propose to show in this paper that differences in the perception of sounds by subjects (i.e subjective) can be revealed with the artificial mouth. For that, we carried out hearing tests, with sounds produced by a trumpet whose mouthpiece depth can be adjusted finely and continuously. A screw with a small thread between the rim and the cup of the mouthpiece allows a continuous adjustment of the cup depth. With this device, very subtle differences in the timbre of the tones can be created, until the threshold of "distinguishability".

The design of the stimulus (pairs of sounds) for the tests, based on [5], is described in section 2. The experimental protocol of three tests, based on [6], and the results, are presented in section 3. Then, preliminary conclusions and perspectives are given in section 4.



## 2. EXPERIMENTAL STUDY

### 2.1. Recording of the sounds

For a brass instrument player, the mouthpiece plays a determining role in the ease of playing and the sound quality. That's why we decided to concentrate our work on this parameter of the instrument. An adaptable depth trumpet mouthpiece, with a screw thread system which increases the mouthpiece cup depth by 0.5 mm each turn, was designed. 11 adjustments of the mouthpiece were considered: from position "0", completely "shallow", to 10, "deep", with a variation of 1 turn between two successive positions (0.5 mm between them). The same trumpet (Yamaha 1335 Bb) was used for all the tests.

We used two ways for producing the sounds: the artificial mouth and a musician. For each mouthpiece adjustment, the notes C4 and D4 were recorded. Three families of sounds were recorded, with the following dynamic<sup>1</sup>:

- **AM**: with the artificial mouth, dynamic *forte* (115dB),
- **MF**: with the musician, dynamic *mezzo forte* (100dB),
- **MP**: with the musician, dynamic *piano* (80dB).

For the recordings (sampling frequency 44100 Hz, 16 bits), a *Sennheiser e604* microphone was placed in the axis of the trumpet, at a distance of one bell radius of the trumpet, and was directly connected to the *Digigram Vx Pocket V2* sound card. The recorded tones were standardized in pitch and amplitude with a signal processing software. The duration of the sound was normalized to 600 ms. The transient regimes (attack and decay) of the sound were eliminated, a 50ms linear amplitude variation was added at the beginning and at the end of the sounds.

### 2.2. Stimuli of the tests

For a given note, for each of the 3 families of 11 sounds, only 5 sounds were selected (the most representative of the tone evolution with respect to the number of turns of the mouthpiece). This limitation of the number of sounds has been done so as to reduce the duration of the tests. The assessment of the difference between sounds has been done by pairwise comparison. The stimulus of the tests was a pair of sounds of the same family (**AM**, **MF** or **MP**), separated by 600ms of silence. All the 10 possible pairs among the 5 sounds were considered. In order to check the coherency of the subject, one pair of identical sounds was added to the stimuli. A total of 11 pairs of sounds, for each family (**AM**, **MF** or **MP**), constituted the stimuli of the tests.

For all tests, the pairs were presented three times to the subject in a random order, so as to check the consistency of the subjects. The subjects listened to the stimuli via a headphone *Audio-Technica ATH-M40* and gave his/her answer by clicking on boxes, via an interface programmed in *VisualBasic6*.

## 3. DESCRIPTION OF THE TESTS - RESULTS

### 3.1. Test 1

With this experiment, we tried firstly to find a threshold of distinguishability of the sounds differentiation, and secondly, to show if the subjective answer of subjects evolves in the same direction whether they are listening to a musician or to the artificial mouth. A total of 20 subjects, including 12 musicians, with no known hearing disorders, performed the first listening test. They had to decide whether the two tones of the pairs were different or not. They listened to all the pairs, that is to say 33 pairs, repeated randomly 3 times as said before. This test was made on the note C4 and D4 series. Thus, each subject assessed a total of 99 pairs for the note C4, and 99 pairs for the note D4.

Three subjects were excluded from the final results because they assessed at least one identical pair as "different". For each pair, subjects' answers were cumulated and put in percentages. Thus, 100% means that all the subjects found that, each time they heard it, the pair of tones was "different", 0% means that the pair has always been evaluated as similar by all the subjects. The results for the remaining 17 subjects for each family of sounds and for the note C4 are shown in figure 1. The first axis of figure 1 represents the number of turns of the mouthpiece for the sound #1 of the pair, the second axis the number of turns of the mouthpiece for the sound #2. The interpolated shading represents the percentage of differences evaluated by the subjects: the darker it is, the higher the difference between tones is. The diagonal of the figures, which is the location of identical pairs, is of course white (0%), because all the incoherent subjects have been excluded.

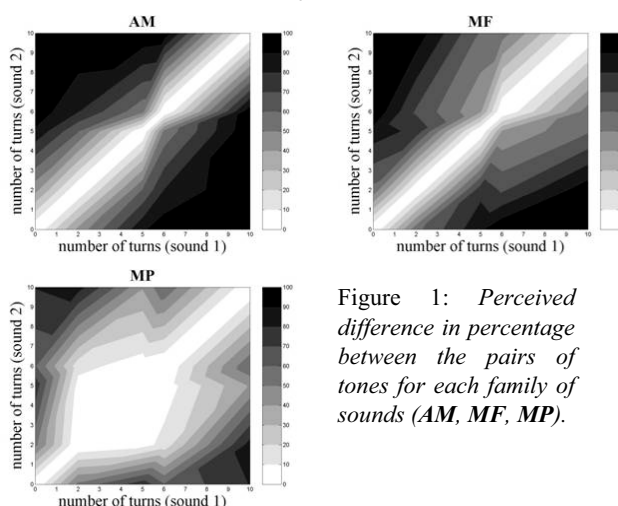


Figure 1: *Perceived difference in percentage between the pairs of tones for each family of sounds (AM, MF, MP).*

First, the trend of results for **AM** and **MF** is similar. The differentiation of timbre is even better than the difference of number of turns of the mouthpiece is high. Perceived differences for **MP** are less marked than for **AM** and **MF** as figures show. It is more ambiguous with **MP** to perceive the difference between the tones heard. The percentage of difference in the **AM** family is higher than with any other families. The threshold of differentiation seems to be lower with sounds played with the **AM**. Thus, it is easier to perceive a variation of cup depth with

<sup>1</sup> the sound level meter being placed just at the bell

the **AM**. The results obtained with the note D4 were quite similar, and are not presented here.

This first test shows finally that subjects perceived differences between sounds. Thus, we projected to improve quantification of difference by a new test (test 2). For the case of **MP**, differences are so small that we decided to exclude it from this new test 2. For the same reason, two pairs of sounds of the families **AM** and **MF** were rejected. Moreover, since the trends of subjective answer are similar for C4 and D4, we chose to use only C4 for the following tests.

### 3.2. Test 2

The aim of this second test was to quantify more finely the perceived differences between the pairs of sounds used in test 1. 23 subjects were asked to say to what degree the tones were different, choosing between "identical", "a little different", "different" and "very different". The answer was coded on an integer scale from 0 (identical) to 3 (very different). To familiarise the subjects with the scale's range, two pairs, one of "identical" tones and one considered as "very different", were made available, before the start of the test.

For each family of sounds (**AM** and **MF**), two identical pairs were added to the stimuli. The total score for these identical pairs was used to assert whether subjects' answers should be excluded from the final results or not. The subjects with a value different of 0 for this total score were eliminated of the test (incoherent). Five of them were excluded for this test 2. All results are shown in table 1. These matrices show the cumulated score for all subjects, expressed as a percentage of the maximum possible score. Thus, the higher the result is, the higher the difference between the corresponding tones is. Black boxes show the pairs that were excluded from this test because the difference between tones was too hard to perceive according to the first listening test.

First of all, the magnitude in percentage of the perceived differences with **MF** is, in general, slightly lower than the perceived differences with **AM**. In other words, it is easier to perceive a difference with the **AM** than with the trumpet player. This result agrees with the first listening test and it gives the possibility for a better quantification of the perceived differences. Secondly, as well as with **AM** and **MF**, the higher the difference between number of turns is, the higher the magnitude of dissimilarity of tone is. Finally, it seems that the magnitude evolves differently according to whether the variation of the number of turns is 0 to 5 or 5 to 10 (non-linearity).

AM		Number of turns (tone 2)					
		0	2	5	6	10	
Number of turns (tone 1)	0	0		50	75	88	
	2		0	25	38	81	
	5	50	25	0		57	
	6	75	38		0	71	
	10	88	81	57	71	0	

MF		Number of turns (tone 2)					
		0	2	5	6	10	
Number of turns (tone 1)	0	0		40	60	75	
	2		0	30	30	69	
	5	40	30	0		26	
	6	60	30		0	23	
	10	75	69	26	23	0	

Table 1: Perceived difference in percentage between the two tones

According to this second test, a better quantification of the perceived difference between trumpet tones has been obtained. The perception of this difference is more noticeable using the **AM** than with a musician playing *forte*. A possible explanation is that a trumpet player adjusts the tone by adapting himself to the mouthpiece. As a conclusion, the artificial mouth could be used as a test bench so as to reveal subtle sound colour differences.

### 3.3. Test 3

The aim of this test was to connect the perceptive differences to a semantic criterion. We have focused on a particular attribute of the timbre, the brightness. For this test, we have removed the identical pairs, and presented the last 48 stimuli to the same subjects as for test 2. They had to define which one of the two tones was the brightest.

The answers of the subjects were considered as valid only if all the answers for the three replications were identical (perfect consistency).

The result are shown in Table 2. Moreover, a quantity called the "confidence" of the comparison *C* was calculated for each pair of sounds. This quantity is the ratio of the number of subjects producing a consistent judgement (three times the same answer) over the total number of subjects. Thus, a confidence of 100 for a pair means that each subject gave the same answer each time he/she hears it.

First of all, the **AM** confidences are higher than the one of the **MF**. For **AM**, all answers converge to the same result: a tone produced by a shallower cup is brighter than the others. Note that this observation is compatible to the usual opinion of trumpet players.

For one pair only (pair 6-10), no conclusion about the brightness attribute can be drawn. For the other pairs, a clear tendency of the assessment of brightness is drawn. For **MF**, although confidence is weaker than for **AM**, the trend looks the same. The **AM** and **MF** lead to opposite results for the two latest pairs. But the confidences are so weak that these results are questionable. A single dimension for explaining the perceptual differences is perhaps not sufficient in this case.

Number of turns		<b>AM</b>			<b>MF</b>		
Tone 1	Tone 2	B	D	C	B	D	C
0	5	17	1	78	9	4	57
0	6	19	1	87	9	5	61
0	10	19	1	87	8	6	61
2	5	13	0	57	14	3	74
2	10	15	1	70	10	4	61
6	2	1	16	74	0	14	61
6	10	9	5	61	1	6	30
10	5	0	16	70	8	1	39

Table 2: Number of subjects who said that tone 1 was brighter (B) or duller (D) than tone 2 for each pair and the confidence (C).

#### **4. CONCLUSIONS**

We have presented in this paper a comparative study of the differentiation of trumpet sounds. Various instruments were defined, by varying the depth of the trumpet mouthpiece, producing continuous subtle sound differences. The sounds were generated in two ways: with an artificial mouth, and with a musician. Three categories of hearing tests were carried out, using pairwise comparisons.

The results obtained either with the artificial mouth or with the musician show the same tendencies. But the threshold of differentiation is lower with sounds produced by the artificial mouth. This can be explained by the faculty of adaptation of the musician to the instrument. Indeed, different instruments played by the same musician can produce very close sounds [7].

As a perspective, similar tests will be carried out using sounds generated by physical modelling. We envisage furthermore to conduct an analysis of the dimensionality of the perceptual difference by multidimensional scaling.

#### **5. ACKNOWLEDGMENTS**

We acknowledge the help of people of the IRCCyN lab and Ecole Centrale de Nantes for their participation to the tests. Authors are indebted to Gilles Pattee and Paul Molina for their help in the manufacturing of the experimental devices.

#### **6. REFERENCES**

- [1] Pratt R.L., Bowsher J.M. "The subjective assessment of trombone quality". *Journal of Sound and Vibration* 57, 425-435 (1978).
- [2] Pratt R.L. and Bowsher J.M. "The objective assessment of trombone quality". *Journal of Sound and Vibration* 65, 521-547 (1979).
- [3] Plitnik G. R, Lawson B.A.. *An investigation of correlations between geometry, acoustic variables, and psychoacoustic parameters for French horn mouthpieces*. *J. Acoust. Soc. Am.* 106, 1111-1125 (1999).
- [4] Petiot J-F., Gilbert G, Teissier F. M.Campbell "Objective analysis of brass instruments using an artificial mouth" *International Symposium on Musical Acoustics ISMA 2001*. 10-14 September 2001 Perugia, Italy (2001).
- [5] Carral S., Campbell D.M. "The influence of the mouthpiece throat diameter on the perception of timbre of brass instruments". *Proceedings of ISMA2002, Mexico*, (2002).
- [6] Wright H. "The acoustics and psychoacoustics of the guitar". *PhD Thesis, University of Wales, Cardiff*, (1996).
- [7] Bertsch M. Variabilities in trumpet sounds. *Proceedings of ISMA97 Institute of Physics, Edinburgh, UK*, 401-406 (1997).

# MODELLING THE LIP REED - COMPUTATIONAL AND EXPERIMENTAL INVESTIGATIONS OF THE TWO-MODE INWARD/OUTWARD STRIKING BEHAVIOUR

Orlando Richards<sup>1</sup>, D. Murray Campbell<sup>1</sup>, Joël Gilbert<sup>2</sup>

<sup>1</sup> School of Physics, University of Edinburgh, Edinburgh EH9 3JZ, UK

<sup>2</sup> Laboratoire d'Acoustique, Université du Maine, Le Mans, France  
richards@ph.ed.ac.uk

## ABSTRACT

The physiology of the vocal folds is very similar to that of the lips of a brass player. This paper adapts a two-mass vocal fold model to represent the behaviour of the lips and compares results obtained from modelling with results obtained from experimental studies of both human and artificial brass players' lips. Of particular interest is the mechanical response of the opening area between the modelled lips - which is directly compared to experimental measurements performed on an artificial mouth. Several important characteristics observed experimentally are reproduced in this analysis, including the presence of a pair of inward / outward striking resonances and the waveforms produced during self-sustained oscillation.

## 1. INTRODUCTION

Experimental measurements of the frequency response of the artificial lips [1] [2] [3] [4] [5] have shown very complex structures. From these structures, it became clear that there was consistently a pair of "inward" and "outward" striking resonances, respectively above and below the playing frequency. Linear stability analysis has shown that a model which contains these two resonances will be able to reproduce the commonly observed "lipping" behaviour, where the brass player can slide a note from above the instrument resonance to below (or vice versa) [5].

The physiology of the vocal folds has a lot in common with the human lips. This paper takes an established model of the vocal folds presented by Lous et al.[6] which has two degrees of freedom, and consequently two modes of oscillation, and compares its behaviour with experimental results obtained using an artificial mouth.

## 2. EXPERIMENTAL MEASUREMENTS

Thorough experimental studies of the behaviour of a set of artificial lips have been carried out in the past few years[2][3]. These studies have produced frequency response data of the artificial lips measured using the apparatus shown in figure 1. The lips are driven by a known oscillating pressure difference, and the resulting lip opening area is recorded by collecting the light from a laser source admitted through the lips.

The mouthpiece shown in the diagram is a transparent mouthpiece that has a window at the front, and the shank protruding to the side. Musical demonstrations have shown that this type of mouthpiece is just as playable as a normal mouthpiece. The pressure difference across the lips,  $\Delta P$ , is recorded by the probe

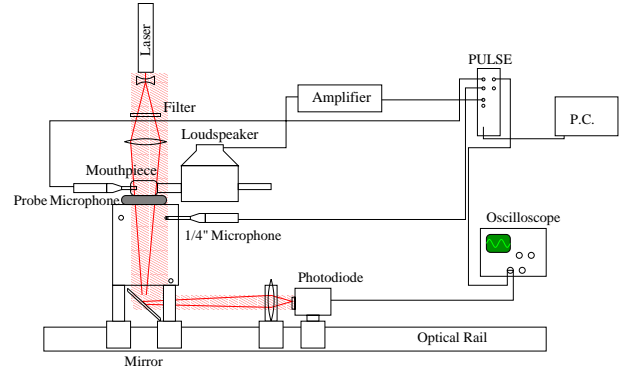


Figure 1: Diagram of experimental setup.

microphone and the 1/4" microphone, and is defined by equation 1.

$$\Delta P = P_{mouth} - P_{mouthpiece} \quad (1)$$

The voltage recorded by the photodiode is directly proportional to the amount of light admitted through the lips. Thus, this value is directly proportional to the opening area between the lips. The frequency response of the lips is defined by equation 2.

$$C(\omega) = \frac{OpeningArea(\omega)}{\Delta P(\omega)} \quad (2)$$

The experimental results obtained take the form of a frequency response plot of the lip opening area. Figure 2 shows one such result, giving the magnitude and phase of the response.

The two vertical lines highlight the two most important resonance frequencies, with opposite "striking" character[5]. In self-sustained oscillation the lips play at a frequency somewhere between these two resonances. It is quite clear, however, that the structure of this response curve is far more complex than that of the displacement of a pair of coupled simple harmonic oscillators.

## 3. VOCAL FOLD MODEL

The Lous model of the vocal folds[6] is a geometrically simple model, which has two degrees of freedom. The model, with the relevant variables labelled, is shown in figure 3.

In order to simplify the calculations, the motion is assumed to be symmetrical about the x-axis. The flow travels in the positive x direction, from the "mouth cavity" out into the open air. A jet is formed by this flow, which separates from the lip channel at the point  $x_s(t)$ .

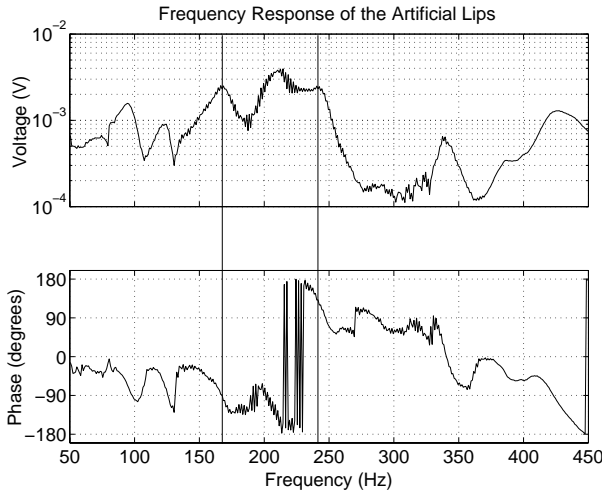


Figure 2: Typical frequency response of the artificial lips' opening area.

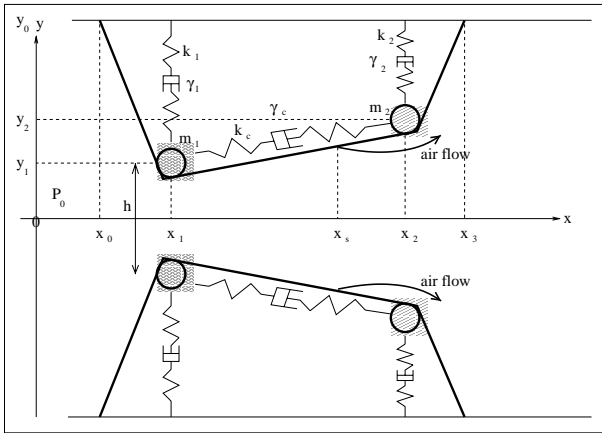


Figure 3: The Lous Vocal Fold Model.

The impulse response of the individual masses is shown in figure 4. It shows that each mass has, as expected, a smooth resonance curve with two peaks, corresponding to the two modes of oscillation.

This structure is clearly quite different from that observed experimentally. The function investigated here is the displacement of each mass, which in many models is linearly proportional to the opening area between the lips. In, for example, the simple model used by Cullen[2] the opening area  $S$  for a given lip displacement  $y$  and an opening width  $b$  is given by:

$$S = 2by \quad (3)$$

However, in the case of the Lous model this function is non-linear, and is given by equation 4.

$$S = 2b[\min(y_1, y_2)] \quad (4)$$

When the frequency response of this function is considered, the results show very similar characteristics to those observed experimentally. Figure 5 shows one such response curve. Note the

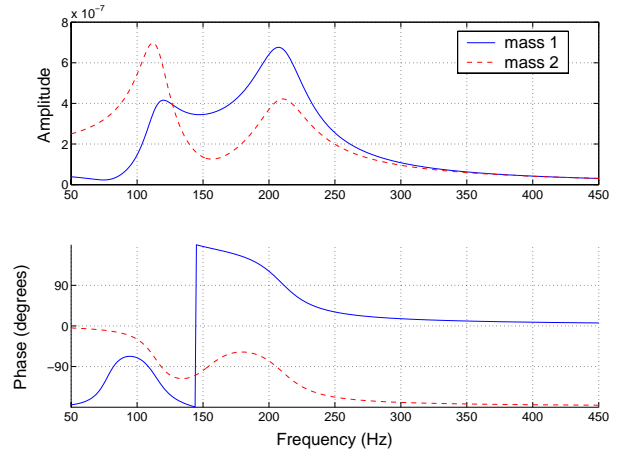


Figure 4: The frequency response of the displacement of the two masses in the Lous model (see figure 3).

two vertical lines representing the outward and inward striking modes. The threshold playing frequency for this configuration was at 161 Hz.

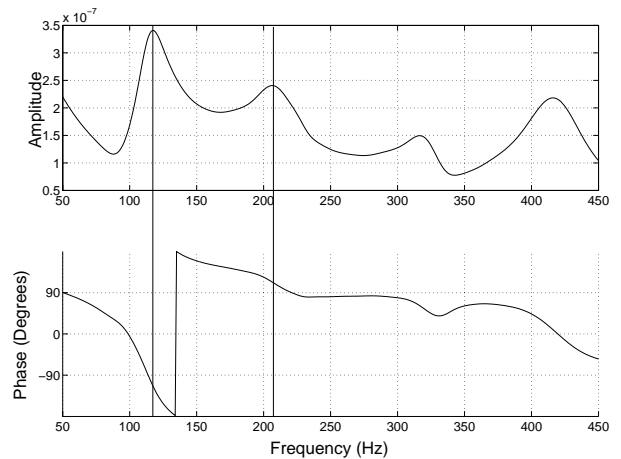


Figure 5: The frequency response of the lip opening area of the Lous model.

This function now shows the two significant peaks observed experimentally, and also shows similar phase characteristics.

In addition to the frequency response data, the trace of the lip opening area during self-sustained oscillation produced a shape of curve similar to that observed experimentally, both with the artificial lips and with human lips (using experiments performed with a high-speed camera). These data are shown in figure 6.

The lip model clearly shows two discontinuities as the height function “swaps” from being the position of one mass to the other. Similar types of discontinuities can be observed in the high speed video recordings of both the human and artificial lips.

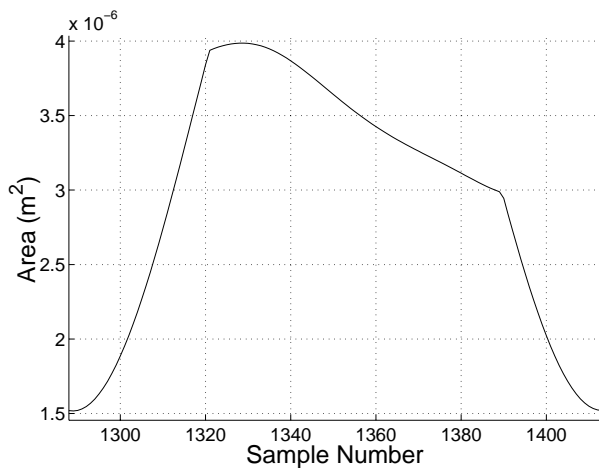


Figure 6: The lip opening area obtained from the Lous model.

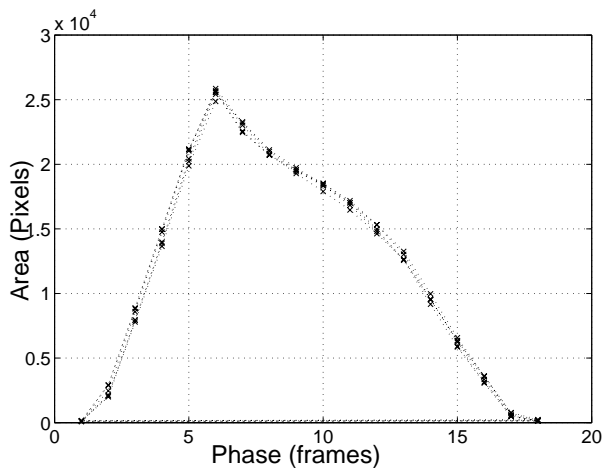


Figure 7: The lip opening area obtained from the high-speed video recordings.

#### 4. FURTHER WORK

Several studies have shown that the lips move in both the  $x$  and  $y$  directions [7][8], but the model used here was restricted to motion only in the  $y$ -direction. Initial investigations of a model which is free to move also in the  $x$ -direction have been very encouraging - providing even more similarities between experimental and computational opening area response curves.

Experimental investigations of the frequency response of an individual point on the lip should also provide further illumination of the problem. Much of the shape of the opening area response curve appears to be from the non-linear function given by equation 4, and as such one would expect to see simpler response curves when looking at an individual point on the lips - as shown in figure 4 for the lip model.

#### 5. CONCLUSIONS

The experimentally observed lip response curve can be reproduced by the Lous model of the vocal folds, taking into account that the lip opening area is a nonlinear function of the individual positions of each mass.

The lip opening area during self-sustained oscillation is also reproducible using this model. The discontinuities in the function observed experimentally also appear when viewing the non-linear area function produced by the simulations.

#### 6. REFERENCES

- [1] Cullen, Gilbert, and Campbell. Brass instruments: Linear stability analysis and experiments with an artificial mouth. *J.Acoust.Soc.Am.*, 86:704–724, 2000.
- [2] J.S. Cullen. *A Study of Brass Instrument Acoustics using an Artificial Reed Mechanism, Laser doppler Anemometry and other techniques*. PhD thesis, The University of Edinburgh, 2000.
- [3] M.A. Neal. *A Study of the Brass Instrument Lip Reed Mechanism using Artificial Lips and Lattice Boltzmann Flow Simulations*. PhD thesis, The University of Edinburgh, 2002.
- [4] M.A. Neal, O.F. Richards, D.M. Campbell, and J. Gilbert. Study of the lip reed destabilisation using an artificial mouth. In *Proc. IoA 2002*, March 2002.
- [5] O. Richards, D. M. Campbell, J. Gilbert, and M. A. Neal. Use of experimental studies in determining a two-mass lip model. In *Forum Acusticum Sevilla 2002*, September 2002.
- [6] N.J.C. Lous, G.C.J. Hofmans, R.N.J. Veldhuis, and A. Hirschberg. A symmetrical two-mass vocal-fold model coupled to vocal tract and trachea, with application to prosthesis design. *Acustica*, 84:1135–1150, 1998.
- [7] D.C. Copley and W.J. Strong. A stroboscopic study of lip vibrations in a trombone. *J.Acoust.Soc.Am.*, 99:1219–1226, 1995.
- [8] S. Yoshikawa and Y. Muto. Lip-wave generation in horn players and the estimation of lip-tissue elasticity. *Acustica/Acta Acustica*, 89:145–162, 2003.



**WOODWINDS**





## **FROM SOUND SYNTHESIS TO INSTRUMENT MAKING : AN OVERVIEW OF RECENT RESEARCHES ON WOODWINDS**

*B. Fabre<sup>1</sup>, A. Hirschberg<sup>2</sup>*

<sup>1</sup> Laboratoire d'Acoustique Musicale, Université Paris 6, boîte courrier 161, 4 place Jussieu F-75252 Paris Cedex France

<sup>2</sup> Department of applied physics, Fluid dynamics laboratory, Eindhoven University of Technology. The Netherlands

fabreb@ccr.jussieu.fr

### **ABSTRACT**

Trying to understand the physics of woodwind instruments has been a challenge for many generations of researchers. Although huge progresses have been achieved, it appears today that the physics of woodwind instruments still keeps an exciting part of mystery.

Since the years 1980s and 1990s, sound synthesis based on simplified descriptions of the time-domain equations allows to produce interesting sounds, even though many aspects are not well understood, especially the effect of geometrical "details" emphasized by instrument makers. Concerning reed instruments, the details of the fluid mechanics in single reed instruments are not well understood, but simplified models of reed mechanics and flow behaviour in the clarinet mouthpiece yielded interesting results on the dynamics of the clarinet. More recently, part of the research turned towards free reed instruments like the harmonica or the mouth organ. Concerning flute-like instruments, some researchers focused on the analysis of specific oscillating regimes, while others focused on the influences on the sound production of the mouth geometry in the flute or of the nicks at the flue exit of flue organ pipes.

A deeper understanding of the effects of the resonator's geometry (cross fingerings, side holes geometry) is also a goal for present researchers and may keep the most useful aspect for instrument makers.

### **1. INTRODUCTION**

Sound synthesis by physical modeling of woodwind instruments has been hugely developed in the last 20 years, starting from the work of McIntyre & al [1] and applied to reed instruments by several authors [2,3] or to the flute [4]. This development, supported by the increase of easily available computer power, is based on simplified descriptions of the physics involved. Woodwind instruments are powered by a static pressure generated by the muscles of the player or by any artificial blower in the case of the organ, and turn the static energy into oscillations using either a combination of mechanical vibrations of reeds sustained by a flow in the case of reed

instruments, either the intrinsic instability of the flow in the case of flute-like instruments. Therefore, the physical description of woodwind instruments should deal with pipe acoustics, mechanical vibrations of reeds and unsteady flows.

### **2. FLUTES**

#### **2.1. A brief history of flute models**

The sound is produced in flute-like instruments by the interaction of an intrinsically unstable jet with a sharp edge called the labium, in the vicinity of an acoustic resonator. The subject has interested researchers since the time of Helmholtz and Rayleigh. Following Powell's approach of the edge-tone [5], feedback loops have been used to describe the self generated oscillations in flute and organ pipes by Coltman [6], Elder [7], Fletcher [8] and Cremer [9] in the sixties and seventies. Those models allowed the first quantitative predictions of the playing frequency as well as the oscillating amplitude and spectra. The work of McIntyre & al. [1] triggered time domain simulation based on a simplified version of these models. In this simplified version, it appeared difficult to relate the model parameters to physical parameters of a flute. Probably because of a misprint, the proposed model did not oscillate with the given set of parameters and showed a monotonously increasing jet deflection added to the desired oscillation, as pointed out by several authors [10,11]. Even if the model was modified to correct these drawbacks, it produced a rather poor non realistic sound.

Models including a better insight into the fluid dynamics of air jets were then developed in the 1990's, leading to a much more realistic sound synthesis [4].

#### **2.2. Where to go ?**

To go one step further probably requires a more detailed analysis of the different aspects involved. A global review of the different problems is presented in [12], focusing on the gap between the rigorous approach proposed by analytical models such as those presented by Howe [13] or Crighton [14] and the simplified lumped models. Based on a hypothesis of localized interactions, lumped models describe each element independently of the others. On the other hand, analytical

models in which the entire flow is described in terms of integral equations can only apply to very simplified geometries, and can only be solved in linear approximation [14]. Analytical models may still be a source of inspiration to enlighten the unanswered problems in lumped models.

### 2.3. Recent developpements

Researches during the last years in the field of flute-like instruments focused on the analysis of a specific part of the model : jet instability [15,16], jet velocity profile [17,18], flow in the jet region [19] while others focused on a specific behavior of the instrument like mouth-tones in flue organ pipes [20,21]. Mouth-tones appear during starting transients of organ pipes and, under special circumstances, may still exist during steady-state. They are characterized by a frequency dependance on the blowing pressure close to that of edge-tones. Measurements of the oscillating amplitude of the mouth-tones showed that they rely upon energy accumulation in the pipe since they show an amplitude about a factor 100 stronger than a normal edge-tone [22], their frequency behaviour indicate a saturation and locking mechanism different from standard pipe-tones oscillations. Another direction followed by researchers was to analyse the effect on the sound production of some geometrical details of the instrument, mostly inspired by the empirical knowledge of the instrument makers.

Despite the interesting sound produced, the model proposed by Verge [4] was unable to take into account some of the geometrical details that instruments makers indicate as important for the sound quality or the playability of the instrument.

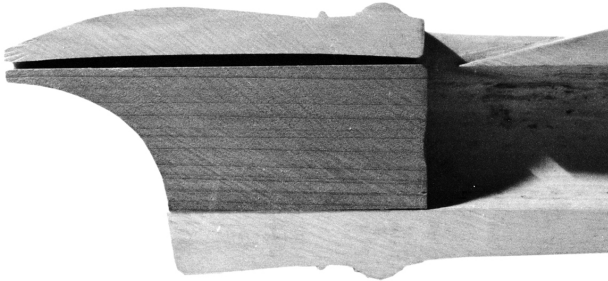


Figure 1 : Longitudinal cut of a recorder showing the shape of the flue channel, the chamfers at the flue exit and the 15° angle of the labium (recorder by D. Bariaux, from the flute collection of M. Castellengo, picture by B. Fabre) .

The work of Ségoufin [18] allowed to go one step further in this direction in the case of the recorder by analysing the effects of the channel geometry and of the chamfers at the end of the channel. Fig. 1 shows the convergence of the flue channel and the 45° chamfers that can be found in an actual recorder. Using flow simulation, Ségoufin [23] showed that the convergence of the channel generates steeper shear layers in the jet than in the case of a straight channel, inducing an efficient frequency dependant jet instability. The length of the channel offers an efficient low-pass filtering of the jet velocity fluctuations [23,24] that helps the stability of the oscillation. The strong stabilizing

effect of the chamfers at the end of the channel was also shown experimentally but has not yet been fully understood.

In the case of a Helmholtz resonator, Dequand [25] studied the influence of the angle of the labium in a transverse flute like geometry of the mouthpiece. Experimental investigation showed that the 60° labium angle found in the modern Boehm flute allows a higher oscillating amplitude than the 15° labium angle found in recorders. The 15° labium angle allows a better production of higher harmonics but also enhances the turbulent noise generated by the jet.

Recent work by Macherey [26] on the influence of the tuning of the acoustic modes a pipe resonator seems to indicate that the results obtained by Dequand can apply to the flute since the jet oscillating movement is dominated by the fundamental component independantly of the tuning, as presented fig. 2.

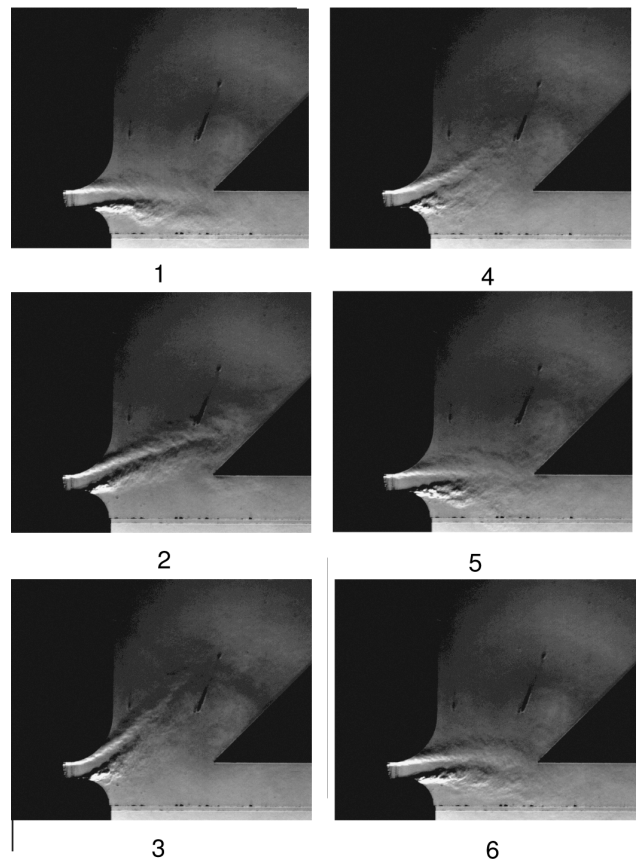


Figure 2 : Six pictures in one period of the oscillation in a Boehm flute like geometry. The figure shows the jet movement from the rounded lips towards a 45° labium. The pipe is placed above and does not appear on the picture. From Macherey [26]

## 3. REED INSTRUMENTS

### 3.1. Single reed instruments

Models of single reed instruments need to include a mechanical description of the reed. The reed is often modeled by

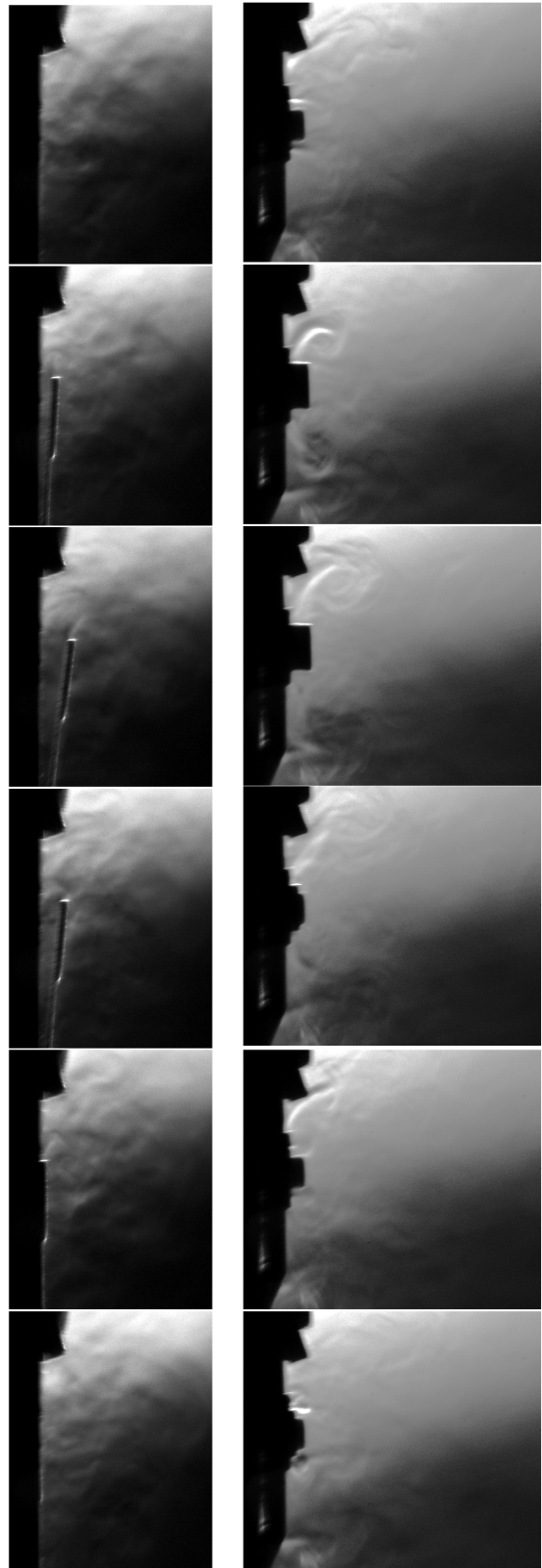
a one mode damped oscillator. For instruments like the clarinet, the playing frequency of the whole instrument is below the reed resonance frequency and the reed is therefore modeled by a spring. It is fascinating to see how this one mode approach of reed mechanics, combined with a simple Bernoulli description of the flow in the reed aperture and a linear acoustic model of the pipe offers a simple model that can predict already quite accurately the behavior of a clarinet [27]. A description of the flow in the reed aperture including flow separation at the tip of the reed has been proposed since 1990 [28] based on a stationary flow description, but it seems that the non-linearity induced by the closing of the reed on the lay is strong enough to mask the weak points of the model.

Recent researches on single reed instruments include the analysis of the effect of the shape of the bore of the pipe, the damping in the pipe as well as in the reed itself [29], a better description of the closing of the reed on the lay [30]. The analysis of the oscillating solutions in the traditional model, together with experiments using an artificial blowing system, showed an interesting analogy with the Helmholtz motion of a bowed string. Recently, Facchinetti & al. [31] proposed an approach in which the reed itself is included in the linear part of the description, restricting the non-linear elements to the flow and the contact forces between reed and lay, considered here as non-linear boundary conditions. This approach allows to determine the modes of the linear part of the system including the reed, yielding interesting results on the harmonicity of the system.

### 3.2. Free reed instruments

Free reed instruments have been very popular amongst researchers during the last years. While the basic description was probably proposed in 1971 by St Hilaire & al. [32], it seems that the experimental work and the model developed by Tarnopolsky & al. [33] together with the experimental results of Cottingham & al. [34] gave an impulse to the researches on free reed instruments. The models used include a description of the pressure fluctuations in blowing reservoir, a mechanical description of the reed as a simple cantilever and a flow through the aperture approximated by a Bernoulli equation, together with a *vena contracta* effect. The detailed description of the area of the aperture between the reed and the backing plate is essential in this model and may be complicated in the case of instruments with curve reeds [35]. In the case of reed organ pipes, the effect of a pipe resonator downstream from the reed has also been studied by Miklos & al. [35]. Taking into account the coupling of two different reeds within the same channel of the harmonica, together with a very simple model of the vocal tract of the player, Millot [36] was able to predict the “drawn bend” playing technique in which a player can play semitones on a diatonic instrument. Millot [37] also developed a simplified model for time domain simulation generating very realistic sound synthesis. On the same line, Hikichi & al. [38] developed a time-domain simulation for the sho.

Figure 3 : transversal (left) and longitudinal (right) view of the flow through the opening of a standard harmonica reed. The figures present 6 pictures covering  $5/6^{\text{th}}$  of the period, centered on the outward opening of the reed.



All the models developed rely on a one mode description of the oscillation of the reed. Measurements of the reed motion in playing conditions indicate that this assumption is valid [33,36]. The description of the flow through the reed opening in terms of a jet may be one of the interesting points to improve. Fig. 3 shows the flow out of a typical harmonica reed (length 15mm, width 2.24 mm, brass of non uniform thickness, free oscillating frequency 267 Hz). The nice moustache shaped vortices generated through the aperture on the sides of the reed may induce both an aerodynamic force on the reed and a non-linear sound source.

#### 4. CONCLUSIONS

The interest for woodwind instruments may come from the fact that their physical description needs to take into account different aspects such as pipe acoustics, fluid dynamics and mechanical vibration. The work of the player on the instrument should also be taken into account if a detailed model is aimed.

While researchers working on single reed instruments have developed the description of the mechanics of the reed, those working on free reed instruments have included the effect of the reservoir cavity and those working on flute-like instruments have studied in details the behavior of the flow.

Considering the high acoustic amplitude of the oscillations in woodwind instruments, non-linear effects at side holes has also been investigated [39] and may show interesting effects when included in the models of woodwind instruments.

Sound synthesis by physical modeling relies on simplified descriptions and may produce fascinating sounds if the proper aspects of the physics of the instrument are grasped, for transient as well as stationary sounds. For the time being, sound synthesis based on physical modeling does not offer the possibility of including the interesting details for the instrument makers. Improving the models so that they can take into account such geometrical details could be a research goal for the next years. At the present time, a deeper understanding of the effects of the resonator's geometry (cross fingerings, side holes geometry) as carried by Wolfe & al. [40] in the case of the flute may keep the most useful aspect for instrument makers

#### 5. REFERENCES

- [1] McIntyre M.E., Woodhouse J., Schumacher R.T. : "On the oscillations of musical instruments", *J. Acoust. Soc. Am.*, 74 (1983) 1325-1343.
- [2] Smith J.O. : "Efficient simulation of the reed-bore and bow-string mechanisms", in *Proceedings of the International Music Conference, The Hague, 1986*, 275-280.
- [3] Adrien J.M., Ducasse E. : "Dynamic modeling of instruments for sound synthesis", in *Proceedings of the International Conference on Acoustics, Belgrade, 1989*, Vol 3, 105-108.
- [4] Verge M.P., Hirschberg A., Caussé R. : "Sound production in recorder-like instruments II, a simulation model" *J. Acoust. Soc. Am.*, 101 (1997) 2925-2939.
- [5] Powell A. : "On the edge-tone" *J. Acoust. Soc. Am.*, 33 (1961) 395-409.
- [6] Coltman J. : "Sounding mechanism of the flute and organ pipe" *J. Acoust. Soc. Am.*, 44 (1968) 983-992.
- [7] Elder S. : "On the mechanism of sound production in organ pipes" *J. Acoust. Soc. Am.*, 54 (1973) 1554-1564.
- [8] Fletcher N.H. : "Sound production by organ flue pipes" *J. Acoust. Soc. Am.*, 60 (1976) 926-936.
- [9] Cremer L. Ising H. : "Die selbstregten schwingungen von Orgelpfeifen" *Acustica* 19 (1967/68) 143-153.
- [10] Fabre B. : PhD dissertation, Le Mans France 1992.
- [11] Valeriu I. : Master's thesis, University of Washington, Seattle, USA 1992.
- [12] Fabre B., Hirschberg A. : "Physical modeling of flue instruments : a review of lumped models" *Acustica Acta-Acustica* 86 (2000) 599-610.
- [13] Howe M. : "Contributions to the theory of aerodynamic sound, with applications to excess jet noise and the theory of the flute" *J. Fluid Mech.* 71 (1975) 625-673.
- [14] Crighton D. : "The edgetone feedback cycle. Linear theory for the operating stages" *J. Fluid Mech.* 234 (1992) 361-391.
- [15] Nolle A.W. : "Sinuous instability of a planar air jet : propagation parameters and acoustic excitation" *J. Acoust. Soc. Am.*, 103.6 (1998) 3690-3705.
- [16] Adachi S. : "Numerical analysis of an air jet" *ISMA* 2001 317-320.
- [17] Yoshikawa S., Keita A. : "Measurements of velocity profiles of the jets issuing from some flue geometries typical of air-jet instruments" *ICA Roma* 2001.
- [18] Segoufin C., Fabre B., Verge M.P., Hirschberg A., Wijnands A.P.J. : "Experimental study of the influence of the mouth geometry on sound production in recorder-like instruments" *Acustica Acta-Acustica* 86 (2000) 649-661.
- [19] Bamberger A. : "Investigations and recent results on flutes with PIV" *ISMA Perugia* 2001.
- [20] Castellengo M. : "Acoustical analysis of initial transients in flute-like instruments" *Acustica Acta-Acustica* 85 (1999) 387-400.
- [21] Miklos A., Angster J. : "Properties of the sound of flue organ pipes" *Acustica Acta Acustica* 86(2000) 611-622.
- [22] Fabre B., Castellengo M. : "Experiments on mouth-tones during transients and steady-state oscillations in a flue organ pipe" *ICA Roma* 2001.
- [23] Segoufin C. : PhD dissertation, Univ. Paris 6, France (2000)
- [24] Verge M.P., Caussé R., Fabre B., Hirschberg A., Wijnands A.P.J., van Steenberghe A. : "Jet oscillations and jet drive in recorder-like instruments" *Acustica Acta Acustica* 2(1994) 403-419.
- [25] Dequand S., Willems J.F.H., Leroux M., Vullings R., van Weert M., Thieulot C., Hirschberg A. : "Simplified models of flue instruments : influence of mouth geometry on the sound source" *J. Acoust. Soc. Am.*, 113.3 (2003)
- [26] Macherey O. : internal report, Paris 2002.
- [27] Kergomard J. : "mechanics of musical instruments" lecture notes for CISM, Springer Verlag 1995.
- [28] Hirschberg A., van de Laar R.W. : "A quasi-stationary model of air flow in the reed channel of single reed woodwind instruments" *Acustica* 70 (1990) 146-154.
- [29] Dalmont J.P., Gilbert J., Kergomard J. : "Reed instruments, from small to large amplitude oscillations and the Helmholtz motion analogy" *Acustica Acta Acustica* 86 (2000) 671-684.
- [30] Olivier S. : PhD dissertation, Le Mans, France 2002.
- [31] Facchinetti M., Boutillon X., Constantinescu A. : "Numerical and experimental modal analysis of the reed and pipe of a clarinet" *J. Acoust. Soc. Am.*, 113.5 (2003) 2874-2883.
- [32] St Hilaire A. O., Wilson T.A., Beavers G.S. : "Aerodynamic excitation of the harmonium reed" *J. Fluid Mech.* 49 (1971) 803-818.
- [33] Tarnopolsky A.Z., Fletcher N.H., Lai J.C.S. : "Oscillating reed valves - an experimental study" *J. Acoust. Soc. Am.*, 108.1 (2000) 400-406.
- [34] Cottingham J.P., Fetzer C.A., "Acoustics of the khaen" *ISMA* 1998 Leavenworth.
- [35] Miklos A., Angster J., Pitsch S., Fletcher N.H. : "Reed vibration in lingual organ pipes without resonator" *J. Acoust. Soc. Am.*, 113.2 (2003) 1081-1091.
- [36] Millot L. PhD dissertation, Univ Paris 6 France 1999
- [37] Millot L. Ambroise D. : "time domain simulation of diatonic harmonica" *J. Acoust. Soc. Am.*, 111.5 (2002) 2376.
- [38] Hikichi T., Osaka N., Itakura F. : "Time domain simulation of the sound production of the sho" *J. Acoust. Soc. Am.*, 113.2 (2003) 1092-1101.
- [39] Dalmont J.P., Nederveen C.J., Dubos V., Olivier S., Meserette V., te Sligte E. : "Experimental determination of the equivalent circuit of an open side hole : linear and non linear behaviour" *Acustica Acta Acustica* 88 (2002) 567-575.
- [40] Wolfe, J., Smith, J., Tann, J. and Fletcher, N.H. (2001) "Acoustic impedance of classical and modern flutes" *Journal of Sound and Vibration*, **243**, 127-144

## EXPERIMENTAL RESEARCH ON DOUBLE REED PHYSICAL PROPERTIES

André Almeida, Christophe Vergez\*, René Caussé, Xavier Rodet

IRCAM; 1, Place Igor Stravinsky; 75004 Paris FRANCE

\*CNRS - Laboratoire de Mécanique et d'Acoustique; 31, chemin Joseph Aiguier; 13402 Marseille

### ABSTRACT

Physical modeling of musical instruments is usually based on simplified assumptions about the behavior of the instrument, so that only the essential information necessary to correctly describe the sound produced by the instrument is kept. Such models are able to describe the sound of single-reed instruments, for example.

A simplified reed model is in fact quite generic and its assumptions can also be applied to double-reed instruments. Such a simple model, however, was proven not to be sufficient, and a double-reed model must include a more complete description of the physics of the reed.

This article presents some of the experimental work being done on double-reed instruments. Measurements such as geometric characterization of the reed aim to allow consolidation of hypothesis previously tested in physical models. The determination of the non-linear characteristic is a key-point in the description of the reed behavior.

### 1. INTRODUCTION

History of physical modeling of reed instruments begins in 1963, when Backus [1] published his first mathematical model of a clarinet. This mathematical model was first applied to sound-synthesis by Schumacher [2]. In spite of its simplicity, this model was able to produce realistic sounds and is currently used in sound synthesis by physical modeling.

In these models, the instrument is seen as a modular system, the exciter (reed and mouthpiece) being modeled separately from the resonator and sharing common physical variables with it. The resonator is usually modeled as a one-dimensional waveguide with boundary conditions that confer the resonance properties of the bore.

Although the bore can have different geometries, a one dimensional waveguide can be described in terms of its input impedance  $Z_{in}(\omega)$  or alternatively its reflection function  $r(t)$ , which can be obtained from the former using a function of its Fourier Transform. This description remains valid as long as we restrict ourselves to linear acoustic propagation.

Modeling of reed-models coupled to conical resonators was tried out by Barjau [3], to study the timbral influence of conical resonators on the behavior of the instrument.

The simplest exciter model consists of a valve controlled by the pressure difference between its inside (reed pressure  $p_r$ ) and its outside (mouth pressure  $p_m$ ). The valve is seen as a harmonic oscillator:

$$m \frac{\partial^2 z}{\partial t^2} + r \frac{\partial z}{\partial t} + k(z - h) = p_r - p_m \quad (1)$$

In this equation,  $m$  is the mass of the valve,  $r$  is its damping and  $k$  its stiffness, all of them considered per unit effective surface.  $z$

is the valve opening. In fact, usually both  $m$  and  $r$  are neglected because playing frequencies are small compared to the reed resonance frequency ( $\omega_r \simeq \sqrt{\frac{k}{m}}$ ).

The pressure difference ( $p_m - p_r$ ) induces a flow through the valve opening section ( $S_r = 2z l_r$ ) which can be described by a simple model like Bernoulli:

$$q = S_r \sqrt{\frac{2}{\rho} (p_m - p_r)} \quad (2)$$

In a clarinet the initial jet produced in the reed channel (between the reed and the mouthpiece) arrives in a much larger chamber and completely loses its kinetic energy without recovering potential energy. The flow is created by the pressure difference between the mouth and the reed, and this ( $p_r$ ) has the same value as the pressure at the input of the bore.

In a double reed the conicity angle is so gentle that the flow can attach to the wall without losing all of its initial kinetic energy by turbulent mixing. Nevertheless, the extended flow which can attach to the reed walls can undergo further head loss before reaching the resonator. Depending on the complexity of the boundary conditions applied to the flow, new phenomena [4] might need to be taken into account, such as jet separation due to greater conicity [5]. Usually these features can be reduced to a head loss establishing a difference between the pressure inside the reed  $p_r$  and the acoustic pressure at the beginning of the bore  $p$ .

These considerations lack experimental evidence. In fact, experimental data about double-reeds is scarce and usually restricted to phenomenological considerations about the time-varying properties of the instrument [6] [7]. A short comparison of this data with the behavior of our model can be found in [8]. Further experimental data and techniques, though in preliminary form are presented in the rest of the article.

### 2. REED CHARACTERIZATION

In a Backus-like wind instrument model, the whole resonator can be characterized at its input by the flow variables  $p$  and  $q$ . Similarly, the two relevant variables from the point of view of the instrument acoustics are the reed output pressure ( $p$ ) and flow ( $q$ ), which therefore establish the coupling between the exciter and the resonator. During a period, the two of them are related by a non-linear function called the *characteristic*.

In the first graph of figure 1 we have plotted the characteristic of a single reed. The reed has a maximum output flow and it is beyond this value that the reed can begin its oscillation. The shape of the actual trajectory of the variables during a period slightly changes with the frequency but for the lowest frequencies it is reasonable to suppose that the dynamic terms in eq. 1 will not have a

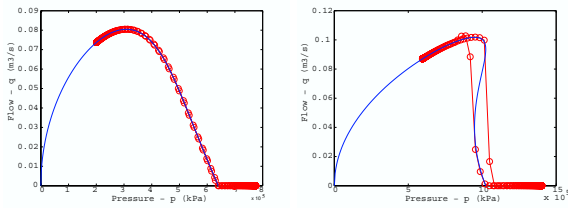


Figure 1: Simulated flow characteristic curves for single-reeds and double-reeds. Markers indicate the trajectory of the instrument's variables during a cycle

big relevance compared to the stiffness and pressure terms. Otherwise, the trajectory will not be superposed to the theoretical curve.

In the case of a double reed, we have seen in section 1 that an additional head-loss must be considered. This fact modifies the characteristic pulling the maximum of the characteristic curve towards the high pressures (fig. 1), so that it can become hysteretic [4]. This in fact can introduce some qualitative changes in the final waveform that will be produced by the instrument [9].

Another way to identify the appearance of hysteresis in the characteristic curve is to analyze a similar curve which relates the pressure to the opening of the reed. By comparing fig. 1 with fig. 2 we see the relationship between the flow characteristic and the reed opening characteristic.

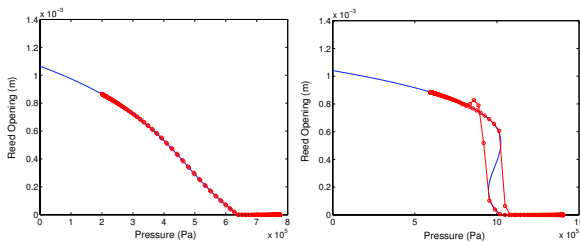


Figure 2: Reed opening characteristic curves calculated with the same model as in figure 1

### 3. EXPERIMENTAL CHARACTERIZATION

In this section we will introduce some experimental methods to try to verify theoretical hypothesis about the flow inside the reed, or the reed characteristics. Rather than direct observation of time variation of physical quantities of the exciter which are often difficult to interpret in terms of physical principles we preferred to simplify the behavior of the instrument so as to gather information about the physical principles involved in the functioning of the instrument.

#### 3.1. Artificial Mouth

In our experiments we study a physical system (instrument) which is usually operated directly by humans. Although the skilled instrumentist has a remarkable proficiency of the control of this system, it is difficult for him to have a prolonged control of all the

variables the system depends on during the whole experiment. Artificial mouths provide easier control over individual parameters while simplifying the observation.

Artificial mouths are currently used in the study of wind instruments. A few examples can be found in literature. It was first used by Backus [10] in the conception of his first clarinet model, and it was adapted and perfected for the study of other reed instruments [11], as well as for brass instruments [12].

**Pressure supply** Lungs provide a pressure source to the reed, which is almost constant during a certain amount of time. In laboratory, lungs are replaced by a compressed air source maintained at a certain pressure level which can be regulated.

**Mouth Cavity** constitutes a resonator whose importance is usually considered as negligible with respect to instrument's impedance, although this hypothesis is still under investigation by C. Fritz.

**Lips** provide a way to control the physical properties of the reed. In particular, by varying the pressure of the lips over the reed, the instrumentist can vary the mass and stiffness of the vibrating end of the reed. Lips are also the main source of damping in equation 1. Special care is thus taken in trying to reproduce the lip's geometry and material properties. Lips are replaced by two cylindrical latex tubes filled with water whose pressure can be controlled.

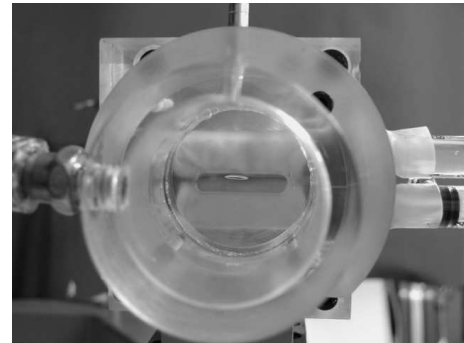


Figure 3: The artificial mouth used in double-reed measurements

The current artificial mouth used in our experiments (fig. 3) is built from *Althuglass* blocks and derived from [13]. The mouth cavity is a cylinder. From one of its bases the mouth's inside can be observed or filmed. The other base is uncovered so that one side of the lips is submitted to the mouth pressure.

The reed is placed between the two latex lips and can be kept in place by a plastic cap which also helps to keep the system leak-proof.

#### 3.2. Determination of the non-linear characteristic

The current artificial mouth provides an easy way to observe the reed opening ( $z$ ) during playing regimes (see [8]) but also in static regimes, for example. For instance, if we can vary the pressure while preventing the reed from oscillating, we are able to determine the whole characteristic curve, from the closed reed until the rest position.

A method of preventing reed oscillations is described by S. Ollivier in his PhD thesis [14]: pressure oscillations that can propagate throughout the reed and be reflected at its end, are damped by a cover with a small perforated diaphragm. This works as an acoustic resistance which prevents all sound waves from being reflected back to the reed tip.

This technique was used successfully [14] to determine the  $q(p)$  characteristic of clarinet and saxophone embouchures in the static regime.

The diaphragm, however, introduces further headloss upstream of the reed. This means that if the diaphragm is undersized, the total characteristic will have the shape of (II) in figure 1, even for a single reed.

### 3.2.1. Experimental setup

Measurement of the reed opening (area and distance between reeds) was based on images captured by a video camera placed in front of the vibrating reed.

Image analysis consists in the recognition of the slit entrance, which is done by selecting the darker area near a point which is user-defined (from one of the pictures of the series), and some simple measurements of area (pixel-counting) and width of the black spot corresponding to the slit.

### 3.2.2. Measured reed opening characteristics

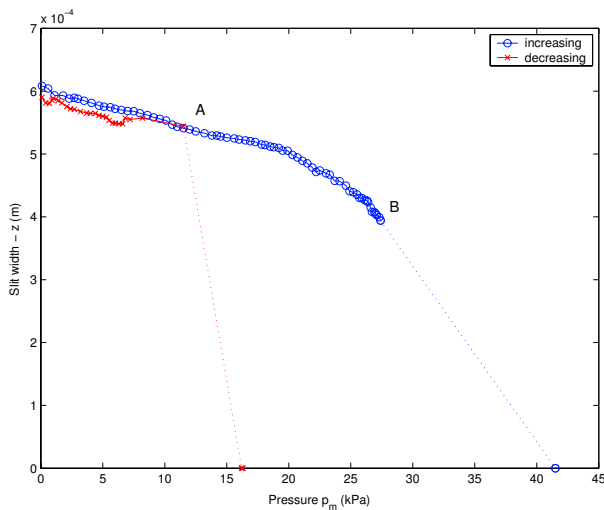


Figure 4: Measured reed opening characteristics

The measured  $z(p)$  characteristic on a double reed (fig. 4) shows invariably a great amount of hysteresis, the closing pressure being almost twice as the opening pressure. Comparison of these results to those obtained on single reeds seems to indicate that a stronger head loss takes place in double reeds generating steeper transitions from open to closed reed.

The experiment itself is demonstrative of this fact: while the reed motion from 0 kPa to point B is difficult to observe, once this point is achieved the reed suddenly shuts. During instrument playing the same is expected to happen when the incoming pressure

wave reaches the reed, assuming a quasi-static theory for the reed behavior.

One advantage of measuring the reed position characteristic instead of the flow characteristic is that it will soon be possible to compare it to a dynamic characteristic (measured in playing condition). In fact it is easier to follow the quick variations of the reed opening than those of the flow.

## 4. REED GEOMETRY

One of the key aspects in describing the flow inside the reed is to precisely know the boundary conditions of the flow. In particular, sudden section variations can induce the formation of a free jet that will dissipate its kinetic energy by turbulent mixing, as in the case of the clarinet. Narrow ducts bring the boundary layers closer together so that they can change the flow description [15]. It is therefore crucial to undertake a complete measurement of the duct geometry, and if possible, its variation during the closing and opening cycle.

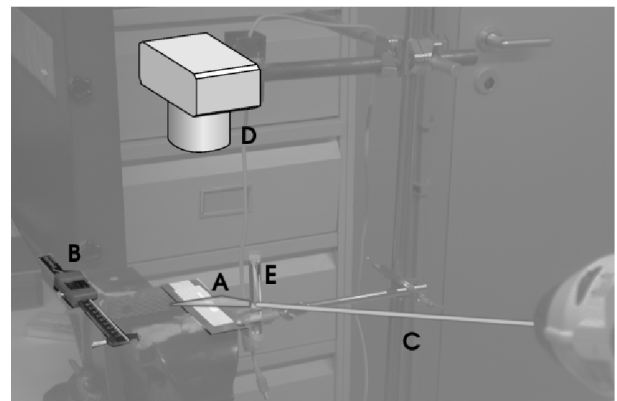


Figure 5: Experimental setup

The inside of several types of double reed was cast into a silicon material. These casts are then used to digitally reconstruct the inside reed profile with the following technique (fig 5):

The cast lies on an accurately moving table (A), whose displacement can be precisely measured (B). The table and the cast are illuminated by a laser beam (C) expanded by a transparent cylinder (E) and striking the table with a small angle (20 deg.). This laser plane would trace an arc of a circumference (due to the presence of E) over the table if the cast wasn't present (the baseline, A on figure 6). Images are captured from above the reed (D), the direction of observation being perpendicular to the table.

Several images (fig. 6) of the laser plane are captured for different displacements of the cast (about 1 mm). These correspond to sections of the reed parallel to each other. The photographs are then inserted into the computer in order to extract the beam deviation at each point. The cast three-dimensional model is reconstructed from the whole set of photographs of the complete reed.



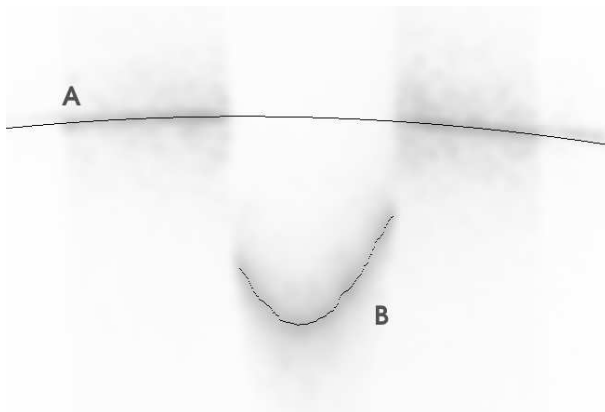


Figure 6: Laser line illuminating the reed cast and computer recognition of the line: A – baseline; B – line deviated by the cast

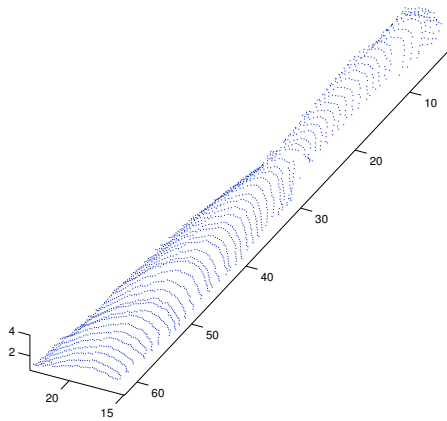


Figure 7: Three-dimensional reconstitution of a reed cast

## 5. CONCLUDING REMARKS

Although the conclusions are rather crude at the moment, we have highlighted the potential of experimentation on reed instruments to a development of the theory of double-reed instruments behavior. The knowledge of the geometry of the reed will allow the formulation of theories and simulation on the flow inside the reed. Further measurements on the variation of pressure along the reed provide a way to validate these theories.

On the other hand, the analysis of the reed characteristic provides a description of its behavior regardless of its causes. It is thus a valuable tool for checking the relevance of the current focus on the flow on the reed behavior, by comparing it to a model based on simplified mechanics for the reed and extended description of the flow.

## 6. ACKNOWLEDGEMENTS

The current experimental work would not have been possible without the technical expertise of Alain Terrier and debating with

G. Lemaitre following his memoir at IRCAM. We would also like to thank J. P. Dalmont and J. Gilbert for fruitful discussions.

A. Almeida's contribution is financed by a scholarship from *Fundação para a Ciência e Tecnologia*, Portugal.

## 7. REFERENCES

- [1] John Backus. Small-vibration theory of the clarinet. *Journal of the Acoustical Society of America*, 1963.
- [2] R. T. Schumacher. Ab initio calculations of the oscillations of a clarinet. *Acustica*, 1981.
- [3] A. Barjau and J. Agulló. Calculation of the starting transients of a double-reed conical woodwind. *Acustica*, 1989.
- [4] C. Vergez and A. Almeida. Modèle physique simple d'instrument de musique à anche double: influence des pertes aéro-dynamiques dans l'anche sur le couplage anche-résonateur. In *Congrès Français d'Acoustique 2002, Lille, France*. Société Française d'Acoustique, 2002.
- [5] A. P. J. Wijnands and A. Hirschberg. Effect of a pipe neck downstream of a double reed. In *Proceedings of the International Symposium on Musical Acoustics*, pages 149–152. Société Française d'Acoustique, 1995.
- [6] Michiko Shimizu, Toshikatsu Naoi, and Tohru Idogawa. Vibrations of the reed and the air column in the bassoon. *Journal of the Acoustical Society of Japan*, 1989.
- [7] A. Ya. Gokhshtein. Self-vibration of finite amplitude in a tube with a reed. *Soviet Physics Dokl.*, 1979.
- [8] André Almeida, Christophe Vergez, René Caussé, and Xavier Rodet. Physical study of double-reed instruments for application to sound-synthesis. In *International Symposium in Musical Acoustics*, Mexico, Mexique, Décembre 2002.
- [9] André Almeida, Christophe Vergez, René Caussé, and Xavier Rodet. Etude des écoulements dans les instruments à vent à anche double, pour application à la synthèse par modèle physique. In *CFA, Congrès Français d'Acoustique, Lille, France*, 2002.
- [10] John Backus. Vibrations of the reed and the air column in the clarinet. *Journal of the Acoustical Society of America*, 1961.
- [11] J. Gilbert. *Etude des Instruments de Musique à Anche Simple: Extension de la Méthode d'Equilibrage Harmonique, Rôle de l'Inharmonicité des Résonances, Mesure des grandeurs d'Entrée*. PhD thesis, Univ. du Maine, 1991.
- [12] Christophe Vergez. *Trompette et Trompettiste: un Système Dynamique Non-linéaire à Analyser, Modéliser et Simuler dans un Contexte Musical*. PhD thesis, Université Paris 6, 2000.
- [13] Vergez C. and Rodet X. Model of the trumpet functioning: real time simulation and experiments with an artificial mouth. In *ISMA Proceedings 1997*.
- [14] Ollivier Sebastien. *Contribution à l'étude des Oscillations des Instruments à Vent à Anche Simple*. PhD thesis, Université du Maine, 2002.
- [15] M. Deverge, X. Pelorson, Vialain C., P.-Y. Lagrée, F. Chen-touf, and J. Willems. Influence of the collision on the flow through in-vitro rigid models of the vocal folds. 2002.

## THE 'VIRTUAL FLUTE': ACOUSTIC MODELLING AT THE SERVICE OF PLAYERS AND COMPOSERS

Andrew Botros, John Smith, Joe Wolfe

School of Physics  
University of New South Wales, Sydney  
J.Wolfe@unsw.edu.au www.phys.unsw.edu.au/music

### ABSTRACT

Among the difficulties facing woodwind players are (i) awkward fingerings for rapid passages, (ii) intonation defects in instruments, and (iii) performing exotic effects such as microtones and multiphonics. In many cases these may be ameliorated by alternative fingerings.

We report the construction and use of a web service for the flute. An expert system was trained by an experienced flutist to determine playability from features of 957 minima in measured acoustic impedance spectra  $Z(f)$  for 76 selected fingerings. Measurements on successively more complicated acoustic systems yielded an accurate waveguide model of  $Z(f)$  of the flute, which generated the minima of the 39,744 different acoustic configurations of the flute. The expert system, coupled with the waveguide model, produces a large database of alternative fingerings, microtone and multiphonic fingerings. The database is accessible to flutists and composers via a user-friendly interface that includes user determined constraints on key combinations and ranks fingerings by playability or pitch. This service, located at <http://www.phys.unsw.edu.au/music/flute> is used hundreds of times per day. We report some of the service's uses and discoveries.

### 1. INTRODUCTION

One of the applied aims of music acoustics is to use the scientific understanding of music and instruments to help musicians. *The Virtual Flute* (TVF) is one such application [1]: it is a widely used web service that supplies flutists and composers with solutions to a wide range of technical problems. These include awkward transitions between notes, intonation and timbre difficulties. It also gives fingerings (key combinations) for microtones (non standard pitches) and multiphonics (chords). We describe briefly the strategies and techniques used to construct TVF. We also report examples of its use. The interest in such examples is that they illustrate the sometimes subtle difficulties faced by musicians and the steps that may be taken to remove them. These in turn illustrate some of the details that must be addressed by scientists aiming to help them.

In *The Virtual Flute*, an expert system relates features of impedance spectra  $Z(f)$  to the perceived musical behaviour of the instrument. A waveguide model, developed and tested on a large database of measurements, predicts the  $Z(f)$  for every possible fingering, determines the pitch and 'playability' of all possible notes and lists possible multiphonic combinations of notes. A musician-friendly interface allows musicians to search the resulting database according to appropriate criteria and constraints.

*The Virtual Flute* is currently used several hundreds of times per day. Here we choose a small number of problems and their solutions to illustrate some effects of acoustical and biomechanical interest and some ways in which the musical possibilities of the instrument have been extended.

#### 1.1. Alternative fingerings

All instruments are imperfect compromises. When a good player rehearses a single phrase many times, s/he may be seeking ways to correct the pitch of one note, to control an inappropriate loudness or stability, or just finding ways to execute or to avoid awkward finger movements. A particular combination of keys depressed is called a fingering. Most players have a repertoire of alternatives, which are used in fast passages or to produce more appropriate pitch and timbre in different circumstances.

For the flute, there are either 13,248 or 26,496 different fingerings, depending on whether the lowest note on the instrument is B3 or C4. We know of no previous attempt to make a complete study.

#### 1.2. Microtones, timbres, multiphonics

Solo and chamber music since the 1950s increasingly calls on woodwind players to play notes that fall between those of standard temperaments, notes with varying timbres and chords [2,3]. Only a subset of the possible combinations of notes are playable on the flute and we know of no previous attempt to list them all. Dick [4] gives an extensive collection of fingerings for these exotic effects but it is far from complete.

The two lowest registers of the flute are usually played with simple fingerings: nearly all of the tone holes downstream from a particular point are open, while all of

those upstream are closed, except for register holes. In cross fingerings, some tone holes downstream from the first open hole are closed. This often increases the end effect and so flattens the note, creating the possibility of a microtone. The inertance at the tone hole affects higher resonances more strongly, so the resonances cease to be harmonic. Higher resonances thus contribute less to the vibration regime, which creates the possibility of a darker timbre. See [5] for a detailed discussion.

Further, the impedance mismatch at a single open hole may partially reflect a travelling wave. The transmitted portion may be reflected at a subsequent open hole. Thus a cross fingering can be considered as a set of resonators with different frequencies. In general they are not in a simple harmonic series, which creates the possibility of the superposition of two or more standing waves to produce a multiphonic.

## **2. STRATEGY AND IMPLEMENTATION**

Because they are open to the air at the embouchure, flutes operate near minima in the acoustic impedance spectrum  $Z(f)$ . The ease of playing the note associated with a minimum in  $Z(f)$  depends on properties of that and other minima. In principle, one might hope to understand this in terms of properties of the jet-bore interaction and a knowledge of the extent to which players control the jet. This is a difficult question. Fortunately, flutists know how hard it is to play a note. So we asked an expert flutist to attempt to play a note corresponding to each of 957 minima identified on the measured  $Z(f)$  data. When the note was playable, it was assigned a playability from 1 to 3, with 0 for unplayable notes.

We expected that the playability of a note associated with a particular minimum might depend on its depth, its bandwidth, the proximity and magnitude of nearby extrema, and whether or not higher minima were harmonically related to it. These were quantified and used as inputs. Three methods were tried to determine playability from these input data. Neural networks were unacceptably slow, even when the input parameter set was reduced. Linear regression was unhelpful and uninformative, partly because of strong correlation among the parameters. A decision tree method, using the C5.0 algorithm suite, an artificial intelligence technique developed by Quinlan [6,7], proved successful. The first tree used only the binary data, 'playable' or 'unplayable'. Training the tree on subsets of the data and testing on others enabled the rejection of unimportant input parameters. The final tree ranks a minimum as unplayable (i) if  $Z > 1.35 \text{ M}\Omega$  or (ii) if  $1.35 \text{ M}\Omega > Z > 0.68 \text{ M}\Omega$  and if the next higher minimum is more than 35% lower, or (iii) if  $0.68 \text{ M}\Omega > Z$  and if the next higher minimum is within 261 Hz. ( $1 \Omega = 1 \text{ Pa.s.m}^{-3}$ )

The quaternary playability ratings (0-3) were used as inputs to Cubist, the continuous version of C5.0. Its output gives playability as a function of the parameters listed above, but again it is not very informative because of the correlation among the parameters.

To obtain playing pitch from the frequency of an impedance minimum measured or calculated at low temperature and humidity is complicated in principle, but here is performed by a simple empirical relation determined by comparing played frequencies with those of the minima. An average embouchure effect is already included in the measurements [8]. This method introduces errors, but they are not greater than the variations among players and instruments.

One dimensional waveguide models to calculate  $Z(f)$  have been made by various authors [9,10]. The parameters for our model were determined by measuring successively more complicated combinations of bores, finger holes and keys. It was then tested on the database of measurements [8,11].  $Z(f)$  was then calculated for all 39,744 fingerings, and the frequency, magnitude, bandwidth and harmonicity of all minima were determined. From these, the expert system constructed a database of about 150,000 possible playing regimes. Inharmonically related minima are used to construct lists of multiphonic possibilities.

The web service itself was constructed according to recommended principles [12,13], and the user interface designed after consideration of the needs and knowledge of flutists and composers, the principal users.

### **2.1. The web service**

Three tools are offered. One allows the user to enter a fingering via a graphical interface and then returns the predicted playable notes with their predicted playability and pitches and the multiphonic possibilities. The second allows input of a note name to search the database for all suitable fingerings and ranks them by intonation or playability, which are included in the displayed output. This tool also allows the user to constrain the search by excluding (or including) any keys that would be inconvenient to use (or not to use, respectively), in the circumstance. The third tool invites input of two or three notes and searches the multiphonic database.

## **3. APPLICATIONS AND SIGNIFICANCE**

### **3.1. Awkward passages and trills**

Flutists write fingerings using the numbers 1,2,3 for the keys usually operated by the long fingers of each hand (left given first), Th for the left thumb key, and then individual names for the other keys. A vertical line separates the two hands. For

instance, the standard fingering for F6 is written Th 1 - 3 | 1 - - D#, with the D# operated by the RH fourth finger.

A trill between the note F6 and A6 is rather awkward using the standard fingerings. The fingering for A6 is Th - 2 - | 1 - - D#. (The reader can appreciate this by attempting a rapid alternation between 1 - 3 and - 2 - with the left hand.) The flutist needing to accomplish this trill sought an alternative fingering for F6, specifying that all the keys used for A6 be included (this ensures that all fingers will move together on the trill). TVF returns Th 1 2 3 | 1 - - tr2 D#, which gives a comfortable trill in which three fingers move in the same sense.

In trills and rapid passages, less than perfect intonation may be tolerated: if a note that lasts 0.1 s, its frequency cannot be resolved to much better than  $\pm 10$  Hz.

### 3.2. Stable transitions

In rapid transitions, there is insufficient time to adjust the embouchure optimally for each note: for a rapid trill, no attempt is made, and for a rapid passage, the embouchure can only change to follow the overall shape of the phrase. A rapid alteration over a large interval can lead to the possibility of 'splitting': the production of an unwanted transient between desired notes. (The possibility of splitting is almost as bad as the effect itself: lack of confidence that the notes will sound properly distracts musicians from interpretive and other issues.)

Flutist Jane Cavanagh reports this example: Stravinsky's *Firebird* requires an acciatura from B5 to E6 to B5. Figure 1 shows why this is difficult. The standard fingering for B5 (also used for B4) will comfortably play F#6, the third harmonic of B4. That for E6 will also play G#5 and A6. For a slow transition, the flutist would shorten and/or quicken the jet to play the E6. How much? Too much to play G#5 but not enough to play A6. S/he would then lengthen and/or slow it enough to play the B5. To play this acciatura (or a trill), there is no time to adjust embouchure: one simply forms an intermediate embouchure and lets the flute fingering select the note. The danger of the split here is that, if the embouchure compromise favours the high note, one risks playing B5-E6-F#6-B6, because the transient unwanted F#6 (the 'split') is only a tone above the higher target. If the compromise embouchure is too low, one will play B5-G#5-B5, or B5-nothing-B5, because the E6 is not a particularly stable note.

This player requested an alternative E6 fingering and found Th 1 2 - | 1 - - D# tr1 tr2. The note is stable and easy to sound, although slightly flat. According to TVF (and players), the minimum immediately below that which supports E6 (Fig 1c) is unplayable, so there is little danger of the E6 'dropping down'. Consequently, the embouchure may be compromised more towards B5 and less to E6, which minimises the chance of sounding F#6. It is a comfortable, safe solution.

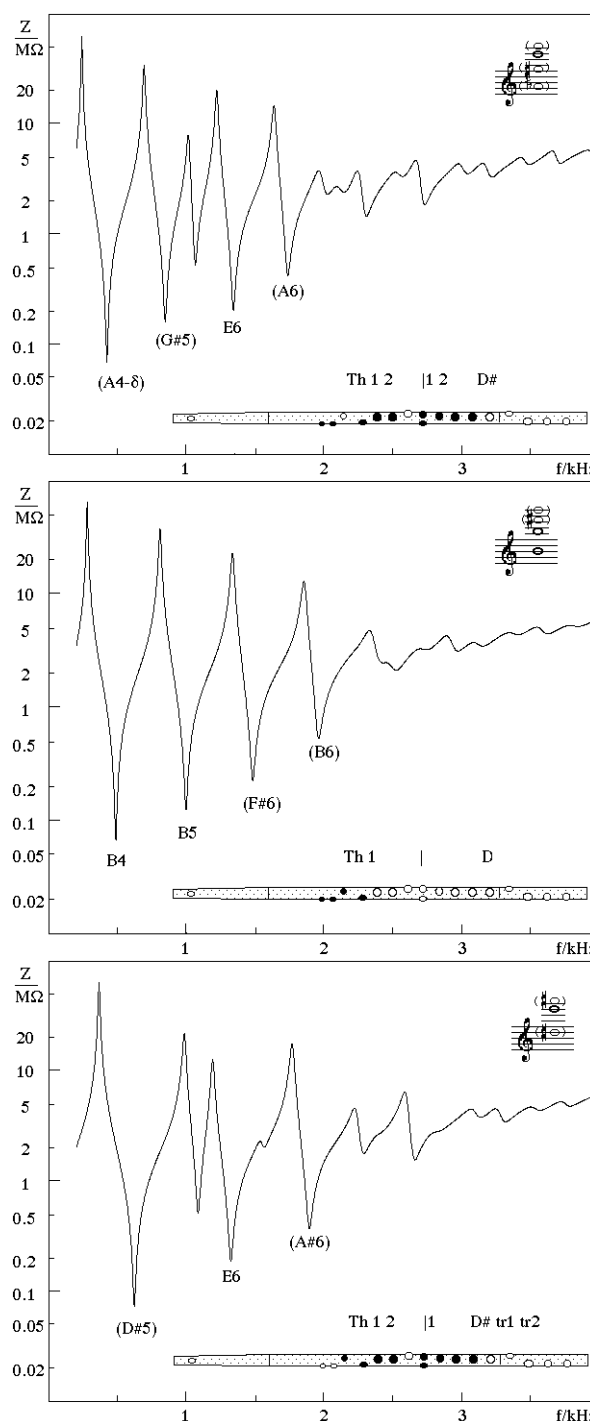


Figure 1:  $Z(f)$  for the standard fingerings for (top) E6 and B5 (middle), and for the alternate E6 fingering

### 3.3. Awkward high passages

High passages are awkward for several reasons. First, the resonances of all wind instruments are inherently weaker

(extrema in  $Z(f)$  are less pronounced) because of visco-thermal damping in the bore. In the flute, this effect is exacerbated by the Helmholtz resonance in the head [11,14]. Second, the individual fingerings are complicated and smooth transitions between them more so. Simple fingerings do not work because either the end effects in the array of open tone holes put them out of tune, or because the wave propagates too far into the array. Indeed, for notes above the tone hole cut off frequency, all notes are overtones of the whole length of the pipe, and several open holes along the length act merely as register holes or tuning perturbations [11,14]. Third, the resonances are closer together, so the danger of undesirable transients, like that discussed above, is greater. Some of the standard fingerings are difficult to play softly, so players seek stable soft fingerings (effectively, those with deeper minima in  $Z(f)$ ). They also seek sequences that are less awkward. The job is even harder when composers call for microtones.

Kathleen Gallagher, who specialises in the contemporary repertoire, cites two examples. The British composer Chris Dench, in *Closing Lemma*, writes a final flourish of high notes landing on a sharp E7. This pitch is well above the tone hole cut off frequency, and well into the 'shorting' range of the Helmholtz resonance, so easily played fingerings are rare. Further, the composer wants a microtone. TVF obliges with 12 - | - - 3 D# tr2.

Welsh composer Richard Barrett, in *What Remains* for flute, bass clarinet and piano calls for a slurred, fast passage sharp C7, sharp B6, E7, flat D7, flat E7, D7, Eb7, Bb6. This player uses standard fingerings for Bb6, D7 and flat D7, but found the rest of the fingerings from TVF, thereby creating a solution to a bar that has produced anxiety and performance approximations for many flutists attempting this work.

### 3.4. High notes and soft high notes

The range of the flute ends somewhere near the middle of the fourth octave, and notes near the end of the range are often difficult to play softly, and sometimes difficult to play in tune. So flutists are keen to seek improvements: minima in  $Z(f)$  that are deeper and closer to the right frequency. TVF offers a fingering for F7 whose minimum is about 30% lower than that of the standard fingering, and which allows even flutists of modest ability to play this very high note, and even play it softly.

### 3.5. Multiphonics

Multiphonics are rare in the low range of wind instruments because an open tone hole acts as a shunt. In the high registers they abound. Composers and flutists routinely use *The Virtual Flute* to find multiphonics and to find how to play them.

### 3.6. Further work

Application to other instruments has begun. The clarinet has a geometry that is almost as standardised as that of the flute's but it is complicated by having very many more fingering possibilities. And the bassoonist among the authors earnestly desires an application to the instrument in which alternative fingerings are most used—and needed.

**Acknowledgments.** We thank Jane Cavanagh, our expert flutist, John Tann for technical assistance, and the Australian Research Council for support.

## 4. REFERENCES

1. Botros, A., Smith, J. and Wolfe, J., "The virtual Boehm flute—a web service that predicts multiphonics, microtones and alternative fingerings", *Acoustics Australia*, 30: 61-65, 2002.
2. L. Berio, *Sequenza*, Suvini Zerboni, Milan, 1958,
3. B. Bartolozzi, *New Sounds for Woodwind*, Oxford Univ. Press, London 1967.
4. Dick, R. *The Other Flute, Multiple Breath Music*, 1989,
5. Fletcher, N. H., "Mode locking in nonlinearly excited inharmonic musical oscillators", *J. Acoust. Soc. Am.* 64: 1566-1569, 1978,
6. Quinlan, J. R., *C4.5: Programs for Machine Learning*, Morgan Kaufman, San Mateo, 1993.
7. Quinlan, J. R. "C5.0: An Informal Tutorial", *Rulequest Research*. <http://www.rulequest.com/see5-unix.html> 2002.
8. Wolfe, J., Smith, J., Tann, J. and Fletcher, N.H., "Acoustic impedance of classical and modern flutes" *Journal of Sound and Vibration*, 243:127-144, 2001.
9. Plitnik, G. R. and Strong, W. J., "Numerical method for calculating input impedance of an oboe", *J. Acoust. Soc. Am.* 65: 816-825, 1979.
10. Caussé, R., Kergomard, J., and Lurton, X., "Input impedance of brass musical instruments - comparison between experiment and numerical models", *J. Acoust. Soc. Am.* 75: 241-254, 1984.
11. Music Acoustics. [www.phys.unsw.edu.au/music](http://www.phys.unsw.edu.au/music)
12. Greenspun, P., Philip and Alex's Guide to Web Publishing, Morgan Kaufman, San Francisco 1999.
13. Nielsen, J., *Designing Web Usability*, New Riders, Indianapolis, 2000.
14. Wolfe, J. and Smith, J. "Cut off frequencies and cross fingering in baroque, classical and modern flutes", *Journal of the Acoustical Society of America*, accepted for publication.

# RELATIONSHIP BETWEEN BLOWING PRESSURE, PITCH, AND TIMBRE OF A SCOTTISH BELLOWS BLOWN BORDER BAGPIPE

Sandra Carral, D. Murray Campbell, Thomas D. Rossing

School of Physics  
University of Edinburgh

scarral@ph.ed.ac.uk, D.M.Campbell@ed.ac.uk, rossing@physics.niu.edu

## ABSTRACT

Bellows blown bagpipes have a long tradition in many European countries, and interest in these instruments has grown in recent years. However, little has been studied about how small changes in the playing parameters affect the way this instrument sounds. It is generally considered that there is a feedback loop in the way wind instruments are played, in which parameters such as blowing pressure and embouchure are changed to adjust the pitch and timbre dynamically. In the case of the bellows blown bagpipes, the only parameter that appears to be controlled by the player for a given fingering is the pressure exerted on the bag of the instrument. This paper describes studies carried out on a small Scottish bellows blown border bagpipe. Analysis of a recording of a performance by an expert player reveals significant fluctuations in pitch during the sounding of a given note, which in turn are related to modulation of the timbre of the sound. The relationship between blowing pressure, pitch and timbre has been investigated using an artificial blowing machine.

## 1. INTRODUCTION

Pipers in general consider that humidity variations in the reed are responsible for the rapid degradation of the reed. In a preliminary study that aimed at finding out how the humidity introduced by the player's breath in mouth-blown pipes affected the pitch and timbre of a chanter reed, recordings of an expert piper were made under two conditions: bellows blown, in which the humidity was considered to remain constant; and mouth blown, in which the humidity was considered to increase over time. The results obtained from this study revealed that the pitch and timbre of the bellows blown chanter vary considerably over time, even when the humidity does not change. Figures 1 and 2 show these variations over the first five minutes of playing.

This implies that there are other significant parameters that affect the pitch and timbre of a given note, apart from changes in humidity. For a given fingering, the only parameter that appears to be changed by the player while playing the bagpipe is the pressure exerted on the bag of the instrument. At this point it was decided to study how the pitch and timbre change with blowing pressure using an artificial blowing machine.

## 2. EXPERIMENTAL SETUP

The artificial blowing machine (Figure 3) that was used is capable of providing a steady pressure through an air pump to a cavity in which the chanter is introduced. A Digitron manometer model 2001P was also connected to measure the pressure given by the

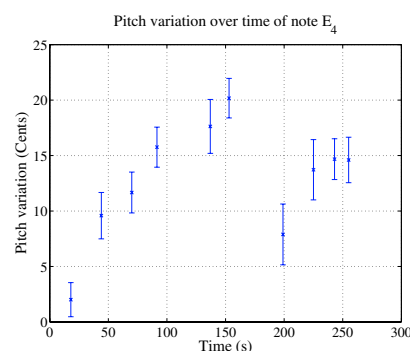


Figure 1: Variations in pitch over time of note  $E_4$  played with bellows

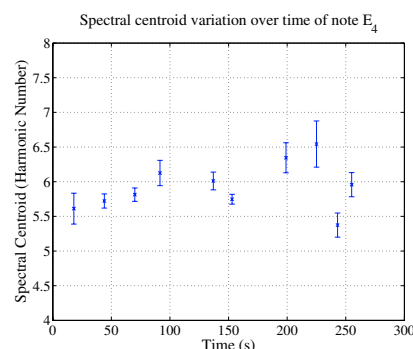


Figure 2: Variations in spectral centroid over time of note  $E_4$  played with bellows

pump. This pressure can be varied from 0 to 80 mBar by adjusting a valve. Figure 4 shows a close up image of the reed inside the cavity of the apparatus.

In the experiment, starting with 0 mBar the pressure is gradually increased until the reed starts vibrating. When the manometer gives a steady measurement, the sound that the chanter produces is then recorded via an Audio-Technica condenser microphone model ATM 31a into a TASCAM DAT recorder model DA-20mkII with a sampling frequency  $f_s = 44.1$  kHz. The pressure is then increased in steps of 2 mBar, and the sound is recorded at each of these points where the manometer gives a steady measurement. When the maximum pressure that the pump can provide is reached (80 mBar) the pressure is then reduced in steps of 2 mBar until the manometer can no longer give a steady measurement (i.e.

the pressure keeps falling even when the valve is kept untouched), at which point the reed eventually stops vibrating.

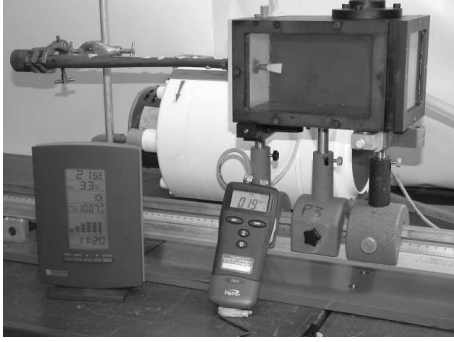


Figure 3: Artificial blowing machine used for the experiments

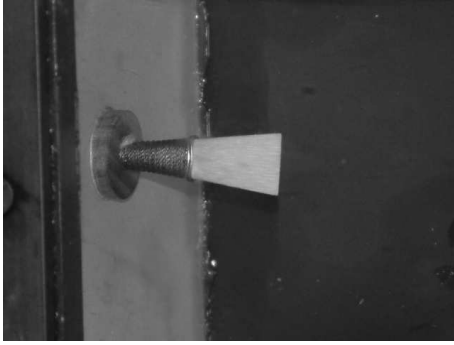


Figure 4: Close up image of the reed inside the apparatus

### 3. CALCULATIONS

The program SNDAN [1] provided by James Beauchamp from the University of Illinois at Urbana-Champaign was used to calculate the pitch variation over time and the spectral centroid variation over time. This program performs a pitch-synchronous phase vocoder analysis, so it tracks frequency deviations of the harmonics of the signal relative to integer multiples of the analysis frequency  $f_a$  provided by the user.

The pitch variation over time is defined as the logarithm of the weighted average frequency deviation:

$$\frac{\sum_{k=1}^5 \frac{A[k] \cdot f_{dev}[k]}{k \cdot f_a}}{\sum_{k=1}^5 A[k]} \quad (1)$$

where  $k$  is the harmonic number,  $A[k]$  is the amplitude of the  $k^{th}$  harmonic,  $f_{dev}[k]$  is the frequency deviation of the  $k^{th}$  harmonic, and  $f_a$  is the analysis frequency. Each harmonic's deviation is weighted according to its instantaneous frequency.

The spectral centroid variation over time<sup>1</sup> is defined as:

<sup>1</sup>Which "...is a measure of perceptual brightness of a sound as it varies with time"

$$\frac{\sum_{k=1}^n k \cdot A[k](t)}{\sum_{k=1}^n A[k](t)} \quad (2)$$

where

$$n = \frac{f_s}{2 \cdot f_a} - 1 \quad (3)$$

is the maximum possible number of harmonics that a given signal can have.

The analysis frequency was selected to be the frequency at which each fingering was supposed to sound, taking into account that this chanter was tuned in a just intonation scale starting from A<sub>4</sub> (440 Hz) with a flat 7<sup>th</sup> tuned at 770 Hz. The lowest note is G<sub>4</sub> tuned at 385 Hz.

The mean  $\mu$  and standard deviation  $\sigma$  of these results were then taken and plotted in graphs of pitch and spectral centroid vs blowing pressure.

Given the fact that the program performs a pitch synchronous analysis, the absolute deviation in frequency of each harmonic should be less than  $f_a/2$ :

$$|f_a - f_1| \cdot n < \frac{f_a}{2} \quad (4)$$

where  $f_1$  is the frequency of the first harmonic of the signal. The percentage of the frequency deviation is:

$$\frac{|f_a - f_1|}{f_a} \cdot 100 \quad (5)$$

For a deviation equivalent to 100 cents, i.e. 6%,

$$n < \frac{50}{6\%} = 8.33 \quad (6)$$

This means that the program will track accurately up to the 8<sup>th</sup> harmonic. In the pitch calculation (equation 1), only the first five harmonics of the signal are used, so in this case, the maximum frequency deviation that can be tolerated is:

$$\frac{50}{n} = 10\% \quad (7)$$

For the spectral centroid calculation, all harmonics are used. To examine how this affects the results obtained, the signal with the highest pitch deviation shown in Figure 9 is taken. In this case,  $f_1 = 616.72$  Hz. If  $f_a = 586.67$  Hz (which was the value used to plot that note), from equation 5 the frequency deviation is 5.12%. Table 1 compares  $\mu$  and  $\sigma$  calculated for the spectral centroid with deviations of 0.00% ( $f_a = f_1 = 616.72$  Hz) and 5.12% ( $f_a = 586.67$  Hz,  $f_1 = 616.72$  Hz) for this particular signal.

Frequency deviation (%)	$\mu$	$\sigma$
0.00	7.6218	0.0853
5.12	7.6516	0.2161

Table 1: Comparison of calculation of the spectral centroid  $\mu$  and  $\sigma$  for frequency deviations of 0.00% and 5.12%

From this it can be concluded that the only difference between these two results is the increase of  $\sigma$  when the frequency deviation

increases. This should be taken into account when analysing the graphs presented in the following section.

#### 4. MEASUREMENTS AND RESULTS

All nine notes of the bagpipe were recorded and analysed as described in the previous section. It was noted that all nine notes played sharp at all the pressures measured. It was also noted by an expert pipe maker that the reed played significantly less loud than an optimum reed would play. It is his opinion that the reason for these is the fact that this particular reed was "soft", and the opening between the blades was slightly narrower than that of an optimum reed. Each note appeared to have a particular profile of pitch and spectral centroid variation with pressure. As an example of this, Figures 5 and 6 show the pitch and spectral centroid variation respectively of note  $E_4$ . All notes had hysteresis, in the sense that the pressure at which the reed had to be subjected before starting vibrating (around 60 mBar) was higher than the smallest steady pressure at which it could play while already vibrating (around 40 mBar).

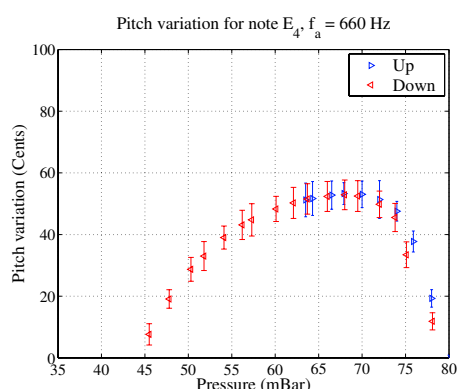


Figure 5: Pitch variation vs blowing pressure of note  $E_4$ .

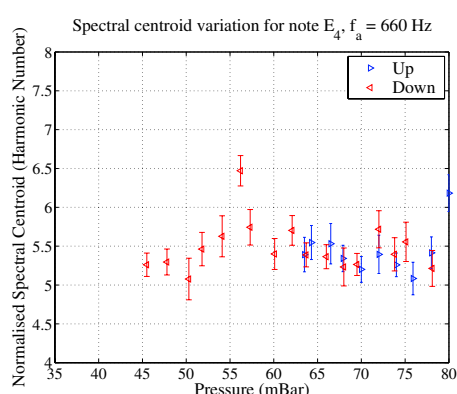


Figure 6: Spectral centroid variation vs blowing pressure of note  $E_4$ .

The note  $D_4$  was selected for further study on the grounds of having the widest variation in spectral centroid at the pressures measured.

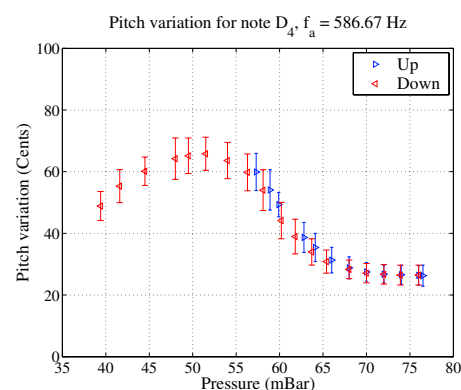


Figure 7: Pitch variation vs blowing pressure of note  $D_4$ .

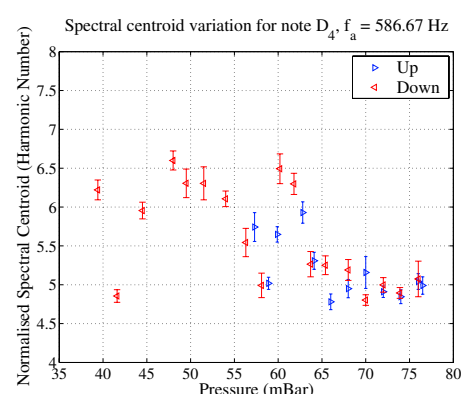


Figure 8: Spectral centroid variation vs blowing pressure of note  $D_4$ .

The temperature and relative humidity in the laboratory were recorded using an Oregon Scientific Deluxe 7 Line Weather Forecaster in four different days. For each day, the measurements of pitch and spectral centroid curves were done twice to find out whether the results obtained were reproducible. The results taken on the same day were essentially the same, although results from different days varied in many ways, even when the temperature and relative humidity conditions varied not more than  $1^\circ\text{C}$  or 4% respectively. Figures 7 and 8 were taken on the 25<sup>th</sup> of April at a temperature of  $18.5^\circ\text{C}$  and a relative humidity of 45%, and Figures 9 and 10 were taken on the 3<sup>rd</sup> of May at a temperature of  $19.5^\circ\text{C}$  and a relative humidity of 36%. Even though the comparison of these figures taken under two different temperature and humidity conditions suggests that the spectral centroid decreased as the humidity increased, this conclusion is not supported by other measurements.

There is a significant increase in pitch and also a significant change in the spectral centroid curve between these two measurements. These could be due to changes in the geometry of the reed. Other parameters such as the previous humidity history on the reed, and ageing of the reed, that were not recorded in these measurements might also be responsible for these changes.

To make sure that these changes were not due to the relative positioning of the reed in the chanter, the note  $D_4$  was recorded several times at a pressure of 60 mBar, repositioning the reed sev-



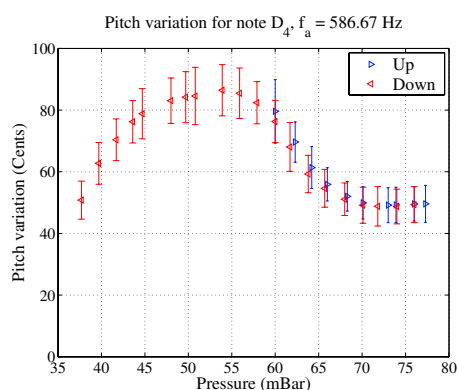


Figure 9: Pitch variation vs blowing pressure of note  $D_4$ .

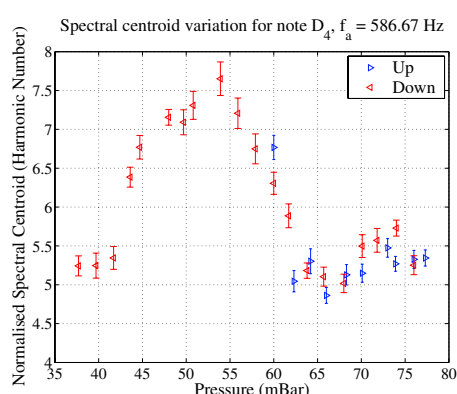


Figure 10: Spectral centroid variation vs blowing pressure of note  $D_4$ .

eral times. The pitch mean varied between 82 and 87 cents above the analysis frequency, but the spectral centroid varied significantly between 6.3 and 6.9 centroid units<sup>2</sup>.

This particular chanter and reed were also played in its bag by an expert player, and measurements of the pressure with the same manometer were recorded. The mean of these measurements was 37.4 mBar, and the standard deviation 1.3 mBar, which means that to start playing, the player has to initially press the bag with a pressure significantly higher to that of normal playing just to start the vibrations of the reed. Also, the player chooses to play in the bottom end of the hysteresis found in the figures presented, where the pitch curve shows the highest slope. This might be to allow pitch and timbre modulations that make musical instruments interesting to the human ear. As an illustration of this, a closer look at Figure 5 reveals that in order to have the 20 cent variation in pitch shown in Figure 1, the player only needed to change the pressure by about 10%.

## 5. CONCLUSIONS AND FUTURE WORK

A preliminary study carried out to find how the humidity from the player's breath affected the sound of the chanter while playing the

bagpipe led to results that suggested that there are other parameters that affect the way this instrument sounds. A study of how the sound changes with blowing pressure was made. It was found that there is a complex relationship between pitch, spectral centroid, and blowing pressure, that involves hysteresis. The measurements recorded on a given day were reproducible, but those made in different days differed significantly. This is possibly due to changes in humidity, geometry, and ageing of the reed.

The results also revealed that this instrument is played in the range in which significant variations in pitch take place when the pressure is changed only by a small percentage, which in turn allows for wide modulations in pitch and timbre.

Future work in this area includes the design and implementation of an air reservoir that can be fed into the artificial blowing machine, previously set up to have certain temperature and relative humidity conditions, to record in a controlled way how the changes in these two parameters affect the results obtained. Also, measurements on how the geometry of the reed changes with playing time will be made, as well as mechanical response curves of the reed and impedance curves of the chanter, with the aim of generating a realistic model of the behaviour of the coupled system composed by the chanter and reed.

Other studies specifically on the reed will include measurements of the area of opening of the reed by shining a laser through its opening, and measurements of its vibrations along its length using a laser vibrometer.

## 6. ACKNOWLEDGEMENTS

We would like to express our gratitude to James Beauchamp for providing the program used in these experiments, for all his support, and for his fruitful comments. Also, to Nigel Richard for providing the chanter and reed, and for his useful discussions about his own experience with his pipes.

This work was supported by the CONACYT scholarship number 146702.

## 7. REFERENCES

- [1] James W. Beauchamp, "Unix workstation software for analysis, graphics, modification, and synthesis of musical sounds," in *Audio Engineering Society*, 1993, p. Preprint 3479.
- [2] R. A. Kendall and E. C. Carterette, "Difference threshold for timbre related to spectral centroid," in *Proceedings of the 4<sup>th</sup> International Conference on Music Perception and Cognition*, 1996.

<sup>2</sup>Roger Kendall in [2] found that the just noticeable difference in spectral centroid for his five component synthetic stimuli was 0.15 centroid units

## THE FREE REED COUPLED TO A PIPE RESONATOR

James P. Cottingham

Physics Department, Coe College  
Cedar Rapids, IA 52402, USA  
jcotting@coe.edu

### ABSTRACT

The free reed coupled to a pipe resonator occurs in various forms of the mouth organs of Asia as well as in some organ pipes. A number of acoustical measurements have been made on this reed-pipe combination, including studies of reed vibration and impedance measurements of the pipes. Particular attention has been paid to the coupling of the reed vibration with the pipe resonator. Although most examples of the free reed pipe employ the reed at the end of a closed tube, as expected in reed wind instruments, the *khaen* and related instruments employ an open tube of effective length  $L$ , with the reed located at approximately  $L/4$ . Most examples of Asian mouth organs are constructed with one note per pipe, as in the pipe organ, but the free-reed pipe with finger holes, exemplified by the *bawu*, is a closed cylindrical pipe with the free reed at one end, in which the effective acoustical length is varied by the use of tone holes. This configuration demonstrates the degree to which the reed frequency can be altered by the pipe resonance frequency.

### 1. INTRODUCTION

Unlike the free reeds found in Western instruments such as the reed organ, accordion, and harmonica, the reeds of the Asian free reed mouth organs are not only coupled to pipe resonators, but are approximately symmetric, so that the same reed can operate on both vacuum and pressure (inhaling and exhaling). Figure 1 shows typical reeds from a sheng and an American reed organ. The sheng, sho, and khaen all employ one reed per pipe, thus requiring a separate pipe for each pitch. Also common in various parts of South and Southeast Asia are free reed pipes which allow change of pitch using finger holes. One version of this type of instrument now common in China is the *bawu*. Detailed general information on the Asian free reed mouth organs is available in the article by Miller [2].

The free reeds used in the Asian mouth organs are cut from a single piece of thin metal, typically brass or a bronze alloy, and set into a bamboo pipe. In the single note per pipe instruments, a finger hole is drilled at a point that destroys the pipe resonance and prevents the reed from sounding unless the hole is closed. Wind is provided by blowing either in or out through the mouthpiece which forms the opening of the air chamber that surrounds the reeds. The instrument is held upright with the air chamber supported by the hands. Fingers or thumbs of both hands are available to close the holes and sound notes. It is typical in playing the instruments that several notes are sounded simultaneously,

some of them serving as drones. See References 2 and 3 for more detailed information.

The frequency of reed vibration is determined by both the reed and the pipe. One or two tuning slots (usually two for the khaen) are cut into the pipe, determining the effective acoustical length. The vibrating frequency of the blown reed can within certain limits be pulled to match the pipe resonance, so that fine tuning is done by means of the position of these tuning slots. In the khaen, reed length only approximately corresponds to sounding frequency, with pipe length apparently used as the prime means for tuning. Measurements taken on a sheng, on the other hand, indicate that the individual reeds are much more carefully tuned to match the pipe resonance [4].

Studies of two characteristics of the Asian free reed mouth organs are summarized in this paper. The first is the degree to which the coupling to the pipe can cause the sounding frequency to deviate from the natural frequency of the reed. The second is the dependence of sounding frequency on blowing pressure.

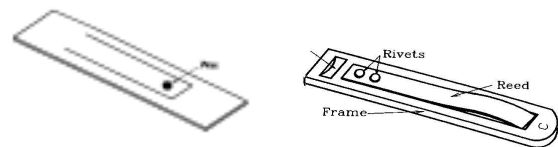


Figure 1. Reeds from a sheng (left) and an American reed organ (right) from Gellerman [1].

### 2. IMPEDANCE CURVES

Impedance curves have been measured for the *bawu*, the khaen, and the sheng following the method of Benade and Ibisi [5]. For khaen pipe impedance measurements, the pipes used were constructed from PVC tubing with dimensions similar to actual khaen pipes. For the sheng, bamboo pipes from a real instrument were used. In the case of the *bawu*, measurements were made on a "bawu" constructed from a piece of PVC pipe with a *bawu* reed attached as well as on actual instruments. A few results for the khaen and sheng are given below. Impedance curves for the *bawu* have been reported elsewhere [4]. The impedance curve measurements for the PVC khaen pipes, one of which is shown in Figure 2, are apparently the first such measurements on this kind of pipe.

In the following discussion, the first few peaks in the impedance curve are interpreted as the resonance frequencies of the pipe. Generally the sounding frequency is expected to be near, but slightly above, the pipe resonance.

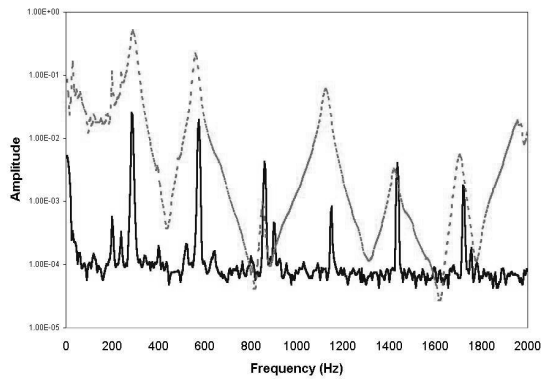


Figure 2a. Impedance curve (dashed) and sound spectrum (solid) of a 59-cm PVC khaen tube with no end sections.

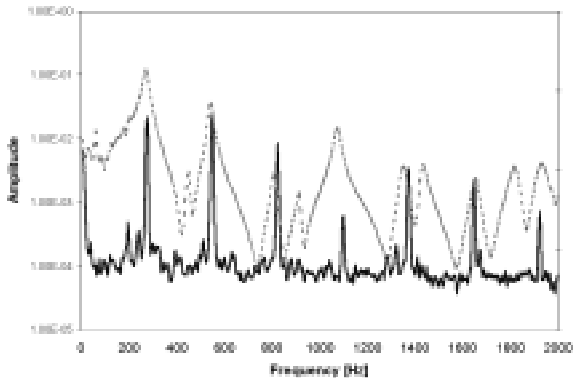


Figure 2b. Impedance curve (dashed) and sound spectrum (solid) of a 59-cm PVC khaen tube with end sections of lengths 11 cm and 35 cm.

### 2.1. Khaen Pipes

The fundamental frequency of the sound spectrum of the PVC khaen pipe (275 Hz) in Figures 2a and 2b is just above the frequency of the first impedance peak (270 Hz), which confirms previous observations that such a free reed pipe will sound at a frequency above the reed frequency and close to a resonant frequency of the pipe. If the length of the tube places the fundamental below the reed frequency, the reed-pipe can sound near the second harmonic of the pipe [3,4]. The difference in tone quality observed in comparing khaen pipes with and without the end sections seems closely related to the differences in the impedance curves for the two cases, as illustrated in the figure.

### 2.2. Sheng Pipes

Sheng pipes are cylindrical over most of their length, but the lower portion in which the reed is mounted is conical. The frequencies of the resonances identified by the impedance peaks are not harmonic. The pattern observed for the sheng is that the sounding frequency of the pipe is above that of the first impedance peak, with the second harmonic of the sound spectrum apparently reinforced by the strong nearby peak in the impedance curve.

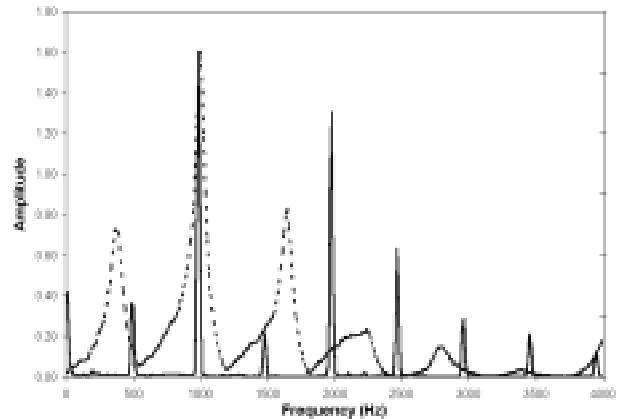
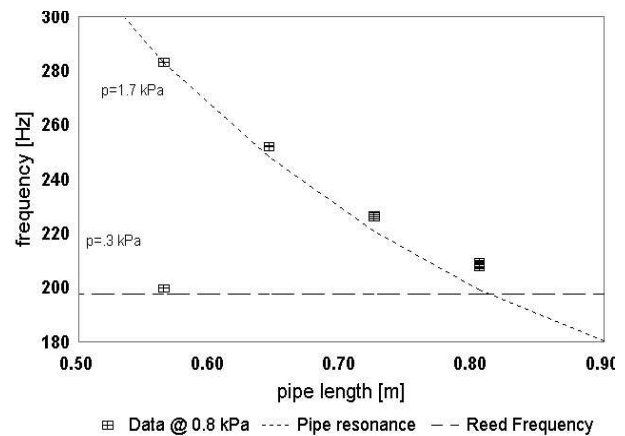


Figure 3. Impedance curve (dashed) and sound spectrum (solid) of a sheng pipe.

## 3. PLAYING FREQUENCY

### 3.1 Frequency and pipe length

Figure 4 shows the general relationship between frequency and pipe length for a khaen pipe. The pipe length was gradually shortened by cutting lengths from the original pipe. As can be seen in the graph, the sounding frequencies follow closely the fundamental pipe frequency, always remaining slightly above it. At the shortest pipe length in this example, the reed did not sound at normal blowing pressure (0.8 kPa), but could be made to sound at +1.7 kPa. At this same length, underblowing (0.3 kPa) caused the reed-pipe to sound at a frequency very close to the reed frequency. The sounding frequency of the reed-pipe combination is somewhat higher than the natural resonance frequencies of



either the reed or the pipe taken alone.

Figure 4. Sounding frequency of a khaen tube as a function of length at 0.8 kPa, except as noted. (Note that this figure is a correction of a result reported earlier in Ref. 3.)

Figure 5 shows the playing frequency of a bawu as a function of pipe resonance frequency. The normally blown notes, obtained both manually and mechanically at around 2.0 kPa, are

generally close to, but slightly above, the measured impedance frequency of the pipe. Underblown notes are close to the natural frequency of the reed. Notes played so high above the reed frequency have a dramatic difference in tone quality compared to those near the reed frequency.

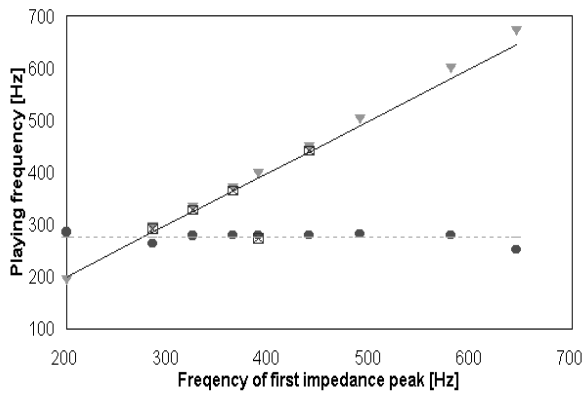


Figure 5. Frequency of a bawu as a function of pipe resonance frequency. Solid elliptical data points from underblowing are near the reed frequency (horizontal line).

### 3.2 Frequency and blowing pressure

Figure 6 shows graphs of sounding frequency as a function of blowing pressure for a khaen pipe as reported earlier [3]. These graphs show a general trend of decreasing frequency with increasing blowing pressure, a trend that was observed and studied in more detail for reeds from a reed organ. [6] Measurements were made for both positive and negative pressure. Although both directions of air flow show the same general trend, the pipes tested did not sound as easily at low positive blowing pressure.

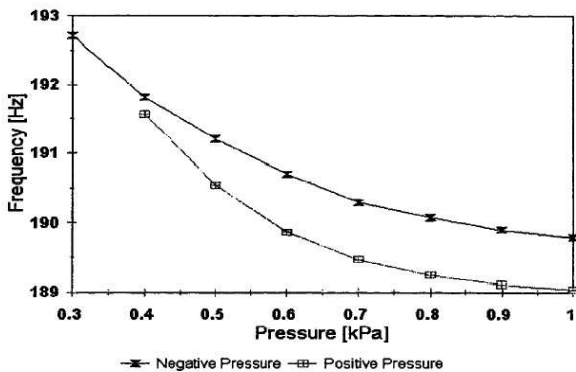


Figure 6. Frequency vs. blowing pressure for a khaen tube, showing both positive(lower curve) and negative (upper curve) blowing pressure.

For positive pressure, 0.1-0.3 kPa more pressure was often needed to initially sound the pipe. The higher pitched pipes seemed to show this difference more than the lower pitched ones. At normal playing pressure for the higher pitched

pipes, the frequencies were very close for positive and negative pressure. At less than normal playing pressure, the difference between positive and negative playing pressure was sometimes as great as 2 Hz.

In the earlier study [3] the dependence of sounding frequency on blowing pressure was studied for only a few pipes, believed to be representative. Since that time questions have been raised as to whether the pattern shown in Figure 6 is universal or even typical. [7] More recent measurements on khaen tubes have shown patterns similar to Figure 6 for some tubes, but very different patterns for other tubes, as shown in Figure 7. Study of these patterns is continuing as this report is being written.

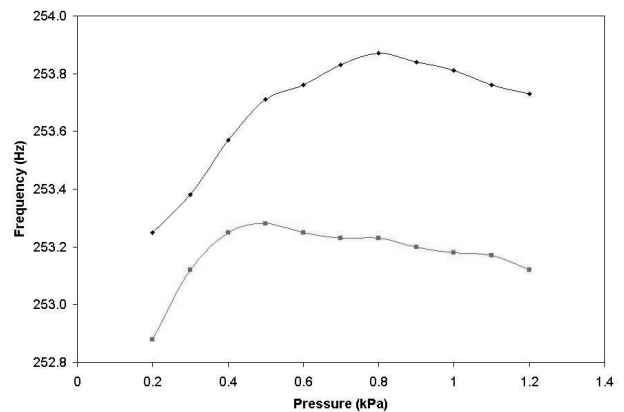


Figure 7. Frequency vs. blowing pressure for a khaen tube, showing both positive (upper curve) and negative (lower curve) blowing pressure.

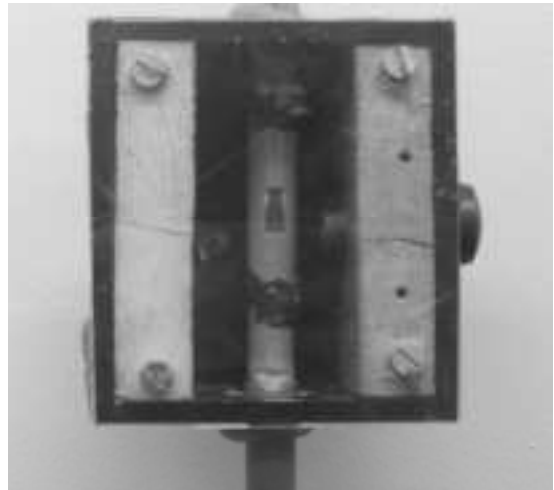


Figure 8. A khaen tube mounted in a laboratory wind chamber with transparent window for use with a laser vibrometer.

#### 4. SUMMARY

The free reeds coupled to pipe resonators in the instruments under consideration seem to behave as "opening" or "outward striking" reeds as discussed by Fletcher [8], with the sounding frequency of the reed-pipe combination is above the natural frequencies of both the reed and the pipe. For the bawu, a free reed pipe with finger holes, the sounding frequency can be as much as an octave above the reed frequency; for the cut-off khæn pipe it can be about half an octave. Previous measurements of reed motion using a laser vibrometer verify that for these instruments the free reed tongue makes only slight excursions in the upstream direction, thus approximating the outward striking reed model [9].

#### 5. ACKNOWLEDGMENTS

The author is grateful to Terry E. Miller of Kent State University for providing examples of high quality khæn, as well as expert advice and opinion on the Asian free reed mouth organs. Thanks are also expressed to Andrew Horner of the Hong Kong University of Science and Technology for obtaining examples of bawu for laboratory use, and to Thomas Rossing of Northern Illinois University for the long-term loan of his sheng, and the use of the NIU laser vibrometer system.

#### 6. REFERENCES

- [1] Gellerman R.F., *The American Reed Organ and the Harmonium*, Vestal Press, 1996.
- [2] Miller, T.E., "Free-Reed Instruments in Asia: A Preliminary Classification," in *Music East and West: Essays in Honor of Walter Kaufmann*, Pendragon, New York, 1981, pp.63-99.
- [3] Cottingham, J.P., and Fetzer C.A., "The Acoustics of the Khæn," *Proc. International Symposium on Musical Acoustics (ISMA98)*, Leavenworth, Washington USA, pp. 261-266, 1998.
- [4] Cottingham, J.P., "Acoustics of a symmetric free reed coupled to a pipe resonator," *Proc. Seventh International Congress on Sound and Vibration (ICSV7)*, Garmisch-Partenkirchen, Germany, pp. 1825-1832, 2000.
- [5] Benade, A.H., and M.I. Ibsi, "Survey of impedance methods and a new piezo-disk-driven impedance head for air columns," *J. Acoust. Soc. Amer.* 81, 1152-1167 (1987).
- [6] Cottingham, J.P., "The motion of air-driven free reeds," *Collected Papers of the 137th meeting of The Acoustical Society of America and the 2nd Convention of the European Acoustics Association: Forum Acusticum*, Berlin, 14-19 March 1999.
- [7] Hikichi, T., Osaka, N., and Itakura, F., "Time-domain simulation of sound production of the sho," *J. Acoust. Soc. Amer.* 113, 1092-1101 (2003).
- [8] Fletcher, N.H. "Excitation Mechanisms in Woodwind and Brass Instruments," *Acustica* 43, 63-72 (1979).
- [9] Busha, M. and Cottingham, J.P., "Experimental investigation of air-driven free reeds using a laser vibrometer system," *J. Acoust. Soc. Amer.* 106, 2288, (1999).



Figure 9. *The khæn.*



Figure 10. *Two examples of bawu.*

## WAVEGUIDE MODELLING OF THE PANPIPES

A. Czyzewski and B. Kostek

Sound & Vision Engineering Department  
Gdansk University of Technology  
Gdansk, Poland  
andcz@sound.eti.pg.gda.pl

### ABSTRACT

Waveguide modelling is nowadays a common technique used in the musical instrument sound synthesis domain. Still, not all instruments can be precisely modeled using this technique. Some simplifications are often required in order to fulfil computational needs. On the other hand, the only way to assess the quality of the synthetic sound resulting from the waveguide model is by means of subjective tests. This paper presents a digital waveguide model of the Panpipes. For the efficient modeling of the Panpipes instrument its structure and its physics were studied and discussed. Principles of the digital waveguide modeling of woodwind instruments were also briefly reviewed. In the paper two digital waveguide models of Panpipes instruments differing from each other in their complexity were presented. Consequently it enabled studying the influence of the decreasing complexity of the model on the resulting synthetic sound quality. The subjective tests performed showed that the simplifications in digital waveguide models introduced reveal no noticeable influence on the sound quality. Comparison of synthetic and real Panpipes sounds was also made and conclusions reached.

### 1. INTRODUCTION

The expansion of digital techniques has led to the development of the sound synthesis techniques based on the digital description of the signals. The physical modeling techniques are a special group of digital methods. They are focused on the structure of the particular instrument and on all the physical phenomena involved in the natural sound generation process. The technique called digital waveguide modeling is a simplified version of mathematical modeling. It is also based on the wave equation describing propagation of acoustic waves in a particular medium. This method usually handles sound generation in real-time. Although the significant simplifications are made in the modeling process, it still retains good quality and reality of synthetic sounds.

The Panpipes belongs to the group of woodwind instruments. It is one of the oldest instruments, and consists of a set of hollow tubes (reeds or bamboo tubes, canes). The instrument is formed by joining the tubes together in a concave curve (as viewed by the player) and setting them on a wooden base. The longest tube is at one end. Each successive tube is slightly shorter than its neighbor, allowing an array of pitches from low to high. As the tubes become shorter they also become narrower. A shorter tube produces a higher pitch. The player blows into the top open end of the tubes. The other end of the tube is usually closed. The

tube bottoms are plugged with either cork or wooden dowels and then further sealed with a plug of beeswax. The beeswax enables the Panpipes to be tuned by either removing some of the wax or inserting and pressing additional wax.

The Panpipes are a set of cylindrical tubes, which means that their diameter does not change along the tube. There is no need to model the shape of the bore in view of the simplicity of the real instrument, thus the modeling process of the Panpipes bore can be simplified as proposed in the literature [1][2].

Two digital waveguide models of the Panpipes were engineered. They differ from each other in their complexity. The strategy behind the so-called "physical" model was to design all essential components of the real instrument in order to produce a synthetic sound perceived subjectively as close to the real one. On the other hand, a "quasi-physical" model should provide an acceptable synthetic sound but the constraint should be put on the simplicity of the design. The models were implemented employing a digital signal processor using the *SynthBuilder* software on the *Next* workstation. This application enabled the modeling of pipe according to the algorithm described before. The models were created on the basis of the digital waveguide models of musical wind instruments as proposed in literature [1][2][3]. Ideas of Välimäki, Cook and other researchers were also followed.

### 2. DIGITAL WAVEGUIDE MODEL OF PANPIPES

The engineered "physical" digital waveguide model of the Panpipes is presented in Fig. 1 and its implementation in Fig. 2 showing the block diagram of this model constructed with the use of *SynthBuilder* tools. It is possible to run this algorithm in real time on a single DSP chip (Motorola 56001). It consists of three basic parts: bore model, jet propagation model, jet-bore interaction model.

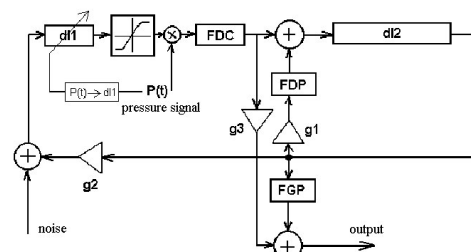


Fig. 1: "Physical" digital waveguide model of the panpipes (single pipe)

Denotations in Fig. 2:

- bore model: delay line  $dl2$ , low pass filter ( $FDP$ ), high pass filter ( $FGP$ ), scaling coefficients  $g1$  ( $-1 < g1 < 0$ ) and  $g3$  ( $0 < g3 < 1$ ),
- jet propagation model: delay line  $dl1$ , scaling coefficient  $g2$  ( $-1 < g2 < 0$ ), element converting air pressure signal into the length of the delay line  $dl1$ , noise generator,
- jet-bore interaction model: non-linear element,  $FDC$  filter (suppressing the  $DC$  offset).

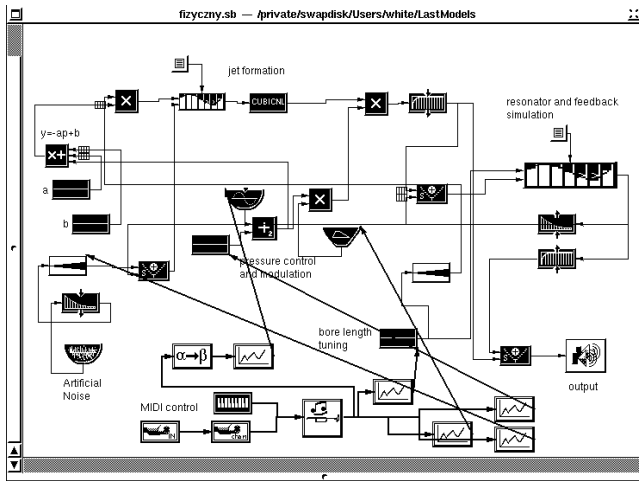


Fig. 2: "Physical" panpipes digital waveguide model implementation in the Synthbuilder environment

### 2.1. The Bore Model

The bore of a single pipe was modeled as proposed in the M. Sc. work of our student [4]. The length of the delay line ( $dl2$ , see Fig. 1), depending on the expected fundamental frequency of the synthetic sound was computed. Length of the delay lines corresponds to the effective length of the tube. The absolute values of the scaling elements were achieved in the tuning process:  $g1 = -0.9403$ ,  $g2 = -0.97$ ,  $g3 = 0.03$ . The phase relations between the direct and reflected waves (at the open and closed end of the bore) strictly determine the sign of each value of the  $g$  coefficient. The  $g1$  coefficient enables control of the phase relations and causes generation of odd multiples of a fundamental mode only. The  $g2$  scaling simulates the phase inversion and the coupling between the travelling waves and the air jet. The  $FGP$  (high pass filter) and  $FDP$  (low pass filter) were implemented as the simple one-pole  $IIR$  filters [4]. They simulate reflections of the travelling waves losses and the dispersive characteristics of the air column together with the reflections.

### 2.2 Jet Propagation Model

The jet propagation model was implemented in its simplified version [2]. In the real instrument a transverse wave is generated in the air jet and gains along its way to the bore edge. This corresponds to the non-linear interaction between the air jet produced by the player and the instrument edge. The amount of the delay  $\delta$  of the transverse wave can be computed according to a simple principle, namely the increase of air pressure decreases the delay  $\delta$  (see Eq. 4), which corresponds to the increase of the velocity of the transverse wave propagation. The effect is that

modulation of the  $P(t)$  pressure signal (see Fig. 1) causes changes in the musical articulation (tremolo, vibrato, and fundamental frequency changes) that are produced in a real instrument analogously. However, in the model implementation, this non-linear process was simplified and resulted in a linear function  $y = ax + b$  (where  $y$  corresponds to the coefficient that scales the length of the delay line ( $dl1$ , see Fig. 1),  $x$  corresponds to the signal  $P(t)$  simulated in the model,  $a = -1.059701$  and  $b = 0.361194$  are coefficients well-chosen to achieve the expected changes of the fundamental frequency in the full range of  $P(t)$  signal changes. The transverse wave gain is simulated by multiplying the non-linear element output by a value proportional to the  $P(t)$ . The delay  $\delta$  of the transverse wave is described as:

$$\delta = \frac{l}{0.5V} = l \sqrt{\frac{2\rho}{P(t)}}, \quad (1)$$

where:

- $l$  - length of the "air jet" (distance between the player's lips and the bore edge),
- $V$  - flow velocity of the transverse wave,
- $\rho$  - air density,
- $P(t)$  - air pressure.

### Jet-Bore Interaction Model

The jet-bore interaction model used in the model is similar to the interaction model proposed by Fletcher and Rossing [5]. The non-linear, sigmoid function describing the interaction was implemented using a polynomial approximation:  $y = a1x + a2x^2 + a3x^3$ , where  $a1 = 0.850746$ ,  $a2 = 0.044776$ ,  $a3 = -0.253731$ ,  $x$  signifies the jet position (corresponding to the bore edge position  $x=0$ ),  $y$  signifies the volume of the jet flow into the bore. The  $FDC$  filter was also added to remove the  $DC$  offset.

### Pressure Signal Model

The pressure signal  $P(t)$  modeling procedure is shown in Fig. 3. The model can be triggered by a constant value of  $P(t)$ , however, it is necessary to manipulate it to achieve all the additional articulation effects listed above. The  $LFO$  signal is added to a constant value for the modulation effects. There is also an envelope added to the  $P(t)$  signal. The external controller (modulation wheel) can manipulate the frequency of the  $LFO$ . The constant value and the attack time of the envelope generator are scaled according to the actual MIDI Velocity message value, coming from the master keyboard that is connected to the model by a MIDI interface.

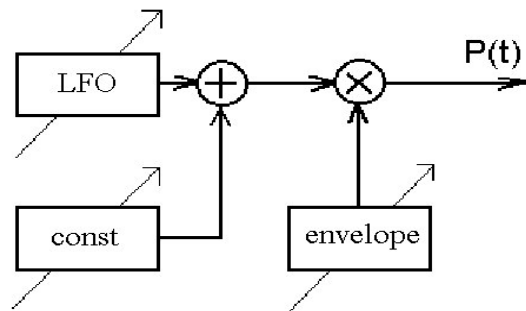


Fig. 3: Pressure signal modeling

### 3. "QUASI-PHYSICAL" DIGITAL WAVEGUIDE MODEL OF THE PANPIPES

The "quasi-physical" model of the Panpipes is presented in Fig. 4. The structure of the "quasi-physical" model is similar to that presented in Fig. 1 (physical model), although the jet model is simplified and the articulation effects (tremolo, vibrato) are produced using some additional *LFO* generators. The tremolo effect is achieved by modulating the amplitude of the output signal and the vibrato effect is achieved by modulating the delay line length, which produces the effect of cyclic fundamental frequency changes (see Fig. 4). Since these models are similar, only the most important parameters of the "quasi-physical" model will be listed. The values of the scaling coefficients are:  $g1=-0.94$ ,  $g2=-0.08$ ,  $g3=1$ . These values were achieved in the tuning process. The interaction between the jet and bore was achieved using polynomial approximation (as above) with the coefficients:  $a1=1$ ,  $a2=-0.014925$ ,  $a3=-0.402985$ . The model and its parameters were also controlled using the master MIDI keyboard.

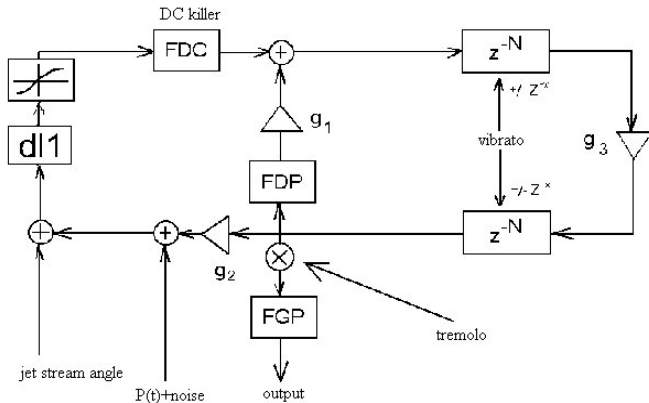


Fig. 4: "Quasi-Physical" digital waveguide model of the panpipes (single pipe)

### 4. RESULTS OF SIMULATIONS

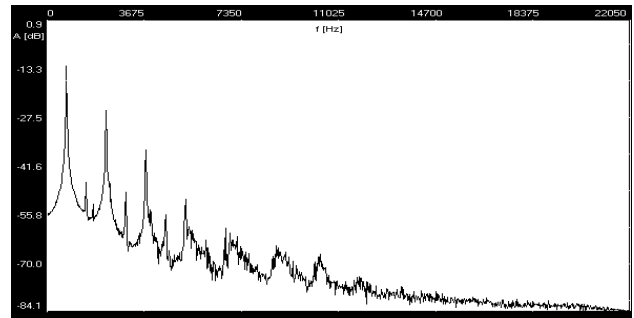
The next step of the experiments carried-out was to check performance of models employing some objective and subjective auditory tests. The goal of the analyses was to compare the quality of the synthetic sounds generated by both models. Time domain analyses show that the "physical" model responses introduced for the different musical performance dynamics are closer to the real Panpipes sounds than these achieved using the "quasi-physical" model. Both models can change the attack time of the output signal according to the velocity changes, but only the "physical" model can change dynamics of the output signal and produce the overshoot effect depending on the velocity changes.

#### 4.1. Spectral Analyses

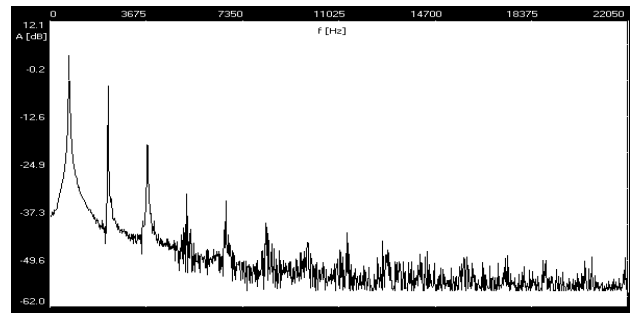
Spectral analyses of the synthetic signals proved that the synthetic sounds spectrum is dominated by odd harmonics, which is a characteristic feature of the instruments such as the

Panpipes (built of pipes with only one open end). In Fig. 5 sample analyses are shown allowing for comparison of real and synthetic sound spectra. On the other hand, attack transients were studied for both waveguide models. The overshoot was seen in the starting transient of the synthetic sound only in the case of a "physical" model. This was obtained for the highest value of the  $P(t)$  signal which may be translated as high velocity value applied on the keyboard. The DC value of  $P(t)$  signal increases with the velocity of key pushing. However, this interaction is not linear. The "quasi-physical" model does not simulate such articulation effects because of the simplifications described above.

#### a. real sound



#### b. synthetic - "physical" model



#### c. synthetic - "quasi-physical" model

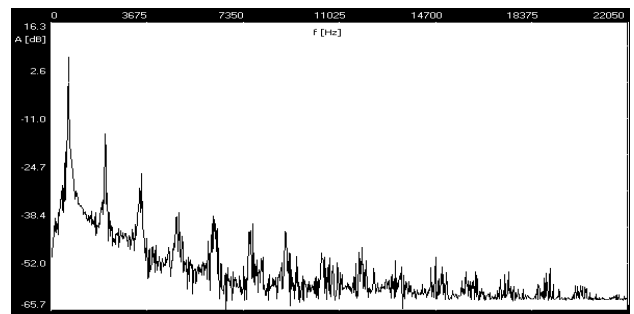


Fig.5: Samples of Panpipes sound spectra

#### 4.2. Subjective Auditory Tests

The parametric auditory tests were carried out to investigate the differences between the quality of the synthetic sounds achieved using both models (see Tab. 1). They were also focused on verifying the optimum values of the parameters of the models (noise signal levels, nominal value of the air pressure signal and



cut-off frequencies of the filters). Thirteen experts were involved in the tests. The synthetic sounds were presented in pairs along with the appropriate natural sounds of the Panpipes. Parameters of the models were assessed in 1-5 point judgement scale. The scores significantly reduced while changing the values of the parameters of the models from their optimum values. In addition, the Fisher test was performed to identify the significant differences between the average values of the judgements assigned to the objects of the test, which allowed identification of the range of the optimum values of each model parameter. In Fig. 6 some results of parametric test analyses are shown. Figures contain comparison of results obtained for "physical" and "quasi-physical" models.

Table. 1 Test questionnaire

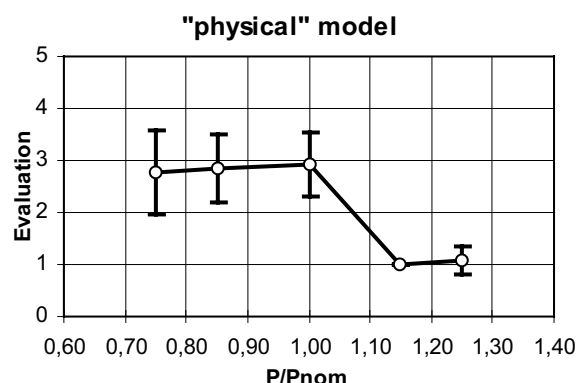
Evaluation/scores	Sound quality as compared to real sound
5	Excellent (no distortions or imperceptible)
4	Very good (distortions perceived but not important)
3	Good (distortions perceived but tolerable)
2	Fair (high level of distortions but passable)
1	Bad (not acceptable distortions)

The synthetic sound quality was perceived as good for the nominal value of the air pressure signal (Fig. 6 a,b). This happened for the "physical" model. On the other hand, for the "quasi-physical" model values higher than the nominal air pressure value, obtained better ratings. As results from other tests, increasing the cut-off frequency above the nominal value of  $f_c$  equal to 5361 Hz causes a decrease in sound quality. On the other hand, decrease of the cut-off frequency up to 4000 Hz does not cause significant decrease in sound quality. Further decreasing of the cut-off frequency causes distortions that are no longer acceptable. The same mean score was obtained for the cut-off frequency equal to 5361 [Hz] for the "quasi-physical" model. However, in this case all scores obtained for values other than that of the nominal cut-off frequency were much worse. Moreover a poor uniformity of experts' ratings should be taken into consideration.

## 5. CONCLUSIONS

Two digital waveguide models of the Panpipes have been proposed in this paper. Both objective analyses and parametric subjective auditory tests have shown that sounds generated using the digital waveguide models of the Panpipes are very realistic and acceptable as to quality. The "physical" model in particular was found to be able to produce very realistic articulation effects. Engineered models, even if not taking into account in full, the interaction of all instrument elements, produce sounds that are very similar to the natural sounds of the Panpipes. Although both models differ from each other in their complexity, their quality was assessed by experts as almost equal. This proves that some simplifications can be performed in a "physical" model with no significant influence on the synthetic sound quality. However, it should be noticed that only single pipes were modeled here. Taking into consideration the interaction between sounds and vibrations coming from various pipes at the same time the complexity of the models would increase significantly. The computational expense of such a model would be too high for performing in real-time, so any possibility of simplifying the model is valuable.

a.



b.

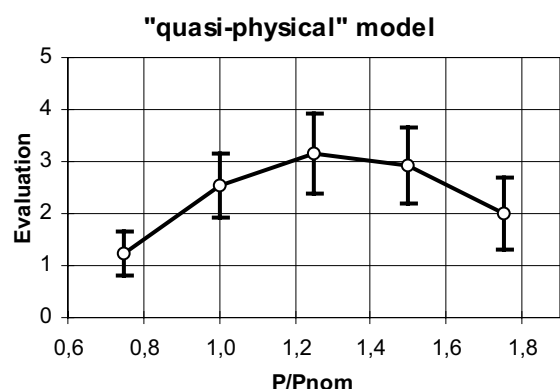


Fig. 6: Comparison of parametric test analyses obtained for "physical" (a) and "quasi-physical" models (b) – searching for the optimum nominal value of the air pressure signal

## 6. REFERENCES

- [1] Czyzewski, A., Jaroszuk J., Kostek B., Digital Waveguide Models of the Panpipes, ISMA'2001, Perugia, Italy, 21-24 September, 2001.
- [2] Czyzewski A., Jaroszuk J., Kostek B., Digital Waveguide Models of the Panpipes; Archives of Acoustics, No. 4, vol. 27, pp. 357 - 371, 2002.
- [3] Smith J. O., Digital Waveguide Modeling of Musical Instruments, An Expansion of the Paper: Physical Modeling Using Digital Waveguides, Computer Music Journal, 16, 4, 74-91, 1992.
- [4] Jaroszuk J., Digital Waveguide Modeling of Wind Instruments Acoustics, M.Sc. Thesis, Sound & Vision Engineering Department, TUG Gdansk, 2000.
- [5] Fletcher N.H., Rossing T. D., The Physics of Musical Instruments, Springer-Verlag, New York, 1991.

# PLAYING FREQUENCY SHIFT DUE TO THE INTERACTION BETWEEN THE VOCAL TRACT OF THE MUSICIAN AND THE CLARINET

Claudia Fritz, Joe Wolfe

Jean Kergomard, René Caussé

School of Physics, UNSW, Sydney  
cfritz@phys.unsw.edu.au

LMA, Marseille and IRCAM, Paris, France

## ABSTRACT

Previous qualitative studies (Mooney [1], Benade [2], Hoekje [3]) confirm musicians' opinions that the vocal tract (VT) affects both timbre and pitch. Johnston, Troup and Clinch [4] modelled the tract as a one peak resonator, which, if tuned to the fundamental  $f_0$  of a clarinet, gives a playing frequency of  $f_0$ . But this result depends upon their particular tract impedance  $Z$ , which is small and real at harmonics of  $f_0$ . In general, the playing frequency is shifted.

We relate the flow and the pressure difference at the reed by the usual non linear Bernoulli's equation in the time domain, simplified as a third order polynomial. In the frequency domain, the impedances of the clarinet and the vocal tract are in series. To obtain an analytical result for the frequency shift, we expand about the threshold oscillation. We compare this result with numerical results from the harmonic balance method. Finally, impedance spectra measured on an artificial VT with a discrete but variable area function are used in this theoretical study. We suggest that tuning the vocal tract to  $f_0$  may be rare and unnecessary.

## 1. PHYSICAL MODELLING

The clarinet is modelled here as a self-sustained oscillator with a linear exciter (the reed) which is coupled nonlinearly to two linear resonators: the pipe and the vocal tract. In previous studies, the tract was often ignored. A sketch of the mouthpiece is shown in Figure 1, which includes the meaning of the physical quantities used. In contrast to most previous models, here the mouth pressure  $p_{mouth}$  is not constant but instead has time variation:

$$p_{mouth} = P_{m0} + p_m(t) \quad (1)$$

where  $P_{m0}$  is the DC component (used alone when the effects of the VT are omitted), which is assumed to be the source, and  $p_m(t)$  is the acoustic component, assumed periodic.

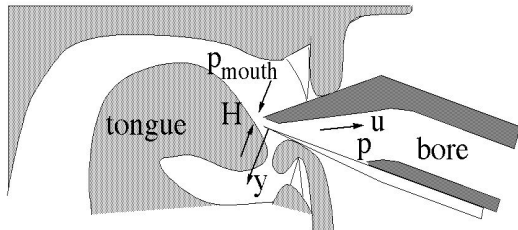


Figure 1: Schematic view of the system with dimensionless physical quantities

## 1.1. The reed

As the reed is not our main interest, we will restrict discussion to the case where the playing frequency is much lower than that of the reed resonance and describe the reed as a simple spring, of stiffness  $k_r$  so

$$k_r y(t) = -(p(t) - p_m(t) - P_{m0}) \equiv -(\Delta p - P_{m0}) \quad (2)$$

## 1.2. The pipe

The pipe is usually characterized by its input impedance, which describes its resonances. High frequencies are not important in our study so, for the modelling only, our 'clarinet' is a cylinder, whose length  $l$  is assumed to include end effects for radiation and the volume velocity due to reed displacement, and in which radiation losses are neglected compared to visco-thermal ones. It has neither tone holes nor bell (which are not important to the oscillation mechanism). Dispersion is as well neglected. We indicate the frequency domain by using capital letters and write the dimensionless equation

$$P(\omega) = Z_p(\omega)U(\omega), \quad (3)$$

The dimensionless input impedance is given by [5]:

$$Z_p(\omega) = i \tan(kl) \quad (4)$$

$$\text{where } kl = \frac{f}{4f_p} - i\psi\eta\sqrt{\frac{f}{f_p}} \quad (5)$$

and where  $\psi \simeq 1.3$  for common conditions in air,  $f_p = c/4l$  is the first resonance frequency of the pipe, and  $\eta$  is a dimensionless loss parameter:  $\eta = \sqrt{l_v l / r^2}$  as derived in ref. [6, Ch.6].

## 1.3. The vocal tract

The vocal tract is modelled as a (linear) impedance  $Z_m$ , as 'seen' by the reed (see the discussion in a companion paper [7]). Flows entering the mouth and the instrument are in opposite directions, so:

$$P_m(\omega) = -Z_m(\omega)U(\omega), \quad (6)$$

Following Johnston et al [4], we approximate the vocal tract as a one peak resonator, an admittedly crude physical model that ignores anatomical details, which are as yet not really well known. We note that only the lowest tract resonance falls in the range in which the instrument has strong harmonics unless played loudly. Further, this allows us to examine Johnston et al's proposition that coincidence or non coincidence of the VT resonance with one of the instrument's resonance may be important.

#### 1.4. The non linear coupling

Assuming some hypotheses, in particular that the system changes sufficiently slowly for Bernoulli's law to be valid and including the volume flow due to the reed displacement in the bore impedance of the bore as described above, the air flow at the reed is related to the pressure difference  $\Delta p$  across it thus:

$$u(t) = \begin{cases} S(t)\sqrt{2|\Delta p - P_{m0}|/\rho} \text{sign}(\Delta p - P_{m0}) & \text{for } y > -H \\ 0 & \text{for } y \leq -H \end{cases} \quad (7)$$

where  $S(t) = (H + y(t))w$  is the cross-sectional area of the opening, determined by the reed width  $w$  and displacement  $y$ .

Denoting dimensionless pressure and flow with a tilde, nondimensionalising pressures by dividing by that which closes the reed,  $P_M$ , impedances by dividing by the characteristic impedance of the bore  $Z_0$ , and defining a dimensionless mouth pressure  $\gamma$ , we write:

$$\tilde{\Delta p} = \frac{\Delta p}{P_M} \quad \text{and} \quad \tilde{u} = \frac{uZ_0}{P_M} \quad (8)$$

$$\gamma = \frac{P_{m0}}{P_M} \quad (9)$$

A dimensionless "embouchure" parameter characterizes the mouthpiece and the mouth position:

$$\zeta = Z_0 w H \sqrt{\frac{2}{\rho P_M}} \quad (10)$$

Substituting dimensionless quantities in equation (7) gives:

$$\tilde{u}(\tilde{\Delta p}) = \zeta(1 + \tilde{\Delta p} - \gamma) \sqrt{|\gamma - \tilde{\Delta p}|} \text{sign}(\gamma - \tilde{\Delta p}) \quad (11)$$

for  $\tilde{\Delta p} > \gamma - 1$  and 0 otherwise.

Hereafter, all parameters are dimensionless and the tilde is omitted. For small oscillations, i.e. close to the oscillation threshold, the previous equation can be expanded as a third-order polynomial:

$$u(\Delta p) = u_{00} + A\Delta p + B\Delta p^2 + C\Delta p^3, \quad (12)$$

where

$$\begin{aligned} u_{00} &= \zeta(1 - \gamma)\sqrt{\gamma}, & A &= \zeta \frac{3\gamma - 1}{2\sqrt{\gamma}}, \\ B &= -\zeta \frac{3\gamma + 1}{8\gamma^{3/2}}, & C &= -\zeta \frac{\gamma + 1}{16\gamma^{5/2}}. \end{aligned} \quad (13)$$

Solving the non linear system composed of equations (3),(6) and (12) is simplified by combining the first two thus:

$$\Delta P = (Z_p + Z_m)U = \mathbb{Z}U \quad (14)$$

The impedances of the pipe and of the VT are thus in series, and  $\mathbb{Z} = Z_p + Z_m$  is the equivalent impedance.

## 2. THEORETICAL INFLUENCE OF THE VT ON THE PLAYING FREQUENCY

Kergomard et al. [5] showed that in the case of the clarinet, the variable truncation method is a good approximation to calculate the spectral envelope easily and analytically. In the first iteration, even harmonics are neglected. In the second, they are calculated from the odd harmonics. Higher harmonics are presumed not to influence lower harmonics so equations can be truncated at the order of the harmonic to be calculated, i.e. the equations are truncated

at the first order when calculating the first harmonic. This solution is substituted into the equations truncated at the third order to calculate the third harmonic and so on.

Here we use the same analytical technique, but with these modifications to the physical situation: the pressure difference across the reed replaces the pressure in the mouth, and the series impedance of clarinet and VT replaces that of the clarinet. We do not expect that the addition of the VT impedance in series will strongly affect the amplitude of odd or even harmonics of pressure in the mouthpiece, unless a vocal tract resonance lies close to a harmonic. However, the VT impedance can have a larger effect on the pressure in the mouth, especially the even harmonics of the played note, and therefore on the pressure difference across the reed. This in turn can affect the playing frequency. Hence we do not neglect even harmonics and the reason for that is now explained.

The variable truncation method is in particular used to obtain easily the playing frequency. Equation (12) truncated to the first order and equation (14) give indeed for the first harmonic:

$$\mathbb{Y}_1 \Delta P_1 = A \Delta P_1 + 3C \Delta P_1 |\Delta P_1|^2 \quad (15)$$

where  $\mathbb{Y} = 1/\mathbb{Z}$  is the admittance of the series combination. This gives

$$|\Delta P_1|^2 = \frac{\mathbb{Y}_1 - A}{3C} \quad (16)$$

This implies that  $\Im(\mathbb{Y}_1) = 0$  because all other terms of this equation are real, and thus gives the playing frequency, called  $\omega_0$ . The threshold pressure is as given by  $A = \mathbb{Y}_1(\omega_0) = A_{10}$ . For the most simplified system, a harmonic pipe for the clarinet (no dispersion) with no VT influence, this implies of course that the playing frequency is equal to the first resonance of the pipe. But if we now add a vocal tract tuned to the first resonance of the pipe, we would expect to obtain the same playing frequency. However, this result is not repeated for numerical solutions of less simplified versions of the problem. These solutions were calculated by the program *Harmbal* developed by Farner et al. [8] which uses the harmonic balance method [9] and obtains the solution for  $N$  harmonics from the solution for  $N - 1$  harmonics.

To see how introduction of the second harmonic produces a frequency shift, we will truncate equation (12) to the second order. The choice of zero in the time domain is arbitrary, so for convenience we choose  $\Delta P_1$  to be real. The following equations are then to be solved simultaneously:

$$\mathbb{Y}_1 \Delta P_1 = A \Delta P_1 + 2B \Delta P_1 \Delta P_2 + 3C \Delta P_1^3 + 6C \Delta P_1 |\Delta P_2|^2$$

$$\mathbb{Y}_2 \Delta P_2 = A \Delta P_2 + B \Delta P_1^2 + 6C \Delta P_1^2 \Delta P_2 + 6C \Delta P_2 |\Delta P_2|^2$$

For simplicity we have chosen to use the Small Oscillations Approximation, used by Worman[10] and Grand et al. [11]. Near the threshold,  $\Delta P_2$  is a second order of  $\Delta P_1$  (Worman [10]) so we can neglect quadratic and higher terms in  $\Delta P_1$  to obtain:

$$\mathbb{Y}_1 - A = 2B \Delta P_2 + 3C \Delta P_1^2 \quad (17)$$

$$(\mathbb{Y}_2 - A) \Delta P_2 = B \Delta P_1^2 \quad (18)$$

So

$$\Delta P_2 = \frac{B \Delta P_1^2}{\mathbb{Y}_2 - A} \quad (19)$$

$$\Delta P_1^2 = \frac{(\mathbb{Y}_1 - A)(\mathbb{Y}_2 - A)}{2B^2 + 3C(\mathbb{Y}_2 - A)} \quad (20)$$

Following the development of Grand et al [11] for conditions close to the threshold, we can write  $A = A_{10} + \delta A$ . Further supposing that the playing frequency remains close to  $\omega_0$  we write  $\omega = \omega_0 + \delta\omega$  and  $\mathbb{Y}_1(\omega) = A_{10} + \delta A_1(\omega)$ . If  $\delta\omega \ll \omega_0$ , this gives  $\delta A_1(\omega) = A_{10} \left( 2iQ \frac{\delta\omega}{\omega_0} \right)$ , where  $Q$  is the dimensionless quality factor of the impedance peak near which the oscillation occurs.  $\mathbb{Y}_2(\omega_0)$  is a priori complex so we write  $\mathbb{Y}_2(\omega)$  in the following form:

$$\mathbb{Y}_2(\omega) = \Re(A_{20}) + i\Im(A_{20}) + \delta A_2(\omega) \quad (21)$$

with  $\delta A_2(\omega) = O(\delta(\omega))$ , which we can neglect in first approximation.

As the left hand side of equation (20) is real, the imaginary part of the right hand side is zero, which gives:

$$\frac{\delta\omega}{\omega_0} = \frac{\delta A}{2A_{10}Q} \frac{2B_2\mathbf{I}}{2B_2\mathbf{R} + 3C(\mathbf{R}^2 + \mathbf{I}^2)} \quad (22)$$

with  $\mathbf{R} = \Re(A_{20}) - A_{10}$  and  $\mathbf{I} = \Im(A_{20})$ .

### 3. MEASUREMENTS

Measurements of the VT impedance were done by using the acoustic impedance spectrometer developed by Smith et al [12]. What is new is the coupling of the VT to the spectrometer and the use of an impedance head mounted inside a clarinet mouthpiece (Figure 2), that can be then coupled to the tract of a human player or to an artificial vocal tract (VT) composed of discrete elements. The artificial tract is modelled on the MRI data of Story and Titze [13] (Figure 3).

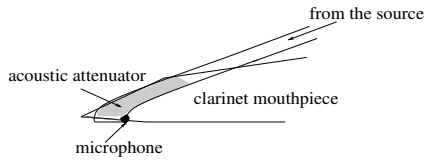


Figure 2: Scheme of the measurement head

As the impedance head has a cross section approximately equivalent to the part of the reed which is inside the player's mouth, we measure the impedance of the VT as "seen" by the reed.

The VT is coupled to a semi-infinite pipe which models the lungs, assumed non-reflective. The glottis can be chosen open or closed (20 or 6 mm diameter) as this varies among musicians, especially between beginners and professionals respectively [14].

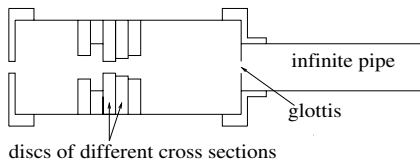


Figure 3: Scheme of the artificial VT

The discrete element tract gives weaker impedance peaks than does a continuous model, but they fall at nearly the same frequencies.

### 4. RESULTS

For experienced players who use their vocal tract, the glottis is nearly closed [14], which increases reflection at the glottis and so enhances VT resonances. We therefore consider only this case, and use the MRI data of Story and Titze [13] which were obtained in speech, where the glottis is almost closed. We present here, in Figure 4, the results for two vowels commonly cited by most of the players: /æ/ as in "had" for the low register and /i/ as in "heed" for the high register. This of course is only an approximation, because the embouchure constrains the player's jaw position.

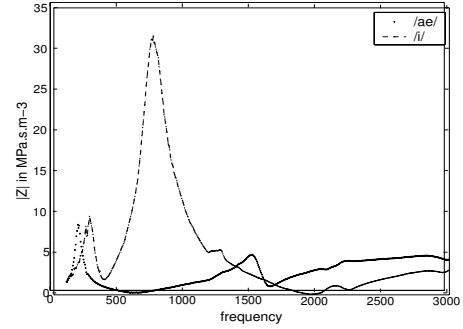


Figure 4: Amplitude of the VT impedance for the vowels /æ/ and /i/.

These results (amplitude and frequency of the resonances) are consistent with previous numerically simulated and experimental results (Hoekje [3], Sommerfeldt and Strong [15]).

The vowel /æ/ has relatively weak resonances so it should not affect much the sound of the clarinet. But the vowel /i/ presents a high peak, at 753 Hz, so we can expect an influence on the pitch around this frequency. The impedance is much higher because the tongue is in a high position which reduces the aperture inside the mouth.

We consider several cases. In one case, the pipe frequency was varied over the range 720-750 Hz: ie on the low frequency side of the strong peak in /i/. The playing frequency varies negligibly for /æ/. For /i/, the playing frequency is less than that for /æ/ by an amount that increases with frequency over this range: ie it increases as the VT impedance increases. Another case used a pipe frequency of 228 Hz, which lies in the middle between the impedance peaks for the first resonances in the two vowels chosen (Figure 4). At this frequency, the vocal tract is inertive for the vowel /i/ and compliant for /æ/. In both cases, the frequency shift is of order 0.2%, and the direction changes with mouth pressure, for reasons that we do not yet understand. We also consider the case where the first resonance frequency of the clarinet is 753 Hz (approximately the note G5), ie when the pipe frequency coincides with the peak in /i/. This case is of interest because of the proposal of formant tuning [4], and it is the one whose results are shown in Figure 5.

As the impedances are dimensionless in our calculation, we have to divide the impedance of the VT by the impedance of the clarinet. We can model it by the general formula of the impedance of one peak resonator:

$$Z_m(f) = iZ_d \frac{k}{k_1^2 - k^2 + i \frac{k k_1}{Q_1}} \quad (23)$$

where  $Z_d$  is the dimensionless characteristic impedance,  $k = 2\pi/f$  and  $k_1 = 2\pi F_1/c$  and  $Q_1$  are respectively the frequency and the quality factor of the resonance. Fitting the model to our measurement gives  $F_1 = 753$  Hz,  $Z_d = 35$  and  $Q_1 = 6$ . We can then calculate the values of the different parameters ( $Q = 14$ ,  $R = 0.056$  and  $I = 0.567$ ) and obtain the shift in the playing frequency from equation (22) (see Figure 5).

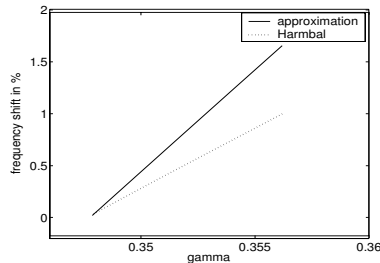


Figure 5: Frequency shift in percent in function of the dimensionless mouth pressure, given by the approximation (22) and by the program Harmbal

The results are compared to those of *Harmbal*. The difference is quite acceptable, so our approximations give a good idea of how the playing frequency evolves for small mouth pressures.

As well as analysing the effects of vocal tract impedance, the *Harmbal* technique can also be used to analyse the effect of changing reed parameters. This is interesting because, to change the pitch, clarinetists move both the tongue and the lower jaw. Lowering the jaw increases the effective length of the reed, decreasing its characteristic frequency. The stiffness and the value of  $H$ , as functions of the force applied to close the reed (the 'jaw force'), were measured directly on a clarinet and reed. Using measured values for modest changes of this jaw force, and inputting the dependent dimensionless parameters to the model described above give changes in playing frequency of the same order as those given in Figure 5 for the effect of the vocal tract. The relative importance of these effects in playing remains, of course, a question to be settled experimentally.

## 5. CONCLUSION

The playing frequency shift obtained in the case of a VT tuned to the first resonance frequency of the clarinet is interesting. If players did tune their tract resonance to coincide with an instrument resonance the playing frequency would shift. However, we doubt that this is what players do. More importantly, this simple case shows a mechanism whereby the playing frequency can be changed by changes to vocal tract geometry. This is important because musicians claim to do it, and model experiments on other instruments show it [7].

On a theoretical point of view, further study will be done in order to improve formula (22) by using an extension of the VTM to fit better to the numerical results of *Harmbal*.

In an other hand, the model reported here neglects several important physical features. Measurements of the impedance of the VT of musicians miming their playing embouchure will be carried out to try to analyse in more detail the role of the tongue and the glottis. The discrete element VT will now be used in a blowing machine to investigate this shift experimentally.

## 6. REFERENCES

- [1] J. Mooney, "The effect of the oral cavity on the tone quality of the clarinet," Ph.D. dissertation, Brigham Young University, 1968.
- [2] A. Benade, "Air column, reed and player's windway interaction in musical instruments," in *Vocal Fold Physiology*, I. Titze and R. Scherer, Eds. The Denver Center for the Performing Arts, 1983.
- [3] P. Hoekje, "Intercomponent energy exchange and upstream/downstream symmetry in nonlinear self-sustained oscillations of reed instruments," Ph.D. dissertation, CaseWestern Reserve University, Cleveland, Ohio, 1986.
- [4] R. Johnston, P. Clinch, and G. Troup, "The role of the vocal tract resonance in woodwind instrument playing," unpublished.
- [5] J. Kergomard, S. Ollivier, and J. Gilbert, "Calculation of the spectrum of self-sustained oscillations using a variable truncation method : application to cylindrical reed instruments," *Acust.- Acta Acust.*, vol. 86, pp. 685–703, 2000.
- [6] A. Hirschberg, J. Kergomard, and G. Weinreich, Eds., *Mechanics of Musical Instruments, Lecture notes CISM*. Springer-Verlag, 1995.
- [7] J. Wolfe, A. Tarnopolsky, N. Fletcher, L. Hollenberg, and J. Smith, "Some effects of the player's vocal tract and tongue on wind instrument sound," in *Proc. SMAC*, Stockholm, Sweden, 2003.
- [8] S. Farner, C. Vergez, and J. Kergomard, "Harmbal: A program for calculating steady-state solutions to nonlinear dynamical autonomous systems by the harmonic balance method. applications to a physical model of the clarinet," *To be submitted to Acustica-Acta Acustica*.
- [9] J. Gilbert, J. Kergomard, and E. Ngoya, "Calculation of the steady-state oscillations of a clarinet using the harmonic balance technique," *J. Acoust. Soc. Amer.*, vol. 86, no. 1, pp. 35–41, 1989.
- [10] W. Worman, "Self-sustained nonlinear oscillations of medium amplitude in clarinet-like systems," Ph.D. dissertation, Case Western Reserve University, 1971.
- [11] N. Grand, J. Gilbert, and F. Laloe, "Oscillation threshold of woodwind instruments," *Acustica*, vol. 82, pp. 137–151, 1996.
- [12] J. Smith, C. Fritz, and J. Wolfe, "A new technique for the rapid measurement of the acoustic impedance of wind instruments," in *Proc. of the Seventh International Congress on Sound and Vibration*, G. Guidati, H. Hunt, H. Heller, and A. Heiss, Eds., vol. III, Garmisch-Partenkirchen, Germany, 4-7 July 2000, pp. 1833 – 1840.
- [13] B. Story, I. Titze, and E. Hoffman, "Vocal tract area functions from magnetic resonance imaging," *J. Acoust. Soc. Amer.*, vol. 100, no. 1, 1996.
- [14] M. S. Mukai, "Laryngeal movement while playing wind instruments," in *Proc. International Symposium on Musical Acoustics*, Tokyo, Japan, 1992, pp. 239–242.
- [15] S. Sommerfeldt and W. Strong, "Simulation of a player-clarinet system," *J. Acoust. Soc. Amer.*, vol. 83, no. 5, pp. 1908–1918, 1988.

## INFLUENCE OF LOSSES ON THE SATURATION MECHANISM OF SINGLE REED INSTRUMENTS

Joël GILBERT, Jean-Pierre DALMONT, Mérouane ATIG

Laboratoire d'Acoustique de l'Université du Maine – UMR CNRS 6613  
Avenue Olivier Mesiaen, 72085 Le Mans cedex 9, France  
joel.gilbert@univ-lemans.fr

### ABSTRACT

The question on what limits the amplitude of the oscillations of clarinet-like instruments is investigated. The influence of the losses on the saturation is shown and discussed. The discussion is based on experimental results coming from an artificial mouth set-up, and on approached theoretical results coming from numerical simulations.

### 1. INTRODUCTION

A lot of papers have been devoted to single-reed instruments (for a first overview, see for example [1] and [2]). If a great attention has been paid to what happens near the threshold of oscillation, only few papers are concerned with the saturation phenomena [3]. When blowing a reed instrument using an artificial mouth, the sound level is limited by the fact that when the blowing mouth overpressure increases the level also increases until a maximum  $P_{extup}$  (saturation or extinction threshold for increasing mouth pressure) beyond which the reed closes suddenly. Then if the mouth overpressure is decreased, the reed oscillates again from a value of the mouth pressure  $P_{thdown}$  (threshold of oscillation for decreasing mouth pressure). The subject of the present paper is to investigate how the losses are responsible of the saturation phenomena. Two tools are used : first is an experiment. using an artificial mouth blowing a clarinet-like instrument. The clarinet is replaced by a straight cylinder which termination can be modified at the open end of the tube in order to vary the losses amount. Second tool is a numerical simulation based on the simplest model of a clarinet-like instrument. These simulations include frequency independent losses.

The present paper is divided into four sections. After this brief introduction, the experimental set-up and the experimental results are presented in section 2.1 and 2.2 respectively. A simplified physical model of the clarinet-like instrument and the simulation method are summarised in section 3.1. Then the simulation results are compared with the experimental results in section 3.2. Finally the preliminary conclusions of this work are discussed section 4.

### 2. EXPERIMENTS

#### 2.1. Experimental set-up

The artificial mouth consists of a Plexiglas box with metal reinforcement [4]. The artificial lip consists of a cylindrical latex balloon of small diameter (10mm) in which a piece of foam

saturated with water is inserted. The lip is fixed on a rigid support which position can be translated vertically by means of a screw. It result mainly on a variation of the reed opening at rest. The mouthpiece is inserted in a metal barrel whose horizontal position can be adjusted. Resonators can be fixed onto the other end of the barrel. The air is supplied by a compressor through a pressure reducing valve.

The pressure  $P_m$  in the mouth is measured by a static pressure sensor. A miniature differential pressure sensor mounted in the wall of the mouthpiece measures the pressure difference  $\Delta p = P_m - p$  between the mouth cavity and the inside of the mouthpiece. The two pressure signals are collected on a computer via a data acquisition card. The experiment starts without blowing pressure ( $\Delta p = 0$ ). The pressure in the mouth cavity  $P_m$  is then increased gradually until the oscillations stop (crescendo case ; see figure 1). Then, the reed closes completely the opening. Starting from the close state, a second experiment can be done, the pressure in the mouth being gradually brought back to zero (decrescendo case). The typical duration of each experiment is 40s.

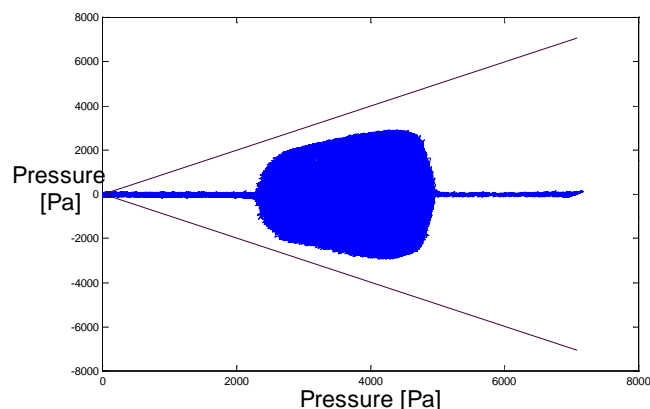


Figure 1: Experimental acoustic pressure (crescendo).  
The mouth pressure and the acoustic pressure in the mouthpiece  
(in Pa) as a function of the mouth pressure (in Pa).

Instead of a clarinet, a tube of 16mm diameter adapted on a clarinet mouthpiece and barrel, is used on which different terminations can be adapted in order to vary the amount of non-linear losses. Two types of terminations are used. First type terminations are pieces of tube with a circular flange of 25mm diameter. They differ from their radius of curvature of the edges.

Four radius of curvature have been machined and used for the experiments :  $r < 0.1\text{mm}$ ,  $r = 0.3\text{mm}$ ,  $r = 1\text{mm}$  and  $r = 4\text{mm}$ . The second type of termination, which tends to approximate a pipe termination without thickness, has a sharp edge (figure 2). These terminations have been extensively studied in [5] by measuring the real part of their impedance  $Z_{end}$  by means of a two microphone method. The measured terminations are the one used in the experiments of the present paper. The sharper the edges of the pipe termination, the more important the losses.

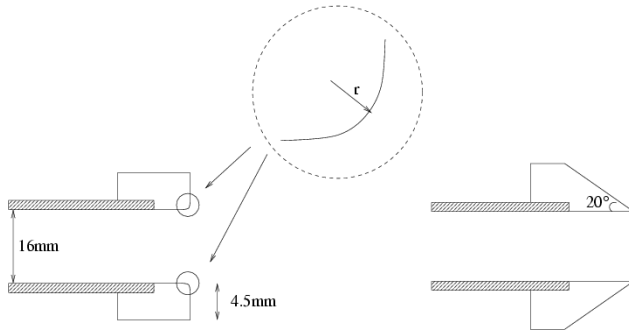


Figure 2: The two types of pipe termination geometry. Left) Tube with rounded edges defined by a radius of curvature  $r$ . Right) Tube with a sharp edge defined by a bevel angle of  $20^\circ$  (unflanged pipe termination).

## 2.2. Experimental results

The experiments are based on the investigation of the acoustic pressure amplitude in the mouthpiece as a function of the mouth pressure. The corresponding curves are displayed figure 3 in two sets, a first set corresponding to an increasing mouth pressure (crescendo) is displayed figure 3a, a second set corresponding to a decreasing mouth pressure (decrescendo) is displayed figure 3b. In each of the two graphs, five curves corresponding to the different terminations are displayed. The present study is based on the analysis of the first oscillation regime of the clarinet-like system (playing frequency around 133 Hz). From the experimental point of view, it is not easy to get the same oscillation regime for every embouchure and every mouth pressure values. Actually, the experimentally observed behaviour is sometimes the second oscillation regime instead of the first one, particularly during the crescendo case, the oscillation first reaches the second regime and then is forced to reach the first regime a fifth and a twelfth below, from the mouth pressure middle range until the saturation. As a consequence figure 3a shows troubled curves around  $P_m = 4000\text{ Pa}$ . It is inconsequential here as the present study is focused on the saturation mechanism. Notice that the first oscillation regime is obtained without difficulty during every decrescendo cases (figure 3b).

Experiments show that the extinction threshold  $P_{extup}$  is significantly influenced by the termination geometry in the increasing pressure (crescendo, figure 3a). The termination with the more rounded edges leading to the larger playing range ( $P_{extup}$  around 10500 Pa). On the contrary, the termination with sharp edges leads to the smaller playing range ( $P_{extup}$  around 8500 Pa). This is explained by the fact that sharp edges lead to a high non linear loss coefficient. From the musical point of view,

the dynamic level and the playing range is increased when the losses are minimised. At the opposite, the mouth pressure  $P_{thdown}$  for which the oscillations appear is not influenced by the termination geometry (decrescendo, figure 3b),  $P_{thdown}$  is about 6000 Pa. Moreover figure 3b shows only slight differences between the curves for different terminations. This is explained by the fact that the different terminations imply non linear losses which are not prominent below the pressure threshold  $P_{thdown}$ .

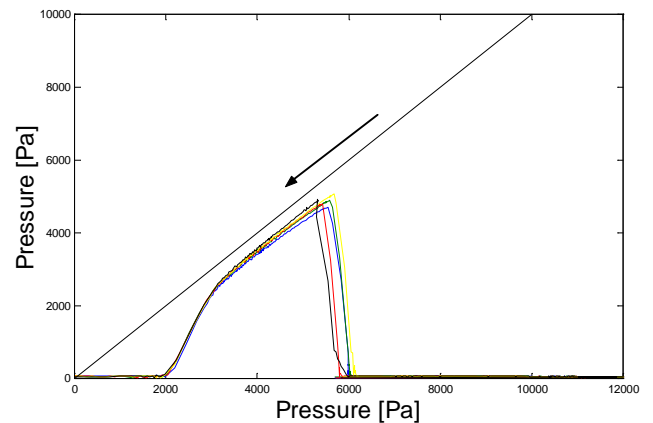
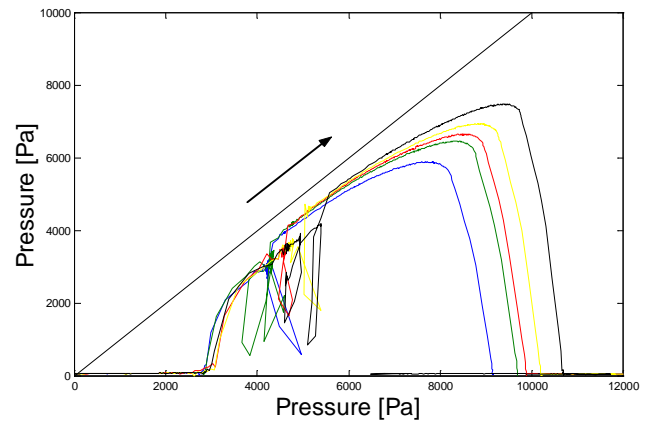


Figure 3: Experimental acoustic pressures corresponding to different terminations : (a) crescendo case, (b) decrescendo case. The mouth pressure and the acoustic pressure in the mouthpiece (in Pa) as a function of the mouth pressure (in Pa).

## 3. SIMULATIONS

### 3.1. Simulation method

The nature of the sound production of single reed instruments is now well understood (see for example [6]). Using an elementary model for the reed and the mouthpiece, coupled with an idealised clarinet, a large range of the musical behaviour of the single reed instruments is described. The elementary model is based on two equations : one for the non linear excitation



mechanism, the reed-mouthpiece system (equation 1) and the one for the resonator, regarded as a linear system (equation 2). The two equations make the coupling between the two following variables :  $u(t)$ , the volume flow entering into the instrument, and  $p(t)$ , the acoustical pressure in the mouthpiece.

$$\begin{cases} u(t) = wH_o(1 - \frac{P_m - p(t)}{P_M})\sqrt{\frac{2(P_m - p(t))}{\rho}} & \text{if } P_m - p(t) \leq P_M \\ u(t) = 0 & \text{if } P_m - p(t) \geq P_M \end{cases} \quad (1)$$

$$\dot{p}(t) = \rho c u(t) + r(t) * (\dot{p}(t) + \rho c u(t)) \quad (2)$$

where  $w$  is the effective width of the reed channel,  $H_o$  the reed opening at rest,  $k$  the reed stiffness,  $P_m$  the mouth pressure,  $\rho$  the air density and  $c$  the speed of sound in free space. The limit value  $P_M$  for which the reed closes the opening is given by  $P_M = kH_o$ . It is the minimum value of the mouth pressure above which the static solution corresponding to the reed blocked against the lay is stable. As a first approximation, the clarinet is approximated with a pure cylinder open at the end. Ignoring losses, the reflection function is a delayed Dirac function :

$$r(t) = -\delta(t - 2\tau) \quad (3)$$

where  $\tau = L/c$ . In that case the convolution equation (equation 2) can be simply rewritten :

$$\dot{p}(t) = \rho c u(t) + p_{inc} \quad (4)$$

The two equations 1 and 4 yield to a non linear equation with only one unknown at the present time  $t$ , the acoustical pressure  $p(t)$  :

$$\dot{p}(t) - \rho c F_{NL}[p(t)] - p_{inc} = 0 \quad (5)$$

where  $F_{NL}$  is the non linear relationship defining  $u(t)$  as a function of  $p(t)$  (equation 1). In the case of the lossless cylindrical tube, assuming that the sampling frequency  $F_s = 1/\Delta t$  is given by  $F_s = 1/2\tau$  (i.e.  $\Delta t = 2\tau$ ), equation 5 yields to :

$$p(n) - \rho c F_{NL}[p(n)] + p(n-1) + \rho c F_{NL}[p(n-1)] = 0 \quad (6)$$

where  $p(n)$  and  $p(n-1)$  are the acoustical pressure at  $t = n\Delta t = 2n\tau$  and  $t = (n-1)\Delta t = 2(n-1)\tau$  respectively. Then giving initial conditions, the acoustical pressure at  $t=0$ , the acoustical pressure can be calculated step by step along time. It allows to get the periodic oscillations corresponding to the fundamental regime of the clarinet-like instrument using the lowest possible sample frequency (2 points per period of oscillation).

Two kind of losses can be taken into account : the linear visco-thermal losses present in the tube and the non linear losses localised at the open end of the tube. As a second approximation for the simulations, one takes only into account the linear losses without dispersion. The attenuation parameter  $\beta$  is assumed independent on the frequency :  $\beta$  is slightly lower than one. A realistic value of  $\beta$  can be estimated by assuming that the attenuation corresponds to the visco-thermal attenuation at the playing frequency which is about 133 Hz :  $\beta = 0.97$ .  $\beta$  represents the cumulative attenuation for a travelling wave along the length  $L$  of the tube, then the reflection function becomes

$$r(t) = -\beta^2 \delta(t - 2\tau) \quad (7)$$

In that case the equation 6 can be simply rewritten :

$$p(n) - \rho c F_{NL}[p(n)] + \beta^2 p(n-1) + \rho c F_{NL}[p(n-1)] = 0 \quad (8)$$

Some simulated acoustic pressures obtained using the simulation method described above and using an increasing mouth pressure  $P_m$  (crescendo case) or a decreasing pressure  $P_m$

(decrescendo case) are done section 3.2 and compared to the experimental results given section 2.2.

### 3.2. Simulation results

The influence of the losses on the saturation mechanism is illustrated figure 4. Simulations are done using different attenuation coefficient  $\beta$  : a realistic value 0.97, and other values 0.96 and 0.94. They are obtained for a mouth pressure  $P_m$  varying linearly from 150 Pa to 15000 Pa during 22.5s (crescendo, figure 4a) and the other way round (decrescendo, figure 4b), they correspond to a medium embouchure ( $P_M = 5700$  Pa).

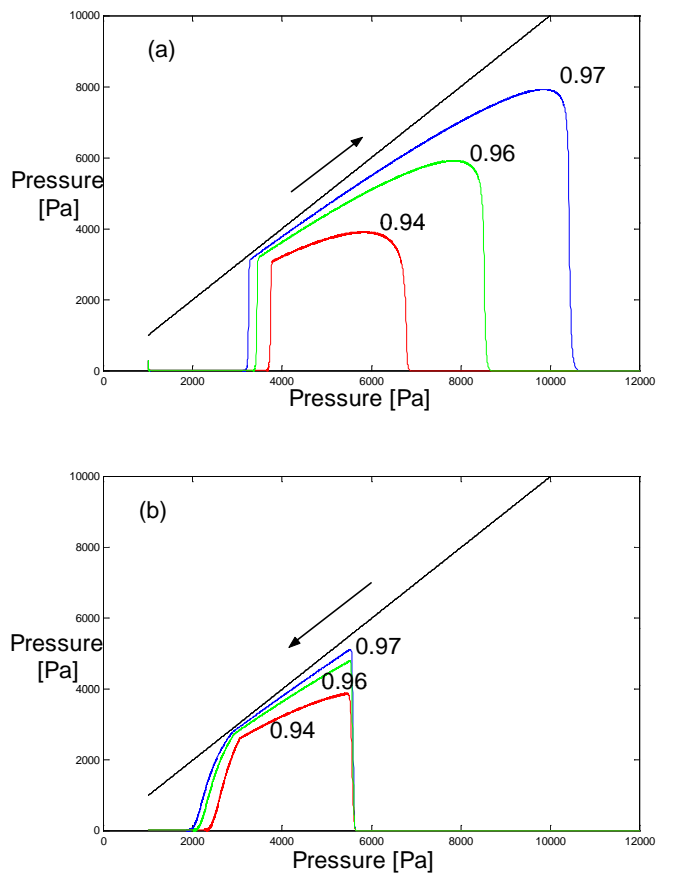


Figure 4: Simulated acoustic pressures corresponding to different attenuation coefficient  $\beta$  values : 0.97, 0.96, 0.94. (a) crescendo case, (b) decrescendo case. The mouth pressure and the acoustic pressure in the mouthpiece (in Pa) as a function of the mouth pressure (in Pa).

Some conclusions can be drawn from the crescendo simulations (figure 4a). In one hand it appears that the mouth pressure  $P_{extup}$  for which the oscillations stops is decreasing when the losses are increasing. It is infinite for  $\beta = 1$  and decreases from 10500 Pa for  $\beta = 0.97$ , to 6750 Pa for  $\beta = 0.94$ , but remains higher than 5700 Pa the value of  $P_M$ . It is clear that  $P_{extup}$  directly depends on the



losses coefficient  $\beta$ . At the opposite, the mouth pressure  $P_{thdown}$  for which the oscillations appear is not influenced by the losses (figure 4b).  $P_{thdown}$  remains always close to  $P_M=5700$  Pa when  $\beta$  is decreasing from 0.97 to 0.94,  $P_{thdown}$  is slightly lower than  $P_M$ . Notice that  $P_{thdown}$  is depending on the way how the decrescendo is simulated : if the decrescendo is run more slowly, then  $P_{thdown}$  reaches the limit value  $P_M$ . The simulations are qualitatively consistent with the experiments discussed section 2, showing the critical part of the amount of losses in the process. This hysteretic phenomena suggests that the clarinet-like system exhibits an inverse bifurcation at the extinction.

#### 4. CONCLUSIONS

It is shown by doing time domain simulations that frequency independent linear losses are sufficient to describe qualitatively the saturation phenomenon observed experimentally using an artificial mouth. The extinction mouth pressure decreases when the losses amount increases during a crescendo process. On the contrary during a decrescendo process the threshold of oscillation is not significantly influenced by losses. This suggest an inverse bifurcation scheme where the losses term is a decisive parameter. Moreover the experiments show that non linear losses have a significant influence on the playing range of a clarinet-like instrument. Especially it is shown that rounded edges may increase the playing range. This fact is well known by instrument makers who prefer to drill conical holes instead of cylindrical holes.

#### 5. REFERENCES

- [1] Nederveen, C. J., Acoustical aspects of woodwind instruments, Northern Illinois University Press, De Kalb, Illinois, 1998.
- [2] Fletcher, N. and Rossing, T. D. , The physics of musical instruments, Springer-Verlag, New-York, 1998.
- [3] Dalmont, J. P., Ducasse, E. and Ollivier, S., Saturation mechanism in reed instruments, Proc. Forum Acusticum, Sevilla, Spain, 2002.
- [4] Gazengel, B. , Caractérisation objective de la qualité de justesse, de timbre et d'émission des instruments à vent à anche simple, thèse de doctorat, Université du Maine, Le Mans, 1994 (text in french).
- [5] Atig, M., Dalmont, J. P., and Gilbert, J., Termination impedance of open-ended cylindrical tubes at high sound pressure level, submitted to C. R. Acad. Sci., 2003.
- [6] Kergomard, J., Elementary considerations on reed-instruments oscillations, in Mechanics of Musical Instruments. Hirschberg A., Kergomard J., Weinreich G. (eds). CISM courses and lectures no.355, Springer-Verlag, Wien, 1995.
- [7] Schumacher, R. T., "Ab initio calculations of the oscillation of a clarinet", Acustica, Vol. 48, 1981, p 71-85.

## VIBRATO OF SINGLE REED INSTRUMENTS

*Joël GILBERT, Laurent SIMON, Jonathan TERROIR*

Laboratoire d'Acoustique de l'Université du Maine – UMR CNRS 6613  
Avenue Olivier Messiaen, 72085 Le Mans cedex 9, France  
joel.gilbert@univ-lemans.fr

### ABSTRACT

Several alto saxophone players' vibratos have been recorded. The signals are analyzed using time-frequency methods in order to estimate the frequency modulation (vibrato rate) and the amplitude modulation (vibrato extent) of each vibrato sample. Time domain simulations of single-reed instruments vibratos are created. The model is controlled by two parameters : the mouth overpressure and a parameter characterizing the reed-mouthpiece system. Preliminary comments and comparisons between the simulated vibratos and recorded vibratos are done.

### 1. INTRODUCTION

Vibrato is one of the common ornaments in occidental classical music, particularly in singing and in wind instruments music. When the instruments are played using vibrato ornaments, deliberate fluctuations in the period and the amplitude of the acoustic pressure signals are applied.

Most of the studies dedicated to vibrato have been concerned with lyric singers (see for example [1], [2], [3]) trying to measure the properties like the vibrato rate (frequency modulation) or the vibrato extent (amplitude modulation), and then to analyse the vibrato structure along time, or to study their pitch perception. Our study is devoted to the single reed wind instruments and particularly to the alto saxophone. Following Christophe Bois (a french professional saxophone player), there are many kinds of vibratos which can be separated in two sets according to the way they are produced : (1) the vibratos "à la machoire", (2) the vibratos "sur l'air". First the aim of the study is to analyse different stable vibratos, by extracting their amplitude modulation and frequency modulation parameters. Secondly, some simulated vibratos based on the physical modelling of a clarinet-like instrument are analysed too.

The present paper is divided in four sections. After this brief introduction, the methods to extract the parameters of the amplitude modulation and of the frequency modulation, are presented in section 2. Then the methods are checked on known test signals, applied to alto saxophone players' vibratos and applied to simulated vibratos in section 3. Finally the preliminary conclusions and the perspectives of this work are discussed in the conclusion, section 4.

### 2. SIGNAL PROCESSING METHODS

The aim of the signal processing we develop in this section is to estimate both the amplitude and the frequency modulation laws of the vibrato signal. In this section, we present the expression of the so-called test signal, we recall a well-known method for estimating its envelope (or amplitude modulation) and we investigate a time-frequency method for estimating the frequency modulation.

#### 2.1. Modelling of test signal

The signal which is used in the following as a test may be written as

$$s(t) = \sum_{n=1}^{N_h} a_n(t) \cos(\phi_n(t)) \quad (1)$$

where  $a_n(t)$  and  $\phi_n(t)$  are respectively the instantaneous amplitude and phase of harmonic  $n$ , and where  $N_h$  is the number of harmonics of the playing frequency. We furthermore suppose that  $a_n(t)$  may be written as

$$a_n(t) = \gamma_n a(t) \quad (2)$$

$\gamma_n$  being the weight in amplitude modulation of harmonic  $n$ , and where the amplitude  $a(t)$  is

$$a(t) = A_0 + \sum_{k=1}^{N_v} A_k \cos(2\pi k F_m t + \psi_k) \quad (3)$$

where  $N_v$  is the number of harmonics of the vibrato frequency. In the following, we note  $\alpha_k$  the amplitude modulation rate of harmonic  $k$  of the vibrato frequency

$$\alpha_k = \frac{A_k}{A_0} \quad (4)$$

Furthermore, in the framework of permanent regime, the instantaneous phase express as

$$\phi_n(t) = 2\pi n F_s t + \sum_{k=1}^{N_v} \frac{n \beta_k F_s}{F_m} \cos(2\pi F_m t + \chi_{nk}) \quad (5)$$

where  $\beta_k$  is the vibrato rate of harmonic  $k$  of the vibrato frequency. In expressions (3) and (5),  $F_s$  is the playing frequency and  $F_m$  is the vibrato frequency,  $\psi_k, \chi_{nk}$  being given phase values. We can associate to each harmonic  $n$  the instantaneous frequency

$$f_i^{(n)}(t) = \frac{1}{2\pi} \frac{d\phi_n(t)}{dt} \quad (6)$$

Inserting (5) in (6) yields

$$f_i^{(n)}(t) = nF_s \left( 1 - \sum_{k=1}^{N_v} \beta_k \sin(2\pi F_m t + \chi_{nk}) \right) \quad (7)$$

In the following, we call  $\beta_1$  the vibrato rate and  $\alpha_1$  the vibrato extent. Figure 1 shows an example of simulated signal  $s(t)$ . Figure 2 shows the associated frequency modulation. We arbitrarily choose each instantaneous frequency law as a sine signal. The most important parameters of the problem are listed in the figures.

One of the aim of the signal processing developed in this paper is to estimate the parameters of equations (2-4) and (7) :  $\gamma_n, A_k, \alpha_k, \psi_k, \beta_k, \chi_{nk}$ .

## 2.2. Amplitude modulation estimation

The first step consists in demodulating the signal  $s(t)$  in order to estimate its amplitude modulation. The used algorithm is the envelope detection. As explained in figure 3, it first squares the signal  $s(t)$ , then low-pass filters the obtained squared signal. The square root of the filtered signal is then proportional to  $a(t)$ . Once  $a(t)$  has been estimated, a synchronous detection allows to estimate the parameters of  $a(t)$  of equations (3-4).

Lastly, the usual assumption that the amplitude modulation  $a_n(t)$  is low-frequency varying while the frequency modulation  $\cos(\phi_n(t))$  is high-frequency varying is made [1].

## 2.3. Frequency modulation estimation

The second step deals with the frequency modulation (vibrato rate). A usual Short-Time Fourier Transform (STFT) is processed to the analytical signal  $z_x(t)$  obtained from  $x(t)$  according to

$$z_x(t) = x(t) + jx(t) \quad (8)$$

where  $x(t)$  is the Hilbert transform of  $x(t)$ . We recall the expression of the STFT

$$\rho_{x,h}(t_0, f) = \int x(t) h^*(t - t_0) e^{-j2\pi ft} dt \quad (9)$$

where  $h(t)$  is chosen window. Then, for each harmonic  $n$  of the playing frequency, linked to a given bandwidth (or frequency spreading)  $\Delta F_n$ , the instantaneous frequency is estimated from [1]

$$\hat{f}_i^{(n)}(t) = \frac{\int_{\Delta F_n} f |\rho_{x,h}(t, f)|^2 df}{\int_{\Delta F_n} |\rho_{x,h}(t, f)|^2 df} \quad (10)$$

where we suppose that the successive bandwidths do not overlap. Even it is well-known that the estimation of the instantaneous frequency from (10) is biased [1], it was proved that this estimation tends to the exact instantaneous frequency when the support of the window tends to infinity. We will consequently use large windows for applying (10).

Once  $f_i^{(n)}(t)$  has been estimated, a synchronous detection allows to estimate the parameters of equations (7).

## 3.RESULTS

In this section we focus on modulation laws such that  $N_v=1$  in equations (3), (5) and (7) (harmonic modulation).

### 3.1 Method Validity

In order to test these methods, several test signals were synthesized, which include real signal modulation rates :  $\alpha_i$  in [5-75]% and  $\beta_i$  in [0,1-10]%.

The analysis of results given by the methods applied to test signals shows that :

- (1) Estimations of modulation frequencies (for amplitude and frequency) imply an error rate less than 1% of the expected  $\alpha_i$ .
- (2) Estimations of central frequencies of the six first harmonics are in the same order of error for  $\alpha_i$  in [5-75]% and  $\beta_i$  in [0,1-2,5]%.
- (3) Estimation error of amplitude modulation decreases with  $\alpha_i$ . For example, for a theoretical  $\alpha_i$  equal to 0,5 the error is less than 1%, and for a theoretical  $\alpha_i$  less than 0,05, the maximum error is around 7%.
- (4) The estimation of the modulation frequency is linked to the choice of  $\alpha_i$ ,  $\beta_i$  and to STFT parameters. Nevertheless, for the first vibrato harmonic estimation, the estimation error is less than 3%.

The main limitation of these methods seems to be for harmonic with very weak amplitude modulation rate compared to other components. For example if the second harmonic amplitude is about 1% of the amplitude of the first harmonic, problems may occur in the estimations of several parameters.

In conclusion, the methods described in section 2 can be consider reliable in most of the cases, despite of some possible further improvements.

### 3.2 Real Signals

Real signals have been recorded by a professional saxophonist. Those different recordings are representative of the main techniques used by woodwinds players to produce a vibrato in occidental classical music. From the player point of view, all these vibratos can be classified in two classes : the vibratos called "sur l'air" and the vibratos called "à la mâchoire", the last one being played mainly with soft tones. All the vibratos are analyzed by estimating the values of the  $\alpha_i$  and  $\beta_i$  parameters.

Several vibratos of the "à la mâchoire" class have been analyzed, the tendencies are  $\alpha_i$  in [5-25]% and  $\beta_i$  in [0,1-1]%. A typical vibrato from the "sur l'air" class has been analyzed, an amplitude modulation rate  $\alpha_i$  equal to 26% and a frequency modulation rate  $\beta_i$  equal to 2% are found. These preliminary results do not indicate a straightforward conclusion, nevertheless it seems that the lower values of both the parameters  $\alpha_i$  and  $\beta_i$  are found in the "à la machoire" vibrato class.

### 3.3 Simulated Signals

The nature of the sound production of single reed instruments is now well understood (see for example [5]). Using an elementary model for the reed and the mouthpiece, coupled with an idealized clarinet, a large range of the musical behavior of the single reed instruments is described. The elementary model is based on two equations : one for the non linear excitation mechanism, the reed-mouthpiece system (equation 11) and the one for the resonator, regarded as a linear system (equation 12). The two equations make the coupling between the two following variables :  $u(t)$ , the volume flow entering into the instrument, and  $p(t)$ , the acoustical pressure in the mouthpiece.

$$\begin{cases} u(t) = wH_o \left(1 - \frac{p_m - p(t)}{P_M}\right) \sqrt{\frac{2(p_m - p(t))}{\rho}} & \text{if } p_m - p(t) \leq P_M \\ u(t) = 0 & \text{if } p_m - p(t) \geq P_M \end{cases} \quad (11)$$

$$p(t) = \rho c u(t) + r(t) * p(t) + \rho c u(t) \quad (12)$$

where  $w$  is the effective width of the reed channel,  $H_o$  the reed opening at rest,  $k$  the reed stiffness,  $p_m$  the mouth pressure,  $\rho$  the air density and  $c$  the speed of sound in free space. The limit value  $P_M$  for which the reed closes the opening is given by  $P_M = kH_o$ . It is the minimum value of the mouth pressure above which the static solution corresponding to the reed blocked against the lay is stable. The reflection function  $r(t)$  of the cylindrical tube takes into account the visco-thermal losses. In order to get oscillations a simulation technique in discrete time-domain is adapted from [6]. Assuming the control parameters ( $P_m$ ,  $H_o$ ,  $k$ ) to be constant, periodic oscillations are obtained in permanent regimes after a short transient. A way to reproduce vibratos by simulations is to use control parameters slowly varying in time. Typically, simulations have been done using control parameters varying harmonically at 5Hz.

Three simulations corresponding to each one of the three control parameters  $P_m$ ,  $H_o$  and  $k$  have been done. The modulation rate of each parameter is equal to 5 Hz, and the modulation extent is equal to 10% of their mean value. Then the three simulated signals have been analyzed using the signal processing methods described in section 2 in order to evaluate the values of  $\alpha_i$  and  $\beta_i$ . The results are :

- (1) An amplitude modulation rate  $\alpha_1$  equal to 9.4% and a frequency modulation rate  $\beta_1$  equal to 0.12% if the control parameter  $P_m$  is modulated harmonically.
- (2) An amplitude modulation rate  $\alpha_1$  equal to 3.3% and a frequency modulation rate  $\beta_1$  equal to 0.22% if the control parameter  $k$  is modulated harmonically.
- (3) An amplitude modulation rate  $\alpha_1$  equal to 3.3% and a frequency modulation rate  $\beta_1$  equal to 0.06% if the control parameter  $H_o$  is modulated harmonically.

These preliminary results show that the mouth pressure mainly controls the amplitude modulation. The reed stiffness mainly controls the frequency modulation. But each control parameter does influence both the amplitude and frequency modulations significantly.

Now the task is to determine which control parameter is the predominant one when the saxophone player is doing a vibrato. At this stage the following assumptions could be done: (1) the "sur l'air" vibrato class is associated to a variation of the control

parameter  $P_m$ , (2) the "à la machoire" vibrato class is associated to a variation of the control parameters  $H_o$  and  $k$ .

## 4. CONCLUSIONS

In this paper some reed instruments vibratos have been studied. Suited signal processing methods have been developed in order to estimate parameters of amplitude and frequency modulations. First the methods have been validated for test signals, then they have applied to real saxophone vibrato sounds, and to simulated clarinet-like vibrato sounds. The methods are able to estimate the characteristics of the vibrato, the vibrato extent and the vibrato rate, with errors less than 5%. Works are in progress for using these methods for classifying different vibratos in large databases.

## 5. REFERENCES

- [1] D'Allessandro, C., and Castellengo M. "The pitch of short-duration vibrato tones", J. Acoust. Soc. Am., Vol. 95, 1994, p1617-1630.
- [2] Prame, E. I. "Measurements of the vibrato rate of ten singers", J. Acoust. Soc. Am., Vol. 96, 1994, p1979-1984.
- [3] Arroabarren, I., Zivanovic, M., Bretos, J., Ezcurra, A., and Carlosena, A., "Measurements of vibrato in lyric singers", IEEE Trans. on Instrumentation and Measurement, Vol. 51, 2002, p 660-665.
- [4] Cohen, L., Time-frequency analysis, Prentice Hall, New-York, 1995.
- [5] Kergomard, J., Elementary considerations on reed-instruments oscillations, in Mechanics of Musical Instruments. Hirschberg A., Kergomard J., Weinreich G. (eds). CISM courses and lectures no.355, Springer-Verlag, Wien, 1995.
- [6] Schumacher, R. T., "Ab initio calculations of the oscillation of a clarinet", Acustica, Vol. 48, 1981, p 71-85.

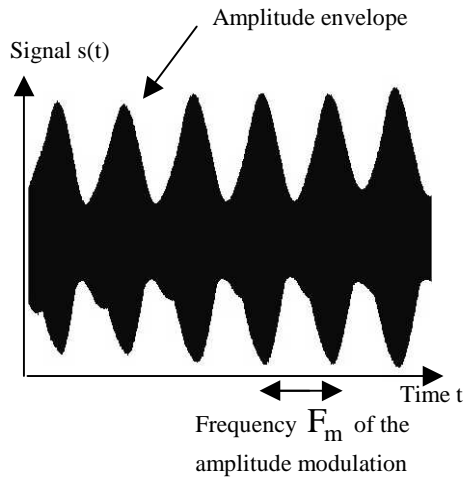


Figure 1: Simulated signal  $s(t)$  defined by equation (3).

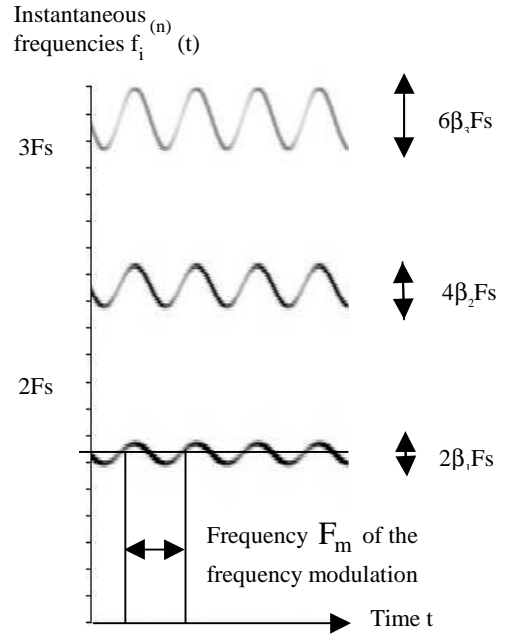


Figure 2: Time-frequency representation of the simulated signal  $s(t)$  of figure 1 according to equation (6).

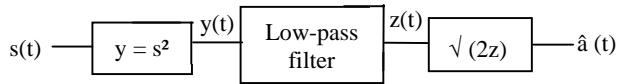


Figure 3: Schematic diagram of envelope detection processing.

## **ACOUSTICAL AND PSYCHOACOUSTICAL INVESTIGATIONS OF THE EFFECT OF CROOK BORE PROFILE ON THE PLAYABILITY OF BASSOONS**

*T.J.W. Hill and D.B. Sharp*

Acoustics Group, Department of Environmental and Mechanical Engineering, Open University,  
Milton Keynes, MK7 6AA, United Kingdom  
T.J.Hill@open.ac.uk, D.Sharp@open.ac.uk

### **ABSTRACT**

Bore profile measurements from a selection of different bassoon crooks (bocals), taken using acoustic pulse reflectometry, are presented and the key differences highlighted. Input impedance measurements of a standard bassoon using various fingerings and the same set of crooks are also presented. Between-crook comparisons are made using modal parameters to characterise the impedance curves. Key features in the input impedance curve thought to influence players' performance on the bassoon are discussed and psychoacoustical investigations of players' appraisals of the effect of different crooks are proposed.

### **1. INTRODUCTION**

The work presented in this paper constitutes an introduction to a series of experiments which follow-up earlier investigations of the effect of crook bore profile on the sound produced by the bassoon [1]. In that work the bore profiles of a selection of crooks produced by a number of manufacturers at various stages throughout the 20th century were measured. Significant differences in bore profile were found between crooks made by the German maker Heckel and other manufacturers, with the exception of a recent crook by Yamaha which closely resembled the Heckel profile. Subsequently, paired comparison listening tests were performed on selected steady-state portions of tones played by two accomplished players on different bassoons. The stimuli were recorded at four different pitches and were processed to account for differences in loudness and transients. The results of the listening tests showed that for certain pairs of crooks a detectable difference in the sound quality was perceived and that this difference was dependent on the pitch of the stimuli. However, no satisfactory correlation was found between the measured differences in crook bore profile and the perceived differences in the sound quality, and as such it was difficult for a link between bore profile and timbre to be established. Problems due to differences in crook length, and hence intonation, were also acknowledged as a complicating factor.

The experiments reported and proposed in this paper aim to address the problems encountered in the previous study and to move the psychoacoustics towards measuring the player's perception of the performance of the crook as opposed to the listener's. The overall aim is still to identify how differences in the bore profile of the crook affect the acoustical and hence musical performance of bassoons and subsequently to identify which acoustical features are desirable and how they might be achieved in practical terms when designing and manufacturing a crook.

### **2. METHODS AND RESULTS**

In this section we briefly describe the experimental and theoretical techniques that are used in this investigation.

#### **2.1. Crooks, Bassoon and Subjects**

For reasons of consistency the impedance measurements we report in this paper and the subsequent psychoacoustics experiments in this study are and will be performed on a standard bassoon, a Boosey and Hawkes, La Fleur instrument, serial number 237. The four crooks (listed in Table 1) for which data are presented in this paper are a representative subset of the large selection of crooks being investigated in the overall study.

#### **2.2. Reflectometry Measurements of Bore Profile**

The bore profiles of the crooks were measured using the non-invasive technique of acoustic pulse reflectometry. This technique is ideally suited to measuring the bore profile of short, gently tapered, virtually circular cross-section ducts, such as bassoon crooks, to within  $\pm 0.1$  mm in radius. The technique involves accurately measuring the input impulse response of the test object. Assuming plane wave propagation and with knowledge of the attenuation of the sound wave in the duct, this allows the bore profile to be computed via a layer-peeling algorithm. A 6 m long, 10 mm diameter, source-tube, with a Knowles electret microphone mounted halfway along its length and a 0.5 m dc-tube were used. This gave an operating bandwidth of around 10 kHz. A schematic diagram of the apparatus is shown in Figure 1. Further details pertaining to this method can be found elsewhere in the literature [2, 3]. The crooks were measured by injecting the sound pulse at the wider end of the crook as this avoids potential problems of a significant jump in the cross-section between the dc-tube and the crook. Bore profiles for four crooks are plotted in Figure 2.

#### **2.3. Impedance Measurements**

A modified, single-microphone, capillary-based impedance apparatus, using a two-calibration-volume approach was used to measure the input impedance of the crooks and the bassoon plus crook. The frequency range was swept in 1 Hz increments from 50 Hz to 5 kHz. Input impedances were measured on the crooks

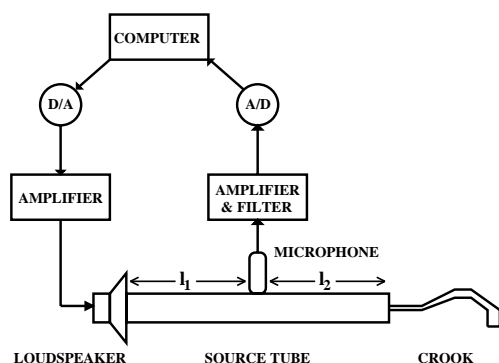


Figure 1: Schematic diagram of the reflectometry apparatus

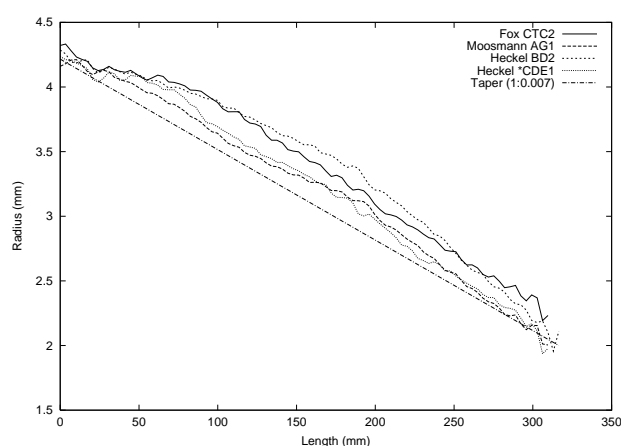


Figure 2: Plots of the bore profile for four crooks.

with a coupler fitted to the narrow end of the crook. The volume of the coupler was chosen to match the volume of an average reed. Similarly, input impedances were measured on crooks when attached to the bassoon when the fingering for certain notes was activated, e.g.  $F_3$ .

The complex impedance data is characterised by fitting, by means of peak-picking, to a simple theoretical model in which the resonances are treated as a linear sum of uncoupled oscillators. This yields resonance frequencies,  $f_n$ ,  $Q$ -values (a measure of the damping),  $Q_n$ , and the acoustic inertance,  $M_n$ , for each of the  $n$  resonances, in a manner similar to that applied to admittance studies of guitars [4]. This enables a quantitative comparison of the input impedances and the acoustic influence of different crooks on the overall input impedance of the whole instrument.

Figure 3 shows the magnitude of the input impedance for the four crooks and Table 1 gives the parameters extracted from these impedance measurements. Figure 4 shows the magnitude of the input impedance for the standard bassoon whilst fingering note  $F_3$  when fitted with the same four crooks.

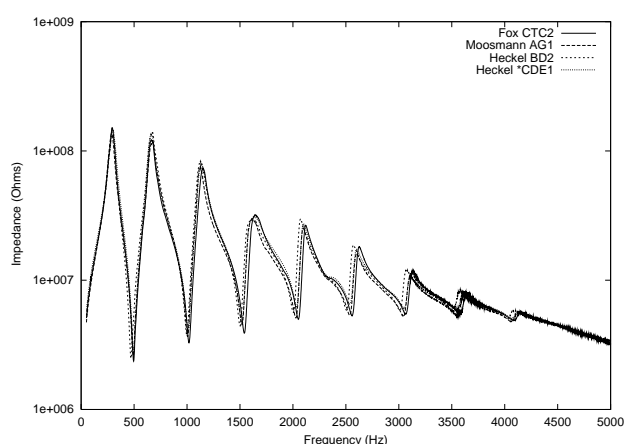


Figure 3: Graphs of the impedance magnitude for four crooks.

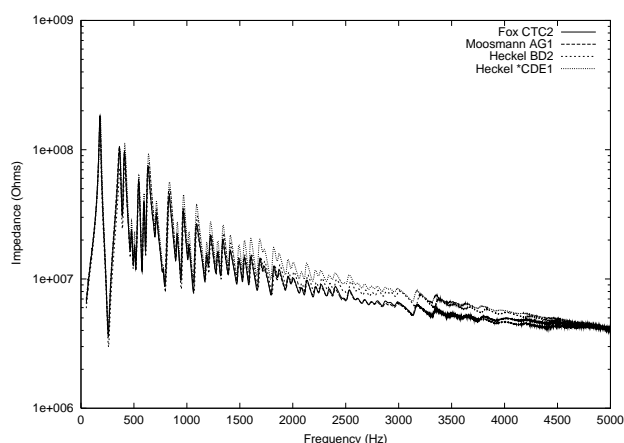


Figure 4: Plots of the impedance magnitude for four crooks on the La Fleur bassoon whilst fingering  $F_3$ .

The plots clearly show that the different crooks profiles influence the impedance of the instrument, particularly in the higher registers where the Heckel crooks are found to produce a higher overall impedance level than the newer crooks by Fox and Moosmann.

## 2.4. Waveform and Spectral Analysis

Recording the subjects whilst they play on the crooks and the standard bassoon during the psychoacoustic tests will provide an additional wealth of data. The psychoacoustic tests and recordings will be carried out in the recital room of the Music Department at the Open University. This will enable us to look for correlations between the subjective appraisal results and the acoustic performance of the crooks plus bassoon. In particular, the nature of the steady state spectrum and the transient responses will be analysed.

Parameter	$f_n$	$Q_n$	$M_n$
Mode (n)	(Hz)		( $\text{kgm}^{-4}$ ) $\times 10^{-12}$
Fox CTC2			
1	294	7	24.2
2	663	12	23.8
3	1144	19	36.3
4	1630	20	66.6
5	2113	40	137.4
6	2613	44	199.1
7	3113	51	398.5
Moosmann AG1			
1	288	6	24.8
2	667	11	22.2
3	1119	20	39.9
4	1598	20	768
5	2088	38	140.9
6	2588	43	236.2
7	3090	50	459.0
Heckel *CDE1			
1	296	7	25.1
2	666	11	18.8
3	1121	18	31.3
4	1591	16	60.3
5	2066	36	113.9
6	2562	39	181.2
7	3058	47	382.3
Heckel BD2			
1	300	6	21.6
2	661	12	20.7
3	1131	18	32.7
4	1609	16	58.9
5	2091	39	134.7
6	2588	39	207.5
7	3097	45	413.4

Table 1: Table of the acoustical parameters extracted from the input impedance of four different crooks.

## 2.5. Psychoacoustical Playing Tests

Psychoacoustical tests to evaluate players' appraisals of a selected number of crooks have been devised. These are based on a paired-comparison paradigm in which players will be asked to assess a particular feature of the performance of the crook when playing a particular passage and indicate which of the pair of crooks is better. In this way the crooks can be subjectively ordered according to their performance with exercises. The exercises devised include assessment of the dynamic or power *fff* achievable on sustained notes (Figure 5a), assessment of the control of a *p* to *ppp* *diminuendo* on sustained notes (Figure 5b), assessment of the ease of speaking or attack of rapidly repeated notes (Figure 5c), assessment of ease of achieving intonation of octaves (Figures 5d and 5e). These tests will be administered in

different playing ranges of the instrument, as in Figures 5a, b and c. An assessment of the performance of each crook in different registers using short excerpts is also proposed. Finally, players will be asked briefly to play *ad lib.* and give a free verbal appraisal as they might do when choosing a crook under normal circumstances.

Due to the inherent ergonomic interaction of the player with the crook and bassoon it is virtually impossible to implement a true 'blind' study. The experimenters aim to keep the pace of the tests and rate of crook changes sufficiently high so that players are less able to track the changes and so make judgments based their immediate experience. The role and influence of the reed is also impossible to factor out between subjects. Barring disasters, subjects will only be allowed to play on one reed throughout the psychoacoustic test session. If time permits players may be able to repeat the experiments on their own instrument. All sessions will be recorded for future cross-analysis of the waveforms and spectra.

## 2.6. Psychoacoustical Listening Tests

There are currently no plans to carry out further listening tests until after the data from the playing tests has been gathered and analysed. Clearly, the recordings from the psychoacoustic playing tests are a potential source of stimuli should further listening test be deemed appropriate.



Figure 5: Sample musical excerpts for use in psychoacoustical playing tests, a) testing volume, b) testing diminuendo control, c) testing attack, d) testing octave intonation and f) testing chromatic octave intonation.



## 2.7. Theoretical Modelling

Using a simple cones and cylinders approach to modelling the profile of the crooks and the standard bassoon, we hope to be able to predict how changes to the crook bore profile affect the input impedance curve and subsequently the parameters that describe a particular resonance feature. This should lead to a clearer understanding of which properties of particular resonances are affected most by certain changes in crook bore profile. Using this approach it will be possible to compare the effect of crook profiles outside of the range of those profiles of crooks in circulation today.

## 3. DISCUSSION

So far, reflectometry measurements indicate that there are a wide range of crook bore profiles. One of the remaining difficulties is acquiring crooks from different (or the same) makers that are of similar length in order to avoid inadvertent subjective judgments based on intonation. Differences in length are apparent both from the reflectometry measurements (Figure 2) and the resonance frequencies derived from input impedance measurements (Figure 3). Discussions with makers and players also suggest that, as a result of the manual nature of the manufacturing process, there is potential for some degree of variation between crooks that are nominally supposed to have the same bore profile. The extent of this variation has yet to be assessed.

Measurements suggest that the input impedances are subtly but critically different. This is reflected in the values of the modal parameters extracted from the data (listed in Table 1). These differences account for the more noticeable differences in the input impedance of the whole instrument (Figure 4).

The task now is to use the psychoacoustical techniques to attempt to correlate perceived differences in playing characteristics with different profiles and subsequently different modal parameters. Having discovered which resonances and parameters have a dominant role in the perceived performance of a crook and bassoon combination it remains to explore theoretically how changes to the crook bore profile map onto changes in the input impedance of the crook and the crook and bassoon combined.

This, of course, assumes that the majority of the acoustical performance of the crook is derived from the bore profile. However, if one talks to any bassoonist or crook maker it will soon become apparent that the received wisdom is that the wall material and wall thickness are perceived to have a significant affect on the performance of a crook and or bassoon. Responding to this aspect would require the application of work similar to that being carried out in our laboratory on brass instruments [5] and would constitute a whole new possible avenue for future research once the role of the bore profile is better understood.

## 4. CONCLUSIONS

The aim of these investigations is to; (1) survey the range of bassoon crook bore profiles in common circulation today, (2) to measure the input impedance characteristics of those crooks in isolation and on a standard bassoon, (3) to measure the subjective appraisal of those crooks in prescribed performance situations, (4) to begin to identify which resonance features are important and (5) to correlate these features with the bore profile of the crook. So far we have succeeded in (1) and (2) and the characterization of the resonance features as required for (4). The psychoacoustical tests required for (3) are in progress and therefore we will be able to report on the outcomes of (5) in the near future. It is anticipated that the results will help the makers of bassoon crooks to focus their efforts in developing the elusive ideal crook and will help players to better match crooks to their instruments.

## 5. ACKNOWLEDGEMENTS

The authors gratefully acknowledge William Waterhouse, for lending us older crooks and for contributions to the design of the psychoacoustic test material, William Ring of Howarths, for advice and supplying a bassoon and crooks, the bassoon makers; Fox, Moosmann, Schreiber and Yamaha for contributions, including the loan of contemporary crooks, and the bassoonists who have volunteered as playing subjects. We also acknowledge the financial support from the Leverhulme Trust.

## 6. REFERENCES

- [1] Sharp, D.B., Wright, H.A.K. and Ring, W., "An acoustical investigation into the effect of the crook profile on the sound produced by the bassoon", *Acustica*, 89(2):137-144, 2003.
- [2] Buick, J.M., Kemp, J., Sharp, D.B., van Walstijn, M., Campbell, D.M., and Smith, R.A. "Distinguishing between similar tubular objects using pulse reflectometry: A study of trumpet and cornet leadpipe" *Meas. Sci. Technol.*, 13:750-757, 2002.
- [3] Sharp, D.B. "Acoustic pulse reflectometry for the measurement of musical wind instruments" PhD Thesis, University of Edinburgh, 1996.
- [4] Hill, T.J.W., Richardson, B.E. and Richardson, S.J. "Acoustical parameters for the characterisation of the classical guitar" accepted for publication in *Acustica* 2002.
- [5] Whitehouse, J.W., Sharp, D.B. and Hill, T.J.W. "Wall vibrations in musical wind instruments", in print, invited article submitted to the *Inst. of Acoustics, Acoustics Bulletin*, summer 2003.

# **RIAM (REED INSTRUMENT ARTIFICIAL MOUTH) A COMPUTER CONTROLLED EXCITATION DEVICE FOR REED INSTRUMENTS**

*Alexander Mayer*

Institute for Musical Acoustics (IWK)  
University of Music Vienna, Austria

mayer@mdw.ac.at

## **ABSTRACT**

This paper describes the development and function of a computer-controlled device to excite reed instruments for music acoustic studies. On the one hand the aim of this artificial „woodwind player“ is a reproducible sound generation as close as possible to the real playing situation, but without the influence of a human player. On the other hand it provides the opportunity for a comparison of different reeds or different embouchure positions, both in conjunction with quantifying their contribution to the timbre. Due to the transparent assembly, recording of motion pictures of the reed oscillation is possible. Using the computer as a closed loop control ensures a reproducible excitation.

## **1. INTRODUCTION**

During the excitation process, the player controls the following embouchure operating values:

- lip contact pressure
- lip position
- air pressure

Normally the player is used to altering these parameters automatically without thinking about it. For quantifying the above mentioned embouchure parameters it is vital to be able to change one operating value while holding the two others constant. This is an impracticable task for human players.

Experiments with a manually driven prototype showed that it was difficult and very time consuming to set up the air pressure and the lip contact pressure manually in order to get a stable sound. Additionally, problems arose if values were altered during the excitation because of an extremely delayed reaction of the system.

One of the reasons for these effects was probably the relatively large volume of the mouth cavity. The volume of about 10 liters was the result of housing the movement parts and various sensors.

In the next step, the mechanical and motor-driven assembly of the artificial mouth with a reduced mouth cavity volume of 0.3 liter was connected to a computer which offered the possibility of varying any parameter independent of the others and reducing the reaction time dramatically.

As the shape, sizes and dimensions of Oboe-, Clarinet- and Bassoon reeds vary to a large extent, it is nearly impossible to design a "multifunctional artificial mouth" for all these instruments. As a first step the artificial mouth was designed to excite clarinets. Still the system should be adaptable for other kinds of reed instruments (e.g. double reeds).

The second prototype was designed with the following goals in mind:

- the cavity should be as small as possible
- the air pressure should be controlled automatically
- the lip contact pressure should be controlled automatically
- a lip positioning system should be implemented

## **2. HARD AND SOFTWARE CONCEPT**

RIAM can be split into three sections:

- Excitation System (mechanical assembly plus sensors)
- Data Interface (transducer, PC data interface)
- Software (application software, run time software)

### **2.1. Excitation System**

Unlike the human oral cavity, the artificial mouth of RIAM is built using transparent plastic. In comparison to the human cavity the new synthetic cavity still has a larger volume and a different surface. Inside the artificial cavity are synthetic lips on an adjustable mounting.

Stepper motors allow a controlled movement in the X and Y axes (see Figure 2). The required amount of air can be supplied by any kind of air pressure source with an output pressure of up to 10 bar. An electronic fine-tuning valve provides accurate air pressure inside the artificial mouth. A large electromagnet (solenoid) simulates the maxillary muscles.

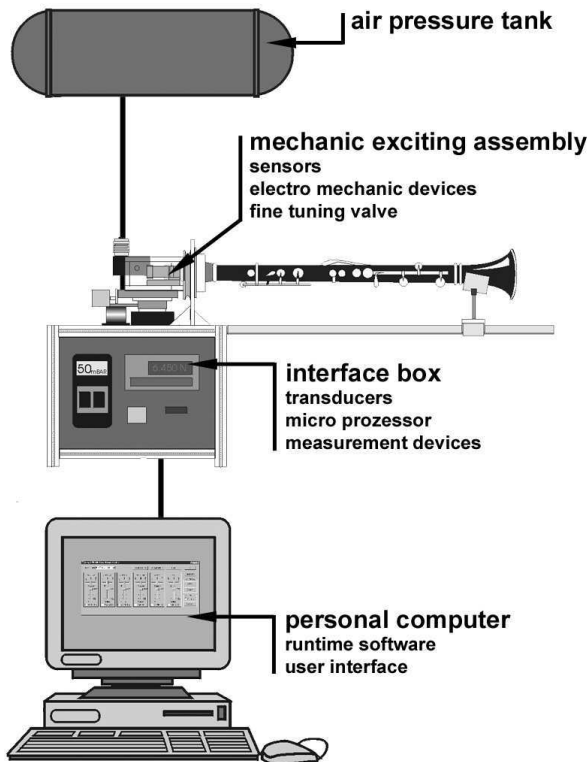


Figure 1: schematic configuration

To provide reproducible operating parameters the following sensors are used:

- air pressure gauge
- lip contact pressure gauge
- lip positioning system

All gauges have an electronic output.

## 2.2. Data Interface

To ensure noise-free signals the measurement values are digitized as near as possible to the mechanical excitation system. These readings are captured by a micro processor.

This processor has four main functions:

- Communicating with the host personal computer
- Controlling of the electromechanical devices
- Reading the measurement values
- Providing a closed-loop control for air pressure and lip contact force

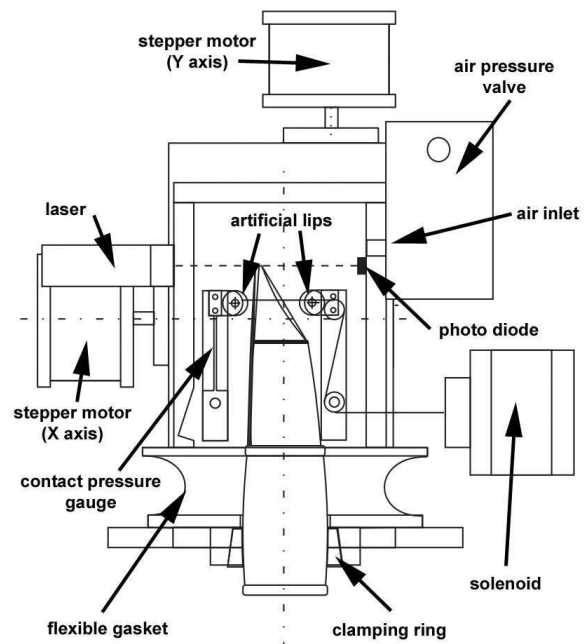


Figure 2: the excitation system.

To provide a sealed seat and to prevent grates on the instrument while mounted, a soft silicon ring clamps the clarinet barrel close to RIAM.

## 2.3. Software

The software can be split into two parts, the application software, running on the PC and the runtime software which is designed for the micro processor located in the data interface.

### 2.3.1. Application Software

The PC software is designed as a graphical user interface. By using graphic scroll bars and input text boxes the user can specify operating conditions. After entering the operating parameters the data are transferred into the memory of the micro computer. The Application software scans the micro processor and displays the current captured operation parameters on screen.

To ensure reproducible experiments these values can be stored on the PC hard disc.

### 2.3.2. Runtime Software

The runtime software has been written in assembler-code. For a real time system such as RIAM, assembler coding provides control over the execution time for a program. Every program step has been time optimized for the system. The runtime software handles the closed-loop algorithm, the stepper motor control and the data transfer to the PC.

### 3. LIMITATIONS OF THE CURRENT DESIGN

After preliminary function tests some limitations of the present version of RIAM have been discovered.

When the reed opening is large the used air pressure valve cannot provide the required amount of air.

It is important to implement the possibility of humidifying the air. With the current setup a playing test is limited to ca. two minutes depending on the thickness of the reed tip.

### 4. THE EXCITATION

After RIAM sets up communication with the PC and calibrates its positioning system, the user is asked to insert the instrument. To prevent damage to the instrument while mounting and to provide a sealed seat, a soft silicon ring clamps the clarinet barrel firmly to RIAM. A threaded cap prevents slippage in the clamping ring and a supporting arm keeps the instrument stationary and fixes it over the whole length.

Because of the different sizes and shapes of the reed instrument types, RIAM initializes the embouchure position each time an instrument is inserted. During this initialization the embouchure system samples the accurate position of the mouthpiece using a laser. This self-adjustment provides reproducible positioning of the artificial lips on the instrument.

After initialization, the user can define the operating values. In many cases the alteration of the operating values is required. Now these adjustments can be simply done during the experiment by moving the graphical scroll bars.

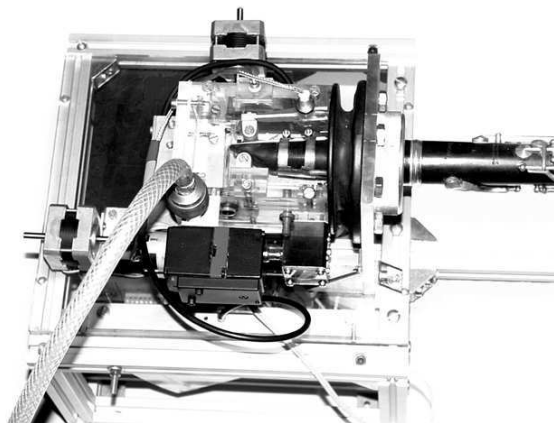


Figure 3: Top View

### 5. APPLICATIONS

#### 5.1. Recording of embouchure operation values

After the successful stabilization of the initial transients, the optimal values of lip contact pressure, lip position and air pressure can be read directly from the PC screen and stored.

#### 5.2. Optical studies

Due to the transparent assembly, stroboscopic recording of slow motion pictures of the reed oscillation is possible.

#### 5.3. Sound analysis

As the used operating values can be stored and reloaded, the main goal of RIAM is to provide an exact and reproducible sound generation. These features offer a convenient possibility to compare different reed characteristics.

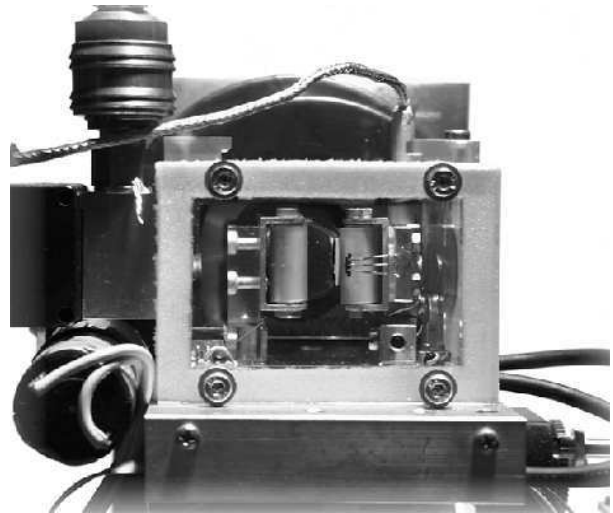


Figure 4: front detail

### 6. PRELIMINARY STUDIES

For an initial investigation with RIAM the differences of the embouchure operation values of three different types of reeds were captured at our institute by Paul Achatz, a professional clarinet player. For all measurements the same mouthpiece, a Wurlitzer W4 (Viennese type) was used.

The reed types:

- RICO plasticover 5
- FIBRACELL medium hard
- LEUTHNER professional

The FIBRACELL reed was shortened 2.5 mm to fit onto the Viennese mouthpiece.

Different embouchure positions were tested by producing tones from e3 to e4.

The procedure starts by adjusting the x- position so that the lip contact gauge is parallel to the reed. This adjustment ensures a correct measurement. The y- position is then defined and an air pressure of 50 mbar (for RICO 35 mbar) is applied. Then the lip contact pressure is increased until the reed oscillation produces a correct sound. *Figure 5* displays the correct lip contact pressure for different y- positions to excite a stable sound.

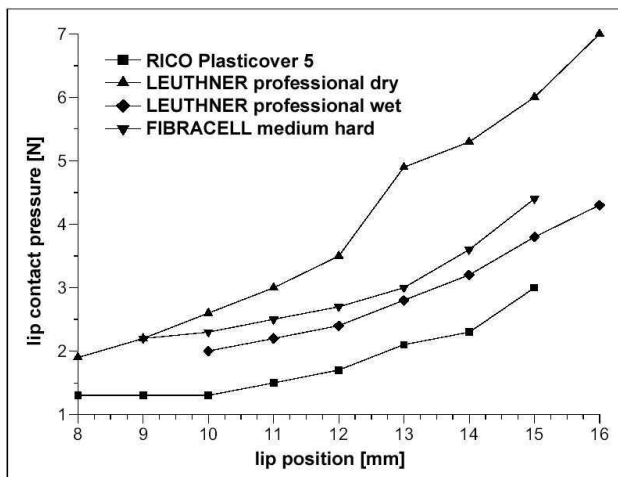


Figure 5: lip contact pressure vs. the lip position (measured from the tip of the mouthpiece)

The largest force is needed exciting the dry LEUTHNER reed. After the reed is soaked in water for a few minutes, the required lip contact pressures can be reduced significantly. Because of the dry air stream through the mouthpiece the tip of the reed dehumidifies very quickly. This effect causes a change of the spring constant of the reed and consequently a change of the reed resonance frequency. For musicians, this case occurs after a long playing pause. With a "dry" reed it is more difficult to play the instrument, which is especially subject to "noise".

In general the lip contact pressure increases with the distance between the lip and the tip of the mouthpiece.

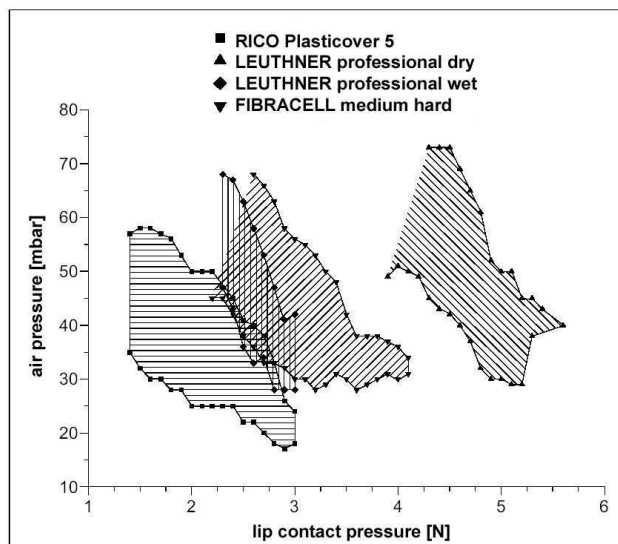


Figure 6: regions of potential sound generation for the tested reeds

To study the interaction between lip contact pressure and air pressure a practical embouchure position on the basis of Figure 5 was selected.

On the one hand the positions were chosen to be in the middle of the useable embouchure region, and on the other hand to provide enough range for variation of the lip contact pressure. The selected lip positions are 13 mm for the RICO reed, 12 mm for the FIBRACELL and the wet LEUTHNER and 11 mm for the dry LEUTHNER reed.

After adjusting the lip position on the reed, the lip force was increased in steps of 0.1 N. For each force value the possible air pressure was varied until the oscillation stops. Figure 6 displays the extracted results.

It should be noted that at low lip contact pressures the reed opening is so large (especially for the FIBRACELL and the dry LEUTHNER reed) that the air pressure valve cannot provide the required amount of air.

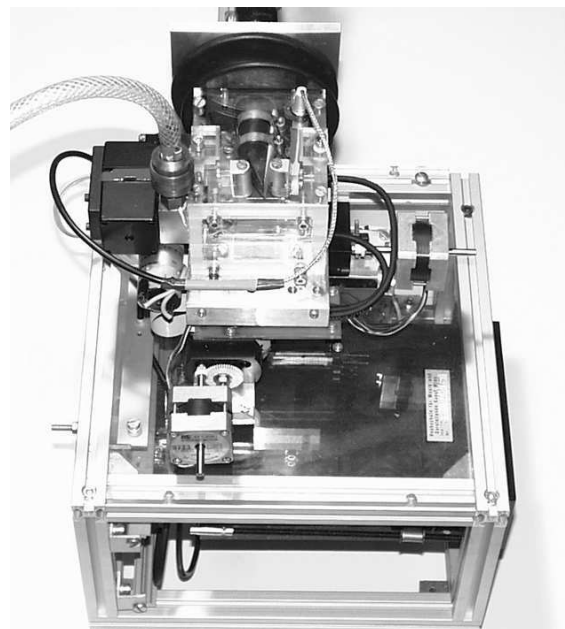


Figure 7: RIAM in use

## 6.2. Discussion of the results

For all tested reeds the determined regions look similar.

When the lip contact force is increased the air pressure must decrease for a stable sound generation.

Maximum and minimum values of the air pressure converge when the lip contact pressure is increased.

## 7. CONCLUSIONS

The presented artificial mouth for reed instruments allows a highly reproducible excitation of clarinets. First studies showed interesting differences between the embouchure parameters of different reeds. Further development at the institute will address the discussed limitations.

## EXPERIMENTAL INVESTIGATION OF CLARINET REED OPERATION

*S. Ollivier, J.-P. Dalmont*

Laboratoire d'Acoustique de l'Université du Maine-UMR CNRS 6613  
Avenue Olivier Messiaen 72085 Le Mans cedex 9, France  
jean-pierre.dalmont@univ-lemans.fr

### ABSTRACT

When the clarinet reed is submitted to a mouth overpressure, reed bends and closes progressively the reed slit. A common and intuitive idea is that the reed curls up to the table which would lead to a progressive reed stiffness increase. However, some recent works suggest that the curling up of the reed to the lay is limited, with the top of the reed touching the table before the lower part [1-4]. To investigate this, an experimental device was build in order to detect the contact area between the reed and the table while being blown by an artificial mouth. Results show that the curling up of the reed to the lay is not systematic.

### 1. INTRODUCTION

A basic model of the clarinet mouthpiece where the reed is modelled as an ideal spring of constant stiffness has been largely used in the literature [5-7]. However, some authors suggest that the vibrating length of the reed and consequently its stiffness shall vary [8]. Analytical [1] and numerical investigation [2-4] suggest that reed stiffness shall not vary so much until the top of the reed touches the lay. The reed stiffness then increases suddenly. The aim of the present paper is to examine how the reed curls up or not to the table and what are the consequences on the non-linear characteristics. The paper first presents, section 2., some theoretical considerations based on a modelling of the reed as a bending beam. Theoretical results are used to enlighten the experimental results, presented section 3, using an original device which gives information on the reed-table interaction.

### 2. THEORETICAL CONSIDERATIONS

Ignoring torsion and transverse bending, the reed can be regarded as a bending beam (see for example [9]). Torsion and transverse bending probably has a certain importance in reed operation. However, considering the reed as a bending beam makes it possible to pose the problems of the curling of the reed. The reed, which is rectilinear, is pressed against the table over a certain length beyond which the table is curved (figure 1). Accurate measurements carried out on modern standard mouthpieces show that the curve is perfectly parabolic [1] that is the radius of curvature of the table is constant. When the reed bends under the effect of a uniform pressure  $\Delta p$ , the contact area between the reed and the table increases only if the radius of curvature of the free reed  $R_{reed}$  is lower or equal to the radius of curvature of the table  $R_{curve}$ . The theory of the beams

[9] makes it possible to write by supposing the width of the reed  $w$  constant:

$$R_{reed}(x) = \frac{2E(x)I(x)}{w\Delta p(L-x)^2} \quad (1)$$

where  $E(x)$  and  $I(x)$  are respectively the Young modulus and the moment of inertia of the reed cross section at abscissa  $x$ ,  $\Delta p$  the pressure difference between both sides of the reed and  $L$  the length of the free part of the reed. In the present paper,  $x=0$  corresponds to the beginning of the free part of the reed which corresponds to the beginning of the curve of the mouthpiece and  $x=L$  corresponds to the tip of the reed (figure 1).

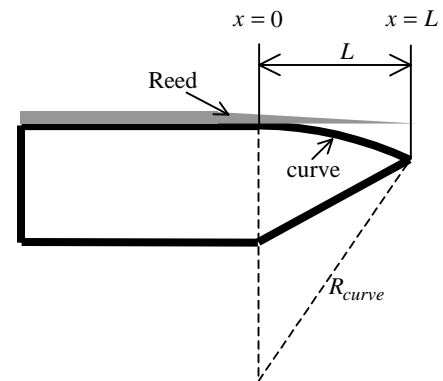


Figure 1: Mouthpiece profile (definitions).

Different cases can be considered. If the reed curvature  $R_{reed}(x)$  is independent on the abscissa  $x$ , the reed deflection is strictly parabolic. Then, the reed has the exactly the same shape as the curve of the table when  $R_{reed} = R_{curve}$ . If the reed curvature  $R_{reed}(x)$  increases the reed curls up to the table, that is the contact point between the reed and the table moves progressively forward to the tip (Figure 2.a). The abscissa of the contact point can be found by solving the following equation :

$$R_{reed}(x) = R_{curve} \quad (2)$$

On the contrary, if the radius of curvature of the reed  $R_{reed}(x)$  decreases with  $x$ , the reed bending is more important near the tip which touches the table whereas there is not contact between the beginning of the curve and the tip (Figure 2.b). If the reed curvature  $R_{reed}(x)$  is not monotonically increasing or decreasing with  $x$  many different situations can occur.

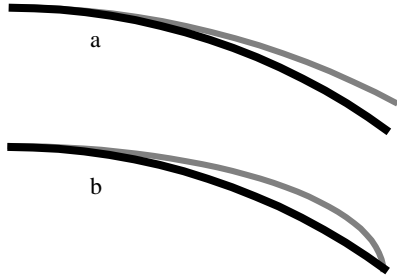


Figure 2: The two “scenarios”  
a) reed curls up to the table  
b) reed tip touches the table

To go further into simplification, the reed is now supposed to have a rectangular cross section and a nominal constant Young modulus  $E_{nom}$ . In that case the reed curvature, as  $I = we^3/12$ , is given by:

$$R_{reed}(x) = \frac{E_{nom}e(x)^3}{6\Delta p L^2(1-x/L)^2} \quad (3)$$

where  $e(x)$  is the reed thickness. Note that this formula is still valid for a non rectangular cross section and for a non constant Young modulus defining an effective thickness as  $e(x) = \sqrt[3]{12 \frac{E(x)I(x)}{wE_{nom}}}$ . Considering the following function for

the reed thickness  $e(x) = e_0(1-x/L)^\beta$  allow us to make some consideration on the reed shape.  $\beta = 0$  corresponds to a reed of constant thickness whereas  $\beta = 1$  corresponds to a reed with a triangular shape. The progressive curling up of the reed to the table is only obtained if  $\beta < 2/3$  (figure 3). If  $\beta > 2/3$  the reed tip first touches the table. The examination of a real reed as done by Walstijn [3-4] and by Ducasse [2] show that the curvature mainly decreases with  $x$ . Indeed the reed profile is closer to the  $\beta = 2$  case than the  $\beta = 2/3$  case. Moreover,  $R_{reed}(x)$  do not vary monotonically: the radius of curvature first decreases and then increases with  $x$ . This is explained by the fact that the thickness at the tip is finite. Then,  $R_{reed}(x)$  tends to infinity when  $x$  tends to  $L$ . Considering the radius of curvature of a real reed (figure 3) it could be said that the reed may in

principle not curl up progressively to the table. This conclusion is probably a bit hasty because the clarinet player presses his lip on the reed. This may result in a curling of the beginning of the reed (near  $x=0$ ). Moreover if the lip presses the reed close enough to the abscissa for which  $R_{reed}(x)$  is minimum, the curling is then possible. This suggest that the curling up of the reed to the table might be possible for a tight embouchure.

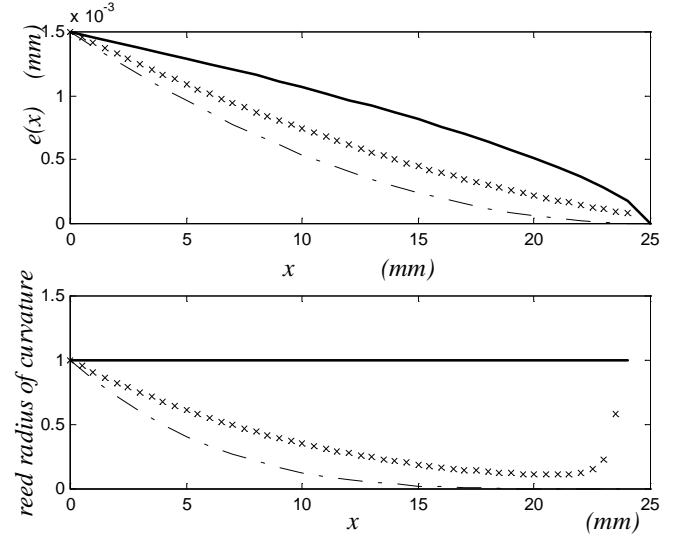


Figure 3: Reed shape and radius of curvature  
up) reed profile.

down) radius of curvature (arbitrary scale).  
continuous line:  $\beta = 2/3$  ; dashed line:  $\beta = 2$  ;  
crosses: real reed (according to Walstijn [3]).

We now investigate the influence of the reed curling on the volume flow characteristic. Neglecting reed damping and inertia and assuming a total dissipation of the kinetic energy of the entering jet, the flow is given by:

$$u = w_j(H_0 - y)\sqrt{2p/\rho} \quad (4)$$

where  $w_j$  is the effective width of the jet (ratio of the jet cross section to the reed opening),  $H_0$  the reed slit opening at rest and  $\rho$  the density of air. In the absence of curling the reed stiffness, defined as  $k = \Delta p/y$  where  $y$  is the deflection at the tip, is theoretically constant ( $y$  is linearly dependant on  $\Delta p$  for a clamped-free bar). When there is curling, the vibrating length decreases and thus the stiffness tends to increase. On the contrary when a point of the higher part of the reed touches the table without curling the stiffness is constant and then increases suddenly. On figure 4 the non-linear characteristics in the case of a constant stiffness and in the case of a variable stiffness is plotted. It is noticeable that when the stiffness becomes too large the reed slit is never totally closed. This seems to be verified in reality: experiments carried with an artificial mouth show that

the volume flow when the reed is “closed” is never completely zero.

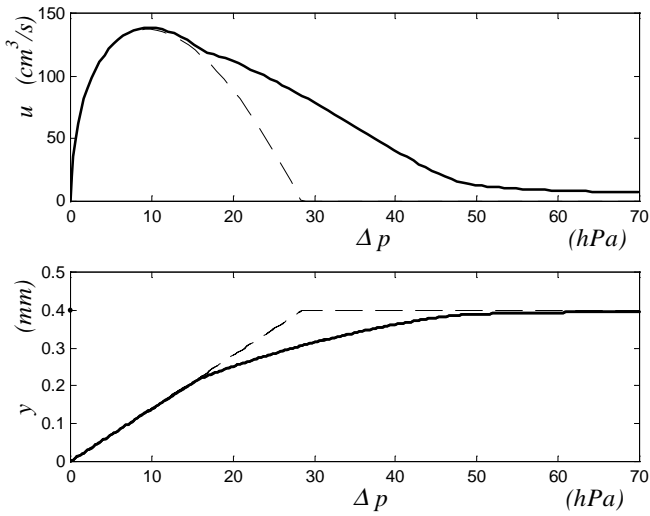


Figure 4: Tip displacement and flow versus pressure  
up) non-linear characteristics (volume flow  
versus pressure difference.  
down) tip displacement versus pressure  
difference.

dashed line : theory with constant stiffness (until closure) ;  
continuous line: theory with variable stiffness (according to  
Walstijn [3,4]);  $H_0 = 0.4\text{mm}$  in both cases.

### 3. EXPERIMENTS

In order to investigate the reed operation some experiments have been carried out using an artificial mouth. The non-linear characteristic is measured in static conditions, the clarinet being replaced by an orifice (for details see [10]). Simultaneously, in order to check if curling occurs, a device designed to evaluate the reed-table interaction has been made.

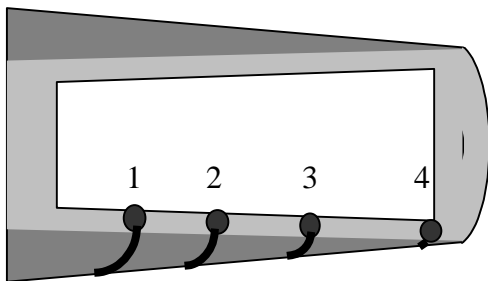


Figure 5: Electrical contacts arrangement on the table.

A series of electrical contacts, realised with a metallized painting, are laid out on the table [11]. The inner surface of the reed is also painted with the same metallized painting. The contacts voltage is fixed to 5V in the absence of contact with the reed which is grounded. When the reed touches a contact its potential falls to 0. The signals resulting from the various contacts are connected to a digital-to-analog converter. Datas are collected on a computer via a data acquisition chart. For the analysis of the results presented here only 4 contacts spaced of 12mm are used (numbered from 1 to 4 see figure 5). This system, which can be used as well in dynamic mode as in static mode, makes it possible at every moment to determine the points of contact between the reed and the table.

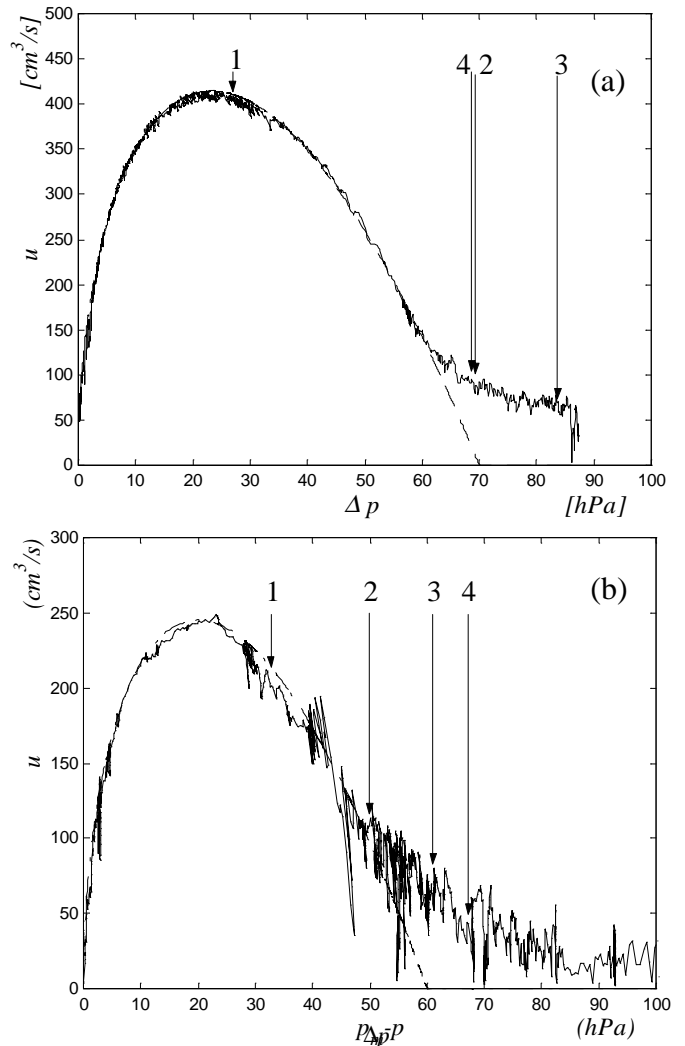


Figure 6: Experimental non-linear characteristics

a) “loose” embouchure.

b) “tight” embouchure.

continuous line: experiment ;

dashed line: theory constant stiffness.

Arrows indicate the pressure for which the electrical contacts close.



Two experiments are presented here. In these two experiments only the pressure exerted by the lip on the reed are different. This results into two different reed opening  $H_0$  and consequently into two different maximum flow (figure 6).

In both cases contact n°1 is the first closed. For the larger opening (figure 6.a) contact n°4 is closed quite simultaneously with contact n°2. This means that the tip of the reed touches the table before the middle of the reed. Finally contact n°3 closes for a higher pressure. In that case it is clear that the reed does not curl up to the table. For the smaller opening (figure 6.b) contacts 1,2,3 and 4 close successively. This suggests that in that case the reed curls up to the table. These results give confirmation that the curling up of the reed to the table might occur only for a tight embouchure. In both experiments the non-linear characteristics follow on its main part the theoretical non-linear characteristics with constant reed stiffness. Theoretical and experimental curves differ only when the reed almost closes the reed channel. Both experimental curves have a similar shape. Indeed, for the tight embouchure the curling up of the reed occurs only when the reed is almost closed which do not result in a consequential change on the non-linear characteristics.

#### 4. CONCLUSION

Our experiments show that the two “scenarios” where the reed tip touches the table and where the reed is curling up to the table can be observed. The first scenario is certainly the more probable as the second one has been only observed for a tight embouchure. This with insight justify the use of a lumped model of the mouthpiece with constant stiffness [5-7]. Our results show that the embouchure has a crucial importance. However, the reed and mouthpiece may also have a great importance. Further experiments with different reeds and mouthpieces have to be done to investigate how much this question might be important for the playability of a clarinet and consequently for the clarinet or saxophone player.

#### 5. REFERENCES

- [1] Gazengel, B., “Caractérisation objective de la qualité de justesse, de timbre et d’émission des instruments à vent à anche simple”, PhD thesis, Université du Maine, Le Mans, France, 1994.
- [2] Ducasse, E., “Modélisation et simulation dans le domaine temporel d’instruments à vent à anche simple en situation de jeu : méthodes et modèles”, PhD thesis, Université du Maine, Le Mans, France, 2001.
- [3] Avanzini, F. and van Walstijn, M., “Modelling the Mechanical Response of the Reed-Mouthpiece-Lip System of a Clarinet. Part I. A One-Dimensional Distributed Model”, submitted for publication, in Acta Acustica, 2003.
- [4] van Walstijn, M. and Avanzini, F. “Modelling the Mechanical Response of the Reed-Mouthpiece-Lip System of a Clarinet. Part II. A Lumped Model”, submitted for publication, in Acta Acustica, 2003.
- [5] Kergomard, J., “Elementary considerations on reed-instruments oscillations, in Mechanics of Musical Instruments,” Hirschberg, A., Kergomard, J., and Weinreich, G. (eds). CISM courses and lectures no. 355, Springer-Verlag, Wien, 1995.
- [6] Ollivier, S., Dalmont, J.P., and Kergomard, J., “Idealized models of reed woodwinds. Part I : analogy with the bowed string,” to be published in Acta Acustica, 2003.
- [7] Ollivier, S., Kergomard, J., and Dalmont, J.P., “Idealized models of reed woodwinds. Part II : on the stability of ‘two step’ oscillations,” to be published in Acta Acustica, 2003.
- [8] Nederveen, C.J., Acoustical aspects of woodwind instruments, Northern Illinois University Press, De Kalb., Illinois, 1998.
- [9] Gere, J.M., Timoshenko, S., Mechanics of Materials, Chapman & Hall, London, 1991.
- [10] Dalmont, J.P., Gilbert, J., Ollivier, S., “Non-linear characteristics of single reed instruments: quasi-static volume flow and reed opening measurements”, to be published in the J. Acoust. Soc. Am, 2003.
- [11] Ollivier, S., “Contribution à l’étude des oscillations des instruments à vent à anche simple : validation d’un modèle élémentaire,” PhD thesis, Université du Maine, Le Mans, France, 2002.

## RESONANCE CURVES AND FREQUENCIES IN THE MULTIHOLED OCARINA

David R. Peterson

Department of Mathematics  
University of Central Arkansas, Conway, AR, U.S.A  
DavidP@mail.uca.edu

### ABSTRACT

The traditional American Indian ocarina, dating back perhaps 5,000 years, consists of a clay vessel with 4 to 10 finger holes and a fipple (window) that splits the air jet created by the player. The ocarina is part of a larger family of whistle-like instruments and toys found in South America [1]. Musical tones are created by covering the holes in various fingering patterns. The tones do not necessarily follow diatonic or chromatic scales. The ocarina acts as a Helmholtz resonator, that is, the vessel volume  $V$  and the geometry of the holes and fipple (primarily the combined surface area) determine the resonance frequencies. In particular,

$$f = K(S/L + \sum(S_j/L_j))^{1/2} \quad (1)$$

where  $S_j$  is the surface area of an open hole and  $L_j$  is the depth, including end-correction, of the hole,  $K = (c/2\pi)/\sqrt{V}$  and  $c$  = speed of sound. For a cylinder of surface area  $S$  and length  $L$ ,  $\rho L/S$  is the acoustic inertance  $M$  ( $\rho$  = air density). The ratio  $S/L$  therefore represents the equivalent quantity  $\rho/M$  for the fipple. For a fipple with complicated geometry there is no obvious direct connection between the actual surface area  $S$  and depth  $L$  of a fipple and the value of  $\rho/M$ , although this is what ocarina builders would like to know.

### 1. INTRODUCTION

Traditional ocarinas were constructed from clay in a wide variety of forms, for example, the so called "sweet potato" in Fig. 1, rounded discs and virtually any animal form.

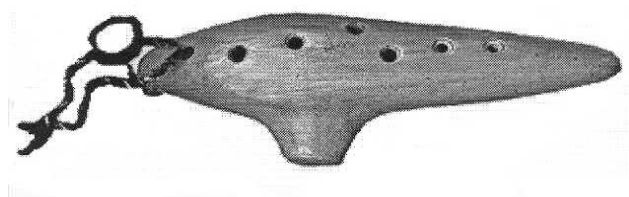


Figure 1: A "Sweet Potato" ocarina from Peru

In construction, clay is pressed into molds for the top and bottom, which are joined before firing. A pointed stick is used to form the fipple and finger holes. Since the volume of the vessel, fipple shape (oblong, circular, or rectangular), finger hole diameter, and finger hole depth is only roughly controlled, the resulting pitches are somewhat unpredictable. Uniformity of pitch seems not to have been a primary concern historically, but,

even so, ocarina bands were observed in Mexico at the time of the Spanish conquest.

Ocarinas are often designed so that the lowest frequency (all holes closed) is an octave below the highest frequency (all holes open). In any case, if the finger holes are the same size and depth (as is most often the case in traditional instruments), from equation (1) it follows that square of the frequency should increase linearly with the number of open holes. Thus western scales are not possible using only open or closed holes because they use the exponential increment  $2^{1/12}$  for a semi-tone.

Modern interest in the ocarina stems from its use among various recording groups as well as mystical use of an ocarina image and synthesized sound in the computer game Legend of Zelda.

Modern ocarinas are made from clay, wood, aluminum and plastic in just about any form. Four or more holes of different diameter are used. The simplest but least efficient design adds a different hole for each pitch of a diatonic scale of one octave. A thumb hole or two can then be added to extend the range and to approximate chromatic scales.

The most common and efficient design uses only 4 finger holes, which makes 16 fingering patterns possible. Given the fipple ratio,  $S/L$ , and the goal of an octave range (between all holes closed and all holes open), Eq. (1) can be used to show mathematically that no choice of finger hole geometry will produce an exact diatonic scale. A common compromise tuning uses hole ratios  $S_j/L_j$ ,  $j = 1, 2, 3$  to approximate a major 2<sup>nd</sup> (only hole 1 open), major 3<sup>rd</sup> (hole 2 open) and a major 5<sup>th</sup> (hole 1 and 3 open).  $S_4/L_4$  is then determined by the octave requirement when all holes are open. If one assumes the theoretical correctness of Eq. (1), cross-fingerings produce a diatonic scale with a maximum error of 1% at resonance, except for the major 7<sup>th</sup> which is significantly sharp in any 4 hole ocarina.

As more holes are opened, blowing pressure increases (a factor of about ten per octave for the ocarinas in this study) and air jet velocity increases. For high air jet velocities the fixed window no longer functions properly, that is, the distance between the air jet opening and the splitting edge becomes relatively too short for effective tone; moreover non harmonic overtones occur. As a result, the practical range of an ocarina is no more than a musical 10<sup>th</sup>.

### 2. RESONANCE CURVES FOR THE OCARINA

The fundamental in an ocarina is much stronger than other harmonics (more than 12 dB difference in sound pressure level in our ocarinas). As blowing pressure increases, the resonance frequency of the fundamental increases, but sound pressure levels of the fundamental stay relatively flat. Even for an ocarina with a distinct resonance peak as in Fig. 2, SPLs vary as

little as 2 dB over a frequency range from 185 to 200 Hz. From a practical point of view this means that a player has an effective frequency range of about a semitone by varying blowing pressure, although over-blowing noticeably increases overtones (sometimes non harmonic) and air jet noise.

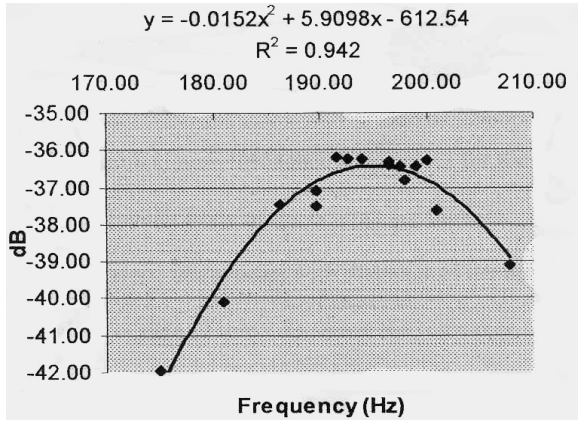


Figure 2: Resonance curve with a distinct maximum.

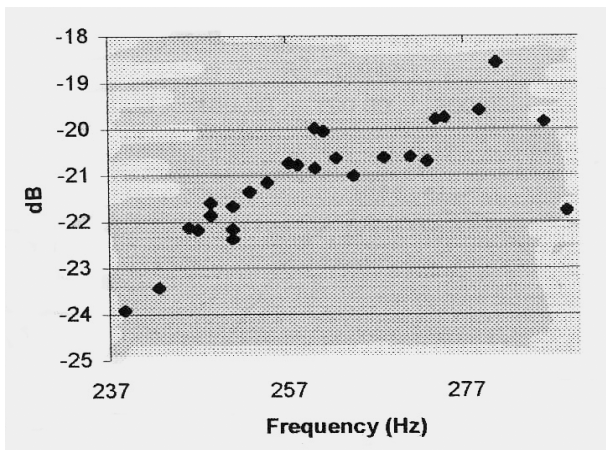


Figure 3: Non distinct resonance maximum.

With a different open-hole configuration on the same ocarina, maximums were less obvious, Fig. 3. In all cases, a quadratic curve fit was used to approximate resonance frequencies.

### 3. THEORETICAL AND EXPERIMENTAL EVIDENCE TO SUPPORT EQ. (1)

Since ocarinas are globular in shape and the overall dimensions are much smaller (4-15 cm) than the wavelengths of its resonance frequencies, it is reasonable to expect that the Helmholtz oscillator model would apply. Indeed, we found the oscillations at the finger holes to be in phase with the fipple.

To facilitate measurements, an ocarina was constructed from a plastic cylinder. A fipple from a penny whistle with a corresponding desired frequency range was installed on the cylinder, see figure 4. A large-capacity compressor with a low-

pressure gauge was used to maintain relatively constant blowing pressure. Sound pressure was measured with a microphone placed about 15 cm above the fipple in a diverse field. A Fast Fourier Transform, FFT, analyzer displayed frequency spectrum decompositions of the pressure signals. Resonance frequencies SPLs were determined from FFT analysis.

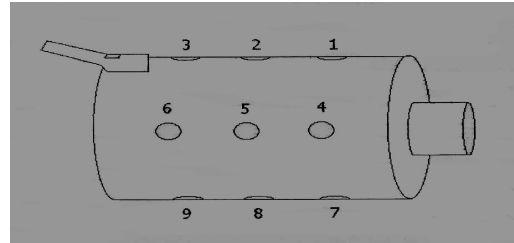


Figure 4: Plastic cylinder ocarina.

Charlie Hind, a skilled craftsman and supplier of walnut ocarina models for our experiments, had suggested that the location of finger holes might play some small role in the tuning of an ocarina. If the Helmholtz model is correct, then hole location should be irrelevant unless the holes and fipple are close enough to influence end corrections in the term  $L_j$ . Holes were drilled as indicated in Fig. 4 and no statistically significant location correlations were identified. The resonance frequencies produced by various holes differed by less than 2%.

Since resistive losses can be ignored for the size of holes used in an ocarina, a theoretical argument similar to that found in Fletcher and Rossing [3] shows that Eq. (1) is approximately correct. When all finger holes are the same diameter and depth, then from (1) the frequency squared is a linear function in the number of open holes,  $m$ ,

$$(2\pi f \sqrt{V/c})^2 = S/L + m (S_j/L_j) \quad (2)$$

With 9 finger holes, a hole diameter of 5.56 mm produced a frequency range somewhat larger than a normal playing range for an ocarina, 194 Hz (all holes closed) to 543 Hz (all holes open). The linear fit was exceptionally close in this case, Fig. 5.

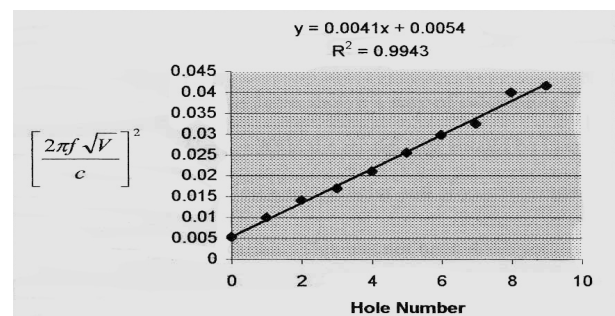


Figure 5: Linear regression for eq. (2), units = meters.

Since the curvature of the ocarina body is typically small compared to the hole size we can assume the finger holes can be modeled as holes with infinite flanges on both sides. For a pipe of radius  $a$ , the end correction for one end is  $\psi \cdot a$ , for some constant  $\psi$  ( $\psi = 0.85$  theoretically, [3]).

Thus

$$L_{\text{corrected}} = L_{\text{actual}} + 2\psi a \quad (3)$$

In our case,  $L_{\text{actual}} = 0.091\text{cm}$ ,  $a = 0.278\text{ cm}$ , and  $S_j/L_j = .407\text{ cm}$  from the slope of the regression curve (Fig. 5). Solving for  $\psi$  in (3) we find close theoretical agreement,  $\psi = .91$ .

#### 4. THE FIPPLE RATIO $S/L = M$

In organ pipes and other fixed lip wind instruments it is well known that the timbre and resonant frequencies of an instrument can be significantly affected by the small vertical displacement of the edge, blowing pressures and the general geometry of the fipple [3]. Ocarina builders have described similar effects in musical terms. Given the wide variability of fipple design in ocarinas, the task of determining  $M$  is difficult.

From (1), the fipple ratio  $S/L$  is empirically determined by the resonance frequency  $f_0$  with all holes closed and the volume  $V$

$$S/L = V(2\pi f_0/c)^2.$$

If an ocarina is tuned to play an octave with all holes open then  $S/L$  can be deduced from (1) without knowing the volume  $V$ ,

$$S/L = (1/3)\sum(S_j/L_j).$$

However, ocarina builders would like some way to predict  $S/L$  from direct fipple measurements.

John Martin [4] derives  $M$  for recorder fipple in the shape of a rectangular wedge of depth  $L$  with inner and outer window areas  $S_{\text{in}}$  and  $S_o$ . Without considering end corrections,

$$M = \rho L \ln(S_o/S_{\text{in}})/(S_o - S_{\text{in}}).$$

Letting  $r = S_o/S_{\text{in}}$ ,

$$M = C\rho L/S_{\text{in}}$$

for  $C = \ln(r)/(r-1)$ .

For wooden ocarinas by Hind,  $C = .48-.63$ . The author has not verified that Martin's formula for  $M$  is useful in ocarinas.

#### 5. CONCLUSIONS

This paper presents a general formula for predicting resonance frequencies in ocarinas using only directly measurable physical quantities. Experimental and theoretical results support the validity of the formula. Although the inertance of the fipple can be deduced empirically, a precise formula that can be used by builders is still not available. Although it may not be theoretically possible to build a four hole ocarina with precisely tuned resonance frequencies, players have a wide latitude in pitch by varying blowing pressure and using partial holes.

#### 3. REFERENCES

- [1] Rawcliffe, S, (1992). Complex Acoustics in Pre-Columbian Flute Systems. "Musical Repercussions of

1492: Encounters in Text and Performance. Smithsonian Institution Press.

- [2] Fletcher, N. H. and Rossing, T. D., (1999). "The Physics of Musical Instruments," 2<sup>nd</sup> edition, Springer-Verlag, New York, p. 227-230.
- [3] Fletcher, N. H., and Douglas, L. M. (1980). Harmonic generation in organ pipes, recorders and flutes. *J. Acoust. Soc. Am.* **68**, 767-771.
- [4] Martin, J. (1994). "The Acoustics of the Recorder." Moeck-Verlag, Celle. 43-46



## MODELING VOCAL-TRACT INFLUENCE IN REED WIND INSTRUMENTS

*Gary P. Scavone*

Center for Computer Research in Music and Acoustics (CCRMA)

Department of Music

Stanford University

`gary@ccrma.stanford.edu`

### ABSTRACT

This paper explores the influence of upstream vocal tract resonances in reed wind instrument performance and modeling. Vocal tract manipulations are a common, though sometimes subtle, performance practice exploited by experienced musicians to produce a variety of important acoustic effects, including contemporary performance techniques such as multiphonics and extended range playing. Several previous acoustic studies have been conducted and most agree that the upstream system can have significant influence under certain circumstances. There is less agreement regarding the importance of this mechanism in “traditional” playing ranges and conditions.

Several digital waveguide structures are proposed to implement this element of the performer-instrument system. The simplest approach involves modeling the oral cavity with a single resonance peak which can be easily controlled to test coupling and reed entrainment, as well as upstream-downstream interactions. The model verifies upstream influence and demonstrates real-time behavior very similar to that experienced in reed wind instrument playing. Multi-resonance vocal tract models are briefly considered and issues of real-time control are discussed.

### 1. BACKGROUND

The 1980s were an active period for acoustic investigation into the role and influence of a player’s vocal tract in wind instrument performance [1, 2, 3, 4, 5]. While a few of these reports included suspect conclusions or demonstrated unfamiliarity with advanced performance practice techniques, a high level of understanding was achieved by the end of the decade.

Clinch et. al. [1] performed X-ray fluoroscopic examinations of vocal tract shape changes involved in the playing of the clarinet, soprano saxophone, and recorder. They noted a strong dependence of note quality on vocal tract shape and, somewhat curiously, concluded “that vocal tract resonant frequencies *must* match the frequency of the required notes in clarinet and saxophone performance.”

Backus [3] made vocal tract impedance measurements and found peak values an order of magnitude less than the impedances of the clarinet air column resonances. He also experimented with a clarinet-like system arranged to sound using a vacuum mechanism located at its downstream end. He observed relatively little change in the resulting waveforms when either human or more sharply tuned resonance structures were placed around the vibrating reed/mouthpiece system. From these results, Backus concluded that “the player’s vocal tract has a negligible influence on the instrument tone.”

By assuming continuity of volume flow, Benade and Hoekje [2, 4, 5] showed that the pressure and flow relationships on each side of the reed can be written as

$$U = \frac{P_d}{Z_d} + \frac{P_d - P_u}{Z_r} \quad -U = \frac{P_u}{Z_u} + \frac{P_u - P_d}{Z_r}, \quad (1)$$

where  $Z_u$  is the input impedance looking upstream from the reed into the player’s windway,  $Z_d$  is the input impedance looking downstream from the reed into the instrument air column, and  $Z_r$  is the nonlinear acoustic impedance of the reed valve. The flow through the reed aperture can then be expressed in terms of the pressure difference  $P_\Delta = P_u - P_d$  and the above equations solved as  $-P_\Delta = ZU$  where

$$Z = \frac{Z_r(Z_d + Z_u)}{Z_r + Z_d + Z_u} = Z_r \parallel (Z_d + Z_u). \quad (2)$$

The reed impedance plays a secondary role in this expression because it tends to be very large in comparison to the other impedances. If the upstream impedance ( $Z_u$ ) is negligible, as was assumed for many years, the system can be accurately described in terms of the air column and reed impedances alone. On the other hand, it is clear that if significant impedance peaks occur in the upstream system, they can influence the behavior of the instrument in important ways. These authors made upstream impedance measurements and found that certain vocal tract configurations can produce strong upstream impedance peaks. In addition, they noted a number of ways in which upstream resonances could have considerable influence on the entrainment of the reed and the resulting sound spectra. With respect to the lack of earlier recognition within the acoustics community of the possible influences of a player’s windway, Benade [4] noted that:

1. every player quickly learns to avoid windway configurations that might adversely affect the instrument response and/or produce undesirable multiphonics;
2. the audible effects of resonance alignment in the player’s windway are rather subtle and not easily recognized in the resulting instrument spectrum;
3. the ability to make use of vocal tract resonances to strengthen or support instrument oscillations is a refinement that typically comes only with many years of performance experience.

In a later study by Wilson [6], upstream resonances were examined during clarinet performance of several musical phenomena. She found that the performer tends to align upstream resonances with the first or second harmonic of a sounding tone, “but

that there were also a number of tones that did not have an airway resonance aligned with a harmonic.” For pitchbend, a large-amplitude vocal tract resonance was used to control the playing frequency. When playing multiphonics, Wilson found that the performer creates a resonance that supports an oscillation at a linear combination of the audible pitch frequencies.

Sommerfeldt and Strong [7] presented a detailed time-domain simulation of a player-clarinet system which included a sixteen segment cylindrical tube approximation for the player’s windway. They explored several vocal tract configurations and found some instances of upstream influence on the resulting sound spectra.

The present study seeks to investigate upstream resonance effects in a real-time synthesis environment. The emphasis here is on capturing the essential features of a generalized single-reed woodwind instrument and developing an upstream model which can be intuitively controlled to test upstream-downstream coupling and reed entrainment.

## 2. THE DOWNSTREAM MODEL

A combination of distributed and lumped system models are utilized in this study. Distributed models are implemented with digital waveguide (DW) techniques [8] which make use of digital delay-lines to efficiently simulate lossless traveling-wave propagation. Linear dispersion and attenuation are commuted and realized at discrete locations within a distributed structure. In the DW context, lumped system approximations are derived in terms of traveling-wave components and implemented with appropriately designed digital “scattering” filters.

### 2.1. The Instrument Air Column

The instrument air column is modeled as a single uniform waveguide of either cylindrical or conical shape and appropriately designed scattering junctions are applied at each of its ends. While more intricate air column structures can be modeled with DW techniques [9, 10, 11], such additional complexity is unnecessary for the purposes of this study.

The block diagram shown in Fig. 1 models traveling-wave propagation within a uniform air column structure. The single digital filter  $\mathcal{R}(z)$  accounts for the combined frequency-dependent losses attributable to radiation, thermal heat conduction, and viscosity along the air column walls.

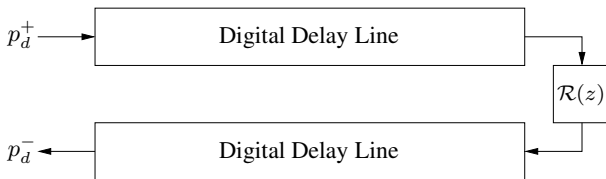


Figure 1: Generalized digital waveguide air column structure.

### 2.2. The Reed Junction

The single-reed woodwind excitation mechanism can be reasonably well modeled as a nonlinear spring because it is normally driven well below its resonance frequency. The flow through the aperture and the movement of the reed are controlled by the difference in pressures on the upstream and downstream sides of the

reed channel,  $p_\Delta = p_u - p_d$ . Making use of the Bernoulli equation for static volume flow and assuming continuity of flow at the reed junction, a memory-less nonlinear function of  $p_\Delta$  can easily be derived [12].

Using DW techniques, this characteristic is transformed into a nonlinear reflection function and implemented via a scattering junction as shown in Fig. 2. The pressure entering the downstream instrument air column is determined as:

$$\begin{aligned} p_d^+ &= p_d^- \cdot r(p_\Delta) + p_u^+ [1 - r(p_\Delta)] \\ &= p_u^+ - [p_u^+ - p_d^-] r(p_\Delta), \end{aligned} \quad (3)$$

where  $r(p_\Delta)$  is the nonlinear reed reflection function. Details regarding the derivation of  $r(p_\Delta)$  in the context of a traveling-wave, scattering theory approach are available elsewhere [13, 10]. Pressure scattering on the upstream side of the reed junction is given by

$$p_u^- = p_d^- - [p_u^+ - p_d^-] r(p_\Delta). \quad (4)$$

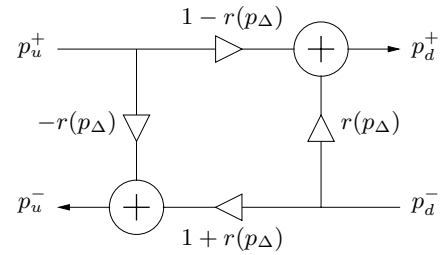


Figure 2: The reed scattering junction.

This study is concerned with the influence of upstream impedance maxima on the operation of *pressure-controlled* wind instrument excitation mechanisms. While a single-reed woodwind system is presented here, other appropriately designed pressure-controlled excitation models can be substituted, such as one based on the brass instrument lip valve. The conditions under which the upstream system might influence a *flow-controlled* mechanism, like that of a flute or recorder, are different and not considered here.

## 3. UPSTREAM WINDWAY MODELS

With a few exceptions [7, 14], most wind instrument simulations have assumed a constant or slowly varying pressure in the player’s mouth and otherwise ignored possible upstream influences. Under these assumptions, the upstream system can be considered a large reservoir driven by a zero-frequency (DC) current source. An electrical circuit analog for such a system is shown in Fig. 3. The current source  $U_l$  represents the player’s lungs, while flow resistance in the lungs and trachea is characterized by  $R_l$ . In general, the lung impedance varies over time based on the vocal fold configuration. The cavity impedance is given by  $Z_c = -j\rho c^2/(V\omega)$ , where  $\rho$  is the mass density of air,  $c$  is the speed of sound in air,  $V$  is the volume of the cavity, and  $\omega$  is the radian frequency. The upstream resistance parameter  $R_u$  characterizes losses in the player’s windway.

The impedance seen by the reed looking upstream is infinite for steady flow but relatively small at higher frequencies. Under these conditions, the reed is controlled by the oscillating pressure on its downstream side and the DC upstream pressure only.

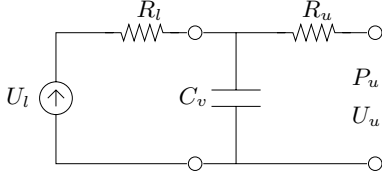


Figure 3: Electrical circuit analog for a traditional upstream windway system.

### 3.1. Windway Resonances

The primary goal of this study was to investigate how upstream resonances might influence the resulting instrument sound and the oscillations of the reed valve. With this in mind, simple vocal tract characterizations having control parameters directly tied to resonance peak and bandwidth features were explored.

An upstream system with a single resonance is represented by the electrical circuit analog of Fig. 4. The impedance seen from the reed is characterized by peaks at DC (set with  $C_v$ ) and at the resonance frequency, which is determined by the components  $L_1$ ,  $C_1$ , and  $R_1$ . Despite the extreme simplicity of this characterization, wind instrument performers are typically making use of just a single resonance in their windway to influence the response of the reed.

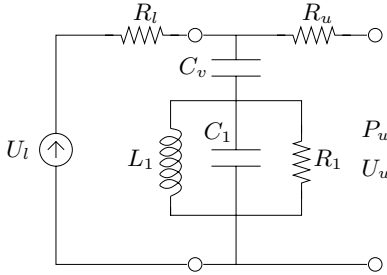


Figure 4: Electrical circuit analog for upstream windway with a single resonance.

Within the digital waveguide context, the lumped impedance representation of the upstream system is converted to a traveling-wave scattering junction expressed in terms of reflectances and transmittances. Figure 5 shows a representative reflectance characteristic when the lung and trachea impedance is assumed infinite.

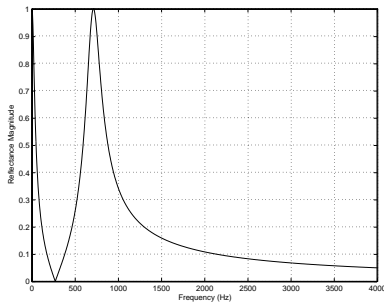


Figure 5: Upstream reflectance derived from the circuit of Fig. 4.

The complete system of Fig. 4 can be transformed to a traveling-wave scattering characterization using a transmission-matrix ap-

proach. If the series combination of the resonant circuit and volume capacitance are represented by an impedance  $Z_s$  and the upstream resistance by  $Z_a = R_u$ , the following matrix approach can be followed:

$$\begin{bmatrix} P_1 \\ U_1 \end{bmatrix} = \begin{bmatrix} 1 & 0 \\ Z_s^{-1} & 1 \end{bmatrix} \begin{bmatrix} 1 & Z_a \\ 0 & 1 \end{bmatrix} \begin{bmatrix} P_2 \\ U_2 \end{bmatrix} \quad (5)$$

$$= \begin{bmatrix} 1 & Z_a \\ Z_s^{-1} & 1 + \frac{Z_a}{Z_s} \end{bmatrix} \begin{bmatrix} P_2 \\ U_2 \end{bmatrix},$$

To render these relationships in the digital waveguide domain, it is necessary to transform the plane-wave physical variables of pressure and volume velocity to traveling-wave variables as

$$\begin{bmatrix} P_1 \\ U_1 \end{bmatrix} = \begin{bmatrix} P_1^+ + P_1^- \\ Z_0^{-1}(P_1^+ - P_1^-) \end{bmatrix}, \quad (6)$$

where  $Z_0$  is the characteristic impedance of the section. Waveguide pressure variables on both sides of the upstream system are then related by an expression of the form

$$\begin{bmatrix} P_1^- \\ P_2^+ \end{bmatrix} = \begin{bmatrix} \mathcal{R}^- & \mathcal{T}^- \\ \mathcal{T}^+ & \mathcal{R}^+ \end{bmatrix} \begin{bmatrix} P_1^+ \\ P_2^- \end{bmatrix}. \quad (7)$$

The process of deriving appropriate discrete-time reflectance and transmittance filters is detailed elsewhere with respect to woodwind tonehole modeling [10]. For the system of Fig. 4, the resulting implementation requires four third-order digital filters.

A simplified, intuitive approach is illustrated by the block diagram of Fig. 6. A single second-order digital resonator is used to model the upstream resonance while the lung pressure component of the model is extracted and simply added to the reflected upstream pressure component. A coupling constant  $g$  is included to control the relative level of upstream influence. The unit delay shown in this signal path is necessary to avoid a delay-free loop through the digital resonance filter and reed scattering junction.

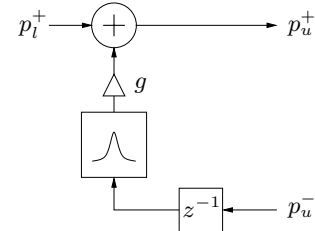


Figure 6: A simplified upstream resonance block diagram.

From this structure, it should be obvious that second-order digital resonators can be cascaded in series to simulate multiple upstream resonances. However, because vocal tract resonances will not typically have harmonic relationships, it is unlikely that a performer would be able to manipulate the upstream system in such a way that multiple upstream resonances could be used to reinforce multiple downstream resonances.

### 3.2. Piecewise Cylindrical Approximations

A distributed acoustic model of the vocal tract can be developed by approximating the dimensions of the upstream windway with a series of concatenated cylindrical pipe sections. In the digital waveguide context, each cylindrical section is efficiently implemented



with a single digital delay-line and a one-multiply scattering junction. This approach was previously used to create an articulatory vocal tract model for the synthesis of singing [15].

With a model capable of accurately simulating arbitrary vocal tract profiles, it is possible to explore general windway shape trends and influences as reported by Clinch et. al. [1]. A multi-segment cylindrical model of the vocal tract was implemented for this study, though its use presented several challenges. In general, it is difficult to predict the way changes in vocal tract shape will affect the resonance structure of the upstream system. Further, the resulting parameter space is complex and requires a well developed, intuitive control interface. Finally, such complexity is unnecessary when one considers that the performer typically makes use of just a single windway resonance to influence the vibrations of the reed.

#### 4. RESULTS AND OBSERVATIONS

The single resonance upstream implementation illustrated in Fig. 6 was combined with an existing digital waveguide saxophone model and the resulting instrument behavior was found to closely parallel that experienced when playing a real saxophone. For example, the first ten or so harmonics of a saxophone can be isolated through the use of vocal tract manipulations. By appropriately controlling the parameters of the upstream model, similar behavior can be demonstrated with the synthesis system. In addition, both the model and saxophone often require re-articulation of notes to break previous reed entrainment.

Figure 7 shows a pair of mouthpiece spectra from the synthesis model produced with and without an upstream resonance. When the upstream resonance was tuned to match the downstream third harmonic, the resulting vibrations of the reed became entrained at that frequency and the sound was heard to jump by a musical twelfth.

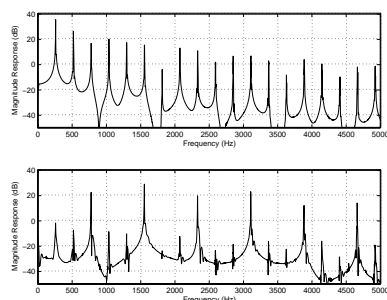


Figure 7: Mouthpiece spectra without upstream resonance (above) and with upstream resonance set to third harmonic frequency (below).

Some questions remain with respect to the role of a player's windway in wind instrument performance. In particular, the extent to which performers make use of vocal tract manipulations within "traditional" playing ranges or during rapid note sequences is unclear. The conclusions of Clinch et. al. [1] appear to overestimate these effects. Instead, observations by this author from saxophone performance experience tend to imply the possible use of broad upstream resonances to reinforce pitch regions, rather than specific notes. Further acoustic study is necessary to clarify these issues.

#### 5. ACKNOWLEDGMENTS

The author would like to thank Julius Smith and Jonathan Abel for helpful discussions on acoustic circuit modeling.

#### 6. REFERENCES

- [1] Clinch, P., Troup, G., and Harris, L., "The importance of vocal tract resonance in clarinet and saxophone performance: A preliminary account", *Acustica*, vol. 50, pp. 280–284, 1982.
- [2] Benade, A. and Hoekje, P., "Vocal tract effects in wind instrument regeneration", *J. Acoust. Soc. Am.*, vol. 71, p. S91, 1982.
- [3] Backus, J., "The effect of the player's vocal tract on woodwind instrument tone", *J. Acoust. Soc. Am.*, vol. 78, no. 1, pp. 17–20, 1985.
- [4] Benade, A. H., "Air column, reed, and player's windway interaction in musical instruments", in *Vocal Fold Physiology, Biomechanics, Acoustics, and Phonatory Control*, ed. Titze, I. R. and Scherer, R. C., Denver Center for the Performing Arts, pp. 425–452, 1985.
- [5] Hoekje, P., *Intercomponent Energy Exchange and Upstream/Downstream Symmetry in Nonlinear Self-Sustained Oscillations of Reed Instruments*, Ph.D. Thesis, Case Western Reserve University, 1986.
- [6] Wilson, T., "The measured vocal tract impedance for clarinet performance and its role in sound production", *J. Acoust. Soc. Am.*, vol. 99, no. 4, pp. 2455–2456, 1996.
- [7] Sommerfeldt, S. and Strong, W., "Simulation of a player-clarinet system", *J. Acoust. Soc. Am.*, vol. 83, no. 5, pp. 1908–1918, 1988.
- [8] Smith, J. O., "Physical modeling using digital waveguides", *Computer Music Journal*, vol. 16, no. 4, pp. 74–91, 1992.
- [9] Välimäki, V., *Discrete-Time Modeling of Acoustic Tubes Using Fractional Delay Filters*, Ph.D. Thesis, Helsinki University of Technology, Faculty of Elec. Eng., Lab. of Acoustic and Audio Signal Processing, Espoo, Finland, Report no. 37, 1995.
- [10] Scavone, G. P., *An Acoustic Analysis of Single-Reed Woodwind Instruments with an Emphasis on Design and Performance Issues and Digital Waveguide Modeling Techniques*, Ph.D. Thesis, Music Dept., Stanford Univ., 1997.
- [11] van Walstijn, M., *Discrete-Time Modelling of Brass and Reed Woodwind Instruments with Applications to Musical Sound Synthesis*, Ph.D. Thesis, Univ. of Edinburgh, 2002.
- [12] McIntyre, M., Schumacher, R., and Woodhouse, J., "On the oscillations of musical instruments", *J. Acoust. Soc. Am.*, vol. 74, no. 5, pp. 1325–1345, 1983.
- [13] Smith, J. O., "Efficient simulation of the reed-bore and bow-string mechanisms", *Proc. Int. Computer Music Conf.*, pp. 275–280, 1986.
- [14] Keefe, D., *On sound production in reed-driven wind instruments*, Technical report, University of Washington, School of Music, Systematic Musicology Program, Seattle, Washington, Report No. 9003, 1990.
- [15] Cook, P., *Identification of Control Parameters in an Articulatory Vocal Tract Model, with Applications to the Synthesis of Singing*, Ph.D. Thesis, Elec. Eng., Stanford Univ., 1990.

# HEAD JOINT, EMOUCHURE HOLE AND FILTERING EFFECTS ON THE INPUT IMPEDANCE OF FLUTES

*John Smith, Joe Wolfe and Michael Green*

School of Physics  
University of New South Wales, Sydney  
J.Wolfe@unsw.edu.au

## ABSTRACT

A study of  $Z(f)$ , the input impedance of the Boehm flute, measured from 200 Hz to 12.5 kHz shows the expected set of strong resonances in the frequency range that corresponds to fundamental frequencies of the playing regime. These frequencies are below the expected cut-off frequency (due to an array of open tone holes) for propagation along the bore of the flute. Above this frequency, in a range that affects the harmonics rather than the fundamental of played notes, the inertive reactance of the tone holes increases with frequency until the standing wave propagates along the tone hole lattice with little attenuation. Harmonic resonances are again evident, but now correspond to resonances of the whole length of the instrument. However the resonances associated with the bore are strongly attenuated over an intermediate frequency range. This appears to be a consequence of a Helmholtz resonator formed by the air in the embouchure hole and the sealed end of the head joint. Experiments with different head joints confirm this mechanism. The envelope of  $Z(f)$  shows a broad maximum near 10 kHz that we attribute to the resonance of the embouchure riser tube.

## 1. INTRODUCTION

Transverse flutes are sealed at one end by a cork or stopper that, in the orchestral flute, is typically positioned about 17 mm from the centre of the embouchure hole. In Figure 1, the volume of air enclosed between the cork and the embouchure hole is labelled  $b$ . It may, in a first approximation, be considered to act as the compliance for a Helmholtz resonator whose mass is that of the air in the embouchure hole,  $a$ . This resonator is effectively in parallel with the bore. It is important that the resonances of the entire instrument in its playing configuration have frequencies in nearly harmonic ratios, so that the higher resonances support the brightness of timbre and loudness in the low register. It is also important because the same fingerings are usually used for notes in both the first and second registers. The global intonation of the instrument depends on the frequency dependences of this resonator, of end effects in the bore, of

the jet drive mechanism, and of the detailed geometry of the head. Diverse aspects of flute acoustics are described by [1-6].

The moveable stopper gives flutists this important advantage over players of other woodwind instruments: the relative tuning and the absolute tuning may be adjusted by separate mechanisms. Using the tuning slide to shorten the overall length of the instrument of course increases the pitch of all notes (with the complication that the pitch increment or proportional change in frequency is greater for notes played with a shorter effective tube length than those played using a longer effective bore). The position of the cork or stopper in the end of the flute may also be adjusted, using a screw. Pushing the cork in further raises the pitch of all notes, but the pitch increment is greater for notes with higher pitch. Thus the flutist whose octaves are narrow, due to the idiosyncrasies of the embouchure-instrument combination, may push the cork in to widen the octaves, and then pull the tuning slide out to compensate for the average pitch increase.

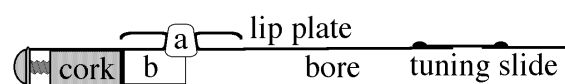


Figure 1: Schematic of a flute head joint.

The fundamental frequencies of notes in the range of the flute fall below 3.2 kHz, but the harmonics extend well beyond this range. To treat the air  $b$  near the stopper as a simple compliance requires that its length be negligible in comparison with the wavelength. This approximation must fail at frequencies of several kHz, where this volume of air may be better approximated by treating it as a waveguide. Similarly, the air  $a$  in the embouchure hole may not be treated as a compact mass for such frequencies. We therefore consider these complications in this paper.

To study the effect of the stopper position, two simple cylindrical flutes were constructed with long head regions. This allowed the stopper to be moved over a wide range. Because of the timing of conferences and deadlines, this work has already been reported at another conference [7], so we present here only a summary of that paper, from which Figure 3 is reproduced with permission.

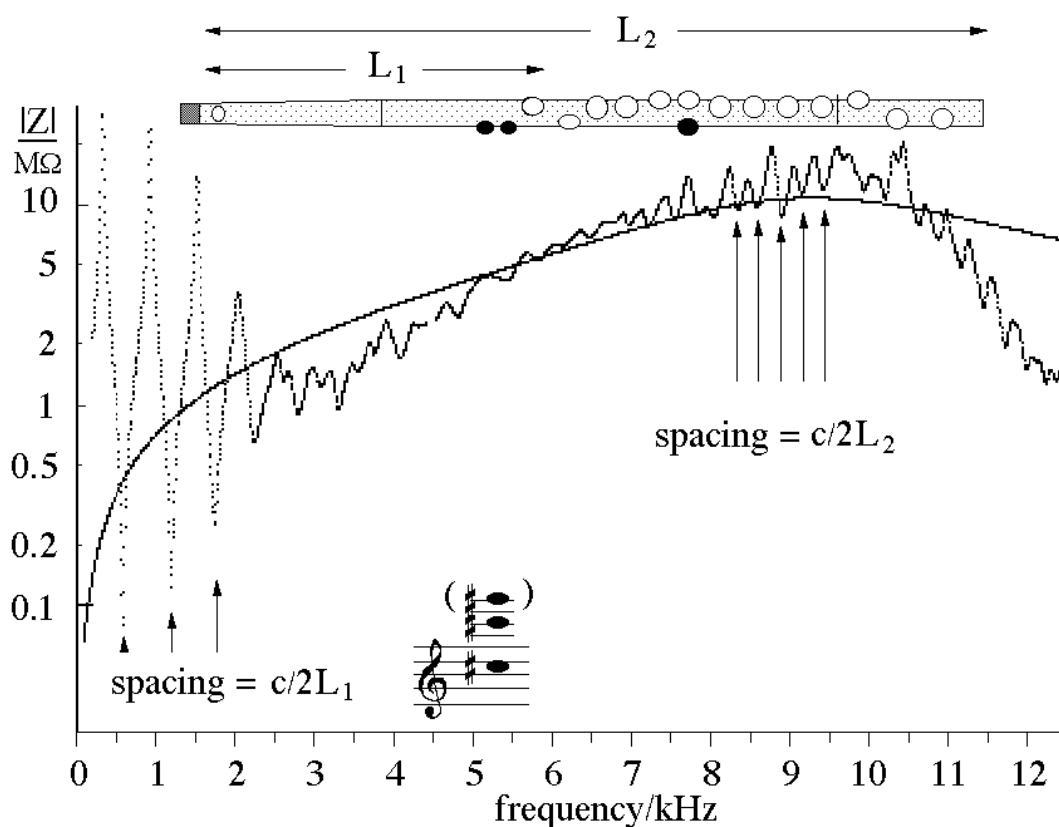


Figure 2: The impedance spectrum of a normal flute, for the fingering normally used to play C#5 and C#6.

## 2. MATERIALS AND METHODS

The cylindrical 'flutes' without tone holes were made from PVC pipe, with internal diameters of 18 and 23 mm. Their lengths were such that they played C4. The normal flute used was a Pearl PF-661: a common, mass-produced instrument. Impedance spectra at the embouchure were measured as described elsewhere [8,9].

## 3. RESULTS AND DISCUSSION

The impedance spectrum  $Z(f)$  for a normal, modern flute (Figure 2) shows several interesting features. The fingering shown is that used for the notes C#5 and C#6, which will also play G#6. For this fingering, almost all of the tone holes are open, and the effective length of the tube  $L_1$  is a little less than half the length of the flute, as shown. The fundamental frequencies of these notes correspond to the first three minima in  $Z(f)$ . Over these three minima and the intervening maxima, the envelope of the curve falls relatively slowly: the resonances become weaker with increasing frequency primarily because of viscothermal losses. Around 2-3 kHz,

however, the resonances become suddenly much weaker. This is due to the inertance of the air in the tone holes, which produces a cut off frequency, above which waves are not reflected at open tone holes [10,11]. The effect of the Helmholtz shunt occurs at slightly higher frequencies—about 5 kHz—as we show using the cylindrical flute without tone holes.

At frequencies above about 7 kHz, resonances reappear. However, their spacing is now that of standing waves over  $L_2$ , approximately the whole length of the instrument. In this frequency range, the inertance of the air in the open tone holes is sufficiently high that the waves 'hardly notice' that they are open. The relatively high cut off frequency of the modern flute is a result of its relatively large tone holes. Clarinets and baroque flutes have much comparatively smaller tone holes, and their cut off frequencies fall within the normal playing range of the instrument, with the result that highest notes are played using standing waves that use almost the entire length of the instrument [9,11].

The solid line in Figure 2 is the theoretical impedance of a truncated cone having the dimensions of the air in the embouchure hole ( $a$  in Figure 1) and including the end effects

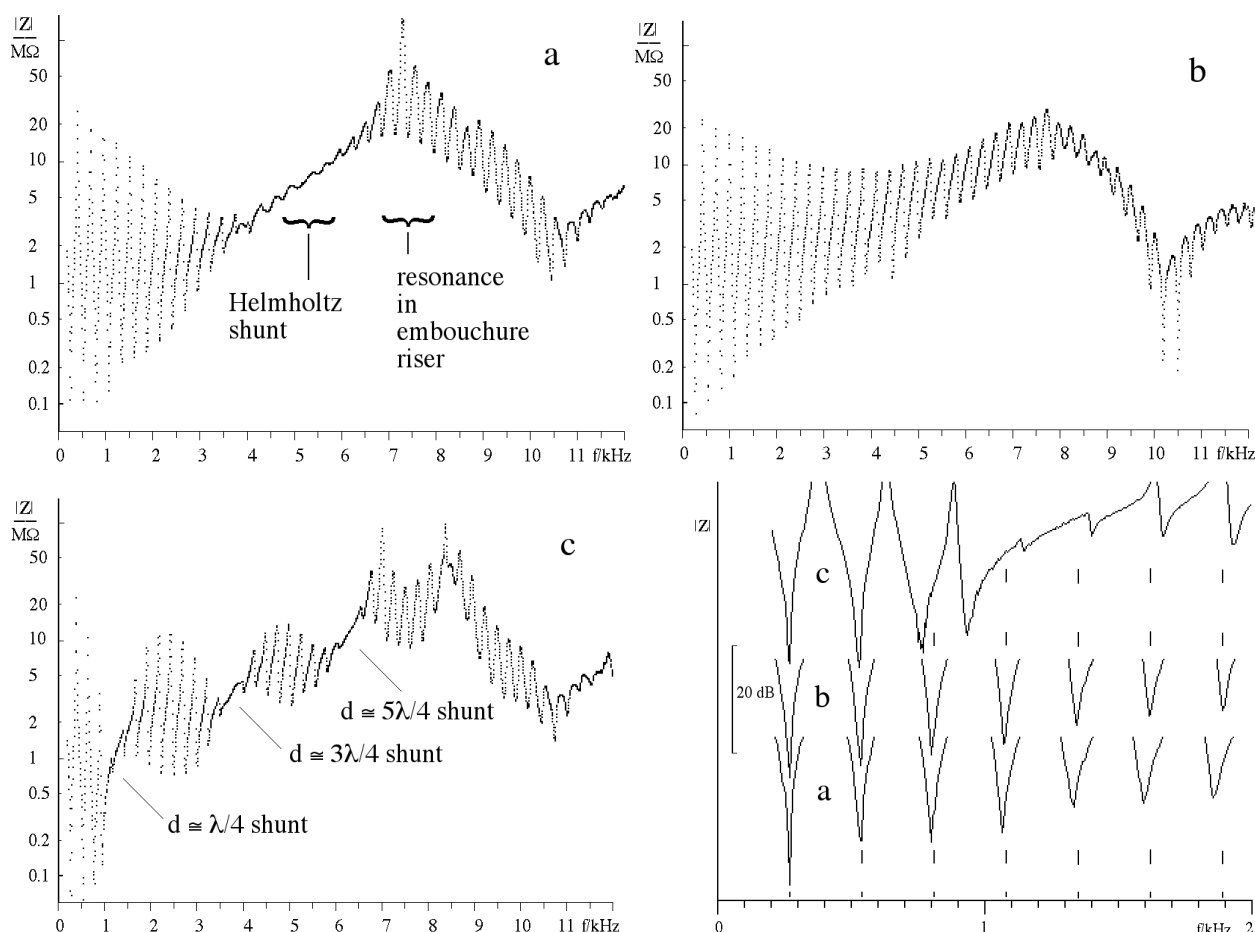


Figure 3: The impedance spectra of flutes with the cork position at (a) 17.5 mm from the embouchure hole; (b) very close to it and (c) at 70 mm from it. (d) shows, on an expanded scale the minima from (a), (b), and (c). Reprinted, with permission, from [7].

due to the baffling of the lip plate and the head tube respectively. We offer this as a possible source of the broad maximum at around 10 kHz. However, the influence of this and other high frequency effects on the air jet is not simple to calculate. For instance, non propagating modes in the flute bore may need to be considered [Tsai, this volume].

To separate the effects of the head joint resonance from those of the tone hole lattice, and to demonstrate the waveguide effect of the air near the cork, we measured  $Z(f)$  on simple cylindrical flutes without tone holes (Figure 3). 3(a) shows the  $Z(f)$  for a simple cylindrical flute with the cork in a typical flute playing position, 17.5 mm from the centre of the embouchure hole. With no tone hole effects, the effect of the upstream shunt is more clearly seen.

Figure 3(b) shows the effect of moving the stopper as close as possible to the embouchure hole. The shunt moves to frequencies beyond the range of our spectrometer in this configuration. Players of Cuban *charanga* music often play

with the cork pushed in close to the embouchure hole so as to facilitate playing notes in the fourth octave of the instrument (2-4 kHz). The penalty for this is that it upsets the relative tuning of the instrument, as shown below.

For Figure 3(c), the stopper is 70 mm from the embouchure hole. Here its waveguide effects are clearly seen. Treating it as a simple closed pipe, its  $\lambda/4$ ,  $3\lambda/4$  and  $5\lambda/4$  minima would be expected at 1.2, 3.6 and 6 kHz. These shunts are indeed seen to reduce the envelope of the extrema due to bore resonances.

We note in passing that, at very high frequencies, the extrema are larger than those for the normal flute (Figure 2). We attribute the weaker resonances in the normal flute in part to the finite radiation losses at each tone hole.

Figure 3(d) shows clearly the compression and expansion of the spacing of the resonances due to withdrawal and insertion of the cork. For this simply cylindrical flute, and with the cork at 17.5 mm, the impedance minima are not

harmonically spaced: such a flute would be better played with the cork inserted further.

#### **4. CONCLUSIONS**

The influence of cork position on the frequencies of impedance minima are in accord with musicians' observations about tuning: greater insertion enlarges intervals. The resonances seen in  $Z(f)$  are determined by the effective length of the instrument. Below the cut off frequency for the tone hole array, this is approximately the length from embouchure to the first open tone hole. At sufficiently high frequencies, the effective length is approximately that of the entire instrument. A broad maximum at around 10 kHz is consistent with a resonance in the embouchure hole.

**Acknowledgments.** We thank John Tann for technical assistance and the Australian Research Council for support.

#### **5. REFERENCES**

1. Benade, A.H., Fundamentals of musical acoustics. Oxford Univ. Press, NY, pp 430-501, 1976.
2. Benade, A.H. and French, J.W., "Analysis of the flute head joint", J. Acoust. Soc. Am., 37: 679-691, 1965.
3. Coltman, J. "Acoustical analysis of the Boehm flute" J. Acoust. Soc. Am., 65: 499-506, 1979.
4. Fletcher, N.H., Strong, W.J., and Silk, R.K. "Acoustical characterization of flute head joints" J. Acoust. Soc. Am., 71: 1255-1260, 1982.
5. Fletcher, N.H. and Rossing, T.D., The Physics of Musical Instruments, 2nd edn. Springer-Verlag, New York, 1998.
6. Nederveen, C.J., Acoustical aspects of wind instruments, Northern Illinois Univ., DeKalb, Ill.), pp 45-78, 1998.
7. Wolfe, J., Smith, J. and Green, M. (2003) "The effects of placement of the head joint stopper on the impedance spectra of transverse flutes". Proc. Eighth Western Pacific Acoustics Conference, Melbourne. (C. Don, ed.) Aust. Acoust. Soc., Castlemaine, Aust.
8. Wolfe, J., Smith, J., Tann, J., and Fletcher, N.H., "Acoustic impedance of classical and modern flutes" J. Sound & Vibration, 243: 127-144, 2001.
9. Music Acoustics. [www.phys.unsw.edu.au/music](http://www.phys.unsw.edu.au/music)
10. Benade, A.H., "On the mathematical theory of woodwind ringer holes", J. Acoust. Soc. Am., 32: 1591-1608, 1960.
11. Wolfe, J. and Smith, J. "Cut off frequencies and cross fingerings in baroque, classical and modern flutes" J. Acoust. Soc. Am., accepted for publication.

# FLUTE PERFORMOLOGY; STATISTICAL ANALYSES AND NUMERICAL SIMULATION OF FLUTE TONE EXCITATION

*Tro, Jan; Bjerkvik, Aslak & Kristiansen, Ulf*

Acoustics,  
Norwegian University of Science and Technology (NTNU)  
NO-7491 Trondheim, Norway  
<tro><bjerkvik><kristian>@tele.ntnu.no

## ABSTRACT

The present analyses are based on a large number of solo flute recordings. Using a near field microphone recording technique it is possible to distinguish between the sound of the shutting key and the following tone transient. For a rapid tone sequence in a professional musical context the precision of the key shutting action is of utmost importance. Furthermore it is assumed to exist a minimum (optimum) time delay between the action of closing (or opening) a hole and the possible start of the correct tone transient based on the behavior of the standing wave build up in the flute tube. Variation of average time delays and deviations is calculated.

In a two-dimensional numerical model of a tube sound field build up we demonstrate tone transient variations as a function of the open or shut hole. Simulation parameters will be compared with the measured values.

The present study, which is part of the ongoing performology projects at the NTNU-Acoustics Lab., emphasizes the advantage of analyzing instrument tones in a musical context.

**Key Words:** Musical Instrument, Performance Analysis, Numerical Simulation, Flute Excitation.

## 1. INTRODUCTION

As a part of the MOSART research program we recorded, during the summer of 2002, 40 versions of the opening movement of Devienne's Concerto no. 7 in E minor for flute and piano, the flute part only, with a professional performer<sup>1</sup>. The performances were recorded in three different rooms, one anechoic chamber, one dry living room and one reverberant chamber. The analyses presented in this paper are all from the anechoic recordings.

Due to the anechoic environment and the recording equipment setup it was possible for some staccato tones to aurally

distinguish between the sound of the physical action of the flute hole key and the following sounding tone transient. The question discussed in this paper concerns the physical behavior of the flute tone buildup in relation to the key action and the physiological performer control.

## 2. DATA AQUISION

### 2.1. Flute tone transient

The figure below (see Figure 1) shows an example of the key action sound followed by the tone transient (staccato  $f_5^\#$ , fundamental frequency  $f_{\text{standard}} = 740.0$  Hz,  $f_{\text{measured}} = 740.2$  Hz).

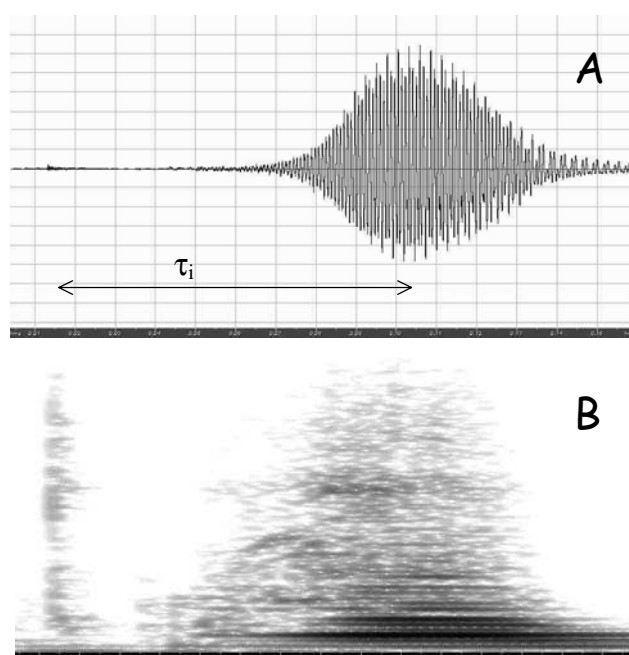


Figure 1: *Staccato flute tone preceded by the key action sound; A: time vs. intensity; B: time vs. frequency.*

Five anechoic performances have been analyzed, each containing a staccato-performed scale-like phrase played twice due to a compositional repetition. The staccato phrase is preceded by a similar legato phrase, all of eight notes. The

<sup>1</sup> "Recording of repeated performances" reported at the [1] Midterm Meeting, task 3 Progress report, "Control and Virtualisation of Musical Instruments".

score notation indicates a tempo close to 132 bpm, i.e. 450 ms per quarter note. In this musical context a single tone in the phrase of eights would have the duration of less than 225 ms. The first staccato tone only has been included in the analyses.

For statistical reasons we define the time interval  $\tau_i$  (see Figure 1, upper part) as the time distance from the start of the key action sound to the maximum level of the following tone. The

recordings were performed during a period of 5 weeks, one recording every week. Due to the intermediate activities of the performer (other recording sessions, laboratory measurements, standard whole day research activities) the performances are considered un-correlated, i.e. not influenced by the previous recording. The table below gives detailed tone information.

## 2.2. Measurements and analyses

Date	Phrase 1, staccato tone 1					Phrase 2, staccato tone 1				
	$\tau_i$ [ms]	Freq.[Hz]	Peak amp.	RMS	Dur.[ms]	$\tau_i$ [ms]	Freq.[Hz]	Peak amp.	RMS	Dur.[ms]
2002	95	740.2	-14.2	-24.3	84	110	741.6	-20.5	-29.6	78
05.07	127	738.9	-25.2	-34.2	71	108	741.3	-14.2	-24.3	88
12.07	96	737.5	-22.9	-33.2	74	71	737.5	-18.0	-25.6	98
19.07	67	739.6	-20.3	-30.6	83	95	742.8	-21.3	-30.8	82
29.07	92	741.2	-26.1	-36.0	53	84	741.2	-23.5	-31.2	77
Avg.	95,4	739,5	-21,7	-31,7	73,0	93,6	740,9	-19,5	-28,3	84,6
Std.	19,1	1,2	4,3	4,1	11,2	14,7	1,8	3,2	2,8	7,7

Table 1: Statistical properties of the flute tones. See explanation in the text.

All the data are measured by use of the Cool Edit Pro program. First column in Table 1 contains the recording date. The following five columns contain the first staccato tone data from phrase 1, such as measured fundamental frequency, peak amplitude (dB), total RMS power and tone duration above an arbitrary reference level of -39 dB, respectively. The last five columns show the similar data for the repeated phrase, phrase 2.

## 3. SIMULATIONS

### 3.1. Simulation method

The simulations have been done using the Transmission Line Modeling (TLM) method. This method discretizes the computational domain in space and time, using a spatial cell-size considerably shorter than the acoustic wavelengths considered. Details of the method can be found in [2].

Basically, on the microscopic level, the method considers the domain to be made up by transmission lines in the form of wave-guides carrying acoustic plane waves, where these waves undergo reflection and transmission at the duct junctions. The acoustic pressure at a junction is derived using the pressures at adjacent nodes only one time step earlier. It is therefore also possible to change the actual geometry of the system as function of time. On the macroscopic level, waves are observed to

propagate through the whole mesh, undergoing typical wave effects like reflection, diffraction, and interference.

The method is an alternative to the finite difference method in the time domain (FDTD), and has the advantages of superior stability, and ease of programming.

### 3.2. Tube excitation

The simulation does not intend to model a real flute, as it is a simple tube-like closed-open resonant system with a Ricker-type wavelet excitation in one end and sound propagation possibilities in the other. The main purpose is to study the acoustical behavior of the tube (flute) tone transient (reflection and propagation) influenced by an open or closed finger hole. This 2-dimentional TLM model is easily changeable to inspect detailed variations in geometry and size. The tube walls are modeled as rigid surfaces with reflection coefficient equal to one. The simulation starts with the excitation in the closed end of the tube, and the signal is observed at a position outside of the tube, in front of and a bit above the opening. The initial condition is with a closed finger hole, and after some time the finger hole is opened, while the wave propagation is still going on in the tube. By low pass filtering and detection of zero-crossings the fundamental frequency of the signal at the receiver position is found, and the opening of the finger hole raises the fundamental by a factor of 12.3%. This corresponds to the actual pitch difference of two semi tones referring to the real flute staccato phrases. As the hole is closed instantly, the resonance frequency changes within 3-4 periods of the fundamental. The simulations are shown in Figure 2 and 3, respectively.

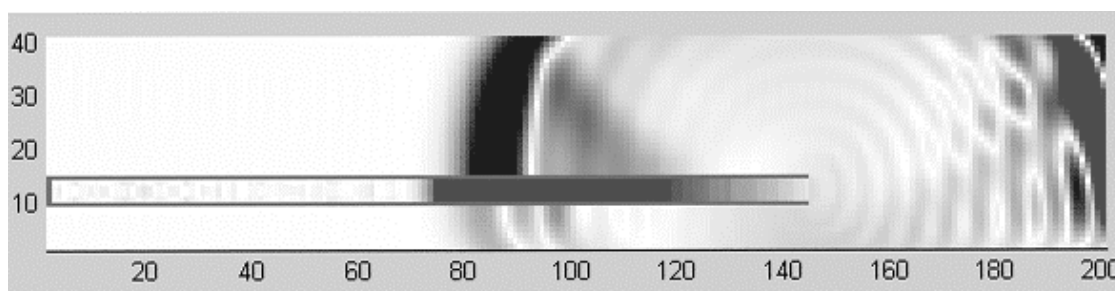


Figure 2: End reflection and sound propagation from a tube. Fundamental frequency  $\approx 660$  Hz.

Figure 2 shows the simulated sound reflection and propagation from the tube end. The geometrical numbers corresponds to the cells in the TLM-mesh, where one cell is  $0.88 \times 0.88$  mm. Figure 3 below shows the reflection and propagation from a similar

tube with one hole. The distance from the tube end to the open hole has been calculated in order to simulate the effect of propagation at an increased pitch by two semi tones.

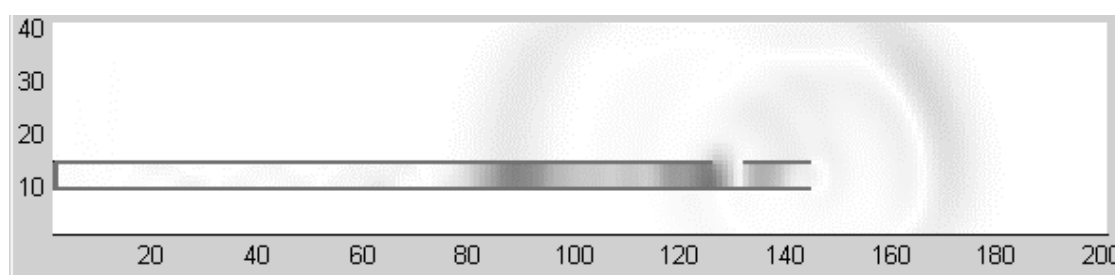


Figure 3: End reflection and sound propagation from a tube with one open hole. Fundamental frequency  $\approx 740$  Hz.

## 4. DISCUSSIONS AND CONCLUSION

Measurements and simulations will be discussed separately.

### 4.1. Staccato tone measurements

The analysis has been concentrated on the first staccato tone ( $f_5^{\#}$ ) in a scale-like phrase preceded by a legato phrase part. A phrase variant later in the movement is included in the analyses. 5 anechoic recordings give us then 10 single staccato tones for analyses as shown in Table 1.

The stability in frequency is remarkable. Through the ten phrases the single tone frequency is on average 740.2 Hz with a standard deviation of 1.8. ISO pitch standard expects 739.99 Hz.

The earlier defined time delay  $\tau_i$  vary between 67 ms and 127 ms with an average of 94.5 ms (standard deviation 18.0 ms). Removing the lowest and the highest value the delay varies from 71 ms to 110 ms. The average value of 94.5 ms seems then reasonably consistent.

The duration of the staccato tones varies between 53 and 98 ms with an average of 78.8 ms (standard deviation 11.8 ms). With a prescribed tempo of 132 bpm the distance between eights tones should be 225 ms. Measured distance values from the analyzed

tone to the next is on average 209.4 ms (standard deviation 5.6 ms), which corresponds well to the “rules“ of music performance.

On average there is little dynamical variations between the phrase 1 staccato tone and the second one, with average total power RMS values -31.7 dB and -28.3 dB, respectively.

Spectral analyses indicate that the key action noise pre-excites the flute tube before the wind pressure produces the musical tone. We have reason to believe the pre-excitation makes it easier to produce the correct pitch, as the expected partials already are present at a very low level.

### 4.2. Simulation results

The TLM model of the tube with an open/closed hole shows that the simulation of a flute with respect to fundamental frequency can be done. However, it must be pointed out that this is a simple 2D tube model and not a designated flute model. If we consider an inside tube plane wave, a 2D model could give the comparable results to the real 3D situation.

### 4.3. Further analyses

In order to compare measured values with the simulation, the simulated signal will be monitored at a position outside of the tube, in front of and a bit above the opening. The comparison of



measured and simulated spectral and time information will be presented at the SMAC03 Conference.

## **5. ACKNOWLEDGEMENT**

Several people have contributed with efforts and comments in the discussions to this presentation. Mentioned should be: Gabriele Boschi, Øyvind Lervik, Peter Svensson, Bård Støfringsdal, Torunn Smevik, John Mango, Vincenzo DiSalvo and the rest of the NTNU Acoustics Group.

## **6. REFERENCES**

- [1] <http://www.diku.dk/musinf/mosart>. Homepage of EU IHP-project “Music Orchestration Systems in Algorithmic Research and Technology”, accessed 14.05.03.
- [2] Y. Kagawa, T. Tsuchiya, B. Fujii, and K. Fujioka, “Discrete Huygens’ model approach to sound wave propagation”, *Journal of Sound and Vibration*, Vol. 218, pp. 419-444, 1998

# RELATING THE HARMONIC-RICH SOUND OF THE CHINESE FLUTE (*DIZI*) TO THE CUBIC NONLINEARITY OF ITS MEMBRANE

Chen-Gia Tsai

Department of Musicology, Humboldt University, Berlin, Germany  
tsai.cc@lycos.com

## ABSTRACT

The *dizi*, a Chinese membrane flute, has a thin membrane covering a hole in the wall of the instrument between the embouchure hole and the first finger hole. The nonlinear membrane produces the rich spectral content that is associated with the characteristic bright timbre of the *dizi*. When the membrane is located near a pressure node of the second harmonic wave in the pipe and thus the driving force is quasi-sinusoidal, *dizi* tones are always dominated by odd-numbered harmonics. We therefore model the membrane as a Duffing oscillator with a hardening spring. This model was tested by two kinds of tones driving the membrane: tones generated by external excitation or by blowing the instrument. For external excitation, the phase plots of the membrane show interlocking spirals, which are predicted by the quasi-sinusoidally driven Duffing oscillator model. For a normal *dizi* tone the agreement is restricted to frequencies < 10 kHz. Rich harmonics above 10 kHz radiated by the membrane, not predicted by our model, may be associated with the jet's sensitivity to the harmonics in the range 0 - 5 kHz generated by the membrane.

## 1. INTRODUCTION

The object of this paper is the membrane flute: a flute with a membrane covering a hole in the wall of its resonator. In contrast to the abundance of membrane-less flutes in numerous musical cultures, only a few membrane flutes exist. The most important of them may be the Chinese flute, the *dizi* (see Figure 1), and the Korean large flute, the *taegum*.

The vibrating membrane brings the bright and buzzing timbre to the flute. Spectra of *dizi* tones are characterized by a formant around 5 kHz [1], which enables the *dizi* to 'cut through' the sound of even large ensembles.

The membrane gives a rich spectral content to the *dizi* at the expense of pitch range. With the membrane tension in a typical playing range, the *dizi* range is restricted to about two octaves plus two notes. Previous impedance measurements on the *dizi* [2] showed that the membrane caused significant admittance

reductions for the bore resonances supporting the two notes immediately beyond this range. Analogously to a string-soundboard system, the vibration modes of the pipe-membrane resonator of the *dizi* are largely damped by the membrane when the pipe's resonances are near the membrane's resonant frequency  $f_m$ , which typically lies in the range 2 - 3 kHz.

Whereas the impedance measurements revealed the linear behaviour of the *dizi* resonator, its harmonic generation stems from its nonlinearity. In this preliminary study, the *dizi* tone for which the membrane is located near a pressure node of the second harmonic wave is simulated by modeling its membrane as a Duffing oscillator.

## 2. BASIC MODEL OF THE MEMBRANE

### 2.1. Timbre changes with pitch

For a membrane flute, the membrane is driven by the acoustic pressure in the resonator and radiates sounds when it vibrates. Because the membrane vibrates more when pressure antinodes lie below it than it does for pressure nodes, its acoustic effects vary with pitch. The inhomogeneous timbre of the *dizi* can be related to the magnitudes of the lowest two harmonics under the membrane, as the acoustic field in the pipe is dominated by low frequencies for soft flute tones. Figure 2 displays three examples of *dizi* spectra and the pressure waves of the lowest two harmonics. As can be observed, when both of them contribute to drive the membrane, the *dizi* tone has a smooth spectrum with a formant at 5 kHz (Figure 2a). When the membrane is located near a pressure node of the second harmonic wave, the *dizi* tone has the same formant but is dominated by odd-numbered harmonics (Figure 2b). When the membrane is located near the pressure nodes of the two lowest harmonics, the *dizi* tone loses its rich harmonics because the membrane hardly vibrates (Figure 2c). Notes pitched higher than this dull tone are characterized by the dramatic recovery of the rich harmonics because the membrane is again located near a pressure antinode of the fundamental wave.

### 2.2. Equation of motion

Among these *dizi* tones with different spectral features, we focus on the one for which the membrane is located near a pressure node of the second harmonic wave (Figure 2b). The membrane is modeled as a Duffing oscillator driven by a quasi-sinusoidal force. Its equation of motion is

$$\ddot{\xi} + r\dot{\xi} + \omega_m^2 \xi + \beta \xi^3 = \frac{G_0}{m} \cos(\omega t + \phi_0) + \frac{G_1}{m} \cos(2\omega t + \phi_1) \quad (1)$$

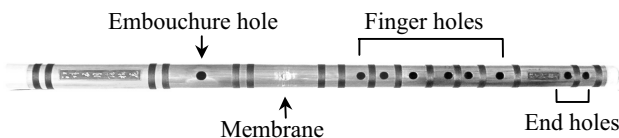


Figure 1: Photo of the *dizi*.

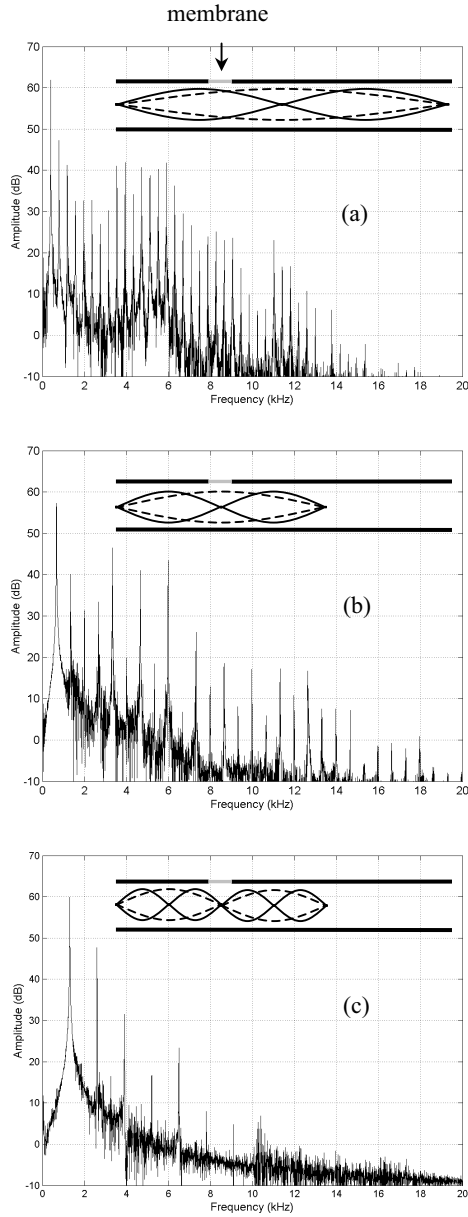


Figure 2: Spectra of dizi tones and sketches of the acoustic pressure waves of the fundamental (dashed lines) and the second harmonic (solid lines). FFT size is 8192. (a) G4 produced by fingering ●●●●●●, first play mode. (b) E5 produced by fingering ●○○○○○, first play mode. (c) E6 produced by fingering ●○○○○○, second play mode.

where  $\xi$  is the effective displacement of the membrane,  $m$  its mass and  $\omega_m$  its resonant frequency. The cubic nonlinear term is suggested by the spectrum shown in Figure 2b, which is dominated by odd-numbered harmonics. Note that the membrane is located at a pressure node of the second harmonic wave. Hence, the force driving the membrane is quasi-sinusoidal;  $G_1/G_0 = O(10^{-2})$ . This is consistent with the fact that a cubic nonlinearity only generates odd-numbered harmonics under a sinusoidal force.

### 2.3. Wrinkling correlates of cubic nonlinearity

A circular membrane with isotropic tension was shown to have the property of a hardening spring [3]. In the case of the *dizi* membrane, its elastic property is complicated by wrinkling. The *dizi* membrane is normally under a uniaxial tensile strain that produces wrinkles, without which, the timbre of the *dizi* will be considered as ‘incorrect’ [4].

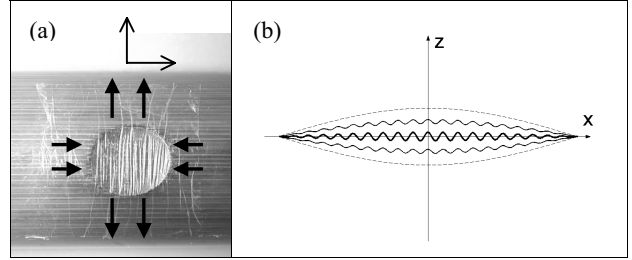


Figure 3: (a) Photo of the dizi membrane. (b) Geometry of the wrinkled membrane in vibration. See the text.

Wrinkles are produced by stretching the membrane in a direction perpendicular to the pipe axis (the  $y$  direction) and compressing it in the direction parallel to the axis (the  $x$  direction: Figure 3a). The behaviour of a wrinkled membrane is governed by the Föppl-von Karman equations, which cannot be solved analytically. Cerda and Mahadevan [5] recently made progress in the geometry and physics of wrinkling by using scaling and asymptotic arguments. The wavelength of wrinkles is determined by a compromise minimising the bending energy and the stretching energy subject to the geometry constraint of inextensibility. As shown in Figure 3b, this constraint in the  $x$  direction is satisfied even for large-amplitude vibrations. This inspired us to describe the motion of the vibrating membrane as a series of strings parallel to the  $y$ -axis. If the membrane is so thin that the bending energy in the  $x$  direction is negligible, the behaviour of these strings is fairly linear until the tension increases for large deformations.

The main effect of wrinkling is to make the membrane behave more linearly by reducing the cubic nonlinearity. If the membrane is unwrinkled due to an isotropic initial tension, the spring constant will be too high for a high initial strain so that the membrane hardly vibrates, or, the cubic nonlinearity will be too high for a low initial strain. In the latter case, we have observed a jump phenomenon in the response curve of the membrane. It leads to hysteresis and discontinuous behaviour of the *dizi*: for the same fingering it either does not sound, or sounds raucously. Wrinkling largely stabilizes sound production.

## 3. METHODS

### 3.1. Experimental study

To measure the sounds radiated by the membrane, a microphone was placed approximately 1 cm above the membrane. A box enclosed the membrane so as to insulate the microphone from sounds radiated at the embouchure hole, finger holes and from the environment. The flute used was a bass *dizi* and the fingering was

●●○○○○ (it has seven finger holes). Some of its physical dimensions are presented in Table 1.

Measurement	Hole length	Hole width	Position
Embouchure hole	1.1	0.95	0
Membrane hole	0.95	0.9	11.9
Third finger hole	1.0	0.9	30.6

Table 1: Physical dimensions (in cm) of the bass dizi.

Two kinds of tones were used to excite the membrane: tones generated by blowing the instrument or by external excitation. Pressure waves comparable with that generated by playing are difficult to produce from loudspeakers without distortion, so the latter was accomplished by singing into the *dizi*, which is an innovative performance technique. In this mode, the embouchure hole is completely covered by the lips.

Producing tones by external excitation was aimed to avoid involving the aerodynamics at the embouchure hole. High harmonics produced by the membrane may affect the jet motion. On the contrary, for the tones produced by singing into the *dizi* it is presumed that the effect of the high harmonics to the glottis is negligible. Falsetto was used for singing into the *dizi* because it produces weaker harmonics than the modal register. Hence, the glottis can be approximated as a source of quasi-sinusoidal tones.

As the acoustic pressure waves recorded above the membrane are approximately proportional to the acceleration of the membrane, they were integrated twice to give the membrane's displacement. The initial velocity was chosen to give a quasi-periodic displacement of the membrane.

### 3.2. Numerical simulations

In numerical simulations, the terms in Eq. (1) are discretised in time with a forward Euler method using time step  $\Delta t = 10^{-5}$  sec. The values  $r = 1700 \text{ sec}^{-1}$ ,  $\omega_m/2\pi = f_m = 2500 \text{ Hz}$ , and  $m = 5 \times 10^{-7} \text{ kg}$  were chosen to fit the response curve of the membrane measured in [2]. The cubic non-linearity, the magnitudes and the phases of the forcing terms were determined by fitting the experimental results.

## 4. RESULTS

Figure 4 gives the experimental (left) and numerical (right) results of the tone produced by the membrane excited by singing into the *dizi*. As the microphone used cannot give the absolute values of acoustic pressure, the membrane's displacement and velocity were plotted in arbitrary units. Fitting the experimental result yields  $\beta = 10^{17} \text{ m}^{-2} \text{ sec}^{-2}$ , the displacement of the membrane of order  $10^{-5} \text{ m}$ , and the acoustic pressure of the fundamental  $G_0/S_m = 100 \text{ Pa}$ , where  $S_m = 0.67 \text{ cm}^2$  is the membrane's area. The membrane's phase plots show interlocking spirals, which were successfully simulated by our model.

Figure 5 gives the experimental and numerical results of the tone produced by playing the *dizi*. Fitting the experimental result yields the acoustic pressure of the fundamental 120 Pa, a value consistent with previous measurements on internal acoustic pressure of flue instruments. Although the membrane's phase

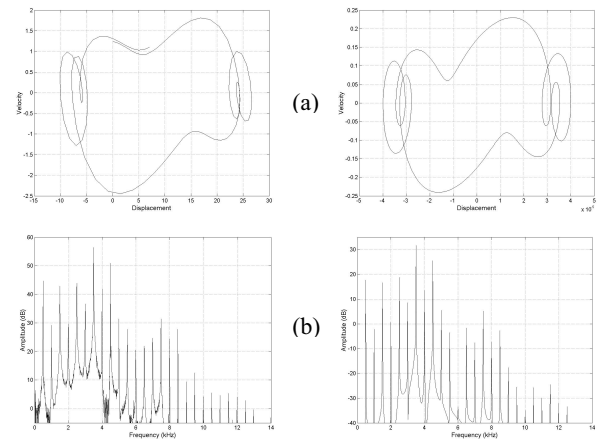


Figure 4: Comparison between the tone radiated by the membrane produced by singing into the *dizi* (left) and stimulation of Eq. (1) (right) with  $G_0 = 6.65 \times 10^{-3} \text{ m} \cdot \text{sec}^{-2}$ ,  $G_1 = 0.03 G_0$ ,  $\omega/2\pi = 500 \text{ Hz}$ ,  $\varphi_0 = 0$ ,  $\varphi_1 = 1$ . (a) Phase plots of the membrane. (b) Spectra of the tones radiated by it.

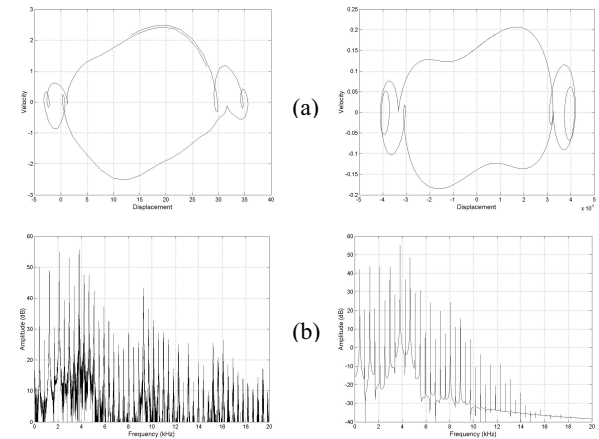


Figure 5: Comparison between the tone radiated by the membrane produced by playing the *dizi* (left) and stimulation of Eq. (1) (right) with  $G_0 = 8 \times 10^{-3} \text{ m} \cdot \text{sec}^{-2}$ ,  $G_1 = 0.02 G_0$ ,  $\omega/2\pi = 424 \text{ Hz}$ ,  $\varphi_0 = 0$ ,  $\varphi_1 = 1$ . (a) Phase plots of the membrane. (b) Spectra of the tones radiated by it.

plots of experimental and numerical results show similar interlocking spirals, the simulated spectrum does not contain rich harmonics above 10 kHz.

Present experimental and numerical results suggest that the first formant at 5 kHz of *dizi* tones can be explained by modeling the membrane as a quasi-sinusoidal driven Duffing oscillator, but the harmonics above 10 kHz in *dizi* tones cannot be predicted without considering more forcing terms in the right hand side of Eq. (1).

## 5. DISCUSSION

Eq. (1) ignores the forcing terms corresponding to high harmonics propagating in the pipe, which are generated by the membrane. If these harmonics are strong enough, they could drive the membrane to generate harmonics above 10 kHz. However, this is not observed in Figure 4b but is noticeable in Figure 5b. It seems that the jet plays a role in sustaining high harmonics in the pipe. Note that when the membrane does not vibrate, the *dizi* tone is not rich in harmonics (Figure 2c). Therefore, the jet alone is not able to produce rich harmonics. We propose that the harmonics above 10 kHz stem from interactions between the two nonlinear mechanisms in the *dizi*: the membrane and the aerodynamics at the embouchure hole.

Rich harmonics in the *dizi* pipe may be contributed by the response of the jet to the harmonics in the 0 - 5 kHz range generated by the membrane. Here we suggest two mechanisms relevant to the jet's sensitivity to these harmonics: the moving separating points of the jet, and its varicose oscillations due to the pressure fluctuations at the flue exit. Several studies have been devoted to the question of whether the jet is responding to the transverse flow velocity, transverse flow displacement or transverse flow acceleration (receptivity problem). In the case of the flute, the lips of the player are rounded, and hence transverse flow acceleration can affect the position of the separation points. Fabre *et al.* [6] pointed out that for a given radius curvature of the edge, a significant contribution of the acceleration can be expected and the jet may be more sensitive to high-frequency harmonics.

Second, high-frequency varicose jet oscillations can be induced by the harmonics generated by the membrane. Verge *et al.* [7] and Ségoufin *et al.* [8] observed a varicose type oscillation of the jet in flow visualization. This oscillation around 3 to 4 kHz was related to an edge-tone feedback loop. For a membrane flute, such varicose jet oscillations might be more significant, because the pressure fluctuations of the harmonics around 3 to 5 kHz generated by the membrane (see Figure 4b) can induce jet velocity fluctuations at the flue exit. According to the jet-drive model [9], high-frequency varicose jet oscillations can introduce rich harmonics into the equivalent pressure difference across the labium.

Finally, the harmonics around 10 to 12 kHz may be amplified by the lowest transverse pipe mode. As can be observed in Figure 2c, turbulence appears coupled to the lowest transverse resonance [10]. Figure 5b also suggests an effect of this transverse pipe mode on the harmonics of the *dizi* tone around 10 kHz. In these *dizi*, the resonator has a diameter of the order 1.6 cm. As the membrane can produce harmonics extending to 15 kHz or even higher frequencies, transverse pipe modes may be excited and affect the motion of the jet as well as the membrane.

## 6. CONCLUSIONS

Our specific experiment on the *dizi* tone for which the membrane is located near a pressure node of the second harmonic wave shows the success of the quasi-sinusoidally driven Duffing oscillator model of the membrane in explaining the *dizi* harmonic generation in the range below 5 kHz, but this model cannot simulate the harmonics above 10 kHz. We relate these harmonics to the jet's sensitivity to the harmonics generated by the membrane in the range 0 - 5 kHz. If the jet amplifies these

harmonics in the pipe, they may in turn drive the membrane to radiate harmonics above 10 kHz. The nonlinear membrane, able to produce high harmonics, brings the question of the high-frequency response of the jet into prominence. This invites further physical studies on membrane flutes.

## ACKNOWLEDGEMENT

The author would like to show his sincere appreciation for helpful comments from Joe Wolfe (University of New South Wales) and Lydia Ayers (Hong Kong University of Science and Technology) on the earlier draft.

## 6. REFERENCES

- [1] Horner, A., Ayers, L., and Law, D., "Synthesis modeling of the Chinese *dizi*, *bawu*, and *sheng*", J. Audio Eng. Soc., 47(12):1076-1087, 1999.
- [2] Tsai, C.G., Wolfe, J., and Smith, J., "Input impedance of the Chinese flute (*dizi*): Linear piston model of its membrane" (in preparation).
- [3] Chobotov, V.A., and Binder, R.C., "Nonlinear response of a circular membrane to sinusoidal acoustic excitation", J. Acoust. Soc. Am., 36:59-71, 1964.
- [4] Thrasher, A., "Di" in The New Grove Dictionary of Musical Instruments, S. Sadie, Ed, Macmillan, London, 1984, Vol. 1, pp. 196.
- [5] Cerda, E., and Mahadevan, L., "Geometry and physics of wrinkling", Phys. Rev. Lett., 90, 074302, 2003.
- [6] Fabre, B., and Hirschberg, A., "Physical modeling of flue instruments: A review of lumped models", Acustica, 86:599-610, 2000.
- [7] Verge, M.P., Fabre, B., Mahu, W.E.A., Hirschberg, A., van Hassel, R., Wijnands, A.P.J., de Vries, J.J., and Hogendoorn, C.J., "Jet formation and jet velocity fluctuations in a flue organ pipe", J. Acoust. Soc. Am., 95:1119-1132, 1994.
- [8] Ségoufin, C., Fabre, B., Verge, M.P., Hirschberg, A., and Wijnands, A.P.J., "Experimental study of the influence of the mouth geometry on sound production in a recorder-like instrument: Windway length and chamfers", Acustica, 86:649-661, 2000.
- [9] Verge, M.P., Caussé, R., Fabre, B., Hirschberg, A., Wijnands, A.P.J., and van Steenbergen, A., "Jet oscillations and jet drive in recorder-like instruments", Acustica, 2:403-419, 1994.
- [10] Verge, M.P., Hirschberg, A., and Caussé, R., "Sound production in recorder-like instrument. II. A simulation model", J. Acoust. Soc. Am., 101:2925-2939, 1997.

## **SOME EFFECTS OF THE PLAYER'S VOCAL TRACT AND TONGUE ON WIND INSTRUMENT SOUND**

*J. Wolfe<sup>1</sup>, A.Z. Tarnopolsky<sup>1</sup>, N.H. Fletcher<sup>1</sup>, L.C.L. Hollenberg<sup>2</sup>, J. Smith<sup>1</sup>*

<sup>1</sup>School of Physics, University of New South Wales, Sydney

<sup>2</sup>School of Physics, University of Melbourne, Melbourne

J.Wolfe@unsw.edu.au    www.phys.unsw.edu.au/music

### **ABSTRACT**

In wind instruments, reeds (including lip reeds) interact with the acoustic impedances of the instrument's bore,  $Z_b$  and the player's vocal tract,  $Z_t$ . The bore is usually narrow and has high  $Q$  resonances whose maxima in  $Z_b$  are large and determine the playing regime to first order. The tract has resonances with lower  $Q$  which act on a small area of the reed. So how do the weak maxima in  $Z_t$  affect the timbre and pitch? We answer this question using a mechanical reed with geometrically simple vocal tracts and lungs to model didjeridu and trombone players.

The small area of the reed (or *moving* area of the lips) sees only weak tract resonances ( $Z_t \ll Z_b$ ) if the tongue is low. The tongue, when raised at the tip, acts as an impedance matching transformer linking this small area to the larger cross sectional area of the lower tract. Different tract configurations give strong effects on timbre and considerable effects on intonation, independently of the reed. The effects are consistent with those reported by players and explain some known intonation effects.

### **1. INTRODUCTION**

Many players of wind instruments talk of the perceived importance of the shape of the mouth on the sound. In the case of the didjeridu, the effect on the timbre is so clear as to be incontestable. Among scientists, however, there is considerable variation in opinion about the effect on pitch [1-4]. In this paper we report experiments on well-characterised model systems: artificial wind instrument players. Using plausible values of the relevant parameters, these show that vocal tract shapes can have important effects on both pitch and timbre.

Why do some scientists doubt the musicians?

First, there is the complication that, when a player changes mouth shape, s/he may also, unconsciously, change lip tension and geometry.

Second, it is difficult to explain the effect. In standard simple models, the acoustic currents on either side of the reed are equal, while the force on the reed depends on the difference in pressure. (We use 'reed' to mean either 'reed' in a woodwind or 'lip-reed' in a lip-reed instrument.) Thus the series combination  $Z_t + Z_b$  acts on the reed. The bore has resonances

with large  $Q$ . For most instruments, the bore is narrow and so has large characteristic impedance  $Z_0$ . How, then, can the relatively weak resonances of the vocal tract have an effect? In the case of the didjeridu, the bore and the tract have comparable dimensions, so the effects may be large. On the trombone, the effect is smaller, but in both cases we argue that it is larger than one might naïvely expect, because of the impedance matching effect of the tongue.

To answer these questions unambiguously, we use an artificial player, so we control vocal tract geometry and reed parameters independently. The reed is a simple cantilever spring. We call this version of the player Phyl, for 'PHYsicist's Lips'. Another version, with fluid-filled latex lips, is called Al, for 'Artificial Lips'. Phyl is less realistic than Al, but she has several advantages. First, she is easy to model mathematically. Second, the reed mass, spring constant and damping are controlled and measured independently of the acoustical experiment. Third, she can be used in the outwards striking mode to model lip reeds (as we do here) or reversed to model woodwinds.

We report measurements on two 'instruments'. One is a simple cylinder, selected from several with different lengths. This is a model of the didjeridu, chosen because of the known effect of the vocal tract on the timbre. We also studied the trombone as an example in which the tract is less well coupled to the bore, because of the mouthpiece constriction. Measurements on a clarinet played with an artificial vocal tract are reported in a companion paper [Fritz et al, this volume].

For simplicity, only geometrically simple vocal tracts are reported here. One is a cylinder, 30 mm in diameter and 180 mm long, representing a vocal tract with the tongue low in the mouth. The other is a cylinder, 9 mm in diameter and 120 mm long (representing the raised tongue) leading to a cone, widening from 9 mm to 30 mm over 60 mm (representing the lower tract). In a related study, (results not shown) we measured the vocal tract of a didjeridu player using MRI. The chosen shapes are idealisations of two tract configurations used in playing that instrument. In the high tongue configuration, the cross-sectional area is small just inside the teeth and above the tongue, and increases towards the lower vocal tract. In the low tongue configuration, there is less variation of area with position along the tract.

## 2. MATERIALS AND METHODS

Figure 1 represents the apparatus schematically. A source of dry compressed air leads to a cylinder, 30 mm diameter and 240 mm long filled with layers of acoustically absorbent material. The acoustic impedance of this cylinder, measured from the downstream end is largely real (lossy) and only weakly frequency dependent. We use it to model the trachea and lungs, whose highly branching structure is expected to have a similar output impedance.

The glottis is modelled by a plate separating the trachea from the vocal tract. The plate has a round hole with smoothed edges. Its diameter is 5 mm, chosen because proficient wind players are reported to keep the vocal folds almost closed while playing.

Downstream from the glottis is the selected vocal tract (see above) followed by the reed. The reed is a mass-loaded brass cantilever, here swinging outwards to model a lip reed. It is mounted in a plate to which the instrument under study may be attached. The didjeridus were sections of PVC pipe, diameter 44 mm and selected lengths. The trombone was a Yamaha, model YBL 321 bass trombone.

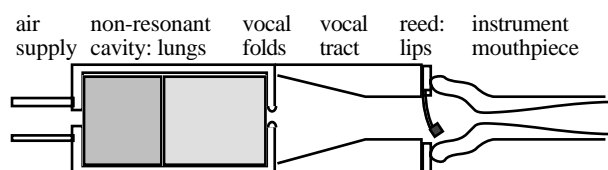


Figure 1: *The artificial lip reed player: not to scale.*

Acoustic impedance was measured using a technique reported elsewhere [5,6]. Sound spectra during playing were measured by a microphone 100 mm from the bell.

## 3. RESULTS AND DISCUSSION

### 3.1. The reed/lip 'sees' only a small area

It is important to note that the area of the reed that moves in the player's mouth is relatively small: rather less than 1 cm<sup>2</sup> for most woodwinds and brass. This is true even for the didjeridu [7].

Consequently the vibrating reed or moving part of the lips is not loaded by the impedance of the instrument measured across the whole area of its mouthpiece. In the simple case of a small piston moving in an infinite baffle, the diameter-matching load 'seen' by the piston can be modelled by an end effect rather like a radiation load: the impedance of an ideally open tube with length 0.8 times the piston radius. For a moving lip section of effective radius  $a$  in the mouth or at the input of an instrument, the impedance 'seen' is that of the instrument, as measured via an aperture with radius  $a$ . For

this reason, the vocal tract and instrument impedances reported here are measured with an impedance head with a small radius. It was taken to be 3.9 mm, which gives an area similar to that estimated from [7], and also because one of the semi-infinite waveguides that we use for calibration has this radius.

### 3.2 Oscillation regimes

The outward striking reed reported here was found to vibrate at frequencies determined by the fundamental or a higher resonance of the instrument-tract system when the frequency of the latter exceed that of the reed by a limited range, as predicted by standard models [8,9]. We call this an instrument-determined regime. Outside this range, the reed vibrates near its own resonant frequency, almost independently of the length of the instrument (a reed-determined regime). For constant reed parameters, gradual lengthening of the pipe produces a pitch falling smoothly as the frequency of the mode of the instrument decreases: an instrument-determined regime. Once the latter falls below the reed frequency, there is a range of lengths over which there is little variation in playing frequency: a reed-determined regime. Beyond this length there is a regime over which the instrument plays at the next higher mode frequency. However, the precise playing frequency depends upon the vocal tract (Figure 2). Depending upon the relationship of the sounding frequency to the maxima and minima of the vocal tract impedance, the imaginary part of the tract impedance  $Z_t$  may be either positive or negative, and thus may either slightly increase or slightly decrease the imaginary part of the dominant bore impedance  $Z_b$ .

Figure 2 shows that both the pitch and the regime transition depend upon the tongue position. For both tracts, the reed dominates at small pipe lengths  $L$ , but the pipe fundamental dominates above  $L = 550$  mm for the high tongue, and above 650 mm for the low tongue. At  $L \approx 1100$  mm the reed begins to dominate again, but for the high tongue alone the second resonance begins to dominate above  $L = 1300$  mm.

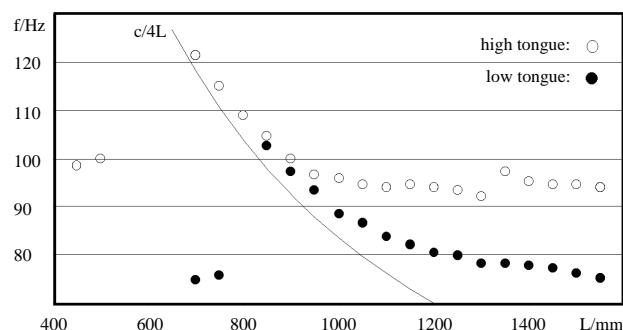


Figure 2. *Playing frequencies  $f$  for 'didjeridu' pipes of different lengths  $L$  played by an artificial playing system with simple vocal tract shapes.*

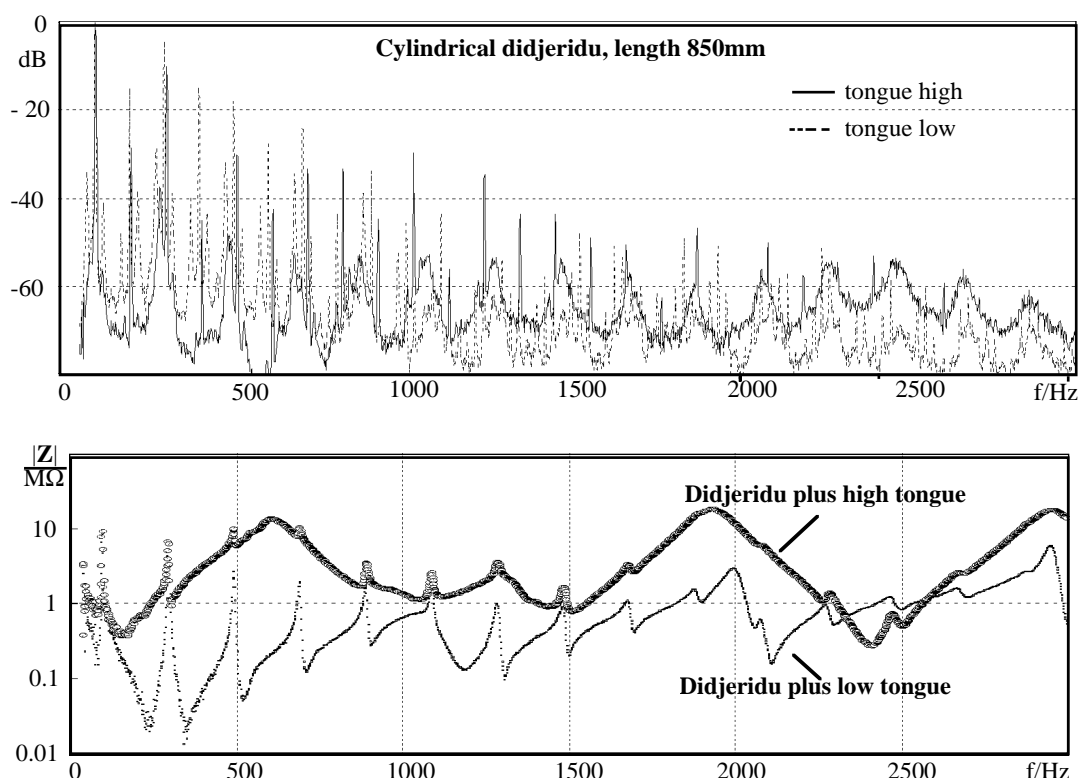


Figure 3. Sound and impedance spectra of a didjeridu played with vocal tracts corresponding to high and low tongue.

### 3.3. Vocal tract dominates didjeridu timbre

Figure 3 compares sound and impedance spectra in an instrument-determined regime for a didjeridu of length 850 mm. On the same axes are shown the sound spectrum and the series impedance  $Z_t + Z_b$  for the two chosen vocal tracts.

The impedance of the bore (not shown separately) is the same for the two, and is a regular series of maxima and minima, spaced at approximately 100 Hz, the frequency of a wave about four times the length of the didjeridu. The minima are not symmetrically spaced with respect to the maxima because  $Z_b$  is measured with a small head, representing the small moving area of the lips. The envelope of the impedance curves is determined by the impedance of the tract. For the raised tongue tract, the maxima are sharper and have higher values of  $Z$  than do those of the low tongue tract.

The spectrum of the note played using the raised tongue shows a stronger formant around 2 kHz, near the frequency of the maximum in  $Z_t + Z_b$ . Qualitatively, this corresponds to the experience of didjeridu players: by raising the tongue close to the roof of the mouth, one can produce a strong formant in the 1–3 kHz range (its exact frequency depends on the detailed shape) [10]. The low tongue sound lacks this formant. (Sound files available at [11].)

As expected, the spectra show strong odd harmonics, with the even harmonics produced due to nonlinear effects in

the reed. The sound files show that Phyl's timbre is breathy due to turbulence at the reed edge, so the resonances (which are not quite harmonic, especially at high frequencies) are excited by this broad band signal, as well as by the strictly harmonic partials of the reed. This is a simple example of the impedance matching effect of the tongue.

Other geometries (results not shown) give comparable effects: for example, a model tract consisting of a cone, narrow at the teeth and widening to meet the lower tract, produces both a strong impedance maximum and a corresponding formant. In this case, the tip of the tongue alone acts as an impedance matcher.

Note too the effect on the pitch (discussed in more detail below): on the one hand, this effect (among others) may be used by musicians for fine pitch adjustment. On the other hand, this effect can explain the intonation problems sometimes produced by double tonguing. In sufficiently rapid staccato passages, players initiate successive notes by alternating the articulations used in speech for [t] and [k]. Unless care is taken to keep the tongue tip high for the [k], the notes tend to alternate slightly in pitch.

### 3.4. Vocal tract influences trombone pitch

Figure 4 shows the spectrum of the sound played on a trombone by the artificial player using the two vocal tracts, in an instrument-determined regime. The shift in pitch, over



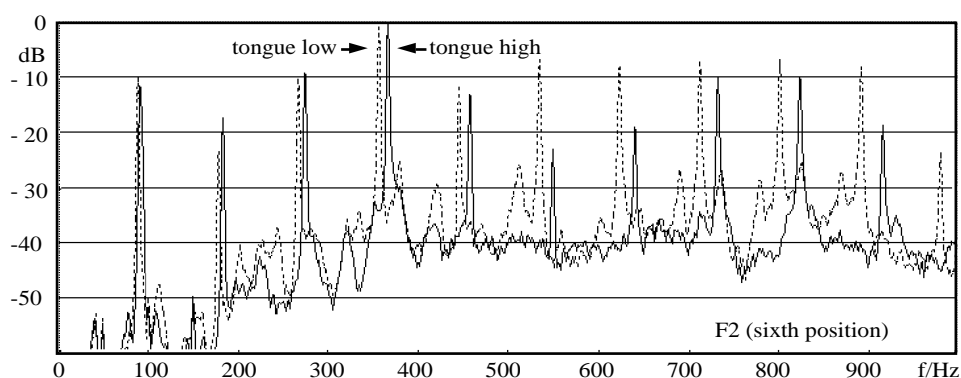


Figure 4. Sound spectra. 'Phyl' plays F2 on the trombone with vocal tracts corresponding to high and low tongue.

the range studied, is typically 20 cents: a musically important effect for intonation. Preliminary measurements on experienced brass players showed a comparable shift in pitch when they were asked to lower the tongue, keeping all else constant. A live brass player can compensate for this with lip tension of course—that she cannot is indeed one of Phyl's few advantages... to physicists.

The two tract configurations give timbres that are distinctly different, but less dramatically so than on the didjeridu (sound files at [11]). This is because the peaks in  $Z_b$  for the trombone are much higher than those for the didjeridu. Not only is the overall bore of the upper part of the instrument narrower than that of the didjeridu, but there is also a constriction in the mouthpiece that produces a formant near the 'pop' frequency of the mouthpiece [1].

#### 4. CONCLUSIONS

In this study of a model player of wind instruments:

1. Vocal tract geometry dominates the timbre of the sound of the didjeridu, and less strongly affects the timbre of the trombone.
2. The tract geometry affects the played pitch by typically 20 cents over both instrument-dominated and reed-dominated regimes in both instruments. It can also cause a transition between different playing registers.
3. Raising the tongue, or the tongue tip, increases the height of peaks in the vocal tract impedance, and so more effectively couples it to the instrument resonances and to the reed or lips. This gives wind players a method of fine pitch adjustment, by variably coupling a largely imaginary impedance. It also explains the intonation problem sometimes introduced by double tonguing.

**Acknowledgments:** We thank John Tann for technical assistance and the Australian Research Council for support.

#### 5. REFERENCES

- [1] Benade, A.H., Fundamentals of Musical Acoustics, Oxford Univ Press, NY, 1976.
- [2] Clinch, P., Troup, G. and Harris, L., "The importance of vocal tract resonance in clarinet and saxophone performance, a preliminary account" *Acustica*, 50:280-284, 1982.
- [3] Backus, J., "The effect of the player's vocal tract on woodwind instrument tone", *J. Acoust. Soc. Am.* 78:17-20, 1985.
- [4] Sommerfeld, S. and Strong, W., "Simulation of a player-clarinet system" *J. Acoust. Soc. Am.* 83:1908-1918, 1988.
- [5] Epps, J., Smith, J.R. and Wolfe, J., "A novel instrument to measure acoustic resonances of the vocal tract during speech" *Measurement Science and Technology*, 8:1112-1121, 1997.
- [6] Wolfe, J., Smith, J., Tann, J. and Fletcher, N.H., "Acoustic impedance of classical and modern flutes" *Journal of Sound and Vibration*, 243:127-144, 2001.
- [7] Hollenberg, L.C.L., "The didjeridu: lip motion and low frequency harmonic generation" *Aust. J. Phys.* 53: 835-850, 2000.
- [8] Fletcher, N.H. "Autonomous vibration of simple pressure-controlled valves in gas flows" *J. Acoust. Soc. Am.* 93: 2172-2180, 1993.
- [9] Fletcher, N.H. and Rossing, T.D., *The Physics of Musical Instruments*, 2nd edn. Springer-Verlag, New York, 1998.
- [10] Fletcher, N., Hollenberg, L., Smith, J. and Wolfe, J. "The didjeridu and the vocal tract", *Proc. International Symposium on Musical Acoustics*, Perugia. D.Bonsi, D.Gonzalez, D.Stanzial, eds, pp 87-90, 2001.
- [11] Music Acoustics, [www.phys.unsw.edu.au/music](http://www.phys.unsw.edu.au/music)

**ORGANS**



# CFD ANALYSIS OF AIR JET DEFLECTION — COMPARISON WITH NOLLE'S MEASUREMENTS

Seiji Adachi

ATR Human Information Science Research Laboratories  
2-2-2 Hikaridai Seika Kyoto 619-0288 Japan  
sadachi@atr.co.jp

## ABSTRACT

Motion of an air jet deflected by sound is a key to understanding sounding mechanism of air-jet driven instruments. The basic mechanism has successfully been explained by several hypothetical models of jet deflection. Our understanding has not, however, reached such a level that the transition among the oscillation modes can be precisely predicted for a given organ flue pipe. This is probably due to conceptual approximations included in the models. To overcome this situation, a more rigorous method based on the Navier-Stokes equations of fluid dynamics is needed. This paper uses computational fluid dynamics (CFD) to directly simulate the wavy motion of a jet deflected by sound. For jets having parabolic and tophat velocity profiles at the flue exit, the deflection amplitude and phase lag behind the sound field are numerically obtained at various distances in the downstream region. The results are compared with those obtained by Nolle's hot-wire measurements.

## 1. INTRODUCTION

Sounding of an air-jet driven instrument is a self-excited oscillation where oscillations of a jet in the mouth and of an aircolumn in the pipe interact with each other. Figure 1 shows an organ flue pipe sounding in the first resonance mode. Here, an aircolumn oscillation in the first resonance mode is schematically illustrated with masses and a spring. An air jet emerging from a flue slit, after traveling through the mouth and being deflected by the sound, impinges on an edge. A part of the airflow coming into the pipe then excites the aircolumn oscillation acoustically. To maintain the sounding, the flow injection into the pipe should be regularly made at an appropriate phase lag behind the aircolumn oscillation.

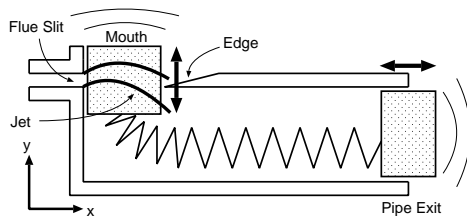


Figure 1: Schematic diagram of an organ flue pipe sounding in the first resonance mode.

According to Elder [1] and Fletcher [2], the jet acts as a volume flow source on the acoustical excitation in the pipe in normal oscillation regimes. This implies that the jet should be deflected

downward when sound pressure has its maximum at the mouth. The phase of the jet deflection can be determined by jet velocity, which can be directly controlled by the air pressure supplied to the pipe. By changing the pressure, we get several oscillation regimes in various resonance modes, or no sounding at all depending on the value of the pressure. To predict the transition among the modes, we have to know how the jet is deflected by the sound, or specifically the phase and magnitude as functions of the traveling distance  $x$ . They also depend on the jet velocity, frequency and amplitude of the sound field.

Due to nonlinearity, it is a formidable task to analytically calculate the phase and magnitude of the deflected jet. Instead, only hypothetical models[3][4][5] have been proposed. These are based on the theory of fluid instability [6] that assumes infinitesimal deflection amplitude, inviscidity of the flow, etc. The motion of the deflected jet predicted by these models does not, however, explain the actual mode transition.

Another approach to obtaining the phase and magnitude is the jet deflection measurement[7][8]. Nolle measured the jet deflection phase and magnitude as functions of the traveling distance  $x$  by hot-wire anemometry[8]. Unfortunately, the results were reported only for one value of the jet velocity. It is thus impossible to predict the mode transition only from his results.

This research aims to calculate the phase and magnitude of the deflected jet numerically from the Navier-Stokes equations. In a previous report[9], it was shown that computational fluid dynamics (CFD) can successfully simulate the motion of the deflected jet. In this paper, the simulated results are compared with those obtained by Nolle's measurement.

## 2. JET DEFLECTION THEORY

The basis for understanding the motion of a jet deflected by sound is the model proposed by Fletcher[3]. Suppose that a jet travels along the  $x$  axis, while it is deflected perpendicular to the traveling direction. The displacement of the jet along the  $y$  axis at time  $t$  can be written as  $\eta(x, t)$ . A uniform sound field oscillating along the  $y$  axis is assumed in the pipe mouth. The acoustic displacement in  $y$  direction is then written as  $Y(t) = Y e^{i\omega t}$ . Fletcher modeled the jet displacement as

$$\eta(x, t) = Y(t) \left[ 1 - e^{\mu x} e^{-i\omega x / V_{ph}} \right], \quad (1)$$

where  $\mu$  is the growth factor of an infinitesimal disturbance imposed on the flow, and  $V_{ph}$  is the phase velocity.

Figure 2 shows  $\eta(x, t)$  calculated from Eq. (1) with assumptions of  $\mu = 0.44 \text{ mm}^{-1}$  and  $\omega / V_{ph} = 0.33 \text{ mm}^{-1}$ . In Fig. 2 (a),

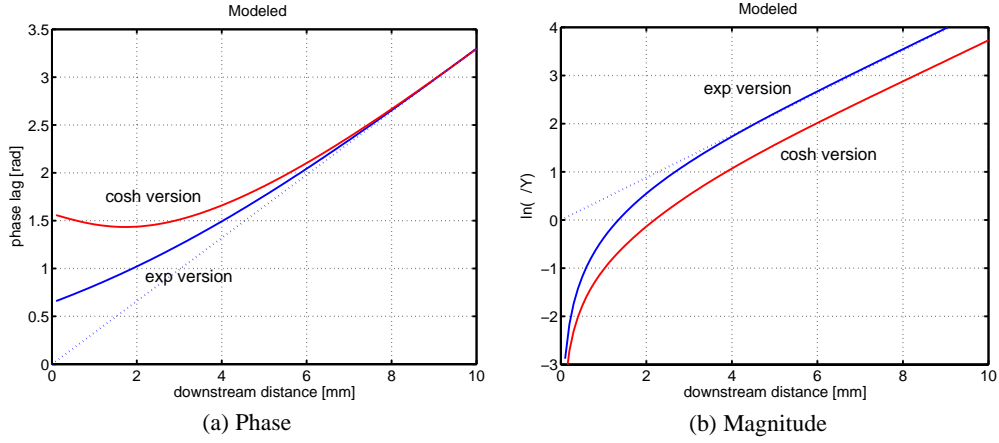


Figure 2: Jet deflection phase and logarithmic magnitude modeled by Eq. (1). Phase is referred to negative acoustic displacement.

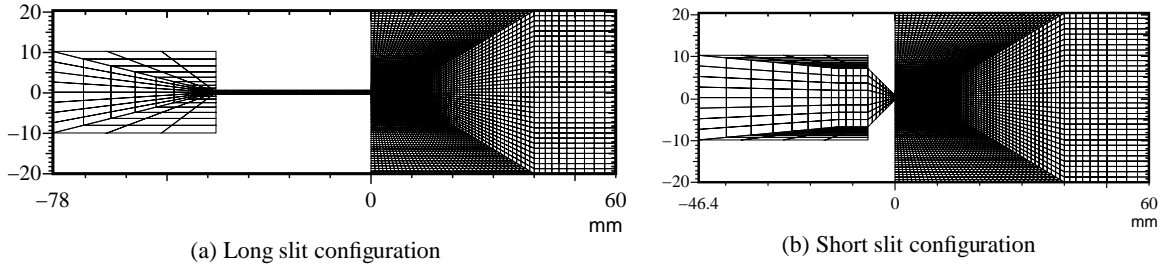


Figure 3: Calculation domains for CFD.

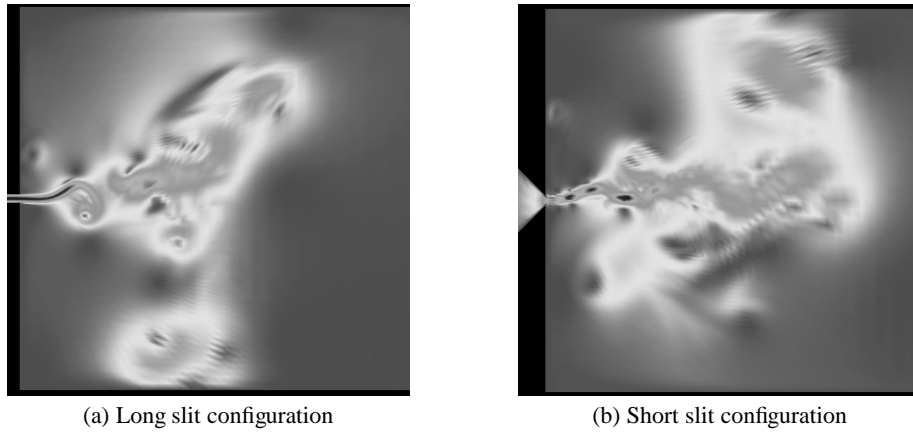


Figure 4: Snapshots of simulated jet deflection.

the phase lagged from  $-Y(t)$  (negative acoustic displacement) is plotted in the radian. In Fig. 2 (b), the logarithmic magnitude of the jet deflection against the acoustic displacement is plotted. The sounding condition is that the jet deflection has the same phase as that of the acoustic displacement. This condition is fulfilled if the edge is placed about 9.4 mm downstream from the flue exit, because it gives  $\pi \approx 3.14$  phase lag in Fig. 2 (a).

### 3. NUMERICAL SIMULATION

The same numerical method as in the previous report[9] is used, except that the outflow boundary condition is replaced with the

convective boundary condition,

$$\begin{cases} \dot{\mathbf{v}} + U_{\text{conv}} \frac{\partial \mathbf{v}}{\partial x} = 0, \\ \dot{p} + U_{\text{conv}} \frac{\partial p}{\partial x} = 0, \end{cases} \quad (2)$$

where velocity field  $\mathbf{v}(\mathbf{x}, t)$  and pressure field  $p(\mathbf{x}, t)$  are assumed to flow out from the boundary with a constant convective velocity  $U_{\text{conv}}$ . This can solve the problem of a numerical divergence that appeared in the previous report.

The calculation domains are shown in Fig. 3 for (a) a long parallel slit and for (b) a short converging slit. These slits have

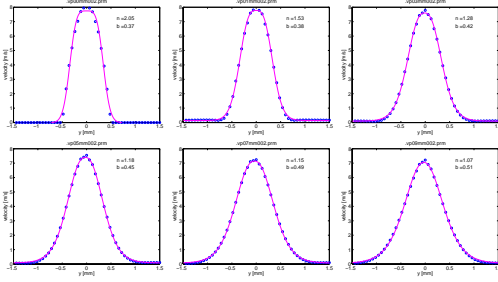


Figure 5: Velocity profiles of a free jet emerging from the long slit.

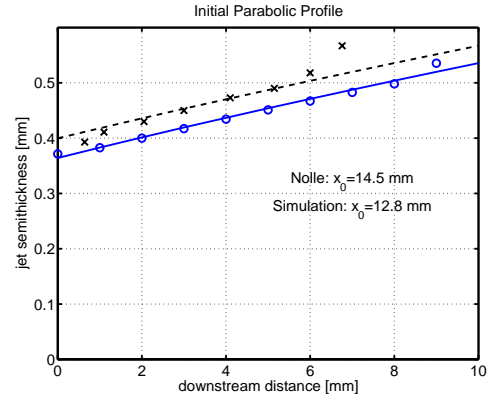


Figure 6: Comparison of jet half-thickness  $b$  between numerical simulation and measurement.

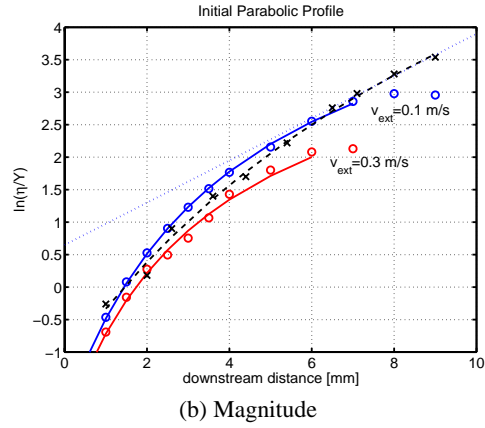
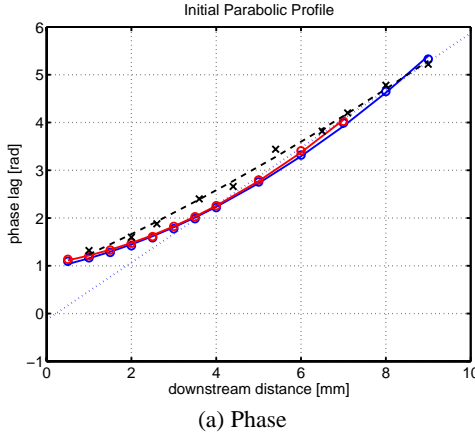


Figure 7: Comparison of jet deflection phase and magnitude between numerical simulation and measurement in long slit configuration.

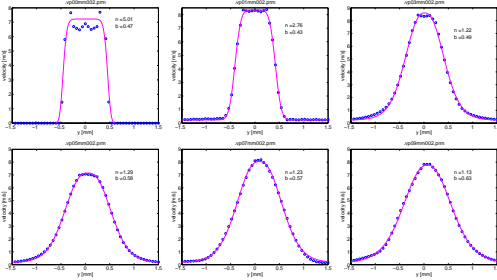


Figure 8: Velocity profiles of a free jet emerging from the short slit.

identical shapes with the ones used in Nolle's measurements. The width of the slits is 1 mm. On the inflow boundary, a constant flow velocity  $U$  is imposed. As in Nolle's measurements,  $U$  was adjusted to give the maximum airflow velocity of 8.2 m/s at the flue exit.

On the upper and lower boundaries in the region downstream from the flue exit, a velocity oscillating sinusoidally along the perpendicular direction is imposed to give acoustical displacement caused by sound deflecting the jet. The magnitude of the velocity was set to 0.1 and 0.3 m/s. These are for 100 and 110 dB sound

pressure levels, respectively.

Snapshots of the calculated flows in the long and short slit configurations are shown in Fig. 4 for a 0.3-m/s acoustic velocity oscillating with a frequency of 300 Hz. In both cases, the wavy motion of a jet deflected by sound is observed. After the jet travels more than a few mm, the deflection amplitude exceeds the slit width. This situation is out of the scope of hypothetical models that assume an infinitesimal amplitude. The flow becomes turbulent after the jet travels about 10 mm. It is observed that the jet motion is also influenced by vortices made by the jet itself. This is an effect that hypothetical models cannot consider.

## 4. SIMULATION RESULTS

### 4.1. Case 1: Long Slit Configuration

In the long slit case, the velocity profile of the jet becomes parabolic at the flue exit. The profile is very similar to the Bickley profile[10] for a theoretical free jet coming out of an infinitesimal slit. Nolle extends the Bickley profile to

$$v(y) = v_p + (v_0 - v_p) \text{sech}^2 \left\{ \left( \frac{y - y_0}{b} \right)^n \right\} \quad (3)$$

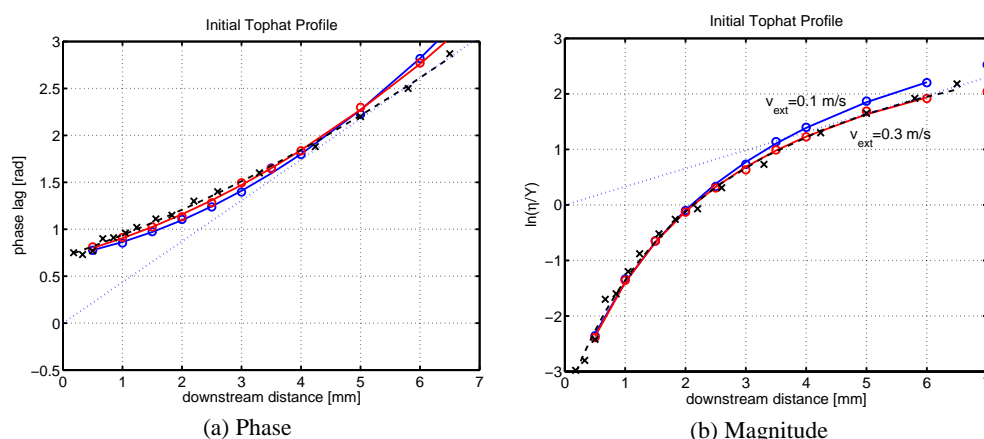


Figure 9: Comparison of jet deflection phase and magnitude between numerical simulation and measurement in short slit configuration.

for analyzing actual velocity profiles, where  $b$  is the half-width of the jet, and  $n$  is a parameter representing the squareness of the profiles. For  $n = 1$ , the original Bickley profile is recovered.

Figure 5 depicts the calculated velocity profiles of a free (undeflected) jet at downstream distances of  $x = 0, 1, 3, 5, 7, 9$  mm. The circles represent calculated values, and the dashed curves are the ones fitted with Eq. (3). As the jet travels,  $n$  approaches 1 from 2.06, and  $b$  increases due to the viscosity.

The dependence of  $b$  on  $x$  is known to be proportional to  $(x + x_0)^{2/3}$  for the Bickley profile, where  $x_0$  is an unknown distance in which the infinitesimal width of a jet grows to the slit width, and therefore it can be used as a fitting parameter. Figure 6 compares calculated  $b$  (marked with  $\circ$ ) with the one measured by Nolle ( $\times$ ). The calculated results are in very good agreement with the measured ones, if we assume that the slit used by Nolle is about 3 % narrower than 1 mm.

Figure 7 depicts (a) the phase and (b) the magnitude of the deflection. The calculated and measured values are plotted with  $\circ$  and  $\times$ , respectively. The solid lines and dashed lines are fitted curves for the calculated and the measured values, respectively. The two solid lines in each figure are for two different amplitudes of the acoustic velocity. The calculated phase curve is in good agreement with the measured one, although the former has a larger curvature. This means that the jet deceleration is larger in the calculation. The calculated magnitude is also in good agreement with the measured one. Note here that there is a difference in the acoustic velocity amplitude. This means nonlinearity, i.e., that the deflection amplitude does not grow linearly as the acoustic velocity amplitude increases.

#### 4.2. Case 2: Short Slit Configuration

In the short slit case, the velocity profile at the flue exit is tophat shaped. Figure 8 depicts the calculated velocity profiles of a free (undeflected) jet at downstream distances of  $x = 0, 1, 3, 5, 7, 9$  mm with fitted curves. The parameter  $n$  representing squareness suddenly drops from 5.01 to 1.13. This means that the profile changes from tophat shape to bell shape.

Figure 9 depicts (a) the phase and (b) the magnitude of the deflection. Both the calculated phase and magnitude are in good agreement with the measured ones. As in the long slit case, the phase curve has a larger curvature, and the magnitude shows non-

linearity.

## 5. CONCLUSION

The phase and magnitude of a jet deflection calculated by CFD are in very good agreement with those obtained by Nolle's flow measurements. In the CFD simulation, nonlinearity was observed. In other words, the deflection amplitude does not grow linearly as the acoustic velocity amplitude increases. However, the phase is not influenced very much by the acoustic velocity amplitude. As a conclusion, CFD is beneficial as a replacement for experimental methods for measuring the motion of a jet deflected by sound.

This research was conducted as part of "Research on Human Communication" with funding from the Telecommunications Advancement Organization of Japan.

## 6. REFERENCES

- [1] Elder, S.A., "On the mechanism of sound production in organ pipes", J. Acoust. Soc. Am. Vol. 54, pp. 1554-1564 1973.
- [2] Fletcher, N.H., "Jet-drive mechanism in organ pipes", J. Acoust. Soc. Am. Vol. 60, pp. 481-483 1976.
- [3] Fletcher, N.H. and Thwaites, S., "Wave propagation on an acoustically perturbed jet", Acustica Vol. 42, pp. 323-334 1979.
- [4] Yoshikawa, S. and Saneyoshi, J., "Feedback excitation mechanism in organ pipes", J. Acoust. Soc. Jpn. Vol. E1, pp. 175-191 1980.
- [5] Adachi, S., "Dynamical modeling of jet deflection mechanism in organ flue pipes", Proc. Int. Symp. on Musical Acoustics (ISMA 2001) pp. 317-320 2001.
- [6] Lord Rayleigh, *The theory of sound* (Macmillan, New York. Reprinted by Dover New York, 1945) Vol. 2, 376-414.
- [7] Yoshikawa, S., "Jet wave amplification in organ pipes", J. Acoust. Soc. Am. Vol. 103, pp. 2706-2717 1998.
- [8] Nolle, A.W., "Sinuous instability of a planar air jet: Propagation parameters and acoustic excitation", J. Acoust. Soc. Am. Vol. 103, pp. 3690-3705 1998.
- [9] Adachi, S., "Numerical Analysis of an air jet: Toward understanding sounding of air-jet driven instruments", Forum Acusticum Sevilla 2002, MUS-04-002-IP, 2002.
- [10] Bickley, W., "The plane jet", Philos. Mag. Vol. 23, pp. 727-731 1937.

## **BREATHING MODES AND SOUND RADIATION OF METALLIC ORGAN PIPES**

*S. Bergweiler<sup>1</sup>, A. Bergner<sup>1</sup>, T. Görne<sup>2</sup>, M. Wegener<sup>3</sup>, R. Gerhard-Multhaupt<sup>3</sup>*

UP Transfer GmbH at the University of Potsdam, Potsdam, Germany (1)

Görne Akustik, Berlin, Germany (2)

University of Potsdam, Department of Physics, ACMP, Potsdam, Germany (3)

bergweil@rz.uni-potsdam.de

### **ABSTRACT**

The tube resonator of an organ pipe has long been considered a perfectly stiff tube. The tube cross section and length, rather than the pipe material, were supposed to influence the sound, but recently this was shown to be wrong. It was found that the pipe surface is not motionless. Ellipsoidal dipole-like oscillations of the upper lip and the upper end of the pipe body were detected. Furthermore, the material does influence the patterns and the magnitude of the pipe-body oscillations.

The sound radiation of a small source will be strongly influenced by the volume flow, caused by its breathing monopole behavior. In organ pipes, however, this has not yet been considered in detail. We measured the breathing motion of the pipe body by means of a ring-shaped piezoelectric sensor film tensioned around the cylindrical pipe resonator. From the length variations of the sensor we obtain an averaged electrical signal for each cross section along the pipe length if pipe-wall breathing occurs. We found a close relationship between the pressure distribution of the air-column resonances inside the pipe and the cross-section variations along the pipe. On pipes with thinner metal walls, stronger breathing of the pipe body was found.

The results are discussed with respect to the relationship between air-column and pipe-body oscillations. Differences between pipes with thicker and thinner walls will also be considered.

### **1. INTRODUCTION**

The simplest physical model of a labial organ pipe consists of a generator coupled with a resonator. In the steady state, resonances occur. The oscillation of the air stream at the lip couples with the standing wave of the air column inside the tube-shaped resonator. Length and diameter of the tube define the fundamental frequency and the relative magnitudes of its higher harmonics. The resulting sound is radiated from the upper open end and the mouth of the pipe. [1, 2, 3]

Organ builders consider the pipe material as very important for the sound quality. Most metallic organ pipes are made of a lead-tin alloy, with lead percentages between 75 and 95%. The higher the lead content the warmer and softer the pipes are considered to sound. Initial research did not support the idea of the material having any influence on the sound [4,5]. Because of the comparably high sound pressures radiated from the pipe openings, it was not considered whether the body of the organ pipe influences the audible sound in any other way apart from the geometrical boundary conditions. The pipe wall was modeled as a perfectly stiff tube providing

well-defined and reproducible boundary conditions for the air column.

Recent investigations revealed various oscillation patterns of the resonator tube itself at the harmonics of the air column. Around the cross section, four nodes were found for all oscillation frequencies. The circumference oscillates as a planar quadrupole. Along the pipe length from the open end to the mouth, the oscillation patterns corresponded to the standing-wave patterns of the air-column harmonics. [6]

Sound radiation strongly depends on the ratio between the size of the oscillating area and the wavelength. In the case of an organ pipe body, tiny surface movements over small areas render sound radiation, at least at lower frequencies, almost impossible. The lateral quadrupole can be modeled as four monopoles at angles of 90°, with adjacent sources at alternate phase. Because of this alternating movement, the air is moving tangentially between the quarters of the quadrupole rather than in radially propagating pressure waves radiated into the far field.

A much more efficient device for radiation is the acoustic monopole with all displacements in phase around the circumference. In organ pipes, breathing motion is thus of great interest. In this case, the source area is the product of the height of the breathing sections and their circumferences. In order to find out if the pipe body itself may radiate sound, we investigated the oscillations of the circumference integrated over sections of the pipe length.

Because of the small surface displacement, the contribution of this surface breathing to the overall pipe sound is rather small. However, variations of the tube-resonator circumference caused by the pressure distribution of the standing waves inside the pipe must also influence the standing waves themselves. In this case, a portion of the energy of the standing wave is fed into the oscillation of the pipe body and is no longer available for sound radiation from the air column. We therefore recorded and compared the sound spectra generated by pipes with different breathing intensities of their bodies.

### **2. MEASUREMENT PROCEDURE**

The measurements were carried out with piezoelectric polymer sensors. When the polymer film is stretched, an electrical voltage is generated between its evaporated electrodes. The sensor is compliant and its voltage signal is proportional to its change of length. The sensor film can also be patterned so that a signal is only detected from its metallized areas. The ribbon-shaped polymer film was slightly tensioned around the pipe body. In order to ensure sufficient and stable contact between



pipe surface and sensor, one end of the polymer film was attached to the pipe with adhesive tape, while the other end was loaded with a small weight. The piezoelectric sensor had a size of 1.5 cm by 11.5 cm and a thickness of 25  $\mu\text{m}$  [7].

Measurements were done on four different pipes at locations 2 cm apart along their lengths, resulting in 25 data points for each pipe. Because the upper lips are slanted, no measurements could be taken there. This slant would have prevented the indispensable good mechanical contact between sensor and pipe surface, still leaving 50 cm of the 60 cm long pipe bodies to be investigated.

### 3. RESULTS AND DISCUSSION

When an organ pipe is blown, the sound starts to build up. After the short attack phase, the steady state is reached very quickly. Now the resonances of the inner air column are fully developed and stable. These air-column resonances are due to the partial reflection of the traveling sound waves at the open end and at the mouth of the pipe. The amplitudes of the forward and backward traveling waves add inside the pipe, constituting a standing wave. For each harmonic of an open organ pipe, a sinusoidal half-wave pattern is found. The first harmonic exhibits one pressure maximum in the pipe center with two minima at the pipe openings. The second harmonic shows two maxima and three minima, etc. [1,3,4].

We studied the circumference oscillations caused by the air pressure inside the pipe. We first investigated two labial principal C (2') organ pipes, P2 and P4, with their fundamental frequency at 263 Hz. Figure 1 shows the signal amplitude along the pipe body, averaging over the elongation around one circumference of the pipe.

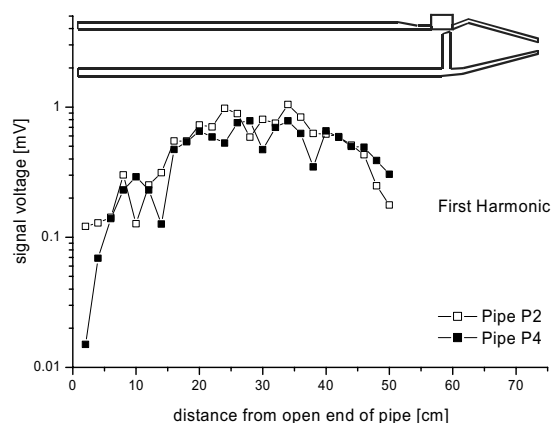


Figure 1: Relative amplitudes of circumference oscillations on two labial organ pipes (P2 and P4) at their first harmonic frequency.

A clear signal with its amplitude extending over two orders of magnitude was observed. For both pipes, the signal profile along the pipe length is almost identical. It clearly decreases towards both openings of the pipe and has one maximum at the center of the pipe body. Figure 2 shows the signal at the frequency of the second harmonic. The range of the signal amplitude from 0.03 to 2 mV is approximately the same as that

of the first harmonic. However, more than only one relative maximum can be seen here. Pipe P4 delivers a rather strong signal at the open end. Towards the mouth, it first reaches a minimum around 10 cm below the open end. The signal then rises twice showing two relative maxima, with minima at 27 cm and near the mouth. P2 is of the same quality concerning the three minima at around 15, 27 and 50 cm. The maxima are, however, different. Between 15 and 50 cm there is rather one high-level region with a small dent in its center than two separate relative maxima.

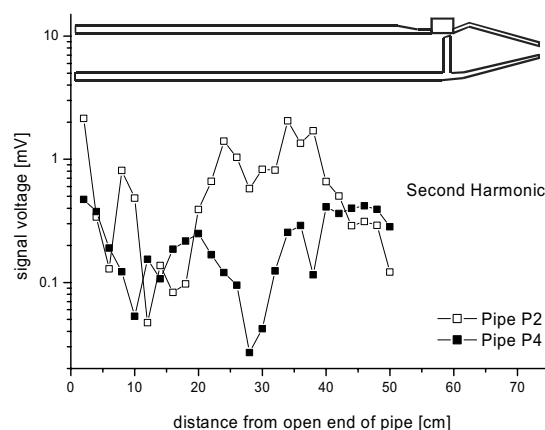


Figure 2: Relative amplitudes of circumference oscillations on two labial organ pipes (P2 and P4) at their second harmonic frequency.

For the first harmonic, the signal detected along the pipe body corresponds very well to the expected standing-wave pressure pattern inside the pipe at the same frequency. At the second harmonic, a clear breathing motion is also found.

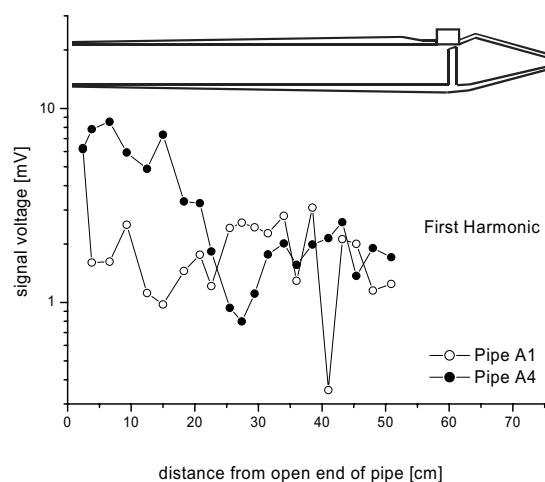


Figure 3: Relative amplitudes of circumference oscillations on two labial organ pipes (A1 and A4) at their first harmonic frequency.

In order to confirm the monopole oscillations of the pipe-body circumference, differently built pipes were also investigated. Length and diameter are unchanged with respect to P1 and P4, but the wall thickness now has a conical profile. The investigated pipes A1 and A4 have been “thinned out”, i.e. their wall thickness decreases from the mouth to the open end from 1 mm to 0.5 mm.

Figure 3 shows the signal amplitude detected on pipes A1 and A4 at the first harmonic frequency. At the open end, the pipe wall is only half as thick as on pipes P2 and P4. For the thinner-walled pipes, the measured signal is approximately 10 times stronger. Towards the mouth where the wall strength increases, the measured signal decreases. A simple geometric function to describe the shape of the signal could not be found.

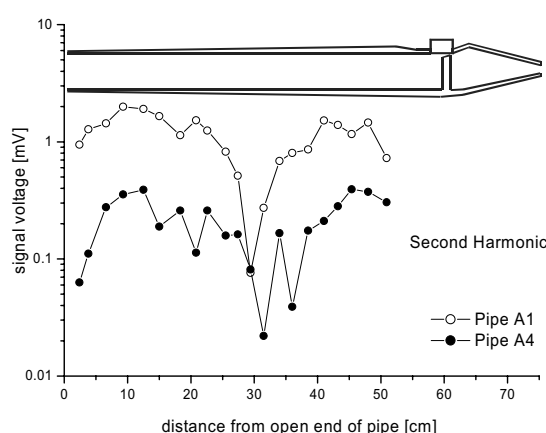


Figure 4: Relative amplitudes of circumference oscillations on two labial organ pipes (A1 and A4) at second harmonic frequency.

For the second harmonic, Figure 4 shows the experimental results of the two thinner-walled pipes. Here the signals of both pipes show the same shape with pipe A4 exhibiting a much smaller amplitude than pipe A1. Both pipes have minima at the open end and at the mouth of the pipe and a third minimum around the pipe center.

#### 4. CONCLUSIONS AND OUTLOOK

In this investigation, the excitation of a monopole breathing of the pipe body was detected for the first time. The circumference of the pipe body oscillates at the frequencies of the air-column resonances. At the first harmonic, the pipes with constant wall profiles show a very good correlation between the inner sound field and the breathing strength of the pipe. At the second harmonic, this also is the case for the pipes with conical wall profiles. The amplitude of the breathing wall oscillation is influenced by the thickness of the pipe wall. Thinner-walled organ pipes show a stronger pressure-induced variation of their circumference than pipes of the same material with thicker walls.

In earlier research [8], we found that, on average, the thinner-walled pipes deliver lower sound-pressure levels at the low harmonics than the pipes with constant wall thickness. The

stronger absorption of the air-column resonance energy by the thinner walls might be responsible for this finding. The modified sound radiation caused by wall vibrations must be further investigated.

All the present preliminary studies must be repeated in order to improve their statistical validity. Measurements on 16 more pipes are in preparation. Furthermore, a series of pipe resonators without the generator part, to be excited with a loudspeaker, will also be investigated with respect to their monopole behavior.

#### 5. ACKNOWLEDGEMENTS

We kindly acknowledge Schuke Orgelbau Potsdam, for making the organ pipes and the laboratory-scale wind supply system available. Furthermore we are indebted to thank Dr. Detlef Zscherpel for many stimulating discussions. We also would like to thank the German Federal Ministry for Economics and Technology (InnoNet Project 16IN0001 and ProInno Project 0203902KBV0) for financial support.

#### 6. REFERENCES

- [1] Rossing, T. and Fletcher, N., “The physics of musical instruments”, 2nd edition, Springer, New York, 1998
- [2] Miklós, A. and Angster, J., “Properties of the sound of flue organ pipes”, *Acta Acoustica*, Vol. 86, No. 4, pp. 611-622, 2000
- [3] Lottermoser, W. und Meyer, J., „Orgelakustik in Einzeldarstellungen“, (“Organ acoustics in individual presentations”), Verlag: Das Musikinstrument, Frankfurt am Main, 1967
- [4] Backus, J. and Hundley, T.C., “Wall vibrations in flue organ pipes”, *J. Acoust. Soc. Am.*, Vol. 39, No. 5, pp. 936-945, 1966
- [5] Boner, C.P. and Newman, R.B., “The effect of wall materials on the steady-state acoustic spectrum of flue pipes”, *J. Acoust. Soc. Am.*, Vol. 12, pp. 83-89, 1940
- [6] Runnemalm, A., Zipser, L. and Franke, H., “Structural vibration modes of a blown organ pipe”, *Acta Acoustica*, Vol. 85, No. 6, pp. 877-882, S. Hirzel Verlag, November 1999
- [7] Wegener M., Gerhard-Multhaupt R., Wirges W., Bergner A. and Bergweiler S., “Breathing modes of woodwind bodies: Experimental detection with ring-shaped piezoelectric-polymer sensors”, *SMAC 03 Proceedings*, Stockholm, 2003
- [8] Görne, T., Zscherpel, D., Zierenberg, M., Bergweiler, S. and Gerhard-Multhaupt, R., „Einflüsse der Wandgestaltung auf den Klang von Prinzipalorgelpfeifen“, (“Effects of the wall-thickness profiles on the sound of principal organ pipes”), 28. DAGA, 2002, Bochum



## **PARTICLE IMAGE VELOCIMETRY (PIV) MEASUREMENTS OF VELOCITY FIELDS AT AN ORGAN PIPE LABIUM**

*Eva-Lena Johansson\*, Lars Benckert and Per Gren*

Division of Experimental Mechanics  
Luleå University of Technology  
SE-971 87 Luleå, Sweden

\*evalena@mt.luth.se

### **ABSTRACT**

A pilot experiment is presented that measures velocity fields in two planes at a blown organ pipe labium for a fundamental tone at 260 Hz. The sound pressure is also measured at the same time as the velocity fields are registered. This makes it possible to follow the change of the velocity field as the sound pressure varies with time. The methods used are stereoscopic particle image velocimetry (PIV) and two-dimensional particle image velocimetry. The difference between the methods is that the first one measures three velocity components by use of two CCD cameras and the second one measures two velocity components with one camera. A double pulsed Nd:YAG laser is used as illuminating source. It gives short light pulses (~13 ns) necessary to resolve the quite high air velocity (~10 m/s). Results show that it is possible to follow a travelling vortex at the organ pipe labium in time as the sound pressure changes. The stereoscopic measurements show that the velocity fields are three-dimensional. The measurements have shown to be repeatable.

### **1. INTRODUCTION**

Velocity field measurements are used as a tool to understand the dynamic behavior of streaming fluids. Many applications are found in engineering, where sound production is one. It is of interest to perform particle image velocimetry (PIV) measurements for three-dimensional velocity fields at high velocities.

A pilot experiment to test a stereoscopic particle image velocimetry set-up is presented, that measures velocity fields in two planes at a blown organ pipe labium for a fundamental tone at 260 Hz. The sound pressure is simultaneously measured as the velocity fields are registered. This makes it possible to follow the change of the velocity fields as the sound pressure varies with time. The methods tested are stereoscopic particle image velocimetry and also two-dimensional particle image velocimetry. The difference between the first method and the second is that the first one measures all three velocity components by use of two CCD cameras and the second one measures two in-plane velocity components with one camera. See for instance Raffel et al. [1] or Hinsch [2] about these measurement methods. Another method that could be used to measure velocities is Laser Doppler Velocimetry (LDV) [3]. This method measures the velocity in one point at a time, but as a continuous function of time. It is not a whole-field measurement method as PIV. PIV measurements are done at a

specific instant of time. Holographic particle image velocimetry [4] is a method that measures the velocities in a volume.

A lot of work has been done earlier on wind instruments, see Fletcher et al. [5]. Flow visualization using Schlieren measurements has been performed as well as numerical simulations of the non-linear flow in wind instruments [6]. Vortexes and acoustic sound fields have recently been visualized by Scanning Laser Doppler Velocity (LDV) measurements [7]. The sound intensity from a blown organ pipe has been measured [8]. Wall vibrations of open organ pipes have been studied by using TV holography, shearography and laser scanning vibrometry [9, 10].

### **2. EXPERIMENTAL METHOD**

The measurement method is a non-intrusive optical method. It is also an indirect method, because tracer particles are seeded to the flow of air and it is the displacement of the particles that one measures. The tracer particles are illuminated with pulsed laser light in a light sheet, twice in a short time interval, and images of the illuminated particles are registered with one or two CCD cameras on separate frames. The displacements are determined with a cross-correlation technique. The two images are divided into small sub images and the mean displacements are determined for each sub image pair. Since the time separation between the images is known, the velocity field can be determined.

Two cooled CCD cameras of type PCO Sencam double shutter with a resolution of  $1280 \times 1024$  pixels, a pixel size of  $6.7 \times 6.7 \mu\text{m}^2$  and a dynamic range of 12 bits were used. They were controlled from a computer via a fibre optic cable. The softwares PivView 1.7 and PivView 2.0 (delivered by PIVTEC GmbH, Göttingen, Germany) were used for calibration of the system and calculation of the velocity fields. Calibration is necessary especially in the stereoscopic arrangement. Both camera images must be adjusted to overlap and different magnification factors over the field of view must be taken into account. A pulsed Nd:YAG laser, Spectron SL804T, was used as a light source. It is a twin cavity model, i.e. it consist of two independent Nd:YAG lasers which can be fired at any time separation. In addition each laser can be double pulsed with time separations ranging from 40  $\mu\text{s}$  to 200  $\mu\text{s}$  with a pulse duration of 13 ns. Up to four recordings are thus possible to obtain. The high velocities in these experiments requires a short time separation between exposures, therefore single pulses from both laser cavities were used. A suitable displacement of particles between two images is 1-10 pixels.

An experimental organ was used with the pipe placed in it, as in [8]. The organ was blown with a fan, whose inlet was fed with smoke from a smoke generator of type SAFEX NEBELGERÄT-FOG GENERATOR F2010. The smoke particles are of  $\mu\text{m}$ -size. The organ pipe is blown with a constant air pressure at 685 Pa (70 millimetre measured on a water gauge). A microphone was placed about 5 cm from the labium to measure the sound pressure. It did not disturb the flow, see Figure 1, where also the stereoscopic camera arrangement is illustrated.

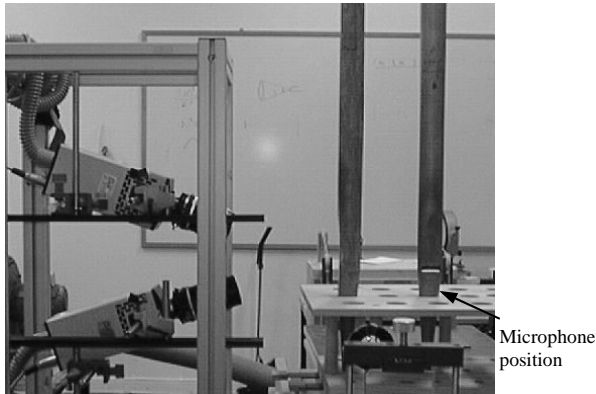


Figure 1. Experimental set-up for 2D-3C PIV. The position of the microphone, as it was during measurements, is shown at the side of the organ pipe.

The flow was first registered with one camera (2D-2C PIV, two dimensions and two velocity components). In this case the velocity field was registered outside the labium, in the middle and from the side of the pipe, see Figure 2. The time separation between images was  $5 \mu\text{s}$  in these measurements. Also 2D-3C (two dimensions and three velocity components) particle image velocimetry was used, which means measurement of three velocity components in a thin sheet. The velocity fields were then registered in two different planes, perpendicular to each other. The two different views are the front view and the side view of the labium. The camera arrangements and the image fields are shown in Figure 3 (a-b). The cameras were arranged according to the angular displacement method [1]. Here the time separation was  $20 \mu\text{s}$ .

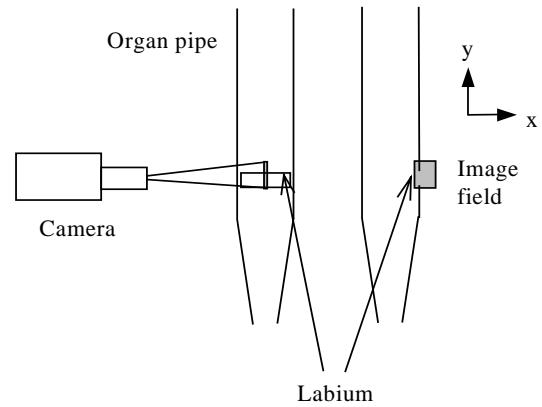


Figure 2. Experimental set-up for 2D-2C PIV. The organ pipe is seen from the front and from the side. The image field is  $14 \times 17 \text{ mm}^2$ .

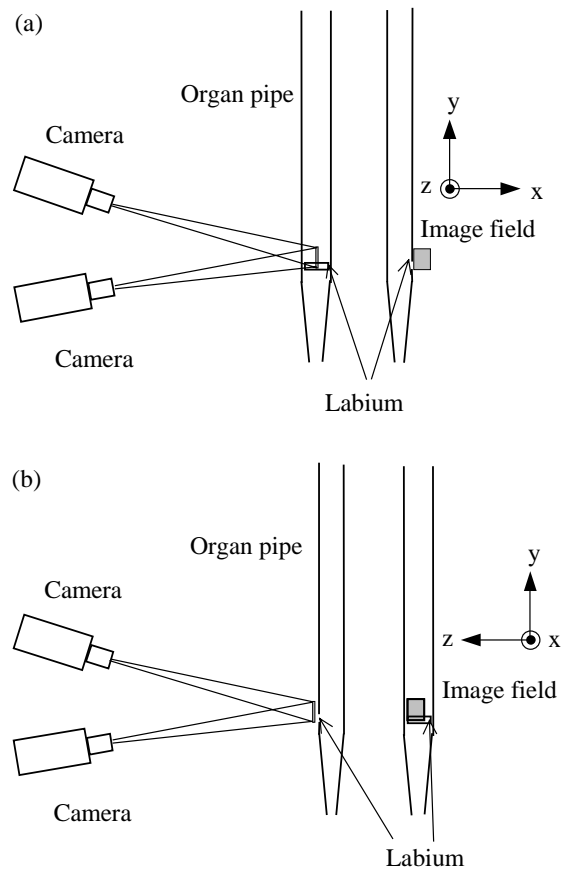


Figure 3. (a) Experimental set-up for 2D-3C PIV. The organ pipe is seen from the front and from the side. The image field is  $23 \times 29 \text{ mm}^2$ . (b) Measurement in a plane perpendicular to the one in (a). The image field is placed 6 mm in front of the pipe.

### 3. RESULTS

The sound pressure curve for one period of the sound at 260 Hz is seen in Figure 4. Five different positions are marked on the curve. The velocity fields at these positions were measured and will be discussed. Some velocity fields, in grayscale, are shown in this paper. To see these and more pictures, coded in colour, we refer to <http://www.sirius.luth.se/expmek/projects.asp?Name=piv>.

Results show that it is possible to follow a travelling vortex at the organ pipe labium in time as the sound pressure changes. At position 1, 2 and 3 on the sound pressure curve a vortex is seen to travel upwards. The mean velocity of the vortex is determined to 7 m/s. Velocities higher than 10 m/s are also registered. Figure 5 (a-b) shows the movement of two vortices. Figure 5 (a) corresponds to position 2 on the sound pressure curve and (b) corresponds to position 3. In Figure 5 (a) the beginning of a new small vortex is seen at the edge of the labium.

The stereoscopic measurements show that the velocity fields are three-dimensional. Figure 6 (a-d) shows two different results at positions 2 and 4 on the sound pressure curve. The two corresponding planes are shown together in (a-b) and (c-d), respectively. At position 2, one vortex is seen in the side view and three vortices are seen in the front view. At position 4 it is seen that air is sucked in-to the labium and at position 5, air is blown out from the labium (no figure is shown).

## 4. DISCUSSION AND CONCLUSIONS

2D-2C PIV and 2D-3C PIV are two methods suitable to study the instantaneous velocity fields outside a blown organ pipe labium. It is possible to follow the change of the velocity fields as the sound pressure varies. For future work it would be desirable to be able to decide at which point on the sound pressure curve the measurement of the velocity field should be done. It is not a trivial problem to trigger the laser to fire in accordance to the sound pressure signal. As it is now, the measurements in time are done randomly. The measurements done at different positions are not done within the same period of the tone, all of the velocity fields originate from different periods. Anyway the velocity field seems to have a special appearance at a fixed point on the sound pressure curve. Repeated measurements support this conclusion, why the velocity field is periodic with the same period as the sound pressure. The stereoscopic measurements done in two different planes are maybe not registered at exactly the same position of the tone, but almost. This affects the comparison between the planes. Future application of the method looks promising.

## 5. ACKNOWLEDGEMENT

The Research Council of Norrbotten (“Norrbottens Forskningsråd”) and The Swedish Research Council supported this work.

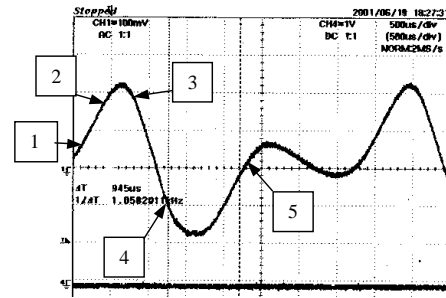
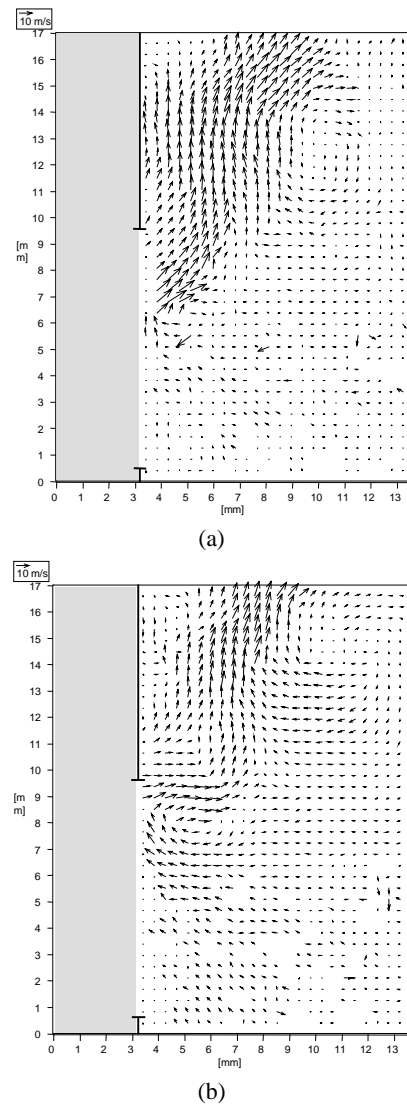


Figure 4. *Sound pressure curve. The frequency is 260 Hz.*



**Figure 5.** *Travelling vortices at the labium measured with 2D-2C PIV. The time separation between the two velocity fields is 400  $\mu$ s, according to the sound pressure curve. One vortex is seen at the upper right corner in (a) and (b). Another vortex is seen at the edge of the labium. The organ pipe is placed between 0-3.2 mm on the horizontal scale. The opening at the labium is placed between 0.5-9.5 mm on the vertical scale.*

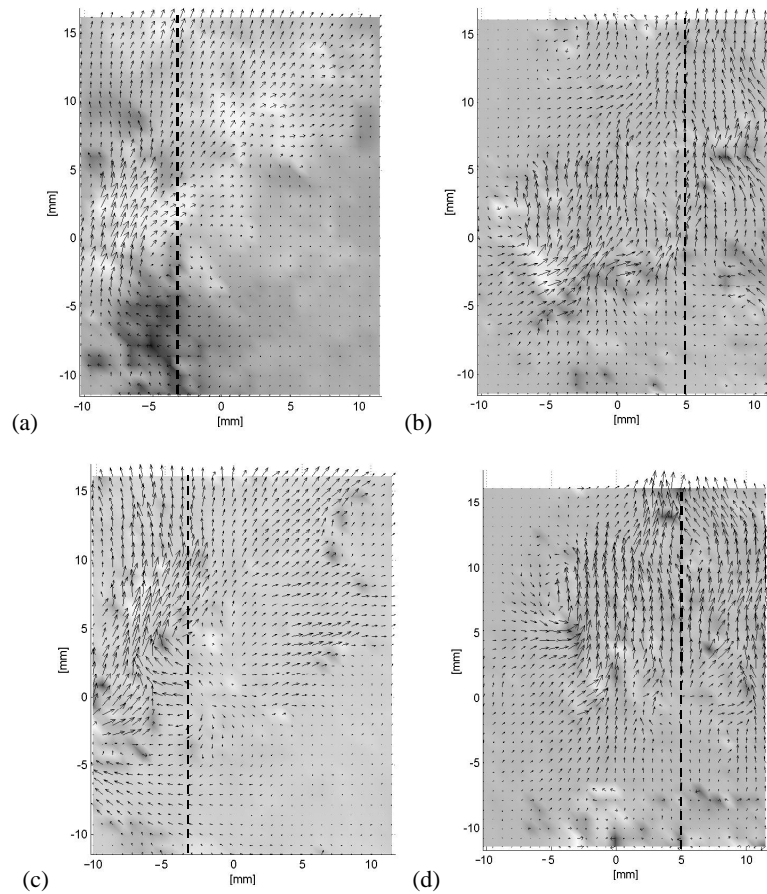


Figure 6. The three-dimensional velocity fields at position 2 (figure a-b) and position 4 (figure c-d) on the sound pressure curve measured with 2D-3C PIV. The in-plane velocity fields are shown with vectors and the out-of-plane velocity fields are shown as a grayscale background. White colour means out-of-plane velocity and black colour means in-to-plane velocity. The velocity is up to 10 m/s. Figure (a) and (c), respectively, shows the side view. The opening at the labium is placed between -3 and -12 mm on the vertical axis. Figure (b) and (d), respectively, shows the front view, in a plane perpendicular to the one in (a) and (c), respectively. The opening at the labium is placed between -6.5 and -12 mm on the vertical scale and all over the horizontal scale. The dashed lines show the intersections between the planes.

## 6. REFERENCES

- [1] Raffel, M., Willert, C. and Kompenhans, J., Particle Image Velocimetry - A Practical Guide, Springer-Verlag, Berlin, 1998.
- [2] Hinsch, K. D., "Particle Image Velocimetry", in: Speckle Metrology, ed. Sirohi R. S., Marcel Dekker, New York, pp. 235-324, 1993.
- [3] Gåsvik, K. J., Optical Metrology, Second edition, John Wiley & Sons, Chichester, 1995.
- [4] Hinsch, K. D., "Three-dimensional particle velocimetry", Measurement Science and Technology, 6:742-753, 1995.
- [5] Fletcher, N. H. and Rossing, T. D., The physics of musical instruments, Second edition, Springer-Verlag, New York Berlin Heidelberg, 1999.
- [6] Hirschberg, A., Chapter 7: "Aero-acoustics of wind instruments", in: Mechanics of musical instruments CISM Udine, Courses and lectures No 355, Springer-Verlag, Wien New York, 1995.
- [7] Zipser, L. and Lindner, S., "Visualisation of Vortices and Acoustic Sound Waves", Proc. 17<sup>th</sup> Int. Congress on Acoustics, Volume 1, Physical Acoustics part B, Ultrasonics, quantum acoustics and physical effect of sound: 24-25, Rome, September 2-7, 2001.
- [8] Runnemalm, A. and Johansson, Ö., "Sound intensity measurements of an open organ pipe", Proc. of the Int. Symposium on Musical Acoustics, ISMA '97, Edinburg, Great Britain, pp. 303-308, 1997.
- [9] Runnemalm, A., "Effects of material choice and tooling methods on structural modes of open organ pipes", Proc. of the Int. Symposium on Musical Acoustics, ISMA '97, Edinburg, Great Britain, pp. 345-352, 1997.
- [10] Runnemalm, A., Zipser, L. and Franke, H., "Structural vibration modes of a blown open organ pipe", Acustica united with Acta Acustica, 85(6):876-881, 1999.

## SPACE AND AIR ECONOMY IN THE ORGAN LOW REGISTER

Johan Liljencrants

Department of Speech, music and hearing  
Kungl Tekniska Högskolan  
jolip@telia.com

### ABSTRACT

The low register in an organ generally commands the space and air supply required. A number of classical and novel measures to economize with these are compared in terms of efficiency in sound level generation and a sideglance at musical usefulness. The comparison includes the source mechanisms of flue, beating and free reeds, pipe and cavity resonators. Designs are presented where a flue pipe is detuned by one semitone by an additional capacitance at its flow node.

### 1. INTRODUCTION

The acoustic power delivered by a monopole source is proportional to the squares of its frequency  $F$  and flow  $U$ . Assuming for reasoning that the sound power delivered from each pipe in a rank should be same this means that pipe flow will have to be inversely proportional to frequency, and at a given efficiency also the supply flow  $S$ . We may represent this with a proportionality  $f \approx 2^{-n/12}$ , where  $n$  is semitone number on a scale of rising frequency, e.g. like the MIDI note numbers. A simple verbal interpretation of this may be: *the lowest octave in a rank will use approximately the same supply flow as all its higher octaves combined*. E.g. a compass of five octaves will use air in the ratios 16 : 8 : 4 : 2 : 1.

The same applies to the lengths of the pipe resonators, while their cross dimensions vary according to mensuration practice. Using a 'halving number'  $M$  (the number of semitones you go along the tonal scale to reach a pipe with half the diameter, typically  $M=18$ ), the pipe cross dimensions vary as  $2^{-n/M}$ . For the total volume of pipes we then have  $V \approx 2^{-n/12-2n/M}$ . Then similarly: *the spatial volume of the lowest octave in a rank will exceed the remaining octaves by 4 times using  $M = 18$ , or 3 times with  $M = 24$* . This underlines the volume occupied by the bass pipes is a prime factor in the space economy.

Sparse piping is common in small secular organs, you omit several notes in the bass register, mostly sharp ones. This may be regarded as an illegal circumvention of the problem. Contrarily however, sparse pipes may be equipped with special devices, 'detuners', to enable one pipe to play more than one note, thus enabling a chromatic compass, but with restrictions on possible simultaneous notes.

An obvious means toward small volume is to select short pipe types. Counting length alone, minimum comes for a Helmholtz type cavity enhancing only the fundamental. For flue pipes you may use quarter wavelength stoppered ones rather than half wavelength open ones. A consequence is then that the harmonic spectrum is reduced to contain essentially only the odd

harmonics. An efficient practice is to play the fundamental with such a pipe in combination with a one octave higher open flue pipe. The latter then fills in the missing odd harmonics of the lower pipe.

The same trick applies to cylindrical quarter wavelength reed pipes (clarinet type), although it is more common to use a conical resonator, about 0.35 wavelengths, resonating near all low harmonics of the exciter. Reed pipes offer a wide range for the voicer in terms of power and timbre, but in the bass the necessary boot volume is not negligible.

### 2. EFFICIENCY MEASUREMENTS

Basic timbral properties are given by the pipe type, but we focus here on a series of measurements to illustrate the efficiency of the pipes, in the physical meaning of acoustic power delivered, as fraction of the blowing power supplied. A disparate set of wooden pipes were measured at varied conditions. Some of these samples are of regular design, borrowed from an organ, others are experimental ones where flue thickness and cut up can be easily varied. Some cases use a reed excited Helmholtz resonator where the cavity is variable by different length frames, clamped together, and brackets for a continuously adjustable port area. The objects are enumerated in Tab. 1 and measured data and some following results pertaining to efficiency are graphically shown in Fig 1. Each measurement included:

- $P_0$ , blowing (foot, boot) pressure in Pa.
- $U_0$ , blowing airflow in liter/sec.
- $F$ , fundamental frequency in Hz.
- $L_a$ , sound pressure level in dB (unweighted) at 25 cm distance from the pipe opening(s).
- $P_e$ , effective sound pressure in kPa at the pressure maximum for the fundamental, inside the resonator. In most cases this pressure waveform is nearly sinusoidal, exceptions are beating reed pipes (pulses) and the narrow flue pipe (square wave with some highpass droop).
- $Q_0$ , low level quality factor for the resonator, from resonance bandwidth and external excitation. This was of less interest as it was found to be always moderately to much higher than the  $Q$  in operation.

The flue width  $D$  (nominal airband thickness) was grossly measured with feeler gauges, but a more reproducible effective value was obtained from the Bernoulli equation as  $D = (U_0 / W) (2 P_0 / \rho)^{-1/2}$ , knowing the cut up width  $W$ . All flues are wedge shaped with about 10 degrees convergence angle, with sharp termination edges and no nicks.



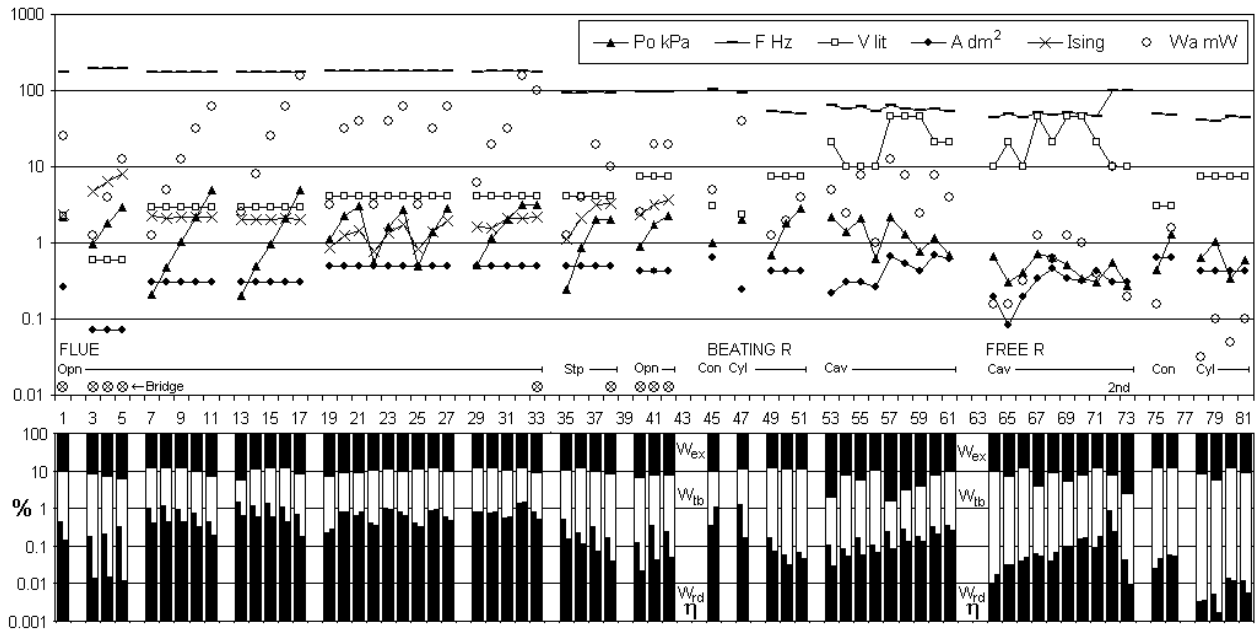


Figure 1: Top: Some dimensional data and measurements for the pipe samples. Bottom: Computed cumulative percentage of input power developed in radiated sound  $W_{rd}$ , resonator loss  $W_{ib}$ , and the excitation mechanism  $W_{ex}$ .  $W_{rd}$  corresponds to efficiency  $\eta$  and is split into a left bar for the result found from external sound, and a right from internal sound pressure.

Sample #	Type	Resonator dim. (mm)	Frequency	Comments
1	Flue, open, roll	855*51*51, H26, D0.85	196	Principal
3-5	Flue, open, bridge	820*27*27, H11, D0.7	196	Cello
7-17	Flue, open	892*55*55	175	Experimental, H and D varied
19-33	Flue, open	845*70*70, H31,	175	Regular, D varied
35-38	Flue, stoppered	825*70*70, H31, D0.73	93	Regular. Same body as #19
40-42	Flue, open, roll	1752*65*65, H30, D0.8	98	Principal
45	Beating reed	Conical 1430*80*80	98	Trombone, tongue 65*12*0.7 mm
47	Beating reed	983*49*49	92	Clarinet, tongue #45
49-51	Beating reed	1745*65*65	49	Clarinet, tongue 130*17*1.5 mm
53-61	Beating reed	Cavity 10/21/46 liter	49	Helmholtz res., port area tuned.
64-73	Free reed	Cavity 10/21/46 liter	49	Helmh. res., tongue 130*10*1.5 mm
75-76	Free reed	Conical 1430*80*80,	49	Trombone. Body #45, tongue #64
78-79	Half free reed	1745*65*65	49	Clarinet. Body #49, tongue #64
80-81	Free reed	1745*65*65	49	Clarinet. Body #49, tongue #64

Table 1: Measurement sample numbers of Fig. 1 and some further characteristics.

The acoustic output power from the pipes can be estimated two ways from these data. An obvious one is to multiply the external intensity (in W/m<sup>2</sup>, derived from  $L_a$ ) by the area of a 25 cm radius sphere around the pipe opening(s). However the sound level varied somewhat with direction, even at the small distance used, which indicates that standing waves in the room interfered to partly disvalidate the measurement. – An alternative way is to use the resonator internal pressure. This pressure applied to the cavity compliance results in a volume flow, essentially all of which passes the pipe opening(s) and exerts the output power in the radiation resistance. When we neglect the fraction of this flow consumed in internal loss mechanisms like viscosity and

wall heating, then for a cavity resonator of volume  $V$  these operations amount to the power

$$W = \omega^4 P_e^2 V^2 / (4 \pi \rho c^5). \quad (1)$$

A complication rises from the  $\omega^4$  factor which means a 12 dB/oct slope when converting internal pressure into delivered power. Experimentally, this could be implemented as a double differentiation of the  $P_e$  signal. This was not done in the present study where in most cases the  $P_e$  signal was essentially sinusoidal. In a few cases (conical reed horn and very narrow ‘cello’ pipe) this was not true, causing a fairly big underestimation of their power, as apparent from Fig. 2, which

compares the output power estimations for all samples, obtained with these two methods.

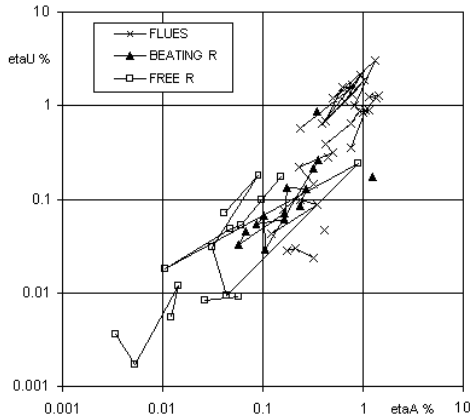


Figure 2: Efficiency estimated from internal pressure vs. that from external SPL.

The second method suggests a speculative extended interpretation, modeling the resonator as in Fig. 3. Assuming a reasonable  $Q$  and neglecting detail refinements, at resonance we can dismiss the reactive elements to have only a resistive divider. This device has  $R_a$  for the useful sound radiation in parallel with  $R_t$  for resonator losses. From resonator volume  $V$  and  $\omega$  we can compute  $R_a$  as the parallel equivalent to the radiation resistance(s) for the opening(s) of the resonator.

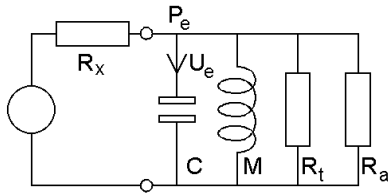


Figure 3: A resonator modeled as a single RMC parallel circuit, with resonance angular frequency  $\omega = (MC)^{-1/2}$  and quality factor  $Q = R/(\omega M) = \omega C/R$ , where  $R$  is the parallel combination of exciter, turbulence and acoustic components.

The resonator is fed through a symbolic resistor  $R_x$ . This represents the exciter, but is only a computational vehicle that is not simply related to the pipe physical dimensions. With a constriction like a reed, part of it can however be interpreted: Differentiating the Bernoulli equation with respect to  $U$ , we find a differential resistance

$$R_x = dP/dU = \rho U/A^2 = 2P/U, \quad (2)$$

simply twice the 'DC flow resistance'.

Loosely conjecturing a driving signal  $P_0$ , fed through the 'pressure divider'  $R_x$  and  $R$ , we can now also compute a dissipated power in  $R_t$ . From  $P$  and  $U$  we may additionally estimate an effective average open area  $A$  through the reed. It must be noted that the power in all three resistors is still far below the supplied blowing power, remarkably almost constantly around 10% of it, whether flue or reed samples. Of the oscillating energy a small and highly variant fraction goes into  $R_a$  to produce useful sound while the rest is lost by turbulence etc. in  $R_t$ . We might call the remaining

90% an exciter loss, partly in  $R_x$ , partly unexplained other input losses. With flues one may see them as converters from static into kinetic energy, inside the resonator converted back and manifested in  $P_e$ .

## 2.1 Flue pipes

For flue pipes the present samples give little tangible hints to any specific dimensional relations connecting to efficiency, notably not even the low level  $Q$ , non-trivial correlations are small. An outstanding exception is however the intonation number, defined by Ising [1] as

$$I = V*(D/H^3)^{1/2} / F, \quad (3)$$

where  $V$  is the initial speed of the air jet, estimable from foot pressure  $P_0$ ,  $D$  its thickness,  $H$  is cut up height, and  $F$  is frequency. Optimal for the flue drive mechanism is said to occur at  $I$  near 2, which appears supported by fig 4. 'Higher' voicing (higher  $V$ ,  $P$ ,  $D$ , lower  $H$ ) normally causes overblowing when  $I > 3$ , here prevented with bridges, extremely so with the very slim pipe #3-5. This renders very prominent higher harmonics, but a weak fundamental. For efficiency in the fundamental, not surprising, normal mensuration appears as broadly optimal. Significantly narrower pipes, or special devices like bridges or freins may still keep up loudness by virtue of the higher harmonics.

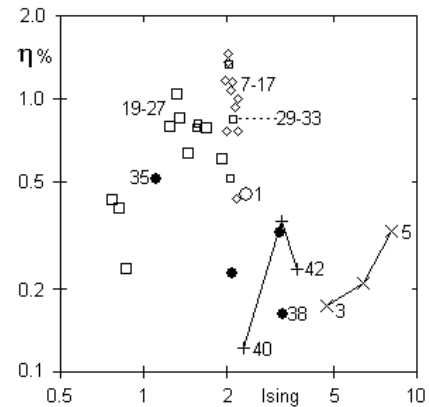


Figure 4: Flue pipe efficiency (external sound) vs. Ising intonation number.

## 2.2 Reed pipes

With beating reed pipes the length and thickness of the tongue are essentially dictated by pitch, pressure, and tongue material, [2]. Remaining parameters, available to control power level and timbre are tongue width and the area of the shallot opening which can be made considerably smaller than the tongue to increase  $R_x$ . With a large  $R_x$  the resonator will operate at a high  $Q$  but with a low pressure and efficiency, and weak harmonics. When instead  $R_x$  is small, then the resonator is heavily damped, higher harmonics from the reed are much transmitted and would render a brutal timbre, and air consumption would be high. - Shallot leathering is an additional option to soften timbre.

Free reeds like in an harmonium are ultimate to conserve space, prominently because they keep pitch without any resonator. Their main drawback is very low efficiency, slow tonal onset,

and that the fundamental is weak relative to the second harmonic. The low sound level can be appreciably incremented using resonators. Since their waveform is two slightly grouped pulses per period tuning the resonator to the second harmonic is particularly effective (samples #72-3). #78-79 tested a shallot with a deep fitting trough rather than a thin plate, blocking the flow during half the cycle, but was a failure in improving the fundamental.

### 3. VOLUME CONSERVATION

There is a continuum of possible resonator designs from a cavity with an opening area  $A$ , varying the neck length  $L$  from a small value up to a quarter wavelength pipe of same cross section, see Fig. 5. For a given resonance, as  $L$  is increased the required volume  $V$  decreases, estimable from the Helmholtz resonance formula.

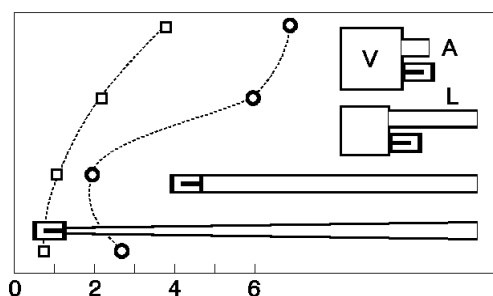


Figure 5: Relative interior (squares) and circumscribed (circles) resonator volume, varying neck length  $L$  at constant frequency and mouth area  $A$ .

The total volume of cavity and neck is however smallest at the extreme where  $L$  is a quarter wavelength. For volume conservation at given sound and supply level this indicates a pipe resonator is always preferred over a Helmholtz resonator. A Helmholtz can be smaller than a pipe only when its opening  $A$  is appreciably less than the pipe area, and this means a correspondingly smaller power handling capacity. An historical circumvention is a 'Wick's cube', one common volume shared by a set of different length ports connected with individual pallets, operable up to almost half an octave.

#### 3.1 Pipe detuners

A conventional work around with sparse piping is to augment some pipes with tone holes, the same principle as used in orchestral woodwinds, such that you can raise them by one semitone.

One dual method proposed here is to connect an additional closed cavity at the flow node. This will instead detune the pipe lower. To lower a pipe one semitone corresponds to making it about 6% longer, so the required extra volume is estimated to be this fraction times the pipe area. Fig. 6 shows a practical implementation. The merit of this method is that the 'tone hole' and its operating mechanism are comparatively small, there is little flow but high pressure at this node. However, the additional device forms a cavity resonator where it is imperative its resonance is higher than the pipe fundamental. Otherwise the pipe interior

will not feel it as a compliance and pipe function will be severely disturbed, in the first place by overblowing.

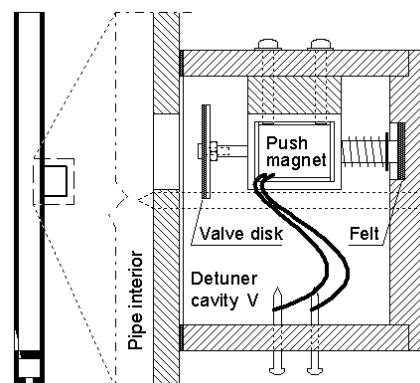


Figure 6: Cavity detuner at a flow node.

A variant method is to use a tube, closed with a valve at one end. The open end impedance of this has a first (resistive) minimum at resonance where the tube is a quarter wavelength. Just below that resonance it is capacitive, with a greater compliance than for the tube volume alone. So placing its open end at the flow node of a regular pipe will detune it lower. Since this detuner is shorter than a quarter pipe wavelength, when the valve is opened the detuner tube will have no action (other than a slight damping) and the pipe returns to its normal pitch.

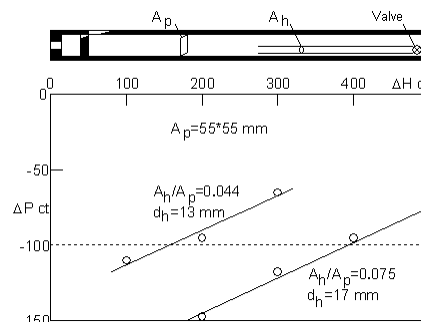


Figure 7: Narrow tube detuner and measured effect.

The graph of Fig. 7 shows measured results. The horizontal axis is how many cents  $\Delta H$  above the basic pipe frequency the auxiliary tube is tuned. The vertical axis  $\Delta P$  shows how many cents the pipe fundamental lowered as consequence. The target of lowering by one semitone is shown with the dotted line and measured points are indicated with circles. The trajectories can not be extended toward smaller  $\Delta H$ . When the detuner resonance becomes too close to the pipe pitch, it will destroy the pressure maximum and the pipe will overblow (cf. action of the middle hole in a harmonic pipe).

### 4. REFERENCES

- [1] Ising, H.: Erforschung und Planung des Orgelklanges. Walcker Hausmitteilung Nr 42, Juni 1971, pp 38-57.
- [2] Liljencrants, J.: Design dimensions for a reed pipe tongue. <http://mmd.foxtail.com/Tech/reedPipeDimensions.html>, 2001.

## FREE REED INSTRUMENTS : CLUES FOR A MINIMAL MODEL

Laurent Millot

ENS Louis Lumière, 7 allée du Promontoire, 93161 Noisy Le Grand Cedex, France  
l.millot@ens-louis-lumiere.fr

### ABSTRACT

Experiments have shown that free reed motion is sinusoidal and can then be described by the reed tip displacement. Taking into account the local rotation of transverse sections, an efficient expression for the section by which air escapes from the instrument will be derived; an escape area which does not predict any closure discontinuity. Using also a quasi-stationary assumption for the air-flow through the reed (assumption of free jet formation), a minimal model for a free reed will be proposed. Details and application in the case of the diatonic harmonica, in which two different free reeds interact, will be given. This particular instrument requires a non-linear description of the vocal tract which will also be described. Listening of time-domain simulations will illustrate that a virtual diatonic harmonica may be able to perform chromatical playing (normal notes, bends and overnotes) and follow temporal modifications of the vocal tract configuration. Some clues for the extension of this model to other free reed instruments will finally be discussed.

### 1. INTRODUCTION

A discussion of time-domain simulation of free reed instruments is proposed on the basis of a model able to explain chromatical playing on a diatonic harmonica. We first review the harmonica model (reed motion, player modelling and related principles). With the help of an analysis of a numerical simulation for a blown note, the model and its extension to other reed instruments is then reviewed. This discussion permits the emergence of a question concerning the eventual inclusion of the acoustic streaming in the sensation of sound. The details for the equations are to be given elsewhere due to their great heaviness.

### 2. MODEL FOR THE DIATONIC HARMONICA

#### 2.1. Model for the musician and the diatonic harmonica

Skilled harmonica players are able to play fully chromatically on a diatonic harmonica and if you want to be able to understand and explain this fact you need to introduce the musician in the model. As shown in [1], the musician uses vowel fricatives in order to produce missing notes (bends, overblows and overdraws) and vowels configurations can be related to the production of each kind of note. The importance of the oral cavity is also demonstrated by x-ray, ultrasonographic and laryngoscopic imaging of players (Howard Levy and Dr Henry Bahnson) while sounding notes on the harmonica [2].

The model for the player is a modified version of the four-tube one proposed by Fant [3] to approximate vowels production: the

cross sections of the four elements are not assumed to be cylindrical but rather rectangular; the palatal constriction and the lip-pal channels longitudinal symmetry axes are different from the back and front cavities ones; the glottis is assumed to be wide open and there is no distinction between the upstream and downstream of it. The model is illustrated by figure 1 and one can note the following successive elements : the back cavity (1) where the supplying over-pressure  $\Delta p_1$  is applied; the palatal constriction (2); the front cavity (3); the lips and harmonica channel (4) and the outside of the instrument (5) where the pressure is assumed to be atmospheric.

The model for the harmonica is quite simple: a channel which constitutes an extension of the lips channel and in which both blown and drawn free reeds are assumed to be encountered in the right vertical plane. This configuration is also presented by figure 1. One can note that both free reeds are figured by piston-like elements with an associated spring. This approximation is discussed in the following paragraph.

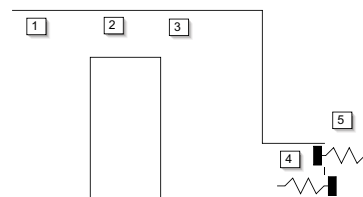


Figure 1: Model of the vocal tract: supply area (1), palatal constriction (2), front cavity (3), lip-pal and harmonica channel (4), outside (5).

#### 2.2. Free reed model

As shown experimentally, for instance in [1, 4, 5, 6], free reed motion remains sinusoidal during all playing modes (with human-like over-pressures for the excitation) which means that, given the reed configuration, the reed can be considered as a cantilever beam moving only on its first transverse mode. As in this case we can derive the displacement of any point of the reed only with the knowledge of the displacement of free tip (for instance), it is possible to describe precisely the reed motion by a mass-spring-damper oscillator with only one parameter: the motion of neutral fiber at free tip of the reed. This is the reason why in the figure 1 both reeds are represented by piston-like and associated spring elements.

As illustrated by the spectrums presented in figure 2, in the case of a simulated blown note, the spectrum for the upper reed neutral fiber  $h_{n,f1}$  is nearly a perfect sinusoid while the spectrum for the over-pressure  $\Delta p_4$  (pressure difference between upstream and downstream of the reeds) contains numerous harmonics. Experimental measurements show exactly the same characteristics

[5]. The rich harmonic content of  $\Delta p_4$  is understandable if we consider that free reeds only modulate the airflow escaping through the reeds: the strong modulation of the airflow causes strong variations of  $\Delta p_4$  and one can observe violent peaks in the  $\Delta p_4$  over-pressure waveforms (see for instance figure 5; right middle or [1, 5]), which may perhaps be qualified as quasi-shockwaves in some cases.

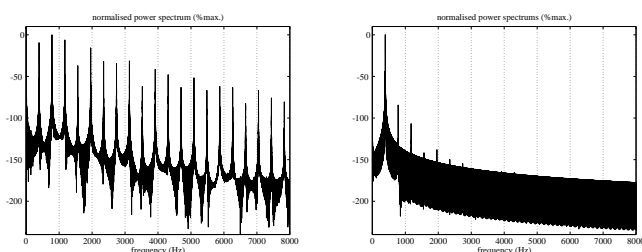


Figure 2: Spectrums (in dB) for the inner over-pressure  $\Delta p_4$  (top) and the deformation of the neutral fiber (bottom) for the upper reed (designed to sound while blowing) free tip during a blown note.

It is important to precise that measurements realized with proximity sensors (which are often non-linear devices) or laser vibrometers may present a non-sinusoidal behaviour and that it can be explained. Indeed, the spectrum given in figure 2 concerns the **neutral fiber** of the reed while the proximity sensors or the laser vibrometer can only access the **upstream** or **downstream** fibers of the reed which are subjects to extension and compression! The definition of these three fibers is illustrated by figure 3. The experimental device may then be a source of confusion if you take its response without any caution because the only fiber which does not suffer from any longitudinal extension is the neutral fiber; upstream and downstream fibers suffer from opposite solicitations whatever free tip position is. Moreover, the transverse sections of the reed suffer from rotation when the reed is moving which means that if you look at a target point of the reed, at rest, with a laser vibrometer in a normal direction relative to the reed, you do not access to the normal velocity of the target point when the reed vibrates: due to the rotation of the transverse sections, the target point also moves in the longitudinal direction. Rotation of transverse sections and longitudinal motion should be observed with the following experiments: observation of a grid of marked points along the length of the upstream (or downstream) face with a fast camera in the normal direction may point out the distortion of the grid; after painting some parallel lines in the thickness of the reed (when the reed is perfectly plane) one may be able to see the distortion and the rotation of these lines with a fast camera in a direction normal to the thickness of the reed. It seems normal that such phenomena would be reduced for reed parts near to the embedded tip of the reed.

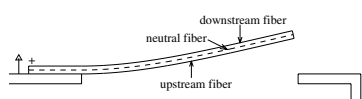


Figure 3: Definition of the upstream, neutral and downstream fibers of a lower free reed (designed to sound while drawing).

Rotation of transverse sections may alter the measurements but it is also responsible for numerous confusions for the proposal of a reed motion model: in literature the reed motion model gives the displacement of the "reed tip" which can differ according to the authors. Indeed, one can only use the mass-spring-damper oscillator approximation (in the case of a striking or free reed) for the neutral fiber displacement not for the upstream or downstream fibers displacements. So, the classical reed motion equation gives or depends on the neutral fiber point of the free tip of the reed, a point whose displacement is quite hard to measure. In such a case, I think a good experimental device may be a strain gauge even if the presence of the strain gauge modifies the behaviour of the reed (increase of the eigenfrequency, added stiffness) [1, 5].

With the discussion of the acoustical flow model, in the next section, we will see that knowing the motion of the neutral, upstream and downstream fibers permits to get an improved description of the flow through to the reed.

### 2.3. Acoustical flow model

In this section we give the principles and the assumptions used in the case of the fourth channel of a G harmonica (see [1, 5] for the reeds characteristics).

From the lungs to the upstream of the reed, the model is 1D but the description of the airflow through the reed is 0D as we consider the same jet velocity across both reeds and unfold the escape areas under both reeds.

In the back cavity (1) we find the over-pressure supply and assume that there is a zero velocity. In the palatal constriction (2) an incompressible and unsteady Bernoulli equation is used taking into account the temporal variation of the geometry of the entire palatal constriction and the formation of a free jet at the input of (2) in (1) in the drawn case and at the output of (2) in (3) in the blown case. For the front cavity (3), we consider a mass conservation, taking into account the temporal variation of the volume of the cavity, in association with an adiabatic assumption. In the lips and harmonica channel (4), an unsteady and incompressible Bernoulli equation is used in which we neglect the kinetic terms (assumed to be quite fewer than the unsteady one); we also introduce a mass conservation between the input of the channel (4) and the downstream of the reeds. Through the reeds, a quasi-stationary flow is assumed with formation of free jet at the downstream of the reeds in the blown case and inside the channel (4) in the drawn case. At the outside (5), the pressure is considered atmospheric. Both reeds motion equations are introduced, using the mass-spring-damper oscillator driven by the over-pressure  $\Delta p_4$ .

These equations are rather classical but new details are related to the definitions of the volume flows escaping or entering through both reeds.

First we take into account the "pumped flows" as first introduced by Thompson [7] because they can represent a significant part of the total flow passing through the reeds, which has been verified within the numerical simulations. Second, we reconsider the sections under the reeds which are necessary to define the flow passing under each reed. Instead of the classical "only front section" assumption (at the free tip of each reed) still used in most of reed models, we consider the real contribution of the front and also the sides contributions to the total section under the reed. Three contributions can be introduced for each reed: a non rectangular but trapezoidal front section which is not normal to the shallot plan, because of the presence of a clearance gap between the shallot

lot window and the reed, and which depends on the downstream fiber (upper reed) or on the upstream fiber (lower reed) evolutions; the two-sides contribution which is related to the downstream (upper reed) or the upstream (lower reed) evolutions and which takes into account the progressive rotation of the outer normals all over the reed, normals which are assumed to indicate the local direction of the free jet; a third algebraic contribution which correspond to the complementary sections between the front and the sides. It is interesting to note that some preliminary visualisations of the air-flow through the reed illustrate the temporal rotation of the free jets all over the reeds.

With this process, we can find the laws for the useful sections (complete escape sections) as functions of the neutral fiber opening of their associated reed. Figure 4 presents the characteristics found for the reeds of channel 4. We can note that, for both reeds, the characteristics are symmetric and present only one minimum point. A further analysis shows that this minimum point corresponds to a plane reed configuration in both cases. So, there is no closing situation for free reed and the useful section increases when the minimum point is passed whatever the reed enters into or escapes from the thickness of the shallot. Moreover, due to the clearance gaps all over the reeds there is no interruption of the airflow and it seems normal to get some thin over-pressure peaks with such "regular" characteristics for the useful sections: the over-pressure falls after passing the plane configuration for the reed. It is important to precise that as we have two different reeds in the channel of the diatonic harmonica, we can encounter some non "peaky" waveforms if the temporal evolutions of the useful sections for both reeds present a great phase difference: if one reed is "wide open" while the other reed is almost "plane", one may not encounter sharp peaks in the over-pressure waveforms.

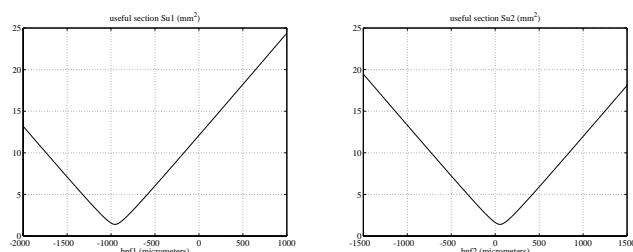


Figure 4: Characteristics of the useful sections by which the air-flow passes under the reed, in the case of the channel 4: (left) upper reed characteristic; (right) lower reed characteristic.

### 3. DISCUSSION AND EXTENSION OF THE MODEL

#### 3.1. Analysis of a numerical simulation

Figure 5 presents an extract (11 ms of the "stationary" part of the note) of the waveforms for most of the physical quantities which are involved in the diatonic harmonica. The tested note is a normal blow with a soft excitation over-pressure. Over-pressure  $\Delta p_1$  corresponds to the excitation signals and varies quite slowly compared to the other signals. The following analysis may be similar for all playing modes (normal draw, drawn bend and overblow) for this channel and also for the other playing modes found on the other channels (blown bend and overdraws on channels 6 to 10), it is just a basis for the discussion.

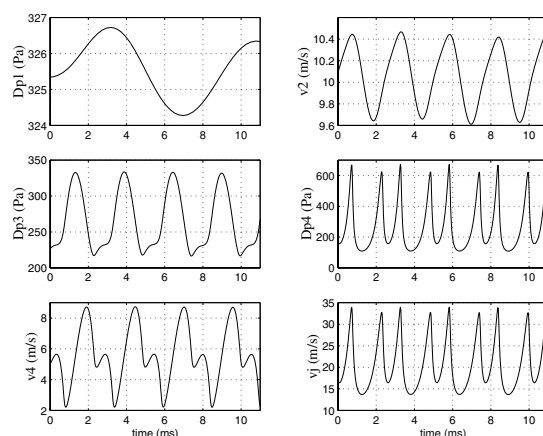


Figure 5: Partial waveforms obtained for a simulated blown note: excitation over-pressure  $\Delta p_1$  (top left), velocity at the end of the palatal constriction  $v_2$  (top right), over-pressure  $\Delta p_3$  in the front cavity (middle left), inner over-pressure  $\Delta p_4$  (middle right), velocity at the entrance of the lippal channel (bottom left), jet velocity  $v_j$  at the reeds downstream (bottom right).

The velocity at the exit of the palatal constriction  $v_2$  has a  $10.07 \text{ m.s}^{-1}$  and the maximal deviation from the mean (for this extract) is  $0.39 \text{ m.s}^{-1}$  which means that we have a significant nonlinear acoustic streaming related to the acoustical speed if we consider the definitions used by Menguy [8]. And we find the same significant nonlinear acoustic streaming in the lips channel (mean velocity:  $5.57 \text{ m.s}^{-1}$ ; maximal deviation:  $3.16 \text{ m.s}^{-1}$ ) and in the free jets (mean velocity:  $20.7 \text{ m.s}^{-1}$ ; maximal deviation:  $13.26 \text{ m.s}^{-1}$ ). This is a good clue to consider that convection is a main phenomena in the oral tract and through the reeds and that separating acoustic streaming and acoustic velocity, during the resolution, is not a good idea. In the case of the free jet, we have such great temporal variations of the total velocity that we do not think that we can distinguish the acoustics from the mean quantities.

On seeing the waveforms for the over-pressure in the front cavity ( $\Delta p_3$ ) and above all at the upstream of the reed ( $\Delta p_4$ ), we can note that these waveforms present great temporal variations even for a 11 ms extract! In such a case, it seems reasonable to consider these over-pressures as acoustical pressures and not to introduce a mean flow and an acoustical field.

At this point, I must precise that I have performed the numerical simulations without any introduction of an acoustical point of view: all these assumptions, principles and equations directly rely on fluid dynamics. And, when I give sounds (over-pressure  $\Delta p_4$  for instance) to listen I just play the calculated waveforms saved as a .wav file. In such listening sessions, the results is then dependent of the capacity of the reproduction system to use the very low-frequency content of the signals. In this case, acoustics is hidden in the signals perception just reveals it.

It seems interesting to investigate again the definition of acoustics in order to see if the low-frequency part of the signal, usually called "mean flow" or acoustic streaming (or even neglected in certain cases), participates to the sensation of sound. Very preliminary listenings done with low-frequency reproduction systems (loudspeakers and even professional headphones), even with fil-

ters bank analysis to separate acoustic streaming from acoustical quantities, make me think that acoustic streaming can be a significant part of the sensation of sound. It seems also important to use (if they are already available) captation, processing and reproduction systems able to take into account the very low frequencies down to 0 Hz, perhaps, to be really able to propose an answer for this question.

Some recent discussions with Hirschberg [9] have pointed out a potential improvement to the model. Indeed, some comparisons between different assumptions for the processing of the flow within a time-varying glottis have shown that the viscous losses may be more significant than the instationary term and that taking a lossy incompressible Bernoulli may be a good improvement to better agree with the experimental results. As the tested geometries are similar to the one of the palatal constriction, for instance, further investigations should consider the introduction of the viscous losses in the description of the palatal constriction and of the lips and harmonica channel. With these corrections, the waveforms in the elements (2) to (4) could be perhaps more "violent". It may be possible to introduce the elements existing at the downstream of the reeds like the thin covers and, why not, the hands of the musician as another aerodynamical extensions of the model.

Keeping these comments in mind, we can now see how to extend the principles used in the harmonica to other reed instruments.

### 3.2. Extension to other reed instruments

The minimal free reed model is given by reed motion, quasi-stationary Bernoulli equation between reed upstream and downstream, pumped and escaping flows.

The extension to instruments like accordion and harmonium may be quite "easy" because, most of the time, these instruments only have one reed per channel and may need a less complicated description of the flow excitation device as the player does not act directly on the reeds. In fact, it is necessary to determine for both instruments what are the elements present at the upstream and at the downstream of the reed.

It seems also possible to apply a simplified harmonica model to organ pipes with free reed by keeping the front cavity and the lips channel and adding a pipe at the downstream of the reed. But, for the pipe some changes are needed. Most of the wind instruments like clarinet, saxophone or sho exhibit a "resonator" whose description is given by a waveguide model, a Green function or a reflexion function which all assume that the acoustic streaming can be neglected! On seeing the results for the diatonic harmonica, it seems interesting to consider the possibility of an acoustic streaming and, following this idea to use adequate Bernoulli and mass conservation descriptions, without any linearisation. This may give access directly to the output volume flow at the output(s) of the pipe. It may also be possible to study how the behaviour of the reed is modified for a metallic striking reed (by using a numerical version of the local motion equations for the reed rather than an approximation by a simple oscillator), and then work on the organ pipes using the extension to the striking reeds.

Extension to the sho can also be considered as we may be able to model the sho as a musician playing a special organ pipe with a free reed. In this case, the model should be a mix between the diatonic harmonica (only the vocal tract part) and the free reed organ pipe.

For clarinet and saxophone instruments, the extension is much more complicated and may be tried after the extension to the or-

gan pipe with a metallic striking pipe. Indeed, the use of wood reed increases the difficulty of the description of the reed because of the anisotropy of the reed mechanical characteristics. But, it seems quite important to try to describe the useful section and the motion of the downstream fiber of the reed in order to improve the description of the flow through the reed, that's to say taking into account the sides contributions to the flow passing the reed. Another relevant question deals with the opportunity to use flow dynamics descriptions, even a simple Bernoulli, for the "resonator" instead of the classical linear descriptions. This idea has already been quasi-suggested by experiments and reflexions of Bouasse [10].

## 4. CONCLUSIONS

Several keypoints (useful sections, use of fluid dynamics rather than linear acoustics, problem of definition of acoustic streaming) have been pointed out which may be used to realize an extension of the model for diatonic harmonica to other reed instruments.

It seems easier to firstly focus the attention to instruments like harmonium and organ pipe. Before considering instruments like clarinet or saxophone, attention should be paid to the extension of free reed characteristics (motion and useful section) to striking metallic reeds.

The 0/1D proposed model may be used to help a 3D model and above all to investigate all the physics involved within free reeds instruments (strange modes, chaos and potential bifurcation, ...). Moreover, some more experiments are needed and an careful lecture of Bouasse's works could be useful.

## 5. REFERENCES

- [1] Millot, L., "Etude des instabilités des valves : application à l'harmonica diatonique", PhD thesis, Université Paris 6, 1999.
- [2] Antaki, J., Bahnson, H., and Burgreen, G., "Acoustic coupling between oral tract and diatonic harmonica: recent observations", *J. Acoust. Soc. Amer.*, Vol. 111(5), 2002, p 2376.
- [3] Fant, G., "Acoustic Theory of Speech Production: With Calculations based on X-Ray Studies of Russian Articulations", Mouton, The Hague-Paris, 1970.
- [4] Cottingham J. P., Lilly J. C. and Reed C. H., "The motion of air-driven free reeds", *Forum Acusticum*, Berlin, 1999.
- [5] Millot, L., Cuesta C. and Valette C., "Experimental results when playing chromatically on a diatonic harmonica", *Acta Acustica*, Vol. 87:262–270, 2001.
- [6] Ricot, D., "Modélisation physique de la vibration d'une anche d'accordéon- application à la synthèse sonore", DEA report, Ircam, 1999.
- [7] Thompson, S. C., "The effect of the reed resonance on woodwind production", *J. Acoust. Soc. Amer.*, Vol. 66:1299–1307, 1979.
- [8] Menguy, L. and Gilbert, J., "Non-linear acoustic streaming accompanying a plane stationary wave in a guide", *Acta Acustica*, Vol. 86:249–259, 2000.
- [9] Hirschberg, A., private communication, 2002.
- [10] Bouasse, H., "Instruments à vent- Tomes I et II", Librairie A. Blanchard, Paris, 1986.

## **SUBJECTIVE EVALUATION OF ORGAN PIPE TIMBRE IN THE STANDARD LISTENER POSITIONS**

*Václav Syrový, Zdeněk Otčenášek, Jan Štěpánek*

Department of Musical Acoustics, Sound Studio of the Faculty of Music AMU, Prague

syrový@hamu.cz, otcenasek@hamu.cz, stepanek@hamu.cz

### **ABSTRACT**

The paper deals with the dependency of tone timbre sensation in the real room on the listener's position relative to the individual organ pipes. Unlike the other musical instruments, in the case of organ three incommutable standard listener positions exist. These positions are closely associated with the subjective tone timbre evaluation of the individual pipe and the whole pipe sounding ensemble too.

The first one is the organmaker's position inside the instrument during the pipe voicing, the second one is the position of the playing organist by the console and the last one is the position of the listener in the church or concert hall auditory. The sound of single pipes (for different stops) was recorded in the positions mentioned above using artificial head, which simulates well the binaural sensation and the acoustic field deformation in the listener vicinity. The digital recording of a tone was carried out for additional two head turns. Afterwards the head was replaced by the pair of omnidirectional microphones and the whole recording procedure was repeated. Selected recorded tones were subjectively compared by listening in headphones.

### **1. INTRODUCTION**

The pipe organ is without question the most complicated musical instrument from view of technical, architectonic and especially acoustical aspects. Concurrently the organ is made from the ensemble of the simplest musical sound sources – labial pipes with the exactly determinated pitch, loudness, timbre and place position in face of listener.

The organ sound, how we know it, for example in the form of plenum or tutti, is a “space” sum of particular pipe sounds. This sum is dependent not only on the quality of individual stops scaling and voicing, but also on the acoustical features of the room – church or concert hall. In contrast to other musical instrument the relationship between the organ and room is compact, changeless and unique, therefore all acoustic measurements and subjective evaluations must be realized “in situ” only. But the results of sound analysis as well as the tone timbre sensation are very different for each position of measurement microphone or listener in the church or hall.

Even though several possibilities of statistical processing of data (for example the time or space averaging) exist, the influence of the distance between the one pipe and microphone or listener position is too high. The above listed three listener positions differentiate primarily just in this distance. The position of organmaker is very close to the tuned and voiced

pipe with its only too concrete sound. Especially by the voicing the organmaker looks for an optimal position of his head, changes this position for another pipes by reason of good tone timbre sensation. Nevertheless he cannot correctly consider and discriminate the loudness and timbre tone proportion between two pipes or two stops, so he confronts very often his feeling with the sensation of his colleague sitting by the console or even in the room. The position of the organist is fixed (excepting moveable consoles), in this position he conceives the registration (selection of stops), the movement and whole performance conception of some musical piece. The sound of single pipes, stops and their combinations is well concrete, clear and balanced in this position too.

The basic sound quality evaluation of organs happens always by the console; the verdicts of organmaker and organist must be identical here. The position of the listener is very various and commensurates with the type, size and acoustical quality of the room (church or concert hall). The sound is less concrete and more spatial here; it highly reflects the acoustical properties of the room. We are often oblivious of the listener position by acoustical measurements of organ but this one is the most important and ultimate for the all in all review of organ sound, its character, quantity, quality, style, musical using etc. At last the listener position in the auditorium, especially its “sound quality” has quite concrete price too and with it connected positive or negative listener motivation.

### **2. EXPERIMENTS**

The main goal of this work was the subjective evaluation of the listener position influence on the pipe tone timbre sensation. The evaluation was supplemented by the pipe tone analysis for each listener position. All experiments were realized on the organ of the Martinů Hall (Faculty of Music in Prague). This concert organ has 41 stops, 3 manuals and pedal with the mechanical action and was built by the Czech firm Rieger-Kloss in 1993 and re-voiced by the German firm Karl Schuke in 2002 (see Fig. 1).

The concert hall is approx. 25 m long, 10 m wide and 10 m high with the reverberation time up to 2.5 sec (160 Hz). The following stops of the 1. manual were chosen for the experiment: Burdon 16', Spitzgambe 8' and Octave 4' on the manual keys: B, e, b, e<sup>1</sup>, b<sup>1</sup>, e<sup>2</sup>, b<sup>2</sup>, e<sup>3</sup> and b<sup>3</sup>, which represented the tones from B<sub>1</sub> to b<sup>4</sup>. The artificial head Cortex C1/TO1 was used for the recording of analyzed tones, two omnidirectional microphones Brüel&Kjaer 4006 with the base 17.5 cm were used for the recording of subjectively evaluated tones. The tones with the duration 4 sec. were recorded and processed in format 44.1 kHz/32 bits by the software Cool Edit Pro 1.2.



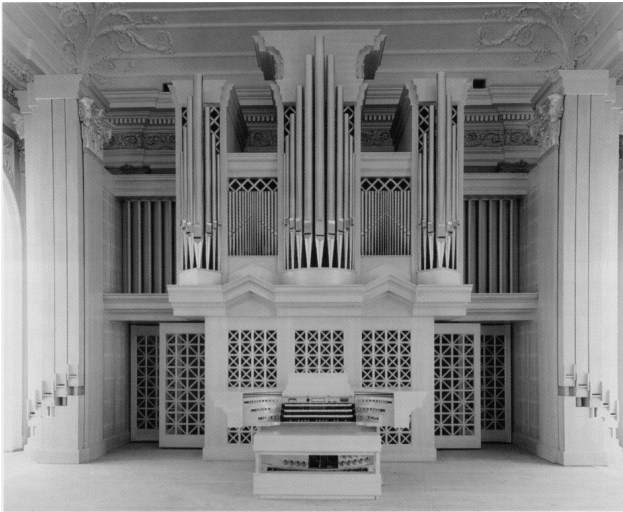


Figure 1: *The organ in the Martinu Concert Hall.*

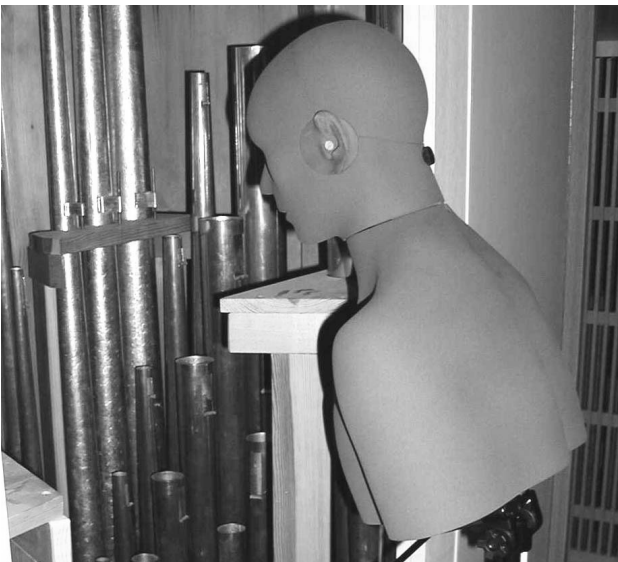


Figure 2: *The organmaker's position inside the organ.*

Fig. 2 shows the basic position of the head with the distance approx. 1 m from sounding pipes. The following two positions were the same but with the  $\pm 45^\circ$  turning round the head axis. Afterwards the microphones were located in the same three positions (related to the ears of the head). The next position of the head and microphones was situated near the console (see Fig. 3) in the distance approx. 7 m from the sounding pipes (with the same angular turning). The last position was in the auditory of the Martinu Hall in the distance approx. 17 m from the console (Fig. 4). In this position no turn was realized. In total 252 tones were recorded. Only the tones recorded by microphones were used for the subjective evaluation.

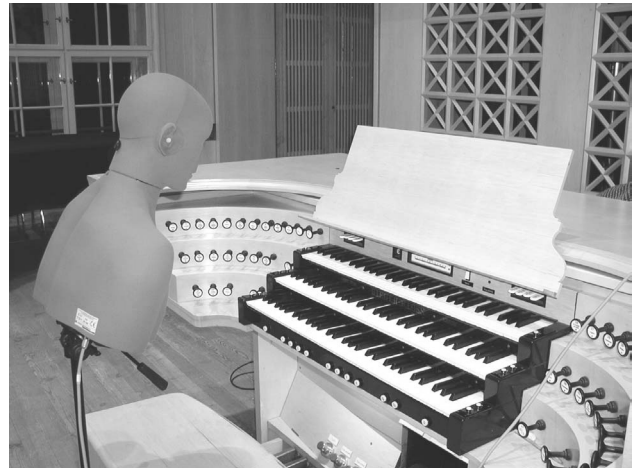


Figure 3: *The organist's position by the console.*



Figure 4: *The listener's position in the auditory.*

For the listening the open headphones Sennheiser HE 60 with the amplifier HEV 70 were used. The following tones were selected: On the keys B,  $e^1$ ,  $b^2$  for the stops: Burdon 16' (sounding B<sub>1</sub>, e,  $b^1$ ), Spitzgambe 8' (sounding B,  $e^1$ ,  $b^2$ ) and Octave 4' (sounding b,  $e^2$ ,  $b^3$ ). The position inside the organ was marked OM (basic middle orientation), OR (right turning), OL (left turning), the position of player by the console PM, PR, PL and only one position in the auditory AM (middle orientation). For tones with the same pitch the general sound dissimilarity in pairs was evaluated with the mark: from 0 (no dissimilarity) up to 5 (maximum dissimilarity) in the loudness, timbre, clarity of transient, noise presence etc.

The substantial simplification of the dissimilarity question comes out from the first view on this specific problem of the organ acoustic measurement and subjective evaluation. Therefore the first listening was restricted only on one person experienced in organ sound problems. On that account the following results have only the preliminary character and next data are currently processed.

### 3. RESULTS

Nine dissimilarity matrixes were obtained as a result of listening tests. The multidimensional scaling method (MDS), model with Euclidean distance was used for their evaluation (overview of models see in [1]). MDS model in general fits stimuli dissimilarities into distances of Euclidean space of appropriate low dimensionality.

In our experiment set of stimuli was represented by tones from the same stop and with the same pitch, and differing only with the recording position. Each set of stimuli includes seven tones: OM, OL, OR, PM, PL, PR, and AM. Two-dimensional solutions, which well reflect the dissimilarities in the most studied sets of tones, were used for the discussion of results.

For all evaluated stops and tones the organmaker's positions was clearly separated from the positions by the console and in the auditory. Dissimilarities were concerned first of all on the clarity of attack transient, timbre and loudness too. Substantially fewer differences were between the console and auditory position as a consequence of the relatively small volume of Martinů Hall. However in these cases the same dissimilarities were found as between the basic middle orientation and turning.

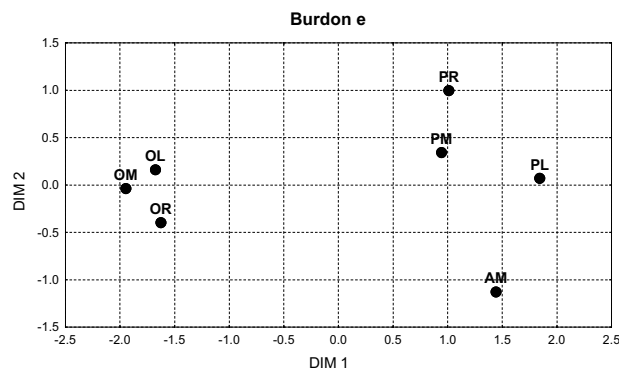


Figure 5: MDS solution for Burdon 16', tone e.

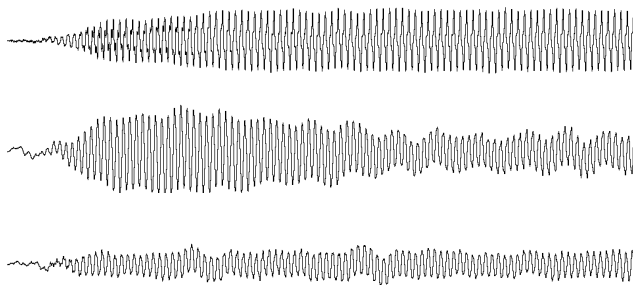


Figure 6: Burdon – attack transient for positions OM-PM-AM

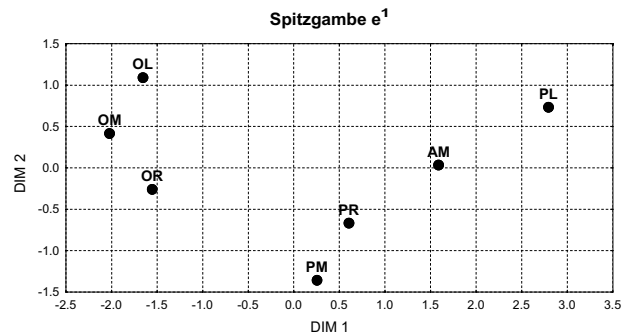


Figure 7: MDS solution for Spitzgambe 8', tone e¹.

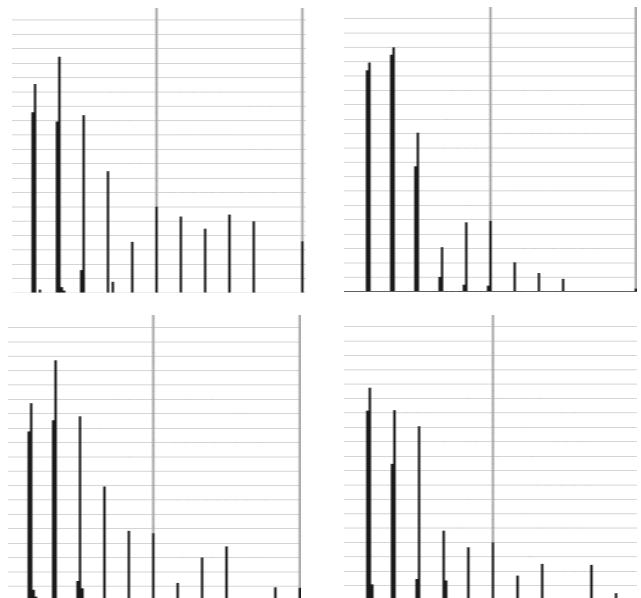


Figure 8: Spitzgambe – spectrum for positions OM-AM-PM-PL

Fig. 5, 7 and 9 show the dislocation of individual recording positions in the two-dimensional psychoacoustic space for given stops and tones. Fig. 6 demonstrates the attack transient differences for the „poor of timbre“ stop Burdon 16'. Especially it's clear to see the characteristic chuff on the beginning of tone in OM position in contrast to PM and AM position. Spectrum differences for the „rich of timbre“ stop Spitzgambe 8' are shown on the Fig. 8. In the upper part of this Figure are the spectra for the positions inside the organ and in the auditory, in the lower part is the interesting difference by the head turning in the console position. The last example on Fig. 10 shows the time envelope differences for the stop Octave 4', which hang together with an influence of the standing waves in the room.

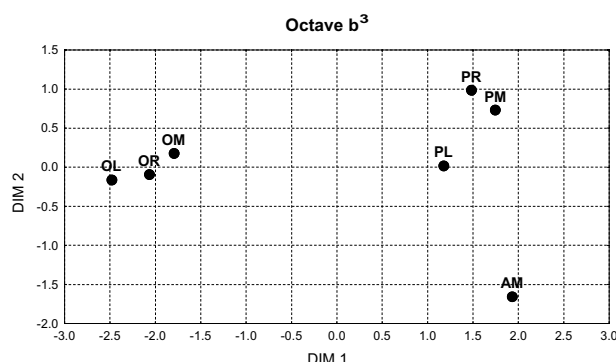


Figure 9: MDS solution for Octave 4', tone  $b^3$ .



Figure 10: Octave – tone envelope for positions OM-PM-AM.

#### 4. CONCLUSION

The attained results (with all these only preliminary character) confirm the high objective and subjective dissimilarities of tone properties in the basic incommutable listener positions by the organ. The substantial differences were found for attack transient character and for the timbre of steady state too but in concrete case of Martinů Concert Hall in far less degree for the loudness of evaluated tones. These sound differences have a big influence by the voicing of single pipes or whole stops, by the organ music performance and evidently by the acoustic measurement. However the organ sound quality is evaluated first from the average listener position in auditory of the hall or church. One of many ways how to eliminate the influence of various listener positions is the averaging of measured data, other way is the simultaneous multi-track recording, subjective evaluation and following statistical processing of all data.

The continuation of this research will be focused on the separated processing of attack transient and timbre dissimilarity in the basic listener positions for more tones, another stops and on an organ in other hall or church. For listening tests will be used more qualified persons and more precisely specified questions about the object of the tone similarity or dissimilarity. This work is closely associated with the documentation method

of acoustic properties of rare historical organs [2-6], developed and used in our Department of Musical Acoustics.

#### 5. ACKNOWLEDGMENT

The research was supported by the Ministry of Education and Youth, Czech Republic (Project No. MSM 511100001).

#### 6. REFERENCES

- [1] McAdams, S., Winsberg, S., Donnadieu, S., De Soete, G., Krimphoff, J., "Perceptual scaling of synthesized musical timbres: common dimensions, specificities, and latent subject classes", *Psychological Research*, 58, 177-192, 1995.
- [2] Štěpánek, J., Otčenášek, Z., and Syrový, V., "Acoustic documentation of church organs", *Proceedings of SMAC 93*, Stockholm, 516-519, 1994.
- [3] Štěpánek, J. and Otčenášek, Z., "Comparison of pipe organ plenum sounds", *Proceedings of ISMA 95*, Dourdan, 86-92, 1995.
- [4] Syrový, V., Otčenášek, Z. and Štěpánek, J., "Acoustic Evaluation of the Reconstruction of Heinrich Mundt Pipe Organs in Prague", *Proceedings of the 17th ICA*, (ISBN 88-88387-03-X), Roma, CD IV (Music), 20-21, 2001.
- [5] Syrový, V., Otčenášek, Z. and Štěpánek, J., "Spectral Characteristics of Czech Baroque Pipe Organs", *Proceedings of ISMA 01*, Perugia, (ISBN 88-900646-0-9), 477-480, 2001.
- [6] Syrový, V., "Ergebnisse der akustischen Vermessung der Teynkirchen-Orgel vor und nach der Restaurierung", *Konferenzbericht IME 8 "Mitteleuropäische Aspekte des Orgelbaus ..."*, Sinzig, Germany (ISBN 3-89564-073-5), 147-153, 2002.

# PERCUSSIONS



## MAKING OF A COMPUTER CARILLON

Matti Karjalainen, Paulo A. A. Esquef, and Vesa Välimäki

Helsinki University of Technology  
Laboratory of Acoustics and Audio Signal Processing, Espoo, Finland  
matti.karjalainen@hut.fi

### ABSTRACT

In this paper we present an analysis, modeling, and synthesis approach to bell sounds. Recorded bell sounds are first analyzed by high-resolution frequency-zooming modal estimation technique, where each partial is described typically by 2-3 submodes in order to include the warble characteristics of envelope beating in the partials. The bells are then modeled by inharmonic digital waveguides (DWGs) in order to achieve a highly efficient yet parametrically controllable synthesis model. The third step is to make a set of bells and related parametric controls in order to build a “computer carillon”. Special means are needed to approximate the strongly inharmonic bell sounds by DWGs, paying particular attention to the accuracy of the lowest partials. The control of bell models in the computerized carillon is through triggering of wavetables that store the initial part of the residual signal obtained in the modal decomposition process. Changing or modulating the modal parameters allows for sound effects that are not possible in real physical bells.

### 1. INTRODUCTION

The aim of this study is to analyze and model bell sounds for efficient real-time synthesis and playing control of a set of bell models, forming a computerized carillon. Full-scale physical models are too complex for the task, so we search for efficient semiphysical or DSP based techniques.

The most characteristic features of bell sounds are an inharmonic set of decaying partials, typically showing temporal envelope fluctuation, resulting in warble sound [1, 2]. Such beating in partials is due to two or more eigenmodes of vibration very close in frequency. Fig. 1 shows the waveform and spectrum of a small handbell, also the spectrum zoomed to the first partial around 1.3 kHz, demonstrating two mode peaks with spacing of about 2.5 Hz.

In Section 2 we first present a parametric analysis technique that is able to estimate with high accuracy the modal parameters of each partial. In Section 3 different synthesis modeling strategies are discussed and their applicability and efficiency is studied to find the best strategies for different bell types. In Section 4, realization of a computerized carillon for real-time synthesis is described, followed by summary and conclusions.

### 2. HIGH-RESOLUTION ANALYSIS OF BELL SOUNDS

The first task is to analyze recordings of target bell sounds to form the basis for synthesis models. We have developed a high-resolution parametric estimation technique based on frequency-zooming autoregressive moving-average method (FZ-ARMA) [3, 4], yielding accurate values for modal frequencies and decay times.

The first step of the procedure requires spectral analysis of the bell sound to roughly determine the frequencies of its prominent

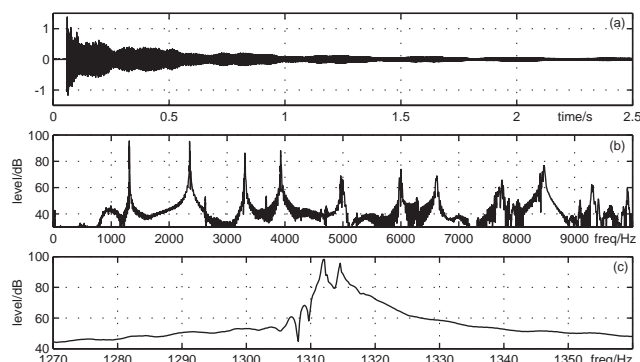


Figure 1: Analysis and modeling of a small bell sound: (a) recorded time-domain signal, (b) magnitude spectrum up to 10 kHz, (c) magnitude spectrum in the modal region around 1313 Hz.

spectral peaks or partials. The idea behind the frequency-zooming modeling is to analyze each partial of the tone separately. To accomplish that for a given partial, the following steps are taken:

1. Down-modulate the original signal to place the spectral peak of interest around 0 Hz, obtaining a complex signal.
2. Apply low-pass filtering to isolate this particular partial. The bandwidth of the filter must be narrow enough to reject neighboring partials.
3. Maximally decimate the low-pass filtered complex signal.
4. Fit a low-order complex-valued ARMA model to the decimated signal.

From the poles of the estimated model one can retrieve the frequencies and decay times of the resonant modes that are present in the analyzed partial, i.e., the frequencies are related to the angles of the poles whereas the decay times are related to the pole radii. More details on the FZ-ARMA analysis can be found in [3]. The advantage of the FZ-ARMA analysis is that it provides means to solve resonance frequencies that occur very close to each other as it happens in bell sounds, see Fig. 1.

As an example, the sound waveform of a hand-bell in Fig. 1, sampled at 44.1 kHz, is analyzed via the FZ-ARMA modeling scheme. The decimated complex-valued signals associated with each partial are modeled through ARMA(2, 4), i.e., two complex poles and four complex zeros. From the pole locations of the models we obtained the frequencies and decay times of the partial modes (two modes per partial in this case). Figure 2 plots the decay envelopes of the lowest partials. Beating is found particularly in the first and second partial. High partials decay relatively fast so that their details are not so important from a perceptual point of view.

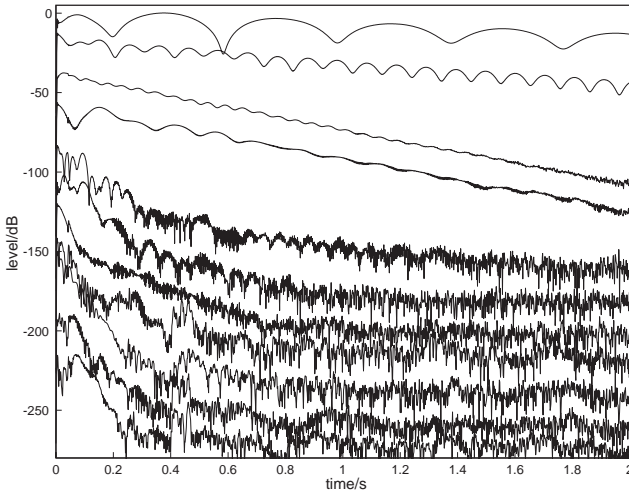


Figure 2: Decay envelopes for partials in bell sound (Fig. 1) from top to down plotted on the dB scale with 20 dB offsets for clarity. Higher partials reach the measurement noise floor.

### 3. EFFICIENT SYNTHESIS MODELS FOR BELLS

When high-quality recordings of bell sounds are available, they can be used directly in sampling synthesis, i.e., in replay from wavetables. This has two drawbacks, however. One is the need of memory for long samples, even tens of seconds. In many cases this is not necessarily a drawback anymore with modern memory technologies. Another problem is the inflexibility of sample-based synthesis if sound features have to be changed at runtime. This was the main motivation to experiment with different efficient parametric synthesis techniques.

#### 3.1. Modal filterbank synthesis

A straightforward method of sound synthesis is to use modal parameters from the FZ-ARMA analysis to build a modal filterbank synthesizer [4]. This is relatively efficient in the handbell case of Fig. 1 where approximately 11 partials is enough for a frequency band of 10 kHz. If a partial consists of two modes, each realized by a filter of order two, the overall filterbank order is about 44. An impulse can be used as the excitation of such a synthesis model. For large low-pitch bells there can be need for filterbank orders of several hundreds. Thus it is attractive to search for even more efficient models.

#### 3.2. Inharmonicizing a digital waveguide

Digital waveguides (DWG) are known as highly efficient models for synthesizing musical instruments that have harmonic spectra [5]. Now we study how to make them inharmonic. DWGs consist basically of a delay loop (see two of them in Fig. 3) which create a comb filter type of spectrum, so that the frequencies of modal resonances are located at frequencies where the phase shift is integer multiple of  $2\pi$ . Inharmonic relationship of modes means nonlinear phase function, which can be obtained by cascading an integer-length ( $L$ ) delay with an allpass filter:

$$H_{\text{delay}}(z) = \frac{a_N + \dots + a_1 z^{-N+1} + z^{-N}}{1 + a_1 z^{-1} + \dots + a_N z^{-N}} z^{-L}. \quad (1)$$

The phase delay will be

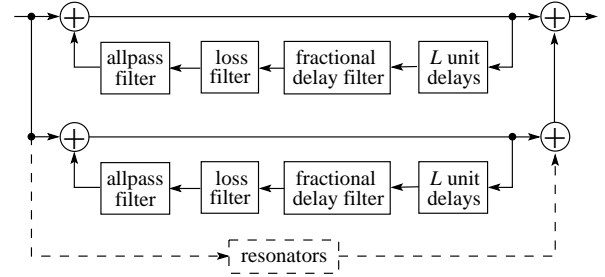


Figure 3: Bell model of dual DWG filters with additional parallel resonators. Each DWG consist of integer delay ( $L$ ), fractional delay for fine tuning of pitch, loss filter, and inharmonicizing allpass filter.

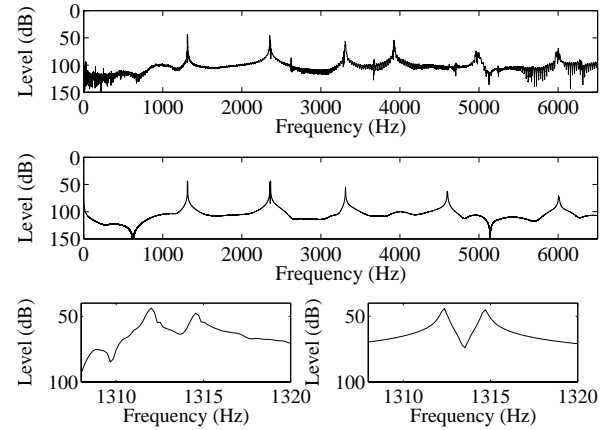


Figure 4: Magnitude spectra of the original handbell (top) and synthesized bell (middle). Zoom in the first partial: original (bottom-left) and synthesized (bottom-right).

$$\tau_{\text{ph}}(\omega) = L + N - \frac{2}{\omega} \arctan \left\{ \frac{\sum_{k=1}^N a_k \sin(k\omega)}{1 + \sum_{k=1}^N a_k \cos(k\omega)} \right\}, \quad (2)$$

where  $a_k$  are the coefficients of the allpass filter, constrained to  $a_0 = 1$ . For efficient realization the allpass order  $N$  must be low. The most interesting case is to use a second order allpass ( $N = 2$ ).

In [6] we developed an automated iterative procedure to fit an inharmonic DWG model, i.e., a feedback loop with a delay plus a second-order allpass loop filter to tune the three lowest partials of a given bell response.

After tuning the modal frequencies, the decay times must be adjusted by a low-pass filter in the waveguide loop to have proper losses at each modal frequency. When a low-order filter is used, typically of first or second order, it can only approximate the general trend of decay time vs. frequency, paying most attention to adjusting the long-ringing lowest partials to decay properly.

Two such inharmonic DWGs must be connected in parallel in order to have two modes for each partial, having a proper frequency difference and decay times to make a desired beating (warble sound). If only one or two partials show remarkable beating, such as in the case of Fig. 1, the second DWG can be avoided by using extra parallel resonators to create the beating for the desired partials in the main DWG.

Figure 4 shows the original and a modeled magnitude spectrum for the handbell introduced in Fig. 1.

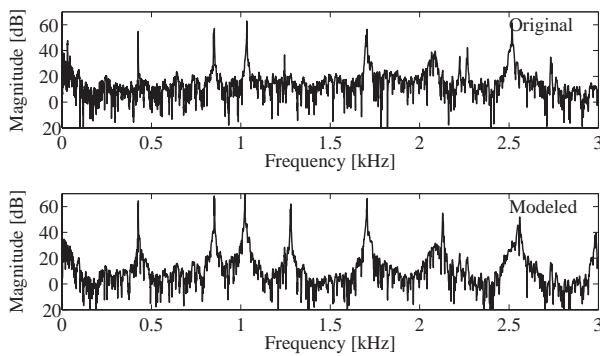


Figure 5: Magnitude spectra for a tuned bell: original (top) and modeled (bottom).

### 3.3. DWG synthesis of tuned bells

The handbell modeled above is an example of bell making where no specific effort is done to increase the harmonicity of partials. In large bells it is common to shape the bells so that many partials are in approximately harmonic frequency relationships [2]. This improves to perceive a definite pitch. The remaining inharmonic ones make the bell-like timbre.

It was found that designing inharmonic DWG models for tuned bells is more difficult than for the handbell using the technique described above. It turns out that the inharmonic partials between approximately harmonic ones tend to get too high Q values, i.e., to decay much slower than desired. This could be compensated for by a loop filter with a magnitude response dip at that frequency, but this leads to high-order loop filters and increased complexity of design.

One choice of compromise could be to let the harmonic components become somewhat less harmonic, yet getting a clearly bell-like sound. This is however not acceptable if a given tuned bell sound must be modeled with a perceptually clear pitch.

A better choice for efficient and relatively accurate modeling of tuned bells is to use digital waveguides only for the realization of the harmonically related partials and to implement remaining low-frequency inharmonic partials by separate parallel resonators.

The upper curve in Fig. 5 depicts the spectral range of 0–3 kHz of a bell from a Belfort bell set<sup>1</sup>. It can be seen that partials 1, 2, 4, 5, etc., form a nearly harmonic set, while partial 3 (just above 1 kHz) is clearly inharmonic. In this case the simplest choice is to model partial 3 as a pair of separate modal resonances and approximate all others by a pair of digital waveguides, designed as in the small bell case. Pairwise modes are needed to realize proper beating envelopes in the partials. The bottom curve in Fig. 5 plots the magnitude spectrum of a model designed this way. The most notable difference is the stronger fourth partial in the synthetic one, which is due to the analysis of model excitation described below.

### 3.4. Excitations

Different ways of obtaining the excitation signal to trigger the hitting of a model are used in different cases. The easiest case is the modal filterbank model, where, for a properly designed ARMA model, the excitation is simply an impulse. If only poles are used to make an all-pole (AR) model, the excitation is obtained by in-

<sup>1</sup>The recordings were kindly provided by Marc Leman.

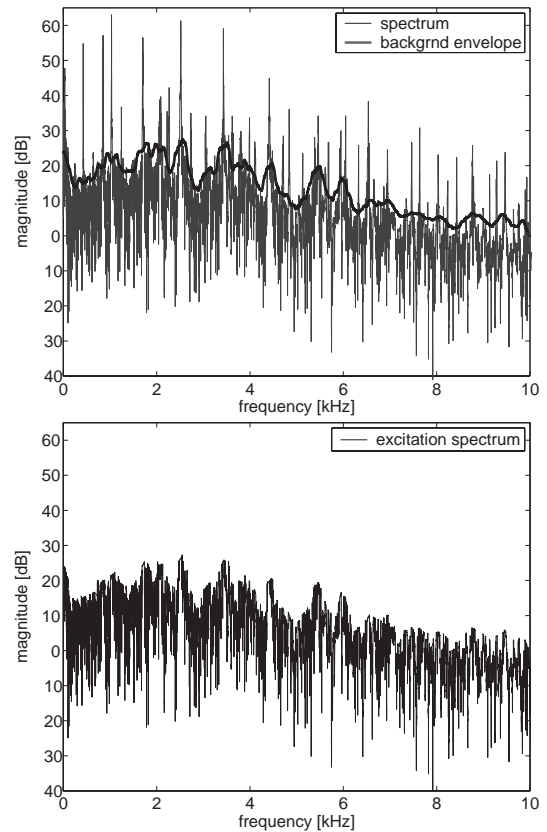


Figure 6: Original and excitation spectra of an inharmonic bell. The excitation is obtained by removing the modal resonances from the complex spectrum of the original sound.

verse filtering the recording and truncating the result to contain the main energy part.

In the digital waveguide cases we have tried the following techniques to get the content of excitation wavetable. A simple way is to use the inverse-filtered residual as mentioned above and to shape it spectrally (e.g., by low-order AR modeling) to yield a proper spectral envelope for the synthetic sound.

Another technique that was applied in the inharmonic DWG modeling of the tuned bell above is to get the excitation from the original sound in the following way:

1. First a long FFT ( $2^{17} = 131072$ ) of the original bell sound is computed;
2. The magnitude and phase are computed and the phase is stored for future use;
3. An estimate of the background spectrum is obtained using the two-pass split-window technique [7];
4. The FFT bins associated with the spectral peaks are replaced with the values of the background spectrum;
5. The modified magnitude spectrum and the original phase are transformed back into the time domain via IFFT;
6. Finally, the resulting excitation signal is windowed: the second half of a Hanning window of length  $2^{17}$  is used for this purpose.



Figure 6 illustrates the procedure used to modify the spectrum of the original bell sound to generate the excitation signals. The magnitude modification is as simple as adopting the spectral envelope curve as an upper magnitude limit excluding the modal resonances.

#### 4. REAL-TIME SYNTHESIS AND CONTROL

Real-time synthesis and playing control of the bell models has been carried out in the BlockCompiler modeling software [8, 9], developed particularly for experimental physical modeling purposes. The BlockCompiler is based on the Common Lisp language for creating and manipulating of block-based models, 'patches', as well as C-code generation and compilation of the patches for efficient run-time execution of the models.

As an example of creating patches in BlockCompiler the modal filterbank model of the handbell can be made by the following script:

```
(defvar bellpatch
  (patch ((wt (.wtable :data *bell-wtable*))
          (.iir (.iir :denom *bell-coeffs*))
          (da (.da)))
    (-> wt iir (inputs da))
    (defun hit () (trigger wt))))
```

where the bell model object created by the form starting from patch is assigned to the variable bellpatch. A wavetable for model excitation is assigned to local variable wt, then the modal filterbank is made to iir, and furthermore sound output (DA-conversion) is bound to da. The line starting by (-> ...) makes interconnections between block outputs and inputs. Finally the function hit is compiled so that when it is called, it triggers the wavetable to feed excitation to the filterbank. Wavetable data \*bell-wtable\* and IIR filterbank denominator coefficients, \*bell-coeffs\*, are assumed to be preanalyzed from a given target sound. When a command (run-patch bellpatch) is executed, the model starts streaming real-time synthesis, and the bell can be triggered by function form (hit).

Inharmonic digital waveguide models can be created in a similar way, although scripting will be somewhat more elaborate. More than 100 such bell models can be executed simultaneously in real time on a 1 GHz computer.

When a set of bells is made by any of the methods described above, a computerized carillon is obtained by making the bells playable through some user interface. A MIDI keyboard can be mapped to the triggering inputs of the bells. Even a computer keyboard may be used in simple demonstrations. The carillon can be played also from sequencer programs through MIDI control or directly from specialized sequencer programs.

The advantage of parametric synthesis models is that sound features can be easily controlled also at runtime. This is important particularly when computer music is created where the potential of modifying sounds is utilized. With synthesis models it is relatively easy to produce sounds that are very difficult or impossible to create by real physical means. One such example is to modulate the frequencies of the modal resonances. Many other digital sound effects can be easily added to the model-based synthesis approach.

#### 5. SUMMARY

In this paper we have investigated the analysis, efficient real-time synthesis, and control of bell sounds, i.e., making of a computerized carillon. The technique used for parametric analysis is based

on high resolution FZ-ARMA modeling which yields modal parameters even for complicated partial behaviors.

For real-time synthesis we have used inharmonic digital waveguides, where the lowest partials are inharmonized by an additional allpass filter in the DWG loop. Two submodels and/or additional parallel resonators are needed to achieve proper decay envelopes of the partials, which is important particularly to make warble sound. Rapidly decaying higher partials do not need as accurate modeling since auditory perception of main timbral features is mostly based on the long-ringing low-frequency partials. There often seems to be only a couple of lowest partials that show strong beating in their envelopes. In such cases a good candidate for efficient and accurate synthesis is to use only one inharmonic digital waveguide and separate parallel resonators for the low-frequency modes to make the envelopes beating.

Finally we have discussed the implementation for real-time synthesis and control of the synthesis models using a physical modeling software called BlockCompiler.

Sound examples are available in:

<http://www.acoustics.hut.fi/demos/smac03/bells>

#### 6. ACKNOWLEDGMENTS

The work of Paulo Esquef has been supported by the EU funded project ALMA (IST-2001-33059) and by the Brazilian National Council for Scientific and Technological Development (CNPq). Our thanks are due to Marc Leman who kindly provided the set of Belfort bell recordings.

#### 7. REFERENCES

- [1] N. H. Fletcher and T. D. Rossing, *The Physics of Musical Instruments*. New York, USA: Springer-Verlag, 1991.
- [2] T. D. Rossing, *Acoustics of Bells*. Striudsborg, PA: Van Nostrand-Reinhold, 1984.
- [3] M. Karjalainen, P. A. A. Esquef, P. Antsalo, A. Mäkitvirta, and V. Välimäki, "Frequency-Zooming ARMA Modeling of Resonant and Reverberant Systems," *J. Audio Eng. Soc.*, vol. 50, no. 12, pp. 1012–1029, Dec. 2002.
- [4] M. Karjalainen, V. Välimäki, and P. A. A. Esquef, "Efficient Modeling and Synthesis of Bell-Like Sounds," *Proc. DAFX-02*, Hamburg, Germany, pp. 181–186, Sept. 2002.
- [5] J. O. Smith, *Principles of Digital Waveguide Models of Musical Instruments*, Ch. 10 in *Applications of Digital Signal Processing to Audio and Acoustics*, (ed. Kahrs and Brandenburg). Kluwer Academic Publishers, 1998.
- [6] P. A. A. Esquef and V. Välimäki, "Design of an Efficient Inharmonic Digital Waveguide Filter for Synthesis of Handbell Sounds," *Proc. FINSIG'03*, Tampere, Finland, May 2003.
- [7] W. A. Struzinski and E. D. Lowe, "A Performance Comparison of Four Noise Background Normalization Schemes Proposed for Signal Detection Systems," *J. Acoust. Soc. Am.*, Vol. 76, no. 6, pp. 1738–1742, Dec. 1984.
- [8] M. Karjalainen, "BlockCompiler: Efficient Simulation of Acoustic and Audio Systems," Preprint 5756 of *114th AES Convention*, Amsterdam, March 2003.
- [9] M. Karjalainen, "Time-Domain Physical Modeling and Real-Time Synthesis Using Mixed Modeling Paradigms," *Proc. SMAC'2003*, Stockholm, Aug. 2003.

## **NORMAL MODES OF THE ELEPHANT BELL**

*R Perrin*

Institute of Fundamental Sciences, Massey University, Palmerston North, New Zealand

*B Deutsch, A Robinson, R Felce and T R Moore*

Department of Physics, Rollins College, Winter Park, FL 32789, USA

*G M Swallowe*

Physics Department, Loughborough University, Loughborough, LE11 3TU, UK

### **ABSTRACT**

The normal modes of a 16-tine elephant bell have been investigated using finite-element modeling, group representation methods and electronic speckle pattern interferometry. The experimental results are in good agreement with the model for about the first ten frequencies, and both are consistent with the predictions of group theory. It is found that the vibration spectrum can be understood by regarding the tines as a set of identical oscillators coupled in series in a closed loop with the hemispherical crown holding them in place, providing the coupling and, perhaps, acting as a sounding board.

### **1. INTRODUCTION**

Beautiful Bangaloreware elephant bells were frequently on sale as souvenirs at exhibitions in the UK in the middle decades of the last century and were often seen on display in the nations' living rooms. Today they have become collectors' items but relatively crude brass bells of similar general type are still available commercially, and it is with one of these that this article is primarily concerned.

The "modern" elephant bell, as shown in Figure 1, consists of a hemispherical shell from whose rim hang roughly identical and equally spaced tines which have a slight inward curvature. There are between 10 and 20 of these, the number increasing with the overall size of the bell and always seeming to be even. There is a caste-in handle at the top of the hemisphere and the bell is rung by means of a clapper consisting of a metal ball suspended from a wire attached to the underside of the hemisphere. This strikes the tines at approximately the point where the hemispherical cap meets the tines. With the Bangaloreware bells the "hemisphere" is rather flattened, the tines are more curved and always seem to be odd in number.

The only previous study of an elephant bell to our knowledge was published in 1944 by Brailsford [1] who looked at a Bangaloreware bell with 15 tines. Looking at the vibration spectrum he found a number of very weak peaks below about 200Hz which he considered to be due to the tines vibrating as individual cantilevers. Starting at 900 Hz he found a sequence of

much more prominent peaks, which he seems to have regarded as being due to the bell as a whole.



Figure 1: *The modern elephant bell.*

### **2. THE FINITE-ELEMENT MODEL**

An elephant bell is harder to model than a conventional one [2, 3] because it does not have complete axial symmetry. It does, however, have a high level of symmetry which can be exploited. We take a "unit cell" to be a vertical segment contained between two planes containing the symmetry axis. These are chosen so that one touches the left hand side of a typical tine at its widest point and the other touches its right-hand neighbour at the corresponding point. The unit cell thus contains one tine plus one gap and that segment of the hemisphere joining them to its pole. If we make a finite-element model of this unit cell then one for the entire bell can be made by copying it  $(r-1)$  times while rotating about the symmetry axis through an angle of  $360/r$  where  $r$  is the number of tines.

To produce the unit cell careful measurements were made of the overall dimensions and profile of a 16-tine bell. The tines and gaps were all measured and averages taken. The unit cell was then modeled by means of the LUSAS package using thin-shell elements chosen to preserve the overall shape of the outside of the bell. The thickness of the tine was taken as a constant 3mm and that of the slice of hemisphere as 4.5 mm.

The bell was about 8 cm tall and 8 cm in diameter at its widest point. The effect of the handle was modeled by constraining the bell to be fixed at the handle's edge. This had the added bonus of making sure that rigid body modes were excluded from the calculation. Typical values for brass of  $8500 \text{ kgm}^{-3}$  for density, 104 GPa for Young's modulus and 0.37 for Poisson's ratio were input to the model.

### 3. SYMMETRY CONSIDERATIONS

#### 3.1 Perturbed bell approach

If the elephant bell did not have inter-tine gaps it would be just one more convex bell with axial symmetry group  $C_{\infty v}$  and would be subject to the usual consequences.[4] The nodal patterns would consist of  $m$  equally spaced "diameters" plus  $n$  circles parallel to the rim. Those with  $m > 0$  would be in degenerate pairs with modal functions varying like  $\sin(m\theta)$  and  $\cos(m\theta)$ , where  $\theta$  is the polar angle, while those with  $m = 0$  would be singlets. The number pairs  $(m, n)$  could be used to specify the modes.

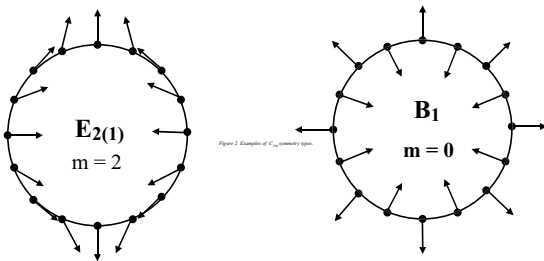


Figure 2. Examples of  $C_{16v}$  symmetry types.

The  $r$  inter-tine gaps constitute a large perturbation with symmetry group  $C_{rv}$  to be applied to this standard convex bell. Because some, but not all, of the original symmetries are now removed, some but not necessarily all of the doublets will become split. One of the present authors (RP) [5] has shown that, in these circumstances, the majority of doublets actually remain as degenerate pairs, although their common frequency may change. Only those with  $m/r = \text{half integer}$ , or non-zero integer, will split. Thus, with 16-tines, only doublets with  $m = 8, 16, \dots$  will split.

#### 3.2 Coupled cantilever approach

Alternatively one could regard the elephant bell as a collection of  $r$  identical cantilevers coupled together in a closed loop by the hemisphere. The collective modes of these cantilevers must be classifiable as symmetry types of the group  $C_{rv}$ . It is possible to construct the appearance of each of these types, as seen in any plane normal to the bell's symmetry axis, from symmetry arguments alone. No information about the coupling forces is required. Details of the method have been given by two of the present authors [6]. With 16 tines there are 4 singlet types and 14 pairs of doublets. Details of some of these are given in Figure 2.

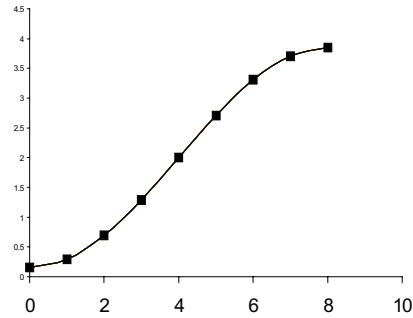


Figure 3. Frequency  $v$   $m$  for vibrating polygon

The analogous problem of  $r$  identical masses at the vertices of a polygon, joined together in pairs by identical springs along the sides to form a closed loop, has previously been solved in detail by one of us (RP) [7]. In this case, because the details of the coupling force were known, it was possible, using group theoretical arguments, to obtain the actual frequencies for the normal modes. When these are plotted in mode order they form a very distinctive "saturation" curve as shown in Figure 3 for the case of 16 sides. This proves to be very significant in understanding the elephant bell, as we shall see.

### 4. FINITE-ELEMENT MODEL RESULTS

LUSAS was used to calculate the frequencies and display the modal forms for all the modes it could find up to about 6 kHz. The results up to 4 kHz are summarised in Table 1. In nearly all cases it was easy to establish an  $m$  value by looking at the mode's behaviour on the hemisphere, although this became harder as  $m$  increased due to evanescence setting in lower down the bell [8]. For  $0 < m < 8$  the modes were all in degenerate pairs, as expected, with frequency differences between pair members never being more than  $\frac{1}{4}$  Hz. Being so close we list only the higher frequency of each pair in Table 1. Modes with  $m = 0$  were all singlets, again as expected. Those with  $m = 8$  were also singlets, not what one expects in a normal bell but which was anticipated in section 3.1 due to the 16-tine perturbation. There was no prediction of Brailsford's low-frequency single-tine cantilever modes. Nor were any modes predicted with  $m > 8$ .

In Figure 4 we plot frequency verses  $m$  for all predicted modes with  $m > 0$  up to 4 kHz. The curves are not even remotely similar to those for a conventional bell. Instead of the frequency rising steadily and indefinitely with  $m$ , the curves reach limiting values at  $m = 8$ . This behaviour is exactly what was described in section 3.2 as being due to a closed loop of identical coupled oscillators. This being the case it should be possible to identify the  $C_{16v}$  symmetry type for each mode by comparing the LUSAS solutions with the group theoretical predictions mentioned in section 3.2. It was quite easy to do this for the first dozen or so modes and the results are incorporated into Table 1. As frequencies got higher and modes more complicated the identification became increasingly difficult. Likewise with identifying values for  $n$ . For modes on the lower curve in Figure

4 it was very easy to see that they had  $n = 0$ , as one would expect. With those on the upper

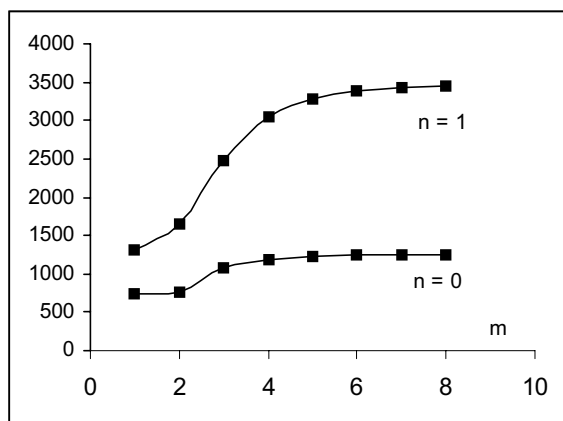


Figure 4. Frequency (Hz) v  $m$  for LUSAS predictions.

curve many appeared to have one nodal circle at around the mid points of the tines. However, because of twisting and/or transverse motion of the tines, it was often difficult to decide where the circle might actually be. Indeed it sometimes appeared to move up and down from tine to tine. In the case of singlet modes it was always very easy to identify both their symmetry types and the location and numbers of their circles

From those LUSAS results so far analysed it is clear that the  $n = 0$  modes on the lower saturation curve are all due to the tines going into fundamental cantilever modes, but in directions varying from tine to tine in a way determined by their symmetry types – essentially by their  $m$  values. The higher modes seem to be due to the tines going into cantilever modes of higher orders plus, in some cases, twisting about their individual axes. Further study using the LUSAS animation facility should produce firmer identifications.

## 5. EXPERIMENTS

In order to compare the predictions of the finite element analysis with the modes of an actual elephant bell, a 16 tine modern bell similar to that shown in Figure 1 was studied using electronic speckle pattern interferometry (ESPI) [9]. The ESPI system images out of plane vibrations by digitally subtracting a speckle interferogram of an object illuminated by coherent radiation before the object begins to vibrate, from one imaged subsequent to its movement.

The system used to image the vibrations of elephant bells was constructed from discrete components on a vibration-isolated optical table that was inside an anechoic chamber. The laser used to illuminate the bell was a diode-pumped, frequency-doubled, Nd:YVO<sub>4</sub> laser with an output of 532nm. The laser was mounted on a vibration isolated optical table outside of the anechoic chamber in order to minimize the ambient noise. The light entered the chamber through a small hole in the wall. All of the data acquisition and analysis was performed by a computer located outside of the chamber.

The vibrations of the bell were driven by a piezoelectric disk that was mounted to either the hemispheric cap or the tines using putty. The piezoelectric driver was connected to a high-quality function generator that produced a sine wave with frequency accuracy and precision exceeding 0.1 Hz. The frequencies of the normal modes of vibration were determined by striking the bell and performing a spectral analysis of the resulting sound. Additionally, the frequency of the function generator was scanned while observing the ESPI image in real time to ensure that no normal modes were neglected.

A typical electronic speckle pattern interferogram is shown in Figure 5. In Figure 5, the bell is vibrating in the (3,0) mode and is viewed both from the side and the top. The dark areas indicate nodes while the light areas indicate antinodes.

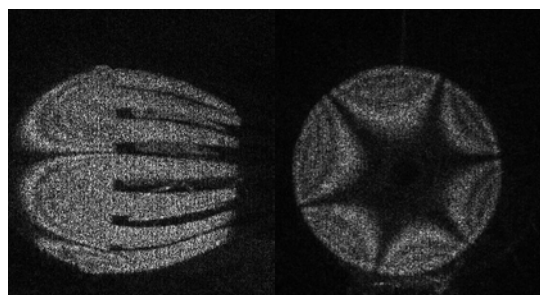


Figure 5: Typical electronic speckle pattern interferogram of a 16-tine modern elephant bell. The view is from the side and top, respectively. The mode is (3,0).

## 6. COMPARISON OF RESULTS

The interpretation of fringe patterns in interferograms of vibrating three dimensional objects is famously difficult. Although a large number of resonant frequencies of the 16-tine bell were detected, it has so far proved possible to fully identify only a few of them. In those cases where  $m$  was identified the degeneracy was always as predicted by group theory. The doublets were all slightly split so, when it is required, we quote the higher value. The lowest frequency modes to be positively identified were a (2, 0) pair at 753 Hz and a (3, 0) pair at 1071 Hz. The LUSAS results were therefore scaled, as in Table 2, to bring its lowest (2, 0) pair into alignment with experiment. This was legitimate because of the use of standard values for density and Young's modulus in the model calculations. If the two lists of results are now matched in sequence, then provided one experimental point is missed out and another is accepted as not having been excited, the agreement of frequencies is excellent up to about 1300 Hz. Above that it is relatively poor and gets progressively worse with further increase in frequencies.

## 7. CONCLUSIONS

The agreement between the finite-element results and the ESPI frequency data for the first set of modes is impressive and suggests that the model is basically sound. The modes that interferometry failed to detect are probably only missing because a more subtle excitation is required. Those modes which

it finds that are not predicted may well be due to non-linear effects. Clearly, a more sophisticated means of identifying the nodal patterns and the symmetry type via interferometry would be a great help in matching the modes up with those predicted by LUSAS. There is little doubt that all of the predictions of group theory will be borne out, always subject to allowances for slight splitting due to small symmetry breaking because of asymmetry in the bell. The failure of the model to give good frequency predictions at higher frequencies is probably because the modes concerned involve the tines twisting about their own axes. The thin shell elements used in the model are probably inadequate to deal with this. In order to arrive at complete agreement, it is probably necessary to develop a more sophisticated model based on true three dimensional elements.

Frequency (Hz)	Degeneracy (S or D)	m	n	Symmetry type
748	D	1	0	E1(1)
765	D	2	0	E2(1)
1087	D	3	0	E3(1)
1181	D	4	0	E4(1)
1197	S	0	1	A1
1221	D	5	0	E5(1)
1241	D	6	0	E6(1)
1251	D	7	0	E7(1)
1254	S	8	0	B1
1316	D	1	1	E1(1)
1661	D	2	1	E2(1)
2467	D	3	1	E3(1)
2901	S	0	1	A2
3044	D	4	1?	E4(1)
3289	D	5	1?	E5(1)
3390	D	6	1?	E6(1)
3432	D	7	1?	E7(1)
3432	S	8	0	B2
3444	S	0	1	A1
3559	D	1	1	E1(1)

Table 1: LUSAS results for the 16-tine bell up to 4000Hz

m	n	Scaled LUSAS frequency (Hz)	Experimental frequency (Hz)
1	0	737	*
2	0	753	753
*	*	*	1004
3	0	1070	1071
4	0	1163	*
0	1	1179	1182
5	0	1202	1206
6	0	1222	1222
7	0	1232	1233
8	0	1235	1242
1	1	1296	1299
*	*	*	1353
*	*	*	1406
2	1	1635	1593
3	1	2429	2050

Table 2: Comparison of scaled LUSAS predictions with interferometric results. An \* marks missing data.

## 8. REFERENCES

- [1] Brailsford H.D., "Some Experiments on an Elephant Bell", J. Acoust. Soc. Am., Vol. 15, 1944, pp.180-187.
- [2] Perrin R., Charnley T. and dePont J., "Normal Modes of the Modern English Church Bell", J. Sound Vib., Vol. 90, 1983, pp. 29-49.
- [3] Rossing T.D., Perrin R., Sathoff H.J. and Peterson R. W., "Vibational Modes of a Tuned Handbell", J. Acoust. Soc. Am., Vol.76, 1984, pp. 1263-1267.
- [4] Perrin R. and Charnley T., "Group Theory and the Bell", J. Sound Vib., Vol. 31, 1973, pp. 411-418.
- [5] Perrin R., "A Group Theoretical Approach to Warble in Ornamented Bells", J. Sound Vib., Vol. 52, 1977, pp. 307-313.
- [6] Perrin R. and Swallowe G. M., "Zero Eigenfrequencies in the Vibrating Polygon", J. Sound Vib., Vol. 174, 1994, pp. 181-189.
- [7] Perrin R., "Group Theory and the Vibrating Polygon", J. Sound Vib., Vol. 25, 1972, pp. 597-607.
- [8] Perrin R. and Gottlieb H. P. W., "Evanesence and Bessel Functions in the Vibrating Circular Membrane" Eur. J. Phys., Vol. 15, 1994, pp. 293-299.
- [9] see for example, R. Jones and C. Wykes, Holographic and Speckle Interferometry, 2<sup>nd</sup> ed., New York, Cambridge, 1989. pp. 165 – 196.

## RAYLEIGH'S BELL MODEL REVISITED

*R Perrin*

Institute of Fundamental Sciences, Massey University, Palmerston North, New Zealand  
rperrin@ts.co.nz

*G M Swallowe*

Physics Department, Loughborough University, Loughborough, LE11 3TU, UK  
G.M.Swallowe@lboro.ac.uk

### ABSTRACT

It is now well over a century since Lord Rayleigh published his model for western-style bells. He used a hyperboloid of revolution plus a flat circular plate for the crown. By limiting himself to inextensional modes of a very restricted type, and exploiting the hyperbola's parametric form, he produced an equation whose roots give the locations of nodal circles. Remarkably this equation involves neither the wall thickness nor physical properties of the bell material and this approach remains the only available analytical way of making such predictions. Although he gave adequate accounts of the derivation and method of solution of his equation, Rayleigh did not present much in the way of comparison of its predictions with experiment. Rather he focussed on using it to explain the fact that the Hum note never has any nodal circles. In the present paper we consider how well profiles of some modern church and handbells can be fitted by hyperbolae. We compare the model's predictions for these bells with data for a range of inextensional modes and report a new, surprisingly accurate, approximate analytical solution of Rayleigh's equation.

### 1. INTRODUCTION

Due to its axial symmetry, it is convenient to discuss a bell using cylindrical polar co-ordinates with  $z$ -axis defined by the axis of symmetry. Thus a typical point  $(r, \hbar, z)$  on the bell undergoes displacements  $(u, v, w)$  in radial, transverse and axial directions. Rayleigh [1] pointed out that normal modes of bells cannot have any nodes in the sense of their being points of zero motion. However, if one considers nodes in the more limited sense of being points of zero amplitude in any one cylindrical polar direction, e.g. radial, then nodal patterns do arise consisting of  $m$  equally spaced "diameters" and  $n$  circles parallel to the rim. This is because axial symmetry requires the normal modes to occur in degenerate pairs, for non-zero  $m$ , whose modal functions, in any one cylindrical polar direction, vary like  $\sin(m\hbar)$  and  $\cos(m\hbar)$  [2].

Rayleigh's professional interest in church bells seems to have gone back to experiments he conducted on the specimens in his local church tower in 1879. His subsequent application of his

general theory for thin curved plates and shells to the strictly inextensional modes of concave bells is well known [1]. There exists only one of these modes for each value on  $m$ . This application is very unusual in that, being based purely on geometry and three inextensibility conditions, it does not predict frequencies but only the locations of nodal circles. Rayleigh's use of this to explain the fact that the Hum ( $m=2$ ) never has any nodal circles while the Tierce ( $m=3$ ) may, or may not, do so is very convincing and remains the best available clue to what is really happening with these modes. However he never explored his model's predictions for higher  $m$  modes and so was not drawn to consider whether they could have more than one nodal circle. The predictions for these higher modes are interesting but prove to be at odds with both experimental and finite-element studies of both church bells and handbells.

### 2. RAYLEIGH'S MODEL

Rayleigh assumed that the profile of a (thin) bell, as seen in any plane containing the symmetry axis, could be approximated by part of a hyperbola with its pole at the bell's shoulder. For convenience we shall use the upper half of the right hand branch of the hyperbola and regard the bell as being stood on its crown, as shown in Figure 1. The complete bell wall is thus the upper half of the hyperboloid of revolution produced by rotating the hyperbola about the  $z$ -axis. The crown Rayleigh considered to be a flat rigid circular plate causing the pole of the hyperbola to be rigidly fixed. Surprisingly no boundary conditions need to be imposed on the rim of the bell in order to solve the equations. Indeed the rim's location is only required at all when one wants to compare the predictions of the model with experiment.

### 3. THE HYPERBOLA

Choosing a plane containing the symmetry axis (i.e. fixed  $\hbar$ ), and retaining cylindrical polar variables, the hyperbola's equation is

$$\frac{r^2}{a^2} - \frac{z^2}{b^2} = 1 \quad (1)$$

where  $a$  and  $b$  have their usual geometrical meanings and are related to the eccentricity  $e$  by  $e^2 = 1 + (b/a)^2$  so that  $e > 1$ . In his model Rayleigh chose to work with the parametric form for the hyperbola:

$$z = b \tan \chi, \quad r = a \sec \chi \quad (2)$$

Geometrical interpretations of  $a$ ,  $b$  and  $\chi$  are shown in Figure 1. Note the role of the point  $(b, 0)$  in defining the angle  $\chi$ . This is not usually discussed in texts on conic geometry. Since the solutions of Rayleigh's model come out in terms of  $\chi$  it is important to note its interpretation and range of  $0 \leq \chi \leq \pi/2$ .

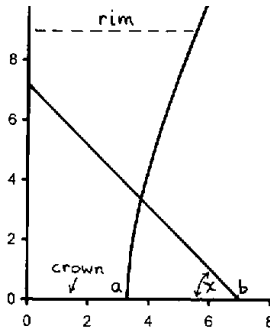


Figure 1: Meaning of the parametric angle  $\chi$

#### 4. SUMMARY OF RAYLEIGH'S THEORY

By considering the change in length of an arbitrary element traced on the surface and imposing axial symmetry, Rayleigh derives three conditions for inextensibility of the element. These are:

$$\frac{\partial w}{\partial z} + \frac{dr}{dz} \frac{\partial u}{\partial z} = 0 \quad (3a)$$

$$\frac{\partial v}{\partial \theta} + u = 0 \quad (3b)$$

$$\frac{\partial w}{\partial \theta} + r \frac{\partial v}{\partial z} + \frac{dr}{dz} \frac{\partial u}{\partial \theta} = 0 \quad (3c)$$

To achieve strict inextensibility all three of these conditions must be satisfied. However, if the element selected lies in the plane of fixed  $z$ , then only the second condition applies. This equation is well known and is sometimes regarded as "the" inextensibility condition [3]. This is because, if one considers the bell's cross-section in a plane of fixed  $z$ , then this is the condition a neutral circle, whose total length remains unchanged throughout the cycle, must satisfy. It requires that if  $u = A(z) \sin(m\chi)$  then  $mv = A(z) \cos(m\chi)$  so the radial and transverse components are locked together. It is well established that all the acoustically important bell modes obey this condition to a good degree of approximation.

Starting from equations (1) and (3), using the known angular form for  $v(z, \chi)$ , converting to parametric forms of the co-

ordinates and imposing the boundary condition at the pole, Rayleigh shows that to get zero motion normal to the bell's surface requires

$$\sin(2\chi) + 2m \tan(m\chi) (e^2 - \cos^2 \chi) = 0 \quad (4)$$

Note that the root  $\chi = 0$  is built into this equation for all values of  $m$  due to the boundary condition at the crown. To locate the nodal circles for the one strictly inextensional mode for each value of  $m$  requires a solution of the equation for that  $m$  value. It is easy to see that no further solutions occur for  $m = 0$  or 1, simply by remembering that  $0 \leq \chi \leq \pi/2$ . In that range  $\sin(2\chi) > 0$  so equation 4 can only have solutions if  $\tan(m\chi) < 0$ , which can never be the case for  $m = 0$  or 1.

#### 5. ASYMPTOTIC SOLUTION

As the eccentricity of the hyperbola increases so the model bell approaches a right circular cylinder. As  $e \rightarrow \infty$  and/or  $m \rightarrow \infty$  the only possibility of solutions of equation 4 is for

$$\tan(m\chi) \rightarrow 0 \quad (5)$$

The limit needs to be from the negative side because  $\sin(2\chi) \geq 0$  and  $(e^2 - \cos^2 \chi) \geq 0$ . Thus

$$\chi \approx 0, \frac{\pi}{m}, \frac{2\pi}{m}, \dots \quad (6)$$

so, depending on  $m$ , there could be any number of nodal circles up to a maximum of  $m/2$  because  $\chi < \pi/2$ . If this asymptotic solution is a reasonably accurate approximation to the exact one, which we show to be the case in the next section, then a nodal circle for  $m=2$  would be ruled out because its location at  $\chi < \pi/2$  puts it at the far end of an infinitely long bell, see Table 1.

Maximum possible number of nodal circles	$m$ values
0	0, 1, 2
1	3, 4
2	5, 6
3	7, 8

Table 1. Possible  $m$  values

#### 6. EXACT SOLUTIONS

It has already been pointed out that  $\chi = 0$  is always a solution of equation 4 and that no other exists for  $m = 0$  or 1. For  $m = 2$  the equation can be rewritten as

$$\sin(2\chi) \left[ 1 + \frac{4}{\cos(2\chi)} (e^2 - \cos^2 \chi) \right] = 0 \quad (7)$$

Thus either  $\sin(2\chi) = 0$  (8)

or  $4e^2 - 1 - 2\cos^2 \chi = 0$  (9)

The latter condition can never be satisfied because  $e > 1$  so the only solutions are  $\chi = 0$ , as expected, and  $\chi = \pi/2$  which is of no practical significance.

Putting  $m = 3$  into equation 4, expanding the multiple angle terms, cancelling  $\sin\chi$  throughout, rewriting the remaining terms in powers of  $\cos\chi$  and collecting them up yields a quadratic equation in  $\cos^2\chi$  :

$$8\cos^4 \chi - 12e^2 \cos^2 \chi + 3e^2 = 0 \quad (10)$$

whose roots can be written

$$\cos^2 \chi = \frac{3}{4}e^2 \left[ 1 \pm \sqrt{1 - \frac{2}{3e^2}} \right] \quad (11)$$

where the upper root is unphysical, leading to  $\cos^2\chi > 1$  as  $e > 1$ . The values of  $\chi$  for the lower root as  $e$  varies are given in Table 2 from which it will be seen that it approaches the asymptotic value of  $60^\circ$  very rapidly as  $e$  increases. When  $e = 2$ , a typical value for church and handbells, the exact value is already less than  $1^\circ$  away. The reason for this is easier to see if one uses the Binomial theorem to expand the square root in equation 11 and then collects terms to give

$$\cos^2 \chi = \frac{1}{4} + \frac{1}{24e^2} + \frac{1}{72e^4} + O\left(\frac{1}{e^6}\right) \quad (12)$$

where the leading term is just the asymptotic value.

If one proceeds in a similar fashion for  $m = 4$  one obtains a different quadratic in  $\cos^2\chi$  whose roots are given by

$$\cos^2 \chi = \frac{1}{6}(4e^2 + 1) \pm \frac{1}{12}\sqrt{64e^4 - 64e^2 + 10} \quad (13)$$

Again the upper root is unphysical and values of  $\chi$  for the lower root are listed in Table 2. As expected the asymptotic value is reached even more quickly and the  $e = 2$  value is now to within half a degree of it.

Because the exact roots of equation 4 are expected to get ever closer to the asymptotic values as  $m$  increases, and it is already so good for  $m = 4$  there may be little point in bothering with it. However we decided to check this for the next two values of  $m$  because they are expected to give two physical roots. Proceeding as before one now obtains cubic equations in  $\cos^2\chi$  which can be solved exactly using Cardin's formula. In each case the three roots were all real but only two were physical. Their algebraic

forms not being very enlightening we limit ourselves to including their values in Table 2.

m→ e↓	3	4	5		6	
1.1	56.83	42.35	33.99	71.38	28.49	59.26
1.5	58.57	43.97	35.32	71.68	29.54	59.65
2.0	59.25	44.49	35.68	71.83	29.79	59.82
5.0	59.89	44.93	35.96	71.97	29.97	59.97
limit	60.00	45.00	36.00	72.00	30.00	60.00

Table 2. Exact solutions in degrees to Rayleigh's equation for a range of values of  $m$  and of eccentricity.

## 7. HYPERBOLIC FITS TO BELL PROFILES

It is well known that both inner and outer profiles of most modern bells are based on either elliptical arcs, circular arcs, or both [3]. Since such curves can never be fitted by a single hyperbola it is tempting to dismiss Rayleigh's model on that basis [4]. However it is not these profiles which are important here but rather that of the neutral bell, which is better approximated by their average. We have therefore tried fitting hyperbolae to the average profiles of two very different modern bells whose details we had previously measured with some accuracy [5,6]. These were a Malmark C5 handbell and a Taylor D5 church bell. The parameters to be fitted were the usual hyperbola parameters  $a$  and  $b$  plus the origin of co-ordinates for the hyperbola as seen from the co-ordinate system for the empirical measurements. The latter were expected to be small and it proved possible to set the  $x$  co-ordinate of the origin to zero. The fitting routine required us to input analytical forms for both the fitting curve and its partial derivatives with respect to the parameters. The results are shown in Figures 2 and 3 from which it can be seen that, in the case of the handbell, the fit is quite good, apart from the region close to the rim. The optimum fit eccentricity was 2.33. When the two points closest to the rim were excluded from the fit this increased to 2.50. In the case of the church bell the fit was worse and had an eccentricity of 1.96. When the three points nearest to the rim were removed the fit improved markedly and the eccentricity went up to 2.19.

## 8. CIRCLE LOCATIONS

### 8.1 The handbell

In Figure 2 we show the hyperbola of best fit to the handbell with lines of fixed  $\chi$  drawn corresponding to asymptotic solutions of Rayleigh's model for various values of  $m$ . From the points where these cut the  $z$ -axis one can see by inspection where nodal circles are predicted. Since the 60 degree line cuts



the axis beyond the bell's rim there should be no nodal circle for  $m = 3$ . There should however be one for  $m = 4$  about a quarter of the way up the bell. This is in good agreement with experiment. However, while Rayleigh's model predicts that this circle should get ever closer to the crown as  $m$  increases, experiment shows that it reaches a limiting point about half way up [5, 6]. When  $m = 8$  is reached Rayleigh is predicting two nodal circles at  $\chi = 22.5^\circ$  and  $45^\circ$  degrees. There is no evidence for a second circle arising in practice.

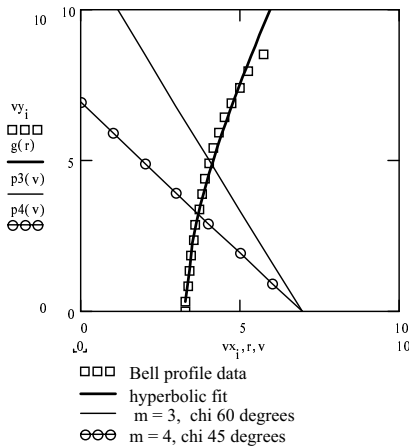


Figure 2: Best fit and theory predictions for a handbell

## 8.2 The church bell

In Figure 3 we show the corresponding diagram for the church bell. Again no circles are predicted for  $m = 2$  or 3 but one is for higher  $m$  values until a second circle is also predicted at  $m = 8$ . This is in contrast to experiment where one finds that  $m = 2$  is the only mode with no circles. There is always a circle for  $m = 3$  and for higher  $m$  values. As with the handbell, experiment shows that the one circle moves to a limiting position near the waist of the bell as  $m$  increases. It never approaches the shoulder.

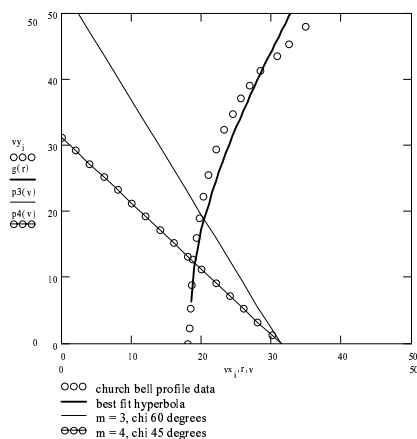


Figure 3: Best fit and theory predictions for a church bell.

## 9. DISCUSSION

Handbells are certainly thin axisymmetric shells and they do not deviate badly from a hyperbolic shape. The correct prediction of zero or one circle for  $m$  values up to 7 is impressive but the failure to predict the correct location of this circle, as  $m$  increases, is a problem as is the prediction of extra circles at higher  $m$  values.. It appears this must be due to the incorrect treatment of the crown. Bells' modal functions do not just disappear at the shoulder but fall to zero at the center of the crown in evanescent fashion [5,7]. An incorrect boundary condition thus seems likely to be to blame but there is no obvious way of correcting it. Exactly the same is true of the church bell but there the situation is worse because the hyperbolic fit is worse and the thickness of the wall varies much more. The failure to predict a circle for the case of  $m = 3$  is a real problem.

## 10. CONCLUSIONS

Rayleigh's model fails when one looks at its predictions in detail but it remains of value for two main reasons. Firstly it does give a qualitative explanation of why all concave bells have (2,0) modes and why, as  $m$  becomes larger, a point is reached where the otherwise expected (m,0) mode is replaced by a second (m,1). Secondly the fact that it predicts only one mode for each  $m$  emphasises the point that the first mode for each  $m$  is strictly inextensional and so differs in a basic way from all the other "inextensional" modes. In addition to this the model remains a remarkable example of Rayleigh's sheer inventive genius. After more than a century a better analytical approach to the bell has yet to be produced.

## 11. REFERENCES

- [1] Strutt J. W. (Lord Rayleigh), "On Bells", Philos. Mag., Vol.29, 1890, pp. 1-17.
- [2] Perrin R. and Charnley T., "Group Theory and the Bell", J. Sound Vib., Vol. 31, 1973, pp. 411-418.
- [3] Rossing T. D. and Perrin R., "Vibrations of Bells", App. Acoust., Vol 20, 1987, pp. 41-70.
- [4] Perrin R., Charnley T., Samson J. and Gottlieb H. P. W., "The Campanoid: an Equation for the Church Bell Profile", J. Sound Vib., Vol. 151, 1991, pp. 163-167.
- [5] Perrin R., Charnley T. and dePont J., "Normal Modes of the Modern English Church Bell", J. Sound Vib., Vol. 90, 1983, pp. 29-49.
- [6] Rossing T. D., Perrin R., Sathoff H.J. and Peterson R.W., "Vibrational Modes of a Tuned Handbell", J. Acoust. Soc. Am., Vol. 76, 1984, pp. 1263-1267.
- [7] Perrin R. and Gottlieb H. P. W., "Evanescent and Bessel Functions in the Vibrating Circular Membrane", Eur. J. Phys., Vol. 15, pp. 293-299.

## **THE HANG: A HAND-PLAYED STEEL DRUM**

*Thomas D. Rossing*

Department of Physics, Northern Illinois University, DeKalb, IL 60115 USA  
rossing@physics.niu.edu

*Uwe J. Hansen*

Department of Physics, Indiana State University, Terre Haute, IN 60115 USA  
u-hansen@indstate.edu

*Felix Rohner and Sabina Schärer*

PANART, Engenhaldenstrasse 131, CH-3012 Bern, Switzerland  
info@hang.ch

### **ABSTRACT**

The HANG is a new steel percussion instrument, consisting of two spherical shells of steel, suitable for playing with the hands. Seven to nine notes are harmonically tuned around a central deep note which is formed by the Helmholtz (cavity) resonance of the instrument body. By means of holographic interferometry we have studied the modes of vibration in a HANG developed by PanArt, Switzerland.

### **1. INTRODUCTION**



Figure 1: *The HANG.*

The Caribbean steelpan is probably the most important new acoustical instrument to develop in the 20<sup>th</sup> century. Since its invention in Trinidad some 50 years ago, improvements in the technology and design have resulted

from research in Europe and the United States in addition to its home country of Trinidad and Tobago [1]. It has also inspired the development of new steel instruments, such as the PANG family of instruments and the hand-played HANG.

The HANG, shown in Figure 1, has nine notes which can be tuned in any tonal system between A3 and G5, including 30 tonal systems suggested by the tuners. The central note is usually tuned a fifth or a fourth below the lowest note of the scale. In this paper we discuss the acoustics of the HANG with special attention to the way in which it vibrates and produces sound.

### **2. HOLOGRAPHIC INTERFEROMETRY**

A hologram is a two-dimensional recording capable of producing a three-dimensional image. It does that by recording the whole wave field, including both the phase and magnitude of the light waves reflected from an object. The phase information is generally converted into intensity information by using a reference beam of coherent light.

In addition to the primary fringes that appear in all holograms due to interference between the object and reference beams, secondary fringes may appear if the object has moved during the exposure. These secondary fringes are widely used to study stress, motion, and vibration. In the experiments to be described, they provide a sort of contour map that indicates how much point has moved between its extremes of deflection, and therefore its amplitude of vibration.

Although holograms recorded on film generally have the highest possible resolution, the use of film is somewhat time consuming. It is much more convenient to create the holographic images electronically, so that they can be viewed as soon as they are created. TV

holography or electronic speckle pattern interferometry allows real-time fringes to be presented on a TV monitor without photographic processing. Our system for TV holography has already been described [2].

### 3. MODES OF VIBRATION

The first five modes of vibration in the G3 note area of the HANG are shown in Figure 2. In the fundamental (0,1) mode, the entire note area moves in a single phase. Next are a pair of (1,1) modes with a nodal line crossing the center of the note area, while a pair of (2,1) modes have two nodal lines across the note. The two (1,1) modes are tuned to two and three times the frequencies of the (0,1) mode.

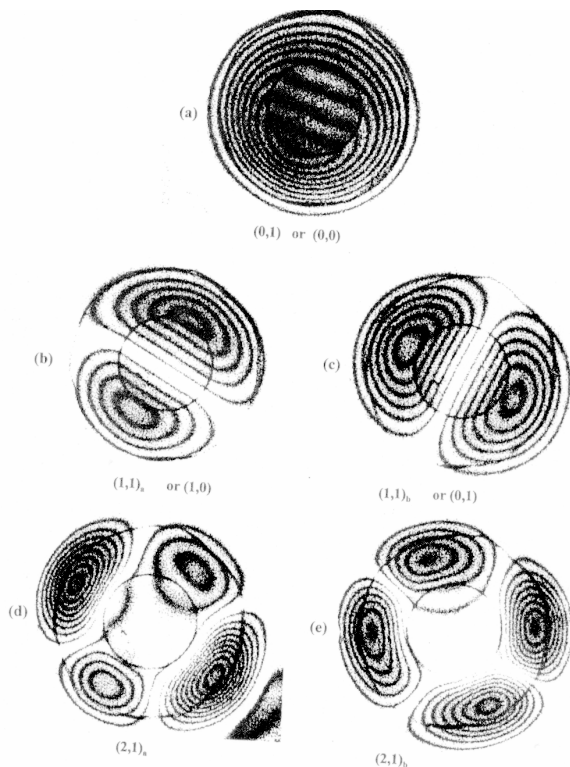


Figure 2: Modes of vibration in the G3 note area.  
(a) (0,1) 189 Hz; (b) (1,1)<sub>a</sub> 390 Hz; (c) (1,1)<sub>b</sub> 593 Hz;  
(d) (2,1)<sub>a</sub> 1418 Hz; (e) (2,1)<sub>b</sub> 1543 Hz.

Similar modes are seen in the E4 note area in Figure 3. If we model the modes as those of a circular plate with a fixed edge, we would logically denote them as (0,0), (1,1)<sub>a</sub>, (1,1)<sub>b</sub>, (2,1)<sub>a</sub> and (2,1)<sub>b</sub>. In this notation, the two numbers give the numbers of nodal circles and nodal diameters, respectively. However, if we use the notation of a rectangular plate with fixed edges, these modes would be called the (0,0), (1,0), (0,1), (1,1)<sub>a</sub> and (1,1)<sub>b</sub> modes. The latter notation, which gives the number of nodes parallel to the two dimensions of the rectangle, is often applied to elliptical plates as well. The note areas of the HANG are actually elliptical, although their eccentricity is small.

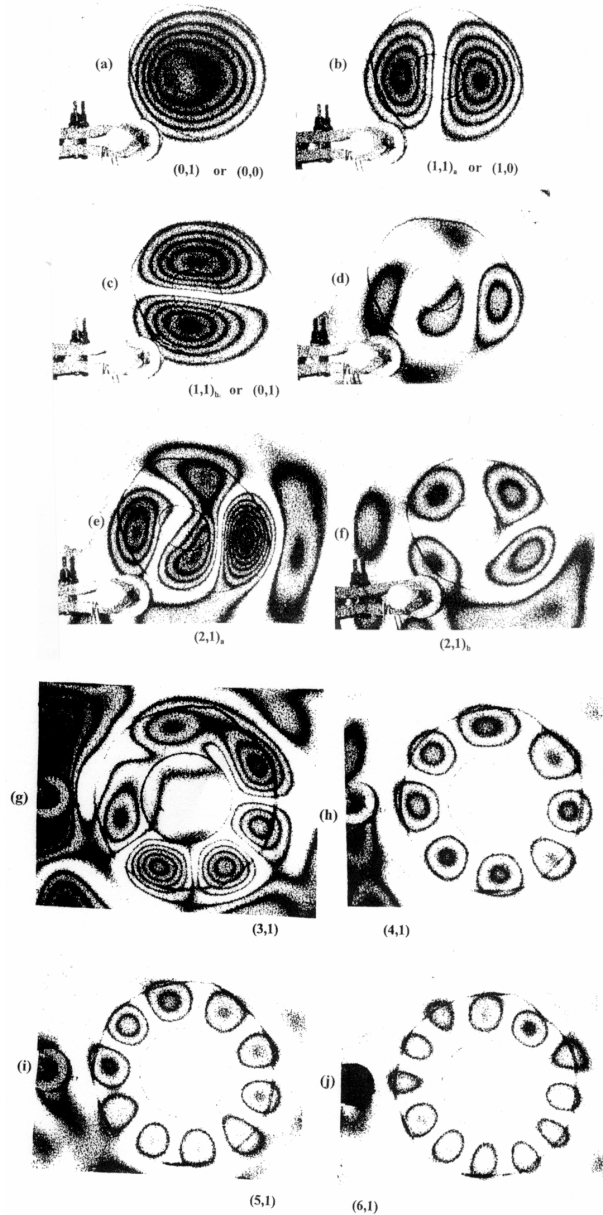


Figure 3: Modes of vibration in the E4 note area  
(a) (0,1) 330 Hz; (b) (1,1)<sub>a</sub> 661 Hz; (c) (1,1)<sub>b</sub> 976 Hz;  
(d) 2110 Hz; (e) (2,1)<sub>a</sub> 2138 Hz; (f) (2,1)<sub>b</sub> 2376 Hz;  
(g) (3,1) 2297 Hz; (h) (4,1) 2618 Hz; (i) (5,1) 3257 Hz;  
(j) (6,1) 3982 Hz.

At higher frequencies, the circular plate notation makes more sense, as shown in Figure 3 g-j, for the higher modes consist of standing waves that appear to propagate parallel to the circumference of the note area.

Figure 4 shows some vibrational modes of the back or lower hemisphere. At 181 Hz, the body flexes, but this mode radiates inefficiently. At 879 Hz mainly the area around the sound hole vibrates, while at higher frequencies, standing waves are observed in a band around the sound hole as well, as seen in Figure 4.

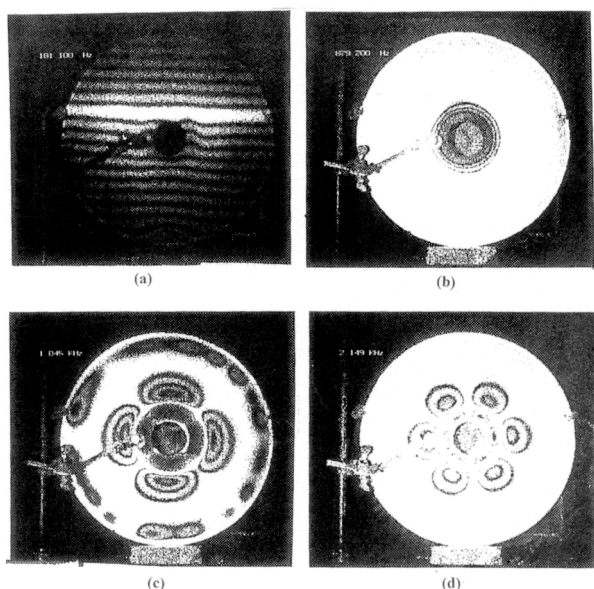


Figure 4: Some vibrational modes of the back.  
(a) 181 Hz; (b) 879 Hz; (c) 1845 Hz; (d) 2149 Hz. The fundamental mode at 87 Hz, which has no nodal lines except at the edge, is not shown.

#### 4. SOUND OF THE HANG

Sound spectra are shown in Figure 5. The HANG was struck with the fleshy part of the hand (upper spectrum) and with the finger tips (lower spectrum) on the central dome. The fundamental at 87 Hz (F2) is clearly seen in both spectra. In the lower spectrum a prominent peak appears at 395 Hz (G4) as well. The fundamental can be tuned from about B1 (62 Hz) to F2 (87 Hz) or higher by changing the spacing between the player's knees.

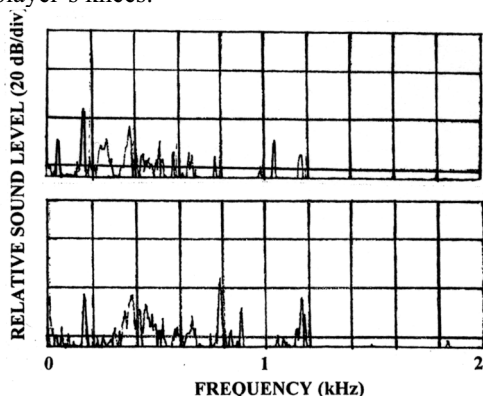


Figure 5: Sound spectra of the HANG.  
In the upper spectrum it was struck with the fleshy part of the hand, while in the lower spectrum it was struck with the finger tips on the central dome. The fundamental at 87 Hz is seen clearly in both spectra.

Recorded examples of the HANG can be heard at  
<<http://www.larkinam.com/MenComNet/Business/Retail/LarkNet/SteelDrums>> .

#### 5. CONCLUSION

The HANG is a new steel percussion instrument suitable for playing with the hands. Each of the nine notes has a fundamental mode of vibration plus two modes with one nodal diameter that are tuned to the octave and the twelfth (two and three times the fundamental frequency). The central note is generally tuned a fifth or a fourth below the lowest note of the scale. Striking the central note also excites a deep sound that can be controlled by positioning the knees.

The modes of vibration can be accurately observed by means of TV holographic interferometry.

#### 6. REFERENCES

- [1] Rossing, T. D., Science of Percussion Instruments, World Scientific, Singapore, 2000. Chapter 10.
- [2] Rossing, T. D., Hansen, U. J., and Hampton, D. S., "Vibrational mode shapes in Caribbean steel pans. I. Tenor and double second, J. Acoust. Soc. Am. 108, 803-812, 2000.



## **VIBRATIONAL MODES OF FIVE-OCTAVE CONCERT MARIMBAS**

*Junehee Yoo and Thomas D. Rossing*

Department of Physics, Northern Illinois University, DeKalb, IL 60115, USA  
yoo@physics.niu.edu, rossing@physics.niu.edu

*Barry Larkin*

Department of Music, Iowa State University, Ames, IA 50014, USA  
blarkin@iastate.edu

### **ABSTRACT**

We compare the bending mode frequencies in two five-octave concert marimbas, one by Yamaha and one by Mallettech. In both instruments, the second mode is accurately tuned to the 4<sup>th</sup> harmonic in the first 3½ octaves, after which the interval decreases. Similarly, the third bending mode is tuned to the 10<sup>th</sup> harmonic in the first 2 octaves, after which the interval decreases. The fourth mode in both instruments varies from the 20<sup>th</sup> harmonic in the lowest bars to about the 6<sup>th</sup> harmonic in the highest bars.

Four to five torsional modes observed in the Mallettech marimba have frequencies interspersed with the bending modes. The lowest torsional mode lies between the two lowest bending modes, while the second torsional mode lies between the second and third bending modes. Coupling between bending and torsional modes is discussed.

### **1. INTRODUCTION**

The term marimba has different meanings in different musical cultures. In eastern and southern Africa it denotes a group of idiophones, some of which are struck and some of which are plucked. In most parts of the World, the term is used to denote the deep-toned orchestral marimba with tuned bars and resonator tubes that evolved from the early Latin American instrument. Beneath each bar is a closed pipe resonator tuned to the fundamental frequency of that bar. A deep arch on the underside of marimba bars allows tuning of the overtones; the first overtone is nominally tuned two octaves above the fundamental [1,2].

### **2. THE MARIMBAS**

Two 5-octave marimbas were used in this study. One was made by Mallettech (see Figure 1) and one by Yamaha. Both have rosewood bars with closed-tube resonators. They are typical of modern marimbas that have large bass bars for concert use over the full 5-octave range.

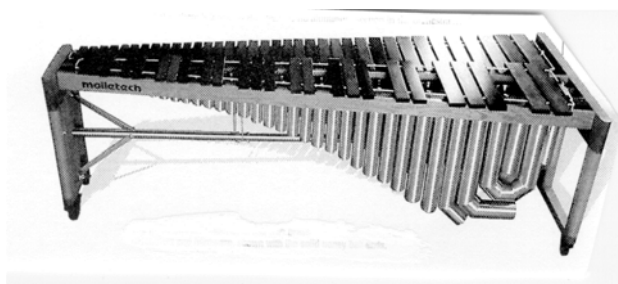


Figure 1: *Mallettech 5-octave concert marimba.*

### **3. MODAL ANALYSIS**

The bars were driven with sinusoidal force by attaching a small magnet to one corner of the bar and applying a sinusoidal magnetic field by means of a coil driven by an audio oscillator and amplifier. Modal shapes were detected by moving a small microphone along the surface of the bar to sample the sound field nearby [3]. For some of the more difficult modes, modal identification was enhanced by using a small accelerometer.

### **4. MODES OF VIBRATION**

#### **4.1. Bending modes**

Relative mode frequencies for the first 4 bending modes in the Mallettech marimba are shown in Figure 2. Frequency ratios are given with respect to the nominal bar frequency, which is always quite close to the measured frequency for the fundamental.

The second bending mode is tuned to four times the nominal frequency in the bars up to D5, after which the ratio slowly decreases to a minimum of about 2.5. Likewise, the third bending mode is tuned to about 10.2 times the nominal frequency up to C4, after which the ratio decreases to less than 5 in the highest bars. The fourth bending mode ranges from 19 times the nominal (fundamental) frequency in the largest bar to 6.1 times the nominal frequency in the next to smallest.

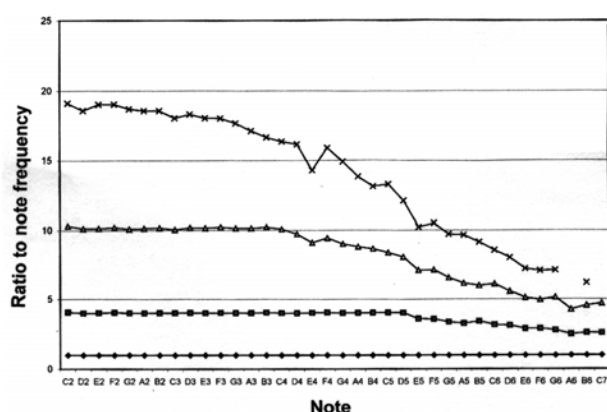


Figure 2: Relative frequencies of the first 4 bending modes in the Malletech marimba. Frequency ratios are given with respect to the nominal bar frequencies.

The second bending mode is tuned to four times the nominal frequency in the bars up to D5, after which the ratio slowly decreases to a minimum of about 2.5. Likewise, the third bending mode is tuned to about 10.2 times the nominal frequency up to C4, after which the ratio decreases to less than 5 in the highest bars. The fourth bending mode ranges from 19 times the nominal (fundamental) frequency in the largest bar to 6.1 times the nominal frequency in the next to smallest.

Relative mode frequencies for the first 4 bending modes in the Yamaha marimba are shown in Figure 3. Frequency ratios are given respect to the nominal bar frequency, which is always quite close to the measured frequency for the fundamental.

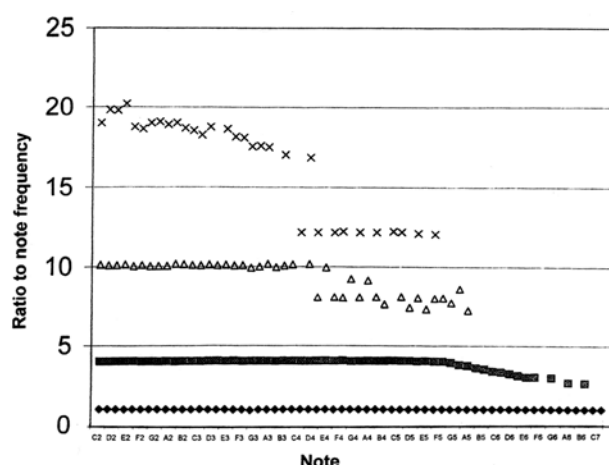


Figure 3: Relative frequencies of the first 4 bending modes in the Yamaha marimba. Frequency ratios are given with respect to the nominal bar frequencies.

The second bending mode is tuned to four times the nominal frequency in the bars up to F5, after which the ratio slowly decreases to a minimum of about 2.6. Likewise, the third bending mode is tuned to about 10.1 times the nominal frequency up to C#4, after which the ratio decreases to about 7 in the highest bars measured. The fourth bending mode ranges

from 19 times the nominal in the largest bar to about 12 in the E5 bar (smaller bars were not measured).

## 4.2. Torsional modes

Torsional mode frequencies for the first five torsional modes in the Malletech bars are shown in Figure 4. Frequency ratios are given respect to the first bending mode frequency, which is always quite close to the nominal bar frequency.

The first torsional mode frequency ranges from about 1.9 times the nominal frequency (largest bars) to about 1.2 times the nominal frequency (smallest bars). The second torsional mode frequency ranges from about 9.4 times the nominal frequency (F3 bar) to 3.9 times the nominal frequency (C7 bar). In the largest bars the ratio is in the range of 8 to 9.

The higher torsional modes (third to fifth) have frequency ratios to the fundamental that vary with bar size, but generally decrease from large to small bars, as shown in Figure 4.

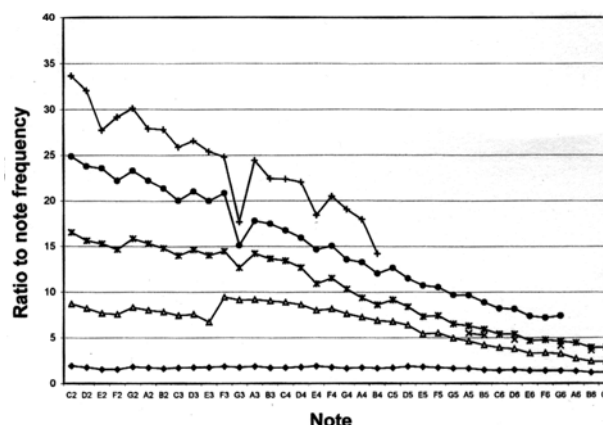


Figure 4: Torsional mode frequencies in the Malletech marimba. Frequency ratios are given with respect to the nominal bar frequencies.

## 5. DISCUSSION

Bork and Meyer [4] investigated the tuning of the third partial (bending mode) to various ratios to the fundamental. They compared synthesized bar sounds in which the third partial was tuned to the following six musical intervals above the third octave: major second, major second +50 cents, minor third, minor third +50 cents, major third, and major third +50 cents. They found a preference for the fourth choice, where the third partial is tuned midway between a major and minor third above the triple octave (i.e., a ratio of 9.88 to the nominal frequency). is in the range of 8 to 9.

In the Malletech marimba, the third partial is tuned about a major third plus 17 cents more than a triple octave above the fundamental, and in the Yamaha marimbas, the third partial is tuned about a major third plus 34 cents more than a triple octave (frequency ratios of 10.1 and 10.2, respectively).

Do torsional modes of vibration contribute much to the timbre of marimba bars? The large bars on these marimbas are quite wide, and thus the torsional modes can radiate an

appreciable amount of sound. In normal playing, the bars are struck near their centers, where the torsional modes have nodes, and thus they will not be excited to any great extent. On the other hand, if the bars are struck away from the center, deliberately or not, the torsional modes could contribute to the timbre.

The first torsional mode, in the larger bars, is between a fifth and an octave above the nominal frequency. A bar would be expected to have a brighter timbre if struck away from the center axis so as to enhance the torsional modes, an effect that some players have noted.

## **6. CONCLUSIONS**

Large 5-octave marimbas, which are becoming increasingly popular with percussionists, have large bars that radiate sound with a large number of partials, due to bending and torsional modes of vibration. In addition to tuning the second partial two octaves above the nominal frequency in all but the smallest bars, marimba tuners appear to tune the third partial in the larger bars to a little more than a major third above the nominal.

Torsional modes of vibration radiate less efficiently than bending modes, but nevertheless they influence the timbre of the lower notes by radiating inharmonic partials when the bar is struck away from the center axis.

## **7. REFERENCES**

- [1] Rossing, T. D., *Science of Percussion Instruments*, World Scientific, Singapore, 2000.
- [2] Fletcher, N. H. and Rossing, T. D., *Physics of Musical Instruments* 2<sup>nd</sup> ed, Springer-Verlag, New York, 1998.
- [3] Rossing, T. D. and Russell, D. A., "Laboratory observation of elastic waves in solids," *American J. Physics* 58, 1153-1162 (1990).
- [4] Bork, I. and Meyer, J., "Zur klanglichen Bewertung von Xylophonen," *Das Musikinstrument* 31(8), 1076, 1982. (English translation in *Percussive Notes* 23(6), 48, 1985).





# PHYSICS-BASED MODELLING



## PHYSICS-BASED MODELING OF MUSICAL INSTRUMENTS

*Vesa Välimäki*

Helsinki University of Technology, Laboratory of Acoustics and Audio Signal Processing  
P.O. Box 3000, FIN-02015 HUT, Espoo, Finland  
vesa.valimaki@hut.fi

### ABSTRACT

Physical models are being developed for musical instruments for two main purposes: research of acoustical properties and sound synthesis. This paper presents an overview of physical modeling of musical instruments. It also proposes a classification of physics-based methods. These include the source-filter, the finite-difference, the mass-spring, the wave digital, the modal, and the digital waveguide models. The methods are closely related to digital signal processing. Current trends and future directions in physical modeling of musical instruments are discussed.

### 1. INTRODUCTION

This paper presents an overview of physics-based modeling of musical instruments. A specific focus of the paper is on sound synthesis methods derived using the physical modeling approach. While first experiments on physics-based sound synthesis were documented 30 year ago, the first products – those by Yamaha – were introduced about 10 years ago. The research in the field has been very active during the last years. An overview of various approaches to physical modeling is given. Finally, current trends and possible future developments will be discussed.

### 2. PHYSICAL MODELING APPROACHES

The physical modeling approaches can be classified into six categories.

1. Source-filter models
2. Finite-difference methods
3. Mass-spring networks
4. Wave digital filters
5. Modal synthesis
6. Digital waveguide modeling

A brief overview of each approach follows.

#### 2.1. Source-Filter Methods

Source-filter methods are a class of signal processing structures that have been extensively used for sound synthesis. A source-filter model is a system where a source signal, typically a spectrally rich periodic waveform, is filtered with a time-varying filter that can be controlled with parameters. While this idea is not necessarily related to physical modeling at all, there are examples of synthesis methods where the source or the filter or both have a clear physical interpretation.

A classical example is a voice-production model for speech and singing synthesis, where the source signal represents the glottal waveform—related to the vibration of the vocal folds—

and the filter has the spectral properties of the vocal tract [1], [2]. The source-filter model was the underlying principle in early analog synthesizers. Recently, this approach has experienced a revival in virtual analog synthesis, which refers to the digital imitation of aged synthesizer sounds.

#### 2.2. Finite-Difference Methods

The finite-difference schemes can be used for solving partial difference equations, such as those describing the vibration of a string, a membrane, or an air column inside a tube. An early example of this approach in physical modeling of musical instruments is the work done by Hiller and Ruiz in early 1970s [3]. This line of research has been continued and extended by Chaigne and others (see, e.g., [4], [5]).

The finite-difference approach leads to a simulation algorithm that is based on a difference equation, which can be programmed with a computer. One advantage is that the parameters are physical variables, which can be varied to learn about the system. Sound synthesis is possible, since the time-domain signal can be observed at one or several points in the system and then converted to an audio signal. Also interaction at any discrete point or many points along the spatial dimension is allowed.

#### 2.3. Mass-Spring Networks

This principle was introduced for musical instrument modeling by Cadoz and his colleagues who developed a system that is based on a computer simulation of mass-spring networks [6]. For example, a vibrating string can be simulated as a mass-spring network by dividing the string into small segments, all of which have a finite mass and elasticity. This yields a network of lumped elements, which together approximate the behavior of the string, which is a distributed system. Using mechanical to electrical analogies and then digitizing these gives a digital system.

#### 2.4. Wave Digital Filters

The background of wave digital filters is in the conversion of analog electronic filters into digital filters, for which Fettweis developed a general theory in the 1970s [7]. In physical modeling of musical instruments, one must first build a mechanical model for the part of the instrument of interest, then convert that to an electrical circuit using certain well known analogies (e.g., mass corresponds to electrical inductance). Finally, the electrical circuit can be discretized, which is usually done using the bilinear transform. This class of models can be seen to be related to mass-spring networks, but there are certain differences, such as the fact that wave digital models typically represent a lumped system, while mass-spring models may

restore the spatial dimension or the distributed nature of the system. Models based on wave digital filters are sometimes used for the excitation part of musical instrument models [8], but are also applicable to the distributed resonator part, such as a woodwind instrument bore [9]. Recently, Sarti and his colleagues have worked on nonlinear, modular wave digital systems [10].

### 2.5. Modal Synthesis

Modal synthesis describes a linear system in terms of its modes of vibration. An early application of this method to modeling of musical instruments and sound synthesis was done by Adrian at IRCAM [11]. In his work, each vibrating mode has a resonance frequency, damping factor, and physical shape specified on a discrete grid. The synthesis is strongly related to vibration measurements of a specific structure or instrument, and this is where the modal data is obtained in the first place.

Cook has extended the idea of modal synthesis to parametric synthesis of percussive sounds [12]. Based on parametric spectral analysis, the method derives a resonator bank and an excitation signal for it. Analysis of several types of excitation allows parametrizing the strike position and style, which can then be used for real-time control.

A novel technique related to modal synthesis is called functional transformation method [13], [14], which also describes a linear system in terms of its modes, but allows deriving accurate models directly based on physics, just as can be done with finite-difference models. The main novelty in functional transformation modeling is to use two different integral transformations (Laplace and Sturm-Liouville) to remove partial derivatives. One of the transformations operates on the temporal and the other on the spatial terms of the partial differential equation.

### 2.6. Digital Waveguide Modeling

Digital waveguide modeling is based on the traveling wave decomposition of vibration in linear structures. In strings, the vibration can be described as a sum of two waveforms traveling in opposite directions. The simulation of this phenomenon with a computer is easy and requires very little operations per sample, since sampled signals are moving in digital delay lines. Losses and dispersion are incorporated using digital lowpass and allpass filters, respectively [15]. Accurate length of the delay lines must be adjusted using interpolation techniques, which are commonly called fractional delay filters [15], [16]. Techniques similar to certain digital waveguide models were proposed in early papers by Kelly and Lochbaum in the context of vocal-tract modeling [17] and more recently by McIntyre, Schumacher, and Woodhouse [18] and by Karplus and Strong [19]. J. O. Smith introduced the term 'digital waveguide' in mid-1980s and developed the general theory [20], [21]. Digital waveguide principles are commonly used in the modeling of the linear resonator part of musical instruments, such as strings [22] and tubes [23].

One advantage of digital waveguide models is that there are methods for calibrating the model parameters based on recorded musical tones [24], [22]. The waveguide approach can also be extended to two and three dimensions to model drums and other multi-dimensional musical systems [25], [26], and [27].

## 3. RECENT TRENDS

Next we look at some current trends in physical modeling. Around mid-1990s, the research reached the point, where most Western orchestral instruments could be synthesized based on a physical model. More recently, many papers have been published on the modeling of ethnic musical instruments. These include, for example, the Turkish tanbur [28], the Ouldémé flute [29], the Tibetan praying bowl [30], and the Finnish kantele [31], among others. We have also recently seen applications of physical modeling techniques to non-musical sound sources. Examples are physical modeling of bird song [32], various everyday sounds, such as those generated by footsteps [33] and beach balls [34], and friction models that can be applied in many cases [35].

Also, combining different physical modeling approaches is becoming an interesting topic. The motivation for this may be the idea of combining the good features of two approaches in a single model [36] or the need to interconnect models that have been designed using different approaches, such as the digital waveguide and the wave digital or the finite difference methods [8], [10], [37].

Another new direction is the subjective evaluation of perceptual features and parameter changes in physics-based synthesis, see, [38], [39], [40], and [41]. This line of research provides musically relevant information on the relations of timbre and the properties of human hearing. These results help in reducing the complexity of synthesis models, because details that are not audible need not be modeled.

The first attempts on audio restoration based on physical models were conducted recently [42]. While this can be successful for single tones, the practical application of such methods for recordings including a mix of several instruments is a challenge for future research. The main problem is high-quality source separation, which is required before this kind of restoration process.

The concept of Structured Audio introduced as part of the MPEG-4 international multimedia standard has opened a new application field for physical models [43]: parametric coding of music, where a program for sound generation of the instruments and control data for playing the instrument are transmitted.

## 4. CONCLUSIONS

Physical modeling of musical instruments has become one of the most active fields of musical acoustics research. There are several approaches to develop a computational model for any given instrument. These approaches were briefly overviewed. The digital waveguide method, together with its variations, is currently the most popular modeling technique, because it leads to computationally efficient algorithms that enable real-time synthesis of many simultaneous voices.

Some current research trends were listed. It can be predicted that in the near future in addition to synthesizing new musical instruments, the physical modeling techniques will be applied to numerous everyday sound sources. This research topic has become popular only a few years ago. Non-musical sounds are of interest because they can be used in human-computer interfaces, in computer games, in sound effects for films and animations, and in virtual reality applications.

## 5. ACKNOWLEDGMENTS

The author would like to thank Dr. Cumhur Erkut, Prof. Matti Karjalainen, and Prof. Augusto Sarti for helpful discussions.

## 6. REFERENCES

- [1] X. Rodet, Y. Potard, and J.-B. Barrière, "The CHANT project: from the synthesis of the singing voice to synthesis in general," *Computer Music J.*, vol. 8, no. 3, pp. 15–31, 1984.
- [2] J. Sundberg, "Synthesizing singing," in *Representations of Musical Signals*. G. De Poli, A. Piccialli, and C. Roads, Eds. MIT Press, Cambridge, MA, 1991, pp. 299–320.
- [3] L. Hiller and P. Ruiz, "Synthesizing musical sounds by solving the wave equation for vibrating objects: Parts I and II," *J. Audio Eng. Soc.*, vol. 19, no. 6, pp. 462–470 and no. 7, pp. 542–550, 1971.
- [4] A. Chaigne and A. Askenfelt, "Numerical simulations of piano strings I: A physical model for a struck string using finite difference methods," *J. Acoust. Soc. Am.*, vol. 95, no. 2, pp. 1112–1118, 1994.
- [5] A. Chaigne and V. Doutaut, "Numerical simulations of xylophones. I. Time-domain modeling of the vibrating bars," *J. Acoust. Soc. Am.*, vol. 101, no. 1, pp. 539–557, 1997.
- [6] J.-L. Florens and C. Cadoz, "The physical model: modeling and simulating the instruments universe," in *Representations of Musical Signals*. G. De Poli, A. Piccialli, and C. Roads, Eds. MIT Press, Cambridge, MA, 1991, pp. 227–268.
- [7] A. Fettweis, "Wave digital filters: theory and practice," *Proc. IEEE*, vol. 74, no. 2, pp. 270–327, 1986.
- [8] S. A. Van Duyne, J. R. Pierce, and J. O. Smith, "Traveling wave implementation of a lossless mode-coupling filter and the wave digital hammer," in *Proc. Int. Computer Music Conf.*, Aarhus, Denmark, pp. 411–418, 1994.
- [9] M. van Walstijn and M. Campbell, "Discrete-time modeling of woodwind instrument bores using wave variables," *J. Acoust. Soc. Am.*, vol. 113, no. 1, pp. 575–585, Jan. 2003.
- [10] A. Pedersini, A. Sarti, and S. Tubaro, "Object-based sound synthesis for virtual environments using musical acoustics," *IEEE Signal Process. Mag.*, vol. 17, no. 6, pp. 37–51, Nov. 2000.
- [11] J.-M. Adrien, "The missing link: modal synthesis," in *Representations of Musical Signals*. G. De Poli, A. Piccialli, and C. Roads, Eds. MIT Press, Cambridge, MA, 1991, pp. 269–297.
- [12] P. R. Cook, "Physically informed sonic modeling (PhISM): synthesis of percussive sounds," *Computer Music Journal*, vol. 21, no. 3, pp. 38–49, 1997.
- [13] L. Trautmann and R. Rabenstein, "Digital sound synthesis based on transfer function models," in *Proc. IEEE Workshop on Applications of Signal Processing to Audio and Acoustics*, New Paltz, NY, pp. 83–86, Oct. 1999.
- [14] L. Trautmann and R. Rabenstein, *Digital Sound Synthesis by Physical Modeling using Functional Transformation Models*. Kluwer, New York, 2003.
- [15] D. A. Jaffe and J. O. Smith, "Extensions of the Karplus-Strong plucked-string algorithm," *Computer Music J.*, vol. 7, no. 2, pp. 56–69, 1983.
- [16] T. I. Laakso, V. Välimäki, M. Karjalainen, and U. K. Laine, "Splitting the unit delay—tools for fractional delay filter design," *IEEE Signal Processing Mag.*, vol. 13, no. 1, pp. 30–60, 1996.
- [17] J. L. Kelly Jr. and C. C. Lochbaum, "Speech synthesis," in *Proc. Fourth Int. Congr. Acoustics*, Copenhagen, Denmark, paper G42, pp. 1–4, Sept. 1962.
- [18] M. E. McIntyre, R. T. Schumacher, and J. Woodhouse, "On the oscillations of musical instruments," *J. Acoust. Soc. Am.*, vol. 74, no. 5, pp. 1325–1345, 1983.
- [19] K. Karplus and A. Strong, "Digital synthesis of plucked-string and drum timbres," *Computer Music J.*, vol. 7, no. 2, pp. 43–55, 1983.
- [20] J. O. Smith, "Physical modeling using digital waveguides," *Computer Music Journal*, vol. 16, no. 4, pp. 74–91, 1992. See: <http://www-ccrma.stanford.edu/~josh/pmudw/>.
- [21] J. O. Smith, "Principles of digital waveguide models of musical instruments," in *Applications of Digital Signal Processing to Audio and Acoustics*, M. Kahrs and K. Brandenburg, Eds. Kluwer, Norwell, MA, 1998, pp. 417–466.
- [22] V. Välimäki, J. Huopaniemi, M. Karjalainen, and Z. Jánosy, "Physical modeling of plucked string instruments with application to real-time sound synthesis," *J. Audio Eng. Soc.*, vol. 44, no. 5, pp. 331–353, May 1996.
- [23] F. Avanzini and D. Rocchesso, "Efficiency, accuracy, and stability issues in discrete-time simulations of single reed wind instruments," *J. Acoust. Soc. Am.*, vol. 111, no. 5, Part 1, pp. 2293–2301, May 2002.
- [24] J. O. Smith, *Techniques for Digital Filter Design and System Identification with Application to the Violin*. Ph.D. Dissertation, Stanford Univ., Stanford, CA, 1983.
- [25] S. A. Van Duyne and J. O. Smith, "Physical modeling with the 2-D digital waveguide mesh," in *Proc. Int. Computer Music Conf.*, Tokyo, Japan, pp. 40–47, 1993.
- [26] F. Fontana and D. Rocchesso, "Physical modeling of membranes for percussion instruments," *Acustica*, vol. 77 no. 3, pp. 529–542, 1998.
- [27] L. Savioja and V. Välimäki, "Reducing the dispersion error in the digital waveguide mesh using interpolation and frequency-warping techniques," *IEEE Trans. Speech and Audio Processing*, vol. 8, no. 2, pp. 184–194, Mar. 2000.
- [28] C. Erkut and V. Välimäki, "Model-based sound synthesis of tanbur, a Turkish long-necked lute," in *Proc. IEEE Int. Conf. Acoust. Speech, Signal Processing*, Istanbul, Turkey, vol. 2, pp. 769–772, June 2000.
- [29] R. de la Cuadra, C. Vergez, and R. Caussé, "Use of physical-model synthesis for developing experimental techniques in ethnomusicology – the case of the Ouldémé flute," in *Proc. Int. Computer Music Conf.*, Gothenburg, Sweden, pp. 53–56, 2002.

- [30] G. Essl and P. Cook, "Banded waveguides on circular topologies and of beating modes: Tibetan singing bowls and glass harmonicas," in *Proc. Int. Computer Music Conf.*, Gothenburg, Sweden, pp. 49–52, 2002.
- [31] C. Erkut, M. Karjalainen, P. Huang, and V. Välimäki, "Acoustical analysis and model-based sound synthesis of the kantele," *J. Acoust. Soc. Am.*, vol. 112, no. 4, pp. 1681–1691, 2002.
- [32] M. Kahrs and F. Avanzini, "Computer synthesis of bird songs and calls," in *Proc. COST-G6 Conf. Digital Audio Effects (DAFx-01)*, pp. 23–27, Limerick, Ireland, Dec. 2001. Available at <http://www.csis.ul.ie/dafx01/>
- [33] P. Cook, "Modeling Bill's gait: analysis and parametric synthesis of walking sounds," in *Proc. AES 22nd Int. Conf. Virtual, Synthetic, and Entertainment Audio*, pp. 73–78, Espoo, Finland, June 2002.
- [34] D. Rocchesso and P. Dutilleul, "Generalization of a 3-D acoustic resonator model for the simulation of spherical enclosures," *EURASIP J. Appl. Signal Processing*, vol. 1, no. 1, pp. 15–26, 2001.
- [35] F. Avanzini, S. Serafin, and D. Rocchesso, "Modeling interactions between rubbed dry surfaces using an elastoplastic friction model," in *Proc. Int. Conf. Digital Audio Effects (DAFx-02)*, pp. 111–116, Hamburg, Germany, Sept. 2002. Available at <http://www.dafx.de/>.
- [36] L. Trautmann, B. Bank, V. Välimäki, and R. Rabenstein, "Combining digital waveguide and functional transformation methods for physical modeling of musical instruments," in *Proc. AES 22nd Int. Conf. Virtual, Synthetic, and Entertainment Audio*, pp. 307–316, Espoo, Finland, June 2002.
- [37] C. Erkut and M. Karjalainen, "Finite difference method vs. digital waveguide method in string instrument modeling and synthesis," in *Proc. Int. Symp. Musical Acoustics (ISMA 2002)*, Mexico City, Mexico, Dec. 2002.
- [38] D. Rocchesso and F. Scalcon, "Bandwidth of perceived inharmonicity for physical modeling of dispersive strings," *IEEE Trans. Speech Audio Processing*, vol. 7, pp. 597–601, Sept. 1999.
- [39] S. Lakatos, P. R. Cook, and G. P. Scavone, "Selective attention to the parameters of a physically informed sonic model," *Acoustics Research Letters Online*, 2000 (published in *J. Acoust. Soc. Am.*, vol. 107, no. 5, pp. L31–L36, 2000).
- [40] H. Järveläinen, V. Välimäki, and M. Karjalainen, "Audibility of the timbral effects of inharmonicity in stringed instrument tones," *Acoustics Research Letters Online*, vol. 2, no. 3, pp. 79–84, 2001. URL: <http://ojps.aip.org/ARLO/>
- [41] H. Järveläinen and T. Tolonen, "Perceptual tolerances for decay parameters in plucked string synthesis," *J. Audio Eng. Soc.*, vol. 49, no. 11, pp. 1049–1059, Nov. 2001. Available at <http://lib.hut.fi/Diss/2003/isbn9512263149/>.
- [42] P. A. A. Esquef, V. Välimäki, and M. Karjalainen, "Restoration and enhancement of solo guitar recordings based on sound source modeling," *J. Audio Eng. Soc.*, vol. 50, no. 4, pp. 227–236, April 2002.
- [43] B. L. Vercoe, W. G. Gardner, and E. D. Scheirer, "Structured audio: creation, transmission, and rendering of parametric sound representations," *Proc. IEEE*, vol. 86, no. 5, pp. 922–940, May 1998.

## A POWER NORMALIZED NON-LINEAR LOSSY PIANO HAMMER

Julien Bensa<sup>1</sup>, Stefan Bilbao<sup>2</sup>, Richard Kronland-Martinet<sup>1</sup> and Julius O. Smith III<sup>3</sup>

<sup>1</sup> Laboratoire de Mécanique et d'Acoustique, Marseille, France

bensa, kronland@lma.cnrs-mrs.fr

<sup>2</sup> Sonic Arts Research Centre (SARC), Queen's University Belfast

s.bilbao@qub.ac.uk

<sup>3</sup> Center for Computer Research in Music and Acoustics (CCRMA) Stanford University

jos@ccrma.stanford.edu

### ABSTRACT

The interaction between a piano string and a striking hammer can be modeled as a system of coupled differential equations. As there is not, in general, an analytic solution to this system, numerical approximation techniques, such as finite differences, are often employed in a simulation setting. In this article, we show that it is also possible to simulate this system through the use of a digital waveguide (to model wave propagation in the string), and a wave digital filter (approximating the mechanics of the hammer). One advantage of such an approach is efficiency, due to the simplicity of the waveguide structure; another, the focus here, is on the stability properties inherent in a scattering-type formulation (of which both waveguides and wave digital filters are examples). These stability properties stem from passivity properties inherent in the model itself, which are preserved through the discretization procedure. In particular, we show that even complex hammer models incorporating strong stiffness and loss nonlinearities may be dealt with using these techniques. Simulations are presented.

### 1. INTRODUCTION

A simple model for the transverse vibration of a struck piano string can be framed in terms of the coupling between a linear resonator (the string itself) and a lumped nonlinear excitation mechanism (the piano hammer) [1][2]. Sound synthesis based on such a model can be carried out in various ways. The equation of motion of the string, which takes the form of a one-dimensional *partial differential equation* (PDE), coupled with a nonlinear *ordinary differential equation* (ODE) describing the hammer can be numerically integrated directly via finite difference methods, as per [1]. Alternatively, the string vibration may be approximated by using a pair of digital delay lines, or digital waveguides [3], which transport wave energy in opposite directions at a fixed speed; loss and dispersion effects may be modeled through the use of terminating digital filters [3][4][5]. Such an approach can be considerably more computationally efficient than classical finite difference methods. The numerical scheme for the hammer, though, when arrived at through a straightforward application of finite differences, can contain instantaneous dependencies, called *delay-free loops*, rendering it effectively not explicitly computable. Implicit methods such as the *K-method* (developed by Borin et al.[6]) and *wave digital filters* (WDFs) [8] can take care of this computability problem, by eliminating the delay-free loops mentioned above.

For the sake of numerical stability, it is useful to have an energy measure (or Lyapunov function) for the discrete system, which

mirrors the energetic behavior of the physical system to be modeled. Such a measure is rather difficult to obtain from time domain finite difference formulations. A scattering representation (such as WDFs), in which the discretization is rewritten in terms of wave variables which are scattered at junctions, can be used to give an easily verifiable numerical stability condition. In the purely *lossless* case, all operations on the signals in the network are either shifts or scattering operations (orthogonal matrix multiplies) at each step in the recursion; the squared sum of all the signals in the network remains constant. Losses can be introduced by simply adding resistive drains at the scattering junctions or the terminating filters; this renders the system more generally *passive*.

In Section 2, we present a short summary of the basic principles of WDFs [8]. In Section 3, we present the standard physical model of the piano hammer/string system. We then show how WDFs can be used to solve this coupled PDE/ODE system, with particular attention paid to nonlinear elements and the necessary power-normalization of wave quantities. Simulation results are also presented.

### 2. WAVE DIGITAL FILTERS

#### 2.1. Wave variables

In order to arrive at a scattering formulation, it is necessary to introduce wave variables [8]. Due to the nonlinearities to be modeled, we make use of power-normalized quantities:

$$\underline{a} = \frac{f + Rv}{2\sqrt{R}} \quad \underline{b} = \frac{f - Rv}{2\sqrt{R}} \quad (1)$$

Here,  $f$  a force and  $v$  a velocity, for an arbitrary positive number  $R$ , known as the port resistance.  $\underline{a}$  and  $\underline{b}$  are the *input* and *output* waves, respectively.

#### 2.2. Wave digital spring and mass

We first apply this change of variables to the equation describing a spring. The relation between the force  $f$  exerted by a spring and its compression velocity  $v$  is given by

$$v = \frac{1}{K} \dot{f} \quad (2)$$

where  $K$  the spring stiffness. By discretizing this equation using the trapezoid rule of numerical integration [7][8] (step size  $T$ ), and choosing  $R = KT/2$ , we arrive at the relation

$$\underline{b}(n) = \underline{a}(n - 1) \quad (3)$$



which is the standard form for a wave digital capacitor (the electrical counterpart of the spring). Thus, the output  $\underline{b}$  at the instant  $n$ , only depends on the input  $\underline{a}$  at the instant  $n - 1$ . Figure 1 shows the wave digital one-port corresponding to a spring. Applying the

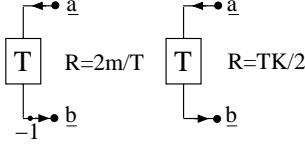


Figure 1: Wave digital mass and spring.

same procedure to a mass  $M$ , defined by  $f = Mdv/dt$ , we get the relation

$$\underline{b}(n) = -\underline{a}(n - 1) \quad (4)$$

with port resistance  $R = 2M/T$ .

### 2.3. Scattering junctions

In order to connect wave digital one-ports such as the spring and mass mentioned previously, it is necessary to make use of scattering junctions (or adaptors, as they are called in WDF terminology). The equations for a scattering junction are restatements of Kirchhoff's connection rules in terms of wave variables.

#### 2.3.1. Parallel and series connections

In terms of power-normalized wave variables  $\underline{a}_i$  and  $\underline{b}_i$ , for  $N$  port resistances  $R_i$ ,  $i = 1, \dots, N$ , the scattering equations are respectively, for a parallel and series connection

$$\underline{b}_i = -\underline{a}_i + \sqrt{G_i} f_J \quad \underline{b}_i = \underline{a}_i - \sqrt{R_i} v_J \quad (5)$$

where  $G_i = 1/R_i$ . The junction force  $f_J$  and the junction velocity  $v_J$  (common to all ports) are given by

$$f_J = \frac{2}{\sum_j G_j} \sum_j \sqrt{G_j} \underline{a}_j \quad v_J = \frac{2}{\sum_j R_j} \sum_j \sqrt{R_j} \underline{a}_j \quad (6)$$

The operations in (5) produce  $N$  outputs  $\underline{b}_i$  from  $N$  inputs  $\underline{a}_i$ ,  $i = 1, \dots, N$ , and can be viewed as an  $N$  by  $N$  matrix multiplication. As long as the port resistances  $R_i$  are chosen positive, the matrix is orthogonal, and thus preserves an  $L^2$  measure of the input signals through the output, i.e.,

$$\sum_{i=1}^N \underline{a}_i^2 = \sum_{i=1}^N \underline{b}_i^2 \quad (7)$$

This energy-preserving property is at the heart of the numerical stability offered by a scattering approach. Even for elements with a nonlinear dependence of the  $R_i$  on the state variables, energy is still preserved.

#### 2.3.2. Elimination of delay-free loops

A special case of the scattering junction occurs when one of the port resistances remains unspecified. For instance, if we choose at port  $q$ , for a parallel and series connection, respectively,

$$G_q = \sum_{i \neq q} G_i \quad R_q = \sum_{i \neq q} R_i \quad (8)$$

the scattering equations (5) above simplify respectively to

$$\underline{b}_q = \frac{1}{\sqrt{G_q}} \sum_{i \neq q} \sqrt{G_i} \underline{a}_i \quad (9)$$

$$\underline{b}_q = -\frac{1}{\sqrt{R_q}} \sum_{i \neq q} \sqrt{R_i} \underline{a}_i \quad (10)$$

Thus the output wave  $\underline{b}_q$  at port  $q$  does not depend on the input wave  $\underline{a}_q$ . In other words, the port is *reflection-free* [8]. This special choice of a free port resistance is necessary in order to avoid delay-free loops, as we shall see in Section 3.3. Graphical representations of series and parallel scattering junctions are shown in Figure 2.

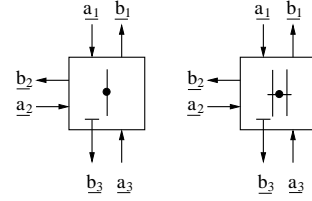


Figure 2: A three-port series scattering junction (left), and a three-port parallel scattering junction (right). A reflection-free port, if present, is indicated by a barred output (port three in this figure).

## 3. APPLICATION OF WDFS TO THE SIMULATION OF THE PIANO HAMMER-STRING INTERACTION

### 3.1. Coupling between the piano string and a nonlinear lossy hammer

We describe in this section the coupled hammer and string model. It consists of a PDE governing the string motion (as presented previously in [5]) coupled with a nonlinear ODE describing the hammer displacement (as proposed by Hunt and Crossley [9]):

$$\begin{aligned} \frac{\partial^2 y_s}{\partial t^2} &= c^2 \frac{\partial^2 y_s}{\partial x^2} - \kappa^2 \frac{\partial^4 y_s}{\partial x^4} - 2b_1 \frac{\partial y_s}{\partial t} + 2b_2 \frac{\partial^3 y_s}{\partial x^2 \partial t} \\ &+ F_H(y_H - y_s) \\ M_H \frac{d^2 y_H}{dt^2} &= -F_H(y_H - y_s) \end{aligned} \quad (11)$$

where

$$F_H(u(t)) = \begin{cases} K_H u^p + K_H \mu u^p \dot{u} & \text{if } u > 0 \\ 0 & \text{if } u \leq 0 \end{cases}, \quad (12)$$

with initial and boundary conditions

$$\begin{aligned} y_s(x, 0) &= y_{s0}(x), \quad \frac{\partial y_s}{\partial t}(x, 0) = v_{s0} \\ y_s(0, t) &= y_s(L, t) = 0, \quad \frac{\partial^2 y_s}{\partial x^2}(0, t) = \frac{\partial^2 y_s}{\partial x^2}(L, t) = 0 \\ y_H(0) &= y_s(x_0, 0), \quad \frac{\partial y_H}{\partial t}(0) = v_{H0} \end{aligned} \quad (13)$$

Here,  $y_s$  is the string displacement,  $y_H$  the hammer displacement,  $c$  the wave speed,  $\kappa$  the stiffness coefficient,  $b_1$  and  $b_2$  the loss parameters,  $M_H$  the hammer mass,  $K_H$  the hammer stiffness,  $p$  the nonlinear stiffness exponent and  $\mu$  the felt loss coefficient.  $x_0$  is the hammer position on the string,  $y_{s0}$  and  $v_{s0}$  are the initial string displacement and velocity and  $v_{H0}$  is the initial hammer velocity.  $L$  is the string length.

This non-linear system does not admit an analytical solution. We show in the next sections that this system can be numerically solved in terms of WDFs.

### 3.2. The non-linear hammer

The hammer force can be actually seen as a sum of two force terms;  $f_H = K_H u^p$ , which depends only on the felt compression and  $f_r = K_H \mu u^p \dot{u}$ , which is related to the compression velocity and introduces loss in the felt. We now discuss these two nonlinearities separately.

Consider a spring-like object defined by the following equation:

$$f(u) = Ku \quad (14)$$

Here,  $f$  is a force, and  $u$  is position; both are functions of time  $t$ .  $K > 0$  is the spring stiffness. Taking a time derivative of both sides of this equation gives

$$\frac{df}{dt} = K \frac{du}{dt} = Kv \quad (15)$$

where  $v$  is velocity, and thus we may write

$$K^{1/2}v = \frac{d}{dt}(K^{-1/2}f) \quad (16)$$

Defining power-normalized variables  $\underline{v} = K^{1/2}v$  and  $\underline{f} = K^{-1/2}f$ , we then obtain

$$\underline{v} = \frac{d\underline{f}}{dt} \quad (17)$$

The spring constant is thus absorbed into the definitions of the variables themselves. Multiplying both sides of (17) by  $\underline{f}$  gives:

$$p = v f = \underline{v} \underline{f} = \underline{f} \frac{d\underline{f}}{dt} = \frac{d}{dt} \left( \frac{1}{2} \underline{f}^2 \right) \quad (18)$$

The left side of the equation can be interpreted as the instantaneous power supplied to the spring, and the right side as the rate of change of the energy

$$E = \frac{1}{2} \underline{f}^2 = \frac{1}{2} K u^2 \quad (19)$$

stored in the spring. Thus all energy supplied to the spring is stored; the spring is lossless, according to such an energy measure. An important point here is that the energy  $E$  is a positive definite function of the state variables (in this case, a quadratic). Suppose, now, that we take (16) as our definition of a spring. We can see that all of the manipulations above still follow, even if  $K = K(u, v, f, t, \dots)$ , as long as  $K$  is a positive function. Thus (16) can be viewed as the definition of a nonlinear lossless spring, if the energy is defined as per (19).

Let us return to the definition of the restoring force in the piano hammer, which is

$$f_H = K_H u^p \quad (20)$$

for  $u > 0$  and  $f_H = 0$  otherwise. Here,  $K_H > 0$  and  $p$  are constants.

Using the definition of a spring given by (16) we define the equivalent hammer felt stiffness  $K_e$  by (see [10] for calculation details):

$$K_e = \frac{1+p}{2} K_H^{1/p} f_H^{(p-1)/p} = \frac{1+p}{2} K_H u^{p-1} \quad (21)$$

which reduces to  $K_e = K_H$  in the linear case, i.e., when  $p = 1$ . The stored energy in the nonlinear spring is thus

$$E = \frac{1}{2} \frac{1+p}{2} K_H u^{p+1} \quad (22)$$

which is again a positive function of  $u$ , when  $u > 0$ .

The force  $f_r = K_H \mu u^p \dot{u}$  is much simpler to deal with; it can be viewed as a nonlinear resistance (or dashpot)  $f_r = R \dot{u}$ , with  $R = K_H \mu u^p$

In sum,  $f_H$  and  $f_r$  are expressed by

$$f_H = K_e(f_H)u \quad (23)$$

$$f_r = \mu f_H \dot{u} \quad (24)$$

### 3.3. Scattering model for the hammer-string interaction

We describe in this section the scattering model for the hammer-string interaction and its connection to a digital waveguide model. In terms of wave variables and scattering junctions, the hammer model defined by (11) and (12) corresponds to the scheme shown in Figure 3.

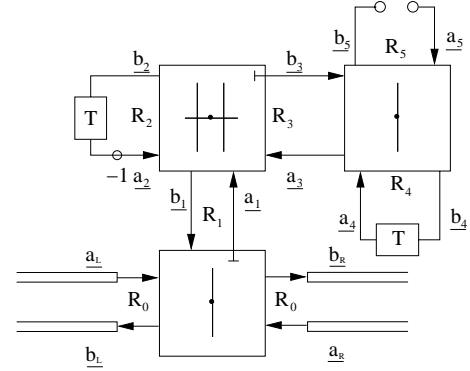


Figure 3: A parallel connection of a mass and a nonlinear lossy spring, top, representing a wave digital hammer, is connected in series with a digital waveguide, bottom.

The upper parallel junction, when disconnected from the lower series junction, is an oscillator (nonlinear and lossy), corresponding to the free vibration of a mass-spring-dashpot system (the hammer). The wave digital port corresponding to the stiffness effects has port resistance  $R_4 = TK_e/2$ ; the lossy port has resistance  $R_5 = \mu f_H$ . Port resistance  $R_2$  (for inertial effects) is given by  $2M_H/T$ .

Connecting a series junctions directly to a parallel junction poses a problem, due to the introduction of delay-free loops;  $a_1$  is calculated from  $b_1$  and vice-versa, as well for  $a_3$  and  $b_3$ . In order to surmount this difficulty, we note that the port resistance  $R_1$  and the port admittance  $G_3$  are left unspecified; we thus can set them to  $2R_0$  and to  $G_1 + G_2$  (where  $G_1 = 1/R_1$  and  $G_2 = 1/R_2$ ) respectively, rendering the port reflection free.

One point requires here special care. The definition of the junction velocity  $v_H$  at the hammer series connection, depends on  $R_4$ , which is a non-linear function of  $f_H$ . At each iteration, a nonlinear equation must be solved using a simple iterative method such as Newton's Method. Nevertheless, due to incomplete convergence of the iterative method, the calculated  $v_H$  is slightly different from the exact solution to the abovementioned equation, the

resulting scattering operation is still orthogonal, and thus energy is preserved.

### 3.4. Simulations

We present simulations of the piano string-hammer interaction. First, perfectly reflecting string terminations, losslessness and stiffness of the string are assumed. In a second part, the hammer is coupled to a lossy and stiff string. The wave digital hammer is decoupled from the digital waveguide when contact is lost (i.e., when a negative value of  $x$  is calculated).

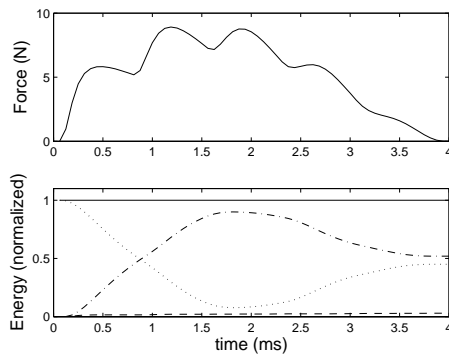


Figure 4: At top, the hammer force curve for a C4 string, and at bottom, the energies of the hammer (dotted), the string (dash-dotted), the loss (dashed) and their total (solid) as a function of time. The total string energy is normalized to unity.

We see in Figure 4, the hammer force and the stored signal energy as a function of time for the C4 note, as well as its partition into hammer, string and lost energies. The hammer energy is calculated from the sum of the squares of the signals  $a_2$  and  $a_4$ , the lost energy from the squared of  $b_5$  and the string energy is simply the squared sum of all the signal values in the digital waveguides, on both sides of the scattering junction. Since there is no loss in the string, the sum of these energies is constant (reflecting perfect losslessness of the model system), to within errors due to machine precision. Figure 5 shows the hysteretic behaviour of the ham-

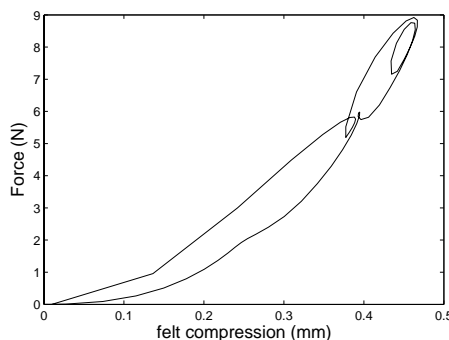


Figure 5: Hysteretic behavior of the force as a function of the felt compression.

mer force as a function of the felt compression indicating losses in the felt. Secondly, we take into account loss and dispersion phenomena in the string using a digital waveguide as defined in [5].

It does not really modify the behavior of the hammer force but it strongly affects the propagation of waves in the string and the resulting tone.

### 4. CONCLUSIONS

In this paper, we have shown how a scattering formulation of the coupling between a piano string and nonlinear lossy hammer can yield a discrete-time simulation with good stability properties. Indeed, the verification of stability amounts to no more than a check on the positivity of the network port resistances. Particular attention was paid to the formulation of the nonlinear hammer, and the means through which a wave digital counterpart may be obtained. The techniques discussed here, in that they rely on iterative numerical methods for solution, share much in common with the K-method proposed in [6] (in that case, table lookups are employed in place of the iterative method). It must be mentioned that the K-method does possess a certain degree of flexibility in the choice of integration method which is not possible in the case of WDFs (which rely exclusively on the trapezoid rule). Here, though, we have access to a simple  $L^2$  energy measure for the discrete simulation; this is not at all evident in the K-method, or in the finite difference methods discussed in [1].

### 5. REFERENCES

- [1] Chaigne, A. and Askenfelt, A. "Numerical Simulations of Struck String I. A Physical Model for a Struck String Using Finite Difference Methods", J. Acoust. Soc. Am., 95(2):1112-1118, 1994.
- [2] Van Duyne, S. A., Pierce, J. R. and Smith, J. O., "Travelling Wave Implementation of a Lossless Mode-Coupling Filter and the Wave Digital Hammer", Proc. Int. Comp. Music Conf., pp. 411-418, 1994.
- [3] Smith, J. O., "Physical Modeling Using Digital Waveguides", Computer Music J., MIT Press, 16(4):74-91, 1992.
- [4] Karjalainen, M., Välimäki, V. and Tolonen, T. "Plucked-String Models: From the Karplus-Strong Algorithm to Digital Waveguides and Beyond", Computer Music J., MIT Press, 22(3):17-32, 1998.
- [5] Bensa, J., Bilbao, S., Kronland-Martinet, R. and Smith, J. O. "The Simulation of Piano String Vibration: From Physical Model to Finite Difference Schemes and Digital Waveguides", J. Acoust. Soc. Am., accepted for publication, 2003.
- [6] Borin, G., De Poli, G. and Rochesso, D. "Elimination of Delay-Free Loops in Discrete-Time Models of Nonlinear Acoustic System", IEEE Trans. Speech and Audio Proc., 8(5):597-605, 2000.
- [7] Sarti, A. and De Poli, G. "Generalized Adaptators with Memory for Nonlinear Structures", Proc. EUSIPCO-96, 3:191-194, 1995.
- [8] Fettweis, A. "Wave Digital Filters: Theorie and Practice", Proc. IEEE, 74(2):270-327, 1986.
- [9] Hunt, K. H. and Crossley, F. R. E. "Coefficient of Restitution Interpreted as Damping in Vibroimpact", ASME J. Appl. Mech., pp.440-445, 1975.
- [10] Bilbao, S., Bensa, J., Kronland-Martinet, R. and Smith, J. O. "The wave digital piano hammer: a passive formulation", Proceedings of the 144th ASA, Cancun, 2002.

# SOUND SYNTHESIS FOR THREE-DIMENSIONAL OBJECTS: DYNAMIC CONTACT BETWEEN TWO ARBITRARY ELASTIC BODIES

*J. Bensoam, R. Caussé, C. Vergez, N. Misdariis and N. Ellis*

Ircam CNRS UMR 9912  
1, place Igor Stravinsky. 75004 Paris. France  
joel.bensoam@ircam.fr

## ABSTRACT

Modalys is a sound synthesis software developed at Ircam for research and musical applications. This software allows one to build virtual instruments based on physical models to obtain the most entire range of expressive variations in the instrument in response to intuitive controls. An instrument, as a complex structure, is described by the mechanical/acoustical interaction of its components (strings, tubes, resonators, soundboard,...).

Some new research have been done recently to extend the sound prediction to three-dimensional objects with the help of numerical methods. In particular, theoretical and numerical treatment of the unilateral and frictionless dynamic contact between two arbitrary elastic bodies was studied and highlighted by simulations implemented in Modalys.

## 1. INTRODUCTION

This paper deal with the dynamic and frictionless contact between two arbitrary elastic bodies. The section 2 is devoted to the formal statement of the two-body contact problem, including equations of motion and contact conditions, and leads to a variational formulation. Section 3 introduces the Poisson function concept which lies at the heart of the reciprocal formulation. This formulation is then numerically solved in section 4.

## 2. FORMAL STATEMENT OF THE PROBLEM

### 2.1. Geometry and conventions

We consider the two-body contact problem show on Fig. (1) where two bodies, (a) and (b), are expected to come into contact during the time interval of interest  $[0, \tau]$ . To simplify notations, a star (\*) is used to represent indifferently body (a) or (b). Let  $\Omega_*$  be an open bounded subset of the three-dimensional Euclidean space  $\mathbb{R}^3$  with a boundary  $\partial\Omega_*$ . The set  $\Omega_*$  is occupied by a linear elastic body (\*) in its undeformed configuration which is referred to an orthogonal Cartesian coordinate system  $Ox_1x_2x_3$ . Surface  $\partial\Omega_*$  of each body is decomposed as usual into three mutually disjoint parts  $\Gamma_d^*$ ,  $\Gamma_n^*$  and  $\Gamma_c^*$ . On  $\Gamma_d^*$  (resp.  $\Gamma_n^*$ ) displacements  $\bar{\mathbf{u}}^*(t)$  (resp. tractions  $\mathbf{t}^*(t)$ ) are given. We denote by  $\Gamma_c^*$  a portion of body (\*) which is a candidate contact surface. The actual surface on which a body comes into contact with the other one is not known in advance, but is contained in the portion  $\Gamma_c^*$  of  $\partial\Omega_*$ . In addition, each body can be subjected to a body force  $\mathbf{f}^*(t)$  (such as gravity for instance).

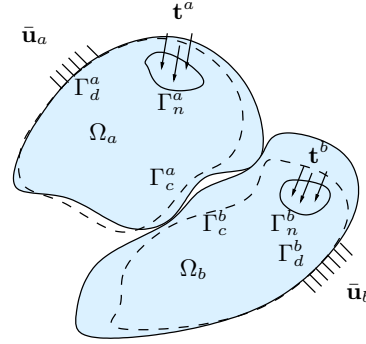


Figure 1: Two elastic bodies (a) and (b) in their undeformed (dash line) and current (solid line) configuration. The actual surface on which the body (a) comes in contact with the other one is not known in advance but is contained in the portion  $\Gamma_c^a$  of its boundary.

The displacement of the the bodies, relative to the fixed spatial frame, at time  $t$ , are represented by a function

$$\mathbf{u} : t \in [0, \tau] \longrightarrow \mathbf{u}(t) = (\mathbf{u}^a(t), \mathbf{u}^b(t)) \in \mathcal{E},$$

where  $\mathbf{u}^*$  is the displacement of body (\*) and  $\mathcal{E}$  the product of Sobolev spaces of each body  $\mathcal{E} = (H^1(\Omega_a))^3 \times (H^1(\Omega_b))^3$ . Throughout this study, standard indicial notation and summation convention are employed. Superposed dots (') indicate differentiation with respect to time and commas (,) denote partial differentiation with respect to  $x_k$ . Thus,  $\dot{u}_i = \frac{\partial u_i}{\partial t}$ ,  $\ddot{u}_i = \frac{\partial^2 u_i}{\partial t^2}$ ,  $u_{i,k} = \frac{\partial u_i}{\partial x_k}$ , etc.

### 2.2. Equations of motion

#### 2.2.1. Contact condition

The contact condition on the relative displacement field  $\mathbf{u}^r = \mathbf{u}^a - \mathbf{u}^b$  of the two-body contact problem is established by Oden and Kikuchi [1] as

$$u_n^r \leq g_{ap}, \quad \text{on } \Gamma_c^a, \quad (1)$$

where  $g_{ap}$  is a given function representing the normalized gap between the two elastic bodies and  $\mathbf{n}$  is the outward unit vector normal to the contact surface  $\Gamma_c^a$ . On the candidate contact surface, the Cauchy stress vector is resolved into normal and tangential parts via

$$\sigma_{kl}n_l = \sigma_n n_k + \sigma_{T_k}, \quad \text{on } \Gamma_c^a. \quad (2)$$

The contact pressure  $\sigma_n$  should be negative for compressive contact that occurs when  $u_n^r = g_{ap}$ . We assume that no frictional tractions in the present discussion; therefore  $\sigma_{T_k} = 0$ . The conditions for normal contact can now be written as

$$u_n^r - g_{ap} \leq 0 \quad (3a)$$

$$\sigma_n \leq 0 \quad (3b)$$

$$\sigma_n(u_n^r - g_{ap}) = 0 \quad (3c)$$

$$\sigma_n \dot{u}_n^r = 0 \quad (3d)$$

which must hold on the contact surface  $\Gamma_c^a$ . Equation (3d) is a statement of the energy conservation during the frictionless contact.

### 2.2.2. Equations of motion

With the contact conditions written and within the framework of linear elasticity the following equations and inequations of motion hold for solid (a) or (b)

$$\rho_\star \ddot{u}_k^\star = \sigma_{kl,l}^\star + \rho_\star f_k^\star \quad \text{in } \Omega_\star \times [0, \tau] \quad (4a)$$

$$\sigma_{kl}^\star = C_{klmn}^\star u_{m,n}^\star \quad \text{in } \Omega_\star \times [0, \tau] \quad (4b)$$

$$\sigma_{kl}^\star n_l^\star = t_k^\star \quad \text{on } \Gamma_n^\star \times [0, \tau] \quad (4c)$$

$$u_k^\star = \bar{u}_k^\star \quad \text{on } \Gamma_d^\star \times [0, \tau] \quad (4d)$$

$$\text{Contact conditions (3)} \quad \text{on } \Gamma_c \times [0, \tau] \quad (4e)$$

The momentum conservation is expressed by equation (4a), while (4b) represents the Hooke's law where  $C_{klmn}^\star$  are the components of the Hooke's tensor of elasticity. Equations (4c) and (4d) are respectively the Neumann and Dirichlet boundary conditions imposed on the surface of the body ( $\star$ ). In this presentation the heat propagation is not considered.

### 2.2.3. Variational formulation

The optimization of Hamilton's functional, on a constraint set that expresses the contact condition, can be used to obtain the formal statement of the two-body dynamic contact problem (4). In this framework, general non-linear programming methods are available: constrained minimization problems can be formulated using saddle point theory where the Lagrange multiplier represents a contact pressure (see [1, 2]). This is done by introducing the space  $\mathcal{W} = \mathcal{E} \times \mathcal{Z} \times \mathcal{N}$  where  $\mathcal{Z}$  is the dual space of displacements on the Dirichlet surfaces while  $\mathcal{N}$  is the admissible set for the Lagrange multipliers  $p_n$  defined by

$$\mathcal{N} = \{p_n \in H^{-1/2}(\Gamma_c) \mid p_n \leq 0 \text{ on } \Gamma_c^a\}. \quad (5)$$

The set  $\mathcal{N}$  is a subset of the dual space of displacements on  $\Gamma_c$  containing negative force. The problem (4) is then equivalent to the determination of the saddle point  $(\mathbf{u}, \boldsymbol{\chi}, \sigma_n) \in \mathcal{W}$  and yields to the Kuhn and Tucker variational formulation [3]

Find  $(\mathbf{u}, \boldsymbol{\chi}, \sigma_n) \in \mathcal{W}$  such that

$$m(\ddot{\mathbf{u}}, \mathbf{v}) + k(\mathbf{u}, \mathbf{v}) = f(\mathbf{v}) \quad \forall \mathbf{v} \in \mathcal{E} \quad (6a)$$

$$\sum_{\star=a,b} (\boldsymbol{\kappa}^\star | \mathbf{u}^\star - \bar{\mathbf{u}}^\star)_{\Gamma_d^\star} = 0 \quad \forall \boldsymbol{\kappa} \in \mathcal{Z} \quad (6b)$$

$$(p_n - \sigma_n | u_n^r - g_{ap} )_{\Gamma_c^a} \geq 0 \quad \forall p_n \in \mathcal{N} \quad (6c)$$

$$(\sigma_n | \dot{u}_n^r)_{\Gamma_c^a} = 0 \quad (6d)$$

where  $f(\mathbf{v})$  represents the forces acting on solids (a) and (b)

$$f(\mathbf{v}) = \sum_{\star=a,b} \left[ (\rho_\star \mathbf{f}^\star | \mathbf{v}^\star)_{\Omega_\star} + (\mathbf{t}^\star | \mathbf{v}^\star)_{\Gamma_n^\star} + (\boldsymbol{\chi}^\star | \mathbf{v}^\star)_{\Gamma_d^\star} + (\sigma_n | v_n^r)_{\Gamma_c^a} \right], \quad \forall \mathbf{v} \in \mathcal{E}. \quad (7)$$

The first equation (6a) represents the principle of virtual work (power) applied to the bodies (a) and (b) subjected, on one hand, to external forces  $(\mathbf{f}^\star, \mathbf{t}^\star)$  and to reaction forces  $\boldsymbol{\chi}^\star$  on their respective Dirichlet surface  $\Gamma_d^\star$ , and on the other hand, to a contact pressure  $\sigma_n$  normal to the contact surface  $\Gamma_c^a$ . In this equation, the bilinear forms

$$m(\mathbf{u}, \mathbf{v}) = \sum_{\star=a,b} \int_{\Omega_\star} \rho_\star u_k^\star v_k^\star dv, \quad \forall \mathbf{u}, \mathbf{v} \in \mathcal{E},$$

$$k(\mathbf{u}, \mathbf{v}) = \sum_{\star=a,b} \int_{\Omega_\star} C_{klmn}^\star u_{m,n}^\star v_{k,l}^\star dv, \quad \forall \mathbf{u}, \mathbf{v} \in \mathcal{E}.$$

are introduced. The second equation (6b) expresses the Dirichlet boundary conditions. Finally, the variational inequality (6c) expresses the unilateral and frictionless contact conditions (3a) to (3c), while (6d) is another way to write (3d). According to this contact condition a non-zero traction may only be generated if the normal velocity  $\dot{u}_n$  is continuous through the contact surface. In other words, during interaction the normal velocities of both bodies must be equal on the contact area, which is quite intuitive.

In fact, the impact between portions of the boundaries of elastic bodies is expected to produce propagating stress and velocity discontinuities. Indeed, just before contact, the relative normal velocity  $\dot{u}_n^r$  could be non-zero: this velocity must thus make a jump to vanish during contact. That is to say that at least one of the bodies endures a brutal change in its velocity in the direction normal to  $\Gamma_c$ . Thus, a particular attention must be dedicated to this additional difficulty.

## 3. RECIPROCAL FORMULATION

To compute a solution of the two-body contact problem in case of stress and velocity discontinuities we will prefer to use an integral representation with Green functions rather than finite difference algorithms such as Newmark and central difference schemes. This method is usually called reciprocal formulation as it involves the inverse of the *elasticity operator* appearing in standard variational statements of linear elastodynamic problems. This inverse operator is the Green function. One of the advantage of this method is that the awkward problem of discontinuities is already treated in the definition of the Green function without the complications of contact problems. Moreover, since the contact pressure occurs only on the contact surface  $\Gamma_c$  the reciprocal formulation uses functions defined only on this surface. It is then often possible to approximate the system using considerably fewer unknowns than with classical formulations.

The purpose of the next subsection is to defined the mathematical tools needed for the reciprocal formulation. A semi-analytical method will also be described to compute those tools. In the following subsection 3.2, the reciprocal formulation will be applied to the two-body contact problem.

### 3.1. The unconstrained problem

#### 3.1.1. Green and Poisson functions

For the time being, let us consider one of the two bodies, say body  $(\star)$  for example, and suppose that the contact pressure  $\sigma_n$  is a given prescribed traction  $\mathbf{t}^\star$  on a surface  $\Gamma_n^\star$  which now includes  $\Gamma_c^\star$  so that the surface of the body is only  $\partial\Omega^\star = \Gamma_n^\star \cup \Gamma_d^\star$ . Other external influences are body force  $\rho_\star \mathbf{f}^\star$  and Dirichlet boundary conditions  $\bar{\mathbf{u}}^\star$  on  $\Gamma_d^\star$ .

If the sources  $\rho_\star \mathbf{f}^\star$ ,  $\mathbf{t}^\star$  and  $\bar{\mathbf{u}}^\star$  are given, the displacement field  $\mathbf{u}^\star$ , solution of the equations (4a) to (4d), is unique and can be expressed by an integral representation<sup>1</sup> using Green and Poisson functions, namely

$$\begin{aligned} u_k^\star(\mathbf{x}; t) = & \int_{\Omega^\star} G_i^k(\mathbf{x}, \mathbf{y}; t) * \rho_\star f_i^\star(\mathbf{y}; t) dv_{\mathbf{y}} \quad (8) \\ & + \int_{\Gamma_n^\star} N_i^k(\mathbf{x}, \mathbf{y}; t) * t_i^\star(\mathbf{y}; t) ds_{\mathbf{y}} + \int_{\Gamma_d^\star} D_i^k(\mathbf{x}, \mathbf{y}; t) * \bar{u}_i^\star(\mathbf{y}; t) ds_{\mathbf{y}} \end{aligned}$$

where the star  $(\star)$  denotes the convolution operation with respect to time. In this formula, the Green function  $\mathbf{G}^k(\mathbf{x}, \mathbf{y}; t)$  is the solution of the equations (4a) to (4d) with the sources  $\bar{\mathbf{t}}^\star = \bar{\mathbf{u}}^\star = 0$ ,  $\rho_\star \mathbf{f}^\star = \delta(t)\delta(\mathbf{x} - \mathbf{y})\mathbf{e}_k$  where  $\mathbf{e}_k$  is  $k$ -th unit basis vector of  $\mathbb{R}^3$ . The Poisson functions  $\mathbf{N}^k$  and  $\mathbf{D}^k$  are the displacement fields corresponding to an impulsive source (force and displacement respectively) placed on the surface of the body ( $\Gamma_n$  and  $\Gamma_d$  resp.).

#### 3.1.2. Modal theory

The major problem of reciprocal method is to find the Green and Poisson functions related to an elastic body. In practice only a few physical systems allow an analytical calculation of such functions. Discontinuities in the fields make difficult to compute pure numerical solutions with impulse sources. Modal theory gives an opportunity to compute semi-analytical function: the Green function  $\mathbf{G}^k$  (and even the Poisson  $\mathbf{N}^k$ ) for any point  $\mathbf{x} \in \bar{\Omega}^\star$  and time  $t$  may be represented by a normal-mode expansion

$$\mathbf{G}^k(\mathbf{x}, \mathbf{y}; t) = \sum_{n=1}^{\infty} \phi_n^\star(\mathbf{x}) Y(t) \frac{\sin \omega_n t}{m_n \omega_n} \phi_n^\star(\mathbf{y}) \cdot \mathbf{e}_k, \quad \mathbf{y} \in \Omega^\star \quad (9)$$

where  $\phi_n^\star$  is the  $n$ -th mode of the body  $(\star)$ . The parameters  $m_n$  and  $\omega_n$  are respectively the modal mass and modal angular frequency associated to the  $n$ -th mode respectively and  $Y(t)$  is the Heaviside function. A similar expression can be built for the Poisson function where the source point  $\mathbf{y}$  lie on the Neumann surface instead of being in the domain  $\Omega^\star$ . The Poisson function  $\mathbf{D}^k$  can also be computed using normal-mode expansion. But, since the modes vanish on the Dirichlet surface  $\Gamma_d^\star$ , a more complicated approach must be used (see Ref. [5] for details).

### 3.2. Two-body contact problem

Applying this result to the variational formulation (6a) and (6b), the displacement and the velocity on the contact surface can be expressed as functions of the contact pressure  $\sigma_n$ . The two-body contact problem is then reduced to the contact conditions (6c) and (6d)

<sup>1</sup> It is important to note that the integral representation (8) has the same form for a point  $\mathbf{x}$  in the domain  $\Omega^\star$  or on the boundary  $\partial\Omega^\star = \Gamma_n^\star \cup \Gamma_d^\star$ . This is an alternative to the integral representation that uses the fundamental solution (free-space Green's function). In this case, a different expression exist depending on the position of the point field  $\mathbf{x}$  (see Ref. [4]).

with only one unknown: the contact pressure and yields to the reciprocal formulation: find  $\sigma_n \in \mathcal{N}$ , such that

$$(p_n - \sigma_n |G_d(\sigma_n) + \bar{g}_{ap})_{\Gamma_c} \geq 0, \quad \forall p_n \in \mathcal{N}, \quad (10a)$$

$$\text{and} \quad (\sigma_n |G_v(\sigma_n) + \bar{u}_n^r)_{\Gamma_c} = 0, \quad (10b)$$

where  $\bar{g}_{ap} = \bar{u}_n^r - g_{ap}$  and

$$G_d(\sigma_n) = \int_{\Gamma_c} N(\mathbf{x}, \mathbf{y}; t) * \sigma_n(\mathbf{y}; t) ds_{\mathbf{y}}, \quad G_v(\sigma_n) = \dot{G}_d(\sigma_n)$$

The Poisson function  $N(\mathbf{x}, \mathbf{y}; t) = N_n^a(\mathbf{x}, \mathbf{y}; t) + N_n^b(\mathbf{x}, \mathbf{y}; t)$  represents the relative Poisson function defined for  $\mathbf{y}$  on the contact surface<sup>2</sup>. The term  $\bar{u}_n^r(\mathbf{x}; t)$  represents the relative displacement due to non contact influences. It is a known function and can be computed using the integral representation (8) for each body. For static problems, the dynamic contact condition (10b) does not exist and the reciprocal variational problem can be alternatively formulated as a constrained minimization problem, on the convex set  $\mathcal{N}$ , of the functional  $F(p_n) = \frac{1}{2} (p_n |G_0(p_n))_{\Gamma_c} + (p_n | \bar{g}_{ap})_{\Gamma_c}$  where  $G_0(p_n)$  and  $N(\mathbf{x}, \mathbf{y})$  is a time-independent Poisson function. An iterative scheme to obtain a solution of such a problem, using a variant of Uzawa's method, can be found in [1]. The dynamic problems are not so straightforward and the reciprocal formulation can be simplified using a time discretization that transforms convolutions into discrete sums.

## 4. NUMERICAL SOLUTION

In this section, a time discretization will be achieved and this will lead to a very simple numerical algorithm described in subsection 4.1 illustrated by a numerical example in 4.2.

### 4.1. Time discretization and algorithm

A time discretization of the two-body contact problem is obtained by introducing a partition of the time domain  $[0, \tau]$  into  $M$  intervals of length  $\Delta t$  such that  $0 = t_0 < t_1 < \dots < t_M = \tau$ , with  $t_{k+1} - t_k = \Delta t$ . In addition, the contact pressure  $\sigma_n$  is postulated, in this model, to be a succession of impulse forces. Thus, the convolutions that appear in the reciprocal formulation (10) can be replaced by discrete sums and can be split, with respect to the contact pressure, into instantaneous and historical terms. Thus, the normalized distance between body (a) and (b), at time  $t_k$ , which should exist in absence of contact, can be evaluated by

$$\hat{u}_n^r(\mathbf{x}; k) = \bar{u}_n^r(\mathbf{x}; k) + \int_{\Gamma_c} \sum_{l=0}^{k-1} N(\mathbf{x}, \mathbf{y}; k-l) \sigma_n(\mathbf{y}, l) ds_{\mathbf{y}} \quad (11)$$

This relative distance can be greater than the normalized gap function on a portion  $\Gamma_c(k)$  of the candidate contact surface  $\Gamma_c$  (see the contact condition (2)). If this surface is not empty, a contact occurs between the time  $t_{k-1}$  and  $t_k$  producing a pressure to avoid the penetration of the bodies. In order to obtain a very simple algorithm, the contact pressure is postulated to act at discrete time  $t_k$  (and not between  $t_{k-1}$  and  $t_k$ ). On the extended contact area  $\Gamma_c(k)$ , which varies on time, the particles velocities can be computed by

$$\dot{u}_n^r(\mathbf{x}; k) = \hat{u}_n^r(\mathbf{x}; k) + \int_{\Gamma_c(k)} \dot{N}(\mathbf{x}, \mathbf{y}; 0^+) \sigma_n(\mathbf{y}; k) ds_{\mathbf{y}} \quad (12)$$

<sup>2</sup> the plus sign  $(+)$  is due to opposite normal unit vectors  $\mathbf{n}^a$  and  $\mathbf{n}^b$ .



where the velocity  $\hat{u}_n^r(\mathbf{x}; k)$  computed<sup>3</sup> by (11) is a known function consisting of external and historical contributions and does not depend on the contact pressure at time  $t_k$ . Finally, according to the dynamical contact condition (3d), equation (12) must vanish in order to create non-zero tractions and give the opportunity to calculate the contact pressure at time  $t_k$  by the integral equation

$$\int_{\Gamma_c(k)} \dot{N}(\mathbf{x}, \mathbf{y}; 0^+) \sigma_n(\mathbf{y}; k) ds_{\mathbf{y}} = -\hat{u}_n^r(\mathbf{x}; k) \quad (13)$$

Finally, a finite element approximation of the problem (4a) to (4d) is considered in order to compute, by (9), semi-analytical Green and Poisson functions using numerical eigenfunctions. In this way the integral equation (13) becomes a linear system to be solved at each sample time (see [3] for details).

#### 4.2. Three-dimensional numerical example

For curved contact surfaces, the unilateral behavior on the boundaries may have a substantial influence on the response of the structures: the structural systems, even in cases of linear elasticity and small deformations, exhibits nonlinear characteristics. The collision between a ring and a slab is considered here as an illustration of such a phenomenon. An elastic ring, subjected to gravity, is dropped with an initial velocity on an elastic slab clamped on its edges. The figure 2 help to see the spatial pressure distribution on the contact surface. The nodes on the candidate contact surface of the ring are numbered from 1 to 9. Computing other simulations, we see that the contact surface extends itself for increasing impact velocity and provides a different behavior of the solids.

#### 5. CONCLUSION

As mention by Talaslidis and Panagiotopoulos [6], due to unilateral constraints, the estimation of the eigenvalue and eigenvector of the two-body system is not possible. Nevertheless, in the present article and within the infinitesimal deformation theory, semi-analytical Green (or Poisson) functions are computed using individual mode expansion for each body. The treatment of wave propagation in the solids is then parted from the contact problem by itself and the reciprocal formulation is used in numerical computations reducing the number of unknown and giving a stable solution. Since the Poisson function is pre-processed, the computational time to solve the contact algorithm remain constant for any desired degree of approximation. Dissipative Green and Poisson functions arising from visco-elastic unconstrained problem are also considered in the contact algorithm. The result is a dissipative system with a dissipative-less contact.

The possibility to predict, with a reasonable computing time, the sound produced by the interaction of two elastic bodies irrespective of the material constitution and geometry constitute the major interest of this study. These accurate distributed contact simulations can also be used to derive the parameters of point-like non-linear phenomenological models usually used in sound synthesis.

<sup>3</sup>To compute a velocity,  $\dot{N}$  is substituted to  $N$  in eq. (11).

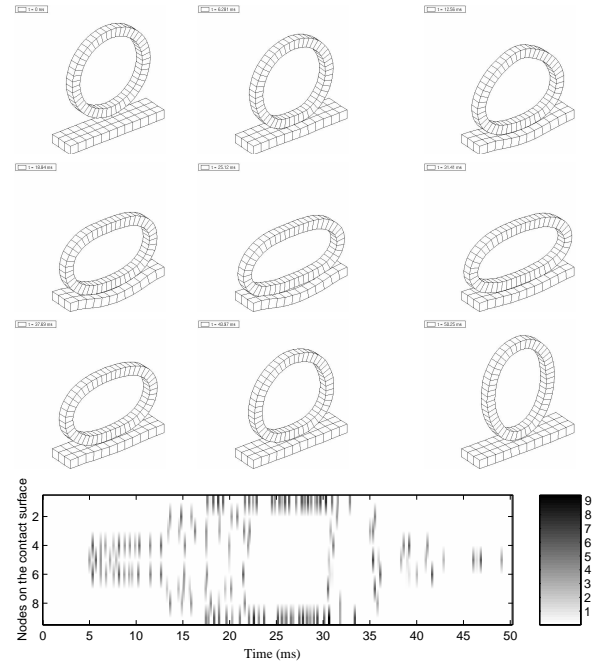


Figure 2: Collision between a ring and a slab and contact pressure (in mPa) on the contact surface. The nodes on the candidate contact surface of the ring are numbered from 1 to 9. When the contact surface extends itself to the nodes 1 (and symmetric 9) the center node 5 is no longer in contact and a gap appears.

#### 6. REFERENCES

- [1] N. Kikuchi and J.T. Oden, *Contact Problems in Elasticity: A Study of variational Inequalities and Finite Element Methods*, Siam, Philadelphia, 1988.
- [2] P.G. Ciarlet, *Introduction à l'analyse numérique matricielle et à l'optimisation*, Masson, Paris, 1990.
- [3] J. Bensoam, "A reciprocal variational approach to the two-body frictionless contact problem in elastodynamics," *International Journal for Numerical Methods in Engineering*, 2003, submitted.
- [4] A.C. Eringen and E.S. Suhubi, *Elastodynamics*, vol. II-linear theory, Academic Press, New York, 1975.
- [5] J. Bensoam, C. Vergez, N. Misdariis, and R. Caussé, "Formulation intégrale et technique des éléments finis appliquées à la synthèse sonore par modèles physiques," in *XVème Congrès Français de Mécanique*, Nancy, 2001, number 453, CFM.
- [6] D. Talaslidis and P. D. Panagiotopoulos, "A linear finite element approach to the solution of variational inequalities arising in contact problems of structural dynamics," *International Journal for Numerical Methods in Engineering*, vol. 18, pp. 1505–1520, 1982.

## MUSICAL APPLICATIONS OF GENERALISED MULTICHANNEL DIGITAL WAVEGUIDES

*Chris Burns, Stefania Serafin*

CCRMA, Department of Music  
Stanford University  
Stanford, CA, 94309  
cburns | serafin@ccrma.stanford.edu

*Matthew Burtner*

VCCM, McIntire Department of Music  
University of Virginia  
Charlottesville, VA, 22903  
mburtner@virginia.edu

### ABSTRACT

We propose different applications in which extensions of digital waveguides have been used in a compositional context.

### 1. INTRODUCTION

One dimensional digital waveguides are a synthesis technique widely used in the computer music community to model waves propagating along different media, such as strings and tubes.

Efficient simulations of different musical instruments, such as plucked, struck and bowed strings, woodwinds and percussions have been built using the waveguide approach. Digital waveguides combine an efficient simulation which provide a low cost realtime implementation to to a meaningful physical interpretation. The idea behind digital waveguides was first introduced in a paper by McIntyre, Schumacher and Woodhouse in the early 80s [1]. The authors discovered that different classes of musical instruments, such as a bowed string, a flute and a clarinet, can be modeled using a similar approach of a nonlinear excitation coupled to a linear resonator. Smith developed this idea and introduced the digital waveguide theory, which has been since widely used in the computer music community [2].

In this paper we propose generalized digital waveguides with different topologies with the intent of creating extended physical models. We built different waveguide structures in which traditional and not traditional excitations are fed into a network of eight independent digital waveguides. The following sections describe a description of these networks as well as different musical applications in which they were used.

### 2. THE EXTENDED WAVEGUIDE STRUCTURE

We started by experimenting with eight independent digital waveguides connected in parallel and excited by different excitation functions, as described below.

#### 2.1. Nonlinear functions as excitations

We started by implementing different nonlinear excitation functions such as a velocity dependent friction curve to reproduce rubbing different hard surfaces and a pressure dependent nonlinear function to reproduce blowing different surfaces. The waveguide resonator was coupled to the nonlinear sustained excitation in a feedback loop.

#### 2.2. Soundfiles and live inputs as excitations

Beyond excitation via mathematical functions, both soundfiles and live audio inputs can be used to drive waveguide networks. For example, we used sampled excitation functions to model rich impulsive excitations such as hit plates and bowls. The excitation was obtained by recording different objects struck at different positions and removing the main frequency components using spectral analysis and inverse filtering. The residual was fed into the waveguide resonator in a feed-forward loop.

The use of soundfiles as excitations also invokes the use of waveguide networks to simulate reverberation; however, more esoteric transformations are also possible. For instance, it is possible to compose continuous transitions between soundfile reverberation and feedback generation, through careful control of delay lengths and gain coefficients

We have also designed networks which are excited by live audio inputs. Depending upon the network topology and system gain, microphones don't even have to be plugged in to excite the network; self-noise at the ADC may be sufficient to set the process in motion. These setups, as in the John Cage realization described in section 6.2, can produce complex and interesting interactions between the activities of a live performer and the output of the network.

### 3. VARIATIONS ON WAVEGUIDE SECTION STRUCTURES

#### 3.1. Peak gain control with nonlinear functions

Traditional waveguide topologies, like other signal processing elements which involve feedback (e.g., IIR filters) are explicitly designed to preserve system stability. However, it is possible to impose at least bounded amplitudes in signal processing systems which do not need traditional criteria for stability. Local peak control can be implemented via waveshaping with nonlinear functions that produce soft clipping. Charles Sullivan presented one such function in his work on physical models of the electric guitar [3]:

$$f(x) = \begin{cases} \frac{2}{3}, & x = 1 \\ x - x^3/3, & -1 < x < 1 \\ -\frac{2}{3}, & x = -1 \end{cases} \quad (1)$$

Related methods for amplitude management include peak limiting compression and the "elastic-mirrors" in Xenakis' GENDYN technique ([4, 5]).



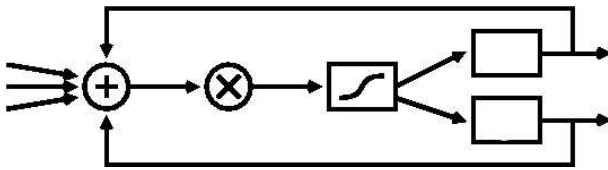


Figure 1: Block diagram for a non-waveguide-like section of a feedback network.

Nonlinear waveshaping functions necessarily color the sonic output of a system. This is especially apparent when nonlinearities are deployed at several different points in a network. While this timbral alteration may seem like a disadvantage, in a compositional context it can just as well be viewed as a desirable feature. After all, peak-managed feedback networks are of interest precisely because they encourage non physical designs with unusual sonic characteristics.

### 3.2. Selective destabilization: waveguides without polarity inversion

Peak-management techniques like nonlinear waveshaping allow a rethinking of the elements and connections within a single waveguide. Many of the waveguides tested in our work feature continuously changing delay lengths, including dynamic delay lengths independent for each rail of a waveguide. Some sections tested even forego the notion of rails, placing delays in configurations which cannot be interpreted physically.

Similarly outside of the domain of physical interpretation, peak management makes it possible to eliminate the typical inversion of polarity as a signal passes between rails of the waveguide [6]. Waveguides which don't utilize sign changes tend to output DC. However, they can be encouraged to produce audible signals if they are perturbed, through changes to the gain coefficients, the delay lengths, or the excitation.

## 4. NETWORK TOPOLOGIES

### 4.1. Circular and "spoke" topologies

Nonlinearities and other forms of peak management facilitate a wide range of network topologies, eliminating concerns about the gain structure of a particular architecture [7]. Our experiments have focused on circular architectures (networks without a particular beginning or end), including structures with "spokes" connecting nonadjacent sections.

## 5. SPATIALIZATION

### 5.1. Spatialization of independent waveguides

Because the primary goal of physical modeling has traditionally been to recreate sounding physical bodies, techniques of waveguide synthesis have largely dealt with exteriors of bodies. One natural extension of the physically-based waveguide network is the use of independent spatial modulation of individual waveguides. By distributing the waveguides of a physically-based system around the listener the notion of "body" as perceived from an exterior orientation, and the perceptually interior notion of "space,"

can be modulated. Spatial modulation of the system allows for an extended notion of the objecthood of the model, and the possibility of transforming it from body into space, or from object into environment. In previous work, the authors have explored extended techniques for physical models by taking advantage of the disassociation of the synthesis and control aspects of the virtual instruments [8, 9].

Building on this work, the physical model of the Tibetan singing bowl suggested an extended approach to spatialization for waveguide networks. A bowl model was implemented allowing each of eight waveguides to be controlled independently. In order to explore the acoustic effect of moving from an exterior to an interior position of the bowl, the impulse response of the bowl was taken from different locations in and around the bowl. Microphone placed inside the center of the bowl, 30cm above the bowl, and 20cm to the side recorded the different impulse responses of the bowl. From these recorded impulse responses, we extracted the frequencies of the main resonances of the instrument, together with the corresponding damping factors, using spectral analysis. The modeling of the multichannel bowl has been discussed in depth in [10].

The resulting instrument, implemented as an extension to the Max/MSP environment, allows simultaneous independent control of the eight fundamental frequencies, eight decay times for the low-pass filters, eight bandwidth for the resonant filters, four dispersion coefficients for the allpass filters, one inlet to input an external source of energy, one excitation position (i.e. where the bowl is hit), one excitation pressure (i.e. how hard it is hit) and one excitation velocity. Eight outlets, each outlet corresponding to a mode of the resonant structure, are sent to spatial processing algorithms for diffusion through a multichannel loudspeaker configuration.

The spatial transformations of the physically-based waveguide networks described here, as in earlier work, represent a desire to explore extended techniques of physical modeling synthesis, in this case using spatial processing. In both projects the possibilities of the embodiment of the model are being broadened. The virtual body is not confined to the same limitations as the physical body, and an extended technique is explored that blurs the boundaries between resonating body and acoustic space.

It was found that multi-channel diffusion of the modes stresses the coherence of the model, perceptually pulling apart the synthesis into constituent parts as the components are treated separately in space. This technique has been identified as an example of Spatio-Operational Spectral (SOS) Synthesis, and discussed in greater detail in another paper ([11]).

### 5.2. Spatialization of circular network topologies

For waveguide networks composed of many discrete sections, one approach to spatialization is to output each section separately. Figure provides a simple example; eight discrete sections of the type are arranged in a circle, with the output of each section routed to its own loudspeaker.

This type of configuration essentially sonifies the propagation of sound through the network, making it possible to hear the influence of particular regions of the network on their adjacencies. While there is no panning or illusion of motion in the traditional sense, cascades of audible activity around the network can produce a variety of interesting spatialization effects.

## 6. MUSICAL APPLICATIONS

### 6.1. That which is bodiless is reflected in bodies II (Burtner)

In the musical composition, *That Which is Bodiless is Reflected in Bodies II*, SOS synthesis is used to explore the threshold between physical and non physical reality. The composition takes as its starting and ending point the physical model bowl as a true acoustic representation of the physical body. In the piece, the physical object is transformed and explored as a multidimensional space that gradually disintegrates into nonphysical reality. The compositional process in the pieces draws on a gradual disembodiment and re embodiment of the acoustic nature of the bowl's physicality.

In order for the physical model to become a transformative emersive environment, the possibility of recreating a spatial representation of the transformational modal bowl is explored in the composition. Changes in modal properties of the bowl effectively alter the size and shape of the bowl. If the physical model bowl were a real bowl it would be seen changing dynamically in space. Extending this principle from an exteriorization of sound to an interior perspective, if the listener is positioned inside the bowl as a type of room, the room would be changing shapes around the listener.

In order for the listener to effectively experience these changes in a performance context, modal transformations of the bowl are linked with spatial propagation of the sound. To accomplish this, each mode of the multichannel bowl discussed above, was assigned to a separate, distinct audio channel. Figure 2 details the implementation of this configuration.

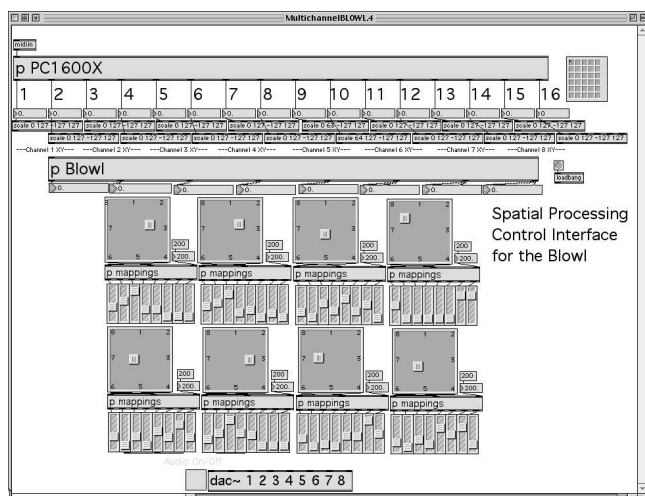


Figure 2: Max/MSP interface for the extended bowl.

The output of the modes are coordinated in a spatial configuration surrounding the listener. As the modes change, the spatial location of the signal changes accordingly. *That which is bodiless is reflected in bodies II* draws the listener close to and then inside the acoustics of the resonating bowl. Once inside the bowl, the modes are multiplied generationally, and the sound environment diverges from any physical representation, becoming an abstract auditory environment built from waveguide networks. *That which is bodiless is reflected in bodies II* offers an initial example of how physically-based modal waveguide synthesis can function as an extended technique in combination with spatial processing.

### 6.2. Cage "Electronic Music for Piano"

Our first application of a peak-managed feedback network was for a realization of John Cage's *Electronic Music for Piano* [12]. In keeping with the increasingly improvisatory nature of Cage's approach to music with live electronics during the 1960s, the handwritten prose score of *Electronic Music for Piano* is suggestive, not prescriptive. Inspired by and in appreciation of Cage and especially dedicatee David Tudor's work in the domain of feedback, we designed this version around a feedback network, implemented using Miller Puckette's Pd software [13]. The feedback network is the most prominent of several parallel signal processing chains applied improvisationally to a live performance of Cage's *Music for Piano 69-84* [14]. The network represents the most extreme form of signal processing in the realization, in that the sustaining, swooping output sounds utterly unlike the piano input.

The feedback section of the instrument passes the two microphone inputs into a circular chain of delay structures, with sixteen delay lines grouped in eight sections. Although each section has two delays, these are not configured as upper and lower rails, and there is only one polarity inversion in the entire structure. Each of the delay lines has a continuously variable length. These lengths are randomly and independently generated for each delay, as are the sweep and sustain times which control the transitions between each new length.

Despite the emphasis on the algorithmic generation of low-level parameters, there is a role for an electronics operator to improvise and intervene during the performance. The operator has access to global scaling factors for each of three delay parameters (delay length, sweep time, sustain time). These scaling factors allow the operator to compress or expand the parameter ranges available to the algorithms. There is also a single parameter controlling all the (identical) gain coefficients of the network. This is certainly the operator's single most influential parameter over the behavior of the network. Finally, the operator has eight selectable output volume presets, each of which independently modifies the output gain stages associated with the eight different loudspeakers, as well as the ability to mute individual loudspeakers. Each preset has its own spatial distribution and weighting of different segments of the feedback network.

The electronics operator, through the parameters mentioned above, and the pianist, via the microphone inputs, can influence the feedback network. However, they do not command it. The network performs in unpredictable ways, sometimes imitating onsets and pitches played at the piano very precisely, sometimes remaining quiet during busy passages, sometimes bursting into noise in the middle of a long silence. Because there is only one polarity inversion in the network, it tends towards the inaudible output of DC. The pianist can perturb the system into audibility by providing an excitation; the electronics operator can encourage the system to sound by raising the gain coefficients near unity, or by seeking a new configuration of delay lengths. The operator can also reliably squelch the feedback network output by turning the gain coefficients down to zero, or by muting the loudspeakers.

The unpredictable behavior of the destabilized feedback network, enhanced by the algorithmic generation of many of its parameters, is the primary feature of the *Electronic Music for Piano* realization. There is a symbiosis of piano, pianist, electronics, and operator; in performance the situation is one of improvising with the electronics, rather than using the electronics to improvise. The electronics are designed to guide the operator's musical choices

just as the operator guides the electronics. The emergent aspects of the electronics' behavior help foster intense listening and communication between pianist and electronics operator in performance.

### 6.3. "Hero and Leander" (Burns)

Following the Cage realization, more recent applied work with generalized waveguide networks utilizing peak management has focussed on the composition of multichannel tape music. In the more fixed environment of tape composition, the indeterminate aspects of the Cage realization's feedback network are less desirable, and so we have implemented a new and more pliable version of the network in Bill Schottstaedt's Common Lisp Music environment [15].

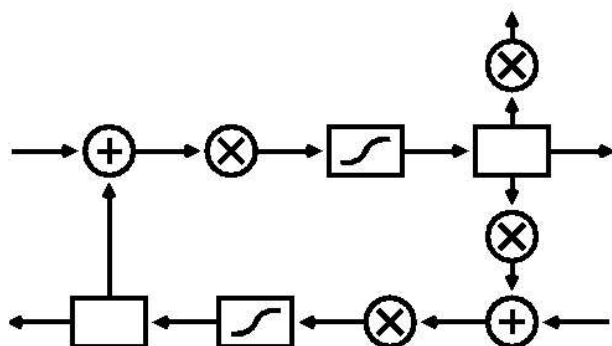


Figure 3: Block diagram for a waveguide-like section of a feedback network including nonlinear waveshaping, used in "Hero and Leander".

Like the Cage realization, the new design is built from a circular arrangement of eight sections. However, each section is much more closely modelled on a traditional waveguide, and therefore more stable and less likely to output DC, than in the Cage realization. The designs include upper and lower rails, and four of the eight sections include a polarity inversion. (If all eight sections included the sign change, the results would be more like a conventional physical model, and less like characteristic feedback sound of the Cage realization).

Figure 3 demonstrates the structure of one the sections which includes the polarity change. Compared to the operator's control over the Cage realization, the control parameters for this network are numerous and low-level. The excitation function is an arbitrary multichannel soundfile. The network provides time-varying envelopes for each of the sixteen delay lines, plus one time-varying envelope which controls all the gain coefficients.

If complex envelopes are used, there can be a large amount of information to specify. However, this parameterization provides for a wide variety of results, with a substantial amount of control over the sonic details of the network's output. Articulation characteristics and other sonic details are not exposed directly to the composer as parameters, but are accessible through the influence of delay lengths and gain coefficients.

## 7. CONCLUSIONS - WAVEGUIDES BEYOND PHYSICAL MODELING

The flexibility of waveguide synthesis allow to create different virtual instruments that are interesting from a musical prospective. This paper described various approaches of composition using digital waveguides, which will be played during the oral presentation.

## 8. REFERENCES

- [1] M. McIntyre, R. Schumacher, and J. Woodhouse, "On the oscillations of musical instruments," *Journal of the Acoustical Society of America*, vol. 74, no. 5, pp. 1325-1345, Nov. 1983.
- [2] Julius O. Smith, "Physical modeling using digital waveguides," vol. 16, no. 4, pp. 74-91, Winter 1992.
- [3] C. Sullivan, "Extending the karplus-strong algorithm to synthesize electric guitar timbres with distortion and feedback," *Computer Music Journal*, vol. 14, no. 3, pp. 26-37, 1990.
- [4] I. Xenakis, *Formalized Music*, Pendragon Press, New York, 1992.
- [5] P. Hoffmann, "The new gendyn program," *Computer Music Journal*, vol. 24, no. 2, pp. 31-38, 2000.
- [6] Julius O. Smith, "Waveguide filter tutorial," 1987, pp. 9-16, Computer Music Association.
- [7] G. Essl and P. Cook, "Banded waveguides on circular topologies and of beating modes: Tibetan singing bowls and glass harmonicas," in *Proc. International Computer Music Conference. ICMA*, 2002, pp. 49-52.
- [8] S. Serafin, M. Burtner, C. Nichols, and S. O'Modhrain, "Expressive controllers for bowed string physical models," in *Proc. DAFX 2001, Limerick, Ireland*, 2001.
- [9] M. Burtner and S. Serafin, "Extended techniques for physical models using instrumental controller substitution," in *Proceedings of ICMC 2001, La Havana, Cuba*, 2001.
- [10] M. Burtner and S. Serafin, "Strictly bowlroom: the physically modeled singing bowl in a transformative immersive environment," in *Proceedings of ISMA, Mexico-City, Mexico*, 2002.
- [11] D. Topper, M. Burtner, and S. Serafin, "Spatio-operational spectral (sos) synthesis," in *Proceedings of Cost-DAFX, Hamburg, Germany*, 2002.
- [12] J. Cage, "Electronic music for piano," .
- [13] M. Puckette, "Pure data," in *Proceedings of the International Computer Music Conference.*, ICMA, 1996, pp. 269-272.
- [14] J. Cage, "Music for piano 69-84," .
- [15] B. Schottstaedt, "Clm - music v meets common lisp," *Computer Music Journal*, vol. 18, no. 2, pp. 30-37, 1994.

## **SYNTHESIS OF VOICED SOUNDS BY MEANS OF WAVEFORM ADAPTIVE PHYSICAL MODELS**

*Carlo Drioli*

Laboratory of Phonetics and Dialectology (IFD)

ISTC-CNR, Italy

`carlo.drioli@csr.fpd.cnr.it`

### **ABSTRACT**

The reproduction of voiced sounds by physical modeling is addressed. A major focus is put on the possibility of fitting a physically constrained model to real voice samples. A source-filter scheme is adopted in which the vocal tract is represented by an all-pole filter and the voice source model relies on a lumped mechano-aerodynamic scheme inspired by the mass-spring paradigm. The vocal folds are represented by a mechanical resonator plus a delay line which takes into account the vertical phase differences. The vocal fold displacement is coupled to the glottal flow by means of a general parametric nonlinear model. An adaptive data-driven identification procedure is outlined, where the parameters of the model are tuned in order to accurately match the target speech waveform. The simultaneous optimization of the source and the vocal tract parameters is discussed. A recursive algorithm based on the Kalman filtering approach is proposed and evaluated. The performance on time varying voiced signals is discussed.

### **1. INTRODUCTION**

Synthesis of speech by numerical methods has evolved considerably since the first experiments in the 1960s. In the first speech synthesis and text to speech conversion systems, the principal concern was to produce an output with a sufficient level of intelligibility. The audio quality of the final result was however often poor and speech sounded unnatural. Intelligibility seems to have reached nowadays a sufficiently high level, and new challenges have emerged. The audio quality of the synthesis, the naturalness of speech and the rendering of the emotions, are among the new targets in speech synthesis technologies.

The source-filter model of speech production, in which a source of excitation is convolved with a filter reproducing the formant structure [1], is today a widespread scheme for synthesis and coding applications. In formant synthesis, a series and/or a parallel of resonances (modelling the vocal tract configuration) is excited by a pulse waveform or by noise. Linear predictive coding (LPC) synthesis is based on the same source-filter scheme, although it provides an automatic analysis procedure to extract the vocal tract filter parameters from the sampled speech waveform. Often speech production is assumed to be a time-varying ARMA process, in the aim of dealing with the time-varying nature of the voiced signal [2]. This modelling approach is effective in representing the nasal and vocal tract transfer functions, but fails to provide a reasonable model of the voice source, and to represent the nonlinear phenomena involved in the voice generation. To overcome this limitation, attempts have been made to refine the original ARMA representation. The searched directions include the embedding of some

kind of refined source model [3]. In many cases, an LF-like model [4] is the preferred choice. The use of physical glottal models has been evaluated as well, although the parametric fitting to sampled waveforms has turned out to be extremely complex in this case. A quasi-articulatory speech synthesizer which uses a one-mass model for the source and a waveguide digital filter model for the vocal tract is described in [5]. In order to fit the model to natural speech, an adaptive procedure to build articulatory parameter vectors for stationary sounds and for transitions is used. To avoid the computational overload required for the solution of finite difference equations describing the vocal tract, a hybrid solution is proposed in [6], in which the glottal excitation is calculated in the time-domain by means of a physiological glottis model, and the vocal tract is modeled in the frequency domain.

Numerical models of the voice source production based on the physiology of the vocal folds have been proposed since 1968 by Ishizaka and Flanagan [7, 8]. In brief, in the IF model each of the vocal folds is represented by two damped mass-spring systems coupled to each other. In addition, a non-linear interaction with the airflow is derived from aerodynamic equations describing the pressure drops from lungs to vocal tract. A wide range of variations and improvements have been proposed since the introduction of the original one- and two-mass models [9, 10, 11, 12, 13]. Although these models contributed substantially to the understanding of the phonation process, their complexity prevented them from being widely adopted in practical coding and synthesis applications.

In this paper, the synthesis of voiced sounds by means of a waveform adaptive physical model is discussed. The speech production model adopted here relies on a source-filter configuration, in which the vocal tract is modeled as a linear filter and the glottal source is modeled as a low-dimensional dynamical model of the vocal folds. The voice production model is introduced in Sec. 2. An adaptive data-driven identification procedure is outlined in Sec. 3: the parameters of the model are tuned recursively in order to accurately match the target speech waveform. The simultaneous optimization of the source and the vocal tract parameters is discussed. The algorithm is evaluated on a voice sample which exhibits time-varying characteristics, and the performance of the algorithm is discussed.

### **2. VOICE PRODUCTION MODEL**

The speech production model adopted here consists of a glottal model, which generates an excitation signal, and a vocal tract model. Usually, a radiation model is also considered at the end of the voice production chain. In the following, we consider the radia-

tion model to be included in the glottis model. In other words, the output of the glottal model is assumed to be the derivative of the glottal flow. The glottal model is based on the physically inspired schemes introduced in a previous study [14], and is reproduced in Fig. 1.

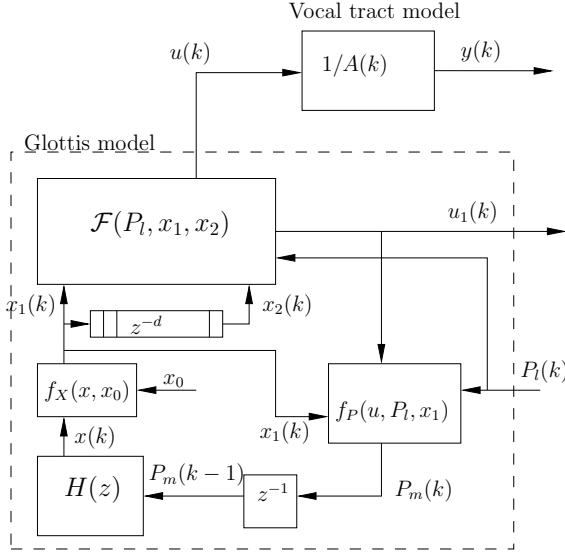


Figure 1: The speech production model for voiced sounds

We briefly recall here the principal characteristics and functional aspects of the glottal model. A more detailed description can be found in [14]. The structure is basically a one-mass model with an embedded parametric nonlinearity. The resonant filter  $H(z)$  represents the oscillating folds, the block  $f_X(x, x_0)$  reproduces the impact distortion on the fold displacement and adds an offset  $x_0$  (the resting position of the folds). The delay line  $z^{-d}$  simulate the propagation of the motion along the thickness of the fold. The block  $f_P(u, P_l, x_1)$  computes the driving pressure  $P_m$  acting on the folds from the flow  $u$  and the fold displacement. Finally, the parametric nonlinearity  $\mathcal{F}(P_l, x_1, x_2)$  represents the flow model, i.e. it converts the glottis area given by the fold displacement into the airflow at the entrance of the vocal tract. Two flow component ( $u_1$  and  $u$ ) are drawn in the scheme:  $u_1$  is a rough flow model computed as a signal proportional to the glottal area function, and  $u$  is the total flow signal which includes the adaptive parametric part. The difference will be further discussed in Section 4.

### 3. ESTIMATION OF THE GLOTTAL SOURCE AND VOCAL TRACT PARAMETERS

The measurement signal  $y(k)$  is described by

$$y(k) = -\sum_{i=1}^N a_i y(k-i) + u(k) + n(k) \quad (1a)$$

$$u(k) = \mathcal{F}(P_l(k), x_1(k), x_2(k)) \quad (1b)$$

$$x_1(k) = \mathcal{V}_1(u(k), P_l(k)) \quad (1c)$$

$$x_2(k) = \mathcal{V}_2(u(k), P_l(k)) \quad (1d)$$

where  $u(k)$  is the flow excitation signal,  $n(k)$  is the measurement noise,  $P_l(k)$  is an estimate of the lung control pressure,  $x_1(k)$  and

$x_2(k)$  represent the oscillating edges of a rough mechanical representation of the vocal folds. The terms  $\mathcal{V}_1$  and  $\mathcal{V}_2$  represent the mechanical parts involved in the oscillation, and contain the resonant second order filter (a mass-spring element) and. This part also contains a delay of at least one sample to make the feedback scheme computable. Given that a parametric model of the flow is used, we can write  $u(k)$  as

$$u(k) = \sum_{i=0}^M w_i(k) \psi_i(P_l(k), x_1(k), x_2(k)). \quad (2)$$

Let us introduce the following vectors:

$$\theta(k)^T = [a_1(k) \ a_2(k) \ \dots \ a_N(k) \ w_0(k) \ w_1(k) \ \dots \ w_M(k)] \quad (3)$$

$$\phi(k)^T = [-y(k-1) \ -y(k-2) \ \dots \ -y(k-N) \ \psi_0(k) \ \psi_1(k) \ \dots \ \psi_M(k)], \quad (4)$$

where  $a_i(k)$ , ( $i = 1 \dots N$ ), are time-varying AR parameters, and  $w_j(k)$ , ( $j = 0 \dots M$ ), are the output layer weights of the parametric nonlinearity which is part of the glottal model embedded in the speech production model. The functions  $\psi_i(k)$  are nonlinear regressors of the inputs  $x_1(k)$ ,  $x_2(k)$ , and  $P_l(k)$ . We can rewrite the first of equations (1) as

$$y(k) = \phi(k)^T \theta(k) + n(k), \quad (5)$$

We note that part of the speech production model, namely the vocal tract and the output layer of the parametric flow model, can now be combined to form a linear ARMA scheme. We rely on this property to propose an adaptive scheme for the simultaneous estimation of the vocal tract model and of the input flow waveform.

We define an estimation signal  $\hat{y}(k|k)$  and a prediction signal  $\hat{y}(k|k-1)$  respectively as

$$\hat{y}(k|k) = -\sum_{i=1}^N a_i(k) y(k-i) + \sum_{i=1}^M w_i(k) \psi_i(k) \quad (6)$$

and

$$\hat{y}(k|k-1) = -\sum_{i=1}^N a_i(k-1) y(k-i) + \sum_{i=1}^M w_i(k-1) \psi_i(k), \quad (7)$$

in which the term  $\sum_{i=1}^M w_i(k-1) \psi_i(k)$  can be viewed as a prediction of the voice source signal at time  $k$ :

$$u(k|k-1) = \sum_{i=1}^M w_i(k-1) \psi_i(k). \quad (8)$$

We can now sketch a recursive identification method to update the parameters  $a_i$  and  $w_i$  to a current estimate, on the basis of the prediction error  $\epsilon(k) = y(k) - \hat{y}(k|k-1)$ . First, however, let us note that the remaining parameters of the glottal model (e.g., the resonance frequency of the mass-spring system, the mass resting position, and other parameters depending on the choice of the model) are hidden in the term  $\psi_i(k)$ . Those parameters can be updated with a separate procedure before the linear regression recursion update. To express this we introduce the terms

$$u'(k|k-1) = \sum_{i=1}^M w_i(k-1) \psi_i(k|k-1), \quad (9)$$

where  $\psi_i(k|k-1)$  are the values of the nonlinear regressors before the adaptation, and

$$\hat{y}'(k|k-1) = - \sum_{i=1}^N a_i(k-1)y(k-i) + u'(k|k-1), \quad (10)$$

is the corresponding predicted output.

Let us now return to the recursive update of the ARMA part of the scheme, and assume that the evolution of the parameters in  $\theta$  can be described by the stochastic equation

$$\theta(k) = \theta(k-1) + q(k), \quad (11)$$

$$\text{cov}[q(k)] = Q, \quad (12)$$

the prediction step (a-priori estimate) is

$$\hat{\theta}(k|k-1) = \hat{\theta}(k-1|k-1) \quad (13)$$

$$\hat{y}(k|k-1) = \phi(k)^T \hat{\theta}(k|k-1) \quad (14)$$

$$\epsilon(k) = y(k) - \hat{y}(k|k-1) \quad (15)$$

and the a-posteriori estimate step is

$$\Sigma(k) = \Sigma(k-1)\phi(k)[R + \phi(k)^T \Sigma(k-1)\phi(k)]^{-1} \quad (16)$$

$$\hat{\theta}(k|k) = \hat{\theta}(k|k-1) + K(k)\epsilon(k) \quad (17)$$

$$\hat{y}(k|k) = \phi(k)^T \hat{\theta}(k|k) \quad (18)$$

$$\Sigma(k) = \Sigma(k-1) - K(k)\phi(k)^T \Sigma(k-1) + Q \quad (19)$$

in which  $q(k)$  is a noise vector with covariance  $Q$ ,  $K(k)$  is the Kalman gain,  $R$  is the variance of the measurement noise  $n(k)$ , and  $\Sigma(k)$  is the covariance of the estimate error. The recursion can be implemented on a sample by sample basis ( $k$  reads as the sample index in this case) or on a signal frame basis (and  $k$  reads as the frame index). The production model identification is applied here on a frame basis, and the sequence of operations that are performed at each frame of the signal reads as

1. Extract the current pitch and run the speech model using the flow and vocal tract parameters from previous frame.
2. Fine tune the mechanical parameters of the glottal model (e.g., fold tension and thickness) with a nonlinear Least Squares procedure.
3. Simultaneously update the glottal flow and the vocal tract parameters with the ARMA recursion described in (11)-(19).

#### 4. EXPERIMENTAL RESULTS

The simultaneous source-vocal tract identification scheme proposed is tested in this section on a time-varying voice signal. The nonlinear regressor layer is chosen to be a physically inspired regressor

$$\psi_0(P_l, x_1, x_2) = \sqrt{P_l} \min\{x_1, x_2\}, \quad (20)$$

and of a set of local gaussian kernels

$$\begin{aligned} \psi_j(P_l, x_1, x_2) &= \exp\left(-\frac{(P_l - m_{1j})^2 + (x_1 - m_{2j})^2 + (x_2 - m_{3j})^2}{\sigma_j^2}\right), \\ j &= 1, \dots, M, \end{aligned} \quad (21)$$

where  $(m_{1j}, m_{2j}, m_{3j})$  is the centroid of the  $j$ th 3-dimensional gaussian kernel,  $\sigma_j$  is the kernel width, and  $M$  is the number of gaussian regressors. The 3-dimensional centroid and width of the gaussian kernels have to be chosen before the identification procedure. In the following examples, the choice was to locate the  $M$  kernels equally spaced along the trajectory described by one period of the target speech signal (i.e., the centroids were selected among input triples  $(P_l, x_1, x_2)$  from a period in the training set). For this experiment, a set of  $M = 50$  gaussian units was used. The signal from the regressor  $\psi_0(P_l, x_1, x_2)$  is a rough version of the glottal flow, and we refer to this flow component as  $u_1 = w_0\psi_0(P_l, x_1, x_2)$ . This signal is useful to monitor the tuning of the mechanical part of the system with the target signal (see Fig. 2).

The voice signal was sampled at 16 bits, 16 kHz, from a male speaker uttering the vowel /a/ with slowly varying pitch (the average pitch being around 140 Hz). The signal was analyzed with the recursive algorithm using non-overlapping frames of 256 samples, corresponding approximately to 2 periods.

The resonance frequency of the filter  $H(z)$  is initially set around the pitch of the voiced sound, computed by a pitch detection algorithm. A driving pressure  $P_l(k)$  is generated as the short-time energy of  $y(k)$ , and the glottal model is run for the duration of the frame. The signals  $u'_1(k|k-1)$ ,  $u'(k|k-1)$ ,  $\hat{y}'(k|k-1)$ . The fold displacement signal  $x_1$  is a quasi-sinusoidal oscillation tuned with the pitch. It is distorted with a zero threshold to generate a discontinuity similar to the one due to the collision of the folds, and that will help the nonlinear layer in estimating the closed-phase of the flow. A second displacement  $x_2$  is generated with a delay-line  $z^{-d}$ , with  $d$  set in the range 1-20. The tuning of the mechanical parts via a LS procedure is performed in order to minimize a distance measure of  $\hat{y}'(k|k-1)$  from  $y(k)$ . The signals  $u_1(k|k-1)$ ,  $u(k|k-1)$ ,  $\hat{y}(k|k-1)$ , are generated after this adaptation. The next step is the adaptation of the parameters  $w_i$  and  $a_i$  of the model via the recursive algorithm described in (11)-(19). An order of 10 was used for the vocal tract filter. This will provide us with the final source signal estimates  $u(k|k)$  and  $\hat{y}(k|k)$ .

The results of the adaptation are shown in Figs. 2 and 3. It can be seen that the rough flow signal  $u_1$  follows the pitch of the target signal and its time-evolution in general. Moreover, the close phases and closure instants are synchronized with the target waveform  $y$ . The second and third signals from top are respectively the source and the speech signal estimates ( $u$  and  $\hat{y}$ ) coming from the simultaneous identification. The picture demonstrates a good reproduction of the target waveform and a coherent estimate of the glottal source, even though some artifacts can be noticed in the estimated signal. The artifacts are mainly due to frame transitions in this case (the figure reproduces 3 training frames). Finally, Fig. 3 shows a comparison between the vocal tract transfer function obtained with autocorrelation LPC and the one obtained with the proposed method. It is evident that the energy contribution due to the voice source present in the LPC filter is noticeably reduced in the filter obtained with the simultaneous source-vocal tract estimation procedure.

As a final remark, we note that the solution shown is not unique, since no target source is available for the voice source. The solution achieved by the algorithm is one of the possible source/vocal tract separations, and in general even a different order of the vocal tract filter could lead to an unrealistic source waveform shape. A possible improvement, under evaluation, is to include an inverse filtering stage based on a covariance LPC analysis. This step could

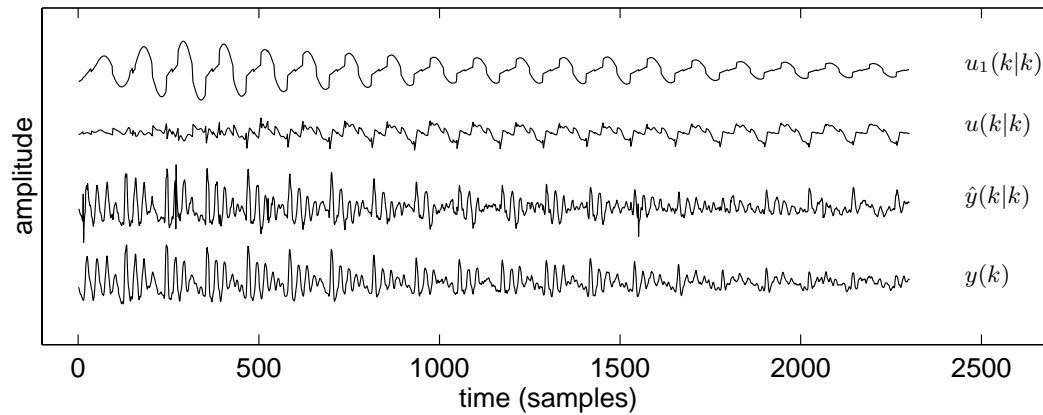


Figure 2: Identification results in the time domain.  $u_1(k)$ : output of the regressor  $\psi_0$ . This signal represents a rough glottal flow derivative, and it is useful to monitor the tuning of the mechanical part of the system with the target signal;  $u(k)$ : estimated voice source;  $\hat{y}(k)$ : reconstructed signal;  $y(k)$ : target signal.

be used to generate an inverse filtered target signal to drive the source signal estimation, and could be used to initialize the recursion.

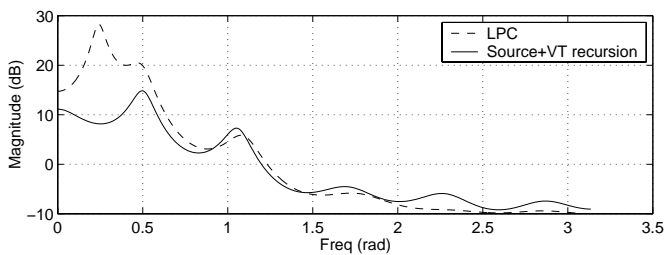


Figure 3: Comparison of the vocal tract transfer functions obtained with LPC and with the proposed method.

## 5. CONCLUSIONS

A speech production model embedding a vocal fold model based on a one-mass schema and enhanced with a data-driven identification component, was discussed. A data-driven analysis/synthesis procedure was described, that allows the model to fit to an arbitrary time-varying speech waveform. The algorithm performs a simultaneous estimate of the voice source and of the vocal tract, on the basis of a rough flow signal generated by the glottal model tuned with the target signal.

## 6. ACKNOWLEDGEMENTS

Part of this research was supported through the European Community Marie Curie Fellowship No. HPMT-2000-00119.

## 7. REFERENCES

- [1] G. Fant, "Some problems in voice source analysis," *Speech Commun.*, vol. 13, pp. 7–22, 1993.
- [2] Y. Miyanaga, N. Miki, and N. Nagai, "Adaptive identification of a time-varying ARMA speech model," *IEEE Transactions on Acoustics, Speech and Signal Processing*, vol. ASSP-34, no. 3, pp. 423–433, June 1986.
- [3] M. Fröhlich, D. Michaelis, and H. W. Strube, "SIM-simultaneous inverse filtering and matching of a glottal flow model for acoustic speech signals," *J. Acoust. Soc. Am.*, vol. 110, no. 1, pp. 479–488, July 2001.
- [4] G. Fant, J. Liljencrants, and Q. Lin, "A four-parameter model of glottal flow," *STL-QPSR*, pp. 1–13, 1985.
- [5] P. Meyer, R. Wilhelms, and H. W. Strube, "A quasiarticulatory speech synthesizer for German language running in real time," *J. Acoust. Soc. Am.*, vol. 86, no. 2, pp. 523–539, August 1989.
- [6] M. M. Sondhi and J. Schroeter, "A hybrid time-frequency domain articulatory speech synthesizer," *IEEE Trans. Acoust. Speech Signal Process.*, vol. ASSP-35, pp. 955–967, 1987.
- [7] J. L. Flanagan and L. L. Landgraf, "Self-oscillating source for vocal-tract synthesizers," *IEEE Trans. Audio and Electroacoustics*, vol. AU-16, pp. 57–64, 1968.
- [8] K. Ishizaka and J. L. Flanagan, "Synthesis of voiced sounds from a two-mass model of the vocal cords," *The Bell Syst. Tech. J.*, vol. 51, no. 6, pp. 1233–1268, July-August 1972.
- [9] K. Ishizaka and J. L. Flanagan, "Acoustic properties of longitudinal displacement in vocal cord vibration," *The Bell Syst. Tech. J.*, vol. 56, no. 6, pp. 889–918, July-August 1977.
- [10] T. Koizumi, S. Taniguchi, and S. Hiromitsu, "Two-mass models of the vocal cords for natural sounding voice synthesis," *J. Acoust. Soc. Am.*, vol. 82, no. 4, pp. 1179–1192, October 1987.
- [11] I. R. Titze, "The physics of small-amplitude oscillations of the vocal folds," *J. Acoust. Soc. Am.*, vol. 83, no. 4, pp. 1536–1552, April 1988.
- [12] N. J. C. Lous, J.C.J. Hofmans, R. N. J. Veldhuis, and A. Hirschberg, "A symmetrical two-mass vocal-fold model coupled to vocal tract and trachea, with application to prosthesis design," *Acta Acoustica*, vol. 84, pp. 1135–1150, 1998.
- [13] J. Liljencrants, "A translating and rotating mass model of the vocal folds," *STL-QPSR*, pp. 1–18, April 1991.
- [14] C. Drioli, "A flow waveform adaptive mechanical glottal model," *STL-QPSR*, vol. 43, pp. 69–79, 2002.

# THE DEVELOPMENT OF A MODULAR PARADIGM FOR THE PHYSICAL MODELLING OF MUSICAL INSTRUMENTS

*Dr. I. Drumm*

The School of Acoustics and Electronic Engineering,  
The University of Salford, Manchester, U.K.

`i.drumm@salford.ac.uk`

## ABSTRACT

The manuscript will describe ongoing research by the author to investigate, develop and evaluate a modular and extensible paradigm for the software based construction of physical models of real musical instruments.

The software makes full use of object orientated programming techniques to construct a user friendly application for the interconnecting of key components of musical instruments such as excitation mechanisms, wave-guides, resonators and environments by using a flexible exchange of parameters beyond the processing of an audio stream. The project aims to consolidate the previous research findings of the wider community and further investigate the relative influence and interconnection of physical components.

## 1. INTRODUCTION

Early sound synthesis techniques such as the addition of multiple harmonic oscillators or the filtering of harmonically rich single oscillators [1] have been complimented in recent years with frequency modulation [2], granular [3] and wave-table synthesis techniques. All techniques have their own strengths and weaknesses when it comes to acoustic simulation and creative potential so many modern synthesizers offer the ability to mix and match.

Modular sound synthesis is not new being originally based on interconnected analogue hardware; it has found new popularity within recent software based synthesizers. However these modular synthesizers do not simulate the underlying mechanical processes of sound generation, so fail to recreate many of the subtleties of real musical instruments.

Physical modeling of musical instruments is where the elements of sound generation are simulated by software in terms of the behavior and interaction of physical mechanisms within virtual musical instruments. The real-time application of sophisticated physical modeling is relatively new having been facilitated by developments in ever more powerful digital hardware. The project aims to explore how a modular approach to physical modelling can be implemented using object orientated programming techniques together with Cakewalk's popular DXi2 application programming interface [4] to facilitate real-time performance and musical acoustics research. The project

not only aims to explore how popular techniques (delay lines, filtering, flow control functions, etc) can be flexibly interchanged, but also how other predictive techniques such as two port analysis [5], wave digital elements [6] and maybe even finite element analysis and ray tracing can be incorporated into a modular framework.

## 2. IMPLEMENTATION

### 2.1. Software Development

It was decided to implement the software as a DXi2.0 plugin for incorporation within popular sequencer packages such as Cakewalk and Sonar. The DXi2.0 API provides classes that take care of the parsing midi note events directly from a keyboard (or recorded sequences) and enable the programmer to generate audio data on the fly for real-time rendering.

For example inheriting from the class CDXi one can override the method

```
CDXi::InitializeNoteEvent(DXiEvent& de)
```

which is called when a new note is pressed. The parameter 'de' is an object that includes an integer 'de.me.m\_byKey' representing the key pressed. The corresponding equal temperament intervals and hence length of main waveguide are given by

$$\frac{f}{f_{root}} = 2^{\pm \frac{n}{12}} = \left( \frac{L}{L + \Delta L} \right)^{\pm 1} \quad (1)$$

where  $n$  is the number of notes relative to a chosen root and  $L + \Delta L$  is the length of the arrays representing the waveguide. An all pass filter was included for fine tuning.

Hence within the method

```
CDXi::Process( ... )
```

the waveguide array can be tapped for each iteration and an audio output buffer set in real-time.



## 2.2. The Base Component

The polymorphic features of object oriented programming facilitate a modular approach to physical modeling. Typically very different components (waveguides, filters, etc) need to have common core elements to enable them to be managed together and interlinked. Such components can be represented by programming objects instantiated from very different classes; that nevertheless are derived from a common base class.

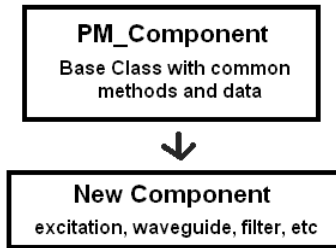


Figure 1: Classes for new components inherit from a PM\_Component base class

In the author's implementation all physical modeling components share the common base class PM\_Component (figure 1) which is itself a derivative of a dialog box class. Hence each sub class can have its own user interface associated with it.

The PM\_Component class contains an object of type PM\_DataObj which will contain all the data associated with a given object. The class from which data objects are instantiated is...

```

class PM_DataObj {
public:
    int type, on, delay_size, delay_size2;
    float y, a,b,c,d;
    float x [MAXSIZE], x2 [MAXSIZE];
}
    
```

Crucially the data object offers the programmer a selection of variables and arrays that he/she may or may not choose to use when developing a new physical modeling component.

For example a waveguide could use the two arrays to represent wave propagation whereas an FIR filter could use arrays to hold an impulse response and a history of previous inputs. Further the arrays could be used to represent respective real and imaginary parts of a set of complex parameters or a complex function across a frequency range.

Clearly there will be redundancy with regards memory, for example a damper component would only need use the y variable to contain a new attenuated output. However as objects link to each other's data via pointers (figure 2), they can be very selective about what information they care to access depending on the type of component they link to. Hence there is no unnecessary exchange of data between iterations.

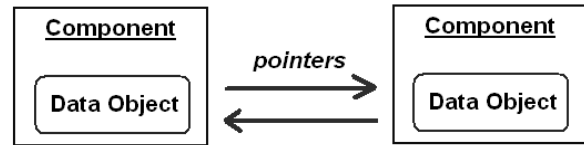


Figure 2: Each component has a data object accessible to others via a pointer

The base class PM\_Component also contains the methods...

Init() called when some parameters are set

NoteStart() called when a new note starts

Iterate() called every sample duration

As these methods are declared as virtual their default functionality can be over-ridden to suit the type of physical modeling component involved.

## 2.3. Linking Components

In order to link components in a processing chain, a set of link objects can be created dynamically by the user. Each link object specifies the component which data will come from and the component which data goes to.

The current simple user interface (figure 3) allows the user to select from a drop down list box a selection of physical modeling components that may be used, i.e. selected and instantiated. Hence he or she can then specify a set of 'from->to' links building up the system.

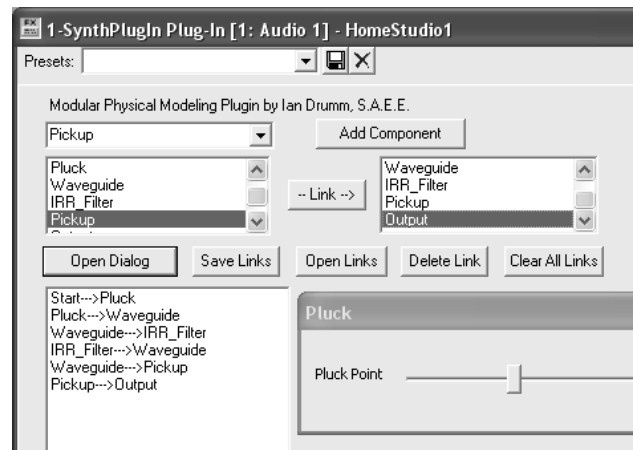


Figure 3: The user can create 'from-> to' links by selecting from instances of components as shown in two list boxes.

When a new note is pressed, the algorithm goes through the list of links and calls all the 'NoteStart()' methods of objects that have been linked to, hence initializing note specific parameters.

Subsequently all 'Iterate()' methods are called repeatedly, i.e. every sample duration, until the note terminates or decays.

For example figure 4 shows a simple string model [7], when all 'NoteStart()' methods are called the 'Pluck' component will set both delay lines. Subsequently when 'Iterate()' methods are

called the 'Pluck' component does nothing, where as the 'Waveguide' component shifts data in delay lines, which are hence accessed by 'Damper', 'Biquad filter' and 'Pickup' components.

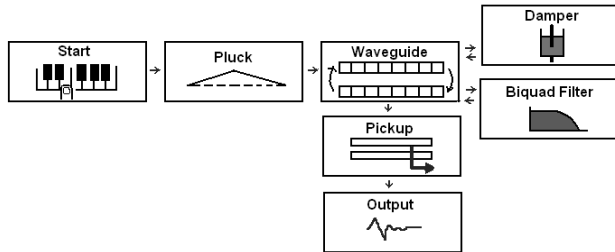


Figure 4: Linking components to represent a simple physical model of a string.

Each component has a dialog box to access important parameters specific to that component. Some times components may need to exchange data or perform calculations when a parameter changes or new data is loaded. For example a 'Data from file' component can be used to load impulse response data into a 'FIR filter' component as shown in figure 5. In such an event the 'Init()' method of each component is called. Surprisingly relatively large (>500 data points) convolutions can be performed easily within large physical models, in real time, given typical modern CPUs (>1GHz).

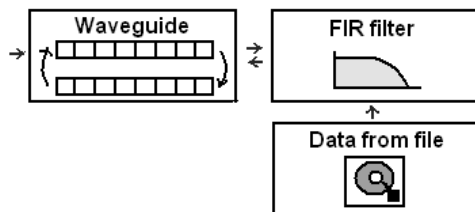


Figure 5: An FIR filter gets impulse response data from a 'Data from file' component.

## 2.4. Options for more advanced models

It is intended that an ever expanding range of component types be added to the plug-in. For example the addition of noise source, single delay and flow control components allow the development of simple wind instrument models. For example a simplified flute model [8] as shown in figure 6 could emulate the interaction of an air reed with the wave guide. 'Tap' and 'Junction' components help with the routing of data.

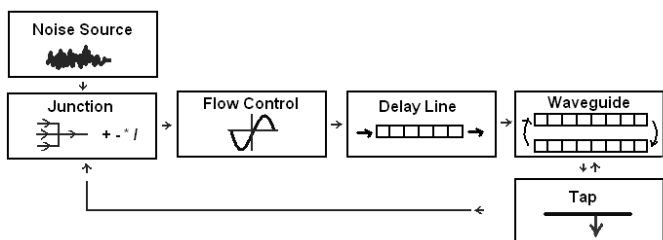


Figure 6: Linking components to represent part of a simplified model of a flute

As suggested earlier the paradigm also lends itself to acoustic prediction beyond the processing of an audio stream. For example there are a variety of methods for predicting the frequency response of a complex impedance termination which can hence be used with a waveguide's characteristic impedance to determine a reflection function. The complex reflection function can in turn be used to calculate the appropriate impulse response hence filter coefficients.

For example the input impedance of the bell of a wind instrument can be determined using two port analysis. This assumes the input impedance of uniform cylindrical section of a pipe of length  $L$  can be represented by

$$\begin{bmatrix} p_0 \\ u_0 \end{bmatrix} = \begin{bmatrix} \cos(kL) & j \frac{\rho_0 c}{S} \sin(kL) \\ j \frac{S}{\rho_0 c} \sin(kL) & \cos(kL) \end{bmatrix} \begin{bmatrix} p_L \\ u_L \end{bmatrix} \quad (2)$$

where  $k$  is wave number. By multiplying the matrices of a large number of sections of differing cross-sectional area  $S$  the input impedance of a conical section can be evaluated. Although the author's implementation allows the linkage of such matrices it also provides a component to multiply multiple such matrices whose cross-sectional areas are informed an array representing the horn shape.

As shown in figure 7 other components link the resulting input impedance to waveguide by invoking an inverse Fourier transform to calculate the appropriate impulse response.

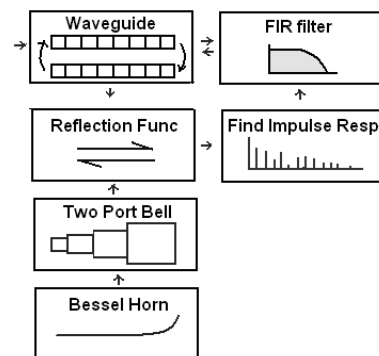


Figure 7: Linking components to represent part of a model of a wind instrument where the complex input impedance of a bell informs the behavior of a FIR filter.

Another way to explore the influence of boundary conditions is by the construction of equivalence circuits [9]. For example the application of circuit theory can be used to model the second order vibration of an acoustic guitar bridge and body [10]. Determination of the corresponding bridge impedance lends itself to the modular approach. The author also aims to explore the application of wave digital elements within the implementation [6].

Polyphony is also possible within the paradigm suggested via the judicious routing of note events to multiple instances of the main waveguide. For instruments with a particularly large number of waveguides (e.g. pianos) the computational expense of managing a large number of waveguide instances can be to some extent avoided by providing components that interpolate between important parameters – though this is still to be explored.

### **3. CONCLUSIONS**

The author seeks to develop a flexible approach to physical modeling within a real-time performance and sequencing environment (i.e. Cakewalk/Sonar). Early implementations have demonstrated the feasibility and merit of such an approach that offers a low CPU overhead between iterations whilst also providing flexibility, well beyond simply processing an audio stream.

### **4. REFERENCES**

- [1] Moog, R. (1965) "Voltage Controlled Electronic Music Modules", Journal of the Audio Engineering Society, Vol. 13, Number 3 pp. 200
- [2] Chowning, J. (1977) "The Synthesis of Complex Audio Spectra by Means of Frequency Modulation," Journal of the Audio Engineering Society 21(7), 1973; reprinted in Computer Music Journal 1(2),.
- [3] Roads, C. "Granular synthesis of sound. In Foundations of Computer Music.", C. Roads and J. Strawn, eds. MIT Press, Cambridge, pp. 145—159, 1985.
- [4] Twelve Tone Systems, "Cakewalk Plug-In Development Kit", [www.directxfiles.com](http://www.directxfiles.com)
- [5] Darlington, P., "Acoustic Two Port Pages", <http://www.geocities.com/drddarlington/twoportsa>
- [6] Smith, J. O., "Finite Difference Methods in Wave Digital Modeling", [ccrma.stanford.edu/~jos/lumped/](http://ccrma.stanford.edu/~jos/lumped/), 2003-03-01
- [7] Karplus, K. & Strong, A.(1983). Digital Synthesis of plucked-string and drum timbres. Computer Music Journal, 7(2), 43-55.
- [8] Cook, Perry, "A Meta-Wind-Instrument Physical Model, and a Meta-Controller for Real Time Performance Control", Proceedings of the ICMC, 1992.
- [9] Beranek, L. – "Acoustics". - New York : American Institute of Physics for the Acoustical Society of America, 1986.
- [10] Cuzzicoli, G and Lombardo, V, "A physical model of a classical guitar including players touch", Computer Music Journal 23, no. 2 (1999): 52-69 (18 pages)

## THE PRINCIPLE OF CLOSED WAVETRAINS, RESONANCE AND EFFICIENCY: PAST, PRESENT AND FUTURE

Georg Essl

Perry R. Cook

Computer & Information Science & Engineering  
University of Florida  
gessler@cise.ufl.edu

Computer Science Department  
Princeton University  
prc@cs.princeton.edu

### ABSTRACT

The principle of closed wavetrains asserts the equivalence of the condition of a traveling wave closing onto itself in phase to the occurrence of a mode. This principle provides a direct conceptual link between spectral descriptions of dynamic responses and a path-based dynamic description. In this paper we present the history and development of the idea since d'Alembert first proposed traveling functional forms to solve the string equation. The subsequent argument between Daniel Bernoulli, Euler and him which led to the development of Fourier analysis and contemporary theories of partial differential equations. Other related developments include the development of chaos theory connected to Poincaré and others, asymptotic solutions associated with Rayleigh, Wenzel, Kramers, Brillouin, and Keller and Kac's famous isospectral problem. Then we discuss how the traveling functions have been utilized in the numerical simulation of musical instruments through work by Julius Smith, Karplus, Strong and other. This work has recently been extended to additional instruments types, in particular idiophones, which not only are more efficient than finite element based simulations but have the desirable property of stability and ease of interpretation under perturbations. We conclude with outlining possible research based on the advantages and drawbacks of the method.

This principle provides a direct conceptual link between modal synthesis and waveguide-style physical models. In addition it suggests the importance of understanding the link between geometry and modes for efficient dynamical simulation. This paper explores these connections with regards to banded waveguide models.

### 1. INTRODUCTION

How do musical instruments behave? What is responsible for the audible aspects of their behavior? How can we predict, recreate and modify this behavior to create music? These questions are at the very core of musical acoustics. In this paper we explore aspects of the evolution of mathematical formulation of the dynamical behavior of sound-

ing objects in general and musical instruments in particular. Within this history a particular principle will be the main focal point of the discussion, namely the *principle of closed wavetrains* also called the *principle of equal phase closure*. Both these phrases can be found in [1] to describe the connection between a closed trajectory of a traveling wave and the occurrence of resonances. More precisely the principle asserts that if a traveling wave closing onto itself in phase a resonant response will result.

This principle is of interest precisely because it links spectral theory with mathematical modeling of the dynamics in a direct way. This is a rarely seen connection in approaches to musical acoustics questions. This paper in part hopes to draw attention to this link by exploring how it has developed over the years and suggest, how in part the separate developments of partial differential equations and functional analysis and dynamical theory can be understood. We will point at separate strands of past and ongoing research and suggest the benefit of bringing them together.

### 2. PAST: FROM D'ALEMBERT TO WAVEGUIDES

The history of the principle of closed wave trains probably starts in the 18th century with d'Alembert's famous first formulation of the perfectly elastic string in it's current form as partial differential equation. Along with it he also presented a solution of two functions traveling left and right<sup>1</sup>. This solution ensued an argument about the validity of the assumptions of the arbitrariness of these functions between d'Alembert, Euler and Daniel Bernoulli. Bernoulli proposed as an alternative solution the sum of sinusoids, yet left open how the coefficients were to be computed. This solution in turn came under criticism by both Euler and d'Alembert. Only with the work of Fourier that then solidified the idea of spectral analysis did Bernoulli's solution recover full acceptance [2].

This early development really produced two focus argu-

<sup>1</sup>Throughout this paper we will give preference to review literature if available. The reader is encouraged to follow the reference of the review articles of books for details and particular publications.

ments. One was concerned with the nature of allowed functions in d'Alembert's solution. The other had to do with the details of spectral theory. The first should then lead via the work of Cauchy, Dirichlet and others to modern functional analysis. These were however for the most part treated separately, a separation which is commonly still seen today.

Maybe this has to do with the localized description of Newton's form of classical mechanics which suggests forming the dynamical equations of a problem as a sum of local forces, which are then to be studied. Alternative forms of describing the classical mechanics were developed through the 18th and 19th century by Euler, Maupertuis, Lagrange, Hamilton and Jacobi. These forms, often called the Lagrangian and Hamiltonian mechanics, emphasizes the finding of trajectories of motion. In particular in the Hamilton's mechanics the evolution, the *flow*, of the dynamics is described by the variables of position and momentum which are driven by the gradient of the energy surface of the system called *the Hamiltonian* [3].

While acoustical problems were arguably an central driving force in the development of physics and mathematics during the 18th and 19th century the focus shifted around the turn of the 19th to the 20th century with the advent of quantum physics.

Physicist faced an inverse problem of sort to the earlier acoustical work. Instead of solving known constituent dynamical equations to match observed spectra, now spectra were observed (of for example black body radiation) and the task was to find dynamical equations that would yield these spectra under upon solution. Of course this happened after the classical dynamical equations failed to yield the correct results. At that time Bohr, Sommerfeld, Einstein and others devised quantization rules based on classical dynamics and Planck's energy quantization to describe the spectra. This work still is basis today for a field called semiclassical physics, which studies how classical methods can be utilized to find quantum mechanical solutions [4].

However there remained startlingly simple problems of classical dynamics for which no general solutions could be found with conventional methods. Among these problems were was the three-body problem as it applies to the motion of the moon in the constellation with the sun and earth. The first calculations date back to Newton, it was not until the late 19th century, that substantial progress was made by George William Hill. His calculation started with a known solution of periodic orbits, closed smooth trajectories, and he would investigate other solutions in its neighborhood. By finding that these periodic orbits are densely distributed among all possible trajectories, Poincaré suggested that periodic orbits were in fact the right starting points for these other possibilities. These possibilities were later found to be potentially chaotic [3].

If a dynamical system can be described by independent

periodic orbits all allowed paths can be represented by a torus topology of the order of independent orbits. This was realized through work by Poincaré and Einstein around the turn of the century. Dynamical systems of this type are called *integrable*. Einstein used the torus structure to both argue that separation of variable is too stringent a condition for the classical solution of dynamical systems and that most dynamical systems don't have a corresponding torus structure. Regardless, a number of integrable systems have been solved by Keller and Rubinow and related work was performed by Brillouin. The procedure of calculating dynamical solutions through quantization on tori topologies are hence called *EBK quantization* after Einstein, Brillouin and Keller. Keller and Rubinow's work in particularly interesting because they provide explicit solutions for the cases of rectangular, circular and elliptical membranes [3]. Recently Chen, Coleman and Zhou presented solutions for stiff bars and plates using this approach [5].

There may be regions in the dynamics where a traveling waves assumption does not hold without reservations. In particular the solution can become singular in some regions. The development of methods treating this problem has a long and somewhat complex history. Early work goes back to Carlini, Liouville and Green and is hence sometimes called Liouville-Green approximation. The connection across singular regions was studied by Gans, Rayleigh, Jeffreys, Wenzel, Kramers and Brillouin and is hence often referred to as WKB or JWKB. The interested reader is referred to [6] for detailed historical context of mathematical developments until the 1970s. The following mathematical theories of relevance are often referred to as *asymptotic theory* and *catastrophe theory*.

These so-called *invariant tori* were then used to study the emergence of chaos in a more general setting by Kolmogoroff, Arnold and Moser in the 1950s and 60s. The *KAM theorem*, named after its contributors, establishes the robustness of tori under small perturbation as long as resonances are sufficiently separated. Similar to Poincaré's idea of starting with periodic orbits, they start with tori and study it's stability under perturbations [4].

There exists an intimate connection between the geometry of the dynamical system and the existence of invariant tori. Exact analytical solutions of arbitrary boundary contours is an unsolved problem in general and hence also this approach is yet limited in the type of geometries that have been solved for. This problem was highlighted by the question Kac posed in the 1960s: "Can we hear the shape of a drum?" [7]. While this question has been answered to be no for specific non-smooth constructions [8], the question remains open for most and very general classes of shapes (like all smooth boundaries).

It is not clear that acousticians were always aware of these developments and how they related to classical acous-

tic problems. However, similar ideas can be found in the acoustics literature of the time. Among the acousticians of the 20th century who developed the idea were Mead [9], Cremer and Heckl [1]. While they state that the approach of finding resonances by studying closed wavetrains works for higher-dimensional problems, only one dimensional problems of strings and bars are explicitly presented.

Keller is known in the violin acoustics community for his work on the bowed string and the friction characteristics he and Friedlander used in their calculations often bears their name. His other work seems to have gone mostly unnoticed. The development of chaos theory did find its way into acoustics [10].

The view of chaos however focuses its attention to the occurrence of chaotic states and the role of attractors and shows little connection to the particular dynamical system under consideration. The study of dynamical non-linearity has mostly focused around localized effects, predominantly excitation mechanisms, like the action of a violin bow on a string or the function of reeds in woodwind instruments [11].

With the advent of digital computers, numerical solutions to dynamical equations developed rapidly in the 20th century. This drive also was used in musical acoustics. Numerical methods that utilize propagation ideas in musical acoustics have focused on the one-dimensional wave-equation, which describes a large class of musical instruments in the western musical tradition [12]. McIntyre, Schumacher, and Woodhouse realized that many of these instruments can be studied as a concatenation of non-linear excitation and linear resonator. They realized that computational effort is focused on the reflection of traveling waves [13]. Karplus and Strong used circular buffers to simulate plucked string sounds which was soon realized to be an accurate discrete simulation of the one-dimensional wave-equation. This approach, usually called *waveguide synthesis* has since been extensively studied by Smith and others and has been used for a range of musical instruments [14, 15].

This sketch of the history of traveling wave physics is by the complexity of the pattern of individual contributions and by nature of the space available here somewhat limited. Many of the cited references contain a wealth of historical context, in particular Gutzwiller's text [3] presents the material in historical context and with focus on the individual contributions.

### 3. PRESENT: BANDED WAVEGUIDES AND THE CONVERGENCE OF PROBLEM-SOLUTIONS

Today we see in some sense a convergence of some of these past developments. In particular modern dynamical theory, spectral theory, numerical methods and filter theory are brought together.

The authors have proposed a method called *banded waveguides*, which attempts at combining the work of dynamic theory of traveling waves with numerical methods like digital waveguide synthesis. The core idea is to expand propagators into band-limited loop dynamics around resonances. The most basic filter structure capturing the idea is depicted in Figure 1. This way of depicting the method hides much of the connection of this structure to the past developed knowledge.

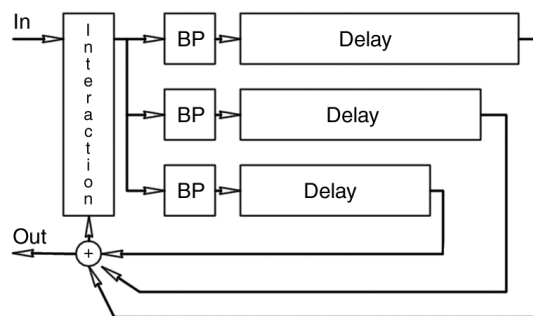


Figure 1: A simple banded waveguide system.

Conceptually this method brings various different ideas together. For one it is a spectral method for its spectral decomposition. It is also a numerical method for close trajectory dynamics for its discretization of loops.

A number of one and two-dimensional problems have been attempted using this method [16]. In particular, the approach is very useful for modeling idiophones of stiff material.

A similar development of the merging of spectral theory and dynamical theory can be observed in recent developments in mathematics where the connection of scattering phenomena on resonances is under scrutiny. In particular it is suggested that propagators are analyzed around resonances making the connection between spectral results and dynamical behavior the starting point of the investigations [17].

The problem of treating regions where the traveling wave approach apparently breaks down or is only approximate has seen much advance. There is ongoing research that studies how to make the asymptotic treatment exact [18, 19]. For entertaining popular treatments of these development, Michael Berry's series of articles are very recommended [20, 21]. Other related directions use complex-valued rays, which simplify similar problems [22].

Other significant developments include recent progress on the isospectral problem when Kac's question was finally answered negatively [8]. Loop dynamics are essential to the progress in this area.

In the realm of numerical methods in musical acoustics

the connection between waveguide synthesis and finite differencing methods has seen detailed investigation by Bilbao [23]. Numerical simulations using waveguide synthesis has reached a level of maturity [14].

However, today, many of these ideas still are only developed in separation and can be seen as a partial convergence only. However, they all seem to be reaching a certain level of individual maturity.

#### 4. FUTURE

Much of the synthesis of these related strands of work has yet to happen and utilized in musical acoustics. In part the problem may be one of translation. This literature spans various areas from pure and applied mathematics, numerical methods, computer science and physics. The various disciplines are not necessarily aware of each others work and use different formalisms in the respective discussion. Yet a continued effort in bringing these ideas together has various advantages. For example waveguide style numerical methods have advantages over finite element methods. They are more efficient. Their stability conditions can be easily observed. The intuitive appeal of closed trajectory description over local description becomes clear when one wants to understand how perturbations to a system affect the response. This intuitive appeal has been praised by various writers in the field. Gutzwiller writes: “[...] all of these ideas deal with relatively elementary questions [...]; as soon as they are understood, some readers may be tempted to call them obvious because of their deceptive simplicity!” [3] Similarly Zworski writes: “The results are technically quite simple, at least by the standards of the subject, and the appeal of this study lies in its connection with applied problems.” [17] Most of this appealing simplicity is however quite unknown to many and one might thus argue that looking into the future may first require connecting with past ideas that haven’t been sufficiently recognized. Gutzwiller makes a related point when he writes: “Most scientists have not participated in the recent development of ideas related to chaos in Hamiltonian systems; they are usually not aware of the many different viewpoints and interpretations, the new problems and methods for their solution, and the novel applications to important experiments.” [3] We hope that this paper helps in pointing towards knowledge that should be beneficial in future studies in musical acoustics.

#### 5. REFERENCES

- [1] L. Cremer, M. Heckl, and E. Ungar, *Structure-Borne Sound*, Springer Verlag, 2nd edition, 1988.
- [2] I. Grattan-Guinness, “Daniel Bernoulli and the varieties of mechanics in the 18th century,” *Nieuw Archief voor Wiskunde*, vol. 5, no. 1, pp. 242–249, September 2000.
- [3] M. C. Gutzwiller, *Chaos in Classical and Quantum Mechanics*, Springer Verlag, New York, 1990.
- [4] M. Brack and R. K. Bhaduri, *Semiclassical Physics*, vol. 96 of *Frontiers in Physics*, Addison-Wesley Publishing, 1997.
- [5] G. Chen, M. P. Coleman, and J. Zhou, “Analysis of Vibration Eigenfrequencies of a Thin Plate by the Keller-Rubinow Wave Method I: Clamped Boundary Conditions With Rectangular or Circular Geometry,” *SIAM Journal on Applied Mathematics*, vol. 51, no. 4, pp. 967–983, August 1991.
- [6] F. W. J. Olver, *Asymptotics and Special Functions*, Academic Press, 1974.
- [7] M. Kac, “Can One Hear the Shape of a Drum?,” *American Mathematical Monthly*, vol. 73, no. 4, pp. 1–23, April 1966.
- [8] T. A. Driscoll, “Eigenmodes of Isospectral Drums,” *SIAM Review*, vol. 39, no. 1, pp. 1–17, March 1997.
- [9] D. J. Mead, “Waves and Modes in Finite Beams: Application of the Phase-Closure Principle,” *Journal of Sound and Vibration*, vol. 171, no. 5, pp. 695–702, 1994.
- [10] W. Lauterborn and U. Parlitz, “Methods of chaos physics and their application to acoustics,” *Journal of the Acoustical Society of America*, vol. 84, no. 6, pp. 1975–1993, December 1988.
- [11] N. H. Fletcher, “The nonlinear physics of musical instruments,” *Rep. Prog. Phys.*, vol. 62, pp. 723–764, 1999.
- [12] N. H. Fletcher and T. D. Rossing, *The Physics of Musical Instruments*, Springer Verlag, New York, 2 edition, 1998.
- [13] M. E. McIntyre, R. T. Schumacher, and J. Woodhouse, “On the oscillation of musical instruments,” *J. Acoust. Soc. Am.*, vol. 74, no. 5, pp. 1325–1344, 1983.
- [14] J. O. Smith, “Digital Waveguide Modeling of Musical Instruments,” draft of unpublished online manuscript, available at <http://ccrma-www.stanford.edu/~jos/waveguide/>, 2002.
- [15] P. R. Cook, *Real Sound Synthesis for Interactive Applications*, A K Peters, Ltd., July 2002.
- [16] G. Essl, *Physical Wave Propagation Modeling for Real-Time Synthesis of Natural Sounds*, Ph.D. thesis, Princeton University, Princeton, NJ, November 2002. Available also as Princeton University Computer Science Technical Report TR-659-02 at <http://ncstrl.cs.princeton.edu/expand.php?id=TR-659-02>.
- [17] M. Zworski, “Resonances in Physics and Geometry,” *Notices of the American Mathematical Society*, vol. 46, no. 3, pp. 319–328, March 1999.
- [18] J. P. Boyd, “The Devil’s Invention: Asymptotic, Superasymptotic and Hyperasymptotic Series,” *Acta Applicandae*, vol. 56, pp. 1–98, 1999.
- [19] C. J. Howls, “Development of Exponential and Hyperasymptotics,” in *Toward the Exact WKB Analysis of Differential Equations, Linear or Non-Linear*, C. J. Howls, T. Kawai, and Y. Takei, Eds. Kyoto University Press, 2000.
- [20] M. Berry, “Why are special functions special?,” *Physics Today*, vol. 54, no. 4, pp. 11–12, April 2001.

## REAL-TIME SYNTHESIS MODELS OF WIND INSTRUMENTS BASED ON PHYSICAL MODELS

*Ph. Guillemin, J. Kergomard, Th. Voinier*

CNRS-Laboratoire de Mécanique et d'Acoustique  
31, chemin Joseph Aiguier. 13402, Marseille cedex 20  
France  
guillem@lma.cnrs-mrs.fr

### ABSTRACT

A real-time synthesis model of wind instruments sounds, based upon a nonlinear physical model, is presented. The model includes a linear part, modelling directly the input impedance of the resonator of the instrument without the travelling waves decomposition, a linear part modelling the reed or lips vibrations and a nonlinear part modelling the interaction between flow, pressure and reed displacement at the mouthpiece. The model itself and its control parameters make an explicit use of the physical parameters, which makes easy and natural its real-time control.

### 1. INTRODUCTION

The calculation of the self-oscillations of instruments such as clarinet has been proposed for the first time by Schumacher [1], using a time domain discretization of the equations, and such a work that does not attempt a real-time implementation has been since widely developed.

In order to perform the calculations in real-time, several methods yielding a time domain formulation of the waves in the resonator have been developed. We can mention the famous Digital Waveguide method (see for example Smith [2] or Välimäki [3]) and Digital Wave Filters [4], that consider the incoming and outgoing waves within each section of a bore and their scattering at the junctions between bores of different sections. Like the Schumacher method, since these methods consider the incoming and outgoing waves, the problem then lays in the formulation of the non-linearity which, whatever the model, can however only be expressed physically in terms of acoustic pressure and flow at the mouthpiece of the instrument.

In this paper, a method of construction of a nonlinear physical synthesis model is proposed. It consists in expressing directly the impedance relationship at the mouthpiece between flow and pressure, which become the input and output of one of the linear parts of the model, respectively. This approach let us process similarly the cases of cylindrical or more complicated bores built by gathering several elementary impedances by using electrical analogies and transmission line formalism. The coupling with the nonlinear characteristics of the reed or the lips can then be done in a natural way and solved explicitly without the use of iterative schemes such as the **K**-Method [5], thanks to a suitable discretization scheme of the reed/lips displacement. We first focus on the case of a cylindrical resonator, which constitutes an approximation of a clarinet bore (see e. g. Kergomard [6] for the notations), and extend the method to other bore geometries [7].

### 2. SIMPLIFIED PHYSICAL MODEL

We first briefly describe the main physical phenomena involved in the construction of the nonlinear physical synthesis model. They are made of an impedance equation linking pressure and flow, a linear oscillator modelling the first mode of vibrations of the reed or the lips, and a nonlinear equation coupling the flow to the pressure and the reed displacement at the mouthpiece.

#### 2.1. Input impedance of a cylindrical lossy bore

The first linear part of the nonlinear synthesis model corresponds to the resonator of the instrument. Assuming that the radius of the bore is large in front of the boundary layers thicknesses, the classical Kirchhoff's theory leads to the value of the complex wavenumber for a plane wave:  $k(\omega) = \frac{\omega}{c} - \frac{i^{3/2}}{2} \alpha c \omega^{1/2}$ . The transfer function of a bore of infinite length between  $x = 0$  and  $x = L$ , which constitutes the propagation filter in a waveguide interpretation, including propagation delay, dispersion and dissipation is then given by:  $F(\omega) = \exp(-ik(\omega)L)$ .

Assuming that the radiation losses are negligible, the input impedance is expressed by:

$$Z_e(\omega) = \frac{P_e(\omega)}{U_e(\omega)} = i \tan(k(\omega)L) \quad (1)$$

#### 2.2. Simple reed model

We use for the reed a classical single mode model. It describes the dimensionless displacement  $x(t)$  of the reed with respect to its equilibrium point  $x = 0$  when it is submitted to a dimensionless acoustic pressure  $p_e(t)$ :  $\frac{1}{\omega_r^2} \frac{d^2 x(t)}{dt^2} + \frac{q_r}{\omega_r} \frac{dx(t)}{dt} + x(t) = p_e(t)$  where  $\omega_r$  and  $q_r$  are the frequency and the quality factor of the reed.

Writing this equation in the Fourier domain yields:

$$\frac{X(\omega)}{P_e(\omega)} = \frac{\omega_r^2}{\omega_r^2 - \omega^2 + i\omega q_r \omega_r} \quad (2)$$

The impulse response satisfies the property  $x(0) = 0$ , which will be useful in the following.

#### 2.3. Nonlinear characteristics

Under classical hypothesis (see e.g. [8] and [6]), the dimensionless acoustic pressure  $p_e(t)$ , the dimensionless acoustic flow  $u_e(t)$  and



the dimensionless reed displacement  $x(t)$  are linked in a nonlinear way at the input of the resonator:

$$\begin{aligned} u_e(t) &= \frac{1}{2}(1 - \text{sign}(\gamma - x(t) - 1))\text{sign}(\gamma - p_e(t)) \\ &\quad \times \zeta(1 - \gamma + x(t))\sqrt{|\gamma - p_e(t)|} \\ &= \mathcal{F}(x(t), p_e(t)) \end{aligned} \quad (3)$$

The parameter  $\zeta$  is characteristic of the whole embouchure and is proportional to the square root of the reed position at equilibrium. The parameter  $\gamma$  is the ratio between the pressure inside the mouth of the player and the static beating-reed pressure. They constitute two important performance parameters since they respectively represent the way the player holds the reed and its blowing pressure inside the instrument. Though, for clarity in the notations, the  $t$  variable is omitted,  $\gamma$  and  $\zeta$  are functions of time.

Combining the reed displacement equation, the impedance relation and the nonlinear characteristics, the acoustic pressure is solution of the set of equations (1), (2) and (3).

### 3. CONSTRUCTION OF THE NONLINEAR SYNTHESIS MODEL FROM THE PHYSICAL MODEL

In order to solve this system of three equations, a different formulation of the impedance relation, compatible with a time-domain implementation, has to be found. For that purpose, the impedance relation is first expressed using a waveguide formalism.

#### 3.1. Expression of the input impedance of the resonator

The input impedance is expressed as a combination of waveguides. For that purpose,  $Z_e(\omega)$  given by eqn. (1) is rewritten as:

$$Z_e(\omega) = \frac{1}{1 + \exp(-2ik(\omega)L)} - \frac{\exp(-2ik(\omega)L)}{1 + \exp(-2ik(\omega)L)} \quad (4)$$

#### 3.2. Non linear synthesis model

The system of equations (1), (2) and (3) let us introduce the reed and the non-linearity as a nonlinear loop linking the output  $p_e$  to the input  $u_e$  of the resonator, as it is shown on figure 1. The output of the model is made of the three coupled variables  $p_e$ ,  $u_e$  and  $x$ . The upper block of the non linear loop models directly the dimensionless input impedance of the resonator according to eqn. (4). It is made of a sum of two elementary waveguides. The upper element corresponds to the first term of equation (4) and the lower element corresponds to the second term. The filter the transfer function of which is  $-F(\omega)^2 = -\exp(-2ik(\omega)L)$  represents the back and forth path of the dimensionless waves, with a sign change at the open end of the instrument.

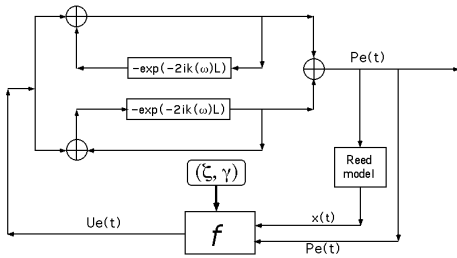


Fig 1: Nonlinear physical synthesis model

In the following, the input impedance and admittance of the cylindrical bore will be denoted respectively by  $\mathcal{C}(\omega)$  and  $\mathcal{C}^{-1}(\omega)$ .

The model is controlled by the length  $L$  of the bore and the parameters  $\zeta(t)$  and  $\gamma(t)$  of the non-linearity. No input signal is necessary since  $\gamma$  is directly proportional to the static pressure inside the mouth of the player.

Assuming again that the radiation impedance is negligible, the external pressure corresponds to the time derivative of the output flow:  $p_{ext}(t) = \frac{du_e(t)}{dt}$ . Moreover, from a perceptual point of view, the losses corresponding to a single travel of the waves between the embouchure and the open end can be ignored.

These simplifications let us express the external pressure as:

$$p_{ext}(t) = \frac{d}{dt}(p_e(t) + u_e(t)) \quad (5)$$

## 4. DISCRETE-TIME SOLUTION OF THE MODEL

### 4.1. Approximation of the input impedance

A time domain equivalent of the inverse Fourier transform of the impedance is required. This time domain formulation will let us compute  $p_e(t)$  as function of  $u_e(t)$ . For that purpose, it is necessary to express the losses through a digital filter. Since only the square of  $F(\omega)$  is needed in eqn. (4), this is done by the use of an approximation of  $F(\omega)^2 = \exp(-2ik(\omega)L)$ . In order to be modified according to the geometry of the resonator, the coefficients of the filter are expressed analytically as functions of the physical parameters, rather than through numerical approximations and minimizations. For that purpose, we use a simple one pole filter, written under the form:

$$\tilde{F}(\tilde{\omega}) = \frac{b_0 \exp(-i\tilde{\omega}D)}{1 - a_1 \exp(-i\tilde{\omega})} \quad (6)$$

where  $f_e$  is the sampling frequency,  $\tilde{\omega} = \frac{\omega}{f_e}$  and  $D = 2f_e \frac{L}{c}$  is the pure delay corresponding to a back and forth path of the waves.

The parameters  $b_0$  and  $a_1$  are calculated so that  $|F(\omega)^2|^2 = |\tilde{F}(\tilde{\omega})|^2$  for two given values of  $\omega$ . The first value  $\omega_1$  is the frequency of the first impedance peak. It insures an exact height of the impedance peak for the fundamental frequency. It is important to preserve this feature for a faithful simulation of the continuous dynamical system, since the linear impedance is coupled with the nonlinear characteristics. It also let the decay time of the fundamental frequency of the approximated impulse response match the exact one, which is important for the transients induced by rapid changes of  $\gamma$  and  $\zeta$ . For the same reasons, the second value  $\omega_2$  corresponds to the frequency of the second impedance peak.

A straightforward calculation using eqn. (4) leads to the difference equation linking  $p_e(n)$  and  $u_e(n)$ :

$$\begin{aligned} p_e(n) &= u_e(n) - a_1 u_e(n-1) - b_0 u_e(n-D) \\ &\quad + a_1 p_e(n-1) - b_0 p_e(n-D) \end{aligned} \quad (7)$$

In the same way, the difference equation corresponding to the admittance of the cylindrical bore can be calculated by changing  $b_0$  into  $-b_0$ .

Figure 2 displays the approximated input impedance as function of frequency superimposed with the exact one (dotted line) ( $L = 0.5m$ ,  $R = 7mm$ ,  $f_e = 44100$ ). The heights of the two first impedance peaks are equal in both cases.

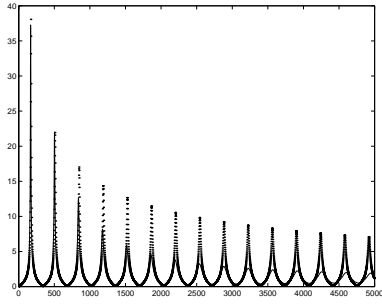


Fig 2: Approximated and exact input impedance (in Hertz)

#### 4.2. Approximation of the reed displacement

Similarly to the impedance relation, the relationship between the acoustic pressure and the reed displacement is discretized in the time domain. In order to keep the property  $x(0) = 0$  of the continuous system when the reed is submitted to a Dirac excitation, we approximate the terms  $i\omega$  and  $-\omega^2$  in the continuous transfer function of the reed, by:  $i\omega \simeq \frac{1}{2}(z - z^{-1})$  and  $-\omega^2 \simeq f_e^2(z - 2 + z^{-1})$ , corresponding to centered numerical differentiation schemes that are both exact for second order polynomials. In this case,  $x(n)$  and  $p_e(n)$  are linked by a difference equation under the form:

$$x(n) = b_{1a}p_e(n-1) + a_{1a}x(n-1) + a_{2a}x(n-2) \quad (8)$$

in which the coefficients are expressed analytically as functions of the reed parameters. We point out that there is no artificial shift of one sample in this discretization scheme.

Figure 3 shows the transfer function of this approximated reed model ( $f_r = 2500\text{ Hz}$ ,  $q_r = 0.2$ ,  $f_e = 44100$ ) superimposed with the exact one (dotted line).

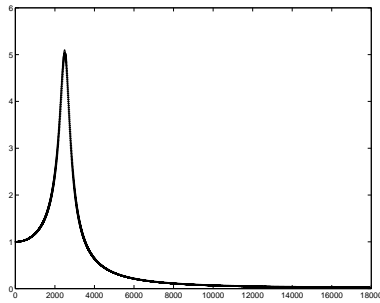


Fig 3: Approximated and exact reed transfer (in Hertz)

#### 4.3. Coupling of the difference equations with the nonlinear characteristics

The sampled formulations of the impulse responses of the reed displacement and of the impedance let us write the sampled equivalent of the continuous system by replacing eqns. (1) and (2) respectively by (7) and (8). Though the system includes an instantaneous nonlinearity, the calculation of  $p_e(n)$  and  $u_e(n)$  can be done explicitly without the use of iterative or table lookup schemes since the computation of  $x(n)$  with equation (8) does not require the knowledge of  $p_e(n)$  (but this of  $p_e(n-1)$  which is known at time  $n$ ). The calculation of the sampled external pressure  $p_{ext}(n)$  is performed by the use of a simple difference between the sum of internal pressure and flow at sample  $n$  and at sample  $n-1$ .

#### 4.4. Extensions of the cylindrical bore model

The explicit resolution scheme mentioned in section (4.3) remains valid as long as the relationship between  $p_e(n)$  and  $u_e(n)$  can be written as:  $p_e(n) = b_{c0}u_e(n) + V$ , where  $V$  includes all the terms of the difference equation that do not depend on the time sample  $n$ . This makes it possible to replace eqn. (7) by others, corresponding to more complex geometries of bores.

We first consider the case of the truncated, divergent, conical bore. In this case, the input impedance is made of a parallel combination of a cylindrical bore of length  $L$  and a length  $x_e$  of "air" corresponding to the distance between the apex and the input:

$$Z_e(\omega) = \frac{1}{\frac{1}{i\omega \frac{x_e}{c}} + \frac{1}{i \tan(k(\omega)L)}} \quad (9)$$

Writing this last equation under the form:  $\frac{P_e(\omega)}{U_e(\omega)} = \frac{i\omega \frac{x_e}{c}}{1 + \frac{i\omega \frac{x_e}{c}}{i \tan(k(\omega)L)}}$  and noting  $\mathcal{D}$  the differentiation operator:  $\mathcal{D} = i\omega$  let us propose the equivalent scheme:

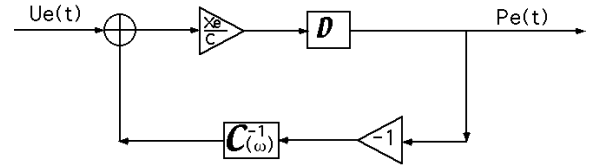


Fig 4: Impedance of a conical bore

In the following, the input impedance of a conical bore will be denoted by  $\mathcal{S}(\omega)$ .

Using e. g. the bilinear transformation for the discretization of  $\mathcal{D} = i\omega$ , eqn. (9) satisfies:  $p_e(n) = b_{c0}u_e(n) + V$ .

The truncated conical bore does not generate impedance peaks the frequencies of which are harmonic of a given fundamental. A solution to this problem in a saxophone bore configuration consists in adding a mouthpiece, the volume of which corresponds to the volume of the missing part of the cone. This mouthpiece can be modelled as an Helmholtz resonator made of a hemispherical cavity of volume  $V$  coupled with a short cylindrical bore of impedance  $C_1(\omega) = ik_1(\omega)L_1$ . The impedance is then given by:

$$Z_e(\omega) = \frac{\frac{1}{Z_2}}{i\omega \frac{V}{\rho c^2} + \frac{1}{Z_1 ik_1(\omega)L_1 + Z_2 S_2(\omega)}} \quad (10)$$

where  $Z_1$  and  $Z_2$  are the characteristic impedances of each bore. Rearranging eqn. (10) let us propose the equivalent scheme:

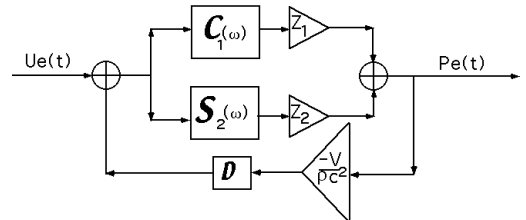


Fig 5: Impedance of a simplified brass bore

Again, the digital version of eqn. (10) is expressed under the form:  $p_e(n) = b_{c0}u_e(n) + V$ .

Figure 6 displays a typical brass bore input impedance, approximated (solid line) and exact (dotted line) together with their corresponding impulse responses.

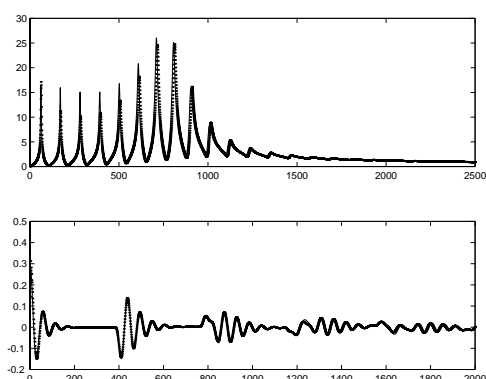


Fig 6: Top: approximated and exact input impedance (in Hertz)  
Bottom: approximated and exact impulse response (in samples)

The Helmholtz resonator parameters are adjusted in order to produce either a harmonic series of impedance peaks in the saxophone case, either a formant in the brass case. For brass instruments, similarly to the radiation, the role of the bell in the input impedance is neglected.

#### 4.5. Example of simulation

Figure 6 shows the pressure  $p_{ext}(t)$  in a saxophone configuration. The attack transient corresponds to an abrupt raising of  $\gamma$ . During the decay,  $\gamma$  decreases linearly towards zero.

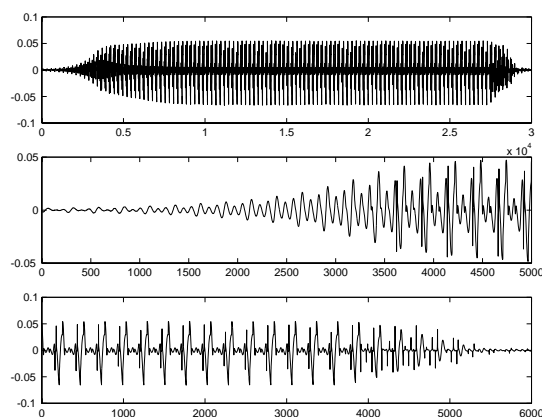


Fig 4: Top: external acoustic pressure (in samples)  
Medium: blow-up of the attack transient (in samples)  
Bottom: blow-up of the decay transient (in samples)

#### 4.6. Real-time synthesis implementation

The nonlinear physical synthesis model has been implemented in real-time in the C language as an external *Max-MSP* object, piloted from MIDI commands given by a *Yamaha WX5* controller. This controller measures, as functions of time, the lip pressure that controls the parameter  $\zeta(t)$ , and the blowing pressure that controls the parameter  $\gamma(t)$ . These informations are received in MIDI format (between 0 and 127) and are normalized in order to correspond

to the range of the physical parameters. The tuning of the model is performed by the use of the MIDI Pitch information coming from the fingering that controls the length  $L$  of the bore. The delay  $D$  is implemented through a circular delay line. Like in real instruments, since the pitch changes with respect to physical parameters such as  $\gamma$ ,  $\zeta$ ,  $\omega_r$  and  $q_r$  and since the real instruments are not perfectly tuned for all the fingerings, it seemed to us unnecessary to implement a fractional delay line with the help of an all-pass filter. In a clarinet or saxophone configuration, the feeling of play of this virtual instrument is comparable to the playing of the real one.

## 5. CONCLUSION

The real-time synthesis model described in this paper has been obtained through a direct transposition of the simplified equations of the physical behavior of the wind instruments. In particular, the straightforward formulation of the input impedance of the bore, avoiding a  $p^+/p^-$  decomposition, let us add to the linear parts of the model a nonlinear loop modelling the nonlinear interaction between pressure, reed displacement and flow as it is expressed physically. The discretized version in time of the coupled system is solved with an explicit scheme. The structure of this scheme makes it possible to extend the cylindrical bore model, by replacing the linear parts of the system by equations obtained by considering more complex geometries of the bore and different reed/lips models [7]. This synthesis model makes it possible to modify in real-time the physical parameters of the instrument, since all the coefficients of the digital filters are explicitly expressed in terms of physical parameters, and to control in real-time the playing parameters.

## 6. REFERENCES

- [1] Schumacher, R.T., "Ab initio calculations of the oscillation of a clarinet", *Acustica*, 48, 71-85 (1981).
- [2] J. O. Smith, "Efficient simulation of the reed-bore and bow-string mechanisms", in *Proceedings of the 1986 International Computer Music Conference*, The Hague. 275-280, Computer Music Association (1986).
- [3] Välimäki, V., and M. Karjalainen. "Digital Waveguide Modelling of Wind Instrument Bores Constructed of Truncated Cones". in *Proc. ICMC 94*, Aarhus. Computer Music Association (1994).
- [4] M. van Walstijn, M. Campbell. "Discrete-time modelling of woodwind instrument bores using wave variables", *J. Acoust. Soc. Am.*, 113, 575-585 (2003).
- [5] G. Borin, G. De Poli, D. Rochesso "Elimination of Delay-free Loops in Discrete-time Models of Nonlinear Acoustic Systems", *IEEE Trans. Sp. Au. Proc.*, 8, 597-606 (2000).
- [6] Kergomard J. "Elementary considerations on reed-instruments oscillations", in *Mechanics of Musical Instruments*, Hirschberg et al. eds., Lectures notes CISM, Springer (1995).
- [7] Ph. Guillemin, J. Kergomard, Th. Voinier, "Procédé de simulation et de synthèse numérique d'un phénomène oscillant", french patent request n°0213682, Oct (2002).
- [8] A. Hirschberg. "Aero-Acoustics of Wind Instruments", in *Mechanics of Musical Instruments*, Hirschberg et al. eds., Lectures notes CISM, Springer (1995).

# TIME-DOMAIN PHYSICAL MODELING AND REAL-TIME SYNTHESIS USING MIXED MODELING PARADIGMS

Matti Karjalainen

Helsinki University of Technology  
Laboratory of Acoustics and Audio Signal Processing  
matti.karjalainen@hut.fi

## ABSTRACT

Three approaches, often used in discrete-time modeling of physical systems, are digital waveguides (DWG) [1], finite difference time-domain schemes (FDTD) [2], and wave digital filters (WDF) [3]. We have shown it feasible to combine these paradigms to a mixed modeling framework [4, 5], making it possible to utilize the best features of each of them. Based on the theoretical framework we have developed a software tool, called the BlockCompiler [6], which is used for high-level description of model structures, automatically compiled to efficient simulation and real-time synthesis. In this paper we present an overview of the mixed modeling paradigm and the BlockCompiler based on it, as well as 1-D and 2-D physical modeling examples simulated in real time.

## 1. MIXED MODELING FRAMEWORK

In time-domain discrete-time modeling of physical systems the task is to approximate the underlying (partial) differential equations by difference equations then to be solved numerically. Formulation of the solution as DSP algorithms makes them computable by efficient software tools, even as real-time simulation. We first introduce DSP formulations of digital waveguides (DWG) and finite difference time-domain schemes (FDTD) as well as their combinations. Then we add wave digital filters (WDF) to this modeling framework.

### 1.1. Wave-based modeling with DWGs

1-D traveling wave formulation is based on the d'Alembert solution of propagation of two opposite direction waves, which properly discretized in time and space [1] yields:

$$y(n, m) = \vec{y}(n - m) + \overleftarrow{y}(n + m) \quad (1)$$

where  $y$  the wave variable and  $n$  and  $m$  are related to time and position, respectively. It follows that the wave propagation can be computed by updating state variables in two delay lines by

$$\vec{y}_{k,n+1} = \vec{y}_{k-1,n} \quad \text{and} \quad \overleftarrow{y}_{k,n+1} = \overleftarrow{y}_{k+1,n} \quad (2)$$

i.e., by simply shifting the samples to the right and left, respectively. Index  $k$  denotes now position and  $n$  is sample index (time). This kind of discrete-time modeling is called Digital Waveguide (DWG) modeling [1]. Since the physical wave variables are split explicitly into directional wave components, we will call such models *W-models* (wave models).

The next step is to take into account the global physical constraints of continuity by Kirchhoff type of rules. This means to formulate the scattering junctions of interconnected ports, with given impedances and wave variables at related ports. For a scattering junction where the physical variables are sound wave pressure  $P$

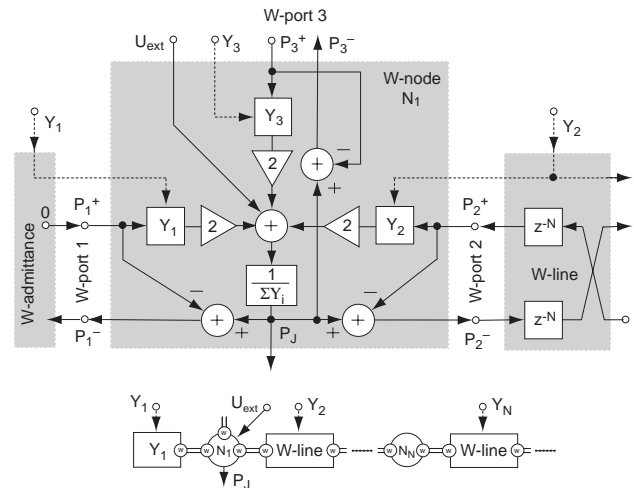


Figure 1: Top: A 3-port scattering junction (W-node  $N_1$ ). Incoming pressures are  $P_i^+$  and outgoing ones  $P_i^-$ . W-port 1 is connected to termination W-admittance  $Y_1$  and port 2 to a two-directional delay line (W-line). Admittance controls are marked by dashed lines. Bottom: Block diagram with abstracted blocks and how they can be connected to form a 1-D DWG waveguide.

and volume velocity  $U$ , and for a parallel admittance model<sup>1</sup> of  $N$  ports, the Kirchhoff constraints become

$$P_1 = P_2 = \dots = P_N = P_J \quad (3)$$

$$U_1 + U_2 + \dots + U_N + U_{ext} = 0 \quad (4)$$

where  $P_J$  is the common pressure of coupled branches and  $U_{ext}$  is an external volume velocity to the junction. When port pressures are represented by incoming wave components  $P_i^+$ , outgoing wave components by  $P_i^-$ , admittances attached to each port by  $Y_i$ , and

$$P_i = P_i^+ + P_i^- \quad \text{and} \quad U_i^+ = Y_i P_i^+ \quad (5)$$

the junction pressure  $P_J$  can be obtained as:

$$P_J = \frac{1}{Y_{tot}} (U_{ext} + 2 \sum_{i=0}^{N-1} Y_i P_i^+) \quad (6)$$

where  $Y_{tot} = \sum_{i=0}^{N-1} Y_i$  is the sum of all admittances to the junction. Outgoing pressure waves, obtained from Eq. (5), are then  $P_i^- = P_J - P_i^+$ . The resulting junction, a *W-node*, is depicted as a DSP structure in the node  $N_1$  of Fig. 1 (top). When admittances  $Y_i$  are frequency-dependent, this diagram can be interpreted as a

<sup>1</sup>Models can be formulated as well for impedances instead of admittances and for series connection, and for different physical variable pairs.

filter structure where the incoming pressures are filtered by the corresponding wave admittances  $Y_i$  times two, and their sum is filtered further by  $1/Y_{\text{tot}}$  to get the junction pressure  $P_J$ .

Two special cases can be noticed on the basis of Eq. (6). First, a (passive) loading admittance is the case with  $Y_i$  where no incoming pressure wave component  $P_i^+$  is associated. This needs no computation except including  $Y_i$  in  $Y_{\text{tot}}$  because  $P_i^+ = 0$ , see the left-hand termination, a *W-admittance*, in Fig. 1. Another issue is the external velocity  $U_{\text{ext}}$  effective to the junction. This is connected directly to the summation at the junction node.

The W-node in Fig. 1 is coupled through *W-ports* to the neighboring elements (port 3 is uncoupled). The right-hand side block is a two-directional delay line, a *W-line*, of admittance  $Y_2$ . The bottom part of the figure depicts a block diagram abstraction of the DSP structure. It also characterizes how waveguides are built as structures of W-line elements connected by W-node junctions.

Notice that the admittances in Fig. 1 may be real-valued or frequency-dependent so that  $Y_i$  and the impedance  $1/\sum Y_i$  can be realized as FIR or IIR filters, or just as real coefficients if all attached admittances are real. The realization of junction nodes, as shown in Fig. 1, is general for any LTI system approximation, also for 2-D and 3-D mesh structures. The delays (see W-line in Fig. 1) between nodes can also approximate fractional delays [7], which is useful particularly with varying length lines. However, delays shorter than a unit delay lead to the problem of delay-free loops, which complicates the situation substantially.

Dashed lines in Fig. 1 are parametric controls for admittances of the network elements. If the DSP blocks are grouped as shown, which is natural in an object-based formulation, the junction W-nodes actually contain most of the computation by implementing wave scattering. The W-node is delegated its admittance parameters through ports from the network elements, W-lines and W-admittances. In a time-varying case the admittance filters (blocks  $Y_1$ ,  $Y_2$ , and  $Y_3$ ) as well as the inverse of their sum  $1/\sum Y_i$  must be updated when the admittance control parameters change.

## 1.2. Finite difference modeling

In the most commonly used way to discretize the wave equation by finite differences the partial derivatives are approximated by second order finite differences

$$y_{xx} \approx (2y_{x,t} - y_{x-\Delta x,t} - y_{x+\Delta x,t})/(\Delta x)^2 \quad (7)$$

$$y_{tt} \approx (2y_{x,t} - y_{x,t-\Delta t} - y_{x,t+\Delta t})/(\Delta t)^2 \quad (8)$$

By selecting the discrete-time sampling interval  $\Delta t$  to correspond to spatial sampling interval  $\Delta x$ , i.e.,  $\Delta t = c\Delta x$ , and using index notation  $k = x/\Delta x$  and  $n = t/\Delta t$ , Eqs. (7) and (8) result in

$$y_{k,n+1} = y_{k-1,n} + y_{k+1,n} - y_{k,n-1} \quad (9)$$

which is a *K-model*, i.e., based on Kirchhoff type of total variables, not wave components. From form (9) we can see that a new sample  $y_{k,n+1}$  at position  $k$  and time index  $n+1$  is computed as the sum of its neighboring position values minus the value at the position itself one sample period earlier.

The behavioral similarity of DWGs vs. FDTDs [11], although being computationally different formulations (W- vs. K-models), hints to expand Eq. (9) to a FDTD type scattering junction for arbitrary port admittances. For a parallel admittance model, corresponding to Eq. (6), Eq. (9) can be formulated for  $N$  ports as

$$P_{J,n+1} = \frac{2}{Y_{\text{tot}}} \sum_{i=0}^{N-1} Y_i P_{i,n} - P_{J,n-1} \quad (10)$$

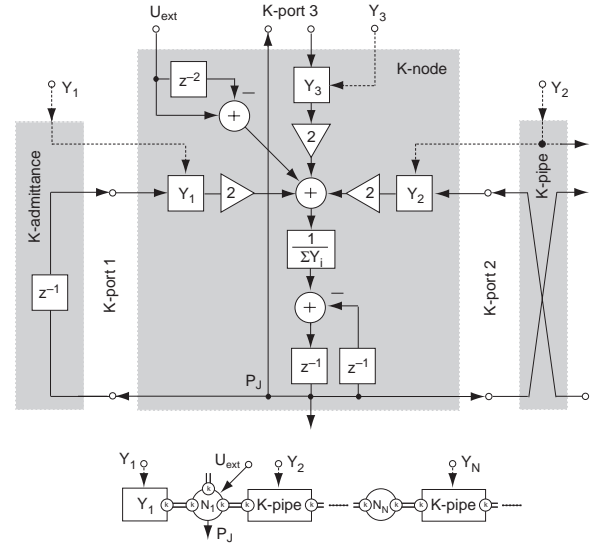


Figure 2: Top: Digital filter structure for finite difference approximation of a 3-port scattering node with port admittances  $Y_1$ ,  $Y_2$  and  $Y_3$  (port 3 not connected). Only total pressure  $P_J$  (K-variable) is explicitly available. Bottom: Block diagram with abstracted blocks to form a 1-D FDTD waveguide.

This is the waveguide mesh formulation as discussed in [8]. Figure 2 depicts a DSP formulation of one such 3-port scattering *K-node* and the way to terminate port 1 by *K-admittance*,  $Y_1$ . This corresponds to the W-model in Fig. 1, except that a wave traveling to the left reflects back from  $Y_1$  one unit delay later than in the DWG case. Notice the feedback through a unit delay. The bottom part of Fig. 2 depicts a block diagram abstraction which shows the conformity with the DWG in Fig. 1.

An essential difference between DWGs of Fig. 1 and FDTDs of Fig. 2 is that while DWG junctions are connected through two-directional delay lines (*W-lines*), FDTD nodes have two unit delays of internal memory, and delay-free *K-pipes* connect ports between nodes (see the right-hand side block in Fig. 2). The DWG and FDTD junction nodes and ports are not directly compatible because they use different type of wave variables.

A further difference in K- vs. W-modeling, in addition to algorithmic and computational precision properties, is the way external excitation has to be inserted into a junction node. For a FDTD junction  $U_{\text{ext}}$  must be fed through filter  $H(z) = 1 - z^{-2}$  (see Fig. 2) in order to initiate impulses traveling to opposite directions. An interesting property of the FDTD waveguide is also its inherent numerical integrating ability, utilized in some modeling tasks [9, 10]. If an impulse excitation into a 1-D waveguide node is inserted through  $H(z) = 1 + z^{-1}$ , there will be step functions propagating to both directions from the excitation point. This integrating property makes it possible to use a pair of variables, such as force and displacement, instead of the physically inherent pair of force and velocity.

## 1.3. Interfacing DWGs and FDTDs

The next question is the possibility to interface wave-based and FDTD-based submodels. In [5] it was shown how to interconnect a lossy 1-D FDTD waveguide with a similar DWG waveguide into a mixed model using a proper interconnection element (adaptor).

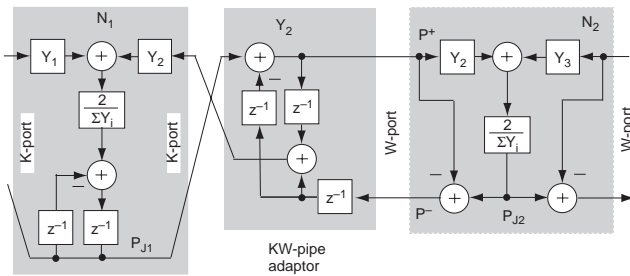


Figure 3: FDTD node (left) and a DWG node (right) forming a part of a hybrid waveguide.  $Y_i$  are wave admittances of W-lines, K-pipes, and adaptor KW-pipes between junction nodes.  $P_j$  are junction pressures,  $P^+$  and  $P^-$  are wave components.

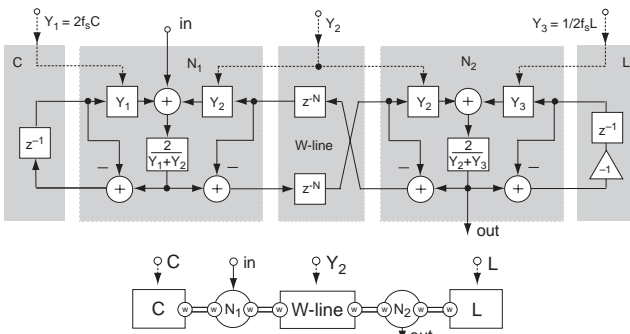


Figure 4: A simple DWG+WDF resonator where a DWG delay line is terminated with a WDF capacitor (left) and inductor (right).

As a generalization, it is possible to make any hybrid model of K-elements (FDTD) and W-elements having arbitrary wave admittances/impedances at their ports.

Figure 3 shows how this can be done in a 1-D waveguide between a K-node  $N_1$  (left) and a W-node  $N_2$  (right). The role of the KW-pipe in the middle of Fig. 3 is to adapt the K-type port of an FDTD node and the W-type port of a DWG node. It is delay-free in left-to-right direction and contains delay in the opposite direction.

Generally the DWG elements are preferable in 1-D modeling due to good numerical properties and possibility of arbitrary (including fractional) delays, while the FDTDs are more efficient in 2-D and 3-D structures, being however more critical in numerical accuracy.

#### 1.4. Interfacing wave digital filters with DWGs

An addition to the mixed modeling above is to adopt Wave Digital Filters (WDF) [3, 11] as discrete-time simulators of lumped parameter elements. Being based on W-modeling (wave variables) they are computationally compatible with the W-type DWGs [11]. A WDF resistor is just a real-valued termination (see  $Y_1$  in Fig. 1, but WDF capacitors and inductors are useful components [3].

As a physically bound choice for the case of this study, a WDF capacitor is realized as a feedback from  $V^-$  wave of a port back to  $V^+$  through a unit delay, having a port admittance  $2f_s C$ . A WDF inductor is a feedback through a unit delay and coefficient -1, having a port admittance  $1/2f_s L$ . Here  $C$  is capacitance,  $L$  is inductance, and  $f_s$  is sample rate (cf. [11]).

Figure 4 shows an example of a model where a DWG delay line is terminated by a WDF capacitor at the left hand side and by

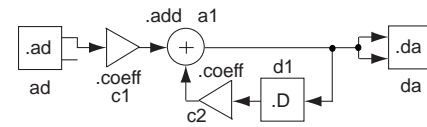


Figure 5: Simple low-pass filtering from sound input to output.

a WDF inductor at the right hand side.

A beneficial property of WDF elements is, since their wave admittances are real-valued, that junctions of such ports remain memoryless in the sense of Fig. 1, i.e.,  $Y_i$  and  $1/\sum Y_i$  are real. On the other hand, more flexibility and efficiency may be achieved in practice by higher order approximations of  $Y_i$  than by using basic WDF components.

WDF elements, being W-models, are not directly compatible with DFTDs that are K-models. However, the compatibility can be realized through a KW-adaptor element if needed.

## 2. REAL-TIME SIMULATION OF MIXED MODELS

The formulation of DWG + FDTD + WDF mixed models above shows directly a way to construct computational physical models based on DSP structures. A software system called the BlockCompiler has been developed that is particularly designed for flexible yet efficient experimentation with physical models [6].

Object-oriented manipulation of blocks and their interactions in the BlockCompiler is implemented in the Common Lisp language. Automatic generation of C source code from interconnected block representation and compilation to a run-time executable provides efficient computation in real time or by sample-by-sample non-realtime simulation.

### 2.1. BlockCompiler features

The main features and functional principles of the BlockCompiler are briefly described as follows:

- **Block structures and patches:** The basic level of block modeling supports DSP with directed data flow, such as adders, multipliers, delays, and digital filters, see Fig. 5 for a simple low-pass filter example. DSP blocks are instantiated by make-forms such as `(.coeff c1)` for a multiplier, `(.ad)` for sound input and `(.da)` for sound output, `(.d)` for a delay, and `(.add)` for an adder. These are chained by forms `(-> (.ad) ...)` from output to input, output to input, etc. A full model is called a *patch*. The patch of Fig. 5 can be created interactively by scripting

```
(patch ((a (.add)))
  (-> (.ad) (.coeff 0.0666) a (inputs (.da)))
  (-> a (.D) (.coeff -0.8668) (input a 1)))
```

It can be started streaming by command `run-patch`. Audio input is then continuously low-pass filtered to audio output. Inputs and outputs of blocks are normally used for synchronous data flow, but inputs may work also asynchronously for parametric control.

- **Macro blocks** can be defined as combinations of more elementary blocks. This is a useful abstraction mechanism whereby the details of the new class objects are hidden.

- **Data types:** The BlockCompiler supports data types {short, long, float, double} and corresponding array types.

- **Multirate support:** Multirate processing is available so that each block can be given a relative sample rate (decimation and interpolation by integer ratio.)



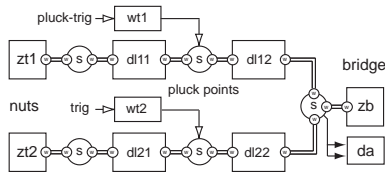


Figure 6: Block diagram of two strings made of delay lines and coupled through a common bridge impedance ( $z_b$ ). Pluck points can be excited from wavetables (wt).

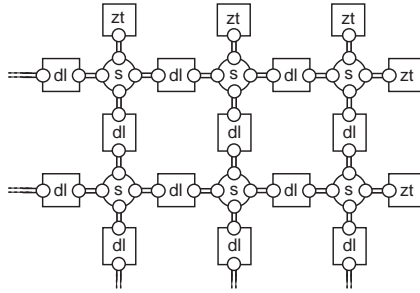


Figure 7: Part of a 2-D rectangular digital waveguide mesh for membrane simulation, composed of delay lines dl, series (impedance) nodes, and terminating impedances zt at boundaries.

• **Code generation and compilation:** Each block of a patch generates inline C code into a file to make a function with related data and declarations. The resulting C file is then compiled by an automatic call to a C compiler.

## 2.2. Physical modeling examples

In physical models the elements are coupled through ports of two-directional interaction. Figure 6 shows a block diagram of a 2-string guitar where the strings are coupled through a common bridge impedance ( $z_b$ ). Each string consists of two delay lines with a pluck point node in between for inserting pluck excitation from a wavetable. The principle of creating a model for the guitar is characterized (only for the upper string) by script:

```
(patch ((zb (.Z :impedance *imped-zb*))
        (zt1 (.Z :impedance *imped-zt1*))
        (wt1 (.wtable *wt-data1*))
        (dl11 (.d-line :delay-length *length11*))
        (dl12 (.d-line :delay-length *length12*))
        ...))
(-s zt (port dl11 0))
(-> wt1 (-s (port dl11 1) (port dl12 0)))
(-> (-s (port dl12 1) (port dl22 1) zb) da)
...)
```

Here the blocks are first instantiated (parameter data shown only symbolically) and bound to symbols used in Fig. 6. Then their ports are series connected by forms `(-s ...ports...)` which return the node objects. Excitations and output are wired unidirectionally to and from node objects by `(-> ...)` forms.

Instead of building a full instrument model, such as 6-string guitar, each string with two polarizations, as a single patch from basic elements, a better strategy is to define macro blocks, layer by layer: First a single polarization element, then two of them for a two-polarization string, further on using six of them, a bridge, and a body filter, to finally define a full guitar as a new macro block.

As another example, Fig. 7 depicts a part of a 2-D waveguide mesh in rectangular shape. It can be composed of W- or K-elements, although K-type FDTD elements are more efficient in 2-D and 3-D digital waveguides. Using KW-adaptors the model can mix both types of elements, e.g., for connecting W-type terminators or fractional delays to an FDTD waveguide mesh. The impedance of each delay can be controlled separately.

## 3. SUMMARY AND CONCLUSIONS

This paper has presented a physical modeling approach where several paradigms are combined to mixed models, including digital waveguides (DWGs) and second-order finite difference time domain models (FDTDs). Furthermore, wave digital filters (WDFs) are applicable, in addition to DWGs, for wave-based modeling (W-modeling). FDTDs, based on Kirchhoff variables (K-modeling), are made compatible with W-models through an adaptor element. The formulation allows for high flexibility in building 1-D, 2-D, and 3-D physical models from interconnected blocks, supporting both spatially distributed and lumped elements. A software tool is developed where such models can be built and executed efficiently.

## 4. ACKNOWLEDGMENT

This work is part of EU ALMA project (IST-2001-33059) and of Academy of Finland project "Technology for Audio and Speech Processing" (SA 53537).

## 5. REFERENCES

- [1] J. O. Smith, "Principles of Waveguide Models of Musical Instruments," in *Applications of Digital Signal Processing to Audio and Acoustics*, ed. M. Kahrs and K. Brandenburg, Kluwer Academic Publishers, Boston 1998.
- [2] J. Strikverda, *Finite Difference Schemes and Partial Differential Equations*, Wadsworth and Brooks, 1989.
- [3] A. Fettweis, "Wave Digital Filters: Theory and Practice," *Proc. IEEE*, 74(2), pp. 270–372, 1986.
- [4] C. Erkut and M. Karjalainen, "Virtual strings based on a 1-D FDTD waveguide model," *Proc. AES 22nd Int. Conf.*, pp. 317–323, Espoo, Finland, 2002.
- [5] C. Erkut and M. Karjalainen, "Finite Difference Method vs. Digital Waveguide Method in String Instrument Modeling and Synthesis," *Proc. ISMA'02*, Mexico City, 2002.
- [6] M. Karjalainen, "BlockCompiler: Efficient Simulation of Acoustic and Audio Systems," *Preprints of AES114th Convention*, Paper 5756, Amsterdam, May 2003.
- [7] T. Laakso, V. Välimäki, M. Karjalainen, and U. K. Laine, "Splitting the Unit Delay—Tools for Fractional Delay Filter Design," *IEEE Signal Processing Magazine*, vol. 13, no 1, pp. 30–60, 1996.
- [8] S. A. Van Duyne and J. O. Smith, "Physical Modeling with the 2-D Digital Waveguide Mesh," *Proc. ICMC'93*, pp. 40–47, Tokyo, Japan, Sept. 1993.
- [9] A. Chaigne, "On the use of finite differences for musical synthesis. Application to plucked stringed instruments," *J. Acoustique*, vol. 5, pp. 181–211, April 1992.
- [10] M. Karjalainen, "1-D digital waveguide modeling for improved sound synthesis," *Proc. IEEE ICASSP'2001*, pp. 1869–1872, Orlando, 2002.
- [11] S. D. Bilbao, *Wave and Scattering Methods for the Numerical Integration of Partial Differential Equations*, PhD Thesis, Stanford University, May 2001.
- [12] A. Sarti and G. De Poli, "Toward Nonlinear Wave Digital Filters," *Proc. IEEE Trans. Signal Processing*, vol. 47, no. 6, pp. 1654–1668, June 1999.

## A NEW METHOD FOR THE CALCULATION OF SELF-SUSTAINED OSCILLATIONS: THE PERTURBATION OF THE HELMHOLTZ MOTION

*J. Kergomard, S. Divoir, S. Farner, C. Vergez*

Laboratoire de Mécanique et d'Acoustique, CNRS  
31 Chemin Joseph Aiguier, 13401 Marseille Cedex 20  
France  
kergomard@lma.cnrs-mrs.fr

### ABSTRACT

When losses are ignored, elementary solutions for the classical models of self sustained instruments, such as reed or bowed string instruments, are pure square or "rectangular" signals, called Helmholtz motion. When losses are introduced, round corner signals are obtained, and the calculation becomes delicate. Ab initio calculation is possible, but methods limited to the steady-state regime make it easier to study the influence of the parameters on the spectrum and the playing frequency: the harmonic balance is well known, but, because losses are small, another iterative technique is suggested. Considering e.g. reed instruments, the Fourier components of the input pressure signal can be divided into two parts: the components with high input impedance, and those with low input impedance (corresponding to the missing harmonics of the rectangular signal). A perturbation method can be obtained by starting from infinite and zero impedances, respectively. A key point is that at each step, frequency is fixed in order to calculate the perturbation, then a new value is calculated using any equation of the harmonic balance system, an excellent candidate being the reactive power defined by Boutillon. In this preliminary study, results are compared for a simplified problem to those of the harmonic balance method, and they are very interesting, especially far from the oscillation thresholds.

### 1. INTRODUCTION

Since Helmholtz, it is well known that the most common sounds of bowed string instruments correspond to a signal close to a pure square or "rectangular" shape (for the signal of the string velocity).

When losses are ignored, solutions of elementary models are pure square or "rectangular" signals, called Helmholtz motion. When losses are introduced, round corner signals are obtained, and the calculation becomes more delicate (see e.g. Woodhouse [1]). Complete computation in the time domain is possible, but taking into account the simplicity of the solutions when no losses are present, an interesting question is whether it is possible to deduce the result with losses from the result without losses by using a perturbation method. The present paper gives a preliminary answer for a similar, but simpler problem: the steady-state, periodic regime of the internal pressure signal for a cylindrical, clarinet-like instrument. It is simple because the nonlinear characteristic, assumed to be independent of time, can be written as a polynomial of the third order, at least at rather low levels of excitation, and because, if the playing frequency is much smaller than the eigenfrequency of the reed, the reed can be regarded as a simple spring without mass and damping. With some classical, complementary

hypotheses (see e.g. Kergomard [2]), the system to be solved is a system of two equations relating the acoustic volume velocity  $u(t)$  at the input of the resonator to the acoustic pressure in the mouthpiece  $p(t)$ . One of them describes the nonlinear excitation mechanism, while the other one describes the resonator, assumed to be linear, as follows:

$$u = u_{00} + Ap + Bp^2 + Cp^3 \quad (1)$$

$$u = h * p, \quad (2)$$

where  $h(t)$  is the impulse response of the resonator, whose Fourier Transform is the input admittance  $Y(\omega)$ , the second equation often being written in the frequency domain:

$$U(\omega) = Y(\omega)P(\omega). \quad (3)$$

(The capital characters are used for the Fourier transform of the quantities of the time domain noted in small characters).

When no losses are considered, the input admittance is infinite for anti-resonance frequencies, and zero for resonance frequencies. If in addition the resonator is cylindrical and radiation entails only a length correction, the anti-resonances correspond to the even harmonics of the oscillation and the resonances to the odd harmonics. With these two conditions, the steady-state solution of the system is a pure square signal, the oscillation frequency being the classical value  $c/4\ell$ , where  $c$  is the speed of sound and  $\ell$  the length of the resonator.

When losses are present, the maxima and minima become finite but the maxima remain large and the minima small as losses are rather weak. When dispersion is taken into account, or if there is a small deviation from the pure cylindrical shape of the resonator, the oscillation frequency, which is an unknown of the system, will in general be close to that of the nondispersive case, and the values of the admittance will not be strongly modified. Thus it is intuitive that a perturbation calculation is possible for both the shape of the signal and the oscillation frequency.

The first step of the reasoning is to avoid infinite or very large quantities, such as the impedance or admittance maxima in the frequency domain, or the maxima of the impulse response in the time domain. A solution consists in considering the frequency domain and dividing the harmonics into two classes: those with high impedance (low admittance) and those with low impedance (high admittance). The even harmonics of the pressure and the odd harmonics of the volume velocity are all small quantities, vanishing for the ideal condition of the pure Helmholtz motion, so they are good basic quantities for a perturbation calculation.



Note however that if a small shift in the oscillation frequency occurs because of dispersion or other causes, a perturbation calculation can become very bad for higher order harmonics. Thus it is essential to treat carefully the problem of the frequency shift. This will be explained in further detail in section 5. In the main part of the paper, we consider first that neither dispersion nor any other cause of frequency shift exist. As a consequence, the oscillation frequency is known and equal to  $c/4\ell$ . Moreover, in order to simplify the study of the problems of convergence for this preliminary study, the admittance is assumed to remain infinite for the even harmonics. The zeroth order solution, i.e. the pure Helmholtz motion, is recapitulated in section 2, then the first and second orders of the loss parameters are derived analytically in section 3. In section 4 the numerical treatment of the iterative procedure is presented as well as the results and a discussion about convergence.

## 2. ZEROth ORDER SOLUTION: THE PURE

### HELMHOLTZ MOTION

The first step of the method is the separation of the even and odd harmonics of the signal, i.e. the symmetrical and antisymmetrical parts (with indices  $s$  and  $a$ , respectively). The two following equations are obtained (see Kergomard et al. [3]) and replace equation (1):

$$u_s = u_{00} + Ap_s + B(p_s^2 + p_a^2) + C(p_s^3 + 3p_s p_a^2) \quad (4)$$

$$u_a = Ap_a + 2Bp_s p_a + C(3p_a p_s^2 + p_a^3). \quad (5)$$

The equations replacing the linear equation (2) are obvious.

The even harmonics of the pressure are then ignored ( $p_s = 0$ ), as explained earlier, and the initial set of equations is replaced by the following:

$$u_a = Ap_a + Cp_a^3 \quad (6)$$

and

$$u_a = h * p_a. \quad (7)$$

If no losses are present, since  $h(t)$  only contains even harmonics and  $p_a$  only contains by definition the odd harmonics of  $p$ , equation (7) leads to  $u_a = 0$ . Then, eliminating in equation (6) the static solution  $p_a = 0$ , the pure Helmholtz motion is found to be

$$p_a = \pm \sqrt{-A/C} \quad (8)$$

where  $C$  is negative [2].  $A = 0$  at the threshold of oscillation. The Fourier components of this square-wave signal are well known. This is the zeroth order solution, and we will denote it  $p_0$ .

The volume velocity  $u_s$  is constant (only the d.c. component exists), and can be deduced by using equation (4).

## 3. FIRST AND SECOND ORDER SOLUTIONS

The basic principle of the method relies on the hypothesis that, for the components of  $h(t)$  existing in the signals  $u_a$  and  $p_a$ ,  $h(t)$  is a first order function of a loss parameter. As an example, for pure cylindrical, sufficiently narrow tubes,  $h(t)$  is proportional to the loss parameter  $\eta$  equal to  $\sqrt{\ell \ell_v}/r$ , where  $\ell_v$  is the characteristic length of the viscous effects [2] and  $r$  the radius of the tube. Expanding the acoustic pressure at successive orders of  $\eta$  i.e. writing

$p_a = p_0 + p_1 + p_2 + \dots$ , it is possible to solve equations (6) and (7). At the first order, the following result is obtained:

$$h * p_0 = Ap_1 + 3Cp_0^2 p_1. \quad (9)$$

Using the zeroth order result (8), it can be simplified to

$$h * p_0 = -2Ap_1. \quad (10)$$

This result is extremely simple to write in the frequency domain since it is linear:

$$P_{1n} = -\frac{1}{2} \frac{Y_n}{A} P_{0n}, \quad (11)$$

the index  $n$  corresponding to the  $n$ th (odd) Fourier component of the signal. It is remarkable that the result for the first harmonic is identical to the result of the "first harmonic method," which consists in the approximation of the unknown signal by its first component only, as follows [2]:

$$P_1 = \frac{1}{3} \sqrt{\frac{Y_1 - A}{C}} = \frac{1}{3} \sqrt{-\frac{A}{C}} \left( 1 - \frac{1}{2} \frac{Y_1}{A} + O\left(\frac{Y_1^2}{A^2}\right) \right). \quad (12)$$

The first term on the right-hand side is the value of the result when no losses exist. The extension of this approximation, called the "Variable Truncation Method" [3], also gives results for higher order harmonics, but these are different from the result (11), as the third harmonic, for example, depends on both  $Y_1$  and  $Y_3$ . In any case, equation (12) allows an intuitive idea of the interest of the method presented in the present paper. The relevant quantities are the ratios  $Y_n/A$ : they are small either if losses are small or if the excitation level  $\gamma$ , directly related to  $A$ , is strong. Near the oscillation threshold, which satisfies exactly  $A = Y_1$  (see Grand et al. [4]), the quantity  $Y_1/A$  approaches unity, and the series expansion (12) is thus not of interest.

A conclusion is that the present method is without interest near the oscillation threshold, and is complementary to the methods valid near the threshold, i.e. the Small Oscillation Method (see Worman [5] and reference [4]) or the more general Variable Truncation Method. We remind that these two methods are exact near the oscillation threshold under conditions related to the relative height of the first impedance peak and the other peaks. On the other hand, the present method is particularly well adapted when  $Y_1/A \ll 1$ . For example, when losses are neglected, the Harmonic Balance Method (see Farner et al. [6]) fails to converge toward the Helmholtz solution, which is given by order 0 of the present method.

Another feature concerning the present method is that the quantities  $Y_n/A$  can be relatively large for the higher order harmonics, since losses in general increase with frequency, but as convergence is obtained (see below), this must be explained by the small influence of the higher order harmonics on the result.

Continuing the procedure, the following nonlinear result is obtained for the second order of the perturbation:

$$h * p_1 = -2Ap_2 + 3Cp_0 p_1^2. \quad (13)$$

The last term can be computed either in the time domain, using sampling, or in the Fourier domain, using the product of infinite series. The second method (with a truncation of the series to a certain number of harmonics) is used in the following because the left-hand side of equation (13) is easily calculated in the frequency domain. If the series are truncated to the first harmonic,

the second-order result is obtained:

$$P_1 = P_{01} \left[ 1 - \frac{Y_1}{2A} + \frac{Y_1^2}{4A^2} \left( 1 - \frac{18}{\pi^2} \right) \right] \quad (14)$$

which differs from that of the first harmonic method (equation (12)). Nevertheless, this equation can provide some useful analytical approximations even for a low order of the truncation.

#### 4. HIGHER ORDER SOLUTIONS

Equation (13) shows the general shape of the higher order solutions:

$$h * p_{m-1} = -2Ap_m + C \times \left( \begin{array}{l} \text{products of three} \\ \text{lower-order solutions} \end{array} \right) \quad (15)$$

which need to be computed numerically. The algorithms are rather simple to establish and therefore not presented here. The product of three series is reduced to a double product for the calculation of the amplitude of the harmonics of the order  $m$  in the loss parameter.

The first property to study is the convergence for the order  $m$  when the number of harmonics increases. The modulus of a few odd harmonics of  $p$ , divided by their value at 100 harmonics, are plotted in figure 1 for order  $m = 5$ ,  $\gamma = 0.4$ , and  $\eta = 0.002$ . It can be seen that for these parameter values (not too close to the oscillation threshold and for rather weak losses), the moduli are converging as the number of harmonics increase.

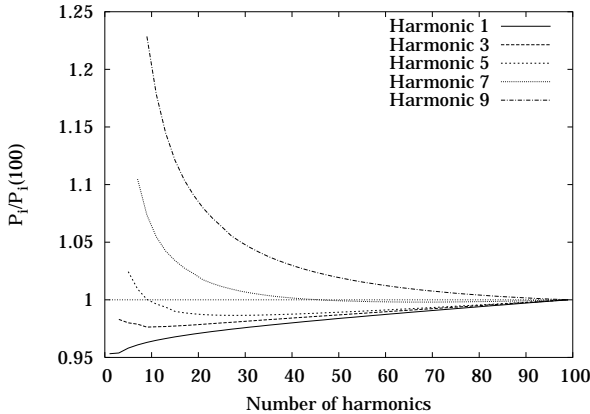


Figure 1: Modulus of the first five odd harmonics of  $p$  (order 5,  $\gamma = 0.4$ ,  $\eta = 0.002$ ) for an increasing number of harmonics, divided by their value at 100 harmonics

The second property to study is the convergence of the first harmonic  $P_1$  as the order of  $\eta$  increases. As expected, the convergence is rather rapid for high excitation levels  $\gamma$  and for low losses. Figure 2 shows the first harmonic of the pressure as  $\gamma$  is varied, for different orders of approximation. Moreover, the solution given by the Harmonic Balance Method (HBM) is plotted for comparison. In this case, losses are rather weak ( $\eta = 0.002$ ), and excepted in the vicinity of the oscillation threshold, few orders are required to converge toward the solution given by the HBM.

Results for the difficult case of rather strong losses ( $\eta = 0.02$ ) are presented in figure 3. As expected, convergence toward the solution given by the HBM is more questionable near the threshold

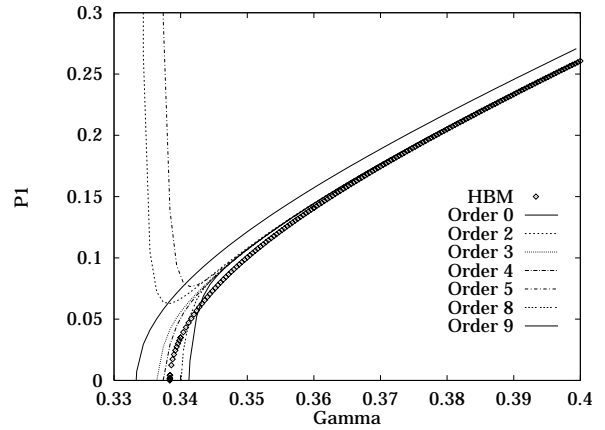


Figure 2: First harmonic of the pressure, when  $\gamma$  is varied, for different orders of approximation compared to the solution given by the HBM ( $\eta = 0.002$ , 50 harmonics)

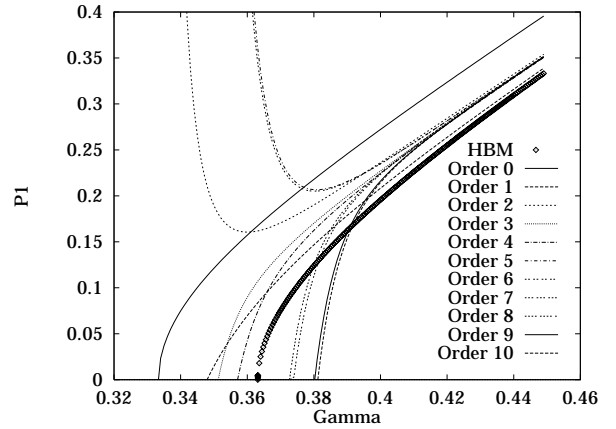


Figure 3: First harmonic of the pressure, when  $\gamma$  is varied, for different orders of approximation compared to the solution given by the HBM ( $\eta = 0.02$ , 50 harmonics)

of oscillation. More surprisingly, however, the converging results far from the threshold deviate from that of the HBM. This has to be further investigated.

In order to solve completely the initial set of equations (1) and (2), it is necessary to calculate the even harmonics, i.e. more generally the low-impedance components of the signal. This is done by a straightforward extension of the above-explained principle: expansion of the volume velocity  $u_s$  at successive orders of the loss parameters and solving of the set of equations (4) and (5).

#### 5. HOW TO TREAT THE QUESTION OF THE PLAYING FREQUENCY?

Another important point is how to calculate the (unknown) oscillation frequency when for instance dispersion occurs. As explained earlier, it is absolutely necessary that, during each step of the iteration, the frequency does not change, otherwise the perturbation calculation is impossible (for higher order harmonics, the error would be unacceptable). Actually, the playing frequency can be

determined by a parallel calculation. At the zeroth order, the frequency is known to be  $c/4\ell$ , and the solution for the amplitudes is known by equation (8). For the first and higher orders, one supplementary equation is necessary. We remark that the "reactive power" equation (see Boutillon and Gibiat [7]) is an excellent choice for such a supplementary equation:

$$\sum_{n=0}^{\infty} n \Im(Y_n) |P_n|^2 = 0. \quad (16)$$

(This is based on the fact that the nonlinear characteristic is independent of time, and is contained in the HBM equations.) After truncating it to the convenient number of harmonics, the frequency can be calculated in each step by noting the admittance  $Y_n$  for the  $n$ th harmonic depends on the frequency. Once the first order approximation of the frequency is determined, the first order approximation of the amplitudes is calculated using the admittance valid for the frequency just obtained. Compared to the simplified case studied in the previous sections, one supplementary step needs to be solved at each order of the iteration.

## 6. GENERAL COMMENTS AND CONCLUSION

The method presented in the paper, the perturbation of the Helmholtz motion, has shown to be efficient except near the oscillation threshold, where the signals involve very few harmonics. This is not a surprise as using a square signal as a starting point is not appropriate for that case so far from a square wave. We notice that most of the self-sustained oscillation instruments have a behaviour of inverse bifurcation, i.e. that the solutions near the oscillation threshold are unstable, thus uninteresting (see e.g. Dalmont et al. [8]). For instruments like a clarinet, having a direct bifurcation, other methods need to be used near the threshold.

It remains to take into account both the even harmonics and the variation of the oscillation frequency with the excitation level. The extension to conical instruments is in principle easy, by separating the small and large impedance components. Concerning bowed string instruments, a generalization is possible, if a nonlinear, time-independent characteristic exists.

The question of transients should be explored. At least for resonators with harmonically related resonances, it seems to be possible to extend the method.

Finally, a major interest for the current method lies in the possibility to get analytical approximations for such nonlinear systems, e.g. at the first or second orders. This may be exploited to study the effect of for instance nonlinear functions that are discontinuous or have a discontinuous derivative, like the violin.

## 7. REFERENCES

- [1] Woodhouse, J., "Self-sustained oscillators", in *Mechanics of musical instruments* (Lecture notes of CISM, Springer), A. Hirschberg et al. eds., pp. 185–228, 1995.
- [2] Kergomard, J., "Elementary considerations on reed-instruments oscillations", in *Mechanics of musical instruments* (Lecture notes of CISM, Springer), A. Hirschberg et al. eds., pp. 229–290, 1995.
- [3] Kergomard, J., Ollivier, S., and Gilbert, J., "Calculation of the spectrum of self-sustained instruments using a variable truncation method: application to cylindrical reed instruments", *Acustica–Acta Acustica* Vol. 86, 685–703, 2000.
- [4] Grand, N., Gilbert, J. and Laloe, F., "Oscillation threshold of woodwind instruments", *Acta Acustica* Vol. 1, 137–151, 1997.
- [5] Worman, W.E., "Self-sustained non-linear oscillations of medium amplitude in clarinet-like systems", PhD thesis, Case Western Reserve Univ., Cleveland, Ohio, 1971.
- [6] Farner, S., Vergez, C., and Kergomard, J., article in preparation.
- [7] Boutillon, X. and Gibiat, V., "Evaluation of the acoustical stiffness of saxophone reeds under playing conditions by using the reactive power approach", *J. Acoust. Soc. Am.*, Vol. 100, 1178–1189, 1996.
- [8] Dalmont, J.P., Gilbert, J., and Kergomard, J., "Reed instruments, from small to large amplitude periodic oscillations and the Helmholtz motion analogy", *Acustica–Acta Acustica*, Vol. 86, 671–684, 2000.

# SIMULATING THE MECHANISM OF SOUND GENERATION IN FLUTES USING THE LATTICE BOLTZMANN METHOD

*Helmut Kühnelt*

Institute of Musical Acoustics  
University of Music and Performing Arts Vienna  
kuehnelt@mdw.ac.at

## ABSTRACT

The sound generation in flute-like instruments, as flutes, recorders and flue organ pipes, is determined by non linear acoustical and fluid dynamical processes, which interact closely. Because of different scales the coupling is rather weak. In addition to that, geometrical parameters of the mouth of the flute as the shape of the labium or the flue exit, where the jet is formed, influence the amplitude and the spectrum of the generated sound considerably. A model for simulating self sustained oscillations in flutes should be able to include weak coupling and strong dependence on boundary conditions.

The lattice Boltzmann method is a rather new method for simulating fluid flow, and as a special discretization of the Boltzmann equation it incorporates fluid dynamics and acoustics intrinsically. In addition to that complex boundary conditions can be modelled very easily. The advantages and shortcomings of the lattice Boltzmann method will be discussed. First results of simulations of a small organ pipe with recorder like dimensions will be presented. They show that the lattice Boltzmann method is able to model self sustained oscillations in flutes.

## 1. INTRODUCTION

Sound generation in flue pipes – flutes, recorders and labial organ pipes – is determined by the interaction of aerodynamic and acoustic phenomena in the mouth of the instrument like vortex shedding at edges which can be both a sound generating and absorbing mechanism.

While simple models can provide insights into the principles of sound generation, until now they can't give more than qualitative predictions in the fields that interest musicians and instrument makers, the amplitude and spectrum of the generated sound.

The simulation of the interaction of aerodynamics and acoustics in flutes leads to several demands:

- The algorithm must be able to accurately track both the sound field and the aerodynamic field, which propagate with disparate velocities and are weakly coupled.
- In flutes the speed of the jet is in most cases considerably lower than 10% of the sound speed. So the used algorithm must cope with very low Mach numbers, which is a non-trivial task for the numerical implementation.
- In low Mach number flow the sound generation is primarily determined by slow vorticity fluctuations which are minute compared to the energy levels of the whole flow.
- In addition to that, geometrical parameters of the mouth of the flute as the shape of the labium or the flue exit, where the

jet is formed, influence the amplitude and the spectrum of the generated sound crucially. For a quantitative prediction their effect on the sound should be modelled realistically.

A model for simulating self sustained oscillations in flutes should be able to include all, weak coupling, small acoustical energies and strong dependence on boundary conditions.

The Lattice Boltzmann method is a quite recent approach for simulating fluid flow, which has proven as a valid and efficient tool in a variety of complex flow problems. In the field of aeroacoustics some fundamental studies have been undertaken showing its validity [1, 2, 3] and only few dealt with applied problems [4, 5]. So the use of the Lattice Boltzmann Method as a tool for computational aeroacoustics can be seen as in its early but encouraging stage.

### 1.1. Lattice Boltzmann Method

The Lattice Boltzmann method (LBM) approximates the Navier-Stokes equations and as a specific discretization of the Boltzmann equation it incorporates fluid dynamics and acoustics intrinsically.

The phase space is discretized spatially and temporally in such a way that the mesoscopic distributions  $f_i$  of the particle populations travel on a regular grid in discrete directions with discrete speeds  $\mathbf{c}_i$ . The nondimensionalized evolution equation of the LBM reads

$$f_i(\mathbf{r} + \mathbf{c}_i, t + 1) = f_i(\mathbf{r}, t) + \Omega_i(f)(\mathbf{r}, t), \quad (1)$$

with the collision term  $\Omega_i(f)(\mathbf{r}, t)$ . This equation can be separated in two steps: The right hand side can be taken as a fully local collision step, the left hand side as the step for propagation to the neighbors on the grid. The structure of (1) shows that the LBM can be implemented easily and is efficient for parallelization.

The conserved macroscopic quantities density  $\rho$  and momentum density  $\mathbf{j} = \rho \mathbf{u}$  are the first and second moments of the distributions  $f_i$ :

$$\rho(\mathbf{r}, t) = \sum_i f_i(\mathbf{r}, t) \quad (2)$$

$$\rho(\mathbf{r}, t) \mathbf{j}(\mathbf{r}, t) = \sum_i \mathbf{c}_i f_i(\mathbf{r}, t) \quad (3)$$

Note that in the isothermal or more correct athermal model used here the temperature is not a conserved quantity. As equation of state that of an ideal gas is chosen:  $p = c_s^2 \rho$ .

The chosen set of lattice velocities  $\mathbf{c}_i$  has to fulfill specific conditions of symmetry and isotropy to recover the desired macroscopic behavior, here the Navier-Stokes equations. The simplest

velocity sets have seven or nine elementary vectors in two dimensions and 15 or 19 populations in three dimensions.

The most simple LB model to implement is the single relaxation time (BGK) model:

$$f_i(\mathbf{r} + \mathbf{c}_i, t + 1) = f_i(\mathbf{r}, t) - \frac{1}{\tau} \left( f_i(\mathbf{r}, t) - f_i^{eq}(\rho(\mathbf{r}, t), \mathbf{u}(\mathbf{r}, t)) \right), \quad (4)$$

with the relaxation time  $\tau$  and the equilibrium distribution  $f_i^{eq}$ , which only depends on the conserved macroscopic quantities. A low Mach number expansion of the Maxwell-Boltzmann distribution, second order in  $\mathbf{u}$  is commonly used as equilibrium distribution in order to approximate the Navier-Stokes equations in the limit for small Mach numbers and small Knudsen numbers and states not too far from equilibrium.

For wave vectors  $\mathbf{k} = 0$  the macroscopic behavior of the LBM can be deduced using a multi-scale (Chapman-Enskog) expansion which leads to the compressible Navier-Stokes equations (up to terms  $\text{Ma}^4$ ):

$$\partial_t \rho + \partial_\alpha \rho u_\alpha = 0 \quad (5)$$

$$\begin{aligned} \partial_t \rho u_\alpha + \partial_\beta (\rho c_s^2 \delta_{\alpha\beta} + \rho u_\alpha u_\beta) = \\ \partial_\beta c_s^2 \rho \left( \tau - \frac{1}{2} \right) (\partial_\alpha u_\beta + \partial_\beta u_\alpha) \end{aligned} \quad (6)$$

$c_s = 1/\sqrt{3}$  is the sound speed of the model,  $\nu = (\tau - \frac{1}{2}) c_s^2$  and  $\lambda = \frac{2}{d} c_s^2 \rho (\tau - \frac{1}{2})$  are the kinematic and the bulk viscosity in  $d$  spacial dimensions. These dimensionless equations can be connected to “the real world” by

$$c_s^{real} = c_s \frac{\delta x}{\delta t}, \quad \nu^{real} = \nu \frac{\delta x^2}{\delta t}, \quad (7)$$

with the lattice spacing  $\delta x$  and the time step  $\delta t$ .

For wave numbers  $\mathbf{k} > 0$  a linear stability analysis [6] shows that up to second order of  $\mathbf{k}$  the acoustic wave propagation is Galilean invariant and the shear and bulk viscosities are independent from  $\mathbf{u}$ . Additionally the stability analysis shows that transverse modes are generally more stable than longitudinal modes and that sound waves propagating in the direction of the mean flow velocity can be quite unstable. As the unstable modes have a small spatial scale, spacial or temporal filtering can be used as a practical means to limit the development of instabilities.

LB models with collision terms with multiple relaxation times [7] are more stable than BGK models. Their free parameters are adjusted to minimize the effect of the lattice symmetry on the macroscopic behavior of the model. In these models the distributions  $f_i$  are transformed from the vector space based upon the discrete velocity set into a vector space based upon the moments of  $f_i$  – the hydrodynamic quantities and their fluxes – where the relaxation parameters of the moments are directly related to the various transport coefficients. Nevertheless due to the transformations, they tend to be more sensitive to the numerics of the computer.

Simulating low viscosity flows with LBM meets a principal problem of stability. Due to the truncated expansion of the equilibrium distribution, the H-theorem of the continuous Boltzmann equation is no longer valid, nevertheless there results a region of stability, which turns out to be rather large for isothermal LBM.

In LB models boundary conditions can be implemented very easily. A rigid wall can be modelled with bounce-back, where all incident populations are reflected exactly 180 degrees,  $f_{out} = f_{in}$ ,  $\mathbf{c}_{out} = -\mathbf{c}_{in}$ , leading to zero velocity at the wall.

In short, the LBM is an approximation of the Navier-Stokes equations which is fully local in space and time, second-order accurate in space and time, pointwise conservative, conditioned to low Mach numbers, unconditionally linearly but only conditionally nonlinearly stable, efficient to serial and parallel computers and can easily handle irregular boundary conditions (within the limits of the regular grid).

## 2. SIMULATING A FLUTE WITH LBM

The sound generation in a small stopped flue pipe with recorder-like proportions was simulated using a three dimensional LBM with 19 populations.

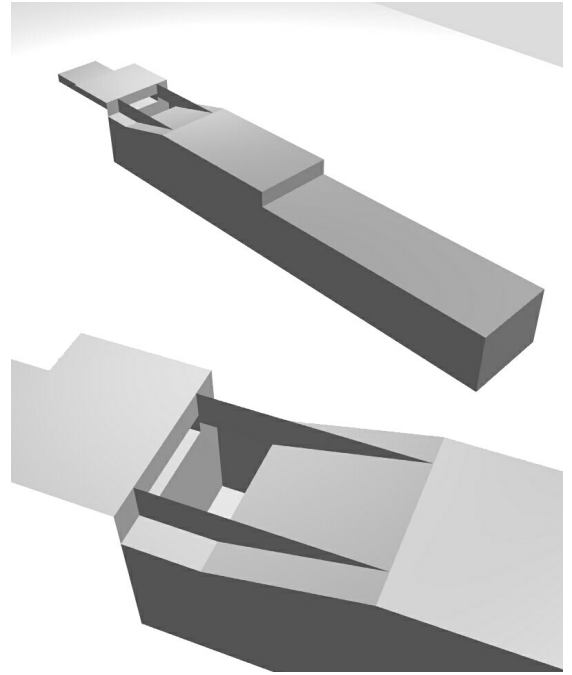


Figure 1: The simulated stopped organ pipe with detailed view of the mouth.

The dimensions are 60 mm  $\times$  7 mm  $\times$  7 mm for the resonator, 15 mm  $\times$  4.5 mm  $\times$  1.2 mm for the flue. The ratio of the distance from flue exit to the labium to the height of the flue exit is about 4, as observed in many recorders of various size and the angle of the labium is approx. 14°. The whole pipe is embedded into a volume of 75 mm  $\times$  7 mm  $\times$  19 mm. Due to the limited computational resources the lattice spacing had to be chosen rather large,  $\delta x = 0.22$  mm.

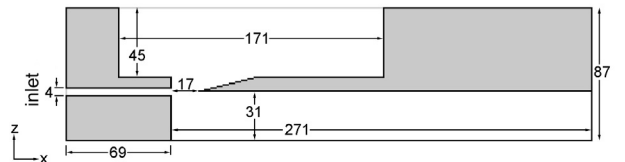


Figure 2: Cross section of the simulated pipe. Dimensions in lattice units.

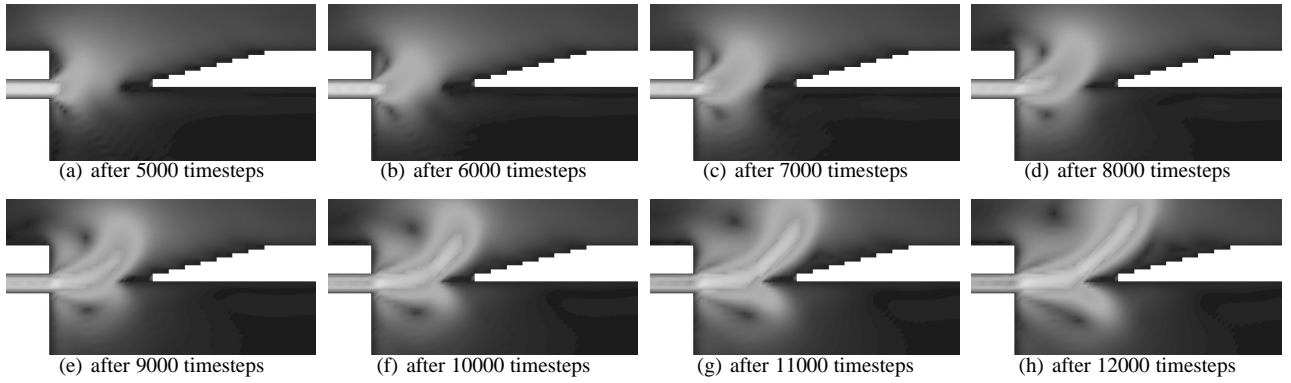


Figure 3: Formation of the jet during start-up. The value of the velocity ranges from blue ( $u = 0$ ) to red (max. velocity). Note that due to the coloring the edge of the labium, where  $u = 0$ , is actually positioned a little more to the left than as it looks.

The isotherm speed of sound  $c_s = 340/\sqrt{1.4}$  m/s was used, resulting in a time step of  $\delta_t = 4.42 \cdot 10^{-7}$  s. The time for rising the flow in the flue was  $10000 \delta_t = 4.42$  ms.

The walls were modelled with the bounce-back boundary condition, at the inlet and outlet the populations entering the volume were determined by the equilibrium distribution.

## 2.1. Formation of the jet at startup

When the pressure rises at the inlet and a flow through the flue develops, at the flue exit a jet is formed due to the effect of viscosity, as shown in fig. 3. The vortices that are shed above and below the flue exit are clearly visible. This shows that with the LBM effects of viscosity emerge naturally, with no needs of special boundary conditions.

Figures 4 - 7 show the velocity profile of the jet at distances of 2, 7, 12 and 17 lattice spacings downstream the flue exit at 11000 timesteps after startup. The jet at the flue exit (fig. 4) has a maximum speed of  $Ma = 0.027$  (7.76 m/s) in its centerline and a velocity profile that matches very well with the theoretical prediction for a jet emerging from a long channel, a Bickley profile

$$U(x, z) = U_0(x) \text{sech}^2(z/b), \quad (8)$$

where  $U_0$  defines the centerline jet velocity and  $b$  the jet half-thickness.

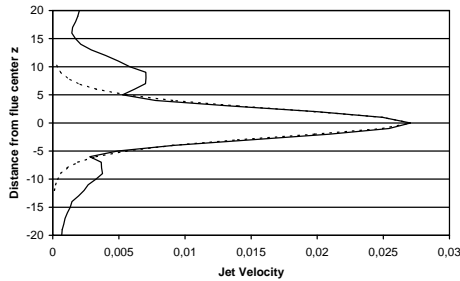


Figure 4: Velocity profile of the jet  $2 \delta_x$  downstream the flue exit. The velocity profile matches very well with the Bickley-profile (dotted).

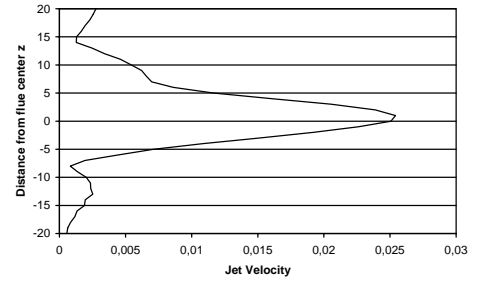


Figure 5: Velocity profile of the jet  $7 \delta_x$  downstream the flue exit.

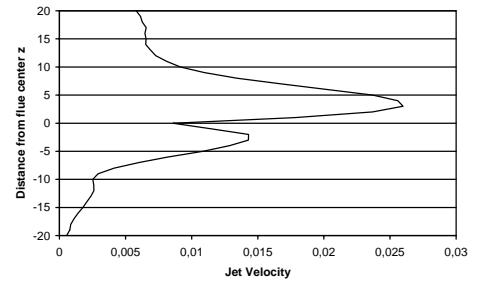


Figure 6: Velocity profile of the jet  $12 \delta_x$  downstream the flue exit.

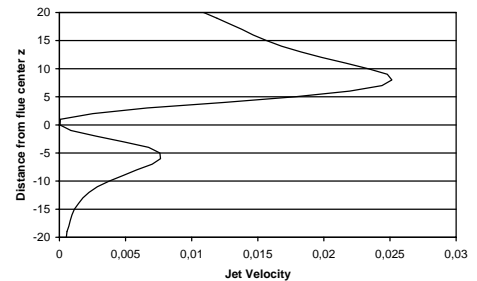


Figure 7: Velocity profile of the jet  $17 \delta_x$  downstream the flue exit. The jet has impinged on the labium.

Because of the higher mean pressure inside the stopped resonator the velocity profile of the jet is not symmetrical.

## 2.2. Steady-state oscillations

Figure 8 shows the density inside the resonator. In this simulation the maximum velocity in the flue was about 5,4 m/s. Already during the rising time an oscillation starts and approaches a steady state. Only the fundamental mode of the pipe is stimulated and its frequency is  $2116.7/\delta_t$ , equivalent 1068.8 Hz, the fundamental frequency of a stopped pipe of 6.73 mm length, which fits well to the length of the used model including an additional end correction caused by the baffles on both sides of the mouth. Inside at half length of the resonator (fig. 8) there is a sound pressure level of 125 dB. In the mouth, where the sound pressure level is 115 dB, the acoustical velocity perpendicular to the jet (fig. 8) has  $\text{Mach} = 0.0003$ .

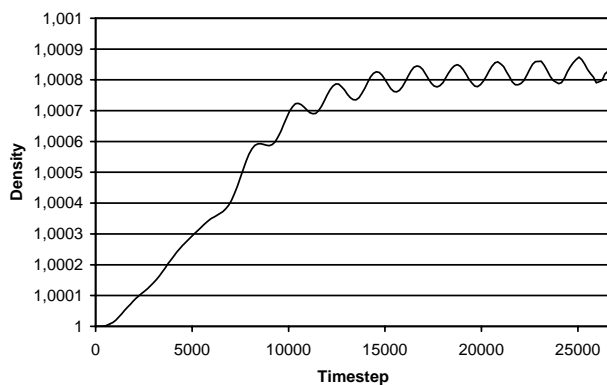


Figure 8: Density at half length of the resonator.

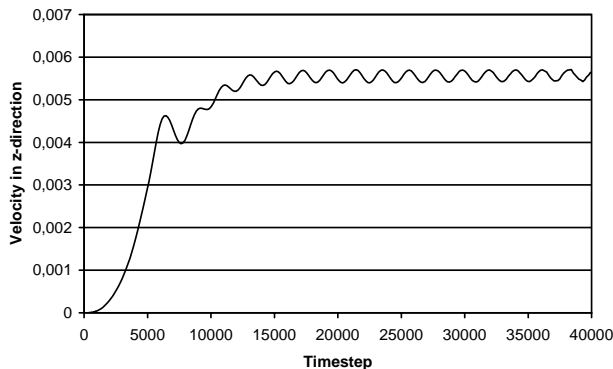


Figure 9: Maximum velocity in z-direction of the jet in the middle of the mouth of the pipe, at 2/3 between flue exit and labium (in Ma).

## 3. CONCLUSIONS

Although some important aspects of the sound generation in flutes like overblowing have been excluded until now and quantitative predictions have not been checked so far, the presented results – the jet velocity, the sound pressure level, the sounding frequency

– are encouraging, because they are within a realistic range. The LBM is still under development and it has a notable potential as tool for aeroacoustic simulations.

## 4. REFERENCES

- [1] Buick, J.M., Greated, C.A. and Campbell, D.M., "Lattice BGK simulation of sound waves", *Europhysics Letters*, 43(3):235-40, 1998.
- [2] Buick, J.M., Buckley, C.L., Greated, C.A. and Gilbert, J., "Lattice Boltzmann BGK simulation of nonlinear sound waves: the development of a shock front", *Journal of Physics A*, 33:3917-28, 2000.
- [3] Haydock, D. and Yeomans, J.M., "Lattice Boltzmann simulations of acoustic streaming", *Journal of Physics A*, 34:5201-13, 2001.
- [4] Wilde, A., "Simulation of sound wave propagation in turbulent flows using a Lattice-Boltzmann scheme", *Proc. Forum Acusticum*, Sevilla, Spain, 2002.
- [5] Skordos, P. and Sussman, G., "Comparison Between Subsonic Flow Simulation and Physical Measurements of Flue Pipes", *Proc. ISMA 1995*, Le Normont, France, pp. 79-85, 1995.
- [6] Lallemand, P. and Lou, L.S., "Theory of the Lattice Boltzmann Method: Dispersion, Dissipation, Isotropy, Galilean Invariance, and Stability", *Physical Review E*, 61(6):6546-62, 2000.
- [7] d'Humières, D., Ginzburg, I., Krafczyk, M., Lallemand, P. and Luo, L.S., "Multiple-relaxation-time lattice Boltzmann models in three dimensions", *Phil. Trans. R. Soc. Lond. A*, 360:437-51, 2002.

## METHODS FOR SYNTHESIZING VERY HIGH Q PARAMETRICALLY WELL BEHAVED TWO POLE FILTERS

Max V. Mathews (m.v.mathews@att.net)

Julius O. Smith (jos@ccrma.stanford.edu)

Center for Computer Research in Music and Acoustics (CCRMA)  
Department of Music, Stanford University  
Stanford, California 94305

### ABSTRACT

Techniques for synthesizing two pole filters are well known. A number of techniques introduce unpleasant sounding transients in the filter response when the frequency or damping of the filter is rapidly changed. We will demonstrate a difference equation for a digital filter in which both the frequency and the damping can be changed without producing discontinuities in the filter output. The technique is based on the well known property of the product of complex numbers. In polar form, the magnitude of the product of two numbers is the product of their magnitudes and the angle of the product is the sum of their angles. Successive multiplies can produce a rotating vector whose real or imaginary parts are samples of constant amplitude sine waves or of exponentially damped sine waves. The frequency and damping of the resulting waves can be changed without changing the amplitude of the waves. These properties can be used to make a digital filter whose input, frequency, and damping can all be functions of time in a useful way. Two alternative structures are additionally proposed, having better numerical properties for low-cost fixed-point implementations. A program to demonstrate some musical applications of these filters will be shown.

### 1. INTRODUCTION

Filters, whose parameters can be varied in time provide an important new resource in musical timbres. High Q filters are also desirable since most musical instruments involve high Q mechanical filters. Unfortunately, tuning a high Q filter can introduce artifacts which change the energy in the filter and produce unpleasant transients in the sound. A mechanical filter consisting of an object on a spring provides a simple example of the problem. The resonant frequency of the object-spring system can be changed by either changing the stiffness of the spring or the mass of the object. But if the mass of the object is changed while the object is moving, the kinetic energy in the object will be changed. Likewise, if the stiffness of the spring is changed while the spring is stretched, the potential energy stored in the spring will be changed. Any change of energy will cause a change in the amplitude of the oscillation.

### 2. OSCILLATOR BASED ON COMPLEX NUMBER MULTIPLICATION

A well known difference equation exists which can compute samples of parametrically well behaved sinusoids [1, 2]. The frequency of the sinusoid can easily be changed without changing the amplitude. The equation is a property of the multiplication of two complex numbers.<sup>1</sup> Complex numbers can be represented as two dimensional vectors in a plane in which the x axis is the real part of the number and the y axis is the imaginary part of the number. The polar coordinate form of the vector is a magnitude and an angle (measured from the x axis). The magnitude of the product of two numbers is the product of the magnitudes of the two numbers and the angle of the product is the sum of the angles of the two numbers.

We will use the following definitions and relations:

$$\begin{aligned} j &\triangleq \sqrt{-1} \\ z &\triangleq \text{a complex number} \\ r &\triangleq |z| \\ \theta &\triangleq \angle z \end{aligned}$$

In terms of real and imaginary components:

$$z = x + jy$$

where

$$\begin{aligned} x &= r \cos(\theta) \\ y &= r \sin(\theta) \end{aligned}$$

Let a sequence of complex numbers

$$z(n), \quad n = 0, 1, 2, 3, \dots$$

be formed from the product of two complex numbers

$$z(n+1) = z_1 z(n), \quad (1)$$

where  $z_1 \triangleq e^{j\theta_1} = \cos(\theta_1) + j \sin(\theta_1)$ . The initial state is taken to be  $z(0) = 1$ , i.e., the initial magnitude and angle are  $r(0) = 1$  and  $\theta(0) = 0$ , respectively. By the rules of complex number multiplication, we have

$$r(1) = r(2) = \dots = r(n) = 1$$

---

<sup>1</sup>[http://www-ccrma.stanford.edu/~jos/mdft/Complex\\_Numbers.html](http://www-ccrma.stanford.edu/~jos/mdft/Complex_Numbers.html)



and

$$\theta(n) = n\theta_1.$$

The imaginary part of  $z(n)$  is the desired sine wave:

$$y(n) = \sin(n\theta_1).$$

The magnitude of the sine wave is always 1. The period of the sine wave is  $2\pi/\theta_1$  samples.

By changing  $\theta_1$ , the period can be changed without affecting the magnitude.

The actual difference equations to compute the sine wave are obtained by writing Eq. (1) as real and imaginary parts. This yields two difference equations which can be extrapolated to compute  $x(n)$  and  $y(n)$ :

$$x(n+1) = x_1x(n) - y_1y(n) \quad (2)$$

$$y(n+1) = y_1x(n) + x_1y(n) \quad (3)$$

where  $x_1 = \cos(\theta_1)$  and  $y_1 = \sin(\theta_1)$ .

### 3. HIGH Q FILTER DIFFERENCE EQUATIONS

#### 3.1. Homogeneous Solution

Equations (1–3) can be modified to compute the response of a finite  $Q$  filter simply by changing  $r_1$  to some value different from unity. From Eq. (1),  $|z(n)|$  will be  $r_1$  raised to the  $n$ th power, and  $y(n)$  will be

$$y(n) = r_1^n \sin(n\theta_1) \quad (4)$$

If  $r_1$  is less than one, Eq. (4) shows the homogeneous solution to Eq. (1) is a sinusoid times a decaying exponential. This solution is the response of a two pole filter.

Equations (2–3) are unchanged except that the coefficients  $x_1$  and  $y_1$  become

$$x_1 = r_1 \cos(\theta_1) \quad (5)$$

$$y_1 = r_1 \sin(\theta_1) \quad (6)$$

If  $y(n)$  is the input to a digital-to-analog converter operating at a sampling rate of  $f_s$  samples per second, then  $x_1$  and  $y_1$  can be written

$$x_1 = e^{-\frac{1}{\tau f_s}} \cos\left(2\pi \frac{f}{f_s}\right) \quad (7)$$

$$y_1 = e^{-\frac{1}{\tau f_s}} \sin\left(2\pi \frac{f}{f_s}\right) \quad (8)$$

where

$$\tau \triangleq \text{time in seconds for filter to decay to } 1/e \quad (9)$$

$$f \triangleq \text{resonant frequency of filter in Hz} \quad (10)$$

$$f_s \triangleq \text{sampling rate in samples per second} \quad (11)$$

Equations (7–10) are valid for  $f$  less than  $f_s/2$ . For  $f$  between  $f_s/2$  and  $f_s$ , the generated frequency will be reflected about  $f_s/2$ .

Negative values of  $\tau$  will generate exponentially increasing sinusoids which can be musically useful.

#### 3.2. Forced Solution

The output of our digital filter is  $y(n)$ . We have not so far provided a mechanism to input a series of samples of a time function into the filter. An input is necessary if we wish to use the filter in a traditional way—that is, to “filter” samples of a sound wave. A number of possibilities exist for adding input samples to our difference equation. We have chosen to add input samples to  $x(n)$ . With this modification, Equations (2–3) become

$$x(n+1) = x_1x(n) - y_1y(n) + u(n) \quad (12)$$

$$y(n+1) = y_1x(n) + x_1y(n) \quad (13)$$

where  $u(n)$  are samples of the input to the filter. The transfer function of the filter is then

$$H(z) \triangleq \frac{Y(z)}{U(z)} = \frac{y_1 z^{-2}}{1 - 2x_1 z^{-1} + (x_1^2 + y_1^2) z^{-2}} \quad (14)$$

$$= \frac{r_1 \sin(\theta_1) z^{-2}}{1 - 2r_1 \cos(\theta_1) z^{-1} + r_1^2 z^{-2}} \quad (15)$$

This is a so-called “all pole” filter, since its two zeros are at  $z = \infty$  and therefore do not affect the magnitude response. This choice of input can be interpreted as driving the poles in *series*, since the transfer functions of series (cascade) filter combinations simply multiply.

We have compared both the sound and the spectrum of our filter output with the outputs of other filter difference equations realizations and we have detected no differences.

We may alternatively add the input samples  $u(n)$  on the right-hand side of Eq. (13) to obtain the transfer function

$$H(z) = \frac{z^{-1} - x_1 z^{-2}}{1 - 2x_1 z^{-1} + (x_1^2 + y_1^2) z^{-2}} \quad (16)$$

$$= \frac{z^{-1} - r_1 \cos(\theta_1) z^{-2}}{1 - 2r_1 \cos(\theta_1) z^{-1} + r_1^2 z^{-2}}. \quad (17)$$

This choice of input introduces a finite zero at  $z = x_1 = r_1 \cos(\theta_1)$ , which is the real part of the location of both poles. This can be interpreted as driving the poles in *parallel*, since denoting the complex conjugate of  $z = x + jy$  by  $\bar{z} = x - jy$ , we have

$$z_1^n + \bar{z}_1^n \leftrightarrow \frac{1}{1 - z_1 z^{-1}} + \frac{1}{1 - \bar{z}_1 z^{-1}} \quad (18)$$

$$= \frac{2 - 2\text{re}\{z_1\} z^{-1}}{1 - 2\text{re}\{z_1\} z^{-1} + |z_1|^2 z^{-2}} \quad (19)$$

$$= 2 \frac{1 - x_1 z^{-1}}{1 - 2x_1 z^{-1} + r_1^2 z^{-2}} = 2zH(z). \quad (20)$$

#### 3.3. State Space Formulation

Rewriting the filter in state-space form,<sup>2</sup> we have

$$\begin{bmatrix} x(n+1) \\ y(n+1) \end{bmatrix} = \begin{bmatrix} x_1 & -y_1 \\ y_1 & x_1 \end{bmatrix} \begin{bmatrix} x(n) \\ y(n) \end{bmatrix} + \begin{bmatrix} b_1 \\ b_2 \end{bmatrix} u(n)$$

<sup>2</sup>[http://www-ccrma.stanford.edu/~jos/filters/-State\\_Space\\_Models.html](http://www-ccrma.stanford.edu/~jos/filters/-State_Space_Models.html)

or

$$\underline{x}(n+1) = \mathbf{A}\underline{x} + \mathbf{B}u(n) \quad (21)$$

$$y(n) = \mathbf{C}^T \underline{x}(n) + Du(n) \quad (22)$$

where  $\mathbf{C}^T = [c_1, c_2] = [0, 1]$  and  $D = 0$ . As is well known, the transfer function of a state-space model (A,B,C,D) is given by

$$H(z) = \mathbf{C}^T(z\mathbf{I} - \mathbf{A})^{-1}\mathbf{B} + D \quad (23)$$

$$= \frac{e_1 z^{-1} + e_2 z^{-2}}{1 - 2r_1 \cos(\theta_1)z^{-1} + r_1^2 z^{-2}}, \quad (24)$$

where

$$e_1 = c_1 b_1 + c_2 b_2 \quad (25)$$

$$e_2 = -c_1(b_1 x_1 + b_2 y_1) + c_2(b_1 y_1 - b_2 x_1). \quad (26)$$

Thus, under all choices of input or output, there is at most one real finite zero at  $z = -e_2/e_1$ .

### 3.4. Phase-Preserving Restrikes

An interesting third (nonlinear) input possibility is to add the input to the *instantaneous magnitude* of  $z(n)$ . This mode is useful for “restriking” a decaying filter oscillation in a *phase-preserving* manner. The result is that the amplitude of a decaying oscillation can be jumped without altering its phase at all.

Adding a real signal  $u(n)$  to the magnitude of  $z(n)$  is equivalent to scaling  $z(n)$  by  $g(n) = u(n)/r(n) + 1$ , where  $r(n) = |z(n)|$ , to get

$$\left[ \frac{u(n)}{r(n)} + 1 \right] z(n) = [u(n) + r(n)]e^{j\theta(n)}.$$

Since amplitude jumps can be perceived as “clicks” when they are too fast, it is useful to delay amplitude jumps until the next zero-crossing of the output  $y(n)$ . Waiting for a zero-crossing in  $y(n)$  is equivalent to waiting for the phase of  $z(n)$  to reach either 0 or  $\pi$ .

Waiting for phase 0 to scale the state  $z(n) = x(n)$  by some gain factor  $g$  is equivalent to adding an input impulse with amplitude  $u(n) = (g-1)|z(n)| = (g-1)x(n)$  to  $x(n)$  at that time. Therefore, another approach to achieving smooth filter restriking is to delay them until the next positive-going zero-crossing in the output signal  $y(n)$ .

### 3.5. Numerical Considerations

Since the difference equations (12–13) are based simply on the multiplication of two complex numbers, their extrapolation is guaranteed to be stable for any value of  $f$  provided the computer arithmetic is perfect. Round-off errors in computer arithmetic will limit the maximum value of  $\tau$ , the accuracy of the resonant frequency, and the stability of the extrapolation in ways we have not studied in detail. Using 64 bit floating point arithmetic seems to be entirely adequate for musical purposes. For lower precision implementations, the alternate forms described in the following two subsections may be considered.

#### 3.5.1. Modified Coupled Form Resonator

Robust behavior in fixed-point implementations using short word lengths, including perfect stability in the undamped case, can be obtained by replacing the complex multiply in Equations (12–13) with a damped version of the so-called “modified coupled form” (MCF) sine oscillator [2]:

$$x(n+1) = r_1[x(n) - \epsilon y(n)] + b_1 u(n) \quad (27)$$

$$y(n+1) = r_1[\epsilon x(n+1) + y(n)] + b_2 u(n) \quad (28)$$

where  $\epsilon = 2 \sin(\theta_1/2)$ , and nominally  $b_1 = 1$  and  $b_2 = 0$ . This recursion is highly insensitive to round-off error. When excited by an impulse ( $u(n) = \delta(n)$ ) with no damping ( $r_1 = 1$ ), the signals  $[x(n), y(n)]$ , viewed as coordinates in the complex plane, follow a fixed *elliptical orbit* over time. As  $\epsilon \rightarrow 0$ , the ellipse approaches a perfect circle. The complex multiply algorithm of Equations (12–13), on the other hand, generates an exact *circle* for all frequencies in the absence of quantization errors.<sup>3</sup> The component sinusoids  $x(n)$  and  $y(n)$  remain samples of pure sinusoids at the same frequency, as in the complex multiply case. The elliptical orbit is due only to the components having a relative phase difference other than 90 degrees. The relative phase approaches 90 degrees as the oscillation frequency (pole angle) approaches zero.

#### 3.5.2. Digital Waveguide Resonator

Another attractive second-order filter structure, based on the “digital waveguide oscillator” [1], is the *digital waveguide resonator* (DWR):

$$x'(n) = gx(n) \quad (29)$$

$$v(n) = c'[x'(n) + y(n)] \quad (30)$$

$$x(n+1) = v(n) - y(n) + \tilde{b}_1 u(n) \quad (31)$$

$$y(n+1) = x'(n) + v(n) + b_2 u(n) \quad (32)$$

where<sup>4</sup>

$$g = r_1^2 \quad (33)$$

$$\tilde{b}_1 = b_1 \sqrt{\frac{1-c'}{1+c'}} \quad (34)$$

$$c' = \sqrt{\frac{1}{1 + \frac{\tan^2(\theta)(1+g)^2 + (1-g)^2}{4g}}} \quad (35)$$

$$\approx 1 - \frac{\tan^2(\theta)(1+g)^2 + (1-g)^2}{8g}. \quad (36)$$

Note that  $c' = \cos(\theta_1)$  when  $g = 1$  (undamped case). Like the MCF, the DWR produces steady sinusoidal oscillations indefinitely, even for short word lengths. This happens because the resonance tuning is controlled by only one coefficient, when the damping goes to zero. As would be the

<sup>3</sup>In the field of *computer graphics*, the MCF has been called the “magic circle” algorithm, because it can be used to recursively draw “circles” on the screen that always close on themselves, even in low-precision arithmetic. While the drawing may look like a circle (when sufficiently many points are computed along its circumference), it is really an ellipse.

<sup>4</sup>[http://www-ccrma.stanford.edu/~jos/waveguide/-Digital\\_Waveguide\\_Oscillator.html](http://www-ccrma.stanford.edu/~jos/waveguide/-Digital_Waveguide_Oscillator.html)

case for any oscillator structure which is controlled by one coefficient affecting tuning only, quantization of that coefficient can only affect tuning as well. Unlike the MCF and complex multiply, which require four multiplies per sample, the DWR requires only two multiplies per sample. Moreover, when the decay is set to  $\tau = \infty$  ( $r_1 = 1$ ), one of the multiplies in the DWR disappears, leaving only *one* multiply per sample for sinusoidal oscillation. As a result, the DWR appears to be best suited for VLSI implementation. As an added bonus, the  $x$  and  $y$  outputs of the DWR are in exact phase quadrature, like the complex-multiply case considered first above. Note, however, that the choice of input (to either the  $x(n)$  or  $y(n)$  state variables) results different amplitude scaling.

Figure 1 shows an overlay of initial impulse responses for the three resonators discussed above. The decay factor was set to  $r_1 = 0.99$ , and the output of each multiplication was quantized to 16 bits, as were all coefficients. The three waveforms sound and look identical. (There are small differences, however, which can be seen by plotting the differences of pairs of waveforms.)

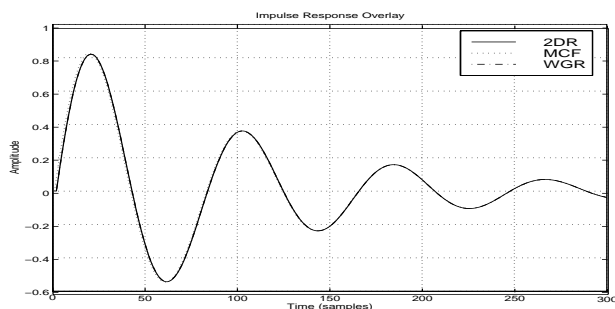


Figure 1: Overlay of three resonator impulse responses, with  $B^T = [1, 0]$  and  $C^T = [0, 1]$ , for the (1) complex-multiply resonator (labeled “2DR” for “2D rotation”), (2) modified coupled form (MCF), and (3) second-order digital waveguide resonator (DWR).

Figure 2 shows the same impulse-response overlay but with  $r_1 = 1$  and only 4 significant bits in the coefficients and signals. The complex multiply oscillator can be seen to decay toward zero due to coefficient quantization ( $x_1^2 + y_1^2 < 1$ ). The MCF and DWR remain steady at their initial amplitude. All three suffer some amount of tuning perturbation.

#### 4. PROGRAM TO PRODUCE AND FILTER SOUND WAVES

To experiment with the timbres that can be synthesized with our high Q filters, we wrote a test program, `filter.cpp`. The program runs on an 800MHz PC running a Linux operating system. The program can

- Compute up to 200 filters whose outputs are summed and sent to a d-to-a converter (16bit, monaural, 44.1kHz) running as a real-time synthesis process.
- Accept impulse inputs to blocks of filters to generate homogeneous filter responses.

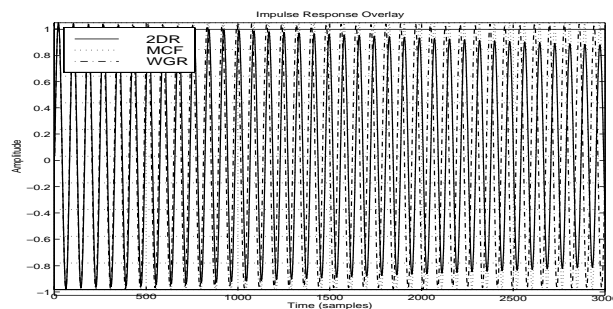


Figure 2: Overlay of three resonator impulse responses, as in Fig. 1, but with  $r_1 = 1$  and quantization of coefficients and signals to 4 significant bits.

- Accept samples from a sound wave put through an a-to-d converter (16bit, monaural, 44.1kHz) running as a real-time effects processor.
- Accept samples from .wav files in the computer hard disk as input.
- Dynamically change the resonant frequencies and damping of blocks of filters in response to either computer keyboard key presses or midi input commands from a midi keyboard.
- Display either waveforms or envelopes of various sampled waves in the computer program

Computations are done in double precision floating point arithmetic. The program has not been carefully optimized. Only about 30 percent of the computer power seems to run all 200 filters.

Tests where parametric changes (both frequencies and decay times) of blocks of filters were suddenly changed showed that neither visible nor audible transients were produced by the parametric changes. Thus it would appear that both frequency and decay can be used as rapidly changing time-varying parameters to form “compositional lines” in compositions.

In the presentation of this paper at the SMAC 03 meeting, we will demonstrate various timbres and effects that can be produced by the filters.

#### 5. CONCLUSIONS

Although no significant compositions employing our high Q parametrically well behaved two pole filters have yet been written, we believe the filters will provide an important new resource for composers, particularly for generating new timbres.

#### 6. REFERENCES

- [1] J. O. Smith and P. R. Cook, “The second-order digital waveguide oscillator,” *Proc. 1992 Int. Computer Music Conf., San Jose*. 1992, pp. 150–153, Comp. Mus. Assoc., <http://www-ccrma.stanford.edu/~jos/wgo/>.
- [2] J. W. Gordon and J. O. Smith, “A sine generation algorithm for VLSI applications,” in *Proc. 1985 Int. Computer Music Conf., Vancouver*. 1985, CMA.

## MODELING AND REAL-TIME SYNTHESIS OF THE KANTELE USING DISTRIBUTED TENSION MODULATION

*Jyri Pakarinen, Matti Karjalainen, and Vesa Välimäki*

Helsinki University of Technology, Laboratory of Acoustics and Audio Signal Processing,  
P.O. Box 3000, FIN-02015 HUT, Espoo, Finland  
jyri.pakarinen@acoustics.hut.fi

### ABSTRACT

Nonlinear behavior of a vibrating string is responsible for acoustical features in some plucked-string instruments, resulting in a characteristic and easily recognizable tone. That is also the case for the Finnish kantele, a traditional plucked-string instrument used in folk music. Earlier works have analyzed the general acoustic properties of the kantele and discussed related sound synthesis techniques. In this study, a novel modeling and sound synthesis method for simulating nonlinear string vibrations with spatially distributed tension modulation is presented. The modeling is conducted through a Digital Waveguide (DWG) approach, using controllable fractional delay elements in implementing the distributed tension modulation nonlinearity. The elongation of the vibrating string is estimated and the result is used in tuning the fractional delay values accordingly. Because of the spatially distributed nature of the approach, control of the string model parameters and observation of its behavior can be implemented at any point along it, in contrast to prior digital waveguide string models. This new approach is applied in constructing a physical model of a five-string kantele. Real-time sound synthesis is implemented using an efficient, block-based modeling tool, the BlockCompiler.

### 1. INTRODUCTION

During the previous years physical modeling has become a more and more tempting sound synthesis approach when the objective is to synthesize the sound of a musical instrument. Possible growth of computational complexity when physical models are used is well compensated by increased sound quality and physically meaningful control data. This study uses a technique called Digital Waveguide modeling (DWG) in establishing a computational model for sound synthesis of nonlinear vibrating strings, in order to produce a physically based sound synthesis of the kantele. The DWG method is widely used in sound synthesis, and it is especially well suited for modeling vibrating strings. An excellent introduction to DWG's used in modeling musical instruments can be found in [1].

### 2. ACOUSTICAL ANALYSIS OF PLUCKED STRINGS

An ideal plucked string with rigid terminations at both ends will produce a harmonic sound, where the frequency of every partial will be an integer multiple of the fundamental frequency. If the string behaves linearly (i.e., a change in the string length does not change the behavior of the vibrational movement), the fundamental frequency will be constant throughout the vibration process. It is well known also that an ideal nonelastic vibrating string can be plucked in such a way that some of the harmonics are missing.

More specifically, if the string is plucked at position  $1/N$  of its length, the resulting motion will lack every  $N$ th harmonic.

The behavior of a nonlinear string is however somewhat different. In an elastic string, the plucking (and vibration) introduces an increase in the length of the string, which results in a growth of tension and furthermore an increase in the frequency of the vibrational movement. As the vibration decays, the effect of the nonlinearity is diminished, and the frequency of the vibration approaches asymptotically the frequency in the linear case.

Also, the behavior of missing harmonics is different in a nonlinear string if the string terminations are nonrigid. The tension modulation in the string will cause excitation of the missing harmonics via the nonrigid string ends. In a way, the energy of other modes will "leak" to the missing modes through the mode coupling in the termination points. The missing harmonics will therefore experience a gradual onset after the pluck, and after that they will decay exponentially like all other harmonics. The generation of missing modes in nonlinear vibrating strings is covered in more detail by Legge and Fletcher [2].

### 3. PLUCKED-STRING MODELS USING DIGITAL WAVEGUIDES

The DWG string model relies on the d'Alembert's solution of the one-dimensional wave equation to divide the wave into two components: the left-proceeding and the right-proceeding wave. The behavior of the string can be seen as the superposition of these two waves. In the DWG method, the string is seen consisting of two delay lines, where the signals travel in opposite directions and proceed to the other delay line when the end of the first one is reached. If the model represents a vibrating string, the reflection of wave components at the endpoints must include a sign change.

Resistive losses of the vibrational movement are modeled with attenuating coefficients somewhere along the delay lines. Frequency-dependent losses in the vibrating string are often modeled with a lowpass filter, called the loop filter, usually implemented at the termination point of the delay line [3], [4]. Since most of the sound radiated from plucked stringed instruments is coming from the vibrating body or the top plate of the instrument, it is logical to consider the output signal as a force signal to the point connecting the body and the string. In the case of a DWG model this would correspond to taking the output as the velocity difference of the two delay lines at the end of the waveguide.

#### 4. ACOUSTICAL ANALYSIS OF THE KANTELE

The kantele is a bridgeless, traditional Finnish plucked string instrument, with usually five metal strings in its basic form. The strings are terminated at one end by metal tuning pins, which are screwed directly into the soundboard. At the opposite end all strings are wound once around a horizontal metal bar called the varras and then knotted. Because of the nonzero distance between the center of the varras and the knot, the vibrations in two polarization planes will have different effective lengths; the varras will be the termination point for horizontal vibration, while the knot will act as a termination for the vertical vibration. This phenomenon causes the total vibration of the string to have two fundamental components with slightly different frequencies, producing beating. The structure of the kantele and the string termination at varras is illustrated in Figure 1. A more detailed structure and acoustical analysis of the kantele can be found in an earlier work [5]. An acoustically improved new design and a study of the history of kantele is presented elsewhere in these proceedings [6].

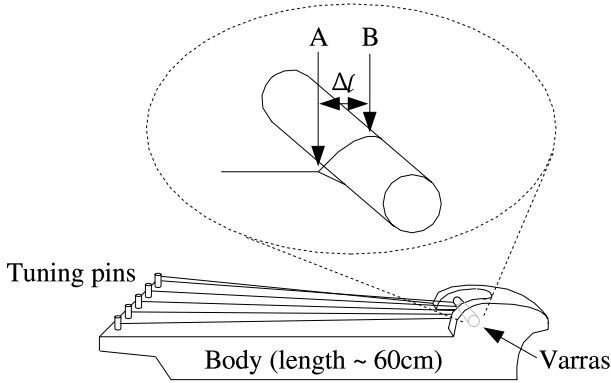


Figure 1: Illustration of the kantele. The string termination at varras is magnified for clarity. *A* denotes the termination point for vertical vibration of the string, while *B* denotes the termination point for horizontal vibration.  $\Delta l$  stands for the distance between *A* and *B*.

#### 5. NOVEL KANTELE STRING MODEL

##### 5.1. Implementing the effects of tension modulation

From the discussion in Section 2, a conclusion can be drawn that simulation of the effects of tension modulation is important if high-quality plucked-string instrument synthesis is to be obtained. Tension modulation in a one-dimensional digital waveguide model is best modeled using fractional delay elements (also known as fractional delay filters). The fractional delay elements are basically allpass filters with adjustable coefficients, being able to produce a controllable delay [7], [8]. They are widely used in the literature with one-dimensional DWG's in tuning the delay lines [3], [9]. The design process of the fractional delay elements is covered in [8].

Previous works [4], [10], [5] use a single fractional delay element in a single-polarization string model for computational efficiency. Physically this would correspond to a single elastic element at the termination point of an otherwise rigid string. An alternative solution can be obtained if the elongation process can be distributed along the delay line, in a similar way that a real

physical string functions, where the elasticity is distributed along the string.

Elongation of the string can be expressed as [2]

$$l_{dev} = \int_0^{l_{nom}} \sqrt{1 + \left(\frac{\partial y}{\partial x}\right)^2} dx - l_{nom} \quad (1)$$

where  $l_{nom}$  is the nominal string length,  $x$  is the spatial coordinate along the string, and  $y$  is the displacement of the string. The first spatial derivative in equation (1) would suggest using slope as a wave variable in the DWG, and thus equation (1) can be approximated for the digital waveguide as [10]

$$L_{dev}(n) = \sum_{k=0}^{\hat{L}_{nom}} \sqrt{1 + [s_r(n, k) + s_l(n, k)]^2} - \hat{L}_{nom} \quad (2)$$

where  $s_r(n, k)$  and  $s_l(n, k)$  are the slope waves at position  $k$  and time instant  $n$ , propagating to the right and to the left, respectively.  $\hat{L}_{nom}$  is the rounded nominal string length. To reduce the computational complexity, equation (2) can be further simplified using a truncated Taylor series expansion to [10]

$$L_{dev}(n) \approx \frac{1}{2} \sum_{k=0}^{\hat{L}_{nom}} [s_r(n, k) + s_l(n, k)]^2 \quad (3)$$

while still maintaining a sufficient accuracy. The approximated delay variation of the total DWG can be obtained from equation (3) as [10]

$$D_{tot}(n) \approx -\frac{1}{2} \sum_{l=n-1-\hat{L}_{nom}}^{n-1} \left(1 + \frac{ES}{F_{nom}}\right) \frac{L_{dev}(l)}{L_{nom}} \quad (4)$$

where  $E$  is Young's modulus,  $S$  is the cross-sectional area of the string, and  $F_{nom}$  is the nominal tension corresponding to the string at rest.

Since the system under consideration uses a distributed set of delay elements, the total delay must be divided by the number of delay elements in the DWG to obtain a delay value for each individual element. The fractional delay element used in the system is a first-order allpass filter of the form

$$A(z) = \frac{-a + z^{-1}}{1 - az^{-1}} \quad (5)$$

where  $a$  is the filter coefficient which defines the length of the delay. Notice that when  $a = 0$  the allpass filter acts as a unit delay. Coefficient  $a$  can be expressed as [7]

$$a = \frac{1 - d_{partial}}{1 + d_{partial}} \quad (6)$$

where  $d_{partial}$  is the delay intended for a single allpass filter. The first order allpass-filter is the best choice for the fractional delay element when delay values around unity are to be obtained [11]. Generally, the approximation of an allpass filter is most accurate when the desired delay is close to the order of the allpass filter. First-order allpass filters also have relatively low computational complexity and zero magnitude response error. The phase response error caused by the allpass filter is not considered to pose a problem since its effect is negligible in the audio frequency range, assuming the sampling frequency to be reasonably high [7].

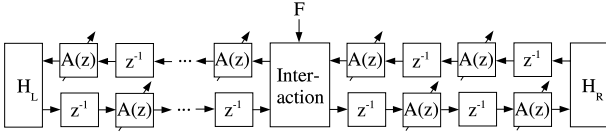


Figure 2: The single-polarization string model.  $A(z)$  denotes an allpass filter, while  $z^{-1}$  denotes a unit delay.  $H_L$  and  $H_R$  are FIR filters modeling the frequency-dependent losses at the left and right string termination points, respectively. The interaction element provides means for inserting a force signal into the string, and its location can be changed.

## 5.2. Single polarization string model

A single-polarization string model constructed from the elements discussed above is illustrated in Figure 2. In this model, both delay lines carry velocity waves, thus allowing a velocity signal of any location on the string to be obtained by summing the left- and right-proceeding wave components at that particular location. Slope waves can be obtained by taking the difference of the wave components and scaling it by a constant coefficient. The unit delays between each allpass filter ensure that no delay-free loops will emerge even if the position of the interaction element is changed.

It is possible to implement an alternative string model, where all delay lines are constructed from allpass filters, resulting in a more homogeneous structure. With this approach however, it must be assured that the structure has at least one unit-delay element inside each loop in order to avoid computability problems. A more in-depth study concerning the construction of the single-polarization model is presented by the authors [12].

## 5.3. Dual polarization string model

The novel synthesis model of a single kantele string is constructed using two single-polarization string models connected through a coupling impedance. The elongation approximations of the strings and the resulting allpass filter coefficient values are evaluated separately for the two string models. The structure of the novel kantele string model is illustrated in Figure 3. In this model,  $v_1(n)$  and  $v_2(n)$  represent the velocity signals coming from the strings vibrating vertically and horizontally, respectively.

It is important to note that while  $v_1(n)$  and  $v_2(n)$  can be obtained anywhere along the string, in this case they are evaluated at the termination points, so that terminal impedances can be used.  $Z_{1bridge}$  and  $Z_{2bridge}$  represent the vertical and horizontal terminal impedances, respectively.  $Z_c$  stands for the coupling impedance from vertical to horizontal string vibration polarization, and  $f_{12}(n)$  represents the corresponding driving force. The forces to the termination caused by the two one-polarizational vibrations are denoted by  $f_1(n)$  and  $f_2(n)$ . The output of the whole two-polarization string model is presented by force signal  $f_{out}(n)$  exerted to the string termination point.

## 6. SYNTHESIS RESULTS

The synthesis results reveal that the behavior of the nonlinear string model is consistent with the theory of elastic strings, discussed in Section 2. The fundamental frequency behaviors of a single-polarization string model and a real kantele tone are compared in

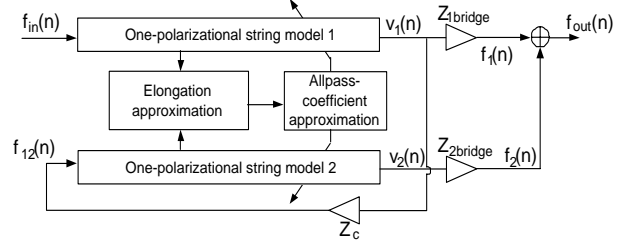


Figure 3: Two-polarization kantele string model. The one-polarizational string model blocks are identical to what is illustrated in Figure 2. Both one-polarizational blocks have different lengths. It is important to note that the coupling between the vibrational polarizations in a real physical system is more complicated but a simplified one-way coupling is used here for clarity.

Figure 4. In this figure, the dash-dotted line approximates the mean value of perceptual detection threshold of an initial pitch glide. The detection threshold in the frequency region of these tones is approximated to be 5.4 Hz [13]. The string model used in this figure had a total delay line length of 55.25 and the allpass coefficient  $a$  was scaled using a constant value of 0.8 in order to simulate the behavior of the recorded sample. The sampling frequency was 44.1 kHz for all string models used in this paper.

The envelope trajectories of the first three partials of a nonlinear plucked string model tone are depicted in Figure 5(a), while the same partials obtained from a linear plucked string model are illustrated in Figure 5(b). As predicted in Section 2, the missing harmonic in the nonlinear case has a gradual increase after the onset of the vibration, and after that it experiences an exponential decay like all other modes. The presence of the heavily attenuated third harmonic in the linear case in Figure 5(b) can be explained by the fact that the excitation to the string was not positioned exactly but only approximately at the location 1/3 of the string's length. The linear string model used in Figure 5(b) was the same as the nonlinear one except that the allpass-coefficient was kept constant during the whole process. The string model used in Fig. 5 had total delay line lengths of 60.5 samples including two third-order low-pass filters (with coefficients  $[-0.0761 \ 0.566 \ 0.566 \ -0.0761]$ ) at both ends as loop filters, and the interaction element was placed between the 20th and 21st delay element. The beating discussed in Section 4 is naturally absent from Fig. 5, since only a single-polarizational string was modeled.

A real-time sound synthesis model of a kantele is constructed using an experimental, block-based, efficient audio-DSP-tool, the BlockCompiler. The algorithm used is efficient enough to process a kantele model with several strings on an ordinary laptop computer at a 44.1 kHz sampling rate. A more detailed description of the BlockCompiler is presented by Karjalainen [14].

## 7. CONCLUSIONS

In this paper we have presented a spatially distributed model of a nonlinear vibrating string. The acoustic features of a real elastic string (fundamental frequency drift and generation of missing harmonics) are modeled in a physically correct manner with this novel approach. The string model is constructed using digital waveguides, and fractional delay filters are used for simulating the nonlinearities. A kantele synthesis model is constructed using two

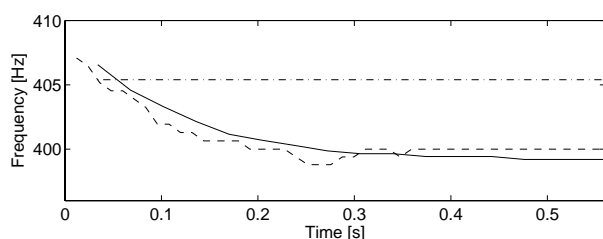


Figure 4: Illustration of the fundamental frequency glide in the synthesized tone (solid line) and in a real kantele tone, obtained via measurements (dashed line). The approximated detection threshold of a pitch drift, illustrated as a dash-dotted line, suggests that the fundamental frequency drifts in both cases are audible.

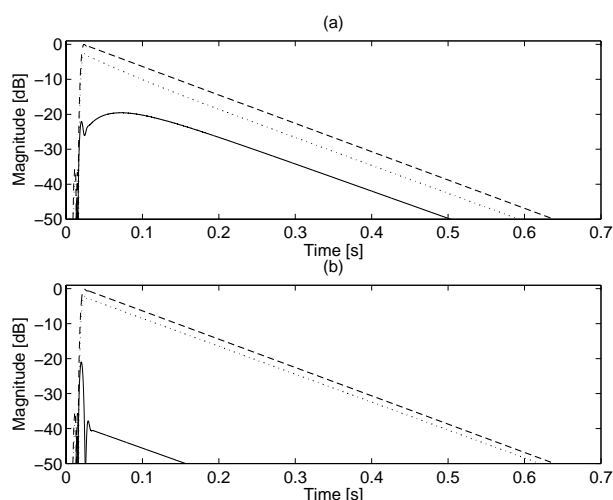


Figure 5: Envelope trajectories of first three harmonics of a synthetic tone in the nonlinear case (a) and in the linear case (b). The string was plucked in both cases at approximately 1/3 of its length. The first harmonic is plotted with a dashed line, the second with a dotted line, and the third with a solid line.

coupled string models for each real kantele string. The advantage of the new approach over previous methods for synthesizing nonlinear strings is its spatially distributed structure, which allows the interaction to the string model to be applied at any point along it.

## 8. ACKNOWLEDGMENTS

This research was done within the ALMA project (ALgorithms for Modelling of Acoustic interactions IST-2001-33059). The ALMA homepage can be found at <http://ftp-dsp.elet.polimi.it/alma/>.

## 9. REFERENCES

- [1] J. O. Smith, "Principles of digital waveguide models of musical instruments," in *Applications of Digital Signal Processing to Audio and Acoustics*, 1997, pp. 417–466.
- [2] K. A. Legge and N. H. Fletcher, "Nonlinear generation of missing modes on a vibrating string," *J. Acoust. Soc. Am.*, vol. 76, pp. 5–12, July 1984.

- [3] D. A. Jaffe and J. O. Smith, "Extensions of the Karplus-Strong plucked string algorithm," *Computer Music Journal*, vol. 7, no. 2, pp. 56–69, summer 1983.
- [4] V. Välimäki, T. Tolonen, and M. Karjalainen, "Plucked-string synthesis algorithms with tension modulation nonlinearity," in *Proc. IEEE Int. Conf. on Acoustics, Speech and Signal Processing*, Phoenix, Arizona, March 15-19, 1999, vol. 2, pp. 977–980.
- [5] C. Erkut, M. Karjalainen, P. Huang, and V. Välimäki, "Acoustical analysis and model-based sound synthesis of the kantele," *J. Acoust. Soc. Am.*, vol. 112, pp. 1681–1691, October 2002.
- [6] J. Pölkki, C. Erkut, H. Penttinen, M. Karjalainen, and V. Välimäki, "New designs for the kantele with improved sound radiation," in *Proc. Stockholm Music Acoustics Conference*, Stockholm, Sweden, August 6-9, 2003.
- [7] V. Välimäki, *Discrete-Time Modeling of Acoustic Tubes Using Fractional Delay Filters*, Doctoral dissertation, Helsinki Univ. of Tech., Acoustics Lab Report Series, Report no. 37, 1995, available on-line at <http://www.acoustics.hut.fi/publications/>.
- [8] T. I. Laakso, V. Välimäki, M. Karjalainen, and U. K. Laine, "Splitting the unit delay - tools for fractional delay filter design," *IEEE Signal Processing Magazine*, vol. 13, no. 1, pp. 30–60, 1996.
- [9] J. O. Smith, *Techniques for Digital Filter Design and System Identification with Application to the Violin*, Ph.D. dissertation, Stanford, California, Stanford University, Dept. of Music, CCRMA Tech. Report no. STAN-M-14, 1983.
- [10] T. Tolonen, V. Välimäki, and M. Karjalainen, "Modeling of tension modulation nonlinearity in plucked strings," *IEEE Transactions on Speech and Audio Processing*, vol. 8, no. 3, pp. 300–310, May 2000.
- [11] V. Välimäki and T. I. Laakso, "Principles of fractional delay filters," in *Proc. International Conference on Acoustics, Speech and Signal Processing*, Istanbul, Turkey, 5-9 June 2000, vol. 6, pp. 3870–3873.
- [12] J. Pakarinen, M. Karjalainen, and V. Välimäki, "Sound synthesis model for a nonlinear vibrating string using distributed fractional delay elements," in *Proc. Finnish Signal Processing Symposium*, Tampere, Finland, May 19, 2003, available on-line at <http://www.cs.tut.fi/finsig03/>.
- [13] H. Järveläinen and V. Välimäki, "Audibility of initial pitch glides in string instrument sounds," in *Proceedings of the International Computer Music Conference*, Havana, Cuba, 17-23 September 2001, pp. 282–285, available on-line at <http://lib.hut.fi/Diss/2003/isbn9512263149/article3.pdf>.
- [14] M. Karjalainen, "BlockCompiler: Efficient simulation of acoustic and audio systems," in *Proc. 114th AES Convention*, Amsterdam, The Netherlands, 22-25 March 2003.

# THE ESTIMATION OF BIRDSONG CONTROL PARAMETERS USING MAXIMUM LIKELIHOOD AND MINIMUM ACTION

Tamara Smyth, Jonathan S. Abel, Julius O. Smith III

Center for Computer Research in Music and Acoustics (CCRMA)  
Stanford University  
tamara/abel/jos@ccrma.stanford.edu

## ABSTRACT

In this research, a method is presented for extracting the control parameters of an avian syrinx synthesis model from recorded birdsong. A look-up table pairs combinations of pressure and tension parameters with the model's corresponding output power spectra. At each time frame, a generalized likelihood ratio fills a pressure-tension matrix indicating similarity between the birdsong power spectrum and the tabulated spectra. Successive pressure-tension matrices are stacked and points exhibiting a good fit to the data align to form trajectories corresponding to changes in pressure and tension over time which can then be used to control the model. In the event a range of trajectories matches the data well, the selected trajectory is that of least action.

## 1. INTRODUCTION

A physical model of the bird's vocal tract was developed using waveguide synthesis techniques for the bronchi and trachea tubes and finite difference methods for the nonlinear vibrating syringeal membranes [1, 2]. In order to judge the model's ability to produce realistic birdsong, and also to improve playability of the model by limiting the parameter space, we have devised a method for extracting the two primary control parameters of the model, pressure and tension, from recorded birdsong.

We employ a *maximum likelihood* approach illustrated in Fig. 3 to extract pressure and tension trajectories. Recorded birdsong is segmented and the power spectra frames are compared to tabulated model power spectra using a likelihood function to indicate goodness of fit. Those control parameter sets having large likelihood at each frame are then aligned to form trajectories over time. Finally, the trajectories are adjusted to account for the ability of the bird to generate and change pressure and tension.

We begin by briefly outlining aspects of the avian syrinx model to give context to the discussion that follows. The maximum likelihood approach is described and the likelihood function detailed. The method is then applied to a field recording of a zebra finch.

## 2. THE SYNTHESIS MODEL

The bird's airway consists of a trachea which divides into the left and right bronchi at its base, and a membrane which forms a valve near the top of each bronchus. During voiced song, the membrane is set into motion by air flow, vibrating at a frequency determined partly by the mass and tension of the membrane and partly by the resonance of the air column to which it is connected [3].

The valve model has the following four variables, illustrated in Fig. 1, which evolve over time during sound production:

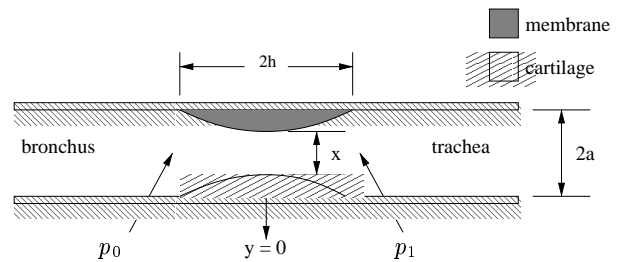


Figure 1: The transverse model of a pressure controlled valve.

1. Pressure on the bronchial side of the valve,  $p_0(t)$ .
2. Air volume flow through the valve channel,  $U(t)$ .
3. Displacement of the membrane,  $x(t)$ .
4. Pressure on the tracheal side of the valve,  $p_1(t)$ .

The model of the valve displacement and the resulting pressure through the constriction is based on the mechanical properties of the membrane and the Bernoulli equation for the air flow. The methods used for digitally simulating the avian vocal tract model are more thoroughly described in [1] and [2], but a signal flow diagram is presented in Fig. 2 for convenience.

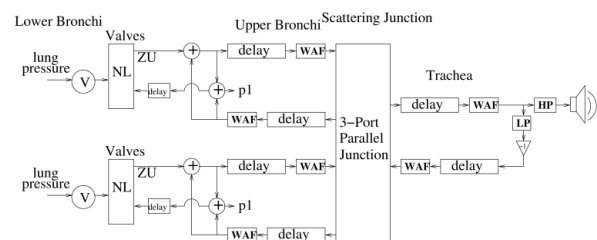


Figure 2: Signal flow diagram of the model

The syrinx shows tremendous variation in structure between different bird species; example values of some anatomical parameters used in the model for various bird sizes are given in Table 2. The two primary control parameters of the model (and the bird) are the blowing pressure from the lungs and the tension of the membrane [4] which the bird controls by contracting the syringeal muscles and by raising the pressure in the interclavicular air sac which encases the syrinx.

There is a definite relationship between the pitch of the sound produced by the bird and the tension of the syringeal membrane.



Fletcher writes the displacement of the membrane as a function of time  $x(t)$  for mode  $n$  as [5]

$$m_n \left[ \frac{d^2 x_n}{dt^2} + 2\kappa \frac{dx_n}{dt} + \omega_n^2 (x_n - x_0) \right] = \epsilon_n F, \quad (1)$$

where the frequency of the first mode  $\omega_1$  is given by

$$\omega_1 = \left( \frac{5T}{\rho_M a H} \right)^{\frac{1}{2}}, \quad (2)$$

with  $T$  being tension,  $\rho_M$  the membrane density,  $a$  the radius of the bronchus,  $H$  the membrane width and  $d$  the membrane thickness with example values given in Table 1. It can be seen therefore, that when the bird increases the tension of the membrane the pitch of the song will also increase. Likewise, an increase in air pressure from the lungs will cause a general increase in amplitude of the produced sound.

anatomical parameters	small	medium	large
membrane density ( $kg/m^3$ )	1000	1000	1000
membrane width ( $mm$ )	1.9	3.5	4.1
membrane thickness ( $\mu m$ )	100	100	100
left bronchus length ( $mm$ )	5	14	30
right bronchus length ( $mm$ )	5	14	30
trachea length ( $mm$ )	17.1	23	35.6
left bronchus radius ( $mm$ )	1.47	2.5	3.5
right bronchus radius ( $mm$ )	1.47	2.5	3.5
trachea radius ( $mm$ )	1.9	3.5	4.1

Table 1: Examples of fixed anatomical parameters for different bird sizes. Though it is the case here, it is not necessary that the left and right bronchus be symmetrical

The mapping of pressure and tension to loudness and pitch respectively is not straightforward however, since nonlinearities intrinsic to the dynamics of the syrinx cause less predictable behaviour [6]. A slight change in one parameter, for instance, can cause effects such as period doubling, mode-locking and transitions from periodic to chaotic behaviour. It would also be somewhat unreasonable to ask a player of the model to control the parameters with the speed and virtuosity of a songbird. It is clear therefore, another mapping strategy is necessary.

### 3. MAXIMUM LIKELIHOOD MODEL

We begin by specifying fixed anatomical parameters of the model corresponding to the bird species whose song we wish to simulate and of which we have a recording. In this case our technique is illustrated making reference to a recording of a zebra finch and makes use of the small bird anatomical parameters from Table 1.

A look-up table is generated by pairing combinations of the control parameters pressure and tension with the model's corresponding output power spectra. Fig. 4 shows an excerpt of the spectrum table for tension ranging from zero to eight at five pressure values. The actual table has many more entries and since it only need be computed once (or at least once per bird species), it can be made as large and dense as is permitted by computer memory.

With the tabulated model spectra in place, the recorded bird-song is processed via a short-time Fourier transform [7] to form a

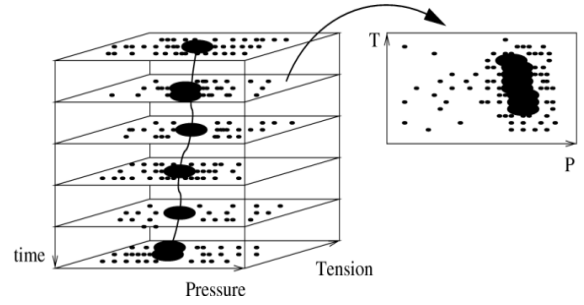


Figure 3: Stack of likelihood images.

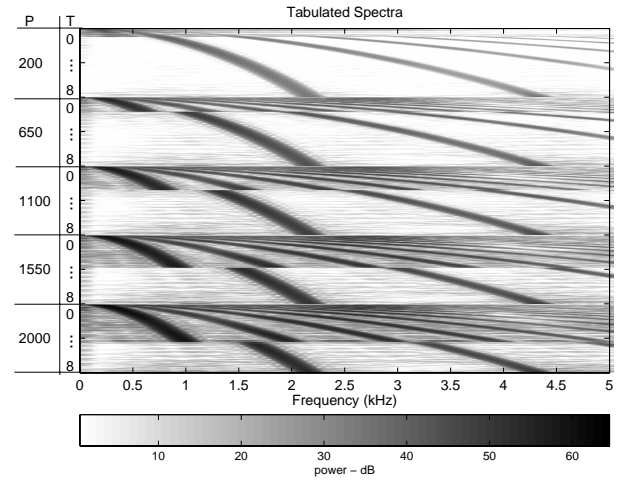


Figure 4: Model output power spectra for different pressure and tension values.

sequence of power spectra over time. An example spectrogram in Fig. 5, taken from a field recording, shows a sequence of gestures for the song of a zebra finch. As is typical of field recordings, it contains a significant amount of background noise concentrated in the low frequencies.

At each time frame, a normalized *log likelihood function* [8] is used to indicate the similarity between the birdsong power spectrum and each of the entries in the spectrum table, filling a pressure-tension matrix similar to the one shown in Fig. 6. The likelihood function used here is normalized so that entries having a value close to one—indicated with dark pixels in Fig. 6—correspond to pressure-tension settings producing spectra very similar to the measured frame spectrum. Those producing entries close to zero—indicated with lighter pixels—have very different spectra from the measured frame under consideration.

The likelihood function was chosen for its statistical properties: In the limit of small estimation errors, its peak location is known to be unbiased with minimum variance [8]. In other words, the likelihood function will, on average, peak at the correct control parameter values, and the peak location will be as insensitive as possible to measurement noise.

We assume that the recorded signal  $s(t)$  consists of the model output  $\mu_\theta(t)$  with measurement and/or modeling error  $\nu(t)$  which

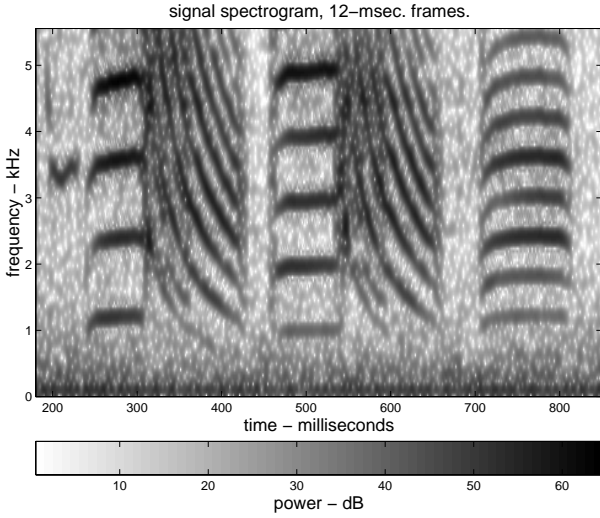


Figure 5: Power spectra for field recording of a zebra finch.

is additive and Gaussian-distributed,

$$s(t) = \alpha \mu_\theta(t) + \nu(t), \quad (3)$$

where  $\alpha$  is an unknown scaling factor and  $\theta = [P \ T]$  is the parameter vector containing pressure  $P$  and tension  $T$ .

Assuming the measured signal is stationary over the duration of an analysis frame, the power spectrum of the measured signal is given by

$$S(\omega) = \alpha^2 M_\theta(\omega) + N(\omega) \quad (4)$$

with  $M_\theta$  representing the model output power spectrum for parameters  $\theta$  and  $N(\omega)$  the noise power spectrum at frequency  $\omega$ . In the case that the noise power  $N(\omega)$  is much smaller than the signal, the probability of observing a power spectrum  $\mathbf{S}$  given control parameters  $\theta$  may be approximated by

$$\begin{aligned} \varphi(\mathbf{S}; \theta) &\approx \mathcal{N}(\alpha^2 \mathbf{M}_\theta, \Sigma) \\ &= \frac{\exp\{-\frac{1}{2}(\mathbf{S} - \alpha^2 \mathbf{M}_\theta)^\top \Sigma^{-1}(\mathbf{S} - \alpha^2 \mathbf{M}_\theta)\}}{\det(2\pi \Sigma)^{\frac{1}{2}}} \end{aligned} \quad (5)$$

where  $\mathbf{S}$  is the stack containing power spectrum bins  $S(\omega_i)$  and similarly  $\mathbf{M}_\theta$  is the stack of model power spectrum bins.

Under the assumption that the additive spectral noise is independent and identically distributed, the log likelihood for a parameter set  $\theta$  given measurements  $\mathbf{S}$  is

$$l(\theta; \mathbf{S}) = -\frac{1}{2\sigma^2}(\mathbf{S} - \alpha^2 \mathbf{M}_\theta)^\top (\mathbf{S} - \alpha^2 \mathbf{M}_\theta). \quad (6)$$

For convenience, we normalize the likelihood so that it ranges from zero, indicating an unlikely fit, to one, indicating a good match:

$$\bar{l}(\theta; \mathbf{S}) = 1 - \frac{(\mathbf{S} - \alpha^2 \mathbf{M}_\theta)^\top (\mathbf{S} - \alpha^2 \mathbf{M}_\theta)}{(\mathbf{S} + \alpha^2 \mathbf{M}_\theta)^\top (\mathbf{S} + \alpha^2 \mathbf{M}_\theta)}. \quad (7)$$

The second term from (7) may be interpreted as the squared distance between the scaled measured data and the table entry, normalized by the squared length of their sum. When the parameters

are such that the measured and model spectra coincide, the numerator above will be small and the likelihood close to one. When the measured and model spectra are very different, the numerator is large—it can never be larger than the denominator as both spectra are positive—and the likelihood is close to zero.

#### 4. MINIMUM ACTION

Typically there will be a range of likelihood ratios that match the data well. The pressure-tension likelihood functions tend to have maxima that are wide in pressure and narrow in tension. On occasion there will be well separated likelihood maxima corresponding to different registers or modes of oscillation with a division between the two. We assume our bird will not expel any unnecessary energy during song performance and in the event of multiple well separated matching maxima we choose the one requiring the least effort on the part of the bird.

Minimum action is introduced into the likelihood function in two ways: one takes into account the effort involved to move from one parameter value to another over time while the other simply incorporates the instantaneous effort where higher values of tension and pressure are considered to require more effort.

For the instantaneous effort we assume that it is more difficult to produce higher values of pressure and tension and represent this added difficulty with a penalty function added to the likelihood function. On the assumption that it is difficult for the bird to rapidly slew control parameters, the sequence of likelihood function maximizers are median filtered to eliminate sporadic, short lived, jumps in the trajectories. A further slew limiting filter is applied to ensure rates of parameter change that are physical plausible.

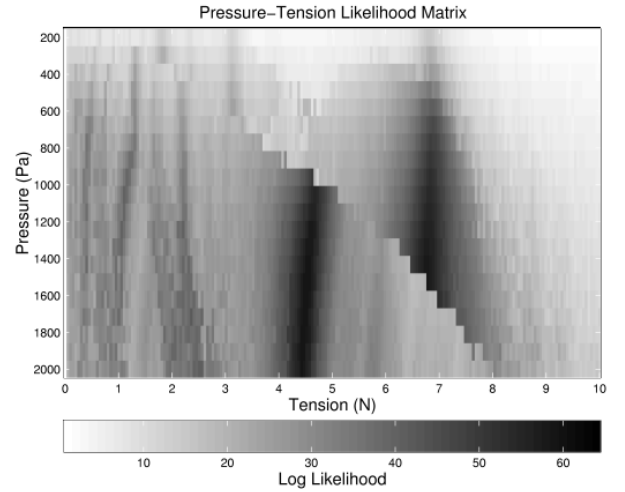


Figure 6: A pressure-tension matrix for one time frame shows two disparate operating registers.

#### 5. CONCLUSIONS

This research serves two purposes: 1) to judge the model's ability to produce realistic birdsong by calibrating it to recorded birdsong and 2) to restrict and scale the control parameter space so as to

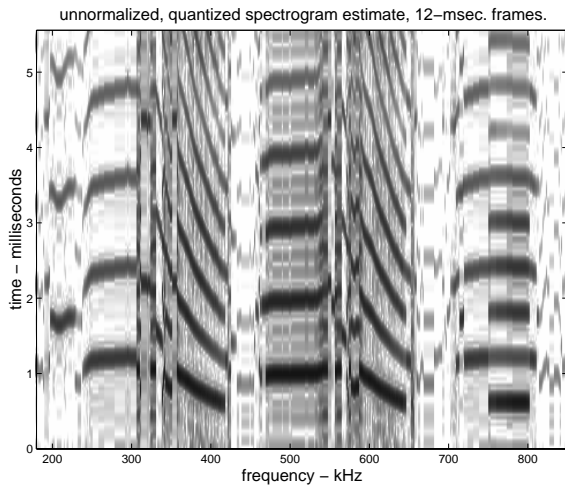


Figure 7: Power spectra based on maximum likelihood control estimates.

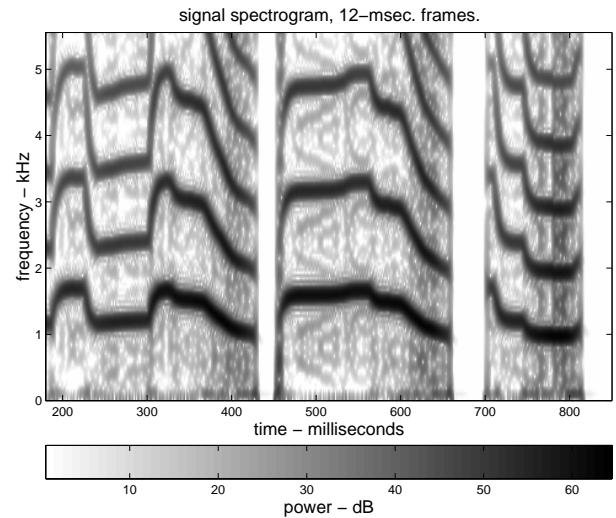


Figure 9: Power spectra of model output using control trajectories from Fig. 8

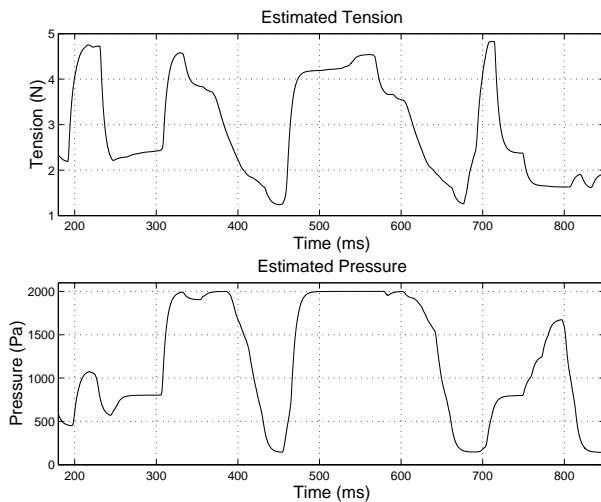


Figure 8: Control trajectories for pressure and tension.

improve the user's ability to interact with the model, e.g., by having a controller that follows predetermined trajectories through the matrix stack.

We applied our method to the zebra finch song shown in Fig. 5. Tabulated power spectra corresponding to the most likely parameters at each time frame are sequenced and shown in Fig. 7. The similarity between the two spectra show very good potential in the model's ability to produce accurate bird-like song.

The final control trajectories extracted from the zebra finch recording are shown in Fig. 8. The spectrogram of the corresponding model output is shown in Fig. 9. Though not identical to either Fig. 5 or Fig. 7 the sound output is perceptually similar and the song gesture is well captured. By mapping the trajectories of Fig. 8 to an input device with two individual continuous controls, the player of the model is able to reproduce bird-like song without requiring the bird's expert technique.

## 6. REFERENCES

- [1] Tamara Smyth and Julius O. Smith, "The sounds of the avian syrinx—are they really flute-like?," in *DAFX 2002 Proceedings*, Hamburg, Germany, September 2002, International Conference on Digital Audio Effects.
- [2] Tamara Smyth and Julius O. Smith, "The syrinx: Nature's hybrid wind instrument," in *CD-ROM Paper Collection*, Cancun Mexico, September 2002, Pan-America/Iberian Meeting on Acoustics.
- [3] Neville H. Fletcher and A. Tarnopolsky, "Acoustics of the avian vocal tract," *Journal of the Acoustical Society of America*, vol. 105, no. 1, pp. 35–49, January 1999.
- [4] Tim Gardner, G Cecchi, M. Magnasco, R. Laje, and Gabriel B. Mindlin, "Simple motor gestures for birdsongs," *Physical Review Letters*, vol. 87, no. 20, pp. 1–4, November 2001.
- [5] Neville H. Fletcher, "Bird song – a quantitative acoustic model," *Journal of Theoretical Biology*, vol. 135, pp. 455–481, 1988.
- [6] M. S. Fee, B. Shraiman, B. Pesaran, and P. P. Mitra, "The role of nonlinear dynamics of the syrinx in the vocalization of a songbird," *Nature*, vol. 395, pp. 67–71, 1998.
- [7] J. B. Allen and L. R. Rabiner, "A unified approach to short-time fourier analysis and synthesis," *Proc. IEEE*, vol. 65, no. 11, pp. 1558–1564, November 1977.
- [8] Louis L. Scharf, *Statistical Signal Processing: Detection, Estimation, and Time Series Analysis*, Addison-Wesley Publishing Company, Inc., 1991.

## **AUTHOR INDEX**

Abel, J S	413
Adachi, S	313
Alipour, F	499
Almeida, A	243
Alonso-Moral, J	549
Amatriain, X	533
Amir, N	189
Ando, Y	475
Arcos, J L	533
Askenfelt, A	67, 91, 151
Astesano, C	671
Atig, M	267
Avanzini, F	95
Badeau, R	715
Bader, R	121
Bank, B	143
Barbancho, A M	517
Barbancho, I	517
Benckert, L	321
Bendiksen, B	561
Bennett, G	13
Bensa, J	365
Bensoam, J	369
Bergner, A	317, 707
Bergweiler, S	317, 707
Bertsch, M	193
Besson, M	671
Beurmann, A	167
Bilbao, S D	365
Bissinger, G	35
Bjerkvik, A	299
Bonada, J	439
Bonsi, D	751
Botros, A	247
Bresin, R	155, 159, 685, 689, 693
Bromage, S R	197
Brown, A W	39
Buen, A	43
Burns, C	373
Burtner, M	373
Campbell, D M	185, 197, 233, 251, 451, 747, 759
Camurri, A	561, 569, 631
Canazza, S	521
Carlsson, P	47, 103
Carral, S	251

Castellengo, M	455
Castro-Sierra, E	591
Caussé, R	243, 263, 369
Chiang, Y C	577
Chilekwa, V	711
Cirotteau, D	561
Cook, P R	385, 677
Cottingham, J P	255
Courtney, P E	107
Čulík, M	87
Czyzewski, A	259
Dahl, S	561, 595, 599, 685, 689
Dall'Osto, D	603
Dalmont, J-P	267, 283
Daniels, A E	213
David, B	715
De Baets, B	635
de Götzen, A	525
De Meyer, H	635
De Poli, G	17
De Voogdt, L	631
Deutsch, B	343
Dillon, R	529
Disley, A C	607
Divoir, S	397
Drioli, C	377
Drumm, I A	381
Dziubinski, M	623
Elejalde-Garcia, M J	549, 719
Ellis, N	369
Erkut, C	133
Esposito, E	125, 723, 755
Esquef, P A A	339
Essl, G	385
Fabre, B	239
Fagnan, L	443
Faraone, G	447
Farner, S	397, 671
Felce, R	343
Fletcher, N H	201, 307
Fontana, F	51
Franco-García, A	719
Franke, H	763
Friberg, A	13, 521, 561, 599
Fritz, C	263
Galembo, A	147, 151, 159
Galluzzo, P M	55

Gäumann, T	163
Geissler, P	59
Gerhard-Multhaupt, R	317, 707
Gilbert, J	229, 233, 267, 271
Giordano, B L	611
Goebl, W	155, 159
Gómez, E	533
Görne, T	317
Gough, C	63
Grachten, M	533
Granqvist, S	459, 595
Gray, C D	451
Greated, C A	451, 747
Gren, P	321
Green, M	295
Griffith, N J L	553
Guettler, K	67, 91
Guillemain, P	389
Hall, D E	727, 729
Hansen, K F	689, 693
Hansen, U J	351
Hanson, R J	731
Henrich, N	455
Hertegård, S	459
Hill, T J W	129, 275, 711
Hirschberg, A	239
Hollenberg, L C L	307
Howard, D M	463, 467, 607, 697
Huitric, H	619
Huovinen, E	615
Imagawa, H	471, 495
Janariz-Larumbe, J	719
Jansson, E V	71
Jelonek, J	75
Jerkert, J	537
Johansson, E-L	321
Johansson, Ö	647
Johansson, S	447
Jordà, S	681
Juslin, P N	513
Kamitani, T	541
Kanno, J	179
Karjalainen, M	133, 339, 393, 409, 739
Kato, K	475
Kausel, W	205
Kenmochi, H	439
Kergomard, J	263, 389, 397

Kim, Y E	479
Kirkwood, B	655
Kiss, J	619
Kjellmo, I	561
Klapuri, A P	587
Kob, M	431
Kostek, B	259, 623
Kouzuki, K	541
Krishnaswamy, A	627
Kristiansen, U	299
Kronland-Martinet, R	365, 671
Kühnelt, H	401
Kuuskankare, M	545
Larkin, B	355
Larsson, H	459
Laurson, M	545
Le Carrou, J-L	229
Lee, M E	483
Leman, M	631, 635
Lesaffre, M	635
Li, A	735
Liljencrants, J	325
Liu, R	553
Llanos-Vazquez, R	549
Løkberg, O J	43
Loscos, A	439
Ludwigsen, D O	209
Łukasik, E	75, 79, 83
Lyu, R Y	577
Macho- Stadler, E	549, 719
Macomber, H K	731
Madison, G	639
Magne, C	671
Marassi, M	723
Marshall, M	685
Martens, J P	635
Martner, O	59
Mathews, M V	13, 405
Matsuda, M	541
Mayer, A	279
Mazzarino, B	561, 631
McCarthy, H	561
Merker, B	639
Mikimoto, S	179
Millot, L	329
Ming, J	667
Mion, L	557

Misdariis, N	369
Molin, N E	703
Moore, T R	213, 343
Moravec, O	643
Morrison, A C	731
Moynihan, B	685
Murphy, P	553
Murtagh, F	667
Nahas, M	619
Naganovski, A	75
Nederveen, C J	217
Niimi, S	471, 495
Noreland, J O D	221
Noson, D	475
Nykänen, A J	647
Ollivier, S	283
Osaka, N	495
Otčenášek, Z	333, 651, 663
Otondo, F	487, 655
Pakarinen, J	409, 739
Pallone, G	671
Parati, L	487
Pasdeloup, V	671
Penttinen, H	133
Perrin, R	343, 347
Peterson, D R	287
Petiot, J F	225, 229
Petrini, K	611
Pettersen, V	491
Poblano, H A	591
Poirson, E	229
Pölkki, J	133
Polotti, P	447
Poulimenos, A	499
Radhakrishnan, N	499
Rajčan, E	87
Rath, M	685
Richard, G	715
Richards, O F	197, 233
Richardson, B E	117, 129
Richardson, S J	129
Rimell, S	697
Rinman, M L	561
Robinson, A	343
Rocchesso, D	7, 95
Rodà, A	521
Rodet, X	243, 443



Rohner, F	351
Rossing, T D	251, 351, 355
Roubeau, B	455
Sakakibara, K-I	471, 495
Sapp, C	13
Scavone, G P	291
Schärer, S	351
Scherer, K R	25
Scherer, R C	499
Schleske, M	59
Schneider, A	167
Schoonderwaldt, E	67, 91
Serafin, S	51, 95, 99, 373
Sharp, D B	275, 711, 735
Shirado, T	659
Shirley, E T	213
Simon, L	271
Sjölander, K	743
Sjölander, P J	503
Skala, J S	171
Skulina, D J	747
Slowinski, R	75
Smith, J	247, 295, 307
Smith III, J O	3, 365, 405, 413
Smith, M J T	483
Smyth, T	413
Stanzial, D	751
Štěpánek, J	333, 643, 651, 663
Story, B H	435
Stulov, A	175
Sujbert, L	143
Sundberg, J	13
Susmaga, R	83
Suzuki, H	179
Swallowe, G M	343, 347
Syrový, V	333, 651
Taguti, T	565
Tanghe, K	635
Tarabusi, V	755
Tardón, L J	517
Tarnopolsky, A Z	307
Tayama, N	471
Terroir, J	271
Timmers, R	569
Tinnsten, M	47, 103
Titze, I R	21
Tro, J	299

Tronchin, L	755
Tsai, C G	303
Urgela, S	87
Välimäki, V	133, 339, 361, 409
van Walstijn, M O	759
Ventura-Miravet, R	667
Vergez, C	243, 369, 397
Vermeulen, V	631
Voinier, T	389
Volpe, G	569, 631
Waadeland, C H	573
Walker, J	553
Wang, C K	577
Wegener, M	317, 707
Westgaard, R H	491
Widmer, G	509, 581
Wirges, W	707
Wolfe, J	247, 263, 295, 307
Woodhouse, J	31, 55, 107, 137
Yanagida, M	659
Yoo, J	355
Young, D	99, 111
Ystad, S	671
Zanon, P	521, 581
Zerbs, C	59
Zipser, L	763
Zwan, P	623



## **GNU FREE DOCUMENTATION LICENSE**

Version 1.2, November 2002

Copyright (C) 2000,2001,2002 Free Software Foundation, Inc.  
59 Temple Place, Suite 330, Boston, MA 02111-1307 USA

Everyone is permitted to copy and distribute verbatim copies  
of this license document, but changing it is not allowed.

### **0. PREAMBLE**

The purpose of this License is to make a manual, textbook, or other functional and useful document "free" in the sense of freedom: to assure everyone the effective freedom to copy and redistribute it, with or without modifying it, either commercially or noncommercially. Secondly, this License preserves for the author and publisher a way to get credit for their work, while not being considered responsible for modifications made by others.

This License is a kind of "copyleft", which means that derivative works of the document must themselves be free in the same sense. It complements the GNU General Public License, which is a copyleft license designed for free software.

We have designed this License in order to use it for manuals for free software, because free software needs free documentation: a free program should come with manuals providing the same freedoms that the software does. But this License is not limited to software manuals; it can be used for any textual work, regardless of subject matter or whether it is published as a printed book. We recommend this License principally for works whose purpose is instruction or reference.

### **1. APPLICABILITY AND DEFINITIONS**

This License applies to any manual or other work, in any medium, that contains a notice placed by the copyright holder saying it can be distributed under the terms of this License. Such a notice grants a world-wide, royalty-free license, unlimited in duration, to use that work under the conditions stated herein. The "Document", below, refers to any such manual or work. Any member of the public is a licensee, and is addressed as "you". You accept the license if you copy, modify or distribute the work in a way requiring permission under copyright law.

A "Modified Version" of the Document means any work containing the Document or a portion of it, either copied verbatim, or with modifications and/or translated into another language.

A "Secondary Section" is a named appendix or a front-matter section of the Document that deals exclusively with the relationship of the publishers or authors of the Document to the Document's overall subject (or to related matters) and contains nothing that could fall directly within that overall subject. (Thus, if the Document is in part a textbook of mathematics, a Secondary Section may not explain any mathematics.) The relationship could be a matter of historical connection with the subject or with related matters, or of legal, commercial, philosophical, ethical or political position regarding them.

The "Invariant Sections" are certain Secondary Sections whose titles are designated, as being those of Invariant Sections, in the notice that says that the Document is released under this License. If a section does not fit the above definition of Secondary then it is not allowed to be designated as Invariant. The Document may contain zero Invariant Sections. If the Document does not identify any Invariant Sections then there are none.

The "Cover Texts" are certain short passages of text that are listed, as Front-Cover Texts or Back-Cover Texts, in the notice that says that the Document is released under this License. A Front-Cover Text may be at most 5 words, and a Back-Cover Text may be at most 25 words.

A "Transparent" copy of the Document means a machine-readable copy, represented in a format whose specification is available to the general public, that is suitable for revising the document straightforwardly with generic text editors or (for images composed of pixels) generic paint programs or (for drawings) some widely available drawing editor, and that is suitable for input to text formatters or for automatic translation to a variety of formats suitable for input to text formatters. A copy made in an otherwise Transparent file format whose markup, or absence of markup, has been arranged to thwart or discourage subsequent modification by readers is not Transparent. An image format is not Transparent if used for any substantial amount of text. A copy that is not "Transparent" is called "Opaque".

Examples of suitable formats for Transparent copies include plain ASCII without markup, Texinfo input format, LaTeX input format, SGML or XML using a publicly available DTD, and standard-conforming simple HTML, PostScript or PDF designed for human modification. Examples of transparent image formats include PNG, XCF and JPG. Opaque formats include proprietary formats that can be read and edited only by proprietary word processors, SGML or XML for which the DTD and/or processing tools are not generally available, and the machine-generated HTML, PostScript or PDF produced by some word processors for output purposes only.

The "Title Page" means, for a printed book, the title page itself, plus such following pages as are needed to hold, legibly, the material this License requires to appear in the title page. For works in formats which do not have any title page as such, "Title Page" means the text near the most prominent appearance of the work's title, preceding the beginning of the body of the text.

A section "Entitled XYZ" means a named subunit of the Document whose title either is precisely XYZ or contains XYZ in parentheses following text that translates XYZ in another language. (Here XYZ stands for a specific section name mentioned below, such as "Acknowledgements", "Dedications", "Endorsements", or "History".) To "Preserve the Title" of such a section when you modify the Document means that it remains a section "Entitled XYZ" according to this definition.

The Document may include Warranty Disclaimers next to the notice which states that this License applies to the Document. These Warranty Disclaimers are considered to be included by reference in this License, but only as regards disclaiming warranties: any other implication that these Warranty Disclaimers may have is void and has no effect on the meaning of this License.

## **2. VERBATIM COPYING**

You may copy and distribute the Document in any medium, either commercially or noncommercially, provided that this License, the copyright notices, and the license notice saying this License applies to the Document are reproduced in all copies, and that you add no other conditions whatsoever to those of this License. You may not use technical measures to obstruct or control the reading or further copying of the copies you make or distribute. However, you may accept compensation in exchange for copies. If you distribute a large enough number of copies you must also follow the conditions in section 3.

You may also lend copies, under the same conditions stated above, and you may publicly display copies.

## **3. COPYING IN QUANTITY**

If you publish printed copies (or copies in media that commonly have printed covers) of the Document, numbering more than 100, and the Document's license notice requires Cover Texts, you must enclose the copies in covers that carry, clearly and legibly, all these Cover Texts: Front-Cover Texts on the front cover, and Back-Cover Texts on the back cover. Both covers must also clearly and legibly identify you as the publisher of these copies. The front cover must present the full title with all words of the title equally prominent and visible. You may add other material on the covers in addition. Copying with changes limited to the covers, as long as they preserve the title of the Document and satisfy these conditions, can be treated as verbatim copying in other respects.

If the required texts for either cover are too voluminous to fit legibly, you should put the first ones listed (as many as fit reasonably) on the actual cover, and continue the rest onto adjacent pages.

If you publish or distribute Opaque copies of the Document numbering more than 100, you must either include a machine-readable Transparent copy along with each Opaque copy, or state in or with each Opaque copy a computer-network location from which the general network-using public has access to download using public-standard network protocols a complete Transparent copy of the Document, free of added material. If you use the latter option, you must take reasonably prudent steps, when you begin distribution of Opaque copies in quantity, to ensure that this Transparent copy will remain thus accessible at the stated location until at least one year after the last time you distribute an Opaque copy (directly or through your agents or retailers) of that edition to the public.

It is requested, but not required, that you contact the authors of the Document well before redistributing any large number of copies, to give them a chance to provide you with an updated version of the Document.

## **4. MODIFICATIONS**

You may copy and distribute a Modified Version of the Document under the conditions of sections 2 and 3 above, provided that you release the Modified Version under precisely this License, with the Modified Version filling the role of the Document, thus licensing distribution and modification of the Modified Version to whoever possesses a copy of it. In addition, you must do these things in the Modified Version:

- A. Use in the Title Page (and on the covers, if any) a title distinct from that of the Document, and from those of previous versions (which should, if there were any, be listed in the History section of the Document). You may use the same title as a previous version if the original publisher of that version gives permission.
- B. List on the Title Page, as authors, one or more persons or entities responsible for authorship of the modifications in the Modified Version, together with at least five of the principal authors of the Document (all of its principal authors, if it has fewer than five), unless they release you from this requirement.
- C. State on the Title page the name of the publisher of the Modified Version, as the publisher.
- D. Preserve all the copyright notices of the Document.
- E. Add an appropriate copyright notice for your modifications adjacent to the other copyright notices.
- F. Include, immediately after the copyright notices, a license notice giving the public permission to use the Modified Version under the terms of this License, in the form shown in the Addendum below.

- G. Preserve in that license notice the full lists of Invariant Sections and required Cover Texts given in the Document's license notice.
- H. Include an unaltered copy of this License.
- I. Preserve the section Entitled "History", Preserve its Title, and add to it an item stating at least the title, year, new authors, and publisher of the Modified Version as given on the Title Page. If there is no section Entitled "History" in the Document, create one stating the title, year, authors, and publisher of the Document as given on its Title Page, then add an item describing the Modified Version as stated in the previous sentence.
- J. Preserve the network location, if any, given in the Document for public access to a Transparent copy of the Document, and likewise the network locations given in the Document for previous versions it was based on. These may be placed in the "History" section. You may omit a network location for a work that was published at least four years before the Document itself, or if the original publisher of the version it refers to gives permission.
- K. For any section Entitled "Acknowledgements" or "Dedications", Preserve the Title of the section, and preserve in the section all the substance and tone of each of the contributor acknowledgements and/or dedications given therein.
- L. Preserve all the Invariant Sections of the Document, unaltered in their text and in their titles. Section numbers or the equivalent are not considered part of the section titles.
- M. Delete any section Entitled "Endorsements". Such a section may not be included in the Modified Version.
- N. Do not retitle any existing section to be Entitled "Endorsements" or to conflict in title with any Invariant Section.
- O. Preserve any Warranty Disclaimers.

If the Modified Version includes new front-matter sections or appendices that qualify as Secondary Sections and contain no material copied from the Document, you may at your option designate some or all of these sections as invariant. To do this, add their titles to the list of Invariant Sections in the Modified Version's license notice. These titles must be distinct from any other section titles.

You may add a section Entitled "Endorsements", provided it contains nothing but endorsements of your Modified Version by various parties--for example, statements of peer review or that the text has been approved by an organization as the authoritative definition of a standard.

You may add a passage of up to five words as a Front-Cover Text, and a passage of up to 25 words as a Back-Cover Text, to the end of the list of Cover Texts in the Modified Version. Only one passage of Front-Cover Text and one of Back-Cover Text may be added by (or through arrangements made by) any one entity. If the Document already includes a cover text for the same cover, previously added by you or by arrangement made by the same entity you are acting on behalf of, you may not add another; but you may replace the old one, on explicit permission from the previous publisher that added the old one.

The author(s) and publisher(s) of the Document do not by this License give permission to use their names for publicity for or to assert or imply endorsement of any Modified Version.

## **5. COMBINING DOCUMENTS**

You may combine the Document with other documents released under this License, under the terms defined in section 4 above for modified versions, provided that you include in the combination all of the Invariant Sections of all of the original documents, unmodified, and list them all as Invariant Sections of your combined work in its license notice, and that you preserve all their Warranty Disclaimers.

The combined work need only contain one copy of this License, and multiple identical Invariant Sections may be replaced with a single copy. If there are multiple Invariant Sections with the same name but different contents, make the title of each such section unique by adding at the end of it, in parentheses, the name of the original author or publisher of that section if known, or else a unique number. Make the same adjustment to the section titles in the list of Invariant Sections in the license notice of the combined work.

In the combination, you must combine any sections Entitled "History" in the various original documents, forming one section Entitled "History"; likewise combine any sections Entitled "Acknowledgements", and any sections Entitled "Dedications". You must delete all sections Entitled "Endorsements."

## **6. COLLECTIONS OF DOCUMENTS**

You may make a collection consisting of the Document and other documents released under this License, and replace the individual copies of this License in the various documents with a single copy that is included in the collection, provided that you follow the rules of this License for verbatim copying of each of the documents in all other respects.

You may extract a single document from such a collection, and distribute it individually under this License, provided you insert a copy of this License into the extracted document, and follow this License in all other respects regarding verbatim copying of that document.

## **7. AGGREGATION WITH INDEPENDENT WORKS**

A compilation of the Document or its derivatives with other separate and independent documents or works, in or on a volume of a storage or distribution medium, is called an "aggregate" if the copyright resulting from the compilation is not used to limit the legal rights of the compilation's users beyond what the individual works permit. When the Document is included in an aggregate, this License does not apply to the other works in the aggregate which are not themselves derivative works of the Document.

If the Cover Text requirement of section 3 is applicable to these copies of the Document, then if the Document is less than one half of the entire aggregate, the Document's Cover Texts may be placed on covers that bracket the Document within the aggregate, or the electronic equivalent of covers if the Document is in electronic form. Otherwise they must appear on printed covers that bracket the whole aggregate.

## **8. TRANSLATION**

Translation is considered a kind of modification, so you may distribute translations of the Document under the terms of section 4. Replacing Invariant Sections with translations requires special permission from their copyright holders, but you may include translations of some or all Invariant Sections in addition to the original versions of these Invariant Sections. You may include a translation of this License, and all the license notices in the Document, and any Warranty Disclaimers, provided that you also include the original English version of this License and the original versions of those notices and disclaimers. In case of a disagreement between the translation and the original version of this License or a notice or disclaimer, the original version will prevail.

If a section in the Document is Entitled "Acknowledgements", "Dedications", or "History", the requirement (section 4) to Preserve its Title (section 1) will typically require changing the actual title.

## **9. TERMINATION**

You may not copy, modify, sublicense, or distribute the Document except as expressly provided for under this License. Any other attempt to copy, modify, sublicense or distribute the Document is void, and will automatically terminate your rights under this License. However, parties who have received copies, or rights, from you under this License will not have their licenses terminated so long as such parties remain in full compliance.

## **10. FUTURE REVISIONS OF THIS LICENSE**

The Free Software Foundation may publish new, revised versions of the GNU Free Documentation License from time to time. Such new versions will be similar in spirit to the present version, but may differ in detail to address new problems or concerns. See <http://www.gnu.org/copyleft/>.

Each version of the License is given a distinguishing version number. If the Document specifies that a particular numbered version of this License "or any later version" applies to it, you have the option of following the terms and conditions either of that specified version or of any later version that has been published (not as a draft) by the Free Software Foundation. If the Document does not specify a version number of this License, you may choose any version ever published (not as a draft) by the Free Software Foundation.

### **ADDENDUM: How to use this License for your documents**

To use this License in a document you have written, include a copy of the License in the document and put the following copyright and license notices just after the title page:

Copyright (c) YEAR YOUR NAME.

Permission is granted to copy, distribute and/or modify this document  
under the terms of the GNU Free Documentation License, Version 1.2  
or any later version published by the Free Software Foundation;  
with no Invariant Sections, no Front-Cover Texts, and no Back-Cover Texts.

A copy of the license is included in the section entitled "GNU  
Free Documentation License".

If you have Invariant Sections, Front-Cover Texts and Back-Cover Texts, replace the "with...Texts." line with this:

with the Invariant Sections being LIST THEIR TITLES, with the  
Front-Cover Texts being LIST, and with the Back-Cover Texts being LIST.

If you have Invariant Sections without Cover Texts, or some other combination of the three, merge those two alternatives to suit the situation.

If your document contains nontrivial examples of program code, we recommend releasing these examples in parallel under your choice of free software license, such as the GNU General Public License, to permit their use in free software.